frontiers | Research Topics

Physical and biogeochemical processes driving methane sources, sinks and emissions in aquatic systems: The past, present and future under global change

Edited by
Daniel F. McGinnis, Yves T. Prairie, Hans-Peter Grossart and Tonya DelSontro

Published in
Frontiers in Environmental Science



FRONTIERS EBOOK COPYRIGHT STATEMENT

The copyright in the text of individual articles in this ebook is the property of their respective authors or their respective institutions or funders. The copyright in graphics and images within each article may be subject to copyright of other parties. In both cases this is subject to a license granted to Frontiers.

The compilation of articles constituting this ebook is the property of Frontiers.

Each article within this ebook, and the ebook itself, are published under the most recent version of the Creative Commons CC-BY licence. The version current at the date of publication of this ebook is CC-BY 4.0. If the CC-BY licence is updated, the licence granted by Frontiers is automatically updated to the new version.

When exercising any right under the CC-BY licence, Frontiers must be attributed as the original publisher of the article or ebook, as applicable.

Authors have the responsibility of ensuring that any graphics or other materials which are the property of others may be included in the CC-BY licence, but this should be checked before relying on the CC-BY licence to reproduce those materials. Any copyright notices relating to those materials must be complied with.

Copyright and source acknowledgement notices may not be removed and must be displayed in any copy, derivative work or partial copy which includes the elements in question.

All copyright, and all rights therein, are protected by national and international copyright laws. The above represents a summary only. For further information please read Frontiers' Conditions for Website Use and Copyright Statement, and the applicable CC-BY licence.

ISSN 1664-8714
ISBN 978-2-8325-2622-4
DOI 10.3389/978-2-8325-2622-4

About Frontiers

Frontiers is more than just an open access publisher of scholarly articles: it is a pioneering approach to the world of academia, radically improving the way scholarly research is managed. The grand vision of Frontiers is a world where all people have an equal opportunity to seek, share and generate knowledge. Frontiers provides immediate and permanent online open access to all its publications, but this alone is not enough to realize our grand goals.

Frontiers journal series

The Frontiers journal series is a multi-tier and interdisciplinary set of open-access, online journals, promising a paradigm shift from the current review, selection and dissemination processes in academic publishing. All Frontiers journals are driven by researchers for researchers; therefore, they constitute a service to the scholarly community. At the same time, the *Frontiers journal series* operates on a revolutionary invention, the tiered publishing system, initially addressing specific communities of scholars, and gradually climbing up to broader public understanding, thus serving the interests of the lay society, too.

Dedication to quality

Each Frontiers article is a landmark of the highest quality, thanks to genuinely collaborative interactions between authors and review editors, who include some of the world's best academicians. Research must be certified by peers before entering a stream of knowledge that may eventually reach the public - and shape society; therefore, Frontiers only applies the most rigorous and unbiased reviews. Frontiers revolutionizes research publishing by freely delivering the most outstanding research, evaluated with no bias from both the academic and social point of view. By applying the most advanced information technologies, Frontiers is catapulting scholarly publishing into a new generation.

What are Frontiers Research Topics?

Frontiers Research Topics are very popular trademarks of the *Frontiers journals series*: they are collections of at least ten articles, all centered on a particular subject. With their unique mix of varied contributions from Original Research to Review Articles, Frontiers Research Topics unify the most influential researchers, the latest key findings and historical advances in a hot research area.

Find out more on how to host your own Frontiers Research Topic or contribute to one as an author by contacting the Frontiers editorial office: frontiersin.org/about/contact

Physical and biogeochemical processes driving methane sources, sinks and emissions in aquatic systems: The past, present and future under global change

Topic editors

Daniel F. McGinnis — University of Geneva, Switzerland
Yves T. Prairie — Université du Québec à Montréal, Canada
Hans-Peter Grossart — University of Potsdam, Germany
Tonya DelSontro — University of Waterloo, Canada

Citation

McGinnis, D. F., Prairie, Y. T., Grossart, H.-P., DelSontro, T., eds. (2023). *Physical and biogeochemical processes driving methane sources, sinks and emissions in aquatic systems: The past, present and future under global change.* Lausanne: Frontiers Media SA. doi: 10.3389/978-2-8325-2622-4

Table of contents

06 Editorial: Sources, sinks, and emissions in aquatic systems: the past, present, and future under global change
Daniel F. McGinnis, Yves T. Prairie, Hans-Peter Grossart and Tonya DelSontro

10 Iterative Forecasting Improves Near-Term Predictions of Methane Ebullition Rates
Ryan P. McClure, R. Quinn Thomas, Mary E. Lofton, Whitney M. Woelmer and Cayelan C. Carey

26 Shelf-Sourced Methane in Surface Seawater at the Eurasian Continental Slope (Arctic Ocean)
Elena Vinogradova, Ellen Damm, Andrey V. Pnyushkov, Thomas Krumpen and Vladimir V. Ivanov

38 Dominance of Diffusive Methane Emissions From Lowland Headwater Streams Promotes Oxidation and Isotopic Enrichment
Andrew L. Robison, Wilfred M. Wollheim, Clarice R. Perryman, Annie R. Cotter, Jessica E. Mackay, Ruth K. Varner, Paige Clarizia and Jessica G. Ernakovich

52 Identifying Sources and Oxidation of Methane in Standing Dead Trees in Freshwater Forested Wetlands
Melinda Martinez, Marcelo Ardón and Mary Jane Carmichael

62 Redox Zone and Trophic State as Drivers of Methane-Oxidizing Bacterial Abundance and Community Structure in Lake Sediments
Sigrid van Grinsven, Dimitri V. Meier, Anja Michel, Xingguo Han, Carsten J. Schubert and Mark A. Lever

84 Spatial Variability and Hotspots of Methane Concentrations in a Large Temperate River
Ingeborg Bussmann, Uta Koedel, Claudia Schütze, Norbert Kamjunke and Matthias Koschorreck

98 Measuring CH_4 Fluxes From Lake and Reservoir Sediments: Methodologies and Needs
Sofia L. D'Ambrosio and John A. Harrison

117 Spatial Mapping of Dissolved Gases in the Danube Delta Reveals Intense Plant-Mediated Gas Transfer
Marie-Sophie Maier, Anna R. Canning, Matthias S. Brennwald, Cristian R. Teodoru and Bernhard Wehrli

133 Lake Sediment Methane Responses to Organic Matter are Related to Microbial Community Composition in Experimental Microcosms
Brittni L. Bertolet, Cristian Koepfli and Stuart E. Jones

143 Relief of Phosphate Limitation Stimulates Methane Oxidation
Thomas P. A. Nijman, André M. Amado, Paul L. E. Bodelier and Annelies J. Veraart

151 Extreme Hydrological Events and Reservoir Methane Emissions
Bradford S. Sherman and Phillip W. Ford

165 Challenges Regionalizing Methane Emissions Using Aquatic Environments in the Amazon Basin as Examples
John M. Melack, Luana S. Basso, Ayan S. Fleischmann, Santiago Botía, Mingyang Guo, Wencai Zhou, Pedro M. Barbosa, Joao H.F. Amaral and Sally MacIntyre

191 Drivers of Anaerobic Methanogenesis in Sub-Tropical Reservoir Sediments
Alistair Grinham, Cathryn O'Sullivan, Matthew Dunbabin, Katrin Sturm, Deborah Gale, William Clarke and Simon Albert

203 Physical Factors and Microbubble Formation Explain Differences in CH_4 Dynamics Between Shallow Lakes Under Alternative States
Sofia Baliña, Maria Laura Sánchez and Paul A. del Giorgio

214 Trait-Based Model Reproduces Patterns of Population Structure and Diversity of Methane Oxidizing Bacteria in a Stratified Lake
Matthias Zimmermann, Magdalena J. Mayr, Damien Bouffard, Bernhard Wehrli and Helmut Bürgmann

229 The Effects of Engineered Aeration on Atmospheric Methane Flux From a Chesapeake Bay Tidal Tributary
Laura L. Lapham, Edward A. Hobbs, Jeremy M. Testa, Andrew Heyes, Melinda K. Forsyth, Casey Hodgkins, Curtis Szewczyk and Lora A. Harris

250 Catchment properties as predictors of greenhouse gas concentrations across a gradient of boreal lakes
Nicolas Valiente, Alexander Eiler, Lina Allesson, Tom Andersen, François Clayer, Camille Crapart, Peter Dörsch, Laurent Fontaine, Jan Heuschele, Rolf D. Vogt, Jing Wei, Heleen A. de Wit and Dag O. Hessen

266 Effects of long-term climate trends on the methane and CO_2 exchange processes of Toolik Lake, Alaska
Werner Eugster, Tonya DelSontro, James A. Laundre, Jason Dobkowski, Gaius R. Shaver and George W. Kling

288 Variability and controls of stable carbon isotopic fractionation during aerobic methane oxidation in temperate lakes
Shoji D. Thottathil, Paula C. J. Reis and Yves T. Prairie

305 Seasonal variability of CO_2, CH_4, and N_2O content and fluxes in small agricultural reservoirs of the northern Great Plains
Sydney A. Jensen, Jackie R. Webb, Gavin L. Simpson, Helen M. Baulch, Peter R. Leavitt and Kerri Finlay

325 Pond greenhouse gas emissions controlled by duckweed coverage
Joseph Rabaey and James Cotner

343 Exploring methane cycling in an arctic lake in Kangerlussuaq Greenland using stable isotopes and 16S rRNA gene sequencing
Sarah B. Cadieux, Ursel M. E. Schütte, Chris Hemmerich, Sarah Powers and Jeffrey R. White

359 Application of concentration and 2-dimensional stable isotope measurements of methane to constrain sources and sinks in a seasonally stratified freshwater lake
Teresa Einzmann, Moritz Schroll, Jan F. Kleint, Markus Greule and Frank Keppler

frontiers | Frontiers in Environmental Science

TYPE Editorial
PUBLISHED 22 May 2023
DOI 10.3389/fenvs.2023.1218878

Check for updates

OPEN ACCESS

EDITED AND REVIEWED BY
Alexandre J. Poulain,
University of Ottawa, Canada

*CORRESPONDENCE
Daniel F. McGinnis,
daniel.mcginnis@unige.ch

RECEIVED 08 May 2023
ACCEPTED 12 May 2023
PUBLISHED 22 May 2023

CITATION
McGinnis DF, Prairie YT, Grossart H-P and DelSontro T (2023), Editorial: Sources, sinks, and emissions in aquatic systems: the past, present, and future under global change.
Front. Environ. Sci. 11:1218878.
doi: 10.3389/fenvs.2023.1218878

COPYRIGHT
© 2023 McGinnis, Prairie, Grossart and DelSontro. This is an open-access article distributed under the terms of the Creative Commons Attribution License (CC BY). The use, distribution or reproduction in other forums is permitted, provided the original author(s) and the copyright owner(s) are credited and that the original publication in this journal is cited, in accordance with accepted academic practice. No use, distribution or reproduction is permitted which does not comply with these terms.

Editorial: Sources, sinks, and emissions in aquatic systems: the past, present, and future under global change

Daniel F. McGinnis[1]*, Yves T. Prairie[2], Hans-Peter Grossart[3,4] and Tonya DelSontro[5]

[1]Aquatic Physics Group, Department F.-A. Forel for Environmental and Aquatic Sciences (DEFSE), Faculty of Science, University of Geneva, Geneva, Switzerland, [2]UNESCO Chair in Global Environmental Change, Université du Québec à Montréal, Montréal, QC, Canada, [3]Department of Experimental Limnology, Leibniz Institute of Freshwater Ecology and Inland Fisheries, Stechlin, Germany, [4]Institute of Biochemistry and Biology, Potsdam University, Potsdam, Germany, [5]Department of Earth and Environmental Sciences, University of Waterloo, Waterloo, ON, Canada

KEYWORDS

methane, ebullition, oxidation, eutrophication, reservoirs, streams, fluxes, ocean

Editorial on the Research Topic
Sources, sinks, and emissions in aquatic systems: the past, present, and future under global change

Methane, a greenhouse gas with a high warming potential, is increasing at an alarming rate (Nisbet et al., 2019). While studies have quantified methane emissions through *in situ* measurements, fewer studies have sought a mechanistic understanding of methane dynamics in aquatic systems (Langenegger et al., 2019). The atmospheric methane contribution from inland and coastal waters remains largely uncertain due to the current mechanistic knowledge gaps and stochastic processes (Bastviken et al., 2011). Methane is unusual in aquatic systems because its oxidation can be nearly as large as its production, highlighting the importance of focusing on both sources and sinks (Thottathil et al., 2019).

The studies in this Research Topic include physical–biogeochemical processes driving methane cycling in both natural and artificial waterbodies, including drivers such as climate warming, eutrophication, and urbanization. Interdisciplinary studies present the effects and feedbacks between methane cycling on the waterbody ecology, physical–biogeochemical cycles, ecology, microbiology, and modeling. Study areas include all types of inland and ocean waters and local, regional, and global upscaling, as well as forecasting. The article types include original research, brief research reports, and reviews.

McClure et al. discussed the potential of near-term ecological forecasting to improve the predicting of sediment methane ebullition rates. The authors developed and tested a near-term, iterative forecasting model of methane ebullition rates in a small eutrophic reservoir. The results show that their refitting approach provides more accurate predictions of methane ebullition rates up to 2 weeks into the future, and it outperforms forecasts without refitting and a persistence null model. The study highlights the need for an improved mechanistic understanding of methane models and future improvements.

Robison et al. quantified stream diffusive methane emissions and compared them to previously published ebullitive emission rates in four lowland headwater streams to

construct a complete methane emission budget. They measured the methane isotopic composition along with the sediment microbial community to investigate production and oxidation across the streams. They show that diffusive methane emissions are 78%–100% of total emissions, and methane oxidation depletes approximately half of the dissolved methane. The authors suggest a conceptual model of methane production, oxidation, and emission from small streams.

Vinogradova et al. investigated the transport of dissolved methane in the Eurasian continental slope and Siberian shelf break during ice melt. The research shows a patchy pattern of methane supersaturation and suggests that sea ice transports methane from the shelf. The study highlights the buffering capacity for seasonal storage of atmospheric and marine methane in the polar mixed layer. It also calculates the potential sea–air flux of methane and describes intrusions of methane plumes from the polar mixed layer into the cold halocline layer.

D'Ambrosio and Harrison critically reviewed 163 peer-reviewed studies that estimate diffusive methane fluxes from lake sediments using sediment incubations, benthic chambers, and modeling approaches. They summarized the advantages and limitations of each method and discussed published comparisons, and they also identified knowledge gaps in understanding lake methane dynamics.

To improve greenhouse gas emission estimates, Grinham et al. examined the methane potential of sediments in mesotrophic and eutrophic sub-tropical reservoirs under different nutrient and organic carbon availabilities. The study shows that these systems are carbon-limited, and the addition of organic carbon significantly increases anaerobic methanogenesis. A comprehensive catchment monitoring program revealed that the frequency of rainfall events is a critical driver of organic matter inputs that drive reservoir methane emissions in the sub-tropical region.

Lapham et al. investigated the effect of engineered aeration on methane dynamics in a eutrophic estuary in Rock Creek, Maryland. The experiment tested the hypotheses that bubble aeration enhances air–water methane flux, and the addition of oxygen will increase aerobic methane oxidation. The results show that regardless of the aeration status, the methane concentrations remained consistently high in all times and locations, establishing the sub-estuary as a source of methane to the atmosphere. The fine-bubble approach showed lower air–water methane fluxes compared to the larger bubble, destratification system.

Submerged macrophytes may affect gas exchange by reducing wind turbulence. Baliña et al. conducted a study in Argentina and revealed that clear vegetated lakes had higher mean annual methane partial pressure (pCH_4) despite having similar mean annual methane diffusive flux. Their results suggest that physical factors such as wind-induced turbulence control these differences in pCH_4 rather than biological factors. The findings indicate that submerged vegetation could dampen wind-induced turbulence and augment pCH_4 in surface waters.

Sherman and Ford presented methane emissions from Cotter Reservoir in Canberra, Australia, during a period of flooding following a long drought. The measurements spanned the first major flood events in 26 years. The floods resulted in hypolimnion warming and the introduction of large amounts of organic carbon. Average methane emissions prior to the flooding were low and uniform across the reservoir, but following the first floods, mean emissions increased dramatically and varied along the reservoir's axis. The authors attributed the changes in methane emissions to both the thermal enhancement of sediment methanogenesis and the supply of fresh organic matter.

In this study, Nijman et al. incubated methane-oxidizing bacteria (MOB) from sediments of four sub-tropical lakes to determine the effects of phosphorus (P) on MOB community composition and methane oxidation. The results show that increases in phosphate concentrations up to 10 μM significantly increased methane oxidation and bacterial biomass P content, while MOB community composition was not affected by phosphate. These effects only occurred at low phosphate concentrations, indicating that high nutrient loads may not mitigate the increased methane production.

Zimmermann et al. aimed to model methane-oxidizing bacteria diversity and niche partitioning based on differences in methane oxidation kinetics and temperature adaptation. The model approach closely reproduced diversity and niche preference patterns of methanotrophs observed in seasonally stratified lakes, but the combination of trait values resulting in coexisting methanotroph communities was limited to very confined regions. The study suggests that natural selection may drive trait values into the specific configurations observed in nature.

Bertolet et al. conducted sediment incubation experiments on 22 lakes to investigate whether variation in microbial community composition is related to the response of sediment methane production to increases in organic matter. The results show that sediment microbial community composition is significantly correlated with sediment methane production responses to organic matter additions. The diversity and richness of the non-methanogen community were found to be the most predictive metrics of the response.

Maier et al. investigated local CO_2 and methane concentrations in the Romanian part of the Danube Delta, determining horizontal gradients in dissolved gas concentrations. Delta-scale concentration patterns were stable across seasons, while small connecting channels were highly influenced by the riparian wetland. The study highlights the effect of plant-mediated gas transfer on dissolved gas concentrations and supports recent studies stressing the need to account for ebullitive gas exchange when assessing metabolism parameters from O_2 in shallow, productive settings.

In this study, genetic and geochemical analyses were used by van Grinsven et al. to investigate the drivers of the distributions, abundances, and community compositions of methane-oxidizing bacteria (MOB) across five lakes in central Switzerland. The results show that methanotrophic abundances peaked in sediments of an oligotrophic lake, and the trophic state at the time of sediment deposition was the best predictor of MOB community structure. Elevated methane fluxes combined with low MOB abundances in surface sediments of eutrophic lakes suggest that a major portion of sedimentary methane bypasses the biological methane filter and escapes to overlying water.

Valiente et al. used a set of chemical, hydrological, climate, and land-use parameters to predict biotic saturation of GHGs in boreal lakes. The predictions were based on surface water samples from 73 lakes in south-eastern Norway covering wide ranges in dissolved organic matter and nutrient concentrations, as well as catchment properties and land use. The study found that catchment

characteristics such as lake size, precipitation, and terrestrial primary production in the watershed control the saturation of GHG in boreal lakes.

In a study of Teardrop Lake in Greenland, Cadieux et al. used stable isotope and 16S rRNA gene amplicon sequencing to determine water column carbon and hydrogen isotopes and microbial community composition. Methane isotopic values were highly enriched in carbon and hydrogen isotopes at 4 m depth, suggesting efficient methanotrophic communities. The researchers suggest that the methane cycling is decoupled from a traditional depth-dependent model, and understanding linkages between depth-dependent microbial dynamics and methane biogeochemistry is necessary to constrain the sensitivity of the methane cycle to future climate change.

Jensen et al. measured diffusive CO_2, methane, and N_2O fluxes from 20 agricultural reservoirs on seasonal and diel timescales. CO_2 concentrations were highest in spring and fall and lowest in mid-summer, while methane was highest in mid-summer, and N_2O was elevated in spring. CO_2 concentrations were affected by factors related to benthic respiration, while methane content was positively correlated with factors that favored methanogenesis, and N_2O concentrations were driven mainly by variation in reservoir mixing. The study estimated mean CO_2-eq flux during the open-water period, ranging from 5,520 to 10,445 mmol m^{-2} $year^{-1}$.

Martinez et al. conducted a stable isotope study to identify sources and sinks of methane in standing dead trees (snags) in freshwater forested wetlands. Their results suggest that snags could be important for methane emission and oxidation and may become more common in coastal areas as marshes migrate into freshwater forested wetlands. They found that methane emissions from snag stem sides and the soil–atmosphere interface were enriched in $\delta^{13}C$, which may point to methane oxidation when moving through the snags. The study highlights the need for further research on the relevance of snags for greenhouse gas cycling at regional and global scales.

Melack et al. evaluated the adequacy of available methane measurements, sampling and field methods, atmospheric measurements, and previously published fluxes and regional estimates to regionalize and constrain the variability of methane fluxes in the Amazon basin. They highlight the need to better understand biogeochemical and physical processes in the Amazon basin to improve mechanistic and statistical models. The authors recommend the application of new remote sensing techniques, increased sampling frequency and duration, experimental studies, and the development of appropriate models for hydrological and ecological conditions. They also suggest the use of advanced methods in microbial ecology and experimental manipulations to strengthen modeling efforts.

Bussman et al. investigated dissolved and atmospheric methane concentrations along 584 km of the Elbe River (Germany). Dissolved methane varied by almost 2.5 orders of magnitude with the hotspots in dissolved and atmospheric concentrations aligning with manmade structures, such as weirs, harbors, and groins. In addition, they compared emission estimates from discrete and continuous sampling approaches. They found that both are sufficient for upscaling methane emissions along rivers but concluded that regions with anthropogenic modifications should be considered in monitoring.

Einzmann et al. used a dual isotope technique to explore methane dynamics in a eutrophic lake in Germany. The stable carbon and hydrogen isotope composition revealed that methane sources and processing varied with stratification and lake depth. Methanogenic pathways differed spatially and seasonally between littoral and pelagic sites, while groundwater inputs of methane were more pronounced during the mixed period. During the stratified period, aerobic methane oxidation in the water column and sulfate-dependent anaerobic methane oxidation in the sediments helped to regulate methane reaching the epilimnion. This study clearly describes how a dual isotope approach of methane in various lake components can provide insight into lake methane dynamics.

Rabaey and Cotner measured GHGs during the ice-free season from 26 ponds in Minnesota (United States) to identify emission drivers from these small waterbodies that have been recognized as significant emitters despite their size. The ponds varied in terms of land use and included natural ones, but all were greenhouse gas sources with methane-dominating emissions. As seen previously, methane emissions positively correlated with phosphorus and anoxia, but in this study duckweed coverage was also a significant predictor with implications for the management of constructed ponds.

Thottathil et al. investigated the variability and controls of stable carbon isotopic fractionation during aerobic methane oxidation in temperate lakes. The authors used experimental incubations of unamended water samples from six temperate lakes at different depths and temperatures to better constrain the natural variability and controls of the isotopic fractionation factor (αox). They found that αox systematically increased from the surface to the deep layers, positively related to the abundance of methane oxidizing bacteria. The authors developed a general model predicting αox that ensures more realistic methane oxidation rates when applying stable carbon isotope-based quantification.

Eugster et al. investigated carbon emissions from an Arctic lake (Toolik Lake, Alaska, United States) using measurements of eddy covariance fluxes and continuous dissolved concentrations of methane and carbon dioxide. Future (30-year) projections suggest increasing soil temperatures will enhance carbon emissions, whereas increasing rainfall intensity will reduce them. The integrated use of eddy covariance and continuous dissolved concentrations allowed the resolution of highly resolved gas exchange coefficients to be compared with gas exchange models, which revealed that the approaches only converge at high wind speeds and that the gas exchange models underpredict true coefficients. The higher coefficients at low wind speeds are attributed to turbulence at the air–water interface being impacted by turbulence generated on land and may be characteristic of other lakes in similar environments.

Author contributions

All authors listed have made a substantial, direct, and intellectual contribution to the work and approved it for publication.

Conflict of interest

The authors declare that the research was conducted in the absence of any commercial or financial relationships that could be construed as a potential conflict of interest.

Publisher's note

All claims expressed in this article are solely those of the authors and do not necessarily represent those of their affiliated organizations, or those of the publisher, the editors and the reviewers. Any product that may be evaluated in this article, or claim that may be made by its manufacturer, is not guaranteed or endorsed by the publisher.

References

Bastviken, D., Tranvik, L. J., Downing, J. A., Crill, P. M., and Enrich-Prast, A. (2011). Freshwater methane emissions offset the continental carbon sink. *Science* 331, 50. doi:10.1126/science.1196808

Langenegger, T., Vachon, D., Donis, D., and McGinnis, D. F. (2019). What the bubble knows: Lake methane dynamics revealed by sediment gas bubble composition. *Limnol. Oceanogr.* 64, 1526–1544. doi:10.1002/lno.11133

Nisbet, E. G., Dlugokencky, E. J., Fisher, R. E., Lowry, D., Michel, S. E., et al. (2019). Very strong atmospheric methane growth in the 4 years 2014–2017: Implications for the Paris Agreement. *Glob. Biogeochem. Cycles* 33, 318–342. doi:10.1029/2018gb006009

Thottathil, S. D., Reis, P. C. J., and Prairie, Y. T. (2019). Methane oxidation kinetics in northern freshwater lakes. *Biogeochemistry* 143, 105–116. doi:10.1007/s10533-019-00552-x

frontiers in Environmental Science

ORIGINAL RESEARCH
published: 01 December 2021
doi: 10.3389/fenvs.2021.756603

Iterative Forecasting Improves Near-Term Predictions of Methane Ebullition Rates

Ryan P. McClure[1], R. Quinn Thomas[1,2], Mary E. Lofton[1], Whitney M. Woelmer[1] and Cayelan C. Carey[1]*

[1]Department of Biological Sciences, Virginia Tech, Blacksburg, VA, United States, [2]Department of Forest Resources and Environmental Conservation, Virginia Tech, Blacksburg, VA, United States

Near-term, ecological forecasting with iterative model refitting and uncertainty partitioning has great promise for improving our understanding of ecological processes and the predictive skill of ecological models, but to date has been infrequently applied to predict biogeochemical fluxes. Bubble fluxes of methane (CH_4) from aquatic sediments to the atmosphere (ebullition) dominate freshwater greenhouse gas emissions, but it remains unknown how best to make robust near-term CH_4 ebullition predictions using models. Near-term forecasting workflows have the potential to address several current challenges in predicting CH_4 ebullition rates, including: development of models that can be applied across time horizons and ecosystems, identification of the timescales for which predictions can provide useful information, and quantification of uncertainty in predictions. To assess the capacity of near-term, iterative forecasting workflows to improve ebullition rate predictions, we developed and tested a near-term, iterative forecasting workflow of CH_4 ebullition rates in a small eutrophic reservoir throughout one open-water period. The workflow included the repeated updating of a CH_4 ebullition forecast model over time with newly-collected data via iterative model refitting. We compared the CH_4 forecasts from our workflow to both alternative forecasts generated without iterative model refitting and a persistence null model. Our forecasts with iterative model refitting estimated CH_4 ebullition rates up to 2 weeks into the future [RMSE at 1-week ahead = 0.53 and 0.48 $\log_e$(mg CH_4 m^{-2} d^{-1}) at 2-week ahead horizons]. Forecasts with iterative model refitting outperformed forecasts without refitting and the persistence null model at both 1- and 2-week forecast horizons. Driver uncertainty and model process uncertainty contributed the most to total forecast uncertainty, suggesting that future workflow improvements should focus on improved mechanistic understanding of CH_4 models and drivers. Altogether, our study suggests that iterative forecasting improves week-to-week CH_4 ebullition predictions, provides insight into predictability of ebullition rates into the future, and identifies which sources of uncertainty are the most important contributors to the total uncertainty in CH_4 ebullition predictions.

Keywords: biogeochemical fluxes, ecological forecasting, freshwater, greenhouse gases, reservoir

OPEN ACCESS

Edited by:
Daniel F. McGinnis, Université de Genève, Switzerland

Reviewed by:
Martin Schmid, Swiss Federal Institute of Aquatic Science and Technology, Switzerland
Dominic Vachon, Umeå University, Sweden

****Correspondence:***
Ryan P. McClure
ryan.mcclure@wsu.edu

Specialty section:
This article was submitted to Biogeochemical Dynamics, a section of the journal Frontiers in Environmental Science

Received: *10 August 2021*
Accepted: *25 October 2021*
Published: *01 December 2021*

Citation:
McClure RP, Thomas RQ, Lofton ME, Woelmer WM and Carey CC (2021) Iterative Forecasting Improves Near-Term Predictions of Methane Ebullition Rates. Front. Environ. Sci. 9:756603. doi: 10.3389/fenvs.2021.756603

INTRODUCTION

Near-term (day to year) ecological forecasting can improve our understanding and quantification of ecosystem processes (Dietze et al., 2018). The repeated updating of models used to generate forecasts (often called data assimilation or data-model fusion; Luo et al., 2011) is crucial for forecasting because it can iteratively improve forecast skill by updating model initial conditions or recalibrating model parameters (Luo et al., 2011; Dietze, 2017a). The iterative process of making a forecast with a model, collecting observations to compare with the forecast, and then updating the forecast models before making a new forecast embodies the scientific method and can substantially improve our representation of ecosystem processes in models (Dietze, 2017b). If the observations match the forecast, the hypothesis (as represented by the forecast model) is supported, otherwise, it provides an opportunity for revising the hypothesis by, e.g., updating model parameters, modifying the model's driver variables, or changing the model's equations. Thus, near-term, iterative forecasting creates a model-data feedback loop that evaluates how effectively a model predicts future ecosystem states, with the forecasts evolving as the ecosystem experiences different environmental conditions.

While near-term, iterative forecasting has been successfully applied to predict other ecological variables, to date the approach has not been broadly used in aquatic biogeochemistry. One biogeochemical process that near-term, iterative forecasts may improve predictions for is methane (CH_4) ebullition, or bubble fluxes of CH_4 from organic-rich sediments to the waterbody surface. Freshwater ecosystems emit large quantities of CH_4 to the atmosphere (currently estimated between 117 and 212 Tg CH_4 yr^{-1}; Saunois et al., 2020). Within human-made reservoirs alone, ebullition rates can vary substantially in emissions, ranging from 1 to 1,000 mg CH_4 m^{-2} d^{-1} (Deemer et al., 2016) and up to 8.9 Tg CH_4 yr^{-1} (Johnson et al., 2021). Among the different types of freshwater CH_4 emissions, ebullition can make up anywhere from 0 to 99.6% of total emissions to the atmosphere (Deemer and Holgerson, 2021) and it is considered one of the most uncertain fluxes in both inland water and global CH_4 budgets (Wik et al., 2016; Saunois et al., 2020).

Ebullition's high spatial and temporal variation makes it difficult to quantify experimentally and create appropriate models, resulting in three challenges that stand in the way of developing robust predictions of CH_4 ebullition fluxes from inland waters. These include 1) model transferability across time and space (i.e., the ability to apply ebullition models across years and ecosystems); 2) identification of the forecast horizons for which future estimates provide useful information (Petchey et al., 2015); and 3) quantification of uncertainty in model predictions. First, while there are multiple different CH_4 ebullition models for inland waters, e.g., process-based models that couple physical, biogeochemical, and bubble plume modules (Schmid et al., 2017), empirical models that use physical, chemical and biological drivers as predictors of CH_4 ebullition fluxes (DelSontro et al., 2016; Aben et al., 2017; Grasset et al., 2021), and auto-regressive (AR) time series models (McClure et al., 2020a), it remains unknown how well they can predict CH_4 ebullition dynamics over time within the same ecosystem. Moreover, given the clear interannual variability in ebullition rates across inland water systems (Burke et al., 2019; Männistö et al., 2019; Linkhorst et al., 2020), quantifying the transferability of CH_4 ebullition model predictions from 1 year to another is critical for CH_4 ebullition modeling. Knowing, for example, if the same model was robust for predicting CH_4 ebullition across multiple years vs. if new models were needed to predict CH_4 ebullition each year would greatly assist CH_4 scaling efforts.

Second, the ability of current CH_4 ebullition models to predict future out-of-sample observations across varying forecast horizons remains untested. An important step for improving the robustness of CH_4 ebullition predictions is to use models to generate out-of-sample predictions for CH_4 ebullition rates at different future horizons (e.g., days, months, or years into the future) and then compare these predictions with observations when they are available. It is possible that CH_4 ebullition models may successfully simulate observed data at a given forecast horizon, but not effectively provide insight as to how far into the future the predictions provide useful information (Petchey et al., 2015). Here, we propose that exploring the transferability and effective forecast horizon of CH_4 ebullition rates using near-term forecasting can serve as a robust tool for improving our understanding of future CH_4 ebullition rate predictions.

Third, near-term iterative forecast workflows need to account for uncertainty in predictions, which provides a critical metric of confidence in forecasts. Moreover, partitioning the different sources of uncertainty can provide insight into model performance and measurements, which has the potential to improve aspects of the model and predictions (Dietze, 2017a; Carey et al., 2021a). In particular, forecast workflows that apply state-space Bayesian methods with iterative model refitting enables the partitioning of sources of uncertainty (e.g., parameters, initial conditions, driver data, and model processes; Dietze, 2017a; Luo et al., 2011), which is crucial for identifying strategies for improving the design for future measurements and models. For example, Thomas et al. (2018) used a state-space hierarchical Bayesian model to forecast biomass change in loblolly pine (*Pinus taeda*) forests in the southeastern United States and then evaluated the relative contribution of different forms of uncertainty to the total forecast uncertainty to guide improvements on future biomass predictions. However, accounting for and partitioning uncertainty still remains uncommon in ecological modeling (Harrison et al., 2017; Lewis et al., 2021), especially in forecasts of future biogeochemical processes like CH_4 ebullition (Lewis et al., 2021). Thus, developing a forecast workflow that implements uncertainty partitioning at every time step will provide key insight to future model development for CH_4 ebullition rates.

The goal of this work was to assess the potential of forecasting CH_4 ebullition as a case study to evaluate its potential more broadly. Given the complexity of ebullition as a biogeochemical process with many different mechanisms that control its fluxes, our goal was to see if we could successfully forecast CH_4, which would support its application to other aquatic biogeochemical processes. We developed an iterative forecasting workflow of

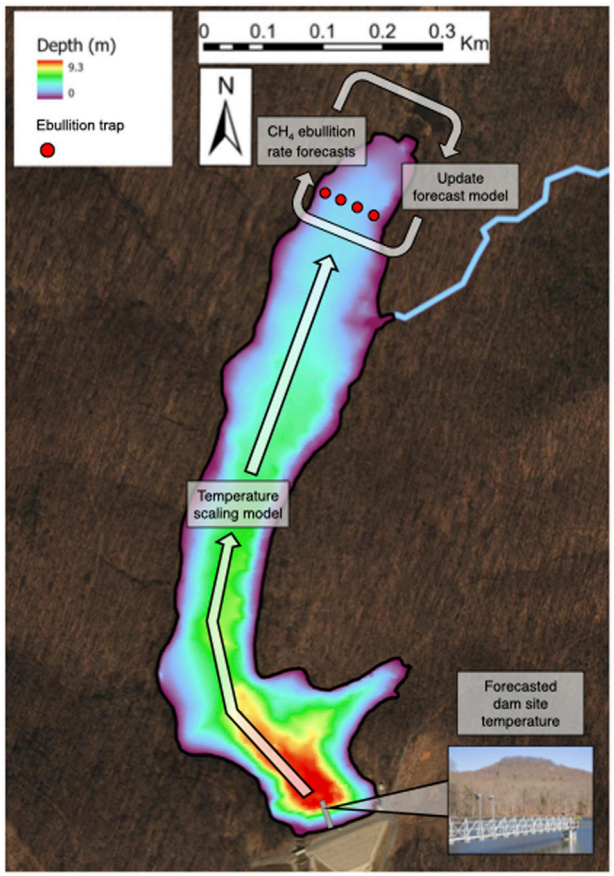


FIGURE 1 | The bathymetry of Falling Creek Reservoir superimposed by a depiction of how our forecast workflow mapped spatially from the dam to the upstream transect where CH_4 ebullition rates were forecasted. Our forecast workflow used water temperature forecasts from the dam site in the reservoir (following Thomas et al., 2020). The water temperature forecasts were scaled to an upstream transect (denoted by red dots on map) to generate near-term iterative CH_4 ebullition rate forecasts. Simultaneously, direct observations from ebullition traps were used to iteratively update the forecast model *via* data assimilation.

weekly CH_4 ebullition rates in a freshwater reservoir up to 2 weeks into the future using forecasted water temperatures, ebullition rate observations, and a state-space model fit in a Bayesian framework with iterative model refitting. We refit our model with new observations to update our ebullition model's states, parameters, initial conditions, and driver data on each model time step and tested our ebullition rate forecast workflow against a similar forecast workflow that did not use iterative model refitting and a persistence null model. We also quantified the contributions of different sources of uncertainty to CH_4 ebullition forecasts at each time step. Our objectives were: 1) develop an iterative, near-term forecasting workflow of CH_4 ebullition rates and apply it to assess a CH_4 ebullition model's interannual transferability; 2) determine the effective forecast horizon of CH_4 ebullition; and 3) quantify and partition the sources of uncertainty in our forecasts to inform future workflow development. Altogether, our goal was to examine the potential of near-term iterative forecasting for improving the representation of CH_4 ebullition in models and providing insight into this important biogeochemical flux.

MATERIALS AND METHODS

Site Description

We developed near-term, real-time, iterative CH_4 ebullition rate forecasts in Falling Creek Reservoir (FCR, **Figure 1**) in summer 2019 and tested the efficacy of different forecasting workflows against observations of CH_4 ebullition rates at different forecast horizons. FCR is a small (0.119 km^2), shallow (Z_{max} = 9.3 m), eutrophic, drinking water reservoir located in southwestern Virginia, United States (37.30°N, 79.84°W). FCR is owned and operated by the Western Virginia Water Authority as a drinking water supply and is in a completely forested watershed (Gerling et al., 2016). FCR's water level was managed to stay at a constant level and did not experience substantial fluctuations during this study (Carey et al., 2021a).

The forecasting workflow used a model developed from a previous summer sampling season (2017) of CH_4 ebullition monitoring data collected at FCR to build and calibrate our forecast models (McClure et al., 2020b). In 2017, four ebullition traps were deployed and monitored weekly from 8 May to 24 October along a shallow upstream transect (McClure et al., 2020a; **Figure 1**). In 2019, the year of this forecasting study, we redeployed all four traps as close as possible to their original locations in 2017 and forecasted measurements collected weekly throughout the summer. Ebullition rates were natural log-transformed (log_e) + 0.1 to meet the assumptions of normality and avoid forecasts of negative ebullition rates in log-space.

Forecast Model and Model-Fitting

Our forecast model was an auto-regressive (AR) time series model with sediment-water interface (SWI) temperatures as a driver:

$$E_t = \beta_0 + \beta_1 E_{t-1} + \beta_2 T_t \quad (1)$$

where E_t log_e (mg CH_4 m^{-2} d^{-1}) is the log_e-transformed mean CH_4 ebullition rate from the four sites at the upstream transect, E_{t-1} log_e (mg CH_4 m^{-2} d^{-1}) is the log_e-transformed CH_4 ebullition rate at the previous measurement (the AR term), and T_t (°C) is the water temperature averaged from measurements at the SWI below the upstream transect between each time step of the model (weekly). There were three parameters in this model: the intercept term (β_0), the parameter governing the effect of the AR term (β_1), and the parameter governing the effect of SWI temperature (β_2). This model was chosen based on prior modeling work at the site, which demonstrated that ≥60% of the total reservoir-wide CH_4 ebullition was emitted from the shallow upstream transect in FCR during the ice-free period, and that there was a strong positive relationship between ebullition and sediment-water interface (SWI) temperatures (McClure et al., 2020a).

TABLE 1 | Definitions of uncertainty sources that can contribute to total forecast uncertainty and what parameter and variables from the **Eqs 2**, **3**, **4**, **6**, **7** correspond to the total uncertainty (derived from Dietze, 2017a).

Source of uncertainty	Definition	Forecast model parameters associated with uncertainty source
Model process	Uncertainty that arises due to the inability of a particular model structure (equations) to represent the real world and reproduce observed conditions. This uncertainty is not associated with a particular mechanism and is represented by adding random noise to forecasts between time-steps	Δt, σ^{proc} **Eq. 3**
Model Parameter	Uncertainty in the model parameter values; represented by randomly sampling from the parameter distributions at the beginning of a forecast	β_0, β_1, β_2 **Eq. 2**
Initial Condition	Uncertainty in the observed conditions when a forecast is created; represented using a distribution of model states at the first model time step	Y_t^E **Eq. 4**
Driver Data	Uncertainty in the forecasted estimates of the model covariates (i.e., sediment-water interface temperatures); represented using an ensemble for model drivers	Y_t^{swi}, σ^{swi}, d_t, ϕ_0, ϕ_1 **Eqs 6**, **7**

We estimated the posterior distributions of the parameters in the model using a state-space Bayesian framework. This framework includes latent states that represent the "true" ebullition rate before observation uncertainty is added. The latent state has a distribution that represents uncertainty in our capacity to model the true ebullition rate. Following **Eq. 1**, the state-spaced framework uses the previous time step's latent state in the AR term:

$$E_t = \beta_0 + \beta_1 E_{t-1}^{latent} + \beta_2 T_t \quad (2)$$

The latent state is normally distributed with a mean equal to the prediction from **Eq. 2** and standard deviation of $\Delta t \sigma_{proc}$:

$$E_t^{latent} \sim N(E_t, \Delta t \sigma^{proc}) \quad (3)$$

σ_{proc} is an unknown parameter that represents process uncertainty that accumulates over a day. Process uncertainty is uncertainty that arises due to the inability of a particular model structure to represent the real world and reproduce observed conditions (**Table 1**, Dietze, 2017a). σ_{proc} is multiplied by the number of days between time steps (Δt) to allow for the standard deviation to scale with the time step length. This was necessary because data were collected approximately weekly but the exact number of days between measurements varied. The observations (Y_t^E) are modeled as a normal distribution with a mean equal to the latent state and standard deviation (σ_t^{obs}) that was set to be the standard error of the mean ebullition rate across the four upstream sites:

$$Y_t^E \sim N\left(E_t^{latent}, \sigma_t^{obs}\right) \quad (4)$$

σ_t^{obs} was time-dependent because standard error of the observations varied by measurement period. Although we include Y_t^E as a source of error, we acknowledge that the actual Y_t^E uncertainty is likely higher due to our inability to include other inherent sources of error (e.g., sample measurement, sample transport, instrument uncertainty, etc.). However, these other inherent sources of uncertainty are likely substantially smaller than the sampling uncertainty currently represented for Y_t^E (**Eq. 4**).

We set the priors for the β_0, β_1, and β_2 parameters as uninformative with normal distributions with a mean of zero and a large standard deviation (1,000). The prior on σ_{proc} was also uninformative with a uniform distribution between 0 and 10,000. State-space models require a prior distribution for the states at the first time step (initial conditions), which we assumed to be normally-distributed with a mean equal to the observed mean Y_0^E ebullition rate and standard deviation equal to the standard error of the mean ebullition rate across the four upstream sites at the first observation period:

$$E_{t=0}^{latent} \sim N\left(Y_{t=0}^E, \sigma_{t=0}^{obs}\right) \quad (5)$$

Our model-fitting process involved four steps. First, we estimated posterior distributions of the parameters using data from summer 2017 that included weekly measurements of CH_4 ebullition rate and SWI temperature using Markov chain Monte Carlo (MCMC) analyses. MCMC analyses are particularly well-suited for forecasting because they numerically estimate probability distributions for model parameter, the latent states, and process uncertainty. These distributions can subsequently be used to quantitatively assess the uncertainty associated with each aspect of the model (parameters, initial conditions, and process error; see **Table 1**). The MCMC analyses were carried out using the "rjags" and "R2jags" packages (Plummer, 2018) within the R statistical environment (R Core Team, 2021). We ran three MCMC chains for 70,000 iterations, including 20,000 initial iterations that were discarded as a burn-in. We assessed convergence using the potential scale reduction factor (PSRF) of the Gelman-Rubin statistic, and parameters were determined to have converged if the PSRF was between 1 and 1.05 (Gelman and Rubin, 1992).

Second, we generated prior distributions for a refitting of the state-spaced model using 2019 data that were derived from posteriors from the 2017 model-fitting. The posterior distributions from the β_0, β_1, and β_2 parameters from the 2017 model-fitting followed a multivariate normal distribution that was used as the prior in the 2019 calibration. The posterior

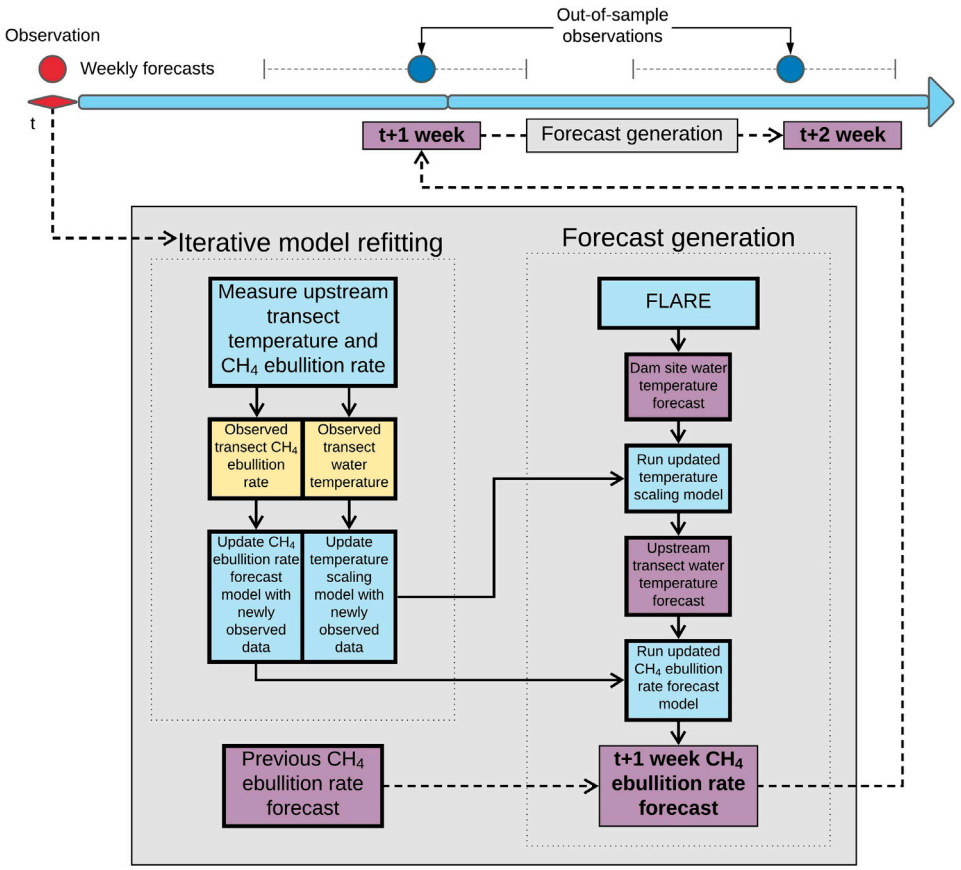


FIGURE 2 | Conceptual illustration of the forecast workflow using iterative model refitting that generates near-term, iterative CH_4 ebullition forecasts. The model refitting stage occurred at the time when new ebullition rates were manually collected from the reservoir. In the shaded part of the figure, the blue boxes represent processes, and the yellow and purple boxes represent the data products that resulted from each process. The yellow boxes are manually-collected data products that were used to update the forecast model and the purple boxes represent forecasted data products.

of σ^{proc} was approximately log-normally distributed in the 2017 model-fitting and we used moment-matching (i.e., a method of matching parameters of the distribution to produce a particular mean and variance) to estimate the parameters for the log-normal prior distribution in the 2019 recalibration.

Third, during the summer of 2019, we refitted the model weekly as new data were collected. The refitting involved starting with the priors from the 2017 model-fitting, appending the new data to the previously collected 2019 data, and re-running the MCMC estimation of posteriors using the 2019 data. The first measurement of 2019 was used as the initial conditions for **Eq. 2**. As a result of this analysis design, we expected the posterior parameter distributions to reflect the prior distributions (i.e., the 2017 posteriors) early in the summer, when data from 2019 were limited, but the posterior parameter distribution would increasingly be influenced by data in 2019 as more data were collected.

Finally, the posterior estimates for the parameters (β_0, β_1, β_2, and σ_{proc}) from each recalibration in 2019 were used to generate 1-week ahead and 2-week ahead forecasts (*Overview of Forecasting Workflow*).

Overview of Forecasting Workflow

Here, we outline the implementation of the forecasting workflow based on the model development and fitting described in *Forecast Model and Model-Fitting*, and then describe how the forecasted driver data were generated in *Forecasting SWI Temperature*. Approximately each week between 17 June and November 7, 2019, we generated forecasts of CH_4 ebullition rates that extended approximately 2 weeks into the future (**Figure 2**). The forecast horizon varied between 13 and 16 days ahead depending on the exact days that the observations were ultimately collected. The forecasts presented here are technically hindcasts because they were generated after the observations were collected; however, a preliminary version of the forecasts were generated using a similar approach in real-time during the summer of 2019 (and thus those are considered true forecasts).

The forecasts were generated using an MCMC approach to numerically represent forecast uncertainty. Because MCMC permits estimation of model parameters, latent states, and process uncertainty parameter as distributions rather than fixed values, an MCMC approach enables estimation of the uncertainty associated with each of these model components by making multiple draws from estimated distributions to

build an ensemble of possible forecast outcomes. Our approach used an ensemble with 210 members. First, to represent initial condition uncertainty, the forecast was initialized using 210 random draws from a normal distribution with a mean equal to the observation at the start of the forecast ($Y_{t=m}$, where m is the week number in the 2019 time series at the time the forecast was initialized) and a standard deviation equal to $\sigma_{t=m}^{obs}$. Second, to represent parameter uncertainty, we randomly drew a set of 210 parameter values from the posterior distributions for each ensemble member from the most recent recalibration. As a result, parameter values varied among ensemble members but were constant over time for a given ensemble member. Third, to represent driver uncertainty, each Bayesian state-space ensemble member was assigned an ensemble member from the sediment-water interface (SWI) temperature forecast (*Forecasting SWI Temperature*). Fourth, using the initial conditions and parameter values described above in steps one and two, respectively, one time step (~1 week) was simulated for each ensemble member. Normal random noise from a distribution with a mean equal to 0 and a standard deviation equal to $\Delta t \sigma^{proc}$ was then added to each ensemble member to account for process uncertainty and generate the 1-week forecast. Finally, the 1-week forecast was used as initial conditions for the second week forecast and step 4 was repeated to generate the 2-week forecast (**Figure 2**). Overall, this numerical forecasting approach quantifies the contribution of initial condition uncertainty, parameter uncertainty, process uncertainty, and driver uncertainty (**Table 1**).

Forecasting SWI Temperature

Because we generated forecasts of future CH_4 ebullition rates, forecasts of the model covariates (i.e., SWI temperatures) were needed as part of our workflow (**Figure 1**, **2**). To produce forecasts of SWI temperature, we used the existing Forecasting Lake And Reservoir Ecosystems (FLARE; Thomas et al., 2020) water temperature forecasting framework and infrastructure deployed in FCR to generate predictions of future water temperatures as driver data for our CH_4 ebullition rate forecasts at all four traps on the transect. FLARE uses near-real time temperature observations, weather forecasts, and a hydrodynamic model (General Lake Model) to forecast water temperatures up to 16 days into the future at the "dam site" at FCR, which was located ~700 m downstream from the ebullition traps (**Figure 1**). To generate SWI forecasts at the upstream ebullition transect, which had a depth of 1–3 m, we developed a temperature scaling model that converted the FLARE forecasts between 1 and 3 m at the dam site to forecasts at the transect. We estimated the posterior distributions of the parameters in the temperature scaling model using a simple (non-state space) Bayesian framework where:

$$T_t = \phi_0 + \phi_1 d_t \quad (6)$$

and

$$Y_t^{swi} \sim N(T_t, \sigma^{swi}) \quad (7)$$

T_t is the predicted upstream transect SWI temperature at time t ϕ_0 and ϕ_1 are the slope and intercept parameters, d_t is the observed mean water temperature between 1 and 3 m at the dam site, and Y_t^{swi} is the observed mean upstream transect SWI. We estimated the posterior distribution for the parameters using a Bayesian framework applied to data from 2017. The temperature scaling model ran three MCMC chains with a burn-in period of 1,000 iterations and a sample size of 10,000 iterations. Prior distributions for the parameters (ϕ_t) were uninformative by using a normal distribution with a mean of zero and a large standard deviation (1,000). The prior distribution for σ^{swi} was also uninformative by using uniform with a large range (0–1,000). Similar to recalibration of the parameters in the ebullition model, the SWI temperature model was iteratively recalibrated in 2019 using the priors derived from the posteriors of the 2017 model-fitting.

To generate the forecast of SWI temperature, first we forecasted water temperature at the dam site using FLARE (Thomas et al., 2020) up to 16-days into the future. This produced a 210-member ensemble with uncertainty primarily derived from uncertainty in weather predictions from the NOAA Global Ensemble Forecasting System and process uncertainty associated with the hydrodynamic lake model underlying FLARE (Thomas et al., 2020). Second, we collected the mean temperature forecasts at 1- and 2-week horizons of the 1 and 3 m depth forecasts for each FLARE member ensemble and applied these values as d_t in **Eq. 6**. Third, we sampled 210 members from the joint posterior distribution of ϕ_0, ϕ_1, and σ^{swi}. Fourth, using sampled ϕ_0 and ϕ_1 and FLARE water temperature forecasts, we predicted the SWI temperature at the upstream site using **Eq. 6**. Finally, for each of the 210 ensemble members we added the normal distributed error from **Eq. 7**. The 210 ensembles of forecasted water temperatures from the scaling model for the upstream transect were then used as driver data for our CH_4 ebullition rate forecast model (T_t) in **Eq. 2**.

Field Data Collection

Approximately every week during the forecast period, we measured CH_4 ebullition rates and SWI temperature manually to update the daily forecasts (**Figure 2**). We collected 10-min SWI temperature data with HOBO temperature loggers (HOBO Pendant Temperature/Light Data Logger, Bourne, MA, United States) deployed below each of the four ebullition traps during the 2017 training period and 2019 forecast period. Each logger was sunk using a stainless-steel weight and a nylon string to sit ~0.1 cm above the SWI. We affixed the bottom logger ~1 m horizontally away from each ebullition trap to prevent potential disturbance of sediments under the traps. We simultaneously downloaded the temperature logger data as ebullition bubbles which had accumulated in the traps since the last sampling date were being collected. The temperature loggers were downloaded using HOBOware version 3.7.13.

The dam site water temperature data (**Figure 1**) were collected using a CTD (Conductivity, Temperature, and Depth) profiler in 2017 and water temperature thermistors in 2019. In 2017, the dam site water temperature depth profiles were collected with the CTD on the same days ebullition rates were collected from the

traps in the upstream transect. The CTD measured temperature every 0.25 s during the profile, resulting in temperature depth profiles at approximately 10-cm resolution through the water column. Further information and all thermistor and CTD data are available in the Environmental Data Initiative (EDI) repository following Carey et al. (2021a) and Carey et al. (2021b).

We sampled the CH_4 ebullition rates at the four upstream traps following McClure et al. (2020b). The ebullition samples from each trap on the transect were extracted across a septum stopper using a needle attached to a 10-ml syringe. We injected 10 ml of ebullition gas into a 20-ml crimped top glass vial that was pre-filled with saturated salt brine solution. A secondary exit syringe extracted the salt brine solution as the sample was injected to generate 10 ml of gas headspace in the vial. Two replicates were collected from each trap on a sampling day if enough gas sample was available, resulting in up to eight possible ebullition rate samples among the four traps. The vials were stored upside down until analysis, so the remaining 10 ml of salt brine solution acted as a barrier to prevent any gas from escaping. We extracted any remaining gas from each ebullition trap using a 30-ml syringe and summed the total volume of ebullition gas collected each week.

We analyzed the manually-collected ebullition gas from the traps for its CH_4 concentration using a Shimadzu Nexus-2030 Gas Chromatography—Flame Ionization Detector (GC-FID; Shimadzu Corporation; Kyoto, Japan) within 24 h of collection (following McClure et al., 2018; McClure et al., 2020b). We determined the observed CH_4 ebullition rate ($\boldsymbol{Y_t^E}$) as follows:

$$Y_t^E = \frac{V_{gas}[CH_4]}{\Delta t A_F} \tag{8}$$

where V_{gas} was the volume of ebullition gas collected in the trap (L), $[CH_4]$ is the CH_4 concentration of the gas (mg CH_4 L^{-1}), Δt is the duration of time the trap was deployed (in days), and A_F is the cross-sectional area of the funnel (0.26 m^2). Following McClure et al. (2020b), we calculated the daily ebullition rates separately for each trap and then averaged the rates from the four traps within the transect to determine a mean daily transect ebullition rate.

Forecast Analysis

To evaluate the interannual transferability of the ebullition model (Objective 1), we compared the skill of the forecast workflow without iterative model refitting with the forecast workflow with iterative model refitting. If the forecast workflow with iterative model refitting performed substantially better than the workflow without iterative refitting, then model transferability from year to year is low. The alternate forecasting workflow without iterative model refitting used the same AR model (**Eq. 2**) and the 2019 CH_4 ebullition rates as initial conditions for each 2-week forecast but sampled parameters from the posteriors that were only based on the 2017 model-fitting. As a result, the parameters did not iteratively update as new data were collected in 2019.

Next, to evaluate the effect of the forecast horizon of CH_4 ebullition rates in our system (Objective 2), we compared the performance of the forecast workflow with iterative model refitting with the persistence null model. If the null model performed better than the forecast workflow with iterative model refitting, then our forecast model of CH_4 ebullition rates was no better than a simple model that assumed next week's rates would be the same as the previous week's rates. The persistence null model was developed using a similar structure as the forecast models and assumed that CH_4 ebullition rates would remain similar into the future with propagated uncertainty. The persistence null model replaced **Eq. 2** with:

$$E_t = E_{t-1}^{latent} \tag{9}$$

The persistence null model used the same MCMC methods for estimating posterior distributions as the forecasting model. Similar to the forecasting model, the null model was fit to 2017 data and the posteriors were used as priors in the weekly recalibration of the model using 2019 data.

For both of the analyses described above, we quantified the Nash-Sutcliffe efficiency (NSE) and root-mean-square-error (RMSE) of the CH_4 ebullition rate forecasts from the forecast workflow with refitting, the forecast workflow without refitting, and the persistence null forecast model. The NSE is a normalized metric that evaluates a model's performance relative to the mean of the observed time series (Nash and Sutcliffe, 1970). We calculated the NSE coefficient (Nash and Sutcliffe, 1970) as follows:

$$\text{NSE} = 1 - \frac{\sum_{t=1}^{N}\left(F_t - Y_t^E\right)^2}{\sum_{t=1}^{N}\left(Y_t^E - \underline{Y^E}\right)^2} \tag{10}$$

where F_t was the mean of the CH_4 ebullition rate forecast ensembles, Y_t^E was the observed mean CH_4 ebullition rate, and $\underline{Y^E}$ was the average of all the observed CH_4 ebullition rates. NSE values range between -∞ to 1, where one indicates a perfect score (i.e., the model perfectly recreates observations; Nash and Sutcliffe, 1970; Moriasi et al., 2007), 0 indicates the model performs the same as the mean of the observations, and <0 indicates the model performs worse than the mean of the observations.

Forecast Uncertainty Partitioning

We quantified the total forecast uncertainty in CH_4 ebullition rate forecasts among all forecast cycles as standard deviation (SD) throughout the forecasting period using the variance of the 210-member ensemble at the 1- and 2-week forecast horizons (Objective 3). Additionally, we partitioned the relative contributions of four different sources of uncertainty, model parameters (β_0, β_1, and β_2), model process error, initial conditions, and driver data (d_t) (Dietze, 2017a) among all forecasts (**Eq. 5**).

We used a One-At-a-Time Sensitivity (OATS) analysis to determine the relative contribution of the uncertainty sources to total uncertainty (as total forecast variance) in each forecast

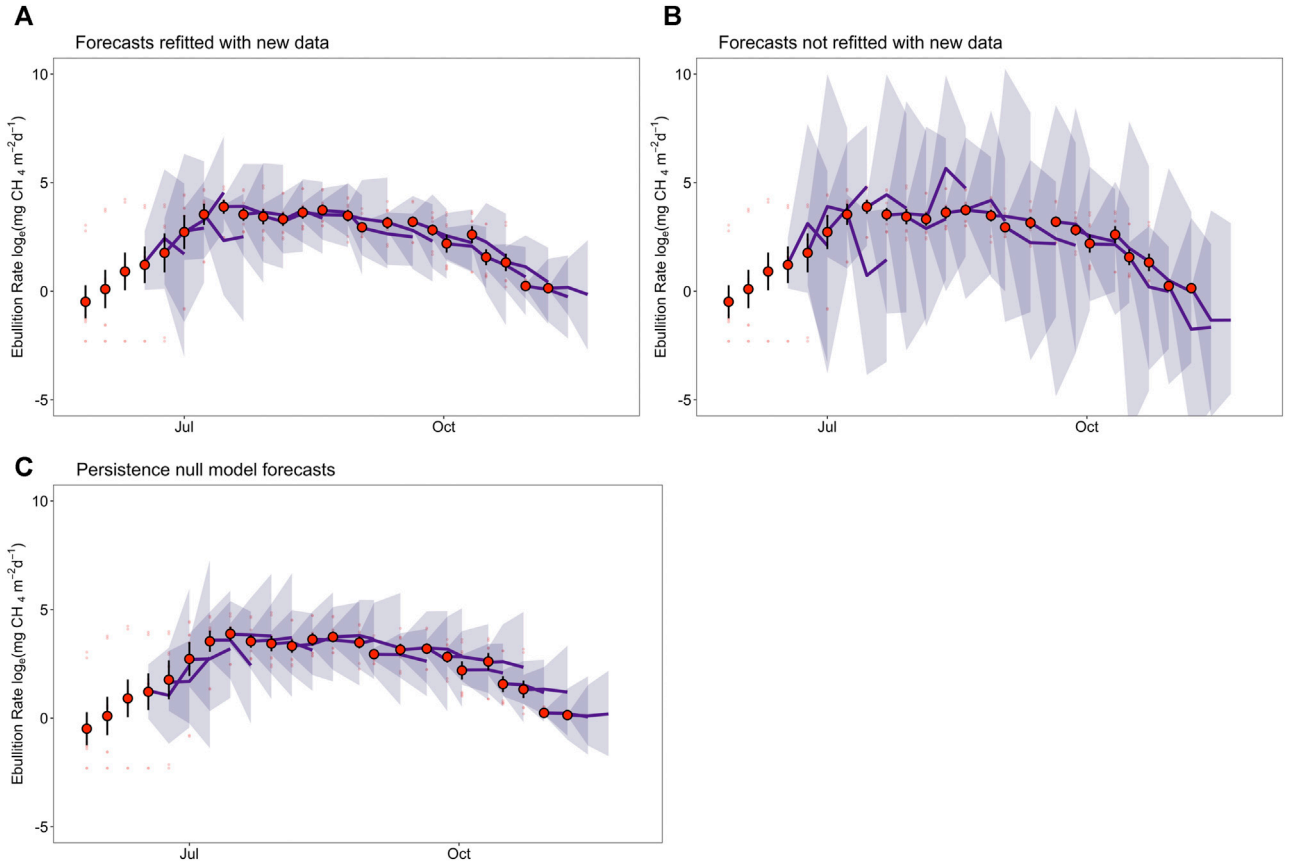


FIGURE 3 | A comparison of weekly forecasted CH_4 ebullition rates in log_e(mg CH_4 m^{-2} d^{-1}) using a workflow in which forecast models were iteratively refitted with new data **(A)**, a workflow in which forecasts were not refitted with new data **(B)**, and a persistence null model **(C)** from 17 June to November 7, 2019. The large red circles plus black error bars represent the observed daily mean transect CH_4 ebullition rate ±1 standard error of the mean from four ebullition traps depicted in **Figure 1**. The small red circles represent the measured CH_4 ebullition rate from each ebullition trap on the transect. The dark purple lines represent the forecasted mean daily ebullition rate from the posterior predictions. The purple shades represent the 95% predictive intervals of the forecasts.

cycle. An OATS analysis holds all sources of uncertainty at their mean except for one, and then numerically evaluates the sensitivity of the forecast to that specific source of uncertainty (Dietze, 2017b). For example, to partition parameter uncertainty, we held all other sources of uncertainty (model process, driver data, and initial condition) at their mean and only allowed the parameter values to vary among ensemble members. The relative proportion of each source of uncertainty was determined by dividing the total variance of each isolated source of uncertainty by the sum of the variance of all uncertainty sources at both the 1- and 2-week forecast horizons across the forecasting period.

Forecast Archiving and Reproducibility

All forecasting driver data (Carey et al., 2021b; Carey et al., 2021c; McClure et al., 2020b), code needed to forecast weekly CH_4 ebullition rates, and the hindcasts generated during the 2019 forecast period are archived either in the Environmental Data Initiative (EDI) repository or Zenodo (McClure et al., 2021). All analyses were run in the R statistical environment version 4.1.0 (R Core Team, 2021).

RESULTS

Observed CH_4 Ebullition Rates

Throughout the forecasting period, we observed high temporal variation in mean CH_4 ebullition rates at FCR's upstream transect (**Figure 3**). Mean ebullition rates at the upstream transect increased from −0.48 to 1.76 log_e (mg CH_4 m^{-2} d^{-1}) from 27 May though 24 June (**Figure 3**). Between 24 June and 15 July, mean CH_4 ebullition rates at the transect continued to increase until the maximum CH_4 ebullition rate for the forecast period was observed on 15 July [3.88 log_e (mg CH_4 m^{-2} d^{-1})]. Between 15 July and 16 October, the observed CH_4 ebullition rates ranged between 1.56 and 3.74 log_e (mg CH_4 m^{-2} d^{-1}). After 16 October, CH_4 ebullition rates dropped to ≤1.32 log_e (mg CH_4 m^{-2} d^{-1}) for the remainder of the forecasting period, which ended on 7 November.

TABLE 2 | Forecast evaluation determined by Nash-Sutcliffe Efficiency (NSE) and root mean square error (RMSE) at 1- and 2-week forecast horizons.The best-performing workflow evaluation statistics (as indicated by the highest NSE and lowest RMSE for each forecast horizon) are highlighted in bold for each horizon.

Workflow	1-week NSE	1-week RMSE	2-week NSE	2-week RMSE
Workflow with iterative model refitting	**0.76**	**0.53 $\log_e$(mg CH_4 m^{-2} d^{-1})**	**0.80**	**0.48 $\log_e$(mg CH_4 m^{-2} d^{-1})**
Workflow without model refitting (using a previous year's parameterization)	–0.23	1.21 $\log_e$ (mg CH_4 m^{-2} d^{-1})	0.60	0.69 $\log_e$ (mg CH_4 m^{-2} d^{-1})
Persistence null model	0.74	0.55 $\log_e$ (mg CH_4 m^{-2} d^{-1})	0.67	0.63 $\log_e$ (mg CH_4 m^{-2} d^{-1})

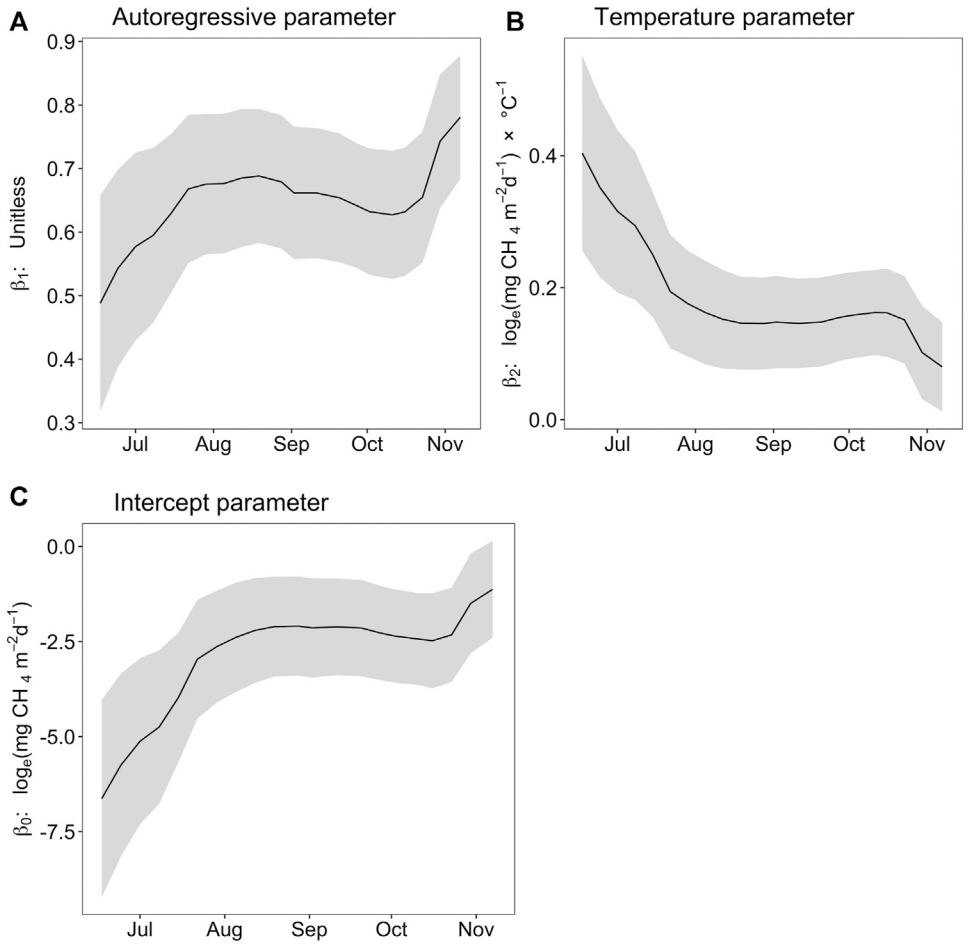


FIGURE 4 | Parameter estimates of β_1, the autoregressive parameter **(A)**, β_2, the sediment-water interface temperature parameter **(B)**, and β_0, the intercept parameter **(C)** of the forecast workflow recalibrated with new data. The black line represents the mean of the parameter ensembles, and the grey area represents the standard deviation of the ensembles (±1 S.D. mean).

Forecast Evaluation and Model Transferability

All three forecast workflows - the forecast model with iterative refitting, the forecast model without refitting, and the null persistence model - generated 95% predictive intervals that encompassed out-of-sample CH_4 ebullition rate observations at both 1- and 2-week forecast horizons (**Figure 3**). However, we found that there were differences in performance among the workflows based on our evaluation metrics (**Table 2**). At both 1- and 2-week forecast horizons, the forecast workflow with iterative model refitting exhibited both higher NSE and lower RMSE values than the forecast workflow without refitting (**Table 2**). Moreover, the forecast workflow with refitting performed better than the null model at both 1- and 2-week forecast horizons (**Table 2**).

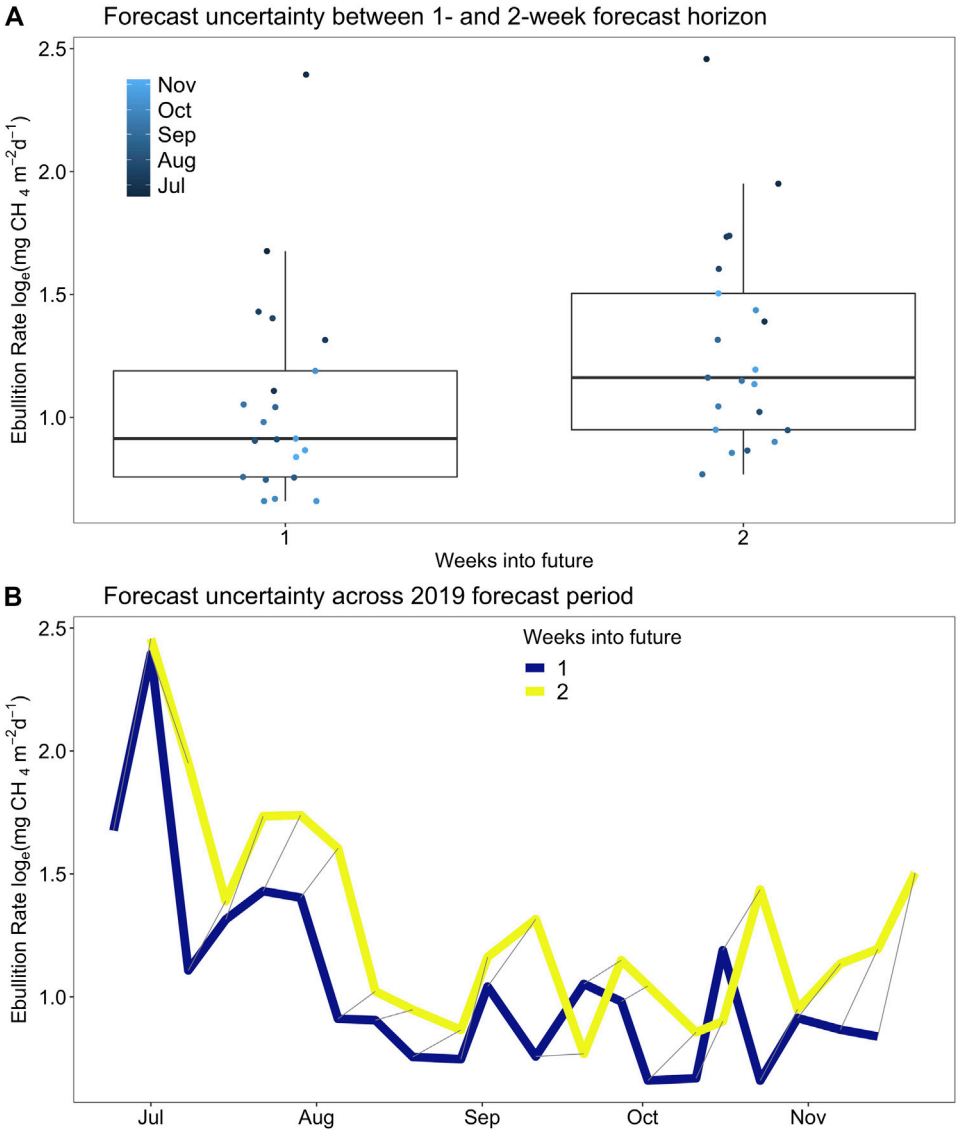


FIGURE 5 | The total forecast uncertainty (as measured by standard deviation of the forecast ensembles) for each week aggregated across forecast cycles for 1 and 2 weeks into the future Panel **(A)**. In panel **(B)**, each different colored line represents the number of weeks into the forecast horizon. The small grey lines are included as a guide to represent each forecast and how the uncertainty of each forecast mapped across the forecasting period.

Our result that the iterative model with refitting performed better than the iterative model without refitting indicates that model parameters estimated from 2017 ebullition rates did a relatively poor job of predicting 2019 ebullition rates, and as such, the model's interannual transferability among years is low. Our finding of low year-to-year transferability informs methods for scaling ebullition models predicting fluxes in one waterbody at one time point to multiple waterbodies over multiple years. Specifically, this result suggests that a single prediction model of ebullition likely will not apply to other years, motivating future work to test this hypothesis in other waterbodies.

Although the forecast workflow without refitting exhibited low transferability across years, the forecast workflow with refitting successfully predicted future CH_4 ebullition rates well because of the evolution of the model parameters throughout the 2019 forecasting period. We observed a substantial evolution of the intercept, AR, and SWI temperature parameters (β_0, β_1, and β_2, respectively) during the 2019 forecast period (**Figure 4**), highlighting how iteratively refitting the model to update the parameters can lead to improved forecast performance. The SWI temperature (β_2) parameter was at its highest value in the early stages of the forecasting period at 0.41 ± 0.15 $\log_e$ (mg CH_4 m^{-2} d^{-1}) × C^{-1} (mean ±1 S.D.) on 17 June, and then steadily decreased throughout the forecasting period to 0.07 ± 0.06 $\log_e$ (mg CH_4 m^{-2} d^{-1}) × C^{-1} by 7 November. This decrease over time coincided with an increase in SWI temperatures, and indicates that the relative importance of the temperature scaling

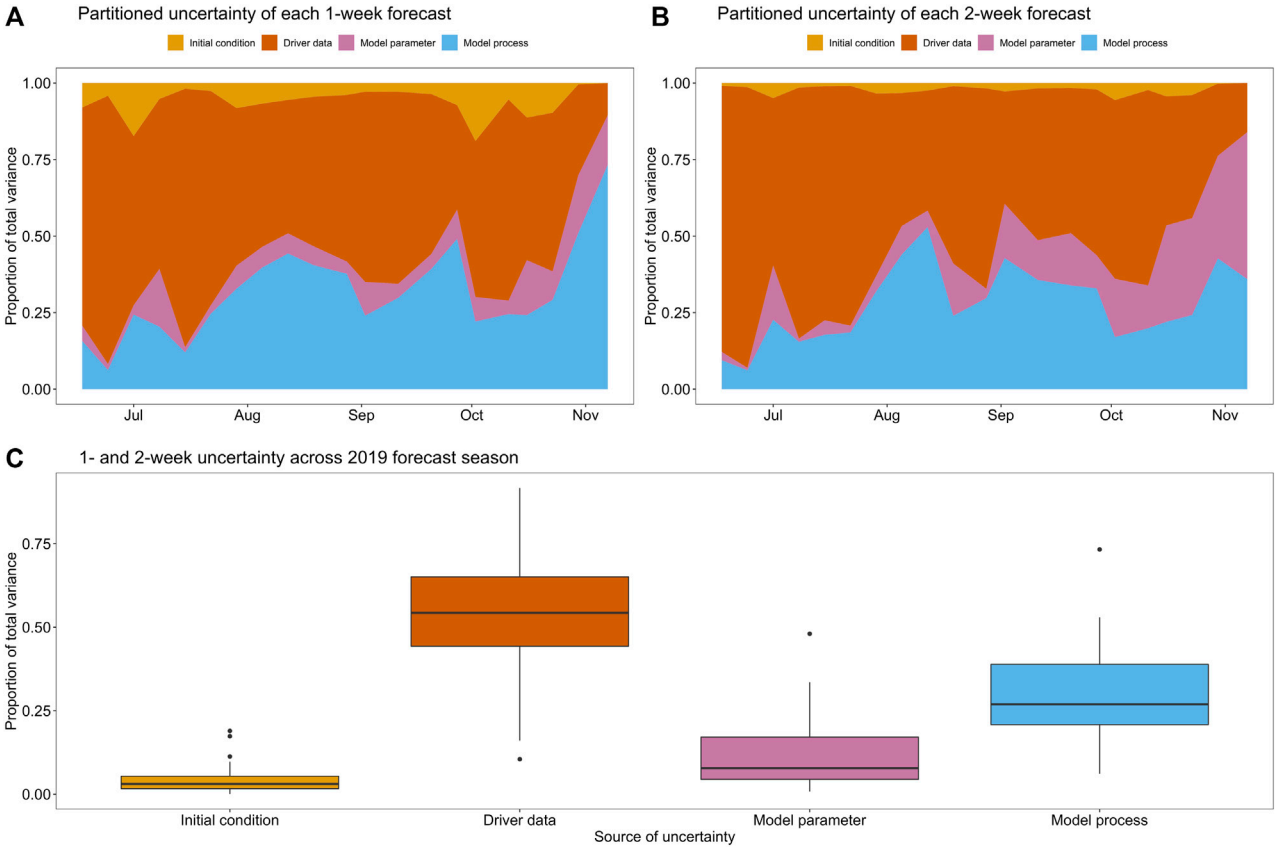


FIGURE 6 | Panel **(A, B)** depicts how the relative contribution of different sources of forecast uncertainty (initial condition, driver, parameter, and process) from the workflow with iterative model refitting evolved over each forecasting cycle starting with the initial day of the forecast cycle 1-week (**A**; *t*+1 in **Figure 2**), and 2-week (**B**; *t*+2 in **Figure 2**) ahead forecasts. Panel **(C)** depicts the same sources of uncertainty aggregated across all of the forecast cycles from *t*+1 and *t*+2 that were evaluated during the 2019 forecast period.

parameter was highest when temperatures at the SWI were low. Conversely, the unitless AR parameter (β_1) was 0.48 ± 0.17 and 0.63 ± 0.09 between 17 June and 2 September, and then steadily increased to a maximum of 0.78 ± 0.09 on 7 November. Finally, the intercept (β_0) parameter changed throughout the forecasting period and was −6.67 ± 2.59 and −2.11 ± 1.26 $\log_e$ (mg CH_4 m^{-2} d^{-1}) between 17 June and 2 September, and then steadily increased to a maximum of −1.11 ± 1.27 $\log_e$ (mg CH_4 m^{-2} d^{-1}) on 7 November. These changes indicate that the relative importance of these three model parameters evolved throughout the forecasting period.

Effective Forecast Horizons

The comparison of the workflows and the persistence null model indicated that our model's effective forecast horizon of CH_4 ebullition with iterative model refitting extended up to 2 weeks into the future (**Table 2**). However, at both 1- and 2-week forecast horizons the null persistence model outperformed the workflow without refitting (**Table 2**). To understand why the forecast workflow with iterative model refitting consistently performed better than the workflow without refitting and the persistence null model, we explored the sources of forecast uncertainty in the workflow with iterative model refitting.

Forecast Uncertainty and Uncertainty Partitioning

Over the forecasting period, the forecast uncertainty (as measured by standard deviation, SD) consistently increased from 1 to 2 weeks into the future, on average by 32% (**Figure 5A**). Simultaneously, total uncertainty in both forecast horizons decreased throughout the forecasting period from June to November (**Figure 5B**). The first forecast (starting 17 June) exhibited the largest uncertainty in both 1- and 2-week forecast horizons, with a SD of 1.67 $\log_e$ (mg CH_4 m^{-2} d^{-1}) at 1-week and 2.46 $\log_e$ (mg CH_4 m^{-2} d^{-1}) at the 2-week horizon (**Figure 5B**). By 15 July, the total forecast SD across the 1- and 2-week horizons decreased to 1.42 and 1.73 $\log_e$ (mg CH_4 m^{-2} d^{-1}) respectively, a 15 and 30% decrease in forecast SD. The total forecast uncertainty continued to decrease though the forecasting season, and by 7 November, the final forecast of the season, the forecast uncertainty was 0.84 $\log_e$ (mg CH_4 m^{-2} d^{-1}) at the 1-

week horizon and 1.50 $\log_e$ (mg CH_4 m^{-2} d^{-1}) at the 2-week horizon.

When partitioned, driver data and model process uncertainty were consistently the largest sources of uncertainty in our forecasts at both 1- and 2-week forecast horizons among all forecasts (**Figure 6**). At the 1-week forecast horizon, driver data uncertainty was the largest source of uncertainty between 17 June and 11 September and then model process uncertainty was the largest source from 11 September to the last forecast on 7 November (**Figure 6A**). At the 2-week forecast horizon, driver data uncertainty was also the largest source of uncertainty between 17 June and 2 September and then model process and parameter uncertainty became the largest sources of uncertainty from 2 September to the last forecast on 7 November (**Figure 6B**). When aggregated across the 2019 period for both horizons, driver data uncertainty contributed a mean of 60% of total forecast uncertainty (**Figure 6C**), indicating that uncertainty in the forecasted water temperatures from FLARE and the uncertainty in the SWI temperature scaling model contributed most to uncertainty in our forecasts. Model process uncertainty was the next highest contributed source of uncertainty at 25% over the entire forecasting period. Both model parameter and initial conditions uncertainty contributed smaller proportions of total variance, with seasonal means of 11 and 4%, respectively (**Figure 6C**).

DISCUSSION

Our CH_4 ebullition forecasting workflow demonstrated that iterative model refitting improved summer CH_4 ebullition rate predictions at both 1- and 2-week forecast horizons (**Table 2**; **Figure 3**). The utility of iterative model refitting was demonstrated by the evolution of the model parameter distributions over time (**Figure 4**) and the improvement of the forecast workflow with refitting over the null model during the forecasting period (**Table 2**). In addition, the forecasts developed by iterative model refitting exhibited lower overall forecast uncertainty as the forecasting period progressed, as indicated by the reduction in the total SD (**Figure 5B**). The primary drivers of uncertainty in the forecasts were driver data and model process. Altogether, our CH_4 ebullition rate forecasts provide insight to: the low transferability of CH_4 ebullition rate prediction models among years (Objective 1), the effective forecast horizon of CH_4 ebullition can extend up to 2 weeks in the future (Objective 2), and that improvements to the driver data and the CH_4 ebullition models themselves would be most useful for improving CH_4 ebullition rate predictions (Objective 3), as discussed below.

Model Interannual Transferability

Our comparison of the forecasting workflows with and without iterative model refitting provided useful insight on the transferability of our CH_4 ebullition prediction models among years. The forecast workflow that relied on the fitted 2017 posterior distributions (without iterative refitting) performed worse than the forecasts with iterative model refitting at both 1- and 2-week horizons (**Table 2**). This difference is likely due to lower overall ebullition rates in 2019 than 2017, which caused the calibrated 2017 posterior distributions to consistently overestimate CH_4 ebullition rates in 2019 (**Figure 3**). These results support previous work observing high interannual variability in CH_4 ebullition rates (Burke et al., 2019; Männistö et al., 2019; Linkhorst et al., 2020), and suggest that adopting a modeling workflow that is iteratively refitted with new incoming data throughout the season will improve CH_4 ebullition predictions. Given our empirical forecast model (**Eq. 2**), its low transferability is not surprising and points to the importance of additional covariates that may be important for driving variability in CH_4 ebullition rates (e.g., Deemer and Holgerson, 2021). The addition of meaningful covariates would likely increase temporal transferability by increasing the mechanistic ability of the model to recreate observed CH_4 ebullition dynamics, as well as decrease total forecast uncertainty, as discussed below.

The evolution of model parameters throughout the forecasting period (**Figure 4**) highlights the ability of iterative refitting to respond to the changing environmental conditions that occurred between June and November. For example, an increase in the observed ebullition rates (**Figure 3**) in early July was concomitant with a decrease in the SWI temperature parameter as the reservoir warmed. Between 15 July and 11 October, both the SWI temperature and AR term parameters remained largely stationary as the ebullition rates exhibited a seasonal increase and then decrease (**Figure 3**). After 11 October, the SWI temperature parameter decreased while the AR term parameter increased to its maximum value. The dynamic parameter values highlight how SWI temperature is likely most important for predicting CH_4 ebullition in early summer, prior to the onset of stable thermal stratification. Conversely, SWI temperatures were much less important during the autumn, when there are large changes occurring week-to-week as water at the SWI undergoes dynamic fall mixing conditions.

Effective Forecast Horizons

The better performance of our forecast workflow with iterative model refitting over the persistence null model at both the 1- and 2-week forecast horizons (**Table 2**) provides insight on how to evaluate the predictive horizon of CH_4 ebullition rates. Although CH_4 ebullition is often considered a stochastic process (Bastviken et al., 2004; though see; West et al., 2016; Bezerra et al., 2020), our study suggests that CH_4 ebullition may be successfully predicted up to 2 weeks ahead at the weekly time step. However, our forecasts do not provide evidence on whether CH_4 ebullition rates can be accurately predicted beyond 2 weeks. Additionally, the 32% increase in the forecast ensemble uncertainty (**Figure 5**) between the 1 and 2-week forecast horizons in our iterative model refitting workflow (**Figure 5A**), indicates that the 2-week forecasts provide less meaningful predictions than the 1-week forecasts. Thus, even if the mean of the forecast ensemble closely matches the out-of-sample predictions at the 2-week horizon, our 2-week forecasts should be interpreted carefully given the substantial increase in the ensemble SD between the 1- and 2-week horizons. Altogether, we advocate for the inclusion of persistence null models and the quantification of forecast

ensemble uncertainty as means for identifying the effective forecast horizon in future forecasting workflows for CH_4 ebullition to inform the performance and meaningful horizon of the models being tested.

Uncertainty Partitioning

Partitioning different sources of uncertainty (initial conditions, parameter, process, and driver uncertainty; Dietze, 2017a) in our CH_4 ebullition rate forecasts allowed us to examine areas where our forecasting workflow with iterative model refitting could be improved (**Figure 6**). The large relative contribution of driver uncertainty in the 1- and 2-week forecasts (**Figures 6A,B**) during the 2019 forecasting period was likely due to uncertainty in the forecasted water temperatures from FLARE and the propagated uncertainty that arose in the SWI temperature scaling model from the downstream dam site to upstream transect site (**Eqs 6**, **7**; *Forecasting SWI Temperature*). Thomas et al. (2020) found that meteorological driver data contributed the largest proportion of uncertainty in FLARE's water temperature forecasts in FCR's surface waters at horizons greater than 2 days into the future. Similarly, Dietze (2017a) found that meteorological driver data uncertainty contributed substantial uncertainty to net ecosystem exchange forecasts at forecast horizons greater than 1 week. Consequently, driver data uncertainty remains an important source of uncertainty that should be quantified in future forecasts of CH_4 ebullition.

We also observed a larger contribution of model process uncertainty at the 1- and 2-week forecast horizons toward the end of the 2019 forecasting period, indicating that improvements to the model itself would improve CH_4 ebullition rate predictions (**Figure 6A**). Model process uncertainty refers to the unexplained variability in the model itself, and encompasses multiple sources of variability in the model, including model structure, parameter heterogeneity, and stochastic variation (Dietze, 2017a). In the case of our forecast workflow for CH_4 ebullition rates, the large contributions from model process uncertainty could have resulted from the model structure, interannual variability that occurred between 2017 and 2019, or other factors that were not accounted for in our state-space model. New forecasts of CH_4 ebullition rates could be improved by specifically partitioning these potential sources of model process uncertainty using a hierarchical framework (Dietze, 2017a; Harris et al., 2018).

Forecasting System Limitations and Areas for Improvement

There are several limitations of our near-term, iterative CH_4 ebullition rate forecasts that should be considered. First, there are many other potential drivers of CH_4 ebullition, such as chlorophyll *a*, nutrients, and water pressure, among others (e.g., DelSontro et al., 2016; West et al., 2016; Harrison et al., 2017; Davidson et al., 2018). Alternative model structures (e.g., DelSontro et al., 2016; Schmid et al., 2017; Peltola et al., 2018; Grasset et al., 2021) could also improve our CH_4 ebullition forecasts and improve their transferability to other freshwater ecosystems and different temporal scales. Because our forecasts relied on an AR model developed from earlier work in FCR (McClure et al., 2020a), we were unable to quantify model selection uncertainty by using an ensemble of models in our forecasting workflow (e.g., process-based ebullition models; Peltola et al., 2018; Schmid et al., 2017), which is an important step for future work. Testing different forecasting workflows with different CH_4 ebullition model covariates and model types in inland water ecosystems at varying temporal and spatial scales will further improve our understanding of this important biogeochemical flux.

In addition to testing other CH_4 ebullition rate models, additional improvements to our forecasting system would also include the addition of automated sensors to improve temporal coverage, incorporation of other statistical methods into the forecasting workflow (e.g., sequential data assimilation methods like particle filters and Kalman filters; Evensen, 2009; Carpenter et al., 1999; Del Moral et al., 2006; Doucet and Johansen, 2009), and other forecast model covariates which might provide more insight to mechanisms of CH_4 ebullition. While our forecasting case study showed that near-term, iterative forecasts with iterative model refitting are possible with manually-collected CH_4 ebullition rates, recent technological improvements in automated sensors hold great potential for advancing the future of CH_4 ebullition forecasting at daily or sub-daily scales by increasing the timescale at which new data can be assimilated and at which forecasts can be made (e.g., Varadharajan et al., 2010; Delwiche and Hemond, 2017; Maher at al., 2019). Together, integrating automated CH_4 ebullition rate sensors, an ensemble of predictive models, and alternate data assimilation methods have the potential to substantially advance forecasting of CH_4 ebullition fluxes at sub-weekly timescales.

Scaling our CH_4 Ebullition Forecasting Workflow to Other Sites

Our near-real time forecasts showed that out-of-sample CH_4 ebullition rates at our littoral transect in FCR were adequately predicted at 1- and 2-week horizons using a state-space Bayesian workflow with iterative model refitting and forecasted SWI temperatures as a model covariate (**Figure 3**). While we acknowledge that we have only applied this forecasting workflow to one reservoir site, we envision that it has the potential to be adapted for predicting CH_4 ebullition in other freshwater ecosystems. Here, we identify three critical components we think would enable others to begin making near-real time forecasts of CH_4 ebullition rates from inland waters and inform ecological understanding of the processes governing ebullition rates:

1) A routine ebullition field monitoring program. The foundation of near-term, iterative forecasting is a coupled model-data feedback loop (Luo et al., 2011; Dietze, 2017b). Developing a field monitoring program that routinely samples ebullition from a waterbody of interest is necessary to develop and iteratively update ebullition forecast models. For example, this could include one automated ebullition trap with high temporal resolution or multiple passive traps that are limited in temporal resolution but are less expensive and allow for more spatial coverage. It is ideal if the monitoring data collection occurs within the maximum time horizon of the forecasted driver data to enable iterative forecast evaluation and model refitting.

2) A model to generate future predictions of ebullition that can be updated as observations become available. While we used a relatively simple state-space model fit in a Bayesian framework to account for the computational requirements to run forecasts with iterative refitting, there are many possible model types and data assimilation methods than can be applied like process-based models (Schmid et al., 2017; Peltola et al., 2018), and machine learning approaches such as neural networks (Abbasi et al., 2020) to develop CH_4 ebullition forecasts. We suggest starting with something simple like a persistence null model (**Eq. 9**) and then adding in additional complexity when resources are available to do so.

3) Forecasted driver data. Depending on model structure, near-real time ebullition forecasts will likely rely on forecasted driver data to predict ebullition at a future time step. In lieu of having access to a water temperature forecasting system as we did for this study, meteorological forecasts (e.g., NOAA's Global Ensemble Forecast System) can be integrated into an ebullition forecasting workflow if the CH_4 ebullition model is driven by meteorological variables such as air temperature, barometric pressure, shortwave radiation, or wind speed (Joyce and Jewell 2003; Tokida et al., 2007; Wik et al., 2014; Peltola et al., 2018; McClure R. et al., 2020). For example, Tokida et al. (2007) showed how decreasing atmospheric pressure triggered substantial increases in CH_4 ebullition from wetlands. Similarly, Wik et al. (2014) associated seasonal CH_4 ebullitive fluxes from thermokarst lakes with shortwave radiation and Joyce and Jewell (2003) suggested that wind speed could influence bottom currents, thereby changing the shear stress at the sediments releasing ebullition bubbles.

There are several additional drivers of ebullition that have the capacity to be applied in a forecasting workflow in addition to those included in this study. However, in order to include a new driver variable in a forecasting workflow, one must produce a forecast of the driver variable, which can add additional uncertainty [e.g., our forecasting application here that translated weather forecasts into future SWI temperatures using FLARE and an empirical scaling model (**Eq. 6**)]. For example, changes in reservoir water level (Beaulieu et al., 2018), chemical and biological drivers such as chlorophyll *a* (West et al., 2016), sedimentation quantity (Wik et al., 2018), sediment quality (Wik et al., 2018), macrophyte abundance, and diel *Chaoborus* spp. migration (Bezerra et al., 2020), are known drivers of ebullition but rarely forecasted. This provides an opportunity for future model studies to begin generating forecasts of these drivers and testing how they perform with near-term forecasts of ebullition. Among the different predictors, chlorophyll *a* may be a useful one to start with as a forecast driver for CH_4 ebullition as there are multiple existing workflows that have generated chlorophyll a forecasts for management (Page et al., 2018; Rousso et al., 2020). Integrating chlorophyll *a* forecasts into CH_4 ebullition forecast workflows, similar to our example of integrating water temperature forecasts to our CH_4 ebullition workflow, would likely improve forecasts of CH_4 ebullition, and enable testing of how well these drivers perform at varying spatial and temporal scales.

Utility of Adopting Near-Term Iterative Forecasting Workflows

In conclusion, we successfully generated near-real time forecasts of CH_4 ebullition rates, a highly variable biogeochemical flux in inland water ecosystems, using forecasted SWI temperatures and near-real time observations of ebullition rates. Further, our forecasts that iteratively updated parameters through model refitting performed better than forecasts that did not update parameters and a persistence null model at both 1- and 2-week forecast horizons, indicating that forecasting workflows with iterative model refitting have the potential to improve our estimates of this highly variable biogeochemical flux up to 2 weeks into the future. Additionally, quantifying and partitioning uncertainty provided an additional line of evidence that iterative forecasting can improve the skill of predictions with time. Uncertainty partitioning showed that our forecast model is highly sensitive to process uncertainty, highlighting the need for more resolved partitioning of variation within our predictive AR model and testing of different CH_4 ebullition predictive models to improve predictions and transferability across multiple spatial and temporal scales. Altogether, we show that near-term iterative forecasting with model refitting and uncertainty partitioning has the potential to improve future CH_4 ebullition rate predictions, an important step to informing our upscaling estimates of CH_4 ebullition fluxes from inland waters to the global carbon cycle.

DATA AVAILABILITY STATEMENT

The original contributions presented in the study are included in the article/supplementary materials, further inquiries can be directed to the corresponding author.

AUTHOR CONTRIBUTIONS

RM and CC developed the original research idea. RM and RT developed the forecasting workflow. WW and ML contributed to code development, field data collection, and forecast model testing. RM wrote the manuscript with equal writing contributions from CC and RT. All authors provided feedback and approved the final version.

FUNDING

This work was supported by the U.S. National Science Foundation (CNS-1737424, DEB-1753639, DBI-1933016, DEB-1926050); the Virginia Tech Global Change Center; and the Fralin Life Sciences Institute.

ACKNOWLEDGMENTS

We thank the Smart Reservoir and FCR Carbon teams for their helpful feedback during this project and the Western Virginia

Water Authority for their long-term support and access to the reservoir. We thank Ashley Mickens for her critical help with data collection and GC-FID analyses. Additionally, we thank Bethany Bookout, Alexandria Hounshell, Abby Lewis, Heather Wander, Rachel Corrigan, James Maze, Dexter Howard, Jacob Wynne, and Nick Hammond for their help with field data collection and Vahid Daneshmand and Renato Figueiredo for their development and maintenance of the FLARE forecast system. Paul Hanson, Erin Hotchkiss, Madeline Schreiber, and GLEON colleagues provided valuable feedback on manuscript development. Finally, as always, we thank Bobbie Niederlehner for helping with the GC-FID and laboratory analysis methods development.

REFERENCES

Abbasi, T., Abbasi, T., Luithui, C., and Abbasi, S. A. (2020). A Model to Forecast Methane Emissions from Topical and Subtropical Reservoirs on the Basis of Artificial Neural Networks. *Water* 12 (1), 145. doi:10.3390/w12010145

Aben, R. C. H., Barros, N., Van Donk, E., Frenken, T., Hilt, S., Kazanjian, G., et al. (2017). Cross continental Increase in Methane Ebullition under Climate Change. *Nat. Commun.* 8 (1), 1–8. doi:10.1038/s41467-017-01535-y

Bastviken, D., Cole, J., Pace, M., and Tranvik, L. (2004). Methane Emissions from Lakes: Dependence of lake Characteristics, Two Regional Assessments, and a Global Estimate. *Glob. Biogeochem. Cycles* 18 (4). doi:10.1029/2004GB002238

Beaulieu, J. J., Balz, D. A., Birchfield, M. K., Harrison, J. A., Nietch, C. T., Platz, M. C., et al. (2018). Effects of an Experimental Water-Level Drawdown on Methane Emissions from a Eutrophic Reservoir. *Ecosystems* 21, 657–674. doi:10.1007/s10021-017-0176-2

Bezerra, M. P., McGinnis, D. F., Bezerra-Neto, J. F., and Barbosa, F. A. R. (2020). Is it Stochastic? Chaoborus Larvae Bioturbation Likely Affect the Timing of Daily Methane (CH4) Ebullitive Flux in a Tropical Reservoir. *Hydrobiologia* 847 (15), 3291–3308. doi:10.1007/s10750-020-04331-w

Burke, S. A., Wik, M., Lang, A., Contosta, A. R., Palace, M., Crill, P. M., et al. (2019). Long-Term Measurements of Methane Ebullition from Thaw Ponds. *J. Geophys. Res. Biogeosci.* 124 (7), 2208–2221.

Carey, C. C., Hounshell, A. G., Lofton, M. E., Birgand, F., Bookout, B. J., Corrigan, R. S., et al. (2021a). *Discharge Time Series for the Primary Inflow Tributary Entering Falling Creek Reservoir, Vinton, Virginia, USA 2013-2021 Ver 7*. Environmental Data Initiative. doi:10.6073/pasta/8d22a432aac5560b0f45aa1b21ae4746

Carey, C. C., Lewis, A. S., McClure, R. P., Gerling, A. B., Chen, S., Das, A., et al. (2021b). *Time Series of High-Frequency Profiles of Depth, Temperature, Dissolved Oxygen, Conductivity, Specific Conductivity, Chlorophyll a, Turbidity, pH, Oxidation-Reduction Potential, Photosynthetic Active Radiation, and Descent Rate for Beaverdam Reservoir, Carvins Cove Reservoir, Falling Creek Reservoir, Gatewood Reservoir, and Spring Hollow Reservoir in Southwestern Virginia, USA 2013-2020 Ver 11*. Environmental Data Initiative. doi:10.6073/pasta/5448f9d415fd09e0090a46b9d4020ccc

Carey, C. C., Woelmer, W. M., Lewis, A. S., Breef-Pilz, A., Howard, D. W., and Bookout, B. J. (2021c). *Time Series of High-Frequency Sensor Data Measuring Water Temperature, Dissolved Oxygen, Pressure, Conductivity, Specific Conductance, Total Dissolved Solids, Chlorophyll a, Phycocyanin, and Fluorescent Dissolved Organic Matter at Discrete Depths in Falling Creek Reservoir, Virginia, USA in 2018-2020 Ver 5*. Environmental Data Initiative. doi:10.6073/pasta/88896f4a7208c9b7bddcf498258edf78

Carpenter, J., Clifford, P., and Fearnhead, P. (1999). Improved Particle Filter for Nonlinear Problems. *IEE Proc. Radar Sonar Navig.* 146 (1), 2–7. doi:10.1049/ip-rsn:19990255

Davidson, T. A., Audet, J., Jeppesen, E., Landkildehus, F., Lauridsen, T. L., Søndergaard, M., et al. (2018). Synergy between Nutrients and Warming Enhances Methane Ebullition from Experimental Lakes. *Nat. Clim Change* 8 (2), 156–160. doi:10.1038/s41558-017-0063-z

Deemer, B. R., Harrison, J. A., Li, S., Beaulieu, J. J., DelSontro, T., Barros, N., et al. (2016). Greenhouse Gas Emissions from Reservoir Water Surfaces: a New Global Synthesis. *BioScience* 66 (11), 949–964. doi:10.1093/biosci/biw117

Deemer, B. R., and Holgerson, M. A. (2021). Drivers of Methane Flux Differ between Lakes and Reservoirs, Complicating Global Upscaling Efforts. *J. Geophys. Res. Biogeosci.* 126 (4). doi:10.1029/2019JG005600

Del Moral, P., Doucet, A., and Jasra, A. (2006). Sequential Monte Carlo Samplers. *J. R. Stat. Soc B.* 68 (3), 411–436. doi:10.1111/j.1467-9868.2006.00553.x

Del Sontro, T., Boutet, L., St-Pierre, A., del Giorgio, P. A., and Prairie, Y. T. (2016). Methane Ebullition and Diffusion from Northern Ponds and Lakes Regulated by the Interaction between Temperature and System Productivity. *Limnol. Oceanogr.* 61, S62–S77. doi:10.1002/lno.10335

Delwiche, K., and Hemond, H. F. (2017). An Enhanced Bubble Size Sensor for Long-term Ebullition Studies. *Limnol. Oceanogr. Methods* 15, 821–835. doi:10.1002/lom3.10201

Dietze, M. C. (2017a). Prediction in Ecology: a First-Principles Framework. *Ecol. Appl.* 27 (7), 2048–2060. doi:10.1002/eap.1589

Dietze, M. C. (2017b). *Ecological Forecasting*. Princeton, NJ: Princeton University Press, 288. ISBN 9781400885459.

Dietze, M. C., Fox, A., Beck-Johnson, L. M., Betancourt, J. L., Hooten, M. B., Jarnevich, C. S., et al. (2018). Iterative Near-Term Ecological Forecasting: Needs, Opportunities, and Challenges. *Proc. Natl. Acad. Sci. USA* 115 (7), 1424–1432. doi:10.1073/pnas.1710231115

Doucet, A., and Johansen, A. M. (2009). "A Tutorial on Particle Filtering and Smoothing: Fifteen Years Later," in *Handbook of Nonlinear Filtering* (New York: Oxford Univ. Press). 12, 676–704.

Evensen, G. (2009). *Data Assimilation: The Ensemble Kalman Filter*. New York, NY: Springer Science & Business Media, 307. ISBN 978-3-642-03710-8.

Gelman, A., and Rubin, D. B. (1992). A Single Series from the Gibbs Sampler Provides a False Sense of Security. *Bayesian Statis.* 4, 625–631.

Gerling, A. B., Munger, Z. W., Doubek, J. P., Hamre, K. D., Gantzer, P. A., Little, J. C., et al. (2016). Whole-catchment Manipulations of Internal and External Loading Reveal the Sensitivity of a century-old Reservoir to Hypoxia. *Ecosystems* 19 (3), 555–571. doi:10.1007/s10021-015-9951-0

Grasset, C., Moras, S., Isidorova, A., Couture, R. M., Linkhorst, A., and Sobek, S. (2021). An Empirical Model to Predict Methane Production in Inland Water Sediment from Particular Organic Matter Supply and Reactivity. *Limnol. Oceanogr.* 66, 3643–3655. doi:10.1002/lno.11905

Harris, D. J., Taylor, S. D., and White, E. P. (2018). Forecasting Biodiversity in Breeding Birds Using Best Practices. *Peer J* 6, e4278.

Harrison, J. A., Deemer, B. R., Birchfield, M. K., and O'Malley, M. T. (2017). Reservoir Water-Level Drawdowns Accelerate and Amplify Methane Emission. *Environ. Sci. Technol.* 51, 1267–1277. doi:10.1021/acs.est.6b03185

Johnson, M. S., Matthews, E., Bastviken, D., Deemer, B., Du, J., and Genovese, V. (2021). Spatiotemporal Methane Emission from Global Reservoirs. *J. Geophys. Res. Biogeosci.* 126. doi:10.1029/2021JG006305

Joyce, J., and Jewell, P. W. (2003). Physical Controls on Methane Ebullition from Reservoirs and Lakes. *Environ. Eng. Geosci.* 9 (2), 167–178. doi:10.2113/9.2.167

Lewis, A. S., Woelmer, W. M., Wander, H. L., Howard, D. W., Smith, J. W., McClure, R. P., et al. (2021). Increased Adoption of Best Practices in Ecological Forecasting Enables Comparisons of Forecastability Across Systems. *Ecological Applications*. (In press). doi:10.1002/eap.2500

Linkhorst, A., Hiller, C., DelSontro, T., Azevedo, G. M., Barros, N., Mendonça, R., et al. (2020). Comparing Methane Ebullition Variability across Space and Time in a Brazilian Reservoir. *Limnol. Oceanogr.* 65 (7), 1623–1634. doi:10.1002/lno.11410

Luo, Y., Ogle, K., Tucker, C., Fei, S., Gao, C., LaDeau, S., et al. (2011). Ecological Forecasting and Data Assimilation in a Data-Rich Era. *Ecol. Appl.* 21 (5), 1429–1442. doi:10.1890/09-1275.1

Maher, D. T., Drexl, M., Tait, D. R., Johnston, S. G., and Jeffrey, L. C. (2019). iAMES: An Inexpensive, Automated Methane Ebullition Sensor. *Environ. Sci. Technol.* 53, 6420–6426. doi:10.1021/acs.est.9b01881

Männistö, E., Korrensalo, A., Alekseychik, P., Mammarella, I., Peltola, O., Vesala, T., et al. (2019). Multi-year Methane Ebullition Measurements from Water and Bare Peat Surfaces of a Patterned Boreal Bog. *Biogeosciences* 16 (11), 2409–2421. doi:10.5194/bg-16-2409-2019

McClure, R. P., Hamre, K. D., Niederlehner, B. R., Munger, Z. W., Chen, S., Lofton, M. E., et al. (2018). Metalimnetic Oxygen Minima Alter the Vertical Profiles of

Carbon Dioxide and Methane in a Managed Freshwater Reservoir. *STOTEN* 636, 610–620.

McClure, R. P., Lofton, M. E., Chen, S., Krueger, K. M., Little, J. C., and Carey, C. C. (2020a). The Magnitude and Drivers of Methane Ebullition and Diffusion Vary on a Longitudinal Gradient in a Small Freshwater Reservoir. *J. Geophys. Res. Biogeosci.* 125 (3). doi:10.1029/2019JG005205

McClure, R. P., Lofton, M. E., Chen, S., Krueger, K. M., Little, J. C., and Carey, C. C. (2020b). *Methane Ebullition and Diffusion Rates, Turbulence, Water Temperature, and Water Depth Data from Falling Creek Reservoir (Virginia, USA) in the Ice-free Period during 2016-2019 Ver 2.* Environmental Data Initiative. doi:10.6073/pasta/c6b1a54e356f5ab093d86dcdb89177ba

McClure, R. P., Thomas, R. Q., Lofton, M. E., Woelmer, W. M., and Carey, C. C. (2021). First Version of Reproducible Forecasts for CH_4 Ebullition Rates at an Upstream Transect in a Eutrophic Reservoir in VA, USA. Available at: https://zenodo.org/badge/latestdoi/346490639.

Moriasi, D. N., Arnold, J. G., Van Liew, M. W., Bingner, R. L., Harmel, R. D., and Veith, T. L. (2007). Model Evaluation Guidelines for Systematic Quantification of Accuracy in Watershed Simulations. *Trans. ASABE* 50 (3), 885–900. doi:10.13031/2013.23153

Munkhammar, J., Mattsson, L., and Rydén, J. (2017). Polynomial Probability Distribution Estimation Using the Method of Moments. *PloS one* 12 (4), e0174573. doi:10.1371/journal.pone.0174573

Nash, J. E., and Sutcliffe, J. V. (1970). River Flow Forecasting through Conceptual Models Part I - A Discussion of Principles. *J. Hydrol.* 10 (3), 282–290. doi:10.1016/0022-1694(70)90255-6

Page, T., Smith, P. J., Beven, K. J., Jones, I. D., Elliott, J. A., Maberly, S. C., et al. (2018). Adaptive Forecasting of Phytoplankton Communities. *Water Res.* 134, 74–85. doi:10.1016/j.watres.2018.01.046

Peltola, O., Raivonen, M., Li, X., and Vesala, T. (2018). Technical Note: Comparison of Methane Ebullition Modelling Approaches Used in Terrestrial Wetland Models. *Biogeosciences* 15 (3), 937–951. doi:10.5194/bg-15-937-2018

Petchey, O. L., Pontarp, M., Massie, T. M., Kéfi, S., Ozgul, A., Weilenmann, M., et al. (2015). The Ecological Forecast Horizon, and Examples of its Uses and Determinants. *Ecol. Lett.* 18 (7), 597–611. doi:10.1111/ele.12443

Plummer, M. (2018). *Rjags: Bayesian Graphical Models Using MCMC*. R Package. Version 4-6, 2016).

R Core Team (2021). *R: A Language and Environment for Statistical Computing*. Vienna, Austria: R Foundation for Statistical Computing. Available at: https://www.R-project.org/.

Rousso, B. Z., Bertone, E., Stewart, R., and Hamilton, D. P. (2020). A Systematic Literature Review of Forecasting and Predictive Models for Cyanobacteria Blooms in Freshwater Lakes. *Water Res.* 182, 115959. doi:10.1016/j.watres.2020.115959

Saunois, M., Stavert, A. R., Poulter, B., Bousquet, P., Canadell, J. G., Jackson, R. B., et al. (2020). The Global Methane Budget 2000-2017. *Earth Syst. Sci. Data* 12, 1561–1623. doi:10.5194/essd-12-1561-2020

Schmid, M., Ostrovsky, I., and McGinnis, D. F. (2017). Role of Gas Ebullition in the Methane Budget of a Deep Subtropical lake: What Can We Learn from Process-Based Modeling. *Limnol. Oceanogr.* 62 (6), 2674–2698. doi:10.1002/lno.10598

Thomas, R. Q., Figueiredo, R. J., Daneshmand, V., Bookout, B. J., Puckett, L. K., and Carey, C. C. (2020). A Near-Term Iterative Forecasting System Successfully Predicts Reservoir Hydrodynamics and Partitions Uncertainty in Real Time. *Water Resour. Res.* 56 (11). doi:10.1029/2019WR026138

Thomas, R. Q., Jersild, A. L., Brooks, E. B., Thomas, V. A., and Wynne, R. H. (2018). A Mid-century Ecological Forecast with Partitioned Uncertainty Predicts Increases in Loblolly pine forest Productivity. *Ecol. Appl.* 28 (6), 1503–1519. doi:10.1002/eap.1761

Tokida, T., Miyazaki, T., Mizoguchi, M., Nagata, O., Takakai, F., Kagemoto, A., et al. (2007). Falling Atmospheric Pressure as a Trigger for Methane Ebullition from Peatland. *Glob. Biogeochem. Cycles* 21 (2). doi:10.1029/2006GB002790

Varadharajan, C., Hermosillo, R., and Hemond, H. F. (2010). A Low-Cost Automated Trap to Measure Bubbling Gas Fluxes. *Limnol. Oceanogr. Meth.* 8 (7), 363–375.

West, W. E., Creamer, K. P., and Jones, S. E. (2016). Productivity and Depth Regulate lake Contributions to Atmospheric Methane. *Limnol. Oceanogr.* 61 (S1), S51–S61. doi:10.1002/lno.10247

Wik, M., Johnson, J. E., Crill, P. M., DeStasio, J. P., Erickson, L., Halloran, M. J., et al. (2018). Sediment Characteristics and Methane Ebullition in Three Subarctic Lakes. *J. Geophys. Res. Biogeosci.* 123 (8), 2399–2411. doi:10.1029/2017JG004298

Wik, M., Thornton, B. F., Bastviken, D., MacIntyre, S., Varner, R. K., and Crill, P. M. (2014). Energy Input Is Primary Controller of Methane Bubbling in Subarctic Lakes. *Geophys. Res. Lett.* 41 (2), 555–560. doi:10.1002/2013GL058510

Wik, M., Thornton, B. F., Bastviken, D., Uhlbäck, J., and Crill, P. M. (2016). Biased Sampling of Methane Release from Northern Lakes: A Problem for Extrapolation. *Geophys. Res. Lett.* 43 (3), 1256–1262. doi:10.1002/2015GL066501

Conflict of Interest: The authors declare that the research was conducted in the absence of any commercial or financial relationships that could be construed as a potential conflict of interest.

Publisher's Note: All claims expressed in this article are solely those of the authors and do not necessarily represent those of their affiliated organizations, or those of the publisher, the editors and the reviewers. Any product that may be evaluated in this article, or claim that may be made by its manufacturer, is not guaranteed or endorsed by the publisher.

Copyright © 2021 McClure, Thomas, Lofton, Woelmer and Carey. This is an open-access article distributed under the terms of the Creative Commons Attribution License (CC BY). The use, distribution or reproduction in other forums is permitted, provided the original author(s) and the copyright owner(s) are credited and that the original publication in this journal is cited, in accordance with accepted academic practice. No use, distribution or reproduction is permitted which does not comply with these terms.

frontiers in Environmental Science

ORIGINAL RESEARCH
published: 28 January 2022
doi: 10.3389/fenvs.2022.811375

Shelf-Sourced Methane in Surface Seawater at the Eurasian Continental Slope (Arctic Ocean)

Elena Vinogradova[1], Ellen Damm[2], Andrey V. Pnyushkov[3,4], Thomas Krumpen[5] and Vladimir V. Ivanov[6,7]*

[1]Shirshov Institute of Oceanology, Russian Academy of Science, Moscow, Russia, [2]Permafrost Research Section, Alfred Wegener Institute for Polar and Marine Research, Potsdam, Germany, [3]International Arctic Research Center, University of Alaska Fairbanks, Fairbanks, AK, United States, [4]Global Institution for Collaborative Research and Education, Hokkaido University, Sapporo, Japan, [5]Sea ice physics Research Section, Alfred Wegener Institute for Polar and Marine Research, Bremerhaven, Germany, [6]Lomonosov Moscow State University, Faculty of Geography, Oceanology Department, Moscow, Russia, [7]Arctic and Antarctic Research Institute, St Petersburg, Russia

This study traces the pathways of dissolved methane at the Eurasian continental slope (ECS) and the Siberian shelf break based on data collected during the NABOS-II expedition in August-September, 2013. We focus on the sea ice-ocean interface during seasonal strong ice melt. Our analysis reveals a patchy pattern of methane supersaturation related to the atmospheric equilibrium. We argue that sea ice transports methane from the shelf and that ice melt is the process that causes the heterogeneous pattern of methane saturation in the Polar Mixed Layer (PML). We calculate the solubility capacity and find that seasonal warming of the PML reduces the CH_4 storage capacity and contributes to methane supersaturation and potential sea-air flux in summer. Cooling in autumn enhances the solubility capacity in the PML once again. The shifts in the solubility capacity indicate the buffering capacity for seasonal storage of atmospheric and marine methane in the PML. We discuss specific pathways for marine methane and the storage capacity of the PML on the ECS as a sink/source for atmospheric methane and methane sources from the Siberian shelf. The potential sea-air flux of methane is calculated and intrusions of methane plumes from the PML into the Cold Halocline Layer are described.

Keywords: methane plumes, polar mixed layer, Eurasian continental slope, sea ice, shelf-basin interaction

OPEN ACCESS

Edited by:
Daniel F. McGinnis, Université de Genève, Switzerland

Reviewed by:
Terry Whitledge, Retired, Fairbanks, AK, United States
Haiyan Jin, Ministry of Natural Resources, China

****Correspondence:***
Elena Vinogradova
vinogradova@ocean.ru

Specialty section:
This article was submitted to Biogeochemical Dynamics, a section of the journal Frontiers in Environmental Science

Received: *08 November 2021*
Accepted: *12 January 2022*
Published: *28 January 2022*

Citation:
Vinogradova E, Damm E, Pnyushkov AV, Krumpen T and Ivanov VV (2022) Shelf-Sourced Methane in Surface Seawater at the Eurasian Continental Slope (Arctic Ocean). Front. Environ. Sci. 10:811375. doi: 10.3389/fenvs.2022.811375

1 INTRODUCTION

The Arctic holds large natural sources of methane (CH_4), especially the Siberian shelf, which is considered as potential sources of this greenhouse gas for the atmosphere. The release of CH_4 from these shallow shelf seas threaten to enhance the current Arctic amplification of global warming (IPCC, 2019). Indeed, warmer seawater as a positive feedback on the climate is discussed to displace gas hydrate stability zones and increase the thawing of subsea permafrost, which acts as a physical barrier to ascending gas (Reagan and Moridis, 2008; Shakhova et al., 2019). Recent acoustic surveys on shelves and along continental slopes revealed significant CH_4 emissions, triggered by an increasing number of submarine gas seepages (Westbrook et al., 2009; Baranov et al., 2020; Chuvilin et al., 2020). These assessments of potential CH_4 release mainly focused on the changes in the submarine CH_4 storage system (Shakhova et al., 2010, Shakhova et al., 2014;

Berchet et al., 2016). Based on these methodological approaches, bottom-up flux CH_4 estimations are strongly imbalanced related to top-down flux estimations (AMAP, 2015), revealing that either the release at the submarine-marine interface or the sea-air CH_4 fluxes is overestimated.

Actually, calculations based on the level of CH_4 supersaturation in surface water related to the atmospheric equilibrium disregard the effects of sea ice and the water transformations coupled to the sea ice cycle on the pathways of CH_4 (Damm et al., 2018). According to recent studies, the transport of shelf-sourced CH_4 by sea ice is a driving mechanism causing the patchy appearance of CH_4 excess in surface waters detected in different Arctic regions (Damm et al., 2015, Damm et al., 2018; Verdugo et al., 2021). Consequently, an assessment of the current sink capacities of certain regions and water masses in the Arctic Ocean is urgently needed to better simulate future climate scenarios.

In the last few decades, Arctic sea ice has sharply declined (Screen and Simmonds, 2010). The longer sea ice-free seasons (Markus et al., 2009; Günther et al., 2015) will have significant consequences for the CH_4 cycle, while the elongated period for a potential net sea-air exchange is just one possibility. Intensive sea ice melt causes an increasing contribution of fresh water in surface waters that dilutes the CH_4 excess. Eventually, warming will amplify the water stratification, and restrict CH_4 fluxes into the atmosphere. Water stratification is known to favor lateral CH_4 transport, which in turn enables CH_4 oxidation in the water column (Mau et al., 2013; Gentz et al., 2014; Myhre et al., 2016; Mau et al., 2017; Silyakova et al., 2020; Damm et al., 2021).

Moreover, changes of temperature and salinity in surface water, controlling the solubility and eventually the storage capacity for CH_4, needs to be considered in assessments of the current CH_4 budget. The Eurasian continental slope (ECS) is a key Arctic region to study this complexity of marine CH_4 pathways and the potential sink capacity of Arctic surface water. The surface water at the ECS comprises the Polar Mixed Layer (PML) on top and the salinity-stratified Cold Halocline Layer (CHL) underneath. In summer, the PML is formed by sea ice melt and Siberian River runoff (Rudels et al., 1996). In winter, ice formation in leads and polynyas alters the characteristics of the PML (Dmitrenko et al., 2009; Krumpen et al., 2011; Iwamoto et al., 2014). The CHL is formed via interaction between inflowing Atlantic water and sea ice (Rudels et al., 2004). The CHL remains close to the Siberian continental slope, receives inflows from surrounding shelves, and is additionally modified through mixing with the PML (Alkire et al., 2017). Both water masses link the shallow shelf with the ECS and highlight the role of the shelf-basin exchange for the validation of the CH_4 sink capacity.

In this study, we provide a first assessment of the seasonal storage capacity of the PML on the ECS. Based on data collected along cross-slope sections in late summer 2013 we point to the seasonal buffer capacity of the PML, which might influence the CH_4 flux. We discuss the ability of the ECS as a sink for CH_4 under the conditions of current sea ice retreat. Further, we describe the formation of CH_4 plumes in the sea ice-influenced PML during the period of pronounced seasonal ice melt and their mixing into the CHL. We show that the CH_4 plumes in the PML on the ECS are induced by the melt of mainly estuarine ice.

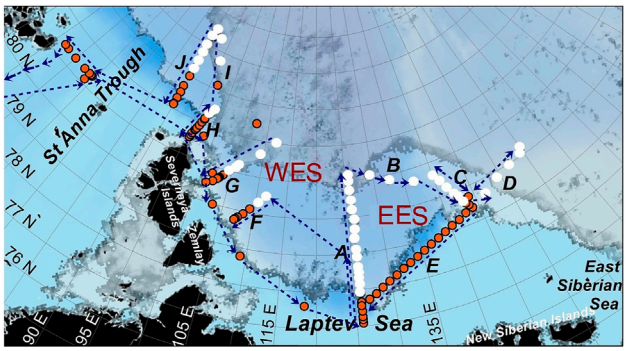


FIGURE 1 | Sea ice concentration [University of Bremen, (Spreen et al., 2008)] on August 15th (light grey/transparent) and September 15th (dark grey/transparent) is shown together with sampling sites in open water (red) and ice-covered (white) regions. Blue arrows indicate the track of the R/V "Akademik Fedorov".

2 MATERIALS AND METHODS

We used CH_4, total alkalinity and thermohaline observations collected at ten sections (**Figure 1**) over the Eurasian continental slope (ECS) of the Arctic Ocean from the St. Anna Trough to the East Siberian Sea during the Nansen and Amundsen Basins Observational System (NABOS, https://uaf-iarc.org/NABOS/) cruise onboard R/V "Akademik Fedorov" from August to September, 2013.

2.1 Satellite-Based Applications to Invest Sea Ice Conditions During Expedition

In order to determine the pathways and source regions of the ice along the sampling sections, we utilized the Lagrangian ice tracking tool, ICETrack. ICETrack makes use of low-resolution sea ice motion and concentration products and has been widely used in previous studies to identify age and origin of sea ice, as well as conditions along pathways (e.g. Belter et al., 2021; Krumpen et al., 2021). A comparison of the satellite-based motion estimates of ICETrack with buoy data has shown that the deviation between real and virtual tracks is rather small (60 ± 24 km after 320 days, Krumpen et al., 2020). For an in-depth method, data product and setup description, we refer to Krumpen et al., 2019).

2.2 Thermohaline Observations, Sampling and Analysis

Profiles of salinity and temperature in the water column were obtained using a conductivity–temperature–depth (CTD) system. The principal device used, was a Sea-Bird SBE911. At selected CTD station a 24-Niskin bottle rosette was used to collect the

water samples for CH_4 and total alkalinity (TA) analysis every 10 m along the top 100 m. Under heavy ice condition sampling was carried out from fractures or leads.

Samples for CH_4 measurements were collected in 30, 100, 200 ml glass vials, taking care to avoid entrainment of bubbles while filling bottles, alkalized up to pH 12, then sealed with rubber stoppers and aluminum caps. To avoid the risk of contamination samples were collected first followed by TA. CH_4 samples were stored in a refrigerator at 4° in the darkness until measuring in the land laboratory within 1 month after the cruise. CH_4 concentrations were measured by using a gas chromatograph with a flame ionization detector (Shimadzu, GA-8A) with an instrumental precision 1%. The analytical error for measurement was 3%.

The CH_4 saturations with respect to atmospheric equilibrium were calculated by applying the equilibrium concentration of CH_4 in sea water with the atmosphere as function of temperature and salinity (Wiesenburg and Guinasso, 1979). We used an atmospheric mole fraction of 1.91 ppm, i.e. the monthly mean from September, 2013 (Data provided by NOAA Global sampling networks, sampling Hydrometeorological Observatory of Tiksi, http://www.esrl.noaa.gov).

The fluxes (F, nMol/m^2 day) of CH_4 across the air-sea interface were calculated in accordance to Wanninkhof (1992), using the equation

$$F = K_w \times (C_w - C_a),$$

where K_w is the gas transfer velocity for CH_4, C_w is the measured CH_4 concentration in surface water, C_a is the equilibrium concentration of CH_4 at surface water temperature and salinity calculated using the measured CH_4 atmospheric mixing ratio and the Bunsen solubility coefficient taken from Wiesenburg and Guinasso, 1979. We have estimated Kw depending on wind speed (u) as described in Wanninkhof (1992):

$$K_w = 0.31 \times u^2 (Sc/660)^{-0.5}$$

Following Wanninkhof (1992), the appropriate Schmidt number (Sc) for CH_4 was calculated using the surface water temperature dependent polynomial relationship.

The relationship between TA and salinity was used to identify the freshwater fractions of sea ice melt or estuarine ice melt waters in the PML (Macdonald et al., 2002; Yamamoto-Kawai et al., 2005; Fransson et al., 2009; Alkire at al., 2019). For TA samples were collected into borosilicate glass flasks (125-ml) pre-treated with saturated mercuric chloride solution (200 µL); the bottles were sealed and stored until following analysis, which was carried out on board by an automated open-cell potentiometric titration (Haraldsson et al., 1997), with precision of ±1 µmol/L.

3 RESULTS

3.1 Weather and Ice Conditions During Sampling: On-Site Observations and Satellite-Based Assessments

Our first five stations near the ice edge covered a route ~80 miles apart the eastern Laptev Sea shelf break for the August 24–26th period. Section A (**Figure 1**, along 126°E longitude) was carried out August 27–28th. No ice was present at the southern stations while mid and northern stations were sampled in an area with ice concentration >90 and 70–80%, respectively. Ice thickness ranged between 70 and 100 cm at the mid stations and 40–60 cm at the northern stations. The ice was first-year ice, substantially rotten and melted from below. For August 29–31st, three northern stations at section C were visited before the termination of sampling due to a consolidated heavy ice pack. Southern stations along the ice edge, were occupied on August 31st. On the next day, the stations along the ice edge towards section D were done. At ~153°E the thickness of the heavy consolidated pack ice reached 2 m. For September 4–6th section E was carried out. On September 8th, we started section F (crossing the Laptev Sea slope at 110°E). On September 10th, section F was interrupted at the middle of the slope by storm conditions. More specifically, the wind speed exceeded 18 m/s and the wave height exceeded 3 m. Work at section G (105°E) started in the marginal ice zone at the northern stations and was finalized at Severnaya Zemlya shelf on September 13th. The same day, we sampled section H at 95°E. Due to the presence of heavy pack ice, section I was started at 84°30′N and, interrupted by a storm, on September 16th. On September 17th we resumed sampling on section J along 90°E. However, a strong storm prevented sampling at the upper slope points. On September 18th and, 19th we sampled the final section across St. Anna Trough.

3.2 Water Mass Properties

A typical vertical structure of surface waters in the Eurasian sector of the Arctic Ocean consists of two layers–the Polar Mixed Layer (PML) and the Cold Halocline Layer (CHL) (Alkire et al., 2017).

The PML extends from the ocean surface to the ~20–55 m depths, and is characterized by vertical uniform distributions of temperature and salinity. Following Jones (2001), the base of the PML is associated with salinities ≤33 psu, but a wide range of temperatures. In line with that, in summer, 2013 the temperature of the PML varied between −1.78 and 2.51°C in the ice-free areas and between −0.137 and −1.781°C in the areas covered by sea ice.

Below the PML, strong vertical gradients of salinity accompanied by negligible gradients of temperature and a relatively weak T–S slope form the CHL. Strong salinity gradients in the CHL suggest the increased density stratification that suppresses diapycnal mixing between the upper and intermediate ocean layers (e.g., Rudels et al., 1996). In 2013, the CHL was localized between 20 and 80 m depths, slightly deepening in the eastern sector of the Makarov Basin. The CHL salinities varied between 33.0 and 34.0 psu (e.g., Alkire et al., 2017), whereas the temperature range was from −1.80°C to −0.1°C.

3.3 CH_4 Distributions

According to regional patterns, in our study, we divided the research area into two sectors: western and eastern ECS.

The western sector (further the western sector of the ECS, WES) comprises the sections located from the St Anna Trough up to the section A at 126°E (**Figure 1**, Sections A, F, G, H, I, J.). The eastern sector (further the eastern sector of the ECS, EES)

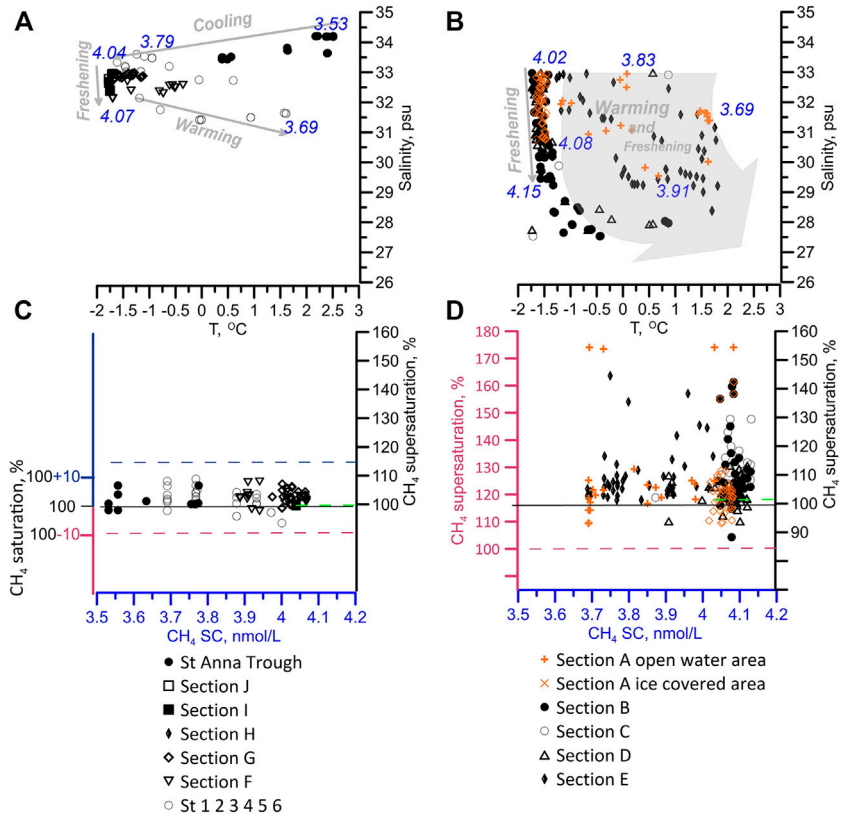


FIGURE 2 | The effect of the CH_4 solubility on the level of CH_4 saturation, related to the atmospheric equilibrium in the PML. The **(A,B)** gives the CH_4 solubility concentration (blue numbers) calculated in relation to the water temperature and salinity. The arrows show the dominant effect of either cooling or warming and freshening in the WES **(A)**, and EES **(B)**. The **(C,D)** shows the shift related to the saturation induced by changing solubility (dashed lines): in blue (cooling), in green (freshening), and in red (warming) in the WES **(C)** and EES **(D)**. The shift in saturation forced by predominantly by warming (left red axes) consisted in real saturation (right black axes) **(D)**. Orange symbols indicate the reference section A. In the WES the enhanced solubility masked the CH_4 supersaturation caused by marine sources. In the EES, CH_4 supersaturation is clearly induced by marine CH_4 sources.

comprises sections located to east from the Lomonosov Ridge (**Figure 1**, Sections B, C, D, E).

In the PML the highest CH_4 concentrations detected were 5.81 nmol/L, which reflected an average CH_4 super-saturation (154%) with respect to the atmospheric equilibrium. The mean CH_4 concentrations increased from 4.03 nmol/L (standard error, SE = 0.18) in the WES up to 4.25 nmol/L (mean, SE = 0.12) in the EES. This corresponded to a slightly increase of the CH_4 super-saturation from 105 to 107% in the WES and EES, respectively. Unlike the WES, where CH_4 saturation was the same for the ice-covered and ice-free areas, in the EES, CH_4 concentration at ice-free stations were 4.23 nmol/L (mean, SE = 0.19) that corresponded to a CH_4 super-saturation of 110.2%. At the ice-covered stations, the mean CH_4 concentration was 4.44 nmol/L (SE = 0.18), which corresponded to a CH_4 super-saturation of 109% at ice-covered stations.

In the CHL the CH_4 concentrations increased from 3.49 nmol/L in the WES to 5.69 nmol/L in the ESL. Those corresponded to CH_4 saturation from 96.7 to 145%. In the WES, the mean CH_4 concentrations were 4.13 nmol/L (SE = 0.19) corresponding to a CH_4 super-saturation of 104%. In the EES mean CH_4 concentration was 4.35 nmol/L (SE = 0.19), which correspond to a CH_4 saturation of 108%.

4 DISCUSSION

When entering through the St Anna Trough, pronounced cooling and freshening by sea ice melt created the PML (Rudels et al., 1996). The direction of the PML circulation is supposed to correspond to the current of warm saline AW underneath, mainly following the coastline eastward (Carmack et al., 2016). The thickness of the PML enhanced from ~20 m at 90°E to ~50 m at 125°E.

In mid of August ~85% of the research area was covered by sea ice while, sea ice progressively reduced to less than ~10% in mid of September. During sampling roughly 15% of the stations on the WES (**Figure 1**) and, 46% of the stations on the EES were still ice covered. The salinity profiles of the PML clearly reflected the different stages of sea ice melt (**Figure 1**, **Figure 4**, **Figure 6**). As the ongoing melt also affects the CH_4 solubility capacity (SC), we discuss the sea ice effects on the CH_4 saturation with respect to the atmospheric equilibrium in detail.

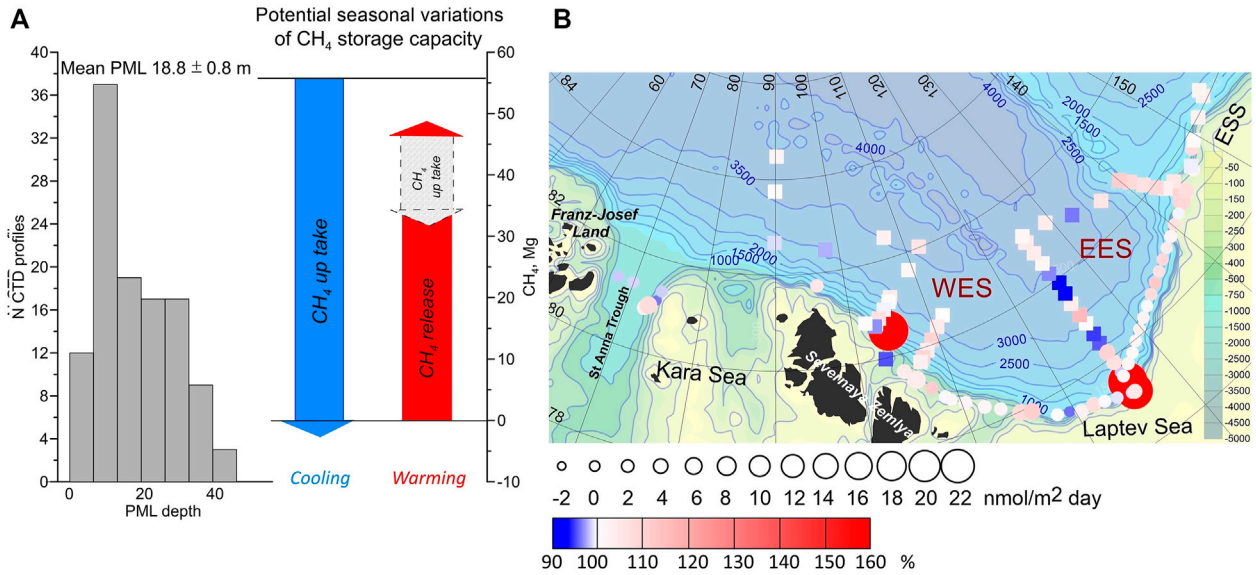


FIGURE 3 | Mean PML depths and the potential CH_4 storage capacity **(A)**; CH_4 flux and saturation related to the atmosphere **(B)**. **(A)** The blue arrow shows the potential CH_4 up-take caused by cooling. Cooling takes place when the water mass enters the polar region and in autumn during the freeze up. The red arrow shows the potential release of CH_4 caused by warming, e.g. as consequences of sea ice retreat. Freshening partly counterbalances the release capacity. The discrepancy between both arrows are caused by variations in the SC calculated with different temperatures in WES and ESS (**Figure 2**). **(B)** CH4 saturation related to the atmospheric equilibrium is shown by colors. Squares and circles show ice-covered and ice-free stations, respectively. The size of circles is related to potential sea-air CH4 fluxes in open water areas.

4.1 CH_4 Solubility Capacity of the Polar Mixed Layer

The cooling of the warm inflowing surface water and coexisting freshening due to sea ice melt or meteoric water enhanced the SC from 3.53 to 4.07 nmol/L in the PML from west to east (**Figures 2A, B**).

In the ice-covered PML in the WES, the SC increased at ~13% mainly by cooling of the water down to near the freezing point (−1.718°C; S 32.963 psu), while the freshening effect remained negligible (<0.1%, ΔS = 0.838 psu). That increase in SC resulted in a slightly CH_4 under-saturation related to the atmospheric equilibrium (**Figure 2**).

In the ice-covered PML in the EES, the water temperature was mostly near the freezing point, while the cooling effect on the SC was still sustained, reflected by the under-saturation at some stations. That pointed to a restricted air-sea exchange mainly hampered by the ice coverage.

By comparison, in the ice-free PML in the WES, a seasonal warming up to 1.608°C, resulted in ~10% less SC, finally reflected in under-saturation down to ~90% (**Figure 2**).

Freshening by sea ice melt increased the SC from 4.02 to 4.08 nmol/L at northern ice-covered stations (**Figures 2A, C**), resulted in negligible increase in the SC (~1%) compared to the effect of simultaneously occurring warming. Under consideration of the variabilities in saturation by changes in the SC, we observed CH_4 supersaturation up to 153% caused by additional CH_4 discharged from marine sources.

A combined effect of freshening and warming was observed in the EES including the reference section A, which served as a boundary between the WES and EES (**Figures 2B, D**). The prevailing impact of warming to the decreased SC (11%) was attributed for all shelf break ice-free stations. By comparison, we observed the largest freshening, in the eastern EES, at the section C, increasing the SC to 4.15 nmol/L, which corresponded to a plus by ~2%.

The variation in the SC revealed the significance of surface warming and coherent freshening due to sea ice melt to the level of CH_4 saturation. Remarkably, the cooling of warm inflowing water in the WES results in an enhanced potential sink capacity for either atmospheric or marine CH_4 sources. However, this potential sink capacity seasonally shrinks by ice melt and subsequent warming of the melt water, while especially the degree of warming in summer, triggers the PML at the ECS switches to acting as a potential source for atmospheric CH_4 (**Figure 3A**).

4.2 The Potential CH_4 Storage Capacity of the Polar Mixed Layer

To assess the variation of potential sources and sink capacities in the upper PML by changing SC we estimated the CH_4 storage capacity within the upper 18.8 m. For the entire area covered by the 2013 NABOS ll observations, we used the average PML depth of 18.8 m determined using high-resolution vertical profiles of the potential density (**Figure 3A**). We just considered the surface layer as a layer mainly favored to be influenced by sea-air gas exchange. Then we multiplied that value to the square of the research area and ΔSC in ng/m^3.

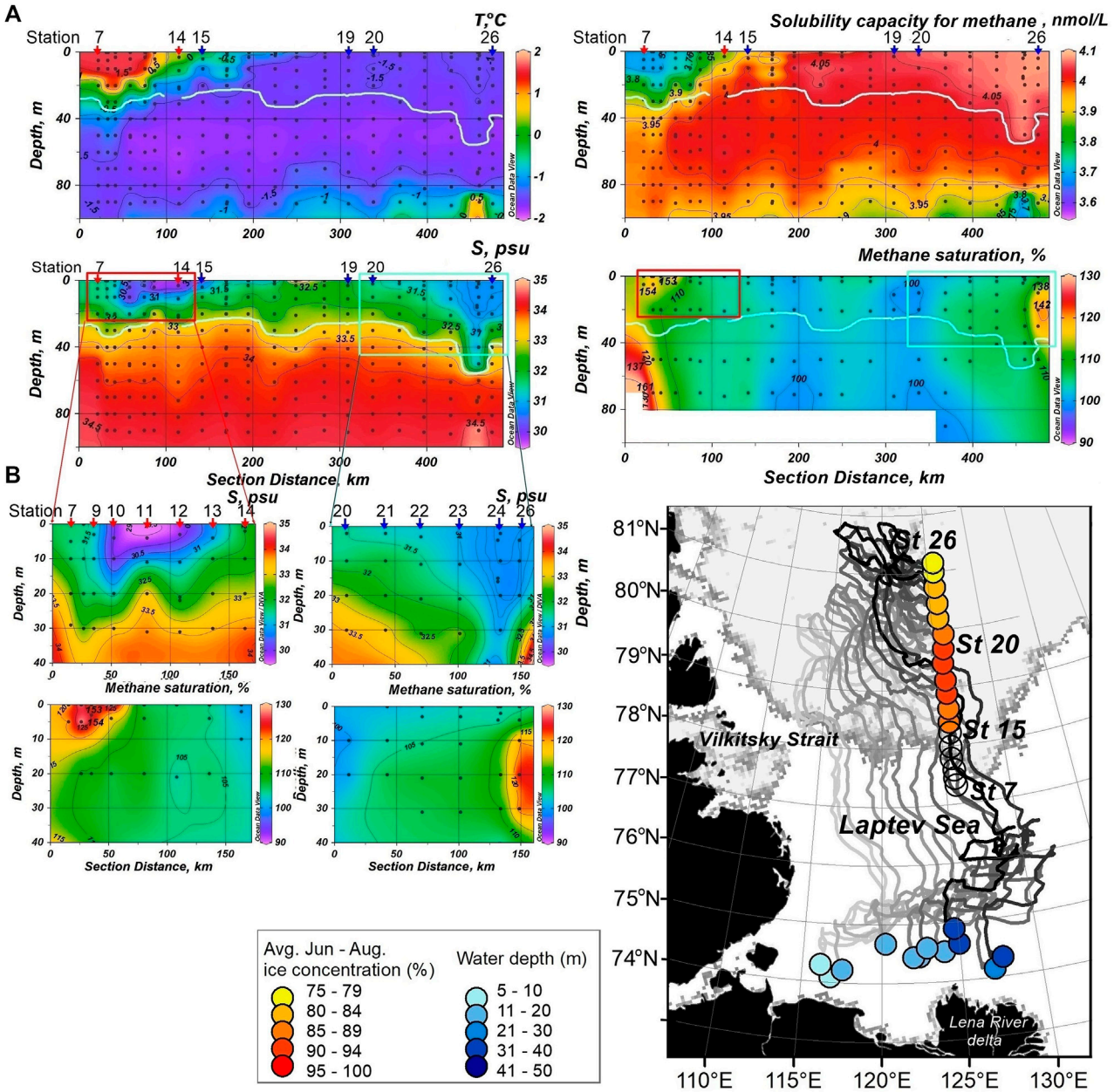


FIGURE 4 | (A) Profiles of temperature, salinity, CH_4 solubility capacity (SC) and saturation along section A (126°E, from south to north). During sampling, stations 7–14 and 15–26 were ice-free [red arrows **(A)**, empty circles **(B)**] and ice covered [blue arrows **(A)**, filled circles **(B)**], respectively. Red and blue squares contour the CH_4 plumes at the southern and northern stations, respectively. Extensions of the red and blue squares are given on the left of the lower panel. The white line gives the boundary between PML and CHL. **(B)** Backward trajectories of sampled sea ice obtained from IceTrack. The color of the end notes provide the corresponding water depths at the formation site. The color of the start nodes provides the June-August ice concentration, averaged along the individual track lines.

The locally restricted cooling of the inflowing warm surface water resulted in a potential CH_4 uptake of ~4.99 Mg (10^6 g) CH_4. We considered this cooling effect exclusively for the region west of 90°E (section J), which corresponded to an area ~30,065 km^2.

In addition, cooling in autumn down to the freezing temperature occurs in the whole research area (335,778 km^2). An assessment of the potential uptake capacity results in ~55.70 Mg of CH_4 (**Figure 3A**).

Under the assumption that the whole area becomes ice free in summer, the seasonal warming will result in 12% less SC tending to balance the relicts of the cooling effect (**Figure 3A**). Then up to ~46.58 Mg (10^6 g) CH_4 might be potentially released from the ECS to the atmosphere. However, in summer 2013, ~66% of the research area was still ice covered, resulting in a two thirds smaller amount.

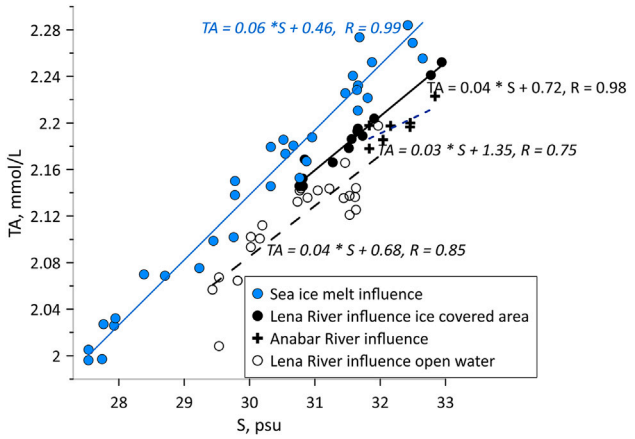


FIGURE 5 | Total alkalinity–salinity plot for PML along the section A and EES sections. Black and empty circles show Lena River ice meltwater fraction at the ice-covered and ice free stations, respectively. Black crosses show Anabar River ice meltwater fraction at the ice-covered stations. Blue circles show the sea ice meltwater fraction. R is the correlation coefficient. Free terms in linear approximation equation $TA\ (S) = kS + TA_{end}$ correspond to alkalinity of meltwater from estuarine ice or sea ice, respectively, pointing to signatures of freshwater sources.

The seasonal changing storage capacity reveals the buffer capacity of the PML for atmospheric or marine-sourced CH_4. While mostly annually balanced, the seasonal stored CH_4 might be reduced by ongoing oxidation in surface water. Studies considering CH_4 oxidation report low oxidation rates in surface waters of other Arctic regions (Mau et al., 2013, Mau et al., 2017; Damm et al., 2015; Uhlig and Loose 2017) but oxidation rate measurements are needed to verify if oxidation acts as CH_4 sink in the PML at the ECS.

Seasonal freshening enhanced the SC just by ~3.2%, resulting in a potential uptake of ~13.17 Mg CH_4. That contribution is small in comparison to the cooling/warming effect on the SC. However, summer sea ice retreat increases the seasonal ice melt at the ECS (Krumpen et al., 2019). That reinforces the freshening effect. In addition, enhanced discharge of Siberian River water (McClelland et al., 2006; Overeem and Syvitski, 2016), which contributes approximately 40% of total freshwater into the Arctic Ocean (Serreze et al., 2006; Haine et al., 2015), will also contribute to increase the CH_4 uptake capacity in the coming decades.

4.3 CH_4 Excess in the Polar Mixed Layer

In summer, the surface water in the central Laptev Sea is reported to be slightly CH_4 supersaturated with spatial restricted hotspots of enhanced CH_4 excess (Thornton et al., 2016). In accordance, we detected CH_4 super-saturation up to ~142% in still ice covered and up to ~154% in ice-free PML. Further, we also revealed a pronounced spatial heterogeneity in the CH_4 excess (**Figure 4A**). Both aspects clearly point to a locally induced CH_4 excess. Hence, we suggest sea ice as the source for CH_4 excess, and the ongoing melt of single ice floes as the process, which causes the heterogeneity in the excess (Damm et al., 2015, Damm et al., 2018; Verdugo et al., 2021). Certain features of local CH_4 release from sea ice into the PML during melt are shown at the section A and discussed in more detail below.

At the southern ice-free stations a CH_4 plume was directly located near the surface of the PML. Remarkably, the plume showed gradients in CH_4 concentration and also in salinity. Both, CH_4 concentration and salinity decreased from south to north (Sts 7–14). That pattern pointed to the formation of the CH_4 plume during the early stage of melt, i.e. when brine charged with CH_4 had been released from sea ice. By comparison, at the northern stations (Sts 12–14) the plume had been subsequently diluted on top during ongoing melt when brine release ceased and remain freshwater discharged. While at the southern stations the ice had being drifted away just before dilution by freshwater started, leaving the plume on top of the PML undiluted (**Figure 4A**).

At the northern ice-covered stations (Sts 25, 26), a CH_4 plume was disposed at the depth range 10–30 m (**Figure 4A**). Notably, the plume position pointed to CH_4 transport dissolved in brine downward during early stages of sea ice melt (Verdugo et al., 2021). Also the lower sea ice concentration at the northern compared to the southern stations (**Figure 4B**), pointed to different stages of ice melt.

This counterintuitive pattern is corroborated by the salinity gradients. Further, tracing the drift pattern, it is obvious that ice at the southern and northern part of the section was formed on the inner Laptev Sea shelf impacted by the Anabar and the Lena River waters, respectively (**Figure 4B**). The ice formed in the Anabar Estuary was less saline because the native winter salinity is < 10 psu (Dmitrenko et al., 2005) than formed in the Lena Estuary, where native winter salinity is 22–28 psu (Dmitrenko et al., 2005). The low salinity of the ice formed in the Anabar estuary caused the relatively slower ice melt at the stations in the middle of the section.

The CH_4 plumes were directly related to initial CH_4 concentration in the ice. CH_4 uptake into sea ice occurs during ice formation from supersaturated seawater (Crabeck et al., 2014; Zhou et al., 2014; Damm et al., 2018). The shallow Laptev Sea shelf is a significant sources of CH_4 (Shakhova et al., 2015; Baranov et al., 2020) and CH_4 super-saturation in shelf water in summer is reported (Bussmann et al., 2017; Sapart et al., 2017; Savvichev et al., 2018).

The river estuaries are characterized by high sedimentation rates (Bauch et al., 2001; Stein et al., 2001; Han, 2014), which exert the dominant control on benthic escape of CH_4 at the sediment-water interface in the shallow Laptev Sea (Puglini et al., 2020). Further, CH_4 uptake during sea ice formation is favored on shallow shelves as cooling during freeze creates convection down to the bottom. This convective mixing enhances the turbulence, initiates resuspension of sediments, and eventually CH_4 release from bottom (Wegner et al., 2017; Damm et al., 2021). Convection also enables rapid transport of CH_4 to the sea surface and hence the uptake into sea ice during freeze events (Damm et al., 2007; Damm et al., 2021).

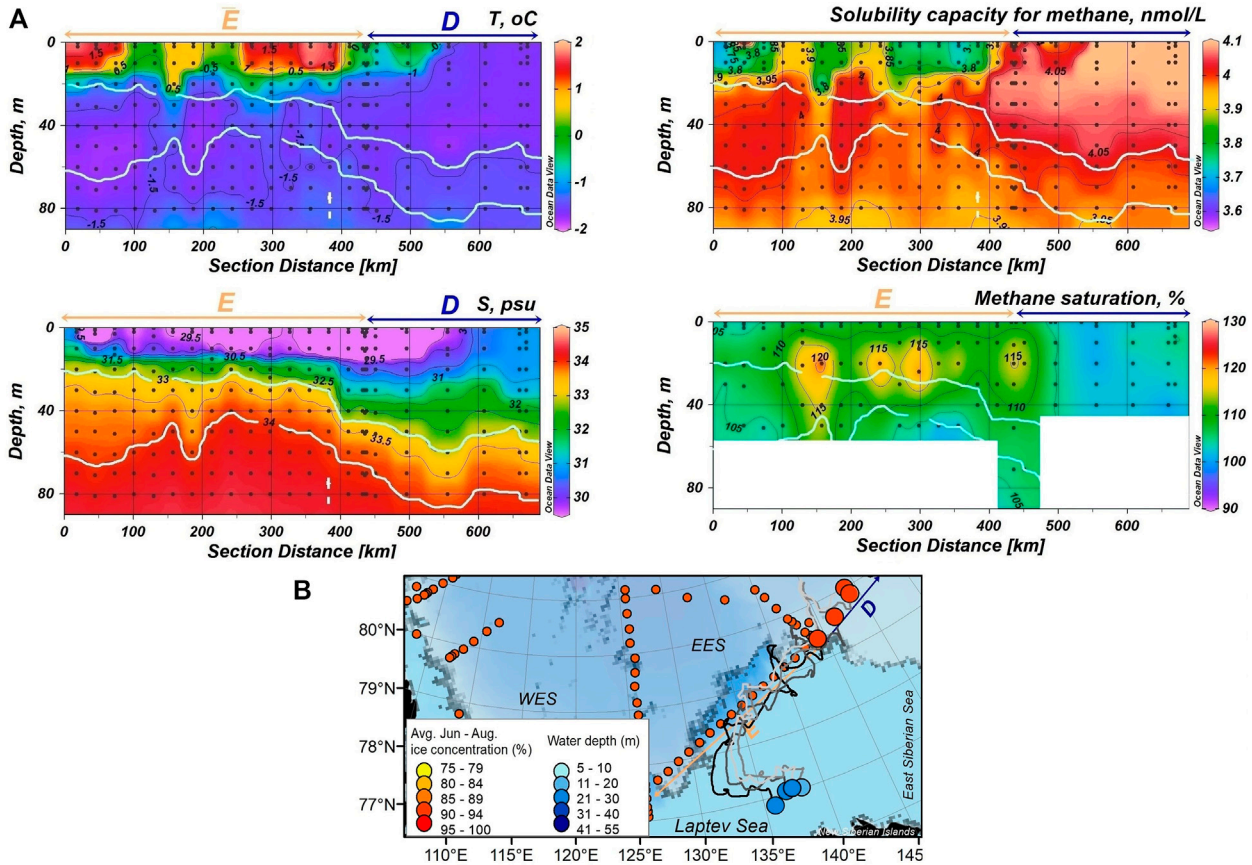


FIGURE 6 | (A) Profiles of temperature, salinity, CH_4 solubility capacity (SC) and saturation along sections E and D (from west to east). Light blue lines show the CHL depths. **(B)** Backward trajectories of sampled sea ice obtained from IceTrack. The color of the start nodes provides the June-August ice concentration, averaged along the individual track lines. The color of the end notes provide the corresponding water depths at the formation site.

The satellite-based backtracking approach of the ice has shown that ice positioned at the northern plume stations was formed in the Anabar-Lena polynya with a water-depth between 30–50 m before it was advected north by prevailing offshore winds (Krumpen et al., 2016, Krumpen et al., 2019) (**Figure 4B**).

In addition, the TA/S ratio at those plume stations (0.72, **Figure 5**) was close to the TA of the Lena River water (0.78 mmol/L from Cooper et al., 2008) clearly pointing to freshening by Lena River ice meltwater fraction. The contribution of ice formed in the estuaries of the large Siberian Rivers to the ice cover in Nansen Basin was reported early (Eicken et al., 2005). Hence, we suggest the existence of ice predominantly formed in the external Lena River estuary on the Laptev Sea shelf and therefore argue for CH_4 uptake from sediments into Lena estuary ice during its formation in autumn. Also at the southern ice-free stations the PML contained Lena River ice meltwater fraction shown by TA/S signal (0.68, **Figure 5**).

In comparison to both plume regions, we detected less CH_4 supersaturation (up to 109%) at ice-covered stations in the middle of the section (Sts 15–19, **Figure 4A**). Backward drift trajectories pointed to the southwestern Laptev Sea shelf with depths ranged from 5 to 30 m, influenced by the Anabar River runoff, as the region for ice formation. The TA/S ratio (**Figure 5**) corroborated the Anabar River waters (Zhulidov and Emetz, 1991) as source water, and the western area of the Laptev Sea as the region for ice formation. The low salinity of the Anabar estuarine-ice caused less CH_4 amount, captured during freezing and the relatively slower ice melt at the stations in the middle of the section.

4.4 The Subsequent Fate of the PML—CH_4 Excess

4.4.1 Potential CH_4 flux to the Atmosphere

As long as a supersaturation of CH_4 in the PML exists, CH_4 might also escape to the atmosphere. Sea-air flux is mainly favored at the end of the ice-free season when cooling and storm events diminish the water stratification. Since the atmosphere potentially acts as final sink for the marine CH_4 that is seasonally stored in sea ice we have calculated the sea-air CH_4 flux.

The PML on the ECS was weakly supersaturated with CH_4, and hence a potential slight net source for the atmosphere during the summer (**Figure 3B**). In total, the CH_4 concentration exceeded the atmospheric equilibrium at 0.22 nmol/L. The average sea-air CH_4 flux, calculated for open water, was 2.0 nmol/m^2day. A slightly higher flux was calculated for the outer shelf of the EES and on the external Laptev Sea shelf at the southern stations along sections A and G (**Figure 3B**). Summarized, the low sea-air flux indicates the ECS as a potential source for atmospheric CH_4 mainly by strong wind loadings, i.e. during storm events.

4.4.2 Dilution of CH_4 Excess in the Polar Mixed Layer and Downward Mixing Into the Cold Halocline Layer

Rapid ice retreat and accompanying strong sea ice melt provided the largest contribution of fresh water to the upper part of the PML in 2013 (Itkin and Krumpen, 2017). Hence, the level of CH_4 excess in the PML was mainly triggered by the dilution with freshwater during later stages of melt. This dilution effect and the potential mixing into deeper water masses are the main processes contributing to keep the estuarine and shelf-sourced CH_4 in the ocean. Apart from oxidation, dilution up to marine CH_4 background values in sea water finally encourage that the ocean acts as sink for marine CH_4 excess in Polar regions (Damm et al., 2021).

We detected CH_4 plumes crossing the boundary between PML and CHL at the ice-free eastern Laptev Sea shelf break (**Figure 6A**). That feature revealed the intrusion of water from the PML, including the CH_4 plume, into the CHL. The increased temperature within those intrusions, related the CHL at surrounding stations, corroborated the PML as the source of the CH_4 plumes (**Figure 6A**). Vertical mixing induced by eddies at the ice edge (Zhao et al., 2014; Pnyushkov et al., 2018) favored the intrusion of water from the PML into the upper CHL and thus the transport of shelf-sourced CH_4 into deeper water masses.

We discussed the plume formation as a result of CH_4 release from sea ice coupled to gravity brine drainage during the first melt stage (see above). Ongoing sea ice melt diluted the plume on top by freshwater discharge. Though, under the warm surface layer, the CH_4 plumes are sustained by the strong density gradient on the top while the vertical mixing between PML and CHL enabled a downward deepening of the CH_4 plumes (**Figure 6A**). The ice edge provides favorable conditions for eddy generation as specifically, convection by water cooling in leads generates a vertical dipole structure with a cyclonic eddy in the upper layer and an anticyclonic eddy in the CHL (Manley and Hunkins, 1985; Gupta et al., 2020; Meneghello et al., 2021). Further studies are needed to verify the role of eddies especially their enhanced lateral and vertical mixing capacity between certain water masses at the EES (Zhao et al., 2014; Pnyushkov et al., 2018) to contribute to the deepening of CH_4 plumes into subsurface waters.

Remarkably, we did not observe CH_4 plumes further east at the ice-covered shelf-break (Section D, **Figure 6A**). At these locations, sea ice melt had just began and CH_4 release from sea ice, was still masked by the enhanced SC of the cold PML water. Further, ice drift trajectories indicated the area of sea ice formation in the shallow Laptev Sea shelf north from the New Siberian Islands (**Figure 6B**). In this area CH_4 supersaturation in seawater as a result of CH_4 release from the sediments under conditions of active turbulence are expected to be low (Puglini et al., 2020). Hence, the just slightly CH_4 super-saturation (up to 108%) corroborate the capturing of low amounts of CH_4 in sea ice on the shelf north from the New Siberian Islands.

CONCLUSION

We found a heterogeneous excess of CH_4 next to the surface in the PML and suggest that sea ice impacts on the amount and pathways of CH_4 on the ECS. On the one side, the cycle of sea ice formation and melt alters the solubility capacity of CH_4 in the surface waters, which ultimately affects its ability to act as a source or sink of atmospheric CH_4. On the other side, sea ice transports shelf-derived CH_4 to the open ocean, which likely acts as a CH_4 sink. It is noteworthy, that the largest CH_4 excess in the PML on the ECS is generated by melt of ice originated in outer river estuaries on the shallow Laptev Sea shelf.

The increased solubility capacity during cooling has shown that the PML on the ECS acts as a potential seasonal sink for atmospheric or marine CH_4. summer ice melt causes surface freshening and subsequent warming. The warming offsets the cooling effect and triggers the switching of the PML to act as a potential source of atmospheric CH_4 in summer. The joint effect of both processes creates the seasonal buffer capacity of the PML. summer sea ice retreat will increase the freshening effect, the buffer capacity and reinforce the sink function of the PML for CH_4.

Finally, Arctic amplification favors perennial sea ice retreat, and hence, we expect that larger amounts of freshwater will dilute the CH_4 excess in surface water which eventually restricts CH_4 flux into the atmosphere.

These linkages should be considered when assessing CH_4 sources and sinks in the changing Arctic.

DATA AVAILABILITY STATEMENT

The datasets presented in this study can be found in online repositories. The names of the repository/repositories and accession number(s) can be found below: https://uaf-iarc.org/nabos/.

AUTHOR CONTRIBUTIONS

EV designed the study. EV and ED wrote the paper. EV sampled and analyzed the CH_4 data. AP sampled and analyzed the physical oceanography data and wrote the oceanography chapter. TK carried out sea ice trajectories and wrote the ice

trajectory part. All authors contributed to the interpretation of the data, the manuscript and the figures.

FUNDING

This study was performed in the framework of the state assignment of IO RAS (theme 0128-2021-0005); NSF funded IARC Program "Nansen and Amundsen Basins Observational System" (NABOS ll; grant #1203473).

ACKNOWLEDGMENTS

We thanked the captain and crew of R/V Akademik Fedorov for their support during the NABOS 2013 cruise. We are grateful to I. Repina for providing wind data. We also thank M. Angelopolous for his comments on an earlier version of this paper. VI acknowledges support by the Interdisciplinary Scientific and Educational School of M.V. Lomonosov Moscow State University Future Planet and Global Environmental Change, AP acknowledges support by the NSF (grant #1724523).

REFERENCES

Alkire, M. B., Jacobson, A., Macdonald, R. W., and Lehn, G. (2019). Assessing the Contributions of Atmospheric/Meteoric Water and Sea Ice Meltwater and Their Influences on Geochemical Properties in Estuaries of the Canadian Arctic Archipelago. *Estuaries and Coasts* 42, 1226–1248. doi:10.1007/s12237-019-00562-w

Alkire, M. B., Polyakov, I., Rember, R., Pnyushkov, A., Ivanov, V., and Ashik, I. (2017). Combining Physical and Geochemical Methods to Investigate Lower Halocline Water Formation and Modification along the Siberian continental Slope. *Ocean Sci.* 13, 983–995. doi:10.5194/os-13-983-2017

AMAP (2015). *Assessment 2015: Human Health in the Arctic*. Oslo, Norway: AMAP. Availableat: https://www.amap.no.

Baranov, B., Galkin, S., Vedenin, A., Dozorova, K., Gebruk, A., and Flint, M. (2020). Methane Seeps on the Outer Shelf of the Laptev Sea: Characteristic Features, Structural Control, and Benthic Fauna. *Geo-mar Lett.* 40, 541–557. doi:10.1007/s00367-020-00655-7

Bauch, H. A., Mueller-Lupp, T., Taldenkova, E., Spielhagen, R. F., Kassens, H., Grootes, P. M., et al. (2001). Chronology of the Holocene Transgression at the North Siberian Margin. *Glob. Planet. Change* 31, 125–139. doi:10.1016/s0921-8181(01)00116-3

Belter, H. J., Krumpen, T., von Albedyll, L., Alekseeva, T. A., Birnbaum, G., Frolov, S. V., et al. (2021). Interannual Variability in Transpolar Drift Summer Sea Ice Thickness and Potential Impact of Atlantification. *The Cryosphere* 15, 2575–2591. doi:10.5194/tc-15-2575-2021

Berchet, A., Bousquet, P., Pison, I., Locatelli, R., Chevallier, F., Paris, J.-D., et al. (2016). Atmospheric Constraints on the Methane Emissions from the East Siberian Shelf. *Atmos. Chem. Phys.* 16, 4147–4157. doi:10.5194/acp-16-4147-2016

Bussmann, I., Hackbusch, S., Schaal, P., and Wichels, A. (2017). Methane Distribution and Oxidation Around the Lena Delta in Summer 2013. *Biogeosciences* 14, 4985–5002. doi:10.5194/bg-14-4985-2017

Carmack, E. C., Yamamoto-Kawai, M., Haine, T. W. N., BaconBluhm, S., Bluhm, B. A., Lique, C., et al. (2016). Freshwater and its Role in the Arctic Marine System: Sources, Disposition, Storage, export, and Physical and Biogeochemical Consequences in the Arctic and Global Oceans. *J. Geophys. Res. Biogeosci.* 121, 675–717. doi:10.1002/2015JG003140

Chuvilin, E., Ekimova, V., Davletshina, D., Sokolova, N., and Bukhanov, B. (2020). Evidence of Gas Emissions from Permafrost in the Russian Arctic. *Geosciences* 10, 383. doi:10.3390/geosciences10100383

Cooper, L. W., McClelland, J. W., Holmes, R. M., Raymond, P. A., Gibson, J. J., Guay, C. K., et al. (2008). Flow-weighted Values of Runoff Tracers (δ18O, DOC, Ba, Alkalinity) from the Six Largest Arctic Rivers. *Geophys. Res. Lett.* 35, L18606. doi:10.1029/2008GL035007

Crabeck, O., Delille, B., Thomas, D. N., Geilfus, N. X., Rysgaard, S., and Tison, J. L. (2014). CO2 and CH4 in Sea Ice from a Subarctic Fjord. *Biogeosciences Discuss.* 11, 4047–4083. doi:10.5194/bgd-11-4047-2014

Damm, E., Bauch, D., Krumpen, T., Rabe, B., Korhonen, M., Vinogradova, E., et al. (2018). The Transpolar Drift Conveys Methane from the Siberian Shelf to the central Arctic Ocean. *Sci. Rep.* 8, 4515. doi:10.1038/s41598-018-22801-z

Damm, E., Ericson, Y., and Falck, E. (2021). Waterside Convection and Stratification Control Methane Spreading in Supersaturated Arctic Fjords (Spitsbergen). *Continental Shelf Res.* 224, 104473. doi:10.1016/j.csr.2021.104473

Damm, E., Rudels, B., Schauer, U., Mau, S., and Dieckmann, G. (2015). Methane Excess in Arctic Surface Water- Triggered by Sea Ice Formation and Melting. *Sci. Rep.* 5, 16179. doi:10.1038/srep16179

Damm, E., Schauer, U., Rudels, B., and Haas, C. (2007). Excess of Bottom-Released Methane in an Arctic Shelf Sea Polynya in winter. *Continental Shelf Res.* 27, 1692–1701. doi:10.1016/j.csr.2007.02.003

Dmitrenko, I. A., Kirillov, S. A., Tremblay, L. B., Bauch, D., and Willmes, S. (2009). Sea-ice Production over the Laptev Sea Shelf Inferred from Historical Summer-To-winter Hydrographic Observations of 1960s-1990s. *Geophys. Res. Lett.* 36, L13605. doi:10.1029/2009GL038775

Dmitrenko, I., Tyshko, K., Kirillov, S., Eicken, H., HolemannKassense, J. H., and Kassens, H. (2005). Impact of Flaw Polynyas on the Hydrography of the Laptev Sea. *Glob. Planet. Change* 48, 9–27. doi:10.1016/j.gloplacha.2004.12.016

Eicken, H., Dmitrenko, I., Tyshko, K., Darovskikh, A., Dierking, W., Blahak, U., et al. (2005). Zonation of the Laptev Sea Landfast Ice Cover and its Importance in a Frozen Estuary. *Glob. Planet. Change* 48, 55–83. doi:10.1016/j.gloplacha.2004.12.005

Fransson, A., Chierici, M., and Nojiri, Y. (2009). New Insights into the Spatial Variability of the Surface Water Carbon Dioxide in Varying Sea Ice Conditions in the Arctic Ocean. *Continental Shelf Res.* 29, 1317–1328. doi:10.1016/j.csr.2009.03.008

Gentz, T., Damm, E., Schneider von DeimlingDeimling, J., Mau, S., McGinnis, D. F., and Schlüter, M. (2014). A Water Column Study of Methane Around Gas Flares Located at the West Spitsbergen continental Margin. *Continental Shelf Res.* 72, 107–118. doi:10.1016/j.csr.2013.07.013

Günther, F., Overduin, P. P., Yakshina, I. A., Opel, T., Baranskaya, A. V., and Grigoriev, M. N. (2015). Observing Muostakh Disappear: Permafrost Thaw Subsidence and Erosion of a Ground-Ice-Rich Island in Response to Arctic Summer Warming and Sea Ice Reduction. *The Cryosphere* 9, 151–178. doi:10.5194/tc-9-151-2015

Gupta, M., Marshall, J., Song, H., Campin, J. M., and Meneghello, G. (2020). Sea-Ice Melt Driven by Ice-Ocean Stresses on the Mesoscale. *J. Geophys. Res. Oceans* 125, e2020JC016404. doi:10.1029/2020JC016404

Haine, T. W. N., Curry, B., Gerdes, R., Hansen, E., Karcher, M., Lee, C., et al. (2015). Arctic Freshwater export: Status, Mechanisms, and Prospects. *Glob. Planet. Change* 125, 13–35. doi:10.1016/j.gloplacha.2014.11.013

Haraldsson, C., Anderson, L. G., Hassellöv, M., Hulth, S., and Olsson, K. (19971997). Rapid, High-Precision Potentiometric Titration of Alkalinity in Ocean and Sediment Pore Waters. *Deep Sea Res. Part Oceanographic Res. Pap.* 44, 2031–2044. doi:10.1016/S0967-0637(97)00088-5

IPCC (2019). *Special Report on the Ocean and Cryosphere in a Changing Climate*. Editors H.-O. Pörtner, D. C. Roberts, V. Masson-Delmotte, P. Zhai, and M. Tignor. Chapter lll. Geneva. Availableat: https://www.ipcc.ch/srocc/chapter/chapter-3-2/.

Itkin, P., and Krumpen, T.(2017). Winter sea ice export from the Laptev Sea preconditions the local summer sea ice cover. *The Cryosphere Discussions*, 1–15. doi:10.5194/tc-2017-28

Iwamoto, K., Ohshima, K. I., and Tamura, T. (2014). Improved Mapping of Sea Ice Production in the Arctic Ocean Using AMSR-E Thin Ice Thickness Algorithm. *J. Geophys. Res. Oceans* 119, 3574–3594. doi:10.1002/2013jc009749

Jones, E. P. (2001). Circulation in the Arctic Ocean. *Polar Res.* 20 (2), 139–146. doi:10.3402/polar.v20i2.6510

Krumpen, T., Belter, H. J., Boetius, A., Damm, E., Haas, C., Hendricks, S., et al. (2019). Arctic Warming Interrupts the Transpolar Drift and Affects Long-

Range Transport of Sea Ice and Ice-Rafted Matter. *Sci. Rep.* 9, 5459. doi:10.1038/s41598-019-41456-y

Krumpen, T., Birrien, F., Kauker, F., Rackow, T., von Albedyll, L., Angelopoulos, M., et al. (2020). The MOSAiC Ice Floe: Sediment-Laden Survivor from the Siberian Shelf. *The Cryosphere* 14, 2173–2187. doi:10.5194/tc-14-2173-2020

Krumpen, T., Gerdes, R., Haas, C., Hendricks, S., Herber, A., Selyuzhenok, V., et al. (2016). Recent Summer Sea Ice Thickness Surveys in Fram Strait and Associated Ice Volume Fluxes. *The Cryosphere* 10, 523–534. doi:10.5194/tc-10-523-2016

Krumpen, T., von Albedyll, L., Goessling, H. F., Hendricks, S., Juhls, B., Spreen, G., et al. (2021). MOSAiC Drift Expedition from October 2019 to July 2020: Sea Ice Conditions from Space and Comparison with Previous Years. *The Cryosphere* 15, 3897–3920. doi:10.5194/tc-15-3897-2021

Krumpen, T., Willmes, S., Morales Maqueda, M. A., Haas, C., Hölemann, J. A., Gerdes, R., et al. (2011). Evaluation of a Polynya Flux Model by Means of thermal Infrared Satellite Estimates. *Ann. Glaciol.* 52 (57), 52–60. doi:10.3189/172756411795931615

Macdonald, R. W., McLaughlin, F. A., and Carmack, E. C. (2002). Fresh Water and its Sources during the SHEBA Drift in the Canada Basin of the Arctic Ocean. *Deep Sea Res. Part Oceanographic Res. Pap.* 49, 1769–1785. doi:10.1016/S0967-0637(02)00097-3

Manley, T. O., and Hunkins, K. (1985). Mesoscale Eddies of the Arctic Ocean. *J. Geophys. Res.* 90 (C3), 4911–4930. doi:10.1029/jc090ic03p04911

Markus, T., Stroeve, J. C., and Miller, J. (2009). Recent Changes in Arctic Sea Ice Melt Onset, Freezeup, and Melt Season Length. *J. Geophys. Res.* 114, C12024. doi:10.1029/2009JC005436

Mau, S., Blees, J., Helmke, E., Niemann, H., and Damm, E. (2013). Vertical Distribution of Methane Oxidation and Methanotrophic Response to Elevated Methane Concentrations in Stratified Waters of the Arctic Fjord Storfjorden (Svalbard, Norway). *Biogeosciences* 10, 6267–6278. doi:10.5194/bgd-10-6461-2013

Mau, S., Römer, M., Torres, M. E., Bussmann, I., Pape, T., Damm, E., et al. (2017). Widespread Methane Seepage along the continental Margin off Svalbard - from Bjørnøya to Kongsfjorden. *Sci. Rep.* 7, 42997. doi:10.1038/srep42997

McClelland, J. W., Déry, S. J., Peterson, B. J., Holmes, R. M., and Wood, E. F. (2006). A Pan-Arctic Evaluation of Changes in River Discharge during the Latter Half of the 20th century. *Geophys. Res. Lett.* 33, L06715. doi:10.1029/2006GL025753

Meneghello, G., Marshall, J., Lique, C., Isachsen, P. E., Doddridge, E., Campin, J.-M., et al. (2021). Genesis and Decay of Mesoscale Baroclinic Eddies in the Seasonally Ice-Covered interior Arctic Ocean. *J. Phys. Oceanogr.* 51, 115–129. doi:10.1175/JPO-D-20-0054.1

Myhre, C. L., Ferré, B., Platt, S. M., Silyakova, A., Hermansen, O., Allen, G., et al. (2016). Extensive Release of Methane from Arctic Seabed West of Svalbard during Summer 2014 Does Not Influence the Atmosphere. *Geophys. Res. Lett.* 43 (9), 4624–4631. doi:10.1002/2016GL068999

Overeem, I., and Syvitski, J. P. M. (2016). Shifting Discharge Peaks in Arctic Rivers, 1977-2007. *Geografiska Annaler: Ser. A, Phys. Geogr.* 92, 285–296. doi:10.1111/j.1468-0459.2010.00395.x

Pnyushkov, A., Polyakov, I. V., Padman, L., and Nguyen, A. T. (201820182). Structure and Dynamics of Mesoscale Eddies over the Laptev Sea continental Slope in the Arctic Ocean. *Ocean Sci.* 14, 1329–1347. doi:10.5194/os-14-1329-2018

Puglini, M., BrovkinRegnier, V. P., Regnier, P., and Arndt, S. (2020). Assessing the Potential for Non-turbulent Methane Escape from the East Siberian Arctic Shelf. *Biogeosciences* 17, 3247–3275. doi:10.5194/bg-17-3247-2020

Reagan, M. T., and Moridis, G. J. (2008). Dynamic Response of Oceanic Hydrate Deposits to Ocean Temperature Change. *J. Geophys. Res.* 113, C12023. doi:10.1029/2008JC004938

Rudels, B., Anderson, L. G., and Jones, E. P. (1996). Formation and Evolution of the Surface Mixed Layer and Halocline of the Arctic Ocean. *J. Geophys. Res.* 101 (C4), 8807–8821. doi:10.1029/96jc00143

Rudels, B., Jones, E. P., Schauer, U., and Eriksson, P. (2004). Atlantic Sources of the Arctic Ocean Surface and Halocline Waters. *Polar Res.* 23 (2), 181–208. doi:10.3402/polar.v23i2.6278

Sapart, C. J., Shakhova, N., Semiletov, I., Jansen, J., Szidat, S., Kosmach, D., et al. (2017). The Origin of Methane in the East Siberian Arctic Shelf Unraveled with Triple Isotope Analysis. *Biogeosciences* 14, 2283–2292. doi:10.5194/bg-14-2283-2017

Savvichev, A. S., Kadnikov, V. V., Kravchishina, M. D., Galkin, S. V., Novigatskii, A. N., Sigalevich, P. A., et al. (2018). Methane as an Organic Matter Source and the Trophic Basis of a Laptev Sea Cold Seep Microbial Community. *Geomicrobiology J.* 35, 411–423. doi:10.1080/01490451.2017.1382612

Screen, J. A., and Simmonds, I. (2010). The central Role of Diminishing Sea Ice in Recent Arctic Temperature Amplification. *Nature* 464 (7293), 1334–1337. doi:10.1038/nature09051

Serreze, M. C., Barrett, A. P., Slater, A. G., Woodgate, R. A., Aagaard, K., Lammers, R. B., et al. (2006). The Large-Scale Freshwater Cycle of the Arctic. *J. Geophys. Res.* 111, C11010. doi:10.1029/2005JC003424

Shakhova, N., Semiletov, I., and Chuvilin, E. (2019). Understanding the Permafrost-Hydrate System and Associated Methane Releases in the East Siberian Arctic Shelf. *Geosciences* 9, 251. doi:10.3390/geosciences9060251

Shakhova, N., Semiletov, I., Leifer, I., Sergienko, V., Salyuk, A., Kosmach, D., et al. (2014). Ebullition and Storm-Induced Methane Release from the East Siberian Arctic Shelf. *Nat. Geosci* 7, 64–70. doi:10.1038/ngeo2007

Shakhova, N., Semiletov, I., Salyuk, A., Yusupov, V., Kosmach, D., and Gustafsson, Ö. (2010). Extensive Methane Venting to the Atmosphere from Sediments of the East Siberian Arctic Shelf. *Science* 327, 1246–1250. doi:10.1126/science.1182221

Shakhova, N., Semiletov, I., Sergienko, V., Lobkovsky, L., Yusupov, V., Salyuk, A., et al. (2015). The East Siberian Arctic Shelf: towards Further Assessment of Permafrost-Related Methane Fluxes and Role of Sea Ice. *Phil. Trans. R. Soc. A.* 373 (2052), 20140451. doi:10.1098/rsta.2014.0451

Silyakova, A., Jansson, P., Serov, P., Ferré, B., Pavlov, A. K., Hattermann, T., et al. (2020). Physical Controls of Dynamics of Methane Venting from a Shallow Seep Area West of Svalbard. *Continental Shelf Res.* 194, 104030. doi:10.1016/j.csr.2019.104030

Spreen, G., Kaleschke, L., and Heygster, G. (2008). Sea Ice Remote Sensing Using AMSR-E 89-GHz Channels. *J. Geophys. Res.* 113, C02S03. doi:10.1029/2005JC003384

Stein, R., Boucsein, B., Fahl, K., Garcia de Oteyza, T., Knies, J., and Niessen, F. (2001). Accumulation of Particulate Organic Carbon at the Eurasian continental Margin during Late Quaternary Times: Controlling Mechanisms and Paleoenvironmental Significance. *Glob. Planet. Change* 31, 87–104. doi:10.1016/s0921-8181(01)00114-x

Thornton, B. F., Geibel, M. C., Crill, P. M., Humborg, C., and Mörth, C.-M. (2016). Methane Fluxes from the Sea to the Atmosphere across the Siberian Shelf Seas. *Geophys. Res. Lett.* 43, 5869–5877. doi:10.1002/2016GL068977

Uhlig, C., and Loose, B. (2017). Using Stable Isotopes and Gas Concentrations for Independent Constraints on Microbial Methane Oxidation at Arctic Ocean Temperatures. *Limnol. Oceanogr. Methods* 15, 737–751. doi:10.1002/lom3.10199

Verdugo, J., Damm, E., and Nikolopoulos, A. (2021). Methane Cycling within Sea Ice; Results from Drifting Ice during Late spring, north of Svalbard. *The Criosphere* 15, 2701–2717. doi:10.5194/tc-15-2701-2021

Wanninkhof, R. (1992). Relationship between Wind Speed and Gas Exchange over the Ocean. *J. Geophys. Res.* 97, 7373–7382. doi:10.1029/92JC00188

Wegner, C., Wittbrodt, K., Holemann, J., Janout, M., Krumpen, T., Selyuzhenok, V., et al. (2017). Sediment Entrainment into Sea Ice and Transport in the Transpolar Drift: A Case Study from the Laptev Sea in winter 2011/2012. *Continental Shelf Res.* 141, 1–10. doi:10.1016/j.csr.2017.04.010

Westbrook, G. K., Thatcher, K. E., Rohling, E. J., Piotrowski, A. M., Pälike, H., and Osborne, A. H. (2009). Escape of Methane Gas from the Seabed along the West Spitsbergen continental Margin. *Geophys. Res. Lett.* 36, L15608. doi:10.1029/2009GL039191

Wiesenburg, D. A., and Guinasso, N. L. (1979). Equilibrium Solubilities of Methane, Carbon Monoxide, and Hydrogen in Water and Seawater. *J. Chem. Eng. Data* 24, 356–360. doi:10.1021/je60083a006

Yamamoto-Kawai, M., Tanaka, N., and Pivovarov, S. (2005). Freshwater and Brine Behaviors in the Arctic Ocean Deduced from Historical Data of $\delta^{18}O$ and

Alkalinity (1929-2002 A.D.). *J. Geophys. Res. Ocean.* 110, C10003. doi:10.1029/2004JC002793

Zhao, M., Timmermans, M.-L., Cole, S., Kishfields, R., Proshutinski, A., and Tolle, J. (2014). Characterizing the Eddies Field in the Arctic Ocean Halocline. *J. Geophys. Res.-Ocean.* 119, 8800–8817. doi:10.1002/2014JC010488

Zhou, J., Tison, J.-L., Carnat, G. N., Geilfus, X., and Delille, B. (2014). Physical Controls on the Storage of Methane in Landfast Sea Ice. *The Cryosphere* 8, 1019–1029. doi:10.5194/tc-8-1019-2014

Zhulidov, A. V., and Emetz, V. M. (1991). *Biogeochemical Regionalization of the USSR. Manuscript*. Rostov on Don: Hydrochemical Institute, 625. p. (in Russian).

Conflict of Interest: The authors declare that the research was conducted in the absence of any commercial or financial relationships that could be construed as a potential conflict of interest.

The reviewer TW declared a shared affiliation with the author AP to the handling editor at time of review.

Publisher's Note: All claims expressed in this article are solely those of the authors and do not necessarily represent those of their affiliated organizations, or those of the publisher, the editors and the reviewers. Any product that may be evaluated in this article, or claim that may be made by its manufacturer, is not guaranteed or endorsed by the publisher.

Copyright © 2022 Vinogradova, Damm, Pnyushkov, Krumpen and Ivanov. This is an open-access article distributed under the terms of the Creative Commons Attribution License (CC BY). The use, distribution or reproduction in other forums is permitted, provided the original author(s) and the copyright owner(s) are credited and that the original publication in this journal is cited, in accordance with accepted academic practice. No use, distribution or reproduction is permitted which does not comply with these terms.

frontiers in Environmental Science

ORIGINAL RESEARCH
published: 31 January 2022
doi: 10.3389/fenvs.2021.791305

Dominance of Diffusive Methane Emissions From Lowland Headwater Streams Promotes Oxidation and Isotopic Enrichment

Andrew L. Robison[1,2], Wilfred M. Wollheim[1], Clarice R. Perryman[3], Annie R. Cotter[1], Jessica E. Mackay[1], Ruth K. Varner[3], Paige Clarizia[3] and Jessica G. Ernakovich[1]*

[1]Department of Natural Resources and the Environment, University of New Hampshire, Durham, NH, United States, [2]Stream Biofilm and Ecosystem Research Laboratory, École Polytechnique Fédérale de Lausanne, Lausanne, Switzerland, [3]Department of Earth Sciences, University of New Hampshire, Durham, NH, United States

Inland waters are the largest natural source of methane (CH_4) to the atmosphere, yet the contribution from small streams to this flux is not clearly defined. To fully understand CH_4 emissions from streams and rivers, we must consider the relative importance of CH_4 emission pathways, the prominence of microbially-mediated production and oxidation of CH_4, and the isotopic signature of emitted CH_4. Here, we construct a complete CH_4 emission budgets for four lowland headwater streams by quantifying diffusive CH_4 emissions and comparing them to previously published rates of ebullitive emissions. We also examine the isotopic composition of CH_4 along with the sediment microbial community to investigate production and oxidation across the streams. We find that all four streams are supersaturated with respect to CH_4 with diffusive emissions accounting for approximately 78–100% of total CH_4 emissions. Isotopic and microbial data suggest CH_4 oxidation is prevalent across the streams, depleting approximately half of the dissolved CH_4 pool before emission. We propose a conceptual model of CH_4 production, oxidation, and emission from small streams, where the dominance of diffusive emissions is greater compared to other aquatic ecosystems, and the impact of CH_4 oxidation is observable in the emitted isotopic values. As a result, we suggest the CH_4 emitted from small streams is isotopically heavy compared to lentic ecosystems. Our results further demonstrate streams are important components of the global CH_4 cycle yet may be characterized by a unique pattern of cycling and emission that differentiate them from other aquatic ecosystems.

Keywords: methane, streams, isotopes, methanogens, methane oxidation, emissions

OPEN ACCESS

Edited by:
Daniel F. McGinnis, Université de Genève, Switzerland

Reviewed by:
Mark Alexander Lever, ETH Zürich, Switzerland
Changhui Wang, Shanxi Agricultural University, China

****Correspondence:***
Andrew L. Robison
andrew.robison@epfl.ch

Specialty section:
This article was submitted to Biogeochemical Dynamics, a section of the journal Frontiers in Environmental Science

Received: *08 October 2021*
Accepted: *30 December 2021*
Published: *31 January 2022*

Citation:
Robison AL, Wollheim WM, Perryman CR, Cotter AR, Mackay JE, Varner RK, Clarizia P and Ernakovich JG (2022) Dominance of Diffusive Methane Emissions From Lowland Headwater Streams Promotes Oxidation and Isotopic Enrichment. Front. Environ. Sci. 9:791305. doi: 10.3389/fenvs.2021.791305

INTRODUCTION

Since the start of the industrial revolution, atmospheric concentrations of methane (CH_4) have increased nearly threefold (Saunois et al., 2020). This atmospheric enrichment of CH_4 is caused predominantly by anthropogenic activities; however, aquatic ecosystems comprise roughly half of all global CH_4 emissions (Rosentreter et al., 2021). Most research into CH_4 emissions and cycling in freshwater systems has occurred in wetlands, lakes, and impoundments, but recent studies have started to highlight the role of rivers and streams in the global CH_4 budget (Stanley et al., 2016; Zhang

et al., 2020). Rosentreter et al. (2021) estimate that streams and rivers emit approximately 30.5 Tg CH_4 yr^{-1} globally, which represents about 20% of the total annual emissions from lakes (151 Tg CH_4 yr^{-1}) or wetlands (149 Tg CH_4 yr^{-1}; Saunois et al., 2020). Methane cycling in small headwater streams, which comprise a majority of river network length (Bishop et al., 2008), represents a gap in our understanding of aquatic CH_4 dynamics. Headwater streams are known to be disproportionately important in the emissions of carbon dioxide within river networks (Hotchkiss et al., 2015; Marx et al., 2017), yet their relative importance regarding CH_4 remains undefined. Additionally, most investigations of CH_4 focus on quantifying CH_4 concentration or flux rather than how CH_4 cycles through the ecosystem (Stanley et al., 2016). As a result, more comprehensive measurements of CH_4 emissions and an improved understanding of CH_4 cycling are needed to accurately include streams in regional and global CH_4 budgets.

The fundamental controls of CH_4 cycling are consistent across aquatic ecosystems, thus we can apply much of what is known about lentic systems to study stream ecosystems. In general, CH_4 is produced via methanogenesis by archaea under anoxic conditions (Chowdhury and Dick, 2013), and the inundated sediments of aquatic environments are generally well-suited for this because of their low redox conditions (e.g., Wik et al., 2018). A key process that consumes CH_4 in surface waters is biological oxidation by bacterial and archaeal methanotrophs, which can function under oxic or anoxic conditions (Conrad, 2009). Oxidation of CH_4 is prevalent in aquatic ecosystems because methanotrophs are generally more productive where there are strong opposing gradients of CH_4 and oxygen, common to aquatic ecosystems (Chowdhury and Dick, 2013). The oxidation of CH_4 can be an important process mitigating CH_4 emissions from aquatic systems (Bastviken et al., 2008; Sawakuchi et al., 2016).

Streams are largely differentiated from lentic waterbodies by the presence of flow, which may affect CH_4 cycling via turbulent mixing and oxygenation of the water column and benthic environment (Trimmer et al., 2010). Previously, the mixing of oxic water into stream sediments was thought to limit methanogenesis, but stream sediments have been shown to support methanogenesis (Sanders et al., 2007; Bodmer et al., 2020). High rates of CH_4 oxidation have also been observed in streams (Shelley et al., 2017), attributed to the strong redox gradient at the sediment-water interface and the introduction of oxygenated waters into the sediments via hyporheic flow (Hampton et al., 2020). However, the relatively rapid mixing of streams and rivers due to flow compared to lentic systems may reduce the proportion of CH_4 oxidized before emissions (Sawakuchi et al., 2016). That is, higher turbulence and gas exchange in streams and rivers may result in less depletion of the CH_4 pool *via* oxidation because of reduced transport time. This may explain why complete oxidation of the dissolved CH_4 pool has been observed in lakes (Bastviken et al., 2008), but not in streams and rivers (Sawakuchi et al., 2016).

The relative importance of CH_4 production and oxidation also affects the isotopic composition of CH_4 (Chanton, 2005; Chanton et al., 2006). The δ^{13}C-CH_4 and δD-CH_4 signature of emitted

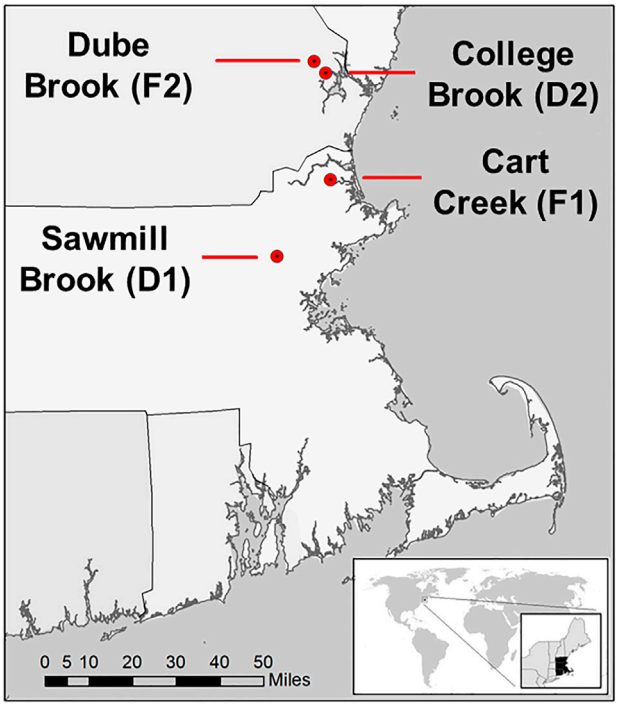


FIGURE 1 | Locations of four study stream reaches in northeast Massachusetts and southeast New Hampshire, United States (Robison et al., 2021).

CH_4 from a particular source (e.g., wetlands, landfills) can be used in atmospheric mixing models to constrain source contributions to bulk atmospheric CH_4 (Schwietzke et al., 2016). For example, CH_4 oxidation exerts a fractionation pattern of δ^{13}C-CH_4 and δD-CH_4 enrichment compared to the source signature of the CH_4 (Chanton et al., 2005). While the exact fractionation can vary significantly (Conrad, 2005), the change in δ^{13}C-CH_4 and δD-CH_4 values typically range from approximately 5–20‰ and 50–250‰, respectively (Whiticar, 1999; Wang et al., 2016). The emission pathway by which gaseous CH_4 leaves aquatic environment also has implications for the isotopic values of the emitted gas (Chanton, 2005). For example, Chanton et al. (1989) established that the δ^{13}C-CH_4 values found within released bubbles were not significantly different from those of the reservoir of CH_4 held within the sediment. Meanwhile, CH_4 that diffuses through sediments and into the water column is more susceptible to oxidation (e.g., Shelley et al., 2017). Thus, the balance of CH_4 emission pathways can be important in determining the isotopic signature of a particular ecosystem (e.g., Sawakuchi et al., 2016) and how that ecosystem is included in atmospheric mixing models (Fisher et al., 2017; Saunois et al., 2020).

To properly understand the role of stream ecosystems in the global CH_4 cycle, there is a need to not only quantify CH_4 fluxes, but also investigate how CH_4 cycles through these systems, using isotopic and microbial analyses. In this paper, we 1) quantify the relative contributions of diffusive and ebullitive emissions of CH_4 from four headwater streams; 2) examine the δ^{13}C-CH_4 and

TABLE 1 | Location, land use, and water quality characteristics of the four streams included in this study. Mean values of runoff, temperature, and stream chemistry are from the period of record.

		F1	F2	D1	D2
Physical descriptors	Latitude (°)	42.77	43.17	42.52	43.13
	Longitude (°)	–70.92	–70.97	–81.18	–70.92
	Area (km^2)	3.9	3.3	4.1	2.3
	Mean observed runoff (cm d^{-1})	0.77	0.68	0.76	0.96
	Slope (m km^{-1})	2.1	1.4	1.7	1.9
	Temperature (°C)	9.9	10.1	10.6	9.7
Land cover	Forest (%)	57.0	59.4	13.7	20.8
	Developed (%)	10.7	7.9	72.8	68.7
	Wetland (%)	18.7	17.3	4.3	0.7
Stream chemistry	Nitrate (mg L^{-1})	0.1	0.2	0.8	0.7
	Chloride (mg L^{-1})	101	62.5	190	321
	DOC (mg L^{-1})	7.3	6.0	4.6	4.2

δD-CH_4 values of CH_4 associated with these two emission pathways; and 3) explore the CH_4-associated microbial community in the stream sediments to provide context for CH_4 cycling. Integrating measurements of CH_4 emissions with an investigation of production and oxidation is needed to understand CH_4 cycling at the ecosystem level. By comparing our results to studies of other aquatic ecosystems such as larger rivers and lakes, we explore how CH_4 cycling in streams may differ and what implications this has for aquatic CH_4 budgets.

MATERIALS AND METHODS

Site Description

This study was conducted in four lowland headwater streams in southeastern New Hampshire and northwestern Massachusetts, United States (**Figure 1**). Watersheds were selected to contrast CH_4 dynamics in the two predominant land use conditions in this region (developed versus forested). These streams have been the focus of previous studies that examined nutrient and carbon cycling and the impact of land use (e.g., Wollheim et al., 2005; Wollheim et al., 2015; Wollheim et al., 2017), and were all monitored for CH_4 ebullition from May through October 2019 (Robison et al., 2021). The watersheds of two streams, Sawmill Brook (D1) and College Brook (D2), are characterized by a relatively developed, suburban landscape, while the other two, Cart Creek (F1) and Dube Brook (F2), are predominantly forest-covered. We group these streams into these two watershed land cover classes for comparison, but recognize the limitation of statistical inference with such a small sample size and mixed land use.

The watersheds range in size from 2.3 to 4.1 km^2, and all streams exhibit relatively shallow slopes (**Table 1**). Mean annual rainfall is 1,280 mm yr^{-1} and mean annual air temperature is 8.9°C (Wollheim et al., 2017). Mean discharge ranges from 25.5 L s^{-1} at D2 to 36.7 L s^{-1} at D1. Stream chemistry is measured as part of the Plum Island Ecosystems LTER project (Morse and Wollheim, 2014; Wollheim et al., 2015). Stream reach characteristics were examined in a concomitant study (Robison et al., 2021). Mean reach depth at baseflow ranged from 7.2 cm at D2 to 14.5 cm at F1, and mean reach width at baseflow ranged from 1.94 m at D2 to 2.83 m at D1. All reaches exhibit shallow slopes of approximately 2 m km^{-1} or less. Benthic substrates included sand, silt, and fine organic matter, while rocks comprised less than 10% of benthic surface area across all sites. Macrophytes were absent from all reaches in this study, eliminating the possibility of CH_4 efflux via plant-mediated transport.

Dissolved CH_4 Sampling and Diffusive Efflux Estimation

Water samples for dissolved CH_4 analysis were collected at each stream using 60 ml syringes fitted with three-way stopcocks. Samples were collected at variable frequencies ranging from multiple samples a week to roughly weekly between June 1 and October 31, 2019. On average, a sample was collected every 6 days at each site. Syringes were rinsed with stream water prior to sample collection. To collect water samples, syringes were filled with approximately 60 ml of stream water from 5 to 10 cm depth below the stream water surface. Syringes were cleared of air bubbles by inverting and expelling bubbles and water until 30 ml of sample water remained. Samples were stored on ice until returned to the laboratory within 6 h. In the laboratory, 30 ml of ambient air was added to each syringe to achieve a 1:1 ratio of sample water to air. Syringes were then shaken for 2 min to equilibrate gases between water and headspace (Magen et al., 2014). The water was then dispelled from the syringe, and the remaining headspace gas was saved for analysis. If the gas samples were not analyzed immediately, they were stored in evacuated glass vials sealed with a rubber septum until analyzed.

Samples were analyzed for CH_4 concentration in the Trace Gas Biogeochemistry Laboratory at the University of New Hampshire. The CH_4 concentration in parts per million by volume (ppmv) was determined using a Shimadzu Gas Chromatograph Flame Ionization Detector. Concentration was standardized using the average area response of ten injections of a standard CH_4 mixture (Northeast Airgas, 2.006 ppmv or Maine Oxy, 1,000 ppmv) to determine instrument precision (Frolking

and Crill, 1994). If multiple samples were collected from a single site, the mean measured concentration was used.

Diffusive fluxes of CH_4 to the atmosphere (F_{CH4}, mmol CH_4 m^{-2} d^{-1}) were calculated as:

$$F_{CH_4} = k_{CH_4} \times \Delta CH_4, \quad (1)$$

where k_{CH4} (m d^{-1}) is the gas transfer velocity for CH_4 and ΔCH_4 is the difference in CH_4 concentration (g m^{-3}) between the water and the air corrected for Henry's Law. We used a constant air CH_4 concentration of 1.94 ppmv based on measurements at the nearby Global Monitoring Laboratory site at the Isle of Shoals, New Hampshire during the monitoring period in 2019 (Earth System Research Laboratory, G. M. D., 2021). The gas exchange rate for CH_4, k_{CH4}, was calculated as:

$$k_{CH_4} = \left(\frac{SC_{CH_4}}{600}\right)^{1/2} \Big/ k_{600}, \quad (2)$$

where SC_{CH_4} is the Schmidt number for CH_4 at a given water temperature and k_{600} (m d^{-1}) is the gas transfer velocity standardized for a Schmidt number of 600. Without direct measurements of gas transfer velocity across a wide range of flow conditions, we estimated k_{600} for each reach based on the relationship following Raymond et al. (2012):

$$k_{600} = 1162 \pm 192 \times S^{0.77 \pm 0.028} \times V^{0.85 \pm 0.045}, \quad (3)$$

where V is the water velocity at time of sampling (m s^{-1}) and S is the channel slope (unitless). The mean slope of each stream reach was found using StreamStats (Ries et al., 2017). Mean daily discharge (Q; L s^{-1}) was available from the long-term monitoring projects (Morse and Wollheim, 2014; Wollheim et al., 2017). Predictive relationships for V from Q were made using the equations for scaling stream geometry at a site (Knighton, 1998):

$$V = 0.287 \times Q^{0.4}. \quad (4)$$

Two or fewer direct measurements of the gas exchange velocity were also made at each site, although generally under relatively low flow conditions (< 50 L s^{-1}). These measurements were made using argon as a conservative gas tracer (Hall and Ulseth, 2020). We used these measurements to roughly evaluate the accuracy of our estimates of k_{600} (**Supplementary Figure S1**).

Ebullitive Sampling and Flux Estimation

Ebullitive CH_4 fluxes were measured during the same time frame as diffusive flux by Robison et al. (2021). Briefly, stationary bubble traps were deployed in triplicate at three to four locations in each stream. Traps were visited at least weekly from June 1 to October 31, 2019, during which the volume of gas collected in each trap was measured and collected for analysis of CH_4 concentration. The flux at each trap was then calculated as the mass of CH_4 emitted over the observation period normalized per unit area under the trap (mmol CH_4 m^{-2} d^{-1}). For this study, mean rates of ebullitive CH_4 flux per measurement period at each stream were used, based on the total number of funnels at a stream.

Isotopic Sampling and Analysis

Gas samples were collected for CH_4 isotopic analysis in the first week of August 2019. Additional samples from F1 and D1 from the first week of September 2018 were also included in analysis. Dissolved CH_4 samples from the surface water were collected in the same manner described above. Additional benthic gas samples were collected by physically disturbing the sediment and collecting released bubbles. A minimum of three sediment gas samples and three surface water dissolved gas samples were collected at each site. All samples were stored in evacuated glass vials sealed with a rubber septum for analysis.

Samples were analyzed for δ^{13}C-CH_4 and δD-CH_4 using an Aerodyne dual tunable infrared laser direct absorption spectrometer (TILDAS; Aerodyne Research Inc, Massachusetts, United States) at the University of New Hampshire. These instruments use high resolution infrared spectrometry to quantify trace gases such as CH_4 (Mcmanus et al., 2011; Nelson and Roscioli, 2015). The TILDAS used here is configured with two 8 μm quantum cascade lasers (QCLs, Alpes Lasers, Switzerland) and a 200 m multipass absorption cell to simultaneously monitor $^{12}CH_4$, $^{13}CH_4$, and CH_3D. The instrument was regularly calibrated with three standard tanks with known isotopic mixing ratios for $^{13}CH_4/^{12}CH_4$ and CH_4/CH_3D. The isotopic composition of the standards was determined using an Aerodyne calibration system. The spectroscopic isotope ratios of four Isometric (now Airgas) CH_4 standards were measured at diluted concentrations ranging from < 1 to 12 ppmv. Keeling plot analysis was used to determine the relationship between the spectroscopic and standard isotope ratios of the Isometric standards. The linear relationship was made to the corresponding measured spectroscopic isotopic ratios of the UNH calibration tanks. The TILDAS is configured with an automated sampling system designed to measure small (≤ 5 ml) injections of high concentration samples by diluting them within the instrument to a target CH_4 mixing ratio of eight ppmv with ultra-zero air. The instrument precision was 0.1‰ for δ^{13}C-CH_4 and 3‰ for δD-CH_3D at the target CH_4 mixing ratio. Samples with very low concentration (<0.01 mM CH_4) can result in erroneous isotopic measurement, and these datapoints (five of 59 samples) were removed prior to statistical analysis.

The percent of CH_4 oxidized between sediment generation and surface water evasion was estimated using the equation:

$$\%\ \text{oxidized} = \frac{\delta^{13}C_{Sample} - \delta^{13}C_{Source}}{(\alpha - 1) \times 1000} \times 100, \quad (5)$$

where $\delta^{13}C_{Sample}$ is the δ^{13}C-CH_4 value found in the surface water sample, $\delta^{13}C_{Source}$ is the δ^{13}C-CH_4 value found in the sediment gas sample, and α is the isotope fractionation factor of CH_4 oxidation. We used two α values to include some uncertainty of isotopic fraction in these stream environments, 1.033 and 1.025 (Tyler et al., 1997; Zhang et al., 2016). This follows previous work estimating the efficiency of CH_4 oxidation in the Amazon River basin (Sawakuchi et al., 2016).

Microbial Sample Collection and Analysis

Sediment cores were collected from the streams for 16S rRNA analysis. A modified Multi Stage Soil Core Sampler (AMS Inc, Idaho, United States), consisting of a stainless steel cylinder and a plastic liner (5 cm diameter), was manually driven into the stream sediments using a sliding weight stand (Wik et al., 2018). Sediment cores were collected the first 2 weeks of July 2019 and processed in the field. Cores were collected at patches in the stream near each set of bubble traps as described in Robison et al. (2021). Four patches at each stream were sampled, except D2 where only three patches were sampled. At each patch, triplicate cores were collected. Sediment collected in the top 2 cm from each core was combined into a composite "surface" sediment sample in a Whirl-Pak sample bag. Similarly, sediment collected between 9 and 11 cm depth was combined into a composite "subsurface" sample. As a result, a total of four composite surface and four composite subsurface samples were collected at each stream except D2, where only three composite samples of each were collected. All tools used to collect cores, including the coring equipment, were sterilized with 70% ethanol between samples and sediment layers to minimize contamination. The depth of 9–11 cm was chosen as the subsurface sample depth because buried rocks or clay layers prevented collection of sediment at depths greater than 12–15 cm in some places. Thus, while 9–11 cm does not represent the maximum or mean depth of the sediment in portions of these streams, it represents a depth layer that could be collected across all sites and is deep enough where complete depletion of oxygen is likely (Crawford et al., 2014). Sediment samples were frozen on-site with liquid nitrogen, stored on ice, and returned to the laboratory within 4 h. Samples were stored in a −80°C freezer until analyzed.

Genomic DNA was extracted from sediment samples using a Qiagen DNeasy PowerSoil kit (Qiagen, Hilden, Germany) with minor changes to the manufacturer's protocol (see Doherty et al., 2020). DNA was amplified by polymerase chain reaction (PCR) using the primers 515f–806r of the V4 region of the 16S rRNA gene to profile bacterial and archaeal communities (Apprill et al., 2015; Parada et al., 2016). Each reaction contained 6 µl DreamTaq Hot Start Green (Thermo Fisher Scientific, Waltham, MA, United States), 2.6 µl sterile water, 0.7 µl forward primer (5 µM), 0.7 µl reverse primer (5 µM), and 2 µl template DNA (10× diluted). DNA amplification was performed using a T100 Thermal Cycler (Bio-Rad, Hercules, CA, United States). The 16S rRNA conditions were: enzyme activation at 95°C for 3 min; followed by 35 cycles of denaturation at 95 °C for 30 s, annealing at 55°C for 30 s, and extension at 72°C for 60 s; then a final extension at 72°C for 12 min.

Gel electrophoresis was used to confirm the presence of the PCR product, which was then quantified using a Quant-iT dsDNA High-Sensitivity Assay Kit and a Qubit 3.0 fluorometer (Thermo Fisher Scientific, Massachusetts, United States). Resulting concentrations ranged from 0.5 to 28 ng μL^{-1}, with sandier sediment samples typically having lower concentrations. PCR products were sent to the Hubbard Center for Genome Studies (University of New Hampshire, New Hampshire, United States) for sequencing by Illumina HiSeq2500 (250 bp reads) with Rapid Run© SBS V2 chemistries (Illumina, San Diego, CA, United States). Sequence reads were demultiplexed using CASAVA.

Sequences were analyzed using QIIME 2 (version 2020.1; Bolyen et al., 2019) on the Premise high performance computing cluster at the University of New Hampshire. Cutadapt was used to remove primers (Martin, 2011). Using DADA2 (Callahan et al., 2016), sequences were truncated at the length where the median Phred score (quality score) fell below 30 (200 bp for forward read; 225 bp for reverse read) and unique sequences were designated as amplicon sequence variants (ASVs). Each sample was then rarefied to 3,400 sequences per sample. Rarefication depths were chosen to ensure at least three samples remained for each depth at each stream. Taxonomy was assigned to ASVs using the SILVA database (release SILVA 138 SSU; Quast et al., 2013; Glöckner et al., 2017). The relative abundances of taxa were calculated after removing chloroplasts, mitochondria, and taxa present in less than 5% of samples.

In this study, we focused primarily on taxa associated with CH_4 production and CH_4 oxidation. Following Hough et al. (2020), we identified methanogens based on classification into the archaeal orders: Methanocellales, Methanobacteriales, and Methanomicrobiales, and the families Methanosarcinaceae and Methanosaetaceae, of order Methanosarcinales (Evans et al., 2019). Similarly, we identified methanotrophs as those from the bacterial orders Methylococcales and Methylomirabilales and the archaeal family Methanoperedenaceae, order Methanosarcinales (Smith and Wrighton, 2019). Taxa from the order Methylococcales are classical aerobic methanotrophs, while those from the order Methylomirabilales are capable of CH_4 oxidation following reduction of nitrate or nitrite (Wu et al., 2011); that is, they are capable of generating oxygen for CH_4 oxidation when in an anoxic environment. Finally, Methanoperedenaceae are a methanotrophic archaea family (formerly known as ANME-2d) known to be capable of CH_4 oxidation via alternative electron donors like nitrate, iron, or manganese (Ettwig et al., 2016; Leu et al., 2020). Despite the indefinite nature of assigning organismal function using 16S sequencing, traits associated with CH_4 cycling are typically conserved and well defined (Martiny et al., 2015), allowing for confidence in these assignments. The relative abundance of individual samples is calculated, from which a mean and standard deviation from all samples collected at a sediment depth in a stream is determined.

Statistical Analyses

All calculations and statistical analyses were performed in MATLAB and Statistics Toolbox Release 2020a (The MathWorks, Inc, Massachusetts, United States), and the significant level was set at $\alpha = 0.05$. Uncertainty in the dissolved CH_4 concentration for each site was determined by the ratio of the standard error (SE) of the measured concentrations to the median concentration (Hojo and Pearson, 1931):

$$\%\ \text{uncertainty} = 1.253 \times \frac{\text{Std Err}}{\text{median } CH_4} \times 100, \qquad (6)$$

TABLE 2 | Summary of measured dissolved methane concentration, estimated methane-specific gas exchange rate, calculated diffusive and ebullitive emissions, measured δ^{13}C-CH_4 and δD-CH_4 values, estimated percent of the dissolved CH_4 oxidized before emission, and the percent abundance of methanogens and methane oxidizing bacteria in the total detected community for the four streams in this study. SD indicates the standard deviation. *Ebullitive methane flux data is from Robison et al. (2021). ^Methanotrophs refers to taxa capable of CH_4 oxidation, whether aerobic or anaerobic.

Variable			F1	F2	S1	S2	Overall
Dissolved CH_4 concentration (μmol CH_4 L^{-1})		Median	0.9	1.6	1.0	1.6	1.1
		Min	0.3	0.8	0.3	0.2	0.2
		Max	13.6	8.5	2.7	16.1	16.1
k_{CH4} (m d^{-1})		Median	4.7	3.4	5.9	4.7	4.8
		Min	4.1	2.2	4.5	4.0	2.2
		Max	8.2	8.3	10.3	11.1	11.1
Diffusive		Median	4.1	4.7	5.9	7.8	5.7
CH_4 flux (mmol CH_4 m^{-2} d^{-1})		Min	1.4	2.2	1.6	1.3	1.3
		Max	64.9	25.7	20.8	70.8	70.8
Ebullitive		Median	0.2	1.3	1.0	0.0	0.6
CH_4 flux* (mmol CH_4 m^{-2} d^{-1})		Min	0.0	0.2	0.01	0.0	0.0
		Max	0.8	4.4	13.5	0.1	13.5
$\delta^{13}CCH_4$ (‰)	Benthic bubble	Mean	−67.8	−66.5	−63.1	−66.0	−65.9
		SD	0.5	0.4	0.6	0.4	0.5
	Surface dissolved	Mean	−51.5	−52.8	−49.5	−55.0	−52
		SD	1.7	0.7	1.1	2.6	1.5
δDCH_4 (‰)	Benthic bubble	Mean	−297	−274	−312	−318	−300
		SD	17	16	21	16	18
	Surface dissolved	Mean	−231	−257	−290	−265	−261
		SD	21	26	42	28	29
% CH_4 oxidized	α = 1.033	Mean	65.2	54.8	54.4	44.0	55.6
		SD	3.7	2.5	2.6	2.4	3.2
	α = 1.025	Mean	49.4	41.5	41.2	33.3	42.1
		SD	2.7	1.8	2.0	1.9	2.1
Methanogens (% abundance)		Mean (0 cm)	0.1	0.2	0.1	0	0.1
		Mean (10 cm)	0.8	0.7	0.3	0.3	0.6
Methanotrophs^ (% abundance)		Mean (0 cm)	1.0	3.2	5.0	4.5	3.5
		Mean (10 cm)	1.6	1.2	4.7	2.5	2.5

which resulted in a unique percent uncertainty at each site. Uncertainty in the gas exchange rate was determined by the standard deviation included in the factors of **Eq. 3**. Simple linear interpolation was used to estimate the rate of diffusive efflux on days without a dissolved CH_4 concentration measurement. Uncertainty in the diffusive CH_4 flux was then estimated by propagating the uncertainty from dissolved CH_4 concentration and gas exchange rates. We summarized CH_4 concentration, gas exchange, and rates of diffusion as medians because of the non-normal distribution of the data. Differences in CH_4 concentration, gas exchange, and diffusive emissions between streams were analyzed using the nonparametric Wilcoxon rank sum test. Trends in CH_4 concentration and diffusion across time were analyzed using the nonparametric Kendall rank correlation coefficient. Isotopic and microbial data were summarized as means because of their small sample sizes and unknown distributions. Differences between streams, depths for microbial samples, and type of sample for isotopes (i.e., benthic or surface water) were compared using two-sample *t*-test or one-way ANOVA.

RESULTS

Dissolved CH_4 Concentration and Diffusive Fluxes

Measured concentrations of dissolved CH_4 in surface water were above saturation (roughly 0.003 μmol CH_4 L^{-1} at 10°C) in all collected samples, with an overall median ±SE of 1.1 ± 0.4 μmol CH_4 L^{-1} (**Table 2**; **Figure 2A**). F2 and D2 had the highest median concentration of CH_4 (1.6 ± 0.9 μmol CH_4 L^{-1}) and F1 had the lowest (0.9 ± 0.3 μmol CH_4 L^{-1}). There was no statistical difference in the median dissolved concentration of CH_4 between watershed land cover classes ($p > 0.05$). We also observed no clear pattern in the dissolved concentration across time at any individual stream ($p = 0.54$). The median k_{CH4} across all sites was 4.8 ± 0.4 m d^{-1}, ranging from 3.4 ± 0.3 m d^{-1} at F2 to 5.9 ± 0.6 m d^{-1} at D1 (**Table 2**; **Figure 2B**). The watershed land cover classes did differ in the estimated gas exchange rates ($p < 0.01$), where the two streams draining developed landscapes, D1 and D2, exhibited significantly higher k_{CH4}. Calculated rates of gas exchange were similar to limited direct measurements in each of the streams (**Supplementary Figure S1**) using short-term continuous injections of a volatile gas tracer (Hall and Ulseth, 2020). Median diffusive CH_4 flux was 5.7 ± 2.3 mmol CH_4 m^{-2} d^{-1} overall (**Table 2**; **Figure 2C**). In individual streams, the median diffusive flux ranged from 4.1 ± 2.1 to 7.8 ± 4.8 mmol CH_4 m^{-2} d^{-1} at F1 and D2, respectively, with the developed watershed class exhibiting a higher rate compared to the forested watershed class ($p < 0.01$). We did not observe any clear temporal pattern in diffusive CH_4 emissions across our monitoring period at any individual site ($p > 0.05$). High diffusive CH_4 fluxes were more strongly associated with high measurements of dissolved CH_4 than with high gas exchange

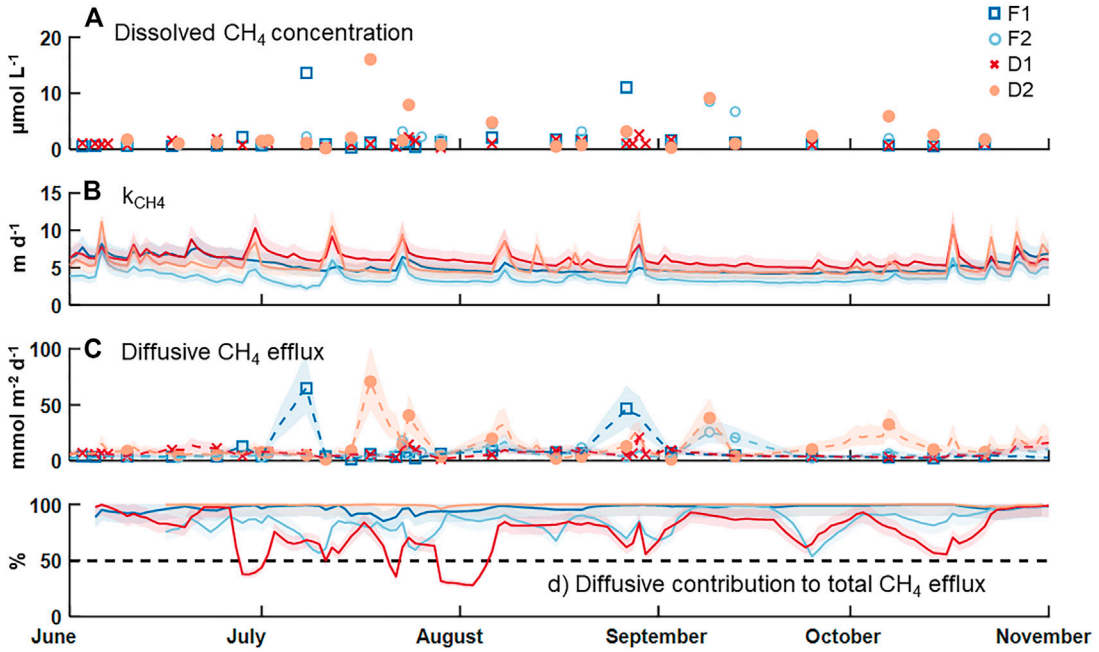


FIGURE 2 | Time series of **(A)** measured dissolved CH_4 concentration, **(B)** estimated gas exchange rate for CH_4, **(C)** estimated diffusive flux rate for CH_4 on days with a concentration measurement (markers) and the days between via linear interpolation (dashed lines), and **(D)** the percent contribution of diffusion to the total CH_4 efflux budget. The shaded areas indicate uncertainty in estimating the gas exchange rate an in linear interpolation of the diffusive emission rates.

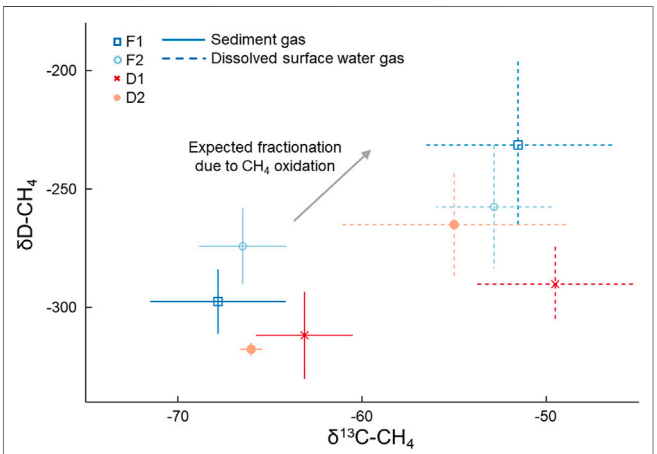


FIGURE 3 | Mean (points) and standard deviation (lines) of $\delta^{13}C$-CH_4 and δD-CH_4 values of samples from sediment gas and dissolved gas in the surface water collected in August 2019. Sediment gas was collected by disturbing the sediment and collecting released bubbles. Points indicate mean values and bars represent the standard deviation. The arrow depicts the expected isotopic fractionation of CH_4 due to oxidation (Chanton et al., 2005).

rates (**Figure 2**). The maximum daily rate of diffusive CH_4 efflux was 70.8 ± 31.4 mmol CH_4 m^{-2} d^{-1} at D2.

Diffusive fluxes of CH_4 were compared to ebullitive fluxes of CH_4 from Robison et al. (2021) during the same period of record (**Table 2**; **Figure 2D**). Across all four streams, the median diffusive CH_4 flux (5.7 ± 2.3 mmol CH_4 m^{-2} d^{-1}) was greater than the median ebullitive CH_4 flux (0.6 ± 0.1 mmol CH_4 m^{-2} d^{-1}). Diffusive emissions of CH_4 comprised approximately 90% of total CH_4 emissions from these four streams over the entire period, ranging from 78% at F2 to nearly 100% at D2. Ebullitive CH_4 flux exceeded diffusive flux only at D1 for short periods (**Figure 2D**). Diffusion accounted for the majority of CH_4 emissions at the other three sites during the entire monitoring period.

Stable Isotopic Composition of CH_4

Benthic gas and surface water gas samples exhibited clear differences in $\delta^{13}C$-CH_4 and δD-CH_4 values (**Table 2**; **Figure 3**). Generally, there was more variability between the type of sample (i.e., benthic or surface water) than between streams. Benthic gas $\delta^{13}C$-CH_4 and δD-CH_4 values averaged across all streams were −65.9 ± 2.0‰ and −300 ± 18‰, respectively. There was some variation in the benthic $\delta^{13}C$-CH_4 values between streams, where D1 exhibited a significantly higher mean $\delta^{13}C$-CH_4 (−63.1 ± 0.6‰) than F1 (−67.8 ± 0.5‰, $p < 0.01$) and F2 (−66.5 ± 0.4‰, $p = 0.02$). More variation was noted in measured δD-CH_4 values, with F2 having the highest mean value of −257 ± 16‰ and D2 having the lowest value of −318 ± 16‰, with only these two sites being significantly different ($p = 0.01$). Dissolved CH_4 $\delta^{13}C$-CH_4 and δD-CH_4 values averaged across all four streams were −52 ± 1.5‰ and −261 ± 29‰, respectively. These were slightly more varied across streams than the benthic samples. For example, $\delta^{13}C$-CH_4 values ranged from −49.5 ± 0.6‰ at D1 to -55.0 ± 2.6‰ at D2 in dissolved CH_4 samples, although no site was significantly different from the others. Meanwhile, dissolved δD-CH_4 ranged

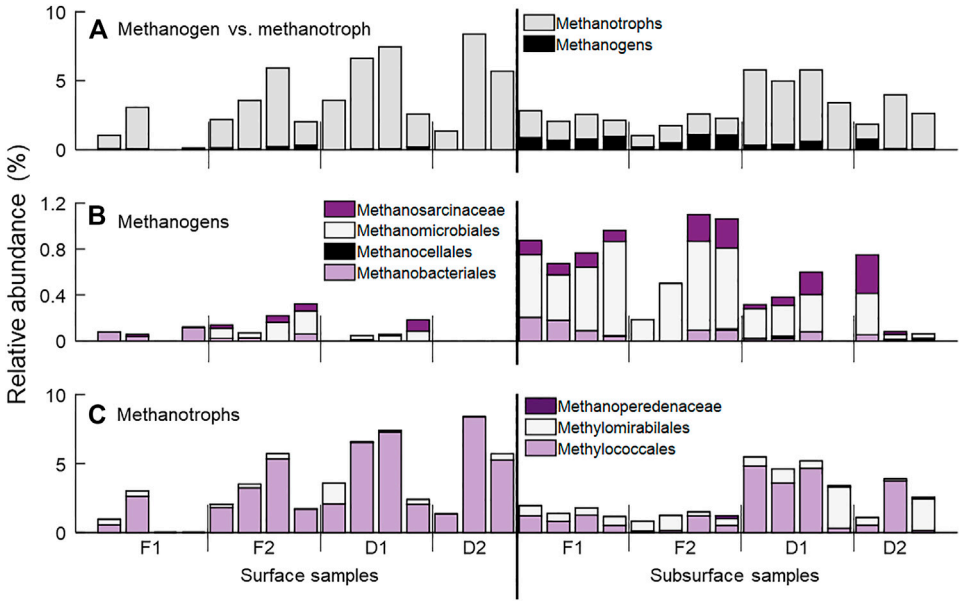


FIGURE 4 | Relative abundance of CH_4-associated taxa at sampling locations. **(A)** All taxa associated with CH_4 production (methanogens, black) and oxidation (methanotrophs, gray). Here, we use the simplified term methanotrophs to refer to those taxa who are capable of CH_4 oxidation through any of a variety of biochemical pathways. **(B)** Archaeal taxa identified as methanogens detected in sediment samples, including the orders Methanomicrobiales, Methanocellales and Methanobacteriales, and the families Methanosarcinales and Methanosaetaceae, both of the order Methanosarcinales. **(C)** Taxa associated with CH_4 oxidation, separated into categories based on potential biochemical pathways. The bacterial order Methylococcales are canonical, aerobic CH_4 oxidizing bacteria. The bacterial order Methylomirabilales are proposed to be capable of CH_4 oxidation following the reduction of nitrite. Finally, methanotrophic archaea from the order Methanosarcinales, family Methanoperedenaceae (formerly known as ANME-2d) are also capable of CH_4 oxidation following the reduction of nitrate, iron, or manganese.

from −257 ± 26‰ at F2 to −290 ± 42‰ at D1, with only these two sites being significantly different (p = 0.04). There was no difference in measured isotopic values between watershed land cover classes when comparing either δ^{13}C-CH_4 or δD-CH_4 between benthic gas and dissolved samples.

Dissolved CH_4 in surface water was more ^{13}C- and D-enriched relative to the sediment gas overall (p < 0.01; **Figure 3**). This amounted to a 14 ± 1.5‰ and 39 ± 29‰ shift towards the heavier isotope for δ^{13}C-CH_4 and δD-CH_4, respectively. The δ^{13}C-CH_4 values for dissolved CH_4 were all significantly higher than sediment CH_4 at each stream, and the δD-CH_4 values were significantly higher than sediment CH_4 at F1 (p = 0.01) and D1 (p = 0.04). Given this enrichment in δ^{13}C-CH_4 values, we estimated the mean proportion of dissolved CH_4 oxidized was 42.1 ± 2.1% when using α = 1.033, and 55.6 ± 2.8% when using α = 1.025 (**Table 2**). The percentage of dissolved CH_4 oxidized in individual streams ranged from a minimum of 33.3 ± 3.1% at D2 using α = 1.025 to 65.2 ± 2.6% at D1 given α = 1.033.

Methane-Associated Microbial Community

Taxa identified as methanogens and methanotrophs were detected across all four streams (**Figure 4A**, **Supplementary Table S1**). Methanogen taxa were detected in 10 of 15 surface sediment samples, and 14 of 15 subsurface samples (**Figure 4B**). These included the archaeal orders Methanosarcinales (families Methanosaetaceae and Methanosarcinaceae), Methanobacteriales (family Methanobacteriacea), Methanomicrobiales (families Methanomicrobiaceae, Methanoregulaceaea, and rice cluster II), and Methanocellales (family Methanocellaceae). As a percent of the total community, methanogens comprised roughly 0.1% of the surface sediment community and 0.6% of the subsurface community, on average. Methanogens comprised a larger percentage of the microbial community in the forested watershed streams than in the developed streams (p = 0.04).

Taxa classified as methanotrophs were detected in 14 of 15 surface samples and all subsurface samples (**Figure 4C**). Taxa from the bacterial orders Methylococcales (families Methylococcaceae and Methylomonaceae), Methylomirabilales (family Methylomirabilaceae), as well as the archaeal order Methanosarcinales (family Methanoperedenaceae) were detected. Methanotrophs comprised a larger fraction of the total microbial community in all samples compared to methanogens, but this may be a result in part of the bias of our primers for bacteria over archaea (Walters et al., 2016). As a percent of the total community, methanotrophs comprised on average 4.3 and 3.6% in surface and subsurface samples, respectively. Aerobic methanotrophs, i.e., Methylococcales, were significantly more abundant in surface sediment samples (p = 0.02), while taxa capable of CH_4 oxidation in anoxic conditions (Methylomirabiales and Methanoperedenaceae) were higher in relative abundance in subsurface samples than in surface samples (p = 0.02). Additionally, methanotroph relative abundance was greater in the two streams draining developed watersheds than the two draining forested watersheds (p < 0.01).

DISCUSSION

Diffusion via turbulent mixing was the dominant pathway of CH_4 emissions from the stream reaches in this study (**Figure 2D**; **Table 2**). This appears more common in small streams compared to larger rivers or lentic ecosystems, where ebullition tends to be more important. The enrichment of CH_4 isotopic values from the benthos to the surface water is likely a result of oxidation, which is supported by the presence of a diverse microbial community capable of CH_4 oxidation. Emitted CH_4 from these streams thus exhibits isotopic values more characteristic of the dissolved CH_4 pool, i.e., heavier than the benthic gas pool. Together, our results suggest CH_4 emission and isotopic patterns in small streams may be unique amongst aquatic ecosystems, and thus may distinguish how small streams should be included in global CH_4 models.

Diffusive Emissions Dominate CH_4 Efflux Budget

Diffusive emissions were the dominant efflux pathway of CH_4 in these four lowland stream reaches. The median diffusive flux is comparable to a summary of 385 streams and rivers (8.22 ± 25.50 mmol CH_4 m^{-2} d^{-1}; Stanley et al., 2016). Total CH_4 emissions were greater than the median of a recent analysis of streams and rivers globally (0.9 mmol CH_4 m^{-2} d^{-1}), but within the 90% range (0.0–35.8 mmol CH_4 m^{-2} d^{-1}; Rosentreter et al., 2021). When compared to lentic waterbodies, the rate of emissions from these four streams is similar on a per area basis (e.g., Holgerson and Raymond, 2016; Sanches et al., 2019). For example, in a variety of lakes and ponds of northern latitudes, total CH_4 emissions ranged from 2.8 to 12.5 mmol CH_4 m^{-2} d^{-1} (Wik et al., 2016b).

The efflux of CH_4 from small streams may be a significant, yet overlooked pathway of carbon fluxes from inland waters. The total aquatic carbon flux for inland waters across North America is estimated to be 24 g C m^{-2} yr^{-1} (Butman et al., 2018), where the flux is normalized for total land area. However, this flux does not include CH_4, as scaling was limited by significant data gaps at the time of estimation. Following scaling methods published previously (Robison et al., 2021), the streams in this study emit roughly 0.08 g CH_4-C m^2 watershed area yr^{-1} when both diffusion and ebullition are considered, less than 1% of the total estimated for inland waters. If the greater radiative forcing of CH_4 relative to CO_2 is taken into account (Saunois et al., 2020), the CO_2-equivalent rate increases to 2.2 g C m^2 watershed area yr^{-1}. Thus, ignoring small stream methane emissions may underestimate watershed carbon emissions by approximately 10%, a significant factor.

Relatively few studies exist with which to compare diffusion and ebullition in lotic systems (**Supplementary Table S2**). Summarizing 26 streams and rivers which considered both pathways, diffusion delivered 68% of total CH_4 emissions on average, but this ranged from 14 to 94% (Stanley et al., 2016). However, it appears smaller streams tend to favor diffusive emissions. For example, diffusion comprised roughly 90% of CH_4 emissions in a small stream in Wisconsin, United States (Crawford et al., 2014). In contrast, studies of larger rivers in the Amazon (Sawakuchi et al., 2014), on the East Qinghai–Tibet Plateau (Zhang et al., 2020), and in urban China (Wang et al., 2021) found diffusion accounted for 64, 21, and 20% of total CH_4 emissions, respectively. Diffusive fluxes generally account for a smaller fraction of the total CH_4 budget in lentic systems too, e.g., 48% for northern lakes and ponds (Wik et al., 2016b).

Land use may affect diffusive CH_4 emissions, where development promotes higher rates of emission. This pattern follows previous studies which linked low oxygen and high organic carbon delivery to higher rates of CH_4 production in urban streams (Stanley et al., 2016; Wang et al., 2021). With only four streams studied and mixed land use within each watershed, the strength of this comparison is narrow. Individual samples from each stream exhibited relatively high concentrations of dissolved CH_4. The median and maximum of dissolved CH_4 concentrations were similar to those found in a yearlong survey of gas concentrations in streams in New Hampshire (0.63 and 13.5 μmol CH_4 L^{-1}; Herreid et al., 2020). Our dataset precludes analysis of what causes these high concentrations, but we have no reason to discard them from our analysis as they fall within ranges observed in streams and rivers locally and globally (Stanley et al., 2016).

The estimation of diffusive CH_4 efflux is limited by the relatively sparse measurements of dissolved CH_4 concentrations and the estimation of gas exchange. The similarity of direct gas exchange measurements to estimates used in this study suggests this latter uncertainty is modest during low flow conditions (**Supplementary Figure S1**). Similarly, while our results likely suffer in accuracy at fine temporal scales (i.e., daily), it does not necessarily indicate the summarized results are inaccurate. Uncertainty due to sampling frequency on estimating seasonal rates of CH_4 emissions in lakes has been examined previously (Wik et al., 2016a); here, a minimum of 17 measurements of dissolved CH_4 concentration were needed to accurately represent seasonal emission patterns from lakes. The minimum number of measurements of dissolved CH_4 concentration in this study is 25. While the standard for lakes may not be the same for lotic ecosystems, we believe our results reflect the typical seasonal behavior at these streams in which diffusion is the dominant emission pathway for CH_4.

Evidence for In-Stream CH_4 Production and Oxidation From Isotopic and Microbial Data

The isotopic and microbial results provide evidence for active CH_4 processing in these streams, with production and oxidation ubiquitous. For example, the presence of ebullition and the detection of methanogens suggests active CH_4 production in the sediment of all four streams. The δ^{13}C-CH_4 and δD-CH_4 values of the sediment-derived gas suggest a combination of acetoclastic (−60‰ to −50‰ δ^{13}C-CH_4 and −400‰ to −250‰ δD-CH_4) and hydrogenotrophic (−110‰ to −60‰ δ^{13}C-CH_4 and −250‰ to −170‰ δD-CH_4) methanogenesis (Whiticar, 1999; Chanton et al., 2005), which is common in aquatic environments (Shelley et al., 2015; Wik et al., 2020). The presence of methanotrophs and an enrichment in both δ^{13}C-CH_4 and δD-CH_4 values between benthic and surface samples suggests

CH_4 oxidation was prevalent across the four streams as well, representing a potentially significant control on emissions. The estimated oxidation proportions are similar, but generally lower than the 57–82% range estimated for large rivers in the Amazon River basin (Sawakuchi et al., 2016) or the 57–100% estimated for lakes in Sweden (Bastviken et al., 2002). The lower oxidation proportion in the streams could be a result of relatively faster turnover of the water column. That is, while the efficiency of CH_4 oxidation could be similar across all aquatic ecosystems, relative fast mixing in small streams may limit the time for CH_4 oxidation to occur. Regarding microbial evidence for CH_4 production and oxidation, detection of microbial taxa via 16S rRNA sequencing can recover dormant or dead microbes (Oliver, 2005), thus the detections do not directly indicate activity. However, combined with the magnitude of CH_4 fluxes and isotopic values, we can confidently infer the presence of microbial CH_4 production and oxidation in the streams.

Alternative explanations for the change in isotopic values are possible. The difference could result from dissolved CH_4 inputs from a different source in the watershed, e.g., the riparian zone (Crawford et al., 2013). If the balance of isotopic values of this other source is distinct from that in the stream sediments, the isotopic values of the dissolved CH_4 in the streams may be confounded by the mixed sources. Additionally, diffusion exerts a fractionation effect (< 3‰ δ^{13}C-CH_4) on CH_4, where lighter CH_4 is preferentially emitted (Knox et al., 1992). This fractionation is much smaller than that of oxidation and the time for diffusion is relative fast in these streams, limiting the impact of this effect. Because isotopic and microbial sampling occurred in August and July, respectively, the results of our oxidation analysis may reflect the conditions of this warmer period of the year. For example, CH_4 isotopes in aquatic ecosystems may be heaviest in the summer (Atkins et al., 2017), possibly as a result of more active microbial oxidation (Shelley et al., 2015). If so, this would indicate we may have measured conditions under which oxidation is most efficient. However, considering the isotopic results in the context of the detection of methane oxidizing microbes, we are confident CH_4 oxidation is prevalent in these streams with the greatest uncertainty around the temporal dynamics of oxidation efficiency.

Mechanisms Driving CH_4 Emission Pathway and Oxidation Potential in Headwater Streams

The dominance of diffusive CH_4 emissions and the relatively lower proportion of CH_4 oxidation appear to distinguish small streams from other aquatic ecosystems. Identifying the factors that drive this difference is thus key to understanding how CH_4 dynamics may differ in small streams. We propose two characteristics that are fundamental in differentiating small streams from larger rivers and from lentic systems: flow and depth. We hypothesize limited bubble formation and CH_4 oxidation results from the unique physical and biogeochemical conditions of small streams caused by increased water exchange between the water column and sediments (hyporheic flow) and short residence time of CH_4 in the water column (gas exchange).

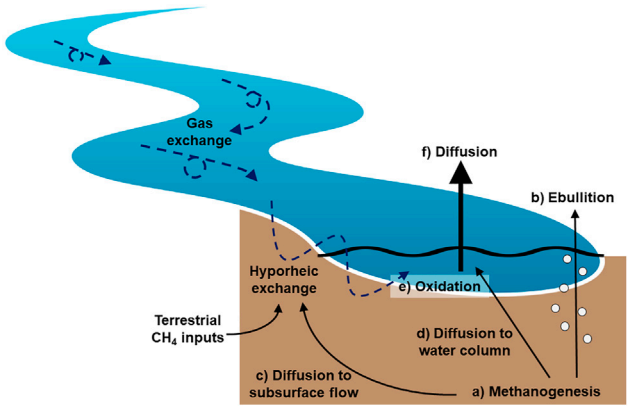


FIGURE 5 | Proposed conceptual model of CH_4 production, transport, oxidation, and emissions in stream ecosystems. The inherent flow and shallow nature of streams promotes hyporheic exchange and high gas exchange rates. This serves to limit bubble formation and promote the transport of dissolved CH_4 out of the sediments *via* diffusion and subsurface flow. While the dissolved CH_4 pool is exposed to oxidation, the proportion of CH_4 that is oxidized is limited by the relatively rapid exchange of water and gases in stream ecosystems. Most CH_4 is emitted via diffusion across the water-air interface in streams, and the limited exposure of this CH_4 pool results in relatively heavy dissolved CH_4 isotopic values. Because diffusive CH_4 emissions dominate the overall emission budget, the mean isotopic value of emitted CH_4 reflects this heavier signature and CH_4 isotopes in streams are enriched relative to other aquatic ecosystems.

Flow provides lotic ecosystems with consistent turbulent mixing, and the relatively shallow nature of small streams propagates this turbulence to the sediment–water interface. These likely limit bubble formation broadly via changes to sediment quality and depth. Because bubble formation is greatly affected by the grain size and physical structure of aquatic sediments (Liu et al., 2016), processes like turbulence which affect the sediment will in turn affect ebullition. For example, the erosional nature of streams (Knighton, 1998) may inhibit ebullition by increasing mean grain size or reducing deposition of organic matter, both of which have been shown to limit ebullition in streams (Crawford et al., 2014; Bodmer et al., 2020). Turbulence also enhances exchange at both the sediment–water and air–water interface within streams (Boano et al., 2014), affecting both bubble formation and oxidation rates. Advective water inputs into and through stream sediments via hyporheic flow (Packman and Salehin, 2003) create patches of oxic and anoxic conditions in close proximity (MahmoodPoor Dehkordy et al., 2019; Nelson et al., 2019). The CH_4 produced in anoxic zones can be transported through sediments by this advective flow (Sobczak and Findlay, 2002), limiting bubble formation further, exposing CH_4 to oxidizing conditions, and decreasing the residence time of CH_4 within the sediment. This advective exchange may ultimately limit the overall potential for CH_4 oxidation. For example, in Amazonian rivers, the extent of CH_4 oxidation was positively related to residence time in surface sediments (Sawakuchi et al., 2016). Oxidation within the water column is also limited by higher rates of gas exchange in streams and rivers

compared to lentic ecosystems (Looman et al., 2021), as does the shallower depth of streams compared to larger rivers (Raymond et al., 2012). For example, 51–100% of the CH_4 in lakes originating in sediments in deeper portions of lakes was oxidized in the water column, while only 24–40% of the CH_4 from shallower areas was oxidized due to the relatively shorter transit time (Bastviken et al., 2008).

We propose a conceptual model of CH_4 production, transport, oxidation, and emission unique to small streams, where CH_4 is emitted primarily through diffusive fluxes and oxidation is relatively limited (**Figure 5**). In this model, 1) CH_4 is primarily produced by methanogens in anoxic sediments. While bubble formation is generally limited in small streams, 2) some CH_4 is emitted *via* ebullition. The bulk of CH_4 production, plus inputs from the upslope catchment via groundwater flow, remains dissolved. In small streams, dissolved CH_4 3) diffuses through the sediments entering hyporheic flow paths, 4) although small amounts of vertical diffusion through the sediments may also occur. Hyporheic flow, which remains primarily anoxic in many systems, moves dissolved CH_4 back to the water column. We propose 5) oxidation primarily occurs near the sediment–water interface, where the redox gradient is greatest and the highest abundance of methanotrophs are detected. In the surface water, CH_4 oxidation is likely limited due to relatively high gas exchange rates. After oxidation, 6) the remaining dissolved CH_4 emitted via diffusion is enriched isotopically relative to that emitted via ebullition. The relative importance of each of these processes will depend on stream characteristics such as slope, water velocity, water depth, and sediment characteristics (i.e., depth, grain size) that influence the degree of hyporheic exchange, hyporheic residence time, redox conditions, and microbial activity. Some of the proposed mechanisms described in this conceptual model were not directly measured (e.g., hyporheic exchange) and require further exploration and testing. We specifically urge the examination of CH_4 cycling and transport within the benthic environment in relation to subsurface flow and redox conditions.

Lotic Ecosystems May Be Isotopically Enriched Relative to Lentic Systems

One important implication of this conceptual model is how streams are considered in global CH_4 models (Dean et al., 2018), particularly with regards to the isotopic values of emitted CH_4. For example, given both the imbalance of emission pathways in this study, as well as the isotopic values of ebullitive and diffusive gases, we calculate mean isotopic values of -55.7 ± 2.1‰ δ^{13}C-CH_4 and -260 ± 36‰ δD-CH_4 for the total CH_4 emitted. The δ^{13}C-CH_4 reflects relatively heavy values compared to global averages of approximately −62‰ δ^{13}C-CH_4 used for aquatic systems (Schwietzke et al., 2016). Considering streams and rivers account for roughly 8% of the global aquatic CH_4 budget (Rosentreter et al., 2021), this difference could be enough to alter the global isotopic signature used for aquatic CH_4 sources.

Very few studies which combine measurements of CH_4 isotopes and emission pathways are available in lotic systems, limiting comparison of our results (**Supplementary Table S2**). The most extensive data in rivers comes from the Amazon, where consideration of both ebullitive and diffusive emissions provides mean δ^{13}C-CH_4 values for total emitted CH_4 of −49.6‰ (Sawakuchi et al., 2016) and −38.4‰ (Sawakuchi et al., 2021). In these large tropical rivers, diffusion comprises a smaller fraction of the total emission budget, but a greater proportion of dissolved CH_4 is oxidized and thus the emitted CH_4 is more isotopically enriched. Our proposed conceptual model allows for these differences, where the higher efficiency of oxidation in larger rivers is enough to counter the higher prevalence of ebullition (Sawakuchi et al., 2021). Further, hyporheic flow is relatively less important in large rivers (Battin et al., 2008), potentially resulting in a greater proportion of CH_4 accumulating in bubbles in river sediments compared to streams. Even fewer studies exist with which to compare δD-CH_4 values. The streams in this study (−260‰) are δD-CH_4 enriched relative to Swedish lentic ecosystems (−310‰; Wik et al., 2020), which further supports the preferred emissions of oxidized CH_4 from streams. More closely comparing lotic δ^{13}C-CH_4 signatures to wetlands of similar latitudes further supports relative isotopic enrichment in lotic systems. Latitudinal patterns have been observed in aquatic δ^{13}C-CH_4 signatures, with enriched values typically characteristic of more tropical environments (Ganesan et al., 2018). The values measured in the present study are enriched relative to wetlands at a similar latitude (approx. −67‰; Fisher et al., 2017). Similarly, δ^{13}C-CH_4 values measured in fluvial portions of the Amazon River basin (Sawakuchi et al., 2016; Sawakuchi et al., 2021) are enriched relative to other tropical wetlands (approx. −60‰; Brownlow et al., 2017). There remains uncertainty in how much aquatic CH_4 emissions are contributing to variation in atmospheric δ^{13}C-CH_4 values (Turner et al., 2019), thus expanding measurement of aquatic CH_4 isotopes remains a valuable endeavor. While many additional measurements across ecosystems will be needed to confirm our proposed model, the possibility of a unique isotopic signature for streams and rivers is significant.

CONCLUSION

This study demonstrates how small streams can emit CH_4 at similar rates to other aquatic ecosystems on a per area basis, but with distinct isotopic signatures compared to lentic systems. The dominance of diffusive emissions to the total CH_4 efflux appears to be characteristic of small streams. Still, the presence of methanogens and methanotrophs highlight the active production and oxidation of CH_4 within stream ecosystems. While oxidation of dissolved CH_4 is limited by the relatively rapid transport of dissolved CH_4 out of the ecosystem, the dominance of diffusive emissions to the overall CH_4 emissions budget ensures the isotopic signature of emitted CH_4 is enriched relative to lentic waterbodies but similar to larger rivers. Consideration of a distinct lotic CH_4 isotopic signature may be critical for accurately incorporating streams and rivers in

regional and global atmospheric mixing CH_4 models. Our proposed conceptual model provides a framework on which to further examine CH_4 production and emissions from streams and how the relative importance of each process varies as a function of stream characteristics. At a global scale, concurrent examination of CH_4 production, oxidation, isotopic values, emissions, and associated microbial communities is needed to determine the generality of our observed patterns in streams. The resultant mechanistic perspectives are required to robustly understand the contribution of lotic ecosystems to the global CH_4 cycle.

DATA AVAILABILITY STATEMENT

The datasets presented in this study can be found in online repositories. The names of the repository/repositories and accession number(s) can be found below: genetic data: https://www.ncbi.nlm.nih.gov/, PRJNA757371. All other data: https://pie-lter.ecosystems.mbl.edu/data

AUTHOR CONTRIBUTIONS

All authors contributed significantly to this manuscript. AR, WW, AC, JM, RV, and JE designed the project. AR, AC, and PC led field sampling and laboratory analyses. CP and RV led isotopic analyses. AC, JM, and JE led microbial laboratory preparation. AR, CP, and AC led data analyses. AR led manuscript development with input from all authors.

FUNDING

Funding for this project comes from the Plum Island Ecosystems LTER NSF Award OCE-1637630, the National Aeronautics and Space Administration Interdisciplinary Science award NNX17AK10G, and the University of New Hampshire College of Life Sciences and Agriculture's Paine Fund. Partial funding was provided by the New Hampshire Agricultural Experiment Station. This is Scientific Contribution Number 2923. This work was supported by the USDA National Institute of Food and Agriculture Hatch Projects NH00659 and NH00667.

ACKNOWLEDGMENTS

We thank the members of the Water Systems Analysis Group and the Trace Gas Biogeochemistry Laboratory at the University of New Hampshire for their assistance in project and manuscript development. We thank Eliza Balch, Sarah Bower, and Christopher Whitney for their support in field work, and Apryl Perry for her assistance in laboratory analyses. We also thank Dr. Joanne Shorter from Aerodyne Research Inc. for access to the dual tunable infrared laser direct absorption spectrometer (TILDAS).

SUPPLEMENTARY MATERIAL

The Supplementary Material for this article can be found online at: https://www.frontiersin.org/articles/10.3389/fenvs.2021.791305/full#supplementary-material

Supplementary Figure S1 | Comparison of measured and estimated gas exchange rates (k_{600}) in the four streams. Gas exchange is measured directly by addition of Argon as a conservative gas tracer. Gas exchange is estimated using Equations 3 and 4 as described in the text. The 1:1 line is displayed as the dashed line.

Supplementary Table S1 | Mean relative abundance (%) of methanogen and methanotroph archaeal and bacterial orders in sediments of the four streams as classified using the SILVA database. Samples are from the surface sediments (0-2 cm depth) or subsurface (9-11 cm depth). nd, no detection. In the order Methanosarcinales the Methanosarcinaceae and Methanosaetaceae families are is classified as methanogens, and the Methanoperedenaceae family are classified as methanotrophs.

Supplementary Table S2 | Rates of diffusive and total CH_4 emissions from a variety of aquatic ecosystems, and $\delta^{13}C$-CH_4 and δD-CH_4 values of emitted CH_4. ^Emitted isotope values are inferred from source signatures and both diffusive and ebullitive emission pathway balances.

REFERENCES

Apprill, A., Mcnally, S., Parsons, R., and Weber, L. (2015). Minor Revision to V4 Region SSU rRNA 806R Gene Primer Greatly Increases Detection of SAR11 Bacterioplankton. *Aquat. Microb. Ecol.* 75, 129–137. doi:10.3354/ame01753

Atkins, M. L., Santos, I. R., and Maher, D. T. (2017). Seasonal Exports and Drivers of Dissolved Inorganic and Organic Carbon, Carbon Dioxide, Methane and δ13C Signatures in a Subtropical River Network. *Sci. Total Environ.* 575, 545–563. doi:10.1016/j.scitotenv.2016.09.020

Bastviken, D., Cole, J. J., Pace, M. L., and Van de Bogert, M. C. (2008). Fates of Methane from Different lake Habitats: Connecting Whole-lake Budgets and CH4emissions. *J. Geophys. Res.* 113, 1–13. doi:10.1029/2007JG000608

Bastviken, D., Ejlertsson, J., and Tranvik, L. (2002). Measurement of Methane Oxidation in Lakes: A Comparison of Methods. *Environ. Sci. Technol.* 36, 3354–3361. doi:10.1021/es010311p

Battin, T. J., Kaplan, L. A., Findlay, S., Hopkinson, C. S., Marti, E., Packman, A. I., et al. (2008). Biophysical Controls on Organic Carbon Fluxes in Fluvial Networks. *Nat. Geosci* 1, 95–100. doi:10.1038/ngeo101

Bishop, K., Buffam, I., Erlandsson, M., Fölster, J., Laudon, H., Seibert, J., et al. (2008). Aqua Incognita: the Unknown Headwaters. *Hydrol. Process.* 22, 1239–1242. doi:10.1002/hyp.7049

Boano, F., Harvey, J. W., Marion, A., Packman, A. I., Revelli, R., Ridolfi, R., et al. (2014). Hyporheic Flow and Transport Processes: Mechanisms, Models, and Bioghemical Implications. *Rev. Geophys.* 52, 1–77. doi:10.1002/2012RG000417.Received

Bodmer, P., Wilkinson, J., and Lorke, A. (2020). Sediment Properties Drive Spatial Variability of Potential Methane Production and Oxidation in Small Streams. *J. Geophys. Res. Biogeosci.* 125, 1–15. doi:10.1029/2019JG005213

Bolyen, E., Rideout, J. R., Dillon, M. R., Bokulich, N. A., Abnet, C., Al-Ghalith, G. A., et al. (2018). QIIME 2: reproducible, interactive, scalable, and extensible microbiome data science. *PeerJ* 6, e27295v2–354.

Brownlow, R., Lowry, D., Fisher, R. E., France, J. L., Lanoisellé, M., White, B., et al. (2017). Isotopic Ratios of Tropical Methane Emissions by Atmospheric Measurement. *Glob. Biogeochem. Cycles* 31, 1408–1419. doi:10.1002/2017GB005689

Butman, D., Striegl, R. G., Stackpoole, S. M., Del Giorgio, P. A., Prairie, Y. T., Pilcher, D. J., et al. (2018). Chapter 14: Inland Waters, in *Second State of the Carbon Cycle Report (SOCCR2): A Sustained Assessment Report*. Washington D. C: U.S. Global Change Research Program. doi:10.7930/SOCCR2.2018.Ch14

Callahan, B. J., McMurdie, P. J., Rosen, M. J., Han, A. W., Johnson, A. J. A., and Holmes, S. P. (2016). DADA2: High-Resolution Sample Inference from Illumina Amplicon Data. *Nat. Methods* 13, 581–583. doi:10.1038/nmeth.3869

Chanton, J., Chaser, L., Glasser, P., and Siegel, D. (2005). "Carbon and Hydrogen Isotopic Effects in Microbial, Methane from Terrestrial Environments," in *Stable Isotopes and Biosphere - Atmosphere Interactions* (San Diego, CA, USA: Elsevier Inc.), 85–105. doi:10.1016/B978-012088447-6/50006-4

Chanton, J. P., Fields, D., and Hines, M. E. (2006). Controls on the Hydrogen Isotopic Composition of Biogenic Methane from High-Latitude Terrestrial Wetlands. *J. Geophys. Res.* 111, 1–9. doi:10.1029/2005JG000134

Chanton, J. P., Martens, C. S., and Kelley, C. A. (1989). Gas Transport from Methane-Saturated, Tidal Freshwater and Wetland Sediments. *Limnol. Oceanogr.* 34, 807–819. doi:10.4319/lo.1989.34.5.0807

Chanton, J. P. (2005). The Effect of Gas Transport on the Isotope Signature of Methane in Wetlands. *Org. Geochem.* 36, 753–768. doi:10.1016/j.orggeochem.2004.10.007

Chowdhury, T. R., and Dick, R. P. (2013). Ecology of Aerobic Methanotrophs in Controlling Methane Fluxes from Wetlands. *Appl. Soil Ecol.* 65, 8–22. doi:10.1016/j.apsoil.2012.12.014

Conrad, R. (2005). Quantification of Methanogenic Pathways Using Stable Carbon Isotopic Signatures: A Review and a Proposal. *Org. Geochem.* 36, 739–752. doi:10.1016/j.orggeochem.2004.09.006

Conrad, R. (2009). The Global Methane Cycle: Recent Advances in Understanding the Microbial Processes Involved. *Environ. Microbiol. Rep.* 1, 285–292. doi:10.1111/j.1758-2229.2009.00038.x

Crawford, J. T., Stanley, E. H., Spawn, S. A., Finlay, J. C., Loken, L. C., and Striegl, R. G. (2014). Ebullitive Methane Emissions from Oxygenated Wetland Streams. *Glob. Change Biol.* 20, 3408–3422. doi:10.1111/gcb.12614

Crawford, J. T., Striegl, R. G., Wickland, K. P., Dornblaser, M. M., and Stanley, E. H. (2013). Emissions of Carbon Dioxide and Methane from a Headwater Stream Network of interior Alaska. *J. Geophys. Res. Biogeosci.* 118, 482–494. doi:10.1002/jgrg.20034

Dean, J. F., Middelburg, J. J., Röckmann, T., Aerts, R., Blauw, L. G., Egger, M., et al. (2018). Methane Feedbacks to the Global Climate System in a Warmer World. *Rev. Geophys.* 56, 207–250. doi:10.1002/2017RG000559

Doherty, S. J., Barbato, R. A., Grandy, A. S., Thomas, W. K., Monteux, S., Dorrepaal, E., et al. (2020). The Transition from Stochastic to Deterministic Bacterial Community Assembly during Permafrost Thaw Succession. *Front. Microbiol.* 11, 2923. doi:10.3389/fmicb.2020.596589

Earth System Research Laboratory, G. M. D. (2021). Carbon Cycle Gases Offshore Portsmouth, New Hampshire (Isles of Shoals), United States. Available at: https://gml.noaa.gov/dv/iadv/index.php?code=nha (Accessed July 1, 2021).

Ettwig, K. F., Zhu, B., Speth, D., Keltjens, J. T., Jetten, M. S. M., and Kartal, B. (2016). Archaea Catalyze Iron-dependent Anaerobic Oxidation of Methane. *Proc. Natl. Acad. Sci. USA* 113, 12792–12796. doi:10.1073/pnas.1609534113

Evans, P. N., Boyd, J. A., Leu, A. O., Woodcroft, B. J., Parks, D. H., Hugenholtz, P., et al. (2019). An Evolving View of Methane Metabolism in the Archaea. *Nat. Rev. Microbiol.* 17, 219–232. doi:10.1038/s41579-018-0136-7

Fisher, R. E., France, J. L., Lowry, D., Lanoisellé, M., Brownlow, R., Pyle, J. A., et al. (2017). Measurement of the 13 C Isotopic Signature of Methane Emissions from Northern European Wetlands. *Glob. Biogeochem. Cycles* 31, 605–623. doi:10.1002/2016GB005504

Frolking, S., and Crill, P. (1994). Climate Controls on Temporal Variability of Methane Flux from a Poor Fen in southeastern New Hampshire: Measurement and Modeling. *Glob. Biogeochem. Cycles* 8, 385–397. doi:10.1029/94gb01839

Ganesan, A. L., Stell, A. C., Gedney, N., Comyn-Platt, E., Hayman, G., Rigby, M., et al. (2018). Spatially Resolved Isotopic Source Signatures of Wetland Methane Emissions. *Geophys. Res. Lett.* 45, 3737–3745. doi:10.1002/2018GL077536

Glöckner, F. O., Yilmaz, P., Quast, C., Gerken, J., Beccati, A., Ciuprina, A., et al. (2017). 25 Years of Serving the Community with Ribosomal RNA Gene Reference Databases and Tools. *J. Biotechnol.* 261, 169–176. doi:10.1016/j.jbiotec.2017.06.1198

Hall, R. O., and Ulseth, A. J. (2020). Gas Exchange in Streams and Rivers. *WIREs Water* 7, 1–19. doi:10.1002/wat2.1391

Hampton, T. B., Zarnetske, J. P., Briggs, M. A., MahmoodPoor Dehkordy, F., Singha, K., Day-Lewis, F. D., et al. (2020). Experimental Shifts of Hydrologic Residence Time in a sandy Urban Stream Sediment-Water Interface Alter Nitrate Removal and Nitrous Oxide Fluxes. *Biogeochemistry* 149, 195–219. doi:10.1007/s10533-020-00674-7

Herreid, A. M., Wymore, A. S., Varner, R. K., Potter, J. D., and McDowell, W. H. (2020). Divergent Controls on Stream Greenhouse Gas Concentrations across a Land-Use Gradient. *Ecosystems* 24, 1299–1316. doi:10.1007/s10021-020-00584-7

Hojo, T., and Pearson, K. (1931). Distribution of the Median, Quartiles and Interquartile Distance in Samples from a Normal Population. *Biometrika* 23, 315–363. doi:10.2307/2332422

Holgerson, M. A., and Raymond, P. A. (2016). Large Contribution to Inland Water CO2 and CH4 Emissions from Very Small Ponds. *Nat. Geosci* 9, 222–226. doi:10.1038/ngeo2654

Hotchkiss, E. R., Hall Jr, R. O., Jr, Sponseller, R. A., Butman, D., Klaminder, J., Laudon, H., et al. (2015). Sources of and Processes Controlling CO2 Emissions Change with the Size of Streams and Rivers. *Nat. Geosci* 8, 696–699. doi:10.1038/ngeo2507

Hough, M., McClure, A., Bolduc, B., Dorrepaal, E., Saleska, S., Klepac-Ceraj, V., et al. (2020). Biotic and Environmental Drivers of Plant Microbiomes across a Permafrost Thaw Gradient. *Front. Microbiol.* 11, 1–18. doi:10.3389/fmicb.2020.00796

Knighton, D. (1998). *Fluvial Forms and Processes: A New Perspective*. First. New York, New York: Hodder Arnold.

Knox, M., Quay, P. D., and Wilbur, D. (1992). Kinetic Isotopic Fractionation during Air-Water Gas Transfer of O2, N2, CH4, and H2. *J. Geophys. Res.* 97, 20335. doi:10.1029/92jc00949

Leu, A. O., Cai, C., McIlroy, S. J., Southam, G., Orphan, V. J., Yuan, Z., et al. (2020). Anaerobic Methane Oxidation Coupled to Manganese Reduction by Members of the Methanoperedenaceae. *ISME J.* 14, 1030–1041. doi:10.1038/s41396-020-0590-x

Liu, L., Wilkinson, J., Koca, K., Buchmann, C., and Lorke, A. (2016). The Role of Sediment Structure in Gas Bubble Storage and Release. *J. Geophys. Res. Biogeosci.* 121, 1992–2005. doi:10.1002/2016JG003456

Looman, A., Maher, D. T., and Santos, I. R. (2021). Carbon Dioxide Hydrodynamics along a wetland-lake-stream-waterfall Continuum (Blue Mountains, Australia). *Sci. Total Environ.* 777, 146124. doi:10.1016/j.scitotenv.2021.146124

Magen, C., Lapham, L. L., Pohlman, J. W., Marshall, K., Bosman, S., Casso, M., et al. (2014). A Simple Headspace Equilibration Method for Measuring Dissolved Methane. *Limnol. Oceanogr.* 12, 637–650. doi:10.4319/lom.2014.12.637

MahmoodPoor Dehkordy, F., Briggs, M. A., Day-Lewis, F. D., Singha, K., Krajnovich, A., Hampton, T. B., et al. (2019). Multi-scale Preferential Flow Processes in an Urban Streambed under Variable Hydraulic Conditions. *J. Hydrol.* 573, 168–179. doi:10.1016/j.jhydrol.2019.03.022

Martin, M. (2011). Cutadapt Removes Adapter Sequences from High-Throughput Sequencing Reads. *EMBnet j.* 17, 10–2809. doi:10.14806/ej.17.1.200

Martiny, J. B. H., Jones, S. E., Lennon, J. T., and Martiny, A. C. (2015). Microbiomes in Light of Traits: A Phylogenetic Perspective. *Science* 350, 350. doi:10.1126/science.aac9323

Marx, A., Dusek, J., Jankovec, J., Sanda, M., Vogel, T., van Geldern, R., et al. (2017). A Review of CO2and Associated Carbon Dynamics in Headwater Streams: A Global Perspective. *Rev. Geophys.* 55, 560–585. doi:10.1002/2016RG000547

Mcmanus, J. B., Zahniser, M. S., and Nelson, D. D. (2011). Dual Quantum cascade Laser Trace Gas Instrument with Astigmatic Herriott Cell at High Pass Number. *Appl. Opt.* 50, A74–A85. doi:10.1364/AO.50.000A74

McManus, J. B., Zahniser, M. S., Nelson, D. D., Shorter, J. H., Herndon, S. C., Jervis, D., et al. (2015). Recent Progress in Laser-Based Trace Gas Instruments: Performance and Noise Analysis. *Appl. Phys. B* 119, 203–218. doi:10.1007/s00340-015-6033-0

Morse, N. B., and Wollheim, W. M. (2014). Climate Variability Masks the Impacts of Land Use Change on Nutrient export in a Suburbanizing Watershed. *Biogeochemistry* 121, 45–59. doi:10.1007/s10533-014-9998-6

Nelson, A. R., Sawyer, A. H., Gabor, R. S., Saup, C. M., Bryant, S. R., Harris, K. D., et al. (2019). Heterogeneity in Hyporheic Flow, Pore Water Chemistry, and Microbial Community Composition in an alpine Streambed. *J. Geophys. Res. Biogeosci.* 124, 3465–3478. doi:10.1029/2019JG005226

Oliver, J. D. (2005). The Viable but Nonculturable State in Bacteria. *J. Microbiol.* 43 Spec No, 93–100.

Packman, A. I., and Salehin, M. (2003). Relative Roles of Stream Flow and Sedimentary Conditions in Controlling Hyporheic Exchange. *Hydrobiologia* 494, 291–297. doi:10.1023/A:1025403424063

Parada, A. E., Needham, D. M., and Fuhrman, J. A. (2016). Every Base Matters: Assessing Small Subunit rRNA Primers for marine Microbiomes with Mock Communities, Time Series and Global Field Samples. *Environ. Microbiol.* 18, 1403–1414. doi:10.1111/1462-2920.13023

Quast, C., Pruesse, E., Yilmaz, P., Gerken, J., Schweer, T., Yarza, P., et al. (2013). The SILVA Ribosomal RNA Gene Database Project: Improved Data Processing and Web-Based Tools. *Nucleic Acids Res.* 41, D590–D596. doi:10.1093/nar/gks1219

Raymond, P. A., Zappa, C. J., Butman, D., Bott, T. L., Potter, J., Mulholland, P., et al. (2012). Scaling the Gas Transfer Velocity and Hydraulic Geometry in Streams and Small Rivers. *Limnol. Oceanogr.* 2, 41–53. doi:10.1215/21573689-1597669

Ries, K. G., III, Newson, J. K., Smith, M. J., Guthrie, J. D., Steeves, P. A., Haluska, T. L., et al. (2017). StreamStats, Version 4. In U.S. Geological Survey Fact Sheet 2017–3046. doi:10.3133/fs20173046

Robison, A. L., Wollheim, W. M., Turek, B., Bova, C., Snay, C., and Varner, R. K. (2021). Spatial and Temporal Heterogeneity of Methane Ebullition in lowland Headwater Streams and the Impact on Sampling Design. *Limnol. Oceanogr.* 66, 4063–4076. doi:10.1002/lno.11943

Rosentreter, J. A., Borges, A. V., Deemer, B. R., Holgerson, M. A., Liu, S., Song, C., et al. (2021). Half of Global Methane Emissions Come from Highly Variable Aquatic Ecosystem Sources. *Nat. Geosci.* 14, 225–230. doi:10.1038/s41561-021-00715-2

Sanches, L. F., Guenet, B., Marinho, C. C., Barros, N., and de Assis Esteves, F. (2019). Global Regulation of Methane Emission from Natural Lakes. *Sci. Rep.* 9, 1–10. doi:10.1038/s41598-018-36519-5

Sanders, I. A., Heppell, C. M., Cotton, J. A., Wharton, G., Hildrew, A. G., Flowers, E. J., et al. (2007). Emission of Methane from Chalk Streams Has Potential Implications for Agricultural Practices. *Freshw. Biol* 52, 1176–1186. doi:10.1111/j.1365-2427.2007.01745.x

Saunois, M., Stavert, A., Poulter, B., Bousquet, P., Canadell, J., Jackson, R., et al. (2020). The Global Methane Budget 2000–2017. *Earth Syst. Sci. Data* 12, 1561–1623. doi:10.5194/essd-12-1561-2020

Sawakuchi, H. O., Bastviken, D., Enrich-prast, A., Ward, N. D., Camargo, P. B., and Richey, J. E. (2021). Low Diffusive Methane Emissions from the Main Channel of a Large Amazonian Run-Of-The-River Reservoir Attributed to High Methane Oxidation. *Front. Environ. Sci.* 9, 1–13. doi:10.3389/fenvs.2021.655455

Sawakuchi, H. O., Bastviken, D., Sawakuchi, A. O., Krusche, A. V., Ballester, M. V. R., and Richey, J. E. (2014). Methane Emissions from Amazonian Rivers and Their Contribution to the Global Methane Budget. *Glob. Change Biol.* 20, 2829–2840. doi:10.1111/gcb.12646

Sawakuchi, H. O., Bastviken, D., Sawakuchi, A. O., Ward, N. D., Borges, C. D., Tsai, S. M., et al. (2016). Oxidative Mitigation of Aquatic Methane Emissions in Large Amazonian Rivers. *Glob. Change Biol.* 22, 1075–1085. doi:10.1111/gcb.13169

Schwietzke, S., Sherwood, O. A., Bruhwiler, L. M. P., Miller, J. B., Etiope, G., Dlugokencky, E. J., et al. (2016). Upward Revision of Global Fossil Fuel Methane Emissions Based on Isotope Database. *Nature* 538, 88–91. doi:10.1038/nature19797

Shelley, F., Abdullahi, F., Grey, J., and Trimmer, M. (2015). Microbial Methane Cycling in the Bed of a Chalk River: Oxidation Has the Potential to Match Methanogenesis Enhanced by Warming. *Freshw. Biol.* 60, 150–160. doi:10.1111/fwb.12480

Shelley, F., Ings, N., Hildrew, A. G., Trimmer, M., and Grey, J. (2017). Bringing Methanotrophy in Rivers Out of the Shadows. *Limnol. Oceanogr.* 62, 2345–2359. doi:10.1002/lno.10569

Smith, G. J., and Wrighton, K. C. (2019). Metagenomic Approaches Unearth Methanotroph Phylogenetic and Metabolic Diversity. *Curr. Issues Mol. Biol.* 33, 57–84. doi:10.21775/cimb.033.057

Sobczak, W. V., and Findlay, S. (2002). Variation in Bioavailability of Dissolved Organic Carbon Among Stream Hyporheic Flowpaths. *Ecology* 83, 3194–3209. doi:10.1890/0012-9658(2002)083[3194:vibodo]2.0.co;2

Stanley, E. H., Casson, N. J., Christel, S. T., Crawford, J. T., Loken, L. C., and Oliver, S. K. (2016). The Ecology of Methane in Streams and Rivers: Patterns, Controls, and Global Significance. *Ecol. Monogr.* 86, 146–171. doi:10.1890/15-1027.1

Trimmer, M., Maanoja, S., Hildrew, A. G., Pretty, J. L., and Grey, J. (2010). Potential Carbon Fixation via Methane Oxidation in Well-Oxygenated River Bed Gravels. *Limnol. Oceanogr.* 55, 560–568. doi:10.4319/lo.2009.55.2.056010.4319/lo.2010.55.2.0560

Turner, A. J., Frankenberg, C., and Kort, E. A. (2019). Interpreting Contemporary Trends in Atmospheric Methane. *Proc. Natl. Acad. Sci. USA* 116, 2805–2813. doi:10.1073/pnas.1814297116

Tyler, S. C., Bilek, R. S., Sass, R. L., and Fisher, F. M. (1997). Methane Oxidation and Pathways of Production in a Texas Paddy Field Deduced from Measurements of Flux, δl3C, and δD of CH4. *Glob. Biogeochem. Cycles* 11, 323–348. doi:10.1029/97gb01624

Walters, W., Hyde, E. R., Berg-Lyons, D., Ackermann, G., Humphrey, G., Parada, A., et al. (2016). Improved Bacterial 16S rRNA Gene (V4 and V4-5) and Fungal Internal Transcribed Spacer Marker Gene Primers for Microbial Community Surveys. *mSystems* 1, 1–10. doi:10.1128/msystems.00009-15

Wang, D. T., Welander, P. V., and Ono, S. (2016). Fractionation of the Methane Isotopologues 13CH4, 12CH3D, and 13CH3D during Aerobic Oxidation of Methane by Methylococcus Capsulatus (Bath). *Geochimica et Cosmochimica Acta* 192, 186–202. doi:10.1016/j.gca.2016.07.031

Wang, G., Xia, X., Liu, S., Zhang, L., Zhang, S., Wang, J., et al. (2021). Intense Methane Ebullition from Urban Inland Waters and its Significant Contribution to Greenhouse Gas Emissions. *Water Res.* 189, 116654. doi:10.1016/j.watres.2020.116654

Whiticar, M. J. (1999). Carbon and Hydrogen Isotope Systematics of Bacterial Formation and Oxidation of Methane. *Chem. Geology.* 161, 291–314. doi:10.1016/S0009-2541(99)00092-3

Wik, M., Johnson, J. E., Crill, P. M., DeStasio, J. P., Erickson, L., Halloran, M. J., et al. (2018). Sediment Characteristics and Methane Ebullition in Three Subarctic Lakes. *J. Geophys. Res. Biogeosci.* 123, 2399–2411. doi:10.1029/2017JG004298

Wik, M., Thornton, B. F., Bastviken, D., Uhlbäck, J., and Crill, P. M. (2016a). Biased Sampling of Methane Release from Northern Lakes: A Problem for Extrapolation. *Geophys. Res. Lett.* 43, 1256–1262. doi:10.1002/2015GL066501.Received

Wik, M., Thornton, B. F., Varner, R. K., McCalley, C., and Crill, P. M. (2020). Stable Methane Isotopologues from Northern Lakes Suggest that Ebullition Is Dominated by Sub-Lake Scale Processes. *J. Geophys. Res. Biogeosci.* 125, 1–13. doi:10.1029/2019JG005601

Wik, M., Varner, R. K., Anthony, K. W., MacIntyre, S., and Bastviken, D. (2016b). Climate-sensitive Northern Lakes and Ponds Are Critical Components of Methane Release. *Nat. Geosci* 9, 99–105. doi:10.1038/ngeo2578

Wollheim, W. M., Mulukutla, G. K., Cook, C., and Carey, R. O. (2017). Aquatic Nitrate Retention at River Network Scales across Flow Conditions Determined Using Nested *In Situ* Sensors. *Water Resour. Res.* 53, 9740–9756. doi:10.1002/2017WR020644

Wollheim, W. M., Pellerin, B. A., Vörösmarty, C. J., and Hopkinson, C. S. (2005). N Retention in Urbanizing Headwater Catchments. *Ecosystems* 8, 871–884. doi:10.1007/s10021-005-0178-3

Wollheim, W. M., Stewart, R. J., Aiken, G. R., Butler, K. D., Morse, N. B., and Salisbury, J. (2015). Removal of Terrestrial DOC in Aquatic Ecosystems of a Temperate River Network. *Geophys. Res. Lett.* 42, 6671–6679. doi:10.1002/2015GL064647

Wu, M. L., Ettwig, K. F., Jetten, M. S. M., Strous, M., Keltjens, J. T., and Niftrik, L. v. (2011). A New Intra-aerobic Metabolism in the Nitrite-dependent Anaerobic Methane-Oxidizing Bacterium Candidatus 'Methylomirabilis Oxyfera'. *Biochem. Soc. Trans.* 39, 243–248. doi:10.1042/BST0390243

Zhang, G., Yu, H., Fan, X., Ma, J., and Xu, H. (2016). Carbon Isotope Fractionation Reveals Distinct Process of CH4 Emission from Different Compartments of Paddy Ecosystem. *Sci. Rep.* 6, 1–10. doi:10.1038/srep27065

Zhang, L., Xia, X., Liu, S., Zhang, S., Li, S., Wang, J., et al. (2020). Significant Methane Ebullition from alpine Permafrost Rivers on the East Qinghai-Tibet Plateau. *Nat. Geosci.* 13, 349–354. doi:10.1038/s41561-020-0571-8

Conflict of Interest: The authors declare that the research was conducted in the absence of any commercial or financial relationships that could be construed as a potential conflict of interest.

Publisher's Note: All claims expressed in this article are solely those of the authors and do not necessarily represent those of their affiliated organizations, or those of the publisher, the editors, and the reviewers. Any product that may be evaluated in this article, or claim that may be made by its manufacturer, is not guaranteed or endorsed by the publisher.

Copyright © 2022 Robison, Wollheim, Perryman, Cotter, Mackay, Varner, Clarizia and Ernakovich. This is an open-access article distributed under the terms of the Creative Commons Attribution License (CC BY). The use, distribution or reproduction in other forums is permitted, provided the original author(s) and the copyright owner(s) are credited and that the original publication in this journal is cited, in accordance with accepted academic practice. No use, distribution or reproduction is permitted which does not comply with these terms.

frontiers in Environmental Science

ORIGINAL RESEARCH
published: 01 February 2022
doi: 10.3389/fenvs.2021.737379

Identifying Sources and Oxidation of Methane in Standing Dead Trees in Freshwater Forested Wetlands

Melinda Martinez[1†]*, *Marcelo Ardón*[1†] *and Mary Jane Carmichael*[2†]

[1]Department Forestry and Environmental Resources, North Carolina State University, Raleigh, NC, United States, [2]Departments of Biology and Environmental Studies, Hollins University, Roanoke, VA, United States

Wetlands are large sources of methane (CH_4), therefore it is vital to understand the pathways, mechanisms, and sources to anticipate future positive feedbacks to climate change. Plant mediated transport of CH_4 from sediment-borne gases is thought to be a major contributor in wetland ecosystems, though few studies have measured standing dead trees (snags). Snags are expected to become more common across the southeastern coast as marshes migrate into freshwater forested wetlands. In this study, our goal was to distinguish the main sources of CH_4 being emitted from snags, that is, from soil or *in situ* origin. The δ^2H and $\delta^{13}C$ stable isotopic composition from various sources was sampled for source determination. We measured CH_4 in various components: emissions from snag stem sides and the soil-atmosphere interface; and concentrations from snag trunk airspace at various heights from ground level (30, 60, and 120 cm), and soil porewater. Potential CH_4 production and oxidation in tree cores from two heights (60 and 120 cm) was also measured to examine the potential for CH_4 generation or oxidation in stems. We found that CH_4 concentrations inside snags (~10–200 ppm) were 2–50 times higher than atmospheric levels, and generally decreased with increasing stem height. The stable isotopes $\delta^{13}C$ and δ^2H showed an enrichment from porewater to soils and snag stems. $\delta^{13}C$ enrichment of CH_4 in snag stems suggests that CH_4 is being oxidized as it moves through snags. The tree core vial incubations showed that very few cores produced small amounts of CH_4 under anaerobic conditions (n = 5 out of 50), and very few cores oxidized CH_4 under more aerobic conditions (n = 5 out of 50). It is possible that a small amount of CH_4 is produced *in-situ* within the heartwood, but it is likely this depends on the density, porosity, and aeration of snags (degree of decay). Our results highlight that high concentrations of CH_4 can persist within the heartwood of snags long after initial decay, and that CH_4 emitted from snags is largely derived from deep wetland soils and oxidized during transport (*via* diffusion) throughout the stem of snags.

Keywords: methane (CH_4), oxidation, ghost forests, freshwater, wetlands

OPEN ACCESS

Edited by:
Hans-Peter Grossart, University of Potsdam, Germany

Reviewed by:
Yves T. Prairie, Université du Québec à Montréal, Canada
Karen Leah Prestegaard, University of Maryland, United States

***Correspondence:**
Melinda Martinez
mmarti13@ncsu.edu

***ORCID:**
Melinda Martinez
orcid.org/0000-0001-6652-9220
Marcelo Ardón
orcid.org/0000-0001-7275-2672
Mary Jane Carmichael
orcid.org/0000-0002-3454-6971

Specialty section:
This article was submitted to Biogeochemical Dynamics, a section of the journal Frontiers in Environmental Science

Received: *06 July 2021*
Accepted: *15 December 2021*
Published: *01 February 2022*

Citation:
Martinez M, Ardón M and Carmichael MJ (2022) Identifying Sources and Oxidation of Methane in Standing Dead Trees in Freshwater Forested Wetlands. Front. Environ. Sci. 9:737379. doi: 10.3389/fenvs.2021.737379

INTRODUCTION

Wetlands play a major role in the global carbon cycle, especially in methane (CH_4) emissions due to the anaerobic conditions created from standing water and saturated soils (Reddy and DeLaune, 2008). CH_4 is an important greenhouse gas because it has a sustained-flux global warming potential 45 times that of carbon dioxide (CO_2), averaged over 100 years (Neubauer and Megonigal, 2015).

CH_4 accounts for about 30% of all long-lived greenhouse gases (GHGs) globally, with a mean residence time of 9 years (Whalen, 2005). Wetlands are the largest natural source of CH_4, contributing as much as 20–30% of the global emissions (Reddy and DeLaune, 2008; Saunois et al., 2020). Freshwater wetlands tend to produce more CH_4 than saline wetlands, because of the abundant sulfate (SO_4^{2-}) found in seawater, which is a preferred electron acceptor and reduces methanogenesis (Reddy and DeLaune, 2008). In freshwater wetlands CH_4 is produced mostly through the acetoclastic pathway, using acetate as the substrate (Conrad, 2005). Once CH_4 is produced there are two relevant fates in wetland ecosystems: consumption by methanotrophs or flux to the atmosphere. The amount emitted to the atmosphere is ultimately a balance between CH_4 production and oxidation as it is transported through the soil-water-plant continuum (Reddy and DeLaune, 2008).

CH_4 pathways to the atmosphere include the soil-atmosphere interface, water-atmosphere interface, or plant-mediated transport to the atmosphere (Carmichael et al., 2014). Many studies have shown that both live and dead herbaceous vegetation contribute a significant amount of CH_4 to the atmosphere (Covey and Megonigal, 2019), and more recent studies have focused on the role of woody vegetation as a CH_4 pathway to the atmosphere (Carmichael et al., 2014; Barba et al., 2018; Martinez and Ardón, 2021). Studies from both upland and wetland ecosystems have shown tree stems to be sources of CH_4 to the atmosphere (Covey and Megonigal, 2019; Vargas and Barba, 2019). While upland ecosystems are generally thought of as CH_4 sinks, studies have shown CH_4 emitted through tree stems can be sourced from within the tree due to wood decomposition, or from deep soil layers and transported through the plant continuum (Megonigal and Guenther, 2008; Covey et al., 2012). Tree stem emissions have been found to be about 42.7 Tg yr^{-1} from the wetland Amazon basin alone, demonstrating the importance of tree stem surfaces (Pangala et al., 2017). While we know more about the source and sink dynamics of soil CH_4 production at broader scales, the biogeochemical pathways of production, oxidation, and pathways of tree stem CH_4 emissions remains poorly understood (Barba et al., 2018).

Fewer studies have focused on CH_4 emissions/pathways from standing dead trees (i.e., snags), which are becoming more common in freshwater forested wetlands across the southeastern United States (White and Kaplan, 2021). These areas with abundant snags are often called ghost forests and are striking features of climate change (Kirwan and Gedan, 2019). White and Kaplan (2021) estimate that 19,480 km^2 of coastal forested wetlands have transitioned to other habitat types from 1986 to 2016, some of which were ghost forests at some point during the transition. Snags have the potential to transport soil produced CH_4 through the root and plant tissue cells to the atmosphere, but CH_4 emitted could also be produced internally due to decomposition (Carmichael and Smith, 2016; Carmichael et al., 2017). As the climate changes, ghost forests are projected to expand in area (Kirwan and Gedan, 2019), and therefore could emit a substantial amount of greenhouse gases to the local and regional carbon cycle (Martinez and Ardón, 2021). It is important to understand the emissions of CH_4 from different pathways for better management in response to a changing climate (Barba et al., 2018).

Stable isotopes ratios (δ^2H-CH_4 and δ^{13}C-CH_4) are useful tools to attribute carbon from different sources and differentiate between gas transport mechanisms (Sanci and Panarello, 2015). The isotopic composition of CH_4 will depend on the metabolic pathway (CO_2 reduction vs. acetate fermentation), and potential oxidation by CH_4 oxidizing bacteria (Barba et al., 2018). Microbially mediated oxidation of CH_4 leaves residual CH_4 enriched (δ^{13}C-CH_4 is more positive). Acetoclastic CH_4 production has δ^{13}C ranging −65 to −50‰, and δ^2H from −400 to −250%, while hydrogenotrophic pathways result in more depleted δ^{13}C values ranging from −110 to −60‰, and δ^2H ranging from −250 to −170‰ (Hornibrook et al., 1997). δ^{13}C and δ^2H values of CH_4 can be altered by secondary processes in anaerobic environments (Hornibrook et al., 2000). Evaporation will lead to observable fractionation, yielding relatively light vapor and δ^2H-CH_4 rich water left behind (more positive) (Michener and Lajtha, 2007). A recent study showed an enrichment of δ^{13}C-CH_4 with increasing tree stem height, estimating that 33% of the CH_4 was oxidized from the lower stem towards the upper stem (Jeffrey et al., 2021). Stable isotopes have not been used to examine sources and potential transformations of CH_4 in snags.

Previously, we showed that snag stem CH_4 fluxes were not as predictable as soil CH_4 fluxes using environmental parameters such as water levels, salinity, and soil sulfate concentrations (Martinez and Ardón, 2021). The disconnect between soil and snag CH_4 drivers was thought to be driven by oxidation taking place within snags. Although soil CH_4 fluxes (5.9 ± 1.9 mg CH_4 m^{-2} hr^{-1}) were 20 times greater than snag CH_4 fluxes (0.3 mg CH_4 m^{-2} hr^{-1}), snag fluxes should still be taken into account given the cumulative GHGs ghost forests stands can potentially contribute.

Our goal in this study was to identify the main sources and pathways of CH_4 emitted from snags in ghost forests by quantifying CH_4 fluxes and concentrations. Stable isotopes, and lab incubation experiments were combined to examine if the CH_4 emitted through the snag stems was soil-derived or produced internally due to heartwood rot. We hypothesized that CH_4 emitted from snag stems was produced in soils, and snags served as conduits to the atmosphere due to the intricate network of open cells within decaying stems. We expected that most of the CH_4 in snags is formed by acetate cleavage (acetoclastic pathway as opposed to CO_2 reduction), therefore we used stable isotope data to examine the degree of oxidation. Lastly, we hypothesized that little CH_4 would be produced from snag tree cores under anaerobic conditions, and CH_4 could be oxidized under higher CH_4 concentrations and aerobic conditions.

MATERIALS AND METHODS

Study Site

Our study took place during the growing season in June and July 2019 on the Albemarle Pamlico Peninsula (APP), in eastern North Carolina. We selected five areas: Palmetto-Peartree

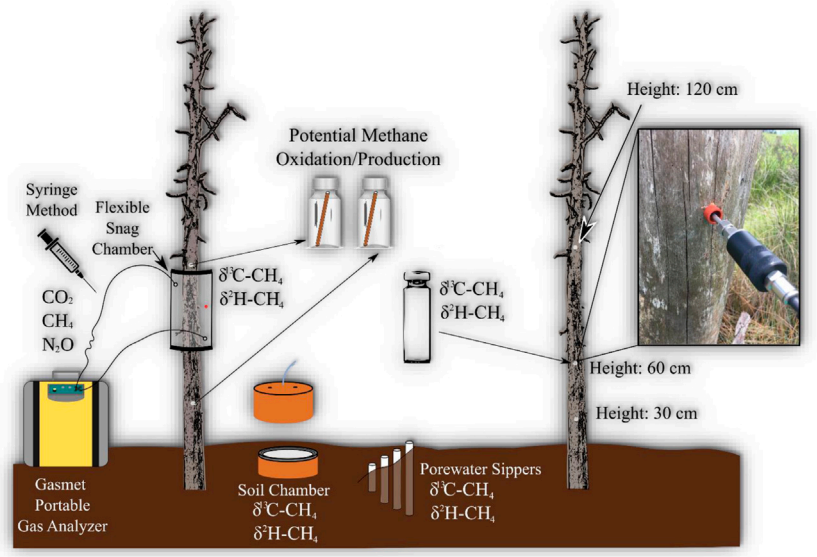


FIGURE 1 | Conceptual diagram of monitoring setup for each site. Gas samples were taken from snag and soil greenhouse gas chambers, and water samples from porewater for dissolved CH_4 concentrations. Red dot on tree chamber is rubber septum which is used when extracting samples with syringe. Snags were drilled at three heights to measure CH_4 concentrations within heartwood of snag. Tree cores were also taken from two heights (60 and 120 cm) for lab incubation experiments to measure potential CH_4 production and oxidation.

Preserve (PPP), Point Peter Rd within the *Alligator* River National Wildlife Refuge (PP), Swanquarter National Wildlife Refuge (SQ), Pocosin Lakes National Wildlife Refuge (PC), and Gull Rock State Game Lands (GR) (Martinez and Ardón, 2021). The coastal wetlands along the APP include non-riverine swamp forests, pocosins, and freshwater and brackish marshes. The APP has generally low salinity (one to seven parts per thousand) and is subject to frequent flooding from wind tides (Manda et al., 2014). More than 50% of the peninsula is within 1.5 m of mean sea level, making it highly vulnerable to sea level rise and saltwater intrusion (Moorhead and Brinson, 1995). The APP has been drained via extensive artificial canals and ditches to improve the agricultural value of the land (Manda et al., 2014), but these canals also allow saltwater to propagate further inland especially during storms, imperiling nearby vegetation communities (Bhattachan et al., 2019). Saltwater intrusion and increasing flooding events have increased the amount of forest die back in the region, creating extensive ghost forests (Smart et al., 2020).

Snag-Stem and Soil CH_4 Emissions

Five snags were selected at each site (n = 25) based on stability (i.e., intact and not at risk of falling). There are different stages of decay for standing dead trees, which can be classified from 1 to 5, with stage 1 being intact and recently deceased while stage 5 being close to falling over (Odion et al., 2011). The snags selected for all sites, except PC, were all pine trees with most of the bark removed classified as stages ranging from 1 to 3. The snags selected at PC were a mixture of pine and cypress trees with most of the bark removed, also ranging from 1 to 3 stages of decay. Snag and soil CH_4 concentrations were measured using clear semi-rigid chambers at various heights ranging from 60–70 cm from ground, depending on optimal sealing conditions (**Figure 1**). The snag-stem chambers were designed after Siegenthaler et al. (2016), which is a flexible type of chamber made from a clear, polycarbonate sheet. Soil chambers (30 cm diameter) were installed 1–2 m a way from snags. The soil chamber tops included a vent tube, internal fan (0.003 m^3/s; Jameco Electronics, Belmont, California, United States), and three sampling ports, two hose barbed connectors for portable gas analyzer tubing (Input/Output air sample) and air-tight tubing (12 inches) with a three-way stopcock for extra gas samples. The soil chambers were inserted 10 cm into the soil and left to stabilize for at least 1 week before taking measurements.

The CH_4 in snag and soils chambers was measured using two different methods: Gasmet portable gas analyzer (Gasmet Technologies, Finland) and the syringe method (**Figure 1**). The Gasmet is capable of analyzing a variety of greenhouse gases, but this study is focused only on CH_4. Chambers were attached for 10–20 min (10 min for snags and 20 for soils), and measuring gas concentrations every 20 s using the Gasmet, or 30–40 min measuring every 5 min using the syringe method. The syringe method was used at times when the Gasmet was not optimal due to either weather or battery failures. Gas samples using syringe method were stored in Exetainer vials (Labco–Lampeter, Wales, United Kingdom). Prior to field use, Exetainer vials were evacuated using a vacuum pump connected to a manifold and flushed repeatedly with ultra-pure N_2 gas. Gas samples were stored in vials and run within a 6-week period, which has been shown to maintain sample concentrations (Sturm et al., 2015). CH_4 gases were analyzed using an Agilent gas analyzer (7890 A GC system - Santa Clara, CA) equipped with a methanizer and Flame ionization Detector for CH_4 analysis. Detailed descriptions of the region, site, and methods can be found in Martinez and Ardón (2021).

CH_4 concentration inside snag heartwood were assessed following a similar protocol to Covey et al. (2012). A 1.27 cm diameter drill bit was used to drill to the center of the tree at three heights (30, 60, and 120 cm). After drilling, each hole was plugged using a rubber septum and pierced with a sampling wand connected to the Gasmet to sample for ~3 min. The air immediately outside the drilled hole was also sampled for comparison and to allow for the higher gas concentration to flow out of the tubing.

Gas samples for stable isotope analysis were sampled once at each site in June 2019 for GR and PP and July 2019 for PC, SQ, and PPP from inside the snag (n = 25) and soil (n = 25) chambers after chamber incubation using a gas tight syringe. Both snag and soil chambers were modified to sample with a syringe either through a rubber septum (snag chambers) or tubing using a three-way stopcock (soil chambers). Heartwood gas samples were also collected for stable isotope analysis with a syringe through a rubber septum 60 cm from ground (n = 25).

Porewater CH_4

Belowground porewater sippers were installed at 30 cm near three snags at each site. Porewater was analyzed to help provide insights into whether CH_4 emitted by stems was produced in soils or groundwater (Barba et al., 2018). Porewater was drawn after snag and soil gas sample collections and measured for δ^{13}C-CH_4, δ^2H-CH_4, and CH_4 concentration. CH_4 concentrations were measured using ultra-high purity N_2 using headspace equilibration methods (Sturm et al., 2015). Approximately 6 ml of porewater was injected into a pre-evacuated 12 ml exetainer. Liquid exetainer samples were stored upside down to prevent gas leakage and placed immediately in a cooler in the field. At the end of each field day collection, 6–7 ml of ultra-pure N_2 gas was added to provide over-pressure preventing access of atmospheric air during transport. Samples were wrapped in aluminum foil, stored upside down, and kept in cool refrigerator (4°C) until lab analysis. Samples were taken out of fridge 24 h prior to GC analysis to reach room temperature to allow equilibration of gases in headspace and water column. The volume of the porewater sample and headspace was determined by weighing the exetainer vial. The concentration of gas in the original water sample was determined by calculating the aqueous concentration in water and headspace after equilibration (Helton et al., 2014).

Porewater samples collected for isotopes δ^2H-CH_4 and δ^{13}C-CH_4 were acidified with HCl acid in the field to a pH < 2 and capped with no headspace bubbles. Two sets of porewater samples were collected per sipper for isotopes δ^2H-CH_4 and δ^{13}C-CH_4, which are analyzed separately. All gas and porewater samples for stable isotope measurements were shipped to UC Davis Stable Isotope Facility. There the stable isotope ratios of carbon (δ^{13}C) and hydrogen (δ^2H) in CH_4 were measured using a ThermoScientific Precon concentration unit interfaced to a ThermoScientific Delta V Plus isotope ratio mass spectrometer (ThermoScientific, Bremen, Germany).

Potential CH_4 Incubations

Snag tree cores were taken (June and July 2019) to provide estimates of CH_4 emissions by incubation to test the potential of wood to produce CH_4 (n = 100; PMP and PMO). Tree cores (5 mm diameter × 10–30 cm length) included the bark (if present), sapwood, and heartwood. Heartwood rot/wet wood conditions provide a conducive habitat for microbial CH_4 production, therefore potential CH_4 production (PMP) from incubations could suggest tree decomposition as an important source of CH_4 (Covey et al., 2012; Barba et al., 2018). Tree cores were taken at two heights (120 and 60 cm) from the five sites, to perform wood incubations to measure potential CH_4 production (n = 50, 25 per each height). Cores were placed in 120 ml serum vials and flushed with N_2 for 8–10 min. Gas samples were taken from the vial at 0, 12, 24, 48, and 72 h after incubating. A separate empty vial was flushed with N_2 as a field blank to measure potential background concentrations. Snag tree cores from GR and PP were run in June 2019 measuring at time points 0, 12, 24, and 48 h, while snag tree cores from PPP, SQ, and PC sites were run in July 2019 measuring at time points 0, 24, 48, and 72 h. The 12 h time point for July incubation was deemed unnecessary, and we extended the incubation to 72 h to determine if a longer incubation was needed to measure change in CH_4 concentration during treatments.

In addition to measuring potential CH_4 produced under anaerobic conditions, snag cores from similar heights (120 and 60 cm from ground) were incubated under higher concentrations of CH_4 to measure potential CH_4 oxidation (PMO) under aerobic conditions (n = 50). Vials were flushed with a gas standard mixture of CO_2, CH_4, and N_2O near ambient levels with a much higher CH_4 concentration. Snag cores from GR and PP were incubated at a CH_4 concentration of ~45 ppm, while snag cores from PPP, SQ, and PC were incubated at a CH_4 concentration of ~120 ppm. The difference in CH_4 concentrations was due to difficulties diluting Pure CH_4 (99.999%). CH_4 can potentially be oxidized by methanotrophs and/or nitrifying bacteria which have an affinity for CH_4 (Chan and Parkin, 2001). Gas samples were taken at similar intervals as the potential CH_4 production incubations. An empty vial flushed with the same gas standard mixture was measured as a field blank to assess potential gas leaks or air seepage inside the vial.

We calculated snag tree core CH_4 fluxes, represented as ng g^{-1} hr^{-1}, using the volume of the vial (minus the volume of the snag tree core) and the weight of the snag tree core as a substitute for area. Criteria were used to filter data using a minimum detectable concentration difference (MDCD) between the initial and final measurements. The MDCD in this study is based on the detection limits of the GC, which is 20% (or 0.2 ppm) for CH_4, so $|\text{Final}_{\text{CH4 Concentration}} - \text{Initial}_{\text{CH4 Concentration}}| > 0.2$ (meets MDCD criteria). Observations that did not meet the criteria were not used (marked as NA). The incubation fluxes were calculated using the HMR approach (*HMR* R package), which uses both linear and non-linear approaches (Pedersen et al., 2010). Only data with significant correlations (p < 0.1) were kept.

Statistics

Due to the lack of normality in the data, Kruskal-Wallis was used to test differences in stable isotopes (δ^{13}C-CH_4 and δ^2H-CH_4) among source types, and heartwood CH_4 concentrations among

TABLE 1 | Environmental conditions (mean ± SE) during sampling across all sites. GR and PP were sampled in June 2019 while PPP, PC and SQ were sampled in July 2019.Water level and salinity values were averaged from the 3 days leading up to sampling. Sulfate samples were taken from porewater sippers.

Site	Air temp (°C)	Soil temp (°C)	Water level (cm)	Salinity (ppt)	Sulfate (mg/L)
PPP	32.7 ± 0.63	24.4 ± 0.16	−5.44 ± 0.73	1.25 ± 0.05	2.39 ± 0.80
PC	34.5 ± 0.55	27.0 ± 0.37	5.95 ± 0.81	2.21 ± 0.01	7.13 ± 1.71
PP	30.0 ± 0.88	21.3 ± 0.38	−19.8 ± 0.61	2.45 ± 0.004	8.90 ± 2.64
GR	27.0 ± 1.12	23.4 ± 0.21	−8.5 ± 0.37	6.06 ± 0.01	125 ± 16.2
SQ	34.5 ± 0.66	26.5 ± 0.17	−8.23 ± 2.98	7.58 ± 0.05	245 ± 72

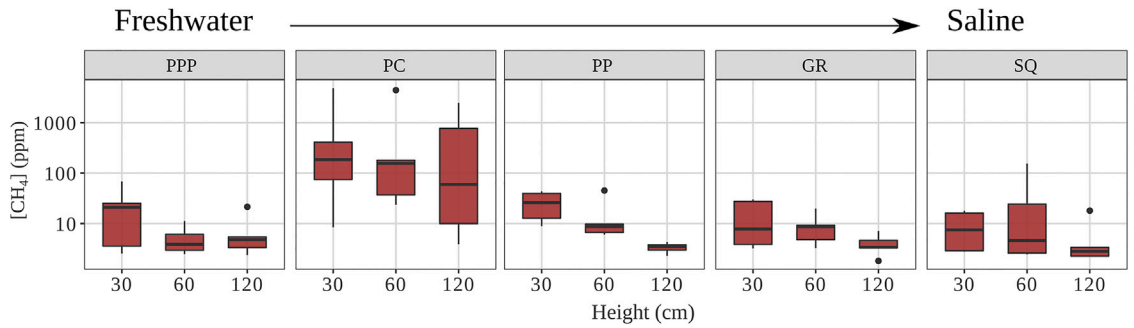


FIGURE 2 | Heartwood CH_4 concentrations for each site (from fresh to saline) and height (PPP—Palmetto Peartree, PC—Pocosin Lakes, PP—Point Peter, GR—Gull Rock, and SQ—Swanquarter). Solid line represents median, whiskers represent 5th and 95th percentiles, and dots are outliers (Note: *y*-axis is log scaled).

sites, and between heights (30, 60, and 120 cm). Dunn's multiple pairwise comparisons were then used for post-hoc analysis when Kruskal-Wallis showed significant differences, with a Bonferroni *p*-value adjustment ($p < 0.05$). Linear regression models were used to assess the relationships between stable isotopes and CH_4 concentrations with all source types (snag chambers, soil chambers, heartwood, and porewater), and also between CH_4 heartwood concentrations and stem height. CH_4 concentration data was log transformed due to lack of normality. All statistical analyses were performed in R program (R Core Team, 2020).

RESULTS

Salinity levels were the lowest at PPP (~1 ppt) and highest at SQ (~7 ppt), with PC, PP, and GR in between, increasing in salinity respectively (**Table 1**). Sulfate concentrations from porewater sippers followed similar patterns as salinity with the lowest concentration in PPP (2.39 mg/L) and highest in SQ (245 mg/L). Air temperature during the sampling period ranged from 27 to 34°C, while soil temperature ranged from 21 to 27°C (**Table 1**). Water levels during the sampling period were highest at PC (~6 cm above ground) and lowest at PP (~20 cm below ground).

Heartwood CH_4

Heartwood CH_4 concentrations differed among sites and between heights ($p < 0.01$, **Figure 2**). Concentrations from PC (mean ± SE: 904 ± 415 ppm) were an order of magnitude higher than all other sites, which were on average 13 ppm ($p < 0.01$, **Figure 2**). For all sites, CH_4 concentrations decreased with increasing height, with measurements from 30 cm being 2–4 times higher than

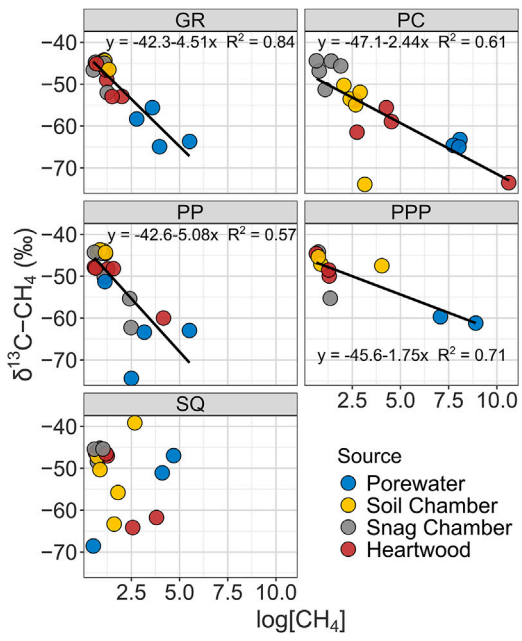


FIGURE 3 | Linear regressions showing relationship between $\delta^{13}C$-CH_4 stable isotopic values with CH_4 concentrations from various sources by study sites. Note all CH_4 concentrations were log transformed.

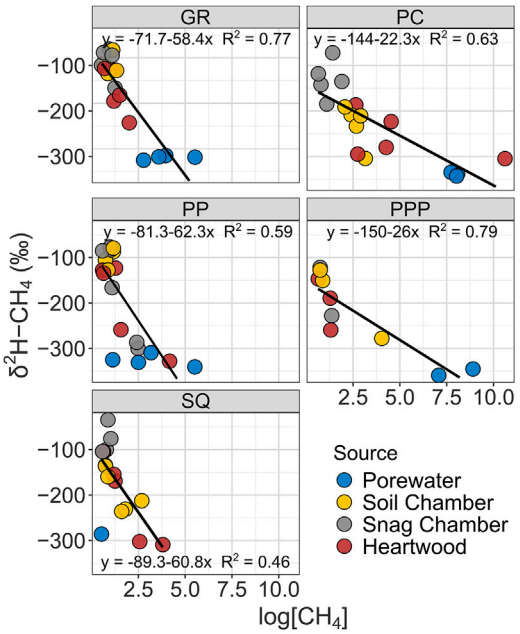


FIGURE 4 | Linear regressions showing relationship between δ^2H-CH_4 stable isotopic values with CH_4 concentrations from various sources by study sites. Note all CH_4 concentrations were log transformed.

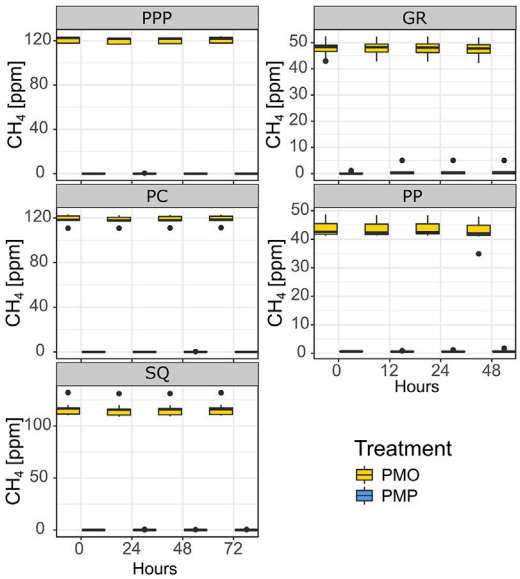


FIGURE 5 | Snag tree core (both heights combined) CH_4 concentrations during incubation experiments. Potential Methane Oxidation—PMO; Potential Methane Production—PMP. GR and PP were incubated in June while PPP, PC, and SQ were incubated in July. Solid line represents median, whiskers represent 5th and 95th percentiles.

measurements from 120 cm (p = 0.01). The linear regression model for CH_4 concentration (log transformed) by height for all sites combined (**Eq. 1**) was significant (p < 0.01) although explained a small amount of variance (r^2=0.04).

$$f(\mathbf{CH_4\ (ppm)}) = -\mathbf{0.01} \times \mathbf{Height\ (cm)} + \mathbf{3.34} \qquad (1)$$

Stable Isotopes

The δ^{13}C-CH_4 value of CH_4 ranged from −74 to −39‰, while δ^2H-CH_4 ranged from -327 to -34‰. Both δ^{13}C-CH_4 and δ^2H-CH_4 stable isotopic values became more enriched (more positive) from porewater < heartwood < soil chamber < snag chamber (**Figures 3**, **4**). Porewater δ^{13}C-CH_4 (mean: −60 ± 1.7‰) and δ^2H-CH_4 (−327 ± 4.8‰) were more depleted than soil chamber, heartwood, and snag chamber values (p < 0.1) (**Figures 3**, **4**). Soil chamber δ^{13}C-CH_4 values (−48 ± 1.5‰) were not significantly different from snag chamber (−47.7 ± 0.9‰; p = 1.0) or heartwood values (-52.2 ± 1.5‰; p = 0.13), but snag chamber values were more enriched than heartwood (p = 0.06). Similarly, soil chamber δ^2H-CH_4 values (−168 ± 14‰) were also within the range of snag chambers (−132 ± 12‰; p = 0.70), and heartwood (−209 ± 14‰; p = 0.53) values, but heartwood values were more depleted than snag chamber values (p = 0.006). Soil chamber δ^{13}C-CH_4 ranged from −73 to −39‰ while δ^2H-CH_4 ranged from -304 to -34‰. Heartwood δ^{13}C-CH_4 ranged from −73 to −44‰, while δ^2H-CH_4 ranged from −327 to −105‰. Overall, there was enrichment in isotopic signature in both δ^{13}C and δ^2H for all source types with decreasing CH_4 concentrations across all sites (**Figures 3**, **4**), except for δ^{13}C from SQ.

Potential CH_4 Incubations

CH_4 concentrations in snag tree core incubations changed very little over time (**Figure 5**). The overall number of snag tree incubation cores that had a measurable flux was 10 out of 100 cores taken. From the measurable fluxes, 5 were from the potential CH_4 oxidation (PMO) treatment, while the other five were from the potential CH_4 production (PMP) treatment (**Figure 5**). The highest CH_4 flux within the PMP treatment was 2.12 ng g^{-1} hr^{-1} for cores 60 cm from ground, while the smallest increase was 0.35 ng g^{-1} hr^{-1} for cores 120 cm from ground. One core from 120 cm height produced a small amount of CH_4 under PMO conditions, 0.5 ng g^{-1} hr^{-1}. The highest oxidized CH_4 within the PMO treatment was -2.5 ng g^{-1} hr^{-1} from 120 cm height core. The sample size was too low to perform any statistical analysis on the incubation flux calculations.

DISCUSSION

Our main goal was to determine the main source of CH_4 found and emitted from snags, and predicted that it was produced in the soil and transported up the stem. We found three lines of evidence to support this hypothesis: 1) there was a decrease in CH_4 concentrations with increasing stem height, 2) the isotopic composition of CH_4 within snags was more enriched in snags relative to porewater, and 3) very little CH_4 was produced or consumed when tree cores were incubated under anaerobic and aerobic conditions, respectively. As expected, most of the CH_4 from snag stems, soil, and porewater was produced through the acetoclastic pathway based on the isotopic signature (δ^{13}C: −45 to

−60‰). Our results show that high concentrations of CH_4 can persist within the heartwood of snags long after initial decay (stage 1) (Odion et al., 2011), and undergo oxidation before being emitted through the stem. The stable isotopes showed enrichment of both δ^{13}C-CH_4 and δ^2H-CH_4 from porewater, to heartwood, to snag chamber indicating that CH_4 was being oxidized throughout this pathway. Although it is important to note that we did not sample water from the various locations, so while the δ^2H-CH_4 pattern is consistent with the δ^{13}C-CH_4 suggesting oxidation, we cannot rule out other water sources. The tree core vial incubations indicated that small amounts of CH_4 can be produced under anaerobic conditions, about 2.12 ng g^{-1} hr^{-1}, but also oxidized under higher CH_4 concentrations (−2.5 ng g^{-1} hr^{-1}). Based on these results, the CH_4 emitted from snags is largely derived from the soil, and progressively oxidized as it passes throughout the stem. It is possible that a small amount of CH_4 is produced *in situ* within the heartwood, but it is likely this depends on the density, porosity, and aeration status of snags (degree of decay and water content). A recent study in forested wetlands showed that gas diffusion barriers may be what ultimately determines the magnitude of stem CH_4 emissions, which in the case of snags is porosity from decay and wood moisture content (Norwood et al., 2021). Overall, our results are consistent with the hypothesis that CH_4 is primarily produced in soils, and is oxidized as it moves along the soil-stem-atmosphere pathway.

Heartwood CH_4

CH_4 concentrations in heartwood varied across the sites. The CH_4 concentrations at PC were higher (904 ± 415 ppm) because there was standing water year-round, unlike all other sites (**Figure 2**; **Table 1**). When drilling into the heartwood at PC, some snags had a small stream of dripping water from within the tree (*personal observation*). The high moisture (and likely low oxygen levels) within the snags were conducive to CH_4 production, which would explain why their concentrations were so much higher than all other sites. The mean heartwood CH_4 concentration for the other sites (~13 ppm) were below those found in snags from a similar region within the APP (100 ppm) (Carmichael et al., 2017). The difference between snags from the Carmichael et al. (2017) study and ours could be due to site differences similar to PC within our own study. The snags from Carmichael et al. (2017) were in standing water year-round.

There was a gradual decrease in CH_4 concentration with increasing stem height (**Figure 2**), which has been found in other studies when measuring heartwood CH_4 concentrations in live and dead trees (Covey et al., 2016; Carmichael et al., 2017), but this decrease also affects tree stem CH_4 fluxes (Pangala et al., 2017; Jeffrey et al., 2019). The decrease in heartwood CH_4 is likely due to distance from source (CH_4 originating from within soils) and increasing oxidation with increasing stem height, which is also why tree-stem CH_4 flux would be affected (Pangala et al., 2017; Jeffrey et al., 2019). Using a linear regression model, we calculated that CH_4 concentrations inside the heartwood would decrease to 0 near 3.34 m (**Eq. 1**). Snags across the study sites ranged in height from 3 to 15 m. Our results suggest that snags can be important areas for CH_4 oxidation. It is important to note that measurements were taken during a relatively warm time of year (**Table 1**), so it is possible that during time periods when the air is cooler, there might be less CH_4 oxidation in the snags (King and Adamsen, 1992).

Stable Isotopes

Stable isotope data from all sites had similar patterns (enrichment from porewater < heartwood < soil chamber < snag chamber) with the exception of δ^{13}C from SQ (**Figure 3**). As we predicted most of the CH_4 produced from each source: snag chamber, heartwood, soil chamber, and porewater, was generated through the acetoclastic pathway which ranges from δ^{13}C ~ −65 to −50‰, and δ^2H ~ −400 to −250%, although a few samples (n = 4) were less than δ^{13}C −65‰ from porewater, soil, and heartwood samples. One sample from heartwood in PC had really high CH_4 concentrations (~40,000 ppm) and a very depleted δ^{13}C signature (−73‰), suggesting that hydrogenotrophic pathway might happen in stems standing in water. The δ^{13}C-CH_4 from various freshwater wetlands have been determined to be within the range of −86‰ to −31‰ (Bréas et al., 2001). A previous study conducted in freshwater wetlands concluded that dissolved CH_4 in porewater at ca. 25−cm depth had δ^2H values of ~ −340‰ or less (Hornibrook et al., 2000), which is also within the range of our study. Overall, the δ^{13}C and δ^2H values indicate that most of the CH_4 measured was produced through the acetate fermentation pathway which is common in most freshwater soils (Bréas et al., 2001).

Both δ^2H and δ^{13}C of porewater CH_4 were significantly depleted compared to all other sources (**Figures 3**, **4**). This would indicate that the CH_4 concentrations from porewater samples were closer in composition to that of the anoxic zone, or anoxic "microsites", leading to lower δ^2H and δ^{13}C (Sugimoto and Fujita, 2006). Porewater CH_4 concentrations are thought to be the best representation of CH_4 production, before any processes (i.e., diffusion and/oxidation) changes the stable isotope signature (Bréas et al., 2001), and therefore those values were used in this study to assess degree of oxidation in heartwood, snag chamber, and soil chamber. The end product of complete CH_4 oxidation is water vapor, which is also why δ^2H becomes enriched (heavier), although rates of hydrogen transfer due to organic matter degradation can also affect δ^2H (Bréas et al., 2001).

Stable isotopes from heartwood and soil chambers were more similar to each other and had wider ranges than snag chambers (**Figures 3**, **4**). Heartwood δ^{13}C and δ^2H were on average similar to the mean porewater δ^{13}C and δ^2H, indicating that the degree of oxidation was less than the pathway from porewater to soil chamber, although there was a wide range for both δ^{13}C and δ^2H (**Figures 3**, **4**). CH_4 oxidation occurred more in samples from snag chambers and were closest to ambient air stable isotopes (−46‰ and −114‰, δ^{13}C and δ^2H respectively), providing further evidence that is consistent with CH_4 continuing to be oxidized as it moves through the snags (**Figures 3**, **4**). A previous study also showed δ^{13}C-CH_4 enrichment with increasing stem height in a flooded forested ecosystem, suggesting oxidation during tree stem transport (Jeffrey et al., 2021). This same study also found methane

oxidizing bacteria (primarily *Methylomonas*) to be abundant within bark representing an important sink (Jeffrey et al., 2021). We have collected evidence of methanotrophs within snags in GR at ~60 cm from ground, although the abundance is not yet known (unpublished data; Carmichael et al. *In Prep*). The degree of oxidation in our study likely depends on the stage of decay of the snags. Later stages of decay (stages 4–5) likely having more porous stems (lower density) therefore increasing oxidation, whereas earlier stages of decay (stages 1–3) may continue emitting CH_4 due to moist tree stems which are more advantageous to methanogens, similar to the snags measured in this study.

The overall positive correlation between δ^2H and $\delta^{13}C$ of CH_4 in freshwater wetlands has also been shown in other studies (Sugimoto and Wada, 1995; Sugimoto and Fujita, 2006). Isotopic fractionation, in both $\delta^{13}C$ and δ^2H, has been shown to decrease with decreasing CH_4 concentrations, which is what we observed in all sites, except SQ (**Figures 3**, **4**) (Riveros-Iregui & King, 2008). It is possible that the higher salinities and thus higher SO_4^{2-} content in the sediments in SQ inhibited methanogenesis because SO_4^{2-} is a preferential electron acceptor in saturated sediments (Weston et al., 2006). If there is less CH_4 (substrate) in the sediment, then there will be less methanotrophy and less enrichment in $\delta^{13}C$ signal (Edmonds et al., 2009).

Potential CH_4 Incubations

Tree cores were incubated under two different simulated conditions to further investigate potential production and/or oxidation in snags internally (heartwood and sapwood). Very few ($n = 10$) cores exhibited a measurable difference in CH_4 from the beginning to the end of the incubation (**Figure 5**). This suggests that any amount of CH_4 that is present in the heartwood is largely soil derived. Under the PMP treatment, the highest measurable CH_4 flux occurred in cores taken from the base of the tree, while in the PMO treatment the highest measurable CH_4 oxidation flux occurred in cores from 120 cm from base of the tree. It is possible that there are more abundant methanogen communities closer to the base where conditions are more conductive for methanogenesis (i.e., higher moisture content, thus lower O_2 availability), but not as much as deep soil layers where majority of the CH_4 is derived. The fact that there was very little change in CH_4 concentrations throughout both treatments at both heights (PMP and PMO) further demonstrates that the majority of the CH_4 emitted from snag stems is largely soil derived (**Figure 5**). A study looking at CH_4 fluxes from stems in the Amazon basin, similarly found that very few of their tree core incubations produced CH_4, and interpreted those results as support for soil as the source of CH_4 (Pangala et al., 2017).

CONCLUSION

Analysis of greenhouse gas (GHG) fluxes from tree stems and snags is still an emerging field, but studies have shown that this pathway, previously unaccounted for in global budgets, is an important source to consider. Although fewer studies have measured the potential of standing dead trees (i.e. snags) to emit GHGs (Carmichael et al., 2017; Jeffrey et al., 2019; Martinez and Ardón, 2021), they have the potential to transport soil produced CH_4 through the plant tissue cells to the atmosphere, but CH_4 emitted could also be produced internally due to decomposition. Across the southeast coastline, many freshwater forested wetlands are rapidly transitioning to marshes due to increasing flooding and saltwater intrusion, leaving behind many snags, collectively referred to as ghost forests. CH_4 dynamics in ghost forests may be more complicated than previously thought due to the various sources and sinks. Our results show that: 1) the majority of CH_4 in soils of these ghost forests is formed through the acetoclastic pathway; 2) the majority of CH_4 being emitted from snags was likely produced deep in the soil, and 3) snags are important locations of CH_4 oxidation.

PERMISSION TO REUSE AND COPYRIGHT

We give permission for figures, tables, and images to be published under a Creative Commons CC-BY licence.

DATA AVAILABILITY STATEMENT

The datasets analyzed for this study can be found in Dryad Digital Repository https://datadryad.org/stash/dataset/doi:10.5061/dryad.xksn02vhg.

AUTHOR CONTRIBUTIONS

MM and MA conceived the study and research methods. Material preparation, data collection and data analysis were performed by MM. The first draft of the manuscript was written by MM with feedback and comments from MA and MC. All authors reviewed, edited, and approved the manuscript to its final form.

FUNDING

This work was funded by the NSF (DEB1713502) as well as North Carolina Sea Grant/SpaceGrant Fellowship (2019).

ACKNOWLEDGMENTS

We thank Destinee Parson, Colin Dail, Cam Phipps, Margaret Maynardie, Kelsey Morton, and Steve Anderson for field and lab assistance. We are also thankful for the Ardón lab for edits on this manuscript.

REFERENCES

Barba, J., Bradford, M. A., Brewer, P. E., Bruhn, D., Covey, K., Haren, J., et al. (2018). Methane Emissions from Tree Stems: a New Frontier in the Global Carbon Cycle. *New Phytol.* 222, 18–28. doi:10.1111/nph.15582

Bhattachan, A., Jurjonas, M. D., Morris, P. R., Taillie, P. J., Smart, L. S., Emanuel, R. E., et al. (2019). Linking Residential Saltwater Intrusion Risk Perceptions to Physical Exposure of Climate Change Impacts in Rural Coastal Communities of North Carolina. *Nat. Hazards* 97, 1277–1295. doi:10.1007/s11069-019-03706-0

Bréas, O., Guillou, C., Reniero, F., and Wada, E. (2001). The Global Methane Cycle: Isotopes and Mixing Ratios, Sources and Sinks. *Isotopes Environ. Health Stud.* 37, 257–379. doi:10.1080/10256010108033302

Carmichael, M. J., Bernhardt, E. S., Bräuer, S. L., and Smith, W. K. (2014). The Role of Vegetation in Methane Flux to the Atmosphere: Should Vegetation Be Included as a Distinct Category in the Global Methane Budget? *Biogeochemistry* 119, 1–24. doi:10.1007/s10533-014-9974-1

Carmichael, M. J., Helton, A. M., White, J. C., and Smith, W. K. (2017). Standing Dead Trees Are a Conduit for the Atmospheric Flux of CH4 and CO2 from Wetlands. *Wetlands* 38, 133–143. doi:10.1007/s13157-017-0963-8

Carmichael, M. J., and Smith, W. K. (2016). Standing Dead Trees: a Conduit for the Atmospheric Flux of Greenhouse Gases from Wetlands? *Wetlands* 36, 1183–1188. doi:10.1007/s13157-016-0845-5

Chan, A. S. K., and Parkin, T. B. (2001). Methane Oxidation and Production Activity in Soils from Natural and Agricultural Ecosystems. *J. Environ. Qual.* 30, 1896–1903. doi:10.2134/jeq2001.1896

Conrad, R. (2005). Quantification of Methanogenic Pathways Using Stable Carbon Isotopic Signatures: a Review and a Proposal. *Org. Geochem.* 36, 739–752. doi:10.1016/j.orggeochem.2004.09.006

Covey, K. R., de Mesquita, C. P. B., Oberle, B., Maynard, D. S., Bettigole, C., Crowther, T. W., et al. (2016). Greenhouse Trace Gases in deadwood. *Biogeochemistry* 130, 215–226. doi:10.1007/s10533-016-0253-1

Covey, K. R., and Megonigal, J. P. (2019). Methane Production and Emissions in Trees and Forests. *New Phytol.* 222, 35–51. doi:10.1111/nph.15624

Covey, K. R., Wood, S. A., Warren, R. J., Lee, X., and Bradford, M. A. (2012). Elevated Methane Concentrations in Trees of an upland forest. *Geophys. Res. Lett.* 39, L15705. doi:10.1029/2012GL052361

Edmonds, J. W., Weston, N. B., Joye, S. B., Mou, X., and Moran, M. A. (2009). Microbial Community Response to Seawater Amendment in Low-Salinity Tidal Sediments. *Microb. Ecol.* 58, 558–568. doi:10.1007/s00248-009-9556-2

Helton, A. M., Bernhardt, E. S., and Fedders, A. (2014). Biogeochemical Regime Shifts in Coastal Landscapes: the Contrasting Effects of Saltwater Incursion and Agricultural Pollution on Greenhouse Gas Emissions from a Freshwater Wetland. *Biogeochemistry* 120, 133–147. doi:10.1007/s10533-014-9986-x

Hornibrook, E. R. C., Longstaffe, F. J., and Fyfe, W. S. (2000). Evolution of Stable Carbon Isotope Compositions for Methane and Carbon Dioxide in Freshwater Wetlands and Other Anaerobic Environments. *Geochimica et Cosmochimica Acta* 64, 1013–1027. doi:10.1016/S0016-7037(99)00321-X

Hornibrook, E. R. C., Longstaffe, F. J., and Fyfe, W. S. (1997). Spatial Distribution of Microbial Methane Production Pathways in Temperate Zone Wetland Soils: Stable Carbon and Hydrogen Isotope Evidence. *Geochimica et Cosmochimica Acta* 61, 745–753. doi:10.1016/S0016-7037(96)00368-7

Jeffrey, L. C., Maher, D. T., Tait, D. R., Reading, M. J., Chiri, E., Greening, C., et al. (2021). Isotopic Evidence for Axial Tree Stem Methane Oxidation within Subtropical lowland Forests. *New Phytol.* 230, 2200–2212. doi:10.1111/nph.17343

Jeffrey, L. C., Reithmaier, G., Sippo, J. Z., Johnston, S. G., Tait, D. R., Harada, Y., et al. (2019). Are Methane Emissions from Mangrove Stems a Cryptic Carbon Loss Pathway? Insights from a Catastrophic forest Mortality. *New Phytol.* 224, 146–154. doi:10.1111/nph.15995

King, G. M., and Adamsen, A. P. S. (1992). Effects of Temperature on Methane Consumption in a Forest Soil and in Pure Cultures of the Methanotroph Methylomonas Rubra. *Appl. Environ. Microbiol.* 58, 2758–2763. doi:10.1128/aem.58.9.2758-2763.1992

Kirwan, M. L., and Gedan, K. B. (2019). Sea-level Driven Land Conversion and the Formation of Ghost Forests. *Nat. Clim. Chang.* 9, 450–457. doi:10.1038/s41558-019-0488-7

Manda, A. K., Giuliano, A. S., and Allen, T. R. (2014). Influence of Artificial Channels on the Source and Extent of saline Water Intrusion in the Wind Tide Dominated Wetlands of the Southern Albemarle Estuarine System (USA). *Environ. Earth Sci.* 71, 4409–4419. doi:10.1007/s12665-013-2834-9

Martinez, M., and Ardón, M. (2021). Drivers of Greenhouse Gas Emissions from Standing Dead Trees in Ghost Forests. *Biogeochemistry* 154, 471–488. doi:10.1007/s10533-021-00797-5

Megonigal, J. P., and Guenther, A. B. (2008). Methane Emissions from upland forest Soils and Vegetation. *Tree Physiol.* 28, 491–498. doi:10.1093/treephys/28.4.491

Moorhead, K. K., and Brinson, M. M. (1995). Response of Wetlands to Rising Sea Level in the Lower Coastal Plain of North Carolina. *Ecol. Appl.* 5, 261–271. doi:10.2307/1942068

Neubauer, S. C., and Megonigal, J. P. (2015). Moving beyond Global Warming Potentials to Quantify the Climatic Role of Ecosystems. *Ecosystems* 18, 1000–1013. doi:10.1007/s10021-015-9879-4

Norwood, M. J., Ward, N. D., McDowell, N. G., Myers-Pigg, A. N., Bond-Lamberty, B., Indivero, J., et al. (2021). Coastal Forest Seawater Exposure Increases Stem Methane Concentration. *J. Geophys. Res. Biogeosci* 126. doi:10.1029/2020JG005915

Odion, D. C., Sarr, D. A., Mohren, S., and Smith, S. (2011). *Monitoring Vegetation Composition, Structure and Function in the parks of the Klamath Network Parks*. Fort Collins, Colorado: National Park Service.

Pangala, S. R., Enrich-Prast, A., Basso, L. S., Peixoto, R. B., Bastviken, D., Hornibrook, E. R. C., et al. (2017). Large Emissions from Floodplain Trees Close the Amazon Methane Budget. *Nature* 552, 230–234. doi:10.1038/nature24639

Pedersen, A. R., Petersen, S. O., and Schelde, K. (2010). A Comprehensive Approach to Soil-Atmosphere Trace-Gas Flux Estimation with Static chambers. *Eur. J. Soil Sci.* 61, 888–902. doi:10.1111/j.1365-2389.2010.01291.x

R Core Team (2020). R: A Language and Environment for Statistical Computing. Vienna, Austria. Available at: http://www.R-project.org/.

Reddy, K. R., and DeLaune, R. D. (2008). *Biogeochemistry of Wetlands Science and Applications*. Boca Raton, FL: CRC Press.

R. H. Michener and K. Lajtha (Editors) (2007). *Stable Isotopes in Ecology and Environmental Science*. 2nd ed. (Malden, MA: Blackwell Pub).

Riveros-Iregui, D. A., and King, J. Y. (2008). Isotopic Evidence of Methane Oxidation across the Surface Water-Ground Water Interface. *Wetlands* 28, 928–937. doi:10.1672/07-191.1

Sanci, R., and Panarello, H. O. (2015). Carbon and Hydrogen Isotopes as Tracers of Methane Dynamic in Wetlands. *Ijg* 06, 720–728. doi:10.4236/ijg.2015.67058

Saunois, M., Stavert, A. R., Poulter, B., Bousquet, P., Canadell, J. G., Jackson, R. B., et al. (2020). The Global Methane Budget 2000–2017. *Earth Syst. Sci. Data* 12, 1561–1623. doi:10.5194/essd-12-1561-2020

Siegenthaler, A., Welch, B., Pangala, S. R., Peacock, M., and Gauci, V. (2016). Technical Note: Semi-rigid chambers for Methane Gas Flux Measurements on Tree Stems. *Biogeosciences* 13, 1197–1207. doi:10.5194/bg-13-1197-2016

Smart, L. S., Taillie, P. J., Poulter, B., Vukomanovic, J., Singh, K. K., Swenson, J. J., et al. (2020). Aboveground Carbon Loss Associated with the Spread of Ghost Forests as Sea Levels Rise. *Environ. Res. Lett.* 15, 104028. doi:10.1088/1748-9326/aba136

Sturm, K., Keller-Lehmann, B., Werner, U., Raj Sharma, K., Grinham, A. R., and Yuan, Z. (2015). Sampling Considerations and Assessment of Exetainer Usage for Measuring Dissolved and Gaseous Methane and Nitrous Oxide in Aquatic Systems. *Limnol. Oceanogr. Methods* 13, 375–390. doi:10.1002/lom3.10031

Sugimoto, A., and Fujita, N. (2006). Hydrogen Concentration and Stable Isotopic Composition of Methane in Bubble Gas Observed in a Natural Wetland. *Biogeochemistry* 81, 33–44. doi:10.1007/s10533-006-9028-4

Sugimoto, A., and Wada, E. (1995). Hydrogen Isotopic Composition of Bacterial Methane: CO2/Hz Reduction and Acetate Fermentation. *Geochimica et Cosmochimica Acta* 59, 1329–1337. doi:10.1016/0016-7037(95)00047-4

Vargas, R., and Barba, J. (2019). Greenhouse Gas Fluxes from Tree Stems. *Trends Plant Sci.* 24, 296–299. doi:10.1016/j.tplants.2019.02.005

Weston, N. B., Dixon, R. E., and Joye, S. B. (2006). Ramifications of Increased Salinity in Tidal Freshwater Sediments: Geochemistry and Microbial Pathways of Organic Matter Mineralization. *J. Geophys. Res.* 111, G01009. doi:10.1029/2005JG000071

Whalen, S. C. (2005). Biogeochemistry of Methane Exchange between Natural Wetlands and the Atmosphere. *ENVIRON. ENG. SCI.* 22, 22. doi:10.1089/ees.2005.22.73

White, E., and Kaplan, D. (2021). Identifying the Effects of Chronic Saltwater Intrusion in Coastal Floodplain Swamps Using Remote Sensing. *Remote Sensing Environ.* 258, 112385. doi:10.1016/j.rse.2021.112385

Conflict of Interest: The authors declare that the research was conducted in the absence of any commercial or financial relationships that could be construed as a potential conflict of interest.

Publisher's Note: All claims expressed in this article are solely those of the authors and do not necessarily represent those of their affiliated organizations, or those of the publisher, the editors and the reviewers. Any product that may be evaluated in this article, or claim that may be made by its manufacturer, is not guaranteed or endorsed by the publisher.

Copyright © 2022 Martinez, Ardón and Carmichael. This is an open-access article distributed under the terms of the Creative Commons Attribution License (CC BY). The use, distribution or reproduction in other forums is permitted, provided the original author(s) and the copyright owner(s) are credited and that the original publication in this journal is cited, in accordance with accepted academic practice. No use, distribution or reproduction is permitted which does not comply with these terms.

frontiers in Environmental Science

ORIGINAL RESEARCH
published: 10 March 2022
doi: 10.3389/fenvs.2022.857358

Redox Zone and Trophic State as Drivers of Methane-Oxidizing Bacterial Abundance and Community Structure in Lake Sediments

Sigrid van Grinsven[1]‡, Dimitri V. Meier[2‡], Anja Michel[2], Xingguo Han[2†], Carsten J. Schubert[1,2] and Mark A. Lever[2]**

[1]Eawag, Swiss Federal Institute of Aquatic Science and Technology, Department of Surface Waters, Research and Management, Kastanienbaum, Switzerland, [2]Institute of Biogeochemistry and Pollutant Dynamics, Swiss Federal Institute of Technology, Zurich, Switzerland

Eutrophication is expected to increase methane production in freshwater sediments worldwide over the coming decades. Methane-oxidizing bacteria (MOB) consume a significant fraction of this sedimentary methane, but the factors that control their distributions and activities are not understood. By combining genetic approaches (*pmo*A, 16S rRNA gene, metagenomics) with geochemical and sedimentological analyses, we investigate the role of trophic state, electron acceptors, oxygen (O_2) and methane fluxes, and potential methylotrophic partner organisms in driving the distributions, abundances, and community compositions of MOB across five lakes in central Switzerland. Although methane fluxes were highest in the eutrophic lakes, methanotrophic abundances peaked in oxic and anoxic sediments of an oligotrophic lake. In all lakes, Type I gammaproteobacterial Methylococcaceae dominated oxic and suboxic bottom water and surface sediments, showing strong correlations with abundances of putatively methylotrophic Methylophilaceae, whereas Type II alphaproteobacterial Methylocystaceae increased in deeper, anoxic sediment layers. Methanotrophic bacteria belonging to the NC10 phylum were predominantly detected within denitrifying sediment of the oligotrophic lake, matching their presumed nitrite-dependent lifestyle. While dominant MOB taxa at the genus-level follow vertical distributions of different aerobic and anaerobic respiration reactions, trophic state at the time of sediment deposition was the best predictor of MOB community structure at the operational taxonomic unit (OTU) level. Elevated methane fluxes combined with low MOB abundances in surface sediments of eutrophic lakes, moreover, support the notion that in eutrophic lakes a major portion of sedimentary methane bypasses the biological methane filter and escapes to overlying water.

Keywords: greenhouse gas emissions, MOB, methanotrophy, microbial community, eutrophication, oligotrophic, methane oxidation, *pmo*A

OPEN ACCESS

Edited by:
Yves T Prairie, Université du Québec à Montréal, Canada

Reviewed by:
Nils Risgaard-Petersen, Aarhus University, Denmark
Dirk de Beer, Max Planck Society, Germany

***Correspondence:**
Sigrid van Grinsven
sigrid.vangrinsven@eawag.ch
Mark A. Lever
mark.lever@usys.ethz.ch

***Present address:**
Xingguo Han, Federal Institute for Forest, Snow, and Landscape Research (WSL), Zürcherstrasse, Switzerland

These authors have contributed equally to this work and share first authorship

Specialty section:
This article was submitted to Biogeochemical Dynamics, a section of the journal Frontiers in Environmental Science

Received: *18 January 2022*
Accepted: *14 February 2022*
Published: *10 March 2022*

Citation:
van Grinsven S, Meier DV, Michel A, Han X, Schubert CJ and Lever MA (2022) Redox Zone and Trophic State as Drivers of Methane-Oxidizing Bacterial Abundance and Community Structure in Lake Sediments. Front. Environ. Sci. 10:857358. doi: 10.3389/fenvs.2022.857358

INTRODUCTION

Freshwater lakes account for 6–16% of natural emissions of the greenhouse gas methane (CH_4) to the atmosphere (Bastviken et al., 2004). Most of this methane is biologically produced in lake sediments. A fraction of this biologically produced methane escapes into the water column by diffusion, ebullition, and advective processes, and is subsequently emitted to the atmosphere (Tranvik et al., 2009; Bastviken et al., 2011; Dean et al., 2018). Methane emissions from lakes to the atmosphere are predicted to increase due to global temperature increases over the coming decades (Dean et al., 2018; Guo et al., 2020; Zhu et al., 2020).

Besides warming, anthropogenic increases in nutrient inputs that enhance primary production and organic carbon loading (eutrophication), can increase methane emissions from lakes (Beaulieu et al., 2019). Hereby enhanced supplies of algal organic carbon stimulate organic matter (OM) mineralization rates and lead to higher respiration rates of the electron acceptors dioxygen (O_2), nitrate (NO_3^-), sulfate (SO_4^{2-}), and metal oxides (Fe(III), Mn(IV)) in lake water and surface sediment. The more rapid depletion of these electron acceptors in lake sediments, combined with the higher OM availability, promotes microbial methane production (methanogenesis) (Fiskal et al., 2019) and results in increased sedimentary methane release under eutrophic conditions (Beaulieu et al., 2019; Sanches et al., 2019).

Most microbially produced methane in lake sediments is microbially oxidized in surface sediments before it can escape to the overlying water. Methane oxidation removes from ~50 to 99% of sedimentary methane, with removal efficiencies being highest in oligotrophic and lowest in eutrophic lakes (D'Ambrosio and Harrison, 2021). Previously, it was believed that lake sedimentary methanotrophy was performed exclusively by aerobic methane-oxidizing bacteria (MOB) within the Alpha- and Gammaproteobacteria (e.g., Auman et al., 2000; Frenzel et al., 1990; Pester et al., 2011; Reim et al., 2012; reviewed in; Knief, 2015). Since then it was shown that Bacteria of the genus *Methylomirabilis* (phylum: NC10) perform anaerobic methane oxidation coupled to nitrite (NO_2^-) reduction (denitrification; Ettwig et al., 2010; Deutzmann et al., 2014), while Archaea of the family Methanoperedenaceae (phylum: Euryarchaeota) couple the anaerobic oxidation of methane to the reduction of NO_3^-, Mn(IV) or Fe(III) (Ettwig et al., 2016; Leu et al., 2020).

Although historically considered to be obligately aerobic, MOB are widespread in O_2-depleted sediments, and in some cases even reach their highest gene copy numbers in anoxic subsurface layers (Rahalkar et al., 2009; Pester et al., 2011; Tsutsumi et al., 2011; He et al., 2021; Lyautey et al., 2021). Recently, members of the gammaproteobacterial genera *Methylobacter* and *Methylomonas* were shown to oxidize methane syntrophically with denitrifying methylotrophic Betaproteobacteria (Methylophilaceae). Hereby the MOB partially oxidize methane to methanol, H_2, or short-chain organic acids (e.g., formate, acetate), which the partner organisms subsequently oxidize to gain energy by denitrification (Beck et al., 2013; Kalyuzhnaya et al., 2013; Oshkin et al., 2014). In addition, several gammaproteobacterial genera (e.g., *Methylomonas*, *Methylobacter*, *Methylomicrobium*) have been shown to directly couple methane oxidation to denitrification under O_2-limiting conditions (Kits et al., 2015b; Cao et al., 2019; van Grinsven et al., 2020a). Recently, stimulation of bacterial methane oxidation rates by iron (III), manganese (IV), and humic compounds has been shown (Oswald et al., 2016; He et al., 2021; van Grinsven et al., 2021) and that certain strains of *Methylomonas* (Gammaproteobacteria) and *Methylosinus* (*Alphaproteobacteria*) can use ferrihydrite minerals as electron acceptors to oxidize methane (Zheng et al., 2020).

The community composition of MOB in lake sediments has so far mainly been studied by microbial enrichment and isolation methods (e.g., Auman et al., 2000; He et al., 2012; Danilova et al., 2016), and by cultivation-independent methods involving fluorescence-in-situ-hybridization (FISH; Rahalkar et al., 2009), sequencing of 16S rRNA genes (Fiskal et al., 2021; Pierangeli et al., 2021), and sequencing of catabolic functional genes (for reviews see (McDonald et al., 2008; Knief, 2015). Hereby *pmo*A, a functional gene that encodes the catalytic subunit of particulate methane monooxygenase (pMMO), an enzyme which performs the initial conversion of methane to methanol, has been widely targeted. The reasons are that *pmo*A is present in almost all known MOB (exception: Beijerinckiaceae), *pmo*A-based phylogenies agree largely with 16S rRNA gene-based phylogenies, and *pmo*A is sufficiently conserved to be suitable for polymerase chain reaction (PCR)-based quantification and sequencing methods.

Even though these methods have greatly advanced knowledge on the distributions of MOB in lake sediments, major knowledge gaps remain. A crucial knowledge gap concerns how increases in sedimentary methane production due to eutrophication and in response to warming impact the activity and community structure of MOB. Moreover, while changes in MOB community structure across oxic-anoxic interfaces are well-studied, little is known about MOB distributions in relation to anaerobic electron acceptors in deeper layers, where MOB often remain abundant. Vertical distributions of these electron acceptors in sediments could shape niches of MOB in ways similar to stratified eutrophic lakes, in which vertical zonations of MOB along redox and methane gradients have been documented (Mayr et al., 2020).

Here we investigate the influence of eutrophication and electron acceptor gradients on the activity, abundance, and community structure of MOB by analyzing sediment cores from five lakes in central Switzerland. These lakes have well-documented trophic histories and today range from oligotrophic (Lake Lucerne) to mesotrophic (Lake Zurich) to eutrophic (Lake Zug, Lake Baldegg, Lake Greifen) (Fiskal et al., 2019). By analyzing sedimentary records that span the entire history of anthropogenic eutrophication starting in the late 19th and early 20th century, we examine if (past) changes in lake trophic state are reflected in MOB community structure at the genus- and operational taxonomic unit (OTU)-level based on *pmo*A sequences today. Based on *pmoA* copy numbers as a proxy for MOB abundance and diffusive fluxes of O_2 and methane in surficial sediment, we investigate whether methane or O_2 availability are key drivers of MOB community size. Using

TABLE 1 | Depth intervals (in cm) of respiration reactions (average ±standard deviation of three stations) across the five lakes (based on **Figure 5** in Fiskal et al., 2019).

	Lake greifen (*eutrophic*)	Lake baldegg (*eutrophic*)	Lake zug (*eutrophic*)	Lake zurich (*mesotrophic*)	Lake lucerne (*oligotrophic*)
Aerobic	0–0.17 ± 0.03	0–0.08 ± 0.02	0–0.23 ± 0.03	0–0.22 ± 0.08	0–0.73 ± 0.25
Denitrification	0–2.5 ± 1.0	0–2.8 ± 1.2	0–7.7 ± 3.1	0–3.3 ± 1.4	0–9.0 ± 2.0
Sulfate reduction	0–5.8 ± 2.0	0–6.2 ± 3.3	0–11.7 ± 3.1	0–10.3 ± 1.2	0–11.0 ± 2.0
Mn(IV) reduction	0.3 ± 0.3–8.2 ± 4.9	0.3 ± 0.3–14 ± 7	0.5 ± 0.0–5.0 ± 0.0	0.3 ± 0.3–24 ± 15	0.7 ± 0.8–bottom
Fe(III) reduction	0.5 ± 0.0–*bottom*	*throughout*	0.5 ± 0.0–*bottom*	0.5 ± 0.0–*bottom*	0.8 ± 0.6–*bottom*
Methanogenesis	*throughout*	*throughout*	*throughout*	2.6 ± 2.4–*bottom*	3.0 ± 1.7–*bottom*

published vertical distributions of respiration reactions (Fiskal et al., 2019), we examine relationships between *in situ* distributions of respiration reactions and MOB abundances and community structure. Finally, we explore the influence of (past) trophic state and dominant respiration reactions on syntrophic partnerships of MOB and methylotrophic partner organisms based on correlations between MOB genera and OTUs from this study and published 16S rRNA gene sequences of methylotrophic bacteria from Han et al. (2020). Our results provide key insights into how eutrophication history and present-day electron acceptor distributions interact to control the community structure and activity of MOB in lake sediments.

MATERIALS AND METHODS

Site Descriptions and Lake Trophic Histories

This study is part of the larger research effort "Lake Eutrophication Impacts on Carbon Accumulations in Sediments" (LEICAS), in which the long-term consequences of eutrophication on sediment biogeochemistry, microbiology, and ecosystem ecology are investigated. LEICAS was initiated in 2016, when Lake Lucerne, Lake Zurich, Lake Zug, Lake Baldegg, and Lake Greifen were each sampled at three stations that covered a water depth gradient from shallow sublittoral to profundal sediments. Biogeochemical, organic geochemical, and 16S rRNA gene-based microbiological data on all stations were published previously by Fiskal et al. (2019, 2021*a*) and Han et al. (2020). An experimental study to investigate impacts of lake "oligotrophication" on sedimentary processes has also been published (Fiskal et al. 2021*b*). Depth profiles of respiration zones are summarized in **Table 1**.

The five lakes all experience seasonal changes in primary production, thermal stratification, and sedimentation (Teranes et al., 1999; Bürgi, 2000; Naeher et al., 2013), but differ in land use and anthropogenic eutrophication histories (Fiskal et al., 2019). Despite minor increases in total P concentrations in the 1960s and 1970s, Lake Lucerne has always remained oligotrophic. Lake Zurich became eutrophic, as evidenced by the development of permanently hypoxic conditions in its deep basin, around 1890 (Naeher et al., 2013), but has been mesotrophic since ~1980 due to improved wastewater management. The three eutrophic lakes became eutrophic at different times (Lake Baldegg: ~1870; Lake Greifen: ~1920; Lake Zug: ~1930) and have remained eutrophic since. The high rates of primary production in Lake Greifen, Lake Baldegg, and Lake Zug are sustained by the retention and recycling of P that was introduced in the 20th century. Despite artificial water column mixing and aeration (Lake Baldegg: since 1982/83; Lake Greifen; since 2009), Lake Baldegg experiences strong decreases in O_2 concentrations over the summer months, and Lake Greifen continues to develop seasonal hypoxia or anoxia below 10 m water depth from June-December (for details see Supplement of Fiskal et al., 2019, and references therein).

Sample Collection

In June and July 2016, three stations that differed in water depth were sampled in each lake (Lake Lucerne: 15, 24, 32 m; Lake Zurich: 25, 45, 137 m; Lake Zug: 25, 35, 50 m; Lake Baldegg: 21, 45, 66 m; Lake Greifen: 15, 24, 32 m) using 15-cm diameter gravity cores (UWITEC, AT). Bottom water temperatures at the time of sampling were 6–7°C at all stations except the shallow (9°C) and deep stations (5°C) in Lake Lucerne. All sites were bioturbated and contained benthic infaunal chironomids and/or oligochaetes (Fiskal et al., 2021a), except the deep, permanently hypoxic station in Lake Zurich. Sediment porewater for downstream measurements of dissolved electron acceptors (nitrate, sulfate, dissolved inorganic carbon) and respiration end products (Mn^{2+}, Fe^{2+}, ammonium) was sampled using rhizons (0.2 µm pore size, Rhizosphere) from a designated core with pre-drilled holes that were taped prior to coring. Solid-phase sediment samples for cell counts, DNA analyses, methane and total organic carbon (TOC) quantifications, and physical property determinations (porosity, density) were taken from an additional core using sterile cut-off syringes. Porewater cores were sampled in 1-cm depth intervals from 0–4 cm, 2-cm intervals from 4–20 cm, and 4-cm intervals from 36–40 cm. The same sampling resolution was applied during solid-phase sediment sampling, except that the top 0–2 cm were sampled at enhanced resolution (0.5 cm depth intervals). For further details on all sampling procedures, see Fiskal et al. (2019).

Additional cores were taken at each station for the measurement of O_2 concentration profiles in surface sediments using Clark-type microsensors (Unisense A/S, DK), macrofaunal

TABLE 2 | (A) *pmo*A primers used in this study. (B) Protocol for qPCR amplification using general *pmo*A primer pair (A189F–Mb661R). During the initial 10 cycles a touch-down PCR was used, during which the annealing temperature decreased in 1°C intervals. The same protocol was used for the NC10-pmoA29F/NC10-pmoA590R primer combination except that the annealing temperature was maintained at 62°C. (C) PCR amplification protocols for sequencing. The same protocol was used for both primer combinations.

(A)

***pmo*A primer name**	**Primer sequence (5′-3′)**	**References**
pmoA A189F	GGN GAC TGG GAC TTC TGG	Holmes et al. (1995)
pmoA_Mb661R	CCG GMG CAA CGT CYT TAC C	Costello and Lidstrom, (1999)
NC10-pmoA239F	GTT GAC GCC GAT CCT GTT	This study
NC10-pmoA590 R	GCA CAT ACC CAT CCC CAT	This study

(B)

	Time (min:s)	**Temperature (°C)**
1. Initial Activation	5:00	95
2. Denaturation	0:15	95
3. Annealing	0:30	*62 → 53*
4. Elongation	0:30	72
Steps 2–4 repeated 10x		
5. Denaturation	0:15	95
6. Annealing	0:30	*52*
7. Elongation	0:30	72
8. Acquisition	0:05	*85*
Steps 5–8 repeated 35x		
6. Denaturation	1:15	*95*
7. Acquisition	*continuous*	*55–95*
8. Cooling	∞	4

(C)

	Time (min:s)	**Temperature (°C)**
1. Initial Activation	5:00	95
2. Denaturation	0:45	95
3. Annealing	0:30	62
4. Elongation	1:00	72
Steps 2–4 repeated 30-50x		
6. Final elongation	5:00	72
8. Cooling	∞	4

community analyses, and sedimentological analyses (including Cs-137 and unsupported Pb-210 for sediment dating; further details and data in Fiskal et al. (2019, 2021*a*)).

Geochemical Analyses

O_2 and methane concentration profiles were published previously by Fiskal et al. (2019). Vertical concentration profiles of O_2 were measured using Clark-type microsensors (Unisense A/S) while methane concentrations were measured by gas chromatography using a flame-ionization detector (for details see Fiskal et al. (2019). Vertical distributions of respiration reactions, based on porewater-dissolved concentrations of O_2, nitrate, sulfate, Mn^{2+}, Fe^{2+} and CH_4, were also determined in Fiskal et al. (2019).

DNA Extraction

DNA was extracted from all solid-phase samples according to Lever et al. (2015). Sediments from Lake Zug, Lake Zurich and Lake Lucerne were extracted according to lysis protocol II. Due to high humic acid concentrations that interfered with post-extraction column-based DNA purification, sediments from Lake Greifen and Lake Baldegg were treated with an additional humic acid removal step prior to purification (lysis protocol III). For detailed protocols, see Han et al. (2020).

Quantification and Sequencing of *pmoA* Genes

*pmo*A was PCR-amplified using the general A189F - Mb661R *pmo*A primer combination (Holmes et al., 1995; Costello and Lidstrom, 1999) and the new NC10-pmoA239F–NC10-pmoA590R primer pair (**Table 2A**). The latter primer pair was specifically designed to amplify *pmo*A sequences of denitrifying methane-oxidizing *Methylomirabilales,* which are not amplified using the general primer pair but were detected in 16S rRNA gene libraries of the five lakes (Han et al., 2020). The general A189F - Mb661R combination was used both for quantitative PCR (qPCR), using complete *pmo*A gene sequences of *Methylococcus capsulatus* as qPCR standards, and for Illumina MiSeq-based community analyses.

For each of the 15 stations, qPCR analyses and sequencing were performed on 7 to 10 samples (**Supplementary Table S1**). Key sample targets included bottom water, sediments above and right below the oxic-anoxic transition in the upper few centimeters, samples from anoxic layers with denitrification and sulfate

reduction (typically to ≤10 cm), and samples from deeper layers where methanogenesis, iron (III) and manganese (IV) reduction were the only detectable respiration reactions (**Table 1**). qPCR was done with SYBR Green I Master Mix on a LightCycler 480 II (Roche Molecular Systems). Each 10-µL reaction mixture consisted of 5 µl Roche Light Cycler Master Mix containing SYBR™ Green, 0.5 µl of each 50 µM primer solution, 1 µl of 1 mg ml^{-1} bovine serum albumin, 2 µl of DNA extract, and 1 µl of molecular-grade water (for qPCR cycler protocol see **Table 2B**). The new NC10-pmoA239F–NC10-pmoA590R was only used for Illumina MiSeq-based community analyses but not quantification due to non-target PCR amplicons in several qPCR products.

*pmo*A sequencing libraries were produced according to the work flow of Han et al. (2020), which included an initial booster PCR to obtain similar amplicon concentrations across all samples, and was followed by tailed-primer PCRs (10 cycles) and index PCRs (8 cycles). For the 25-µl PCR reaction mixtures the hot start version of the TaKaRa Ex Taq DNA polymerase was used. Reaction mixtures consisted of 2.5 µl 10x Ex Taq Buffer, 2 µl dNTP solution (2.5 mM each), 0.75 µl of each primer mixture (10 µM concentrations), 2 µl of bovine serum albumin (1 mg ml^{-1}), 0.125 µl of TaKaRa Ex Taq HS, 2 µl of DNA extract, and 14.9 µl of molecular-grade water (for PCR protocols see **Table 2C**). Paired-end sequencing (600 cycles) was done using a MiSeq Personal Sequencer (Illumina, San Diego, CA).

Amplicon Sequence Data Processing

All DNA sequence data were processed according to the pipeline outlined in Han et al. (2020). Briefly, raw reads were quality-checked by FastQC, followed by read end trimming by seqtk. Trimmed reads were then merged into amplicons by flash (max mismatches density, 0.15) and primer sites removed by usearch (in-silico PCR). Quality filtering was done by prinseq (GC range, 30–70; Min Q mean, 20). OTUs were then clustered according to 97% similarity thresholds (proxy for species-level) to a final number of 927 representative sequences using the USEARCH otutab (), which was also used to remove chimeric sequences. OTU sequences were then used for phylogenetic and bioinformatic analyses.

*pmo*A Sequences From Lake Metagenomes

To identify potential blind spots or phylogenetic biases of the *pmo*A primer combinations used, we performed complementary *pmo*A analyses on lake sedimentary metagenomes. Metagenomes of DNA extracts from five sediment depths of the deepest station in each lake were sequenced at the Joint Genome Institute (JGI; Berkeley, CA, United States; **Supplementary Table S1**). Paired sequence reads were generated on an Illumina NovaSeq S4 sequencer in 2 × 150 bp mode. Assembly and annotation were performed by the standard automated pipeline of the JGI (see **Supplementary Material**) and loaded into the Integrated Microbial Genomes and Metagenomes (IMG/M) platform (Chen et al., 2021) for exploration and systematic gene search. Potential *pmoA* genes from all 25 metagenomes were identified by the AMO Pfam motif (PF02461) detected in the encoded proteins by the IMG annotation pipeline (Chen et al., 2021) resulting in 105 genes in total. The sequences were downloaded and dereplicated (100% nucleotide sequence identity) with Vsearch (v.2.14.1; Rognes et al., 2016) using standard settings, resulting in 81 unique sequences. *pmoA* genes were distinguished from similar *amoA* (ammonia monooxygenase subunit A genes) based on their placement in phylogenetic trees (see below).

*pmo*A Phylogenetic Analyses

Taxonomic assignments were performed using a newly constructed, comprehensive and up-to-date *pmo*A sequence alignment database in ARB (Ludwig et al., 2004). This database included published *pmo*A amplicon and metagenome sequences and was initially based on an alignment produced on a subset of sequences using ClustalW in SeaView. This gene data base has since been expanded to include >5,000 *pmo*A sequences in addition to representatives of *pmo*A-like RA21 and *pxm*A (putative copper-containing monooxygenase) and *amo*A gene clusters. In the process of database expansion, the overall alignment has been updated and optimized. All amplicon sequences obtained with the general *pmo*A and NC10-specific primer pairs and metagenomic *pmo*A sequences were added and aligned to the curated *pmo*A database. De-novo phylogenetic trees, calculated using ARB Neighbour-Joining with Jukes-Cantor Correction (1,000 bootstraps), were then used to taxonomically classify all *pmo*A OTUs to the genus-level. Tree calculations were based on a ~470-base pair region that corresponds to the amplified region of the A189F-Mb661R primer pair.

Sequence Annotations and Accession Numbers

All *pmo*A OTU taxonomic assignments are shown in **Supplementary Material S1**. Amplicon sequences are publicly accessible at the NCBI Sequence Read Archive (SRA) under Bioproject ID PRJNA785131. Samples used for metagenomes can be found under the ID Gs0142423 on JGI GOLD (https://gold.jgi.doe.gov/, Mukherjee et al., 2021). Metagenomic datasets are publicly available at the JGI genome portal (https://genome.jgi.doe.gov/portal/) under the proposal Id 504756 and at NCBI (PRJNA620348–PRJNA620356, PRJNA620360–PRJNA620364, PRJNA654670–PRJNA654680).

Data Visualizations and Statistical Analyses

Diversity and richness indices were calculated with the functions "diversity" and "specnumber" in the R-package vegan (v. 2.5–7 (Oksanen et al., 2020). Kruskal–Wallis tests, combined with Dunn's posthoc tests with Bonferroni P correction, were performed to check for significant differences in methane concentrations, *pmo*A copy numbers, and *pmo*A/16S rRNA gene ratios in relation to trophic state using R stats version 4.0.3 and the R-package FSA (Ogle et al., 2021). Non-parametric Kruskal–Wallis tests were used instead of One-way Analyses of Variance (ANOVA) due to non-normal data distributions. To test for significant relationships between MOB community composition and sediment depth, used as a

proxy for geochemical gradients, and trophic state at the time of sediment deposition, Permutational Multi-variate Analyses Of Variance (PERMANOVA) were performed on genus- and OTU-level community compositions. PERMANOVAs were performed in R with the adonis2 () function in vegan based on Bray-Curtis dissimilarities (9,999 permutations). An Analysis of Similarity (ANOSIM; Bray-Curtis, 9,999 permutations) was used to test for significant differences in MOB communities between individual trophic state categories (eutrophic, mesotrophic, oligotrophic) using the anosim () function in vegan. Non-linear Multi-Dimensional Scaling (NMDS) analyses based on Bray-Curtis dissimilarities (Beals, 1984) were performed using the 'metaMDS' function of vegan and used to examine community dissimilarities between samples. Similarity percentage (SIMPER) analyses with the 'simper' function (999 permutations) in vegan were used to identify genus-level taxa and OTUs that contribute significantly to community dissimilarities between sample categories (i.e., trophic state, respiration zone). To identify potential syntrophic interactions between methanotrophic and methylotrophic microorganisms, correlations between the abundances of dominant MOB taxa and OTUs and potentially methylotrophic bacteria were determined based on Spearman's rank correlation coefficients. The latter were calculated according to Lloréns-Rico et al. (2021) with the correlation. R script (https://github.com/raeslab/benchmark_microbiome_transformations/tree/master/scripts/, accessed on 3 July 2021).

All plots were generated with ggplot2 R-package (https://ggplot2.tidyverse.org; Wickham (2016)), basic R plotting functions, LibreOffice Calc, and Microsoft Excel.

Diffusive Fluxes of Methane and O_2

Diffusive porewater fluxes of methane and O_2 across the sediment-water interface were calculated from vertical concentration profiles using a one-dimensional reaction-transport model (Müller et al., 2003; equation 5) applying published diffusion coefficients (D_{O2} (5°C): 1.25×10^{-5} cm^2 s^{-1} (Müller et al., 2003); D_{CH4} (5°C): 9.5×10^{-6} cm^2 s^{-1} (Lerman, 1979)). An empirical formation factor F of 1.2 (Maerki et al., 2004) was used to correct for porosity and tortuosity of the sediment.

Thermodynamic Calculations

Standard Gibbs energies of potential aerobic and denitrifying methanotrophic reactions, and widespread, potentially competing aerobic organotrophic and lithotrophic reactions, were calculated based on ΔG_r° values published in Thauer *et al.* (1977). The range of *in situ* Gibbs energies (ΔG_r') of these reactions in lake sediments was calculated for a range of environmentally relevant educt and product concentrations according to the equation

$$\Delta G_r' = \Delta G_r^\circ + RT \ln Q_r$$

where R is the universal gas constant (0.008314 kJ mol^{-1} K^{-1}), T is standard temperature (298.15K), and Q_r is the reaction quotient. For further details, see **Table 5**.

RESULTS

Methane Concentration Profiles and Potential for Aerobic Methanotrophy

Porewater-dissolved methane concentrations increased with trophic state, with sediment depth, and in several cases with station water depth (Lake Zug, Lake Zurich, Lake Lucerne; **Figure 1A**). Eutrophic lakes (Lakes Greifen, Baldegg, and Zug) had higher methane concentrations than the oligotrophic Lake Lucerne ($p < 0.001$, Kruskal–Wallis test followed by a Dunn's post hoc test). The highly eutrophic Lake Greifen and Lake Baldegg individually also had higher methane concentrations than Lake Lucerne ($p < 0.05$, same test).

All stations in the eutrophic lakes and the hypoxic deep station in Lake Zurich displayed steep increases in methane concentrations from the sediment surface downward. This and the concave-down shapes of these concentration profiles indicate that net methane production sets in within the top 1 cm of sediment at these stations. These stations also had elevated methane concentrations all the way to the shallowest sampling interval (0–0.5 cm sediment depth). By contrast, methane concentrations at the middle and shallow stations in mesotrophic Lake Zurich and all stations in oligotrophic Lake Lucerne remained at lower levels (<0.5 mM) in the top cm. These stations only showed strong methane concentration increases, combined with downward concavity indicative of net methane production, below 2–4 cm.

Matching the methane concentration profiles, modeled methane fluxes increase with trophic state (**Figure 2A**; **Table 3**). The highest methane fluxes were detected at the deepest stations of all lakes except the year-round artificially aerated Lake Baldegg. By contrast dissolved O_2 fluxes into sediments did not change clearly with trophic state (**Figure 2B**). O_2 fluxes were consistently higher in eutrophic Lake Baldegg and Lake Zug compared to oligotrophic Lake Lucerne. The lowest O_2 fluxes were measured at the seasonally and permanently hypoxic deep stations of Lake Greifen and Lake Zurich, respectively. Ratios of methane to O_2 fluxes reflect the high methane fluxes and low O_2 fluxes at these two deep hypoxic stations (**Figure 2C**), where six times more (Lake Greifen) or equal amounts of methane (Lake Zurich) diffuse to the sediment surface as can be consumed by aerobic methane oxidation under the standard 1:2 stoichiometry of methane to O_2. This is not the case for the remaining 13 stations, where – assuming 1:2 stoichiometry – at most 6–30% of O_2 consumption can be accounted for by aerobic methane oxidation.

Trends in Absolute and Relative Abundances of MOB

Copy numbers of *pmo*A, which we used as a proxy for MOB abundance, generally ranged from 10^4 to 10^6 g^{-1} wet sediment and had their highest values in the top 10 cm (**Figure 1B**). Hereby, pmoA copy numbers varied between and within stations, but did not show consistent trends in relation to redox conditions or sediment depth. Consequently, *pmo*A

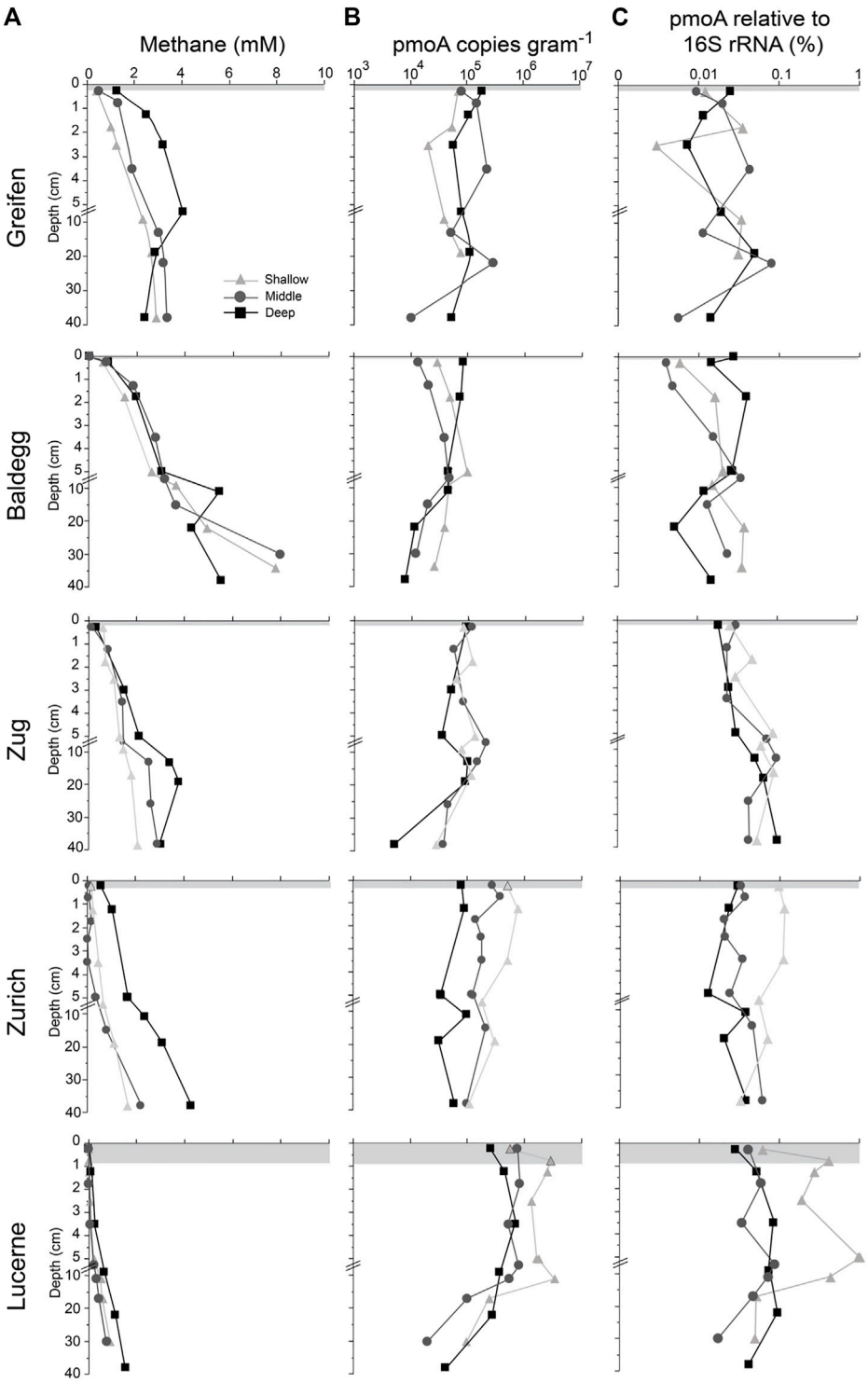


FIGURE 1 | Methane, O_2 and MOB dynamics in sediments of the three lakes. **(A)** methane concentrations profiles and depth of O_2 penetration (gray area below sediment surface). **(B)** Absolute abundances of *pmoA* as determined by qPCR. **(C)** Relative contribution of MOB to the total microbial community, estimated from ratios of *pmoA* to total 16S rRNA gene copies. Note the log-scale in (B) and (C).

copy numbers did not change significantly from oxic sediments to the shallowest samples below the depth of O_2 depletion ($p > 0.05$, here and following paragraphs: Kruskal–Wallis with Dunn's post hoc test). Furthermore, several sites had bimodal distributions, with surface and subsurface sedimentary *pmo*A copy number peaks, with the

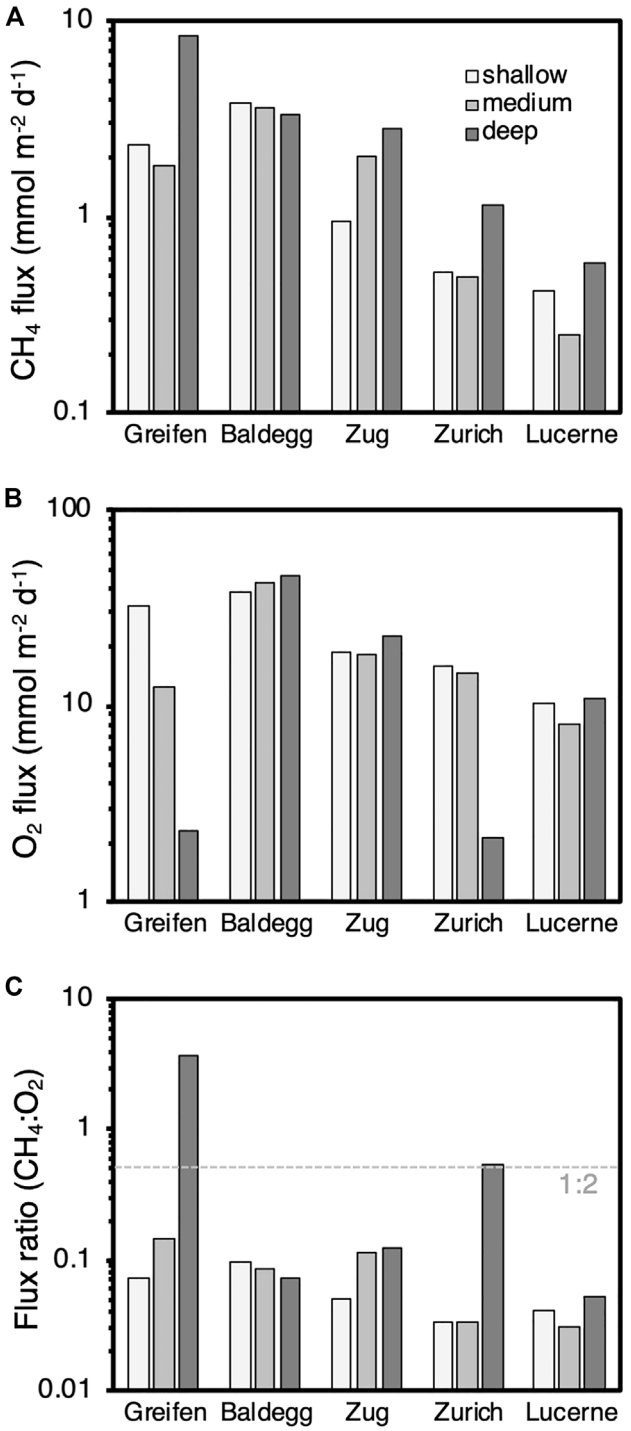


FIGURE 2 | Modeled diffusive fluxes of **(A)** methane and **(B)** O_2, and **(C)** diffusive flux ratios (CH_4:O_2) for all lake stations. The dashed line in (C) indicates a 1:2 flux ratio of CH_4 to O_2. Values below this value indicate a sufficiently high O_2 flux for the complete oxidation of all upward diffusing CH_4 to bicarbonate (HCO_3^-). Values above this dashed line (only deep hypoxic stations of Lake Greifen and Lake Zurich) indicate insufficient O_2 influx to oxidize all CH_4 to bicarbonate.

latter generally found in the zone of net methane production (methanogenesis zone).

Despite having the lowest methane fluxes (**Figure 2**; **Table 3**), Lake Lucerne had the highest *pmo*A copy numbers (**Figure 1B**, $p < 0.001$). These were up to 10-fold higher compared to the other lakes, both within and below the O_2 penetration depth. By contrast, in Lake Baldegg, which had the highest methane fluxes (with Lake Greifen) and highest O_2 fluxes (**Table 3**; **Figure 2**), and the shallowest O_2 penetration (**Table 1**), *pmo*A copy numbers were the lowest of all lakes. These trends were statistically supported. The oligotrophic lake (Lake Lucerne) had significantly higher *pmo*A copy numbers than the combined eutrophic lakes ($p < 0.001$), but not Lake Zurich. Both Lake Zurich and Lake Lucerne also had higher *pmo*A copy numbers when individually compared to Lake Baldegg ($p < 0.05$ and $p < 0.001$, respectively).

The contribution of MOB to the total microbial community, expressed in % based on the ratio between *pmo*A and 16S rRNA gene copy numbers, ranged from ~0.005 to 1% and was also highest in Lake Lucerne (**Figure 1C**). The highest values were reached at the shallow station in Lake Lucerne, despite the low methane concentrations (<2 mM; **Figure 1A**) and low methane fluxes (**Table 3A**) at this station. As for *pmo*A copies, Lake Lucerne had significantly higher contributions of MOB compared to the eutrophic lakes ($p < 0.05$), and when compared individually to Lake Baldegg ($p < 0.01$).

Phylogenetic Diversity of Methanotrophic Bacteria Based on *pmo*A

Phylogenetic analyses of *pmo*A sequences obtained by amplicon and metagenome sequencing revealed a phylogenetically diverse MOB assemblage (**Figure 3**). Groups detected include Type I and Type II MOB, Methylomirabilales, and less known *pmo*A-like gene clusters (RA21-like, pxma (putative copper-containing monooxygenase)).

Within the gammaproteobacterial Type I methanotrophs, diverse Type Ia and Type Ib OTUs dominated. All of these OTUs cluster more or less closely with Type Ia and Type Ib genera of the family Methylococcaceae, with the exception of several (represented by OTU_130) that cluster in the phylogenetic vicinity of Candidatus Crenothrix polyspora. Even though the latter is not phylogenetically separated from typical Type Ia Methylococcaceae *pmo*A (**Figure 3**) or 16S rRNA gene sequences (**Supplementary Figure S3**), it is often placed in its own family (Crenotricaceae) due to its distinct morphology. In addition to Type Ia and Type Ib *pmo*A sequences, Type I OTUs belonging to an unknown group (OTU_834) and the USC-gamma cluster were detected. Furthermore, one subcluster that was closely related to *Methylobacter tundripaludicum* was only detected by metagenome sequencing. Closest relatives of the detected Type I MOB OTUs were isolated or sequenced from diverse aquatic freshwater and marine water columns and sediments, as well as wetland and terrestrial soils.

TABLE 3 | (A) Modeled CH_4 and O_2 fluxes and flux ratios by lake and station. (B) Lake-specific average ±standard deviation (SD) of modeled CH_4 and O_2 fluxes and flux ratios shown in (A). At the standard stoichiometry for aerobic methane oxidation 2 O_2 are reduced per CH_4 oxidized. Thus, at a flux ratio of 0.03, approximately 6% of O_2 that enters sediments is consumed by aerobic methane oxidation, assuming that all methane is oxidized in sediments *via* the standard stoichiometry of aerobic methane oxidation.

(A)

	Shallow			Middle			Deep		
	CH_4 flux	O_2 flux	Flux ratio	CH_4 flux	O_2 flux	Flux ratio	CH_4 flux	O_2 flux	Flux ratio
	mmol m^{-2} d^{-1}	mmol m^{-2} d^{-1}	CH_4: O_2	mmol m^{-2} d^{-1}	mmol m^{-2} d^{-1}	CH_4: O_2	mmol m^{-2} d^{-1}	mmol m^{-2} d^{-1}	CH_4: O_2
Greifen	2.34	32.71	0.07	1.83	12.56	0.15	8.48	2.32	3.65
Baldegg	3.76	38.28	0.10	3.62	42.72	0.08	3.29	46.14	0.07
Zug	0.96	18.64	0.05	2.03	18.01	0.11	2.83	22.57	0.13
Zurich	0.53	15.79	0.03	0.49	14.59	0.03	1.16	2.12	0.55
Lucerne	0.42	10.26	0.04	0.25	8.10	0.03	0.58	10.99	0.05

(B)

	Average ± SD		
	CH_4 flux	O_2 flux	Flux ratio
	mmol m^{-2} d^{-1}	mmol m^{-2} d^{-1}	CH_4: O_2
Greifen	4.21 ± 3.70	15.86 ± 15.46	1.29 ± 2.05
Baldegg	3.56 ± 0.24	42.38 ± 3.94	0.08 ± 0.01
Zug	1.94 ± 0.94	19.74 ± 2.47	0.10 ± 0.04
Zurich	0.73 ± 0.37	10.83 ± 7.57	0.20 ± 0.30
Lucerne	0.41 ± 0.16	9.78 ± 1.50	0.04 ± 0.01

Within the alphaproteobacterial Type II MOB, which had a lower OTU diversity than the gammaproteobacterial Type I MOB, *pmo*A sequences were dominated by the *pmoA*1 and *pmo*A2 clusters (collectively also known as Type IIa MOB). *pmo*A1 and *pmo*A2 encode different isoenzymes of pMMO and are found in the genera *Methylocystis* and *Methylosinus*, some members of which have both genes. In addition, we detected sequences that clustered with the genus *Methylocapsa* (also known as Type IIb cluster) and the less known USC-alpha cluster. Despite the known discrimination of the A1809/Mb66a primer pair against USC-alpha and *Methylocapsa*-like *pmo*A (Knief, 2015), metagenome sequencing did not yield any missing OTUs or phylogenetic clusters. The majority of Type II MOB sequences cluster with isolates and environmental sequences from terrestrial and wetland soils.

The new NC10-specific pmoA29F/590R primer combination detected sequences that cover the known phylogenetic diversity of NC10-*pmo*A. The fact that NC10 were also detected by metagenome sequencing, including one sequence with 100% sequence identity to Candidatus Methylomirabilis limnetica, indicates that this group occurred in significant numbers in certain samples (discussed more later). Detected NC10-*pmo*A sequences clustered with ones that were previously recovered from water-logged soils and aquatic sediments.

Two additional, *pmo*A-like clusters (RA21-like, *pxma*) were only detected by metagenome sequencing, matching past observations that the general A1809/Mb66a misses both of these divergent, functionally poorly understood *pmo*A clusters. The recovered sequences diverge strongly from previously published RA21-like or pxma metagenome sequences and are thus of unknown taxonomic origin.

Lake-specific Trends in *pmo*A OTU Richness, Diversity and Evenness

The methanotrophic community detected with the general A1809/Mb66a *pmo*A primer pair showed a similar OTU richness across the five lakes (**Figure 4A**; $p > 0.05$, Kruskal–Wallis test followed by a Dunn's post hoc test). The diversity and evenness was, however, significantly lower in oligotrophic Lake Lucerne compared to each of the other lakes (**Figures 4B,C**; $p < 0.001$, same tests). This indicates that, despite harboring a comparable total number of OTUs, MOB communities in Lake Lucerne are dominated by few highly abundant OTUs. By contrast, the other four lakes shared a similar, higher evenness and diversity of OTUs. Richness and diversity comparisons were not performed on NC10, as only 19 OTUs belonging to this phylum were recovered, most of which were unique to sediments of Lake Lucerne.

Depth Zonation and Trophic Preference of Methanotrophic Communities

*pmo*A taxonomic compositions based on the general A1809/Mb66a *pmo*A primer pair showed systematic trends in relation to sediment depth and to a lesser degree trophic state (**Figure 5**). Clear trends within lakes in relation to water depth or from oxic to anoxic sediment layers within the same sediment cores were absent.

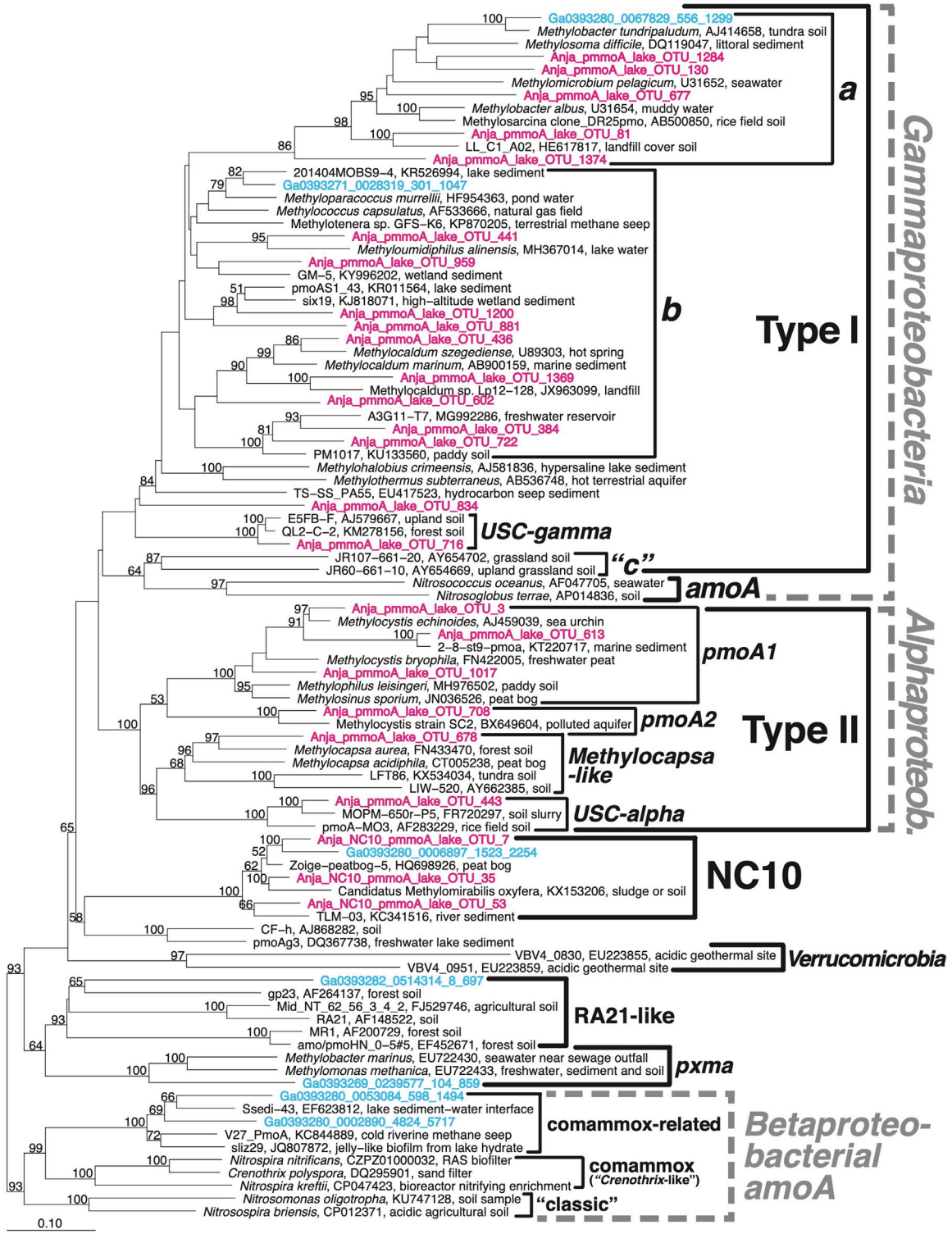


FIGURE 3 | Neighbour-joining phylogenetic tree of *pmo*A amplicon sequences obtained using the general A1809/Mb66a and NC10-specific pmoA29F/590R primer combinations (pink) as well as metagenomic *pmo*A sequences (blue). The latter are only shown in cases where metagenomic analyses revealed the presence of *pmo*A (sub)clusters that were not detected by amplicon sequencing. Branching patterns with ≥50% bootstrap support (1,000 replicate calculations) are indicated at branch nodes.

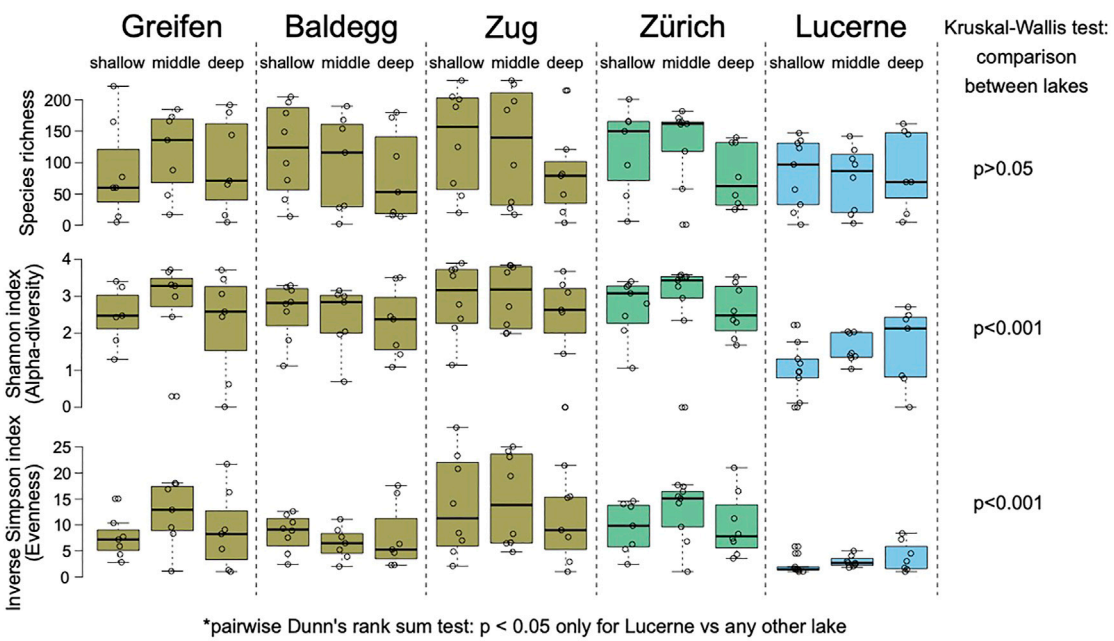


FIGURE 4 | OTU Richness (total number of OTUs), Shannon Index (diversity), and Inverse Simpson Index (evenness) of *pmo*A sequences across the different lakes and sampling stations. The colors represent the current trophic states: eutrophic (brown), mesotrophic (green) and oligotrophic (blue). Far right: results of Kruskal–Wallis test with Dunn's posthoc test showing that the Shannon and Inverse Simpson Indices differ significantly between Lake Lucerne and the other four lakes, but not between the other four lakes.

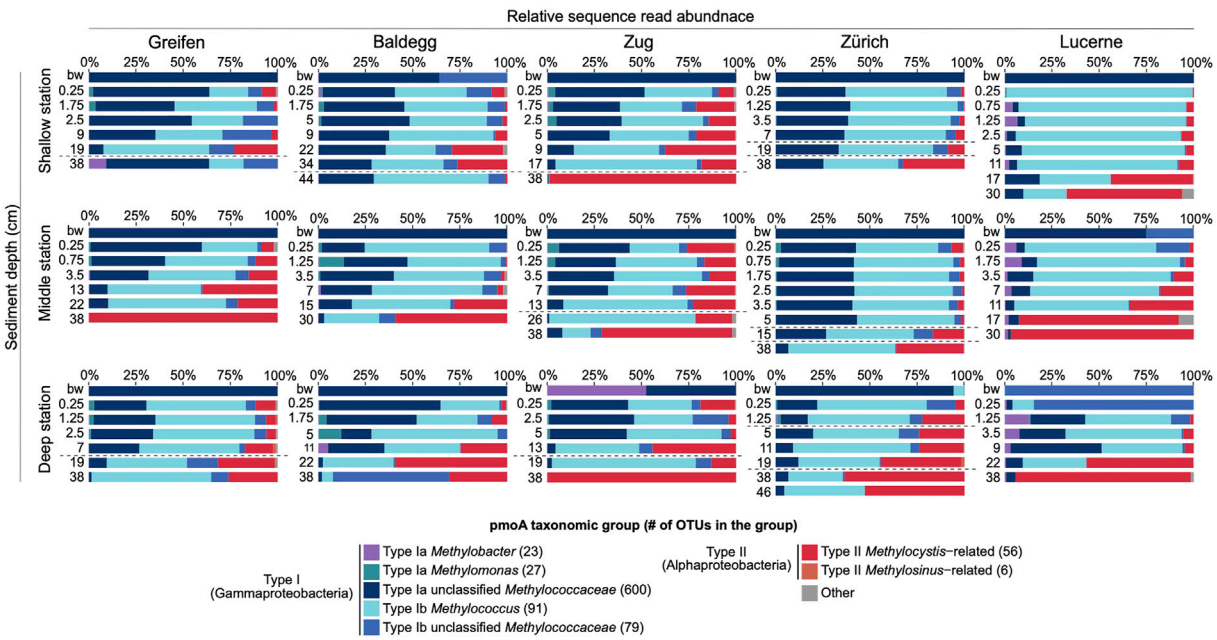


FIGURE 5 | Barcharts showing depth distributions of dominant genus-level *pmo*A taxa/clades across lakes and stations (*x*-axis: percentage of total *pmo*A reads per sample; *y*-axis: sediment depth in cm; bw = bottom water). OTUs that could not be assigned to any known MOB genera were termed "Unclassified" (Type Ia/Type Ib Unclassified Methylococcaceae). Stations are ordered from shallow (top row) to deep (bottom row). Dashed horizontal lines indicate transitions from oligotrophic to eutrophic for Lake Greifen, Lake Baldegg, Lake Zug, and Lake Zurich, at stations where the deepest recovered samples were deposited when these lakes were still oligotrophic. A second dashed horizontal line in shallower layers of Lake Zurich indicates the transition from eutrophic to mesotrophic around 1980. Note: measurable O_2 concentrations (>1–2 μM) were only present in the shallowest sediment sample from 0.25 cm, except at the shallow station in Lake Lucerne where O_2 was measurable at 0.25 and 0.75 cm sediment depth.

Type I methanotrophic communities in all five lakes were generally dominated by three taxonomic groups, termed Type Ia Unclassified Methylococcaceae, Type Ib *Methylococcus*, and Type Ib Unclassified Methylococcaceae (**Figure 5**). Bottom water was dominated by Type Ia Unclassified Methylococcaceae (in most cases >95% of reads). Exceptions are the deep stations in Lake Zug and Lake Lucerne, which are dominated by Type Ia *Methylobacter* and Type Ib Unclassified Methylococcaceae *pmo*A sequences, respectively. Communities shift systematically from bottom water into sediments, where *pmo*A sequences that cluster with the genus *Methylococcus* (Type Ib), which were nearly absent from bottom water, emerge as a second dominant group.

Percentages of Type Ia Unclassified Methylococcaceae are on average higher in sediments of today's eu- and mesotrophic lakes compared to oligotrophic Lake Lucerne. Percentages of this group also decrease gradually with sediment depth at most stations, although these decreases do not closely match depth distributions of O_2 or anaerobic respiration reactions, or past shifts in trophic state. Similar depth- or trophic state-related changes in Type Ib *Methylococcus*-type *pmo*A contributions are less evident, though, notably, this cluster drops in relative abundances in deep sediment layers of oligotrophic Lake Lucerne and most deep oligotrophic layers of today's eutrophic lakes. The third major Type I cluster (Type Ib Unclassified Methylococcaceae) fluctuates in percentages without clear trends in relation to O_2 or respiration zone, sediment depth, past or present trophic state. Other Type I clusters that accounted for significant, but minor percentages of *pmo*A reads included Type Ia *Methylomonas*- and *Methylobacter*-like sequences, Type Ib *Methylocaldum*-like sequences, and Unclassified Type I-sequences (**Figure 5**). Read percentages of these groups also did not show clear trends in relation to O_2 or respiration zone, sediment depth, past or present trophic state.

The general decreases in Type I *pmo*A sequence percentages with sediment depth coincided with strong increases in facultative Type II methanotrophs that mainly grouped with the *Methylocystis*-type pmoA1 cluster (**Figure 5**). This cluster was almost absent from bottom water but – independent of trophic state - became dominant below the depths of O_2, nitrate, and sulfate depletion in iron-reducing and methanogenic sediment layers.

Comparative Analyses of MOB Based on 16S rRNA Gene Sequences

We checked whether sedimentary trends in *pmo*A sequences were reproducible in the complementary 16S rRNA gene data of Han et al. (2020), and how MOB that were missed by the general A1809/Mb66a *pmo*A primer pair compared in relative abundances (**Supplementary Figure S1**). These analyses confirm the shift in dominance from gammaproteobacterial to alphaproteobacterial MOB with increasing sediment depth (and age) observed in *pmo*A sequence compositions. Moreover, in sediments of Lake Lucerne, members of Candidatus Methylomirabilia (NC10) dominate shallow sediments along with Type Ia Methylococcaceae. Methylomirabilia furthermore account for up to ~30% of methanotrophic 16S reads in deep sediment layers of the eutrophic lakes, and even dominate sediments below 5 cm depth in Lake Zurich. All Methylomirabilia-related 16S rRNA gene sequences could be assigned to the order Methylomirabilales. Most reads in Lake Lucerne belong to the genus Methylomirabilis, while most reads in the other lakes group with the uncharacterized Sh765B-TzT-35 cluster.

A striking difference to the *pmo*A analyses was the much lower percentage of Type Ib in the 16S rRNA gene data set. In addition, alphaproteobacterial Type II were dominated by 16S rRNA sequences that cluster with the mostly methylotrophic genus *Methyloceanibacter* (family: Methyloligellaceae), which only includes one confirmed methanotrophic member that, however, lacks *pmo*A (*M.oceanibacter methanicus*; Vekeman et al., 2016). By comparison, percentages of sequences related to facultatively methanotrophic *Methylocystis* are much lower, though these also increase with sediment depth. Lastly, 16S rRNA gene data indicate the presence of low read fractions (~0.1%) of Type III methanotrophs (Methylacidiphilaceae; Verrucomicrobia) in surface layers of the middle stations in Lake Baldegg and Lake Lucerne.

Taxonomic and OTU-Level Environmental Clustering of *pmo*A Sequences

A Non-linear Multi-dimensional scaling (NMDS) ordination of samples based on major taxa recovered with the general A1809/Mb66a *pmo*A primer pair confirms the main inference from **Figure 5** that MOB communities at the genus-level are more strongly structured in relation to sediment depth than trophic state (**Figure 6A**). This is confirmed based on the results of a PERMANOVA (**Table 4**). These show that while both sediment depth and trophic state have a significant impact on MOB community structure at the genus-level (both $p < 0.001$), depth explains a higher portion of the observed community variation ($R^2 = 0.22$) than trophic state ($R^2 = 0.16$). Complementary ANOSIM analyses, moreover, show that trophic state at the time of deposition only shows significant differences between samples that were deposited under oligotrophic vs. eutrophic conditions ($R = 0.30$, $p < 0.001$), but not between eutrophic and mesotrophic ($R = 0.08$, $p > 0.05$) or mesotrophic and oligotrophic conditions ($R = -0.16$, $p > 0.05$).

The pattern shifts when NMDS analyses are performed at the OTU-level ("species-level"; **Figure 6B**). Here trophic state is more strongly correlated with community structure than sediment depth, as indicated by the clear separation of oligotrophic Lake Lucerne from the other four lakes. By contrast, OTU compositions of sediment samples that were deposited under mesotrophic conditions in Lake Zurich are highly similar to samples deposited under eutrophic conditions in Lake Zurich or the other presently eutrophic lakes. Interestingly, OTU samples from the deep oligotrophic layers in Lake Zug and one deep oligotrophic layer in Lake Greifen cluster most closely with oligotrophic communities from Lake Lucerne (**Figure 6B**), suggesting that trophic state at the time of deposition is the key driver of MOB community structure at

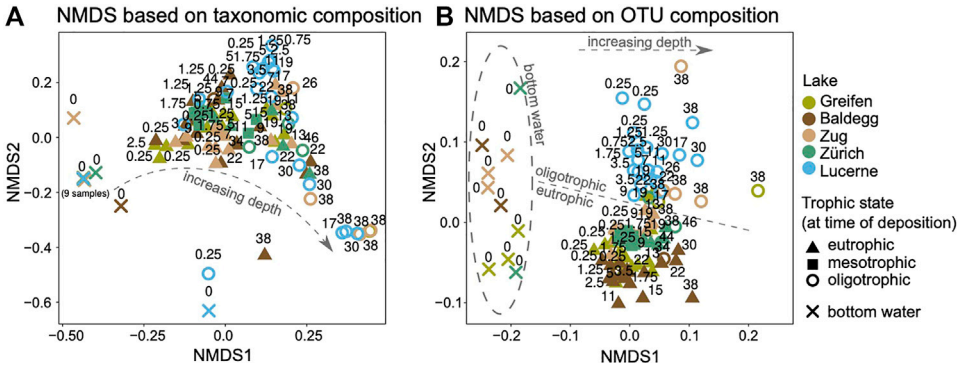


FIGURE 6 | Non-linear multi-dimensional scaling (NMDS) ordination of sediment and water samples based on **(A)** taxonomic groups shown in **Figure 5**, and **(B)** OTUs (only general A1809/Mb66a *pmo*A primer pair). Sediment depths of key samples (in cm) are written into both panels. The low OTU diversity (19 OTUs in total, mainly Lake Lucerne) did not allow for an NMDS analysis of NC10 *pmo*A sequences.

TABLE 4 | Permutational Multi-variate Analysis of Variance (PERMANOVA) results for differences in community composition in relation to trophic state at time of deposition and sediment depth (as a proxy for vertical respiration zone gradients). Taxa-level tests were used as a proxy for MOB community trends at the genus-level, while OTU-level tests were used as a proxy for community trends at the species-level. [*** indicates $p < 0.001$.].

		Degrees of freedom	Sums of squares	Mean squares	F-model	R^2	*p*
Taxa	Trophic state	2	1.71	0.85	12.34	0.16	***
	Sediment depth	1	2.2	2.2	31.78	0.21	***
	Residuals	95	6.56	0.07	0.63		
	Total	98	10.46	1			
OTUs	Trophic state	2	7.34	3.67	15.54	0.23	***
	Sediment depth	1	2.68	2.68	11.36	0.08	***
	Residuals	95	22.42	0.24	0.69		
	Total	98	32.44	1			

the OTU-level. This is confirmed based on a PERMANOVA test (**Table 4**), which shows that while both sediment depth and trophic state have a significant impact on MOB community structure at the OTU-level (both $p < 0.001$), trophic state explains a much higher portion of the observed community variation ($R^2 = 0.23$) than sediment depth ($R^2 = 0.08$).

Further OTU-level analyses, reveal that the three main *pmo*A clusters (**Figure 5**; Type Ia unclassified Methylococcaceae, Type Ib *Methylococcus*, Type II *Methylocystis*) in eu- and mesotrophic lakes are dominated by a larger number of OTUs than in Lake Lucerne (**Supplementary Figure S2**). Most of these dominant OTUs in the eu- and mesotrophic lakes are shared among these lakes. By contrast, as already indicated by **Figure 4**, Lake Lucerne is dominated by a smaller number of OTUs with very high relative abundances. These dominant OTUs in Lake Lucerne represent a subset of the OTUs that dominate sediments of the eu- and mesotrophic lakes. Additional similarity percentage (SIMPER) analyses reveal that some OTUs are highly abundant in oligotrophic samples of Lake Lucerne and deep oligotrophic layers of Lakes Greifen, Baldegg, and Zug, but nearly absent from sediment layers that were deposited under eutrophic conditions (e.g. Methylococcaceae OTU2, *Methylocystis*-related OTU3; **Supplementary Figure S2**).

Potential Environmental and Biological Drivers of MOB Communities

Abundance analyses of *pmo*A copy numbers and *pmo*A/16S ratios in relation to respiration reactions and trophic state confirm both the absence of a clear *pmo*A copy number relationship with respiration zone as well as the clear relationship between *pmo*A copy number and trophic state (**Figure 7A**). On average, *pmo*A copy numbers increase by a factor of 8 and *pmo*A/16S ratios increase by a factor of 4 from sediment samples that were deposited under eutrophic conditions to ones that were deposited under oligotrophic conditions. Both increases are significant ($p < 0.001$, Kruskal–Wallis followed by Dunn's post hoc test).

In addition, dominant *pmo*A taxonomic groups (**Figure 5**) and their most abundant OTUs show clear patterns in relation to vertical respiration zone and to a lesser degree trophic state (**Figure 7A**). The observed patterns in relation to respiration

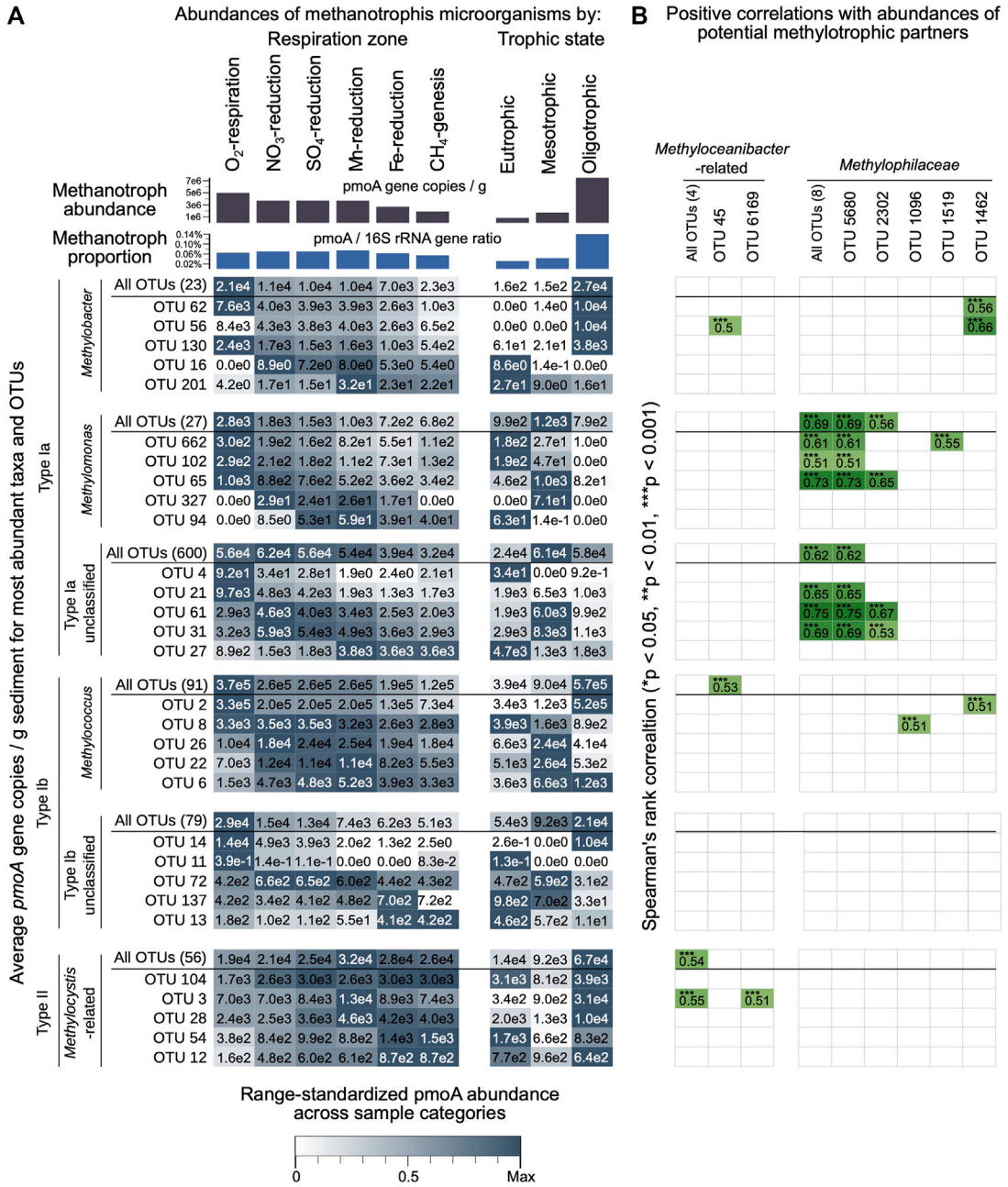


FIGURE 7 | (A) Total *pmo*A copy numbers, relative abundances of *pmo*A relative to 16S rRNA gene copy numbers (bar charts at top), and calculated gene copy numbers of dominant *pmo*A taxa and their five most abundant OTUs across different respiration zones and in relation to lake trophic state at the time of sediment deposition (remaining graph). Total *pmo*A copy numbers and *pmo*A/16S rRNA gene percentages are averages of values shown in **Figures 1B,C**, respectively. Gene copy numbers of dominant *pmo*A taxa and OTUs were calculated by multiplying relative *pmo*A abundances by total *pmo*A copy numbers per gram of wet sediment. The heatmap color intensity reflects the standardized average pmoA copy numbers per taxon or OTU, with highest intensity representing the highest average copy number within each comparison (respiration zone, trophic state). **(B)** Spearman correlation matrix of calculated *pmo*A copy numbers per taxon or dominant OTU (calculated as in (A)) vs. calculated 16S rRNA gene copy numbers of dominant methylotrophic taxa (Methylophilaceae, Methyloceanibacter-related) and their dominant OTUs as determined by multiplying 16S rRNA gene sequence contributions by qPCR-based total 16S rRNA gene copy numbers (all 16S data from Han et al., 2020). Spearman's rank correlation coefficients of ≥0.5 are shaded in green and listed in the graph. Asterisks indicate significance level (*$p < 0.05$; **$p < 0.01$; ***$p < 0.001$).

zone explain the observed significant correlations of *pmo*A community structure at the genus- and OTU-level with sediment depth, which *per se* is not a likely community driver (see previous section). The Type Ia MOB genera *Methylobacter* and *Methylomonas* and Type Ib genus *Methylococcus*, and dominant OTUs within all three genera, have their highest calculated average *pmo*A abundances in oxic sediments. By contrast, the Type Ia Unclassified Methylococcaceae and Type

II *Methylocystis*, and several dominant OTUs within these groups, have peak *pmo*A abundances in denitrifying, sulfate- and manganese-reducing (Unclassified Type Ia) and in manganese- and iron-reducing and methanogenic layers (*Methylocystis*) (**Figure 7A**). With respect to abundances in relation to trophic state, we generally observe that Type Ia *Methylobacter* and Type II *pmo*A sequences, and their dominant OTUs, reach their peak abundances under oligotrophic conditions, whereas Type Ia *Methylomonas* and Unclassified Methylococcaceae, and their dominant OTUs, reach their highest abundances under meso- and eutrophic conditions. Highly similar patterns to those in **Figure 7A** were observed when calculated absolute abundances of dominant taxa and OTUs were substituted with relative abundances (**Supplementary Figure S4**).

Calculated *pmo*A abundances of major MOB taxa and their dominant OTUs correlate strongly with major methylotrophic taxa and their dominant OTUs (**Figure 7B**). Type Ia Unclassified Methylococcaceae, Type Ia *Methylomonas*, and Type Ib Methylococcus, as well as dominant OTUs within these three groups, show strong positive Spearman's correlations (Rho>0.5, $p < 0.001$) with 16S rRNA gene-based abundances of Methylophilaceae and dominant OTUs of Methylophilaceae. In addition, matching their observed *pmo*A peak abundancess in deeper layers, *pmo*A abundances of *Methylocystis* and one of its dominant OTUs (OTU_3) are correlated with 16S gene-based abundances of *Methyloceanibacter* and one of its dominant OTUs (OTU_45). Nonetheless, *pmo*A OTUs with highest abundances in the oxic or denitrifying sediment layers (Type Ia and Type Ib MOB) were much more likely to correlate with methylotrophic OTUs than *pmo*A OTUs reaching peak abundances in deeper anoxic layers (Type II). Among *pmo*A OTUs with peak abundances in the oxic or denitrifying layer, 19 and 22%, respectively, showed a significant positive correlation (Rho>0.5, $p < 0.05$) with methylotrophic 16S OTUs. This proportion dropped to 10 and 9% for OTUs most abundant in the sulfate and manganese reduction zones, and was 0 and 2%, respectively, in the iron reduction and methanogenesis zones. Moreover, of the 64 *Methylocystis* OTUs, it was only the aforementioned OTU_3 (**Figure 7B**) that showed significant correlations with *Methyloceanibacter*.

We found no clear relationship between trophic state and the percentage of *pmo*A OTUs that correlate significantly with the percentage of methylotrophic 16S OTUs (Rho>0.5, $p < 0.05$). Based on calculated absolute abundances, 10 and 12% of *pmo*A OTUs with peak abundances in sediments deposited under eutrophic and oligotrophic conditions, respectively, were significantly correlated with methylotrophs.

DISCUSSION

Methanotrophic bacteria play a key role in mediating methane emissions from lakes across the world (Bastviken et al., 2008; Thottathil et al., 2018). Although eutrophication enhances organic carbon inputs to lake sediments (Heathcote and Downing, 2012; Anderson et al., 2014) and increases lake sedimentary methane production and emissions (Beaulieu et al., 2019; Fiskal et al., 2019), its effects on the activity, abundance, and community structure of sedimentary MOB is not understood. By performing detailed quantitative and phylogenetic analyses on MOB communities in sediment cores from five lakes that span the past centuries, and by analyzing this community data in the context of trophic history, present-day respiration zone distributions, O_2 and methane fluxes, we produce novel insights into the potential controls on MOB communities in lake sediments. We summarize major findings in the following paragraphs and discuss these in further detail in the subsequent thematically structured subsections.

Summary of Major Findings

Matching measured methane concentrations (**Figure 1A**) and modeled methane production profiles (Fiskal et al., 2019), we observe clear increases in surface sedimentary methane fluxes in eutrophic lakes (**Figure 2A**; **Table 3**). Yet, gene copy number-based estimates indicate that MOB are on average 8-fold more abundant and account for 4-fold higher fractions of the total microbial community in samples deposited under oligotrophic compared to eutrophic conditions (**Figure 7**). An insufficient supply of O_2 can be ruled out as a first-order explanation as, except at the hypoxic deep stations in Lake Greifen and Lake Zurich, only a minor fraction (6–30%) of the diffusive flux of O_2 can be accounted for by aerobic methane oxidation assuming the standard 2:1 stoichiometry of O_2:CH_4 (**Figure 2C**).

Matching previous studies on lake sediments (Rahalkar et al., 2009; Pester et al., 2011; Tsutsumi et al., 2011; He et al., 2021; Lyautey et al., 2021), *pmo*A copy numbers do not change significantly from oxic to anoxic sediments (**Figure 1B**). Based on calculated *pmo*A gene copy numbers of individual MOB genera, certain Type II MOB taxa (mainly *Methylocystis*) even reach peak abundances in deep methanogenic and metal reducing sediment (**Figure 5**; **Supplementary Figure S1**). The observation of high or even elevated *pmo*A copies below the oxic-anoxic transition is at odds with cultivation data, which indicate that the vast majority of alpha and gammaproteobacterial MOB, including all Methylocystaceae, are obligate aerobes (Bowman, 2014). This raises questions concerning whether these *pmo*A sequences belong to catabolically active, dormant, inactive, or even dead cells.

While Type II MOB dominate deeper layers, Type I MOB (Methylococcacea) are the major group in oxic and suboxic bottom water and surface sediments (**Figure 6**), matching other studies on freshwater surface sediments (e.g., Rahalkar et al., 2009; Lyautey et al., 2021). Hereby the (near) absence of Type Ib, but not Type Ia, MOB in overlying water suggests a habitat preference of Type Ib for sediments. Similar to previous studies (Yang et al., 2016; He et al., 2021; Lyautey et al., 2021), *Methylococcus*-type *pmo*A dominate Type Ib communities. By contrast, *Methylobacter*-type Type Ia sequences, which frequently dominate lake sediments elsewhere (Tsutsumi et al., 2011; Reim et al., 2012; Yang et al., 2016), are less abundant. Instead, the majority of Type Ia sequences fall outside of known genera ('Type Ia Unclassified Methylococcaceae'). Some of these sequences cluster loosely with Candidatus Crenothrix polyspora

(**Figure 3**), raising questions regarding their identity as filamentous Crenotrichaceae or unicellular (mostly coccoid) Methylococcaceae. Phylogenetic trees based on both *pmo*A and 16S rRNA gene sequences, in which Crenotrichaceae (Crenothrix polyspora) group with well-known Methylococcaceae isolates (**Figure 3**, **Supplementary Figure S3**) could not resolve this issue. Besides Type I and Type II MOB taxa, we detect NC10-type denitrifying methanotrophs (Methylomirabilota) based on 16S rRNA gene analyses (**Supplementary Figure S1**). Members of the type genus *Methanomirabilis* occur at similar relative abundances to Type I methanotrophs in denitrifying sediments of Lake Lucerne, whereas uncultivated groups of Methylomirabilota (mainly Sh765B−TzT−35) occur at significant abundances in deeper, nitrate-depleted, fully anoxic layers of most lakes.

While the drivers of (uncultivated) Methylomirabilota communities remain uncertain, Type I and Type II MOB taxa at the genus-level show vertical distributions that match distributions of major respiration reactions (**Figure 7A** and **Supplementary Figure S4**). This raises the possibility that distributions of MOB genera in lake sediments reflect genus-level differences in the ability to live without O_2 and respire different anaerobic electron acceptors. Moreover, OTU-level analyses indicate lake trophic state as a major driver of MOB diversity and community structure at the species-level (**Figure 4**, **6B** & **7A**). Potential explanations are that differences in anabolic nutrient regimes or micro-scale habitat heterogeneity impact MOB communities at the species-level. By contrast, based on correlation analyses of MOB taxa and potential methylotrophic partner organisms (Results text), we find no evidence that co-dependencies of MOB on syntrophic partners vary with trophic state. Instead, correlations between MOB and methylotrophic bacterial OTUs follow clear taxonomic and environmental trends, being most frequently observed within Type I taxa that dominate oxic and suboxic surface sediments.

Explanations for the Higher MOB Gene Copy Numbers and Percentages Under Low CH_4 fluxes

The order of magnitude higher *pmo*A copy numbers in oligotrophic Lake Lucerne compared to the eutrophic lakes (**Figure 1B** & **7A**), show parallels with quantitative data on total microbial community size. Total 16S rRNA gene copy numbers were also highest in Lake Lucerne (Han et al., 2020) and were generally supported by microscopic cell counts which indicated higher microbial cell abundances in Lake Lucerne and Lake Zurich than in the three eutrophic lakes (Fiskal et al., 2019). These trends seem paradoxical given that the higher deposition and burial rates of organic carbon in the eutrophic lakes sustain higher total respiration and methanogenesis rates throughout cores from these lakes (Fiskal et al., 2019). A possible explanation is that microbial cell-specific energy requirements are higher in eutrophic lake sediment, e.g. due to enhanced physiological stress from elevated toxic contaminant loads. Yet, though more research is needed, previous studies suggest minor effects of anthropogenic toxin contamination on sediment microbial communities (Chen et al., 2014; Di Cesare et al., 2020). Notably also, the shallow and medium station in Lake Zurich are located in a Zinn (Sn)-polluted area (Lennartz, 2010), and yet had high cell counts and high qPCR values of *pmo*A and total 16S genes.

An alternative explanation is that – matching the higher microbial activity - sediments of eutrophic lakes have higher microbial growth rates, but that these coincide with higher rates of mortality, e.g. due to viral lysis or predation. Though we lack data on viral lysis rates, previous work has shown high abundances of oligochaetes (Tubificidae) to 20 cm sediment depth in the three eutrophic lakes and absence of these worms from all but the sediment surface in Lake Lucerne (Fiskal et al., 2021a). Gut microbiome analyses suggest protein-rich diets that are consistent with microbial grazing as a major food source of tubificids (Fiskal et al., 2021a; de Valk et al., 2017). While lake sedimentary invertebrates are known to stimulate growth of MOB in surface sediments ("microbial gardening"), leading to MOB becoming a major food source of these invertebrates in some lakes (Kiyashko et al., 2001; Deines et al., 2007; Jones and Grey, 2011), none of the stations in this study show evidence for MOB gardening (Fiskal et al., 2021a). We thus propose that non-selective grazing by tubificids causes higher mortality and ultimately results in lower abundances of microorganisms, including MOB, in sediments of the eutrophic lakes.

While non-selective grazing by oligochaetes explains lower absolute abundances of MOB, it does not explain the lower relative abundances (percentages) of MOB in the eutrophic lakes (**Figure 1C**, **7A**, and **Supplementary Figure S2**). These lower percentages are particularly striking given the steep, overlapping O_2 and CH_4 concentration gradients in the top 0.5 cm of eutrophic lakes (**Figure 1A**), which imply high potential for aerobic methanotrophy. In the following paragraphs, we evaluate three potential hypotheses to explain the lower percentages of MOB in eutrophic lake sediments with high methane fluxes.

Direct observations on sediment cores from the eutrophic lakes revealed the presence of gas bubbles starting just below the 1 to 2 cm thick, flocculent surface layer. While gas bubbles also appeared in sediment of Lake Lucerne and the shallow and medium stations in Lake Zurich, these bubbles were restricted to deeper, more compacted sediment layers and less numerous in these locations. Based on these observations, it is possible that most methane in sediments of eutrophic lakes is present in gas bubbles rather than bioavailable dissolved form. These methane bubbles may bypass the "biological methane filter" in oxic surface sediments by rapid transit through the flocculent surface layer followed by ebullition into overlying water, explaining why methane oxidation only supports a small percentage of the microbial community in eutrophic lake sediments. The importance of ebullitive release of methane from lake sediments to overlying water and the atmosphere is well-known and especially high for shallow and/or eutrophic lakes (Thebrath et al., 1993; Schubert et al., 2012), though little is known about how ebullitive losses quantitatively compare to biological consumption by MOB in lake sediments.

TABLE 5 | Gibbs energies of potential aerobic and denitrifying methanotrophic reactions, organotrophic reactions, and lithotrophic reactions. We include Gibbs energies under standard conditions (ΔG_r°), and for a range of environmentally relevant educt and product concentrations ($\Delta G_r'$ (range), see footnote below table) assuming standard temperature, pressure, and pH (Note: the impact of *in situ* temperature, pressure, and pH on Gibbs energy yields is negligible within the range of calculated educt and product concentrations).

Reaction	kJ mol^{-1}	
	ΔG_r°	$\Delta G_r'$ (*range*)
Methanotrophic		
$CH_4 + 2\ O_2 \rightarrow HCO_3^- + H^+ + H_2O$	-813	-811 to -732
$CH_4 + O_2 \rightarrow 0.5\ CH_3COO^- + 0.5\ H^+ + H_2O$	-391	-394 to -343
$CH_4 + O_2 \rightarrow COO^- + 1.5\ H_2 + H^+$	-340	-449 to -397
$CH_4 + 0.5\ O_2 \rightarrow CH_3OH$	-125	-136 to 99
$CH_4 + 2.67\ NO_2^- + 1.67\ H+ \rightarrow HCO_3^- + 1.33\ N_2 + 2.33\ H_2O$	-923	-829 to -730
Organotrophic		
glucose $+6\ O_2 \rightarrow 6\ HCO_3^- + 6\ H^+$	-2,843	-3,015 to -281
aspartic acid $+3\ O_2 + 2\ H_2O \rightarrow 4\ HCO_3^- + NH_4^+ + 3\ H^+$	-1,351	-1,475 to -1,361
guanine $+2\ O_2 + 10\ H_2O \rightarrow 5\ HCO_3^- + 5\ NH_4^+$	-1,006	-1,186 to -1,100
lactate $+3\ O_2 \rightarrow 3\ HCO_3^- + 2\ H^+$	-1,322	-1,357 to -1,243
acetate $+2\ O_2 \rightarrow 2\ HCO_3^- + H^+$	-844	-846 to -761
Lithotrophic		
$NH_4^+ + 1.5\ O_2 \rightarrow NO_2^- + 2\ H^+ + H_2O$	-274	-343 to -278
$NO_2^- + 0.5\ O_2 \rightarrow NO_3^-$	-74	-74 to -31
$H_2 + 0.5\ O_2 \rightarrow H_2O$	-237	-203 to -160

Electron donor and acceptor concentrations (educt concentrations):
Methanotrophic:
Max: {CH_4} = 10 mM; {O_2} = {NO_2^-} = 100 μM; Min: {CH_4} = 1 μM; {O_2} = {NO_2^-} = 1 nM

Organotrophic:
Max: {organic compound} = {O_2} = 100 μM; Min: {organic compound} = {O_2} = 1 nM

Lithotrophic:
Max: {NH_4^+} = 10 mM; {O_2} = {NO_2^-} = {H_2} = 100 μM; Min: {NH_4^+} = 1 μM; {O_2} = {NO_2^-} = {H_2} = 1 nM

Concentrations of reaction products (product concentrations):
{CH_3OH} = {formate} = {acetate} = {NO_3^-} = 1 μM; {H_2} = 10 nM; {HCO_3^-} = 2 mM; {N_2} = 100 μM

Given the high sedimentation rates of labile microalgal biomass (Han et al., 2020) and shallow depletion of O_2 and nitrate in the three eutrophic lakes (**Table 1**), competition for O_2 or nitrate between MOB and other microorganisms could also explain the lower MOB percentages in eutrophic lakes. Thermodynamic calculations (**Table 5**) indicate that aerobic organotrophic microorganisms have substantially higher energy yields than aerobic or denitrifying MOB. Organotrophs could thus outcompete MOB for O_2 and nitrate, and thereby suppress methane consumption rates and the efficiency of the biological methane filter in the eutrophic lakes. By comparison, sediments of Lake Lucerne have deeper O_2 and nitrate penetration (**Table 1**) and receive less labile algal organic matter than the eutrophic lakes (Han et al., 2020). Here competition for O_2 or nitrate could be less intense due to stronger electron donor limitation of organotrophs, and lead to MOB being major O_2 consumers. In Lake Lucerne, MOB may even have energetic advantages over competing lithotrophic nitrifying bacteria (**Table 5**), which are major microbial community members in this lake (Han et al., 2020). Reduced competition for O_2 and nitrate could also explain why MOB effectively deplete upward-diffusing methane in the surface centimeters of Lake Lucerne and the oxic shallow and medium stations of Lake Zurich.

The third hypothesis concerns potential changes in dominant methanotrophic reactions in relation to trophic state. Besides performing the complete oxidation of methane to CO_2, MOB are known to under certain conditions only partially oxidize methane to low molecular weight intermediates, such as methanol, H_2, formate, or acetate, which are then utilized by denitrifying partner organisms (Kalyuzhnaya et al., 2013; Beck et al., 2013; Oshkin et al., 2014; Hernandez et al., 2015). The factors that determine whether MOB perform complete or partial oxidation are not understood. O_2 concentrations may affect the MOB genera involved, but not necessarily the occurrence of syntrophic reactions (Beck et al., 2013; Hernandez et al., 2015; Oshkin et al., 2014). Compared to the complete oxidation of methane to CO_2, the Gibbs energies of partial oxidation reactions are ~6-fold (methanol) or 3- to 4-fold (formate, acetate) lower (**Table 5**). Higher contributions of energetically less favorable partial methane oxidation reactions in the eutrophic lakes could thus contribute to the lower MOB percentages in the latter. Yet, while we observe strong correlations between calculated *pmo*A copy numbers of

certain Type I genus-level taxa and OTUs with calculated 16S gene copy numbers of Methylophilaceae (**Figure 7B**), the percentage of taxa or OTUs with such correlations does not change in relation to trophic state.

In conclusion, based on available data, enhanced oligochaete grazing is a plausible reason for the lower absolute abundances of MOB in eutrophic lakes, whereas the lower percentages of MOB in eutrophic lakes can be explained with enhanced methane ebullition and/or outcompetition of MOB for O_2 by aerobic organotrophs. By contrast, based on our correlation analyses, enhanced energy-sharing with syntrophic partner organisms is less likely to drive the lower percentages of MOB in eutrophic lakes.

Role of Respiration Zone in Structuring Major MOB Taxa

Analyses of *pmo*A genus-level taxa distributions indicate strong overlaps in community structure between different trophic states, and thus argue against the existence of distinct oligotrophic or eutrophic MOB taxa (**Figure 5** & **6A**). Instead, the highly significant correlation of sediment depth with taxon-level MOB community structure, combined with the clear taxon-specific differences in distributions relative to vertical respiration zones, point to respiration zone as a key driver of MOB community composition at the genus-level (**Figure 5**, **6A**, and **7A**).

Interestingly, the Type Ia genera *Methylobacter* and *Methylomonas* and Type Ib genus *Methylococcus*, and dominant OTUs within these genera, had their highest calculated average *pmo*A abundances in oxic sediments (**Figure 7**), even though at least members of *Methylobacter* and *Methylomonas* have been linked to facultative anaerobic metabolism with or without partner organisms (*Methylomonas*: NO_2^-, NO_3^-, ferrihydrite (Kits et al., 2015b, 2015a; Zheng et al., 2020)); *Methylobacter*: NO_3^- (Smith et al., 2018; van Grinsven et al., 2020a)). Other MOB, including the Unclassified Type Ia Methylococcaceae have peak *pmo*A abundances in suboxic layers (**Figure 7**), suggesting that members of this paraphyletic group might couple methane oxidation to nitrate reduction. Syntrophic interactions between unclassified Type Ia Methylococcaceae and *Methylomonas* and methylotrophic Methylophilaceae with denitrifying potential were previously proposed (Beck et al., 2013; Cao et al., 2019; van Grinsven et al., 2020b) and would match found correlations between *pmo*A abundances of both groups and 16S rRNA gene-based abundances of Methylophilaceae (**Figure 7B**).

While the observed distributions of Type I taxa are generally consistent with previous studies, the observed trends in Type II taxa are more difficult to reconcile. Type II alphaproteobacterial Methylocystaceae sequences dominated deep anoxic sediments of all lakes (**Figure 6**). It remains unclear whether these deep *Methylocystis*-related *pmoA* sequences derive from metabolically active cells, resting (dormant) or inactive cells, or dead organisms. For this DNA to be from dead cells, DNA of *Methylocystis* would need to be more effectively preserved than DNA of Type I methanotrophs, e.g. via shielding by more degradation-resistant cell walls. Members of *Methylocystis* produce lipoidal cysts as resting stages, which are compositionally distinct from the carbohydrate-rich ("*Azotobacter*-type") cell walls of cysts produced by most Methylococcaceae (Bowman 2014). These lipoidal cysts may be more degradation-resistant in lake sediments than *Azotobacter*-type cysts. Yet, enhanced stability of resting stages, which requires substantiation, does not explain why dominant *Methylocystis*-related OTUs reach their highest gene copy numbers in anoxic layers where respiration is dominated by metal reduction and methanogenesis (**Figure 7A**), or why previous studies have reported increases in relative abundances and active assimilation of methane-C by Type II methanotrophs in anoxic sediment (Yang et al., 2019; He et al., 2012). A potential explanation is that Type II *Methylocystis*-related MOB oxidize methane *via* strictly anaerobic associations with partner organisms. Yet, only one *Methylocystis* OTU (out of 64) showed a significant correlation with a methylotrophic bacterial OTU (genus Methyloceanibacteria; **Figure 7B** and related text). Thus, deep Type II MOB might depend less on syntrophic interactions than their Type I counterparts in shallower layers, or not at all. Future research will reveal whether members of *Methylocystis* are involved in methane oxidation, e.g. coupled to metal reduction, as was previously shown for members of *Methylosinus*, a sister genus of *Methylocystis* (Zheng et al., 2020), or even subside on substrates other than methane, such as acetate or ethanol as was previously shown for (however aerobic) members of this genus (Haque et al., 2020; Oshkin et al., 2020).

Lake Trophic State as a Driver of MOB Communities at the Species-Level

While *pmo*A-based community structure at the genus-level was similar across different trophic states, analyses at the OTU-level indicate trophic state as a major driver of MOB community structure at the species-level (**Figure 6B**). Sediments of the oligotrophic Lake Lucerne have a significantly lower OTU diversity and evenness than sediments of the meso- and eutrophic lakes (**Figure 4**) and are dominated by a small number of OTUs that are also present though not dominant in eu- and mesotrophic lakes (**Supplementary Figure S2**). Interestingly, as previously demonstrated for 16S rRNA gene-based analyses of bacterial communities (Han et al., 2020), the trophic state at the time of sediment deposition appears to better predict the present-day MOB community structure than the present-day trophic state of the lake in numerous cases. This is indicated by the fact that OTU community fingerprints of several deep samples from Lake Zug and Lake Greifen, that were deposited under oligotrophic conditions, cluster with samples from the always oligotrophic Lake Lucerne (**Figure 6B**). This legacy effect was most evident in a Type Ib Methylococcaceae-related (OTU_2) and a Type II *Methylocystis*-related OTU (OTU_3). These OTUs dominated sediment samples from Lake Lucerne and had

high relative abundances in deep oligotrophic samples from Lake Zug and Lake Greifen, while being nearly absent from all other samples (**Supplementary Figure S2**).

Our results indicate that MOB community structure is controlled by different environmental variables on different phylogenetic levels. The strong community structuring of MOB genus-level taxa in relation to respiration zones could reflect differences in electron acceptor use or methylotrophic partners among these taxa. By contrast, the clear structuring of OTU-based communities relative to trophic state suggests that additional factors control MOB communities at the species or strain-level, such as differences in enzyme and transporter affinities in relation to nutrient regimes or competition with other microorganisms for O_2. The low community alpha-diversity and evenness in oligotrophic Lake Lucerne, where organic matter is more degraded and contains lower fractions of algal organic carbon, could reflect lower geochemical niche diversity, reduced availability of biosynthetic nutrients and reduced competition for O_2. In comparison, higher availability of nutrients needed for biomass production and higher diversity of microniches with distinct redox conditions could support higher numbers of co-existing OTUs and higher evenness in eutrophic lake sediments.

CONCLUSION

Although eutrophication is expected to increase lacustrine methane emissions worldwide, its effects on the methanotrophic and wider carbon-cycling microbial community are not well understood. Across five lakes in central Switzerland that range in present-day trophic state from highly eutrophic to oligotrophic, and differ significantly in trophic histories, we observe the highest *pmo*A copy numbers and contributions of MOB to total microbial communities under oligotrophic conditions. This observation is remarkable given the higher methane fluxes in the eutrophic lakes and considering that O_2 fluxes into sediments vastly exceed the amount required for complete mineralization of methane at most stations. Potential explanations include that most methane produced in eutrophic sediments "bypasses" MOB communities by ebullition into overlying water and/or that MOB are outcompeted for O_2 by organotrophic microorganisms with higher *in situ* energy yields in eutrophic lakes. In addition, microbial community size based on gene copy numbers may not represent a reliable proxy for MOB activity, suggesting that follow-up studies in which methanotrophic activity is measured are needed.

The consistent depth zonation of "aerobic" MOB in suboxic and anoxic sediments suggests that a much higher proportion of MOB taxa is capable of anaerobic metabolism than previously assumed. The observed OTU-level community structuring according to trophic state at the time of sediment deposition, moreover, indicates a legacy effect of eutrophication on methanotrophic communities. Correlation analyses of MOB and potential methylotrophic partner organisms suggest that syntrophic interactions between MOB and methylotrophs are most important in oxic and denitrifying sediment, and less important in deeper layers where O_2 and nitrate are presumed to be absent. Future research will reveal whether Type II MOB that increase in deep, Fe-reducing and methanogenic layers engage in an unknown form of methanotrophy, and, if so, how methane oxidation is thermodynamically possible in the same sediment layers in which methane is also produced.

DATA AVAILABILITY STATEMENT

The datasets presented in this study can be found in online repositories. The names of the repository/repositories and accession number(s) can be found in the article/ **Supplementary Material**.

AUTHOR CONTRIBUTIONS

ML designed the study. AM and XH performed the laboratory analyses. DM, SvG, ML, and CS analyzed the data. ML, SvG, and DM wrote the manuscript with input from all co-authors.

FUNDING

This study was funded by the Swiss National Science Foundation (project 205321_163371 "Role of bioturbation in controlling microbial community composition and biogeochemical cycles in marine and lacustrine sediments" awarded to ML).

ACKNOWLEDGMENTS

We thank Beat Müller (Eawag) for assistance with diffusive flux calculations, Nathalie Dubois, Alois Zwyssig, Alfred Lück, and Irene Brunner for sampling assistance (all Eawag), Annika Fiskal, Philip Eickenbusch, and Lorenzo Lagostina (all ETH Zurich) for technical support, and Silvia Kobel, Aria Minder, and Jean-Claude Walser from the Genetic Diversity Centre (GDC; ETH Zurich) for assistance with next-generation sequencing and bioinformatic analyses.

SUPPLEMENTARY MATERIAL

The Supplementary Material for this article can be found online at: https://www.frontiersin.org/articles/10.3389/fenvs.2022.857358/full#supplementary-material

REFERENCES

Anderson, N. J., Bennion, H., and Lotter, A. F. (2014). Lake Eutrophication and its Implications for Organic Carbon Sequestration in Europe. *Glob. Change Biol.* 20, 2741–2751. doi:10.1111/gcb.12584

Auman, A. J., Stolyar, S., Costello, A. M., and Lidstrom, M. E. (2000). Molecular Characterization of Methanotrophic Isolates from Freshwater lake Sediment. *Appl. Environ. Microbiol.* 66, 5259–5266. doi:10.1128/aem.66.12.5259-5266.2000

Bastviken, D., Cole, J. J., Pace, M. L., and van de Bogert, M. C. (2008). Fates of Methane from Different lake Habitats: Connecting Whole-lake Budgets and CH4emissions. *J. Geophys. Res.* 113, a–n. doi:10.1029/2007JG000608

Bastviken, D., Cole, J., Pace, M., and Tranvik, L. (2004). Methane Emissions from Lakes: Dependence of lake Characteristics, Two Regional Assessments, and a Global Estimate. *Glob. Biogeochem. Cycles* 18, a–n. doi:10.1029/2004GB002238

Bastviken, D., Tranvik, L. J., Downing, J. A., Crill, P. M., and Enrich-Prast, A. (2011). Freshwater Methane Emissions Offset the Continental Carbon Sink. *Science* 331, 50. doi:10.1126/science.1196808

Beals, E. W. (1984). Bray-curtis Ordination: An Effective Strategy for Analysis of Multivariate Ecological Data. *Adv. Ecol. Res.* 14, 1–55. doi:10.1016/S0065-2504(08)60168-3

Beaulieu, J. J., DelSontro, T., and Downing, J. A. (2019). Eutrophication Will Increase Methane Emissions from Lakes and Impoundments during the 21st century. *Nat. Commun.* 10, 3–7. doi:10.1038/s41467-019-09100-5

Beck, D. A. C., Kalyuzhnaya, M. G., Malfatti, S., Tringe, S. G., Glavina del Rio, T., Ivanova, N., et al. (2013). A Metagenomic Insight into Freshwater Methane-Utilizing Communities and Evidence for Cooperation between theMethylococcaceaeand theMethylophilaceae. *PeerJ* 1, e23. doi:10.7717/peerj.23

Bowman, J. P. (2014). The Family Methylococcaceae. *The Prokaryotes: Gammaproteobacteria* 9783642389, 411–440. doi:10.1007/978-3-642-38922-1_237

Buergi, H. R., and Stadelmann, R. (2000). für, R. S.-I. V., and 2000, undefinedChange of phytoplankton diversity during long-term restoration of Lake Baldegg (Switzerland). *SIL Proc. 1922-2010* 27, 574–581. doi:10.1080/03680770.1998.11901300

Cao, Q., Liu, X., Ran, Y., Li, Z., and Li, D. (2019). Methane Oxidation Coupled to Denitrification under Microaerobic and Hypoxic Conditions in Leach Bed Bioreactors. *Sci. Total Environ.* 649, 1–11. doi:10.1016/j.scitotenv.2018.08.289

Chen, I.-M. A., Chu, K., Palaniappan, K., Ratner, A., Huang, J., Huntemann, M., et al. (2021). The IMG/M Data Management and Analysis System v.6.0: New Tools and Advanced Capabilities. *Nucleic Acids Res.* 49, D751–D763. doi:10.1093/NAR/GKAA939

Chen, J., He, F., Zhang, X., Sun, X., Zheng, J., and Zheng, J. (2014). Heavy Metal Pollution Decreases Microbial Abundance, Diversity and Activity within Particle-Size Fractions of a Paddy Soil. *FEMS Microbiol. Ecol.* 87, 164–181. doi:10.1111/1574-6941.12212

Costello, A. M., and Lidstrom, M. E. (1999). Molecular Characterization of Functional and Phylogenetic Genes from Natural Populations of Methanotrophs in Lake Sediments. *Appl. Environ. Microbiol.* 65, 5066–5074. doi:10.1128/aem.65.11.5066-5074.1999

D'Ambrosio, S., and Harrison, J. A. (2021). Methanogenesis Exceeds CH4 Consumption in Eutrophic lake Sediments. *Limnol. Oceanogr. Lett.* 6, 173–181. doi:10.1002/lol2.10192

Danilova, O. V., Suzina, N. E., Van De Kamp, J., Svenning, M. M., Bodrossy, L., and Dedysh, S. N. (2016). A New Cell Morphotype Among Methane Oxidizers: A Spiral-Shaped Obligately Microaerophilic Methanotroph from Northern Low-Oxygen Environments. *ISME J.* 10, 2734–2743. doi:10.1038/ismej.2016.48

Dean, J. F., Middelburg, J. J., Röckmann, T., Aerts, R., Blauw, L. G., Egger, M., et al. (2018). Methane Feedbacks to the Global Climate System in a Warmer World. *Rev. Geophys.* 56, 207–250. doi:10.1002/2017RG000559

Deines, P., Bodelier, P. L., and Eller, G. (2007). Methane-derived Carbon Flows through Methane-Oxidizing Bacteria to Higher Trophic Levels in Aquatic Systems. *Environ. Microbiol.* 9, 1126–1134. doi:10.1111/j.1462-2920.2006.01235.x

Deutzmann, J. S., Stief, P., Brandes, J., and Schink, B. (2014). Anaerobic Methane Oxidation Coupled to Denitrification Is the Dominant Methane Sink in a Deep lake. *Proc. Natl. Acad. Sci. USA* 111, 18273–18278. doi:10.1073/pnas.1411617111

de Valk, S., Khadem, A. F., Foreman, C. M., van Lier, J. B., and de Kreuk, M. K. (2017). Physical and Biochemical Changes in Sludge Upon Tubifex Tubifex Predation. *Environ. Technol.* 38, 1524–1538. doi:10.1080/09593330.2016.1236150

Di Cesare, A., Pjevac, P., Eckert, E., Curkov, N., Miko Šparica, M., Corno, G., et al. (2020). The Role of Metal Contamination in Shaping Microbial Communities in Heavily Polluted marine Sediments. *Environ. Pollut.* 265, 114823. doi:10.1016/j.envpol.2020.114823

Ettwig, K. F., Butler, M. K., Le Paslier, D., Pelletier, E., Mangenot, S., Kuypers, M. M. M., et al. (2010). Nitrite-driven Anaerobic Methane Oxidation by Oxygenic Bacteria. *Nature* 464, 543–548. doi:10.1038/nature08883

Ettwig, K. F., Zhu, B., Speth, D., Keltjens, J. T., Jetten, M. S. M., and Kartal, B. (2016). Archaea Catalyze Iron-dependent Anaerobic Oxidation of Methane. *Proc. Natl. Acad. Sci. USA* 113, 12792–12796. doi:10.1073/pnas.1609534113

Farhan Ul Haque, M., Xu, H.-J., Murrell, J. C., and Crombie, A. (2020). Facultative Methanotrophs - Diversity, Genetics, Molecular Ecology and Biotechnological Potential: a Mini-Review. *Microbiol. (United Kingdom)* 166, 894–908. doi:10.1099/mic.0.000977

Fiskal, A., Anthamatten, E., Deng, L., Han, X., Lagostina, L., Michel, A., et al. (2021a). Carbon Sources of Benthic Fauna in Temperate Lakes across Multiple Trophic States. *Biogeosciences* 18, 4369–4388. doi:10.5194/bg-18-4369-2021

Fiskal, A., Gaillard, A., Giroud, S., Malcic, D., Joshi, P., Sander, M., et al. (2021b). Effects of Macrofaunal Recolonization on Biogeochemical Processes and Microbiota a Mesocosm Study. *Water* 13, 1599. doi:10.3390/w13111599

Fiskal, A., Deng, L., Michel, A., Eickenbusch, P., Han, X., Lagostina, L., et al. (2019). Effects of Eutrophication on Sedimentary Organic Carbon Cycling in Five Temperate Lakes. *Biogeosciences* 16, 3725–3746. doi:10.5194/bg-16-3725-2019

Frenzel, P., Thebrath, B., and Conrad, R. (1990). Oxidation of Methane in the Oxic Surface Layer of a Deep lake Sediment (Lake Constance). *FEMS Microbiol. Lett.* 73, 149–158. doi:10.1016/0378-1097(90)90661-910.1111/j.1574-6968.1990.tb03935.x

Grinsven, S., Sinninghe Damsté, J. S., Engelmann, J. C., Harrison, J., Villanueva, L., and Villanueva, L. (2020a). Methane Oxidation in Anoxic lake Water Stimulated by Nitrate and Sulfate Addition. *Environ. Microbiol.* 22, 766–782. doi:10.1111/1462-2920.14886

Grinsven, S., Sinninghe Damsté, J. S., Polerecky, L., Villanueva, L., and Villanueva, L. (2020b). Nitrate Promotes the Transfer of Methane-derived Carbon from the Methanotroph Methylobacter Sp. To the Methylotroph Methylotenera Sp. in Eutrophic lake Water. *Limnol. Oceanogr.* 66, 878–891. doi:10.1002/lno.11648

Guo, M., Zhuang, Q., Tan, Z., Shurpali, N., Juutinen, S., Kortelainen, P., et al. (2020). Rising Methane Emissions from Boreal Lakes Due to Increasing Ice-free Days. *Environ. Res. Lett.* 15, 064008. doi:10.1088/1748-9326/ab8254

Han, X., Schubert, C. J., Fiskal, A., Dubois, N., and Lever, M. A. (2020). Eutrophication as a Driver of Microbial Community Structure in lake Sediments. *Environ. Microbiol.* 22, 3446–3462. doi:10.1111/1462-2920.15115

He, R., Wooller, M. J., Pohlman, J. W., Quensen, J., Tiedje, J. M., and Leigh, M. B. (2012). Shifts in Identity and Activity of Methanotrophs in Arctic Lake Sediments in Response to Temperature Changes. *Appl. Environ. Microbiol.* 78, 4715–4723. doi:10.1128/AEM.00853-12

He, R., Wang, J., Pohlman, J. W., Jia, Z., Chu, Y.-X., Wooller, M. J., et al. (2021). Metabolic Flexibility of Aerobic Methanotrophs under Anoxic Conditions in Arctic lake Sediments. *ISME J.* 16, 78–90. doi:10.1038/s41396-021-01049-y

Heathcote, A. J., and Downing, J. A. (2012). Impacts of Eutrophication on Carbon Burial in Freshwater Lakes in an Intensively Agricultural Landscape. *Ecosystems* 15, 60–70. doi:10.1007/s10021-011-9488-9

Hernandez, M. E., Beck, D. A. C., Lidstrom, M. E., and Chistoserdova, L. (2015). Oyxgen Availability is a Major Factor in Determining the Composition of Microbial Communities Involved in Methane Oxidation. *Peer J.* 3, e801. doi:10.7717/peerj.801

Holmes, A. J., Costello, A., Lidstrom, M. E., and Murrell, J. C. (1995). Evidence that Participate Methane Monooxygenase and Ammonia Monooxygenase May Be Evolutionarily Related. *FEMS Microbiol.Lett.* 132, 203–208. doi:10.1111/j.1574-6968.1995.tb07834.x

Jones, R. I., and Grey, J. (2011). Biogenic Methane in Freshwater Food Webs. *Freshw. Biol.* 56, 213–229. doi:10.1111/j.1365-2427.2010.02494.x

Kalyuzhnaya, M. G., Yang, S., Rozova, O. N., Smalley, N. E., Clubb, J., Lamb, A., et al. (2013). Highly Efficient Methane Biocatalysis Revealed in a Methanotrophic Bacterium. *Nat. Commun.* 4, 1–7. doi:10.1038/ncomms3785

Kits, K. D., Campbell, D. J., Rosana, A. R., and Stein, L. Y. (2015a). Diverse Electron Sources Support Denitrification under Hypoxia in the Obligate Methanotroph Methylomicrobium Album Strain BG8. *Front. Microbiol.* 6, 1–11. doi:10.3389/fmicb.2015.01072

Kits, K. D., Klotz, M. G., and Stein, L. Y. (2015b). Methane Oxidation Coupled to Nitrate Reduction under Hypoxia by the GammaproteobacteriumMethylomonas Denitrificans, Sp. Nov. Type Strain FJG1. *Environ. Microbiol.* 17, 3219–3232. doi:10.1111/1462-2920.12772

Kiyashko, S., Narita, T., and Wada, E. (2001). Contribution of Methanotrophs to Freshwater Macroinvertebrates: Evidence from Stable Isotope Ratios. *Aquat. Microb. Ecol.* 24, 203–207. doi:10.3354/ame024203

Knief, C. (2015). Diversity and Habitat Preferences of Cultivated and Uncultivated Aerobic Methanotrophic Bacteria Evaluated Based on pmoA as Molecular Marker. *Front. Microbiol.* 6, 1346. doi:10.3389/fmicb.2015.01346

Lennartz, S. (2010). Zinn in Den Sedimenten Des Zürichsees. PhD thesis. Germany: Univ. of Tübingen.

Lerman, A. (1979). *Geochemical Processes: Water and Sediment Environments*. New York, NY: John Wiley & Sons.

Leu, A. O., Cai, C., McIlroy, S. J., Southam, G., Orphan, V. J., Yuan, Z., et al. (2020). Anaerobic Methane Oxidation Coupled to Manganese Reduction by Members of the Methanoperedenaceae. *ISME J.* 14, 1030–1041. doi:10.1038/s41396-020-0590-x

Lever, M. A., Torti, A., Eickenbusch, P., Michaud, A. B., Säntl-Temkiv, T., Jørgensen, B. B., et al. (2015). A Modular Method for the Extraction of DNA and RNA, and the Separation of DNA Pools from Diverse Environmental Sample Types. *Front. Microbiol.* 6, 476. doi:10.3389/fmicb.2015.00476

Lloréns-Rico, V., Vieira-Silva, S., Gonçalves, P. J., Falony, G., and Raes, J. (2021). Benchmarking Microbiome Transformations Favors Experimental Quantitative Approaches to Address Compositionality and Sampling Depth Biases. *Nat. Commun.* 12. doi:10.1038/s41467-021-23821-6

Ludwig, W., Strunk, O., Westram, R., Richter, L., Meier, H., Yadhukumar, A., et al. (2004). ARB: A Software Environment for Sequence Data. *Nucleic Acids Res.* 32, 1363–1371. doi:10.1093/nar/gkh293

Lyautey, E., Billard, E., Tissot, N., Jacquet, S., and Domaizon, I. (2021). Seasonal Dynamics of Abundance, Structure, and Diversity of Methanogens and Methanotrophs in Lake Sediments. *Microb. Ecol.* 82, 559–571. doi:10.1007/s00248-021-01689-9

Maerki, M., Wehrli, B., Dinkel, C., and Müller, B. (2004). The Influence of Tortuosity on Molecular Diffusion in Freshwater Sediments of High Porosity 1 1Associate Editor: M. L. Machesky. *Geochimica et Cosmochimica Acta* 68, 1519–1528. doi:10.1016/j.gca.2003.09.019

Mayr, M. J., Zimmermann, M., Guggenheim, C., Brand, A., and Bürgmann, H. (2020). Niche Partitioning of Methane-Oxidizing Bacteria along the Oxygen-Methane Counter Gradient of Stratified Lakes. *ISME J.* 14, 274–287. doi:10.1038/s41396-019-0515-8

McDonald, I. R., Bodrossy, L., Chen, Y., and Murrell, J. C. (2008). Molecular Ecology Techniques for the Study of Aerobic Methanotrophs. *Appl. Environ. Microbiol.* 74, 1305–1315. doi:10.1128/AEM.02233-07

Mukherjee, S., Stamatis, D., Bertsch, J., Ovchinnikova, G., Sundaramurthi, J. C., Lee, J., et al. (2021). Genomes OnLine Database (GOLD) v.8: Overview and Updates. *Nucleic Acids Res.* 49, D723–D733. doi:10.1093/nar/gkaa983

Müller, B., Wang, Y., Dittrich, M., and Wehrli, B. (2003). Influence of Organic Carbon Decomposition on Calcite Dissolution in Surficial Sediments of a Freshwater lake. *Water Res.* 37, 4524–4532. doi:10.1016/S0043-1354(03)00381-6

Naeher, S., Gilli, A., North, R. P., Hamann, Y., and Schubert, C. J. (2013). Tracing Bottom Water Oxygenation with Sedimentary Mn/Fe Ratios in Lake Zurich, Switzerland. *Chem. Geology.* 352, 125–133. doi:10.1016/j.chemgeo.2013.06.006

Ogle, D., Doll, J., Wheeler, P., and Dinno, A. (2021). FSA: Fisheries Stock Analysis. R package version 0.9.1, Available at: https://github.com/droglenc/FSA.

Oksanen, J., Blanchet, F. G., Friendly, M., Kindt, R., Legendre, P., and McGlinn, D. (2020). Vegan: Community Ecology Package: R Package Version 2.5-7. Available at: https://scholar.google.com/scholar?hl=en&as_sdt=0%2C5&q=vegan%3A+Community+Ecology+Package.+R+++package+version+2.5-7&btnG= [Accessed January 11, 2022].

Oshkin, I. Y., Beck, D. A., Lamb, A. E., Tchesnokova, V., Benuska, G., McTaggart, T. L., et al. (2014). Methane-fed Microbial Microcosms Show Differential Community Dynamics and Pinpoint Taxa Involved in Communal Response. *ISME J.* 9, 1119–1129. doi:10.1038/ismej.2014.203

Oshkin, I. Y., Miroshnikov, K. K., Grouzdev, D. S., and Dedysh, S. N. (2020). Pan-genome-based Analysis as a Framework for Demarcating Two Closely Related Methanotroph Genera Methylocystis and Methylosinus. *Microorganisms* 8, 768. doi:10.3390/microorganisms8050768

Oswald, K., Milucka, J., Brand, A., Hach, P., Littmann, S., Wehrli, B., et al. (2016). Aerobic Gammaproteobacterial Methanotrophs Mitigate Methane Emissions from Oxic and Anoxic lake Waters. *Limnol. Oceanogr.* 61, S101–S118. doi:10.1002/lno.10312

Pester, M., Schleper, C., and Wagner, M. (2011). The Thaumarchaeota: an Emerging View of Their Phylogeny and Ecophysiology. *Curr. Opin. Microbiol.* 14, 300–306. doi:10.1016/j.mib.2011.04.007

Pierangeli, G. M. F., Domingues, M. R., Jesus, T. A. d., Coelho, W. S., Pompêo, M. L. M., Saia, F. T., et al. (2021). Higher Abundance of Sediment Methanogens and Methanotrophs Do Not Predict the Atmospheric Methane and Carbon Dioxide Flows in Eutrophic Tropical Freshwater Reservoirs. *Front. Microbiol.* 12, 1–15. doi:10.3389/fmicb.2021.647921

Rahalkar, M., Deutzmann, J., Schink, B., and Bussmann, I. (2009). Abundance and Activity of Methanotrophic Bacteria in Littoral and Profundal Sediments of lake Constance (Germany). *Appl. Environ. Microbiol.* 75, 119–126. doi:10.1128/AEM.01350-08

Reim, A., Lüke, C., Krause, S., Pratscher, J., and Frenzel, P. (2012). One Millimetre Makes the Difference: High-Resolution Analysis of Methane-Oxidizing Bacteria and Their Specific Activity at the Oxic-Anoxic Interface in a Flooded Paddy Soil. *ISME J.* 6, 2128–2139. doi:10.1038/ismej.2012.57

Rognes, T., Flouri, T., Nichols, B., Quince, C., and Mahé, F. (2016). VSEARCH: A Versatile Open Source Tool for Metagenomics. *PeerJ* 4, e2584. doi:10.7717/PEERJ.2584/FIG-7

Sanches, L. F., Guenet, B., Marinho, C. C., Barros, N., and de Assis Esteves, F. (2019). Global Regulation of Methane Emission from Natural Lakes. *Sci. Rep.* 9, 1–10. doi:10.1038/s41598-018-36519-5

Schubert, C. J., Diem, T., and Eugster, W. (2012). Methane Emissions from a Small Wind Shielded lake Determined by Eddy Covariance, Flux chambers, Anchored Funnels, and Boundary Model Calculations: A Comparison. *Environ. Sci. Technol.* 46, 4515–4522. doi:10.1021/es203465x

Smith, G. J., Angle, J. C., Solden, L. M., Borton, M. A., Morin, T. H., Daly, R. A., et al. (2018). Members of the Genus Methylobacter Are Inferred to Account for the Majority of Aerobic Methane Oxidation in Oxic Soils from a Freshwater Wetland. *MBio* 9, 1–17. doi:10.1128/mBio.00815-18

Teranes, J. L., McKenzie, J. A., Lotter, A. F., and Sturm, M. (1999). Stable Isotope Response to lake Eutrophication: Calibration of a High-Resolution Lacustrine Sequence from Baldeggersee, Switzerland. *Limnol. Oceanogr.* 44, 320–333. doi:10.4319/lo.1999.44.2.0320

Thauer, R. K., Jungermann, K., and Decker, K. (1977). Energy Conservation in Chemotrophic Anaerobic Bacteria. *Bacteriol. Rev.* 41, 100–180. doi:10.1128/br.41.1.100-180.1977

Thebrath, B., Rothfuss, F., Whiticar, M. J., and Conrad, R. (1993). Methane Production in Littoral Sediment of Lake Constance. *FEMS Microbiol. Ecol.* 102, 279–289. doi:10.1111/j.1574-6968.1993.tb05819.x

Thottathil, S. D., Reis, P. C. J., del Giorgio, P. A., and Prairie, Y. T. (2018). The Extent and Regulation of Summer Methane Oxidation in Northern Lakes. *J. Geophys. Res. Biogeosci.* 123, 3216–3230. doi:10.1029/2018JG004464

Tranvik, L. J., Downing, J. A., Cotner, J. B., Loiselle, S. A., Striegl, R. G., Ballatore, T. J., et al. (2009). Lakes and Reservoirs as Regulators of Carbon Cycling and Climate. *Limnol. Oceanogr.* 54, 2298–2314. doi:10.4319/lo.2009.54.6_part_2.2298

Tsutsumi, M., Kojima, H., and Fukui, M. (2012). Vertical Profiles of Abundance and Potential Activity of Methane-Oxidizing Bacteria in Sediment of Lake Biwa, Japan. *Microb. Environ.* 27, 67–71. doi:10.1264/jsme2.ME11285

van Grinsven, S., Oswald, K., Wehrli, B., Jegge, C., Zopfi, J., Lehmann, M. F., et al. (2021). Methane Oxidation in the Waters of a Humic-Rich Boreal lake Stimulated by Photosynthesis, Nitrite, Fe(III) and Humics. *Biogeosciences* 18, 3087–3101. doi:10.5194/bg-18-3087-2021

Vekeman, B., Kerckhof, F.-M., Cremers, G., de Vos, P., Vandamme, P., Boon, N., et al. (2016). New Methyloceanibacter Diversity from North Sea Sediments Includes

Methanotroph Containing Solely the Soluble Methane Monooxygenase. *Environ. Microbiol.* 18, 4523–4536. doi:10.1111/1462-2920.13485

Wickham, H. (2016). *ggplot2: Elegant Graphics for Data Analysis*. New York, NY: Springer-Verlag.

Yang, Y., Chen, J., Tong, T., Li, B., He, T., Liu, Y., et al. (2019). Eutrophication Influences Methanotrophic Activity, Abundance and Community Structure in Freshwater Lakes. *Sci. Total Environ.* 662, 863–872. doi:10.1016/j.scitotenv.2019.01.307

Yang, Y., Zhao, Q., Cui, Y., Wang, Y., Xie, S., and Liu, Y. (2016). Spatio-temporal Variation of Sediment Methanotrophic Microorganisms in a Large Eutrophic lake. *Microb. Ecol.* 71, 9–17. doi:10.1007/s00248-015-0667-7

Zheng, Y., Wang, H., Liu, Y., Zhu, B., Li, J., Yang, Y., et al. (2020). Methane-Dependent Mineral Reduction by Aerobic Methanotrophs under Hypoxia. *Environ. Sci. Technol. Lett.* 7, 606–612. doi:10.1021/acs.estlett.0c00436

Zhu, Y., Purdy, K. J., Eyice, Ö., Shen, L., Harpenslager, S. F., Yvon-Durocher, G., et al. (2020). Disproportionate Increase in Freshwater Methane Emissions Induced by Experimental Warming. *Nat. Clim. Chang.* 10, 685–690. doi:10.1038/s41558-020-0824-y

Conflict of Interest: The authors declare that the research was conducted in the absence of any commercial or financial relationships that could be construed as a potential conflict of interest.

Publisher's Note: All claims expressed in this article are solely those of the authors and do not necessarily represent those of their affiliated organizations, or those of the publisher, the editors and the reviewers. Any product that may be evaluated in this article, or claim that may be made by its manufacturer, is not guaranteed or endorsed by the publisher.

Copyright © 2022 van Grinsven, Meier, Michel, Han, Schubert and Lever. This is an open-access article distributed under the terms of the Creative Commons Attribution License (CC BY). The use, distribution or reproduction in other forums is permitted, provided the original author(s) and the copyright owner(s) are credited and that the original publication in this journal is cited, in accordance with accepted academic practice. No use, distribution or reproduction is permitted which does not comply with these terms.

frontiers in Environmental Science

ORIGINAL RESEARCH
published: 11 March 2022
doi: 10.3389/fenvs.2022.833936

Spatial Variability and Hotspots of Methane Concentrations in a Large Temperate River

Ingeborg Bussmann[1]*, *Uta Koedel*[2], *Claudia Schütze*[3], *Norbert Kamjunke*[4] and *Matthias Koschorreck*[5]

[1]Departments of Marine Geochemistry and Shelf Sea System Ecology, Alfred-Wegener-Institut, Helmholtz Zentrum für Polar- und Meeresforschung, Bremerhaven, Germany, [2]Department Monitoring and Exploration Technologies, Helmholtz Centre for Environmental Research UFZ, Leipzig, Germany, [3]Department Computational Hydrosystems, Helmholtz Centre for Environmental Research UFZ, Leipzig, Germany, [4]Department River Ecology, Helmholtz Centre for Environmental Research UFZ, Magdeburg, Germany, [5]Department Lake Research, Helmholtz Centre for Environmental Research UFZ, Magdeburg, Germany

Rivers are significant sources of greenhouse gases (GHGs; e.g., CH_4 and CO_2); however, our understanding of the large-scale longitudinal patterns of GHG emissions from rivers remains incomplete, representing a major challenge in upscaling. Local hotspots and moderate heterogeneities may be overlooked by conventional sampling schemes. In August 2020 and for the first time, we performed continuous (once per minute) CH_4 measurements of surface water during a 584-km-long river cruise along the German Elbe to explore heterogeneities in CH_4 concentration at different spatial scales and identify CH_4 hotspots along the river. The median concentration of dissolved CH_4 in the Elbe was 112 nmol L^{-1}, ranging from 40 to 1,456 nmol L^{-1} The highest CH_4 concentrations were recorded at known potential hotspots, such as weirs and harbors. These hotspots were also notable in terms of atmospheric CH_4 concentrations, indicating that measurements in the atmosphere above the water are useful for hotspot detection. The median atmospheric CH_4 concentration was 2,033 ppb, ranging from 1,821 to 2,796 ppb. We observed only moderate changes and fluctuations in values along the river. Tributaries did not obviously affect CH_4 concentrations in the main river. The median CH_4 emission was 251 µmol m^{-2} d^{-1}, resulting in a total of 28,640 mol d^{-1} from the entire German Elbe. Similar numbers were obtained using a conventional sampling approach, indicating that continuous measurements are not essential for a large-scale budget. However, we observed considerable lateral heterogeneity, with significantly higher concentrations near the shore only in reaches with groins. Sedimentation and organic matter mineralization in groin fields evidently increase CH_4 concentrations in the river, leading to considerable lateral heterogeneity. Thus, river morphology and structures determine the variability of dissolved CH_4 in large rivers, resulting in smooth concentrations at the beginning of the Elbe versus a strong variability in its lower parts. In conclusion, groin construction is an additional anthropogenic modification following dam building that can significantly increase GHG emissions from rivers.

Keywords: greenhouse gas, methane, Elbe River, groins, emission, fluxes, continuous sampling, large scale

OPEN ACCESS

Edited by:
Tonya DelSontro,
University of Waterloo, Canada

Reviewed by:
Bernhard Mayer,
University of Calgary, Canada
Daniele Kasper,
Federal University of Rio de Janeiro, Brazil

***Correspondence:**
Ingeborg Bussmann
Ingeborg.bussmann@awi.de

Specialty section:
This article was submitted to Biogeochemical Dynamics, a section of the journal Frontiers in Environmental Science

Received: *12 December 2021*
Accepted: *04 February 2022*
Published: *11 March 2022*

Citation:
Bussmann I, Koedel U, Schütze C, Kamjunke N and Koschorreck M (2022) Spatial Variability and Hotspots of Methane Concentrations in a Large Temperate River. Front. Environ. Sci. 10:833936. doi: 10.3389/fenvs.2022.833936

1 INTRODUCTION

Awareness regarding the significant contributions of inland waters, such as lakes, reservoirs, or rivers, to the global CH_4 budget (103 Tg CH_4 $year^{-1}$) has been increasing (Rosentreter et al., 2021); however, relatively few studies have investigated CH_4 dynamics in flowing waters (Bastviken et al., 2011). Streams and rivers have garnered much attention as the sources of atmospheric CH_4 (Stanley et al., 2016). Regardless of being well-aerated, lotic waters are typically oversaturated with CH_4 compared to water in equilibrium with atmospheric CH_4, resulting in significant diffusive emissions to the atmosphere (Stanley et al., 2016). However, the precise quantification of these CH_4 emissions is challenging because of large spatiotemporal heterogeneities. The magnitude of these diffusive emissions depends on the water turbulence, physical gas transfer coefficient, and CH_4 partial pressure difference between water and the atmosphere (Donelan et al., 2002).

Dissolved CH_4 concentrations are rather variable and depend on the balance between the input of CH_4 to water and its loss. While outgassing to the atmosphere is the most important CH_4 loss process, microbial CH_4 consumption in the water is relatively slow (Matoušů et al., 2019). The main sources of CH_4 are in-stream production in anoxic sediments and import from riparian areas (Rasilo et al., 2017). The hydrologic linkage to suitable habitats such as inundated floodplains and wetlands delivers CH_4 to the river channel (Stanley et al., 2016). Recently, possible phytoplankton-mediated CH_4 production under oxic conditions has been discussed (Tang et al., 2016).

However, localized input of CH_4 to streams is not simple to detect, because outgassing is a rapid process, resulting in a short residence time of CH_4 in stream water (in River Elbe less than a day). Furthermore, the low solubility of CH_4 in the water coupled with its rapid water–atmosphere exchange can lead to pronounced heterogeneities in CH_4 concentrations along the river gradient. Any CH_4 input to a stream is lost to the atmosphere within a short flow distance, resulting in the local control of CH_4 concentrations in streams (Stanley et al., 2016).

Conventional assessments of spatial heterogeneity in streams rely on discrete sampling, restricting the amount of possible data and spatial resolution. In a previous study also along the Elbe, large-scale patterns and hotspots of elevated CH_4 concentrations have been revealed (Matoušů et al., 2019). In particular, harbors, dammed river sections, and tributary inflows are the well-known CH_4 emission hotspots (Maeck et al., 2013), which are often neglected in conventional sampling schemes. Therefore, upscaling based on such conventional datasets entails a high degree of uncertainty, because the employed approaches may overlook local hotspots and the spatial extent of such hotspots may be poorly defined.

A number of approaches can be used to quantify CH_4 concentrations and detect CH_4 emission hotspots. To measure dissolved CH_4 at a high spatial resolution, several degassing systems coupled with cavity ring-down spectroscopy have been used (Gonzalez-Valencia et al., 2014). Alternatively, *in-situ* CH_4 sensors can be used to map CH_4 (Canning et al., 2021). Moreover, CH_4 point emission sources can be identified based on atmospheric measurements using a hyperspectral camera (Gålfalk et al., 2016) or mobile gas analyzer (Karion et al., 2013). Atmospheric CH_4 measurements from autonomous boats have been used to map CH_4 emissions from freshwaters (Dunbabin and Grinham 2017).

To this end, we scanned a 584 km longitudinal transect along the Elbe—Germany's third largest river—including the mouth of several tributaries. We simultaneously and continuously measured dissolved and atmospheric CH_4 concentrations using a degassing system connected to a greenhouse gas analyzer. In addition, we measured basic hydrographic parameters. This allowed a novel and high spatial resolution of about 4000 data points. The present study aimed to quantify CH_4 concentrations in and identify CH_4 hotspots along the river channel. By analyzing a quasi-continuous dataset of CH_4 concentrations we tried to identify and characterize possible sources of CH_4, which is hardly possible with single water samples along the river. Finally, by monitoring the CH_4 mixing ratio in the atmosphere in parallel, we explored the potential effects of fluctuating atmospheric CH_4 concentrations on the calculated CH_4 emissions, the possibility of detecting hotspots based on atmospheric measurements and thus to improve the estimation of the diffusive CH_4 flux from the Elbe.

2 MATERIALS AND METHODS

2.1 Study Area: German Elbe and its Tributaries

River Elbe is 1,094-km-long, flowing from the Czech Republic to the North Sea. The catchment area spans 148,268 km^2, and the mean annual discharge is 861 $m^3 s^{-1}$ at the mouth. The present study covers the German part of the river between the Czech border (Elbe km-0) and Geesthacht weir (Elbe km-586). Discharge at the gauge Magdeburg at the time of the study was 241 $m^3 s^{-1}$, which is close to the average low value (231 $m^3 s^{-1}$) and 44% of the annual mean (554 $m^3 s^{-1}$). Elbe flows through several land use types, including highly urbanized zones, agricultural regions, and near-natural areas. Major tributaries are the rivers Schwarze Elster, Mulde, Saale, and Havel. Here, we primarily focused on the effects of Havel on dissolved CH_4 in the Elbe. Additional information on the tributaries is provided in the **Supplementary Material**.

2.2 Vessel Cruise and Water Sampling

Sampling was performed using the research vessel Albis, which is 15-m-long and has a draft of only 45 cm. We used the Lagrangian approach in which sampling was performed according to the travel time of the river water. The cruise started on 4 August 2020, in Schmilka (Elbe km-4) and was completed on 12 August 2020, in Geesthacht (Elbe km-584, **Figure 1**). The positions recorded by GPS (longitude and latitude) were converted to "Elbe kilometer" together with information on the lateral distance to the middle of the navigation channel (https://atlas.wsv.bund.de/bwastr-locator/client/).

At 23 stations, a transect across the river channel was sampled (left-hand shore, middle, and right-hand shore, **Figure 1**). Each

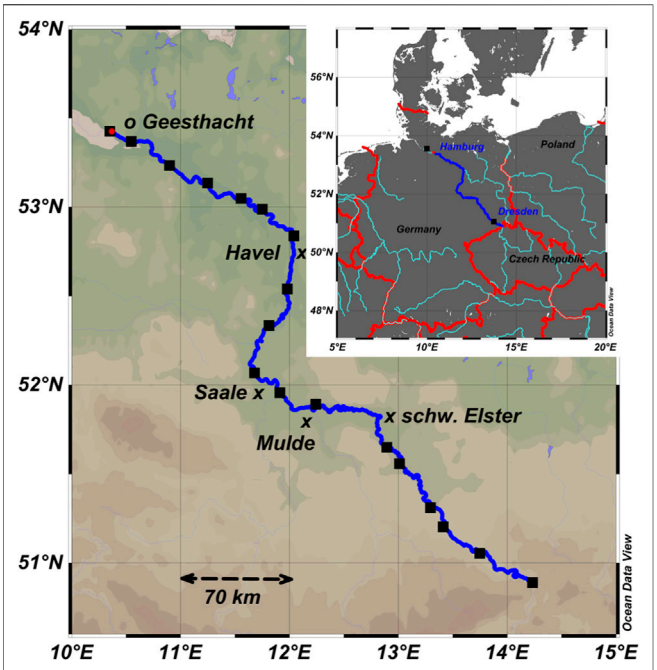


FIGURE 1 | Map of the studied part of German. The inlet shows the location of the Elbe (blue) within Europe (red border lines) and other rivers (light blue).

time the anchor was set, sampling was performed for approximately 10 min. In addition, river water was pumped continuously from the vessel bottom to a pool, which provided water to all continuous measurement devices.

For CH_4 analyses, 30 ml water samples were collected with a horizontal water sampler (Hydro-Bios, Germany) and 60 ml plastic syringes. A headspace of 30 ml ambient air was created, and the syringes were vigorously shaken for 2 min. The equilibrated headspace was transferred to evacuated Exetainer vials (Labco, United Kingdom), and the equilibration temperature was measured by inserting a thermometer in the remaining water sample in the syringe. Air samples were collected for subsequent headspace correction.

Gas samples in the Exetainer vials were analyzed using a gas chromatograph equipped with a flame ionization detector (SRI 8610, SRI Instruments, Torrance U.S.A.). Certified mixtures of 10.01 ppm CH_4 in N_2 were used as the standards. CH_4 concentrations in the water samples were calculated based on the mixing ratios in equilibrated headspace samples corrected for CH_4 concentrations in the applied air headspace according to Henry's law.

2.3 Continuous Measurements

2.3.1 Dissolved CH_4

Dissolved CH_4 concentrations in the continuous water supply were measured with a dissolved gas extraction unit and a laser-based analytical greenhouse gas analyzer (GGA; both LosGatosResearch, San Jose, CA, United States). The degassing unit drew water from the water basins (as described above) at a flow rate of ~1.5 L min^{-1}. CH_4 was extracted from the water via a hydrophobic membrane and hydrocarbon-free carrier gas on the other side of the membrane (synthetic air, flow rate = 0.5 L min^{-1}). The carrier gas, including the extracted CH_4, was then forwarded to the inlet of the gas analyzer. The time offset between the drawing in of water and stable recording on the GGA was predetermined in the laboratory. The total offset (water supply + instrument offset) was 87 s.

The degassing efficiency depends on the ratio of water flow to gas flow, in addition to the water temperature. In the laboratory, the efficiency had been determined at various ratios. During the cruise, the water flow decreased due to the clogging of the filters. The ppm values obtained from the GGA were corrected for extraction efficiency at the respective water-to-gas flow ratios. Only data for which the fit flag of the GGA was "3" and data that were obtained when the vessel was moving (see next section) were used. Data were recorded each second and averaged per minute. Sampling times were from morning until late afternoon.

To convert the relative concentrations (ppm) given by the GGA to absolute concentrations (nmol L^{-1}), CH_4 concentrations measured in discrete water samples were used to calculate the conversion factor (20.21 nmol L^{-1} ppm^{-1}). Previous tests have shown that this set-up had a precision of 7.3% (unpublished data I. Bussmann). Dissolved CO_2 concentrations are presented in the **Supplementary Material**.

2.3.2 Atmospheric CO_2 and CH_4

GHG concentrations in ambient air were measured with the LI-7810 $CH_4/CO_2/H_2O$ Trace Gas Analyzer (LI-COR Biosciences, Lincoln, NE, United States), which is a laser-based gas analyzer that uses optical feedback cavity-enhanced absorption spectroscopy. The analyzer was installed on the top deck of the research vessel, and measurements were obtained continuously at the sampling frequency of 1 Hz. Due to the internal flow rate and the use of a 2 m tube, there was a small delay of 1 s between the tube inlet and the detector. The analyzer provides the dry mole fractions of CH_4 [ppb] and CO_2 [ppm] in air corrected for both spectroscopic interference and dilution due to water vapor. Unpublished tests of the device setup under ambient air conditions showed a precision of 1.5% for CO_2 measurements and 0.7% for CH_4 measurements.

All sampled data were averaged over 1 min, quality-checked and flagged in terms of low-quality or non-interesting values (e.g., outliers, power-up data, or vessel in the harbor) and merged with the position data. For spatial analysis, only data obtained when the vessel was moving (flag 1 = good and flag 2 = 1) were considered. The data of the night-time stops were used to study the influence of the atmospheric diurnal cycle.

2.3.3 Hydrographic Parameters

A portable pocket FerryBox (4H-Jena, Germany) was used to record the hydrographic parameters and positions using the following sensors: Seabird SBE45 thermosalinograph, Aanderaa oxygen optode, Meinsberg pH electrode, Seapoint Chlorophyll Fluorometer (SCF), and Seapoint Turbidity Meter. The water flow was 3–4 L min^{-1}. Data were saved once per minute.

On some days, the pump of the ferry box did not work properly. Thus, only data obtained when the flow rate was >1 L min^{-1} were used. Data obtained when the system was

rinsed with freshwater from the vessel were manually filtered and discarded. The oxygen sensor broke on August 10.

Data on the water discharge of Elbe were obtained from https://hochwasservorhersage.sachsen-anhalt.de for the nearest water gauges at Magdeburg, Wittenberg, Barby-Saale, and Tangermünde. Data on flow velocity were provided by A. Schoel, Bundesanstalt für Gewässerkunde, Koblenz, Germany.

2.4 Flux Calculations, Mixing, and Upscaling

Diffusive CH_4 emissions (J) where calculated using the following equation:

$$J\ (mmol\ m^{-2} d^{-1}) = k_{CH4} \times (C_{aq} - C_{eq})$$

where k is the median gas transfer coefficient (k_{CH4} = 2.32 m d^{-1}, calculated based on the data published by Matoušů et al. (2019), ranging from 0.37 to 8.81 m d^{-1}, n = 8); C_{aq} is the measured CH_4 concentration in the water; and C_{eq} is the CH_4 concentration in the water that is in equilibrium with the atmosphere.

The equilibrium concentration was calculated using two methods. First, we calculated C_{eq} based on the data of the respective dissolved CH_4 concentration and water temperature (n = 61) at single stations. Salinity was set to 0.01 PSU (practical salinity unit). For atmospheric CH_4 concentration, a fixed value of 1938.5 ppb was used (annual mean at Zugspitze, Germany, (https://www.umweltbundesamt.de/daten/klima/atmosphaerische-treibhausgas-konzentrationen).

Second, we used continuously measured dissolved CH_4 concentrations at the respective water temperature. Salinity was set to 0.01 PSU. For further flux calculation, the actual measured atmospheric CH_4 concentration was used. From all 4,298 sampling points, the median and range were calculated.

To calculate the total diffusive flux from Elbe, we fitted a polynomial to the width *versus* Elbe kilometer data published by Mallast et al. (2020) (**Supplementary Figure S1**) for determining Elbe width per kilometer (w). We averaged the diffusive flux per kilometer (J_{km}). Harbors were excluded from this calculation. The total diffusive flux per kilometer (J_{tot}) was calculated using the following equation and finally summed up from km-9 to km-584:

$$J_{tot}\ (mol\ d^{-1}) = \sum J_{km} \times (w \times 1000\ m)$$

We modeled CH_4 concentrations at the inflow of three major tributaries using a simple mass balance model. The expected dilution of the tributary water was calculated from the discharge data of the tributaries and Elbe assuming conservative mixing (**Table 2**).

To integrate the area under the curve, KaleidaGraph (Synergy, version 4.5) was used. Diffusive flux (μmol m^{-2} d^{-1}) was plotted against distance (Elbe kilometer in meters, x-axis), resulting in a cumulative flux (mol m^{-1} d^{-1}). **Figure 6** and **Figure 8** were obtained with QGIS (QGIS.org, 2022. QGIS Geographic Information System. QGIS Association), Bing Aerial (2022, Basemap for QGIS) and **Figure 5** with Google Earth pro (7.3.4.8248).

To estimate atmospheric flux on windy and calm nights without horizontal wind flow, we used the approach proposed by Barkwith et al. (2020). Based on the discretization model of the near-surface atmosphere into boxes, where each box is treated similar to an open flux chamber with an inlet for the ambient air and an outlet to generate a continuous gas flow, gas flux can be estimated. Assuming fully mixed air within the boxes and no horizontal wind within the measurement height, the flux can be calculated as the difference between the observed and background gas concentration within the assumed box volume.

3 RESULTS

3.1 Overall Distribution of CH_4

The median dissolved CH_4 concentration in Elbe was 112 nmol L^{-1}, ranging from 40 to 1,456 nmol L^{-1} (**Table 1**, **Supplementary Figure S2**). The median CH_4 concentration in equilibrium with the atmosphere was 2.8 nmol L^{-1}, indicating that Elbe water was always supersaturated. Dissolved CO_2 concentrations are presented in **Supplementary Figure S3**. We observed large-scale patterns of GHG concentrations both along the river course and in specific regions with elevated dissolved CH_4 concentrations, such as harbors and some tributaries.

In the Elbe channel near the Czech border (near km-4), CH_4 concentration was rather high (250 nmol L^{-1}). In the first 120 km, dissolved CH_4 concentration decreased steadily, albeit without marked variability (50–100 nmol L^{-1}) (**Figure 2A**). In the middle part, dissolved CH_4 concentration fluctuated between 50 and 110 nmol L^{-1}. In this part of the river, we observed large variability, with several distinct small peaks (**Figure 3**). There was a clear increase in CH_4 concentration to approximately 200 nmol L^{-1} after km-430 (**Figure 2A**). Starting from Elbe km-560, CH_4 concentrations increased further toward the weir Geesthacht, reaching very high values up to 1,000 nmol L^{-1} (**Figure 2A**).

The median diffusive CH_4 flux from the water to atmosphere along the Elbe course was 251 μmol m^{-2} d^{-1}, ranging from 66 to 3,709 μmol m^{-2} d^{-1} (**Table 1**; **Figure 2B**). The distribution of diffusive flux along the river reflected the distribution of CH_4 concentration, with the maxima at harbors, near the shore, and upstream of the weir (**Supplementary Figure S4**). The comparison of calculations based on the continuous measurements of dissolved and atmospheric CH_4 and water temperature *versus* the calculations based on single water samples and the overall German atmospheric CH_4 concentration revealed near identical median values but narrower ranges (**Table 1**).

3.2 Atmospheric CH_4

The mean atmospheric CH_4 concentration along the Elbe course was 2,034 ± 54 ppb (**Figure 2A**). The time series showed a distinct sawtooth pattern. Apparently, the deviation from the atmospheric baseline is related to the time of day, with more or less increased concentrations in the early morning hours, followed by a slow decrease to the normal conditions during the day.

To analyze the temporal behavior of atmospheric gas concentrations and distinguish between temporal and spatial patterns, longer observation periods at a fixed location were required. For that purpose, we used continuous measurements during the night-time stops in harbors, for instance, a 12-h stop at Elbe km-200 near Dessau. A substantial increase of approximately

TABLE 1 | Comparison of the discrete and continuous measurements of dissolved and atmospheric CH_4 and resulting CH_4 emission estimates.

	Discrete sampling	Continuous measurements
n_{water}	57	3,786
CH_4 concentration range (nmol L^{-1})	5–1,639	40–1,456
CH_4 concentration median (nmol L^{-1})	112	112
Median equilibrium concentration (nmol L^{-1})	2.634	2.813
n_{atm}	1	479k
Atmospheric CH_4 range (ppb)		1,821–2,796
Atmospheric CH_4 median (ppb)	1,951[a]	2,033
Median (range) of diffusive CH_4 flux (μmol m^{-2} d^{-1})	248 (4–3,796) n = 61	251 (66–3,709) n = 3,543[b]
Total diffusive CH_4 emission (mol d^{-1})[c]	27,791	28,747

[a]*Annual mean value at the Zugspitze station (https://www.umweltbundesamt.de/daten/klima/atmosphaerische-treibhausgas-konzentrationen).*
[c]*Value based on the total river surface area (A) of 112 km^2 (see Materials and Methods).*
[b]*This value is less than that for n_{water} due to data gap; when water temperature data were missing, the daily mean was used for calculation.*

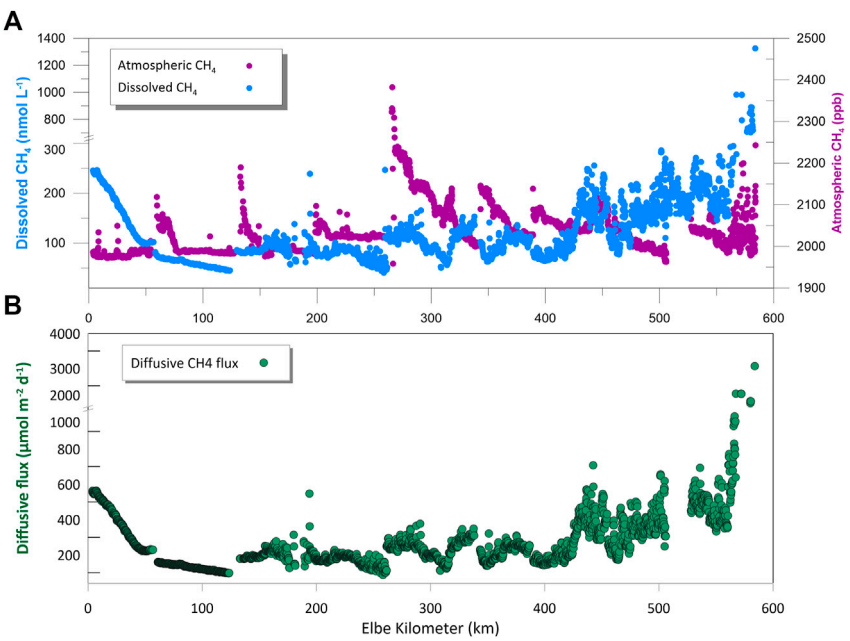


FIGURE 2 | Atmospheric (ppb) and dissolved CH_4 (nmol L^{-1}) concentration **(A)** and diffusive CH_4 emissions (μmol m^{-2} d^{-1}) *versus* river km **(B)** Only data obtained when the vessel was moving at the speed of >4 kn were considered; tributaries were excluded.

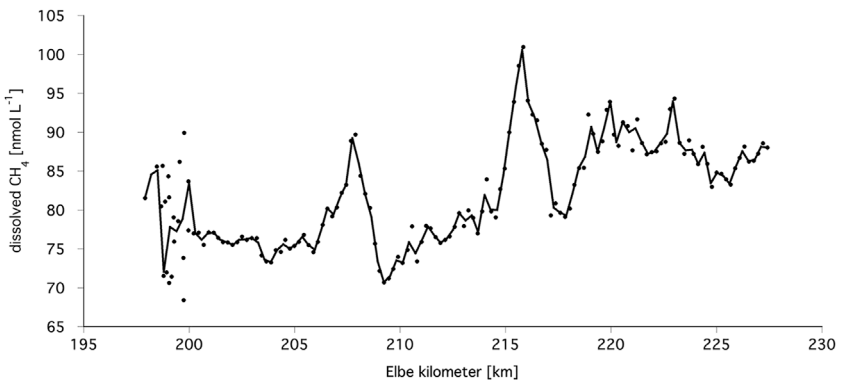


FIGURE 3 | Small-scale heterogeneity of dissolved CH_4 along a selected reach around km-210. Data from **Figure 2** were used; interpolated line is shown.

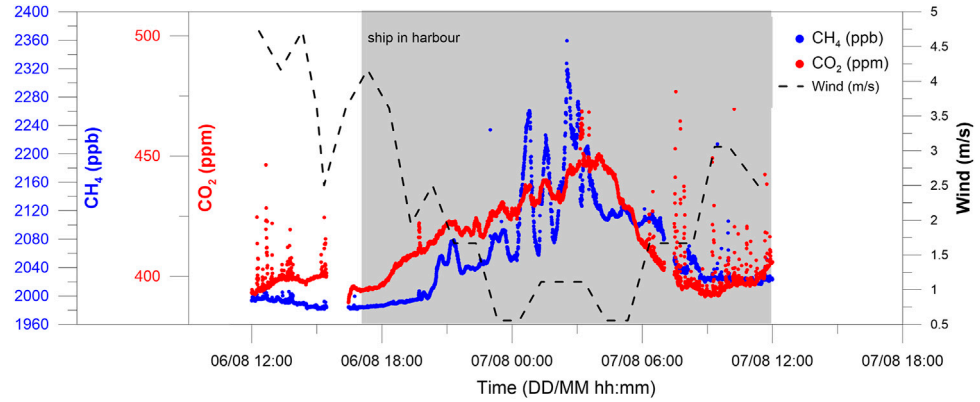


FIGURE 4 | Variability in the atmospheric greenhouse gas concentrations during a diurnal cycle compared to the wind conditions measured in the surrounding at Elbe km-200. Wind data were obtained from https://www.timeanddate.de/wetter/deutschland.

15% in the mixing ratio for both gases during the night may be attributed to the still active (and more or less stable) emission sources, consistent with atmospheric accumulation processes due to low dynamics in the near-surface layers (wind velocity <2 m s^{-1}; data from the Elster weather station, Elbe).

Furthermore, the diurnal cycle (**Figure 4**) reflected the causes of the observed patterns of and jumps in atmospheric CH_4 concentrations depicted in **Figure 2A**. The atmospheric CH_4 data appeared to be clearly affected by the diurnal wind situation. After a calm night with low winds in the morning hours, extreme increases in atmospheric CH_4 concentrations were observed in the harbors. Moreover, the cruise often started with higher CH_4 concentrations in the morning hours compared to the latest values measured on the previous day at the same location. In the further course of the day, the values gradually stabilized, resulting in the typical sawtooth pattern, as shown in **Figure 2A**. Hence, to use atmospheric CH_4 measurements as an indicator of potential emission sources, the knowledge of meteorological conditions and the diurnal cycle at selected locations is necessary.

In addition to this regular pattern, some locations with increased atmospheric CH_4 concentrations were detected during the continuous measurements. In particular, while staying in harbors or passing larger urban areas (such as the cities of Dresden or Magdeburg), increased CH_4 concentrations were observed. Interestingly, according to the elevated dissolved CH_4 concentrations, zones with increased atmospheric values were measured (e.g., upstream of the weir Geesthacht, at km-560: maximum concentration = 2,250 ppb).

3.3 Small-Scale Variability

We also observed small-scale variability of dissolved CH_4. A typical mid-river section (**Figure 3**) exemplified some noise but also distinct concentration peaks. For instance, at km-207 and km-215, two small peaks were observed with an increase from 75 to 90 nM and from 80 to 100 nM, respectively. More such small peaks were observed from km-260 to km-300 (not shown).

These locally elevated CH_4 concentrations are difficult to explain. A possible reason is that the vessel occasionally approached one of the river sides, where concentrations were higher. However, there was no correlation between the distance of the vessel from the central waterway and the dissolved CH_4 concentration. Thus, the peaks cannot be explained by lateral vessel movements. In addition, CH_4 concentration was not correlated with flow velocities above 0.8 m s^{-1} (**Supplementary Figure S5**).

3.4 Lateral Variations

CH_4 concentrations in the water samples taken near the shore were significantly higher than those in the middle of the river (**Supplementary Figure S6**, Wilcoxon rank sign test, paired data, $n = 19$, $p = 0.01$ for right shore vs. middle and $p = 0.05$ for left shore versus middle). The mean CH_4 concentration at the 18 sites was 300 ± 393 nmol L^{-1} near the shore and 228 ± 350 nmol L^{-1} in the middle, indicating a difference of 32%.

Based on high-resolution measurements, we observed either no difference (Schmilka, **Figure 5A**, 31%), a symmetric distribution of the lateral increase (Rogätz, **Figure 5B**, 25%), a one-sided increase (Werben, **Figure 5C**, 31%), or a linear increase (13%) in dissolved CH_4 in the lateral transects. Elevated CH_4 concentrations near the shore were more pronounced and more variable in the lower reaches of the river (**Supplementary Figure S6**). We compared the different patterns of the lateral CH_4 distribution in Schmilka (no difference), Rogätz (symmetric), and Werben (one-sided) based on the aerial photographs of the sites (provided by Googpe Earth Pro for 24 June 2016; 6 August 2020; and 15 September 2016). In Schmilka, no obstacles were noted at the shore line. Meanwhile, groins were visible on both sides in Rogätz and in Werben only at the left river shore.

3.5 Hotspots

The highest dissolved CH_4 concentrations were recorded in the harbors (Dresden, Mühlberg, Leopoldshafen, Niedgripper Schleuse, Wittenberg, and Dömitz), with a median of 828 nM, ranging from 284 to 2,136 nM. Accordingly, the diffusive flux in the harbors was nearly six times higher than that in the river itself, with a median of 1,655, ranging from 806 to 3,010 μmol m^{-2} d^{-1}.

Additionally, elevated CH_4 concentrations were noted as the course approached Geesthacht weir on August 12 (**Figure 6**).

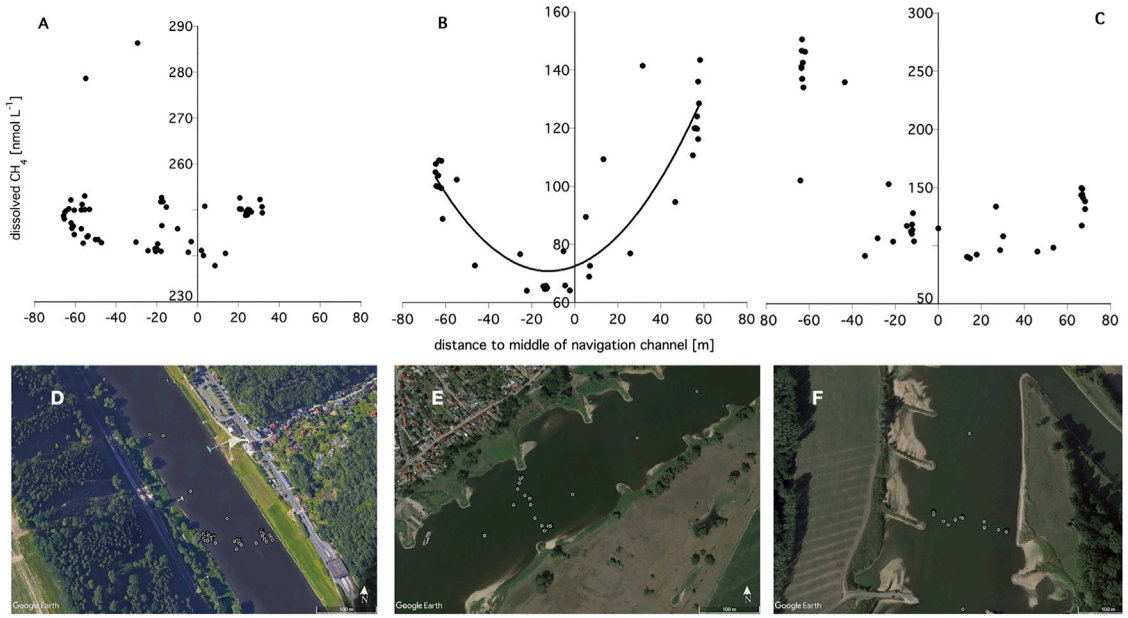


FIGURE 5 | Dissolved CH_4 concentration at lateral transects in Schmilka **(A and D**, km-4**)** Rogätz **(B and E**, km-351**)** and Werben **(C and F**, km-422**)**. Aerial photographs were retrieved from Google Earth Pro, dots indicate the ship's position.

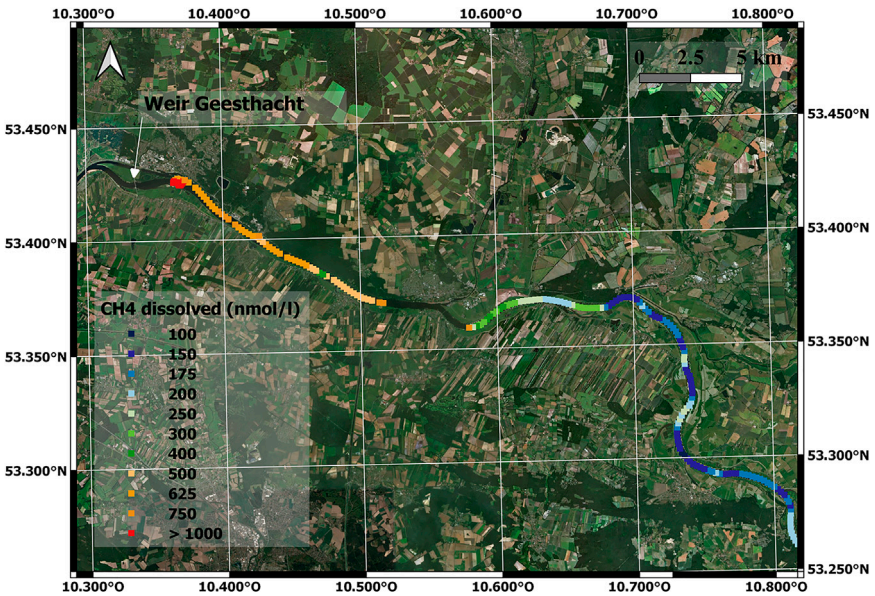


FIGURE 6 | Dissolved CH_4 concentration upstream of the weir Geesthacht. Map base: Bing Aerial.

Intermediate CH_4 concentrations (minimum = 154 nM) were recorded until 24 km before the weir, and the value increased toward the weir, reaching the maximum concentration of 1,127 nM (km-555 to km-590). Conductivity and temperature slightly increased toward the weir, while chlorophyll and turbidity decreased. The diffusive flux of CH_4 increased toward the weir, from values below 700 μmol m^{-2} d^{-1} at Elbe km < 567 to values exceeding 1,500 μmol m^{-2} d^{-1} at Elbe km > 576.

Likewise, atmospheric CH_4 concentrations also increased toward the weir (**Figure 7**), although no direct correlation with dissolved CH_4 concentration or diffusive CH_4 flux was noted.

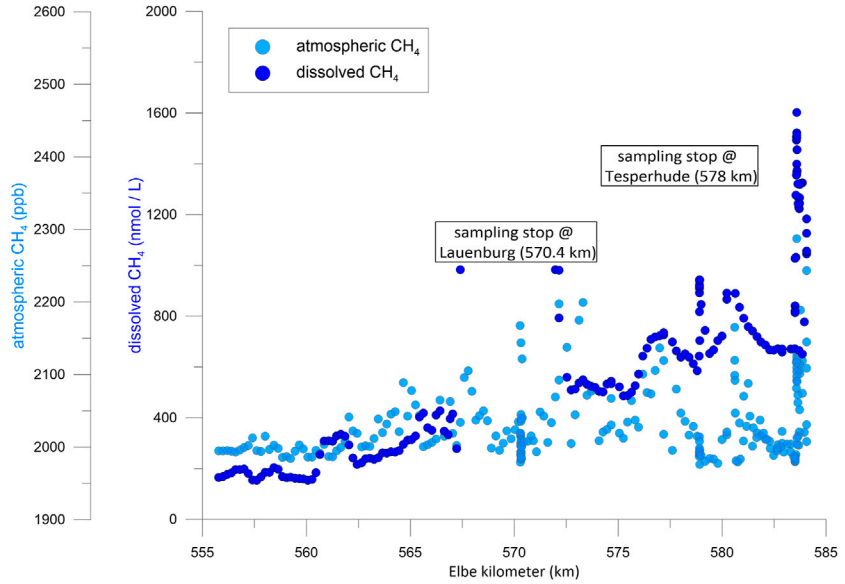


FIGURE 7 | Atmospheric CH_4 and dissolved CO_2 and CH_4 concentrations upstream of the weir Geesthacht.

TABLE 2 | CH_4 budget at tributary inflows.

	Schwarze Elster	Mulde	Saale	Havel
Q_{Elbe} (m^3 s^{-1})	218[a]	218[a]	233.6[b]	269[c]
$Q_{Tributary}$ (m^3 s^{-1})	1.38	11	24.4	5.5
Q ratio (E/T)	158	20	10	49
CH_4 Elbe upstream (nM)	85 (79–91) *n* = 4	112 (110–114) n = 9	109 (107–112) n = 6	165 (152–176) *n* = 4
CH_4 tributary (nM)	147 (78–165) n = 17	394 (380–401) n = 13	124 (112–153) n = 14	256 (227–271) *n* = 14
CH_4 Elbe downstream:				
Measured [nM]	72 (71–82) n = 11	s110 (108–113) n = 10	121 (114–127) n = 6	149 (132–245) n = 6
Expected [nM]	85	126		167

[a]*Gauge Wittenberg.*
[b]*Gauge Barby–Saale.*
[c]*Gauge Tangermünde.*
Expected downstream concentrations were calculated based on Elbe + Tributary data assuming conservative mixing.
Q_{Elbe} was obtained from https://hochwasservorhersage.sachsen-anhalt.de/.
For CH_4 concentrations, the median value, range, and number of sampling points are indicated.

3.6 Tributaries

Tributaries showed little effect on CH_4 concentrations in the main river. CH_4 concentrations downstream of tributary inflows were similar to the concentrations upstream (**Table 2**; **Figure 8**). Discharge of Havel was about 2% of the Elbe discharge. Compared with the value in the upstream region of Elbe (165 nM), CH_4 concentration in the upstream region of Havel was higher (256 nM). However, in the downstream region, CH_4 concentration rapidly decreased within 1.2 km (149 nM) (**Table 2** and **Figure 8**). The CH_4 concentration predicted assuming conservative mixing was 167 nM. Similar trends of a negligible influence were also noted in the other tributaries (**Supplementary Figures S7, S8** and **Table 2**).

Interestingly, we observed a small hotspot with elevated CH_4 approximately 3 km upstream of the mouth of Havel (**Figure 8**). Along a reach of ~2.5 km, CH_4 concentrations were nearly 1.7 times elevated. A detailed inspection of the cruise track revealed that the vessel had been steaming close to an area of large groin fields on the left-hand shore (**Figure 8**).

3.7 Flux and Upscaling

We applied a weighted approach to calculate the total diffusive flux of CH_4 from Elbe to the atmosphere, taking into account the fact that the width of the river increases from the Czech border toward Geesthacht weir (112 m at km-10–282 m at km-497), with a final increase in CH_4 concentration towards the weir. The weighted approach revealed a total area of 112 km^2, resulting in the emission of 28,747 mol CH_4 d^{-1} (**Table 1**), which is equivalent to 0.46 t CH_4 d^{-1}. The calculation of total daily emissions based on discrete water sampling data revealed a similar value (0.43 t CH_4 d^{-1}). Thus, the spatial resolution of discrete sampling was sufficient to estimate correct total emission.

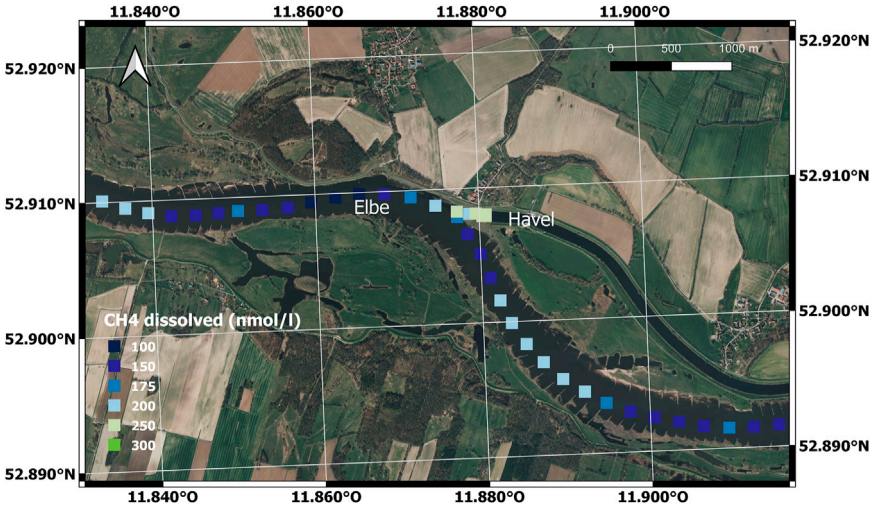


FIGURE 8 | CH_4 concentration at the mouth of Havel. Map base: Bing Aerial.

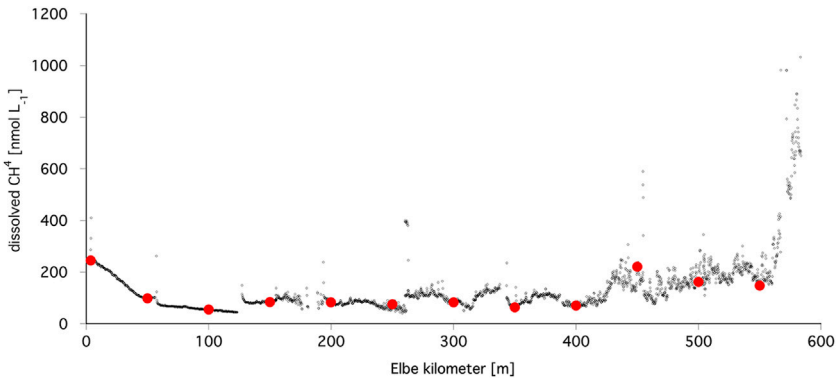


FIGURE 9 | Comparison between the continuously measured dissolved CH_4 concentration (small black dots) and the concentration (red circles) at every 50 km.

To evaluate the benefit of high-resolution CH_4 data for upscaling, we subsampled our continuous dataset of dissolved CH_4 assuming sampling every 10, 20, 50, or 100 km. The "all" dataset considered only sampling at the river, excluding harbors, and no transects, resulting in a total of 2,740 data points. The starting point at km-3 and endpoint at km-584 were included in all cases. As a result, the following average values of dissolved CH_4 and number of data points were recorded: 137 ± 116 nM (std error = 2%) and n = 2,665 for the "all" dataset; 148 ± 183 nM (std error = 24%) and n = 59 for the every 10 km dataset; 158 ± 231 nM (std error = 43%) and n = 29 for the every 20 km dataset; 209 ± 341 nM (std error = 95%) and n = 13 for the every 50 km dataset; and 290 ± 462 nM (std error = 175%) and n = 7 for the every 100 km dataset, respectively. The average values increased from the "all" dataset (137 nM) toward the every 100 km dataset (290 nM); however, the standard deviation and standard error also increased markedly. As shown in **Figure 9**, with the example of the "every 50 km" data set, the background and median values could be easily covered with less frequent sampling. However, the peaks and extremes could be rarely covered.

The relevance of different sampling densities to the calculation of diffusive flux was estimated by determining the area under the curve of the diffusive flux along Elbe. The cumulative diffusive flux along Elbe, as measured with continuous sampling, was 177 mol m^{-1} d^{-1}. With sampling every 10, 20, 50, and 100 km, the cumulative diffusive fluxes were mostly higher at 174, 183, 191, and 255 mol m^{-1} d^{-1}, respectively. Sampling at 10 and 20 km yielded comparable results to continuous sampling. However, inadequate sampling at 50 and 100 km resulted in the overestimation of diffusive flux by 8–44%.

4 DISCUSSION

The Elbe River was consistently oversaturated with CH_4 (related to water in equilibrium with atmospheric CH_4), rendering it a

steady source of the emission of this GHG to the atmosphere. This result is consistent with literature (Stanley et al., 2016) and supports the view that in addition to small streams, which receive CH_4 from riparian soils (Leng et al., 2021), larger rivers must also be considered CH_4 sources. Our emission estimate of 251 μmol m^{-2} d^{-1} (153 t y^{-1} in total) is almost double than a previous estimate (131 μmol m^{-2} d^{-1} or 97 t y^{-1}, Matoušů et al., 2019). However, the estimated flux from Elbe was comparable to that recorded from other large German rivers, including Rhine (119 μmol m^{-2} d^{-1}; Wilkinson et al., 2019) and Danube (209–370 μmol m^{-2} d^{-1}; Canning et al., 2021; Maier et al., 2021). This study was conducted in August 2020; therefore, seasonal differences in water discharge, water temperature and CH_4 concentrations were not considered.

4.1 Methods

The comparison of CH_4 emission calculation based on either continuous or discrete data proved that conventional discrete sampling is sufficient to scale up emissions to the entire river. Furthermore, we did not observe a diurnal pattern of CH_4 concentrations in the water, indicating that the time of day need not be considered in discrete sampling schemes. Thus, continuous CH_4 data from a river cruise are not affected by short term temporal fluctuations and useful to identify the spatial patterns of this GHG.

Typically, a constant atmospheric mixing ratio is used to calculate the concentration gradient at the water–atmosphere interface. Although we observed some variability in atmospheric CH_4, this had a minor effect on flux calculation and upscaling. The median CH_4 concentration was 4% higher than the reference measurements at Zugspitze. At Germany's highest peak, the measured values are particularly representative of the background pollution of the atmosphere and largely unaffected by local sources (https://www.umweltbundesamt.de/daten/klima/atmosphaerische-treibhausgas-konzentrationen). Using that value as the reference atmospheric concentration for flux calculations, the median CH_4 flux would be 251 μmol m^{-2} d^{-1}, which is identical to the value we obtained based on the *in-situ* data. Therefore, for the German Elbe, continuous measurements of atmospheric CH_4 are not required to obtain a reliable flux estimate.

The conversion of concentration data to diffusive emission requires the knowledge of gas transfer velocity (K_{600}, the gas transfer velocity for CO_2 at 20°C). In the present study, we did not measure K but used previously published data calculated from simultaneous flux and concentration measurements (Matoušů et al., 2019). Our K_{600} of 2.35 m d^{-1} for German Elbe is similar to the values reported for other large rivers, including Danube (median = 0.69, range = 0.2–3.4 m d^{-1}) (Maier et al., 2021). A similar K_{600} of 2.53 m d^{-1} was obtained using the standard empirical calculation of K_{600} based on flow velocity and slope (Raymond et al., 2012). Although the use of a constant K_{600} for the entire river would surely introduce some bias, we consider the possible error to be rather small. Flow conditions were rather uniform along the river channel. The mean flow velocity during the cruise was 0.9 ± 0.2 m s^{-1} (**Supplementary Figure S5**) based on data derived from a river model (Andreas Schöl, pers. com.). Thus, as K_{600} fluctuated within a rather narrow range, the effect of K_{600} variations on total CH_4 emission estimates should be minor. An exception might be the reach directly upstream of the weir at Geesthacht, where the flow velocity was ~0.2 m s^{-1} [K_{600} = 2.1, according to Raymond et al. (2012)], and the use of a constant K_{600} (2.32) may have slightly overestimated diffusive emissions.

However, while the longitudinal heterogeneities of K_{600} probably had a minor impact on total CH_4 emissions, this may not be true for lateral transects. Previous comparisons of K_{600} in the middle of the river and near the shore along Magdeburg have indicated approximately 40% lower K_{600} values near the river banks (Koschorreck, unpublished data). However, a lower K_{600} near the shore may be balanced by a higher K_{600} at groin heads, where water flow is typically turbulent. Thus, small-scale quantification of K_{600} using drifting floating chambers (Lorke et al., 2015) is essential to better assess gas transfer velocities at large rivers.

Our data show that lateral heterogeneity is definitely relevant to the assessment of dissolved CH_4 concentrations. Here, we emphasize the effects of measurement strategies. First, our longitudinal dataset may be affected by the exact position of the vessel in the river during the cruise. Second, when obtaining discrete samples from a river for CH_4 quantification, it is important to sample water from not only the middle of the river but also sides—a fact already known for the measurement of other water parameters (Weigold and Baborowski 2009).

Furthermore, the lateral extension (width) of the river must also be considered when CH_4 emissions are scaled up to the entire river. For instance, we compared two sites (km-75 versus km-311) with similar diffusive CH_4 fluxes (146 μmol m^{-2} d^{-1}) but with different widths (132 *versus* 189 m). At the wider site, the total diffusive flux was approximately 1.5 times higher (28 *versus* 19 mol d^{-1}). Overlooking different widths and simply applying the mean flux to the entire river area would assign greater weight to measurements in the upstream area (narrower), thus underestimating the total emissions. As Elbe becomes broader toward Geesthacht and the CH_4 concentrations increase, the total CH_4 flux of this area is high both due to high CH_4 concentration and large surface area.

This study was conducted at mean water level. It is currently unclear what influence the water level has on the flow conditions at the groins. Further seasonal studies are needed here.

4.2 Hotspot Occurrence and Extension

Since the flow velocity of Elbe was rather uniform (with the exception of reaches upstream the weir), any pronounced deviation from the baseline CH_4 concentration should be caused by the changes in source strength. However, as our data show it is not trivial to distinguish a point source of CH_4 from a "hot moment," which may create CH_4 plumes. We observed different shapes of CH_4 peaks during our cruise which we conceptualize in **Figure 10**. A point source should result in a stationary hotspot with declining concentration downstream due to outgassing. Meanwhile, a "hot moment" would result in a parcel of water with elevated CH_4 concentration, which moves downstream, losing CH_4 to the atmosphere on its way. Thus, information on the source of

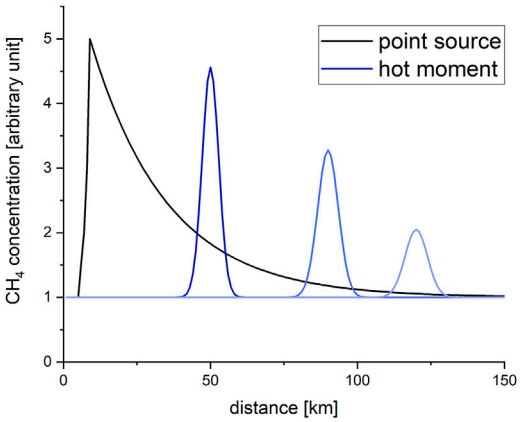


FIGURE 10 | Shape of a hypothetical CH_4 hotspot depending on its origin. The point source curve was calculated as described by Crawford et al. (2014), assuming k_{600} = 2.32 m d^{-1}, water depth = 1 m, and flow velocity = 0.72 m s^{-1}. The blue lines indicate the downstream movement of a CH_4 plume created by a "hot moment."

elevated CH_4 can be gained by analyzing continuous CH_4 concentration dataset, as discussed below.

4.2.1 Weirs and Harbors as Hotspots

Weirs affect CH_4 concentrations both in the upstream and downstream reaches. Thus, weirs act as a point source. The higher CH_4 concentration at the start of our cruise was probably caused by the weir at Usti, approximately 40 km upstream of our starting point in Schmilka. This speculation is supported by our observation of elevated CH_4 at Geesthacht weir as well as earlier observations (Matoušů et al., 2019). Assuming that CH_4 oxidation is slow [6–10 times slower than diffusive loss (Heilweil et al., 2016; Matoušů et al., 2019)], CH_4 outgassing must be the major loss process and the impact of a weir as a point source should be evident up to 100 km downstream (**Figure 10**). This is consistent with our observation of "normal" concentrations nearly 60 km downstream of Schmilka, which is 100 km downstream of the weir. Thus, in addition to the dammed section, weirs increase CH_4 concentrations also in reaches downstream of the weir.

As expected, CH_4 concentrations and emissions were high upstream of the Geesthacht weir (with emissions of >1,500 µmol m^{-2} d^{-1} at the weir *versus* the median of only 251 µmol m^{-2} d^{-1} for the entire river). The surface area before the weir (km > 576) is ~4 million m^2 (estimated based on a Google Earth Pro image), and as the diffusive flux was high, the region accounted for 28% to the total diffusive CH_4 emissions from Elbe. The trapping of sediments upstream of river dams triggers high CH_4 production in the sediment (Maeck et al., 2013), resulting in extreme CH_4 emissions (DelSontro et al., 2010). At such sites, CH_4 emissions are typically dominated by ebullition—a process not considered in the present study. Thus, at least in the dammed section, our CH_4 emission estimation based solely on diffusion probably underestimated the actual value. While continuous CH_4 concentration measurements are suitable to detect CH_4 concentration hotspots, they are not suitable to quantify emissions at hotspots where ebullition occurs. However, ebullition also increases CH_4 concentration in the water due to CH_4 loss from rising bubbles (DelSontro et al., 2010). Thus, we believe that continuous CH_4 concentration measurements allow the detection of sites with intensive ebullition.

At harbors, we observed high diffusive fluxes, which were approximately 6 times greater than in the river itself. These observations corroborate the results reported by Matoušů et al. (2019). In the harbor basins with mostly stagnant water, organic material accumulates, resulting in higher CH_4 concentrations and diffusive fluxes. We estimated the areas of the harbors Dresden, Mühlberg, Dessau, Niegripper Schleuse, Wittenberg and Dömitz using Google Earth Pro and calculated a total area of 404,974 m^2. However, as their respective areas were small, these harbors accounted for only 2% to the total flux in Elbe. Thus, the river itself accounts for 70% of the diffusive flux. These flux estimates for harbors can be considered the maximum values, since we used the same K for harbors as that for the flowing river. These results were consistent with our harbor flux estimates based on atmospheric CH_4 accumulation during the night, which showed that CH_4 fluxes in the harbor and river were quite similar. Thus, in harbors, high CH_4 concentrations are counterbalanced by low K values and may be neglected from the quantification of total CH_4 emissions from the river.

4.2.2 Hot Moments and Small-Scale Variability

We frequently observed small peaks of dissolved CH_4 for which we could find no straightforward explanation (**Figure 3**). Interestingly, we observed these small peaks only in areas with groins. As discussed below, groin fields are the possible sources of CH_4. Between the groin heads, the shear stress of the main current leads to an energy input into the groin fields, resulting in eddies detaching from the groin heads. Furthermore, they promote energy and mass exchange between the main and the groin field flow (Kleinwächter et al., 2017). In the context of the present study, this implies that at the head of the groins, CH_4-rich eddies were released, which then traveled along Elbe, becoming smaller with time (**Figure 10**).

In our analysis, we probably overestimated the size of these small peaks because the vessel was moving with the current. When the vessel steaming downstream at ~3.6 m s^{-1} was passing a CH_4 plume drifting at 0.9 m s^{-1} in the same direction, it likely stayed longer in the plume than when the water was not moving. As a result, the spatial extent of these plumes may have been overestimated.

4.2.3 Tributaries

The inflow of four tributaries (Schwarze Elster, Mulde, Saale, and Havel) did not markedly increase CH_4 concentrations in the main river below the confluence, even though CH_4 concentration within the tributaries were significantly higher than that in the mainstream, as also observed in a similar study in 2017 (Matoušů et al., 2019). This is not surprising considering the lower relative discharge of the tributaries than that of Elbe (**Table 2**). Only Saale contributed a considerable amount of water (10% of the Elbe

discharge), but its CH_4 concentrations were only marginally elevated compared to those in Elbe.

Another possible explanation for the minor influence of the tributaries is that the vessel mainly measured concentrations in the middle of the river. Thus, we may have missed the plumes of the tributaries, when their input was flowing parallel to the shore. For Saale, where conductivity is elevated, water mainly flows along the left shoreline and complete mixing occurs only after 100 km (Kamjunke et al., 2021). In future studies, the inflow of tributaries should be better followed along the shore line.

Low contribution to riverine CH_4 is probably also true for backwaters, which may exhibit extremely high CH_4 concentrations (Staniek 2019). In River Danube, CH_4 exchange between floodplain waters and the river was driven by hydrology, and significant amounts of CH_4 were flushed into the river when the water level was lowering (Sieczko et al., 2016). However, under stagnant low-water conditions, as in the present study, most floodplain waters are disconnected from the river, with little water exchange.

4.2.4 Atmospheric Measurements as a Tool for Hotspot Detection

The measurement of CH_4 concentrations in the atmosphere directly above the water surface has been used to identify the hotspots of CH_4 emissions and even calculate emission rates (Dunbabin and Grinham 2017). We observed elevated atmospheric CH_4 concentrations in harbors and in reaches upstream of a weir, confirming that atmospheric measurements can be useful to identify emission hotspots. However, the calculation of fluxes based on our atmospheric CH_4 data was only possible under specific environmental conditions. Our analyses revealed a considerable effect of diurnal meteorological conditions on the atmospheric CH_4 mixing ratio, which prevented quantitative interpretation with respect to aquatic emissions. As an exception, measurements at night, when the vessel was anchored in the harbors, showed elevated atmospheric CH_4. Using a virtual open chamber approach (Barkwith et al., 2020), an emission rate of 8.4 $\mu mol\ m^{-2}\ h^{-1}$ (=202 $\mu mol\ m^{-2}\ d^{-1}$) was calculated in the quiet nighttime hours. This value is close to the diffusive flux of 251 $\mu mol\ m^{-2}\ d^{-1}$ (**Table 1**). In daylight hours, when the wind conditions were more complex and when the vessel was cruising along the river, atmospheric data were rather stable and did not allow for the tracking of small-scale variability and spots with locally elevated aquatic CH_4 concentrations.

4.3 Large-Scale Patterns and Effects of Groins

In addition to the above hotspots, we observed interesting large-scale patterns. Before km-130, the variability of dissolved CH_4 was rather low. Despite the longitudinal trend, we did not observe small-scale fluctuations. Further, there was an evident change in dissolved CH_4 around km-130. Notably, this observation coincided with the first appearance of groins. To improve navigability, groins have been constructed all along the downstream reaches of Elbe from km-122. These groin fields give rise to a high spatiotemporal diversity of sedimentation regimes (Henning and Hentschel 2013).

The hypothesis that groins increase the variability of riverine CH_4 was supported by our lateral transect data, which showed elevated CH_4 concentrations near the shore only in the presence of groins. This is plausible because groins create areas of reduced flow velocity, resulting in the sedimentation of suspended particles (Pusch and Fischer 2006). These accumulated sediments act as the sites of intensive organic matter mineralization and, probably, methanogenesis (Schwartz and Kozerski 2003). Assuming that groin fields are the relevant sources of CH_4, the CH_4 concentrations in the river may be regulated by 1) CH_4 production in a respective groin field and 2) water exchange between the groin field and the middle of the river.

The lateral variability of CH_4 concentration was more pronounced in the downstream reaches of the river (**Supplementary Figure S6**), implying higher CH_4 production in these downstream reaches or lower water exchange between the banks and middle of the river, resulting in CH_4 accumulation in the groin fields. The second explanation is more plausible given the greater width of the river (**Supplementary Figure S1**), combined with lower flow velocity. Evidently, the presence of groin fields increases riverine CH_4 concentrations, although the magnitude of this effect depends on site conditions.

It is well known that damming increases CH_4 emissions from rivers (Maeck et al., 2013). We show in this study that damming is not the only mechanism by which human alterations increase riverine CH_4 emissions. We conclude that the construction of groins is an additional mechanism by which anthropogenic modifications significantly increase CH_4 emissions from rivers.

5 CONCLUSION

Besides the conventional assessments of spatial heterogeneity in streams based on discrete sampling, we presented data from a new approach continuously investigating large-scale patterns and hotspots of elevated CH_4 concentrations along the Elbe River. We observed large-scale patterns of GHG concentrations both along the river course and in specific regions with elevated dissolved CH_4 concentrations, such as harbors, some tributaries and the weir. The River Elbe was consistently oversaturated with CH_4 (related to water in equilibrium with atmospheric methane) and had to be considered as a CH_4 source with an emission rate estimated at 251 $\mu mol\ m^{-2}\ d^{-1}$.

High-spatial resolution measurements of dissolved CH_4 in the River Elbe revealed that weirs increased CH_4 concentrations not only upstream, but also downstream of a weir. At these hotspots not only elevated CH_4 concentrations in the water but also in the atmosphere were observed, confirming that atmospheric measurements can be useful to identify emission hotspots.

The inflow of four tributaries did not significantly increase CH_4 concentrations in the main river below the confluence. However, to fully assess the impact of tributaries on riverine

CH_4 spatially resolved sampling downstream of the confluence areas is necessary.

Groin fields appeared to be an unexpected but important source of high small-scale variability. We could clearly distinguish between river reaches without groins and lower and constant CH_4 concentration and river reaches with groins with a high variability of dissolved CH_4. Thus, the CH_4 concentration in the river is regulated by a complex interplay of 1) CH_4 originating from upstream reaches, 2) CH_4 production in a respective groin field, and 3) water exchange between the groin field and the middle of the river. These interactions result in significant lateral CH_4 concentration profiles with higher dissolve CH_4 concentrations near to the shore as well as in hitherto unknown small scale CH_4 concentration fluctuations along the river. Future work aiming to quantify CH_4 emissions from rivers needs to take into account this variability.

The direct comparison of our discrete and continuous measurements proved that conventional discrete sampling is sufficient to estimate an upscaled methane emission rate for the entire river. However, our data also clearly show the importance of the acquisition of regions with small-scale anomalies based on high resolution sampling strategies. The here proposed continuous sampling is valuable to survey the entire river system or at least the vulnerable regions, which can be of great relevance in case of extreme hydrological events.

DATA AVAILABILITY STATEMENT

The datasets presented in this study can be found in the pangea repository at the following address: https://doi.pangaea.de/10.1594/PANGAEA.939900.

AUTHOR CONTRIBUTIONS

All authors listed have made a substantial, direct, and intellectual contribution to the work and approved it for publication.

FUNDING

This study was part of the Helmholtz Program Changing Earth, ST4.1: "Fluxes and transformation of energy and matter in and across compartments;" and ST5.2 "Water resources and environment." We acknowledge funding from the Helmholtz Association in the framework of the Helmholtz funded observation system MOSES (Modular Observation Solutions for Earth Systems) and from the Initiative and Networking Fund of the Helmholtz Association through the project "Digital Earth" (funding code ZT-0025).

ACKNOWLEDGMENTS

We thank Sven Bauth, Erik Evers, Heike Goretzka, Hannah Jebens, and Ute Link, and for help during field and laboratory work.

SUPPLEMENTARY MATERIAL

The Supplementary Material for this article can be found online at: https://www.frontiersin.org/articles/10.3389/fenvs.2022.833936/full#supplementary-material

REFERENCES

Barkwith, A., Beaubien, S. E., Barlow, T., Kirk, K., Lister, T. R., Tartarello, M. C., et al. (2020). Using Near-Surface Atmospheric Measurements as a Proxy for Quantifying Field-Scale Soil Gas Flux. *Geosci. Instrum. Method. Data Syst.* 9 (2), 483–490. doi:10.5194/gi-9-483-2020

Bastviken, D., Tranvik, L. J., Downing, J. A., Crill, P. M., and Enrich-Prast, A. (2011). Freshwater Methane Emissions Offset the continental Carbon Sink. *Science* 331 (6013), 50. doi:10.1126/science.1196808

Canning, A., Wehrli, B., and Körtzinger, A. (2021). Methane in the Danube Delta: the Importance of Spatial Patterns and Diel Cycles for Atmospheric Emission Estimates. *Biogeosciences* 18 (12), 3961–3979. doi:10.5194/bg-18-3961-2021

Crawford, J. T., Lottig, N. R., Stanley, E. H., Walker, J. F., Hanson, P. C., Finlay, J. C., et al. (2014). CO_2 and CH_4 Emissions from Streams in a Lake-Rich Landscape: Patterns, Controls, and Regional Significance. *Glob. Biogeochem. Cycles* 28 (3), 197–210. doi:10.1002/2013gb004661

DelSontro, T., McGinnis, D. F., Sobek, S., Ostrovsky, I., and Wehrli, B. (2010). Extreme Methane Emissions from a Swiss Hydropower Reservoir: Contribution from Bubbling Sediments. *Environ. Sci. Technol.* 44 (7), 2419–2425. doi:10.1021/Es9031369

Donelan, M. A., Drennan, W. M., Saltzman, E. S., and Wanninkhof, R. (2002). *Gas Transfer at Water Surfaces*. Washington, USA: American Geophysical Union. doi:10.1029/GM127

Dunbabin, M., and Grinham, A. (2017). Quantifying Spatiotemporal Greenhouse Gas Emissions Using Autonomous Surface Vehicles. *J. Field Rob.* 34 (1), 151–169. doi:10.1002/rob.21665

Gålfalk, M., Olofsson, G., Crill, P., and Bastviken, D. (2016). Making Methane Visible. *Nat. Clim Change* 6, 426–430. doi:10.1038/nclimate2877

Gonzalez-Valencia, R., Magana-Rodriguez, F., Gerardo-Nieto, O., Sepulveda-Jauregui, A., Martinez-Cruz, K., Walter Anthony, K., et al. (2014). *In Situ* measurement of Dissolved Methane and Carbon Dioxide in Freshwater Ecosystems by off-Axis Integrated Cavity Output Spectroscopy. *Environ. Sci. Technol.* 48 (19), 11421–11428. doi:10.1021/es500987j

Heilweil, V. M., Solomon, D. K., Darrah, T. H., Gilmore, T. E., and Genereux, D. P. (2016). Gas-Tracer Experiment for Evaluating the Fate of Methane in a Coastal Plain Stream: Degassing versus In-Stream Oxidation. *Environ. Sci. Technol.* 50 (19), 10504–10511. doi:10.1021/acs.est.6b02224

Henning, M., and Hentschel, B. (2013). Sedimentation and Flow Patterns Induced by Regular and Modified Groynes on the River Elbe, Germany. *Ecohydrol.* 6 (4), 598–610. doi:10.1002/eco.1398

Kamjunke, N., Rode, M., Baborowski, M., Kunz, J. V., Zehner, J., Borchardt, D., et al. (2021). High Irradiation and Low Discharge Promote the Dominant Role of Phytoplankton in Riverine Nutrient Dynamics. *Limnol. Oceanogr.* 66, 2648–2660. doi:10.1002/lno.11778

Karion, A., Sweeney, C., Pétron, G., Frost, G., Michael Hardesty, R., Kofler, J., et al. (2013). Methane Emissions Estimate from Airborne Measurements over a Western United States Natural Gas Field. *Geophys. Res. Lett.* 40 (16), 4393–4397. doi:10.1002/grl.50811

Kleinwächter, M., Schröder, U., Rödiger, S., Hentschel, B., and Anlauf, A. (2017). *Alternative Buhnenformen in der Elbe - hydraulische und ökologische Wirkungen. Kapitel 3: Buhnen an der Elbe und ihre Umgestaltung*. Stuttgart: Schweizerbart.

Koschorreck, M., Prairie, Y. T., Kim, J., and Marcé, R. (2021). Technical Note: CO_2 Is Not like CH_4 - Limits of and Corrections to the Headspace Method to Analyse pCO_2 in Fresh Water. *Biogeosciences* 18 (5), 1619–1627. doi:10.5194/bg-18-1619-2021

Leng, P., Kamjunke, N., Li, F., and Koschorreck, M. (2021). Temporal Patterns of Methane Emissions from Two Streams with Different

Riparian Connectivity. *J. Geophys. Res. Biogeosci.* 126 (8), e2020JG006104. doi:10.1029/2020JG006104

Lorke, A., Bodmer, P., Noss, C., Alshboul, Z., Koschorreck, M., Somlai-Haase, C., et al. (2015). Technical Note: Drifting versus Anchored Flux chambers for Measuring Greenhouse Gas Emissions from Running Waters. *Biogeosciences* 12 (23), 7013–7024. doi:10.5194/bg-12-7013-2015

Maeck, A., DelSontro, T., McGinnis, D. F., Fischer, H., Flury, S., Schmidt, M., et al. (2013). Sediment Trapping by Dams Creates Methane Emission Hot Spots. *Environ. Sci. Technol.* 47 (15), 8130–8137. doi:10.1021/es4003907

Maier, M.-S., Teodoru, C. R., and Wehrli, B. (2021). Spatio-temporal Variations in Lateral and Atmospheric Carbon Fluxes from the Danube Delta. *Biogeosciences* 18 (4), 1417–1437. doi:10.5194/bg-18-1417-2021

Mallast, U., Staniek, M., and Koschorreck, M. (2020). Spatial Upscaling of CO_2 Emissions from Exposed River Sediments of the Elbe River during an Extreme Drought. *Ecohydrology* 13, e2216 (6). doi:10.1002/eco.2216

Matoušů, A., Rulík, M., Tušer, M., Bednařík, A., Šimek, K., Bussmann, I., et al. (2019). Methane Dynamics in a Large River: a Case Study of the Elbe River. *Aquat. Sci.* 81 (1), 12. doi:10.1007/s00027-018-0609-9

Pusch, M., and Fischer, H. (2006). *Stoffdynamik und Habitatstruktur in der Elbe*. Berlin: Weißensee Verlag.

Rasilo, T., Hutchins, R. H. S., Ruiz-González, C., and del Giorgio, P. A. (2017). Transport and Transformation of Soil-Derived CO_2, CH_4 and DOC Sustain CO_2 Supersaturation in Small Boreal Streams. *Sci. Total Environ.* 579, 902–912. doi:10.1016/j.scitotenv.2016.10.187

Raymond, P. A., Zappa, C. J., Butman, D., Bott, T. L., Potter, J., Mulholland, P., et al. (2012). Scaling the Gas Transfer Velocity and Hydraulic Geometry in Streams and Small Rivers. *Limnol. Oceanogr.* 2, 41–53. doi:10.1215/21573689-1597669

Rosentreter, J. A., Borges, A. V., Deemer, B. R., Holgerson, M. A., Liu, S., Song, C., et al. (2021). Half of Global Methane Emissions Come from Highly Variable Aquatic Ecosystem Sources. *Nat. Geosci.* 14 (4), 225–230. doi:10.1038/s41561-021-00715-2

Schwartz, R., and Kozerski, H.-P. (2003). Entry and Deposits of Suspended Particulate Matter in Groyne Fields of the Middle Elbe and its Ecological Relevance. *Acta Hydrochim. Hydrobiol.* 31 (4-5), 391–399. doi:10.1002/aheh.200300496

Sieczko, A. K., Demeter, K., Singer, G. A., Tritthart, M., Preiner, S., Mayr, M., et al. (2016). Aquatic Methane Dynamics in a Human-Impacted River-Floodplain of the Danube. *Limnol. Oceanogr.* 61, S175–S187. doi:10.1002/lno.10346

Staniek, M. (2019). *Distribution of Greenhouse Gas Concentrations along Two Characteristic Elbe Segments*. Germany: Martin Luther University Halle-Wittenberg. BSc Bachelor Thesis.

Stanley, E. H., Casson, N. J., Christel, S. T., Crawford, J. T., Loken, L. C., and Oliver, S. K. (2016). The Ecology of Methane in Streams and Rivers: Patterns, Controls, and Global Significance. *Ecol. Monogr.* 86 (2), 146–171. doi:10.1890/15-1027.1

Tang, K. W., McGinnis, D. F., Ionescu, D., and Grossart, H.-P. (2016). Methane Production in Oxic lake Waters Potentially Increases Aquatic Methane Flux to Air. *Environ. Sci. Technol. Lett.* 3 (6), 227–233. doi:10.1021/acs.estlett.6b00150

Weigold, F., and Baborowski, M. (2009). Consequences of Delayed Mixing for Quality Assessment of River Water: Example Mulde–Saale–Elbe. *J. Hydrol.* 369 (3), 296–304. doi:10.1016/j.jhydrol.2009.02.039

Wilkinson, J., Bodmer, P., and Lorke, A. (2019). Methane Dynamics and thermal Response in Impoundments of the Rhine River, Germany. *Sci. Total Environ.* 659, 1045–1057. doi:10.1016/j.scitotenv.2018.12.424

Conflict of Interest: The authors declare that the research was conducted in the absence of any commercial or financial relationships that could be construed as a potential conflict of interest.

Publisher's Note: All claims expressed in this article are solely those of the authors and do not necessarily represent those of their affiliated organizations, or those of the publisher, the editors and the reviewers. Any product that may be evaluated in this article, or claim that may be made by its manufacturer, is not guaranteed or endorsed by the publisher.

Copyright © 2022 Bussmann, Koedel, Schütze, Kamjunke and Koschorreck. This is an open-access article distributed under the terms of the Creative Commons Attribution License (CC BY). The use, distribution or reproduction in other forums is permitted, provided the original author(s) and the copyright owner(s) are credited and that the original publication in this journal is cited, in accordance with accepted academic practice. No use, distribution or reproduction is permitted which does not comply with these terms.

frontiers in Environmental Science

REVIEW
published: 29 March 2022
doi: 10.3389/fenvs.2022.850070

Measuring CH_4 Fluxes From Lake and Reservoir Sediments: Methodologies and Needs

Sofia L. D'Ambrosio and John A. Harrison*

School of the Environment, Washington State University Vancouver, Vancouver, WA, United States

Accurately quantifying the diffusive flux of CH_4 between sediments and the overlying water column is crucial when constructing CH_4 budgets in lakes and reservoirs. Although a variety of *ex situ* and *in situ* techniques exist for determining this flux, no reviews have provided a comprehensive, comparative overview of these approaches or discussed implications of measurement method on flux estimation. Here, we critically review methods applied in 163 peer-reviewed studies to estimate diffusive CH_4 fluxes from lake sediments, including sediment incubations, benthic chambers, and modeling approaches applied in the sediment or water column. For each method, we summarize the approach, discuss limitations and advantages, and summarize published comparisons between different methods. In addition, we examine how method limitations have likely shaped knowledge gaps in current understanding of lake CH_4 dynamics. Finally, we call for the development and application of new methods, along with additional testing and intercomparison of existing methods, in order to advance understanding of lake CH_4 fluxes.

Keywords: methane, sediment methane flux, sediment methanogenesis, CH_4 flux, flux measurement

OPEN ACCESS

Edited by:
Daniel F. McGinnis,
Université de Genève, Switzerland

Reviewed by:
Dominic Vachon,
Umeå University, Sweden
Maciej Górka,
University of Wrocław, Poland

****Correspondence:***
Sofia L. D'Ambrosio
sofia.dambrosio@wsu.edu

Specialty section:
This article was submitted to Biogeochemical Dynamics, a section of the journal Frontiers in Environmental Science

Received: *07 January 2022*
Accepted: *09 March 2022*
Published: *29 March 2022*

Citation:
D'Ambrosio SL and Harrison JA (2022) Measuring CH_4 Fluxes From Lake and Reservoir Sediments: Methodologies and Needs. Front. Environ. Sci. 10:850070. doi: 10.3389/fenvs.2022.850070

1 INTRODUCTION

Lakes and reservoirs are collectively responsible for an estimated 9%–27% (70–175 Tg) of global methane (CH_4) emissions annually (Rosentreter et al., 2021). The majority of CH_4 in these ecosystems is thought to be produced in sediments (Peeters et al., 2019), where high organic carbon availability and anoxic conditions favor methanogenesis (Bastviken, 2009). Methane in sediments can then cross the sediment-water interface (SWI) via diffusion or ebullition (bubbling) into the water column, from whence it may ultimately reach the atmosphere. Typically, up to 50% of CH_4 emissions from lakes and reservoirs occurs via diffusion rather than ebullition (Bastviken et al., 2004; Bastviken et al., 2008; Deemer et al., 2016). Although bubbling from sediments is certainly an important pathway for CH_4 transport (DelSontro et al., 2010; Beaulieu et al., 2016), here we focus on the diffusive flux of CH_4 from sediments, which is a critical component of understanding lentic greenhouse gas cycling and emissions.

Methane diffusion from lake and reservoir sediments is highly variable in both space and time. In a synthesis of measurements from 23 lakes and reservoirs, diffusive CH_4 fluxes across the SWI varied up to three orders of magnitude across and within systems (Adams, 2005). The wide variability in rates is due, in part, to physical and biological factors that influence rates of CH_4 production (methanogenesis) and oxidation (methanotrophy) within sediments, as well as controls on the diffusive transport of CH_4 out of sediments. For example, greater sediment CH_4 production rates have been linked to higher lake productivity (West et al., 2016; D'Ambrosio and Harrison, 2021), warmer temperatures (Duc et al., 2010), organic matter availability (Berberich et al., 2019; Praetzel

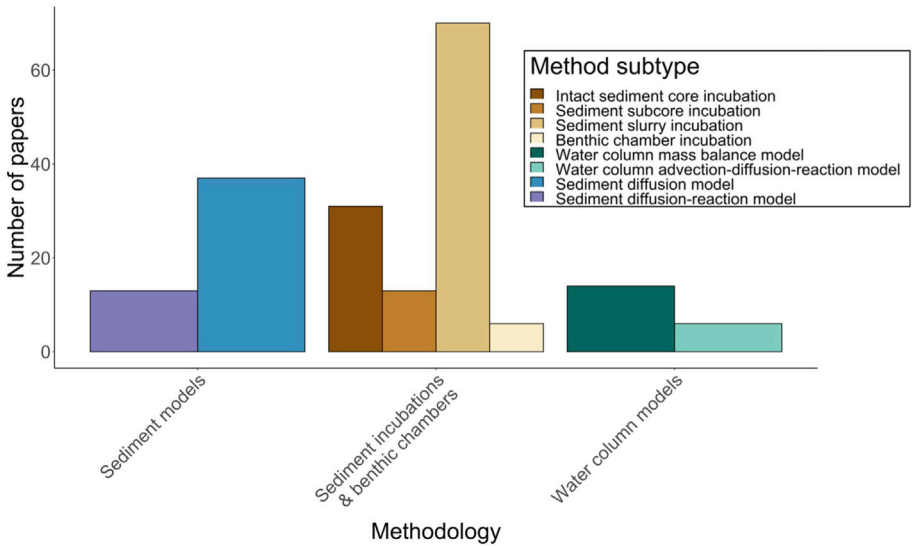


FIGURE 1 | Number of studies measuring sediment methanogenesis and/or the flux of CH_4 from sediments. Broad subcategories of methodology are shown in legend. Ten sediment incubation studies are excluded from the plot because incubation subtype could not be determined, however they are included in the Supplementary Data File of references (**Supplementary Table S1**).

et al., 2020), and anoxic conditions above and within sediments (Liikanen and Martikainen, 2003; Huttunen et al., 2006). Methane oxidation, which can consume significant amounts of CH_4 at the SWI or deeper in the sediment profile, is controlled by the availability of CH_4 and electron acceptors such as oxygen, nitrate, iron oxides, manganese oxides, and sulfate (Kuivila et al., 1988; Clayer et al., 2016; van Grinsven et al., 2020). The diffusive release of CH_4 out of sediments is, in turn, influenced by the net supply of CH_4 (i.e., production—oxidation), and can be affected by conditions and processes above sediments such as the CH_4 concentration in water overlying sediments, oxidation at the sediment surface (Bosse et al., 1993; Rolletschek, 1997), near-bed turbulence (D'Ambrosio, 2022), surface waves (Hofmann et al., 2010), and sediment resuspension (Bussmann, 2005).

The wide range of methods used to measure the CH_4 diffusion from sediments may play an important role in the large variability in reported fluxes. Approaches such as sediment incubations, sediment models, and water column models have differing spatiotemporal resolutions, sampling requirements, and limitations, all of which influence resulting flux measurements. Although explicit comparisons of multiple approaches for measuring CH_4 emission across the air-water interface have been extensive (St. Louis et al., 2000; Schubert et al., 2012; Deemer et al., 2016), there is no similar synthesis of methods for measuring for CH_4 diffusion across the SWI. A critical examination of methodologies used to estimate this flux is needed to: 1) understand the advantages and disadvantages of current approaches; 2) recognize how limitations of common techniques shape gaps in our current view of CH_4 dynamics in lakes and reservoirs; and 3) identify future method developments needed to advance understanding of the supply and transport of CH_4 in lacustrine systems.

Here, we critically review methodologies from 163 studies reporting CH_4 diffusive flux and/or methanogenesis in lake or reservoir sediments (references provided in the **Supplementary Data File**). From these studies, we classify typical methods for measuring this flux into three broad categories: sediment incubations and benthic chambers, modeling approaches applied in the sediment, and modeling approaches applied in the water column. We summarize each approach, describe the utility, advantages, and disadvantages for each, and examine previous studies explicitly comparing measurements from multiple techniques. Finally, we discuss how existing approaches have shaped knowledge gaps in lacustrine CH_4 cycling, and we provide recommendations for future methodological developments needed to improve the quantification of sediment CH_4 flux and its role in lake and reservoir carbon budgets.

2 METHODOLOGIES

2.1 Sediment Incubations & Benthic Chambers

2.1.1 Approach Summary

Sediment incubations have historically been the most common approach for estimating diffusive CH_4 fluxes from lake sediments (**Figure 1**). Incubation-based estimates can be categorized as *ex situ* sediment incubations, typically performed in the lab, or *in situ* incubations, usually performed by deploying benthic chambers to the lakebed.

Ex situ incubations are the most common and measure CH_4 flux *in vitro* from intact sediment cores, subcores, or sediment-water slurries (**Figure 1**). Intact cores can be collected via piston, gravity, or box coring, and may be segmented into smaller

subcores prior to incubation (Mudroch and MacKnight, 1991). Slurries are subsampled from a core or sediment grab and then homogenized prior to incubation, often through mixing with lake water or deionized water. Sediment cores, subcores, or slurries are placed in incubation chambers, such as acrylic tubes for cores (Sturm et al., 2014) or glass vials for subcores or slurries (Wagener et al., 1990), then sealed with gastight stoppers. Vial headspaces above sediments may be filled partially or completely with lake water or deionized water. Anoxic or oxic conditions are then established in the chambers prior to incubation, depending on the study objectives. Anoxic incubations are often flushed and evacuated with an inert gas (e.g., N_2 or He; Liikanen et al., 2002a; Praetzel et al., 2020), whereas oxic incubations use air (Sweerts et al., 1991; Chmiel et al., 2016). Incubations usually take place either in a temperature-controlled water bath (Kelly and Chynoweth, 1981) or at *in situ* depth in the water column (Algesten et al., 2005). Core incubation chambers are often, although not always, equipped with a magnetic stirrer that gently mixes water above the core without disturbing the SWI (Frenzel et al., 1990; Leal et al., 2007). Some core incubations also use constant flow-through systems that pump lake water from an outside reservoir into the overlying water of cores. This maintains oxic or anoxic conditions throughout the incubation and prevents the accumulation or depletion of compounds that may alter CH_4 production or consumption rates (Liikanen et al., 2002d; Bussmann, 2005).

A small subset of incubations is performed *in situ* using a benthic chamber approach (sometimes called a static chamber; **Figure 1**). Benthic chambers are open-bottomed boxes or cylinders constructed of acrylic, steel, or plastic, and are implanted several centimeters into the sediment for *in situ* incubation (Viollier et al., 2003). Chambers can be installed manually with scuba divers (Duchemin et al., 1995) or using a benthic lander, which is designed to implant the chamber remotely after being lowered to a lake bottom (Devol, 1987; Kuivila et al., 1988; Urban et al., 1997; Maerki et al., 2009). Chamber designs often include pumps or paddles that continuously circulate water within a chamber throughout the incubation (Devol, 1987; Colas et al., 2021).

Incubation duration varies substantially, in part as a function of technique. *Ex situ* incubations typically last days (Jones et al., 1982; Hershey et al., 2015) to weeks (Liikanen et al., 2002b; Dan et al., 2004); however some can last months (Martinez-Cruz et al., 2017; Valle et al., 2018) to years (Nozhevnikova et al., 2007; Isidorova et al., 2019). Benthic chamber deployments are usually shorter, lasting from hours to a day (Kuivila et al., 1988; Urban et al., 1997). Incubations are generally sampled at multiple time points to determine CH_4 concentrations, with the rate of change in concentrations over time used to calculate fluxes. For *ex situ* incubations, headspace gas or water overlying sediment can be sampled using syringes, or flow from an external reservoir may be used to push water out of the incubation chamber to be sampled. For benthic chambers, samples of water are extracted either manually via tubing/pumps to the surface (Yavitt et al., 1992; Duchemin et al., 1995) or automatically with programmable syringes (Devol, 1987; Kuivila et al., 1988; Urban et al., 1997; Maerki et al., 2009).

Samples collected during incubations are analyzed for CH_4 concentration using gas chromatography or laser absorption spectrometry. Samples in the gas phase can be analyzed immediately. Samples in liquid phase are first prepared using headspace equilibration, a technique which injects an inert gaseous headspace (often ultrapure helium), and then agitates the water in order to equilibrate dissolved CH_4 with the gaseous phase prior to analysis (McAullife, 1971; Magen et al., 2014). Henry's law is then used to determine the amount of CH_4 originally present in the liquid phase.

The rate at which CH_4 is produced in the incubation over time is used to estimate sediment diffusive flux. In benthic chambers, intact core, and some subcore incubations, the production rate is typically expressed in areal units (i.e., CH_4 produced per m^2 of core horizontal cross-sectional area incubated) and therefore assumed to be equivalent to diffusive CH_4 flux across the SWI (J_{SWI}). In slurry and some subcore incubations, production rates are typically measured in gravimetric or volumetric units (i.e., CH_4 produced per liter or gram of dried sediment). Volumetric or gravimetric production rates can be converted to a flux by assuming rates are constant over a specified sediment depth of active methanogenesis (z_{act}), then multiplying by the sediment bulk density (ρ). In some cases, one point measurement of CH_4 production is assumed to be representative of the active zone of methanogenesis in the sediment profile (**Figure 2A**; West et al., 2016; Berberich et al., 2019). In other cases, vertical changes in methanogenesis are accounted for by integrating measurements of gravimetric or volumetric CH_4 production made at multiple depths throughout the sediment profile (**Figure 2B**; Murase and Sugimoto 2002; Liu et al., 2019).

2.1.2 Approach Advantages

Incubations and benthic chambers provide a highly controlled, customizable environment for researchers to manipulate environmental conditions, and thus they are often used to evaluate drivers of CH_4 processing (**Table 1**). For example, previous incubation studies have investigated how sediment CH_4 flux and/or methanogenesis rates respond to shifting temperatures (Zeikus and Winfrey, 1976; Duc et al., 2010), nutrient concentrations (Stadmark and Leonardson, 2007; Rodriguez et al., 2018), organic matter deposition (West et al., 2012; Grasset et al., 2018), oxygen availability (Liikanen et al., 2002c; Liikanen and Martikainen, 2003), and supply of electron acceptors likely to be involved in CH_4 oxidation (Karvinen et al., 2015; Rissanen et al., 2017). These experimental manipulations are impractical or impossible to apply in most benthic chamber experiments, yet they are important for identifying which environmental drivers exert control on methanogenesis and methanotrophy within lake sediments (Bastviken, 2009; Borrel et al., 2011). Additionally, incubations are unique in that they can be used to partition out gross rates of CH_4 production and oxidation, rather than net rates. This is usually done by injecting the incubation with isotopically-labeled methanogenic or methanotrophic substrate (e.g., ^{14}C-labeled acetate/bicarbonate or $^{14}CH_4$, respectively) and tracking the radioactivity and concentration of CH_4 in the incubation over time (Kuivila et al., 1989; Nüsslein et al., 2001; Pimenov et al., 2010).

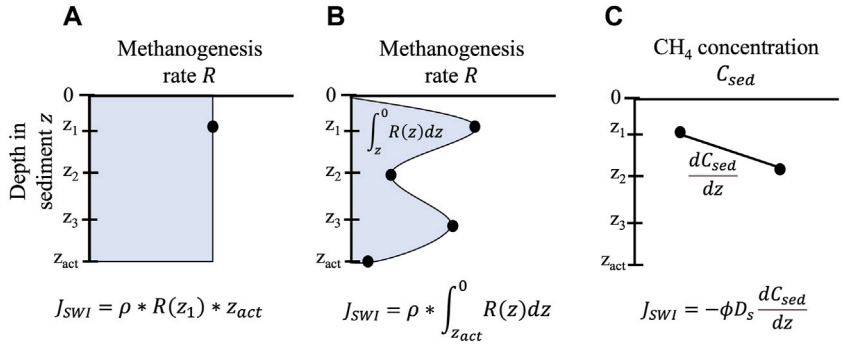


FIGURE 2 | Multiple approaches for measuring diffusive flux from sediments (J_{SWI}) using point measurements of methanogenesis (R) or CH_4 concentrations (C_{sed}) in the sediment column. Points indicate discrete measurements taken at depths z, with z_{act} denoting the sediment depth below which methanogenesis is considered negligible. The SWI is where $z = 0$. Note that all axes are not drawn to scale. Below each panel, the equation for flux is shown, with ρ indicating sediment bulk density, ϕ sediment porosity (**Eq. 1**), and D_s sediment diffusivity (**Eq. 1**). **(A)** Converting one measurement of CH_4 production into flux by assuming methanogenesis is constant with depth. **(B)** Determining flux by integrating a vertical profile of CH_4 production measured at multiple depths. An arbitrary vertical profile is shown as an example. **(C)** Determining flux with a diffusion model (Fick's first law, **Eq. 1**).

TABLE 1 | Summary of procedures, recommended applications, and limitations of each method used to measure diffusive CH_4 flux from lake sediments.

Methodology	Procedure	Recommended Applications	Limitations
Sediment incubations & benthic chambers	Measure CH_4 accumulation or consumption in benthic chambers or *ex situ* incubations of intact cores, subcores, or sediment slurries	- Evaluate effects of potential drivers on relative rates of sediment flux - Compare relative fluxes between multiple sites or time periods	- Possible stimulation/inhibition of methanogenesis/methanotrophy - Sediment disturbance artifacts - Isolation from water column and BBL processes, altered physical mixing
Sediment models	Estimate flux using profile of CH_4 concentrations in sediment column	- Diffusion models: Fast, simple flux estimates to compare across study sites or time periods - Diffusion-reaction models: Depth-specific information on zones of sediment methanogenesis & methanotrophy	- Error associated with concentration gradient estimation near SWI - Excludes sediment surface processes - Sediment disturbance artifacts
Water column models	Estimate flux based on CH_4 concentration profiles in the water column	- Mass balance models: Construct lake-wide CH_4 budget - Advection-diffusion-reaction models: Examine long-term (e.g., seasonal) changes in lake-wide CH_4 cycling	- Little information on drivers behind CH_4 dynamics - Assumptions of spatial homogeneity - Potentially data-intensive

Incubations are also popular in part due to their simplicity, reproducibility, and relatively simple sampling requirements. Benthic chambers and/or *ex situ* incubation containers are generally constructed from low-cost materials and incubations can be repeated with sediments from (or at) multiple sampling locations, time points, and study systems (**Table 1**). Furthermore, CH_4 flux from an incubation can be determined from just a few samples of CH_4 concentrations over time, typically just a few hours to a day, or less. Other approaches, such as water column models (**Section 2.3**), often require significantly more data such as sediment ebullition estimates, temperature profiles in the water column, and/or CH_4 oxidation measurements.

Lastly, although here we focus on methods for measuring CH_4 diffusion from sediments, an advantage of incubations is that some set-ups can be modified to measure diffusion and ebullition simultaneously (Liikanen et al., 2002c). While a full discussion of these incubation designs is beyond the scope of this review, the capacity to measure diffusive and ebullitive flux from sediments can be advantageous given bubbling is an important CH_4 transport pathway in many lakes and reservoirs (DelSontro et al., 2011, 2015).

2.1.3 Approach Limitations

An important limitation of incubations and benthic chambers is that they provide a spatiotemporal snapshot of CH_4 diffusion from sediments. Rates from this method are relevant to the sediment incubated, which typically has a surface area of a few square centimeters to a square meter or less (**Figure 3**). Assumptions that flux estimates based on incubations are applicable lake-wide are questionable, given previous work has found significant differences in sediment CH_4 production and fluxes between profundal and littoral sites (Liikanen et al., 2003;

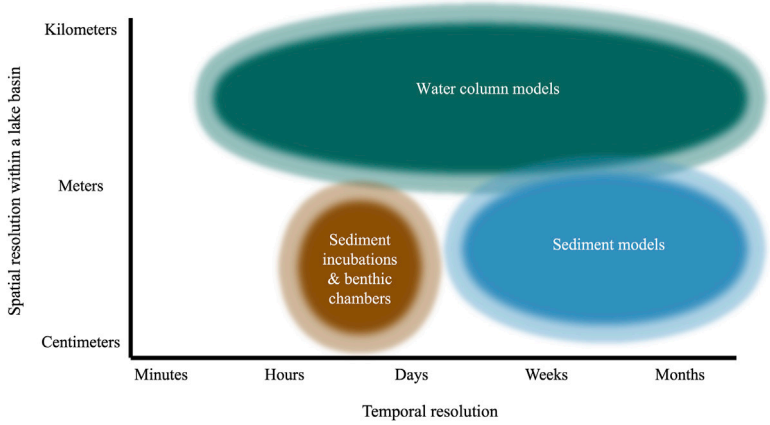


FIGURE 3 | Conceptual map showing the typical temporal and spatial resolution of common methodologies included in **Figure 1**. Temporal resolution represents the typical time period over which measurements from each method are made or averaged over. Spatial resolution indicates the spatial scale over which measurements from each method are made or averaged across within an individual lake basin.

Li et al., 2021) or between locations with different organic matter inputs (Berberich et al., 2019; Praetzel et al., 2020). Rate estimates based on incubations also represent a flux averaged only over the incubation duration, usually hours or days (**Figure 3**). Incubations therefore do not generally account for temporal shifts across seasons (Nüsslein and Conrad, 2000; Itoh et al., 2015) or during lake stratification and mixing (Liikanen et al., 2002b; Vachon et al., 2019). Additionally, volumetric or gravimetric CH_4 production rates measured in incubations are often converted into a flux by assuming rates are constant over a specified active layer depth (**Figure 2A**). This assumption runs counter to many studies demonstrating that methanogenesis changes significantly with lake sediment depth (Chan et al., 2005; Lofton et al., 2015; Yang et al., 2017; Praetzel et al., 2020).

Ex situ incubations and benthic chambers also largely isolate sediments from lake-scale processes that may influence flux across the SWI (**Table 1**). For example, internal waves can drive fluctuations in turbulence and mixing in the boundary layer overlying sediments (Henderson, 2016). These fluctuations in near-bed conditions have been demonstrated to influence fluxes of oxygen, nitrate, and CH_4 across the SWI on hourly to daily time scales (Lorke et al., 2003; Brand et al., 2008; Bryant et al., 2010; D'Ambrosio, 2022). Internal waves can also drive redox changes at the SWI, which may influence within-sediment rates of methanogenesis and methanotrophy (Frindte et al., 2013; Frindte et al., 2015). The effects of such boundary layer and surface sediment dynamics on flux are not considered within traditional incubation setups. Furthermore, although surface waves and sediment resuspension have also been tied to variations in diffusive CH_4 release from lake sediments (Bussmann, 2005; Hofmann et al., 2010), only one study has simulated the effects of resuspension in their incubation microcosm design (Bussmann 2005).

For *ex situ* incubations specifically, sampling artifacts from sediment collection and preparation are important to consider (**Table 1**). Previous work has posited that sediment slurrying can stimulate methanogenesis (Kelly and Chynoweth, 1980; Frenzel et al., 1990) or inhibit methanotrophy (Su et al., 2019) compared to *in situ* rates (**Table 1**). In contrast, intact and subcore incubations avoid slurrying in order to preserve sediment layering and structure, in part because methanogenesis and methanotrophy change significantly with sediment depth (Chan et al., 2005; Martinez-Cruz et al., 2018). However, in gas-rich sediments, stratigraphy can be significantly disturbed by core sampling due to changes in hydrostatic pressure and temperature during core withdrawal (Dück et al., 2019b). It is similarly challenging to collect cores in soft-bottom sediments without altering sediment structure (Blomqvist, 1991). Given these limitations, incubations are best suited for measuring relative (rather than absolute) rates of diffusive CH_4 release from sediments (**Table 1**).

Lastly, fluxes estimated with incubations are sensitive to incubation duration because conditions within the chamber can change over time. For example, oxygen may be depleted over the course of benthic chamber incubations (Duchemin et al., 1995), which may affect rates of CH_4 production and oxidation given the sensitivity of methanogens and methanotrophs to oxygen availability (Borrel et al., 2011; Thottathil et al., 2019). Such oxygen depletion can be avoided by limiting the duration of benthic chamber deployments (Urban et al., 1997) and by monitoring oxygen concentrations in benthic chambers. For *ex situ* incubations, an initial lag phase of CH_4 production may also occur as methanogens or methanotrophs acclimate to vial conditions and/or compete with other microorganisms present (Torres et al., 2011; Grasset et al., 2021). However, lag phases are not observed in all incubations (Chan et al., 2005; Valle et al., 2018; Li et al., 2020). Furthermore, CH_4 production may decrease over time in long-term incubations (Isidorova et al., 2019), likely due to the gradual depletion of methanogenic precursors such as acetate. Consequently, *ex situ* incubations that are shorter than a typical lag phase or long enough to deplete methanogenic substrates may underestimate rates of CH_4 release from sediments.

2.2 Sediment CH_4 Models

2.2.1 Approach Summary

Modeling CH_4 in the sediment column is a common method for estimating CH_4 flux across the SWI of lakes and reservoirs (**Figure 1**). Sediment models for estimating CH_4 fluxes across the SWI can be considered as falling into one of two main categories: 1) diffusion models, which estimate CH_4 flux solely based on molecular diffusion; and 2) diffusion-reaction models, which also account for the effects of microbial reactions and/or bioirrigation on CH_4 flux (**Figure 1**). In the former case, flux is estimated between two discrete depths in the sediment column using Fick's first law of diffusion (**Figure 2C**):

$$J = -\phi D_s \frac{dC_{sed}}{dz} \tag{1}$$

where J is CH_4 flux in the sediment, ϕ is sediment porosity, D_s is diffusivity of CH_4 in the sediment, and $\frac{dC_{sed}}{dz}$ is the CH_4 concentration gradient across sediment depth z (Berner, 1980). For J to be representative of flux across the SWI (J_{SWI}), the CH_4 concentration gradient should be measured as close to the SWI as possible. Sediment porosity is either measured directly or estimated based on literature values, which typically range from 0.8 to 0.99 in lake sediments (Frenzel et al., 1990; Carignan and Lean, 1991; Langenegger et al., 2019). Sediment diffusivity D_s is determined by correcting the molecular diffusivity of CH_4 in pure water at *in situ* temperature (D_0) for sediment tortuosity using the relationship $D_s = D_o\phi^2$. Another approach corrects diffusivity using the relationship $D_s = \frac{D_o}{\Theta^2}$, where tortuosity ($\Theta^2$) is estimated as a function of sediment porosity (Lerman, 1979; Berner, 1980). Lastly, the diffusivity of low-solubility compounds such as CH_4 may be increased by the presence of gas voids in the sediment column; in these cases, D_0 can be corrected for sediment porosity and volumetric water content (W_c) using the relationship $D_s = D_o\frac{W_c^{7/3}}{\phi^2}$ (Flury et al., 2015).

Beyond molecular diffusion considered in **Eq. 1**, processes such as bioirrigation or microbial reactions may also affect CH_4 distribution in sediments. A more comprehensive diffusion-reaction model can account for how these processes work in concert with molecular diffusion to influence CH_4 concentrations in the sediment. Normally, such a diffusion-reaction model is applied at many discrete vertical layers in the sediment column, rather than the two discrete depths considered in the diffusion model of **Eq. 1**. First, the effect of molecular diffusion on CH_4 distribution throughout the sediment column is considered, according to Fick's second law of diffusion:

$$\frac{dC_{sed}}{dt} = \frac{d}{dz}\left(\phi D_s \frac{dC_{sed}}{dz}\right) \tag{2}$$

where t is time. Second, an additional term R is commonly included to account for how net microbial CH_4 production and/or oxidation in each sediment layer affect the distribution of CH_4 (Rahalkar et al., 2009; Clayer et al., 2018):

$$\frac{dC_{sed}}{dt} = \frac{d}{dz}\left(\phi D_s \frac{dC_{sed}}{dz}\right) + R \tag{3}$$

R can be solved for numerically or analytically. A popular approach involves using differential equation-solving software, such as PROFILE (Berg et al., 1998) or REC (Lettmann et al., 2012), to numerically solve for R in each layer, given inputs of measured sediment CH_4 concentration profiles.

In some cases, an additional term is added to **Eq. 3** to account for the effects of bioirrigation on CH_4 transport (Bartosiewicz et al., 2016, 2021; Clayer et al., 2016). Bioirrigation and bioturbation describe how biologically driven water circulation through sediments and sediment mixing, respectively, affect solute transport between sediment porewater and the overlying water (Kristensen et al., 2012). Burrows serve as conduits between the sediment porewater and the overlying water, creating a concentration gradient that drives additional diffusive transport of CH_4:

$$\frac{dC_{sed}}{dt} = \frac{d}{dz}\left(\phi D_s \frac{dC_{sed}}{dz}\right) + \phi\alpha(C_0 - C_{sed}) + R \tag{4}$$

where α is the intensity of bioirrigation and C_0 is the CH_4 concentration measured at the SWI. Estimates of α for CH_4 in lake sediments can be made based on sediment diffusivity, depth below the SWI, and the radius of the tubes formed by burrowing animals (Boudreau, 1984; Clayer et al., 2016). Lastly, assuming steady state conditions reduces **Eq. 4** to:

$$0 = \frac{d}{dz}\left(\phi D_s \frac{dC_{sed}}{dz}\right) + \phi\alpha(C_0 - C_{sed}) + R \tag{5}$$

From **Eq. 5**, there are multiple routes to calculate a flux across the SWI. Both PROFILE and REC solve for a depth profile of R in volumetric units, which can be depth-integrated into an flux across the SWI (**Figure 2B**; Norði et al., 2013; Bartosiewicz et al., 2016; Clayer et al., 2016). Alternatively, another technique assumes a constant rate for R in between the SWI and the lower end of the diffusion-reaction zone in the sediment column (z_{max}, i.e., where the porewater CH_4 concentration remains unchanged with depth). Using these assumptions, **Eq. 3** can be solved analytically for flux across the SWI (Epping and Helder, 1997; Müller et al., 2003):

$$J_{SWI} = \phi\sqrt{2RD_s(C_0 - C_{max})} \tag{6}$$

where C_{max} is the CH_4 concentration at z_{max} based on measured porewater CH_4 concentration profiles (Pasche et al., 2011; Müller et al., 2012; Steinsberger et al., 2017, 2019).

All sediment models covered here require measurements of CH_4 concentrations in the sediment porewater, which can be obtained a variety of ways. The simplest technique is collecting an intact sediment core, subsampling into core slices by depth, then measuring CH_4 concentration in each subsample using headspace equilibration (**Section 2.1.1**). Another technique measures CH_4 concentrations using a small probe inserted at various depths in the sediment core (Bussmann and Schink, 2006). Here, methane from the sediment diffuses across the permeable membrane of a probe inserted at a specific sediment depth, and a constant flow of carrier gas to the probe flushes the CH_4 to a gas chromatograph for

determination of concentration. Other approaches rely on the extraction of sediment porewater, which can be analyzed for CH_4 concentration with headspace equilibration (**Section 2.1.1**). Porewater can be extracted with squeezers, metal or plastic devices that use pistons or gas pressure to compress sediment and force out interstitial porewater. Porewater from different depths in a core may be extracted using squeezers on various core subsections (Reeburgh, 1967) or by using squeezers built to compress entire cores and fitted with ports at various sampling depths (Jahnke, 1988). A recently developed technique involves using a modified squeezer to subsample sediment from different depths into copper tubing, then centrifuging aliquots from the tubes to extract the porewater (Tyroller et al., 2016). Alternatively, small, porous Rhizon tubes can be inserted into different depths of the sediment. Porewater is then drawn into the tubes using suction from an attached vacuum pump, syringe, or evacuated test tube. Rhizons were originally developed for use in terrestrial soils, but have subsequently been adapted to sample porewater in saturated sediments from aquatic systems (Seeberg-Elverfeldt et al., 2005).

Porewater may also be sampled without collecting a core by deploying a "peeper" directly into the sediment (Hesslein, 1976). Peepers are acrylic samplers containing an array of small wells spaced several centimeters apart in the vertical. Sampling wells are filled with anoxic water and covered with a permeable membrane made of cellulose-acetate or polysulfone. Peepers are typically left in the sediment for several weeks to equilibrate via dialysis, then sampled and analyzed for CH_4 using headspace equilibration.

2.2.2 Approach Advantages

Sediment models are highly customizable depending on the lake system and level of sampling effort required. For example, a simple diffusion model (**Eq. 1**) to estimate flux requires sample collection as basic as measuring one CH_4 concentration gradient close to the SWI. Due to these relatively simple data requirements, sediment diffusion models are often employed as a fast, easy way to compare fluxes across multiple lakes (Adams, 2005; Huttunen et al., 2006), sampling sites (Zhang et al., 2020; Li et al., 2021), or time periods (**Table 1**; Rolletschek 1997).

In contrast, more sophisticated diffusion-reaction models (**Eqs 3–5**) can be constructed to account for the effects of microbial CH_4 production, oxidation, bioturbation, and/or bioirrigation on CH_4 transport out of sediments. Although these more comprehensive models require detailed sampling of CH_4 concentrations in the sediment column, their implementation can be made easier with freely available software used to solve the differential equations involved, such as PROFILE or REC (Berg et al., 1998; Lettmann et al., 2012). Diffusion-reaction models also can be used to solve for depth profiles of methanogenesis and methanotrophy in the sediment, which are powerful tools for examining the locations, controls, and microbial communities involved in CH_4 supply and transport (**Table 1**). For example, comparing rates of CH_4 production and oxidation in the sediment profile with observed fluxes across the SWI can highlight the importance of methanotrophy in substantially reducing CH_4 release into the hypolimnion (Koschorreck et al., 2008; Rahalkar et al., 2009; Norði et al., 2013).

2.2.3 Approach Limitations

Estimates from sediment modeling rely on porewater CH_4 concentrations (**Eq. 1**), which are the net result of equilibration with the surrounding sediment column and overlying water. Measurements are therefore only representative of the sediment sampled (usually centimeters to a meter or less) and its close surroundings (likely several meters; **Figure 3**). Accordingly, assumptions that measurements from sediment models characterize fluxes lake-wide should be interpreted with caution, given the significant spatial variability in sediment CH_4 dynamics across different sites within the same lake (**Section 2.1.3**).

Moreover, flux estimates from sediment models should be considered an average across weeks to months (**Figure 3**), the time scale on which equilibration of CH_4 concentrations in sediments typically occurs (Harper et al., 1997). Therefore, similar to incubations, these estimates do not account for short-term fluctuations in processes that may influence CH_4 diffusion across the SWI (**Section 2.1.3**). Unless modeling is repeated across multiple dates and sites, changes across seasons due to changing temperature, deposition of organic matter, or other environmental factors (Thebrath et al., 1993; Murase and Sugimoto, 2002; Yang et al., 2018) are also not considered. This seasonal variability may be particularly pronounced in lakes that thermally stratify and develop seasonal hypolimnetic hypoxia, as the resulting shifts in oxygen availability to surface sediments can profoundly influence sediment CH_4 oxidation and flux (Liikanen et al., 2003).

Typical techniques for measuring CH_4 concentrations in porewater, required for sediment modeling, also come with logistical hurdles and sampling artifacts (**Table 1**). Peepers can be challenging to deploy, since they require 1–3 weeks for equilibration and may need to be installed by scuba divers (Hesslein, 1976; Bufflap and Allen, 1995). Gas loss is a common sampling artifact during sediment core collection (Paull et al., 2000), peeper extraction (Adams, 2005), and headspace equilibration (Tyroller et al., 2016), resulting in underestimated CH_4 concentrations (and therefore inaccurate gradients). Exposure of sediment cores and/or peepers to oxygen during collection (Bufflap and Allen, 1995) is another potential problem that may stimulate methanotrophy and therefore influence sampled concentrations. Applying noble gas tracer (Tyroller et al., 2016) or freeze coring (Dück et al., 2019a) methods to analyze CH_4 concentrations in sediments may address some of these sampling artifacts.

In particular, sediment diffusion models (**Eq. 1**) are inherently limited by the spatial resolution of porewater sampling. The CH_4 gradient used in **Eq. 1** should be measured as close to the SWI as possible, because CH_4 concentrations can change rapidly within just a few millimeters of the sediment surface (Bussmann and Schink, 2006). However, accurately sampling CH_4 concentrations close to the SWI can be challenging with conventional porewater

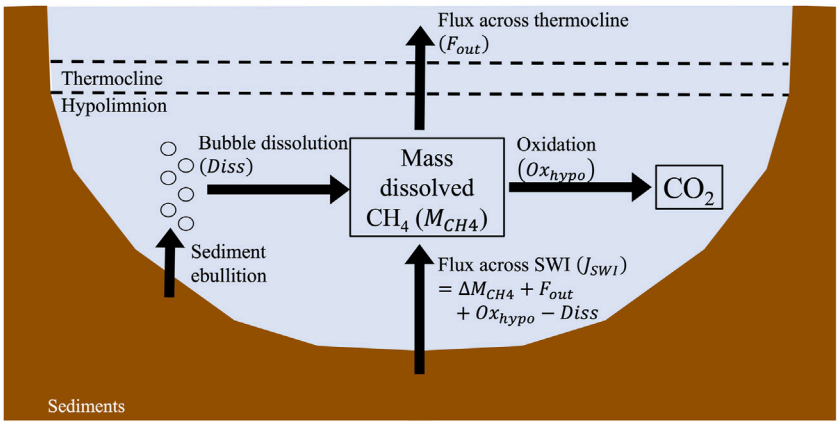


FIGURE 4 | Example mass balance model of a lake hypolimnion. Note arrows are not drawn to scale. See text for details (**Section 2.3**).

measurement techniques (**Table 1**). For example, peeper samplers are typically limited to a vertical resolution of a centimeter or more (Harper et al., 1997), making it difficult to accurately measure steep gradients near the SWI. Furthermore, the surface sediments where CH_4 gradients are steepest can be inadvertently lost when using some conventional coring techniques (Shirayama and Fukushima, 1995; Ostrovsky, 2000), especially in soft, unconsolidated sediments (Blomqvist, 1991). To resolve this issue, CH_4 gradients at the SWI are sometimes calculated based on concentrations in the rest of the porewater profile using linear regression or exponential models (Schubert et al., 2011; Maeck et al., 2013; Zhang et al., 2020). Alternatively, a CH_4 gradient measured between the overlying water and the uppermost sampled point in the sediment profile may be a suitable substitute for the SWI gradient (Klump et al., 2009).

2.3 Water Column Modeling

2.3.1 Approach Summary

The diffusion of CH_4 from sediments is an important component of many models simulating CH_4 dynamics in all or part of the lake water column. Many water column models rely on other methods described in this paper, such as incubations or sediment modeling (**Sections 2.1**, **2.2**), to estimate the flux of CH_4 across the SWI and use the measured value as model input. In this section, we focus on water column modeling approaches that estimate CH_4 diffusive flux from sediments through mathematical expressions within the model structure, rather than previously described methods. These water column models can be classified into two groups: 1) mass balances used to calculate CH_4 mass quantities in the water column; and 2) advection-diffusion-reaction models used to simulate CH_4 concentrations in the water column (**Figure 1**).

Mass balances are the most common water column model used to quantify CH_4 diffusion from sediments (**Figure 1**). Researchers applying a mass balance approach create a conceptual model of the sources, sinks, and transformations affecting the mass of CH_4 present in the water column. Most often, this mass balance is focused on the lake hypolimnion during thermal stratification. The exchange of gases and solutes between the epilimnion and hypolimnion is significantly slowed throughout the stratification period, often resulting in CH_4 accumulation below the thermocline (Eckert and Conrad, 2007). The hypolimnion during stratification can therefore be thought of as a largely closed system with sediments as the primary source of accumulating CH_4. As an example, a simple conceptual model outlining the sources, sinks, and transformations of CH_4 in the lake hypolimnion during thermal stratification is shown in **Figure 4**. Using this model, a mass balance can be used to link the observed rate of change in the mass of dissolved CH_4 in the hypolimnion over time (ΔM_{CH4}) to the diffusive flux of CH_4 from sediments (J_{SWI}):

$$\Delta M_{CH4} = J_{SWI} + Diss - F_{out} - Ox_{hypo} \quad (7)$$

where $Diss$ is the rate of dissolution from CH_4 bubbles present in the hypolimnion, F_{out} is the CH_4 flux out of the hypolimnion across the thermocline, and Ox_{hypo} is the rate of CH_4 oxidation in the hypolimnion. J_{SWI} can therefore be mathematically solved for by determining all the other terms in **Eq. 7** expressed in units of flux (e.g., mmol m^{-2} d^{-1}). $Diss$ is typically calculated as a function of ebullition measured from inverted funnel traps (Addess and Effler, 1996; Vachon et al., 2019). F_{out} can be estimated with Fick's first law applied across the thermocline (Kelly et al., 1988):

$$F_{out} = -K_z \frac{dC_{wc}}{dz} \quad (8)$$

where K_z is the eddy diffusivity within the thermocline and $\frac{dC_{wc}}{dz}$ is the CH_4 concentration gradient across the thermocline. K_z is often estimated by measuring heat exchange between the epilimnion and hypolimnion (Powell and Jassby, 1974; Addess and Effler, 1996; Matthews et al., 2005). Incubations are often used to quantify Ox_{hypo} (Rudd et al., 1974; Bastviken et al., 2008). However, some researchers simplify **Eq. 7** by assuming $Diss$ (Rudd and Hamilton, 1978), F_{out} (Bédard and Knowles, 1991), and/or Ox_{hypo} (Vachon et al., 2019) are small enough to be considered insignificant in their lake system.

The ΔM_{CH4} term is determined by tracking the increasing mass of dissolved CH_4 in the hypolimnion throughout the

stratification period. Typically, the hypolimnion is divided into horizontal layers, and CH_4 concentrations are monitored over time at a point within each layer. Water samples are collected periodically from each layer, usually with a Van Dorn sampler or tubing attached to a pump at the surface, then analyzed for CH_4 concentrations using gas chromatography or laser absorption spectrometry. Assuming each layer is horizontally well-mixed, ΔM_{CH4} can therefore be determined over time interval Δt:

$$\Delta M_{CH4} = \frac{\Delta\left(\sum C_{wc,i} V_i\right)}{A_{hypo}\Delta t} \quad (9)$$

where A_{hypo} is the sediment surface area below the hypolimnion, V_i is the volume of hypolimnion layer i, and $C_{wc,i}$ is the measured CH_4 concentration in layer i of the water column.

A small subset of water column models that include a term for diffusive CH_4 flux from sediments are advection-diffusion-reaction models. We will provide a brief overview here, however readers are referred to previous detailed descriptions for a full discussion of these models (Durisch-Kaiser et al., 2011; Tan et al., 2015; Stepanenko et al., 2016; Sabrekov et al., 2017; Schmid et al., 2017). These models consider how molecular diffusion affects CH_4 transport in the water column, similar to how diffusion and diffusion-reaction models in the sediment consider the effects of molecular diffusion in the sediment profile (**Section 2.2.1**). However, unlike sediment models, advection is often included as an important term influencing CH_4 transport in the water column. The diffusive flux of CH_4 from sediments is usually included as a reaction term within the advection-diffusion-reaction model and can be solved for in multiple ways. In models that contain separate modules for the sediment and the water column, flux can be calculated using empirical relationships between methanogenesis and easily-measured sediment characteristics, such as temperature, labile carbon content, and/or pH (Stepanenko et al., 2011; Tan et al., 2015; Sabrekov et al., 2017). Methanogenesis rates can then be depth-integrated to estimate of flux out of sediments (**Figure 2B**). In models that only contain a water column module, flux can be parameterized by comparing observed and modeled CH_4 concentration profiles in the water column (Durisch-Kaiser et al., 2011; Schmid et al., 2017).

2.3.2 Approach Advantages

Water column models are useful for determining the flux of CH_4 across the SWI without relying on direct measurements of CH_4 concentrations within the sediment porewater. Accordingly, these models avoid potential artifacts when sampling sediments for CH_4, such as the escape of gases, loss of surface sediments, or oxygen exposure during sediment collection (**Section 2.2.3**). Water column models also provide flux estimates integrated over space and time (**Figure 3**), which can be advantageous when researchers are more concerned with observing system-wide CH_4 dynamics than quantifying small-scale processes within the sediment or at the SWI (**Table 1**). For example, coupling CH_4 mass balance information from the hypolimnion with monitoring of surface emissions can track whether CH_4 released from sediments is ultimately stored, oxidized, or emitted (Matthews et al., 2005; Bastviken et al., 2008). Furthermore, some water column models can simultaneously determine the contribution of diffusion and ebullition to flux from lake sediments (Tan et al., 2015; Stepanenko et al., 2016), which can be advantageous in systems where bubbling is significant. For example, by modeling CH_4 concentrations in the water column of Lake Kinneret, authors determined that ebullition was the primary pathway for surface CH_4 emission and that methanotrophs oxidized the vast majority of dissolved CH_4 in the water column (Schmid et al., 2017).

Another advantage of water column models is that they are highly customizable. On one hand, more terms could be added to the mass balance represented by **Eq. 7** as needed, such as source terms for water column CH_4 production (Donis et al., 2017; Günthel et al., 2020) and/or release from CH_4 seeps (Schmid et al., 2007; Bornemann et al., 2016). However, more complicated models may require more sampling effort (**Table 1**). For example, advection-diffusion-reaction models of CH_4 concentrations in the water column typically require more data than mass balances, such as meteorological information (Tan et al., 2015) and/or detailed temperature profiles (Sabrekov et al., 2017). On the other hand, modeling and sampling effort can sometimes be significantly simplified, for example in lakes where the last three terms in **Eq. 7** can be considered negligible. In these cases, a mass balance can be performed with only lake bathymetry information and multiple hypolimnetic CH_4 concentration profiles measured throughout lake stratification (**Eq. 9**).

2.3.3 Approach Limitations

When using water column models, it is important to consider the desired temporal resolution for model output. Water column models can be run on a range of time steps from minutes to months (**Figure 3**), depending on the level of data input and amount of computational time available. Many models also often assume spatial homogeneity of CH_4 fluxes from sediments (**Table 1**). For example, mass balances similar to **Eqs 7–9** typically provide no information on the flux of CH_4 from sediments not in contact with the hypolimnion, such as shallow littoral regions that can be significant sources of CH_4 in many lakes and reservoirs (Encinas Fernández et al., 2016). Nevertheless, **Eqs 7–9** can be adjusted for use in other layers of the water column in order to estimate the diffusive CH_4 flux from sediments lake-wide (Strayer and Tiedje, 1978) or specifically from sediments in contact with the epilimnion and/or metalimnion (Bastviken et al., 2008).

In contrast, advection-diffusion-reaction models applied in the water column focus on the basin-wide distribution of CH_4, and therefore some do consider spatial heterogeneity in flux. For example, researchers applying an advection-diffusion-reaction model in the water column of Lake Kuivajärvi estimated CH_4 release from sediments for five different depth zones (littoral to profundal) throughout a 6 month period (Stepanenko et al., 2016). Similarly, some advection-diffusion-reaction models account for how methanogenesis rates may vary spatially across sediment layers due to changing substrate quality and quantity (Tan et al., 2015). However, others assume CH_4 diffusion from sediments is spatiotemporally constant throughout the entire

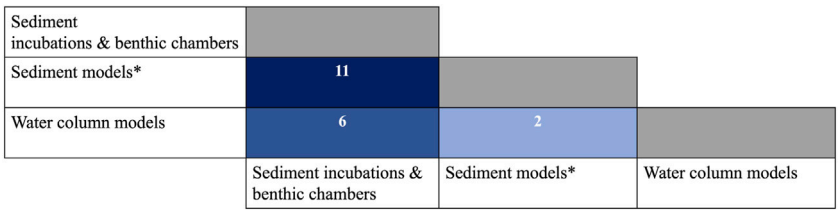


FIGURE 5 | Matrix showing number of studies that have compared multiple methodologies for calculating the diffusive flux of CH_4 from sediments. Blue boxes show number of existing studies, with lighter blue indicating fewer studies and darker blue indicating a larger number of studies. Asterisk indicates that there are $n = 4$ studies, not shown in the matrix here, that compared fluxes between two subtypes of sediment models (diffusion and diffusion-reaction models). All comparative studies are identified in the Supplementary data file (**Supplementary Table S1**).

lake (Durisch-Kaiser et al., 2011), which is not the case in many lakes and reservoirs (Bastviken et al., 2008; Berberich et al., 2019).

Water column models are also limited in their ability to determine drivers of diffusive CH_4 flux from sediments (**Table 1**). Mass balances say little about the possible controls on flux unless they are combined with other data, such as organic carbon deposition rates, temperature profiles, or oxygen concentrations. Similarly, advection-diffusion-reaction models in the water column often rely on model parameterization or empirical equations to calculate flux across the SWI, neither of which directly link CH_4 dynamics to causal drivers. In contrast, other methodologies (such as incubations performed under different experimental conditions) can directly test how CH_4 flux changes with shifting environmental variables.

3 METHODOLOGICAL COMPARISONS

As described above, each method for measuring the diffusive flux of CH_4 from lake sediments has particular advantages, limitations, and capacities to answer scientific questions about lacustrine CH_4 cycling. When choosing which method is appropriate for one's work, previous studies explicitly comparing results from multiple approaches are informative. Careful method intercomparisons are useful in that when results from different approaches are comparable, they can build confidence in our ability to estimate CH_4 fluxes. Alternatively, when method intercomparisons reveal vastly divergent flux estimates across different techniques, they can highlight whether certain approaches are associated with systematic biases and indicate important areas for further investigation. Examples of such comparison studies are limited, comprising just 13% of our dataset (**Figure 5**; **Section 4.4**). In this section, we focus on this small subset of comparative studies to highlight a few important insights into the implications of method choice for the estimation of sediment CH_4 fluxes.

3.1 Sediment Diffusion Models and Surface Sediment Processes

Previous comparisons of incubations and diffusion models applied in the sediment (Fick's first law, **Eq. 1**) emphasize the challenge of accurately measuring processes near the SWI. Compared to sediment incubations, sediment diffusion models are reported to sometimes overestimate (Sweerts et al., 1991; Sinke et al., 1992; Li et al., 2018) and sometimes underestimate (Frenzel et al., 1990; Thebrath et al., 1993) the diffusive flux of CH_4 from sediments. The discrepancy between incubation and diffusion model-based estimates may stem from several causes. For example, sediment concentration profiles cannot capture how rapid processes at the sediment surface may influence flux (Urban et al., 1997) and (**Table 1**). Sediments near the SWI are often an important location for sediment CH_4 oxidation (Frenzel et al., 1990; Schubert et al., 2011; Hershey et al., 2014) or methanogenesis (Winfrey and Zeikus, 1979; Liikanen et al., 2002b; Dan et al., 2004), driving rapid changes in CH_4 concentrations within just a few millimeters or centimeters of the SWI (Bussmann and Schink. 2006). These concentration changes may be unresolvable by the limited spatial resolution of porewater samples (Harper et al., 1997), resulting in measurement error for sediment diffusion model-based estimates (**Table 1**). In contrast, incubation using benthic chambers or intact cores measure CH_4 accumulation above the SWI, and therefore they incorporate the potential effects of rapid surface processes on flux. Intact core incubations or benthic chambers may therefore be preferable to a sediment diffusion modeling approach in systems where significant CH_4 processing in the sediment occurs within several millimeters of the SWI.

3.2 Incubation Effects on Microbial Rates

Comparisons between sediment incubations and other approaches suggest that incubations may overestimate fluxes by stimulating methanogenesis and/or inhibiting methanotrophy. For example, in Lake Constance, sediment fluxes based on slurry incubations were 3–4 times larger than estimates from sediment diffusion modeling (1,400 and 369 μmol CH_4 m^{-2} d^{-1}, respectively; Frenzel et al., 1990). In a eutrophic maar lake, incubation-based sediment fluxes (16 mmol CH_4 m^{-2} d^{-1}) were about tenfold higher than sediment diffusion model estimates (1.5 mmol CH_4 m^{-2} d^{-1}; Fahrner et al., 2008). Similarly, other studies report larger estimates of CH_4 diffusive fluxes from incubations than hypolimnetic mass balances. In Frain's Lake and Third Sister Lake, flux estimates based on incubations performed between 0 and 20 cm sediment depth were 2–5 times higher than flux estimates based on a

hypolimnetic mass balance (Kelly and Chynoweth, 1980). Incubations measured a sediment flux of 2,600 μmol CH_4 m^{-2} d^{-1} in the profundal zone of Blelham Tarn, 2–10 times higher than flux estimates from a hypolimnetic mass balance (235–1,244 μmol CH_4 m^{-2} d^{-1}; Jones and Simon 1981). The overestimation of methanogenesis by sediment incubation has also been noted in studies of other flooded soils (Blodau and Moore, 2003), where some incubation-based rates of CH_4 production in peatland soils were found to be more than 10 times larger than estimates from sediment modeling. Sediment collection and handling prior to incubation may disturb sediment microstructure, possibly stimulating methanogenesis by providing better contact for methanogens to access substrate (Kelly and Chynoweth, 1980). Incubation preparation (e.g., sediment slurrying or headspace flushing) may also stimulate CH_4 production by degassing or diluting compounds that would otherwise inhibit methanogens (Kelly and Chynoweth, 1980).

Larger sediment fluxes as a result of stimulated methanogenesis may be further compounded by the possible inhibition of CH_4 oxidation by sediment slurrying, which may destroy aggregates important for methanotrophs and their syntrophic partners (Su et al., 2019). Methanotrophy is also positively correlated with CH_4 availability (Thottathil et al., 2019), so degassing during sediment core sampling or incubation preparation could slow CH_4 oxidation compared to *in situ* rates. The possible effects of incubation on methanogenesis and methanotrophy suggests that this approach may be more suitable for comparing relative rather than absolute fluxes.

3.3 Comparing CH_4 Flux & CH_4 Production

Comparing fluxes across methods also highlights the difference between measurements of CH_4 flux and CH_4 production. Confusingly, these terms are sometimes used interchangeably in the literature, despite the fact that the former technically refers to the rate of CH_4 transport across a plane (e.g., the SWI) and the latter represents a rate of methanogenesis. The confusion in terminology is further compounded by the fact that CH_4 production rates measured at discrete depths throughout the sediment profile can be depth-integrated into a flux out of sediments (**Figures 2A,B**). Previous studies have reported similar estimates of depth-integrated CH_4 production from sediment diffusion-reaction modeling (**Eqs 3–5**) and flux across the SWI from sediment diffusion models (**Eq. 1**; Bartosiewicz et al., 2016; Steinsberger et al., 2019). However, other studies have noted a mismatch between estimates of CH_4 diffusion based on sediment diffusion models and depth-integrated methanogenesis based on sediment diffusion-reaction models, attributing the difference to some produced CH_4 being oxidized anaerobically (Norði et al., 2013) or forming bubbles (Adler et al., 2011) in the sediment profile before it could diffuse into the water column. Others have calculated sediment ebullition specifically as the difference between depth-integrated methanogenesis and the diffusive CH_4 flux across the SWI (Langenegger et al., 2019).

Depth-integrated production also may not accurately represent flux if the sampling spatial resolution is too coarse to capture significant changes in methanogenesis within the sediment profile (**Figure 2B**). Methanogenesis can double or triple within just a few centimeters in the sediment column of some lakes (Chan et al., 2005; Yang et al., 2017), yet depth integration often assumes CH_4 production is constant across sediment layers ranging in thickness from 3 to 5 cm (Bretz and Whalen, 2014; Berberich et al., 2019) to 20 cm or more (West et al., 2016). In these cases, depth-integrated production may be significantly different from flux. The possibility of misrepresenting flux by depth-integrating methanogenesis rates further underscores the advantage of approaches that measure the release of CH_4 from sediments without sampling sediments directly, such as benthic chambers.

3.4 Sediment Depth Matters

Lastly, considering what sediment depths are characterized by a method is important when comparing techniques. The majority (60%) of incubation studies in our dataset base sediment CH_4 flux or production measurements on samples taken from a sediment depth ≤20 cm. This is important because when using methods reliant on sediment sampling, such as sediment modeling or some incubations, fluxes may be underestimated if sampling excludes depths with significant methanogenesis. For example, Kelly and Chynoweth (1980) reported fluxes measured with core incubations sectioned from 0 to 3 cm in the sediment column were 2–4 times lower than fluxes measured with cores sectioned from 0 to 20 cm. Although the authors attribute the stark difference in fluxes to a possible artificial stimulation of methanogenesis in deeper layers of incubated sediment (**Section 3.2**), there are multiple examples in the literature of active and significant methanogenesis deep in the sediment profile. Production rates from 25 to 30 cm in the sediment profile of oligotrophic Lake Constance were observed to be almost as high as those from surface sediments (Rothfuss et al., 1997). Similarly, methanogenesis from 90 to 130 cm in the sediments of mesotrophic Lake Ätäskö were comparable to rates observed at 10–30 cm (Rissanen et al., 2017), and the highest methanogenesis rates were observed below 50 cm in cores from a thermokarst lake (Heslop et al., 2015) and an acidic lake (Koschorreck et al., 2008).

Taken together, these examples suggest that the common assumption of negligible methanogenesis in deep sediments is incorrect, at least some of the time. Highly organic-rich sediment columns (e.g., those within thermokarst lakes) may exhibit significant methanogenesis beyond surface sediments, whereas sandy, porous sediment columns may not have the carbon stores to support such microbial activity deeper in the profile. Alternatively, highly acidic or basic lakes may contain surface sediments with a pH that inhibits methanogenesis; yet methanogens may be active deeper in the sediment profile where conditions are more favorable. The control that sampled sediment depth exerts on flux estimates from some *ex situ* approaches highlights the advantage of methodologies that consider the entire sediment column in their measurements, such as *in situ* methods or techniques that estimate flux based on water column measurements.

4 RECOMMENDATIONS & FUTURE DIRECTIONS

The strengths and limitations of each method for measuring diffusive CH_4 flux from sediments should influence one's choice of approach for different research applications. Thus far, we have focused on limitations of individual methods (**Section 2**) or between pairs or small groups of methods (**Section 3**). Here, we take a broader perspective to 1) discuss how limitations across the full suite of approaches have shaped gaps in current understanding of lacustrine CH_4 cycling; and 2) recommend future methodological developments needed to address these gaps.

4.1 Short-Term Temporal Variability

Little is known about short-term (sub-hourly) variation in diffusive CH_4 fluxes from sediments, largely because most available approaches operate on hourly to monthly or seasonal time scales (**Figure 3**). A better characterization of short-term variability is necessary for identifying the implications of temporal resolution on measured fluxes. For example, previous studies have stressed the possibility of under- or over-estimating surface emissions from reservoirs and impounded rivers due to inadequate sampling frequency (Maeck et al., 2014; Wik et al., 2016; Harrison et al., 2017; Marcon et al., 2019). No similar studies exist for CH_4 diffusion from lake sediments, despite recent evidence that diffusive flux can change significantly within hours (D'Ambrosio, 2022). Advancing understanding of short-term variability would therefore be instructive when determining the appropriate method and sampling frequency for future work.

Flux gradient approaches are promising, emerging tools for characterizing short-term variability in CH_4 fluxes. Such methods can be applied to measure fluxes on a time scale of minutes to hours across the lake bottom boundary layer (BBL), a region of the water column extending up to several meters above the lakebed and a zone where currents are affected by friction with sediments (Henderson, 2016). Although flux measured in the BBL is not technically equivalent to flux across the SWI, estimates from the BBL are valuable because they quantify the rate at which CH_4 is transported from sediments into the lake interior, from which it may ultimately be emitted to the atmosphere. Using a flux gradient technique, flux estimates are made *in situ* by combining measurements in the BBL of vertical concentration gradients, turbulent mixing, and temperature stratification (McGillis et al., 2011). Recently, the method has been adapted for use in a lake BBL for the first time (D'Ambrosio, 2022), whereas previous applications have focused on fluxes of momentum, oxygen, or total alkalinity in marine BBLs (Reidenbach et al., 2006; McGillis et al., 2011; Turk et al., 2015; Takeshita et al., 2016). This methodological advancement allowed for the estimation of CH_4 fluxes on an hourly basis within the BBL of a eutrophic reservoir, revealing significant sub-daily variations in CH_4 transport (D'Ambrosio, 2022).

The development of other techniques that operate on a short temporal scale would also be helpful, such as eddy correlation (eddy flux) techniques that have already been developed for fluxes of other dissolved gases such as CO_2 and O_2 across the SWI (Berg et al., 2013; Kokic et al., 2016). Unfortunately, eddy flux techniques require *in situ* concentration measurements with a temporal resolution <1 s (Donis et al., 2015), which are beyond the capability of dissolved CH_4 instruments at present; response times for aqueous CH_4 sensors are, at this writing, limited to 12 s–40 min response times (Damgaard and Revsbech, 1997; Webb et al., 2016; Xiao et al., 2020). The development of aqueous CH_4 sensors with faster response times would facilitate the development of eddy correlation approaches for measuring CH_4 flux from lakebeds. Alternatively, relaxed eddy accumulation techniques avoid the need for fast-response sensors and have been used to measure fluxes of oxygen, temp, and suspended matter across the SWI in a shallow riverine lake (Lemaire et al., 2017). However, both eddy flux and relaxed eddy accumulation approaches perform best in consistently turbulent conditions, and therefore may be of limited utility in lakes and reservoirs where near-bed turbulence is intermittent (Simpson et al., 2011; Henderson, 2016). Flux gradient approaches, adapted for use in moderately stratified lake BBLs (D'Ambrosio, 2022), may be the best alternative in these cases.

4.2 Boundary Layer Dynamics

Methodological limitations have also obscured the relationship between BBL conditions and SWI CH_4 diffusion. In stratified lakes and reservoirs, internal waves and seiches can drive changes in BBL mixing and biogeochemistry that occur on timescales of minutes to hours (Wüest and Lorke, 2003; Bernhardt et al., 2014). It is well-established that such periodic changes in BBL turbulence exert significant control on the diffusive flux of other redox-active solutes to and from sediments, such as oxygen and nitrate (Lorke et al., 2003; Brand et al., 2008, 2009; Bryant et al., 2010). However, most available approaches for measuring CH_4 diffusion from sediments cannot capture how such boundary layer processes influence flux. Current techniques largely rely on *ex situ* analyses (**Table 1**) performed on hourly to seasonal time scales (**Figure 3**). Consequently, boundary layer conditions have been largely overlooked as a potential factor influencing the diffusive flux of CH_4 out of sediments.

Future work that couples BBL observations with CH_4 flux measurements from sediments in space and time is needed to investigate how boundary layer dynamics may influence the rate and timing of CH_4 transport into the water column. For example, flux gradient approaches do not isolate sediments from lake-scale processes in the boundary layer that may influence flux (D'Ambrosio, 2022), unlike *ex situ* techniques such as sediment incubations. Application of the flux gradient approach has illustrated how fluctuations in BBL turbulent mixing may exert an important control on CH_4 transport from sediments into the water column (D'Ambrosio, 2022). The development of eddy flux and/or relaxed eddy accumulation techniques may also be helpful in this regard (**Section 4.1**). However, further measurements in other lake systems and a closer examination of potential causal links between boundary layer dynamics and CH_4 transport are still needed. For example, on seasonal time scales, methanotrophs can regulate the upwards flux of CH_4 in the water column by

responding readily to changes in concentrations of CH_4 and electron acceptors (Graf et al., 2018; Mayr et al., 2020a; Mayr et al., 2020b). On shorter time scales, it is unknown if methanotrophs exert a similar control on CH_4 flux from sediments in response to fluctuating concentrations of CH_4 and electron acceptors in the BBL.

4.3 Developing Modeling Approaches

Available methods for measuring diffusive CH_4 flux across the SWI rely on direct sampling of the sediments or the water column. Our capacity to measure flux is therefore limited in lakes that are remote, seasonally inaccessible, or ice-covered. Moreover, a sampling bias towards measurements made over short-term deployments and during the summer months is likely, as noted in the literature of surface CH_4 emissions from lakes (Wik et al., 2016; Jansen et al., 2020). Consequently, current estimates of the diffusive flux of CH_4 from sediments are focused on physically accessible lakes and reservoirs, likely during the warmer months. Expanding the spatiotemporal coverage of measurements would provide novel insight into the variability and controls on CH_4 release from lake sediments in a wide variety of lakes and reservoirs.

Developing models that estimate CH_4 diffusion from sediments using easily-measured lake characteristics, rather than measurements of CH_4 concentrations in the sediments and/or water column, could improve the spatiotemporal coverage of methane flux estimates. Multiple models of surface CH_4 emissions from easily-measured lake characteristics have been created (Bastviken et al., 2004; Harrison et al., 2021). Similar techniques for predicting CH_4 diffusion from lake sediments have not been developed, yet there is evidence that some basic lake characteristics could be useful in predicting sediment diffusive flux. For example, a recent study successfully modeled sediment CH_4 production as a function of particulate organic matter supply and reactivity (Grasset et al., 2021). Moreover, a recent meta-analysis of over 60 lakes and reservoirs suggests sediment CH_4 production rates can be linked to trophic status (D'Ambrosio and Harrison, 2021), which can be readily measured on site with surface water sampling. Exploring the power of lake characteristics to predict CH_4 diffusion from sediments could elucidate how the supply of CH_4 to the lake water column potentially changes across seasons, latitudes, lake types, and other system characteristics, uninhibited by direct sampling effort.

4.4 Expanding Method Comparisons

Of the 163 studies included in this review, just 13% (n = 22) used multiple methods to estimate CH_4 diffusion from sediments (**Figure 5**; **Supplementary Table S1**). Approximately half of the comparative studies in our dataset compare the most popular approaches (sediment incubations and sediment diffusion models; **Figure 1**; **Supplementary Table S1**). To our knowledge, less common methods such as water column models have fewer direct comparisons (**Figure 5**). Comparisons between approaches in one or multiple lakes are common in studies of CH_4 surface emission (Schubert et al., 2012; Podgrajsek et al., 2014; Deemer et al., 2016; Sanches et al., 2019), and oxidation in the water column or sediments (Bastviken et al., 2002; Su et al., 2019), but are uncommon in the study of CH_4 diffusion from sediments. More method comparisons would benefit the field because observed agreement or deviation between approaches highlights methodological limitations and potential caveats when considering estimates between studies.

5 CONCLUSION

The diffusive flux of CH_4 from sediments is a critical source of CH_4 to lake and reservoir ecosystems, which collectively contribute significantly to global greenhouse gas emissions. Here, we critically assess the most popular methods for quantifying CH_4 diffusion from sediments, including incubations, diffusion and diffusion-reaction models applied in the sediment, and mass balance and advection-diffusion-reaction models applied in the water column. We also discuss lessons learned from the small body of studies that directly compare some of these methods, including 1) estimating flux across the SWI with sediment diffusion models is challenging because these models are quite sensitive to surface sediment CH_4 concentration gradients, which are difficult to measure at an appropriate spatial resolution; 2) incubation-based approaches can bias flux estimates by stimulating methanogenesis and/or inhibiting methanotrophy in sediments; 3) depth-integrating methanogenesis rates to estimate flux can lead to error if the sampling spatial resolution is not fine enough to resolve changes in CH_4 production with depth; and 4) most studies estimate flux based on sampling shallow sediments (<20 cm depth), and therefore may not consider the possibility of significant CH_4 production demonstrated deeper in the sediments of some systems. Furthermore, we explore how methodological limitations have shaped knowledge gaps regarding the rate and timing of CH_4 supply to lake interiors. Specifically, the coarse spatiotemporal resolution of most established methods contributes to a poor understanding of the short-term variability of diffusive flux from sediments and the potential control of boundary layer conditions. Furthermore, the spatiotemporal coverage of diffusive flux estimates from different systems is likely biased towards physically accessible lakes sampled during the summer months.

We also identify several important avenues for future methodological advancement. *In situ* approaches with sub-hourly temporal resolution are needed to address questions of short-term variability and the role of boundary layer conditions. Recent applications of flux gradient techniques and possible future adaptations of eddy correlation or relaxed eddy accumulation approaches could be useful tools to this end. Expanding CH_4 flux measurements using these techniques can help inform models that predict diffusive flux from sediments using basic lake characteristics, possibly improving the future spatiotemporal coverage of estimates. More quantitative comparisons between techniques at the finest and coarsest spatiotemporal resolution considered here (cm/min scales and whole lake/seasonal scales, respectively) would highlight additional strengths weaknesses of additional methods, point out additional knowledge gaps, and clarify the implications of methodological approach for flux estimation.

AUTHOR CONTRIBUTIONS

SD performed the literature review and wrote the manuscript. JH provided scientific and editorial support.

FUNDING

This work was supported by funding from the NSF GRFP #1347973 and #1842493 to SD and funding from NSF DEB 1355211 and NSF DISES 2109259 to JH.

ACKNOWLEDGMENTS

The authors thank Kevan Moffett, David Butman, Stephen Henderson, and multiple reviewers for their helpful feedback on this manuscript.

SUPPLEMENTARY MATERIAL

The Supplementary Material for this article can be found online at: https://www.frontiersin.org/articles/10.3389/fenvs.2022.850070/full#supplementary-material

REFERENCES

Adams, D. D. (2005). "Diffuse Flux of Greenhouse Gases - Methane and Carbon Dioxide - at the Sediment-Water Interface of Some Lakes and Reservoirs of the World," in *Greenhouse Gas Emissions—Fluxes and Processes*. Editors M. Garneau, A. Tremblay, C. Roehm, and L. Varfalvy (Springer Berlin Heidelberg), 129–153. doi:10.1007/978-3-540-26643-3_6

Addess, J. M., and Effler, S. W. (1996). Summer Methane Fluxes and Fall Oxygen Resources of Onondaga Lake. *Lake Reservoir Manage.* 12, 91–101. doi:10.1080/07438149609354000

Adler, M., Eckert, W., and Sivan, O. (2011). Quantifying Rates of Methanogenesis and Methanotrophy in Lake Kinneret Sediments (Israel) Using Pore-Water Profiles. *Limnol. Oceanogr.* 56, 1525–1535. doi:10.4319/lo.2011.56.4.1525

Algesten, G., Sobek, S., Bergström, A.-K., Jonsson, A., Tranvik, L. J., and Jansson, M. (2005). Contribution of Sediment Respiration to Summer CO_2 Emission from Low Productive Boreal and Subarctic Lakes. *Microb. Ecol.* 50, 529–535. doi:10.1007/s00248-005-5007-x

Bartosiewicz, M., Laurion, I., Clayer, F., and Maranger, R. (2016). Heat-Wave Effects on Oxygen, Nutrients, and Phytoplankton Can Alter Global Warming Potential of Gases Emitted from a Small Shallow Lake. *Environ. Sci. Technol.* 50, 6267–6275. doi:10.1021/acs.est.5b06312

Bartosiewicz, M., Maranger, R., Przytulska, A., and Laurion, I. (2021). Effects of Phytoplankton Blooms on Fluxes and Emissions of Greenhouse Gases in a Eutrophic lake. *Water Res.* 196, 116985. doi:10.1016/j.watres.2021.116985

Bastviken, D., Cole, J. J., Pace, M. L., and Van de Bogert, M. C. (2008). Fates of Methane from Different lake Habitats: Connecting Whole-lake Budgets and CH_4 emissions. *J. Geophys. Res.* 113, a–n. doi:10.1029/2007JG000608

Bastviken, D., Cole, J., Pace, M., and Tranvik, L. (2004). Methane Emissions from Lakes: Dependence of lake Characteristics, Two Regional Assessments, and a Global Estimate. *Glob. Biogeochem. Cycles* 18, a–n. doi:10.1029/2004GB002238

Bastviken, D., Ejlertsson, J., and Tranvik, L. (2002). Measurement of Methane Oxidation in Lakes: A Comparison of Methods. *Environ. Sci. Technol.* 36, 3354–3361. doi:10.1021/ES010311P

Bastviken, D. (2009). "Methane," in *Encyclopedia of Inland Waters* (Academic Press), 783–805. doi:10.1016/b978-012370626-3.00117-4

Beaulieu, J., McManus, M., and Nietch, C. (2016). Estimates of Reservoir Methane Emissions Based on a Spatially-Balanced Probabilistic-Survey. *Limnol. Oceanogr.* 61, S27–S40. doi:10.1109/JPHOT.2015.XXXXXXX10.1002/lno.10284

Bédard, C., and Knowles, R. (1991). Hypolimnetic O_2 Consumption, Denitrification, and Methanogenesis in a Thermally Stratified lake. *Can. J. Fish. Aquat. Sci.* 48, 1048–1054.

Berberich, M. E., Beaulieu, J. J., Hamilton, T. L., Waldo, S., and Buffam, I. (2019). Spatial Variability of Sediment Methane Production and Methanogen Communities within a Eutrophic Reservoir: Importance of Organic Matter Source and Quantity. *Limnol. Oceanogr.* 65, 1336–1358. doi:10.1002/lno.11392

Berg, P., Long, M. H., Huettel, M., Rheuban, J. E., McGlathery, K. J., Howarth, R. W., et al. (2013). Eddy Correlation Measurements of Oxygen Fluxes in Permeable Sediments Exposed to Varying Current Flow and Light. *Limnol. Oceanogr.* 58, 1329–1343. doi:10.4319/lo.2013.58.4.1329

Berg, P., Risgaard-Petersen, N., and Rysgaard, S. (1998). Interpretation of Measured Concentration Profiles in Sediment Pore Water. *Limnol. Oceanogr.* 43, 1500–1510. doi:10.4319/lo.1998.43.7.1500

Berner, R. (1980). *Early Diagenesis: A Theoretical Approach*. Princeton, NJ: Princeton University Press.

Bernhardt, J., Kirillin, G., and Hupfer, M. (2014). Periodic Convection within Littoral lake Sediments on the Background of Seiche-Driven Oxygen Fluctuations. *Limnol. Oceanogr.* 4, 17–33. doi:10.1215/21573689-2683238

Blodau, C., and Moore, T. R. (2003). Experimental Response of Peatland Carbon Dynamics to a Water Table Fluctuation. *Aquat. Sci. - Res. Across Boundaries* 65, 47–62. doi:10.1007/s000270300004

Blomqvist, S. (1991). Quantitative Sampling of Soft-Bottom Sediments: Problems and Solutions. *Mar. Ecol. Prog. Ser.* 72, 295–304. doi:10.3354/meps072295

Bornemann, M., Bussmann, I., Tichy, L., Deutzmann, J., Schink, B., and Pester, M. (2016). Methane Release from Sediment Seeps to the Atmosphere Is Counteracted by Highly Active Methylococcaceae in the Water Column of Deep Oligotrophic Lake Constance. *FEMS Microbiol. Ecol.* 92, fiw123–11. doi:10.1093/femsec/fiw123

Borrel, G., Jézéquel, D., Biderre-Petit, C., Morel-Desrosiers, N., Morel, J.-P., Peyret, P., et al. (2011). Production and Consumption of Methane in Freshwater lake Ecosystems. *Res. Microbiol.* 162, 832–847. doi:10.1016/j.resmic.2011.06.004

Bosse, U., Frenzel, P., and Conrad, R. (1993). Inhibition of Methane Oxidation by Ammonium in the Surface Layer of a Littoral Sediment. *FEMS Microbiol. Ecol.* 13, 123–134. doi:10.1016/0168-6496(93)90030-B10.1111/j.1574-6941.1993.tb00058.x

Boudreau, B. P. (1984). On the Equivalence of Nonlocal and Radial-Diffusion Models for Porewater Irrigation. *J. Mar. Res.* 42, 731–735. doi:10.1357/002224084788505924

Brand, A., Dinkel, C., and Wehrli, B. (2009). Influence of the Diffusive Boundary Layer on Solute Dynamics in the Sediments of a Seiche-Driven lake: A Model Study. *J. Geophys. Res.* 114, 1–12. doi:10.1029/2008JG000755

Brand, A., McGinnis, D. F., Wehrli, B., and Wüest, A. (2008). Intermittent Oxygen Flux from the interior into the Bottom Boundary of Lakes as Observed by Eddy Correlation. *Limnol. Oceanogr.* 53, 1997–2006. doi:10.4319/lo.2008.53.5.1997

Bretz, K., and Whalen, S. (2014). Methane Cycling Dynamics in Sediments of Alaskan Arctic Foothill Lakes. *Iw* 4, 65–78. doi:10.5268/IW-4.1.637

Bryant, L. D., Lorrai, C., McGinnis, D. F., Brand, A., Est, A. W., and Little, J. C. (2010). Variable Sediment Oxygen Uptake in Response to Dynamic Forcing. *Limnol. Oceanogr.* 55, 950–964. doi:10.4319/lo.2010.55.2.0950

Bufflap, S. E., and Allen, H. E. (1995). Sediment Pore Water Collection Methods for Trace Metal Analysis: A Review. *Water Res.* 29, 165–177. doi:10.1016/0043-1354(94)E0105-F

Bussmann, I. (2005). Methane Release through Resuspension of Littoral Sediment. *Biogeochemistry* 74, 283–302. doi:10.1007/s.10.1007/s10533-004-2223-2

Bussmann, I., and Schink, B. (2006). A Modified Diffusion-Based Methane Sensor and its Application in Freshwater Sediment. *Limnol. Oceanogr. Methods* 4, 275–283. doi:10.4319/lom.2006.4.275

Carignan, R., and Lean, D. R. S. (1991). Regeneration of Dissolved Substances in a Seasonally Anoxic lake: The Relative Importance of Processes Occurring in the Water Column and in the Sediments. *Limnol. Oceanogr.* 36, 683–707. doi:10.4319/lo.1991.36.4.0683

Chan, O. C., Claus, P., Casper, P., Ulrich, A., Lueders, T., and Conrad, R. (2005). Vertical Distribution of Structure and Function of the Methanogenic Archaeal

Community in Lake Dagow Sediment. *Environ. Microbiol.* 7, 1139–1149. doi:10.1111/j.1462-2920.2005.00790.x

Chmiel, H. E., Kokic, J., Denfeld, B. A., Einarsdóttir, K., Wallin, M. B., Koehler, B., et al. (2016). The Role of Sediments in the Carbon Budget of a Small Boreal lake. *Limnol. Oceanogr.* 61, 1814–1825. doi:10.1002/lno.10336

Clayer, F., Gobeil, C., and Tessier, A. (2016). Rates and Pathways of Sedimentary Organic Matter Mineralization in Two Basins of a Boreal lake: Emphasis on Methanogenesis and Methanotrophy. *Limnol. Oceanogr.* 61, S131–S149. doi:10.1002/lno.10323

Clayer, F., Moritz, A., Gélinas, Y., Tessier, A., and Gobeil, C. (2018). Modeling the Carbon Isotope Signatures of Methane and Dissolved Inorganic Carbon to Unravel Mineralization Pathways in Boreal lake Sediments. *Geochimica et Cosmochimica Acta* 229, 36–52. doi:10.1016/j.gca.2018.02.012

Colas, F., Baudoin, J.-M., Bonin, P., Cabrol, L., Daufresne, M., Lassus, R., et al. (2021). Ecosystem Maturity Modulates Greenhouse Gases Fluxes from Artificial Lakes. *Sci. Total Environ.* 760, 144046. doi:10.1016/j.scitotenv.2020.144046

D'Ambrosio, S. L., and Harrison, J. A. (2021). Methanogenesis Exceeds CH_4 Consumption in Eutrophic lake Sediments. *Limnol Oceanogr Lett.* 6, 173–181. doi:10.1002/lol2.10192

D'Ambrosio, S. L. (2022). *Methane Flux from Lacustrine Sediments: Advancing Methodologies, Determining Drivers, and Characterizing Variability across Spatiotemporal Scales*.

Damgaard, L. R., and Revsbech, N. P. (1997). A Microscale Biosensor for Methane Containing Methanotrophic Bacteria and an Internal Oxygen Reservoir. *Anal. Chem.* 69, 2262–2267. doi:10.1021/ac9611576

Dan, J., Kumai, T., Sugimoto, A., and Murase, J. (2004). Biotic and Abiotic Methane Releases from Lake Biwa Sediment Slurry. *Limnology* 5, 149–154. doi:10.1007/s10201-004-0124-7

Deemer, B. R., Harrison, J. A., Li, S., Beaulieu, J. J., DelSontro, T., Barros, N., et al. (2016). Greenhouse Gas Emissions from Reservoir Water Surfaces: A New Global Synthesis. *Bioscience* 66, 949–964. doi:10.1093/biosci/biw117

DelSontro, T., Kunz, M. J., Kempter, T., Wüest, A., Wehrli, B., and Senn, D. B. (2011). Spatial Heterogeneity of Methane Ebullition in a Large Tropical Reservoir. *Environ. Sci. Technol.* 45, 9866–9873. doi:10.1021/es2005545

DelSontro, T., Mcginnis, D. F., Sobek, S., Ostrovsky, I., and Wehrli, B. (2010). Extreme Methane Emissions from a Swiss Hydropower Reservoir: Contribution from Bubbling Sediments. *Environ. Sci. Technol.* 44, 2419–2425. doi:10.1021/es9031369

DelSontro, T., McGinnis, D. F., Wehrli, B., and Ostrovsky, I. (2015). Size Does Matter: Importance of Large Bubbles and Small-Scale Hot Spots for Methane Transport. *Environ. Sci. Technol.* 49, 1268–1276. doi:10.1021/es5054286

Devol, A. H. (1987). Verification of Flux Measurements Made with *In Situ* Benthic chambers. *Deep Sea Res. A. Oceanographic Res. Pap.* 34, 1007–1026. doi:10.1016/0198-0149(87)90050-1

Donis, D., Flury, S., Stöckli, A., Spangenberg, J. E., Vachon, D., and McGinnis, D. F. (2017). Full-scale Evaluation of Methane Production under Oxic Conditions in a Mesotrophic lake. *Nat. Commun.* 8, 1661. doi:10.1038/s41467-017-01648-4

Donis, D., Holtappels, M., Noss, C., Cathalot, C., Hancke, K., Polsenaere, P., et al. (2015). An Assessment of the Precision and Confidence of Aquatic Eddy Correlation Measurements. *J. Atmos. Ocean. Technol.* 32, 642–655. doi:10.1175/JTECH-D-14-00089.1

Duc, N. T., Crill, P., and Bastviken, D. (2010). Implications of Temperature and Sediment Characteristics on Methane Formation and Oxidation in lake Sediments. *Biogeochemistry* 100, 185–196. doi:10.1007/s10533-010-9415-8

Duchemin, E., Lucotte, M., Canuel, R., and Chamberland, A. (1995). Production of the Greenhouse Gases CH_4 and CO_2 by Hydroelectric Reservoirs of the Boreal Region. *Glob. Biogeochem. Cycles* 9, 529–540. doi:10.1029/95GB02202

Dück, Y., Liu, L., Lorke, A., Ostrovsky, I., Katsman, R., and Jokiel, C. (2019a). A Novel Freeze Corer for Characterization of Methane Bubbles and Assessment of Coring Disturbances. *Limnol. Oceanogr. Methods* 17, 305–319. doi:10.1002/lom3.10315

Dück, Y., Lorke, A., Jokiel, C., and Gierse, J. (2019b). Laboratory and Field Investigations on Freeze and Gravity Core Sampling and Assessment of Coring Disturbances with Implications on Gas Bubble Characterization. *Limnol. Oceanogr. Methods* 17, 585–606. doi:10.1002/lom3.10335

Durisch-Kaiser, E., Schmid, M., Peeters, F., Kipfer, R., Dinkel, C., Diem, T., et al. (2011). What Prevents Outgassing of Methane to the Atmosphere in Lake Tanganyika? *J. Geophys. Res.* 116, G02022. doi:10.1029/2010JG001323

Eckert, W., and Conrad, R. (2007). Sulfide and Methane Evolution in the Hypolimnion of a Subtropical lake: A Three-Year Study. *Biogeochemistry* 82, 67–76. doi:10.1007/s10533-006-9053-3

Encinas Fernández, J., Peeters, F., and Hofmann, H. (2016). On the Methane Paradox: Transport from Shallow Water Zones rather Than *In Situ* Methanogenesis Is the Major Source of CH_4 in the Open Surface Water of Lakes. *J. Geophys. Res. Biogeosci.* 121, 2717–2726. doi:10.1002/2016JG003586

Epping, E. H. G., and Helder, W. (1997). Oxygen Budgets Calculated Fromin Situ Oxygen Microprofiles for Northern Adriatic Sediments. *Continental Shelf Res.* 17, 1737–1764. doi:10.1016/S0278-4343(97)00039-3

Fahrner, S., Radke, M., Karger, D., and Blodau, C. (2008). Organic Matter Mineralisation in the Hypolimnion of an Eutrophic Maar lake. *Aquat. Sci.* 70, 225–237. doi:10.1007/s00027-008-8008-2

Flury, S., Glud, R. N., Premke, K., and McGinnis, D. F. (2015). Effect of Sediment Gas Voids and Ebullition on Benthic Solute Exchange. *Environ. Sci. Technol.* 49, 10413–10420. doi:10.1021/acs.est.5b01967

Frenzel, P., Thebrath, B., and Conrad, R. (1990). Oxidation of Methane in the Oxic Surface Layer of a Deep lake Sediment (Lake Constance). *FEMS Microbiol. Ecol.* 73, 149–158. doi:10.1111/j.1574-6968.1990.tb03935.x

Frindte, K., Allgaier, M., Grossart, H.-P., and Eckert, W. (2015). Microbial Response to Experimentally Controlled Redox Transitions at the Sediment Water Interface. *PLoS One* 10, e0143428. doi:10.1371/journal.pone.0143428

Frindte, K., Eckert, W., Attermeyer, K., and Grossart, H.-P. (2013). Internal Wave-Induced Redox Shifts Affect Biogeochemistry and Microbial Activity in Sediments: A Simulation experiment. *Biogeochemistry* 113, 423–434. doi:10.1007/s10533-012-9769-1

Graf, J. S., Mayr, M. J., Marchant, H. K., Tienken, D., Hach, P. F., Brand, A., et al. (2018). Bloom of a Denitrifying Methanotroph, ' Candidatus Methylomirabilis Limnetica', in a Deep Stratified lake. *Environ. Microbiol.* 20, 2598–2614. doi:10.1111/1462-2920.14285

Grasset, C., Mendonça, R., Villamor Saucedo, G., Bastviken, D., Roland, F., and Sobek, S. (2018). Large but Variable Methane Production in Anoxic Freshwater Sediment upon Addition of Allochthonous and Autochthonous Organic Matter. *Limnol. Oceanogr.* 63, 1488–1501. doi:10.1002/lno.10786

Grasset, C., Moras, S., Isidorova, A., Couture, R. M., Linkhorst, A., and Sobek, S. (2021). An Empirical Model to Predict Methane Production in Inland Water Sediment from Particular Organic Matter Supply and Reactivity. *Limnol. Oceanogr.* 66, 3643–3655–13. doi:10.1002/lno.11905

Günthel, M., Klawonn, I., Woodhouse, J., Bižić, M., Ionescu, D., Ganzert, L., et al. (2020). Photosynthesis-driven Methane Production in Oxic lake Water as an Important Contributor to Methane Emission. *Limnol. Oceanogr.* 65, 2853–2865–13. doi:10.1002/lno.11557

Harper, M. P., Davison, W., and Tych, W. (1997). Temporal, Spatial, and Resolution Constraints for *In Situ* Sampling Devices Using Diffusional Equilibration: Dialysis and DET. *Environ. Sci. Technol.* 31, 3110–3119. doi:10.1021/es9700515

Harrison, J. A., Deemer, B. R., Birchfield, M. K., and O'Malley, M. T. (2017). Reservoir Water-Level Drawdowns Accelerate and Amplify Methane Emission. *Environ. Sci. Technol.* 51, 1267–1277. doi:10.1017/CBO9781107415324.00410.1021/acs.est.6b03185

Harrison, J. A., Prairie, Y. T., Soued, C., and Mercier-Blais, S. (2021). Year-2020 Global Distribution and Pathways of Reservoir Methane and Carbon Dioxide Emissions According to the Greenhouse Gas from Reservoirs (G- Res) Model. *Glob. Biogeochem. Cycles*, 0–3. doi:10.1029/2020GB006888.This

Henderson, S. M. (2016). Turbulent Production in an Internal Wave Bottom Boundary Layer Maintained by a Vertically Propagating Seiche. *J. Geophys. Res. Oceans* 121, 2481–2498. doi:10.1002/2015JC011071.Received

Hershey, A. E., Northington, R. M., Hart-Smith, J., Bostick, M., and Whalen, S. C. (2015). Methane Efflux and Oxidation, and Use of Methane-Derived Carbon by Larval Chironomini, in Arctic lake Sediments. *Limnol. Oceanogr.* 60, 276–285. doi:10.1002/lno.10023

Hershey, A. E., Northington, R. M., and Whalen, S. C. (2014). Substrate Limitation of Sediment Methane Flux, Methane Oxidation and Use of Stable Isotopes for Assessing Methanogenesis Pathways in a Small Arctic lake. *Biogeochemistry* 117, 325–336. doi:10.1007/s10533-013-9864-y

Heslop, J. K., Walter Anthony, K. M., Sepulveda-Jauregui, A., Martinez-Cruz, K., Bondurant, A., Grosse, G., et al. (2015). Thermokarst lake Methanogenesis along a Complete Talik Profile. *Biogeosciences* 12, 4317–4331. doi:10.5194/bg-12-4317-2015

Hesslein, R. H. (1976). An *In Situ* Sampler for Close Interval Pore Water Studies1. *Limnol. Oceanogr.* 21, 912–914. doi:10.4319/lo.1976.21.6.0912

Hofmann, H., Federwisch, L., and Peeters, F. (2010). Wave-induced Release of Methane: Littoral Zones as Source of Methane in Lakes. *Limnol. Oceanogr.* 55, 1990–2000. doi:10.4319/lo.2010.55.5.1990

Huttunen, J. T., Väisänen, T. S., Hellsten, S. K., and Martikainen, P. J. (2006). Methane Fluxes at the Sediment–Water Interface in Some Boreal Lakes and Reservoirs. *Boreal Environ. Res.* 11, 27–34.

Isidorova, A., Grasset, C., Mendonça, R., and Sobek, S. (2019). Methane Formation in Tropical Reservoirs Predicted from Sediment Age and Nitrogen. *Sci. Rep.* 9, 1–9. doi:10.1038/s41598-019-47346-7

Itoh, M., Kobayashi, Y., Chen, T.-Y., Tokida, T., Fukui, M., Kojima, H., et al. (2015). Effect of Interannual Variation in winter Vertical Mixing on CH_4 dynamics in a Subtropical Reservoir. *J. Geophys. Res. Biogeosci.* 120, 1246–1261. doi:10.1002/2015JG002972

Jahnke, R. A. (1988). A Simple, Reliable, and Inexpensive Pore-Water Sampler1. *Limnol. Oceanogr.* 33, 483–487. doi:10.4319/lo.1988.33.3.0483

Jansen, J., Thornton, B. F., Wik, M., MacIntyre, S., and Crill, P. M. (2020). Temperature Proxies as a Solution to Biased Sampling of Lake Methane Emissions. *Geophys. Res. Lett.* 47. doi:10.1029/2020GL088647

Jones, J. G., and Simon, B. M. (1981). Differences in Microbial Decomposition Processes in Profundal and Littoral Lake Sediments, with Particular Reference to the Nitrogen Cycle. *Microbiology* 123, 297–312. doi:10.1099/00221287-123-2-297

Jones, J. G., Simon, B. M., and Gardener, S. (1982). Factors Affecting Methanogenesis and Associated Anaerobic Processes in the Sediments of a Stratified Eutrophic Lake. *Microbiology* 128, 1–11. doi:10.1017/CBO9781107415324.00410.1099/00221287-128-1-1

Karvinen, A., Lehtinen, L., and Kankaala, P. (2015). Variable Effects of Iron (Fe (III)) Additions on Potential Methane Production in Boreal Lake Littoral Sediments. *Wetlands* 35, 137–146. doi:10.1007/s13157-014-0602-6

Kelly, C. A., and Chynoweth, D. P. (1980). Comparison of *In Situ* and *In Vitro* Rates of Methane Release in Freshwater Sediments. *Appl. Environ. Microbiol.* 40, 287–293. doi:10.1128/aem.40.2.287-293.1980

Kelly, C. A., and Chynoweth, D. P. (1981). The Contributions of Temperature and of the Input of Organic Matter in Controlling Rates of Sediment Methanogenesis1. *Limnol. Oceanogr.* 26, 891–897. doi:10.4319/lo.1981.26.5.0891

Kelly, C. A., Rudd, J. W. M., and Schindler, D. W. (1988). Carbon and Electron Flow via Methanogenesis, SO42- NO3-, Fe3+, and Mn4+ Reduction in the Anoxic Hypolimnia of three lakes. *Arch. Hydrobiol Beih Ergebn Limnol* 31, 333–344.

Klump, J. V., Fitzgerald, S. A., and Waplesa, J. T. (2009). Benthic Biogeochemical Cycling, Nutrient Stoichiometry, and Carbon and Nitrogen Mass Balances in a Eutrophic Freshwater bay. *Limnol. Oceanogr.* 54, 692–712. doi:10.4319/lo.2009.54.3.0692

Kokic, J., Sahlée, E., Brand, A., and Sobek, S. (2016). Low Sediment-Water Gas Exchange in a Small Boreal lake. *J. Geophys. Res. Biogeosci.* 121, 2493–2505. doi:10.1002/2016JG003372

Koschorreck, M., Wendt-Potthoff, K., Scharf, B., and Richnow, H. H. (2008). Methanogenesis in the Sediment of the Acidic Lake Caviahue in Argentina. *J. Volcanology Geothermal Res.* 178, 197–204. doi:10.1016/j.jvolgeores.2008.06.017

Kristensen, E., Penha-Lopes, G., Delefosse, M., Valdemarsen, T., Quintana, C., and Banta, G. (2012). What Is Bioturbation? the Need for a Precise Definition for Fauna in Aquatic Sciences. *Mar. Ecol. Prog. Ser.* 446, 285–302. doi:10.3354/meps09506

Kuivila, K. M., Murray, J. W., Devol, A. H., Lidstrom, M. E., and Reimers, C. E. (1988). Methane Cycling in the Sediments of Lake Washington. *Limnol. Oceanogr.* 33, 571–581. doi:10.4319/lo.1988.33.4.0571

Kuivila, K. M., Murray, J. W., Devol, A. H., and Novelli, P. C. (1989). Methane Production, Sulfate Reduction and Competition for Substrates in the Sediments of Lake Washington. *Geochimica et Cosmochimica Acta* 53, 409–416. doi:10.1016/0016-7037(89)90392-x

Langenegger, T., Vachon, D., Donis, D., and McGinnis, D. F. (2019). What the Bubble Knows: Lake Methane Dynamics Revealed by Sediment Gas Bubble Composition. *Limnol. Oceanogr.* 64, 1526–1544. doi:10.1002/lno.11133

Leal, J. J. F., Dos Santos Furtado, A. L., De Assis Esteves, F., Bozelli, R. L., and Figueiredo-Barros, M. P. (2007). The Role of Campsurus Notatus (Ephemeroptera: Polymitarcytidae) Bioturbation and Sediment Quality on Potential Gas Fluxes in a Tropical lake. *Hydrobiologia* 586, 143–154. doi:10.1007/s10750-006-0570-9

Lemaire, B. J., Noss, C., and Lorke, A. (2017). Toward Relaxed Eddy Accumulation Measurements of Sediment-Water Exchange in Aquatic Ecosystems. *Geophys. Res. Lett.* 44, 8901–8909. doi:10.1002/2017GL074625

Lerman, A. (1979). *Geochemical Processes: Water and Sediment Environments*.

Lettmann, K. A., Riedinger, N., Ramlau, R., Knab, N., Böttcher, M. E., Khalili, A., et al. (2012). Estimation of Biogeochemical Rates from Concentration Profiles: A Novel Inverse Method. *Estuarine, Coastal Shelf Sci.* 100, 26–37. doi:10.1016/j.ecss.2011.01.012

Li, B., Gu, Q., Miao, Y., Luo, W., Xing, P., and Wu, Q. L. (2020). Methane Distribution Patterns along a Transect of Lake Fuxian, a Deep Oligotrophic lake in China. *Environ. Sci. Pollut. Res.* 27, 25848–25860. doi:10.1007/s11356-019-06098-7

Li, L., Fuchs, A., Ortega, S. H., Xue, B., and Casper, P. (2021). Spatial Methane Pattern in a Deep Freshwater lake: Relation to Water Depth and Topography. *Sci. Total Environ.* 764, 142829. doi:10.1016/j.scitotenv.2020.142829

Li, L., Xue, B., Yao, S., Tao, Y., and Yan, R. (2018). Spatial-temporal Patterns of Methane Dynamics in Lake Taihu. *Hydrobiologia* 822, 143–156. doi:10.1007/s10750-018-3670-4

Liikanen, A., Flöjt, L., and Martikainen, P. (2002a). Gas Dynamics in Eutrophic Lake Sediments Affected by Oxygen, Nitrate, and Sulfate. *J. Environ. Qual.* 31, 338–349. doi:10.2134/jeq2002.3380

Liikanen, A., Huttunen, J. T., Murtoniemi, T., Tanskanen, H., Väisänen, T., Silvola, J., et al. (2003). Spatial and Seasonal Variation in Greenhouse Gas and Nutrient Dynamics and Their Interactions in the Sediments of a Boreal Eutrophic lake. *Biogeochemistry* 65, 83–103. doi:10.1023/A:1026070209387

Liikanen, A., Huttunen, J. T., Valli, K., and Martikainen, P. J. (2002b). Methane Cycling in the Sediment and Water Column of Mid-boreal Hyper-Eutrophic Lake Kevätön, Finland. *fal* 154, 585–603. doi:10.1127/archiv-hydrobiol/154/2002/585

Liikanen, A., and Martikainen, P. J. (2003). Effect of Ammonium and Oxygen on Methane and Nitrous Oxide Fluxes across Sediment-Water Interface in a Eutrophic lake. *Chemosphere* 52, 1287–1293. doi:10.1016/S0045-6535(03)00224-8

Liikanen, A., Murtoniemi, T., Tanskanen, H., Väisänen, T., and Martikainen, P. J. (2002c). Effects of Temperature and Oxygen Availability on Greenhouse Gas and Nutrient Dynamics in Sediment of a Eutrophic Mid-boreal lake. *Biogeochemistry* 59, 269–286. doi:10.1023/A:1016015526712

Liikanen, A., Tanskanen, H., Murtoniemi, T., and Martikainen, P. J. (2002d). A Laboratory Microcosm for Simultaneous Gas and Nutrient Flux Measurements in Sediments. *Boreal Environ. Res.* 7, 151–160.

Liu, L., Sotiri, K., Dück, Y., Hilgert, S., Ostrovsky, I., Uzhansky, E., et al. (2019). The Control of Sediment Gas Accumulation on Spatial Distribution of Ebullition in Lake Kinneret. *Geo-mar Lett.* 40, 453–466. doi:10.1007/s00367-019-00612-z

Lofton, D. D., Whalen, S. C., and Hershey, A. E. (2015). Vertical Sediment Distribution of Methanogenic Pathways in Two Shallow Arctic Alaskan Lakes. *Polar Biol.* 38, 815–827. doi:10.1007/s00300-014-1641-4

Lorke, A., Müller, B., Maerki, M., and Wüest, A. (2003). Breathing Sediments: The Control of Diffusive Transport across the Sediment-Water Interface by Periodic Boundary-Layer Turbulence. *Limnol. Oceanogr.* 48, 2077–2085. doi:10.4319/lo.2003.48.6.2077

Maeck, A., DelSontro, T., McGinnis, D. F., Fischer, H., Flury, S., Schmidt, M., et al. (2013). Sediment Trapping by Dams Creates Methane Emission Hot Spots. *Environ. Sci. Technol.* 47, 8130–8137. doi:10.1021/es4003907

Maeck, A., Hofmann, H., and Lorke, A. (2014). Pumping Methane Out of Aquatic Sediments - Ebullition Forcing Mechanisms in an Impounded River. *Biogeosciences* 11, 2925–2938. doi:10.5194/bg-11-2925-2014

Maerki, M., Müller, B., Dinkel, C., and Wehrli, B. (2009). Mineralization Pathways in lake Sediments with Different Oxygen and Organic Carbon Supply. *Limnol. Oceanogr.* 54, 428–438. doi:10.4319/lo.2009.54.2.0428

Magen, C., Lapham, L. L., Pohlman, J. W., Marshall, K., Bosman, S., Casso, M., et al. (2014). A Simple Headspace Equilibration Method for Measuring Dissolved Methane. *Limnol. Oceanogr.* 12, 637–650. doi:10.4319/lom.2014.12.637

Marcon, L., Bleninger, T., Männich, M., and Hilgert, S. (2019). High-frequency Measurements of Gas Ebullition in a Brazilian Subtropical Reservoir-Identification of Relevant Triggers and Seasonal Patterns. *Environ. Monit. Assess.* 191. doi:10.1007/s10661-019-7498-9

Martinez-Cruz, K., Leewis, M.-C., Herriott, I. C., Sepulveda-Jauregui, A., Anthony, K. W., Thalasso, F., et al. (2017). Anaerobic Oxidation of Methane by Aerobic Methanotrophs in Sub-arctic lake Sediments. *Sci. Total Environ.* 607-608, 23–31. 608. doi:10.1016/j.scitotenv.2017.06.187

Martinez-Cruz, K., Sepulveda-Jauregui, A., Casper, P., Anthony, K. W., Smemo, K. A., and Thalasso, F. (2018). Ubiquitous and Significant Anaerobic Oxidation of Methane in Freshwater lake Sediments. *Water Res.* 144, 332–340. doi:10.1016/j.watres.2018.07.053

Matthews, D. A., Effler, S. W., and Matthews, C. M. (2005). Long-term Trends in Methane Flux from the Sediments of Onondaga Lake, NY: Sediment Diagenesis and Impacts on Dissolved Oxygen Resources. *archiv_hydrobiologie* 163, 435–462. doi:10.1127/0003-9136/2005/0163-0435

Mayr, M. J., Zimmermann, M., Dey, J., Brand, A., Wehrli, B., and Bürgmann, H. (2020a). Growth and Rapid Succession of Methanotrophs Effectively Limit Methane Release during lake Overturn. *Commun. Biol.* 3. doi:10.1101/707836

Mayr, M. J., Zimmermann, M., Dey, J., Wehrli, B., and Bürgmann, H. (2020b). Lake Mixing Regime Selects Apparent Methane Oxidation Kinetics of the Methanotroph Assemblage. *Biogeosciences* 17, 4247–4259. doi:10.5194/bg-17-4247-2020

McAullife, C. (1971). GC Determination of Solutes by Multiple Phase Equilibration. *Chem. Tech.* 1, 46–51.

McGillis, W. R., Langdon, C., Loose, B., Yates, K. K., and Corredor, J. (2011). Productivity of a Coral Reef Using Boundary Layer and Enclosure Methods. *Geophys. Res. Lett.* 38, a–n. doi:10.1029/2010GL046179

Mudroch, A., and MacKnight, S. D. (1991). "Bottom Sediment Sampling," in *Handbook of Techniques for Aquatic Sediments Sampling*, 29–95.

Müller, B., Wang, Y., Dittrich, M., and Wehrli, B. (2003). Influence of Organic Carbon Decomposition on Calcite Dissolution in Surficial Sediments of a Freshwater lake. *Water Res.* 37, 4524–4532. doi:10.1016/S0043-1354(03)00381-6

Müller, B., Bryant, L. D., Matzinger, A., and Wüest, A. (2012). Hypolimnetic Oxygen Depletion in Eutrophic Lakes. *Environ. Sci. Technol.* 46, 9964–9971. doi:10.1021/es301422r

Murase, J., and Sugimoto, A. (2002). Seasonal and Spatial Variations of Methane Production in Mesotrophic lake Sediments (Lake Biwa, Japan). *SIL Proc. 1922-2010* 28, 971–974. doi:10.1080/03680770.2001.11901861

Norði, K. à., Thamdrup, B., and Schubert, C. J. (2013). Anaerobic Oxidation of Methane in an Iron-Rich Danish Freshwater lake Sediment. *Limnol. Oceanogr.* 58, 546–554. doi:10.4319/lo.2013.58.2.0546

Nozhevnikova, A. N., Nekrasova, V., Ammann, A., Zehnder, A. J. B., Wehrli, B., and Holliger, C. (2007). Influence of Temperature and High Acetate Concentrations on Methanogenensis in lake Sediment Slurries. *FEMS Microbiol. Ecol.* 62, 336–344. doi:10.1111/j.1574-6941.2007.00389.x

Nusslein, B., Chin, K.-J., Eckert, W., and Conrad, R. (2001). Evidence for Anaerobic Syntrophic Acetate Oxidation during Methane Production in the Profundal Sediment of Subtropical Lake Kinneret (Israel). *Environ. Microbiol.* 3, 460–470. doi:10.1046/j.1462-2920.2001.00215.x

Nüsslein, B., and Conrad, R. (2000). Methane Production in Eutrophic Lake Plußsee: Seasonal Change, Temperature Effect and Metabolic Processes in the Profundal Sediment. *fal* 149, 597–623. doi:10.1127/archiv-hydrobiol/149/2000/597

Ostrovsky, I. (2000). The Upper-Most Layer of Bottom Sediments: Sampling and Artifacts. *Fundam. Appl. Limnol. (Archiv Hydrobiol.* 55, 243–255.

Pasche, N., Schmid, M., Vazquez, F., Schubert, C. J., Wüest, A., Kessler, J. D., et al. (2011). Methane Sources and Sinks in Lake Kivu. *J. Geophys. Res.* 116, G03006. doi:10.1029/2011JG001690

Paull, C. K., Lorenson, T. D., Dickens, G., Borowski, W. S., Ussler, W., and Kvenvolden, K. (2000). Comparisons of *In Situ* and Core Gas Measurements in ODP Leg 164 Bore Holes. *Ann. N. Y. Acad. Sci.* 912, 23–31. doi:10.1111/j.1749-6632.2000.tb06756.x

Peeters, F., Encinas Fernandez, J., and Hofmann, H. (2019). Sediment Fluxes rather Than Oxic Methanogenesis Explain Diffusive CH4 Emissions from Lakes and Reservoirs. *Sci. Rep.* 9. doi:10.1038/s41598-018-36530-w

Pimenov, N. V., Kallistova, A. Y., Rusanov, I. I., Yusupov, S. K., Montonen, L., Jurgens, G., et al. (2010). Methane Formation and Oxidation in the Meromictic Oligotrophic Lake Gek-Gel (Azerbaijan). *Microbiology* 79, 247–252. doi:10.1134/S0026261710020177

Podgrajsek, E., Sahlée, E., Bastviken, D., Holst, J., Lindroth, A., Tranvik, L., et al. (2014). Comparison of Floating Chamber and Eddy Covariance Measurements of lake Greenhouse Gas Fluxes. *Biogeosciences* 11, 4225–4233. doi:10.5194/bg-11-4225-2014

Powell, T., and Jassby, A. (1974). The Estimation of Vertical Eddy Diffusivities below the Thermocline in Lakes. *Water Resour. Res.* 10, 191–198. doi:10.1029/WR010i002p00191

Praetzel, L. S. E., Plenter, N., Schilling, S., Schmiedeskamp, M., Broll, G., and Knorr, K.-H. (2020). Organic Matter and Sediment Properties Determine in-lake Variability of Sediment CO_2 and CH_4 Production and Emissions of a Small and Shallow lake. *Biogeosciences* 17, 5057–5078. doi:10.5194/bg-17-5057-2020

Rahalkar, M., Deutzmann, J., Schink, B., and Bussmann, I. (2009). Abundance and Activity of Methanotrophic Bacteria in Littoral and Profundal Sediments of Lake Constance (Germany). *Appl. Environ. Microbiol.* 75, 119–126. doi:10.1128/AEM.01350-08

Reeburgh, W. S. (1967). An Improved Interstitial Water Sampler1. *Limnol. Oceanogr.* 12, 163–165. doi:10.4319/lo.1967.12.1.0163

Reidenbach, M. A., Monismith, S. G., Koseff, J. R., Yahel, G., and Genin, A. (2006). Boundary Layer Turbulence and Flow Structure over a Fringing Coral Reef. *Limnol. Oceanogr.* 51, 1956–1968. doi:10.4319/lo.2006.51.5.1956

Rissanen, A. J., Karvinen, A., Nykänen, H., Peura, S., Tiirola, M., Mäki, A., et al. (2017). Effects of Alternative Electron Acceptors on the Activity and Community Structure of Methane-Producing and Consuming Microbes in the Sediments of Two Shallow Boreal Lakes. *FEMS Microbiol. Ecol.* 93, 1–16. doi:10.1093/femsec/fix078

Rodriguez, M., Gonsiorczyk, T., and Casper, P. (2018). Methane Production Increases with Warming and Carbon Additions to Incubated Sediments from a Semiarid Reservoir. *Inland Waters* 8, 109–121. doi:10.1080/20442041.2018.1429986

Rolletschek, H. (1997). Temporal and Spatial Variations in Methane Cycling in Lake Müggelsee. *fal* 140, 195–206. doi:10.1127/archiv-hydrobiol/140/1997/195

Rosentreter, J. A., Borges, A. V., Deemer, B. R., Holgerson, M. A., Liu, S., Song, C., et al. (2021). Half of Global Methane Emissions Come from Highly Variable Aquatic Ecosystem Sources. *Nat. Geosci.* 14, 225–230. doi:10.1038/s41561-021-00715-2

Rothfuss, F., Bender, M., and Conrad, R. (1997). Survival and Activity of Bacteria in a Deep, Aged lake Sediment (Lake Constance). *Microb. Ecol.* 33, 69–77. doi:10.1007/s002489900009

Rudd, J. W. M., Hamilton, R. D., and Campbell, N. E. R. (1974). Measurement of Microbial Oxidation of Methane in lake Water. *Limnol. Oceanogr.* 19, 519–524. doi:10.4319/lo.1974.19.3.0519

Rudd, J. W. M., and Hamilton, R. D. (1978). Methane Cycling in a Eutrophic Shield lake and its Effects on Whole lake Metabolism 1. *Limnol. Oceanogr.* 23, 337–348. doi:10.4319/lo.1978.23.2.0337

Sabrekov, A. F., Runkle, B. R. K., Glagolev, M. V., Terentieva, I. E., Stepanenko, V. M., Kotsyurbenko, O. R., et al. (2017). Variability in Methane Emissions from West Siberia's Shallow Boreal Lakes on a Regional Scale and its Environmental Controls. *Biogeosciences* 14, 3715–3742. doi:10.5194/bg-14-3715-2017

Sanches, L. F., Guenet, B., Marinho, C. C., Barros, N., and de Assis Esteves, F. (2019). Global Regulation of Methane Emission from Natural Lakes. *Sci. Rep.* 9, 1–10. doi:10.1038/s41598-018-36519-5

Schmid, M., Batist, M. D., Granin, N. G., Kapitanov, V. A., McGinnis, D. F., Mizandrontsev, I. B., et al. (2007). Sources and Sinks of Methane in Lake Baikal: A Synthesis of Measurements and Modeling. *Limnol. Oceanogr.* 52, 1824–1837. doi:10.4319/lo.2007.52.5.1824

Schmid, M., Ostrovsky, I., and McGinnis, D. F. (2017). Role of Gas Ebullition in the Methane Budget of a Deep Subtropical lake: What Can We Learn from Process-Based Modeling? *Limnol. Oceanogr.* 62, 2674–2698. doi:10.1002/lno.10598

Schubert, C. J., Diem, T., and Eugster, W. (2012). Methane Emissions from a Small Wind Shielded Lake Determined by Eddy Covariance, Flux Chambers,

Anchored Funnels, and Boundary Model Calculations: A Comparison. *Environ. Sci. Technol.* 46, 4515–4522. doi:10.1021/es203465x

Schubert, C. J., Vazquez, F., Lösekann-Behrens, T., Knittel, K., Tonolla, M., and Boetius, A. (2011). Evidence for anaerobic oxidation of methane in sediments of a freshwater system (Lago di Cadagno). *FEMS Microbiol. Ecol.* 76, 26–38. doi:10.1111/j.1574-6941.2010.01036.x

Seeberg-Elverfeldt, J., Schlüter, M., Feseker, T., and Kölling, M. (2005). Rhizon Sampling of Porewaters Near the Sediment-Water Interface of Aquatic Systems. *Limnol. Oceanogr. Methods* 3, 361–371. doi:10.4319/lom.2005.3.361

Shirayama, Y., and Fukushima, T. (1995). Comparisons of Deep-Sea Sediments and Overlying Water Collected Using Multiple Corer and Box Corer. *J. Oceanogr.* 51, 75–82. doi:10.1007/bf02235937

Simpson, J. H., Wiles, P. J., and Lincoln, B. J. (2011). Internal Seiche Modes and Bottom Boundary-Layer Dissipation in a Temperate lake from Acoustic Measurements. *Limnol. Oceanogr.* 56, 1893–1906. doi:10.4319/lo.2011.56.5.1893

Sinke, A. J. C., Cornelese, A. A., Cappenberg, T. E., and Zehnder, A. J. B. (1992). Seasonal Variation in Sulfate Reduction and Methanogenesis in Peaty Sediments of Eutrophic Lake Loosdrecht, The Netherlands. *Biogeochemistry* 16, 43–61. doi:10.1007/bf02402262

Stadmark, J., and Leonardson, L. (2007). Greenhouse Gas Production in a Pond Sediment: Effects of Temperature, Nitrate, Acetate and Season. *Sci. Total Environ.* 387, 194–205. doi:10.1016/j.scitotenv.2007.07.039

Steinsberger, T., Müller, B., Gerber, C., Shafei, B., and Schmid, M. (2019). Modeling Sediment Oxygen Demand in a Highly Productive lake under Various Trophic Scenarios. *PLoS One* 14, e0222318–23. doi:10.1371/journal.pone.0222318

Steinsberger, T., Schmid, M., Wüest, A., Schwefel, R., Wehrli, B., and Müller, B. (2017). Organic Carbon Mass Accumulation Rate Regulates the Flux of Reduced Substances from the Sediments of Deep Lakes. *Biogeosciences* 14, 3275–3285. doi:10.5194/bg-14-3275-2017

Stepanenko, V., Mammarella, I., Ojala, A., Miettinen, H., Lykosov, V., and Vesala, T. (2016). LAKE 2.0: A Model for Temperature, Methane, Carbon Dioxide and Oxygen Dynamics in Lakes. *Geosci. Model. Dev.* 9, 1977–2006. doi:10.5194/gmd-9-1977-2016

Stepanenko, V. M., Machul'skaya, E. E., Glagolev, M. V., and Lykossov, V. N. (2011). Numerical Modeling of Methane Emissions from Lakes in the Permafrost Zone. *Izv. Atmos. Ocean. Phys.* 47, 252–264. doi:10.1134/S0001433811020113

St. Louis, V. L. V. L., Kelly, C. a., Duchemin, É., Rudd, J. W. M., and Rosenberg, D. M. (2000). Reservoir Surfaces as Sources of Greenhouse Gases to the Atmosphere: A Global Estimate. *Bioscience* 50, 766. doi:10.1641/0006-3568(2000)050[0766:rsasog]2.0.co;2

Strayer, R. F., and Tiedje, J. M. (1978). *In Situ* methane Production in a Small, Hypereutrophic, Hard-Water lake: Loss of Methane from Sediments by Vertical Diffusion and Ebullition 1. *Limnol. Oceanogr.* 23, 1201–1206. doi:10.4319/lo.1978.23.6.1201

Sturm, K., Yuan, Z., Gibbes, B., Werner, U., and Grinham, A. (2014). Methane and Nitrous Oxide Sources and Emissions in a Subtropical Freshwater Reservoir, South East Queensland, Australia. *Biogeosciences* 11, 5245–5258. doi:10.5194/bg-11-5245-2014

Su, G., Niemann, H., Steinle, L., Zopfi, J., and Lehmann, M. F. (2019). Evaluating Radioisotope-based Approaches to Measure Anaerobic Methane Oxidation Rates in Lacustrine Sediments. *Limnol. Oceanogr. Methods* 17, 429–438. doi:10.1002/lom3.10323

Sweerts, J.-P. R. A., Bär-Gilissen, M.-J., Cornelese, A. A., and Cappenberg, T. E. (1991). Oxygen-consuming Processes at the Profundal and Littoral Sediment-Water Interface of a Small Meso-Eutrophic lake (Lake Vechten, The Netherlands). *Limnol. Oceanogr.* 36, 1124–1133. doi:10.4319/lo.1991.36.6.1124

Takeshita, Y., McGillis, W., Briggs, E. M., Carter, A. L., Donham, E. M., Martz, T. R., et al. (2016). Assessment of Net Community Production and Calcification of a Coral Reef Using a Boundary Layer Approach. *J. Geophys. Res. Oceans* 121, 5655–5671. doi:10.1002/2016JC011886

Tan, Z., Zhuang, Q., and Walter Anthony, K. (2015). Modeling Methane Emissions from Arctic Lakes: Model Development and Site-level Study. *J. Adv. Model. Earth Syst.* 7, 459–483. doi:10.1002/2014MS000344

Thebrath, B., Rothfuss, F., Whiticar, M. J., and Conrad, R. (1993). Methane Production in Littoral Sediment of Lake Constance. *FEMS Microbiol.* 102, 279–289. doi:10.1111/j.1574-6968.1993.tb05819.x

Thottathil, S. D., Reis, P. C. J., and Prairie, Y. T. (2019). Methane Oxidation Kinetics in Northern Freshwater Lakes. *Biogeochemistry* 143, 105–116. doi:10.1007/s10533-019-00552-x

Torres, I. C., Inglett, K. S., and Reddy, K. R. (2011). Heterotrophic Microbial Activity in lake Sediments: Effects of Organic Electron Donors. *Biogeochemistry* 104, 165–181. doi:10.1007/s10533-010-9494-6

Turk, D., Yates, K., Vega-Rodriguez, M., Toro-Farmer, G., L'Esperance, C., Melo, N., et al. (2015). Community Metabolism in Shallow Coral Reef and Seagrass Ecosystems, Lower Florida Keys. *Mar. Ecol. Prog. Ser.* 538, 35–52. doi:10.3354/meps11385

Tyroller, L., Tomonaga, Y., Brennwald, M. S., Ndayisaba, C., Naeher, S., Schubert, C., et al. (2016). Improved Method for the Quantification of Methane Concentrations in Unconsolidated Lake Sediments. *Environ. Sci. Technol.* 50, 7047–7055. doi:10.1021/acs.est.5b05292

Urban, N. R., Dinkel, C., and Wehrli, B. (1997). Solute Transfer across the Sediment Surface of a Eutrophic lake: I. Porewater Profiles from Dialysis Samplers. *Aquat. Sci.* 59, 1–25. doi:10.1007/pl0000130210.1007/bf02522546

Vachon, D., Langenegger, T., Donis, D., and McGinnis, D. F. (2019). Influence of Water Column Stratification and Mixing Patterns on the Fate of Methane Produced in Deep Sediments of a Small Eutrophic lake. *Limnol. Oceanogr.* 64, 2114–2128. doi:10.1002/lno.11172

Valle, J., Gonsior, M., Harir, M., Enrich-Prast, A., Schmitt-Kopplin, P., Bastviken, D., et al. (2018). Extensive Processing of Sediment Pore Water Dissolved Organic Matter during Anoxic Incubation as Observed by High-Field Mass Spectrometry (FTICR-MS). *Water Res.* 129, 252–263. doi:10.1016/j.watres.2017.11.015

van Grinsven, S., Sinninghe Damsté, J. S., Harrison, J., and Villanueva, L. (2020). Impact of Electron Acceptor Availability on Methane-Influenced Microorganisms in an Enrichment Culture Obtained from a Stratified Lake. *Front. Microbiol.* 11. doi:10.3389/fmicb.2020.00715

Viollier, E., Rabouille, C., Apitz, S. E., Breuer, E., Chaillou, G., Dedieu, K., et al. (2003). Benthic Biogeochemistry: State of the Art Technologies and Guidelines for the Future of *In Situ* Survey. *J. Exp. Mar. Biol. Ecol.* 285-286, 5–31. –286. doi:10.1016/S0022-0981(02)00517-8

Wagener, S., Schulz, S., and Hanselmann, K. (1990). Abundance and Distribution of Anaerobic Protozoa and Their Contribution to Methane Production in Lake Cadagno (Switzerland). *FEMS Microbiol. Lett.* 74, 39–48. doi:10.1111/j.1574-6968.1990.tb04050.x

Webb, J. R., Maher, D. T., and Santos, I. R. (2016). Automated, *In Situ* Measurements of Dissolved CO_2, CH_4, and δ_{13} C Values Using Cavity Enhanced Laser Absorption Spectrometry: Comparing Response Times of Air-Water Equilibrators. *Limnol. Oceanogr. Methods* 14, 323–337. doi:10.1002/lom3.10092

West, W. E., Coloso, J. J., and Jones, S. E. (2012). Effects of Algal and Terrestrial Carbon on Methane Production Rates and Methanogen Community Structure in a Temperate lake Sediment. *Freshw. Biol.* 57, 949–955. doi:10.1111/j.1365-2427.2012.02755.x

West, W. E., Creamer, K. P., and Jones, S. E. (2016). Productivity and Depth Regulate lake Contributions to Atmospheric Methane. *Limnol. Oceanogr.* 61, S51–S61. doi:10.1002/lno.10247

Wik, M., Thornton, B. F., Bastviken, D., Uhlbäck, J., and Crill, P. M. (2016). Biased Sampling of Methane Release from Northern Lakes: A Problem for Extrapolation. *Geophys. Res. Lett.* 43, 1256–1262. doi:10.1002/2015GL066501

Winfrey, M. R., and Zeikus, J. G. (1979). Microbial Methanogenesis and Acetate Metabolism in a Meromictic lake. *Appl. Environ. Microbiol.* 37, 213–221. doi:10.1128/aem.37.2.213-221.1979

Wüest, A., and Lorke, A. (2003). Small-scale Hydrodynamics in Lakes. *Annu. Rev. Fluid Mech.* 35, 373–412. doi:10.1146/annurev.fluid.35.101101.161220

Xiao, S., Liu, L., Wang, W., Lorke, A., Woodhouse, J., and Grossart, H.-P. (2020). A Fast-Response Automated Gas Equilibrator (FaRAGE) for Continuous *In Situ* Measurement of Methane Dissolved in Water. *Hydrol. Earth Syst. Sci. Discuss.*, 1–28. doi:10.5194/hess-2020-67

Yang, Y., Chen, J., Li, B., Liu, Y., and Xie, S. (2018). Anaerobic Methane Oxidation Potential and Bacteria in Freshwater Lakes: Seasonal Changes and the Influence

of Trophic Status. *Syst. Appl. Microbiol.* 41, 650–657. doi:10.1016/j.syapm.2018.08.002

Yang, Y., Li, N., Wang, W., Li, B., Xie, S., and Liu, Y. (2017). Vertical Profiles of Sediment Methanogenic Potential and Communities in Two Plateau Freshwater Lakes. *Biogeosciences* 14, 341–351. doi:10.5194/bg-14-341-2017

Yavitt, J. B., Angell, L. L., Fahey, T. J., Cirmo, C. P., and Driscoll, C. T. (1992). Methane Fluxes, Concentrations, and Production in Two Adirondack beaver Impoundments. *Limnol. Oceanogr.* 37, 1057–1066. doi:10.4319/lo.1992.37.5.1057

Zeikus, J. G., and Winfrey, M. R. (1976). Temperature Limitation of Methanogenesis in Aquatic Sediments. *Appl. Environ. Microbiol.* 31, 99–107. doi:10.1128/aem.31.1.99-107.1976

Zhang, L., Liao, Q., Gao, R., Luo, R., Liu, C., Zhong, J., et al. (2021). Spatial Variations in Diffusive Methane Fluxes and the Role of Eutrophication in a Subtropical Shallow lake. *Sci. Total Environ.* 759, 143495. doi:10.1016/j.scitotenv.2020.143495

Conflict of Interest: The authors declare that the research was conducted in the absence of any commercial or financial relationships that could be construed as a potential conflict of interest.

Publisher's Note: All claims expressed in this article are solely those of the authors and do not necessarily represent those of their affiliated organizations, or those of the publisher, the editors, and the reviewers. Any product that may be evaluated in this article, or claim that may be made by its manufacturer, is not guaranteed or endorsed by the publisher.

Copyright © 2022 D'Ambrosio and Harrison. This is an open-access article distributed under the terms of the Creative Commons Attribution License (CC BY). The use, distribution or reproduction in other forums is permitted, provided the original author(s) and the copyright owner(s) are credited and that the original publication in this journal is cited, in accordance with accepted academic practice. No use, distribution or reproduction is permitted which does not comply with these terms.

frontiers in Environmental Science

ORIGINAL RESEARCH
published: 31 March 2022
doi: 10.3389/fenvs.2022.838126

Spatial Mapping of Dissolved Gases in the Danube Delta Reveals Intense Plant-Mediated Gas Transfer

Marie-Sophie Maier[1,2], Anna R. Canning[3], Matthias S. Brennwald[4], Cristian R. Teodoru[1,5] and Bernhard Wehrli[1,2]*

[1]Institute of Biogeochemistry and Pollutant Dynamics, Department of Environmental Systems Science, ETH Zurich, Zurich, Switzerland, [2]Department Surface Waters–Research and Management, Eawag, Swiss Federal Institute of Aquatic Science and Technology, Kastanienbaum, Switzerland, [3]GEOMAR Helmholtz-Zentrum für Ozeanforschung Kiel, Kiel, Germany, [4]Department of Water Resources and Drinking Water, Eawag, Swiss Federal Institute of Aquatic Science and Technology, Dübendorf, Switzerland, [5]Romanian National Institute of Marine Geology and Geoecology (GeoEcoMar), Bucharest, Romania

Global estimates see river deltas and estuaries contributing about equally to CO_2 and CH_4 emissions as lakes and reservoirs, despite a factor 6 smaller surface area. Assessing the horizontal gradients in dissolved gas concentrations from large river reaches to connecting canals and wetland lakes remains a challenge in many deltaic systems. To elucidate the processes affecting local CO_2 and CH_4 concentrations in the Romanian part of the Danube Delta, we mapped dissolved O_2, N_2, He and Ar using a portable gas-equilibration membrane-inlet mass spectrometer (GE-MIMS), along with CO_2, CH_4, water temperature and conductivity. We measured the concentrations along the aquatic continuum from a small houseboat during two campaigns, in spring and autumn, to capture different hydrological and plant growth conditions. Delta-scale concentration patterns were comparably stable across seasons. Small connecting channels were highly influenced by the riparian wetland, which was strongest in the eastern part of the biosphere reserve. These sites represented the delta's CO_2 and CH_4 hotspots and showed clear signs of excess air, i.e., supersaturation of dissolved noble gases with respect to air-saturated water. As the adjacent wetland was permanently inundated, this signal was likely caused by root aeration of *Phragmites australis*, as opposed to traditional excess air formation via water table fluctuations in the unsaturated zone. The special vegetation setting with reed growing on floating peat coincided with the highest CO_2 and CH_4 concentrations (>700 µmol/L CO_2 and 13 µmol/L CH_4, respectively) observed in an adjacent channel. Shallow lakes, on the other hand, were major sites of photosynthetic production with O_2 oversaturation reaching up to 150% in spring. The observed deficit in non-reactive gases (He, Ar and N_2) indicated that the lakes were affected by O_2 ebullition from macrophytes. According to our estimations, this ebullitive flux decreased O_2 concentrations by up to 2 mg/L. This study highlights the effect of plant-mediated gas transfer on dissolved gas concentrations and supports recent studies stressing the need to account for ebullitive gas exchange when assessing metabolism parameters from O_2 in shallow, productive settings.

Keywords: carbon cycle, greenhouse gases, noble gases, plant-mediated gas transfer, ebullition, excess air, Danube Delta, membrane-inlet mass spectrometry

OPEN ACCESS

Edited by:
Yves T. Prairie, Université du Québec à Montréal, Canada

Reviewed by:
Patrick Höhener, Aix Marseille Université, France
Núria Catalán, UMR8212 Laboratoire des Sciences du Climat et de l'Environnement (LSCE), France

****Correspondence:***
Marie-Sophie Maier
marie-sophie.maier@usys.ethz.ch

Specialty section:
This article was submitted to Biogeochemical Dynamics, a section of the journal Frontiers in Environmental Science

Received: *17 December 2021*
Accepted: *14 March 2022*
Published: *31 March 2022*

Citation:
Maier M-S, Canning AR, Brennwald MS, Teodoru CR and Wehrli B (2022) Spatial Mapping of Dissolved Gases in the Danube Delta Reveals Intense Plant-Mediated Gas Transfer. Front. Environ. Sci. 10:838126. doi: 10.3389/fenvs.2022.838126

1 INTRODUCTION

The release of greenhouse gases from deltaic and estuarine systems cannot be neglected, but the spatial variability of these emissions is poorly understood (Cai, 2011). For CH_4, the most recent global emission estimate from deltas and estuaries is 4.95 TgC $year^{-1}$ (Borges and Abril, 2011), which equals 25% of the efflux from rivers and streams (0.02 PgC $year^{-1}$, Stanley et al., 2016). It represents only 3.5–6.3% of the CH_4 flux from lakes and reservoirs (0.139–0.078 PgC $year^{-1}$, depending on lake size distribution, DelSontro et al., 2018). Global CO_2 emission estimates from deltas and estuaries of 0.27 ± 0.23 PgC $year^{-1}$ (Laruelle et al., 2010) are only one order of magnitude smaller than the oceanic and terrestrial CO_2 sink (2.5 and 3.4 PgC $year^{-1}$, Friedlingstein et al., 2020). These estimates are smaller than estimated global CO_2 emissions from rivers (0.48–0.85 PgC $year^{-1}$, Lauerwald et al., 2015) but in a similar range as emissions from lakes and reservoirs (0.32–0.58 PgC $year^{-1}$, Raymond et al., 2013; Holgerson and Raymond, 2016). These estimates indicate a very active role of river deltas and estuaries because they exhibit 6 times smaller surface areas when compared to lakes and reservoirs (Laruelle et al., 2010; Holgerson and Raymond, 2016).

The increase of global surface temperatures, its adverse effects for humans and the biosphere (IPCC, 2021), and the potential failure of the Paris agreement (Sachs, 2019) all demand a solid understanding of carbon budgets. In this context, Deemer et al. (2016) identified the lack of adequate spatial coverage as a stumbling block for calculating global greenhouse gas emissions from reservoirs. In contrast to the open ocean or large lakes and rivers, many freshwater systems such as small streams or small lakes can show quite strong horizontal concentration gradients (McGinnis et al., 2016; Natchimuthu et al., 2016). In addition, differences in gas exchange parameters depend on channel slope and morphometry and can change over a small distance (Ulseth et al., 2019; Hall and Ulseth, 2020). The drivers of steep concentration changes can be manifold, ranging from groundwater inflow (Horgby et al., 2019) to changes in depth (Natchimuthu et al., 2016) and hydrodynamics (McGinnis et al., 2016) or organic matter availability (Battin et al., 2008). An additional factor that has so far gained little attention is plant-mediated gas transfer. Recent observations point to oxygen ebullition via photosynthesis (Koschorreck et al., 2017) and other studies suggested specific gas-transfer mechanisms for reed stands, which deserve detailed analysis under field conditions (Brix et al., 1996; Sorrell and Brix, 2013).

River deltas are complex sites, where many of these drivers may govern steep spatial gradients of dissolved (greenhouse) gases across different waterscapes and may introduce large uncertainty to any upscaling approach (Abril and Borges, 2019; Maier et al., 2021). Along with the identification of emission hotspots in single systems, it is therefore vital to understand the processes affecting the spatiotemporal variability of greenhouse gas concentrations in order to improve extrapolation to unsampled territory.

The Danube Delta, Romania, shows very large concentration gradients of dissolved CO_2 and CH_4 with hotspots in some small channels (Maier et al., 2021). Based on these discrete measurements, steep spatial gradients remain unresolved and potential emission hotspots may be undetected. High-resolution portable sensors measuring dissolved gases such as CO_2 and CH_4 specifically provide a more detailed spatial picture (Canning A. R et al., 2021). Earlier studies showed horizontal gradients in CO_2 and CH_4 concentrations across Danube Delta lakes (Pavel et al., 2009), as well as daily cycles in CH_4 concentrations (Canning A et al., 2021).

While spatial mapping of only CO_2 and CH_4 gives direct indication on the location of potential emission hot spots, measurements of additional gas species can shed further light on the processes that cause or affect these greenhouse gas patterns. Portable membrane-inlet mass spectrometers (MIMS) allow measurements of several dissolved gases in the field (Brennwald et al., 2016) and thus allow to complement greenhouse gas measurements with measurements of noble gases, O_2 and N_2. As noble gases are not affected by biological processes, this allows to get a more detailed view on the physical and biological drivers of the dissolved gas variability. Ar, which has similar solubility characteristics as O_2, is used in oceanography to account for O_2 changes due to physical processes such as waves or degassing (Craig and Hayward, 1987). Recent studies suggest that physical processes like ebullition also play a role in O_2 dynamics in shallow lakes (Koschorreck et al., 2017).

This study builds on a 2-year field campaign at discrete sites in the Danube Delta, which quantified carbon fluxes to the atmosphere (Maier et al., 2021). Here we adopt a same high-resolution mapping approach that allowed Canning A et al. (2021) to identify spatial patterns of methane emissions in the Delta. In order to identify physically and biologically driven gas-transfer mechanisms in more detail, we continuously mapped the spatial distribution of a broad set of dissolved gases (CO_2, CH_4, O_2, N_2, He and Ar) in the Danube Delta. We aimed at 1) identifying spatial patterns and horizontal gradients across the different deltaic waterscapes during two seasons, 2) applying noble gas measurements for constraining physical and biological processes in emission hotspots of greenhouse gases at terrestrial-aquatic boundaries, and 3) quantifying ebullition as a confounding factor in estimates of ecosystem metabolism.

2 MATERIALS AND METHODS

2.1 Study Site

Flowing over 2,850 km and receiving water from 19 different European countries, the Danube River discharges into the Black Sea through a three-arm delta, the Danube Delta. It is Europe's second largest river delta after the Volga wetlands on the Caspian Sea and located at the border of Ukraine to eastern Romania. Runoff from the Carpathian Mountains and the Alps determines the seasonality of the river's hydrology, where peak discharge in spring is followed by low discharge in autumn (**Supplementary Figure S1**). These changes in hydrology directly translate into changes in water level in the delta, leading to flooding of the wetland area in spring and subsequent drainage in autumn.

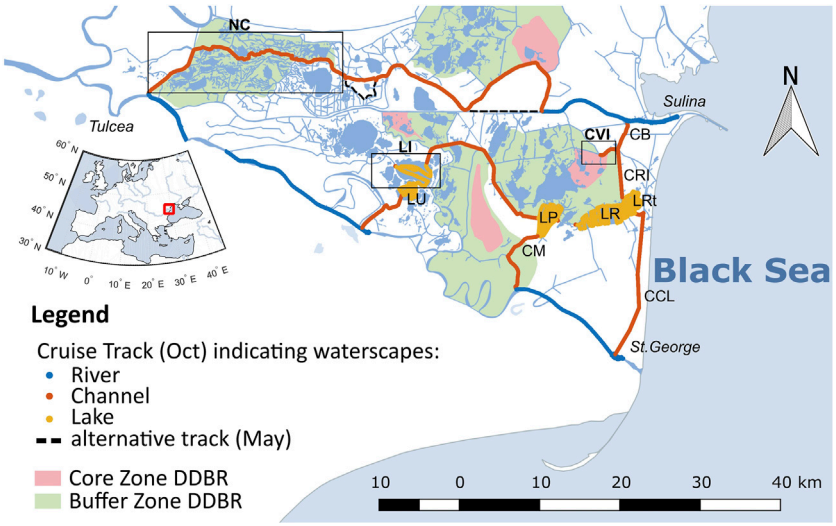


FIGURE 1 | Southern part of the Danube Delta with cruise tracks of the sampling campaign in October 2017. Colors indicate the different waterscapes (blue = river, orange = channel, yellow = lake). The black dotted line indicates where the sampling track in May 2017 differed from October 2017. Red and green areas show the location of core and buffer zones of the Danube Delta Biosphere Reserve (Gastescu, 2013). Boxes indicate specifically discussed sites: NC, northern channels, LI, Lake Isac, CVI, Canal Vatafu-Imputita. Other abbreviations stand for LU, Lake Uzlina (*Lake Isaccel*), LP, Lake Puiu, LR, Lake Rosu, LRt, Lake Rosulet, CM, Canal Mocanului (*Canal Mocansca*), CB, Canal Busurca, CRI, Canal Rosu-Imputita, CCL, Canal Cordon Litoral (*Canal Tataru*). Names refer to (Gastescu, 2013), italic names indicate deviating names on maps.google.ch. For mapping details see *Methods* section.

Between the main river branches, the delta consists of vast reed areas and shallow flow-through lakes, which are connected to the main branches via small natural and artificial channels (**Figure 1**). The river water generally enters the delta at the West and flows back into the river in the East close to the Black Sea. However, depending on the water level fluctuations, direction of flow is also known to reverse in some of the eastern channels (Irimus, 2006). With respect to the 20-years average, the Danube River showed below average discharge throughout most of the monitoring year 2017 (**Supplementary Figure S1**; ICPDR (2019)).

The Danube Delta is a Ramsar Wetland Site and a World heritage site (UNEP-WCMC (UN Environment Programme World Conservation Monitoring Centre), 2021). Since 1998, it is part of the transboundary UNESCO Biosphere Reserve (UNESCO, 2021). The Danube Delta Biosphere Reserve (DDBR, **Figure 1**) aims to protect the deltas' diversity of flora and fauna. To this end, about 9% of the deltas' area classifies as strictly protected core zone with another 48% representing buffer zones surrounding the core areas (UNESCO, 2021), where tourism and reed harvesting are restricted.

About 23% of the 220,000 ha reed area represent potential harvesting areas (Covaliov et al., 2010). The reed, predominantly consisting of *Phragmites australis* (Hanganu et al., 2002), is either used as cattle food by locals or professionally harvested by private companies during winter. Burning of the remaining crop parts increases future yield and prevents succession by other plants (Covaliov et al., 2010). Reed grows on reed peat, consisting of a network of viable rhizomes. Initially, this reed peat forms an about 1 m thick floating layer with no contact to the underlaying mineral soil. In Romanian, this is called "plaur". Bottom contact establishes as the peat grows thicker or during low water levels (Hanganu et al., 2002). Both harvesting and burning increases the buoyancy of the plaur and the reed density (Covaliov et al., 2010), yet reduce the abundance of old and broken reed culms, which play an important role in oxygenating the rhizome (Sorrell and Brix, 2013).

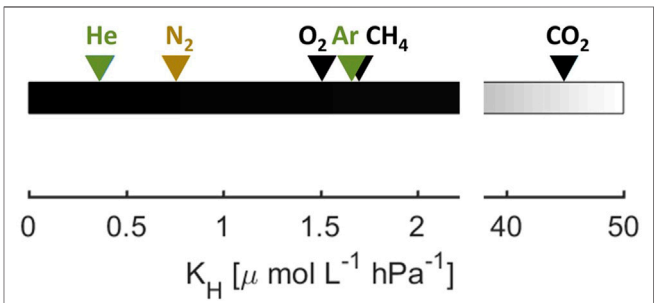


FIGURE 2 | Calculated Henry constants of selected gases for T = 15°C and standard pressure. Noble gases are shown in green, biogenic gases and greenhouse gases are shown in black. N_2 is considered as not significantly altered by metabolism in this study and therefore shown in ocher.

As road infrastructure through the delta is lacking, ships and boats are the most important means of transport there. This boat traffic likely enhances gas exchange in some of the small, highly frequented channels, as well as in the main branches.

2.2 Measured Gas Species

For this study, we complemented CO_2 and CH_4 measurements with measurements of dissolved noble gases (He and Ar), O_2 and N_2. Noble gases such as He and Ar help to understand the

physical changes affecting all dissolved gas concentrations. As most poorly soluble gas in the water (**Figure 2**), He is affected most strongly by gas bubbles rising through the water column. On their way through to the surface, less soluble gases from the surrounding water replace more soluble gases initially present in the bubble (McGinnis et al., 2006), which is called stripping. We expected to see such a stripping effect for He during ebullition, i.e., enhanced gas transfer to the atmosphere via bubbles.

The solubility properties of Ar are very similar to those of O_2 and comparable to N_2 (about 2:1). It is therefore often used to account for physical changes affecting these gases or to improve measurement accuracy by employing O_2:Ar or N_2:Ar ratios (Craig and Hayward, 1987; Groffman et al., 2006). O_2:Ar ratios are frequently used in the ocean for quantifying net community production (Craig and Hayward, 1987; Tortell et al., 2015) but also in ice cores (Zhou et al., 2014).

In combination, noble gases can indicate the presence of excess air, i.e., an observed surplus of dissolved gas in excess to atmospheric equilibrium concentrations with air-like gas composition (Heaton and Vogel, 1981). This phenomenon is traditionally observed in unconfined groundwater bodies, where air entrapment during a rising groundwater table leads to an increase in hydraulic pressure, allowing the water to take up more gas and thus partially or fully dissolving the trapped gas bubble (Aeschbach-Hertig et al., 1999). This presence of excess air can raise the O_2 and N_2 saturation beyond expectation in river banks and groundwater (Mächler et al., 2013).

The concentration of O_2 represents an indicator for the ecosystem metabolism, i.e., autotrophic versus net heterotrophic conditions. *In-situ* O_2 concentrations are often used as a measure for net primary productivity, i.e., primary production–respiration. Different methods include the measurement of diel O_2 changes in streams and lakes (Staehr et al., 2012; Hall et al., 2016; Bernhardt et al., 2018).

Since our measurement system was not sensitive enough to resolve small biogenic changes in N_2 from the comparably large N_2 background concentration of air-saturated water, we used molecular nitrogen as a third conservative gas species in this study.

2.3 Sampling

We continuously measured the concentrations of dissolved gases (CO_2, CH_4, He, Ar, O_2, N_2) in the southern part of the Danube Delta during two field campaigns in May and October 2017. The journey of our sensor-equipped houseboat covered the different waterscapes of the delta, i.e., main river branches, small channels and large flow-through lakes (**Figure 1**). The size of our houseboat prevented accessibility of shallower lakes or narrower channels (**Supplemenatry Figure S2**). Due to time constraints, the paths in May and October deviate slightly in the northern part of the mapping area.

For the analysis of dissolved He, Ar, O_2 and N_2, we used a membrane-inlet mass spectrometer (MIMS) from Gasometrix (Brennwald et al., 2016) in combination with a submergible pump and a membrane-equilibrator. The total number of datapoints per gas species amounted to ~8,600 in May and ~8,900 in October. We filled gasbags with a known composition of pressurized air enriched with CO_2 and CH_4 and used those as standard gas mixture during the field trip. This standard gas and ambient air were measured in regular intervals (every fifth and 10th sample batch, respectively, with 1 sample batch representing five individual measurements) to ensure data accuracy. The partial pressures and concentrations of the gases dissolved in water were quantified from the raw MIMS data following the procedures described in Brennwald et al. (2016). Given the large concentration gradients in the delta, we performed the calculations for individual measurements. Where necessary, e.g., to compare gases measured by different detectors, averages and standard deviations were calculated for the closest five measurements (i.e., 1 sample batch). Standard/ambient air measurements were performed along the journey, therefore introducing regular gaps in the dissolved concentration maps. Ambient air measurements of He, Ar, N_2 and O_2 were processed the same way as other samples and used as quality control. The standard deviation varied <1.7% for Ar and O_2, ~0.5% for N_2 and <7% for He. Average ambient air measurements were up to about 2% (N_2, Ar, O_2) or 3.5% (He) smaller than global values (see **Supplementary Table S1**).

In addition to the MIMS, we used a set-up with combined flow-through sensors, which included CONTROS HydroC® CO_2 FT and CONTROS HydroC® CH_4 FT sensors (formerly Kongsberg Maritime Contros GmbH, Kiel, Germany; now -4H- JENA Engineering GmbH, Jena, Germany) to measure CO_2, and CH_4, respectively. The setup also included a SBE 45 micro thermosalinograph (Sea-Bird Scientific, Bellevue, WA, United States) to measure temperature and conductivity on-board. For details please refer to Canning A. R et al. (2021). This part of the data is available via the Pangaea database (Canning et al., 2020) and details on CH_4 concentrations were previously published by Canning A et al. (2021). We recorded GPS position, depth and *in-situ* temperature with a Lowrance HDS5 sonar.

2.4 Data Analysis

2.4.1 Calculation of Saturation Concentrations

We calculated the saturation concentrations for the different gas species according to the temperature-salinity-solubility relations for He (Weiss, 1971), O_2 (Garcia and Gordon, 1992), N_2 and Ar (Hamme and Emerson, 2004), CO_2 (Weiss, 1974) and CH_4 (Wiesenburg and Guinasso Jr, 1979). For the actual partial pressure in the atmosphere, we used 400 ppm for CO_2 and 1,840 ppb for CH_4. Since we are working in freshwater, we set salinity to 0 for the calculations. A comparison of the Henry coefficients at 15°C and standard pressure shows that He is the least soluble of the investigated gases (**Figure 2**), followed by N_2, while O_2, Ar and CH_4 have very similar solubility, and CO_2 is the most soluble gas by far.

2.4.2 Classification Into Waterscapes and Definition of Striking Sites

In the data analysis, we took a closer look at the three different waterscapes, i.e., river, channel and lakes (**Figure 1**) that were classified as specified in Maier et al. (2021). In brief, the main branches of the River Danube belong to the river class, while old

cut-off meanders and small channels with a low flow velocity are defined as channels. The lake class includes the shallow delta lakes. In addition to these three waterscapes, we evaluated three sites, where we found extreme values of dissolved gas concentrations: Lake Isac, Canal Vatafu-Imputita and a combination of channels in the north (see boxes in **Figure 1**). These sites are representative of different areas within the delta with prominent characteristics.

The northern channels cut through the Sontea-Fortuna lake complex in the north of the delta and include Canal Mila 35, Canal Sontea and Garla Sontea (Gastescu, 2013). Especially in the western-most part of the northern channel complex, the canals are bordered by river levees (**Supplementary Figure S8**). The vegetation is a mix of natural floodplain forest, mixed reed mace and pure reed vegetation on mineral and organic soils. In some places, the river levees are used for wood extraction, cattle grazing and small vegetable gardens (Hanganu et al., 2002). These channels are representative for most small channels in this area.

Canal Vatafu-Imputita is situated in the Rosu-Puiu complex in the eastern part of the delta (Oosterberg et al., 2000) at the border of the Vatafu-Lungulet core protection zone and the surrounding buffer zone. This area is situated in a depression zone and lies below sea level (Gastescu, 2013). As a result, the area is permanently inundated (**Supplementary Figure S8**). The dominant vegetation is reed, which mainly occurs on plaur. However at the Easternend of the channel also "mineral soils" and "salinized soils" occur (Hanganu et al., 2002), which may reflect the evolution of the delta over time (Panin, 1996). Judging from vegetation and elevation maps, the channels in the Matita-Merhei lake complex in the North shows similar characteristics (Hanganu et al., 2002; Gastescu, 2013).

Lake Isac belongs to the Gorgova-Uzlina lake complex in the fluvial part of the delta and has a residence time of about 12 days (Oosterberg et al., 2000). With about 10.2 km^2 it is the deltas' fourth largest lake with respect to open water surface area and has an average water depth of 2.4 m (Oosterberg et al., 2000). It was categorized as large and turbid lake by Oosterberg et al. (2000) and as "intermediate" type lake showing "a combination of clear water, submerged vegetation, suspended solids and algal blooming" by Coops et al. (1999). This matches our recent observations, where Lake Isac had abundant submerged vegetation in spring and early summer, while later in the year it showed signs of an algal bloom (Maier et al., 2021). Examples of lakes in the delta showing similar characteristics are Lake Fortuna and Lake Gorgova (Coops et al., 1999). Apart from Lake Isac, the other mapped lakes were classified as "turbid" with less abundant submerged vegetation (Coops et al., 1999; Oosterberg et al., 2000).

2.4.3 Estimation of Excess Air and Equilibration Temperature

To estimate the excess air present in our system, we used both a visual approach for three of the locations, where enough data was present, as well as the "nobelfit"-routine (Brennwald, 2020).

For the visual approach, which is helpful to understand the concept of excess air, we plotted He concentrations against Ar concentrations in ccSTP/g (cubic centimeters at standard conditions per mass of water, 1 ccSTP = 1/22,414 Mol). We included the line that represents air saturated water samples (ASW) equilibrated at different temperatures, as well as a line indicating the concentration changes of ASW when excess air, A, increases at a certain temperature, T_w.

The unfractionated excess air model (UA-model) is the simplest concept to describe the excess air phenomenon. It assumes complete dissolution of an entrapped air bubble as described by:

$$C_i = C_i^{ASW}\left(T_w, p\right) + A \cdot z_i \tag{1}$$

where C_i is the dissolved gas concentration of species i. C_i^{ASW} is the concentration in water in equilibrium with air (air saturated water), which is a function of the equilibration temperature, T_w and ambient pressure, p. The factor z_i refers to the volume fraction in dry air of the respective gas i and A denotes the initially entrapped amount of dry air per unit mass of water (Aeschbach-Hertig et al., 2008).

Using the script "noblefit.m" (Brennwald, 2020), which is based on a χ^2 regression model, we employed He, Ar and N_2 as tracers to solve **Eq. 1** for A and T_w. While a positive A-value indicates a surplus of gas dissolved in the water, a negative A-value can be interpreted as a sign for degassing, e.g., by gas stripping via ebullition.

Since He concentrations in our system are likely affected by ebullition, we also used traditional O_2:Ar ratios to disentangle the biologically produced amount of O_2 from physical changes in dissolved gas saturations.

2.4.4 O_2 Estimation From O_2:Ar Ratio

Given their similar solubility (**Figure 2**), O_2 and Ar concentrations are affected in a similar way by physical changes, such as changes in temperature and pressure or gas stripping. Biological processes, i.e., O_2 production or consumption via photosynthesis or respiration, on the other hand do not affect Ar concentrations, thereby creating a difference in the O_2:Ar ratio. In environments where ebullition or air entrapment play a large role and in the absence of other Ar sources or sinks, the O_2:Ar ratio can be used to disentangle the biologically induced O_2 changes from physical changes (Craig and Hayward, 1987).

We calculated $\Delta O_2/Ar$, the biologically induced disequilibrium of O_2 with respect to Ar from the O_2 and Ar saturation ($O_{2,sat}$, Ar_{sat}) by rearranging the equation used by Zhou et al. (2014):

$$\Delta O_2 \Big/ Ar = \frac{[O_2]/[Ar]}{[O_2]_{eq}/[Ar]_{eq}} - 1 = \frac{[O_2]\big/[O_2]_{eq}}{[Ar]\big/[Ar]_{eq}} - 1 = \frac{O_{2,sat}}{Ar_{sat}} - 1\ , \tag{2}$$

where $[O_2]$ and $[Ar]$ are the measured concentrations and $[O_2]_{eq}$ and $[Ar]_{eq}$ denote the concentrations in air equilibrated water.

The amount of O_2 associated to biological activity thus follows as:

$$[O_2]_{bio} = \Delta O_2 \Big/ Ar \cdot [O_2]_{eq} \tag{3}$$

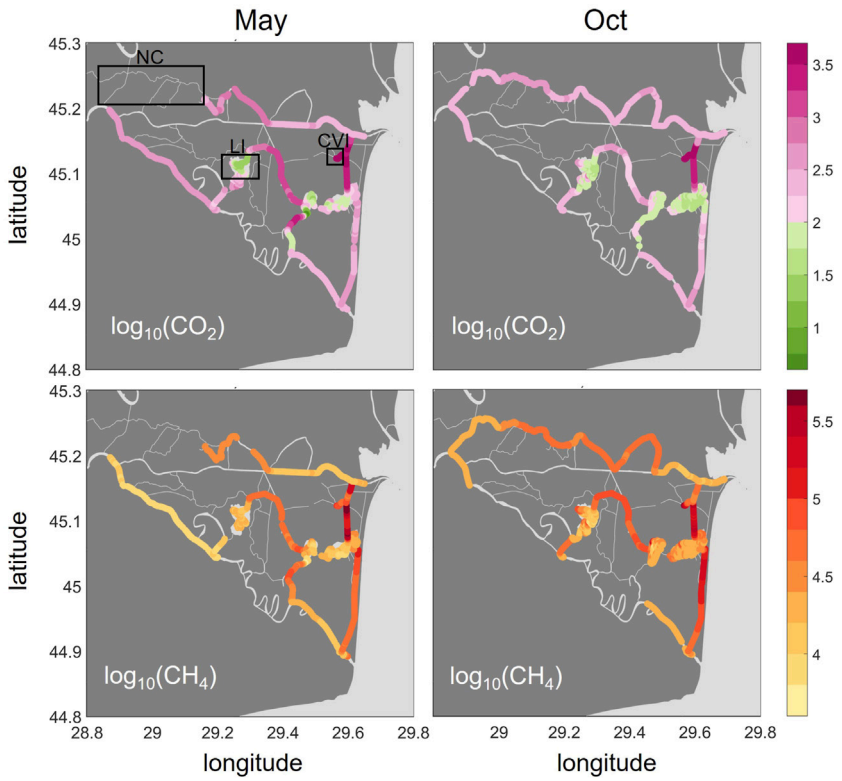


FIGURE 3 | Spatial distribution of greenhouse gas saturations (%) as CO_2 (top row) and CH_4 (bottom row) in May and October 2017 presented as $\log_{10}$ (). Color coding: pink for CO_2 represents oversaturation (>2), green indicates undersaturation. CH_4 is oversaturated throughout the delta. The boxes in the upper left graph indicate the locations of the Northern Channels (NC), Lake Isac (LI) and Canal Vatafu-Imputita (CVI). The two plots for CH_4 were adapted from Canning A et al. (2021).

and can be either positive (photosynthesis) or negative (respiration). We calculated the difference between the measured O_2 concentration and the concentration expected from the O_2:Ar ratio by adding the biological O_2 to the equilibration concentration:

$$[O_2]_{dif} = [O_2]_{meas} - \left([O_2]_{bio} + [O_2]_{eq}\right) \quad (4)$$

Negative $[O_2]_{dif}$ implies that O_2 is missing with respect to what we would expect at Ar saturations of 100%.

2.4.5 Spatial Maps and Statistical Analysis

We used Matlab R2017a and R2017b to create the figures and conduct statistical analyses. For the spatial maps, we updated publicly available shape files for Romania and Ukraine (Mapcruzin, 2016; https://mapcruzin.com/, last access: 13 December 2016) using the OpenLayers plugin in QGIS. This data sources contains imformation from openstreetmap.org, which is made available under the Open Database License (ODbL) at https://opendatacommons.org/licenses/odbl/1.0/). To compare the concentrations and saturations in the three different waterscapes and three additional sites of interest, we used the "distributionPlot.m" function (Jonas, 2021). Source code from the "noblefit"-package (Brennwald, 2020) was run on GNU Octave (version 4.2.1).

3 RESULTS

3.1 Dissolved Greenhouse Gases: CO_2 and CH_4

Both CO_2 and CH_4 showed very large concentration ranges and steep gradients across the delta with a hotspot area in the East that persisted across seasons (**Figure 3**). As the green colors indicate, CO_2 was undersaturated in many parts of the lakes in both seasons with a median across all lakes of 96% saturation in May and 65% in October. We encountered exceptions for the western lake areas close to the inflow, which receive water from wetlands and channels. These channels, as well as the river main branches, were oversaturated in CO_2 across seasons (median in May and October: 279 and 283%, respectively, in the river branches and 1,270%, respectively, 270% in the channels). Compared to the river reaches, the oversaturation in the channels showed a larger range (**Supplementary Table S3**). The highest concentrations were found in Canal Vatafu-Imputita (median: 3,000% and 4,400% in May and October, respectively, **Supplementary Table S4**) and the adjoining channels, Canal Busurca (leading north) and Canal Rosu-Imputita (leading south to Lake Rosu, **Figure 1**). While Canal Busurca showed high concentrations along the whole

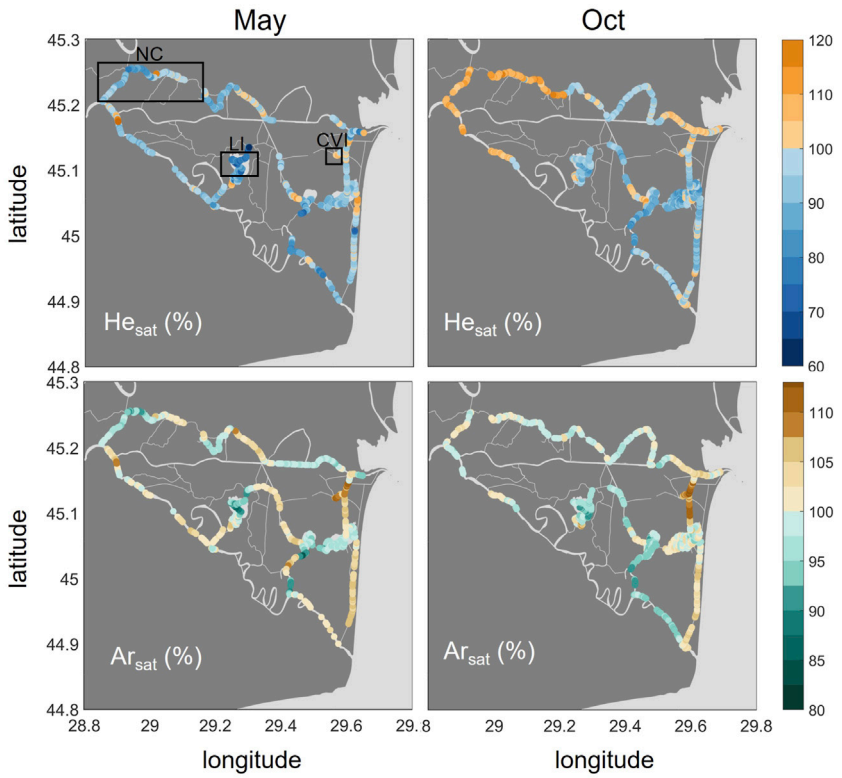


FIGURE 4 | Spatial distribution of He (top row) and Ar (bottom row) in % saturation in May and October 2017. Oversaturation is shown in orange/brown and undersaturation in blue/turquoise. Please note the different ranges of the color bars. The boxes in the upper left graph indicate the locations of the Northern Channels (NC), Lake Isac (LI) and Canal Vatafu-Imputita (CVI).

channel stretch in May, concentration dropped along the channel in October, indicating the reversal of flow direction along the first part of the channel.

CH_4 was oversaturated in all parts of the delta, with the lowest saturations occurring in the main branches of the Danube (median: 10,700 and 18,000% in May and October, **Figure 3** and **Supplementary Table S3**) followed by the lakes (median: 16,600 and 22,300% in May and October, respectively). Channels showed the highest CH_4 saturations (median: 41,200 and 57,700% in May and October, respectively). In contrast to CO_2, the highest CH_4 saturations were not found in Canal Vatafu-Imputita directly, but rather in Canal Rosu-Imputita. Canal Cordon-Litoral showed elevated CH_4 partial pressures that covered a long stretch especially in October. CO_2 was only mildly oversaturated in this channel.

3.2 Noble Gases: He and Ar

The noble gases, He and Ar (**Figure 4**), generally showed undersaturation conditions in lakes, with the strongest undersaturation occurring in Lake Isac for both gases in May (median: 77 and 91%, respectively). The strongest oversaturation, in contrast, was found in small channels. While the highest He saturations were observed in the Northern Channels in October (median: 108%), the eastern channels around Canal Vatafu-Imputita showed the maximum Ar saturations in both seasons (median: 108% in May and 112% in October). Along the stretch of this channel, we observed both under and oversaturated conditions with respect to He.

3.3 O_2 and N_2

O_2 saturations covered a large range from 19% to 162% in May and 5.2% to 139% in October (**Figure 5**). The main river branches were slightly undersaturated in both seasons with a median of 90 and 92% in May and October, respectively. In contrast to the other gases, O_2 saturations were highest in the lakes, especially in Lake Isac (median: 147% in May). The CO_2 hotspot, Canal Vatafu-Imputita, had the lowest O_2 saturations. The saturations were as low as 19% in May and 5% in October at that spot and adjoining channels, which is less than 2 mg/L and therefore too low for the survival of most fish species.

The N_2 saturations we observed ranged between 74 and 111% in May and 87–108% in October (**Figure 5**). N_2 was generally undersaturated in the lakes, while some of the channels showed oversaturation. N_2 saturations were elevated in the channels downstream of small settlements and lodging houses, for example in the channel leading from the main river to Lake Uzlina (Canal Uzlina) and the channel entering Lake Puiu from the west (Canal Caraorman). The strongest oversaturation in both May and October (median: 109 and 108%, respectively) was found in the CO_2 hotspot, Canal Vatafu-Imputita.

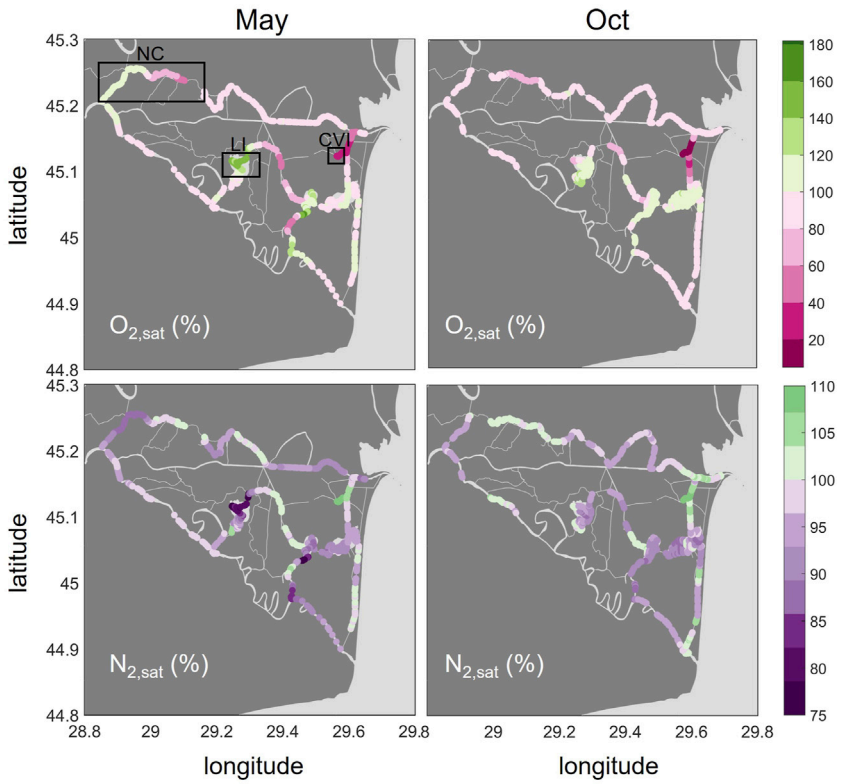


FIGURE 5 | Spatial distribution of O_2 (top row) and N_2 (bottom row) in % saturations in May and October 2017. Oversaturation is shown in green, undersaturation in purple and pink. Please note the different ranges of the colorbars. The boxes in the upper left graph indicate the locations of the Northern Channels (NC), Lake Isac (LI) and Canal Vatafu-Imputita (CVI).

4 DISCUSSION

4.1 From Patterns to Processes

The simultaneous analysis of different dissolved gas concentrations at high spatial resolution allows us to identify systematic patterns of concentration anomalies across the waterscapes of the Danube Delta. Comparing reactive with non-reactive gas concentrations, we identify relevant physical and biological processes such as excess air formation (Kipfer et al., 2002), ebullition (Brennwald et al., 2005; McGinnis et al., 2006) and ecosystem metabolism (Staehr et al., 2012). Two features in the concentration maps (**Figures 3–5**) deserve special attention. In the Eastern channels (Canal Busurca, Canal Rosu-Imputita and Canal Vatafu-Imputita; **Figure 1**) we observed hotspots of CH_4 and CO_2 concentrations (**Figure 3**). The clear oversaturation of non-reactive gases such as Ar and N_2 in this area could help us to identify potential drivers of these emission hotspots (**Figures 4**, **5**). By contrast, the survey revealed a general under-saturation of dissolved CO_2 in lakes (**Figure 3**). Here, changes in diel O_2 concentrations could allow estimating the intensity of photosynthesis (Staehr et al., 2012). However, the observed under-saturation of He, Ar and N_2 (**Figures 4**, **5**) points to a non-biological sink of dissolved gases that could affect primary production estimates based on O_2 concentrations.

A statistical display of the individual measurements in May and October reveals a broad distribution of measured values (**Figure 6**). The plot summarizes all data grouped according to waterscapes in the left panel, while the right-hand side presents only data from "boxed" areas in **Figure 1**: the Northern Channels, the hotspot channel Canal Vatafu-Imputita in the East and Lake Isac in the center of the study area. Part of the variability is caused by dramatic concentration changes at the local level (**Figures 3**, **5**). The small channels in the vicinity of Canal Vatafu-Imputita are a case in point: here, the hydrology is characterized by stagnant conditions with very slow flow velocities. Sudden changes in discharge in the main river can even reverse the flow direction and introduce water from the Sulina main branch to an area that otherwise receives water from the delta. In contrast to the main branch, the water from the delta has a strong signature from the reed and elevated greenhouse gas concentrations. Therefore, dissolved gas concentrations of CO_2, CH_4 and O_2 change abruptly along channel junctions. In the Northern Channels, the gradients were more gradual. There, larger concentration changes show a relation to channel junctions. We observed similar broad concentrations shifts in lakes such as Lake Isac. Here, greenhouse gas concentrations were highest in the East, where water was entering from a small connecting channel with Canal Litcov and from riparian reed beds. O_2 showed the opposite trend with lowest concentrations in

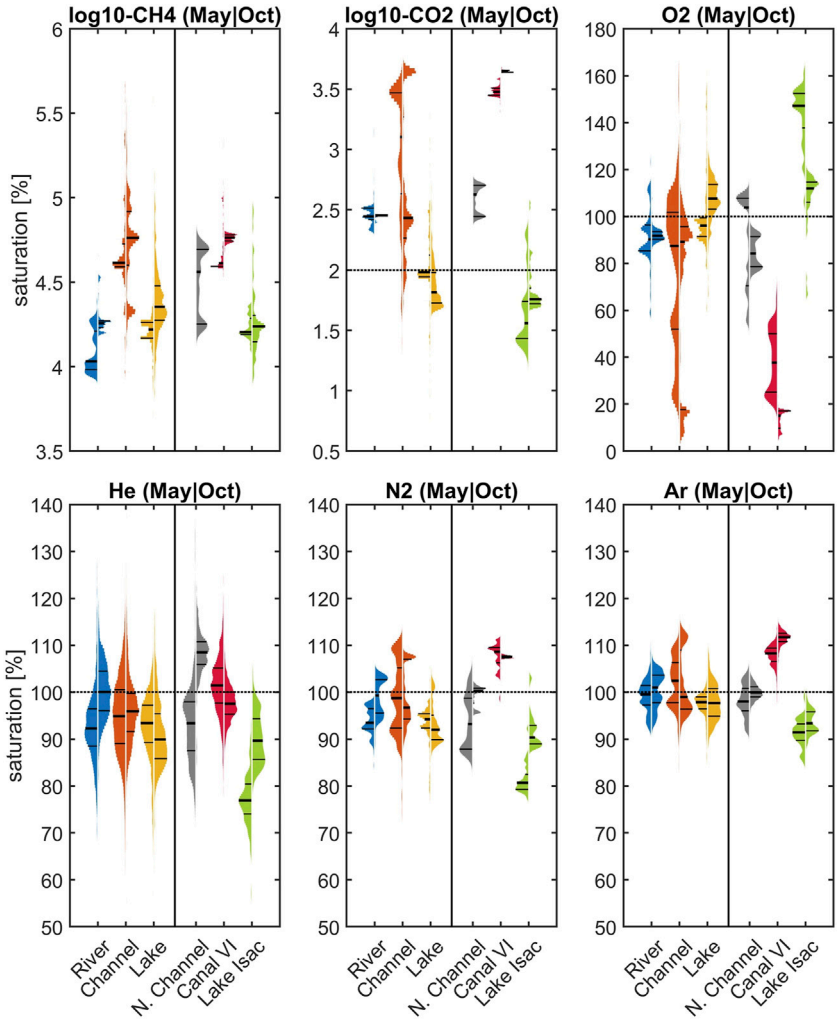


FIGURE 6 | Variability in CH_4, CO_2, O_2, He, N_2 and Ar saturations with respect to different waterscapes (river, channel, lake) and three selected areas in May (left distribution) and October (distribution on the right). Horizontal lines in the distributions mark the 25th, 50th and 75th percentile. Horizontal dotted lines represent 100% saturation. In case of CH_4 this line is below the selected plotted area. Please note the different scaling of the *y*-axis and the representation of CH_4 and CO_2 as $\log_{10}$ (). See boxes in **Figure 1** for the location of the specific areas Northern Channels, Canal Vatafu-Imputita and Lake Isac and **Supplementary Tables S3 and S4**.

the East. Wind-driven gas exchange drove re-equilibration and therefore, the dissolved gas signatures supplied by the lakes to the outflow channels changed gradually with increasing distance from the lake source.

The comparison of dissolved gas patterns across waterscapes yields valuable diagnostic insights (**Figure 6**). Focusing on non-reactive gases, the reaches of the Danube River remained close to saturation, whereas parts of the channels and most prominently Canal Vatafu-Imputita remained clearly oversaturated with respect to Ar and N_2 during both seasons. Therefore, an effective mechanism of excess air formation seems to be present in some of the small channels that form hot spots of potential greenhouse gas emissions. By contrast, lakes in general, and especially Lake Isac, showed a tendency towards undersaturation in their non-reactive gas concentrations. This undersaturation in He and N_2 in Lake Isac was more pronounced in May (77 and 81% for He and N_2, respectively) compared to October (~90% for both He and N_2) and indicates that a stripping mechanism is active in the transfer of unreactive gases to the atmosphere.

As expected, the O_2 and CO_2 patterns revealed heterotrophic characteristics of the main branches of the Danube River (**Figure 6**) with oversaturation of CO_2 and general O_2 deficits. The channels showed the same heterotrophic pattern but with a very broad distribution that could potentially be traced to their interaction with the littoral zone and the reed beds. Lake Isac, by contrast, showed evidence for intense photosynthesis in the summer, with around 150% O_2 saturation and lower autotrophy in October with about 110% O_2.

To discuss possible sources and sinks of unreactive gases, we will address a few hypotheses that could help identifying the role of different physical processes in generating the observed patterns in the Danube Delta (**Figure 7**). In the context of excess air in channels, several studies documented the role of water table

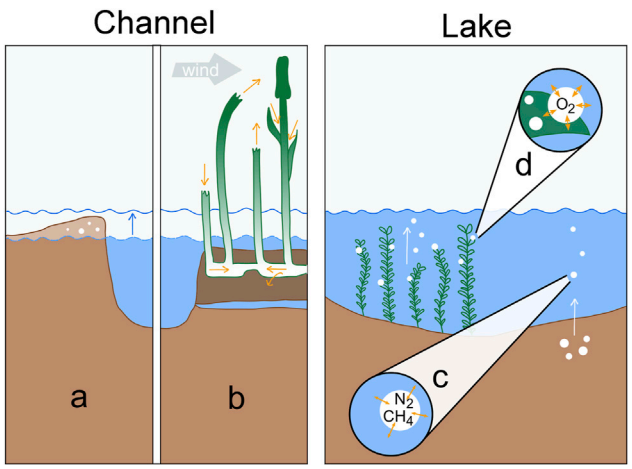


FIGURE 7 | Processes determining dissolved gas concentrations in channels (left) and shallow lakes (right): **(A)** Excess air formation via water table fluctuation in riverbanks. **(B)** Convective sediment aeration by *Phragmites australis* in permanently inundated reed areas. The two left culms illustrate venturi-induced convection, the right two culms represent humidity-induced convection. **(C)** Gas stripping by CH_4 bubbles rising from anoxic sediments. **(D)** Gas stripping by O_2 bubbles forming on macrophyte leaves during intensive photosynthesis.

fluctuations in unconfined groundwater bodies (e.g., Kipfer et al., 2002; Mächler et al., 2013). In the Eastern Danube Delta, however, floating reed vegetation is a much more prominent feature of the littoral zone than sand bars or riparian soils, which calls for another supersaturation formation hypothesis. In lakes, the release of methane bubbles at the sediment-water interface could drive gas ebullition to the atmosphere and result in dissolved gas deficits (McGinnis et al., 2006). Alternatively, accumulating oxygen bubbles at the surface of submerged macrophytes would provide an additional pathway for the loss of unreactive gases in the water column (Long et al., 2020).

4.2 Excess Air Is Tracing Emission Hotspots Near Reed Beds

The solubility of gases decreases with increasing temperature. The temperature sensitivity of this equilibrium process varies between different gases (**Figure 8**). While the solubility of He decreases by about 6% when the water temperature increases from 10 to 30°C, Ar solubility will diminish by 33%. This contrasting behavior can be used to estimate the amount of excess air, i.e., the excess in dissolved atmospheric gases, caused by dissolving air bubbles in water. Plotting the data from our surveys in **Figure 8** reveals significant excess air components in the samples of Canal Vatafu-

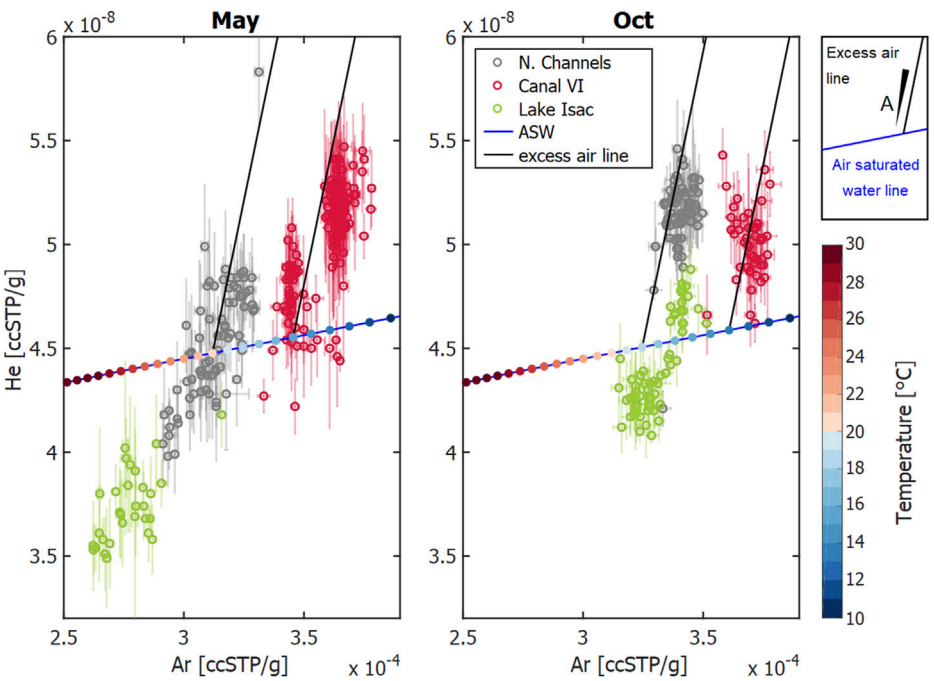


FIGURE 8 | He vs. Ar concentration in ccSPT/g, i.e., cubic centimeter of gas at standard pressure and temperature per gram of water in samples from the indicated locations in May and October 2017. The open circles show the average data from different observation sites, standard deviations are shown as error bars. The blue lines represent the concentrations in air-saturated water (ASW) at different temperatures; with temperature in °C represented as color-coded dots at 1°C increments. The solid black lines represent the excess-air lines for temperatures that fit well with the measured data: T = 20°C and T = 15°C (May), and T = 18°C and T = 13°C (Oct). The amount of dissolved air, A, increases with increasing distance from the ASW line.

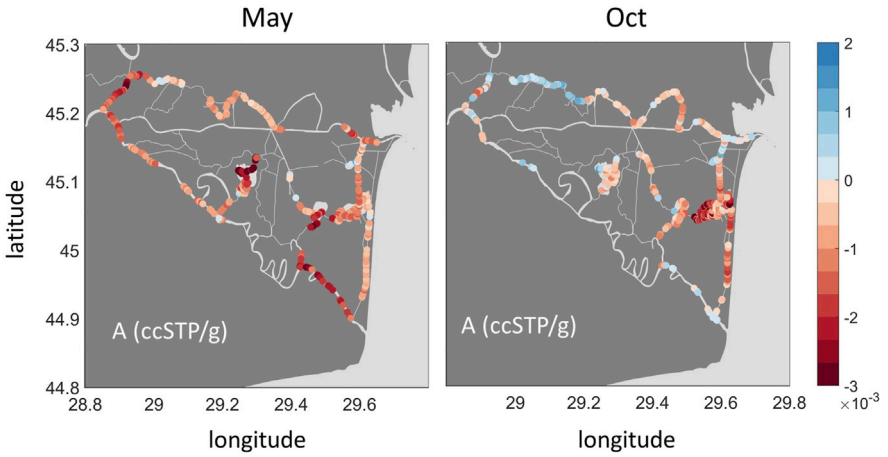


FIGURE 9 | Spatial variability in the estimates of excess air *A* for May (left) and October (right).

Imputita during both seasons, while the Northern Channels only show consistent excess air in October. The data from Lake Isac, by contrast, indicate significant gas loss (**Figure 8**).

Knowledge regarding the geomorphological and ecological context of the different sites helps in the identification of processes that cause the observed patterns in **Figure 8**. The Northern Channels are framed by riverbanks representing a potential setting for excess air formation via water table fluctuations (**Supplementary Figure S8**). During rising water table, entrapped bubbles in the unsaturated zone dissolve and increase local concentrations above saturation (Kipfer et al., 2002). Both campaigns in spring and autumn took place during falling water level (**Supplementary Figure S1**), when we expect previously enriched water to exfiltrate from the riverbanks back into the channels (**Figure 7A**). Once in the channel, gas exchange ensures re-equilibration of the oversaturated water with the atmosphere. In addition, tourist boats navigate the Northern Channels extensively from spring through summer and autumn, enhancing gas exchange, but defining a causal link would require time-resolved monitoring of excess air and boat traffic.

Canal Vatafu-Imputita, on the other hand, is situated in a depression zone framed by permanently inundated reed beds (**Supplementary Figure S8**). We were thus initially surprised to find supersaturated conditions at this location, especially since it is one of very few locations showing excess air in both seasons (**Figure 9**). While the excess air signal in October was comparable to the Northern Channels, the equilibration temperature was about 5°C lower (**Figure 8**; **Supplementary Figure S6**). As there are no adjacent riverbanks and rather little traffic at Canal Vatafu-Imputita, we found only two potential drivers for the excess air signal at this location: rapid heating or convective gas addition via reed vegetation.

As indicated by the difference between equilibrium temperature obtained from the UA-model and the *in-situ* measured temperature (**Supplementary Figure S7**), the equilibration could have taken place at an approximately 5°C lower temperature in the sun sheltered reed, with the water parcel heating rapidly without changing its gas content once reaching the channel (**Supplementary Figure S4**). The channels within reed beds are rather wind sheltered environments as long as the main wind direction is perpendicular to the channel orientation. However, during sporadic measurements of daily temperature cycles in the channel, we only observed temperature fluctuations up to 2°C over the course of 1 day. Therefore, it seems unlikely that rapid heating would lead to the observed excess air signals.

We can therefore hypothesize that the plant physiology of the dominating reed species was the relevant cause of the oversaturation (**Figure 7B**). Equipped with aerenchyma (i.e., tissue with air channels, e.g., Baldantoni et al. (2009)), *Phragmites australis* transports O_2 in order to aerate its root zone (e.g., Brix et al., 1996). Aerating the root zone is vital for plants living in water logged or inundated soils, since anoxic sediment environments promote several adverse redox reactions (DeLaune and Reddy, 2008). The transportation mechanisms affect all gases present in air and wetland sediments (Sorrell and Brix, 2013). This way, He, Ar and N_2 are pumped into the root zone together with O_2 and could be used as tracers for plant-mediated oxygen supply.

Convective flow in plants is driven by a pressure gradient within the plant. The two most important gas transport processes in *Phragmites australis* are venturi-induced convection and humidity-induced convection (Armstrong et al., 1992). Venturi-induced flow is driven by wind blowing across the culms, thereby creating a pressure differential that sucks air out of tall dead culms. Short broken culms act as inflow and lead air along the underground root system to tall culms. The effectiveness of this process increases with wind speed (Armstrong et al., 1992). Humidity-induced flow works best during hot and dry days, since it relies on the pressure difference created by moistening of the air inside the plants living green shoots. Dead and broken culms act as efflux sites in this case (Armstrong et al., 1996). According to field measurements shortly above the water table, the pressure inside live culms is up to 2% higher than ambient air pressure

(Arkebauer et al., 2001). The exchange of gases between plant and rhizome is governed by diffusion (Armstrong et al., 1996).

Assuming the plants provide enough air to their root system to saturate the surrounding water with dissolved gases, we can estimate the level of noble gas oversaturation to be expected. The plaur which *Phragmites australis* grows on is about 0.8–1.3 m thick, so it is reasonable to assume that the root systems reach a depth of 1 m below water level. At this depth, the local hydrostatic pressure is about 10^4 Pa higher than atmospheric pressure. If the plants would provide enough air to this depth to saturate the water phase at this increased pressure, we would expect 10% oversaturation when comparing it to water equilibrated at local atmospheric pressure. This is approximately the amount of oversaturation we observed for He, Ar and N_2 in May and October in Canal Vatafu-Imputita (**Supplementary Figure S5**).

Based on field measurements, Brix et al. (1996) estimated the total gas exchange by *Phragmites australis* to 9–11 L m^{-2} h^{-1}. Assuming an air-like gas composition in the gas transport system of the plant and a dissolution of 10% of the gas transported by the total flux observed by Brix et al. (1996), would mean that 1.5–3.5 h were sufficient to supply the amount of N_2 and Ar to the root systems needed to create the observed oversaturation.

If reed beds play a significant role in the injection of excess air and high concentrations of CH_4 and CO_2, then how can we explain the different patterns observed in the GHG and excess air maps (**Figures 3**, **9**)? Canal Vatafu-Imputita drains a core protection zone of the Danube Delta Biosphere Reserve, which is populated by *Phragmites australis*, while other core zones generally protect other vegetation types. In the core zone, harvesting and burning of the reed is not permitted, thus we expect more dead and broken culms that can function as efflux culms for the convective flow in this area, together with more degradable organic matter. Brix et al. (1996) report 280 dead and 85 living culms per square meter in their study area. At sites that are harvested and burnt we would expect the ratio to be shifted towards living culms as dead culms are removed regularly, which might restrict sediment aeration. A functioning soil aeration results in the oxidation of reduced species near the root zone, e.g., oxidation of CH_4 produced during organic matter degradation to CO_2 (DeLaune and Reddy, 2008). Looking at the maps in **Figure 3**, the high ratio of CO_2 to CH_4 indicates that CH_4 oxidation could be an important process in Canal Vatafu-Imputita. This seems plausible, considering that biofilms inhabiting the root surfaces of *Phragmites australis* consist to about one-third of bacteria capable of oxidizing CH_4 (Faußer et al., 2012). This could explain the buildup of high CO_2 concentrations in the water phase below the floating plaur which subsequently drain into Canal Vatafu-Imputita. The adjacent Canal Rosu-Imputita is draining the buffer area, where reed harvesting is allowed within limits. It shows higher CH_4 and lower CO_2 concentrations than Canal Vatafu-Imputita, especially in spring. The oversaturation of Ar, N_2 and He is also less in this channel during the early growing season, which may indicate that nearby reed beds are managed and O_2 transfer during the early growing season is hampered, resulting in a reduced oxidation capacity in the root zone.

Once the supersaturated water reaches the channel, diffusive re-equilibration with the atmosphere would decrease the oversaturation towards equilibrium. Intense boat traffic would enhance gas exchange and ebullition could strip the gases even below equilibrium. A combination of these processes might explain the comparably low He saturations observed at Canal Vatafu-Imputita (**Figure 6**).

4.3 Gas Loss by Ebullition in Shallow Lakes

In contrast to the channels, we observed undersaturation of He, Ar and N_2 in the lakes, especially in Lake Isac. This coincided with a CO_2 undersaturation and an O_2 oversaturation. The undersaturation of He, Ar and N_2 indicates that gas stripping by ebullition affects the dissolved gas concentrations, since a rising bubble exchanges gas with the surrounding water column and thereby strips dissolved gases depending on their solubility (Brennwald et al., 2005; McGinnis et al., 2006). Accordingly, in Lake Isac the hardly soluble He showed the strongest undersaturation, followed by the more soluble N_2 and Ar (compare **Figures 2** and **6**). As O_2 and Ar exhibit similar solubilities, undersaturation of Ar indicates that O_2 must be affected by gas stripping. We calculated the effect on O_2 concentration via O_2:Ar ratios (**Eq. 4** and **Figure 10**). For oversaturated O_2 conditions in May, we found a linear relation with missing $O_{2,dif}$ down to about 2.5 mg/L at 150% saturation.

Gas ebullition is the most likely cause for the observed oxygen deficit and there are two potential drivers of such a process: CH_4 ebullition from the sediment (**Figure 7C**) and O_2 ebullition from macrophyte leaves (**Figure 7D**). Evaluating the dataset from Maier et al. (2020) showed that CH_4 ebullition was most often present in lakes and channels, where it occurred in 43 and 42% cases of flux measurements around the year (Maier et al., 2020). However, with a depth of only about 1.5–4 m, the sampled delta lakes are comparably shallow (Oosterberg et al., 2000), which limits the contact time between water column and the rising gas bubble, thus restricting gas exchange (McGinnis et al., 2006). A pure CH_4 bubble with an initial size of 2 mm would still contain 70% of the initial CH_4 if released from 4 m depth. Larger bubble diameter or shallower release depth would increase the percentage of initially CH_4 transported (Greinert and McGinnis, 2009). CH_4 bubbles released from the sediment usually contain large amounts of N_2. Assuming the minimum amount of CH_4 needed to trigger the rise of a bubble through the sediment would result in an approximate CH_4:N_2 composition of 35:65% (Langenegger et al., 2019). A CH_4/N_2 bubble released in a lake with 2 m depth would transport on average about 5.3 µg O_2 per bubble to the atmosphere (**Supplementary Figure S10**). Thus, about 0.8 million methane bubbles per m^2 would have to be released to the atmosphere from a fully mixed water column of 2 m depth to account for the buildup of a daily oxygen deficit of 2 g m^{-3}. This would equal a CH_4 flux of 3.1 mol m^{-2} day^{-1}, which is about 60 times higher than the maximum total CH_4 flux measured in lakes and more than 2,000 times higher than the median total CH_4 flux from lakes in the Danube Delta (Maier et al., 2021). In the case of CH_4 ebullition being the sole cause of O_2 reduction, we would expect gas stripping to be strongest after macrophyte die-off or in autumn when large amounts of easily

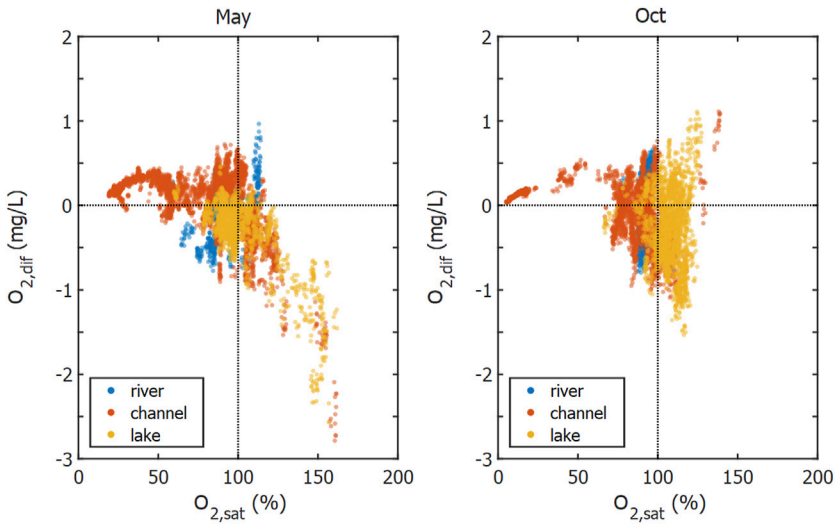


FIGURE 10 | O_2 concentration difference of O_2 calculated from O_2:Ar ratio (**Eq. 4**). Color coding indicates the different waterscapes. Negative values of $O_{2,dif}$ occur for samples with significant undersaturation in the Ar concentration.

degradable material are available. Considering the large fluxes needed and the unusual timing, it is unlikely for CH_4 ebullition to be the dominant process reducing the saturation of dissolved gases in May and we therefore turn our attention to photosynthesis.

In spring, the bottom of Lake Isac was covered by macrophytes, many of them reaching close to the water surface (**Supplementary Figure S11**). If photosynthesis is very productive, bubbles containing N_2 and a lot of O_2 form on the leave surface of macrophytes and can be released via ebullition (Koschorreck et al., 2017). In contrast to CH_4 bubbles rising from the sediment, these O_2 bubbles spent considerably longer time in contact with the water column until they detach and rise to the surface. This process would also explain the quasi-linear relationship between observed oversaturation and estimated amount of missing O_2, assuming that stronger oversaturation coincided with more O_2 bubble formation and increased release to the surface. Strong oversaturation together with missing O_2 was almost exclusively observed in the lakes (**Supplementary Figure S9**), especially in Lake Isac and Lake Puiu in spring where median O_2 saturation was 147 and 115%, respectively. Both lakes are also the sites where He and Ar saturations were lowest with median saturations of 76.9 and 91.4% in Lake Isac, and 87.5 and 96.9% in Lake Puiu, respectively. Temperature-corrected, specific conductivity was lower in these lakes than in the main river (**Supplementary Figure S3**). This may also indicate high primary productivity because intense photosynthesis takes up CO_2, thus increasing pH, shifting the carbonate equilibrium, and leading to calcite precipitation and a decrease of specific conductivity (Dittrich et al., 2004; Ostrofsky and Miller, 2017).

The combined measurements of non-reactive gases and O_2 thus indicate that photosynthesis was even higher than indicated by *in-situ* O_2 oversaturation. Whether the inter-lake differences are caused by differences in submerged macrophyte abundance (Coops et al., 1999) or caused by differences in macrophyte species (Niculescu et al., 2020) cannot be concluded without further research. In any case, the current findings support several recent studies that highlight the importance of considering ebullitive gas exchange when estimating metabolism from diel O_2 concentration measurements in shallow ecosystems and propose to constrain ebullition rates using funnels or modelling the gas exchange from noble gas measurements (Koschorreck et al., 2017; Howard et al., 2018; Long et al., 2020). The reduction of daily net O_2 production estimates by ebullitive O_2 fluxes is estimated to about 1–21% (Howard et al., 2018).

4.4 Implications for Process Analysis and Upscaling

High-resolution mapping of biogenic and inert dissolved gases across the waterscapes of the Danube Delta revealed a broad range in the saturation state of the greenhouse gases CO_2 and CH_4 (**Figure 3**). The main river reaches showed the expected behavior of a net heterotrophic ecosystem metabolism with slight supersaturation in both gases (**Figure 6**).

The channels in a delta system represent the reactive pipes transferring water from lakes and wetlands back into the main river and finally to the sea. Measuring the patterns of unreactive gases in channels provided additional insights: Signals of excess air in a canal close to floating natural *Phragmites* stands provided evidence for convective gas transfer into the root zone and for intensified CH_4 oxidation resulting in elevated levels of CO_2 at comparatively low CH_4 concentration. This preliminary assignment of most plausible processes to a set of dissolved gas patterns may help in guiding further research into the "black-box" of terrestrial-aquatic linkages at densely vegetated aquatic-terrestrial boundaries.

In comparison to the river reaches and channels, the shallow lakes were dominated by photosynthesis with clear CO_2 deficits and

O_2 oversaturation (**Figures 3**, **5**). In these highly productive systems (Durisch-Kaiser et al., 2011; Maier et al., 2021), non-reactive gases gave clear evidence for O_2 ebullition from macrophytes, a process that deserves further attention. Ebullitive loss of O_2 to the atmosphere complicates the estimation of net ecosystem production in shallow lakes (Koschorreck et al., 2017), beds of macrophytes and with floating vegetation (Kleinschroth et al., 2021). Such plant communities in freshwater systems remain a significant challenge for efforts to upscale net CO_2 exchange.

The current discussion and global synthesis of the carbon transfer along the land-ocean aquatic continuum (LOAC, Regnier et al., 2013) is still dominated by active pipe models (Cole et al., 2007; Abril and Borges, 2019). Such a river engineering approach falls short of capturing the dramatic changes in the biomorphology of large river corridors of the last century. Surveys identified a loss of around 80% of the riparian wetlands in the lower Danube River corridor (Csagoly et al., 2016). On a global scale, preliminary estimates arrive at a loss of wetland area in the range of 17–50% between 1970 and 2008 depending on the region (Dixon et al., 2016). Loss or restoration of riparian wetland areas will certainly affect the greenhouse gas budgets of large river systems, but adequate measurements and models are needed to derive reliable estimates.

Based on this case study, we conclude, that adding non-reactive gas tracers to the toolbox of biogeochemical analysis offers significant potential for disentangling physical and biological processes in deltaic systems. Our analysis identifies root aeration of *Phragmites australis* reed beds as a plausible process leading to the oversaturation of small channels with non-reactive gas species as well as greenhouse gases. Furthermore, we highlight the effect of O_2 ebullition on dissolved gas concentrations in shallow lakes and the risk of underestimating metabolic rates derived from O_2 concentrations.

DATA AVAILABILITY STATEMENT

The datasets presented in this study can be found in the following online repositories: The data set with the MIMS measurements presented (i.e. He, Ar, O_2 and N_2) and accompanying metadata files are available via the ETH Research Collection at https://doi.org/10.3929/ethz-b-000537695 (Maier et al., 2022). The CO_2, CH_4, temperature and conductivity data have been uploaded to PANGAEA, available at: https://doi.pangaea.de/10.1594/PANGAEA.925080 (last access: 20.01.2021, Canning et al., 2020).

AUTHOR CONTRIBUTIONS

MSM, AC and BW conceptualized the present study. MSM, AC, CT and MB participated in field work. AC processed and analyzed the CO_2 and CH_4 data, MSM processed and analyzed the other dissolved gases. MSM conducted the excess air model calculations with support from MB. MSM prepared the figures, supplementary material, and, together with BW, drafted the manuscript. All authors engaged in discussing and editing the paper.

FUNDING

This work was supported by the Swiss State Secretariat for Education, Research and Innovation (SERI; grant no. 15.0068). The research leading to these results has received funding from the European Union's Horizon 2020 research and innovation program under the Marie Skłodowska-Curie Actions (grant no. 643052; C-CASCADES project).

ACKNOWLEDGMENTS

The authors thank Tim Kalvelage, Alexander Mistretta, Till Breitenmoser and our Romanian houseboat crew for their support during fieldwork. We thank the entire 4H- JENA team for their support with the CH_4 and CO_2 sensors, as well as Dan McGinnis and Rolf Kipfer for fruitful discussions and suggestions.

SUPPLEMENTARY MATERIAL

The Supplementary Material for this article can be found online at: https://www.frontiersin.org/articles/10.3389/fenvs.2022.838126/full#supplementary-material

REFERENCES

Abril, G., and Borges, A. V. (2019). Ideas and Perspectives: Carbon Leaks from Flooded Land: Do We Need to Replumb the Inland Water Active Pipe? *Biogeosciences* 16 (3), 769–784. doi:10.5194/bg-16-769-2019

Aeschbach-Hertig, W., El-Gamal, H., Wieser, M., and Palcsu, L. (2008). Modeling Excess Air and Degassing in Groundwater by Equilibrium Partitioning with a Gas Phase. *Water Resour. Res.* 44 (8), 1-12. doi:10.1029/2007wr006454

Aeschbach-Hertig, W., Peeters, F., Beyerle, U., and Kipfer, R. (1999). Interpretation of Dissolved Atmospheric noble Gases in Natural Waters. *Water Resour. Res.* 35 (9), 2779–2792. doi:10.1029/1999wr900130

Arkebauer, T. J., Chanton, J. P., Verma, S. B., and Kim, J. (2001). Field Measurements of Internal Pressurization in Phragmites Australis (Poaceae) and Implications for Regulation of Methane Emissions in a Midlatitude Prairie Wetland. *Am. J. Bot.* 88 (4), 653–658. doi:10.2307/2657065

Armstrong, J., Armstrong, W., Beckett, P. M., Halder, J. E., Lythe, S., Holt, R., et al. (1996). Pathways of Aeration and the Mechanisms and Beneficial Effects of Humidity- and Venturi-Induced Convections in Phragmites Australis (Cav.) Trin. Ex Steud. *Aquat. Bot.* 54 (2), 177–197. doi:10.1016/0304-3770(96)01044-3

Armstrong, J., Armstrong, W., and Beckett, P. M. (1992). Phragmites Australis: Venturi- and Humidity-Induced Pressure Flows Enhance Rhizome Aeration and Rhizosphere Oxidation. *New Phytol.* 120 (2), 197–207. doi:10.1111/j.1469-8137.1992.tb05655.x

Baldantoni, D., Ligrone, R., and Alfani, A. (2009). Macro- and Trace-Element Concentrations in Leaves and Roots of Phragmites Australis in a Volcanic lake in Southern Italy. *J. Geochemical Exploration* 101 (2), 166–174. doi:10.1016/j.gexplo.2008.06.007

Battin, T. J., Kaplan, L. A., Findlay, S., Hopkinson, C. S., Marti, E., Packman, A. I., et al. (2008). Biophysical Controls on Organic Carbon Fluxes in Fluvial Networks. *Nat. Geosci* 1 (2), 95–100. doi:10.1038/ngeo101

Bernhardt, E. S., Heffernan, J. B., Grimm, N. B., Stanley, E. H., Harvey, J. W., Arroita, M., et al. (2018). The Metabolic Regimes of Flowing Waters. *Limnology and Oceanography* 63, S99–S118. doi:10.1002/lno.10726

Borges, A. V., and Abril, G. (2011). "Carbon Dioxide and Methane Dynamics in Estuaries," in *Treatise on Estuarine and Coastal Science*. Editors E. Wolanski, and D. McLusky (Waltham: Academic Press), 119–161. doi:10.1016/b978-0-12-374711-2.00504-0

Brennwald, M. S. (2020). *Noblefit - Quantitative Interpretation of Enivronmental Tracer Data* [Online]. GitHub.com. Available at: https://github.com/brennmat/noblefit (Accessed 05 29, 2021).

Brennwald, M. S., Kipfer, R., and Imboden, D. M. (2005). Release of Gas Bubbles from lake Sediment Traced by noble Gas Isotopes in the Sediment Pore Water. *Earth Planet. Sci. Lett.* 235 (1), 31–44. doi:10.1016/j.epsl.2005.03.004

Brennwald, M. S., Schmidt, M., Oser, J., and Kipfer, R. (2016). A Portable and Autonomous Mass Spectrometric System for On-Site Environmental Gas Analysis. *Environ. Sci. Technol.* 50 (24), 13455–13463. doi:10.1021/acs.est.6b03669

Brix, H., Sorrell, B. K., and Schierup, H.-H. (1996). Gas Fluxes Achieved by *In Situ* Convective Flow in Phragmites Australis. *Aquat. Bot.* 54 (2), 151–163. doi:10.1016/0304-3770(96)01042-x

Cai, W.-J. (2011). Estuarine and Coastal Ocean Carbon Paradox: CO2 Sinks or Sites of Terrestrial Carbon Incineration? *Annu. Rev. Mar. Sci.* 3 (1), 123–145. doi:10.1146/annurev-marine-120709-142723

Canning, A., Maier, M.-S., Wehrli, B., and Körtzinger, A. (2020). [Dataset]. Seasonal High-Resolution Sensor Data for pCO2, pCH4, O2 and Temperature/salinity within the Danube Delta, Romania in 2017. Available at: https://doi.pangaea.de/10.1594/PANGAEA.925080. Accessed from 20 January, 2021.

Canning, A. R., Fietzek, P., Rehder, G., and Körtzinger, A. (2021). Technical Note: Seamless Gas Measurements across the Land-Ocean Aquatic Continuum - Corrections and Evaluation of Sensor Data for CO2, CH4 and O2 from Field Deployments in Contrasting Environments. *Biogeosciences* 18 (4), 1351–1373. doi:10.5194/bg-18-1351-2021

Canning, A., Wehrli, B., and Körtzinger, A. (2021). Methane in the Danube Delta: the Importance of Spatial Patterns and Diel Cycles for Atmospheric Emission Estimates. *Biogeosciences* 18 (12), 3961–3979. doi:10.5194/bg-18-3961-2021

Cole, J. J., Prairie, Y. T., Caraco, N. F., McDowell, W. H., Tranvik, L. J., Striegl, R. G., et al. (2007). Plumbing the Global Carbon Cycle: Integrating Inland Waters into the Terrestrial Carbon Budget. *Ecosystems* 10 (1), 171–184. doi:10.1007/s10021-006-9013-8

Coops, H., Hanganu, J., Tudor, M., and Oosterberg, W. (1999). Classification of Danube Delta Lakes Based on Aquatic Vegetation and Turbidity. *Hydrobiologia* 415 (0), 187–191. doi:10.1007/978-94-017-0922-4_26

Covaliov, S., Doroftei, M., and Hanganu, J. (2010). Danube Delta Biosphere Reserve (DDBR): Reed Dynamics within Actual Context. *Adv. Environ. Sci.* 2 (1), 69–79.

Craig, H., and Hayward, T. (1987). Oxygen Supersaturation in the Ocean: Biological versus Physical Contributions. *Science* 235 (4785), 199–202. doi:10.1126/science.235.4785.199

Csagoly, P., Magnin, G., and Hulea, O. (2016). "Lower Danube Green Corridor," in *The Wetland Book: II: Distribution, Description and Conservation*. Editors C. M. Finlayson, G. R. Milton, R. C. Prentice, and N. C. Davidson. (Dordrecht: Springer Netherlands), 1–6. doi:10.1007/978-94-007-6173-5_251-1:

Deemer, B. R., Harrison, J. A., Li, S., Beaulieu, J. J., DelSontro, T., Barros, N., et al. (2016). Greenhouse Gas Emissions from Reservoir Water Surfaces: A New Global Synthesis. *BioScience* 66 (11), 949–964. doi:10.1093/biosci/biw117

DeLaune, R. D., and Reddy, K. R. (2008). *Biogeochemistry of Wetlands: Science and Applications*. Boca Raton: CRC Press.

DelSontro, T., Beaulieu, J. J., and Downing, J. A. (2018). Greenhouse Gas Emissions from Lakes and Impoundments: Upscaling in the Face of Global Change. *Limnol Oceanogr Lett.* 3 (3), 64–75. doi:10.1002/lol2.10073

Dittrich, M., Kurz, P., and Wehrli, B. (2004). The Role of Autotrophic Picocyanobacteria in Calcite Precipitation in an Oligotrophic Lake. *Geomicrobiology J.* 21 (1), 45–53. doi:10.1080/01490450490253455

Dixon, M. J. R., Loh, J., Davidson, N. C., Beltrame, C., Freeman, R., and Walpole, M. (2016). Tracking Global Change in Ecosystem Area: The Wetland Extent Trends index. *Biol. Conservation* 193, 27–35. doi:10.1016/j.biocon.2015.10.023

Durisch-Kaiser, E., Doberer, A., Reutimann, J., Pavel, A., Balan, S., Radan, S., et al. (2011). Organic Matter Governs N and P Balance in Danube Delta Lakes. *Aquat. Sci.* 73 (1), 21–33. doi:10.1007/s00027-010-0156-5

Faußer, A. C., Hoppert, M., Walther, P., and Kazda, M. (2012). Roots of the Wetland Plants Typha Latifolia and Phragmites Australis Are Inhabited by Methanotrophic Bacteria in Biofilms. *Flora - Morphol. Distribution, Funct. Ecol. Plants* 207 (11), 775–782. doi:10.1016/j.flora.2012.09.002

Friedlingstein, P., O'Sullivan, M., Jones, M. W., Andrew, R. M., Hauck, J., Olsen, A., et al. (2020). Global Carbon Budget 2020. *Earth Syst. Sci. Data* 12 (4), 3269–3340. doi:10.5194/essd-12-3269-2020

Garcia, H. E., and Gordon, L. I. (1992). Oxygen Solubility in Seawater: Better Fitting Equations. *Limnol. Oceanogr.* 37 (6), 1307–1312. doi:10.4319/lo.1992.37.6.1307

Gastescu, P. (2013). *Map of the Danube Delta Biosphere Reserve*. 1:240000. Tulcea, Romania: Danube Delta Biosphere Reserve Authority DDBRA.

Greinert, J., and McGinnis, D. F. (2009). Single Bubble Dissolution Model - the Graphical User Interface SiBu-GUI. *Environ. Model. Softw.* 24 (8), 1012–1013. doi:10.1016/j.envsoft.2008.12.011

Groffman, P. M., Altabet, M. A., Böhlke, J. K., Butterbach-Bahl, K., David, M. B., Firestone, M. K., et al. (2006). Methods for Measuring Denitrification: Diverse Approaches to a Difficult Problem. *Ecol. Appl.* 16 (6), 2091–2122. doi:10.1890/1051-0761(2006)016[2091:mfmdda]2.0.co;2

Hall, R. O., Tank, J. L., Baker, M. A., Rosi-Marshall, E. J., and Hotchkiss, E. R. (2016). Metabolism, Gas Exchange, and Carbon Spiraling in Rivers. *Ecosystems* 19 (1), 73–86. doi:10.1007/s10021-015-9918-1

Hall, R. O., and Ulseth, A. J. (2020). Gas Exchange in Streams and Rivers. *WIREs Water* 7 (1), e1391. doi:10.1002/wat2.1391

Hamme, R. C., and Emerson, S. R. (2004). The Solubility of Neon, Nitrogen and Argon in Distilled Water and Seawater. *Deep Sea Res. Oceanographic Res. Pap.* 51 (11), 1517–1528. doi:10.1016/j.dsr.2004.06.009

Hanganu, J., Dubyna, D., Zhmud, E., Grigoras, I., Menke, U., Drost, H., et al. (2002). *Vegetation of the Biosphere Reserve "Danube Delta" - with Transboundary Vegetation Map on a 1:150000 Scale*. Romania, Ukraine and RIZA: Danube Delta National Institute, M.G. Kholodny - Institute of Botany & Danube Delta Biosphere ReserveThe Netherlands. RIZA rapport 2002.049, Lelystad, ISBN 9036954797.

Heaton, T. H. E., and Vogel, J. C. (1981). "Excess Air" in Groundwater. *J. Hydrol.* 50, 201–216. doi:10.1016/0022-1694(81)90070-6

Holgerson, M. A., and Raymond, P. A. (2016). Large Contribution to Inland Water CO2 and CH4 Emissions from Very Small Ponds. *Nat. Geosci* 9 (3), 222–226. doi:10.1038/ngeo2654

Horgby, Å., Canadell, M. B., Ulseth, A. J., Vennemann, T. W., and Battin, T. J. (2019). High-Resolution Spatial Sampling Identifies Groundwater as Driver of CO 2 Dynamics in an Alpine Stream Network. *J. Geophys. Res. Biogeosci.* 124 (7), 1961–1976. doi:10.1029/2019JG005047

Howard, E. M., Forbrich, I., Giblin, A. E., Lott, D. E., III, Cahill, K. L., and Stanley, R. H. R. (2018). Using Noble Gases to Compare Parameterizations of Air-Water Gas Exchange and to Constrain Oxygen Losses by Ebullition in a Shallow Aquatic Environment. *J. Geophys. Res. Biogeosci.* 123 (9), 2711–2726. doi:10.1029/2018JG004441

ICPDR (2019). [Dataset]. Danube River Basin Water Quality Database. Available at: http://www.icpdr.org/wq-db/. Accessed from 29 October, 2019.

IPCC (2021). *Climate Change 2021: The Physical Science Basis*. Contribution of Working Group I to the Sixth Assessment Report of the Intergovernmental Panel on Climate Change. Cambridge University Press.

Irimus, I. (2006). "The Hydrological Regime of the Danube in the Deltaic Sector," in *Danube Delta: Genesis and Biodiversity(*. Editors C. Tudorancea and M. M. Tudorancea (Leiden, Netherlands: Backhuys Publishers), 53–64.

Jonas (2021). Violin Plots for Plotting Multiple Distributions (distributionPlot.M) [Online]. Available at: https://www.mathworks.com/matlabcentral/fileexchange/23661-violin-plots-for-plotting-multiple-distributions-distributionplot-m. MATLAB Central File Exchange (Accessed January 17, 2021).

Kipfer, R., Aeschbach-Hertig, W., Peeters, F., and Stute, M. (2002). Noble Gases in Lakes and Ground Waters. *Rev. Mineralogy Geochem.* 47 (1), 615–700. doi:10.2138/rmg.2002.47.14

Kleinschroth, F., Winton, R. S., Calamita, E., Niggemann, F., Botter, M., Wehrli, B., et al. (2021). Living with Floating Vegetation Invasions. *Ambio* 50 (1), 125–137. doi:10.1007/s13280-020-01360-6

Koschorreck, M., Hentschel, I., and Boehrer, B. (2017). Oxygen Ebullition from Lakes. *Geophys. Res. Lett.* 44 (18), 9372–9378. doi:10.1002/2017gl074591

Langenegger, T., Vachon, D., Donis, D., and McGinnis, D. F. (2019). What the Bubble Knows: Lake Methane Dynamics Revealed by Sediment Gas Bubble Composition. *Limnol Oceanogr* 64 (4), 1526–1544. doi:10.1002/lno.11133

Laruelle, G. G., Dürr, H. H., Slomp, C. P., and Borges, A. V. (2010). Evaluation of Sinks and Sources of CO2 in the Global Coastal Ocean Using a Spatially-Explicit Typology of Estuaries and continental Shelves. *Geophys. Res. Lett.* 37 (15), L15607(1-6). doi:10.1029/2010gl043691

Lauerwald, R., Laruelle, G. G., Hartmann, J., Ciais, P., and Regnier, P. A. G. (2015). Spatial Patterns in CO2 evasion from the Global River Network. *Glob. Biogeochem. Cycles* 29 (5), 534–554. doi:10.1002/2014gb004941

Long, M. H., Sutherland, K., Wankel, S. D., Burdige, D. J., and Zimmerman, R. C. (2020). Ebullition of Oxygen from Seagrasses under Supersaturated Conditions. *Limnol Oceanogr* 65 (2), 314–324. doi:10.1002/lno.11299

Mächler, L., Peter, S., Brennwald, M. S., and Kipfer, R. (2013). Excess Air Formation as a Mechanism for Delivering Oxygen to Groundwater. *Water Resour. Res.* 49 (10), 6847–6856. doi:10.1002/wrcr.20547

Maier, M.-S., Teodoru, C. R., and Wehrli, B. (2021). Spatio-temporal Variations in Lateral and Atmospheric Carbon Fluxes from the Danube Delta. *Biogeosciences* 18 (4), 1417–1437. doi:10.5194/bg-18-1417-2021

Maier, M.-S., Teodoru, C. R., and Wehrli, B. (2020). [Dataset]. "Spatio-temporal Variations of Lateral and Atmospheric Carbon Fluxes from the Danube Delta (Dataset)," in *A 2-year Dataset of Measured Concentrations and Fluxes* (ETH Zurich). Available at: http://hdl.handle.net/20.500.11850/416925. doi:10.3929/ethz-b-000416925

mapcruzin (2016). Mapcruzin.com [Online]. Available at: https://mapcruzin.com/free-romania-arcgis-maps-shapefiles.htmwww.openstreetmap.org/ (Accessed 12 13, 2016).

McGinnis, D. F., Bilsley, N., Schmidt, M., Fietzek, P., Bodmer, P., Premke, K., et al. (2016). Deconstructing Methane Emissions from a Small Northern European River: Hydrodynamics and Temperature as Key Drivers. *Environ. Sci. Technol.* 50 (21), 11680–11687. doi:10.1021/acs.est.6b03268

McGinnis, D. F., Greinert, J., Artemov, Y., Beaubien, S., and Wüest, A. (2006). Fate of Rising Methane Bubbles in Stratified Waters: How Much Methane Reaches the Atmosphere? *J. Geophys. Res. Oceans* 111 (C9), C09007(1-15). doi:10.1029/2005JC003183

Natchimuthu, S., Sundgren, I., Gålfalk, M., Klemedtsson, L., Crill, P., Danielsson, Å., et al. (2016). Spatio-temporal Variability of lake CH4 Fluxes and its Influence on Annual Whole lake Emission Estimates. *Limnol. Oceanogr.* 61 (S1), S13–S26. doi:10.1002/lno.10222

Niculescu, S., Boissonnat, J.-B., Lardeux, C., Roberts, D., Hanganu, J., Billey, A., et al. (2020). Synergy of High-Resolution Radar and Optical Images Satellite for Identification and Mapping of Wetland Macrophytes on the Danube Delta. *Remote Sensing* 12 (14), 2188. doi:10.3390/rs12142188

Oosterberg, W., Staras, M., Bogdan, L., Buijse, A. D., Constantinescu, A., Coops, H., et al. (2000). *Ecological Gradients in the Danube Delta Lakes: Present State and Man-Induced Changes*. Lelystad: RIZA the Netherlands, Danube Delta Natinal Institute Romania and Danube Delta Biosphere Reserve Authority Romania. RIZA rapport nr. 2000.015.

Ostrofsky, M. L., and Miller, C. (2017). Photosynthetically-mediated Calcite and Phosphorus Precipitation by Submersed Aquatic Vascular Plants in Lake Pleasant, Pennsylvania. *Aquat. Bot.* 143, 36–40. doi:10.1016/j.aquabot.2017.09.002

Panin, N. (1996). Danube Delta - Genesis, Evolution and Sedimentology. *Geo-Eco-Marina* 1, 11–34.

Pavel, A., Durisch-Kaiser, E., Balan, S., Radan, S., Sobek, S., and Wehrli, B. (2009). Sources and Emission of Greenhouse Gases in Danube Delta Lakes. *Environ. Sci. Pollut. Res. Int.* 16 Suppl 1 (1), S86–S91. doi:10.1007/s11356-009-0182-9

Raymond, P. A., Hartmann, J., Lauerwald, R., Sobek, S., McDonald, C., Hoover, M., et al. (2013). Global Carbon Dioxide Emissions from Inland Waters. *Nature* 503 (7476), 355–359. doi:10.1038/nature12760

Regnier, P., Friedlingstein, P., Ciais, P., Mackenzie, F. T., Gruber, N., Janssens, I. A., et al. (2013). Anthropogenic Perturbation of the Carbon Fluxes from Land to Ocean. *Nat. Geosci* 6, 597–607. doi:10.1038/ngeo1830

Sachs, N. M. (2019). The Paris Agreement in the 2020s: Breakdown or Breakup. *Ecol. LQ* 46, 865. doi:10.15779/Z38H708140

Sorrell, B. K., and Brix, H. (2013). "Gas Transport and Exchange through Wetland Plant Aerenchyma," in *Methods in Biogeochemistry of Wetlands*. Editors R. DeLaune, K. Reddy, C. Richardson, and J. Megonigal (Madison WI: Soil Science Society of America), 177–196.

Staehr, P. A., Testa, J. M., Kemp, W. M., Cole, J. J., Sand-Jensen, K., and Smith, S. V. (2012). The Metabolism of Aquatic Ecosystems: History, Applications, and Future Challenges. *Aquat. Sci.* 74 (1), 15–29. doi:10.1007/s00027-011-0199-2

Stanley, E. H., Casson, N. J., Christel, S. T., Crawford, J. T., Loken, L. C., and Oliver, S. K. (2016). The Ecology of Methane in Streams and Rivers: Patterns, Controls, and Global Significance. *Ecol. Monogr.* 86 (2), 146–171. doi:10.1890/15-1027

Tortell, P. D., Bittig, H. C., Körtzinger, A., Jones, E. M., and Hoppema, M. (2015). Biological and Physical Controls on N2, O2, and CO2distributions in Contrasting Southern Ocean Surface Waters. *Glob. Biogeochem. Cycles* 29 (7), 994–1013. doi:10.1002/2014GB004975

Ulseth, A. J., Hall, R. O., Boix Canadell, M., Madinger, H. L., Niayifar, A., and Battin, T. J. (2019). Distinct Air-Water Gas Exchange Regimes in Low- and High-Energy Streams. *Nat. Geosci.* 12 (4), 259–263. doi:10.1038/s41561-019-0324-8

UNEP-WCMC (UN Environment Programme World Conservation Monitoring Centre) (2021). World Heritage Datasheet - Danube Delta [Online]. Available at: http://world-heritage-datasheets.unep-wcmc.org/datasheet/output/site/danube-delta/ (Accessed 07 27, 2021).

UNESCO (2021). Ecological Sciences for Sustainable Development. Danube Delta. [Online]. Available at: http://www.unesco.org/new/en/natural-sciences/environment/ecological-sciences/biosphere-reserves/europe-north-america/romaniaukraine/danube-delta/ (Accessed 07 26, 2021).

Weiss, R. F. (1974). Carbon Dioxide in Water and Seawater: the Solubility of a Non-ideal Gas. *Mar. Chem.* 2 (3), 203–215. doi:10.1016/0304-4203(74)90015-2

Weiss, R. F. (1971). Solubility of Helium and Neon in Water and Seawater. *J. Chem. Eng. Data* 16 (2), 235–241. doi:10.1021/je60049a019

Wiesenburg, D. A., and Guinasso, N. L., Jr (1979). Equilibrium Solubilities of Methane, Carbon Monoxide, and Hydrogen in Water and Sea Water. *J. Chem. Eng. Data* 24 (4), 356–360. doi:10.1021/je60083a006

Zhou, J., Delille, B., Brabant, F., and Tison, J.-L. (2014). Insights into Oxygen Transport and Net Community Production in Sea Ice from Oxygen, Nitrogen and Argon Concentrations. *Biogeosciences* 11 (18), 5007–5020. doi:10.5194/bg-11-5007-2014

Conflict of Interest: The authors declare that the research was conducted in the absence of any commercial or financial relationships that could be construed as a potential conflict of interest.

Publisher's Note: All claims expressed in this article are solely those of the authors and do not necessarily represent those of their affiliated organizations, or those of the publisher, the editors and the reviewers. Any product that may be evaluated in this article, or claim that may be made by its manufacturer, is not guaranteed or endorsed by the publisher.

Copyright © 2022 Maier, Canning, Brennwald, Teodoru and Wehrli. This is an open-access article distributed under the terms of the Creative Commons Attribution License (CC BY). The use, distribution or reproduction in other forums is permitted, provided the original author(s) and the copyright owner(s) are credited and that the original publication in this journal is cited, in accordance with accepted academic practice. No use, distribution or reproduction is permitted which does not comply with these terms.

frontiers in Environmental Science

ORIGINAL RESEARCH
published: 31 March 2022
doi: 10.3389/fenvs.2022.834829

Lake Sediment Methane Responses to Organic Matter are Related to Microbial Community Composition in Experimental Microcosms

Brittni L. Bertolet[1,2]*, *Cristian Koepfli*[1] *and Stuart E. Jones*[1]

[1]Department of Biological Sciences, University of Notre Dame, Notre Dame, IN, United States, [2]Department of Ecology and Evolutionary Biology, University of California, Irvine, Irvine, CA, United States

Lake sediment microbial communities mediate carbon diagenesis. However, microbial community composition is variable across lakes, and it is still uncertain how variation in community composition influences sediment responses to environmental change. Sediment methane (CH_4) production has been shown to be substantially elevated by increased lake primary productivity and organic matter supply. However, the magnitude of the response of CH_4 production varies across lakes, and recent studies suggest a role for the microbial community in mediating this response. Here, we conducted sediment incubation experiments across 22 lakes to determine whether variation in sediment microbial community composition is related to the response of sediment CH_4 production to increases in organic matter. We sampled the 22 lakes across a gradient of pH in order to investigate lakes with variable sediment microbial communities. We manipulated the incubations with additions of dried algal biomass and show that variation in the response of CH_4 production to changes in organic matter supply is significantly correlated with metrics of sediment microbial community composition. Specifically, the diversity and richness of the non-methanogen community was most predictive of sediment CH_4 responses to organic matter additions. Additionally, neither metrics of microbial abundance nor preexisting organic matter availability explained meaningful variation in the response. Thus, our results provide experimental support that differences in sediment microbial communities influences CH_4 production responses to changes in organic matter availability.

Keywords: methanogenesis, structure-function links, microbial community structure, eutrophication, sediment carbon cycling

OPEN ACCESS

Edited by:
Yves T. Prairie, Université du Québec à Montréal, Canada

Reviewed by:
Sophie Crevecoeur, Environment and Climate Change, Canada
Annika Vaksmaa, Royal Netherlands Institute for Sea Research (NIOZ), Netherlands

***Correspondence:**
Brittni L. Bertolet
brittni.bertolet@uci.edu

Specialty section:
This article was submitted to Biogeochemical Dynamics, a section of the journal Frontiers in Environmental Science

Received: *13 December 2021*
Accepted: *11 March 2022*
Published: *31 March 2022*

Citation:
Bertolet BL, Koepfli C and Jones SE (2022) Lake Sediment Methane Responses to Organic Matter are Related to Microbial Community Composition in Experimental Microcosms. Front. Environ. Sci. 10:834829. doi: 10.3389/fenvs.2022.834829

1 INTRODUCTION

Methane (CH_4) production in lake sediments fuels lake greenhouse gas emissions and is a contributor to atmospheric CH_4 concentrations (Bastviken et al., 2011). Variation in CH_4 production across lakes has been shown to be correlated with multiple biotic and abiotic variables, including temperature (Duc et al., 2010; Yvon-Durocher et al., 2014; de Jong et al., 2018), stratification dynamics (Fallon et al., 1980; Ford et al., 2002), organic matter availability and lability (West et al., 2012; West et al., 2015; DelSontro et al., 2016; Grasset et al., 2018), and microbial community composition (Bertolet et al., 2019). Understanding sources of variation in lake CH_4

production has improved our ability to predict how lake CH_4 production and emission may change under future environmental change scenarios.

Recent work has highlighted the role of autochthonous organic matter (OM) in fueling anaerobic decomposition and CH_4 production across lakes (Deemer et al., 2016; West et al., 2016). Thus, the global eutrophication of inland waters is expected to increase lake CH_4 emissions (Davidson et al., 2018; DelSontro et al., 2018; Sepulveda-Jauregui et al., 2018; Beaulieu et al., 2019). However, the magnitude of the response of lake CH_4 dynamics to increases in autochthonous OM has been shown to differ across lakes at both the laboratory (West et al., 2015) and ecosystem (Bertolet et al., 2020) scales. Determining sources of variation in the relationship between autochthonous OM and lake CH_4 production is thus essential for constraining future predictions of lake CH_4 dynamics.

Variation in the response of lake CH_4 production to autochthonous OM supply may be related to the same factors that influence CH_4 production, such as temperature, oxygen dynamics, or historic OM availability. However, during eutrophication, sediment temperature and anoxia are often stabilized due to increased stratification (Foley et al., 2012; Müller et al., 2012), and variation in the CH_4 production response to increases in OM remains evident even in laboratory experiments when temperature and anoxia are constant (West et al., 2015). Preexisting OM availability may influence the response if increases in autochthonous OM primes the carbon pool and allows for the use of previously unavailable OM (Guenet et al., 2010; Zhang et al., 2017). However, few studies have tested this in lake sediments.

Cross-lake differences in the sediment microbial community are another potentially important source of variation in sediment responses to incoming autochthonous OM. Advances in our ability to observe and quantify microbial communities have revealed tremendous diversity in sediment microbial community composition both within and across lakes (Steger et al., 2011; Bertolet et al., 2019; Orland et al., 2020; Wang et al., 2020). CH_4 is produced via the anaerobic metabolism of methanogenic archaea (hereafter referred to as "methanogens"). However, methanogens can utilize only a limited number of substrates (acetate, CO_2/H_2, formate, methylated compounds, etc.) and are reliant on other members of the microbial community (hereafter referred to as "non-methanogens") to breakdown complex autochthonous OM into methanogenesis precursors (Nozhevnikova et al., 2007; Liu and Whitman, 2008). Because of these complex biogeochemical interactions, community composition and abundance have the potential to influence sediment responses to increases in autochthonous OM.

Comparative studies have provided substantial support for the role of microbial community composition in influencing sediment CH_4 and CO_2 production (Torres et al., 2011; Ji et al., 2016; Bertolet et al., 2019; Xia et al., 2020; Yang et al., 2020). For example, in north temperate lakes, community composition of the non-methanogen community was significantly related to lake CH_4 production after accounting for variation in primary productivity across 14 lake sediments (Bertolet et al., 2019). Additionally, Torres et al. (2011) showed that heterotrophic activity was related to microbial biomass in three lake sediments that differed in trophic status. However, few studies have experimentally tested the influence of microbial community composition on sediment function or considered how microbial community composition may interact with changing OM conditions to influence sediment function.

Here, we test the hypothesis that microbial community composition influences the response of lake CH_4 production to autochthonous OM. To do so, we designed sediment slurry incubation experiments with variable microbial community composition and OM supply. To capture variation in microbial community composition, we conducted incubations across 22 lake sediments, chosen along a pH gradient (range: 3.9–7.4) at the sediment-water interface, which has been previously shown as an environmental determinant of microbial community composition (Bertolet et al., 2019). We predicted that metrics of both microbial community composition and abundance would be correlated with the magnitude of the response of CH_4 production to OM additions. Our experimental design allows for a mechanistic understanding of the role of microbial communities in sediment carbon processing and thus could help to predict future CH_4 production using quantitative metrics of sediment microbial communities.

2 METHODS AND MATERIALS

2.1 Experimental Design

Lakes were located in northern Wisconsin, United States. We sampled 13 lakes between June and August 2019 and an additional 9 lakes between July and August 2020 (**Table 1**). During each sampling season, the sampled lakes represented the full range of the pH gradient. To construct sediment slurry incubations, we sampled sediment and hypolimnetic water from the deepest point of every lake. Sediment was collected from the top 15 cm of the sediment surface with an Eckman dredge and hypolimnetic water was collected from 0.25 m above the sediment surface with a Van Dorn water sampler. There was some degree of atmospheric oxygen exposure during sampling for both hypolimnion water samples and sediment samples, however we attempted to mitigate the length of exposure. Hypolimnion water samples were sealed immediately after collection the field. Sediment samples were collected in 5-gallon open-air buckets. Upon return to the laboratory, sediment was sampled from the bottom of the bucket for construction of sediment incubations and construction occurred within 5 h of collection. Prior to construction, all samples were stored in the dark at 4°C.

We constructed experimental sediment incubations in 300 ml glass serum bottles containing 50 ml of sediment and 50 ml of anoxic hypolimnion water. To quantify the difference in CH_4 production under increased OM supply, we conducted triplicate incubations with and without additions of OM. For incubations treated with the addition, we added 20 mg of dried algal biomass (*Scenedesmus obliquus*). *S. obliquus* was grown in Bold's Basal Medium under constant aeration with atmospheric carbon dioxide concentrations. To generate a homogeneous dried

TABLE 1 | Summary of environmental variables of sampled lakes, including pH and dissolved oxygen (DO) concentration at the sediment-water interface, sediment organic matter content (OM %), and epilimnion chlorophyll *a* concentration (chl *a*).

Lake name (ID)	Latitude	Longitude	Year	pH	DO (mg L^{-1})	OM (%)	chl a (μg L^{-1})
Birch (BH)	46.21790	−89.83819	2020	7.1	0.07	21.0	10.6
Bolger (BO)	46.23012	−89.49446	2019	6.6	0.18	26.7	12.1
Brandy (BY)	45.90675	−89.70108	2019	6.9	0.16	24.1	30.8
Brown (BR)	46.21793	−89.47365	2019	7.3	0.09	28.5	10.4
Crampton (CR)	46.20989	−89.47357	2019	6.0	0.71	26.5	6.2
Cranberry (CB)	46.23244	−89.56998	2019	3.9	0.29	36.7	3.3
Crystal Bog (CYB)	46.00800	−89.60570	2020	4.3	0.5	38.1	21.7
Horsehead (HH)	46.23325	−89.71534	2020	7.3	0.08	20.0	9.3
Hummingbird (HB)	46.24367	−89.50590	2019	4.9	0.38	35.9	6.6
Johnson (JS)	45.89971	−89.72118	2019	6.7	0.11	24.4	11.0
Misty (MI)	46.25265	−89.48140	2020	5.5	0.13	40.3	10.1
Morris (MO)	46.25709	−89.52120	2019	7.0	0.23	26.0	13.4
Nichols (NH)	46.10372	−89.68792	2020	5.6	0.09	35.2	9.9
North Gate (NG)	46.25873	−89.49735	2019	3.5	0.16	36.7	18.3
Paul (PA)	46.25261	−89.50357	2019	5.8	0.24	33.3	3.2
Peter (PE)	46.25288	−89.50359	2019	6.3	0.41	36.4	4.6
Street (SE)	46.09621	−89.70341	2020	5.2	1.09	31.2	7.5
Trout Bog (TB)	46.04127	−89.68613	2020	4.2	0.16	38.6	15.0
Tenderfoot (TF)	46.21787	−89.52921	2019	6.8	0.13	26.3	10.5
Tender Bog (TR)	46.22994	−89.52722	2020	3.9	0.17	43.3	8.7
Ward (WA)	46.25829	−89.51732	2019	7.4	0.17	25.1	3.4
West Long (WL)	46.23591	−89.50156	2020	5.8	0.15	36.1	9.9

material for additions, we centrifuged the wet material in 40 ml batches at 4,000 rpm for 10 minutes, extracted the pellet, and dried the pellet for 7 days. All dried material was added to a single vial and homogenized before addition to incubations. After additions, we capped and sealed the serum bottles with rubber septa and aluminum crimp seals and homogenized the sediment slurries by manual shaking for 1 min. We then purged the headspace of each incubation with N_2 gas for 5 min to maintain anoxic conditions. We incubated the bottles in the dark at 4°C to simulate conditions at the bottom of a lake and we incubated the bottles for approximately 28 days.

2.2 Net Methane Production

During the length of the incubation period, we estimated net CH_4 production rates from each incubation by iteratively sampling from the headspace for CH_4 concentration. The first sampling occurred 24 h after purging the headspace and sealing the incubations. We then sampled every 3–5 days, as well as at end of incubation (approximately 28 days), for a minimum of 4 sampling points for each incubation (**Supplementary Figure S1**). To sample for CH_4 concentration, we extracted 10 ml of headspace gas using a 25-gauge needle pierced through the rubber septa. Samples were immediately injected into airtight glass vials for measurement of CH_4 concentration on an Agilent 6890 Gas Chromatograph with parameters previously described in West et al. (2016). We then added 10 ml of N_2 back to the headspace to maintain pressure. We inferred net rates of CH_4 production, after accounting for the headspace dilution, from the slope of a linear regression fit to the time-series (**Supplementary Figure S1**). For incubations in which CH_4 did not accumulate over time ($N = 4$), we assumed a net CH_4 production of zero.

2.3 Microbial Community Composition and Abundance

During the initial collection of lake sediments for construction of incubations, we sampled approximately 1 g of sediment for analysis of microbial community composition and abundance. Sediments were stored in sterile plastic 1.5 ml cryovial tubes at −80°C until DNA extraction. We conducted a single DNA extraction for each lake using 0.25 g of sediment and the DNeasy PowerSoil Pro kit (Qiagen, Hilden, DE) according to manufacturer instructions. The extracted DNA was used as template for 16S rRNA paired-end gene sequencing to determine differences in community composition. Extracted DNA was also used as template in digital droplet polymerase chain reactions (ddPCR) of the 16S rRNA gene and the alpha subunit of methyl coenzyme reductase (mcrA) gene to determine total bacterial + archaeal abundance and methanogen abundance, respectively.

For 16S rRNA paired-end gene sequencing, the V4 region of the 16S rRNA gene was amplified in a 15 μl PCR reaction with dual indexed primers: 515F (5′-GTGCCAGCMGCCGCGGTAA-3′) and 806R (5′-GGACTACHVGGGTWTCTAAT- 3′) (Kozich et al., 2013). Amplified DNA served as template for high-throughput paired-end (2 × 250 bp) sequencing on an Illumina MiSeq v2 Standard flow cell at the Michigan State University Research Technology Support Facility. Sequencing resulted in 1,279,135 high-quality reads across all lake samples. Raw sequence reads are available at the NCBI Sequence Read Archive (Accession # PRJNA813558). To determine differences in microbial community composition, we used the mothur (version 1.44.3) bioinformatics pipeline for merging of paired-end reads, quality filtering, clustering, and taxonomic classification (Kozich et al., 2013). To determine community

membership, operational taxonomic units (OTUs) were defined at 97% similarity using the *dist.seqs* command and a 0.03 cutoff. Representative sequences for each OTU were aligned and classified against the RDP classifier database (version 18) (Wang et al., 2007).

To quantify abundance of the 16S rRNA gene and mcrA gene, we conducted ddPCR using the BioRad QX200 Droplet Digital PCR system. The indicator genes were amplified in separate 20 µl ddPCR reactions using a BioRad C1000 Touch thermocycler with EvaGreen as the reporting dye. For amplification of the 16S rRNA gene, each reaction contained 2 µl of 1/100 diluted sediment DNA template, 1X Q200 ddPCR EvaGreen Supermix, and 0.1 µM of each primer targeting 16S rRNA: 338F (5′-ACTCCTACGGGA GGCAG-3′) and 805R (5′-GACTACCAGGGTATCTAATC- 3′) (Yu et al., 2005). For amplification of the mcrA gene, each reaction contained 1 µL of 1/10 diluted sediment DNA template, 1X Q200 ddPCR EvaGreen Supermix, and 0.25 µM of each primer targeting mcrA: mcrAqF (5′-AYGGTATGGARCAGTACGA- 3′) and mcrAqR (5′-TGVAGRTCGTABCCGWAGAA-3′) (West et al., 2012). Thermocycling conditions for both indicator genes are reported in **Supplementary Table S1**. Additionally, for both assays, we performed three technical replicates on a subset of the samples to verify precision. Technical replicates indicated high precision of the assays (**Supplementary Figure S2**), and we normalized copy numbers to copies per gram of sediment to be comparable across samples.

2.4 Lake Environmental Variables

During sampling for construction of incubations, we measured dissolved oxygen concentration and pH at the sediment-water interface using a YSI Professional Plus Multiparameter meter (Yellow Springs Instruments, Yellow Springs, OH, United States). We also collected additional sediment to quantify sediment OM content and epilimnion water for quantification of water column chlorophyll *a* (chl *a*) concentrations, as metrics of differences in OM availability and lake trophic status. We quantified percent OM of sediment using loss on ignition measurements of dried sediment samples (Heiri et al., 2001). To quantify water column chl *a*, we used particles from 450 ml of the epilimnion sample captured on a 0.7 µm glass fiber filter and we analyzed the sample using methanol extraction and fluorometry (Welschmeyer, 1994).

2.5 Statistical Analyses

We conducted all statistical analyses in R (R Core Team, 2018) using the base and vegan (Oksanen et al., 2017) packages. To quantify variation in sediment microbial community composition across the 22 lakes, we first rarified every sample to 39,948 sequence reads to be comparable across sample sequencing depths. We then identified methanogen OTUs by the presence of "Methano" in taxonomic assignments, as a conservative means of identifying methanogens, and manually curated our list of putative methanogen genera for known methanogen taxa. Some methanogenic microbes were likely not identified based on this method (Kharitonov et al., 2021), but our approach did allow for estimation of relative sequence recovery of known methanogenic groups. We then conducted the following analyses for both the methanogen and non-methanogen community.

To quantify variation in microbial community composition across the 22 lakes, we standardized OTU matrices of both communities to reflect relative sequence recovery and generated pairwise Bray-Curtis dissimilarity matrices of each community using the *vegdist* function. We then generated principal coordinates for each community based on the Bray-Curtis dissimilarity matrices using the *cmdscale* function. The first principal coordinate axes (PCoA 1) represent 40.6 % and 29.2% of the variation in the methanogen and non-methanogen community, respectively. We also tested for effects of environmental conditions on community composition using permutational multivariate ANOVA (PERMANOVA) tests using the adonis function in R (Anderson, 2001). We evaluated significance of the PERMANOVA statistic using 1000 permutations of the dissimilarity matrices for each community. To quantify differences in microbial community diversity and richness, we also calculated the Shannon Diversity Index and community richness, or the sum of OTUs present in each sample. Thus, we used the Shannon Index, community richness, and the PCoA 1 scores for both communities as metrics of community composition in subsequent analyses.

To quantify the response of sediment CH_4 production to the OM additions across the 22 lakes, we calculated the difference in mean net CH_4 production between incubations with and without OM additions (ΔCH_4 production) for every lake. We also quantified the maximum percent utilization of OM additions by calculating the total CH_4 produced through the length of the experiment divided by the amount of OM supplied. For the dried autochthonous OM supplied, we assumed a carbon content of 61.5% based on measurements from West et al. (2015). Finally, we determined significant correlations between the log-transformed ΔCH_4 production and metrics of microbial community composition and abundance using simple linear regressions. We used the log-transformation to abide by assumptions of normally distributed data. We also determined the correlation between log-transformed ΔCH_4 production and metrics of preexisting OM supply (sediment OM %, and water column chl *a* concentration). Data, metadata, and code for all analyses are available on GitHub at https://github.com/brittnibertolet/CH4response2OM.

3 RESULTS

3.1 Microbial Community Composition and Abundance

Sampling along a gradient of pH resulted in sediment incubations with variable microbial communities. After rarifying, sequencing recovered 367 methanogen OTUs and 26,494 non-methanogen OTUs. Methanogen reads represented 1.5% of the total sequence reads and the relative sequencing reads of methanogens ranged from 0.7 % to 2.8% across all lakes. As hypothesized from previous work (Bertolet et al., 2019), the composition of both

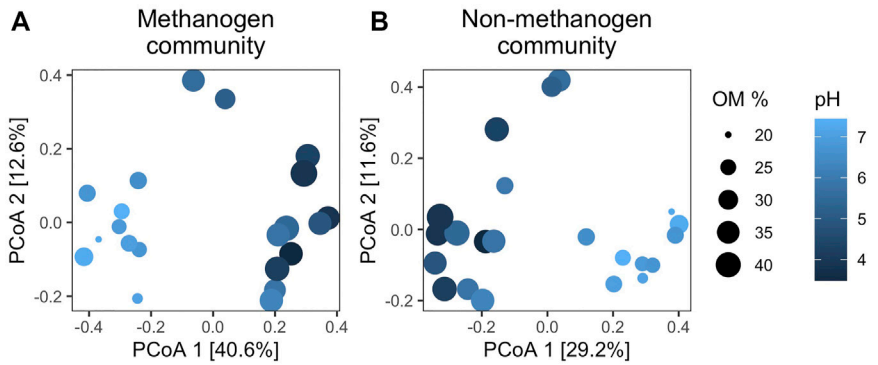


FIGURE 1 | First two principal coordinates of the methanogen community composition **(A)** and the non-methanogen community composition **(B)**. Permutational analysis of variance indicated that methanogen community composition was significantly related to pH ($F_{22,1}$ = 9.24, p = 0.001) and sediment organic matter content ($F_{22,1}$ = 8.58, p = 0.001). Similarly, non-methanogen community composition was also significantly related to ($F_{22,1}$ = 5.77, p = 0.001) and sediment organic matter content ($F_{22,1}$ = 6.01, p = 0.001).

the methanogen and non-methanogen community was significantly related to pH and sediment OM (**Figure 1**). As such, PCoA Axis 1 of both communities was significantly correlated with pH (methanogen: R^2 = 0.73, p < 0.001, non-methanogen: R^2 = 0.69, p < 0.001) and OM (methanogen: R^2 = 0.71, p < 0.001, non-methanogen R^2 = 0.76, p < 0.001). Additionally, the relative abundances of different methanogen genera (**Supplementary Figure S2**) and non-methanogen phyla (**Supplementary Figure S3**) varied across lakes.

Microbial richness and diversity varied significantly across the lake samples as well as between the methanogen and non-methanogen communities. Methanogen richness ranged from 13 to 60 OTUs, while non-methanogen richness ranged from 1,404 to 6,059 OTUs. Methanogen Shannon Index ranged from 1.7 to 2.8, while non-methanogen ranged from 4.9 to 7.3. Additionally, neither methanogen richness nor diversity were significantly correlated with environmental variables (pH, sediment OM %, or chl *a* concentration). In contrast, non-methanogen richness and Shannon Index were both significantly correlated with both pH and sediment OM % (**Supplementary Table S2**).

Digital droplet PCR of the 16S rRNA and mcrA genes also indicated variation in the total bacterial + archaeal abundance and methanogen abundance across lakes (**Supplementary Figure S4**). Total bacterial + archaeal abundance ranged from 3.07×10^5 to 1.22×10^8 copies per gram wet sediment. However, total bacterial + archaeal abundance was not related to sediment pH nor sediment OM %. Instead, total bacterial + archaeal abundance was significantly correlated with water column chl *a* concentration (R^2 = 0.24, p < 0.05; **Supplementary Figure S5**). Similarly, methanogen abundance ranged from 3.31×10^5 to 1.79×10^7 copies per gram wet sediment and was significantly correlated with 16S rRNA copy number (R^2 = 0.26, p < 0.05) and water column chl *a* concentration (R^2 = 0.19, p < 0.05; **Supplementary Figure S4**). However, the relative sequence reads of methanogens, derived from the 16S rRNA Illumina sequencing, was not related to ddPCR estimates of microbial abundance nor chl *a* concentration. Additionally, neither differences in community composition nor abundance were related to sample year (**Supplementary Table S4**).

3.2 Methane Production Responses to Organic Matter Additions

Rates of CH_4 production were variable across lakes and were significantly influenced by autochthonous OM additions. OM additions increased the net CH_4 production rate across all lakes (Kruskal-Wallis test: χ^2 = 73.2, p < 0.001; **Figure 2**). However, the magnitude of the response (ΔCH_4 production) varied and ranged from 1.1 to 27.3 μmol CH_4 L sediment slurry^{-1} day^{-1}. Additionally, maximum potential utilization of OM ranged from 0.28 % to 7.1% of algal carbon added to a slurry.

Variation in the ΔCH_4 production was related to differences in both metrics of sediment microbial community composition and pH across the sampled lake sediments (**Figure 3**). Specifically, the Shannon Diversity Index and richness of the non-methanogen explained the most amount of variation in ΔCH_4 production, and pH and metrics of methanogen community composition were also significantly correlated with the log-transformed ΔCH_4 production (**Table 2**). However, neither abundance metrics nor environmental variables related to OM supply (sediment OM % or water column chl *a*) explained variation in ΔCH_4 production, despite significant influences of sediment OM % on both methanogen and non-methanogen community composition (**Figure 1**). Additionally, the sample year did not influence patterns ΔCH_4 production (**Supplementary Table S2**).

4 DISCUSSION

Lake CH_4 production and emission are consistently positively related to lake primary productivity and trophic status, but, in both laboratory and field scenarios, there exists large variation in the magnitude of the temporal response of CH_4 dynamics to increases in OM (West et al., 2015; Yakimovich et al., 2018; Bertolet et al., 2020; Yang et al., 2020). Understanding sources of

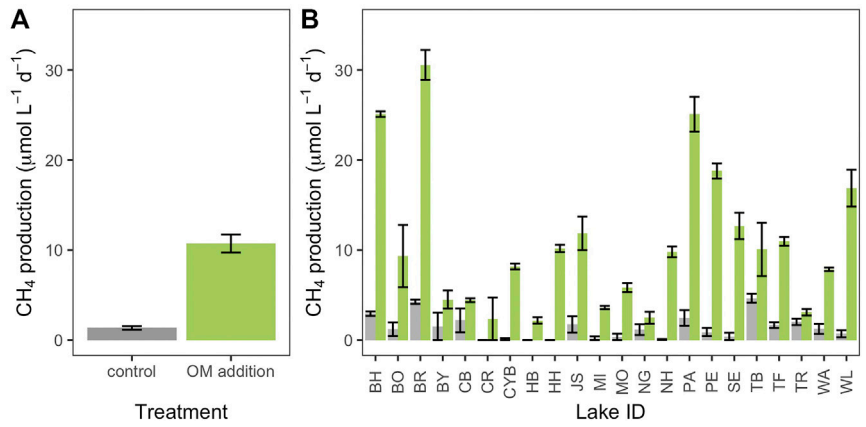


FIGURE 2 | Net methane (CH_4) production rates of sediment slurry incubations across organic matter (OM) additions (grey: control; green: OM addition). OM additions significantly increased the net CH_4 production rate across all lakes (**(A)**; KruskalWallis test: $\chi^2 = 73.2$, $p < 0.001$). However, the magnitude of increase was variable across lakes **(B)**. Error bars indicate one standard error.

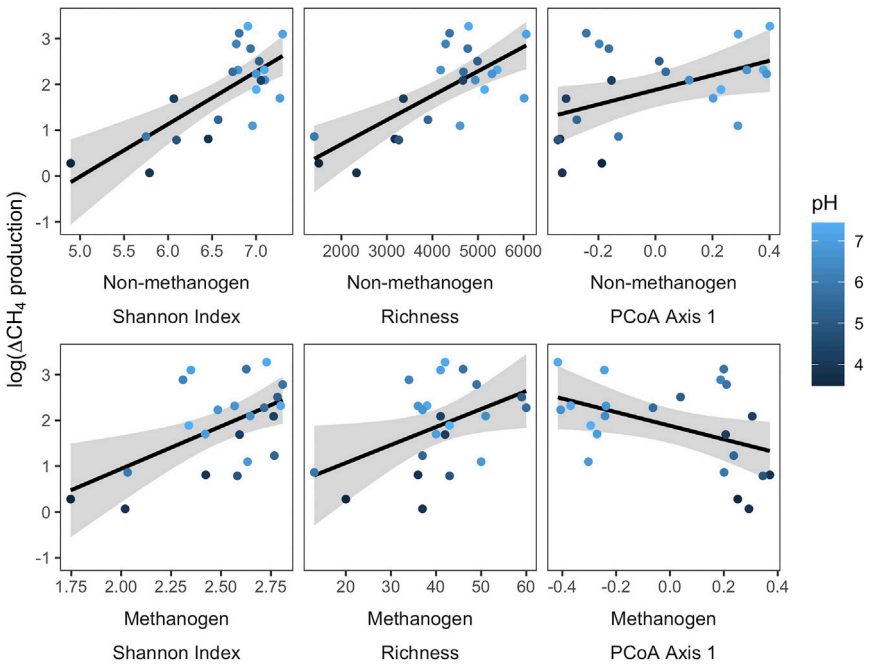


FIGURE 3 | Correlations between the log-transformed difference in net methane production amongst organic matter additions (ΔCH_4 production) and metrics of microbial community composition. Statistics are reported in **Table 2**.

this variation is essential for making quantitative predictions under future environmental change scenarios (DelSontro et al., 2018). In the present study, we show that variation in the response of lake CH_4 production to increases in OM is correlated with pH-mediated differences in sediment microbial community composition (**Figure 3**). Specifically, metrics of the non-methanogen community composition were the best predictors of CH_4 production responses to increasing OM, especially as compared to the methanogen community or other variables hypothesized to influence CH_4 responses to OM, such as preexisting OM availability and metrics of microbial abundance (**Table 2**). By comparing multiple metrics of community composition, as well as specifically investigating both the methanogen and non-methanogen community, we provide critical evidence of how lake sediment responses to environmental change may be improved by incorporating variation in microbial community composition.

A growing body of literature describes the links between lake sediment microbial community composition and lake pH and OM content (Kotsyurbenko et al., 2004; Bertolet et al., 2019; Orland

TABLE 2 | Summary statistics of linear regressions between the log-transformed difference in net CH_4 production between organic matter additions (ΔCH_4 production) and environmental and microbial predictors.

Response	Predictor	R^2	*p*-value
log (ΔCH_4 production)	Non-methanogen Shannon Index*	0.52	<0.001
	Non-methanogen richness*	0.52	<0.001
	pH*	0.35	<0.01
	Methanogen Shannon Index*	0.32	<0.01
	Non-methanogen PCoA 1*	0.21	<0.05
	Methanogen PCoA 1*	0.20	<0.05
	Methanogen richness*	0.19	<0.05
	OM %	0.14	0.08
	chl a	0.06	0.26
	average control CH4 production	0.04	0.31
	16S copies	0.01	0.61
	mcrA copies	0.004	0.76

Predictors are ordered by the coefficient of determination (R^2) and significant relationships are indicated with a "".*

et al., 2020). We reproduce established patterns in lake sediment microbial community assembly, in which the methanogen and non-methanogen communities are differentiated across pH and sediment OM% (**Figure 1**). Further, as previous research has established that lakes have variable CH_4 production responses to changes in OM (West et al., 2015; Grasset et al., 2018), we used this gradient of pH to test the hypothesis that sediment microbial community composition influences the effect size of the CH_4 production and OM relationship.

In our study, there was substantial variation in the CH_4 production response to OM additions (**Figure 2**). The difference in net CH_4 production between incubations with and without additions of OM (ΔCH_4 production) ranged from 1.1 to 27.3 μmol CH_4 L sediment $slurry^{-1}$ day^{-1}. As we hypothesized, variation in ΔCH_4 production was significantly correlated with pH-mediated differences in microbial community diversity, richness, and composition (**Table 2**). Specifically, lakes with microbial communities associated with higher pH environments had greater CH_4 production responses to additions in OM (**Figure 3**). While it is difficult to disentangle the effects of pH and microbial community composition on ΔCH_4 production, previous research does suggest that pH structures the differences in microbial community composition across lakes (Xiong et al., 2012; Bertolet et al., 2019; Orland et al., 2020) and that the mechanistic relationship between pH and CH_4 production relies on pH effects on competitive interactions between methanogens and other fermenting bacteria (Phelps and Zeikus, 1984; Ye et al., 2012). Additionally, in a replicated common garden experiment with contrasting pH environments, microbial community composition influenced rates of CH_4 and CO_2 production independent of the pH environment (Bertolet et al., in press).

Our results suggest that relationships between microbial community composition and pH may be used to predict the response of sediment CH_4 production to changes in OM. Specifically, information about variation in the non-methanogen community was most predictive of function, and so we suggest that syntrophic interactions, or the supply of substrate by one group to another, between microbial functional groups in lake sediments are likely an important control on rates of CH_4 production. Production of methanogenesis precursors has previously been shown to be limiting (Kotsyurbenko et al., 2004) and methanogens are reliant on heterotrophic and acetogenic bacteria for the conversion of complex organic material into substrates that can be utilized (Liu and Whitman, 2008). However, we still lack the ability to identify the functional capacity of various microbial groups, so quantifying these interactions remains difficult.

Further research is needed to identify how variation in microbial community diversity and composition relates to functional diversity within the microbial community, and how interactions between members may lead to differences in emergent function. Currently, few OTUs in our dataset can be functionally identified based on taxonomy or other means. Metagenomic analyses have made significant strides in functionally defining sediment microorganisms (Vavourakis et al., 2018; Rathour et al., 2020), however few studies have measured ecosystem function in conjunction with metagenomic characterization or identified statistical relationships that can be used for prediction. Additionally, measurements of microbial metabolic traits, either *in situ* or in laboratory, and at both population and community scales, would greatly improve our ability to differentiate important microbial function groups and incorporate their variation across space and time into understanding of ecosystem function.

In the absence of the ability to constrain microbial functional groups, we suggest that aggregated metrics of microbial community composition, such as diversity metrics, richness, and composition scores, may be used to distinguish possible sediment responses to environmental change. Interestingly, diversity and richness metrics explained more variation than composition scores, indicating that evenness of composition is potentially less informative than richness. This approach to establishing links between microbial community diversity and ecosystem function that uses OTU richness and diversity is supported by other studies that suggest that taxonomically resolved information of microbial communities is not predictive of sediment function (Ji et al., 2016; Orland et al., 2020), and which highlight the need to move beyond taxonomy in order to identify metrics of functional groups that can be used in predictive models (Hall et al., 2018). Additionally, we also find that estimates of microbial abundance from ddPCR were not related to differences in ΔCH_4 production (**Table 2**). This is consistent with previous research indicating that changes in sediment CH_4 production due to changes in OM supply are likely due to changes in per cell activity and not changes in abundance (West et al., 2012).

It is worth noting that we also tested for effects of preexisting OM conditions on ΔCH_4 production, as previous work has hypothesized that temporal response of lake CH_4 production to eutrophication may be related to current or historical trophic state (Bertolet et al., 2020; Yang et al., 2020). However, we found that there were no significant correlations between the strength of the response and metrics of preexisting OM availability

(sediment OM % and water column chl *a*; **Table 2**). Further, we observed no evidence of a priming effect, as the maximum potential utilization of the algal supplied carbon never exceeded even 10%. In temperate lakes, sediment carbon pools are highly recalcitrant and primarily consisting of allochthonous derived material (Sobek et al., 2009), which may decouple the effect of preexisting OM availability from current responses to incoming autochthonous OM.

By conducting experimental manipulations of 22 lake sediments, we provide a direct line of evidence supporting links between lake pH, sediment microbial community composition, lake trophic status, and sediment CH_4 production. Specifically, we see that microbial community composition and pH are correlated and positively predict the response of lake CH_4 production to increases in OM. Previous research has begun to highlight the importance of incorporating variation in sediment microbial communities into ecosystem conceptual and predictive models (Graham et al., 2016; Hall et al., 2018), and, as the global eutrophication of inland freshwater ecosystems is likely to increase CH_4 production (DelSontro et al., 2018; Beaulieu et al., 2019), understanding sources of variation in the magnitude of change is thus critical for predicting future lake carbon cycling. We encourage further research that identifies important microbial functional groups and that utilizes relationships between the environment, microbial community composition, and ecosystem function to understand and predict variation in lake CH_4 production and emission.

DATA AVAILABILITY STATEMENT

Data and metadata presented in the study are deposited in the Zenodo repository: https://doi.org/10.5281/zenodo.6368660. Raw sequence reads are available at the NCBI Sequence Read Archive (Accession # PRJNA813558).

AUTHOR CONTRIBUTIONS

BB and SJ developed research design and hypotheses. BB collected field data and conducted experiments with guidance from SJ. CK and BB conducted molecular analyses. BB conducted statistical analyses with guidance from SJ and CK. BB wrote initial manuscript. All authors contributed to data interpretation, provided written feedback, and approved the final version.

FUNDING

This research was supported by the National Science Foundation under Grants 1754363, 1754561, 1547866, and 2109350.

ACKNOWLEDGMENTS

We thank Sydney Louden, Gabriella Marines-Chio, Carly Olson, Randi Notte, and Ceara Talbot for assisting in field data collection. The University of Notre Dame Environmental Research Center provided logistic support.

SUPPLEMENTARY MATERIAL

The Supplementary Material for this article can be found online at: https://www.frontiersin.org/articles/10.3389/fenvs.2022.834829/full#supplementary-material

REFERENCES

Anderson, M. J. (2001). A New Method for Non-Parametric Multivariate Analysis of Variance. *Austral Ecol.* 26 (1), 32–46. doi:10.1111/j.1442-9993.2001.01070.pp.x

Bastviken, D., Tranvik, L. J., Downing, J. A., Crill, P. M., and Enrich-Prast, A. (2011). Freshwater Methane Emissions Offset the Continental Carbon Sink. *Science* 331 (6013), 50. doi:10.1126/science.1196808

Beaulieu, J. J., DelSontro, T., and Downing, J. A. (2019). Eutrophication Will Increase Methane Emissions from Lakes and Impoundments during the 21st century. *Nat. Commun.* 10, 1375. doi:10.1038/s41467-019-09100-5

Bertolet, B. L., Olson, C. R., Szydlowski, D. K., Solomon, C. T., and Jones, S. E. (2020). Methane and Primary Productivity in Lakes: Divergence of Temporal and Spatial Relationships. *J. Geophys. Res. Biogeosci.* 125 (9), e2020JG005864. doi:10.1029/2020JG005864

Bertolet, B. L., West, W. E., Armitage, D. W., and Jones, S. E. (2019). Organic Matter Supply and Bacterial Community Composition Predict Methanogenesis Rates in Temperate lake Sediments. *Limnol Oceanogr Lett.* 4 (5), 164–172. doi:10.1002/lol2.10114

Davidson, T. A., Audet, J., Jeppesen, E., Landkildehus, F., Lauridsen, T. L., Søndergaard, M., et al. (2018). Synergy between Nutrients and Warming Enhances Methane Ebullition from Experimental Lakes. *Nat. Clim Change* 8, 156–160. doi:10.1038/s41558-017-0063-z

de Jong, A. E. E., in 't Zandt, M. H., Meisel, O. H., Jetten, M. S. M., Dean, J. F., Rasigraf, O., et al. (2018). Increases in Temperature and Nutrient Availability Positively Affect Methane-Cycling Microorganisms in Arctic Thermokarst lake Sediments. *Environ. Microbiol.* 20 (12), 4314–4327. doi:10.1111/1462-2920.14345

Deemer, B. R., Harrison, J. A., Li, S., Beaulieu, J. J., DelSontro, T., Barros, N., et al. (2016). Greenhouse Gas Emissions from Reservoir Water Surfaces: A New Global Synthesis. *BioScience* 66, 949–964. doi:10.1093/biosci/biw117

DelSontro, T., Beaulieu, J. J., and Downing, J. A. (2018). Greenhouse Gas Emissions from Lakes and Impoundments: Upscaling in the Face of Global Change. *Limnol Oceanogr Lett.* 3, 64–75. doi:10.1002/lol2.10073

DelSontro, T., Boutet, L., St-Pierre, A., del Giorgio, P. A., and Prairie, Y. T. (2016). Methane Ebullition and Diffusion from Northern Ponds and Lakes Regulated by the Interaction between Temperature and System Productivity. *Limnol. Oceanogr.* 61, S62–S77. doi:10.1002/lno.10335

Duc, N. T., Crill, P., and Bastviken, D. (2010). Implications of Temperature and Sediment Characteristics on Methane Formation and Oxidation in lake Sediments. *Biogeochemistry* 100, 185–196. doi:10.1007/s10533-010-9415-8

Fallon, R. D., Harrits, S., Hanson, R. S., and Brock, T. D. (1980). The Role of Methane in Internal Carbon Cycling in Lake Mendota during Summer Stratification. *Limnol. Oceanogr.* 25 (2), 357–360. doi:10.4319/lo.1980.25.2.0357

Foley, B., Jones, I. D., Maberly, S. C., and Rippey, B. (2012). Long-Term Changes in Oxygen Depletion in a Small Temperate lake: Effects of Climate Change and Eutrophication. *Freshw. Biol.* 57, 278–289. doi:10.1111/j.1365-2427.2011.02662.x

Ford, P. W., Boon, P. I., and Lee, K. (2002). Methane and Oxygen Dynamics in a Shallow Floodplain Lake: The Significance of Periodic Stratification. *Hydrobiologia* 485, 97–110. doi:10.1023/a:1021379532665

Graham, E. B., Knelman, J. E., Schindlbacher, A., Siciliano, S., Breulmann, M., Yannarell, A., et al. (2016). Microbes as Engines of Ecosystem Function: When Does Community Structure Enhance Predictions of Ecosystem Processes? *Front. Microbiol.* 7, 214. doi:10.3389/fmicb.2016.00214

Grasset, C., Mendonça, R., Villamor Saucedo, G., Bastviken, D., Roland, F., and Sobek, S. (2018). Large but Variable Methane Production in Anoxic Freshwater Sediment upon Addition of Allochthonous and Autochthonous Organic Matter. *Limnol. Oceanogr.* 63, 1488–1501. doi:10.1002/lno.10786

Guenet, B., Neill, C., Bardoux, G., and Abbadie, L. (2010). Is There a Linear Relationship between Priming Effect Intensity and the Amount of Organic Matter Input? *Appl. Soil Ecol.* 46, 436–442. doi:10.1016/j.apsoil.2010.09.006

Hall, E. K., Bernhardt, E. S., Bier, R. L., Bradford, M. A., Boot, C. M., Cotner, J. B., et al. (2018). Understanding How Microbiomes Influence the Systems They Inhabit. *Nat. Microbiol.* 3, 977–982. doi:10.1038/s41564-018-0201-z

Heiri, O., Lotter, A. F., and Lemcke, G. (2001). Loss on Ignition as a Method for Estimating Organic and Carbonate Content in Sediments: Reproducibility and Comparability of Results. *J. Paleolimnology* 25, 101–110. doi:10.1023/a:1008119611481

Ji, Y., Angel, R., Klose, M., Claus, P., Marotta, H., Pinho, L., et al. (2016). Structure and Function of Methanogenic Microbial Communities in Sediments of Amazonian Lakes with Different Water Types. *Environ. Microbiol.* 18 (12), 5082–5100. doi:10.1111/1462-2920.13491

Kharitonov, S., Semenov, M., Sabrekov, A., Kotsyurbenko, O., Zhelezova, A., and Schegolkova, N. (2021). Microbial Communities in Methane Cycle: Modern Molecular Methods Gain Insights into Their Global Ecology. *Environments* 8, 16. doi:10.3390/environments8020016

Kotsyurbenko, O. R., Chin, K.-J., Glagolev, M. V., Stubner, S., Simankova, M. V., Nozhevnikova, A. N., et al. (2004). Acetoclastic and Hydrogenotrophic Methane Production and Methanogenic Populations in an Acidic West-Siberian Peat Bog. *Environ. Microbiol.* 6 (11), 1159–1173. doi:10.1111/j.1462-2920.2004.00634.x

Kozich, J. J., Westcott, S. L., Baxter, N. T., Highlander, S. K., and Schloss, P. D. (2013). Development of a Dual-Index Sequencing Strategy and Curation Pipeline for Analyzing Amplicon Sequence Data on the MiSeq Illumina Sequencing Platform. *Appl. Environ. Microbiol.* 79, 5112–5120. doi:10.1128/AEM.01043-13

Liu, Y., and Whitman, W. B. (2008). Metabolic, Phylogenetic, and Ecological Diversity of the Methanogenic Archaea. *Annu. N.Y Acad. Sci.* 1125, 171–189. doi:10.1196/annals.1419.019

Müller, B., Bryant, L. D., Matzinger, A., and Wüest, A. (2012). Hypolimnetic Oxygen Depletion in Eutrophic Lakes. *Environ. Sci. Technol.* 46, 9964–9971. doi:10.1021/es301422r

Nozhevnikova, A. N., Nekrasova, V., Ammann, A., Zehnder, A. J. B., Wehrli, B., and Holliger, C. (2007). Influence of Temperature and High Acetate Concentrations on Methanogenensis in lake Sediment Slurries. *FEMS Microbiol. Ecol.* 62, 336–344. doi:10.1111/j.1574-6941.2007.00389.x

Oksanen, J., Guillaume Blanchet, F., Friendly, M., Kindt, R., Legendre, P., McGlinn, D., et al. (2017). Vegan: Community Ecology Package. R package version 2.4-2. Available at: https://CRAN.R-project.org/package=vegan (Accessed November 18, 2021).

Orland, C., Yakimovich, K. M., Mykytczuk, N. C. S., Basiliko, N., and Tanentzap, A. J. (2020). Think Global, Act Local: The Small-Scale Environment Mainly Influences Microbial Community Development and Function in lake Sediment. *Limnol Oceanogr* 65, S88–S100. doi:10.1002/lno.11370

Phelps, T. J., and Zeikus, J. G. (1984). Influence of pH on Terminal Carbon Metabolism in Anoxic Sediments from a Mildly Acidic lake. *Appl. Environ. Microbiol.* 48, 1088–1095. doi:10.1128/aem.48.6.1088-1095.1984

R Core Team (2018). *R: A Language and Environment for Statistical Computing*. Vienna, Austria: R Foundation for Statistical Computing. URL https://www.R-project.org/ (Accessed November 18, 2021).

Rathour, R., Gupta, J., Mishra, A., Rajeev, A. C., Dupont, C. L., and Thakur, I. S. (2020). A Comparative Metagenomic Study Reveals Microbial Diversity and Their Role in the Biogeochemical Cycling of Pangong lake. *Sci. Total Environ.* 731, 139074. doi:10.1016/j.scitotenv.2020.139074

Sepulveda-Jauregui, A., Hoyos-Santillan, J., Martinez-Cruz, K., Walter Anthony, K. M., Casper, P., Belmonte-Izquierdo, Y., et al. (2018). Eutrophication Exacerbates the Impact of Climate Warming on lake Methane Emission. *Sci. Total Environ.* 636, 411–419. doi:10.1016/j.scitotenv.2018.04.283

Sobek, S., Durisch-Kaiser, E., Zurbrügg, R., Wongfun, N., Wessels, M., Pasche, N., et al. (2009). Organic Carbon Burial Efficiency in Lake Sediments Controlled by Oxygen Exposure Time and Sediment Source. *Limnol. Oceanogr.* 54 (6), 2243–2254. doi:10.4319/lo.2009.54.6.2243

Steger, K., Premke, K., Gudasz, C., Sundh, I., and Tranvik, L. J. (2011). Microbial Biomass and Community Composition in Boreal lake Sediments. *Limnol. Oceanogr.* 56 (2), 725–733. doi:10.4319/lo.2011.56.2.0725

Torres, I. C., Inglett, K. S., and Reddy, K. R. (2011). Heterotrophic Microbial Activity in Lake Sediments: Effects of Organic Electron Donors. *Biogeochemistry* 104, 165–181. doi:10.1007/s10533-010-9494-6

Vavourakis, C. D., Andrei, A.-S., Mehrshad, M., Ghai, R., Sorokin, D. Y., and Muyzer, G. (2018). A Metagenomics Roadmap to the Uncultured Genome Diversity in Hypersaline Soda lake Sediments. *Microbiome* 6, 168. doi:10.1186/s40168-018-0548-7

Wang, Q., Garrity, G. M., Tiedje, J. M., and Cole, J. R. (2007). Naïve Bayesian Classifier for Rapid Assignment of rRNA Sequences into the New Bacterial Taxonomy. *Appl. Environ. Microbiol.* 73 (16), 5261–5267. doi:10.1128/AEM.00062-07

Wang, W., YujunYi, Y., Yang, Y., Zhou, Y., Zhang, S., Wang, X., et al. (2020). Impact of Anthropogenic Activities on the Sediment Microbial Communities of Baiyangdian Shallow Lake. *Int. J. Sediment Res.* 35, 180–192. doi:10.1016/j.ijsrc.2019.10.006

Welschmeyer, N. A. (1994). Fluorometric Analysis of Chlorophyll a in the Presence of Chlorophyll B and Pheopigments. *Limnol. Oceanogr.* 39 (8), 1985–1992. doi:10.4319/lo.1994.39.8.1985

West, W. E., Coloso, J. J., and Jones, S. E. (2012). Effects of Algal and Terrestrial Carbon on Methane Production Rates and Methanogen Community Structure in a Temperate Lake Sediment. *Freshw. Biol.* 57, 949–955. doi:10.1111/j.1365-2427.2012.02755.x

West, W. E., Creamer, K. P., and Jones, S. E. (2016). Productivity and Depth Regulate Lake Contributions to Atmospheric Methane. *Limnol. Oceanogr.* 61, S51–S61. doi:10.1002/lno.10247

West, W. E., McCarthy, S. M., and Jones, S. E. (2015). Phytoplankton Lipid Content Influences Freshwater Lake Methanogenesis. *Freshw. Biol.* 60, 2261–2269. doi:10.1111/fwb.12652

Xia, P., Zhang, J., Liu, J., and Yu, L. (2020). Shifts of Sediment Bacterial Community and Respiration along a Successional Gradient in a Typical Karst Plateau Lake Wetland (China). *J. Ocean. Limnol.* 39, 880–891. doi:10.1007/s00343-020-0073-y

Xiong, J., Liu, Y., Lin, X., Zhang, H., Zeng, J., Hou, J., et al. (2012). Geographic Distance and pH Drive Bacterial Distribution in Alkaline lake Sediments across Tibetan Plateau. *Environ. Microbiol.* 14 (9), 2457–2466. doi:10.1111/j.1462-2920.2012.02799.x

Yakimovich, K. M., Emilson, E. J. S., Carson, M. A., Tanentzap, A. J., Basiliko, N., and Mykytczuk, N. C. S. (2018). Plant Litter Type Dictates Microbial Communities Responsible for Greenhouse Gas Production in Amended Lake Sediments. *Front. Microbiol.* 9, 2662. doi:10.3389/fmicb.2018.02662

Yang, Y., Chen, J., Tong, T., Xie, S., and Liu, Y. (2020). Influences of Eutrophication on Methanogenesis Pathways and Methanogenic Microbial Community Structures in Freshwater Lakes. *Environ. Pollut.* 260, 114106. doi:10.1016/j.envpol.2020.114106

Ye, R., Jin, Q., Bohannan, B., Keller, J. K., McAllister, S. A., and Bridgham, S. D. (2012). pH Controls over Anaerobic Carbon Mineralization, the Efficiency of Methane Production, and Methanogenic Pathways in Peatlands across an Ombrotrophic-Minerotrophic Gradient. *Soil Biol. Biochem.* 54, 36–47. doi:10.1016/j.soilbio.2012.05.015

Yu, Y., Lee, C., Kim, J., and Hwang, S. (2005). Group-Specic Primer and Probe Sets to Detect Methanogenic Communities Using Quantitative Real-Time Polymerase Chain Reaction. *Biotechnol. Bioeng.* 89 (6), 670–679. doi:10.1002/bit.20347

Yvon-Durocher, G., Allen, A. P., Bastviken, D., Conrad, R., Gudasz, C., St-Pierre, A., et al. (2014). Methane Fluxes Show Consistent Temperature Dependence across Microbial to Ecosystem Scales. *Nature* 507, 488–491. doi:10.1038/nature13164

Zhang, X., Han, X., Yu, W., Wang, P., and Cheng, W. (2017). Priming Effects on Labile and Stable Soil Organic Carbon Decomposition: Pulse Dynamics over Two Years. *PLoS ONE* 12 (9), e0184978. doi:10.1371/journal.pone.0184978

Conflict of Interest: The authors declare that the research was conducted in the absence of any commercial or financial relationships that could be construed as a potential conflict of interest.

Publisher's Note: All claims expressed in this article are solely those of the authors and do not necessarily represent those of their affiliated organizations, or those of the publisher, the editors and the reviewers. Any product that may be evaluated in this article, or claim that may be made by its manufacturer, is not guaranteed or endorsed by the publisher.

Copyright © 2022 Bertolet, Koepfli and Jones. This is an open-access article distributed under the terms of the Creative Commons Attribution License (CC BY). The use, distribution or reproduction in other forums is permitted, provided the original author(s) and the copyright owner(s) are credited and that the original publication in this journal is cited, in accordance with accepted academic practice. No use, distribution or reproduction is permitted which does not comply with these terms.

frontiers | Frontiers in Environmental Science

BRIEF RESEARCH REPORT
published: 01 April 2022
doi: 10.3389/fenvs.2022.804512

Relief of Phosphate Limitation Stimulates Methane Oxidation

Thomas P. A. Nijman[1], André M. Amado[2], Paul L. E. Bodelier[3] and Annelies J. Veraart[1]*

[1]Department of Aquatic Ecology and Environmental Biology, Radboud Institute for Biological and Environmental Sciences (RIBES), Radboud University, Nijmegen, Netherlands, [2]Laboratory of Aquatic Ecology, Institute of Biology, Federal University of Juiz de Fora, Juiz de Fora, Brazil, [3]Department of Microbial Ecology, Netherlands Institute of Ecology (NIOO-KNAW), Wageningen, Netherlands

Aquatic ecosystems such as shallow lakes and wetlands are important emitters of the greenhouse gas methane (CH_4). Increased phosphorus (P) loading is expected to increase CH_4 production in these ecosystems. This increased CH_4 production can potentially be mitigated by increased CH_4 oxidation, but how P availability affects methane-oxidizing bacterial (MOB) community composition and potential CH_4 oxidation remains to be tested. Here, we incubated MOB from sediments of four subtropical lakes of different trophic states for 7 days at different phosphate (PO_4^{3-}) concentrations to determine the effects of P on MOB community composition and potential CH_4 oxidation. We measured CH_4 consumption daily and compared CH_4 oxidation during the exponential growth phase. Furthermore, we determined MOB community composition at the end of the incubations using qPCR of the *pmoA* gene. To test for differences in N and P uptake, we determined bacterial biomass N and P content. We found that increases in PO_4^{3-} concentrations until 10 µM significantly increased CH_4 oxidation. PO_4^{3-} also increased bacterial biomass P content, while N content was not affected. MOB community composition was not affected by PO_4^{3-} but more strongly correlated to lake of origin, likely due to the short duration of the incubations. Our results show that PO_4^{3-} can not only stimulate CH_4 oxidation indirectly through increased CH_4 production, but also directly by increasing MOB growth. Importantly, these effects only occur at low PO_4^{3-} concentrations, indicating that at high nutrient loads the increased CH_4 oxidation will likely not mitigate the increased CH_4 production.

Keywords: methane oxidation, phosphate, eutrophication, methane, aquatic sediment, freshwater, methanotroph, microbial community composition

OPEN ACCESS

Edited by:
Yves T. Prairie, Université du Québec à Montréal, Canada

Reviewed by:
Malak M. Tfaily, University of Arizona, United States
Tapan Kumar Adhya, KIIT University, India

****Correspondence:***
Thomas P. A. Nijman
tom.nijman@ru.nl

Specialty section:
This article was submitted to Biogeochemical Dynamics, a section of the journal Frontiers in Environmental Science

Received: *29 October 2021*
Accepted: *17 February 2022*
Published: *01 April 2022*

Citation:
Nijman TPA, Amado AM, Bodelier PLE and Veraart AJ (2022) Relief of Phosphate Limitation Stimulates Methane Oxidation. Front. Environ. Sci. 10:804512. doi: 10.3389/fenvs.2022.804512

INTRODUCTION

Methane (CH_4) is the second most important greenhouse gas, contributing to 16–25% of global warming (IPCC, 2014). Microbial processes in aquatic ecosystems, such as wetlands and shallow lakes, are the main source of this greenhouse gas, accounting for over 50% of global CH_4 emissions (Rosentreter et al., 2021). Currently, the nutrient status of many shallow lake ecosystems is changing because of eutrophication, which is expected to increase shallow lake CH_4 emissions (Aben et al., 2017; Davidson et al., 2018), mostly driven by phosphorus (P) and nitrogen (N) enrichment in water and sediment (Correll, 1998). While interactions between N cycling and CH_4 emissions have been well studied (Bodelier and Steenbergh, 2014), we still lack understanding about the effects of P on CH_4 emissions.

CH_4 cycling in shallow lakes is largely driven by the sediment microbiome. In the anoxic zone of the sediment, methanogens produce CH_4 (Conrad, 2007). Subsequently, a large part of the produced CH_4 is mitigated by methane-oxidizing bacteria (MOB), which consume CH_4 mostly aerobically, converting CH_4 into CO_2. In freshwater ecosystems with high concentrations of alternative electron acceptors, such as nitrate and sulfate, CH_4 can also be converted anaerobically (Deutzmann, 2020). This study focuses on aerobic MOB, which belong to the Gammaproteobacteria (type I), Alphaproteobacteria (type II), and Verrucomicrobia, of which type I and type II MOB are dominant in most freshwater lakes. These MOB differ in their phylogeny, physiology, biochemistry, and morphology (Semrau et al., 2010). While both perform the same process—CH_4 oxidation—they prefer different environments. Type I MOB are most abundant in stable environments with high substrate availability while type II are most abundant in environments with disturbances such as heat waves and desiccation and low substrate availability (Ho et al., 2013). CH_4 oxidation by MOB is the sole biological CH_4 sink (Adamsen and King, 1993), and it is therefore important to know how MOB react to disturbances such as eutrophication.

The accumulation of phosphate (PO_4^{3-}) in aquatic ecosystems can affect CH_4 oxidation. In a field study, higher potential CH_4 oxidation rates were found in sediments that had higher PO_4^{3-} concentrations (Veraart et al., 2015). Increased [PO_4^{3-}] is also hypothesized to indirectly affect CH_4 oxidation rates by changing the MOB community. It has been suggested that type I MOB thrive in eutrophic environments with high [PO_4^{3-}] while type II MOB compete better in more oligotrophic environments with low [PO_4^{3-}] (Ho et al., 2013). One of the reasons for this is that type II MOB generally harbor more enzymes which liberate P from organic molecules and have membranes with lower P content (Veraart et al., 2015). Changes in the dominant type of MOB can potentially also lead to changes in CH_4 oxidation rates (Reis et al., 2020; Nijman et al., 2021), thereby altering the mitigation capacity of the MOB community.

Only one study has addressed the direct relationship between [PO_4^{3-}] and MOB functioning (Sawakuchi et al., 2021). In this study, surface water MOB from ice-covered lakes oxidized more CH_4 at 500 μg/L (~5 μM) PO_4^{3-} than without PO_4^{3-} in long-term incubations at 4 °C. However, the specific conditions of this experiment make it difficult to apply to MOB from other ecosystems. Most important, the dominant MOB in the ice-covered lake experiment are very rare outside of arctic regions (50.3% *Methylobacter tundripaludum* and 44.6% *Methylovulum psychrotolerans*). Second, the CH_4 oxidation rates were very low (2.5–29.4 μmol CH_4 L^{-1} d^{-1}), compared to many other MOB communities, such as those in lake sediments (e.g. Shelley et al., 2015). Finally, the question arises whether higher PO_4^{3-} concentrations would further increase potential CH_4 oxidation rates, and up to which concentration PO_4^{3-} could still be the limiting growth factor for MOB.

Therefore, we still lack a good understanding of the direct relationship between [PO_4^{3-}] and CH_4 oxidation. Other studies of MOB, which showed effects of PO_4^{3-} on CH_4 oxidation rates (Veraart et al., 2015) and on the type of MOB (Ho et al., 2013), were based on correlative field observations, and thus only showed an indirect relationship between [PO_4^{3-}] and MOB functioning. Since many biogeochemical variables are correlated, the relationship between [PO_4^{3-}] and CH_4 oxidation found in these studies could also have been due to other variables, such as organic matter content (Czepiel et al., 1995) or N availability (Bodelier and Laanbroek, 2004). Furthermore, since increased [PO_4^{3-}] stimulates lake CH_4 emissions, likely through enhanced CH_4 production (Aben et al., 2017; Davidson et al., 2018), oxidation may also be indirectly stimulated by PO_4^{3-} due to higher CH_4 availability. However, considering that bacteria need P for growth, and especially type I MOB since they contain phospholipid-rich stacked membranes (Bodelier et al., 2009), it is likely that PO_4^{3-} also directly affects MOB, especially at low PO_4^{3-} concentrations.

Here, we investigated the effect of PO_4^{3-} concentration on potential CH_4 oxidation and MOB community composition. We expected increases in PO_4^{3-} concentration would increase potential CH_4 oxidation. Furthermore, we expected that increases in PO_4^{3-} concentration would favor type I MOB over type II MOB.

METHODS

To test the effects of [PO_4^{3-}] on potential CH_4 oxidation and MOB community composition, we incubated MOB from four different subtropical lake sediments in 48 microcosms at different [PO_4^{3-}], analyzing CH_4 oxidation rates during exponential growth and final MOB community composition (**Figure 1**).

Sediment Sampling and Inoculum Preparation

Four subtropical lake sediments in south-eastern Brazil were sampled in april 2019 to obtain different MOB communities for the microcosms (**Supplementary Table S1**). We sampled Funil lake (latitude, longitude: 2231′31″S, 44°33′1″W), Manacás lake (2146′43″S, 4322′8″W), Botanical Garden lake of Universidade Federal de Juiz de Fora (UFJF; 2143′55″S, 4322′14″W), and Chapéu D'Uvas lake (CDU; 2134′55″S, 4333′16″W). The lakes were chosen because of their different trophic state. Funil lake (Pacheco et al., 2015) and Manacás lake (Lawall et al., 2005) are eutrophic, UFJF botanical garden lake is mesotrophic (Nunes et al., 2021) and CDU lake is oligotrophic (Almeida et al., 2019). We took one sediment core from each lake with a Uwitech corer (ø 60 mm), of which we sliced off the top 2 cm (~56.5 ml), and used those for the microcosms. While one core is not enough for a representative picture of the community of a single lake sediment, the use of single cores from four different lakes allowed us to investigate the relationship between [PO_4^{3-}] and CH_4 oxidation for MOB communities with different community composition.

The sediments were used to prepare inocula for the microcosms. The sliced sediment was first diluted with lake water from the corresponding lake to obtain a total volume of

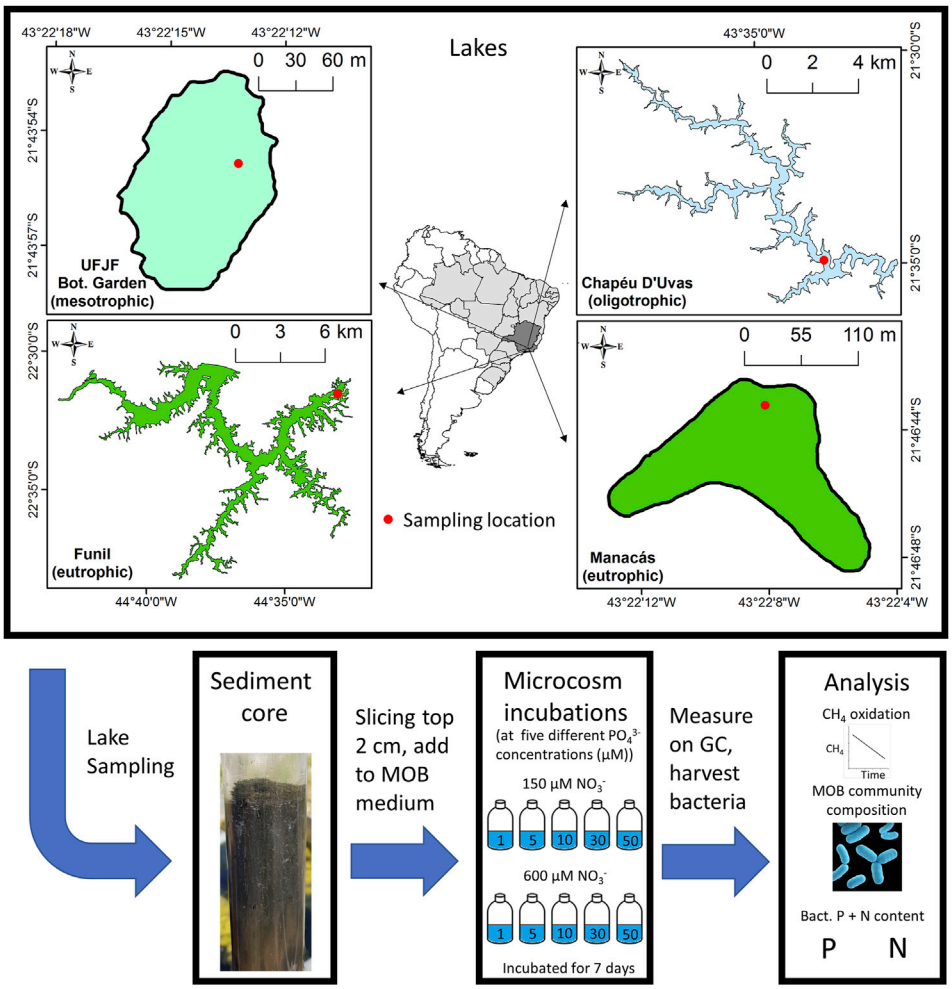


FIGURE 1 | Sampling sites and experimental design.

150 ml, and homogenized using a blender. While blending could have lysed some cells, the low speed of the blender was likely not enough to significantly affect the microbial community. After mixing, the suspended sediment was pipetted into 15 ml falcon tubes and centrifuged at 4,000 rpm for 5 min. Then, the supernatant, containing a large number of bacteria, was taken. The supernatant was filtered through 1.2 μm glass fiber filters to remove most protozoa and remaining sediment particles, and the filtrate was used as inoculum for the microcosms.

Microcosms

We used microcosms to test how [PO_4^{3-}] affected MOB growth and community composition. We prepared Nitrate Mineral Salts (NMS) medium specific for MOB (Whittenbury et al., 1970, ATCC 1306) with 10 μM copper and five different PO_4^{3-} concentrations (1, 5, 10, 30, and 50 μM, added as KH_2PO_4 and $NaHPO_4$ in a 1:2.5 ratio). We also used two different NO_3^- concentrations (150 and 600 μM, added as KNO_3) to control for effects of N and N:P ratio, and included a negative control (0 μM PO_4^{3-} and 0 μM NO_3^-, no inoculum added) and positive control (1 mM PO_4^{3-} and 1 mM NO_3^-), resulting in twelve microcosms per lake. The PO_4^{3-} and NO_3^- concentrations were chosen based on comparable concentrations in mesotrophic to eutrophic freshwater sediments (Geurts et al., 2008; Veraart et al., 2015). We ran one series of microcosm experiments per lake, yielding four replicates per combination of [PO_4^{3-}] and [NO_3^-]. Microcosms were prepared by adding 57 ml NMS medium and 3 ml inoculum of the respective lake to 120 ml serum bottles. Bottles were closed with butyl stoppers and capped, after which 10% of the total headspace was replaced with CH_4 (purity grade 4.5). This left an oxygen (O_2) concentration of 18.9%. We incubated the microcosms in the dark for 7 days at 20°C, while stirring continuously. Because MOB use O_2 in a 2:1 ratio to oxidize CH_4, there was not enough O_2 in the microcosms to completely consume all CH_4. However, we found that in all microcosms, the [CH_4] still decreased after the time of exponential growth, indicating that O_2 was not yet depleted. It was also unlikely CH_4 decreased because of anaerobic oxidation of methane (AOM), as described below.

Since the microcosms had a much higher O_2 concentration than is present in sediments (Wang et al., 2014), we did not aim to show how sediment MOB would respond to increased [PO_4^{3-}]. Rather, the aim was to show how model MOB communities would respond to different PO_4^{3-} concentrations. Using an initially high [O_2] had two advantages. First, it allowed the MOB to reach exponential growth because they could consume the majority of CH_4 before O_2 would become limiting. Second, it prevented AOM and methanogenesis. For AOM, 2% O_2 decreased CH_4 oxidation of '*Candidatus* Methylomirabilis oxyfera' by 60% within 22 h without recovery (Kampman et al., 2018), while 5% O_2 caused '*Candidatus* Methanoperedens nitroreducens' to be outcompeted by *Methylobacter*, an aerobic MOB (Guerrero-Cruz et al., 2018). Also, while some methanogens can survive O_2 exposure (Peters and Conrad, 1995), these only showed activity after 15 days without O_2. Therefore, it is unlikely there was AOM or methanogenesis in the microcosms.

To determine CH_4 consumption rates, we measured CH_4 concentration in the headspace directly after CH_4 addition and once per day afterwards. The CH_4 concentration was measured by taking 1 ml of the headspace and injecting into a Bruker 450-GC (Bruker Technologies, Australia) equipped with a flame ionization detector. The concentration was calculated by comparing to a standard curve. Furthermore, 1 ml of medium was taken daily for MOB analysis, although these samples were not used because the number of cells was too low for DNA extractions.

CH_4 Oxidation During Exponential Growth

To estimate CH_4 oxidation rates, we calculated the rate at which CH_4 decreased per day per ml of medium, accounting for removal of water and air from the microcosms (supplementary methods). Surprisingly, there was no CH_4 oxidation in the microcosms of mesotrophic UFJF botanical garden lake. Little data on this lake are available thus far, but potential MOB inhibitors such as low pH, high NH_4^+ and humic substance concentration have not been observed. However, one possibility is the lakes' high oxygen concentration (11 mg/L, Nunes et al., 2021) may have prevented most CH_4 production, exemplified by very low CH_4 emissions (3.39 mg CH_4 m^{-2} day^{-1} September 2021, personal communication Nasário and Barros), and thereby the development of an active MOB community, which remains to be experimentally confirmed. Because of the lack of CH_4 oxidation, we removed those microcosms from our analysis. For the remaining microcosms, we used the time of exponential growth to compare CH_4 oxidation at different PO_4^{3-} concentrations, based on the day with the largest decrease. All incubations had >0.75% CH_4 (12 μM CH_4 in the water) left after this day, which is not yet limiting (Shelley et al., 2015). Exponential growth occurred 1 day earlier for the eutrophic sediments than for the oligotrophic sediment (**Supplementary Figure S4**).

MOB Community Composition

To evaluate MOB community composition, we harvested the bacteria from the microcosms after 7 days. Thirty ml of the final medium was filtered through 0.2 μm filters, using half for DNA extractions. Filters of the positive control were used to test the DNA extraction method, while the negative control was not filtered as there was no bacterial growth. Four filters were accidently lost during transportation and the remaining 26 filters were used for qPCR. Bacteria were scraped off the filters using sterile cell scrapers (Greiner Bio-One 541070) and DNA was extracted with the DNeasy PowerSoil kit (Qiagen 12888-100) according to manufacturer's instructions with one modification: bead-beating was performed using a Powerlyzer for 45 s at 2,500 rpm. We then determined copy number of type Ia (*Methylobacter*, *Methylomonas*), type Ib (*Methylocaldum*, *Methylococcus*) and type II (*Methylosinus*, *Methylocella*, *Methylocystis*) MOB by qPCR using different primers for the *pmoA* gene, according to Kolb et al. (2003) with some small modifications (**Supplementary Table S2**), using iQ SYBR® Green Supermix as mastermix. All samples and standards were measured in triplicate on a BioRad iQ5 Multicolour Real-Time PCR detection system (Vers. 2.0, BioRad, Gothenburg Sweden), on which we checked the melt curves.

Bacterial Biomass N and P Content

To investigate whether the PO_4^{3-} concentrations changed the N and P content of the MOB, we filtered 10 ml of the final medium through two 0.7 μm glass fiber filters per microcosm. Filters were weighted before and after filtering, and bacterial N and P concentration was determined from the bacterial biomass retained on the filters after potassium persulfate digestion (Carmouze, 1994). N concentration in bacterial biomass was measured on a total organic carbon analyzer, equipped with a TNM-1 total nitrogen module (TOC-V CPN, Shimadzu), whereas P in bacterial biomass was measured spectrophotometrically (Lambda 365 UV/VIS, Perkin Elmer) by the ascorbic acid method (Mackereth et al., 1979). Filters were pre-combusted (550°C for 4 h) before filtration and oven dried before analysis (60°C for >24 h). The filtration method for microbial biomass nutrient contents using 0.7 μm pore size filters may not account for all the microbial community - smaller cells may pass through filters - but a previous study showed an average 80% retention of bacterial community using this pore size (They et al., 2017). Because the main available carbon substrate for microbial growth was CH_4, and because we used NMS medium specific for MOB, we assumed that MOB were the predominant bacteria, and hence bacterial biomass N and P content was closely related to MOB N and P content. Also, because most CH_4 was consumed in all incubations, similar total growth of MOB had taken place, indicating that N and P content per cell were related to total N and P content of the bacterial community. However, these results should be interpreted with caution, because P could also have formed suspended particles, increasing P content of the filters.

Statistical Analysis

Statistical analyses were performed in R 3.6.3 (R Core Team, 2019). To analyze how [PO_4^{3-}] affected CH_4 oxidation during exponential growth, we calculated potential CH_4 oxidation rates at different [PO_4^{3-}] (supplementary methods). Next, we

determined which model fit the data best to compare effects of [PO_4^{3-}] on CH_4 consumption for the different lakes. We tested a linear regression, a nonlinear least-squares regression using the *nls* function, and a segmented regression using the *segmented* function (Muggeo, 2003). Based on a comparison of AIC values (**Supplementary Table S3**), the best-fitting model was the nonlinear least-squares regression, which we further analyzed. We also compared the nonlinear least-squares regression for 150 and 600 µM NO_3^- separately (**Supplementary Figure S1**), but since the differences between these models were small, we finally used one model combining all data.

To determine at which PO_4^{3-} concentrations CH_4 oxidation rates during exponential growth significantly differed from each other, we determined the confidence intervals (CIs) of CH_4 oxidation at different PO_4^{3-} concentrations and calculated the *p*-value at which CIs of different concentrations overlapped.

Relative abundance of different MOB types was calculated by dividing the copy number per MOB type by the copy number of all MOB. To achieve normality, the proportions of MOB type Ia and II were logit transformed while the type Ib proportion was log transformed. Linear models were used to test the effects of [PO_4^{3-}] [NO_3^-], and lake of origin on relative abundance of different MOB types, and the *emmeans* function (Lenth et al., 2020) was used for post-hoc between-lake comparisons. We also inspected the relationship between N:P ratio and proportions of MOB (**Supplementary Figure S2**), but found no clear patterns.

Bacterial P content was log-transformed to achieve normality and linear models were used to test the effects of NO_3^- and PO_4^{3-} on bacterial N content and log-transformed bacterial P content. A similar model comparison to CH_4 oxidation showed the best fitting model was a linear regression rather than a nonlinear least-squares regression or segmented regression (**Supplementary Table S4**). Similar to CH_4 oxidation, we compared the models for 150 and 600 µM NO_3^- separately (**Supplementary Figure S3**), but finally decided to combine all data since the differences between the models were very small.

RESULTS

To investigate the effects of [PO_4^{3-}] on model MOB communities, 30 microcosms from three different lakes (Manacás, Funil, CDU) were incubated at five different PO_4^{3-} concentrations (1–50 µM), while a fourth lake (UFJF botanical garden) yielded no MOB growth and was therefore removed from the analysis.

CH_4 oxidation increased with [PO_4^{3-}] (**Figure 2**). Interestingly, PO_4^{3-} stimulated CH_4 oxidation during exponential growth mostly at low [PO_4^{3-}] up to 10 µM, as shown by the good fit of the nonlinear least-squares regression to the CH_4 oxidation data (**Supplementary Table S3**). Analysis of confidence intervals showed that CH_4 oxidation at 1 µM PO_4^{3-} was significantly lower than at all higher concentrations (5 µM: $p = 0.0036$; 10, 30, and 50 µM: $p < 0.0001$) while CH_4 oxidation at 5 µM PO_4^{3-} was significantly lower than at 30 µM ($p = 0.0051$) and 50 µM PO_4^{3-} ($p = 0.0039$), and slightly lower at 10 µM PO_4^{3-} than at 50 µM PO_4^{3-} ($p = 0.048$). There was no effect of [NO_3^-] or lake of origin on CH_4 oxidation.

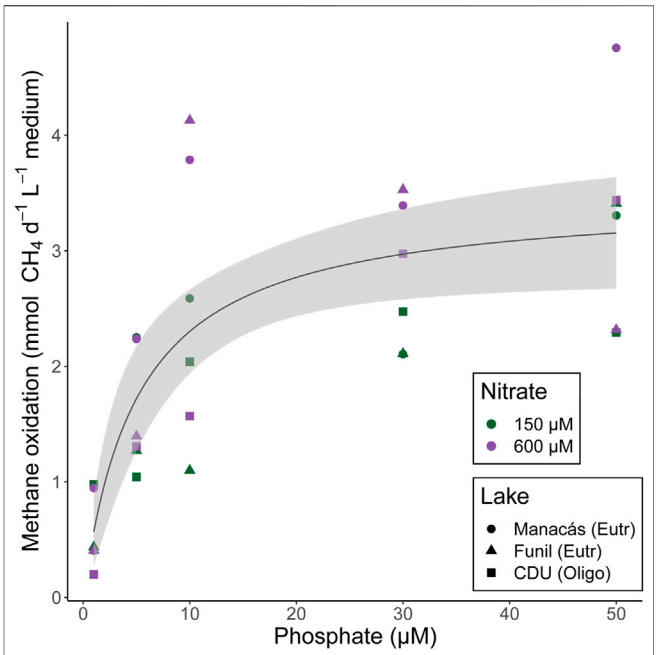


FIGURE 2 | CH_4 oxidation per day per ml of medium at different [PO_4^{3-}] and [NO_3^-] during exponential growth phase of MOB from Manacás lake, Funil lake, and CDU lake. Fitted line according to nonlinear least-squares regression, shading represents 95% confidence interval. Individual measurements are shown, colours represent [NO_3^-] treatments, shapes represent lake of origin, $n = 30$.

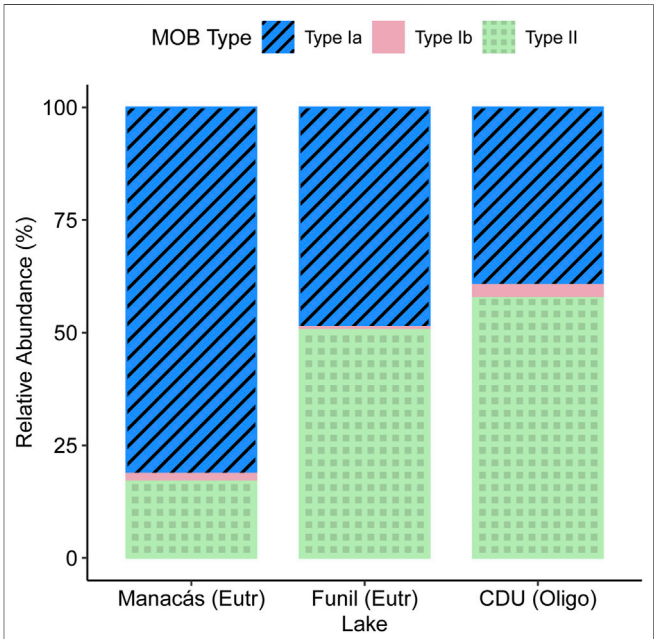


FIGURE 3 | proportional abundance of different types of MOB per lake based on qPCR copy number of the *pmoA* gene at the end of microcosm incubations. Different colours represent different types of MOB, $n = 26$.

The change in CH_4 oxidation did not coincide with changes in relative abundance of different MOB types, which were mostly influenced by the lake of origin (**Supplementary Table S5**;

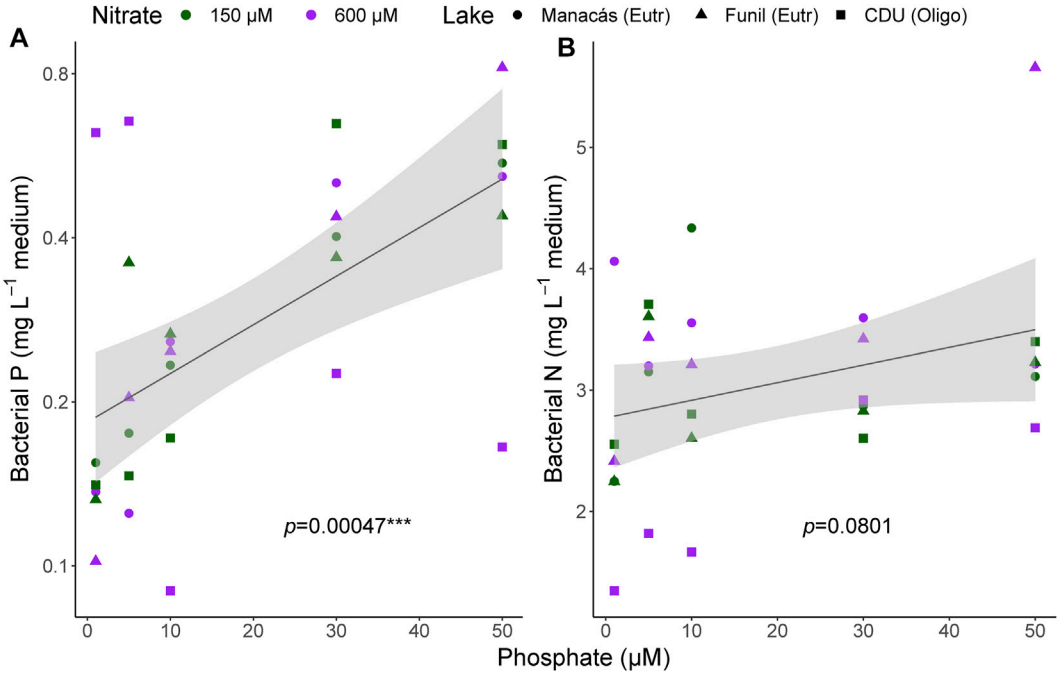


FIGURE 4 | Bacterial P (log-transformed, **(A)** and bacterial N **(B)** content per litre of medium at the end of the microcosm incubations. Fitted line according to linear regression, shading represents 95% confidence interval. Individual measurements are shown, colours represent [NO_3^-] treatments, shapes represent lake of origin, n = 30.

Figure 3). Most MOB were either type Ia (58.8%) or type II (39.6%), while only a small percentage was type Ib (1.7%). Type Ia MOB were more abundant in the Manacás microcosms than in the CDU microcosms ($p < 0.05$) but not influenced by [NO_3^-] or [PO_4^{3-}] concentrations. Type II MOB showed the opposite trend and were more abundant in the CDU lake microcosms than in the Manacás microcosms ($p < 0.05$), while also not being affected by [NO_3^-] or [PO_4^{3-}]. Type Ib were more abundant in the Manacás and CDU microcosms than in the Funil microcosms ($p < 0.05$ for both, **Supplementary Table S5**). Interestingly, the number of type Ib MOB significantly decreased at higher [NO_3^-] ($p = 0.05$, **Supplementary Table S5**) but since the abundance of type Ib was relatively low, this had little impact on overall community composition.

Bacterial P content showed a strong relationship with [PO_4^{3-}] ($p = 0.00047$, **Figure 4A**), while bacterial N content (**Figure 4B**) was not influenced by either [NO_3^-] or [PO_4^{3-}]. In contrast to CH_4 oxidation rates, the increase in bacterial P content was also observed at high [PO_4^{3-}] and not only at low concentrations, as there was a linear relationship between the log transformed bacterial P content and [PO_4^{3-}].

DISCUSSION

In our microcosm experiment, we found that increased [PO_4^{3-}] led to an increase in potential CH_4 oxidation rates, in agreement with our hypothesis. This was likely because MOB incorporated more P to increase their growth rates, as shown by the increase in bacterial P biomass content at higher [PO_4^{3-}]. However, the [PO_4^{3-}] did not affect the relative abundance of different types of MOB.

PO_4^{3-} increased CH_4 oxidation during exponential growth in a nonlinear way, indicating that PO_4^{3-} was likely the limiting growth factor for the MOB communities at low concentrations. Increasing PO_4^{3-} to concentrations up to 10 µM relieved MOB from PO_4^{3-} limitation and thereby increased their growth. This is in line with previous research showing higher rates of CH_4 oxidation in systems with higher PO_4^{3-} availability (Veraart et al., 2015; Nijman et al., 2021). Increased P content suggested that bacteria used more P at higher PO_4^{3-}, possibly to invest in rRNA to increase their growth rate - as suggested in the growth rate hypothesis (Elser et al., 2000) - thereby increasing CH_4 oxidation rates. At PO_4^{3-} concentrations above 10 µM, P on the filters still increased but this did not coincide with increased CH_4 oxidation, possibly because bacteria stored the excess PO_4^{3-} in organic and inorganic molecules inside the cytoplasm (Kulakovskaya, 2014) rather than investing in new cells. Likely, another limiting factor was preventing faster growth of MOB, such as copper (Semrau et al., 2010) or maximum growth rate (Ho et al., 2013). Future studies could investigate if PO_4^{3-} concentrations lower than 1 µM, which are common in surface waters (Geurts et al., 2008), limit CH_4 oxidation even more.

It is not clear whether the response of the model MOB communities in our experiment would be comparable to the response of sediment MOB communities, as those generally experience much lower O_2 concentrations (Wang et al., 2014). Interestingly, MOB communities in the water column have the highest growth rates at low [O_2], and the question remains whether the effects of PO_4^{3-} that we found in this experiment would also be found at low [O_2]. A future experiment at lower initial [O_2], in which [O_2] is closely monitored and added when necessary, could give further insight into these dynamics.

Since the increased CH_4 oxidation in the microcosms was only apparent at low PO_4^{3-} concentrations, the direct effect of PO_4^{3-} on CH_4 oxidation might contribute little to the CH_4 cycle in highly eutrophic lakes. Rather, these lakes might be more strongly influenced by an increase in methanogenesis because of higher algal carbon decomposition (West et al., 2012) and decreased oxygen (Bastviken et al., 2004). If MOB in sediments are stimulated by PO_4^{3-} in a comparable way to those in the microcosms, that may be one of the reasons why CH_4 emissions are higher in eutrophic lakes (Aben et al., 2017; Davidson et al., 2018), while MOB are a more effective CH_4 filter in mesotrophic lakes where they still benefit from increased PO_4^{3-} concentrations (Veraart et al., 2015).

Our results are in line with the increased CH_4 oxidation rates found in P-amended incubations of surface water from ice-covered lakes (Sawakuchi et al., 2021). In both studies, adding 5 μM PO_4^{3-} increased CH_4 oxidation rates. In contrast, the rates in our experiment were on average about 100-fold higher (0.19–4.75 mmol CH_4 d^{-1} L^{-1} vs. 0.0025–0.029 mmol CH_4 d^{-1} L^{-1}), and type II MOB were far more abundant (40% vs. <5%). That is likely because our model communities originated from freshwater sediments, which often harbour highly active MOB communities (Oremland and Culbertson, 1992).

Increased [PO_4^{3-}] had little effect on MOB community composition, which was more related to the lake of origin. The eutrophic Manacás lake had a higher proportion of type Ia MOB, while the oligotrophic CDU lake had more type II MOB. This is in line with predictions that type I MOB are better competitors and thrive in high nutrient environments, while type II are better stress-tolerators that can deal with low nutrient conditions (Ho et al., 2013). However, the fact that MOB community composition did not change in response to [PO_4^{3-}] was in contrast with these predictions. Most likely, the short duration of 1 week for our experiment explains this result, which was too short to change MOB community composition. Future research could simulate MOB growth at different [PO_4^{3-}] for a longer period to see possible shifts in community composition.

The microcosms did not show relationships between N:P ratio and CH_4 oxidation, bacterial N and P content, and MOB community composition (**Supplementary Figures S1–3**). Likely, this was because [PO_4^{3-}] was limiting and therefore driving most changes in the microcosms, while changes in MOB community composition would require more time. A future experiment using concentrations of NO_3^- and PO_4^{3-} that are not limiting, e.g., 100–600 μM NO_3^- and 10–100 μM PO_4^{3-}, could provide further insight into the effects of N:P ratio on CH_4 oxidation.

To conclude, we show that MOB originating from lake sediments can be PO_4^{3-} limited and show a nonlinear response to increased PO_4^{3-} concentrations, indicating that they can potentially mitigate increased methanogenesis in mesotrophic lakes that become more eutrophic.

DATA AVAILABILITY STATEMENT

The datasets presented in this study can be found in online repositories. The names of the repository/repositories and accession number(s) can be found below: (10.17026/dans-x59-warf) (DANS EASY).

AUTHOR CONTRIBUTIONS

TN, AA, and AV designed the experiment. TN and AA carried out the practical work, with support from PB for the qPCR analyses. All authors discussed the results and contributed to the final manuscript.

FUNDING

AV was funded by Aquafarm 2.0. This work was partly funded by an Erasmus + Grant awarded to TN, by Brazil's National Council for Scientific and Technological Development (CNPq), for providing Productivity grants to AA (PQ 310033/2017-9 and PQ 312772/2020-2), and by the PROPP-UFJF Reverse Sandwich Program.

ACKNOWLEDGMENTS

We thank Icaro Barbosa for sampling Chapéu D'Uvas and helping with slicing, Layla Fonseca, Alisa Shubina, and Annemiek Tiekstra for help with molecular analyses, José Paranaiba for help plotting the sampling locations, Jonas Nasário and Nathan Barros for providing CH_4 emission data of the UFJF botanical garden lake, and Fons Smolders for advising on porewater PO_4^{3-} concentrations.

SUPPLEMENTARY MATERIAL

The Supplementary Material for this article can be found online at: https://www.frontiersin.org/articles/10.3389/fenvs.2022.804512/full#supplementary-material

REFERENCES

Aben, R. C. H., Barros, N., Van Donk, E., Frenken, T., Hilt, S., Kazanjian, G., et al. (2017). Cross continental Increase in Methane Ebullition under Climate Change. *Nat. Commun.* 8, 1–8. doi:10.1038/s41467-017-01535-y

Adamsen, A. P. S., and King, G. M. (1993). Methane Consumption in Temperate and Subarctic forest Soils: Rates, Vertical Zonation, and Responses to Water and Nitrogen. *Appl. Environ. Microbiol.* 59, 485–490. doi:10.1128/aem.59.2.485-490.1993

Almeida, R. M., Paranaíba, J. R., Barbosa, Í., Sobek, S., Kosten, S., Linkhorst, A., et al. (2019). Carbon Dioxide Emission from Drawdown Areas of a Brazilian Reservoir Is Linked to Surrounding Land Cover. *Aquat. Sci.* 81, 68. doi:10.1007/s00027-019-0665-9

Bastviken, D., Cole, J., Pace, M., and Tranvik, L. (2004). Methane Emissions from Lakes: Dependence of lake Characteristics, Two Regional Assessments, and a Global Estimate. *Glob. Biogeochem. Cycles* 18, a–n. doi:10.1029/2004GB002238

Bodelier, P. L. E., Bär Gillisen, M.-J., Hordijk, K., Sinninghe Damsté, J. S., Rijpstra, W. I. C., Geenevasen, J. A. J., et al. (2009). A Reanalysis of Phospholipid Fatty

Acids as Ecological Biomarkers for Methanotrophic Bacteria. *ISME J.* 3, 606–617. doi:10.1038/ismej.2009.6

Bodelier, P. L. E., and Laanbroek, H. J. (2004). Nitrogen as a Regulatory Factor of Methane Oxidation in Soils and Sediments. *FEMS Microbiol. Ecol.* 47, 265–277. doi:10.1016/S0168-6496(03)00304-0

Bodelier, P. L., and Steenbergh, A. K. (2014). Interactions between Methane and the Nitrogen Cycle in Light of Climate Change. *Curr. Opin. Environ. Sustainability* 9-10, 26–36. doi:10.1016/j.cosust.2014.07.004

Carmouze, J. P. (1994). *O metabolismo dos ecossistemas aquáticos: fundamentos teóricos, métodos de estudo e análises químicas*. São Paulo: Edgard Blucher.

Caspers, H., Heron, J., and Talling, J. F. (1979). F. J. H. Mackereth, J. Heron & J. F. Talling: Water Analysis: Some Revised Methods for Limnologists. - with 4 fig., 120 Pp. Far Sawrey, Ambleside: Freshwater Biological Association Scientific Publication No. 36. 1978. I SBN 900386 31 2. £ 2. 50. *Int. Revue Ges. Hydrobiol. Hydrogr.* 64, 456. doi:10.1002/iroh.19790640404

Conrad, R. (2007). Microbial Ecology of Methanogens and Methanotrophs. *Adv. Agron.* 96, 1–63. doi:10.1016/S0065-2113(07)96005-8

Correll, D. L. (1998). The Role of Phosphorus in the Eutrophication of Receiving Waters: A Review. *J. Environ. Qual.* 27, 261–266. doi:10.2134/jeq1998.00472425002700020004x

Czepiel, P. M., Crill, P. M., and Harriss, R. C. (1995). Environmental Factors Influencing the Variability of Methane Oxidation in Temperate Zone Soils. *J. Geophys. Res.* 100, 9359–9364. doi:10.1029/95JD00542

Davidson, T. A., Audet, J., Jeppesen, E., Landkildehus, F., Lauridsen, T. L., Søndergaard, M., et al. (2018). Synergy between Nutrients and Warming Enhances Methane Ebullition from Experimental Lakes. *Nat. Clim Change* 8, 156–160. doi:10.1038/s41558-017-0063-z

Deutzmann, J. S. (2020). *Anaerobic Utilization of Hydrocarbons, Oils, and Lipids*. Berlin, Germany: Springer International Publishing AG. doi:10.1007/978-3-319-50391-2

Elser, J. J., Sterner, R. W., Gorokhova, E., Fagan, W. F., Markow, T. A., Cotner, J. B., et al. (2000). Biological Stoichiometry from Genes to Ecosystems. *Ecol. Lett.* 3, 540–550. doi:10.1046/j.1461-0248.2000.00185.x

Geurts, J. J. M., Smolders, A. J. P., Verhoeven, J. T. A., Roelofs, J. G. M., and Lamers, L. P. M. (2008). Sediment Fe:PO4ratio as a Diagnostic and Prognostic Tool for the Restoration of Macrophyte Biodiversity in Fen Waters. *Freshw. Biol.* 53, 2101–2116. doi:10.1111/j.1365-2427.2008.02038.x

Guerrero-Cruz, S., Cremers, G., van Alen, T. A., Op den Camp, H. J. M., Jetten, M. S. M., Rasigraf, O., et al. (2018). Response of the Anaerobic Methanotroph " Candidatus Methanoperedens Nitroreducens" to Oxygen Stress. *Appl. Environ. Microbiol.* 84, 1–17. doi:10.1128/AEM.01832-18

Ho, A., Kerckhof, F.-M., Luke, C., Reim, A., Krause, S., Boon, N., et al. (2013). Conceptualizing Functional Traits and Ecological Characteristics of Methane-Oxidizing Bacteria as Life Strategies. *Environ. Microbiol. Rep.* 5, 335–345. doi:10.1111/j.1758-2229.2012.00370.x

IPCC (2014). *Climate Change 2014: Synthesis Report*. Geneva, Switzerland: IPCC. doi:10.1017/CBO9781107415324

Kampman, C., Piai, L., Temmink, H., Hendrickx, T. L. G., Zeeman, G., and Buisman, C. J. N. (2018). Effect of Low Concentrations of Dissolved Oxygen on the Activity of Denitrifying Methanotrophic Bacteria. *Water Sci. Technol.* 77, 2589–2597. doi:10.2166/wst.2018.219

Kolb, S., Knief, C., Stubner, S., and Conrad, R. (2003). Quantitative Detection of Methanotrophs in Soil by Novel pmoA -Targeted Real-Time PCR Assays. *Appl. Environ. Microbiol.* 69, 2423–2429. doi:10.1128/AEM.69.5.2423-2429.2003

Kulakovskaya, T. (2014). Phosphorus Storage in Microorganisms: Diversity and Evolutionary Insight. *Biochem. Physiol.* 04. doi:10.4172/2168-9652.1000e130

Lawall, S., Tamiozzo Pereira Torres, F., and Rocha, G. C. (2005). Diagnostic and proposal of recovery of the lake Manacás watershed, campus of the federal university of Juiz de Fora, Minas Gerais. *Soc. Nat.* 1, 494–501. Available at: http://www.seer.ufu.br/index.php/sociedadenatureza/article/view/9726/5842.

Lenth, R., Buerkner, P., Herve, M., Love, J., Riebl, H., and Singmann, H. (2020). Emmeans: Estimated Marginal Means, Aka Least-Squares Means. *Aka Least-Squares Means*. Available at: https://cran.r-project.org/package=emmeans.

Muggeo, V. M. R. (2003). Estimating Regression Models with Unknown Break-Points. *Statist. Med.* 22, 3055–3071. doi:10.1002/sim.1545

Nijman, T. P. A., Davidson, T. A., Weideveld, S. T. J., Audet, J., Esposito, C., Levi, E. E., et al. (2021). Warming and Eutrophication Interactively Drive Changes in the Methane-Oxidizing Community of Shallow Lakes. *Isme Commun.* 1, 3–6. doi:10.1038/s43705-021-00026-y

Nunes, P., Roland, F., Amado, A. M., da Silva Resende, N., and Cardoso, S. J. (2022). Responses of Phytoplanktonic Chlorophyll-A Composition to Inorganic Turbidity Caused by Mine Tailings. *Front. Environ. Sci.* 9, 605838. doi:10.3389/fenvs.2021.605838

Oremland, R. S., and Culbertson, C. W. (1992). Importance of Methane-Oxidizing Bacteria in the Methane Budget as Revealed by the Use of a Specific Inhibitor. *Nature* 356, 421–423. doi:10.1038/356421a0

Pacheco, F. S., Soares, M. C. S., Assireu, A. T., Curtarelli, M. P., Roland, F., Abril, G., et al. (2015). The Effects of River Inflow and Retention Time on the Spatial Heterogeneity of Chlorophyll and Water-Air CO2 Fluxes in a Tropical Hydropower Reservoir. *Biogeosciences* 12, 147–162. doi:10.5194/bg-12-147-2015

Peters, V., and Conrad, R. (1995). Methanogenic and Other Strictly Anaerobic Bacteria in Desert Soil and Other Oxic Soils. *Appl. Environ. Microbiol.* 61, 1673–1676. doi:10.1128/aem.61.4.1673-1676.1995

R Core Team (2019). *R: A Language and Environment for Statistical Computing*. Vienna, Austria: R Core Team. Available at: http://www.r-project.org.

Reis, P. C. J., Thottathil, S. D., Ruiz-González, C., and Prairie, Y. T. (2020). Niche Separation within Aerobic Methanotrophic Bacteria across Lakes and its Link to Methane Oxidation Rates. *Environ. Microbiol.* 22, 738–751. doi:10.1111/1462-2920.14877

Rosentreter, J. A., Borges, A. V., Deemer, B. R., Holgerson, M. A., Liu, S., Song, C., et al. (2021). Half of Global Methane Emissions Come from Highly Variable Aquatic Ecosystem Sources. *Nat. Geosci.* 14, 225–230. doi:10.1038/s41561-021-00715-2

Sawakuchi, H. O., Martin, G., Peura, S., Bertilsson, S., Karlsson, J., and Bastviken, D. (2021). Phosphorus Regulation of Methane Oxidation in Water from Ice-Covered Lakes. *J. Geophys. Res. Biogeosci* 126, 1–13. doi:10.1029/2020jg006190

Semrau, J. D., Dispirito, A. A., and Yoon, S. (2010). Methanotrophs and Copper. *FEMS Microbiol. Rev.* 34, 496–531. doi:10.1111/j.1574-6976.2010.00212.x

Shelley, F., Abdullahi, F., Grey, J., and Trimmer, M. (2015). Microbial Methane Cycling in the Bed of a Chalk River: Oxidation Has the Potential to Match Methanogenesis Enhanced by Warming. *Freshw. Biol.* 60, 150–160. doi:10.1111/fwb.12480

They, N. H., Amado, A. M., and Cotner, J. B. (2017). Redfield Ratios in Inland Waters: Higher Biological Control of C:N:P Ratios in Tropical Semi-arid High Water Residence Time Lakes. *Front. Microbiol.* 8, 1505. doi:10.3389/fmicb.2017.01505

Veraart, A. J., Steenbergh, A. K., Ho, A., Kim, S. Y., and Bodelier, P. L. E. (2015). Beyond Nitrogen: The Importance of Phosphorus for CH 4 Oxidation in Soils and Sediments. *Geoderma* 259-260, 337–346. doi:10.1016/j.geoderma.2015.03.025

Wang, C., Shan, B., Zhang, H., and Rong, N. (2014). Analyzing Sediment Dissolved Oxygen Based on Microprofile Modeling. *Environ. Sci. Pollut. Res.* 21, 10320–10328. doi:10.1007/s11356-014-2875-y

West, W. E., Coloso, J. J., and Jones, S. E. (2012). Effects of Algal and Terrestrial Carbon on Methane Production Rates and Methanogen Community Structure in a Temperate lake Sediment. *Freshw. Biol.* 57, 949–955. doi:10.1111/j.1365-2427.2012.02755.x

Whittenbury, R., Phillips, K. C., and Wilkinson, J. F. (1970). Enrichment, Isolation and Some Properties of Methane-Utilizing Bacteria. *J. Gen. Microbiol.* 61, 205–218. doi:10.1099/00221287-61-2-205

Conflict of Interest: The authors declare that the research was conducted in the absence of any commercial or financial relationships that could be construed as a potential conflict of interest.

Publisher's Note: All claims expressed in this article are solely those of the authors and do not necessarily represent those of their affiliated organizations, or those of the publisher, the editors and the reviewers. Any product that may be evaluated in this article, or claim that may be made by its manufacturer, is not guaranteed or endorsed by the publisher.

Copyright © 2022 Nijman, Amado, Bodelier and Veraart. This is an open-access article distributed under the terms of the Creative Commons Attribution License (CC BY). The use, distribution or reproduction in other forums is permitted, provided the original author(s) and the copyright owner(s) are credited and that the original publication in this journal is cited, in accordance with accepted academic practice. No use, distribution or reproduction is permitted which does not comply with these terms.

frontiers | Frontiers in Environmental Science

ORIGINAL RESEARCH
published: 13 May 2022
doi: 10.3389/fenvs.2022.893180

Extreme Hydrological Events and Reservoir Methane Emissions

Bradford S. Sherman[1,2]* *and Phillip W. Ford*[3]

[1]CSIRO Land and Water, Canberra, ACT, Australia, [2]Reservoir Doctors Pty Ltd., Duffy, ACT, Australia, [3]CSIRO Oceans and Atmosphere, Canberra, ACT, Australia

Floating chamber measurements of CH_4 emissions from Cotter Reservoir (Canberra, Australia) were performed on five occasions between October 2010 and April 2012. The timing of the measurements spanned the first major flood events that followed drought-breaking rains that ended the Millenium Drought in southeast Australia. The flood events were the largest in 26 years and followed the 3 lowest flow years on record. The floods warmed the hypolimnion of this normally monomictic reservoir by ~8°C during the first summer and by ~3°C during the second summer of the study compared to "normal" summer hypolimnion temperatures. In addition, the floods carried large amounts of vegetation and soil that had accumulated in the catchment during previous years. Average CH_4 emissions prior to the flooding were low (4.3 mg-CH_4 m^{-2} d^{-1}) and relatively uniform across 8 measurement sites spaced along the long axis of the reservoir. Following the first floods, which occurred during spring and summer 2010–2011, the mean reservoir CH_4 emission increased to 99 mg-CH_4 m^{-2} d^{-1} with emissions at the upstream end of the reservoir approximately 100 times greater than emissions near the dam wall. The following year (2011–2012) average emissions were lower (30 mg-CH_4 m^{-2} d^{-1}) and the longitudinal gradient weakened. A major flood occurred in autumn 2012 and warmed the hypolimnion by ~3 C, but emissions did not change much in response. We hypothesize that the changes in mean reservoir CH_4 emission can be attributed to both thermal enhancement of sediment methanogenesis by a factor of 2–7, and to the supply of fresh organic matter from the catchment by a factor of 3.

Keywords: methane-CH_4, reservoir, hydrology, flood, climate change, spatiotemporal variability

OPEN ACCESS

Edited by:
Daniel F. McGinnis,
Université de Genève, Switzerland

Reviewed by:
Ryan P. McClure,
Virginia Tech, United States
Luana S. Basso,
National Institute of Space Research (INPE), Brazil

***Correspondence:**
Bradford S. Sherman
BradfordS.Sherman@icloud.com

Specialty section:
This article was submitted to Biogeochemical Dynamics, a section of the journal Frontiers in Environmental Science

Received: *10 March 2022*
Accepted: *21 April 2022*
Published: *13 May 2022*

Citation:
Sherman BS and Ford PW (2022) Extreme Hydrological Events and Reservoir Methane Emissions. Front. Environ. Sci. 10:893180. doi: 10.3389/fenvs.2022.893180

1 INTRODUCTION

Methane in the atmosphere is a strong absorber of infra-red (7.6 μm) radiation and is the second most radiatively active atmospheric gas after CO_2. Increases in CH_4 concentration in the atmosphere affect the Earth's radiation balance and contribute to global warming. The global average atmospheric concentration of methane has increased from approximately 700 ppb at the start of the industrial era to 1880 ppb in 2020. The trajectory of concentration was not one of unbroken rise, with a 7-year plateau from 2000 to 2007. Most of the increase has been attributed to human activities particularly to leakage from oil, coal, and natural gas extraction, rice paddies, reservoirs, land fills, and emissions from farmed ruminants. These anthropogenic emissions are added to the pre-existing natural emissions from lakes (albeit now often perturbed from pristine conditions by human modified nutrient inputs), wetlands, and geologic emissions (Etiope and Schwietzke, 2019). The

global methane emissions are predominantly balanced by an atmospheric sink term due to reaction with OH radical in the troposphere with a methane lifetime of 9.1 years (Prather et al., 2012), and controlled largely by the concentration of OH.

The post 2007 increase in the atmospheric CH_4 inventory has been attributed to changes in the strength of both the natural and anthropogenic components as well as changes in the tropospheric oxidation rate, but these attributions remain uncertain and in some cases contradictory (Turner et al., 2019; Lan et al., 2021). There are only limited, globally available, parameters (CH_4 concentration, $\delta C^{13}CH_4$, and δD^2CH_4) available to deconvolve the global (or twin hemisphere) concentration signal, while several sources share common isotopic characteristics. The alternative bottom-up approach to source identification suffers from an inability to enumerate all the sources in each category of emitter, as well as a lack of precision in quantifying the individual emissions, or to model them accurately. Consequently, there is a mismatch between the two approaches which has not been resolved yet, as well as substantial uncertainties in estimating the size of the various sources.

Irrespective of the sources of the CH_4, consideration of the global warming equivalents (Lynch et al., 2020) shows that for times shorter than 100 years, CH_4 mitigation strategies can produce reductions in global warming faster than equi-molar CO_2 reductions due to the much longer residence time of CO_2 vis a vis the lifetime of CH_4 (Shindell et al., 2012; Turner et al., 2019; Lynch et al., 2020). The benefits of prompt CH_4 mitigation (i.e., well before 2050) have now been recognized in the policy sphere and adopted recently as an international priority measure at COP 26 (albeit with some nations abstaining).

Reduction in methane emission from reservoirs have emerged now as a potentially promising mitigation opportunity. Reservoirs as well as ponds and lakes are now included in the global GHG accounting protocols, and quantified reductions are recognized as contributions to agreed national commitments. Furthermore, since reservoirs are engineered structures, there is potential scope to implement changes in their operating rules designed to lower CH_4 emissions. Aesthetic, environmental conservation, and biodiversity considerations may limit similar manipulations for natural lakes and ponds. In addition, the mitigation methods appropriate for reservoirs may not carry over to lakes, given the different drivers controlling CH_4 emissions in the two types of systems (Deemer and Holgerson, 2021).

In light of the evidence (discussed further below) that increased catchment loads, implicitly containing terrestrial organic carbon, lead to increased CH_4 emissions, catchment manipulation to limit carbon-rich sediment inputs is another potential mitigation mechanism. The obstacle to implementation of mitigation measures in either the catchment, or the reservoir itself, is the lack of the underpinning and integrated mechanistic understanding (Deemer et al., 2016; Saunois et al., 2020; Rosentreter et al., 2021).

So far, attempts to determine global emissions have relied largely on scaling up, using an average emission extrapolation approach [critically reviewed in DelSontro et al. (2011)], or modelling using morphometric characteristics such as reservoir depth or surface area. These characteristics have been identified by regression analysis of available emission data sets as having predictive capacity. Productivity (trophic status), as measured by chlorophyll concentration is also used as a predictor (Deemer et al., 2016). This variable represents supply of autochthonous organic carbon delivered to the sediments. Allochthonous carbon (in particulate form) is another possible source of metabolizable organic carbon which can be transformed to CH_4 within the sediments. The evidence for the involvement of allochthonous carbon in CH_4 emission in reservoirs is presently limited and involves only a limited number of systems. It shows, however, that high rates of ebullition lead to high total areal fluxes of CH_4 (Aben et al., 2017), and that high C burial rates are associated with high rates of ebullition (Sobek, et al., 2012).

Ebullition of CH_4 has been observed to be the dominant flux pathway in many reservoirs (Beaulieu et al., 2020). As the source of ebullitive emissions is the organic carbon present in the sediments, there should be a strong correlation between spatial distribution of organic C rich sediments and the ebullition rate. High CH_4 fluxes were observed in Lake Wohlen (DelSontro et al., 2010), a relatively shallow run-of-river hydroelectric reservoir receiving nutrient rich treated wastewater. The CH_4 ebullition flux was unevenly distributed longitudinally along the reservoir. The dissolved CH_4 concentration in the well-mixed water column, on the other hand, increased monotonically from the riverine input end to the dam wall. Further investigation of the sediment properties of Lake Wohlen (Sobek et al., 2012) showed that there were high sedimentation rates of particulate organic matter in the middle section of the reservoir. Sediment pore water gas saturation—a prerequisite for ebullition—was greatest in these regions.

The strongest association between the location of allochthonous inputs and elevated CH_4 ebullitive emissions comes from hydroacoustic measurements in Lake Kariba, (DelSontro et al., 2011). The bubble fluxes in deltaic region, where there were significant terrestrial inputs (though not quantified), were of order ten times those in a bay which lacked riverine inflows. Similar enhanced bubble fluxes were seen at the downstream ends of a series of shallow impoundments (forebays) in the Saar River (Maeck et al., 2013), where the sediment deposition was greater than at the upstream end of the pool where the river entered. Furthermore, there was a statistically significant exponential correlation between CH_4 ebullitive flux and the measured sediment accumulation rate. Musenze et al. (2014) observed strong spatial gradients in CH_4 concentration (and by inference CH_4 emissions) in 3 subtropical reservoirs of varying catchment characteristics, surface area and morphology. The direction of the gradients was, however, the reverse of Maeck et al., 2013), being highest at the riverine input end and lowest at the dam wall end. The upstream/downstream gradient of CH_4 concentration was attributed to the selective deposition of larger, catchment-derived organic particles at the upstream end. Similar higher upstream/lower downstream gradient in CH_4 ebullition fluxes

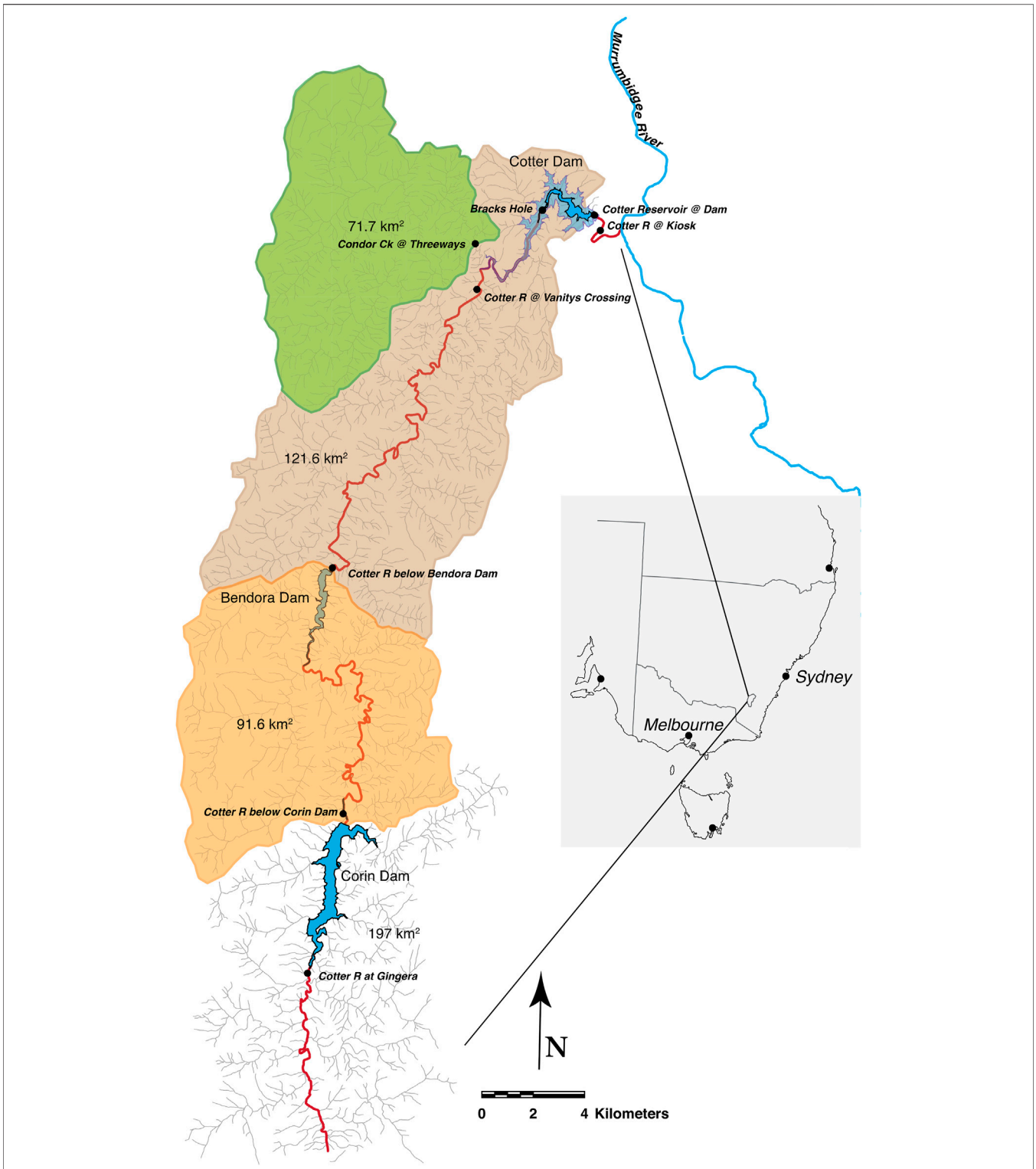


FIGURE 1 | Cotter Reservoir catchment showing hydrologic gauging stations and upstream reservoirs. Shaded areas denote catchment areas: orange between Corin and Bendora Dams; brown between Bendora and Cotter Dams not including Condor Ck; green Condor Ck subcatchment. Original full surface level of Cotter Reservoir is shown in dark blue and for enlarged Cotter Dam in light blue.

was observed in a small reservoir (McClure et al., 2020) and by the authors in two subtropical reservoirs in Australia (Sherman et al., 2012).

In all these examples the rate of input of particulate organic carbon was either constant (Lake Wohlen) or not considered. In semi-arid areas, the water and associated sediment inflows are

episodic with a single large flood event filling the reservoir. If the association of higher ebullitive CH_4 fluxes with zones of high organic sediment deposition is universally valid, then higher fluxes would be expected post flood and from the zones of greatest deposition—namely the river delta area of the reservoir (Yang, 2019). In this paper we explore this hypothesis taking advantage of fortuitous measurements on a freshwater reservoir before and after two such flood events.

2 MATERIALS AND METHODS

2.1 Site Description

Cotter Reservoir is a water supply reservoir for the city of Canberra, the capital of Australia, located at 35.320148°S, 148.939043°E, roughly 1/3 of the way between Sydney and Melbourne. At the time of the measurements, the reservoir was controlled by the original dam constructed in 1912 and enlarged to 4 GL in 1951. The full surface level (FSL) of the reservoir was 500.79 m AHD corresponding to a surface area of 47.7 ha and volume of 3.9 GL. During November 2009—October 2013, the reservoir was enlarged again to a volume of 79 GL and surface area of ca. 264 ha by construction of a new 83 m-tall dam with a full supply level of 550.8 m.

The total catchment area is 482 km^2 of which 290 km^2 comprises mid- and upper catchments supplying 2 dams, Bendora Dam and Corin Dam, located 23 and 39 river km, respectively, upstream of Cotter Dam (**Figure 1**). The mid- and upper-catchments have been protected from development within the Namadgi National Park since 1984 and vegetation there consists largely of native vegetation (e.g., eucalypt woodlands, grasslands) (Alluvium Consulting, 2020) with some limited cleared area used historically for grazing. This contrasts with most of the lower catchment immediately adjacent to Cotter Dam which has been extensively modified by forestry activities consisting of extensive pine plantations and a network of unsealed access roads. The mid- and upper-catchments comprise predominantly well-drained red Earth soils whereas the lower catchment largely consists of highly erodible yellow earths and yellow podzolics (Wade et al., 2013).

The principal gauged sources of inflow to Cotter Reservoir are Condor Creek, with a catchment of ca. 72 km^2 and in which the forestry plantations represent most of the land use; discharge from the mid- and upper-catchments that pass through Bendora Dam into the Cotter River; and discharge from the lower catchment between Bendora Dam and the gauging station at Vanitys Crossing located upstream of the confluence of the Cotter River and Condor Ck. With an area of 122 km^2 this part of the Lower Cotter catchment comprises a mixture of native vegetation within the Namadgi National Park and pine plantations. The locations of the gauging stations are shown in **Figure 1** and **Supplementary Table S1**.

2.2 Field Measurements

All floating chamber and water column profile measurements were performed from the CSIRO boat at 8–9 sites (CD01—CD09) located approximately along the axis of the reservoir (**Figure 2**). The boat was positioned at each site approximately using a handheld GPS at which point the boat was anchored and allowed to swing on the anchor line in response to changes in wind conditions. The floating chamber was tethered to the boat with a rope approximately 5 m long which allowed the chamber to move independently of the boat across the water surface (within limits); this minimized boat-induced chamber motions relative to the water surface that could potentially disturb the water beneath the chamber and potentially impact diffusive flux measurements. In practice, this means that each chamber measurement should be considered as representing the characteristic flux emanating from the area across which the chamber moved during the deployment.

2.2.1 Floating Chamber Gas Flux Measurements

Methane (and CO_2) fluxes between the water and the atmosphere were measured by recirculating air continuously at 5.5 ± 0.5 L/min through the headspace of a floating chamber and measuring this air continuously (approximately every 5 s) during a deployment of minimum duration 15-min using a Picarro G1301 $CO_2/CH_4/H_2O$ gas analyzer. The system is based on that used by Hydro Québec (Lambert and Fréchette, 2005) but with several modifications to improve performance including the implementation of the Picarro CRDS rather than using other gas analyzer technology. Technical details regarding the system are given in Zhao et al. (2015).

A minimum of two repeat deployments were performed at each site during each field trip. At sites with ebullition, deployments sometimes had to be truncated because the CH_4 concentration exceeded the measurement capabilities of the Picarro G1301: either the maximum detection limit was exceeded, or the rate of change of concentration was such that the instrument would not record values at a satisfactory rate. In such cases, additional deployments were undertaken at a site to ensure a minimum of 30 min of useable data had been acquired.

Each deployment was manually inspected for evidence of bubble evasion into the chamber—this was clearly seen as rapid substantial increases in CH_4 concentration in the headspace gas (**Supplementary Figure S1**) without corresponding changes in CO_2 concentrations. Where the data showed only a diffusive flux of CH_4, the flux was computed using a linear best fit regression to the data to yield dCH_4/dt. When ebullition was evident, end point concentrations were taken as the concentrations measured at least 15 min apart and the flux calculated as $(M_f—M_0)/\Delta t$ where M_f and M_0 are the final and initial masses of CH_4 in the chamber measured Δt seconds apart. If a deployment had been truncated due to ebullition (necessitating additional deployments as described above), a conservative estimate of the minimum total flux was determined using the end point concentrations and assuming $\Delta t = 900$ s (rather than the shorter actual measurement duration), i.e., we assumed no further emission occurred following the last usable data point. The ebullitive contribution to the total flux was calculated as the total flux less the estimated diffusive flux based on extrapolation of the diffusive portion of the deployment data.

All gas flux measurements were accompanied by meteorological data measured concurrently on the boat using

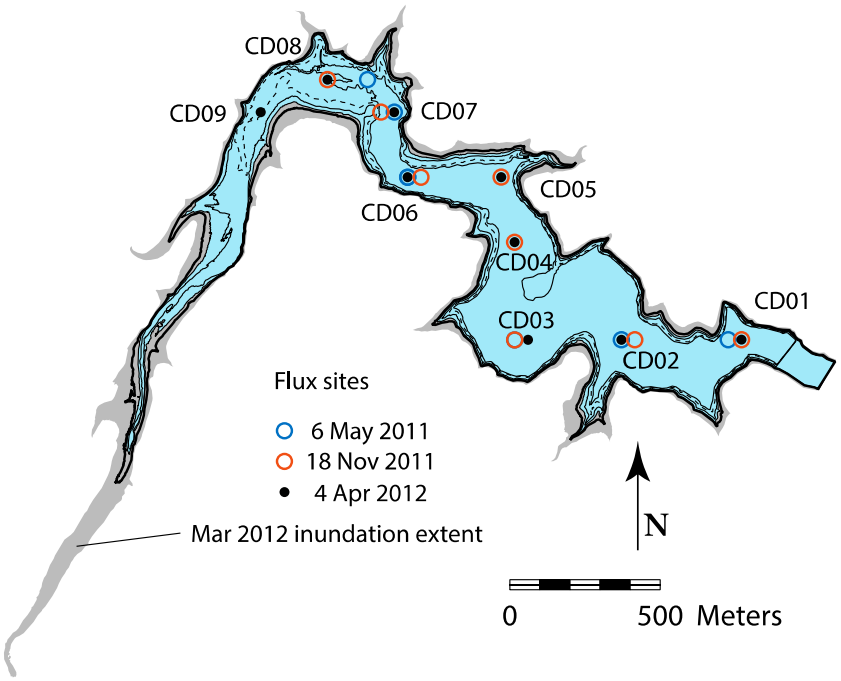


FIGURE 2 | Cotter dam GHG flux measurement sites on 6 May 2011, 18 November 2011, 4 April 2012. Maximum extents of inundation are shown as blue shaded area (504 m contour) for December 2010 and gray shaded area (512 m contour) for March 2012. Dashed line is 500 m; other contours are at 498, 502, 506 (bold) m.

a Kestrel 4500 Pocket Weather meter (barometric pressure, air temperature, relative humidity, wind speed and direction). The Kestrel 4500 was deployed on a tripod with the axis of the wind sensor approximately 0.9–0.98 m above the water surface and logged every 20 s.

Areal mean fluxes, $\bar{F}$, for each field trip were computed by weighting the flux measured at each site by the proportional contribution of the surface area of the reservoir in proximity to each site to the total reservoir surface area on the day of measurement. The boundaries between areas were defined as the approximate midpoint between measurement sites.

$$\bar{F} = \frac{\sum_i A_i F_i}{\sum_i A_i}$$

where F_i is the flux of a gas measured at site i and A_i is the corresponding subarea of the reservoir.

2.2.2 Dissolved Gas Measurements

The spatial and temporal distribution of dissolved methane was measured by collecting water samples for laboratory analysis. During flux chamber deployments, triplicate samples per measurement site were taken from a depth of 5–10 cm below the water surface during the interval between chamber deployments. Depth profiles of dissolved methane were measured by collecting triplicate samples at 2–5 depths spanning the water column at sites CD02, CD04, CD06 and CD08. Sample depths were contingent upon the water column depth at each site and were selected to ensure samples were collected near the air-water interface (0.05 m) and near the sediment-water interface (~0.5 m above the bottom). Additional samples within the water column were chosen to resolve potential gradients in dissolved methane based on inspection of water column temperature and dissolved oxygen profiles. For profiles with obvious underflows (identified by a decrease in temperature and increase in dissolved oxygen), the bottom samples were taken approximately 0.5 m above the upper boundary of the underflow. Samples were pumped from depth using a Rule bilge pump and garden hose for sufficient time to purge the hose and then the stream of water was sampled using a thrice-rinsed syringe. All water samples were stored in 12.4 mL Exetainers filled with 6.5–7.5 mL of sample plus 0.5 mL of $ZnCl_2$ preservative, leaving a headspace of 4.9–5.9 mL. All samples were sent to the Monash University Water Studies Centre for analysis of CH_4 concentration using gas chromatography. No dissolved methane samples were collected during the 6 May 2011 field trip.

2.2.3 Water Column Physical Profiles

A Yellow Springs Instruments (YSI) 6600v2 water quality sonde measured temperature, dissolved oxygen, conductivity, pH, chlorophyll-a fluorescence, phycocyanin fluorescence and turbidity. The profiler was lowered in approximately 1 m intervals and held stationary for approximately 30 s at each depth before being lowered to the next depth. Sensors were sampled every 1 s and the average, median, minimum, and maximum values for each depth computed as well as the standard deviation and variance.

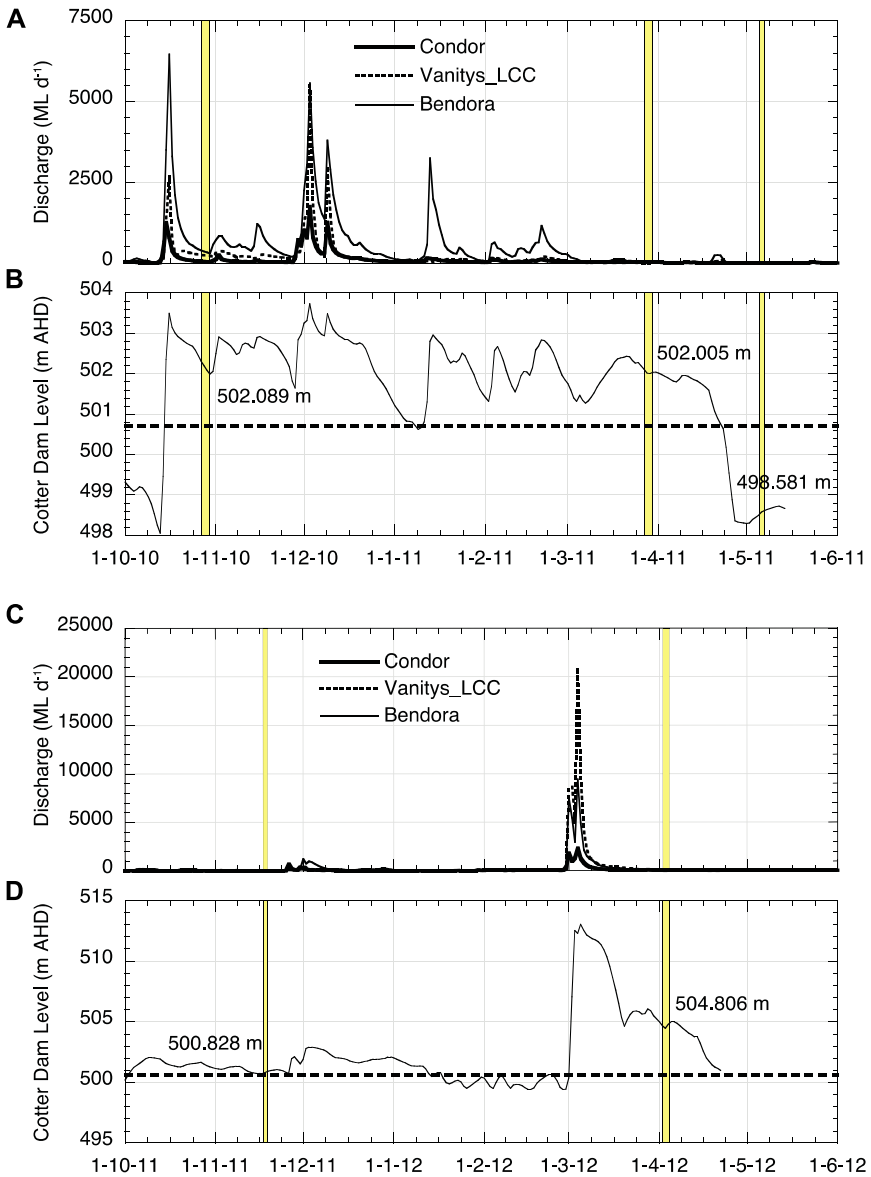


FIGURE 3 | Cotter Dam daily inflows and reservoir water levels during **(A,B)** 2010–2011; and **(C,D)** 2011–2012. Inflow data are for Condor Ck (bold), Lower Cotter Catchment at Vanitys Crossing (thin dashed line), and Cotter River below Bendora Dam (thin solid line). Discharge from the Lower Cotter Catchment was calculated as the gauged flow at Vanitys Crossing less the discharge from Bendora Dam. Heavy dashed line denotes crest of old dam. Yellow bars denote field trips and the corresponding water levels are shown as m AHD. Source data courtesy Dylan Evans, ALS, and Bureau of Meteorology << http://www.bom.gov.au/waterdata/>>.

Dissolved oxygen data within a layer were trimmed to eliminate transients associated with the relatively slow response time of the dissolved oxygen sensor.

2.3 Hydrologic Data

Hydrologic data (discharge, temperature, conductivity, and turbidity) were routinely measured every 15 min at several sites (station ID in parentheses) within the local catchment area of Cotter Reservoir: Condor Ck (410733); Cotter R. downstream of Bendora Dam (410747); Bracks Ck (340013); Cotter R. at Vanitys Crossing (410725); and downstream of Cotter Dam (410700). The water level in Cotter Dam (410704) was also recorded every 15 min. Locations of the sites are shown in **Figure 1** and **Supplementary Table S1**.

3 RESULTS

3.1 Hydrologic Conditions

Reservoir inflow and water levels are shown in **Figure 3**. The period of the study experienced the highest annual runoff in 26 years and followed the three driest years on record (2007–2009, data not shown). The flood events during

TABLE 1 | Areal mean (±s.d.) and annual methane fluxes from Cotter Reservoir and the fractional contribution of ebullition to the total flux.

Date	Reservoir surface area	Mean Areal CH_4 flux	Annual CH_4 flux	Fraction as ebullition
	[Ha]	[mg-CH_4 m^{-2} d^{-1}]	[t-CH_4 y^{-1}]	[%]
29 October 2010	54.6	4.25 (2.18)	0.86	33
29 March 2011	54.2	99.1 (21.8)	20	78
6 May 2011	39.6	9.20 (2.32)	1.9	86
18 November 2011	48.4	29.8 (12.0)	6.0	50
4 April 2012	67.0	31.6 (12.1)	6.4	74

October 2010 and December 2010 discharged 114 GL into the reservoir. This compares with a very similar amount of 118 GL from the March 2012 flood. The 2010 inflows, which raised the water level several metres above the top of the old dam (RL 500.79 m), originated approximately 15% from the Condor Ck, 25% from the Lower Cotter catchment at Vanitys Ck with the remaining 60% originating in the catchment upstream of Bendora Dam (**Supplementary Figure S2**). In contrast to the 2010 floods, the March 2012 flood originated 10% from Condor Ck, 57% from the Lower Cotter catchment at Vanitys Ck, and the remaining 34% from the upper catchment. The March 2012 flood caused the water level to rise approximately 2 m over the top of the partially-constructed new dam (RL 511.3 m) inundating soil and vegetation for the first time (**Supplementary Figure S3**). Importantly, the new dam had increased the nominal volume, and residence time, of the reservoir by a factor of ~3 compared to the previous year.

The temperature of the inflow has a profound effect on how the inflow enters the water column of the reservoir. Inflow temperature data were available for the full duration of the project at Condor Ck but only for the 2011–2012 measurement season at Vanitys Crossing. During the 2010–2011 measurement season, the water temperature in Condor Ck was 10–12°C during the October 2010 event, 15 ± 1°C from early November 2010 through mid-December 2010, and during the smaller inflow events in January 2011 the temperature varied in the range 17–20°C. During 2011–2012, there was a single large event during March 2012 at which time the temperature in Condor Ck was 14–15°C and the Cotter R at Vanitys was 1°C warmer.

From December 2011—May 2012 the temperature of the Cotter River at Vanitys Crossing was consistently 1–2°C warmer than the water in Condor Ck (**Supplementary Figure S4**). This pattern reflects the influence of the less-steep terrain and sparser vegetation cover in the Condor Ck subcatchment which allow relatively more nighttime cooling in Condor Ck. A similar pattern is expected to hold during the 2010–2011 season as well.

3.2 Gas Flux Measurements

Floating chamber measurements of CH_4 fluxes were performed at most stations during each of the five field trips. Westerly winds blowing along the axis of the water surface towards the dam prevailed during the first four trips (October 2010–November 2011, **Supplementary Figure S5**) and from the south and west during the final trip (April 2012). Wind speed during individual measurements varied from 0.2 to 3.0 m s^{-1} and averaged 1.2, 1.4, 0.8, 2.1 and 0.9 m s^{-1} for each field trip, respectively. Such conditions would produce a persistent surface drift current towards the dam that supplemented the water motions in the dam driven by inflows and outflows. Areal mean CH_4 fluxes for each trip are given in **Table 1**.

3.2.1 CH_4 Fluxes

The average and standard deviation of all CH_4 flux measurements are shown in **Figure 4** and the corresponding surface layer dissolved methane concentrations in **Figure 5**. Vertical profiles of dissolved methane at sites CD02, 04, 06, and 08 are shown in **Figure 6**. During the first field trip (October 2010), measured fluxes were low and there was only a slight spatial gradient between sites CD01 and CD07 with fluxes increasing in the upstream direction in the range 0.1–0.2 mmol CH_4 m^{-2} d^{-1}. Dissolved CH_4 varied from 0.10–0.15 μmol L^{-1} at these sites with little appreciable longitudinal variability. Ebullition was encountered only once during a single chamber deployment at site CD08 (where dissolved CH_4 was 0.18 μmol L^{-1}) and this increased the flux markedly to 0.7 mmol CH_4 m^{-2} d^{-1}. This was the only bubble event captured during the October 2010 trip despite some visual evidence of bubble activity in the vicinity of CD07 and CD08. There was no evidence of ebullition upstream of CD08.

The CH_4 fluxes measured during trip 2 (29 March 2011, mid-autumn) had increased markedly everywhere with a much more pronounced spatial gradient; the highest flux at site CD07 (32.3 ± 5.2 mmol m^{-2} d^{-1}) was more than 100 times the lowest flux at site CD01 (0.28 ± 0.019 mmol m^{-2} d^{-1}). Bubbles were conspicuous at all times at sites CD06 - CD08 and were occasionally seen at CD05 and CD03. Only four chamber deployments did not record a bubble event and site CD01 was the only site without any bubble event reported. Similarly, dissolved CH_4 exhibited a very pronounced longitudinal gradient, increasing from 0.31 μmol L^{-1} at CD01 to >2.6 μmol L^{-1} at sites CD07 and CD08.

By late autumn (6 May 2011), after significant seasonal cooling of the water column had taken place (**Figure 7**), the fluxes had diminished at all sites. Fluxes measured at sites CD01 to CD06 were the lowest during the project but the 100:1 gradient of fluxes from upstream to downstream persisted. Bubble activity in May 2011 was pronounced at both sites CD07 and CD08, but absent from all other sites.

The following late spring trip (November 2011) found higher fluxes everywhere compared to May 2011, but the strength of the longitudinal gradient had diminished to approximately 10:1 and the strength of the corresponding gradient in dissolved CH_4 had also diminished. Again, ebullition was present at just the upstream sites

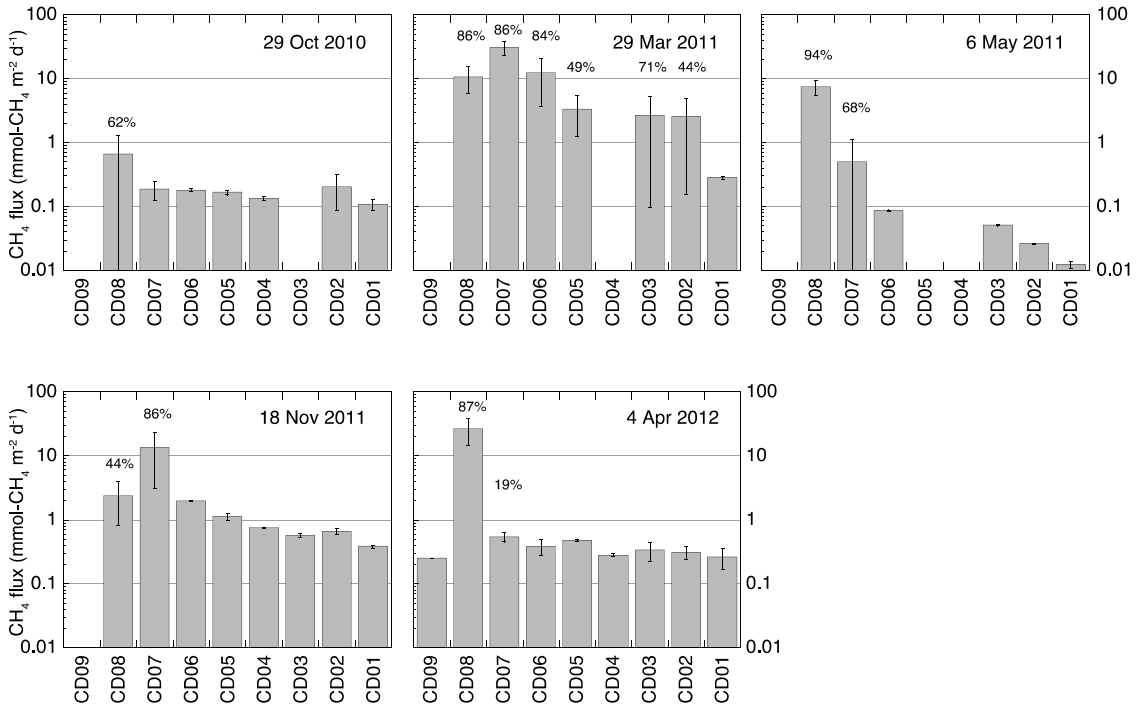


FIGURE 4 | Average 15-min methane fluxes (mmol-CH_4 m^{-2} d^{-1}) measured at each site during the five field trips: 29 October 2010. 29 March 2011, 6 May 2011, 18 November 2011, 4 April 2012. Missing bars indicate no measurement performed. Percentages above bars are the fraction of the measured fluxes attributable to ebullition. Error bars denote one sample standard deviation.

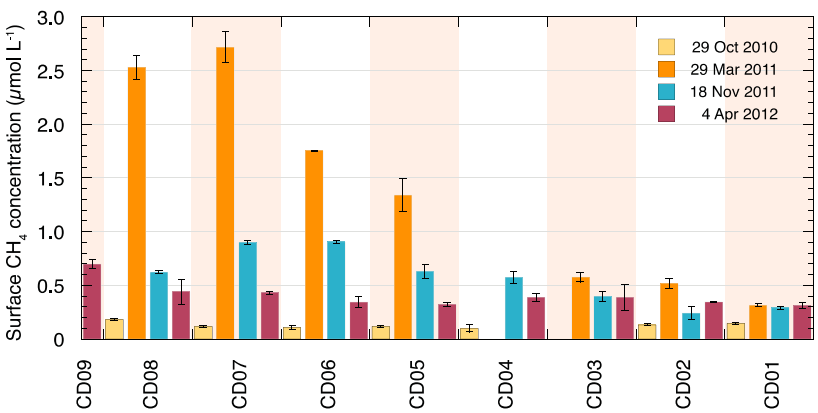


FIGURE 5 | Dissolved methane concentration just below the water surface during the flux chamber measurements on 29 October 2010 (beige), 29 March 2011 (orange), 18 November 2011 (blue) and 4 April 2012 (violet). Note that site CD04 was not measured in March 2011 and CD03 was not measured in October 2010. Site CD09 is upstream, site CD01 is downstream.

CD07 and CD08. Ebullition was the dominant mode of emission at CD07.

By the following autumn (April 2012), the gradient in fluxes had returned to close to the level originally observed in October 2010 (neglecting site CD08). Ebullition was the dominant (87%) component of the total CH4 flux at CD08. The gradient in dissolved CH_4 also weakened by a further factor of 2 compared to that observed in November 2011. Notably, both fluxes and dissolved CH_4 were consistently higher in April 2012 compared to October 2010 and this may relate to the difference in water temperatures at the times of the two field trips (discussed below).

In November 2011, ebullition was most intense at site CD07 whereas during April 2012 bubble activity was mainly at CD08. In April 2012, significant bubble activity was observed over extensive areas in the vicinity of site CD09, a newly inundated

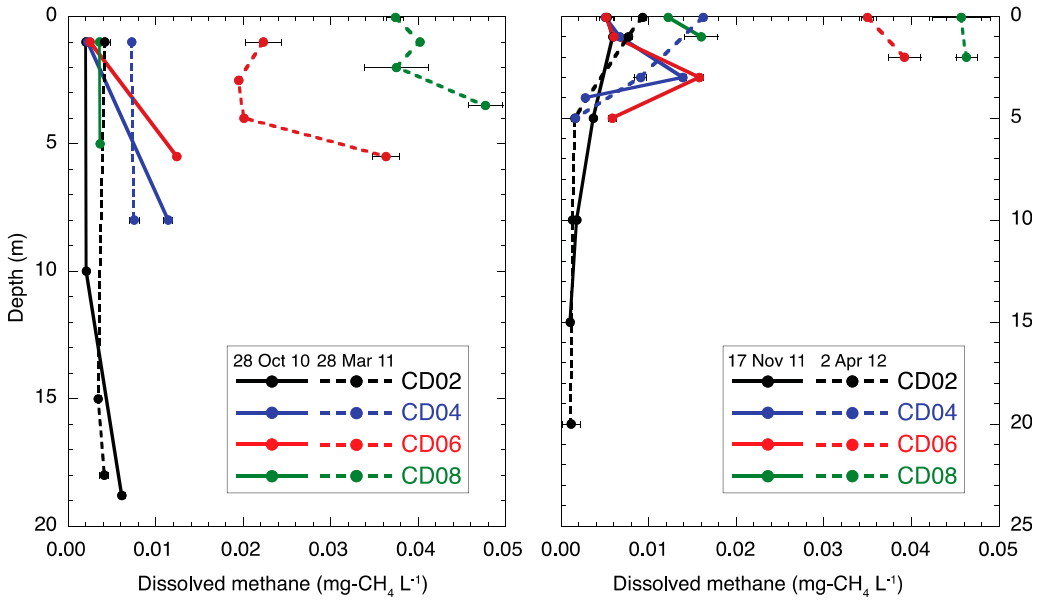


FIGURE 6 | Depth profiles of dissolved CH_4 on 28 October 2010 (solid), 28 March 2011 (dashed), 17 November 2011 (solid), and 2 April 2012 (dashed) at sites CD02 (black), CD04 (blue), CD06 (red) and CD08 (green). Error bars denote 1 standard deviation (n = 2).

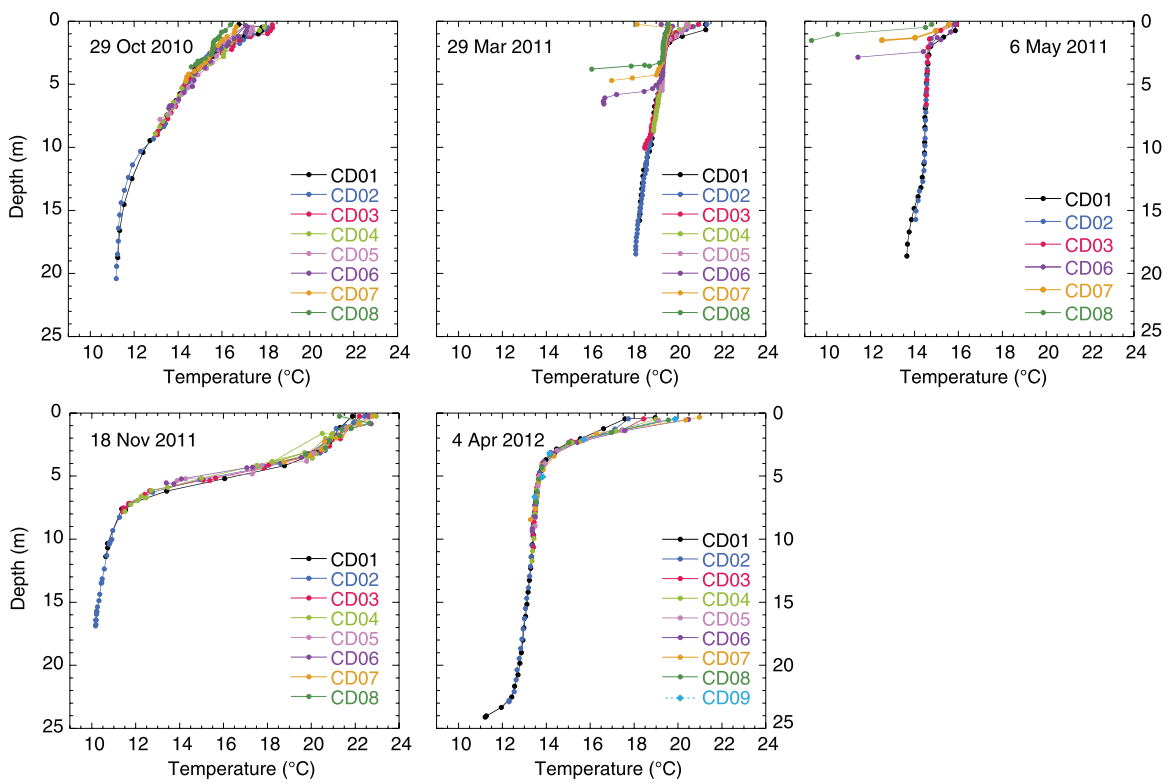


FIGURE 7 | Water column temperature profiles at each site during the five field trips: 29 October 2010. 29 March 2011, 6 May 2011, 18 November 2011, 4 April 2012.

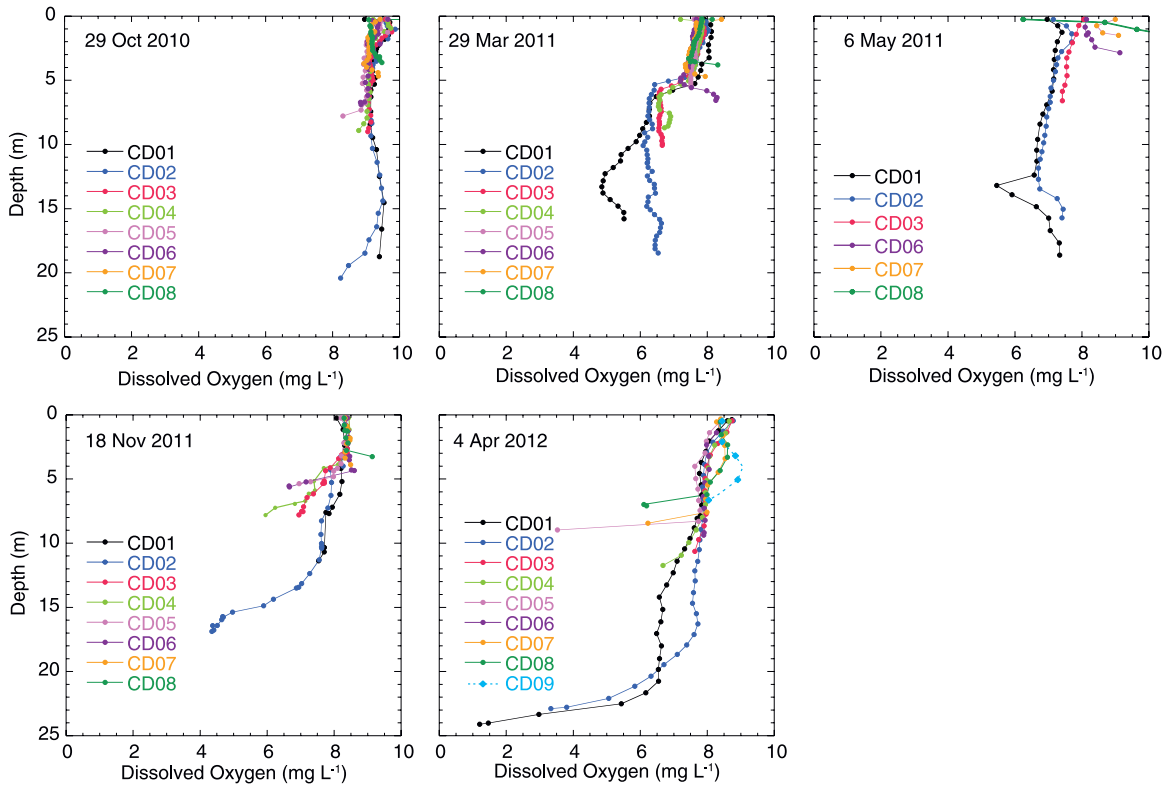


FIGURE 8 | Water column dissolved oxygen profiles at each site during the five field trips: 29 October 2010. 29 March 2011, 6 May 2011, 18 November 2011, 4 April 2012.

and possible deposition zone, but was not detected in the flux chamber measurements.

3.2.2 Areal Mean CH_4 fluxes

Averaged over the surface of the reservoir, the areal mean CH_4 flux increased by a factor of 23 from 4.25 mg-CH_4 m^{-2} d^{-1} in October 2010 to 99.1 mg-CH_4 m^{-2} d^{-1} in March 2011 following the first two flood events before decreasing to 9.20 mg-CH_4 m^{-2} d^{-1} in mid-autumn (**Table 1**). Mean areal CH_4 fluxes during 2011–2012 were the same (*t*-test of means, $p = 0.95$) at 29.8 and 31.6 mg-CH_4 m^{-2} d^{-1} before and after the March 2012 flood.

3.3 Reservoir Stratification

Temperature profile data (**Figure 7**) show that inflow events caused extensive mixing throughout the water column of the reservoir. The 29 October 2010 profile shows a hypolimnion temperature of 11°C—about 1°C warmer than similar observations in preceding years (unpublished data)—but with evidence of extensive disturbance and mixing of the water column over the top 10 m. By 29 March 2011, the hypolimnion temperature had increased to 18°C and the temperature gradient was linear from top-to-bottom, a condition that can only be caused by significant whole-water column mixing which presumably was the result of the December 2010 flood and the follow-up runoff event in January 2011. Autumnal cooling of the water column typically begins in April in this region and by 6 May 2011 seasonal cooling had caused full mixing throughout the water column which had cooled to 14°C at the bottom.

During 2011–2012, the water column exhibited a "typical" late spring temperature profile on 18 November 2011 with a hypolimnion temperature of 10°C and a very strong thermocline from 3 to 8 m depth. Following the March 2012 flood event, the 4 April 2012 profile shows that, despite the very large volume of inflow arriving at the dam in March (>120,000 mL), there was only limited warming of the hypolimnion to 11–13°C. The lack of greater hypolimnetic warming compared to the December 2010—January 2011 flood events was likely a consequence of the relatively warm inflow temperature (14–16°C) that would constrain the inflow to enter the reservoir, after entrainment of surface layer water, to the uppermost 5–10 m. The temperature at the sediment-water interface did not exceed ca. 13°C during the 2011–2012 season.

The strong difference between thermal stratification characteristics between years, with 2010–2011 at least 5°C warmer than 2011–2012, could be expected to have a substantial impact on any thermally regulated microbial processes in the reservoir such as methanogenesis.

The dissolved oxygen profiles (**Figure 8**) are consistent with this description of the physical mixing processes within the water column. Water column dissolved oxygen seldom fell below 6 mg-O_2 L^{-1}, a highly unusual condition close to the sediment-water

interface in a monomictic reservoir. (Note that oxygen profiles were not measured at the deepest part of the reservoir, thus local hypoxia cannot be excluded.) Dissolved oxygen was <4 mg O_2 L^{-1} on only one occasion (4 April 2012)—at sites CD01 and CD02 when the reservoir was at its deepest during the project.

The very weak vertical gradients in dissolved oxygen during 2010–2011suggest a combination of relatively high rates of vertical mixing and/or very low *in situ* oxygen demand in the hypolimnion. Given the elevated temperatures at depth during this season, and the recent large supply of organic matter, low oxygen demand seems less likely. Profiles from both 18 November 2011 and 4 April 2012 trips showed stronger gradients in dissolved oxygen close to the bottom of the water column indicating that sediment oxygen demand exceeded the turbulent diffusive supply of oxygen from above to a greater extent in 2011–12 compared to 2010–11.

Thermal stratification exhibited little longitudinal variability at depth with only minor divergences from one end of the reservoir to the other during each field trip apart from the measurements on 29 March 2011 and 6 May 2011 (**Figure 7**). At stations CD06, CD07, and CD08 a cold underflow is apparent in the lowest 2 m of each profile. This underflow was characterised also by relatively elevated dissolved oxygen concentrations (**Figure 8**). During the week prior to 29 March 2011, steady inflow to Cotter Reservoir from Bendora Dam averaged 0.6 m^3 s^{-1} and 0.4 m^3 s^{-1} from Condor Ck with temperatures in both streams steadily decreasing from 17 to 14°C. Just prior to 6 May, total inflow was 0.6 m^3 s^{-1} and a cold change in weather had decreased the stream temperature to 7–9°C, again consistent with the temperature of the underflow in the upper reaches of the reservoir and the development of a relatively colder lower 5 m of the water column further downstream. We note also that the seasonality and the observed temperature and dissolved oxygen differences are both tell-tale indicators of differential cooling (Wells and Sherman, 2001; Doda et al., 2022).

The biogeochemical consequences are that water from the upstream end of the reservoir, which is enriched in methane relative to the downstream stations (**Figure 6**), is translocated by a density current to deeper waters downstream. The overlying waters are effectively displaced upwards forming a methane-depleted surface layer flowing upstream towards the littoral area. This temperature differential was not seen during the final field trip (4 April 2012) when the seasonality was theoretically appropriate, but the weather was 3–5°C warmer than the prior year. Also, at this time the reservoir was 5 m deeper and the littoral zone—the source of the cooler and methane-enriched water had moved further upstream beyond station CD9 and was not detected by the sampling at this station.

Especially noteworthy is that the water column at the upstream littoral sites where the highest CH_4 fluxes were measured was always well oxygenated at the deepest point in the profile. This is consistent with the CH_4 production occurring in the sediments at these sites. The gravity currents moving methane enriched water downstream as a subsurface flow will transfer oxygenated littoral waters to the deeper reaches downstream also.

4 DISCUSSION

The profound hydrologic events caused by drought breaking rains in the catchment were followed by a substantial increase in methane emissions across the entire reservoir. As we show below, part of this increase is due to the observed changes in the stratification and sediment temperature produced by the inflows. A larger part of the increased emissions is attributed to the delivery of large amounts of allochthonous particulate organic carbon by the flood pulses.

4.1 Temperature and Stratification Effects

The impact of the large inflow volumes in late spring—early summer of 2010 on the relatively small reservoir was to completely mix the water column (**Figure 7**). In addition to the two large floods, inflow averaged >550 mL d^{-1} from September 2010 through February 2011. The nearly linear temperature stratification—as opposed to the more typical stratification of progressively increasing dT/dz as one approaches the bottom of the surface mixing layer from below—seen in other years (data not shown) in this monomictic reservoir confirms that profound mixing occurred. This mixing effect raised the bottom temperature from its typical seasonal value of ca. 10–18°C throughout the length of the reservoir.

The evidence indicates that the combined impact of the large inflow events on temperature stratification and the increased deposition of catchment organic matter was responsible for the 23-fold increase, relative to the first measurement on 29 October 2010, in reservoir CH_4 emissions observed following the first runoff event in late 2010 and the 7-fold increase observed the following year. It is significant that during the second year of the study, the large inflow event occurred in early autumn (March 2012) rather than late spring (mid-October 2010) because thermal stratification in the reservoir was stronger—the top to bottom temperature difference was 10–12°C for the second event compared to just 6°C for the first event. The stronger stratification and deeper water column appear to have prevented mixing all the way to the bottom of the water column in 2012 although there was sufficient mixing energy to create a linear temperature gradient. During 2012, the hypolimnion temperature was just 13°C compared to 18°C during the previous year.

Seasonal temperature differences alone cannot explain the variability in CH_4 emissions, as emissions were higher in November 2011 than in April 2012 despite the water column being cooler in November. The higher average wind speed (**Supplementary Figure S5**) during the November 2011 measurements would be expected to enhance the diffusive flux and partially compensate for a decrease in methane production rate due to the colder water temperatures. As well, ebullition may have been additionally suppressed by the 4 m deeper water column in April.

Assuming measurements of thermal mediation of methane production by other researchers (Duc et al., 2010; Lofton et al., 2014) are applicable to Cotter Reservoir, we suggest that temperature effects alone increased methane emissions by 2–7 times following the 2010–2011 floods and by 1.3–2 times following the March 2012 flood. If we assume the higher estimates for each year, then the increased supply of catchment organic matter accounted for an additional increase in emissions by a factor of 3.3–3.5 during both years.

4.2 Delivery of Allochthonous Organic Carbon

The supply of catchment organic matter has been hypothesized to be responsible for consistent spatial patterns of CH_4 emissions by the authors in other storages in Australia (Sherman et al., 2012) and elsewhere (**Section 1**). The 2010 inflow was, we suggest, an event which delivered unusually large amounts of reactive organic matter to the reservoir.

The late 2010 inflow event was the first significant inflow event since the onset of the Millennium Drought of 2002–2009 in eastern Australia. Much of the catchment vegetation was *Eucalyptus* spp. which shed their leaves annually and, under conditions of extreme drought die off, adding further to the accumulated leaf litter. Under drought conditions there would have been an unusually large build up of organic matter. In addition, the lower catchment was only slowly recovering from the effects of the devastating 2003 Canberra bushfire. Landscape recovery activities undertaken prior to the floods had left substantial piles of debris in a highly disturbed, erosion-prone Lower Cotter subcatchment (Wade et al., 2013). It is reasonable to expect that the drought-breaking runoff transported a particularly large amount of eroded soil and terrestrial organic matter which had been accumulating in the catchment over the preceding years. This sediment and organic matter would be deposited in the reservoir with much of it focused in the upstream reaches of the water body as the inflow decelerated and heavier particulates fell out to the bottom. Such an increase of organic matter towards the upstream end of the reservoir is consistent with our observations of increasing CH_4 fluxes as the upstream end of the reservoir was approached (**Figure 4**).

The impact of the 2003 Canberra bushfire—which devasted the Cotter catchment—should be considered as well. In addition to the relatively high hillside and gully erosion potential of the landscape arising from historical forestry operations close to the reservoir, the bushfire destroyed most of the vegetation in this area and burned hot enough to change the soil properties in a way that would further exacerbate erosion. Post-fire activities in the nearby catchment included large scale harvesting of salvageable timber (Wade et al., 2013) with the consequence that at the time of our measurements most of the immediate catchment consisted mainly of grasses and scrubby vegetation (e.g., blackberries) and occasional log piles. We assume that both the bushfire itself and the post-fire management activities further increased the susceptibility of the catchment to erosion and added to the supply of readily eroded or transported organic matter.

4.3 Increased CH_4 Fluxes and Increased Ebullition Post Deposition Events

Even after allowing for the different temperature effects after the 2 flood events, average methane emissions were up to 3.5 times greater than before the floods. These effects are most clearly seen at Site CD08 where the CH_4 flux is the largest of all sites post flood and increased by a factor of about 100. This increase represents the transition from a flux characteristic of an "old" reservoir (4.3 mg-CH_4 m^{-2} d^{-1}) to the much higher and ebullition-dominated fluxes (99 mg-CH_4 m^{-2} d^{-1}) similar to those of the allochthonous influenced sites in the lake Wohlen (DelSontro et al., 2010) and Saar River impoundments (Maeck et al., 2013) (discussed in Section1).

Emissions at site CD08 had been the only ebullition emissions before the flood whereas ebullition occurred at six of the seven sites measured following the first flood. At 4 of these post-flood sites, ebullition was the dominant contributor (relative to diffusion) to the total flux (**Figure 4**). The effect of the floods was to extend the higher flux and ebullition-rich zone further into the dam towards the dam wall.

The behavior of CD08 is noteworthy in that ebullition was the larger component of the total CH_4 flux on all 5 sampling visits, even though the magnitude of the flux varied by a factor of 20 across the measurements. Furthermore, the site was always in oxygenated water (**Figure 8**). We attribute this effect to its location in the river delta section of the reservoir—the region of trapping of incoming particulate organic debris even under regular or low flow conditions—providing a continuing input of fresh reactive organic matter.

4.4 Implications

There are 2 major implications from this work: methane fluxes from "old" reservoirs (those where the original *in situ* supply of reactive organic carbon, inundated on dam construction, has been exhausted) may be stimulated by episodic events. This increase is a step change in the total CH_4 flux and persists for some time. These episodic events deliver uneven distributions of new, reactive allochthonous carbon to the reservoir which support higher rates of CH_4 emission reflecting the sedimentation pattern of the new material within the reservoir. The distribution of sediment within the reservoir is dependent on the residence time of the flood pulse within the reservoir, the inflow sediment concentration, and the sedimentation rate of the material in the pulse. Consequently, the location of sediment zones (and high emission areas) may vary from event to event and change location and extent within the reservoir depending on the source and size of the flood.

Much of the existing data on reservoir CH_4 emissions are based on studies with limited temporal coverage, i.e., based on time-limited field measurement campaigns that cannot realistically be expected to incorporate interannual to decadal hydrographic perturbations.

Our results suggest that major episodic hydrological disturbances can have a large impact on measured reservoir CH_4 emissions and that these effects persist for at least a year. The timing of field measurements relative to hydrological events should be considered when extrapolating from brief periods of field observations to decadal and longer

estimates of reservoir emissions used in Greenhouse Inventory accounting.

Furthermore, better understanding of catchment properties, especially the reactivity and quantities of mobilizable particulate organic carbon, is necessary for predicting reservoir emissions in the face of climate change.

DATA AVAILABILITY STATEMENT

The raw data supporting the conclusion of this article will be made available by the authors, without undue reservation.

AUTHOR CONTRIBUTIONS

BSS and PWF developed the experimental design and performed all the sampling and data analysis. BSS wrote the preliminary report with assistance from PWF including preparation of all figures. Both authors wrote the main manuscript text, interpreted the data, discussed the results, and reviewed the manuscript.

FUNDING

Financial support for the "Cotter Dam Methane Emissions" project was provided by Icon Water (formerly ACTEW) and CSIRO's Integrated Water Systems stream in the Urban Water theme. Financial support for publication was provided by the University of Canberra Centre for Applied Water Science and Reservoir Doctors Pty Ltd.

ACKNOWLEDGMENTS

The authors would like to thank Icon Water and Marco Bottari (Icon Water) for permission and support to conduct this work at Cotter Reservoir; Jim Brophy (CSIRO) and Danny Hunt (CSIRO) for their valuable technical support in carrying out the field work; and to Drs. Todd Scicluna and Perran Cook (Monash University Water Studies Centre) for performing the gas chromatography. Special thanks to Dr. Jon Sanderman for valuable comments on the project reports which formed the basis of this manuscript. We also wish to thank two reviewers for their very helpful and insightful comments which have led to a substantially improved manuscript.

SUPPLEMENTARY MATERIAL

The Supplementary Material for this article can be found online at: https://www.frontiersin.org/articles/10.3389/fenvs.2022.893180/full#supplementary-material

REFERENCES

Aben, R. C. H., Barros, N., van Donk, E., Frenken, T., Hilt, S., Kazanjian, G., et al. (2017). Cross Continental Increase in Methane Ebullition under Climate Change. *Nat. Commun.* 8, 1682. doi:10.1038/s41467-017-01535-y

Alluvium Consulting (2020). *Cotter Catchment Actions for Clean Water Plan*. Canberra: Alluvium Consulting.

Beaulieu, J. J., Waldo, S., Balz, D. A., Barnett, W., Hall, A., Platz, M. C., et al. (2020). Methane and Carbon Dioxide Emissions from Reservoirs: Controls and Upscaling. *J. Geophys Res. Biogeosci* 125, e2019JG005474. doi:10.1029/2019JG005474

Deemer, B. R., Harrison, J. A., Li, S., Beaulieu, J. J., DelSontro, T., Barros, N., et al. (2016). Greenhouse Gas Emissions from Reservoir Water Surfaces: A New Global Synthesis. *BioScience* 66, 949–964. doi:10.1093/biosci/biw117

Deemer, B. R., and Holgerson, M. A. (2021). Drivers of Methane Flux Differ between Lakes and Reservoirs, Complicating Global Upscaling Efforts. *Biogeosciences* 126, e2019JG005600. doi:10.1029/2019jg005600

DelSontro, T., Kunz, M. J., Kempter, T., Wüest, A., Wehrli, B., and Senn, D. B. (2011). Spatial Heterogeneity of Methane Ebullition in a Large Tropical Reservoir. *Environ. Sci. Technol.* 45, 9866–9873. doi:10.1021/es2005545

DelSontro, T., McGinnis, D. F., Sobek, S., Ostrovsky, I., and Wehrli, B. (2010). Extreme Methane Emissions from a Swiss Hydropower Reservoir: Contribution from Bubbling Sediments. *Environ. Sci. Technol.* 44, 2419–2425. doi:10.1021/es9031369

Doda, T., Ramón, C. L., Ulloa, H. N., Wüest, A., and Bouffard, D. (2022). Seasonality of Density Currents Induced by Differential Cooling. *Hydrol. Earth Syst. Sci.* 26, 331–353. doi:10.5194/hess-26-331-2022

Duc, N. T., Crill, P., and Bastviken, D. (2010). Implications of Temperature and Sediment Characteristics on Methane Formation and Oxidation in Lake Sediments. *Biogeochemistry* 100, 185–196. doi:10.1007/s10533-010-9415-8

Etiope, G., and Schwietzke, S. (2019). Global Geological Methane Emissions: An Update of Top-Down and Bottom-Up Estimates. *Elem. Sci. Anthropocene* 7, 47. doi:10.1525/elementa.383

Lambert, M., and Fréchette, J.-L. (2005). "Analytical Techniques for Measuring Fluxes of CO2 and CH4 from Hydroelectric Reservoirs and Natural Water Bodies," in *Greenhouse Gas Emissions - Fluxes and Processes: Hydroelectric Reservoirs and Natural Environments*. Editors A. Tremblay, L. Varfalvy, C. Roehm, and M. Garneau (Berlin, Heidelberg: Springer Berlin Heidelberg), 37–60. doi:10.1007/978-3-540-26643-3_3

Lan, X., Basu, S., Schwietzke, S., Bruhwiler, L. M. P., Dlugokencky, E. J., Michel, S. E., et al. (2021). Improved Constraints on Global Methane Emissions and Sinks Using δ13C-CH4. *Glob. Biogeochem. Cycles* 35, e2021GB007000. doi:10.1029/2021gb007000

Lofton, D. D., Whalen, S. C., and Hershey, A. E. (2014). Effect of Temperature on Methane Dynamics and Evaluation of Methane Oxidation Kinetics in Shallow Arctic Alaskan Lakes. *Hydrobiologia* 721, 209–222. doi:10.1007/s10750-013-1663-x

Lynch, J., Cain, M., Pierrehumbert, R., and Allen, M. (2020). Demonstrating GWP*: A Means of Reporting Warming-Equivalent Emissions that Captures the Contrasting Impacts of Short- and Long-Lived Climate Pollutants. *Environ. Res. Lett.* 15, 044023. doi:10.1088/1748-9326/ab6d7e

Maeck, A., DelSontro, T., McGinnis, D. F., Fischer, H., Flury, S., Schmidt, M., et al. (2013). Sediment Trapping by Dams Creates Methane Emission Hot Spots. *Environ. Sci. Technol.* 47, 8130–8137. doi:10.1021/es4003907

McClure, R. P., Lofton, M. E., Chen, S., Krueger, K. M., Little, J. C., and Carey, C. C. (2020). The Magnitude and Drivers of Methane Ebullition and Diffusion Vary on a Longitudinal Gradient in a Small Freshwater Reservoir. *J. Geophys. Res. Biogeosciences* 125, e2019JG005205. doi:10.1029/2019jg005205

Musenze, R. S., Grinham, A., Werner, U., Gale, D., Sturm, K., Udy, J., et al. (2014). Assessing the Spatial and Temporal Variability of Diffusive Methane and Nitrous Oxide Emissions from Subtropical Freshwater Reservoirs. *Environ. Sci. Technol.* 48, 14499–14507. doi:10.1021/es505324h

Prather, M. J., Holmes, C. D., and Hsu, J. (2012). Reactive Greenhouse Gas Scenarios: Systematic Exploration of Uncertainties and the Role of Atmospheric Chemistry. *Geophys. Res. Lett.* 39, L09803. doi:10.1029/2012gl051440

Rosentreter, J. A., Borges, A. V., Deemer, B. R., Holgerson, M. A., Liu, S., Song, C., et al. (2021). Half of Global Methane Emissions Come from Highly Variable Aquatic Ecosystem Sources. *Nat. Geosci.* 14, 225–230. doi:10.1038/s41561-021-00715-2

Saunois, M., Stavert, A. R., Poulter, B., Bousquet, P., Canadell, J. G., Jackson, R. B., et al. (2020). The Global Methane Budget 2000–2017. *Earth Syst. Sci. Data* 12, 1561–1623. doi:10.5194/essd-12-1561-2020

Sherman, B., Ford, P., Hunt, D., and Drury, C. (2012). *Reservoir Methane Monitoring and Mitigation - Little Nerang and Hinze Dam Case Study*. Brisbane: Urban Water Security Research Alliance. Available at: https://publications.csiro.au/rpr/pub?pid=csiro:EP124042.

Shindell, D., Kuylenstierna, J. C. I., Vignati, E., van Dingenen, R., Amann, M., Klimont, Z., et al. (2012). Simultaneously Mitigating Near-Term Climate Change and Improving Human Health and Food Security. *Science* 335, 183–189. doi:10.1126/science.1210026

Sobek, S., DelSontro, T., Wongfun, N., and Wehrli, B. (2012). Extreme Organic Carbon Burial Fuels Intense Methane Bubbling in a Temperate Reservoir. *Geophys. Res. Lett.* 39, L01401. doi:10.1029/2011gl050144

Turner, A. J., Frankenberg, C., and Kort, E. A. (2019). Interpreting Contemporary Trends in Atmospheric Methane. *Proc. Natl. Acad. Sci. U.S.A.* 116, 2805–2813. doi:10.1073/pnas.1814297116

Wade, A., White, I., Worthy, M., Gill, A. M., Mueller, N., Taylor, P., et al. (2013). Land Management Impacts on Water Quality Following Fire in a Major Water Supply Catchment. *Australas. J. Water Resour.* 16, 121–139. doi:10.7158/w10-841.2013.16.2

Wells, M. G., and Sherman, B. (2001). Stratification Produced by Surface Cooling in Lakes with Significant Shallow Regions. *Limnol. Oceanogr.* 46, 1747–1759. doi:10.4319/lo.2001.46.7.1747

Yang, L. (2019). Contrasting Methane Emissions from Upstream and Downstream Rivers and Their Associated Subtropical Reservoir in Eastern China. *Sci. Rep.* 9, 8072. doi:10.1038/s41598-019-44470-2

Zhao, Y., Sherman, B., Ford, P., Demarty, M., DelSontro, T., Harby, A., et al. (2015). A Comparison of Methods for the Measurement of CO2 and CH4 Emissions from Surface Water Reservoirs: Results from an International Workshop Held at Three Gorges Dam, June 2012. *Limnol. Oceanogr. Methods* 13, 15–29. doi:10.1002/lom3.10003

Conflict of Interest: The authors declare that the research was conducted in the absence of any commercial or financial relationships that could be construed as a potential conflict of interest. At the time the project was undertaken (2010-2012), both BSS and PWF were solely employed by CSIRO. Reservoir Doctors Pty Ltd. is a sole proprietor company established in 2014 by BSS to facilitate undertaking part-time ad hoc consulting work following his departure/retirement from CSIRO in late 2013. BSS continues as a visiting scientist at CSIRO and an Adjunct Associate Professor at the Centre for Applied Water Science, University of Canberra, Bruce, ACT, Australia.

Publisher's Note: All claims expressed in this article are solely those of the authors and do not necessarily represent those of their affiliated organizations, or those of the publisher, the editors and the reviewers. Any product that may be evaluated in this article, or claim that may be made by its manufacturer, is not guaranteed or endorsed by the publisher.

Copyright © 2022 Sherman and Ford. This is an open-access article distributed under the terms of the Creative Commons Attribution License (CC BY). The use, distribution or reproduction in other forums is permitted, provided the original author(s) and the copyright owner(s) are credited and that the original publication in this journal is cited, in accordance with accepted academic practice. No use, distribution or reproduction is permitted which does not comply with these terms.

frontiers | Frontiers in Environmental Science

REVIEW
published: 19 May 2022
doi: 10.3389/fenvs.2022.866082

Challenges Regionalizing Methane Emissions Using Aquatic Environments in the Amazon Basin as Examples

John M. Melack[1,2], Luana S. Basso[3], Ayan S. Fleischmann[4], Santiago Botía[5], Mingyang Guo[6], Wencai Zhou[1], Pedro M. Barbosa[1,7], Joao H.F. Amaral[1,8] and Sally MacIntyre[1,9]*

[1]Earth Research Institute, University of California, Santa Barbara, Santa Barbara, CA, United States, [2]Bren School of Environmental Science and Management, University of California, Santa Barbara, Santa Barbara, CA, United States, [3]General Coordination of Earth Science, National Institute for Space Research, São José dos Campos, Brazil, [4]Mamirauá Institute for Sustainable Development, Tefé, Brazil, [5]Biogeochemical Signals Department, Max Planck Institute for Biogeochemistry, Jena, Germany, [6]Department of Earth, Atmospheric and Planetary Sciences, Purdue University, West Lafayette, IN, United States, [7]Groupe de Recherche Interuniversitaire en Limnologie, Département des Sciences Biologiques, Université du Québec à Montréal, Montreal, QC, Canada, [8]Engineering School of Sustainable Infrastructure & Environment, University of Florida, Gainesville, FL, United States, [9]Department of Ecology, Evolution and Marine Biology, University of California, Santa Barbara, Santa Barbara, CA, United States

OPEN ACCESS

Edited by:
Hans-Peter Grossart, University of Potsdam, Germany

Reviewed by:
Renato Campello Cordeiro, Fluminense Federal University, Brazil
Bernhard Wehrli, ETH Zürich, Switzerland

***Correspondence:**
John M. Melack
melack@bren.ucsb.edu

Specialty section:
This article was submitted to Biogeochemical Dynamics, a section of the journal Frontiers in Environmental Science

Received: *30 January 2022*
Accepted: *25 April 2022*
Published: *19 May 2022*

Citation:
Melack JM, Basso LS, Fleischmann AS, Botía S, Guo M, Zhou W, Barbosa PM, Amaral JHF and MacIntyre S (2022) Challenges Regionalizing Methane Emissions Using Aquatic Environments in the Amazon Basin as Examples. Front. Environ. Sci. 10:866082. doi: 10.3389/fenvs.2022.866082

Key challenges to regionalization of methane fluxes in the Amazon basin are the large seasonal variation in inundated areas and habitats, the wide variety of aquatic ecosystems throughout the Amazon basin, and the variability in methane fluxes in time and space. Based on available measurements of methane emission and areal extent, seven types of aquatic systems are considered: streams and rivers, lakes, seasonally flooded forests, seasonally flooded savannas and other interfluvial wetlands, herbaceous plants on riverine floodplains, peatlands, and hydroelectric reservoirs. We evaluate the adequacy of sampling and of field methods plus atmospheric measurements, as applied to the Amazon basin, summarize published fluxes and regional estimates using bottom-up and top-down approaches, and discuss current understanding of biogeochemical and physical processes in Amazon aquatic environments and their incorporation into mechanistic and statistical models. Recommendations for further study in the Amazon basin and elsewhere include application of new remote sensing techniques, increased sampling frequency and duration, experimental studies to improve understanding of biogeochemical and physical processes, and development of models appropriate for hydrological and ecological conditions.

Keywords: wetlands, floodplains, methane fluxes, remote sensing, inundation, modeling

1 INTRODUCTION

Emissions of methane from inland aquatic ecosystems are large and highly variable (Saunois et al., 2020; Rosentreter et al., 2021). Hence, estimating regional and global emissions is important and challenging. Bottom-up extrapolations often lack sufficient measurements for robust estimates. Simulation models of fluxes and aircraft or satellite analyses of atmospheric concentrations and emissions have other limitations and uncertainties (Ma et al., 2021). Tropical wetlands, in particular, are large, natural sources of methane

and their interannual variations in area contribute to varying atmospheric concentrations (Nisbet et al., 2016; Pandey et al., 2017). As the climate warms, the role of tropical wetlands is likely to be enhanced (Zhang et al., 2017). With aquatic ecosystems extending over about 20% of its area (Junk et al., 2011), the Amazon basin represents a major proportion of tropical methane emissions. Hence, we use the Amazon basin as a data-rich, tropical region, and take advantage of its extensive and varied aquatic environments to illustrate and evaluate regionalization approaches, data requirements and results. The challenges considered for the Amazon basin are general to regionalization efforts elsewhere, and lessons learned can be applied to other regions, such as the warming arctic (Wik et al., 2016) or African wetlands (Lunt et al., 2021).

Aquatic ecosystems contribute to large fluxes of carbon in the Amazon basin. High rates of primary production, respiration and methanogenesis lead to fluxes of carbon dioxide and methane to the atmosphere from rivers, lakes, floodplains and other wetlands (Richey et al., 2002; Melack et al., 2004; Melack et al., 2009; Forsberg et al., 2017; Pangala et al., 2017). Though remote sensing of inundation (e.g., Hamilton et al., 2002; Parrens et al., 2019; Prigent et al., 2020) and aquatic habitats (Hess et al., 2003, 2015), inundation modeling (e.g., Coe et al., 2007; Paiva et al., 2013), and measurements of gas concentrations and fluxes in rivers, reservoirs, lakes and wetlands are available (Melack, 2016; Barbosa et al., 2020), considerable uncertainty and information gaps remain. Key challenges to regionalization of methane fluxes in the Amazon basin are the large seasonal variation in inundated areas and habitats, the wide variety of aquatic ecosystems throughout the Amazon basin, and the variability in methane fluxes in time and space. Further issues stem from the various types of methods used and difficulties estimating ebullitive fluxes.

Regionalization can be done at several scales from that of floodplain lakes and wetland types to large regions to the whole Amazon basin. Habitat-specific fluxes can be combined with estimates of habitat areas and their seasonal variations. Mechanistic models can provide an alternative way to estimate regional fluxes. Results from aircraft and satellite measurements of gas concentrations combined with atmospheric transport models can offer integrated regional estimates.

To examine challenges regionalizing methane emissions in the Amazon basin we first consider the hydrological variability and the variety of aquatic ecosystems and their spatial extent. Next the adequacy of sampling and of field methods plus atmospheric measurements, as applied to the Amazon basin, are discussed, followed by a summary of published fluxes. Then, understanding of relevant biogeochemical and physical processes in Amazon aquatic environments and their incorporation into mechanistic and statistical models are examined. Prior and current regional estimates using bottom-up and top-down approaches are reviewed and critiqued. Lastly, recommendations for further study are made.

2 HYDROLOGICAL VARIABILITY AND INUNDATION ESTIMATES

The hydrological Amazon basin extends over ~6 million km^2 with major rivers including the Solimões, Madeira, Negro and Japurá joining to form the mainstem Amazon River with annual discharge up to about 20% of global fluvial inputs to oceans. Recent reviews and analyses offer valuable perspectives on hydrological conditions in the Amazon basin of relevance to regionalization of methane fluxes. Fassoni-Andrade et al. (2021) provide a comprehensive review of the water cycle, associated hydrological processes and relevant remote sensing advances in the Amazon basin with its high rates of precipitation, extensive floodplains, diverse tropical forests, complex topography, and large variations in freshwater storage and discharge. Melack and Coe (2021) focus on hydrological aspects of Amazon floodplains in relation to ecological processes. Fleischmann et al. (2021) present an intercomparison of 29 inundation datasets for the Amazon basin derived from remote sensing-based products, hydrological models and multi-source products, and illustrate the variety and divergences among the datasets currently available (**Figures 1**, **2**).

Variations in rainfall and large changes in river stage and discharge combined with backwater effects and flood propagation result in seasonal and interannual variations in extent of inundation of thousands of lakes, floodplains and other wetlands (Meade et al., 1991; Espinoza et al., 2009; Paiva et al., 2013). Annual amplitude variation in river water levels can be as high as 15 m (Fassoni-Andrade et al., 2021). Particularly high or low rainfall is linked to ENSO events and strong warming of surface waters in the tropical North Atlantic (Marengo and Espinoza 2016). Moreover, the hydrology of the Amazon is not stationary, and positive trends in maximum river water levels across the central basin are evident (Gloor et al., 2013; Barichivich et al., 2018), with several record-breaking floods in the last decade registered in cities such as Manaus (Espinoza et al., 2021). The hydrology of floodplains and other wetlands combines inputs from local catchments with regional-scale fluxes and is characterized by variations in the amplitude, duration, frequency, and predictability of inundation and a seasonally flooded ecotone, called the aquatic-terrestrial transition zone, that often contains woody and herbaceous vegetation (Melack and Coe 2021).

Inundation extent can be simulated with process-based models, and models have been applied at the scale of specific lakes (Ji et al., 2019), floodplain reaches (Wilson et al., 2007; Rudorff et al., 2014 a,b; Pinel et al., 2019) and the whole basin (e.g., Coe et al., 2007; Yamazaki et al., 2011; Miguez-Macho and Fan 2012; Paiva et al., 2013). Apers et al. (2022) used literature-based parameters for natural peatlands to develop and integrate a tropical peatland hydrology module into a global land surface model; global meteorological reanalysis data were used as inputs. In the Amazon basin both lowland and Andean peatland hydrology were simulated; both need further validation.

Temporal (from static to monthly intervals, up to a few decades) and spatial (at resolutions from 12.5 m to 25 km) changes in water level and inundation can be detected with remote sensing techniques, as summarized in Fleischmann et al. (2021). Long-term, maximum inundated area for the basin <500 m asl is estimated as ~600000 ± ~82,000 km^2 using synthetic aperture radar (SAR)-based products, though subregional products suggest a basin-wide underestimation of ~10%. Minimum inundation extent using SAR-based products is

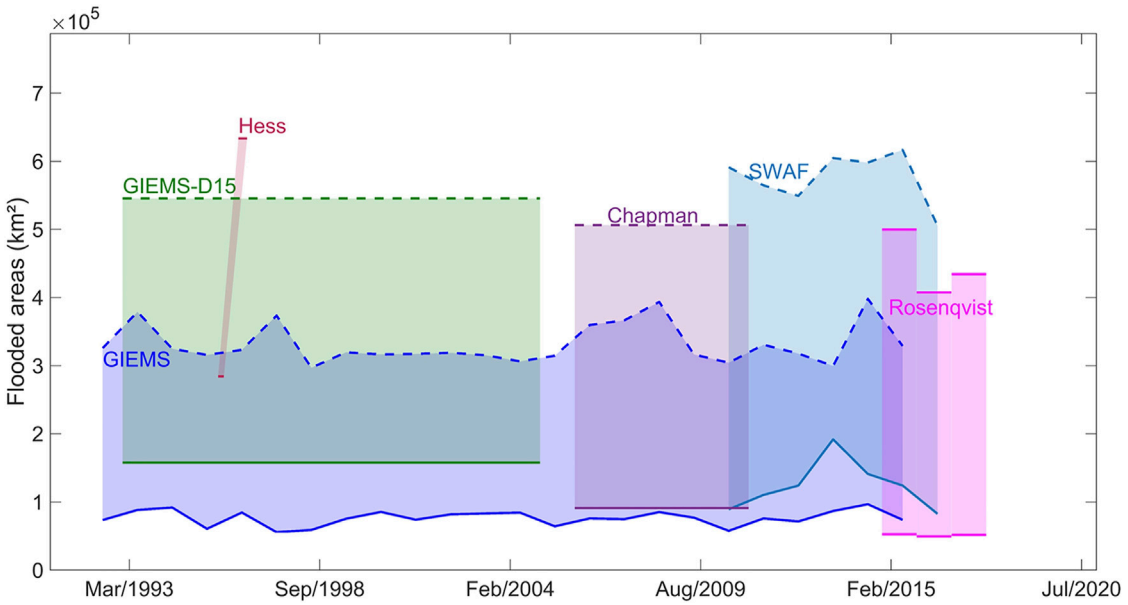


FIGURE 1 | Maximum and minimum inundated areas for Amazon basin <500 m asl based on different remote sensing and analysis techniques. GIEMS: Prigent et al. (2020), GIEMS-D15: Fluet-Chouinard et al. (2015), Chapman: Chapman et al. (2015), SWAF: Parrens et al. (2019), Rosenqvist: Rosenqvist et al. (2020), Hess: Hess et al. (2015).

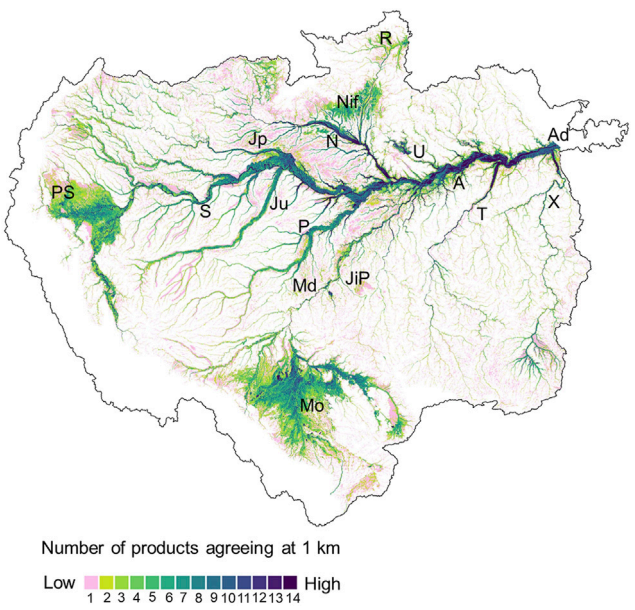


FIGURE 2 | Hydrological Amazon basin with inundated areas shown for basin <500 m asl based on different remote sensing and analysis techniques. Each 1 km pixel shows the number of basin-scale inundation datasets (total of 14 products were assessed) that agree that the pixel is floodable, according to Fleischmann et al. (2021). Rivers and wetlands mentioned in the text: Solimões—S, Madeira—Md, Negro—N, Japurá—Jp, Juruá—Ju, Purus—P, Amazonas—A, Tapajós—T, Xingu—X, Ji-Paraná—JiP, Uatumã—U, Llanos de Moxos - Mo, Pacaya-Samiria - PS, Negro interfluvial wetlands - Nif, Roraima—R, Amazon delta wetlands—Ad.

estimated as 139,300 ± 127,800 km^2. Differences among products arise from differing characteristics of sensors, periods of acquisitions, spatial resolution, and data processing algorithms. Especially large uncertainties exist for interfluvial wetlands (Llanos de Moxos, Pacaya-Samiria, *campinas* and *campinaranas* in the Negro basin, Roraima), where inundation tends to be shallower and more variable in time than along riverine floodplains.

While quite useful, remote sensing and modeling results do have limitations. Gauges of river stage are widely spaced, and floodplains are ungauged with a few exceptions; satellite-borne altimeters have wide spacing along tracks, though work fairly well for rivers. Gravity anomaly sensors based on the GRACE missions (Tapley et al., 2004) have been used to monitor changes in floodplain water storage at the basin scale (Alsdorf et al., 2010). For monitoring inundation dynamics, passive microwave has coarse spatial resolution, and SAR data have limited temporal or spatial coverage, though new sensors offer repeated regional coverage. Forthcoming missions, such as the Surface Water and Ocean Topography (SWOT) and the NASA-ISRO Synthetic Aperture Radar (NISAR) missions, will provide useful data to monitor the extent and water levels of Amazonian wetlands. Topographic and bathymetric data at high vertical resolution are fundamental to understand the dynamics of floodplain water storage, but they are rare, though improved digital elevation models are now becoming available (see https://eop-cfi.esa.int/index.php/docs-and-mission-data/dem for list; including the Copernicus global 30 m product; O'Loughlin et al., 2016; Nardi et al., 2019; Fassoni-Andrade et al., 2020).

3 AQUATIC SYSTEMS AND THEIR SPATIAL EXTENT IN AMAZON BASIN

Aquatic ecosystems in the basin range from small streams to large rivers fringed by floodplains, lakes and seasonally flooded forests and savannas. Topographic, climatic, and landscape features range from Andean highlands in the west to lowlands across the central and eastern basin. Based on information available for climate, hydrology, water, sediments and plants, Junk et al. (2011) classified 14 major types of natural wetlands in the lowland Amazon. The amplitude, duration, frequency and predictability of inundation are key criteria in their classification, though these hydrological aspects have insufficient spatial and temporal data for many parts of the basin. Furthermore, a functional classification of these aquatic ecosystems in terms of their relevance to methane biogeochemistry and flux, as encouraged by Sahagian and Melack (1998), is lacking. Hence, our first challenge to regionalizing methane emissions concerns the appropriate characterization of the varied systems, their spatial extent and temporal variability.

Based on available measurements of methane emission and areal extent, seven types of aquatic systems will be considered: streams and rivers, lakes, seasonally flooded forests, seasonally flooded savannas and other interfluvial wetlands, herbaceous plants on riverine floodplains, peatlands, and hydroelectric reservoirs. Aquatic habitats with insufficient information about methane fluxes include coastal freshwater wetlands, such as the wetlands on Marajós Island in the Amazon delta, agricultural ponds (Macedo et al., 2013), road-blocked streams (Leitão et al., 2018), tank bromeliads and cultivated rice. More broadly, retarded drainage can lead to saturated soils without standing water throughout the basin with unknown extent or duration. Estimates of areal extent, judged as the most reliable with caveats, are provided. General issues are the regional boundaries represented by different datasets, as well as inherent limitations of the methods and their validation.

Given the Amazon basin's immense scale, variability and difficult access, remote sensing approaches are essential to characterize the aquatic systems. Aquatic habitats range in dimension from headwater streams (<1 m across) to ponds and large lakes to floodplains tens of kilometers wide to wetlands covering tens of thousands of km^2, adding further challenges. Passive and active microwave, laser, visible and near-infrared and gravity anomaly detection systems have been applied in the Amazon basin (Melack 2004; Fassoni-Andrade et al., 2021). SAR techniques are of particular utility because inundation under vegetation and relevant types of aquatic vegetation can be detected, and data can be acquired during day or night and under clouds (e.g., Kasischke et al., 1997; Silva et al., 2015). Melack and Hess (2010) and Hess et al. (2015) used the methodology described in Hess et al. (2003) to determine floodable area, inundated area, and areal extent of major habitats permanently or periodically inundated in the lowland Amazon basin based on mosaics of SAR data obtained during low and high river stages in 1995 and 1996. Open water and herbaceous and woody plants within floodable regions were distinguished at a spatial resolution of about 100 m. High-resolution airborne videography and laser altimetry were used to validate the classifications (Hess et al., 2002). Other remotely sensed products that characterize aquatic habitats are available for specific locations (e.g., Silva et al., 2010; Renó et al., 2011; Hawes et al., 2012; Arnesen et al., 2013; Ferreira-Ferreira et al., 2015).

3.1 Rivers and Streams

Allen and Pavelsky (2018) used Landsat and river stage data to determine river widths at mean annual discharge and judged their estimates accurate for widths wider than 90 m. Since the HydroBASINS dataset used for the river network is derived from a single flow direction algorithm, it cannot represent braided channels, such as occur in some reaches of Amazonian rivers. Their river channel, surface area estimate within the Amazon basin is ~58,000 km^2. Mouthbays of rivers, such as the Tapajós, Xingu, Tefé and Coari, were considered lakes, and the analysis did not include the whole delta. Combining their river channel area with estimates for the delta (9,500 km^2, Castello et al., 2013 plus L.L. Hess, personal communication) and mouthbays of the Tapajós and Xingu (3,800 km^2, Sawakuchi et al., 2014) results in a river channel area of 77,500 km^2. An analysis for drainage areas from 1 to 431,000 km^2 and channels >2 m in width used hydraulic geometry and the drainage network to estimate the Amazon basin (excluding the delta and mouthbays) to have a combined area of about 60,000 km^2 (Beighley and Gummadi 2011). Given that this procedure included smaller rivers than Allen and Pavelsky's analysis and used independent data, the two estimates are quite similar. As another example, Rasera et al. (2008) developed empirical relationships between drainage area and channel widths combined with river lengths derived from a digital river network to determine the area of streams and rivers in the Ji-Paraná River basin. Assuming their relationship applied to the whole lowland Amazon basin, an area of 23,000 km^2 would result for rivers from third to sixth order, similar to that estimated by Beighley and Gummadi (2011) for rivers in that size range. These estimates do not include headwater streams (zero or first orders) that require high resolution topography quite difficult to obtain under forest canopies or labor-intensive surveying. Riparian corridors, often with saturated soils, periodically flooded (Chambers et al., 2004), are also not included.

Large Amazon rivers are typically considered "white waters" with near-neutral pH and relatively high suspended sediment and nutrient concentrations (e.g., Amazon, Madeira, Purus, Juruá and Japurá), "black waters" with low pH, nutrients and suspended sediments and high dissolved organic carbon (e.g., Negro, Uatumã), and "clear waters" with low to neutral pH and low nutrients, suspended sediments and dissolved organic carbon (e.g., Tapajós and Xingu) (Mayorga and Aufdenkampe 2002; Junk et al., 2011). These three types of river water were classified for 6th to 11th order rivers based on field observations and visual inspection of optical images by Venticinque et al. (2016). Smaller rivers and streams are likely to vary considerably in chemical composition, but regional characterization is lacking.

3.2 Lakes

If calculated as the difference between SAR analysis of open water areas at ~100 m resolution for a period with near-maximum inundation in the central lowland Amazon basin (Hess et al., 2015) minus the river channel areas for rivers wider than 90 m (Allen and Pavelsky 2018), an area of ~20,000 km^2 results. Since the river channel areas were derived for the whole basin and the SAR analysis applies only to the basin <500 asl, the lake area is probably under estimated. The HydroLAKES database (Messager et al., 2016) subsetted for the Amazon basin has a lake area of ~23,000 km^2. This data set for lakes >0.1 km^2 used several data sources, including the SRTM waterbody data (Slater et al., 2006), and underwent manual removal of river and wetland polygons and other corrections.

Using side-looking airborne radar imagery acquired mostly during periods of low to moderate inundation by *Projecto RadamBrasil* (e.g., Departmento Nacional da Produção Mineral), Sippel et al. (1992) measured lake areas on the mainstem floodplain from 51° to 70° W and along the lower 400 km of the Japurá, Purus, Negro and Madeira rivers totaling ~11,800 km^2.

Radar mosaics and maps generated from these images, both at 1:250,000 scale, allowed areas ≥~0.05 km^2 to be estimated. Hamilton et al. (1992) found that the areas of lakes on the Amazon floodplains appear to follow the Pareto distribution, with censorship and truncation on both ends, which indicates that the lakes are statistically self-similar and that descriptive statistics for the lakes will vary with the scale of observation.

Seasonal and interannual variations in inundation lead to a range of lake areas and associated depths that are not represented by the available regional estimates. Results for well-studied lakes provide an indication of variations: Calado, 2–8 km^2 (Lesack and Melack 1995), Janauacá, 23–390 km^2 (Pinel et al., 2015), Curuai, 850–2,250 km^2 (Rudorff et al., 2014a); these values include some flooded vegetation at high stages. Limnological and ecological conditions in Amazon floodplain lakes are reviewed in Melack and Forsberg (2001), Melack et al. (2009), Melack et al. (2021), and Junk (1997).

3.3 Seasonally Flooded Forests

The SAR-based analysis used by Hess et al. (2015) is well validated for detection of inundated forests. By combining the proportion of woody vegetation (forest, woodland and shrubs) compared to total inundated areas at the time of the high (70%) and low (62%) water levels analyzed by Hess et al. with the maximum (631,000 km^2) and minimum (53,000 km^2) inundated areas from Parrens et al. (2019), maximum (442,000 km^2) and minimum (~33,000 km^2) flooded forest areas can be estimated. Seasonally flooded forests vary considerably in species diversity and composition, biomass and productivity depending on fertility of the sediments, duration of inundation and ecological factors not fully understood (Junk et al., 2010). Most flooded forests are associated with white-water rivers, and called *várzea* forests. Those along black-water rivers are called *igapó* forests, cover up to ~84,000 km^2, and those near clear-water rivers that include *várzea* and *igapó* forests, are estimated to cover up to ~50,000 km^2, based on the maximum flooded forest area calculated above and proportional areas from Melack and Hess (2010).

3.4 Seasonally Flooded Savannas and Other Interfluvial Wetlands

Seasonally inundated savannas with a variety of herbaceous plants and palms and other trees occur in Roraima (Brazil) and Llanos de Moxos (Bolivia) (Melack and Hess 2010; Junk et al., 2011). Interannual maxima, minima and mean inundation over an 8-year period in these two regions are provided by Hamilton et al. (2002): Roraima (16,500, 250 and 3,000 km^2) and Llanos de Moxos (83,000, 6,100 and 34,000 km^2). The Rupununi savannas, near Roraima are similar, and may reach a maximum area of ~15,000 km^2 (Junk et al., 2011).

Other interfluvial wetlands occur in several regions within the Amazon basin and are not well studied (Junk et al., 2011). In the middle Negro basin ~30,000 km^2 of wetlands with sedges, other aquatic plants, patches of palm, mainly *Mauritia flexuosa*, and open water occur; Frappart et al. (2005) estimated a similar inundated area for this region. A time series of SAR data was used to determine inundation duration, extent and vegetation in the Cuini (minimum, 784 km^2; maximum, 964 km^2), and Itu (minimum, 550 km^2; maximum, 762 km^2) wetlands, both located near the middle Negro River (Melack et al., 2009; Belger et al., 2011). Fleischmann et al. (2020) compared several inundation datasets for the Negro interfluvial wetlands associated with *campinas* and *campinaranas* (Rossetti et al., 2017), with maximum inundation extent reaching up to 20,000 km^2. The muted variation in area of these wetlands is likely owed to the limited hydrological connection to the rivers. Between the Purus and Madeira rivers wetland patches a few hectares to ~150 km^2, totaling approximately 5,000 km^2 occur (Junk et al., 2011).

3.5 Herbaceous Plants on Riverine Floodplains

Herbaceous plants are abundant throughout the white-water floodplains of the Amazon basin. These plants grow profusely on sediments during low water and as rooted emergent and as free-floating plants, as inundation and water depths increase seasonally (Junk and Piedade 1997). Common C4 grasses are *Echinochloa polystachya, Paspalum repens* and *Paspalum fasciculatum*; other plants include the C3 grass, *Hymenachne amplexicaulis*, rice (*Oryza perennis*), and the genera *Eichhornia, Ludwigia, Neptunia, Salvinia,* and *Pistia* (Engle et al., 2008; Silva et al., 2013). SAR and other remotely sensed imagery can detect these plants, though their seasonal succession, growth and decline require time-series data. Also, narrow bands of floating plants fringing lakes and rivers and intermingled with woodlands can limit their accurate measurement. For the lowland basin, the combination of the proportion of inundated area represented by herbaceous vegetation in white-water river catchments and areas inundated permit an estimated area during high water of approximately 25,000 km^2 (Melack and Hess 2010; Hess et al., 2015). As an example of areal variations, in floodplain lakes totaling ~9,400 km^2 along the eastern Amazon River, herbaceous

plant coverage ranged from 770 to 2,900 km^2, based an analysis of Radarsat and MODIS images over 2 years (Silva et al., 2013). Herbaceous plants are rarely abundant in black-water river systems, and tend to be only moderately common in clear-water rivers (Junk et al., 2011).

Insufficient information is available to determine basin-wide variations and differences.

3.6 Peatlands

Among the floodplain and other wetlands delineated in **sections 3.3–3.5**, some are likely to be peatlands, though the classification of organic-rich soils in the region as peats is not standardized, and sampling is insufficient to determine their extent. Gumbricht et al. (2017) defined peat as a soil having at least 50% organic matter in the upper 0.3 m, while others have used different criteria, for example to identify minerotrophic and ombrotrophic sites (Lähteenoja et al., 2009). Among the possible peatlands based on the analysis by Gumbricht et al. (2017), the Pacaya-Samiria wetlands in the Peruvian lowlands, composed of seasonally flooded forests, palm swamps and peatlands, have had their inundated area and peat fairly well characterized (Lähteenoja et al., 2012; Jensen et al., 2018). By combing multi-sensor remote sensing with forest censuses and cores of peat thickness Draper et al. (2014) estimated that peatlands cover 35,600 ± 2,130 km^2 in the Pastaza-Marañon foreland basin (located in the Pacaya-Samiria region). A portion of this area is included within wetland areas described earlier, though during the period of the high water represented in Hess et al. (2015) fluvial flooding had receded in the Peruvian lowlands. Evidence for peat accumulation is also provided by sampling in parts of the Negro and Madre de Dios river basins, and suggested by model results (summarized in Gumbricht et al., 2017). However, the hybrid expert system used by Gumbricht et al. to estimate the regional distribution of wetlands and peatlands is not consistent with other estimates of inundation (Fleischmann et al., 2021), perhaps because of overestimation of soil moisture by the topographic index used or large rainfall in 2011, the year used. Their designation of floodplains and other wetlands as peatlands requires considerably more evidence, though recent studies are detecting peats scattered through the basin (e.g., Winton et al., 2021)

3.7 Hydroelectric Reservoirs

Hydroelectric reservoirs currently in the Amazon basin cover approximately 4,575 km^2 (Almeida et al., 2019; Kemenes et al., 2007 for Balbina). In Bolivia (50 km^2), Ecuador (35 km^2) and Peru (103 km^2) almost all are above 1,000 m asl while in Brazil all are <500 m asl. The area of reservoirs (~2,600 km^2) estimated by Messager et al. (2016) is too low. Plans for more hydroelectric systems, especially in the Andes, could considerably expand their area (Almeida et al., 2019) and have substantial ecological consequences (Forsberg et al., 2017).

4 METHANE MEASUREMENT METHODS

4.1 Sampling Issues

The majority of the studies in Amazonian aquatic environments, albeit sampled infrequently and usually in open waters of lakes or rivers, represent considerable effort given the immense area and remoteness of the basin. Few studies covered a complete hydrological cycle, and rarely included diel variations or multiple years. Related limnological, hydrological and meteorological measurements were seldom done concurrently, limiting the ability to evaluate the role of ecological factors, thermal structure and other processes on CH_4 fluxes and concentrations. Regions or habitats with few or no data include the Llanos de Moxos, coastal freshwater wetlands, riparian zones along streams, small reservoirs associated with agriculture, cultivated rice in Roraima and elsewhere, and habitats above 500 m. The recent findings of significant fluxes from trees, especially when inundated, included measurements in several types of forests (Pangala et al., 2017) and seasonal variations (Gauci et al., 2021), and point to the need for considerably more data on fluxes from trees given the large diversity of trees. Among hydroelectric reservoirs, measurements are available for a few (summarized in Melack et al., 2004; Guerin et al., 2006; Barros et al., 2011; Kemenes et al., 2016), but only Balbina reservoir has data collected from multiple reservoir and downstream stations as well as measurements of fluxes associated with turbines over a year (Kemenes et al., 2007, 2011). Abril et al. (2005) provide comparable, long-term data for Petit Saut reservoir in French Guyana.

4.2 Field Methods

4.2.1 Diffusive CH_4 Fluxes

Floating chambers of various designs have been used to measure diffusive fluxes based on deployments of often less than 30 min on regional surveys and at specific locations (e.g., Barlett et al., 1988; Devol et al., 1990; Kemenes et al., 2007; Barbosa et al., 2016, 2020). As CH_4 accumulated in the chambers, sequential samples are removed or the gas is circulated from the chamber to a portable instrument measuring CH_4 continuously; analytical methods are described below. An alternative approach is to calculate the diffusive flux (F) based on measurements of concentration of methane in the water and estimation of gas exchange velocity (k) using the following equation:

$$F = k\left(C_w - C_{eq}\right)$$

where C_w is the observed dissolved CH_4 concentration and C_{eq} is the CH_4 concentration in equilibrium with the atmosphere. To estimate k, MacIntyre et al. (2019) and MacIntyre et al. (2021) provide theoretical and empirical evidence for the validity of the surface renewal model, though most studies in Amazon lakes used wind-based equations (Engle and Melack 2000; Barbosa et al., 2016), which are likely to underestimate fluxes by a factor of two or more. For large rivers, equations for k often incorporate current velocity and/or wind speed (Alin et al., 2011), while equations applied to streams and small rivers use hydraulic parameters, such as slope and velocity (Raymond et al., 2012). In small rivers, the dominant driver for near-surface turbulence driving gas exchange has thresholds which vary with current speed and wind speed (Guseva et al., 2021). Using data from montane streams, Ulseth et al. (2019) found that turbulent diffusion is important in low-energy streams and that

entrainment of air bubbles in high-energy streams enhanced gas exchange.

4.2.2 Fluxes *via* Woody and Herbaceous Plants

Pangala et al. (2017) and Gauci et al. (2021) attached chambers to tree trunks to estimate methane fluxes from the trees at several locations during a 1-month period of rising water and in seasonal deployments at several locations, respectively. Given the considerable variations in fluxes from the trees, large diversity of trees, and difficulty of extrapolating to whole trees and then forests, many more measurements of both fluxes and forest characteristics are needed to characterize fluxes from flooded and upland trees.

Although plant-mediated transport is known to occur via herbaceous plants (e.g., Villa et al., 2020), it has not been consistently observed, albeit seldom sampled, in Amazon lakes or wetlands. Wassmann et al. (1992) did not detect different fluxes between chambers with or without mats of *Paspalum repens*, a dominant floating grass with few roots reaching the sediments. Among the few measurements by Bartlett et al. (1988), floating mats of *Eichornia* or *Paspalum* had no or slight enhancement compared to open water, while rooted *Victoria regia* growing in shallow water did emit more CH_4 than open water, as would be expected based on other studies of water lilies (Dacey 1981). In *Eichornia* stands in the southern Amazon and Pantanal, Oliveira Junior et al. (2020) found that diffusive CH_4 emissions were much higher when the plants were rooted, but that emissions from free-floating plant mats were lower than those from nearby open water. In interfluvial wetlands with shallow water in the Negro basin, Belger et al. (2011) reported higher fluxes in chambers covering emergent, rooted plants at one seasonally inundated site but not at another, permanently flooded site.

4.2.3 Ebullitive CH_4 Flux

Most estimates of ebullitive CH_4 fluxes in Amazon lakes have been made using floating chambers during a short deployment. Devol et al. (1988), Devol et al. (1990) and Sawakuchi et al. (2014) used floating chambers with discrete sampling of gas and estimated ebullition indirectly by subtracting diffusive fluxes, calculated from an estimated gas transfer velocity and CH_4 concentration gradient, from combined ebullitive and diffusive fluxes. Alternatively, chambers can be coupled to a portable gas analyzer to obtain high-frequency measurements, and CH_4-enriched bubbles detected from abrupt increases in gas concentration (Crill et al., 1988; Wassmann et al., 1992; Barbosa et al., 2021). Submerged inverted funnels (bubble traps) deployed for hours to days integrate episodic fluxes. Acoustic methods to detect bubbles in the water column and estimate ebullition (DelSontro et al., 2011; Linkhorst et al., 2020) have seldom been used in the Amazon. Barbosa et al. (2021) made the most complete set of measurements to date in both vegetated habitats and open water over 2 years using floating chambers with high frequency measurements and bubble traps, and during falling water, a hydroacoustic echo sounder was employed to detect bubbles.

The variability of ebullition introduces considerable uncertainty in estimates of ebullitive and total CH_4 flux, and the three approaches have different problems. Floating chambers cover a small area and are typically deployed for less than 30 min; very small bubbles cannot be detected. Bubble traps also cover small areas, and bubble volumes of less than ~1 ml are difficult to measure. Hydroacoustic surveys capture bubbles at high spatial resolution but for only a short time interval, although moored acoustic transponders could be deployed. All three approaches are likely to underestimate ebullition.

4.2.4 CH_4 Concentrations

Until recently, almost all samples from the atmosphere, bubble traps, floating chambers and dissolved in water were assayed in a gas chromatograph equipped with a flame ionization detector. Gas samples for analyses of dissolved CH_4 were obtained using a headspace technique by vigorous shaking of water and air in the sampling syringe (Hamilton et al., 1995). A customized system used during the 1980s employed a gas filter correlation technique (Sebacher and Harriss 1982) with the infrared detector inside the floating chamber to generate a continous record of concentration changes. Portable, off-axis integrated cavity output spectrometers (e.g., products of Los Gatos Research, Inc. and Picarro, Inc.) are now available to measure gas samples directly from floating chambers, from equilibrators receiving water pumped from rivers or lakes, or after headspace extraction in samples. However, the equilibration time between water and gas in equilibrators varies among designs and concentrations.

4.2.5 Environmental Variables

Factors relevant to interpretation of methane fluxes include meteorological variables, stratification and mixing, dissolved oxygen, nutrient and other solute concentrations, current velocities and water depths, underwater light attenuation, chlorophyll and dissolved and particulate carbon concentrations, and sediment characteristics. Time-series of vertical profiles of temperature and dissolved oxygen measured with moored sensors are especially important given the strong diel variations typical of these tropical locations. Seldom do such measurements accompany those of fluxes; exceptions include Barbosa et al. (2020).

4.3 Atmospheric Measurements

4.3.1 Eddy Covariance and Tower-Based Measurements

Eddy covariance is now widely used to measure methane fluxes in wetlands (Dalmagro et al., 2019; Delwiche et al., 2021) and lakes (e.g., Schubert et al., 2012; Podgrajsek et al., 2016), and has been used in short campaigns to measure CO_2 fluxes in an Amazon lake (Polsenaere et al., 2013) and reservoir (Souza do Vale et al., 2016). Two studies provide methane fluxes over upland forests using tower-based measurements. Carmo et al. (2006) used a profiling system based on mixing ratio measurements at three sites in the Amazon. Querino et al. (2011) provides one of the few eddy covariance estimates over upland forest at a site north of Manaus. Both studies focused on within canopy gradients and the uppermost inlet was not more than 10 m above the canopy. A recent study using a profiling system of atmospheric mixing ratio measurements at the Amazon Tall Tower Observatory (ATTO) suggest a nighttime source of methane from flooded forests along

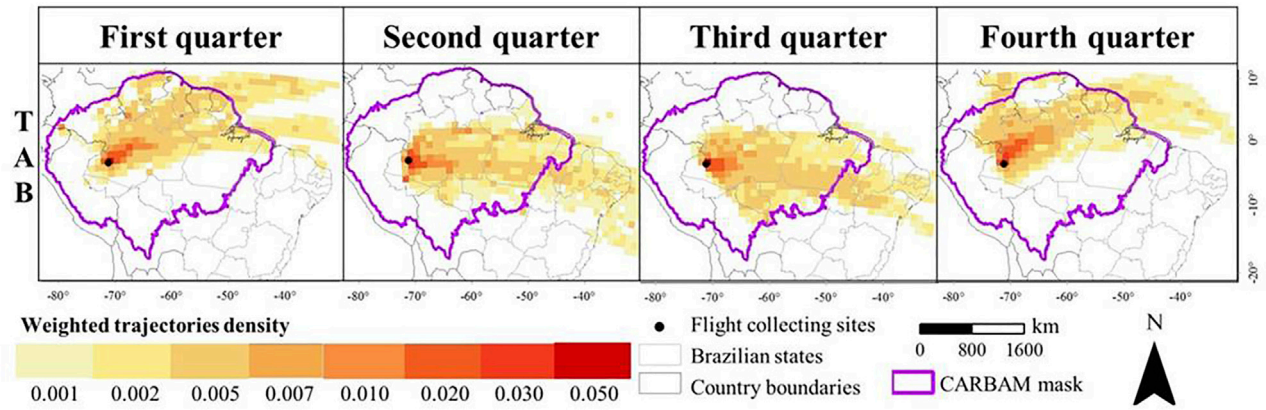


FIGURE 3 | Weighted mean quarterly regions of influence for 2010 through 2018 for the TAB site (5.9°S, 70.0°W). Adapted from Cassol et al. (2020) and Basso et al. (2021), where methods are explained.

the Uatumã River (Botía et al., 2020a). An eddy covariance flux tower is now measuring CO_2 and CH_4 fluxes in a natural palm peatland near Iquitos, Peru (Griffis et al., 2020).

4.3.2 Airborne Sampling and Analysis

Airborne sampling of methane and other gases, followed by assays of concentrations, and in some cases, isotopic composition, in the lower atmosphere, when combined with atmospheric transport models, have provided integrated calculations of methane fluxes over subregions of the Amazon basin (Miller et al., 2007; Beck et al., 2012; Basso et al., 2016; Wilson et al., 2016; Basso et al., 2021; Wilson et al., 2021). For example, Basso et al. (2021) reported seasonal and annual CH_4 fluxes based on measurements of atmospheric CH_4 in vertical profiles from ~300 m to 4.4 km collected about twice per month from 2010 through 2018 at sites located in the southeastern, northeastern, southwest-central and northwest-central Brazilian Amazon basin. The fluxes, estimated with a column budgeting technique, include all sources and sinks within the area traversed by air masses flowing from the Atlantic coast to each site, representing regional scales of ~10^5–10^6 km^2. For each of the sites' quarter-yearly resolved air-mass trajectory, density weighted regions of influence were calculated (Cassol et al., 2020), as illustrated for site TAB in the northwest-central Amazon basin (**Figure 3**). These weighted trajectories show that areas closer to the flights have greater influence than more distant regions, and that the air mass trajectories vary by season. Hence, attributing the fluxes to sources requires incorporating these spatial and temporal differences.

Results reported by Basso et al. (2021) indicate that wetlands are likely the major source of methane, at least for seasons and sites with extensive inundated areas. Other sources include fires, anthropogenic emissions from enteric fermentation by cattle (Crippa et al., 2019) and urban areas, termites (van Asperen et al., 2021), and, perhaps, emissions associated with canopies of upland forests (Carmo et al., 2006; Martinson et al., 2010). Carbon monoxide measured concomitantly with CH_4 was used to estimate CH_4 emissions from biomass burning. Uptake by soils also occurs (Keller et al., 2005). Though each of these upland fluxes have uncertainties and regionalization challenges, we are not examining these issues here.

4.3.3 Satellite Sensors

Satellite retrievals of atmospheric concentrations of CH_4 are now available from several sensing systems (e.g., SCIAMACHY, Frankenbert et al., 2011; GOSAT, Webb et al., 2016; Parker et al., 2020; TROPOMI, Yu et al., 2021; AIRS onboard the NASA/AQUA satellite, Ribeiro et al., 2016). For example, Webb et al. (2016) found good agreement in the seasonal patterns from airborne vertical profiles extrapolated through the atmosphere and remote sensing data from GOSAT. When combined with inverse modeling and subsetted, these analyses permit estimates of methane emissions in the Amazon basin (e.g., Frankenberg et al., 2008; Tunnicliffe et al., 2020). Evaluations of these approaches are provided by several recent studies (e.g., Parker et al., 2018).

5 METHANE FLUX MEASUREMENTS

In parallel with **section 3** on areal extent, available estimates of methane emissions are summarized for seven types of aquatic systems: streams and rivers, lakes, seasonally flooded forests, seasonally flooded savannas and other interfluvial wetlands, herbaceous plants on riverine floodplains, peatlands, and hydroelectric reservoirs. A final section identifies major gaps. Fluxes judged as representative of each habitat and that span seasonal variations are selected, if possible. Values are usually expressed in mass of CH_4, not molar units, and converted to daily rates by simple multiplication, as needed.

Most of the published data have expressed averaged values as arithmetic mean fluxes, and these are used here. However, since diffusive and especially episodic fluxes are not normally distributed, arithmetic means are biased toward higher values, and standard deviations often suggest unrealistic negative fluxes. As discussed by Rosentreter et al. (2021) and others, expressing

results as medians with interquartile ranges offers an alternative that represents the spread. Geometric means, while statistically sensible for these skewed data, are seldom used (e.g., Barbosa et al., 2020). Applying an approach, such as Monte Carlo uncertainty analysis, would be appropriate, except very few of the published datasets include the individual measurements required to do such analysis. For example, Melack et al. (2004) were able to calculate means and Monte Carlo-based uncertainties for habitat-specific methane emissions with individual measurements reported in Devol et al. (1990).

5.1 Rivers and Streams

Methane emissions based on floating chambers deployed in the Amazon River and major tributaries during low and high water, in most cases, reported by Sawakuchi et al. (2014) ranged from ~0.2 to 297 mg CH_4 m^{-2} d^{-1} with averages (as mg CH_4 m^{-2} d^{-1}): Amazon (21.6), Solimões (5), Negro (8.6), Madeira (0.6), Tapajós (38), Xingu (96), Preto (1.4) and Para (5). Barbosa et al. (2016) measured diffusive CH_4 fluxes using floating chambers and estimated fluxes based on the concentration of the gas in the water and calculated gas exchange coefficients along a 700-km transect including four stations in the Negro River and 21 of its tributaries at low and high water plus six stations on a 1100-km transect of the Solimões-Amazon River and one on the Maderia River occupied four times. Fluxes ranged from ~0.2 mg CH_4 m^{-2} d^{-1} in the Solimões (during early falling water) to ~3,900 mg CH_4 m^{-2} d^{-1} in the Jutaí River during low falling water with averages (as mg CH_4 m^{-2} d^{-1}): Amazon and Solimões (18), Negro River and tributaries (54), Madeira (6.4), Purus (6.4), Juruá (5), Japurá (9.6). While ebullition may occur in rivers, as suggested by Sawakuchi et al. (2014), the indirect method used may be compromised by the wide ranges of gas exchange velocities expected in turbulent rivers.

Measurements in tributaries were made near their confluence with the Negro, Amazon or Solimões, and no upper reaches of rivers were sampled.

Additional data for the Solimões and Amazon rivers include those by Richey et al. (1988), who combined measurements of dissolved CH_4 concentrations in the main stem with estimates of air–water gas exchange to estimate a diffusive evasion of 3.2 mg CH_4 m^{-2} d^{-1}, which is similar to 2.7 mg CH_4 m^{-2} d^{-1}determined by Bartlett et al. (1990), but lower than measurements by Sawakuchi et al. (2014) and Barbosa et al. (2016). In the Uatumã River, downstream of Balbina dam, emission was 2,200 mg CH_4 m^{-2} d^{-1} (Kemenes et al., 2007), a value far above other rivers, with the exception of the Jutaí River. Interactions between the fringing floodplains and river channels are not well understood, though a gradient of increasing methane toward the margins of the Solimões River suggests inputs from the floodplains (Richey et al., 1988; Bartlett et al., 1990; Devol et al., 1994).

In a perennial first-order stream in the upper Xingu catchment, average fluxes based on floating chambers deployed monthly for a year were 108 ± 25 mg CH_4 m^{-2} h^{-1} or 2,600 ± 600 mg CH_4 m^{-2} d^{-1} (Neu et al., 2011). These very high fluxes could reflect input of groundwater high in CH_4, and may have over-estimated emissions because stationary chambers in streams can increase turbulent exchange. No other fluxes from streams are available. For comparison, average fluxes of 18 mg CH_4 m^{-2} d^{-1} summarized in Stanley et al. (2016) for tropical and subtropical streams are much lower. Clearly, many more measurements are needed.

5.2 Lakes

Several studies have focused on open waters of lakes, though few included a complete year, adequately measured diffusive and ebullitive fluxes and rarely sampled diel variations. Over 2 years, nearly monthly measurements in an embayment and open water area of Lake Janauacá, located in *várzea* of the central basin, CH_4 fluxes were made with floating chambers connected to an off-axis integrated cavity output spectrometer and inverted funnels to capture bubbles (Barbosa et al., 2020; Barbosa et al., 2021). Diffusive fluxes, with measurements over diel periods combined for both sites, averaged ~27 mg CH_4 m^{-2} d^{-1}, and when combined with ebullition averaged 85 mg CH_4 m^{-2} d^{-1}; diel variations were observed often with higher values during the day.

In *várzea* Lake Camaleão on Marchantaria Island in the Solimões River, Wassmann et al. (1992) deployed floating chambers connected to an automated system assaying CH_4 concentrations during a range of water levels, each with at least 3 days of sequential measurements, allowing bubble detection, and reported an average flux of 29 mg CH_4 m^{-2} d^{-1}. Diel variations were not observed. As part of regular sampling over 18 months in two lakes on the floodplain of the Negro River and six on the floodplain of the Solimões River (Forsberg et al., 2017), Devol et al. (1990) reported average fluxes of 44 mg CH_4 m^{-2} d^{-1}. Average diffusive fluxes during high water in *várzea* Lake Calado were 8.3 mg CH_4 m^{-2} d^{-1} (Crill et al., 1988), during rising water averaged 6.6 mg CH_4 m^{-2} d^{-1}, increased up to 220 mg CH_4 m^{-2} d^{-1} during passage of a rare cold front, while during falling water averaged 54 mg CH_4 m^{-2} d^{-1}; total flux averaged 163 mg CH_4 m^{-2} d^{-1} during falling water (Engle and Melack 2000).

As part of a transect along the Solimões and Amazon rivers, Barbosa et al. (2016) reported an overall average of 59 mg CH_4 m^{-2} d^{-1}, ranging below detection to 298 mg CH_4 m^{-2} d^{-1} for 10 lakes, including white waters and black waters, sampled during four hydrological phases. Sawakuchi et al.'s (2014) few measurements of total fluxes from the eastern *várzea* Lake Curuai averaged 18 mg CH_4 m^{-2} d^{-1}.

5.3 Seasonally Flooded Forests

Methane fluxes within seasonally flooded forests occur from water surfaces, from the trunks of trees and from exposed soils during low water periods. In the flooded forests fringing Lake Janauacá, Barbosa et al. (2020) recorded an average of 110 mg CH_4 m^{-2} d^{-1}, based on floating chamber and bubble trap measurements. Diffusive CH_4 fluxes within flooded forest measured by Wassmann et al. (1992) ranged from 1 to 12 mg CH_4 m^{-2} d^{-1}, and ebullition averaged 69 mg CH_4 m^{-2} d^{-1}. Fluxes at four water levels with floating chambers by Gauci et al. (2021) ranged as follows (expressed as mg CH_4 m^{-2} d^{-1}) for plots along the Solimões (43–55 except for a high water value of 450), Negro

(12–19) and Tapajós (36–55) rivers. Based on measurements with floating chambers in inundated *igapó* forests along the Jaú River Rosenqvist et al. (2002) calculated a mean annual emission of methane 30 mg CH_4 m^{-2} d^{-1}.

Fluxes through trees in seasonally flooded forests can be high and quite variable when expressed per unit area of emitting surface. Based on sampling transects in twelve 0.4 ha forested plots along the Negro, Amazon, Madeira and Tapajós rivers during a period of rising water, Pangala et al. (2017) reported fluxes for mature and young trees per unit area of stem surface from 0.33 to 337 mg CH_4 m^{-2} h^{-1} and 0.39–581 mg CH_4 m^{-2} h^{-1}, respectively. Similar measurements at four water levels in plots along the Solimões, Negro and Tapajós rivers by Gauci et al. (2021) ranged as follows (expressed as mg CH_4 m^{-2} h^{-1} per unit area of stem surface): Solimões (0.013–78.9), Negro (0.005–50.5) and Tapajós (-0.004–69.7). Soil CH_4 fluxes when the water table was below the surface in these plots were low and often negative, ranging from uptake of ~1 mg CH_4 m^{-2} d^{-1} to evasion of ~1 mg CH_4 m^{-2} d^{-1} (Gauci et al., 2021).

5.4 Seasonally Flooded Savannas and Other Interfluvial Wetlands

The Pantanal wetland can serve as a surrogate for the savanna wetlands in the Llanos de Moxos (Bolivia), which lack measurements of methane fluxes. Regular vertical profiles of methane and other gases obtained by aircraft from March 2017 to September 2019 in the Pantanal were combined with a planetary boundary layer budgeting technique to calculate a regional CH_4 flux of 50 mg CH_4 m^{-2} d^{-1} averaged over 1 year, assuming a planetary boundary layer-free troposphere exchange time of 3 days (Gloor et al., 2021). This flux integrates emissions from lakes, rivers and wetlands plus enteric fermentation by cattle and fires. Floating chambers deployed at five sites over a year in a Pantanal floodplain near the Miranda River yielded an average flux of 142 mg CH_4 m^{-2} d^{-1} (Marani and Alvala 2007).

Mean emission of monthly measurements with floating chambers in numerous wetlands near Boa Vista (Roraima) of about 14 mg CH_4 m^{-2} d^{-1} seem rather low compared to other similar Amazonian habitats (Jati 2014), perhaps because ebullition was not captured. Emissions from cultivated rice in Roraima are not available. In the mid-Negro basin, Belger et al. (2011) measured methane uptake on unflooded lands, evasion from flooded areas as diffusive and ebullitive fluxes with chambers and funnels, and as transport through rooted plants. Emission from wetland areas averaged 77 mg CH_4 m^{-2} d^{-1}.

5.5 Herbaceous Plants on Riverine Floodplains

As water levels rise on riverine floodplains, herbaceous plants form floating mats. Several studies have deployed floating chambers to measure methane fluxes from the water surface or, rarely, from plants on the surface. In mats of floating herbaceous plants, Barbosa et al. (2020) measured an average diffusive CH_4 flux of 53 mg CH_4 m^{-2} d^{-1} and estimated an average ebullition of 97 mg CH_4 m^{-2} d^{-1}, totaling 150 mg CH_4 m^{-2} d^{-1}. Diffusive fluxes within similar mats reported by Bartlett et al. (1988; 1990) were similar, averaging 42 and 44 mg CH_4 m^{-2} d^{-1}, respectively. Wassmann et al. (1992) reported diffusive fluxes from ~2 to 28 mg CH_4 m^{-2} d^{-1}, average ebullition of 23 mg CH_4 m^{-2} d^{-1} and did not detect plant-mediated transport via floating mats of *Paspalum repens*.

5.6 Peatlands

Fluxes in palm-dominated peatlands and nearby habitats in the western Amazon basin are variable and can be high. Eddy covariance measurements in a natural palm (*Mauritia flexuosa*) peatland near Iquitos (Peru) over a 2-year period averaged 22 g C m^{-2} y^{-1} (= ~80 mg CH_4 m^{-2} d^{-1}) (Griffis et al., 2020). Teh et al. (2017) measured fluxes in the Pastaza–Marañón basin in forests, a *Mauritia flexuosa*-dominated palm swamp, and a mixed palm swamp during wet and dry seasons in four campaigns. Among all data, diffusive CH_4 emissions averaged ~48 ± 4 mg CH_4 m^{-2} d^{-1}; fluxes in the *M. flexuosa* palm swamp averaged ~49 ± 5 mg CH_4 m^{-2} d^{-1} (assuming their notation, CH_4–C, means the mass of C in the CH_4). As noted by the authors, their estimates of ebullition from short deployments of static chambers are probably not representative. In the same region, del Aguila-Pasquel (2017) sampled 8 times over 8 months spanning wet and dry seasons in a palm swamp and reported a mean flux of 73 ± 5.4 mg CH_4 m^{-2} d^{-1} (n = 129). In peatlands in the Madre de Dios River basin (Peru) Winton et al. (2017) found that open canopy Cyperaceae-dominated areas emitted 4.7 ± 0.9 mg CH_4 m^{-2} h^{-1} (=113 ± 22 mg CH_4 m^{-2} d^{-1}), and *Mauritia flexuosa* palm-dominated areas emitted 14.0 ± 2.4 mg CH_4 m^{-2} h^{-1} (= 336 ± 58 mg CH_4 m^{-2} d^{-1}) during a short period in 1 month. That CH_4 can be emitted through *M. flexuosa* trunks suggests that emissions from palm-dominated peatlands based on soil flux chambers underestimate fluxes (van Haren et al., 2021). CH_4 fluxes were significantly correlated to pneumatophore density in *M. flexuosa* stands (van Lent et al., 2019).

5.7 Hydroelectric Reservoirs

Several hydroelectric reservoirs have measurements available while most, usually smaller ones, do not. In Balbina reservoir, measurements of diffusive and ebullitive fluxes from multiple stations within the reservoir (average 63 mg CH_4 m^{-2} d^{-1}), degassing at the turbines and downstream were made over a year, when combined produce an annual CH_4 emission of 97 Gg for the whole system, excluding methane oxidation in the river (Kemenes et al., 2007). Additional measurements at Samuel and Curua-Una reservoirs indicated the significance of degassing at the turbines and downstream (Kemenes et al., 2016). Based on measurements using drifting chambers during four periods in the first 2 years after filling of the Belo Monte hydroelectric system, Bertassoli et al. (2021) reported averages of 104 and 283 mg CH_4 m^{-2} d^{-1}, and whole systems annual totals of 20 and 50 Gg CH_4. About half the flux was attributed to ebullition, and degassing in turbines was deemed minor.

Paranaíba et al. (2021) combined measurements of diffusive methane fluxes and calculations of gas exchange velocities with floating chambers at several sites and concentrations of methane

sampled and analyzed on continuous transects through the Curuá-Una reservoir. During the rainy season with rising water levels, they reported average fluxes of 9.6 mg CH_4 m^{-2} d^{-1} (range from 1.4 to 112) and during the drier season with falling water levels average fluxes of 14.4 mg CH_4 m^{-2} d^{-1} (range from 1.3 to 69). As part of a study of organic carbon burial in Curuá-Una reservoir, Quandra et al. (2021) found methane dissolved in pore water to be above saturation in about one quarter of their measurements, indicating a potential for ebullition. Porewater concentrations were similar during periods with rising and falling water, varied spatially, but were not related to C:N ratios or organic carbon burial rates.

Emission from other Brazilian reservoirs based on overall average diffusive and ebullitive emissions from the surfaces of ten reservoirs within southern portions of the basin, as summarized in Deemer et al. (2016) is ~80 mg CH_4 $m^{-2}d^{-1}$; this value does not include degassing through turbines or below the dam. Estimating the emissions from the reservoirs in Bolivia, Ecuador and Peru is more difficult because no measurements exist and temperatures will be less at higher elevations and the watersheds differ from conditions in Brazil; a value of half that from Deemer et al. (2016) is suggested. The extent that the reservoir emissions represent net emissions, i.e., emissions additional to those associated with the undammed rivers, are uncertain, with estimates at Belo Monte (Bertassoli et al., 2021) and Balbina (Kemenes et al., 2011); upland forest soils, before being inundated, are likely to be sinks for methane.

5.8 Major Gaps

The seasonally flooded ecotone, called the aquatic-terrestrial transition zone, is a varying mixture of bare soil and cover by herbaceous and woody plants exposed during periods of low water. Areas occupied by the aquatic-terrestrial transition zone are especially large in regions with shallow seasonal flooding, such as in savannas. Few measurements of methane flux or related processes are available for these periods in the Amazon (Pangala et al., 2017; Gauci et al., 2021); those of Smith et al. (2000) for the Orinoco floodplain are relevant. Microbial activity in response to desiccation (Conrad et al., 2014) and CH_4 oxidation in exposed sediments on Amazon floodplains (Koschorreck 2000) have also been examined.

Sediments exposed as reservoir levels decline are analogous to the aquatic-terrestrial transition zone. Experimental measurements of methane emissions from sediment cores from a tropical Brazilian reservoir exposed to drying and rewetting indicated enhanced emissions from sediments with overlying water removed and when rewetted compared to sediments that had overlying water (Kosten et al., 2018). A comparative study for several types of aquatic systems including ones in tropical climates by Paranaíba et al. (2022) found emissions from portions of inland waters exposed to the atmosphere as water levels decline were consistently higher than emissions in nearby uphill soils. Statistical analyses revealed that methane emissions were negatively related to organic matter content and positively related to moisture of the sediments.

Riparian zones along streams often have soils with high water content but without standing water and occur throughout the Amazon basin. Topographic features are illustrated in Nobre et al. (2011). These environments are likely sources of methane emission. For example, soils in upland forests can release CH_4, depending on soil moisture levels (Sihi et al., 2021).

6 BIOGEOCHEMICAL AND PHYSICAL PROCESSES

Interpretation and modeling of methane fluxes requires understanding of the key processes; hence we discuss aspects of these processes with a focus on conditions relevant to the Amazon basin. Methane emissions reflect differences between CH_4 production by methanogens and consumption by methanotrophs, and physical processes. Environmental factors that influence biological rates include water temperature, dissolved oxygen, trophic status and substrate availability. Wind, diel variations in thermal structure and physical processes such as convective and shear-driven mixing alter gas distributions and transfer velocities. CH_4 can reach the atmosphere by three pathways: via diffusive fluxes at the air-water interface, via bubbles that form in the sediment, rise through the water column and are emitted to the atmosphere (ebullition), and through the vascular systems of herbaceous and woody aquatic plants. Ebullitive fluxes depend on bubble formation and hydrostatic pressure over the sediment, while diffusive fluxes depend on concentration gradients and turbulence. Here, we examine understanding of relevant biogeochemical and physical processes in Amazon aquatic environments.

6.1 Biogeochemical Processes

The biogeochemical and microbial processes involved in the production and consumption of methane are known though uncertainties remain (e.g., Segers 1998; Borrel et al., 2011; Bridgham et al., 2013; Schlesinger and Bernhardt 2013). However, the quantitative importance of these processes varies among habitats and regions, and needs further study in aquatic environments within the Amazon basin. The availability to methanogens of the varied organic compounds present in Amazonian waters has not been characterized, though studies of the use of these substances for metabolism, in general, are available (e.g., Waichman 1996; Mayorga et al., 2005; Amaral et al., 2013; Ward et al., 2013; Vihermaa et al., 2014). Using samples from sediment cores obtained in an Amazon reservoir and two other tropical reservoirs in Brazil and incubated over about 2 years, Isidorova et al. (2019) found that rates of CH_4 production had a strong statistical relation to sediment total nitrogen content and age of the sediment. Given the variations of sediment characteristics in Amazon floodplains and reservoirs (Hedges et al., 1986; Martinelli et al., 2003; Smith et al., 2003; Guyot et al., 2007; Moreira-Turcq et al., 2013; Cardoso et al., 2014; Sobrinho et al., 2016), further studies will likely reveal different methane production rates associated with these variations.

CH_4 oxidation has been measured in a tropical reservoir (Guérin and Abril 2007) and inferred to occur in floodplain

lakes (Crill et al., 1988; Engle and Melack 2000) or exposed sediments (Koschorreck 2000). Based on stable isotopic mass balances of CH_4, Sawakuchi et al. (2016) estimated substantial rates of CH_4 oxidation in large Amazonian rivers, and found that genetic markers for methane oxidizing bacteria were positively correlated with CH_4 oxidation. Using incubations and measurements of δ^{13}C-CH_4 in a *várzea* lake, Barbosa et al. (2018) found that a large fraction of dissolved CH_4 was oxidized with volumetric CH_4 oxidation rates ranging from ~1 to 175 mg CH_4 m^{-3} d^{-1}. Heavier values of δ^{13}C-CH_4 in surface waters when compared to bottom waters and sediment bubbles corroborate these high rates. They also found that CH_4 oxidation had a positive relation with CH_4 concentration and the presence of dissolved oxygen.

The microbial assembles in floodplain lakes (e.g., Melo et al., 2019) including methanogens and methanotrophs have received limited investigation in the Amazon (e.g., Finn et al., 2020; Bento et al., 2021; Gontijo et al., 2021). Conrad et al. (2010, 2011) and Ji et al. (2016) examined microbial communities and measured rates of methanogenesis in sediments by incubating sediment slurries from different floodplain lakes; CH_4 production was found to be mainly hydrogenotrophic based on isotopic fractionation. However, the congruence of laboratory incubations of sediment slurries with CH_4 production in intact sediments is unclear. More study is needed relating microbial activity to environmental conditions, such as the examination of responses to desiccation by Conrad et al. (2014). Anaerobic oxidation of methane and microbial methane production in oxygenated water also need attention, as indicated by studies elsewhere (e.g., Caldwell et al., 2008; Grossart et al., 2011; Roland et al., 2016). For example, Gabriel et al. (2020) used slurries of flooded Amazon forest soils to demonstrate the potential for anaerobic methane oxidation by Fe(III) reduction.

6.2 Physical Processes

In the warm waters of the Amazon basin, high latent heat fluxes lead to convective mixing while diurnal heating under strong insolation leads to periods of stable stratification (e.g., Augusto-Silva et al., 2019). Exchange of methane between surficial water and overlying atmosphere depends on the concentration gradient between air and water and on physical processes at the interface, usually parameterized as a gas transfer velocity (k). Gas transfer velocities are influenced by atmospheric stability and, in water, are altered by currents, wind and convection, as well as rain, temperature and organic surficial films. Melack (2016) summarized estimates of k available for rivers and lakes in the Amazon basin. Results reported by Ulseth et al. (2019) indicate quite large k values can occur in high-energy montane streams due to bubble entrainment. Recent studies by MacIntyre et al. (2019) and MacIntyre et al. (2021) have used near-surface measurements of dissipation rates of turbulent kinetic energy and hydrodynamic theory to calculate k under low wind conditions in open water and within flooded forests.

Though gas transfer velocity can be parameterized based on wind speed (Wanninkhof 1992; Cole and Caraco 1998), the dependence of k on the dissipation rate of turbulent kinetic energy (ϵ) has theoretical and empirical evidence. The surface renewal model, $k = c_1\ (\epsilon\nu)^{1/4})\ Sc^{-n}$ has an explicit dependence on dissipation rates, where dissipation rates have units of $m^2\ s^{-3}$, ν is kinematic viscosity ($m\ s^{-2}$), Sc is the Schmidt number, n is −1/2 or −2/3, and c_1 is an empirical coefficient. Dissipation rates depend on the shear just below the air-water interface and are augmented if cooling or heating are appreciable relative to shear (MacIntyre et al., 2021). This model has been applied to Amazon flooded forests (MacIntyre et al., 2019) and reservoirs (MacIntyre et al., 2021) and confirmed with indirect estimates of k using results of experiments with floating chambers (Amaral et al., 2020).

Stratification within tropical lakes and reservoirs can be appreciable as a result of intense heating when winds are light (e.g., Augusto-Silva et al., 2019). In that case, near-surface values of dissipation rate can be higher than observed under cooling. With stratification retarding the downward mixing of heat, much of the turbulence produced by wind is dissipated. Values of k computed using the surface renewal model during heating averaged 10 cm h^{-1} but reached 18 cm h^{-1} for winds up to 4 m s^{-1}, were independent of wind speed, and increased with heating (MacIntyre et al., 2021). Hence, the fluxes estimated from wind-based models for many of the lakes in the Amazon basin are likely underestimated.

CH_4 ebullition, a major mechanism for evasion to the atmosphere, is regulated by the production and accumulation of CH_4 in sediments and processes leading to the release of bubbles from the sediments. Release of bubbles can be influenced by variations in hydrostatic pressure caused by a drop in atmospheric pressure or drop in water level. Other factors include currents, waves, shear-stress at the sediment-water interface and possibly sediment disturbances by benthic organisms (Barbosa et al., 2021).

Vertical and horizontal water movements connect littoral, pelagic and benthic regions of lakes and wetlands (MacIntyre and Melack 1995) and are likely to influence CH_4 concentrations and fluxes. One-dimensional (e.g., DYRESM, Yeates and Imberger 2003) and three-dimensional (e.g., AEM3D, Hodges and Dallimore 2019) hydrodynamic models include processes induced by surface heat fluxes, wind, inflows and outflows. One-dimensional models characterize a lake as a single water column in the vertical and are computationally efficient permitting long-term and regional applications. Three-dimensional models divide a lake into grids in three directions, resolve spatial variability of thermal structure, internal waves, horizontal exchanges and calculate dissipation rates of turbulent kinetic energy, a key term in the surface renewal model of gas exchange. An example of an application of a three-dimensional model to a floodplain lake illustrates spatial differences in diel cycles of stratification and mixing (**Figures 4A–D**), and circulations driven by wind-induced basin-scale internal waves when the near-surface water is stratified (**Figures 4E,F**). Three-dimensional hydrodynamic modeling has demonstrated that diel differences in water temperature between floating plant mats and open water as well as basin-scale motions can cause lateral exchanges linking vegetated habitats to open water (Amaral et al., 2021). Higher CH_4 concentrations in

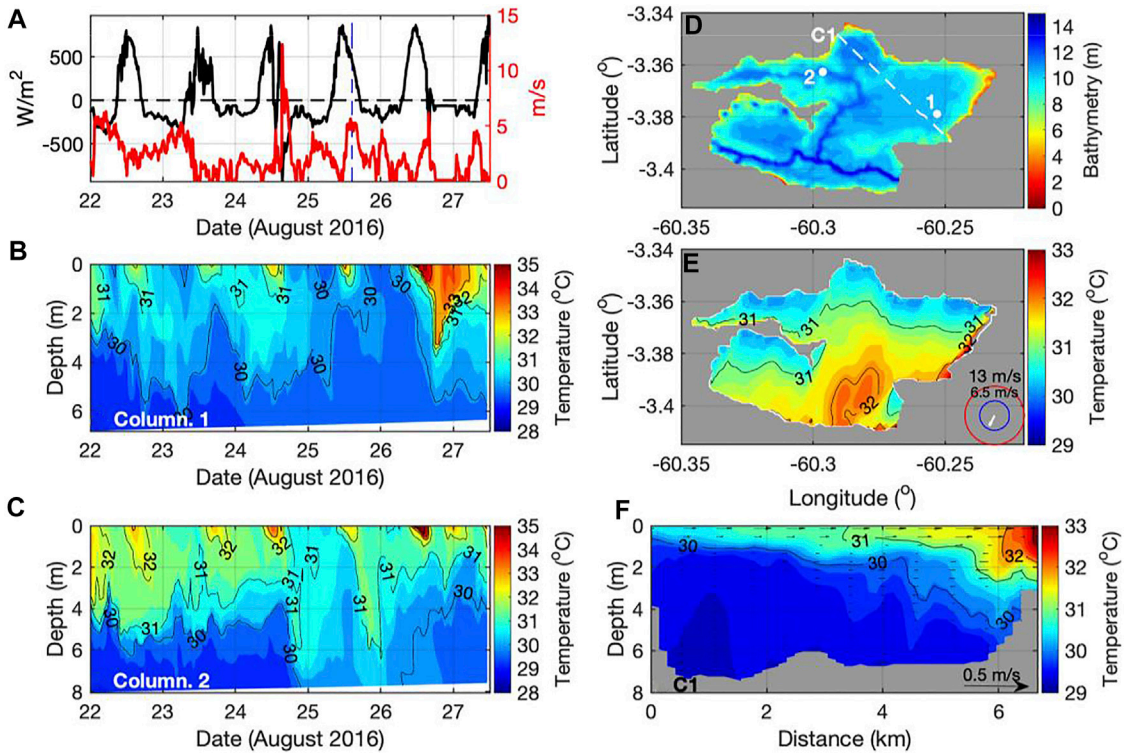


FIGURE 4 | Three-dimensional modeling of thermal structure in Lake Janauacá. **(A)** The net heat flux and wind speed at site one on map in panel d; **(B,C)** AEM3D simulated temperatures of water column at sites 1,2 over 5 days; **(D)** bathymetry of Lake Janauacá, white dots indicate sites 1,2 shown in panels b and c, and white dashed line marks orientation of transect C1; **(E)** AEM3D simulated near-surface temperatures at the time marked by the vertical blue dashed line in panel a (25 August 2016, 14:29:30 h); **(F)** AEM3D simulated temperatures and horizontal velocities along transect C1 at the time marked by the vertical blue dashed line in panel a (25 August 2016, 14:29:30 h). Numbered black lines in panels b, c, e and f are the isotherms at 1°C intervals. Application of AEM3D to Lake Janauacá is described in Amaral et al. (2021).

herbaceous plant mats than in open water suggest that vegetated habitats can be sources of CH_4 to other regions (Bartlett et al., 1988; Barbosa et al., 2020).

7 MODELING METHANE EMISSIONS

7.1 Wetland Models

In a summary of results from the Wetland and Wetland CH_4 Inter-comparison of Models Project (WETCHIMP), Melton et al. (2013) stated that the models disagreed in their simulations of wetland areal extent and methane emissions, in both space and time, and had parameter and structural uncertainty, and noted that lakes and rivers were not included. Moreover, mechanistic models of methane production and evasion appropriate for tropical floodplains are not available (Riley et al., 2011), though relevant conceptual models have been proposed (Cao et al., 1996; Potter 1997; Potter et al., 2014). While several models have potentially useful components or formulations (e.g., Walter and Heimann 2000; Tang et al., 2010; Bloom et al., 2012; Wania et al., 2013; Ringeval et al., 2014; Tan et al., 2015; Lu et al., 2016), no spatially explicit model exists that incorporates the inundation dynamics, ecological characteristics and limnological conditions of tropical floodplains and wetlands. Of special importance is inclusion of plant functional groups common in these habitats combined with appropriate algorithms to estimate their productivity, as these plants supply most of the organic carbon subsequently released as methane (Melack and Engle 2009; Melack et al., 2009). Algorithms are required that simulate stratification and mixing of the water column with concomitant influence on the extent of anoxia and on air-water gas exchange.

Current regional biogeochemical models of methane emissions from wetlands calculate grid-averaged methane fluxes based on soil temperature and carbon availability or heterotrophic respiration. Examples of these models include the Joint United Kingdom Land Environment Simulator (JULES) (Clark et al., 2011; McNorton et al., 2016), the Lund-Potsdam-Jena model (LPJ-WSL; Sitch et al., 2003; Zhang et al., 2016), a CH_4 biogeochemistry model based on the Integrated Biosphere Simulator (TRIPLEX-GHG; Zhu et al., 2014), the LPX-Bern model (Ringeval et al., 2014), a revision of TEM-MDM (Liu et al., 2020) and WetCHARTs (Bloom et al., 2017), JPL-WHyMe (Wania et al., 2010), the Dynamic Land Ecosystem Model (DLEM, Zhang et al., 2017), and CLM4Me (Riley et al., 2011; Meng et al., 2012). A methane model for Amazon peatlands is under development (Yuan et al., 2020). One problem with these models is their use of molecular diffusion through soil layers that

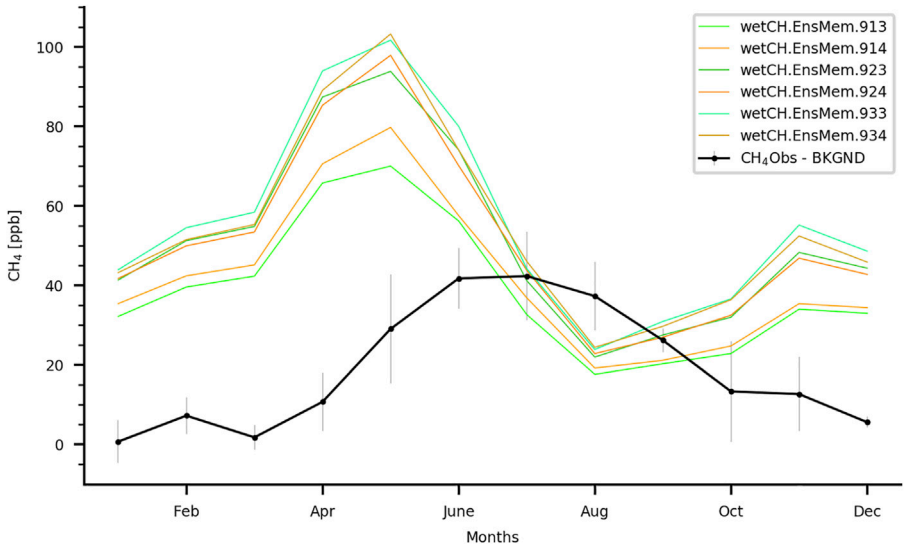


FIGURE 5 | Seasonal cycle of the regional signal (as measurements - background concentration) for simulated and observed mixing ratios of CH_4 at ATTO, expressed as parts per billion (ppb). The observed mixing ratios at ATTO (measurement height 79 m) are shown as a black line and the error bars represents ±1 sigma (standard deviation). This methodology was applied for CO_2 at ATTO by Botía et al. (2021). The background concentrations are from the inversion available via the Copernicus Atmosphere Monitoring Service (CAMS) (Segers and Houweling 2020). For the simulated and observed mixing ratios, only daytime values (13:00–17:00 h local time) were used to ensure well-mixed conditions in the planetary boundary layer. WetCHARTs v1.3.1 is used for the simulated contribution of wetlands to the integrated CH_4 signal at ATTO. The set of WetCHARTs ensemble members show different temperature dependence factors for the CH_4 respiration fraction (Q_{10}) and different wetland extents.

is not appropriate for the turbulence-based gas transfer needed for conditions with surface inundation. Inundation is usually simulated as overland hillslope flows and an approximated terrain model, and does not represent the large seasonal inundation variations and hydrologic fluxes present in the Amazon basin. Climatic inputs are typically obtained from reanalysis products with insufficient temporal resolutions to force diel processes. The plant functional groups included do not represent the aquatic plants common in the Amazon basin. Furthermore, these models do not explicitly include biogeochemical processes, such as methanogenesis and methane oxidation, or physical processes, such as mixing through the water, lateral exchanges, ebullition, or air-water exchange via turbulent mixing. Also, they do not simulate dissolved oxygen concentrations and thus the impact of dissolved oxygen on the methane oxidation or prescribe bulk dissolved oxygen concentrations to the grids (Wania et al., 2010; Riley et al., 2011).

Results from an atmospheric transport model and ATTO mixing ratios (Botia et al., 2020) were compared to six versions of the extended ensemble available in WetCHARTs v1.3.1 (Bloom et al., 2017) to account for variability in wetland extent and the temperature-dependent CH_4 respiration fraction (Q_{10}) (**Figure 5**). All WetCHARTs' simulations used precipitation from ERA5 (C3S, 2017) to drive the temporal variability of methane emissions and the CARDAMOM model for heterotrophic respiration, but the wetland spatial extent was varied. The simulations ending in three used the Global Lakes and Water Database (Lehner and Döll 2004) and those ending in four used the sum of all wetland and freshwater land cover types in GLOBCOVER (Bontemps et al., 2011). Each pair of simulations had a different temperature dependence of the CH_4 respiration fraction (Q_{10}), according to the second digit of each simulation (Q_{10} = 1,2,3). The variability in the WetCHARTs simulations indicates that when using a different wetland extent but the same temperature dependence of the CH_4 respiration fraction (Q_{10}), the effect on the integrated CH_4 signal can be about 10 ppb (i.e., lines 913 and 914). This effect seems to be larger at lower Q_{10} values. When using a different Q_{10} and the same wetland extent (e.g., line 914 with 924 or 934), the differences are larger when comparing the Q_{10} = 1 with the Q_{10} = 2 simulations than between the Q_{10} = 2 and Q_{10} = 3 simulations. Furthermore, these comparisons suggest that WetCHARTs fluxes for the ATTO footprint are too high, and that the seasonality of WetCHART-derived mixing ratios at ATTO are 1 month out of phase when compared to the ATTO observations. When accounting for transport errors (not shown here), the simulated wetland signal at ATTO is still higher than the observations (Botia et al., 2020).

7.2 Lake Models

Potter et al. (2014) built a model for Amazon floodplain lakes based on the supply of organic carbon, as a key factor determining methane production. The LAKE model (Stepanenko et al., 2016) includes most major processes operative in lakes, but the methane module has only been tested on a small boreal lake. Zimmermann et al. (2021) used measurements and a one-dimensional physical model of a small temperate lake to examine how seasonal or more frequent thermocline deepening influenced methane emission and consumption by methanotrophs. Though conceptually

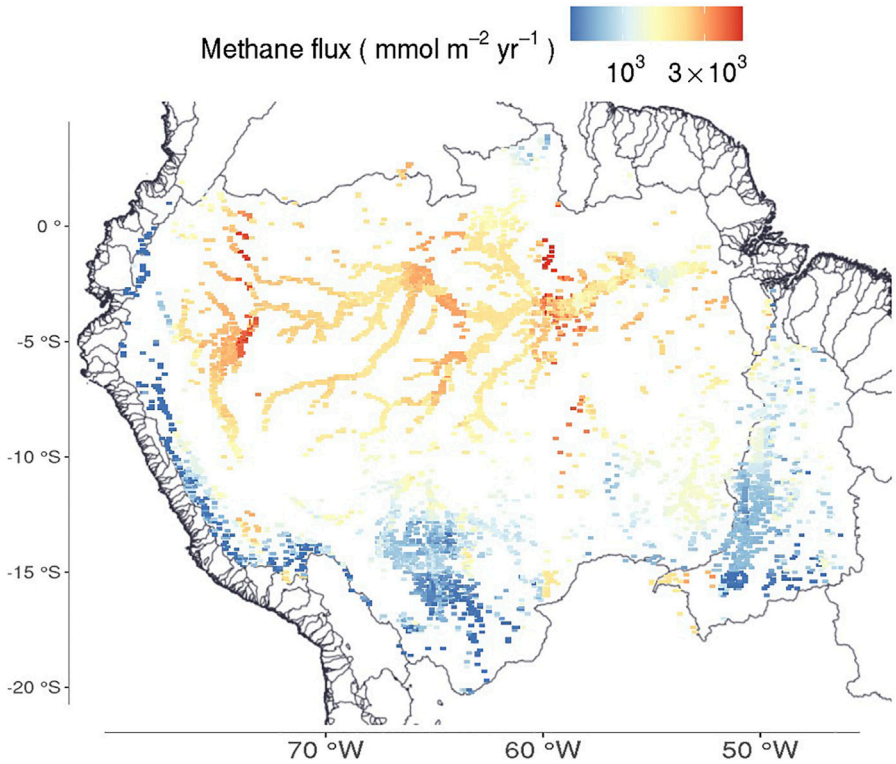


FIGURE 6 | Mean annual methane fluxes for only lakes, expressed as mmoles of CH_4 m^{-2} y^{-1}, weighted averaged by lake area within 0.5° × 0.5° grid cells for 2004 through 2006 as modeled by ALBM (Tan et al., 2015; Guo et al., 2020). Both the Amazon and Tocantins basins are shown.

relevant, this model would require revision because diel cycles of stratification and mixing are common in shallow Amazon lakes.

The Arctic Lake Biogeochemical Model (ALBM) is a one-dimensional process-based, biogeochemical model that simulates the thermal and methane dynamics of lakes (Tan et al., 2015). The model has been applied to arctic and boreal lakes on seasonal time scales (Tan et al., 2015; Guo et al., 2020), but the thermal module and several other aspects need revisions for conditions in shallow, warm waters. In **section 6.2** we discuss alternative models of the relevant physical processes. By combining sensitivity analyses and calibration and validation with appropriate data, the models have been shown to perform reasonably well for specific lakes. However, to apply these models on a regional scale is more difficult as success depends on the calibration and validation sites being representative of the region, and on the availability of data for lakes in the region. An application of ALBM to the Amazon basin produced reasonable results for open water of lakes that further modifications are likely to improve (**Figure 6**). The parameters used for the Amazon basin were calibrated with data from two well-studied floodplain lakes (Janauacá and Calado) with relevant references cited above.

Several biogeochemical and physical processes need to be incorporated or improved in mechanistic methane models for floodplain lakes. New formulations of gas transfer velocity and inclusion of lateral exchanges and diel stratification and mixing, as described in **section 6**, are recommended. Developing parameterizations for fluxes through trees and herbaceous plants, oxic methane production, anaerobic methane oxidation and supply of carbon by autotrophic growth and hydrological inputs are challenging but important. To improve modeling of ebullition, inclusion of changes in hydrostatic pressure and from disturbances of the sediments may help.

7.3 Statistical Models and Analyses

Statistical models offer another approach for estimating lake and reservoir emissions, albeit with limitations related to data availability

DelSontro et al. (2016) analyzed the relationship between emission rates and the predictor variables of lake size, chlorophyll a, total phosphorus and total nitrogen using simple and multiple linear regression for lake and reservoirs distributed around the world. Though tropical reservoirs were included, Amazon floodplain lakes are not represented in this analysis. Among the variables evaluated only chlorophyll a had a positive effect on total methane emission. For comparison, a statistical model applied to Lake Janauacá found variables related to CH_4 production (temperature, dissolved organic carbon) and consumption (dissolved nitrogen, oxygenated water column), as important to dissolved CH_4 concentrations (Barbosa et al., 2020).

Using eddy covariance data from wetland sites largely in the north temperate zone, Knox et al. (2021) applied several statistical techniques to examine the importance of a variety of physical and biological predictors of the timing and magnitude of CH_4 fluxes. While quite informative with regard to the wetlands included, the

TABLE 1 | Methane emission for reach of the mainstem Solimões-Amazon rivers and floodplains from 73.57° W, 4.5° S (confluence of Marañón and Ucayali rivers) to 51.4° W, 0.46° S (Gurupá Island). Areas of aquatic habitats from Melack and Hess (2010) and of rivers from Allen and Pavelsky (2018). Mg = 10^6 g.

River channel
Area, 11,470 km^2.
Average flux, 20 mg CH_4 m^{-2} d^{-1} (Sawakuchi et al., 2014 for Amazon; Barbosa et al., 2016 for Solimões).
Total area flux, 230 Mg CH_4 d^{-1}.
Floodplain lakes (open water)
Areas: high water, 10,370 km^2; low water, 5,700 km^2 (open water minus river channel areas)
Average flux, 42 mg CH_4 m^{-2} d^{-1} (Barbosa et al., 2021, diffusive and ebullitive fluxes)
Low water areal total, 435 Mg CH_4 d^{-1}.
High water areal total, 114 Mg CH_4 d^{-1}.
Floating herbaceous aquatic plants
Areas: high water, 9,800 km^2; low water, 6,200 km^2
Average flux, 118 mg CH_4 m^{-2} d^{-1} (Barbosa et al., 2021, diffusive and ebullitive fluxes)
High water areal total, 1,156 Mg CH_4 d^{-1}.
Low water areal total, 732 Mg CH_4 d^{-1}.
Seasonally inundated forests
Fluxes from water surface
Areas: high water, 51,300 km^2; low water, 16,400 km^2 (includes shrubs, woodland, and forest)
Average flux, 58 mg CH_4 m^{-2} d^{-1} (Barbosa et al., 2021, diffusive and ebullitive fluxes)
High water areal total, 2,975 Mg CH_4 d^{-1}.
Low water areal total, 950 Mg CH_4 d^{-1}.
Fluxes from tree stems
Average flux, 145 mg CH_4 m^{-2} d^{-1} (Pangala et al., 2017; average for sites along Amazon and Solimões rivers)
High water areal total, 7,440 Mg CH_4 d^{-1}.
Low water areal total, 2,380 Mg CH_4 d^{-1}.

only site in tropical South America is in the Pantanal, a seasonal savanna wetland. Though the Pantanal shares similarities to the Moxos wetlands, the majority of floodplain and other wetlands in the Amazon basin are not represented in the analyses.

While it is well known that all models have biases from limitations and assumptions within the models and as a result of the data used in calibration and validation, given the logistic and scientific challenges with measurements in the vast and complex Amazon basin, models of all types can surely contribute to understanding and projections of methane emissions.

8 PREVIOUS AND CURRENT ESTIMATES OF REGIONAL EMISSIONS FOR AMAZON BASIN

8.1 Bottom-Up Approaches

Estimates of methane fluxes at different spatial scales illustrate varied approaches and limitations. Early estimates of regional methane fluxes made for the mainstem Solimões-Amazon floodplain and the whole basin were limited by lack of data on areas of inundation and aquatic habitats and few measurements of fluxes (e.g., Bartlett et al., 1988; Devol et al., 1990). The first estimates that incorporated remote sensing of inundation and habitat areas were done by Melack et al. (2004) for the mainstem Solimões-Amazon floodplain and a 1.77 million km^2 area in the central basin (Hess et al., 2003). They combined habitat-specific methane fluxes with seasonal changes in the area of aquatic habitats, derived from active and passive microwave remote sensing, and applied Monte Carlo error propagation to establish uncertainties. By assuming similar fluxes by habitat and adding approximations for particular regions (e.g., Moxos), an extrapolation to whole lowland basin was made. For the central basin quadrant, annual emission was estimated as 9 ± 1.7 Tg CH_4, and if extrapolated to the basin below 500 m asl, resulted in approximately 29 Tg CH_4 y^{-1}. The largest omission from these estimates is evasion from seasonally flooded forests. The measurements of emissions for trees, extrapolated to the Amazon basin, by Pangala et al. (2017; 15.1 ± 1.8 to 21.2 ± 2.5 Tg CH_4 y^{-1}) and Gauci et al. (2021; 12.7 to 21.1 Tg CH_4 y^{-1} for inundated trees plus 2.2 to 3.6 Tg CH_4 y^{-1} for riparian zones with water tables below the surface) substantially increase regional fluxes. However, considerable uncertainty in these estimates stems from the lack of adequate data on the abundance and emitting surface areas of the trees and the high variability in fluxes per unit area of trees.

As part of the Science Panel for the Amazon (SPA) report, released at COP26 (Gatti L. et al., 2021; Mahli et al., 2021), J. Melack, L. Basso and S. Pangala provided bottom-up estimates of methane emission from aquatic environments in the combined hydrological Amazon and Tocantins basins, and for the Amazon forest biome. A total area of aquatic habitats for these two basins of 970,500 km^2 was used to generate their bottom-up estimate of approximately 51 Tg CH_4 y^{-1}. However, this estimate does not include seasonal and interannual variations or a rigorous uncertainty analysis. A second estimate of methane emissions was done for the Amazon biogeographic province that encompasses tropical forests in much of Amapá, French Guiana, Guyana, Suriname, and southern Venezuela and eastern Colombia that drains into the Orinoco River (Albert et al., 2021). This estimate had added uncertainty because of the lack of data for most of the northeastern areas outside of the hydrological Amazon basin.

Improvements needed in bottom-up estimates are inclusion of seasonal variations in flooding and aquatic habitats, as noted in **sections 2**,**3**, and more measurements of all fluxes, summarized in **section 4**. An example of doing so is provided by Barbosa et al. (2021) for a floodplain lake with fringing inundated forests and herbaceous plants. They combined seasonal variations in ebullitive, diffusive and tree-mediated fluxes with variations in water depths and areal coverage of aquatic habitats, i.e., weighting fluxes by seasonal variations in habitat areas and habitat-specific fluxes. This approach was especially important for ebullition for which the fraction of total emission from water surfaces varied from 1% (rising and high water) to 89% (low water) in open water of the lake, and from 73% (rising water) to 93% (falling water) in flooded forests.

An example of the challenges and compromises in regionalization is offered for a reach of the mainstem Solimões-Amazon rivers and associated floodplains (**Table 1**). The values in **Table 1** provide a sense of the relative importance of different habitats as sources of methane to the atmosphere based on areal fluxes and habitat areas for low and high water conditions. However, the fluxes should be viewed with caution because of the uncertainties associated with the data and calculations. As summarized in **section 5**, several studies provide measurements of methane fluxes from water surfaces in river channels and floodplain habitats. Those selected here were judged representative and offering the most complete data. To fully use data from all studies is not possible because actual datasets are not available in most publications. The fluxes from trees are especially difficult to extrapolate because of the large variance in per tree fluxes and the very limited measurements of the surface areas of trees. Fluxes from floodplain soils during low water periods are not included.

In an analysis for the reach of the mainstem Solimões-Amazon floodplain from 54° to 70° W, annual fluxes of 1.7 ± 0.4 Tg CH_4 were calculated with 67% of the uncertainty attributed to habitat-specific fluxes and 33% owed to uncertainties in areal estimates of inundation and vegetative cover (Melack et al., 2004). To do so, the methane emission rate per unit area for the mainstem Solimões-Amazon floodplain, representing a mixture of habitats, and using a mean annual flooded area of 42,700 km^2 (determined as monthly means from Sippel et al. (1998) summed over 12 months and divided by 12) was estimated as ~40 Mg CH_4 km^{-2} y^{-1}.

8.2 Top-Down Estimates With Aircraft Sampling

Several aircraft campaigns provide methane flux estimates for different regions and periods. Beck et al. (2012) estimated fluxes for the lowland Amazon during November as 36 ± 12 mg CH_4 m^{-2} d^{-1} and during May as 43 ± 19 mg CH_4 m^{-2} d^{-1}. Miller et al. (2007) collected vertical profiles of methane over 4 years at sites near Santarém and Manaus and calculated average emissions of ~27 mg CH_4 m^{-2} d^{-1}. Wilson et al. (2016) applied the TOMCAT model using aircraft vertical profiles and estimated methane emissions of 36.5 to 41.1 Tg CH_4 y^{-1}in 2010 and 31.6 to 38.8 Tg CH_4 y^{-1} in 2011 for an area of 5.8 × 10^6 km^{-2}; non-combustion emissions represented 92–98% of total emissions. Pangala et al. (2017) estimated emissions of 42.7 ± 5.6 Tg CH_4 y^{-1} for an area of 6.77 × 10^6 km^2 based on vertical profiles from 2010 to 2013; 10% of emission was attributed to biomass burning.

The most comprehensive record is provided by Basso et al. (2021), who used lower-troposphere vertical profiles of methane concentration from four sites in the Brazilian Amazon basin between 2010 and 2018 and a column budget technique to calculate emissions of 46.2 ± 10.3 Tg CH_4 y^{-1} with no temporal trend. This finding of no temporal trend during a period with exceptionally high and low river stages and varying inundation areas suggests further examination of how methane fluxes could have varied through these years.

Basso et al. (2021) used the methodology of Gatti L. V. et al. (2021) to estimate fluxes for three subregions and combined these as a weighted flux scaled to an area of 7.25 million km^2, a region that includes parts of Venezuela, and all of Suriname, French Guyana and Guiana plus coastal watersheds in Brazil and upper Tocantins basin. The large region to the west of their sampling locations near Tefé and Tabatinga was not sampled and has some environments not represented by the regions to the east, such as the Peruvian peatlands and Andean highlands. Based on concurrent measurements of carbon monoxide, 17% of the sources were attributed biomass burning and 83% mainly to wetlands. Causes for seasonality in wetland fluxes and for the larger signals in the northeast are not fully understood, indicating that more studies are needed.

8.3 Top-Down Estimates Using Satellite Data

Based on SCIAMACHY data, Bergamaschi et al. (2009) calculated total Amazon emissions of 47.5 to 53.0 Tg CH_4 y^{-1} in 2004 for an area of 8.6 × 10^6 km^2. Based on an inversion model, Fraser et al. (2014) estimated an emission of 59.0 ± 3.1 Tg CH_4 y^{-1} from tropical South America (approximately ~9.7 × 10^6 km^2) in 2010. Tunnicliffe et al. (2020) using inverse modelling estimates and GOSAT measurements reported mean emissions for the Brazilian Amazon wetlands (and not clearly defined) lower than other estimates (9.2 ± 1.8 Tg CH_4 y^{-1}). Wilson et al. (2021) using GOSAT data and an inverse model estimated total emissions from natural, agricultural and biomass burning sources of 38.2 ± 5.3 (between 2010 and 2013) and 45.6 ± 5.2 Tg CH_4 y^{-1} (between 2014 and 2017) for the Amazon basin (approximately ~6.0 × 10^6 km^2). Given the different regions represented and the mixture of sources, it is difficult to compare these estimates with each other or with the aircraft or bottom-up values.

8.4 Model Results

Methane emissions for the Amazon basin, extracted from the WetCharts ensemble of wetland models (Bloom et al. (2017) at monthly resolution for 2009 and 2010 by Basso et al. (2021), are 39.4 ± 10.3 Tg CH_4 y^{-1}, and results are similar to emissions derived from aircraft samples except for the northeastern portion of the basin. Gedney et al. (2019) provided estimates of methane flux for the Amazon basin using the JULES model that varied from ~24 to ~58 Tg CH_4 y^{-1}, a rather wide range that stems from problems with inundation estimates and parameterization of

methane fluxes. As part of an application of ALBM to global lakes (Guo et al., 2020), an estimate for only lakes in the Amazon and Tocantins basins, based a static lake area from Messager et al. (2016) and calibration with data from lakes Janauacá and Calado, yielded estimates of ~0.7 Tg CH_4 y^{-1} and ~0.1 Tg CH_4 y^{-1}, respectively. This estimate is similar to the estimate of ~0.7 Tg CH_4 y^{-1} in Mahli et al. (2021) for the same regions based on extrapolation of bottom-up measurements of fluxes and similar lakes areas.

9 FURTHER STUDIES AND RECOMMENDATIONS

Given that an important source of uncertainty in the global methane budget is attributed to emissions from wetlands and other inland waters (Saunois et al., 2020), further improvements in measurements and the understanding of large sources of methane emissions from aquatic ecosystems in the Amazon basin and similar systems elsewhere are clearly a priority. Our review has identified several key ways to do so: 1) Application of remote sensing techniques to better characterize the spatial extent and temporal variations in inundation and aquatic habitats. 2) Increased sampling frequency and duration of methane fluxes and related environmental conditions in all aquatic systems using a combination of approaches including ground-based, aircraft and satellite measurements. 3) Conducting experimental studies to improve understanding of biogeochemical and physical processes. In particular, more studies of the complex roles of microbial assembles and their response to environmental conditions, and of methane emissions in relation to qualities of organic matter and biogeochemical conditions in sediments would improve predictive capabilities. 4) Further development of models appropriate for hydrological and ecological conditions throughout the Amazon basin.

Current hydrological models provide estimates of variations in inundation, and remote sensing products include inundated areas, though the longest time-series underestimate areas in some habitats and high-resolution products are temporally sparse. Mapping inundated lands during low water season poses special challenges in the Amazon basin (Fleischmann et al., 2021). Biogeochemical wetland models do not incorporate key processes and need to use better inundation estimates. For example, Fleischmann et al. (2021) judged that the WAD2M product used in several global methane models does not represent well the inundation dynamics of various wetland complexes in the Amazon basin. Large uncertainties stem from the paucity of measurements of methane fluxes throughout the Amazon basin. Particularly large gaps exist for the Llanos de Moxos, peatlands throughout the Amazon basin, coastal systems, interfluvial wetlands and habitats above 500 m. Streams and medium-sized rivers have very few data. Measurements during low water periods in exposed areas with herbaceous plants and floodable forests are rare. Measurements above and below the dams are available for few hydroelectric projects. Diel, seasonal and interannual variations are very seldom documented. To evaluate potential impacts of increased temperatures and atmospheric CO_2 concentrations on different plants and other organisms would benefit from a combination of experiments and modeling. With the increased availability of *in situ* sensors and automatic recording systems, improved temporal coverage is possible, though logistic challenges remain. The results from an observing system, as suggested by Bloom et al. (2016) for the Amazon basin, would provide valuable data.

As illustrated for specific lakes or subregions, spatially and temporally representative measurements combined with remote sensing-based inundation and habitat estimates can produce seasonally-weighted fluxes (e.g., Rosenqvist et al., 2002; Barbosa et al., 2021). Mechanistically correct and properly calibrated models provide a complementary approach. Models of autotrophic productivity as a source of the organic carbon that fuels methanogenesis and influences other conditions need to use functional traits appropriate to the ecology of the Amazon. Expanded use of hydrological models linked to carbon supply from uplands to aquatic systems (e.g., Lauerwald et al., 2017; Hastie et al., 2019) is also recommended.

Recent results can be used to develop robust regional estimates of methane fluxes from aquatic environments in the Amazon basin, and these approaches can be applied elsewhere. Multiyear measurements of methane concentrations obtained from aircraft (e.g., Basso et al., 2021) and towers, such as the ATTO facility (e.g., Botía et al., 2020), when combined with atmospheric transport models, provide spatially integrated methane concentrations in the regions of influence. However, attributing sources of the methane requires examination of the inundated area and methane fluxes represented by the gridded regions of influence. A critical aspect is applying uncertainty analyses that incorporate natural variability and evaluate systematic biases of the measurements.

Indeed, incorporating all these approaches to an area as vast and diverse as the Amazon basin is a daunting challenge. Though serendipity and national and international initiatives will continue to influence research opportunities, we suggest a few examples. Promising planned remote sensing missions are SWOT and NISAR (mentioned in **section 2**). The SWOT mission will simultaneously measure surface water elevation, slope and extent and provide the basis for calculations of river discharge and monitoring of lake water levels. NISAR will complement other SAR missions by providing global 12-days coverage of L-band radar, which penetrates forest canopies to detect inundation under seasonally flooded forests. Cost-effective sampling designs depend on institutional infrastructure, interested and trained personnel, funding and international coordination. Hence, many studies were concentrated in the vicinity of research institutes or universities or were conducted as surveys along major rivers. Less accessible or remote regions or habitats, such as the Llanos de Moxos, other interfluvial wetlands and Andean slopes, are likely to be significant sources of methane and will require extra effort and expense. In contrast, streams and medium-sized rivers are surprisingly under-sampled given their proximity to established research centers. Applications of advanced methods in microbial ecology and experimental manipulations, including characterization of methanogenic and methanotrophic assembles and their temporal variability in abundance and activity, would strengthen modeling efforts and predictive understanding. Creative individuals will

continue to develop new ideas and methods and venture into unexplored areas.

AUTHOR CONTRIBUTIONS

The ideas represented in our review evolved from discussions among all co-authors over several years. JM developed and wrote the manuscript and all co-authors contributed with results and revisions.

FUNDING

National Aeronautics and Space Administration (NASA grant NNX17AK49G) and the US National Science Foundation (NSF DEB grant 1753856) to JM and SM supported data analysis and writing by JM, SM, and WZ. Sao Paulo Research Foundation (FAPESP grants 2018/14006-4 and 2019/23654-2) supported data analysis by LB. Bundesministerium für Bildung und Forschung (grants 01LB1001A and 01LK1602A) and the International Max Planck Research School for Global Biogeochemical Cycles (IMPRS-gBGC) supported data analysis and writing by SB.

ACKNOWLEDGMENTS

SB acknowledges the ATTO team running the site, and Jost Lavric and David Walter for data handling and processing, and thanks Anthony A. Bloom for providing version 1.3.1 of WetCHARTs for the STILT simulations.

REFERENCES

Abril, G., Guérin, F., Richard, S., Delmas, R., Galy-Lacaux, C., Gosse, P., et al. (2005). Carbon Dioxide and Methane Emissions and the Carbon Budget of a 10-year Old Tropical Reservoir (Petit Saut, French Guiana). *Glob. Biogeochem. Cycles* 19, 1–16. doi:10.1029/2005gb002457

Albert, J., Hoorn, C., Malhi, Y., Phillips, O., Encalada, A. C., Steege, H., et al. (2021). "The Multiple Viewpoints for the Amazon: Geographic Limits and Meanings," in *Amazon Assessment Report*. Editors C. Nobre, A. Encalada, E. Anderson, F. H. Roca Alcazar, and M. Bustamante (New York, USA: United Nations Sustainable Development Solutions Network). www.theamazonwewant.org/spa-reports.

Alin, S. R., Rasera, M. d. F. F. L., Salimon, C. I., Richey, J. E., Holtgrieve, G. W., Krusche, A. V., et al. (2011). Physical Controls on Carbon Dioxide Transfer Velocity and Flux in Low-Gradient River Systems and Implications for Regional Carbon Budgets. *J. Geophys. Res.* 116, G01009. doi:10.1029/2010jg001398

Allen, G. H., and Pavelsky, T. M. (2018). Global Extent of Rivers and Streams. *Science* 361, 585–588. doi:10.1126/science.aat0636

Almeida, R. M., Shi, Q., Gomes-Selman, J. M., Angarita, H., Barros, N., Forsberg, B. R., et al. (2019). Reducing the Greenhouse Gas Footprint of Amazon Hydropower with Optimal Dam Planning. *Nat. Comm*. doi:10.1038/s41467-019-12179-5

Alsdorf, D., Han, S.-C., Bates, P., and Melack, J. (2010). Seasonal Water Storage on the Amazon Floodplain Measured from Satellites. *Remote Sens. Environ.* 114, 2448–2456. doi:10.1016/j.rse.2010.05.020

Amaral, J. H. F., Melack, J. M., Barbosa, P. M., Borges, A. V., Kasper, D., Cortés, A. C., et al. (2021). Inundation, Hydrodynamics and Vegetation Influence Carbon Dioxide Concentrations in Amazon Floodplain Lakes. *Ecosystems*. doi:10.1007/s10021-021-00692-y

Amaral, J. H. F., Melack, J. M., Barbosa, P. M., MacIntyre, S., Kasper, D., Cortes, A. C., et al. (2020). Carbon Dioxide Fluxes to the Atmosphere from Waters within Flooded Forests in the Amazon Basin. *J. Geophys. Res. Biogeosci.* 125, e2019JG005293. doi:10.1029/2019jg005293

Amaral, J., Suhett, A., Melo, S., and Farjalla, V. (2013). Seasonal Variation and Interaction of Photodegradation and Microbial Metabolism of DOC in Black Water Amazonian Ecosystems. *Aquat. Microb. Ecol.* 70, 157–168. doi:10.3354/ame01651

Apers, S., De Lannoy, G. J. M., Baird, A. J., Cobb, A. R., Dargie, G. C., del Aguila Pasquel, J., et al. (2022). Tropical Peatland Hydrology Simulated with a Global Land Surface Model. *J. Adv. Model. Earth Sys* 14, e2021MS002784. doi:10.1029/2021MS002784

Arnesen, A. S., Silva, T. S. F., Hess, L. L., Novo, E. M. L. M., Rudorff, C. M., Chapman, B. D., et al. (2013). Monitoring Flood Extent in the Lower Amazon River Floodplain Using ALOS/PALSAR ScanSAR Images. *Remote Sens. Environ.* 130, 51–61. doi:10.1016/j.rse.2012.10.035

Augusto-Silva, P. B., MacIntyre, S., de Moraes Rudorff, C., Cortés, A., and Melack, J. M. (2019). Stratification and Mixing in Large Floodplain Lakes along the Lower Amazon River. *J. Gt. Lakes. Res.* 45, 61–72. doi:10.1016/j.jglr.2018.11.001

Barbosa, P. M., Farjalla, V. F., Melack, J. M., Amaral, J. H. F., da Silva, J. S., and Forsberg, B. R. (2018). High Rates of Methane Oxidation in an Amazon Floodplain Lake. *Biogeochemistry* 137, 351–365. doi:10.1007/s10533-018-0425-2

Barbosa, P. M., Melack, J. M., Amaral, J. H. F., Linkhorst, A., and Forsberg, B. R. (2021). Large Seasonal and Habitat Differences in Methane Ebullition on the Amazon Floodplain. *J. Geophys. Res. Biogeosci.* 126, e2020JG005911. doi:10.1029/2020JG005911

Barbosa, P. M., Melack, J. M., Amaral, J. H. F., MacIntyre, S., Kasper, D., Cortés, A., et al. (2020). Dissolved Methane Concentrations and Fluxes to the Atmosphere from a Tropical Floodplain Lake. *Biogeochemistry* 148, 129–151. doi:10.1007/s10533-020-00650-1

Barbosa, P. M., Melack, J. M., Farjalla, V. F., Amaral, J. H. F., Scofield, V., and Forsberg, B. R. (2016). Diffusive Methane Fluxes from Negro, Solimões and Madeira Rivers and Fringing Lakes in the Amazon Basin. *Limnol. Oceanogr.* 61, S221–S237. doi:10.1002/lno.10358

Barichivich, J., Gloor, E., Peylin, P., Brienen, R. J. W., Schöngart, J., Espinoza, J. C., et al. (2018). Recent Intensification of Amazon Flooding Extremes Driven by Strengthened Walker Circulation. *Sci. Adv.* 4, eaat8785. doi:10.1126/sciadv.aat8785

Barros, N., Cole, J. J., Tranvik, L. J., Prairie, Y. T., Bastviken, D., Huszar, V. L. M., et al. (2011). Carbon Emission from Hydroelectric Reservoirs Linked to Reservoir Age and Latitude. *Nat. Geosci.* 4, 593–596. doi:10.1038/ngeo1211

Bartlett, K. B., Crill, P. M., Sebacher, D. I., Harriss, R. C., Wilson, J. O., and Melack, J. M. (1988). Methane Flux from the Central Amazonian Floodplain. *J. Geophys. Res.* 93, 1574–1582. doi:10.1029/jd093id02p01571

Bartlett, K., Crill, P. M., Bonassi, J., Richey, J. E., and Harriss, R. (1990). Methane Flux from the Amazon River Floodplain: Emissions during Rising Water. *J. Geophys. Res.* 95 (16), 773788. doi:10.1029/jd095id10p16773

Basso, L. S., Gatti, L. V., Gloor, M., Miller, J. B., Domingues, L. G., Correia, C. S. C., et al. (2016). Seasonality and Interannual Variability of CH_4 Fluxes from the Eastern Amazon Basin Inferred from Atmospheric Mole Fraction Profiles. *J. Geophys. Res. Atmos.* 121, 168–184. doi:10.1002/2015jd023874

Basso, L. S., Marani, L., Gatti, L. V., Miller, J. B., Gloor, M., Melack, J., et al. (2021). Amazon Methane Budget Derived from Multi-Year Airborne Observations Highlights Regional Variations in Emissions. *Commun. Earth Environ.* 2, 246. doi:10.1038/s43247-021-00314-4

Beck, V., Chen, H., Gerbig, C., Bergamaschi, P., Bruhwiler, L., Houweling, S., et al. (2012). Methane Airborne Measurements and Comparison to Global Models during BARCA. *J. Geophys. Res.* 117, a–n. doi:10.1029/2011JD017345

Beighley, R. E., and Gummadi, V. (2011). Developing Channel and Floodplain Dimensions with Limited Data: a Case Study in the Amazon Basin. *Earth Surf. Process. Landforms* 36, 1059–1071. doi:10.1002/esp.2132

Belger, L., Forsberg, B. R., and Melack, J. M. (2011). Carbon Dioxide and Methane Emissions from Interfluvial Wetlands in the Upper Negro River Basin, Brazil. *Biogeochemistry* 105, 171–183. doi:10.1007/s10533-010-9536-0

Bento, M. d. S., Barros, D. J., Araújo, M. G. d. S., Da Róz, R., Carvalho, G. A., do Carmo, J. B., et al. (2021). Active Methane Processing Microbes and the Disproportionate Role of NC10 Phylum in Methane Mitigation in Amazonian Floodplains. *Biogeochemistry* 156, 293–317. doi:10.1007/s10533-021-00846-z

Bergamaschi, P., Frankenberg, C., Meirink, J. F., Krol, M., Villani, M. G., Houweling, S., et al. (2009). Inverse Modeling of Global and Regional CH_4 Emissions Using SCIAMACHY Satellite Retrievals. *J. Geophys. Res.* 114, D22301. doi:10.1029/2009JD012287

Bertassoli, D. J., Sawakuchi, H. O., de Araújo, K. R., de Camargo, M. G. P., Alem, V. A. T., and Pereira, T. S. (2021). How Green Can Amazon Hydropower Be? Net Carbon Emission from the Largest Hydropower Plant in Amazonia. *Sci. Adv.* 7, eabe1470.

Bloom, A. A., Bowman, K. W., Lee, M., Turner, A. J., Schroeder, R., Worden, J. R., et al. (2017). A Global Wetland Methane Emissions and Uncertainty Dataset for Atmospheric Chemical Transport Models (WetCHARTs Version 1.0). *Geosci. Model. Dev.* 10, 2141–2156. doi:10.5194/gmd-10-2141-2017

Bloom, A. A., Lauvaux, T., Worden, J., Yadav, V., Duren, R., Sander, S. P., et al. (2016). What Are the Greenhouse Gas Observing System Requirements for Reducing Fundamental Biogeochemical Process Uncertainty? Amazon Wetland CH_4 Emissions as a Case Study. *Atmos. Chem. Phys.* 16, 15199–15218. doi:10.5194/acp-16-15199-2016

Bloom, A. A., Palmer, P. I., Fraser, A., and Reay, D. S. (2012). Seasonal Variability of Tropical Wetland CH_4 Emissions: the Role of the Methanogen-Available Carbon Pool. *Biogeosciences* 9, 2821–2830. doi:10.5194/bg-9-2821-2012

Bontemps, S., Defourny, P., van Bogaert, E., Arino, O., Kalagirou, V., and Ramos Peres, J. (2011). Globcover Products Description and Validation Report. Technical report, ESA. URL: epic.awi.de/id/eprint/31014/16/GLOBCOVER2009_284 (Validation_Report_2-2.pdf.285.

Borrel, G., Jézéquel, D., Biderre-Petit, C., Morel-Desrosiers, N., Morel, J.-P., Peyret, P., et al. (2011). Production and Consumption of Methane in Freshwater Lake Ecosystems. *Res. Microbiol.* 162, 832–847. doi:10.1016/j.resmic.2011.06.004

Botía, S., Galkowski, M., Marshall, J., Koch, T., Lavric, J. V., Walter, D., et al. (2020b). *Six Years of Atmospheric CO_2, CH_4 and CO at the Amazon Tall Tower Observatory: A New Opportunity to Study Processes on Seasonal and Inter-annual Scales.* Abstract GC009-0013. Fall 2020 American Geophysical Union conference.

Botía, S., Gerbig, C., Marshall, J., Lavric, J. V., Walter, D., Pöhlker, C., et al. (2020a). Understanding Nighttime Methane Signals at the Amazon Tall Tower Observatory (ATTO). *Atmos. Chem. Phys.* 20, 6583–6606. doi:10.5194/acp-20-6583-2020

Bridgham, S. D., Cadillo-Quiroz, H., Keller, J. K., and Zhuang, Q. (2013). Methane Emissions from Wetlands: Biogeochemical, Microbial, and Modeling Perspectives from Local to Global Scales. *Glob. Change Biol.* 19, 1325–1346. doi:10.1111/gcb.12131

C3S (2017). ERA5: Fifth Generation of ECMWF Atmospheric Reanalyses of the Global Climate. URL: https://cds.climate.copernicus.eu/cdsapp#!/home.

Caldwell, S. L., Laidler, J. R., Brewer, E. A., Eberly, J. O., Sandborgh, S. C., and Colwell, F. S. (2008). Anaerobic Oxidation of Methane: Mechanisms, Bioenergetics, and the Ecology of Associated Microorganisms. *Environ. Sci. Techn.* 42, 6791–6799.

Cao, M., Marshal, S., and Gregson, K. (1996). Global Carbon Exchange and Methane Emission from Natural Wetlands: Application of a Process-Based Model. *J. Geophys. Res.* 101 (14399-14), 414. doi:10.1029/96jd00219

Cardoso, S. J., Enrich-Prast, A., Pace, M. L., and Roland, F. (2014). Do models of Organic Carbon Mineralization Extrapolate to Warmer Tropical Sediments? *Limnol. Oceanogr.* 59, 48–54.

Carmo, J. B. d., Keller, M., Dias, J. D., Camargo, P. B. d., and Crill, P. (2006). A Source of Methane from Upland Forests in the Brazilian Amazon. *Geophys. Res. Lett.* 33, L04809. doi:10.1029/2005gl025436

Cassol, H. L. G., Domingues, L. G., Sanchez, A. H., Basso, L. S., Marani, L., Tejada, G., et al. (2020). Determination of Region of Influence Obtained by Aircraft Vertical Profiles Using the Density of Trajectories from the HYSPLIT Model. *Atmosphere* 11, 1073. doi:10.3390/atmos11101073

Castello, L., McGrath, D. G., Hess, L. L., Coe, M. T., Lefebvre, P. A., Petry, P., et al. (2013). The Vulnerability of Amazon Freshwater Ecosystems. *Conserv. Lett.* 6, 217–229. doi:10.1111/conl.12008

Chambers, J. Q., Tribuzy, E. S., Toledo, L. C., Crispim, B. F., Higuchi, N., J. dos Santos, J., et al. (2004). Respiration from a Tropical Forest Ecosystem: Partitioning of Sources and Low Carbon Use Efficiency. *Ecol. Applic* 14, S72–S88.

Chapman, B., Mcdonald, K., Shimada, M., Rosenqvist, A., Schroeder, R., and Hess, L. (2015). Mapping Regional Inundation with Spaceborne L-Band SAR. *Remote Sens.* 7, 5440–5470. doi:10.3390/rs70505440

Clark, D. B., Mercado, L. M., Sitch, S., Jones, C. D., Gedney, N., Best, M. J., et al. (2011). The Joint UK Land Environment Simulator (JULES), Model Description - Part 2: Carbon Fluxes and Vegetation Dynamics. *Geosci. Model. Dev.* 4, 701–722. doi:10.5194/gmd-4-701-2011

Coe, M. T., Costa, M. H., and Howard, E. (2007). Simulating the Surface Waters of the Amazon River Basin: Impacts of New River Geomorphic and Dynamic Flow Parameterizations. *Hydrol. Process.* 22, 2542–2553.

Cole, J. J., and Caraco, N. F. (1998). Atmospheric Exchange of Carbon Dioxide in a Low-Wind Oligotrophic Lake Measured by the Addition of SF6. *Limnol. Oceanogr.* 43, 647–656. doi:10.4319/lo.1998.43.4.0647

Conrad, R., Ji, Y., Noll, M., Klose, M., Claus, P., and Enrich-Prast, A. (2014). Response of the Methanogenic Microbial Communities in Amazonian Oxbow Lake Sediments to Desiccation Stress. *Environ. Microbiol.* 16, 1682–1694. doi:10.1111/1462-2920.12267

Conrad, R., Klose, M., Claus, P., and Enrich-Prast, A. (2010). Methanogenic Pathway, 13C Isotope Fractionation, and Archaeal Community Composition in the Sediment of Two Clear-Water Lakes of Amazonia. *Limnol. Ocean.* 55, 689–702. doi:10.4319/lo.2009.55.2.0689

Conrad, R., Noll, M., Claus, P., Klose, M., Bastos, W. R., and Enrich-Prast, A. (2011). Stable Carbon Isotope Discrimination and Microbiology of Methane Formation in Tropical Anoxic Lake Sediments. *Biogeosciences* 8, 795–814. doi:10.5194/bg-8-795-2011

Crill, P. M., Bartlett, K. B., Wilson, J. O., Sebacher, D. I., Harriss, R. C., Melack, J. M., et al. (1988). Tropospheric Methane from an Amazonian Floodplain Lake. *J. Geophys. Res.* 93, 1564–1570. doi:10.1029/jd093id02p01564

Crippa, M., Oreggioni, G., Guizzardi, D., Muntean, M., Schaaf, E., Lo Vullo, E., et al. (2019). *Fossil CO_2 and GHG Emissions of All World Countries*. doi:10.2760/655913

Dacey, J. W. H. (1981). Pressurized Ventilation in the Yellow Waterlily. *Ecology* 62, 1137–1147. doi:10.2307/1937277

Dalmagro, H. J., Zanella de Arruda, P. H., Vourlitis, G. L., Lathuillière, M. J., de S. Nogueira, J., Couto, E. G., et al. (2019). Radiative Forcing of Methane Fluxes Offsets Net Carbon Dioxide Uptake for a Tropical Flooded Forest. *Glob. Change Biol.* 25, 1967–1981. doi:10.1111/gcb.14615

Deemer, B. R., Harrison, J. A., Li, S., Beaulieu, J. J., DelSontro, T., Barros, N., et al. (2016). Greenhouse Gas Emissions from Reservoir Water Surfaces: A New Global Synthesis. *BioScience* 66, 949–964. doi:10.1093/biosci/biw117

del Aguila-Pasquel, J. (2017). *Methane Fluxes and Porewater Dissolved Organic Carbon Dynamics from Different Peatland Types in the Pastaza-Marañon Basin of the Peruvian Amazon*. Houghton, MI: Michigan Technological University. Open Access Master's thesis. doi:10.37099/mtu.dc.etdr/494

DelSontro, T., Beaulieu, J. J., and Downing, J. A. (2018). Greenhouse Gas Emissions from Lakes and Impoundments: Upscaling in the Face of Global Change. *Limnol. Oceanogr. Lett.* 3, 64–75. doi:10.1002/lol2.10073

DelSontro, T., Kunz, M. J., Kempter, T., Wüest, A., Wehrli, B., and Senn, D. B. (2011). Spatial Heterogeneity of Methane Ebullition in a Large Tropical Reservoir. *Environ. Sci. Technol.* 45, 9866–9873. doi:10.1021/es2005545

Delwiche, K. B., Knox, S. H., Malhotra, A., Fluet-Chouinard, E., McNicol1, G., Feron, S., et al. (2021). FLUXNET- CH4: A Global, Multi-Ecosystem Dataset and Analysis of Methane Seasonality from Freshwater Wetlands. *Earth Sys. Sci. Data Disc.* doi:10.5194/essd-2020-307

Departamento Nacional da Produção Mineral (1978). *Projeto RadamBrasil. Folha SA 20: Manaus*. Rio de Janeiro, Brazil: Departamento Nacional da Produção Mineral.

Devol, A. H., Richey, J. E., Clark, W. A., King, S. L., and Martinelli, L. A. (1988). Methane Emissions to the Troposphere from the Amazon Floodplain. *J. Geophys. Res.* 93, 1583–1592. doi:10.1029/jd093id02p01583

Devol, A., Richey, J., Forsberg, B., and Martinelli, L. (1994). "Environmental Methane in the Amazon River Floodplain," in *Global Wetlands: Old World and New*. Editor W. J. Mitsch (Elsevier), 151–165.

Devol, A., Richey, J., Forsberg, B., and Martinelli, L. (1990). Seasonal Dynamics in Methane Emissions from the Amazon River Floodplain to the Troposphere. *J. Geophys. Res.* 95, 417–426. doi:10.1029/jd095id10p16417

Draper, F. C., Roucoux, K. H., Lawson, I. T., Mitchard, E. T. A., Honorio Coronado, E. N., Lähteenoja, O., et al. (2014). The Distribution and Amount of Carbon in the Largest Peatland Complex in Amazonia. *Environ. Res. Lett.* 9. doi:10.1088/1748-9326/9/12/124017

Engle, D. L., Melack, J. M., Doyle, R. D., and Fisher, T. R. (2008). High Rates of Net Primary Production and Turnover of Floating Grasses on the Amazon Floodplain: Implications for Aquatic Respiration and Regional CO_2 Flux. *Glob. Change Biol.* 14, 369–381. doi:10.1111/j.1365-2486.2007.01481.x

Engle, D., and Melack, J. M. (2000). Methane Emissions from the Amazon Floodplain: Enhanced Release during Episodic Mixing of Lakes. *Biogeochemistry* 51, 71–90. doi:10.1023/a:1006389124823

Espinoza, J.-C., Marengo, J. A., Schongart, J., and Jimenez, J. C. (2021). The New Historical Flood of 2021 in the Amazon River Compared to Major Floods of the 21st Century: Atmospheric Features in the Context of the Intensification of Floods. *Weather Clim. Extrem.* 35, 100406. doi:10.1016/j.wace.2021.100406

Espinoza Villar, J. C., Guyot, J. L., Ronchail, J., Cochonneau, G., Filizola, N., Fraizy, P., et al. (2009). Contrasting Regional Discharge Evolutions in the Amazon Basin (1974-2004). *J. Hydrology* 375, 297–311. doi:10.1016/j.jhydrol.2009.03.004

Fassoni-Andrade, A. C., Fleischmann, A. S., Papa, F., Paiva, R. C. D., Wongchuig, S., Melack, J. M., et al. (2021). Amazon Hydrology from Space: Scientific Advances and Future Challenges. *Rev. Geophys.* 59, e2020RG000728. doi:10.1029/2020RG000728

Fassoni-Andrade, A. C., Paiva, R. C. D. d., Rudorff, C. d. M., Barbosa, C. C. F., and Novo, E. M. L. d. M. (2020). High-resolution Mapping of Floodplain Topography from Space: A Case Study in the Amazon. *Remote Sens. Environ.* 251, 112065. doi:10.1016/j.rse.2020.112065

Ferreira-Ferreira, J., Silva, T. S. F., Streher, A. S., Affonso, A. G., de Almeida Furtado, L. F., Forsberg, B. R., et al. (2015). Combining ALOS/PALSAR Derived Vegetation Structure and Inundation Patterns to Characterize Major Vegetation Types in the Mamirauá Sustainable Development Reserve, Central Amazon Floodplain, Brazil. *Wetl. Ecol. Manage* 23, 41–59. doi:10.1007/s11273-014-9359-1

Finn, D. R., Ziv-El, M., van Haren, J., Park, J. G., del Aguila-Pasquel, J., Urquiza–Muñoz, J. D., et al. (2020). Methanogens and Methanotrophs Show Nutrient-dependent Community Assemblage Patterns across Tropical Peatlands of the Pastaza-Marañón Basin, Peruvian Amazonia. *Front. Microbiol.* 11, 746. doi:10.3389/fmicb.2020.00746

Fleischmann, A. S., Paiva, R. C. D., Collischonn, W., Siqueira, V. A., Paris, A., Moreira, D. M., et al. (2020). Trade-Offs between 1-D and 2-D Regional River Hydrodynamic Models. *Water Resour. Res.* 56. doi:10.1029/2019WR026812

Fleischmann, A. S., Papa, F., Fassoni-Andrade, A., Melack, J. M., Wongchuig, S., Paiva, R. C. D., et al. (2021). How Much Inundation Occurs in the Amazon River Basin? *Remote Sens. Environ. Prepr.* doi:10.1002/essoar.10508718.1

Fluet-Chouinard, E., Lehner, B., Rebelo, L. M., Papa, F., and Hamilton, S. K. (2015). Development of a Global Inundation Map at High Spatial Resolution from Topographic Downscaling of Coarse-Scale Remote Sensing Data. *Remote Sens. Environ.* 158, 348–361. doi:10.1016/j.rse.2014.10.015

Forsberg, B. R., Dunne, T., Melack, J. M., Venticinque, E., Goulding, M., Barthem, R., et al. (2017). Potential Impact of New Andean Dams on the Amazon Fluvial Ecosystems. *PLOS One* 12 (8), e0182254.

Forsberg, B. R., Melack, J. M., Richey, J. E., and Pimentel, T. P. (2017). Planktonic Photosynthesis and Respiration in Amazon Floodplain Lakes. *Hydrobiologia* 800, 187–206.

Frankenberg, C., Aben, I., Bergamaschi, P., Dlugokencky, E. J., Van Hees, R., Houweling, S., et al. (2011). Global Column-Averaged Methane Mixing Ratios from 2003 to 2009 as Derived from SCIAMACHY: Trends and Variability. *J. Geophys. Res. Atmos.* 116, 1–12. doi:10.1029/2010JD014849

Frankenberg, C., Bergamaschi, P., Butz, A., Houweling, S., Meirink, J. F., Notholt, J., et al. (2008). Tropical Methane Emissions: A Revised View from SCIAMACHY Onboard ENVISAT. *Geophys. Res. Lett.* 35. doi:10.1029/2008GL034300

Frappart, F., Seyler, F., Martinez, J.-M., Leon, J. G., and Cazenave, A. (2005). Flooplain Water Storage in the Negro River Basin Estimated from Microwave Remote Sensing of Inundated Area and Water Levels. *Remote Sens. Environ.* 99, 387–399.

Fraser, A., Palmer, P. I., Feng, L., Bösch, H., Parker, R., Dlugokencky, E. J., et al. (2014). Estimating Regional Fluxes of CO_2 and CH_4 Using Space-Borne Observations of XCH4: XCO2. *Atmos. Chem. Phys.* 14, 12883–12895.

Gabriel, G. V. M., Oliveira, L. C., Barros, D. J., Bento, M. S., Neu, V., Toppa, R. H., et al. (2020). Methane Emission Suppression in Flooded Soil from Amazonia. *Chemosphere* 250, 126263. doi:10.1016/j.chemosphere.2020.126263

Gatti, L., Melack, J., Basso, L. S., Restrepo-Coupe, N., Pangala, S., Saleska, S. R., et al. (2021a). "Amazon Carbon Budget. Cross-Chapter," in *Amazon Assessment Report*. Editors C. Nobre, A. Encalada, E. Anderson, F. H. Roca Alcazar, and M. Bustamante (New York, USA: United Nations Sustainable Development Solutions Network). Available at: www.theamazonwewant.org/spa-reports.

Gatti, L. V., Basso, L. S., Miller, J. B., Gloor, M., Domingues, L. G., Cassol, H. L. G., et al. (2021b). Amazonia as a Carbon Source Linked to Deforestation and Climate Change. *Nature* 595, 388–393.

Gauci, V., Figueiredo, V., Gedney, N., Pangala, S. R., Stauffer, T., Weedon, G. P., et al. (2021). Non-flooded Riparian Amazon Trees Are a Regionally Significant Methane Source. *Phil. Trans. R. Soc. A*, 3802020044620200446. doi:10.1098/rsta.2020.0446

Gedney, N., Huntingford, C., Comyn-Platt, E., and Wiltshire, A. (2019). Significant Feedbacks of Wetland Methane Release on Climate Change and the Causes of Their Uncertainty. *Environ. Res. Lett.* 14, 084027. doi:10.1088/1748-9326/ab2726

Gloor, M., Brienen, R. J. W., Galbraith, D., Feldpausch, T. R., Schöngart, J., Guyot, J. L., et al. (2013). Intensification of the Amazon Hydrological Cycle over the Last Two Decades. *Geophys. Res. Lett.* 40, 1729–1733. doi:10.1002/grl.50377

Gloor, M., Gatti, L. V., Wilson, C., Parker, R. J., Boesch, H., Popa, E., et al. (2021). Large Methane Emissions from the Pantanal during Rising Water-Levels Revealed by Regularly Measured Lower Troposphere CH_4 Profiles. *Glob. Biogeochem. Cycles* 35, e2021GB006964. doi:10.1029/2021GB006964

Gontijo, J. B., Paula, F. S., Venturini, A. M., Yoshiura, C. A., Borges, C. D., Moura, J. M. S., et al. (2021). Not just a Methane Source: Amazonian Floodplain Sediments Harbour a High Diversity of Methanotrophs with Different Metabolic Capabilities. *Molec. Ecol.* 30, 2560–2572.

Griffis, T. J., Roman, T. D., Wood, J. D., Deventer, M. J., Fachin, L., Rengifo, J., et al. (2020). Hydrometeorological Sensitivities of Net Ecosystem Carbon Dioxide and Methane Exchange of an Amazonian Palm Swamp Peatland. *Agric. For. Meteorol.* 295. doi:10.1016/j.agrformet.2020.108167

Grossart, H.-P., Frindte, K., Dziallas, C., Eckert, W., and Tang, K. W. (2011). Microbial Methane Production in Oxygenated Water Column of an Oligotrophic Lake. *Proc. Nat. Acad. Sci.* 108, 19657–19661.

Guérin, F., and Abril, G. (2007). Significance of Pelagic Aerobic Methane Oxidation in the Methane and Carbon Budgets of a Tropical Reservoir. *J. Geophys. Res. Biogeosci.* 112. doi:10.1029/2006JG000393

Guérin, F., Abril, G., Richard, S., Burban, B., Reynouard, C., Seyler, P., et al. (2006). Methane and Carbon Dioxide Emissions from Tropical Reservoirs: Significance of Downstream Rivers. *Geophys. Res. Lett.* 33. doi:10.1029/2006GL027929

Gumbricht, T., Roman-Cuesta, R. M., Verchot, L., Herold, M., Wittmann, F., Householder, E., et al. (2017). An Expert System Model for Mapping Tropical Wetlands and Peatlands Reveals South America as the Largest Contributor. *Glob. Chang. Biol.* 23, 3581–3599. doi:10.1111/gcb.13689

Guo, M., Zhuang, Q., Tan, Z., Shurpali, N., Juutinen, S., Kortelainen, P., et al. (2020). Rising Methane Emissions from Boreal Lakes Due to Increasing Ice-free Days. *Environ. Res. Lett.* 15, 064008. doi:10.1088/1748-9326/ab8254

Guseva, S., Aurela, M., Cortés, A., Lotsar, E., MacIntyre, S., Mammarella, I., et al. (2021). Physical Drivers of Near-Surface Turbulence in a Regulated River. *Water Resour. Res.* 57, e2020WR027939.

Guyot, J. L., Jouanneau, J. M., Soares, L., Boaventura, G. R., Maillet, N., and Lugane, C. (2007). Clay Mineral Composition of River Sediments in the Amazon Basin. *Catena* 71, 340–356.

Hamilton, S. K., Melack, J. M., Goodchild, M. F., and Lewis, W. M., Jr. (1992). "Estimation of the Fractual Dimension of Terrain from Lake Size Distributions," in *Lowland Floodplain Rivers: Geomorphological Perspectives*. Editors P. A. Carling and G. E. Petts (New York: John Wiley & Sons), 145–163.

Hamilton, S. K., Sippel, S. K., and Melack, J. M. (2002). Comparison of Inundation Patterns Among Major South American Floodplains. *J. Geophys. Res.* 107–D20. doi:10.29/2000JD000306

Hamilton, S., Sippel, S., and Melack, J. M. (1995). Oxygen Depletion and Carbon Dioxide Production in Waters of the Pantanal Wetland of Brazil. *Biogeochemistry* 30, 115–141.

Hastie, A., Lauerwald, R., Ciais, P., and Regnier, P. (2019). Aquatic Carbon Fluxes Dampen the Overall Variation of Net Ecosystem Productivity in the Amazon

Basin: An Analysis of the Interannual Variability in the Boundless Carbon Cycle. *Glob. Chang. Biol.* 25, 2094–2111. doi:10.1111/gcb.14620

Hawes, J. E., Peres, C. A., Riley, L. B., and Hess, L. L. (2012). Landscape-scale Variation in Structure and Biomass of Amazonian Seasonally Flooded and Unflooded Forests. *For. Ecol. Manage.* 281, 163–176.

Hedges, J. I., Clark, W. A., Quay, P. D., Richey, J. E., Devol, A., and Santos, U. (1986). Composition and Fluxes of Particulate Organic Material in the Amazon River. *Limnol. Oceanogr.* 31, 717–738.

Hess, L. L., Melack, J. M., Affonso, A. G., Barbosa, C., Gastil, M., and Novo, E. M. L. M. (2015). Amazonian Wetlands: Extent, Vegetative Cover, and Dual Season Inundation Area. *Wetlands* 35, 745–756.

Hess, L. L., Melack, J. M., Novo, E. M. L. M., Barbosa, C. C. F., and Gastil, M. (2003). Dual-season Mapping of Wetland Inundation and Vegetation for the Central Amazon Basin. *Remote Sens. Environ.* 87, 404–428.

Hess, L. L., Novo, E. M. L. M., Slaymaker, D. M., Holt, J., Steffen, C., Valeriano, D. M., et al. (2002). Geocoded Digital Videography for Validation of Land Cover Mapping in the Amazon Basin. *Int. J. Remote Sens.* 7, 1527–1556.

Hodges, B. R., and Dallimore, C. (2019). *Aquatic Ecosystem Model: AEM3D, User Manual.* Australia: Hydronumerics. Docklands.

Isidorova, A., Grasset, C., Mendonça, R., and Sobek, S. (2019). Methane Formation in Tropical Reservoirs Predicted from Sediment Age and Nitrogen. *Sci. Rep.* 9, 11017. doi:10.1038/s41598-019-47346-7

Jati, S. R. (2014). *Emissão de CO_2 e CH_4 nas savanas úmidas de Roraima*. Manaus, Brazil: M.Sc. thesis. Instituto Nacional de Pesquisas da Amazonia.

Jensen, K., McDonald, K., Podest, E., Rodriguez-Alvarez, N., Horna, V., and Steiner, N. (2018). Assessing L-Band GNSS-Reflectometry and Imaging Radar for Detecting Sub-canopy Inundation Dynamics in a Tropical Wetlands Complex. *Remote Sens.* 10, 1431. doi:10.3390/rs10091431

Ji, X., Lesack, L. F. W., Melack, J. M., Wang, S., Riley, W. J., and Shen, C. (2019). Seasonal Patterns and Controls of Hydrological Fluxes in an Amazon Floodplain Lake with a Surface-Subsurface Processes Model. *Water Resour. Res.* 55, 3056–3075. doi:10.1029/2018WR023897

Ji, Y., Angel, R., Klose, M., Claus, P., Marotta, H., Pinho, L., et al. (2016). Structure and Function of Methanogenic Microbial Communities in Sediments of Amazonian Lakes with Different Water Types. *Environ. Microbiol.* 18, 5082–5100. doi:10.1111/1462-2920.13491

W. J. Junk (Editor) (1997). "*Central Amazon Floodplain: Ecology of a Pulsing System*, (Berlin, Germany: Spinger), 126

Junk, W. J., and Piedade, M. T. F. (1997). "Plant Life in the Floodplain with Special Reference to Herbaceous Plants," in *Central Amazon Floodplain: Ecology of a Pulsing System*. Editor W. J. Junk (Berlin, Germany: Spinger: Ecological Studies), 126, 147–185.

Junk, W. J., Piedade, M. T. F., Schöngart, J., Cohn-Haft, M., Adeney, J. M., and Wittmann, F. (2011). A Classification of Major Naturally-Occurring Amazonian Lowland Wetlands. *Wetlands* 31, 623–640.

Junk, W. J., Piedade, M., Wittmann, F., Schöngart, J., and Parolin, P. (Editors) (2010). *Amazonian Floodplain Forests: Ecophysiology, Ecology, Biodiversity and Sustainable Management* (Berlin, Germany: Springer). Ecological Studies 210.

Kasischke, E. S., Melack, J. M., and Dodson, M. C. (1997). The Use of Imaging Radar for Ecological Applications-A Review. *Remote Sens. Environ.* 59, 141–156.

Keller, M., Varner, R., Dias, J. D., Silva, H., Crill, P., Oliveira, R. C., et al. (2005). Soil–atmosphere Exchange of Nitrous Oxide, Nitric Oxide, Methane, and Carbon Dioxide in Logged and Undisturbed Forest in the Tapajos National Forest, Brazil. *Earth Interact.* 9 (23), 1–28.

Kemenes, A., Forsberg, B. R., and Melack, J. M. (2011). CO_2 Emissions from a Tropical Hydroelectric Reservoir (Balbina, Brazil). *J. Geophys. Res. Biogeosci.* 116, G03004. doi:10.1029/2010JG001465

Kemenes, A., Forsberg, B. R., and Melack, J. M. (2016). Downstream Emissions of CH_4 and CO_2 from Amazon Hydroelectric Reservoirs (Tucuruí, Samuel and Curuá-Una). *Inland Waters* 6, 295–302.

Kemenes, A., Forsberg, B. R., and Melack, J. M. (2007). Methane Release below a Hydroelectric Dam. *Geophys. Res. Lett.* 34, L12809.

Knox, S. H., Bansal, S., McNicol, G., Schafer, K., Sturtevant, C., Ueyama, M., et al. (2021). Identifying Dominant Environmental Predictors of Freshwater Wetland Methane Fluxes across Diurnal to Seasonal Time Scales. *Glob. Change Biol.* 27, 3582–3604. doi:10.1111/gcb.15661

Koschorreck, M. (2000). Methane Turnover in Exposed Sediments of an Amazon Floodplain Lake. *Biogeochemistry* 50, 195–206.

Kosten, S., van den Berg, S., Mendonça, R., Paranaíba, J. R., Roland, F., Sobek, S., et al. (2018). Extreme Drought Boosts CO_2 and CH_4 Emissions from Reservoir Drawdown Areas. *Inland waters*. 8, 329–340. doi:10.1080/20442041.2018.1483126

Lähteenoja, O., Reátegui, Y. R., Räsänen, M., Torres, D. D. C., Oinonen, M., and Page, S. (2012). The Large Amazonian Peatland Carbon Sink in the Subsiding Pastaza-Marañón Foreland Basin, Peru. *Glob. Change Biol.* 18, 164–178. doi:10.1111/j.1365-2486.2011.02504.x

Lähteenoja, O., Ruokolainen, K., Schulman, L., and Alvarez, J. (2009). Amazonian Floodplains Harbour Minerotrophic and Ombrotrophic Peatlands. *Catena* 79, 140–145.

Lauerwald, R., Regnier, P., Camino-Serrano, M., Guenet, B., Guimberteau, M., Ducharne, A., et al. (2017). ORCHILEAK (Revision 3875): a New Model Branch to Simulate Carbon Transfers along the Terrestrial-Aaquatic Continuum of the Amazon Basin. *Geosci. Model. Dev.* 10, 3821–3859. doi:10.5194/gmd-10-3In821-2017

Lehner, B., and Döll, P. (2004). Development and Validation of a Global Database of Lakes, Reservoirs and Wetlands. *J. Hydrol.* 296, 1–22.

Leitão, R. P., Zuanon, J., Mouillot, D., Leal, C. G., Hughes, R. M., Kaufmann, P. R., et al. (2018). Disentangling the Pathways of Land Use Impacts on the Functional Structure of Fish Assemblages in Amazon Streams. *Ecography* 41, 219–232.

Lesack, L. F. W., and Melack, J. M. (1995). Flooding Hydrology and Mixture Dynamics of Lake Water Derived from Multiple Sources in an Amazon Floodplain Lake. *Water Resour. Res.* 31, 329–345.

Linkhorst, A., Hiller, C., DelSontro, T., Azevedo, G., Barros, N., Mendonça, R. F., et al. (2020). Comparing Methane Ebullition Variability across Space and Time in a Brazilian Reservoir. *Limnol. Oceanogr.* 65, 1623–1634. doi:10.1002/lno.11410

Liu, L., Zhuang, Q., Oh, Y., Shurpali, N. J., Kim, S., and Poulter, B. (2020). Uncertainty Quantification of Global Net Methane Emissions from Terrestrial Ecosystems Using a Mechanistically Based Biogeochemistry Model. *J. Geophys. Res. Biogeosci* 125, e2019JG005428. doi:10.1029/2019JG005428

Lu, X., Zhuang, Q., Liu, Y., Zhou, Y., and Aghakouchak, A. (2016). A Large-Scale Methane Model by Incorporating the Surface Water Transport. *J. Geophys. Res. Biogeosci.* 121. doi:10.1002/2016JG003321

Lunt, M. F., Palmer, P. I., Lorente, A., Borsdorff, T., Landgraf, J., Parker, R. J., et al. (2021). Rain-fed Pulses of Methane from East Africa during 2018–2019 Contributed to Atmospheric Growth Rate. *Environ. Res. Lett.* 16, 024021.

Ma, S., Worden, J. R., Bloom, A. A., Zhang, Y., Poulter, B., Cusworth, D. H., et al. (2021). Satellite Constraints on the Latitudinal Distribution and Temperature Sensitivity of Wetland Methane Emissions. *AGU Adv.* 2, e2021AV000408. doi:10.1029/2021AV000408

Macedo, M. N., Coe, M. T., DeFries, R., Uriarte, M., Brando, P. M., Neill, C., et al. (2013). Land-use-driven Stream Warming in Southeastern Amazonia. *Philos. Trans. R. Soc. Lond B Biol. Sci.* 368, 20120153. doi:10.1098/rstb.2012.0153

MacIntyre, S., Amaral, J. H. F., Barbosa, P. M., Cortés, A., Forsberg, B. R., and Melack, J. M. (2019). Turbulence and Gas Transfer Velocities in Sheltered Flooded Forests of the Amazon Basin. *Geophys. Res. Lett*. doi:10.1029/2019GL083948

MacIntyre, S., Amaral, J. H., and Melack, J. M. (2021). Turbulence in the Upper Mixed Layer under Light Winds: Implications for Fluxes of Climate-Warming Trace Gases. *J. Geophys. Res. Oceans* 126, e2020JC017026. doi:10.1029/2020JC017026

MacIntyre, S., and Melack, J. M. (1995). Vertical and Horizontal Transport in Lakes: Linking Littoral, Benthic, and Pelagic Habitats. *J. N. Amer. Benth. Soc.* 14, 599–615.

Malhi, Y., Melack, J., Gatti, L. V., Ometto, J., Kesselmeier, J., Wolff, S., et al. (2021). "Chapter 6 – Biogeochemical Cycles: Carbon and Other Elements," in *Amazon Assessment Report*. Editors C. Nobre, A. Encalada, E. Anderson, F. H. Roca Alcazar, and M. Bustamante (New York, USA: United Nations Sustainable Development Solutions Network). Available at: www.theamazonwewant.org/spa-reports.

Marani, L., and Alvala, P. C. (2007). Methane Emissions from Lakes and Floodplains in Pantanal, Brazil. *Atmos. Environ.* 41, 1627–1633.

Marengo, J. A., and Espinoza, J. C. (2016). Extreme Seasonal Droughts and Floods in Amazonia: Causes, Trends and Impacts. *Intern. J. Clim.* 36, 1033–1050.

Martinelli, L. A., Victoria, R. L., de Camargo, P. B., Piccolo, M. C., Mertes, L., Richey, J. E., et al. (2003). Inland Variability of Carbon–Nitrogen Concentrations and $\delta^{13}C$ in Amazon Floodplain (Várzea) Vegetation and Sediment. *Hydrol. Process.* 17, 1419–1430.

Martinson, G. O., Werner, F. A., Scherber, C., Conrad, R., Corre, M. D., Flessa, H., et al. (2010). Methane Emissions from Tank Bromeliads in Neotropical Forests. *Nat. Geosci.* 3, 766–769.

Mayorga, E., Aufdenkampe, A. K., Masiello, C. A., Krusche, A. V., Hedges, J. I., Quay, P. D., et al. (2005). Young Organic Matter as a Source of Carbon Dioxide Outgassing from Amazonian Rivers. *Nature* 436, 538–541. doi:10.1038/nature03880

Mayorga, E., and Aufdenkampe, A. (2002). *Processing of Bioactive Elements in the Amazon River System. Ecohydrology of South American Rivers and Wetlands*. IAHS Special Publication 6, 1–23.

McNorton, J., Gloor, E., Wilson, C., Hayman, G. D., Gedney, N., Comyn-Platt, E., et al. (2016). Role of Regional Wetland Emissions in Atmospheric Methane Variability. *Geophys. Res. Lett.* 43, 11433–11444. doi:10.1002/2016GL070649

Meade, R. H., Rayol, J. M., Conceição, S. C. Da., and Natividade, J. R. G. (1991). Backwater Effects in the Amazon River Basin. *Environ. Geol. Water Sci.* 18, 105–114. doi:10.1007/BF01704664

Melack, J. M., Amaral, J. H. F., Kasper, D., Barbosa, P. M., and Forsberg, B. R. (2021). Limnological Perspectives on Conservation of Aquatic Ecosystems in the Amazon Basin. *Aquat. Cons. Mar. Freshw. Ecosys.* 31, 1041–1055.

Melack, J. M. (2016). "Aquatic Ecosystems," in *Interactions between Biosphere, Atmosphere and Human Land Use in the Amazon Basin*. Editors L. Nagy, B. R. Forsberg, and P. Artaxo (Berlin, Germany: Springer), 227, 117–145.)*Ecol. Stud.*

Melack, J. M., and Coe, M. T. (2021). Amazon Floodplain Hydrology and Implications for Aquatic Conservation. *Aquat. Cons. Mar. Freshw. Ecosys.* 31, 1029–1040.

Melack, J. M., and Engle, D. (2009). An Organic Carbon Budget for an Amazon Floodplain Lake. *Verh. Intern. Ver. Limnol.* 30, 1179–1182.

Melack, J. M., and Forsberg, B. (2001). "Biogeochemistry of Amazon Floodplain Lakes and Associated Wetlands," in *Biogeochemistry of the Amazon Basin*. Editors M. E. McClain, R. L. Victoria, and J. E. Richey (Oxford, U.K.: Oxford University Press), 235–276.

Melack, J. M., Hess, L. L., Gastil, M., Forsberg, B. R., Hamilton, S. K., Lima, I. B. T., et al. (2004). Regionalization of Methane Emissions in the Amazon Basin with Microwave Remote Sensing. *Glob. Change Biol.* 10, 530–544.

Melack, J. M., and Hess, L. L. (2010). "Remote Sensing of the Distribution and Extent of Wetlands in the Amazon Basin," in *Amazonian Floodplain Forests: Ecophysiology, Ecology, Biodiversity and Sustainable ManagementEcological Studies*. Editors W. J. Junk, M. Piedade, F. Wittmann, J. Schöngart, and P. Parolin (Berlin, Germany: Springer), 210, 43–59.)

Melack, J. M., Novo, E. M. L. M., Forsberg, B. R., Piedade, M. T. F., and Maurice, L. (2009). "Floodplain Ecosystem Processes,". Editors J. Gash, M. Keller, and P. Silva-Dias (Washington, D.C: American Geophysical Union. Geophys. Monogr. Series), 186, 525–541.*Amaz. Glob. Change*

Melack, J. M. (2004). "Remote Sensing of Tropical Wetlands," in *Manual of Remote Sensing*. Editor S. Ustin. 3rd ed. (New York, USA: John Wiley & Sons), 4, 319–343.

Melo, M. L., Bertilsson, S., Amaral, J. H. F., Barbosa, P. M., Forsberg, B. R., and Sarmento, H. (2019). Flood Pulse Regulation of Bacterioplankton Community Composition in an Amazonian Floodplain Lake. *Freshw. Biol.* 64, 108–120.

Melton, J. R., Wania, R., Hodson, E. L., Poulter, B., Ringeval, B., Spahni, R., et al. (2013). Present State of Global Wetland Extent and Wetland Methane Modelling: Conclusions from a Model Inter-comparison Project (WETCHIMP). *Biogeosciences* 10, 753–788.

Meng, L., Hess, P. G. M., Mahowald, N. M., Yavitt, J. B., Riley, W. J., Subin, Z. M., et al. (2012). Sensitivity of Wetland Methane Emissions to Model Assumptions: Application and Model Testing against Site Observations. *Biogeosciences* 9, 2793–2819. doi:10.5194/bg-9-2793-2012

Messager, M. L., Lehner, B., Grill, G., Nedeva, I., and Schmitt, O. (2016). Estimating the Volume and Age of Water Stored in Global Lakes Using a Geo-Statistical Approach. *Nat. Commun.* 7, 13603–13611. doi:10.1038/ncomms13603

Miguez-Macho, G., and Fan, Y. (2012). The Role of Groundwater in the Amazon Water Cycle: 1. Influence on Seasonal Streamflow, Flooding and Wetlands. *J. Geophys. Res.* 117 (D15). doi:10.1029/2012JD017539

Miller, J. B., Gatti, L. V., d'Amelio, M. T. S., Crotwell, A. M., Dlugokencky, E. J., Bakwin, P., et al. (2007). Airborne Measurements Indicate Large Methane Emissions from the Eastern Amazon Basin. *Geophys. Res. Lett.* 34. doi:10.1029/2006GL029213

Moreira-Turcq, P., Bonnet, M. P., Amorim, M., Bernardes, M., Lagane, C., Maurice, L., et al. (2013). Seasonal Variability in Concentration, Composition, Age, and Fluxes of Particulate Organic Carbon Exchanged between the Floodplain and Amazon River. *Glob. Biogeochem. Cycles* 27, 119–130.

Nardi, F., Annis, A., Di Baldassarre, G., Vivoni, E. R., and Grimaldi, S. (2019). GFPLAIN250m, a Global High-Resolution Dataset of Earth's Floodplains. *Sci. Data* 6, 180309. doi:10.1038/sdata.2018.309

Neu, V., Neill, C., and Krusche, A. V. (2011). Gaseous and Fluvial Carbon Export from an Amazon Forest Watershed. *Biogeochemistry* 105, 133–147.

Nisbet, E. G., Dlugokencky, E. J., Manning, M. R., Lowry, D., Fisher, R. E., France, J. L., et al. (2016). Rising Atmospheric Methane: 2007–2014 Growth and Isotopic Shift. *Glob. Biogeochem. Cycles* 30, 1356–1370. doi:10.1002/2016GB005406

Nobre, A. D., Cuartas, L. A., Hodnett, M., Renn, C. D., Rodrigues, G., Silveira, A., et al. (2011). Height above the Nearest Drainage—A Hydrologically Relevant New Terrain Model. *J. Hydrol.* 404, 13–29. doi:10.1016/j.jhydrol.2011.03.051

O'Loughlin, F. E., Paiva, R. C. D., Durand, M., Alsdorf, D. E., and Bates, P. D. (2016). A Multi-Sensor Approach towards a Global Vegetation Corrected SRTM DEM Product. *Remote Sens. Environ.* 182, 49–59.

Oliveira Junior, E. S., van Bergen, T. J. H. M., Nauta, J., Budiša, A., Aben, R. C. H., Weideveld, S. T. J., et al. (2020). Water Hyacinth's Effect on Greenhouse Gas Fluxes: A Field Study in a Wide Variety of Tropical Water Bodies. *Ecosystems*. doi:10.1007/s10021-020-00564-x

Paiva, R. C. D., Buarque, D. C., Collischonn, W., Bonnet, M. P., Frappart, F., Calmant, S., et al. (2013). Large-scale Hydrologic and Hydrodynamic Modeling of the Amazon River Basin. *Water Resour. Res.* 49, 1226–1243. doi:10.1002/wrcr.20067

Pandey, S., Houweling, S., Krol, M., Aben, I., Monteil, G., Nechita-Banda, N., et al. (2017). Enhanced Methane Emissions from Tropical Wetlands during the 2011 La Niña. *Sci. Rep.* 7, 45759. doi:10.1038/srep45759

Pangala, S. R., Enrich-Prast, A., Basso, L. S., Peixoto, R. B., Bastviken, D., Hornibrook, E. R. C., et al. (2017). Large Emissions from Floodplain Trees Close the Amazon Methane Budget. *Nature* 552, 230–234. doi:10.1038/nature24639

Paranaíba, J. R., Aben, R., Barros, N., Quadra, G., Annika Linkhorst, A., Amado, A. M., et al. (2022). Cross-continental Importance of CH_4 Emissions from Dry Inland-Waters. *Sci.Total Environ.* 814, 151925.

Paranaíba, J. R., Barros, N., Almeida, R. M., Linkhorst, A., Mendonça, R., do Vale, R., et al. (2021). Hotspots of Diffusive CO_2 and CH_4 Emission from Tropical Reservoirs Shift through Time. *J. Geophys. Res. Biogeosci.* 126, e2020JG006014. doi:10.1029/2020JG006014

Parker, R. J., Boesch, H., McNorton, J., Comyn-Platt, E., Gloor, M., Wilson, C., et al. (2018). Evaluating Year-To-Year Anomalies in Tropical Wetland Methane Emissions Using Satellite CH_4 Observations. *Remote Sens. Environ.* 211, 261–275. doi:10.1016/j.rse.2018.02.011

Parker, R. J., Wilson, C., Bloom, A. A., Comyn-Platt, E., Hayman, G., McNorton, J., et al. (2020). Exploring Constraints on a Wetland Methane Emission Ensemble (WetCHARTs) Using GOSAT Satellite Observations. *Biogeosciences* 17, 5669–5691.

Parrens, M., Bitar, A. A., Frappart, F., Paiva, R., Wongchuig, S., Papa, F., et al. (2019). High Resolution Mapping of Inundation Area in the Amazon Basin from a Combination of L-Band Passive Microwave, Optical and Radar Datasets. *Int. J. Appl. Earth Obs. Geoinf.* 81, 58–71. doi:10.1016/j.jag.2019.04.011

Pinel, S., Bonnet, M., da Silva, J., Sampaio, T. C., Garnier, J., Catry, T., et al. (2019). Flooding Dynamics within an Amazonian Floodplain: Water Circulation Patterns and Inundation Duration. *Water Resour. Res. 2019WR026081*. doi:10.1029/2019WR026081

Pinel, S., Bonnet, M. P., Santos da Silva, J., Daniel Moreira, D., Calmant, S., Satgé, F., et al. (2015). Correction of Interferometric and Vegetation Biases in the SRTMGL1 Spaceborne DEM with Hydrological Conditioning towards Improved Hydrodynamics Modeling in the Amazon Basin. *Remote Sens.* 7, 16108–16130. doi:10.3390/rs71215822

Podgrajsek, E., Sahlée, E., Bastviken, D., Natchimuthu, S., Kljun, N., Chmiel, H. E., et al. (2016). Methane Fluxes from a Small Boreal Lake Measured with the Eddy Covariance Method. *Limnol. Oceanogr.* 61, S41–S50. doi:10.1002/ln0.10245

Polsenaere, P. D. J., Detandt, G., Vidal, L. O., Pérez, M. A. P., Marieu, V., and Abril, G. (2013). Thermal Enhancement of Gas Transfer Velocity of CO_2 in an Amazon Floodplain Lake Revealed by Eddy Covariance Measurements. *Geophys. Res. Lett.* 40, 1–7.

Potter, C. S. (1997). An Ecosystem Simulation Model for Methane Production and Emission from Wetlands. *Glob. Biogeochem. Cycles* 11, 495–506.

Potter, C. S., Melack, J. M., and Engle, D. (2014). Modeling Carbon Dynamics and Methane Emissions from Amazon Floodplain Ecosystems. *Wetlands* 34, 501–511.

Prigent, C., Jimenez, C., and Bousquet, P. (2020). Satellite-derived Global Surface Water Extent and Dynamics over the Last 25 Years (GIEMS-2). *J. Geophys. Res. Atmos.* 125, 1–18. doi:10.1029/2019JD030711

Quadra, G. R., Sobek, S., Paranaíba, J. R., Isidorova, A., Roland, F., do Vale, R., et al. (2020). High Organic Carbon Burial but High Potential for Methane Ebullition in the Sediments of an Amazonian Hydroelectric Reservoir. *Biogeosciences* 17, 1495–1505.

Querino, C. A. S., Smeets, C. J. P. P., Vigano, I., Holzinger, R., Moura, V., Gatti, L. V., et al. (2011). Methane Flux, Vertical Gradient and Mixing Ratio Measurements in a Tropical Forest. *Atmos. Chem. Phys.* 11, 7943–7953.

Rasera, M. F. F. L., Ballester, M. V. R., Krusche, A. V., Salimon, C., Montebelo, L. A., Alin, S. R., et al. (2008). Estimating the Surface Area of Small Rivers in the Southwestern Amazon and Their Role in CO_2 Outgassing. *Earth Interact.* 12, 1–16. doi:10.1175/2008EI257.1

Raymond, P. A., Zappa, C. J., Butman, D., Bott, T. L., Potter, J., Mulholland, P., et al. (2012). Scaling the Gas Transfer Velocity and Hydraulic Geometry in Streams and Small Rivers. *Limnol. Oceanogr Fluids Environ.* 2, 41–53. doi:10.1215/21573689-1597669

Renó, V. F,, Novo, E. M. L. M., Suemitsu, C., Rennó, C. D., and Silva, T. S. F. (2011). Assessment of Deforestation in the Lower Amazon Floodplain Using Historical Landsat MSS/TM Imagery. *Remote Sens. Environ.* 11, 3446–3456.

Ribeiro, I. O., de Souza, R. A. F., Andreoli, R. V., Kayano, M. T., and dos Santos Costa, P. (2016). Spatiotemporal Variability of Methane over the Amazon from Satellite Observations. *Adv. Atmos. Sci.* 33, 852–864.

Richey, J., Devol, A., Wofsy, S. C., Victoria, R., and Ribeiro, M. N. G. (1988). Biogenic Gases and the Oxidation and Reduction of Carbon in Amazon River and Floodplain Waters. *Limnol. Oceanogr.* 33, 551–561.

Richey, J. E., Melack, J. M., Aufdenkampe, A. K., Ballester, V. M., and Hess, L. L. (2002). Outgassing from Amazonian Rivers and Wetlands as a Large Tropical Source of Atmospheric CO_2. *Nature* 416, 617–620. doi:10.1038/416617a

Riley, W. J., Subin, Z. M., Lawrence, D. M., Swenson, S. C., Torn, M. S., Meng, L., et al. (2011). Barriers to Predicting Changes in Global Terrestrial Methane Fluxes: Analyses Using CLM4Me, a Methane Biogeochemistry Model Integrated in. *CESM. Biogeosci. Disc.* 8, 1733–1807.

Ringeval, B., Houweling, S., van Bodegom, P. M., Spahni, R., van Beek, R., Joos, F., et al. (2014). Methane Emissions from Floodplains in the Amazon Basin: Challenges in Developing a Process-Based Model for Global Applications. *Biogeosciences* 11, 1519–1558. doi:10.5194/bg-11-1519-2014

Roland, F., Darchambeau, F., Morana, C., Crowe, S. A., Thamdrup, B., and Borges, A. V. (2016). Anaerobic Methane Oxidation in an East African Great Lake (Lake Kivu). *Biogeosci. Disc.*, 1–27. doi:10.5194/bg-2016-300

Rosenqvist, A., Forsberg, B. R., Pimentel, T., Rauste, Y. A., and Richey, J. E. (2002). The Use of Spaceborne Radar Data to Model Inundation Patterns and Trace Gas Emissions in the Central Amazon Floodplain. *Int. J. Remote Sens.* 23, 1303–1328.

Rosenqvist, J., Rosenqvist, A., Jensen, K., and McDonald, K. (2020). Mapping of Maximum and Minimum Inundation Extents in the Amazon Basin 2014–2017 with ALOS-2 PALSAR-2 ScanSAR Time-Series Data. *Remote Sens.* 12, 1326. doi:10.3390/rs12081326

Rosentreter, J. A., Borges, A. V., Deemer, B. R., Holgerson, M. A., Liu, S., Song, C., et al. (2021). Half of Global Methane Emissions Come from Highly Variable Aquatic Ecosystem Sources. *Nat. Geosci.* 14, 225–230. doi:10.1038/S41561-021-00715-2

Rossetti, D. F., Gribel, R., Rennó, C. D., Cohen, M. C. L., Moulatlet, G. M., Cordeiro, C. L. de. O., et al. (2017). Late Holocene Tectonic Influence on Hydrology and Vegetation Patterns in a Northern Amazonian Megafan. *Catena* 158, 121–130. doi:10.1016/j.catena.2017.06.022

Rudorff, C. M., Melack, J. M., and Bates, P. M. (2014a). Flooding Dynamics on the Lower Amazon Floodplain: 1. Hydraulic Controls on Water Elevation, Inundation Extent and River-Floodplain Discharge. *Water Resour. Res.* 50, 619–634.

Rudorff, C. M., Melack, J. M., and Bates, P. M. (2014b). Flooding Dynamics on the Lower Amazon Floodplain: 2. Seasonal and Interannual Hydrological Variability. *Water Resour. Res.* 50, 635–649.

Sahagian, D., and Melack, J. M. (Editors) (1998). *Global Wetland Distribution and Functional Characterization: Trace Gases and the Hydrologic Cycle*. Stockholm, Sweden: IGBP Report, 46.

Saunois, M., Stavert, A. R., Poulter, B., Bousquet, P., Canadell, J. G., Jackson, R. B., et al. (2020). The Global Methane Budget: 2000-2017. *Earth Syst. Sci. Data* 12, 1561–1623. doi:10.5194/essd-12-1561-2020

Sawakuchi, H. O., Bastviken, D., Sawakuchi, A. O., Krusche, A. V., Ballester, M. V., and Richey, J. E. (2014). Methane Emissions from Amazonian Rivers and Their Contribution to the Global Methane Budget. *Glob. Chang. Biol.* 20, 2829–2840. doi:10.1111/gcb.12646

Sawakuchi, H. O., Bastviken, D., Sawakuchi, A. O., Ward, N. D., Borges, C. D., Tsai, S. M., et al. (2016). Oxidative Mitigation of Aquatic Methane Emissions in Large Amazonian Rivers. *Glob. Chang. Biol.* 22, 1075–1085. doi:10.1111/gcb.13169

Schlesinger, W. H., and Bernhardt, E. S. (2013). *Biogeochemistry*. Amsterdam: Elsevier.

Schubert, C. J., Diem, T., and Eugster, W. (2012). Methane Emissions from a Small Wind Shielded Lake Determined by Eddy Covariance, Flux Chambers, Anchored Funnels, and Boundary Model Calculations: A Comparison. *Environ. Sci. Techn.* 46, 4515–4522.

Sebacher, D. I., and Harriss, R. C. (1982). A System for Measuring Methane Fluxes from Inland and Coastal Wetland Environments. *J. Environ. Qual.* 11, 34–37.

Segers, A., and Houweling, S. (2020). Description of the CH_4 Inversion Production Chain. *Tech. Rep. Copernic. Atmos. Monit. Serv*. CAMS73_2018SC1_D73.5.2.2-2019_202001_production_chain_v1.

Segers, R. (1998). Methane Production and Methane Consumption: A Review of Processes Underlying Wetland Methane Fluxes. *Biogeochemistry* 41, 23–51. doi:10.1023/A:1005929032764

Sihi, D., Xu, X., Ortiz, M. S., O'Connell, C. S., Silver, W. L., López-Lloreda, C., et al. (2021). Representing Methane Emissions from Wet Tropical Forest Soils Using Microbial Functional Groups Constrained by Soil Diffusivity. *Biogeosciences* 18, 1769–1786. doi:10.5194/bg-18-1769-2021

Silva, T. S., Melack, J. M., and Novo, E. M. (2013). Responses of Aquatic Macrophyte Cover and Productivity to Flooding Variability on the Amazon Floodplain. *Glob. Chang. Biol.* 19, 3379–3389. doi:10.1111/gcb.12308

Silva, T. S. F., Costa, M. P. F., and Melack, J. M. (2010). Spatio-temporal Variability of Macrophyte Cover and Productivity in the Eastern Amazon Floodplain: a Remote Sensing Approach. *Remote. Sens. Environ.* 114, 1998–2010.

Silva, T. S. F., Melack, J., Streher, A. S., Ferreira-Ferreira, J., and Furtado, L. F. A. (2015). "Capturing the Dynamics of Amazonian Wetlands Using Synthetic Aperture Radar: Lessons Learned and Future Directions," in *Advances in Wetland Classification and Mapping*. Editors R. W. Tiner, V. Klemas, and M. W. Lang (Oxford, U.K: Taylor and Francis Publ.), 455–472.

Sippel, S. J., Hamilton, S. K., Melack, J. M., and Novo, E. M. M. (1998). Passive Microwave Observations of Inundation Area and the Area/stage Relation in the Amazon River Floodplain. *Int. J. Remote Sens.* 19, 3055–3074.

Sippel, S. J., Hamilton, S. K., and Melack, J. M. (1992). Inundation Area and Morphometry of Lakes on the Amazon River Floodplain, Brazil. *Arch. Hydrobiol.* 123, 385–400.

Sitch, S., Smith, B., Prentice, I. C., Arneth, A., Bondeau, A., Cramer, W., et al. (2003). Evaluation of Ecosystem Dynamics, Plant Geography and Terrestrial Carbon Cycling in the LPJ Dynamic Global Vegetation Model. *Glob. Change Biol.* 9, 161–185. doi:10.1046/j.1365-2486.2003.00569

Slater, J. A., Garvey, G., Johnston, C., Haase, J., Heady, B., Kroenung, G., et al. (2006). The SRTM Data 'finishing' Process and Products. *Photogramm. Eng. Remote Sens.* 72, 237–247. doi:10.14358/PERS.72.3.237

Smith, L. K., Melack, J. M., and Hammond, D. E. (2003). Carbon, Nitrogen and Phosphorus Content and ^{210}Pb-Derived Burial Rates in Sediments of an Amazon Floodplain Lake. *Amazoniana* 17, 413–436.

Smith, L., Lewis, W., and Chanton, J. P. (2000). Methane Emissions from the Orinoco River Floodplain, Venezuela. *Biogeochemistry* 51, 113–140.

Sobrinho, R. L., Bernardes, M. C., Abril, G., Kim, J.-H., Zell, C. I., Mortillaro, J.-M., et al. (2016). Spatial and Seasonal Contrasts of Sedimentary Organic Matter in Floodplain Lakes of the Central Amazon Basin. *Biogeosciences* 13, 467–482. doi:10.5194/bg-13-467-2016

Souza do Vale, R., Silva de Santana, R. A., Silva, J. T., Miller, S. D., Ferreira de Souza, R. A., Picanço, G. A. S., et al. (2016). Eddy Covariance Measurements of Latent Heat, Sensible Heat, Momentum and CO_2 Fluxes on the Reservoir of the Hydroelectric Plant Curuá-Una, PA. *Ciência Nat.* 38, 15–20.

Stanley, E. H., Casson, N. J., Christel, S. T., Crawford, J. T., Loken, L. C., and Oliver, S. K. (2016). The Ecology of Methane in Streams and Rivers: Patterns, Controls, and Global Significance. *Ecol. Monogr.* 86, 146–171.

Stepanenko, V., Mammarella, I., Ojala, A., Miettinen, H., Lykosov, V., and Vesala, T. (2016). LAKE 2.0: a Model for Temperature, Methane, Carbon Dioxide and Oxygen Dynamics in Lakes. *Geosci. Model. Dev.* 9, 1977–2006.

Tan, Z., Zhuang, Q., and Walter Anthony, K. (2015). Modeling Methane Emissions from Arctic Lakes: Model Development and Site-level Study. *J. Adv. Model. Earth Syst.* 7, 459–483. doi:10.1002/2014MS000344

Tang, J., Zhang, Q., Shannon, R. D., and White, J. R. (2010). Quantifying Wetland Methane Emissions with Process-Based Models of Different Complexity. *Biogeosciences* 7, 3817–3837.

Tapley, B. D., Bettadpur, S., Watkins, M., and Reigber, C. (2004). The Gravity Recovery and Climate Experiment: Mission Overview and Early Results. *Geophys. Res. Lett.* 31, 1–4. doi:10.1029/2004GL019920

Teh, Y. A., Murphy, W. A., Berrio, J.-C., Boom, A., and Page, S. E. (2017). Seasonal Variability in Methane and Nitrous Oxide Fluxes from Tropical Peatlands in the Western Amazon Basin. *Biogeosciences* 14, 3669–3683. doi:10.5194/bg-14-3669-2017

Tunnicliffe, R. L., Ganesan, A. L., Parker, R. J., Boesch, H., Gedney, N., Poulter, B., et al. (2020). Quantifying Sources of Brazil's CH_4 Emissions between 2010 and 2018 from Satellite Data. *Atmos. Chem. Phys.* 20, 13041–13067.

Ulseth, A. J., Hall, R. O., Boix Canadell, M., Madinger, M. L., Niayifar, A., and Battin, T. J. (2019). Distinct Air–Water Gas Exchange Regimes in Low-And High-Energy Streams. *Nat. Geosci.* 12, 259–263.

van Asperen, H., Alves-Oliveira, J. R., Warneke, T., Forsberg, B., Araújo, A. C., and Notholt, J. (2021). The Role of Termite CH_4 Emissions on Ecosystem Scale: a Case Study in the Amazon Rain Forest. *Biogeosciences* 18, 2609–2625.

van Haren, J., Brewer, P. E., Kurtzberg, L., Wehr, R. N., Springer, V. L., Espinoza, R. T., et al. (2021). A Versatile Gas Flux Chamber Reveals High Tree Stem CH_4 Emissions in Amazonian Peatland. *Agric. For. Meteorol.* 307, 108504. doi:10.1016/j.agrformet.2021.108504

van Lent, J., Hergoualc'h, K., Verchot, L., Oenema, O., and van Groenigen, J. W. (2019). Greenhouse Gas Emissions along a Peat Swamp Forest Degradation Gradient in the Peruvian Amazon: Soil Moisture and Palm Roots Effects. *Mitig. Adapt. Strateg. Glob. Change* 24, 625–643. doi:10.1007/s11027-018-9796-x

Venticinque, E., Forsberg, B., Barthem, R., Petry, P., Hess, L. A., Mercado, A., et al. (2016). An Explicit GIS-Based River Basin Framework for Aquatic Ecosystem Conservation in the Amazon. *Earth Syst. Sci. Data* 8, 651–661.

Vihermaa, L. E., Waldron, S., Garnett, M. H., and Newton, J. (2014). Old Carbon Contributes to Aquatic Emissions of Carbon Dioxide in the Amazon. *Biogeosciences* 11, 3635–3645.

Villa, J. A., Ju, Y., Stephen, T., Rey-Sanchez, C., Wrighton, K. C., and Bohrer, G. (2020). Plant-mediated Methane Transport in Emergent and Floating-Leaved Species of a Temperate Freshwater Mineral-Soil Wetland. *Limnol. Oceanogr.* 65, 1635–1650.

Waichman, A. V. (1996). Autotrophic Carbon Sources for Heterotrophic Bacterioplankton in a Floodplain Lake of Central Amazon. *Hydrobiologia* 341, 27–36.

Walter, B. P., and Heimann, M. (2000). A Process-Based, Climate-Sensitive Model to Derive Methane Emissions from Natural Wetlands: Application to Five Wetland Sites, Sensitivity to Model Parameters, and Climate. *Glob. Biogeochem. Cycles* 14, 745–765.

Wania, R., Melton, J. R., Hodson, E. L., Poulter, B., Ringeval, B., Spahni, R., et al. (2013). Present State of Global Wetland Extent and Wetland Methane Modelling: Methodology of a Model Inter-comparison Project (WETCHIMP). *Geosci. Model. Dev.* 6, 617–641.

Wania, R., Ross, I., and Prentice, I. C. (2010). Implementation and Evaluation of a New Methane Model within a Dynamic Global Vegetation Model: LPJ-WHyMe V1. 3.1. Geosci. *Model. Dev.* 3, 565–584.

Wanninkhof, R. (1992). Relationship between Gas Exchange and Wind Speed over the Ocean. *J. Geophys. Res.* 97, 7373–7381.

Ward, N. D., Keil, R. G., Medeiros, P. M., Brito, D. C., Cunha, A. C., Dittmar, T., et al. (2013). Degradation of Terrestrially Derived Macromolecules in the Amazon River. *Nat. Geosci.* 6, 530–533. doi:10.1038/ngeo1817

Wassmann, R., Thein, U. G., Whiticar, M. J., Rennenberg, H., Seiler, W., and Junk, W. J. (1992). Methane Emissions from the Amazon Floodplain: Characterization of Production and Transport. *Glob. Biogeochem. Cycles* 6, 3–13.

Webb, A. J., Bösch, H., Parker, R. J., Gatti, L. V., Gloor, E., Palmer, P. I., et al. (2016). CH_4 Concentrations over the Amazon from GOSAT Consistent with *In Situ* Vertical Profile Data. *J. Geophys. Res.* 121, 11006–11020. doi:10.1002/2016JD025263

Wik, M., Varner, R. K., Walter Anthony, K., MacIntyre, S., and Bastviken, D. (2016). Climate-sensitive Northern Lakes and Ponds Are Critical Components of Methane Release. *Nat. Geosci*. doi:10.1038/NGEO2578

Wilson, C., Chipperfield, M. P., Gloor, M., Parker, R. J., Boesch, H., McNorton, J., et al. (2021). Large and Increasing Methane Emissions from Eastern Amazonia Derived from Satellite Data, 2010-2018. *Atmos. Chem. Phys.* 21, 10643–10669.

Wilson, C., Gloor, M., Gatti, L. V., Miller, J. B., Monks, S. A., McNorton, J., et al. (2016). Contribution of Regional Sources to Atmospheric Methane over the Amazon Basin in 2010 and 2011. *Glob. Biogeochem. Cycles* 30, 400–420. doi:10.1002/2015GB005300

Wilson, M. D., Bates, P. D., Alsdorf, D., Forsberg, B., Horritt, M., Melack, J., et al. (2007). Modeling Large-Scale Inundation of Amazonian Seasonally Flooded Wetlands. *Geophys. Res. Lett.* 34, L15404. doi:10.1029/2007GL030156

Winton, R. S., Flanagan, N., and Richardson, C. J. (2017). Neotropical Peatland Methane Emissions along a Vegetation and Biogeochemical Gradient. *PLoS One* 12 (10), e0187019. doi:10.1371/journal.pone.0187019

Winton, S., Benavides, J. C., Mendoza, E., Hastie, A. T., Restrepo Canola, J. F., Ortega, A. G. H., et al. (2021). *Diverse Carbon-Rich Peatlands in the Amazonia and Orinoquia of Colombia*. Washington, D.C.: AGU Fall 2021 meeting. abstract B51C-07.

Yamazaki, D., Kanae, S., Kim, H., and Oki, T. (2011). A Physically Based Description of Floodplain Inundation Dynamics in a Global River Routing Model. *Water Resour. Res.* 47, W04501.

Yeates, P. S., and Imberger, J. (2003). Pseudo Two-dimensional Simulations of Internal and Boundary Fluxes in Stratified Lakes and Reservoirs. *Intern. J. River Basin Manage.* 4, 297–319. doi:10.1080/15715124.2003.9635214

Yu, X., Millet, D. B., and Henze, D. K. (2021). How Well Can Inverse Analyses of High-Resolution Satellite Data Resolve Heterogeneous Methane Fluxes? Observing System Simulation Experiments with the GEOS-Chem Adjoint Model (V35). *Geosci. Model. Dev.* 14, 7775–7793. doi:10.5194/gmd-14-7775-2021

Yuan, F., Ricciuto, D. M., Xu, X., Roman, D. T., Wood, J. D., Lilleskov, E., et al. (2020). *Modeling Methane Emissions in an Amazonian Palm Swamp Peatland with the E3SM Land Model*. AGU Fall 2020 meeting. abstract GC009-0011.

Zhang, B., Tian, H., Lu, C., Chen, G., Pan, S., Anderson, C., et al. (2017). Methane Emissions from Global Wetlands: An Assessment of the Uncertainty Associated with Various Wetland Extent Data Sets. *Atmos. Environ.* 165, 310–321. doi:10.1016/j.atmosenv.2017.07.001

Zhang, Z., Zimmermann, N. E., Stenke, A., Li, X., Hodson, E. L., Zhu, G., et al. (2017). Emerging Role of Wetland Methane Emissions in Driving 21st Century Climate Change. *Proc. Natl. Acad. Sci. U. S. A.* 114, 9647–9652. doi:10.1073/pnas.1618765114

Zhang, Z., Zimmermann, N. E., Kaplan, J. O., and Poulter, B. (2016). Modeling Spatiotemporal Dynamics of Global Wetlands: Comprehensive Evaluation of a New Sub-grid TOPMODEL Parameterization and Uncertainties. *Biogeosciences* 13, 1387–1408. doi:10.5194/bg-13-1387

Zhu, Q., Liu, J., Peng, C., Chen, H., Fang, X., Jiang, H., et al. (2014). Modelling Methane Emissions from Natural Wetlands by Development and Application of the TRIPLEX-GHG Model. *Geosci. Model. Dev.* 7, 981–999.

Zimmermann, M., Mayr, M. J., Bürgmann, H., Eugster, W., Steinsberger, T., Wehrli, B., et al. (2021). Microbial Methane Oxidation Efficiency and

Robustness during Lake Overturn. *Limnol. Oceanogr. Lett.* 6, 320–328. doi:10.1002/lol2.10209

Conflict of Interest: The authors declare that the research was conducted in the absence of any commercial or financial relationships that could be construed as a potential conflict of interest.

Publisher's Note: All claims expressed in this article are solely those of the authors and do not necessarily represent those of their affiliated organizations, or those of the publisher, the editors and the reviewers. Any product that may be evaluated in this article, or claim that may be made by its manufacturer, is not guaranteed or endorsed by the publisher.

Copyright © 2022 Melack, Basso, Fleischmann, Botía, Guo, Zhou, Barbosa, Amaral and MacIntyre. This is an open-access article distributed under the terms of the Creative Commons Attribution License (CC BY). The use, distribution or reproduction in other forums is permitted, provided the original author(s) and the copyright owner(s) are credited and that the original publication in this journal is cited, in accordance with accepted academic practice. No use, distribution or reproduction is permitted which does not comply with these terms.

frontiers | Frontiers in Environmental Science

ORIGINAL RESEARCH
published: 31 May 2022
doi: 10.3389/fenvs.2022.852344

Drivers of Anaerobic Methanogenesis in Sub-Tropical Reservoir Sediments

Alistair Grinham[1], Cathryn O'Sullivan[2], Matthew Dunbabin[3], Katrin Sturm[4], Deborah Gale[4], William Clarke[1] and Simon Albert[1]*

[1]School of Civil Engineering, The University of Queensland, Brisbane, QLD, Australia, [2]Commonwealth Scientific and Industrial Research Organisation (CSIRO), Canberra, ACT, Australia, [3]School of Electrical Engineering and Robotics, Queensland University of Technology, Brisbane, QLD, Australia, [4]Seqwater, Brisbane, QLD, Australia

Anaerobic methanogenesis is dependent on key macronutrients (carbon, nitrogen and phosphorus) and trace metals (including iron, nickel and cobalt) to drive methane production. Reservoir derived methane emissions have correlated to eutrophication status, with elevated emissions associated with more eutrophic systems. Additionally, sediment organic matter can enhance methane emissions, particularly through the ebullition pathway. As such, it is critical to understand how organic carbon and nutrient inputs into reservoir water columns and sediments drive methanogenesis to improve flooded land greenhouse gas emission estimates. In this study we examine the methane potential of sediments in mesotrophic (Little Nerang Dam) and eutrophic (Lake Wivenhoe) sub-tropical reservoirs under different nutrient and organic carbon availabilities using biological methane potential (BMP) tests. BMP tests were conducted with sediments incubated under anaerobic conditions using replicate controls (reservoir bottom waters) or treatments (excess nutrient and/or organic carbon availability). The results indicated that these systems are carbon limited. The addition of organic carbon significantly increases anaerobic methanogenesis by 20-fold over controls. Analysis of sediment samples from the reservoirs showed that both reservoirs were replete in key macronutrient and trace metal content for methanogenesis. Finally, a comprehensive catchment monitoring program of Little Nerang Dam measuring catchment inflow events, lateral transport of forest litter, and bulk atmospheric deposition showed that catchment inflows and lateral transport of forest litter were strongly linked to rainfall and accounted for more than 99% of the total annual load. This suggests the frequency of rainfall events is a critical driver of organic matter inputs that drive reservoir methane emissions in the humid, sub-tropical region.

Keywords: catchment loading, lateral litter inputs, atmospheric deposition, methanogenesis drivers, reservoir sediments

OPEN ACCESS

Edited by:
Daniel F. McGinnis,
Université de Genève, Switzerland

Reviewed by:
Guangchao Zhuang,
Ocean University of China, China
Bernhard Wehrli,
ETH Zürich, Switzerland

****Correspondence:***
Alistair Grinham
a.grinham@uq.edu.au

Specialty section:
This article was submitted to Biogeochemical Dynamics, a section of the journal Frontiers in Environmental Science

Received: *11 January 2022*
Accepted: *20 April 2022*
Published: *31 May 2022*

Citation:
Grinham A, O'Sullivan C, Dunbabin M, Sturm K, Gale D, Clarke W and Albert S (2022) Drivers of Anaerobic Methanogenesis in Sub-Tropical Reservoir Sediments. Front. Environ. Sci. 10:852344. doi: 10.3389/fenvs.2022.852344

1 INTRODUCTION

Methane is the second most potent greenhouse gas and contributes up to 25% of global warming (Etminan et al., 2016). Aquatic systems account for up to 50% of global methane emissions (Rosentreter et al., 2021) with artificial reservoirs recognised as major contributors to this emissions source (Bastviken et al., 2011; Deemer et al., 2016; Harrison et al., 2021). Reservoir derived methane emissions have repeatedly been shown to be correlated with eutrophication status,

with elevated emissions associated with more eutrophic systems (Deemer et al., 2016; DelSontro et al., 2018; Beaulieu et al., 2019). Additionally, sediment organic matter can enhance methane emissions, particularly through the ebullition pathway (Grinham et al., 2018; Berberich et al., 2019). As such, it is crucial to understand how eutrophication status and sediment organic matter in freshwater reservoirs drives methanogenesis to improve flooded land greenhouse gas emission estimates.

Methane production from anaerobic methanogenesis is dependent on key macronutrients including carbon for energy production, nitrogen for protein biosynthesis and phosphorus for nucleic acid synthesis and co-enzyme production (Takashima et al., 1990; Hullebusch et al., 2019). In addition, the enzymatic pathway in methanogenesis is highly metal rich (Zerkle et al., 2005) and all methanogens require iron, nickel and cobalt (Jarrell and Kalmokoff, 1988; Wang et al., 2019) with iron involved in virtually all metalloenzymes (Glass and Orphan, 2012). Eutrophication will increase nitrogen and phosphorus inputs to reservoir sediments whereas organic matter loading will increase carbon availability to reservoir sediments. However, a key area of uncertainty lies in how these sediment methanogenic communities respond to these competing drivers and which of these nutrients is limiting methane production. Reservoir sediments are highly reducing environments (Brannon et al., 1985) generally dominated by metal-rich silt or clay particles (Morris and Fan, 1998; van Rijn, 2012) and there is an extensive body of literature examining metal cycling in freshwater sediments (Boudreau, 1999; Ehrlich et al., 2015; Bianchi, 2021). However, there is a second area of uncertainty as there are few studies that examine the availability of these key trace metals for microbial uptake in sub-tropical reservoir sediments.

A third area of uncertainty in sub-tropical reservoirs lies in the loading of key macronutrients (including carbon, nitrogen and phosphorus) to the sediment zone. These depositional environments can receive macronutrient loading through multiple pathways including: catchment inflow events (Burford et al., 2012; Michalak, 2016); lateral transport of forest litter to stream networks or reservoir shoreline (Tonin et al., 2017); and atmospheric deposition directly into the reservoir surface waters (Tipping et al., 2014; Kanakidou et al., 2016). However, there are limited studies that have examined the relative contribution of all three pathways to reservoir macronutrient loading.

To address these three areas of uncertainty the objectives of this study are as follows: 1) examine the methane potential of sediments in sub-tropical reservoirs under different nutrient and organic carbon availabilities; 2) characterise reservoir sediments in terms of key macronutrient and trace metal availability for anaerobic methanogenesis; and 3) quantify key macronutrient loading to reservoirs from multiple pathways across the annual cycle.

2 MATERIALS AND METHODS

2.1 Description of Study Sites

Lake Wivenhoe and Little Nerang Dam are located in South East Queensland, Australia and the primary use for both reservoirs is urban water supply (**Figures 1A,B**). Lake Wivenhoe is located on the Brisbane River system and is the largest reservoir in the region with construction completed in 1985 (**Figure 1C**). Reservoir surface area at full supply level (FSL) is 10,750 ha with a storage capacity of 1.17×10^9 m^3. The catchment area is 7,020 km^2 and is a relatively degraded catchment with more than 50% modified from natural condition (Gale, 2016). Construction of Little Nerang Dam was completed in 1961 and is located on the Nerang River system (**Figure 1D**). Reservoir surface area at full supply level (FSL) is 49 ha with a storage capacity of 6.71×10^6 m^3. The catchment area is 35 km^2 and is a relatively unmodified catchment with only 17% modified from natural condition (Gale, 2016). The natural condition of both catchments was dominated by dry and wet sclerophyll forest consisting typically of mixed eucalypt, casuarina, and wattle forest (Hubble et al., 2010; Kemp et al., 2019). Catchment modification of both reservoirs is primarily for agriculture and is dominated by grazing land use (QLUMP, 2018) and reservoir water quality in this region is strongly correlated with their catchment land use (Burford et al., 2007). The highly modified catchment of Lake Wivenhoe has resulted in it being characterised as eutrophic whilst the relatively unmodified catchment of Little Nerang Dam has resulted in this reservoir being characterised as mesotrophic (Rigosi et al., 2015).

2.2 Biological Methane Potential of Reservoir Sediments

To address study objective 1, a series of biological methane potential (BMP) tests on sediments from the eutrophic reservoir, Lake Wivenhoe, and the mesotrophic reservoir, Little Nerang Dam, were conducted:

1) to investigate whether reservoir sediments can act as an inoculum to initiate methane production;
2) to assess the impact of adding nutrients and organic carbon, in the form of cellulose, on the sediment methane generation rate.

Sediments were sampled from four sites in Lake Wivenhoe (**Figure 1C**) and three sites in Little Nerang Dam (**Figure 1D**) covering riverine (inflow), transition and lacustrine zones in January and February 2009 (**Supplementary Figure S3**). Sediment samples for BMP tests were collected from each reservoir sampling site using a 250 cm^2 Van Veen sediment grab (K.C Denmark A/S, Silkeborg, Denmark) and transferred to ziplock bags. As much as possible, air was excluded from the bags and they were stored on ice for transport back to the laboratory. Sediments were divided into two subsamples; one for analysis and another for use as inoculum for biological methane tests described below. Samples were stored at 4°C for a maximum of 24 h prior to processing. Sediment samples from all sites were subjected to moisture content, volatile solids analysis and particle size analysis. Total solids and moisture content were determined gravimetrically after drying to constant weight at 110°C. While volatile solids (VS.) were determined by combusting the dried samples at 550°C for 2 h (APHA, 2005). Particle size

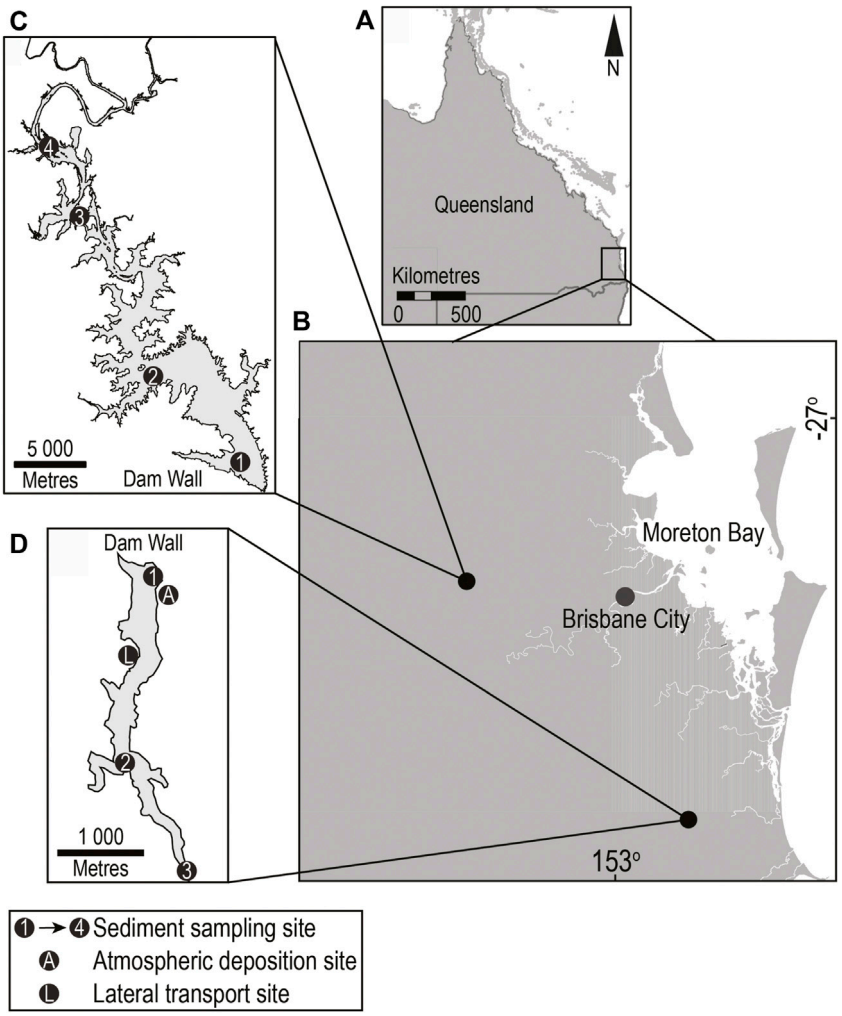


FIGURE 1 | Study area relative to **(A)** Queensland, Australia and **(B)** South East Queensland showing location of sampling sites on **(C)** Lake Wivenhoe and **(D)** Little Nerang Dam.

distribution was analysed using the laser diffraction method (Malvern Mastersizer 2000E, Malvern Instruments Ltd., UK) where samples were sonicated for 1 min prior to analysis to ensure true particle size was measured (Sperazza et al., 2004). Percent sand (2 mm–63 μm fraction), silt (63–2 μm fraction) and clay (<2 μm fraction) were then derived for each sample and classified following Folk (1974). Sediment characterisation data from BMP sampling sites is presented in **Supplementary Table S1**.

The methane producing potential of the sediments was measured under ideal conditions according to the method of Owen et al. (1979). Three treatments were conducted on sediments from each sample site with a minimum of five replicates per site. In each replicate treatment 10 g of sediment was place in a 160 ml Wheaton serum bottle. This served as both substrate and inoculum for the BMP tests. For the baseline treatment (Sediments), 100 ml of reservoir bottom water and 0.1 ml of the redox indicator, Rezasurin, were added to the serum bottle. In the second treatment (Sediments + Nutrients), the impact of the addition of excess nutrients (including ammonia, phosphate, cobalt, iron and nickel) was tested by replacing the lake water with 100 ml of BMP media (Owen et al., 1979). In the third treatment (Sediments + Nutrients + Cellulose), the impact of the addition of labile carbon and nutrients was tested by adding 1 g of 50 μm microcrystalline cellulose (Sigma-Aldrich Pty Ltd., North Ryde, NSW, Australia) along with 100 ml of BMP media.

Preparation of the BMP nutrient solution is a complex, multistep process designed to ensure the final solution and headspace are free from dissolved and gaseous oxygen. Full details of how to prepare the solution can be found in Owen et al. (1979). The final solution concentrations used in the sediment + nutrient and sediment + nutrient + cellulose treatments are described in **Table 1**.

All bottles were sealed with butyl rubber stoppers and aluminium crimp seals after purging with nitrogen gas to create an anaerobic head space. The bottles were incubated at 38°C. It is acknowledged

TABLE 1 | Nutrient concentration in biological methane potential (BMP) test solution prepared according to Owen et al. (1979).

Assay Reagent	Final Solution Concentration (g/L)
Resazurin	0.001
$(NH_4)_2HPO_4$	0.08
$CaCl_2.2H_2O$	0.25
NH_4Cl	0.40
$MgCl_2.6H_2O$	1.80
KCl	1.30
$MnCl_2.4H_2O$	0.02
$CoCl_2.6H_2O$	0.03
H_3BO_3	0.006
$CuCl_2.2H_2O$	0.003
$Na_2MoO_4.2H_2O$	0.003
$ZnCl_2$	0.002
$FeCl_2.4H_2O$	0.37
$Na_2S.9H_2O$	0.5
Biotin	0.00002
Folic acid	0.00002
Pyridoxine hydrochloride	0.0001
Riboflavin	0.00005
Thiamin	0.00005
Nicotinic acid	0.00005
Pantothenic acid	0.00005
B12	0.000001
p-aminobenzoic acid	0.00005
Thioctic acid	0.00005
$NaHCO_3$	4.67

that this temperature is significantly higher than ambient temperatures experienced reservoir bottom waters, however, this was chosen to assess the maximal rates of methane generation from the sediments. The vast majority of research using BMP tests comes from experiments assessing the degradability of organic materials for anaerobic digestion. These tests are generally conducted at mesophilic temperatures (30–38°C) because this temperature range is sufficient to support significant microbial activity (Raposo et al., 2012). Psychrophilic temperatures (<20°C) generally result in a decrease in microbial activity. While thermophilic temperatures (45–60°C) may further increase methane generation rates the improvements are not large enough to justify their use. The rates of methane generation recorded in the BMP tests are unlikely to occur at the temperatures observed in the reservoir bottom waters (14–21°C, **Supplementary Figure S3**), but the impact of the addition of carbon and nutrients on the volume of methane produced is likely to be similar regardless of temperature.

The bottles were sampled weekly for gas volume by connection to a water filled manometer for a minimum of 7 weeks. At each sampling event, a 10 ml sample of the head space gas was collected for analysis of methane content by gas chromatography (GC). The methane content of the gas samples (v/v%) was measured using a Perkin Elmer Autosystem GC as described previously (APHA, 2005; O'Sullivan et al., 2005).

2.3 Reservoir Sediment Macronutrient and Trace Metal Content

To address study objective 2, undisturbed sediment cores for macronutrient and metal content analysis were collected from each BMP sampling site using a gravity corer (Envco Environmental Equipment Suppliers, Australia) and acrylic liners (69 mm inner diameter, 500 mm long). Sediment porewaters were extracted in the field directly from the cores using 0.2 µm sippers (Rhizon CSS samplers, Rhizosphere Research Products B.V., Netherlands) positioned laterally through pre-drilled holes into the acrylic liner. Porewaters were passively drawn out of the sediments using evacuated 12 ml exetainers (Lab Co., Ceredigion, UK) with samples then stored on ice for transport to the laboratory. Porewater samples were analysed for macronutrient and trace metal content and were assumed to represent the dissolved fraction. Sediment samples for the total fraction were manually collected directly into sterile 250 ml glass jars from the upper 10 cm of each sediment core. Samples were placed on ice in the dark for transport to the laboratory. Analysis of key macronutrient (TOC, TN and TP) and metal content was undertaken at the National Association of Testing Authorities (NATA) accredited laboratory, Environmental Analysis Laboratory (EAL), Southern Cross University, Lismore, Australia and followed the methodology of Rayment and Lyons (2010). Sediment TOC and TN analysis was undertaken using a CNS-2000 Combustion Analyzer (LECO Corporation, United States) and TP and metal content (Method APHA 3125; APHA, 2005) was analysed by inductively coupled plasma mass spectrometry (ICP-MS). Porewater dissolved organic carbon (DOC) was analysed using a LECO CNS-2000 Combustion Analyzer (Method APHA 5310-B; APHA, 2005), ammonia and phosphate were analysed using flow-injection analysis (FIA) colorimetry (Lachat QuikChem 8,000) (Method APHA 4500; APHA, 2005) and trace metals were analysed using ICP-MS (Method APHA 3125; APHA, 2005).

2.4 Macronutrient Loading to Little Nerang Dam

To address study objective 3, a series of field campaigns were undertaken to monitor each of the reservoir loading pathways as previously described in the Introduction section. Macronutrient loading due to lateral transport of forest litter and from bulk atmospheric deposition were both monitored over the 2010 annual cycle. Loading due catchment inflows was monitored over a 5 year period from 2009 to 2013 (**Supplementary Figure S6**). It should be noted that sampling events for the lateral transport, catchment inflow and atmospheric deposition were somewhat infrequent and therefore these data are subject to considerable uncertainty, both spatially and temporally. They do, however, provide an estimate of the magnitude of the different input pathways relative to each other. Detailed methodology for each pathway is provided in the sections below.

2.4.1 Macronutrient Loading due to Lateral Transport of Forest Litter

Lateral transport of forest litter (expressed as g m^{-1} shoreline d^{-1} rather than lateral transport velocity) was monitored at a single site located on the western shoreline of Little Nerang Dam approximately 2 m above reservoir full supply level

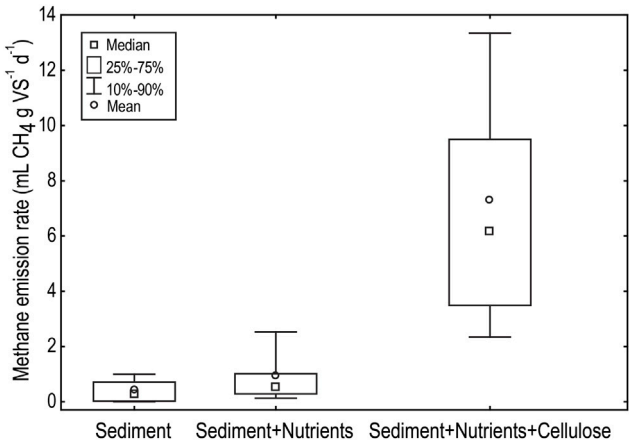


FIGURE 2 | Biological methane potential of sediments from Little Nerang Dam and Lake Wivenhoe when incubated in reservoir bottom waters (Sediment), BMP media (Sediment + Nutrients) or BMP media supplemented with the organic carbon, cellulose (Sediment + Nutrients + Cellulose).

(**Figure 1D**). Lateral traps were constructed from stainless wire frames (250 by 250 mm) with a nylon mesh (10 mm pore size) bag on the downhill side. Traps were deployed parallel to the shoreline and spaced approximately 5 m apart. Each trap sampled a ground length of 0.25 m and samples were collected at approximately monthly intervals. Trap contents were transferred to sealed bags, transported to the laboratory and then dried to a constant weight at 60°C. Dry weights (g) were normalised to the ground sampling length (m) and deployment time (d) with rates expressed as (g m^{-1} d^{-1}). In addition, litter samples from February, March and October were analysed for key macronutrient (TOC, TN and TP) and metal content using at the NATA accredited EAL, Southern Cross University, Lismore, Australia. TOC and TN analysis was undertaken using a CNS-2000 Combustion Analyzer (LECO Corporation, United States) following In-house method S4a (NATA, 2021). TP and metal content was analysed by inductively coupled plasma optical emission spectrometry (ICP-OES) following Method APHA 3125 (APHA, 2005).

Additional details of the catchment are provided in **Supplementary Material**. To further understand forest litter transport, a permanent transect was established in western catchment area of Little Nerang Dam starting immediately upslope of the lateral transport monitoring site. Three additional monitoring sites were located along an altitudinal gradient (400 m—high; 300 m—mid; and 200 m—low) as shown in **Supplementary Figure S2**. At each site vegetation surveys, vertical forest litter fall rates monitoring and soil characterisation were undertaken with detailed methodology described in **Supplementary Material Sections S1.2 to S1.4** and findings presented in **Supplementary Material Sections S2.2 to S2.4 and S2.6**.

2.4.2 Macronutrient Loading due to Catchment Inflows

The study region is in the humid sub-tropics where the majority of rainfall occurs during summer months (December to February) and more than 50% of the total annual rainfall occurs through heavy rainfall days (**Supplementary Figure S1**) due to localised storm activity or major rainfall events such as east coast lows (Dowdy et al., 2013). In addition, daily rainfall totals in excess of 100 mm are observed several times across the annual cycle in the Little Nerang Dam catchment (**Supplementary Figure S1**). These major rainfall events, in combination with the steep catchment (**Supplementary Figure S2**), results in high energy inflows to the reservoir capable of transporting large quantities of dissolved and particulate matter. Access to reservoir inflow points during high flows is limited by health and safety risks and, therefore, only a single inflow was sampled during the 2010 monitoring period. However, five additional event sampling campaigns were undertaken over a 5 year period from 2009 to 2013 (**Supplementary Figure S6**). For each campaign, sampling was undertaken on the reservoir as close as possible to catchment inflow points. Samples were collected approximately 30 cm below the water surface using MilliQ water washed high density polyethylene (HDPE) sample containers following state sampling guidelines (DES, 2018). Sub-surface sampling minimised the likelihood of sampling large (<10 mm) particulate organic matter from lateral litter transport in the upper catchment regions. Samples were placed on ice for transport to the laboratory and macronutrient analyses were conducted by the NATA accredited EAL, Southern Cross University, Lismore, Australia. TOC was analysed using a CNS-2000 Combustion Analyzer (Method APHA 5310-B; APHA, 2005) and TN and TP were analysed using flow-injection analysis (FIA) colorimetry (In-house method W4; NATA, 2021).

2.4.3 Bulk Atmospheric Deposition Rates of Macronutrients

Bulk deposition of the macronutrients TOC, TN and TP was monitored at a single site located in a forest clearing near the wall of Little Nerang Dam following the methodology detailed in Huston et al. (2009). Samplers were constructed of polyvinyl chloride (PVC) funnels (110 mm diameter, surface area = 0.0095 m^2) inserted into a 2 L HDPE plastic bottle wrapped in aluminium foil to exclude light. Funnels and bottles were washed using Milli-Q water prior to deployment. Samplers were housed in PVC pipes (90 mm diameter, 300 mm length), mounted 2 m above the ground level and a minimum of 50 m from surround forest. Three replicate samples were collected on a weekly to monthly frequency over a 10 month period (Feb–December 2010). Field and rinsate blanks were used for quality control (DES, 2018). Sealed sample bottles with 100 ml Milli-Q water were deployed alongside field samplers for each deployment. In addition, a new sampler was processed alongside the deployed samplers during field collection. All samples were placed on ice for transport directly to the laboratory with all macronutrient analyses conducted by the NATA accredited Queensland Health, Forensic and Scientific Services (QHFSS), Brisbane, Australia. TOC was analysed using a Shimadzu TOC-L carbon analyser and TN and TP were analysed using flow-injection analysis (FIA) colorimetry (APHA, 2005). Bulk atmospheric deposition rates of individual macronutrients (mg m^{-2} d^{-1}) were calculated using

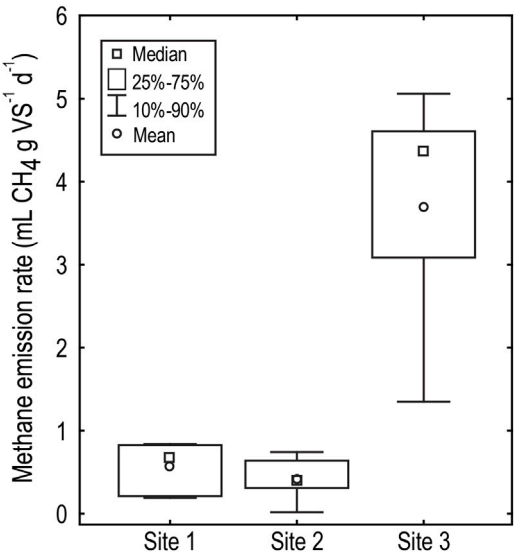


FIGURE 3 | Biological methane potential (mL g VS^{-1} d^{-1}, mL of methane produced per gram of volatile solids added to the incubation per day, where volatile solids represents the degradable organic material and is measured by combustion at 550°C) of sediments from three sampling sites in Little Nerang Dam when incubated with nutrient media. Site locations are shown in **Figure 1D**.

the mass of TOC, TN or TP (mg) deposited over the deployment time (d) and normalised to the funnel surface area (m^2).

2.4.4 Annual Scaling of Macronutrient Loading Rates

Annual loading rates of total organic carbon, total nitrogen and total phosphorus were estimated for three loading pathways: catchment inflow, later litterfall transport and atmospheric deposition using the following approaches:

Annual catchment inflow loading was calculated using the 2010 inflows (**Figure 4A**) and the median concentration of TOC, TN and TP from event monitoring campaigns (**Figure 5**). Loading was expressed as tonnes per year (t y^{-1}) and the uncertainty range was generated using the interquartile range in inflow macronutrient concentrations (**Figure 5**).

Annual loading due to lateral transport of leaf litter was calculated from the median transport rates (**Figure 4B**) and the forest litter macronutrient content (**Table 3**) to generate annual transport rates of TOC, TN and TP per metre. These per metre rates were then scaled to the catchment by the combined lengths of the reservoir shoreline and the higher order stream network (34.2 km total). Loading was expressed as tonnes per year (t y^{-1}) and the uncertainty range was generated using the interquartile range in lateral transport rate (**Figure 4B**) and the upper and lower litter macronutrient content (**Table 3**).

Annual loading due to atmospheric deposition was calculated using the annual median bulk deposition rates of TOC, TN and TP (**Figure 6**) and the annual average reservoir surface area for 2010. Loading was expressed as tonnes per year (t y^{-1}) and the uncertainty range was generated using the interquartile range in macronutrient bulk deposition rate (**Figure 6**).

As noted above, these estimates are based on data collected at discrete sampling points spread out in both time and space. They are not intended to provide a precise nutrient budget of the reservoirs. Rather, they have been conducted to provide an estimate of the difference in magnitude between the three different input pathways.

2.5 Statistical Analysis

Statistical analyses of sediment BMP tests and forest litter lateral transport rates using factorial or one-way analysis of variances (ANOVAs) were performed using the software program Statistica 13 (Dell Inc., 2016). Raw sediment BMP normalised methane production rate data was first classified into individual reservoirs (Little Nerang Dam; Lake Wivenhoe) and treatment (sediment; sediment and nutrients; sediment, sediment, nutrients and cellulose) and these categories were used as the categorical predictors with sediment BMP normalised gas production rates as the continuous variable. A factorial ANOVA was used to examine differences between reservoirs and/or treatment, however, no significant interaction was found between sediment BMP tests at the reservoir level ($F_{(1,\ 128)} = 1.27$, $p = 0.261$) and differences were examined at the treatment level. In addition, no significant interaction was observed between sites within each reservoir for individual treatments with the exception of the nutrient treatments in Little Nerang Dam and a one-way ANOVA was used to examine site differences. To examine the effect of precipitation on forest litter lateral transport rates, raw data was first pooled into two categories (runoff or no runoff) depending if catchment runoff occurred in the deployment period. A one-way ANOVA was used to examine differences in forest litter lateral transport rates and these categories were used as the categorical predictors. Post hoc tests were performed using Fisher's least significant difference (LSD) test (Zar, 1984). The non-parametric Kruskal–Wallis (KW) test was used as the continuous data failed to satisfy the assumptions of normality or homogeneity of variance even after transformation.

3 RESULTS

3.1 Biological Methane Potential of Reservoir Sediments

Reservoir sediments incubated with both organic carbon and nutrient rich media had significant higher methane generation rates ($F_{(2,\ 128)} = 100.50$, $p < 0.001$) compared with sediment incubated in bottom water and only nutrient rich media (**Figure 2**). The median methane generation rate from sediments incubated with organic carbon was 6.2 (IQR: 3.5–9.5) ml g VS^{-1} d^{-1} (mL of methane produced per Gram of volatile solids added to the incubation per day, where volatile solids represents the degradable organic material and is measured by combustion at 550°C) with a maximum rate of 25.8 ml g VS^{-1} d^{-1}. Median methane generation rates from sediments incubated without organic carbon were an order of magnitude lower (**Figure 2**). The median methane generation rate from sediments incubated in bottom waters was 0.29 (IQR: 0.02–0.71) ml g VS^{-1} d^{-1} with a maximum rate of 1.7 ml g VS^{-1} d^{-1}. The median methane generation rate from sediments incubated in nutrient media only was 0.52 (IQR:

TABLE 2 | Total and dissolved fractions of selected key sediment macronutrient and trace metals from Lake Wivenhoe and Little Nerang Dam.

Reservoir	Fraction	Parameter	Unit	Average	Upper	Lower
Lake Wivenhoe	Total	Organic carbon	%	3.4	3.9	3.0
		Nitrogen	%	0.341	0.405	0.308
		C:N		9.97	9.63	9.74
		Phosphorus	mg kg^{-1}	1,044.0	1,132.5	983.9
		Cobalt	mg kg^{-1}	21.0	21.8	20.7
		Iron	mg kg^{-1}	47,736	50,056	44,414
		Nickel	mg kg^{-1}	24.6	26.5	23.5
	Dissolved	Organic carbon	mg L^{-1}	72.9	85.8	62.2
		Ammonia	mg L^{-1}	39.2	44.3	36.7
		Phosphate	mg L^{-1}	0.078	0.097	0.068
		Cobalt	mg L^{-1}	0.013	0.020	0.010
		Iron	mg L^{-1}	20.7	23.0	18.2
		Nickel	mg L^{-1}	0.010	0.013	0.006
Little Nerang	Total	Organic carbon	%	12.67	25.5	3.38
		Nitrogen	%	0.257	0.306	0.195
		C:N		49.30	83.33	17.33
		Phosphorus	mg kg^{-1}	711.1	909.1	602.9
		Cobalt	mg kg^{-1}	18.1	19.1	16.6
		Iron	mg kg^{-1}	35,565	36,721	34,895
		Nickel	mg kg^{-1}	18.8	19.0	18.5
	Dissolved	Organic carbon	mg L^{-1}	63.6	71.3	52.3
		Ammonia	mg L^{-1}	51.6	54.1	48.5
		Phosphate	mg L^{-1}	0.068	0.082	0.061
		Cobalt	mg L^{-1}	0.009	0.014	0.006
		Iron	mg L^{-1}	22.1	35.2	13.9
		Nickel	mg L^{-1}	0.010	0.014	0.008

0.28–1.01) ml g VS^{-1} d^{-1} with a maximum rate of 5.1 ml g VS^{-1} d^{-1}. Whilst the addition of nutrient rich media led to a small increase in the methane generation compared to sediments incubated in bottom waters, however, this increase is not statistically significant (**Figure 2**).

The high level of variability in methane generation rates observed in sediments from Little Nerang Dam under the nutrients treatment (**Figure 3**) is primarily due to different responses from the sediments from the headwaters of the dam (Site 3 **Figure 1D**). The addition of nutrients to sediments from the two sites closer to the dam wall (Site 1 and 2 **Figure 1D**) had little impact on methane generation whilst the addition of nutrients to the sediments from the headwaters led to a significant, order of magnitude, increase ($F_{(2, 15)} = 10.90$, $p < 0.005$) in the methane generation rate (**Figure 3**).

3.2 Reservoir Sediment Macronutrient and Trace Metal Content

Total and dissolved fractions of key macronutrients and trace metals were detected in all reservoir sediments sampled (**Table 2**). Macronutrients and trace metals in the total sediment fraction were similar for all parameters between Lake Wivenhoe and Little Nerang Dam with the exception of organic carbon and carbon to nitrogen ratio (C:N). Average organic carbon content and C:N were one order of magnitude lower in Lake Wivenhoe compared to Little Nerang Dam (**Table 2**). Dissolved fractions of sediment macronutrients and trace metals were similar across all parameters between the reservoirs and average ammonia and iron concentrations exceeded 39 and 20 mg L^{-1}, respectively (**Table 2**).

3.3 Macronutrient Loading to Little Nerang Dam

Monitoring of forest litter lateral transport rates over the annual cycle included five separate inflows events closely associated with major catchment rainfall (**Figure 4A**). Elevated rates of lateral transport were observed following each catchment runoff event with the exception of the May event (**Figure 4B**). Significantly higher rates (KW $H_{(1,32)} = 14.7$, $p < 0.001$) of forest litter lateral transport were observed following runoff events as opposed to no runoff events (**Supplementary Figure S10**) where median lateral transport rates (4.7 g m^{-1} d^{-1}) following catchment runoff were over one order of magnitude higher than rates where no runoff occurred (0.4 g m^{-1} d^{-1}). It is assumed the lateral transport rates observed at the shoreline site are representative of the catchment given the relatively constant hillslope (**Supplementary Figure S7**) and similar rates of vertical forest litterfall across the altitudinal gradient (**Supplementary Figure S8**).

Analysis of forest litter macronutrient content indicated this to be a major source of organic carbon to reservoir sediments. Total organic carbon content were two to three orders of magnitude higher than total nitrogen and total phosphorus, respectively (**Table 3**). Average nitrogen content was 0.8%, phosphorus was 0.04% and organic carbon was over 50%. The elevated carbon contents and high carbon to nitrogen ratios suggest that this material is relatively degradable. In addition, forest litter was found to contain detectable quantities of the key trace metals, with iron content two

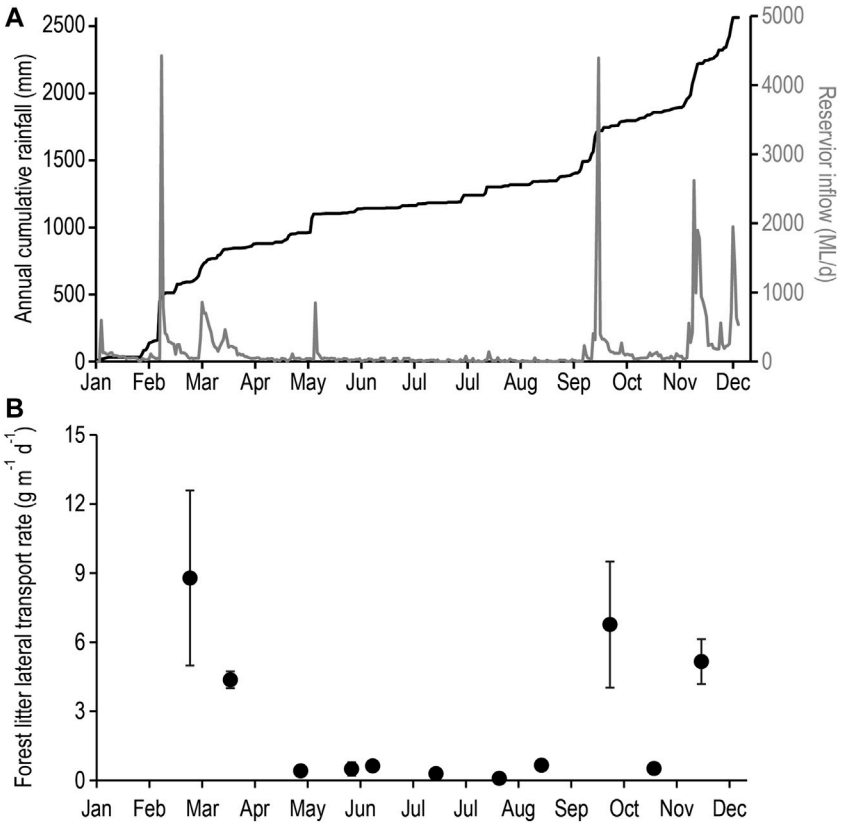


FIGURE 4 | (A) Cumulative rainfall (black line) and catchment inflow (grey line); and **(B)** forest litter lateral transport rate per unit shoreline (g m^{-1} shoreline d^{-1}) from Little Nerang Dam across the 2010 annual cycle.

TABLE 3 | Forest litter macronutrient and mineral content from thee sampling events during lateral transport monitoring at Little Nerang Dam.

Parameter	Units	Average	Upper	Lower
Carbon	%	52.5	52.9	52.1
Nitrogen	%	0.83	0.96	0.67
C:N		63.25	55.10	77.76
Phosphorus	%	0.04	0.05	0.03
Cobalt	mg kg^{-1}	0.6	1	0.2
Iron	mg kg^{-1}	201	343	130

orders of magnitude higher than and cobalt (**Table 3**). Forest litter collected in lateral traps consisted almost exclusively of eucalypt leaves and eucalypts were the dominant canopy trees at all sites surveyed (**Supplementary Table S4**).

Monitoring of catchment inflow events over six separate inflows events across a 5 year monitoring period revealed a consistent pattern with total phosphorus concentrations and order of magnitude lower than total nitrogen and two orders of magnitude below total organic carbon concentrations (**Figure 5**). Median TP, TN and TOC concentrations of inflows were 0.180 (IQR: 0.110–0.200), 0.995 (IQR: 0.787–1.135) and 10.5 (IQR: 9.0–11.3) mg L^{-1}, respectively (**Figure 5**).

Bulk atmospheric deposition rates of macronutrients across the annual cycle revealed a consistent pattern with TP rates an order of magnitude lower than TN and TOC rates (**Figure 6**). Median daily rates of TP, TN and TOC bulk deposition were 0.152 (IQR: 0.073–0.240), 1.658 (IQR: 1.082–2.093) and 4.296 (IQR: 3.183–5.650) mg m^{-2} d^{-1}, respectively (**Figure 6**).

Annual scaling of macronutrient loading to Little Nerang Dam across all three pathways was dominated by catchment inflows following major rainfall events. These inflows accounted for 57% of TOC annual loading, 88% of TN annual loading and 96% of TP annual loading (**Table 4**). Lateral litter transport accounted for 42% of TOC annual loading, 11% of TN annual loading and 3% of TP annual loading (**Table 4**). Atmospheric deposition was a relatively minor pathway and accounted for less than 1% of TOC, TN, and TP annual loading (**Table 4**). Estimated annual loading for TOC was highly variable with the interquartile range almost three times the median rate whereas the interquartile range was less than the median rate for both TN and TP (**Table 4**).

4 DISCUSSION

Understanding how sediment methanogenic communities respond to nutrient and organic carbon loading is essential to refine global methane budgets and manage emissions from

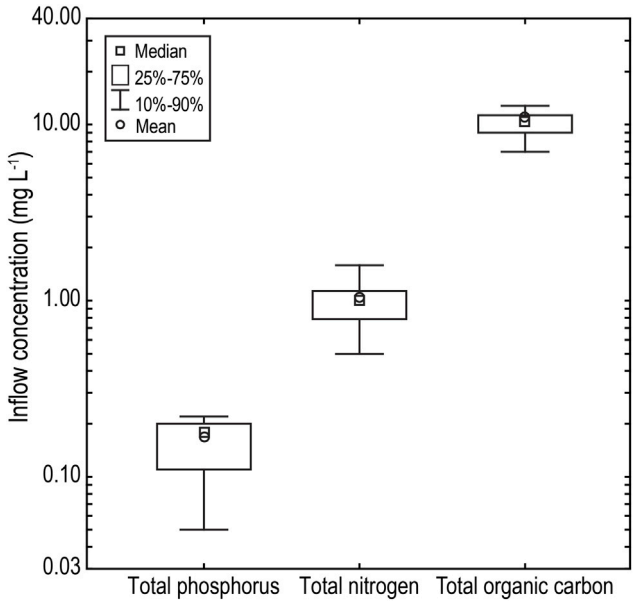


FIGURE 5 | Macronutrient (TP, TN and TOC) concentration of catchment inflow waters to Little Nerang Dam over a 5 year monitoring period from 2009 to 2013.

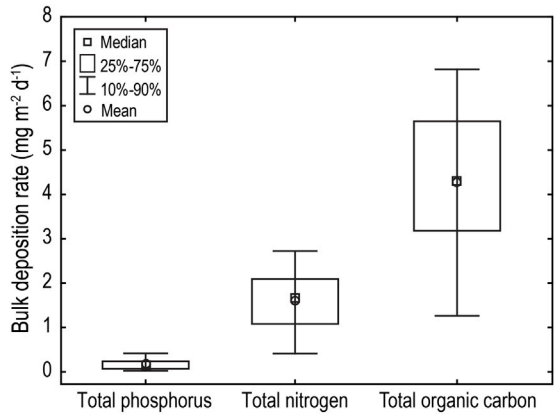


FIGURE 6 | Average daily bulk atmospheric deposition of macronutrients (TP, TN and TOC) to Little Nerang Dam over a 10 month monitoring period from Febuary to December 2010.

flooded lands. This study demonstrated that all reservoir sediments tested contain native, hydrolytic, acidogenic and methanogenic microbial communities capable of degrading the organic carbon present in the sediments and generating methane. In addition, the laboratory tests demonstrated organic carbon is a key limiting macronutrient to methanogenic communities in the sediments of both the eutrophic and mesotrophic reservoirs. In all cases, adding a readily degradable form of organic carbon led to a significant increase in methane generation, directly supporting the findings of Grasset et al. (2018) who demonstrated the addition of fresh organic carbon greatly stimulated methane production in freshwater anoxic sediments. Given all reservoir sediments sampled in this study were replete in key macronutrient and trace metal content for methanogenesis (**Table 2**), organic carbon loading to the sediment zone will, therefore, likely stimulate *in situ* methanogenic communities. This is supported by Boon and Mitchell (1995) who demonstrated a 400%–500% increase in methanogenesis rates when freshwater sediments from southeast Australia were incubated with eucalypt leaves under ambient temperatures. Together, these findings suggest organic carbon loading is an important driver of anaerobic methanogenesis in mesotrophic and eutrophic sub-tropical reservoirs. This has been demonstrated in temperate freshwater lakes, impoundments, reservoirs and coastal sediments (Kelly and Chynoweth, 1981; Maeck et al., 2013; Tittel et al., 2019; Jilbert et al., 2021).

The significant response in BMP tests between sites observed in the nutrient treatment from Little Nerang Dam is a key finding. Sediments from sites further from the dam wall had elevated volatile solids contents (**Supplementary Table S1**) and displayed increased methane generation rate upon addition of nutrient solution without cellulose addition (**Figures 2**, **3**). Similar spatial heterogeneity in methane ebullition has been reported by DelSontro et al. (2011) in tropical reservoir, Lake Kariba.

This is likely due to the proximity of these sediments to catchment inflow points which are rich in organic carbon in the form of forest litter (**Supplementary Table S1**). These sediments are, therefore, more nutrient limited (and less carbon limited) than the sediments closer to the dam wall which contain lower organic matter content and are, potentially, carbon limited (**Supplementary Table S1**). This nutrient limitation in sediments adjacent catchment inflows has important implications for reservoir emissions as these are major ebullition zones (Grinham et al., 2018) accounting for over 90% of total reservoir emissions (Grinham et al., 2011). Any increase in reservoir nutrient loading, in areas where organic carbon is not limiting, would likely stimulate *in situ* sediment methanogenesis as well as total reservoir emissions. This provides one potential mechanism as to how eutrophication will exacerbate inland water methane emissions and supports the findings of regional and global correlation studies (Bastviken et al., 2004; Deemer et al., 2016; DelSontro et al., 2016; West et al., 2016; Beaulieu et al., 2019). An additional observation in terms of macronutrient limitation lies in the ratio of available nitrogen (ammonia) to phosphorus (phosphate) observed in the reservoir sediment porewaters. The N:P ratio ranged from 503 in Lake Wivenhoe to 759 in Little Nerang Dam (**Table 2**) and is one to two orders of magnitude higher than N:P ratio from cellular elemental stoichiometry for methanogens which ranges between 5 and 19 (Takashima et al., 1990). This suggests relative phosphorus limitation occurs in sediment porewaters and is a potential contributing factor to the strong relationship found between TP and methane emissions globally (Deemer et al., 2016; DelSontro et al., 2016; Beaulieu et al., 2019).

Scaling of annual macronutrient loading to Little Nerang Dam highlighted the importance of lateral transport of forest litter as an organic carbon loading pathway contributing almost 50% of

TABLE 4 | Annual macronutrient loading to Little Nerang Dam reservoir from three pathways: catchment inflow; lateral litter transport; and atmospheric deposition.

Pathway	Parameter	Median (t y^{-1})	25th Percentile (t y^{-1})	75th Percentile (t y^{-1})
Catchment inflows	Total organic carbon	612.36	524.88	659.02
	Total nitrogen	58.03	45.90	66.19
	Total phosphorus	10.50	6.42	11.66
Lateral litter transport	Total organic carbon	460.42	223.05	2,981.30
	Total nitrogen	7.28	4.05	38.34
	Total phosphorus	0.35	0.21	1.72
Atmospheric deposition	Total organic carbon	0.71	0.52	0.93
	Total nitrogen	0.27	0.18	0.34
	Total phosphorus	0.03	0.01	0.04
Total annual loading	**Total organic carbon**	**1,073.49**	**748.46**	**3,641.25**
	Total nitrogen	**65.58**	**50.12**	**104.88**
	Total phosphorus	**10.87**	**6.64**	**13.42**

the total annual load (**Table 4**). The high carbon content and C:N ratio of the organic material entering Little Nerang Dam *via* lateral transport suggests that this material is relatively fresh and highly degradable. Therefore, this loading pathway of organic carbon to reservoirs is an important consideration to improve understanding of reservoir methane generation and emissions (Tittel et al., 2019). The significantly higher forest litter lateral transport rates observed following runoff events supports the finding that precipitation is the major control of plant litter dynamics in tropical biomes (Tonin et al., 2017). From the data collected in this study it is not possible to comment on whether methane emission event corresponded with rainfall events because there was no coordinated schedule of methane sampling following rainfall events. It is highly likely that there will be a delay between organic matter deposition due to rainfall events and methane emission events. Organic matter inflows can be expected to be highly sporadic and coincide with high rainfall events, but the microbial processing of organic matter that is deposited in bottom waters and sediments involves several steps (solubilisation, acidification and methanogenesis) which are influenced by factors other than rainfall inflows. The degradation of highly lignified material is likely to be slow, particularly under anaerobic conditions, and therefore methane emissions are likely to occur over longer timescales and may not be correlated with inflow events (Xu et al., 2019).

Bulk atmospheric deposition was a minor macronutrient loading pathway to Little Nerang Dam reservoir (**Table 4**). This is supported by Adams et al. (2014) who found atmospheric deposition to be an insignificant loading pathway in a southeast Australian agricultural catchment. However, the ubiquitous nature of atmospheric deposition across the catchment will likely increase productivity of the forest and contribute to reservoir loading *via* litterfall. The contribution of atmospheric deposition to productivity has been observed in the tropical forests of French Guinea (van Langenhove et al., 2020). Catchment inflow was the major loading pathway to Little Nerang Dam for all macronutrients monitored (**Table 4**). The importance of this pathway for loading of organic carbon, nitrogen and phosphorus to stream networks and reservoirs is well established (Burford et al., 2007; O'Brien et al., 2016; Johnson et al., 2018). Catchment inflows and later transport of forest littler accounted for more than 99% of the total TOC, TN and TP annual load to Little Nerang Dam (**Table 4**). It is, therefore, important that future evaluations of macronutrient loading to reservoirs, particularly in the sub-tropics and tropical regions, consider both loading pathways in their assessments. This is of critical importance given the projected increase in global reservoirs (Günther et al., 2015), with over 3,700 future hydropower dams either planned or under construction (Zarfl et al., 2015), and the increase in rainfall driven eutrophication over the 21st century (Sinha et al., 2017).

In conclusion, this study demonstrated the importance of understanding the complex interplay between eutrophication and organic carbon loading in driving methane emissions from reservoir sediments. All sediments tested from these sub-tropical reservoirs were capable of methanogenesis and this was primarily limited by organic carbon. In sediments with elevated organic carbon content, nutrient limitation was observed, and this provides a potential mechanism for past studies that have demonstrated strong, positive relationships between eutrophication and methane emissions. Sediments from mesotrophic and eutrophic reservoirs were replete in key macronutrients (TOC, TN and TP) and trace metals (Fe, Ni and Co.) required for anaerobic methanogenesis. Finally, annual loading of macronutrients to the Little Nerang Dam reservoir was dominated by catchment inflows and lateral transport of forest litter. Based on these findings we suggest methane emission modelling and importantly mitigation from flooded lands takes into account the role of organic carbon as a driver of emissions alongside eutrophication.

DATA AVAILABILITY STATEMENT

The original contributions presented in the study are included in the article/**Supplementary Material**, further inquiries can be directed to the corresponding author.

AUTHOR CONTRIBUTIONS

All authors contributed to the conceptualization of the study. AG coordinated the study, conducted field sampling and analysed

samples. MD contributed to the field sampling events. CS conducted biological methane potential tests and analysed laboratory samples. KS and DG contributed to the field sampling events and chemical analysis. All authors contributed to the interpretation of the results. AG produced the draft manuscript and all authors contributed to the editing of the draft.

FUNDING

Field monitoring campaigns, laboratory studies and sample analysis undertaken in this study were funded by Queensland Bulk Water Supply Authority, trading as Seqwater.

ACKNOWLEDGMENTS

The authors would like to acknowledge the financial and logistical support provided by Queensland Bulk Water Supply Authority, trading as Seqwater. Field and laboratory assistance was provided by N. Cutts, B. Knowles and P. Maxwell. Floristic surveys were undertaken by D. Jinks (Gold Coast Botany).

SUPPLEMENTARY MATERIAL

The Supplementary Material for this article can be found online at: https://www.frontiersin.org/articles/10.3389/fenvs.2022.852344/full#supplementary-material

REFERENCES

Adams, R., Arafat, Y., Eate, V., Grace, M. R., Saffarpour, S., Weatherley, A. J., et al. (2014). A Catchment Study of Sources and Sinks of Nutrients and Sediments in South-East Australia. *J. Hydrol.* 515, 166–179. doi:10.1016/j.jhydrol.2014.04.034

APHA (2005). *Standard Methods for the Examination of Water and Wastewater*. 21st ed. Washington, DC: American Public Health Association (APHA), American Water Works Association (AWWA) and Water Environment Federation-WEF.

Bastviken, D., Cole, J., and PaceTranvik, M. L. (2004). Methane Emissions from Lakes: Dependence of Lake Characteristics, Two Regional Assessments, and a Global Estimate. *Glob. Biogeochem. Cycles* 18, GB4009. doi:10.1029/2004gb002238

Bastviken, D., Tranvik, L. J., Downing, J. A., Crill, P. M., and Enrich-Prast, A. (2011). Freshwater Methane Emissions Offset the Continental Carbon Sink. *Science* 331, 50. doi:10.1126/science.1196808

Beaulieu, J. J., DelSontro, T., and Downing, J. A. (2019). Eutrophication Will Increase Methane Emissions from Lakes and Impoundments During the 21st Century. *Nat. Commun.* 10, 1375. doi:10.1038/s41467-019-09100-5

Berberich, M. E., Beaulieu, J. J., Hamilton, T. L., Waldo, S., and Buffam, I. (2019). Spatial Variability of Sediment Methane Production and Methanogen Communities within a Eutrophic Reservoir: Importance of Organic Matter Source and Quantity. *Limnol. Oceanogr.* 65, 1–23. doi:10.1002/lno.11392

Bianchi, T. S. (2021). The Evolution of Biogeochemistry: Revisited. *Biogeochemistry* 154, 141–181. doi:10.1007/s10533-020-00708-0

Boon, P. I., and Mitchell, A. (1995). Methanogenesis in the Sediments of an Australian Freshwater Wetland: Comparison with Aerobic Decay, and Factors Controlling Methanogenesis. *FEMS Microbiol. Ecol.* 18 (3), 175–190. doi:10.1111/j.1574-6941.1995.tb00175.x

Boudreau, B. P. (1999). Metals and Models: Diagenic Modelling in Freshwater Lacustrine Sediments. *J. Paleolimnol.* 22, 227–251. doi:10.1023/a:1008144029134

Brannon, J. M., Chen, R. L., and Gunnison, D. (1985). "Sediment-Water Interactions and Mineral Cycling in Reservoirs," in *Microbial Processes in Reservoirs*. Editor D. Gunnison (Dordrecht: Springer Netherlands), 121–134. doi:10.1007/978-94-009-5514-1_7

Burford, M. A., Johnson, S. A., Cook, A. J., Packer, T. V., Taylor, B. M., and Townsley, E. R. (2007). Correlations Between Watershed and Reservoir Characteristics, and Algal Blooms in Subtropical Reservoirs. *Water Res.* 41, 4105–4114. doi:10.1016/j.watres.2007.05.053

Burford, M. A., Green, S. A., Cook, A. J., Johnson, S. A., Kerr, J. G., and O'Brien, K. R. (2012). Sources and Fate of Nutrients in a Subtropical Reservoir. *Aquat. Sci.* 74, 179–190. doi:10.1007/s00027-011-0209-4

Deemer, B. R., Harrison, J. A., Li, S., Beaulieu, J. J., DelSontro, T., Barros, N., et al. (2016). Greenhouse Gas Emissions from Reservoir Water Surfaces: A New Global Synthesis. *BioScience* 66, 949–964. doi:10.1093/biosci/biw117

DelSontro, T., Kunz, M. J., Kempter, T., Wüest, A., Wehrli, B., and Senn, D. B. (2011). Spatial Heterogeneity of Methane Ebullition in a Large Tropical Reservoir. *Environ. Sci. Technol.* 45, 9866–9873. doi:10.1021/es2005545

DelSontro, T., Boutet, L., St-Pierre, A., del Giorgio, P. A., and Prairie, Y. T. (2016). Methane Ebullition and Diffusion from Northern Ponds and Lakes Regulated by the Interaction Between Temperature and System Productivity. *Limnol. Oceanogr.* 61, S62–S77. doi:10.1002/lno.10335

DelSontro, T., Beaulieu, J. J., and Downing, J. A. (2018). Greenhouse Gas Emissions from Lakes and Impoundments: Upscaling in the Face of Global Change. *Limnol. Oceanogr. Lett.* 3, 64–75. doi:10.1002/lol2.10073

DES (2018). *Monitoring and Sampling Manual: Environmental Protection (Water) Policy*. Brisbane, Australia: Queensland Department of Environment and Science.

Dowdy, A. J., Mills, G. A., Timbal, B., and Wang, Y. (2013). Changes in the Risk of Extratropical Cyclones in Eastern Australia. *J. Clim.* 26 (4), 1403–1417. doi:10.1175/jcli-d-12-00192.1

Ehrlich, H. L., Newman, D. K., and Kappler, A. (Editors) (2015). *Ehrlich's Geomicrobiology*. 6th ed. (Boca Raton: CRC Press). doi:10.1201/b19121

Etminan, M., Myhre, G., Highwood, E. J., and Shine, K. (2016). Radiative Forcing of Carbon Dioxide, Methane, and Nitrous Oxide: A Significant Revision of the Methane Radiative Forcing. *Geophys. Res. Lett.* 43, 12614–12623. doi:10.1002/2016gl071930

Folk, R. L. (1974). *Petrology of Sedimentary Rocks*. Austin, TX, USA: Hemphill Pub. Co.

Gale, D. (2016). *Diatoms as Indicators of Ecological Change in Freshwater Reservoirs of South East Queensland*. PhD Thesis. Brisbane: School of Civil Engineering, The University of Queensland. doi:10.14264/uql.2016.64

Glass, J. B., and Orphan, V. J. (2012). Trace Metal Requirements for Microbial Enzymes Involved in the Production and Consumption of Methane and Nitrous Oxide. *Front. Microbio.* 3, 61. doi:10.3389/fmicb.2012.00061

Grasset, C., Mendonça, R., Villamor Saucedo, G., Bastviken, D., Roland, F., and Sobek, S. (2018). Large but Variable Methane Production in Anoxic Freshwater Sediment Upon Addition of Allochthonous and Autochthonous Organic Matter. *Limnol. Oceanogr.* 63, 1488–1501. doi:10.1002/lno.10786

Grinham, A., Dunbabin, M., Gale, D., and Udy, J. (2011). Quantification of Ebullitive and Diffusive Methane Release to Atmosphere From a Water Storage. *Atmos. Environ.* 45 (39), 7166–7173. doi:10.1016/j.atmosenv.2011.09.011

Grinham, A., Dunbabin, M., and Albert, S. (2018). Importance of Sediment Organic Matter to Methane Ebullition in a Sub-Tropical Freshwater Reservoir. *Sci. Total Environ.* 621, 1199–1207. doi:10.1016/j.scitotenv.2017.10.108

Günther, G., Lehner, B., Lumsdon, A. E., MacDonald, G. K., Zarfl, C., and Liermann, C. R. (2015). An Index-Based Framework for Assessing Patterns and Trends in River Fragmentation and Flow Regulation by Global Dams at Multiple Scales. *Environ. Res. Lett.* 10, 015001. doi:10.1088/1748-9326/10/1/015001

Harrison, J. A., Prairie, Y. T., Mercier-Blais, S., and Soued, C. (2021). Year-2020 Global Distribution and Pathways of Reservoir Methane and Carbon Dioxide Emissions According to the Greenhouse Gas from Reservoirs (G-Res) Model. *Glob. Biogeochem. Cycles* 35, e2020GB006888. doi:10.1029/2020gb006888

Hubble, T. C. T., Docker, B. B., and Rutherfurd, I. D. (2010). The Role of Riparian Trees in Maintaining Riverbank Stability: A Review of Australian Experience and Practice. *Ecol. Eng.* 36, 292–304. doi:10.1016/j.ecoleng.2009.04.006

Hullebusch, E. D. V., Yekta, S. S., Calli, B., and Fermoso, F. G. (2019). "Biogeochemistry of Major Elements in Anaerobic Digesters: Carbon, Nitrogen, Phosphorus, Sulfur and Iron," in *Trace Elements in Anaerobic Biotechnologies*. Editors F. G. Fermoso, E. D. V. Hullebusch, G. Collins, J. Roussel, A. P. Mucha, and G. Esposito (London, UK: IWA Publishing). doi:10.2166/9781789060225

Huston, R., Chan, Y. C., Gardner, T., Shaw, G., and Chapman, H. (2009). Characterisation of Atmospheric Deposition as a Source of Contaminants in Urban Rainwater Tanks. *Water Res.* 43, 1630–1640. doi:10.1016/j.watres.2008.12.045

Jarrell, K. F., and Kalmokoff, M. L. (1988). Nutritional Requirements of the Methanogenic Archaebacteria. *Can. J. Microbiol.* 34 (5), 557–576. doi:10.1139/m88-095

Jilbert, T., Cowie, G., Lintumäki, L., Jokinen, S., Asmala, E., Sun, X., et al. (2021). Anthropogenic Inputs of Terrestrial Organic Matter Influence Carbon Loading and Methanogenesis in Coastal Baltic Sea Sediments. *Front. Earth Sci.* 9, 716416. doi:10.3389/feart.2021.716416

Johnson, E. R., Inamdar, S., Kan, J., and Vargas, R. (2018). Particulate Organic Matter Composition in Stream Runoff Following Large Storms: Role of POM Sources, Particle Size, and Event Characteristics. *J. Geophys. Res. Biogeosci.* 123, 660–675. doi:10.1002/2017jg004249

Kanakidou, M., Myriokefalitakis, S., Daskalakis, N., Fanourgakis, G., Nenes, A., Baker, A. R., et al. (2016). Past, Present, and Future Atmospheric Nitrogen Deposition. *J. Atmos. Sci.* 73 (5), 2039–2047. doi:10.1175/jas-d-15-0278.1

Kelly, C. A., and Chynoweth, D. P. (1981). The Contributions of Temperature and of the Input of Organic Matter in Controlling Rates of Sediment Methanogenesis. *Limnol. Oceanogr.* 26, 891–897. doi:10.4319/lo.1981.26.5.0891

Kemp, J., Olley, J., and Capon, S. (2019). "An Environmental History of Moreton Bay Hinterlands," in *Moreton Bay Quandamooka & Catchment: Past, Present, and Future*. Editors I. R. Tibbetts, P. C. Rothlisberg, D. T. Neil, T. A. Homburg, D. T. Brewer, and A. H. Arthington (Brisbane, Australia: The Moreton Bay Foundation).

Maeck, A., DelSontro, T., McGinnis, D. F., Fischer, H., Flury, S., Schmidt, M., et al. (2013). Sediment Trapping by Dams Creates Methane Emission Hot Spots. *Environ. Sci. Technol.* 47 (15), 8130–8137. doi:10.1021/es4003907

Michalak, A. M. (2016). Study Role of Climate Change in Extreme Threats to Water Quality. *Nature* 535, 349–350. doi:10.1038/535349a

Morris, G., and Fan, J. (1998). *Reservoir Sedimentation Handbook: Design and Management of Dams, Reservoirs and Watersheds for Sustainable Use*. London, UK: McGraw-Hill.

NATA (2021). Environmental Analysis Laboratory - Office of Research. Southern Cross University Accreditation Number 14960. Available at: https://nata.com.au/find-organisation/ (Accessed December, 2021).

O'Brien, K. R., Weber, T. R., Leigh, C., and Burford, M. A. (2016). Sediment and Nutrient Budgets Are Inherently Dynamic: Evidence from a Long-Term Study of Two Subtropical Reservoirs. *Hydrol. Earth Syst. Sci.* 20, 4881–4894. doi:10.5194/hess-20-4881-2016

O'Sullivan, C. A., Burrell, P. C., Clarke, W. P., and Blackall, L. L. (2005). Structure of a Cellulose Degrading Bacterial Community During Anaerobic Digestion. *Biotechnol. Bioeng.* 92 (7), 871–878. doi:10.1002/bit.20669

Owen, W. F., Stuckey, D. C., Healy, J. B., Young, L. Y., and McCarty, P. L. (1979). Bioassay for Monitoring Biochemical Methane Potential and Anaerobic Toxicity. *Water Res.* 13 (6), 485–492. doi:10.1016/0043-1354(79)90043-5

QLUMP (2018). Queensland Land Use Mapping Program (QLUMP) of the Department of Science, Information Technology and Innovation (DSITI). Available at: https://www.qld.gov.au/environment/land/vegetation/mapping/qlump (Accessed October, 2021).

Raposo, F., De la Rubia, M. A., Fernández-Cegrí, V., and Borja, R. (2012). Anaerobic Digestion of Solid Organic Substrates in Batch Mode: An Overview Relating to Methane Yields and Experimental Procedures. *Renew. Sustain. Energy Rev.* 16 (1), 861–877. doi:10.1016/j.rser.2011.09.008

Rayment, G. E., and Lyons, D. J. (2010). *Soil Chemical Methods - Australasia*. Melbourne, Australia: CSIRO Publishing.

Rigosi, A., Hanson, P., Hamilton, D. P., Hipsey, M., Rusak, J. A., Bois, J., et al. (2015). Determining the Probability of Cyanobacterial Blooms: The Application of Bayesian Networks in Multiple Lake Systems. *Ecol. Appl.* 25, 186–199. doi:10.1890/13-1677.1

Rosentreter, J. A., Borges, A. V., Deemer, B. R., Holgerson, M. A., Liu, S., Song, C., et al. (2021). Half of Global Methane Emissions Come From Highly Variable Aquatic Ecosystem Sources. *Nat. Geosci.* 14, 225–230. doi:10.1038/s41561-021-00715-2

Sinha, E., Michalak, A. M., and Balaji, V. (2017). Eutrophication Will Increase During the 21st Century as a Result of Precipitation Changes. *Science* 357 (6349), 405–408. doi:10.1126/science.aan2409

Sperazza, M., Moore, J. N., and Hendrix, M. S. (2004). High-Resolution Particle Size Analysis of Naturally Occurring Very Fine-Grained Sediment Through Laser Diffractometry. *J. Sediment. Res.* 74, 736–743. doi:10.1306/031104740736

Takashima, M., Speece, R. E., and Parkin, G. F. (1990). Mineral Requirements for Methane Fermentation. *Crit. Rev. Environ. Control* 19 (5), 465–479. doi:10.1080/10643389009388378

Tipping, E., Benham, S., Boyle, J. F., Crow, P., Davies, J., Fischer, U., et al. (2014). Atmospheric Deposition of Phosphorus to Land and Freshwater. *Environ. Sci. Process. Impacts* 16, 1608–1617. doi:10.1039/c3em00641g

Tittel, J., Hüls, M., and Koschorreck, M. (2019). Terrestrial Vegetation Drives Methane Production in the Sediments of Two German Reservoirs. *Sci. Rep.* 9, 15944. doi:10.1038/s41598-019-52288-1

Tonin, A. M., Gonçalves, J. F., Bambi, P., Couceiro, S. R. M., Feitoza, L. A. M., Fontana, L. E., et al. (2017). Plant Litter Dynamics in the Forest-Stream Interface: Precipitation Is a Major Control Across Tropical Biomes. *Sci. Rep.* 7, 10799. doi:10.1038/s41598-017-10576-8

van Langenhove, L., Verryckt, L. T., Bréchet, L., Courtois, E. A., Stahl, C., Hofhansl, F., et al. (2020). Atmospheric Deposition of Elements and its Relevance for Nutrient Budgets of Tropical Forests. *Biogeochemistry* 149, 175–193. doi:10.1007/s10533-020-00673-8

van Rijn, L. C. (2012). *Principles of Sedimentation and Erosion Engineering in Rivers, Estuaries and Coastal Seas*. Netherlands: Aqua Publications.

Wang, T., Li, Z., Chen, X., and Long, X.-E. (2019). Effects of Nickel and Cobalt on Methane Production and Methanogen Abundance and Diversity in Paddy Soil. *PeerJ* 7, e6274. doi:10.7717/peerj.6274

West, W. E., Creamer, K. P., and Jones, S. E. (2016). Productivity and Depth Regulate Lake Contributions to Atmospheric Methane. *Limnol. Oceanogr.* 61, S51–S61. doi:10.1002/lno.10247

Xu, N., Liu, S., Xin, F., Zhou, J., Jia, H., Xu, J., et al. (2019). Biomethane Production from Lignocellulose: Biomass Recalcitrance and Its Impacts on Anaerobic Digestion. *Front. Bioeng. Biotechnol.* 7, 191. doi:10.3389/fbioe.2019.00191

Zar, J. H. (1984). *Biostatistical Analysis*. USA: Prentice-Hall.

Zarfl, C., Lumsdon, A. E., Berlekamp, J., Tydecks, L., and Tockner, K. (2015). A Global Boom in Hydropower Dam Construction. *Aquat. Sci.* 77, 161–170. doi:10.1007/s00027-014-0377-0

Zerkle, A. L., House, C. H., and Brantley, S. L. (2005). Biogeochemical Signatures Through Time as Inferred from Whole Microbial Genomes. *Am. J. Sci.* 305 (6-8), 467–502. doi:10.2475/ajs.305.6-8.467

Conflict of Interest: Authors KS and DG were employed by Seqwater.

The remaining authors declare that the research was conducted in the absence of any commercial or financial relationships that could be construed as a potential conflict of interest.

Publisher's Note: All claims expressed in this article are solely those of the authors and do not necessarily represent those of their affiliated organizations, or those of the publisher, the editors and the reviewers. Any product that may be evaluated in this article, or claim that may be made by its manufacturer, is not guaranteed or endorsed by the publisher.

Copyright © 2022 Grinham, O'Sullivan, Dunbabin, Sturm, Gale, Clarke and Albert. This is an open-access article distributed under the terms of the Creative Commons Attribution License (CC BY). The use, distribution or reproduction in other forums is permitted, provided the original author(s) and the copyright owner(s) are credited and that the original publication in this journal is cited, in accordance with accepted academic practice. No use, distribution or reproduction is permitted which does not comply with these terms.

frontiers | Frontiers in Environmental Science

BRIEF RESEARCH REPORT
published: 23 June 2022
doi: 10.3389/fenvs.2022.892339

Physical Factors and Microbubble Formation Explain Differences in CH_4 Dynamics Between Shallow Lakes Under Alternative States

Sofia Baliña[1], Maria Laura Sánchez[1] and Paul A. del Giorgio[2]*

[1]Departamento de Ecología, Genética y Evolución, Facultad de Ciencias Exactas y Naturales, Universidad de Buenos Aires. Instituto de Ecología, Genética y Evolución de Buenos Aires (IEGEBA - CONICET/UBA), Ciudad Autónoma de Buenos Aires, Argentina, [2]Département des science biologiques, Université du Québec à Montréal, Montréal, QC, Canada

Submerged macrophytes play a key role in maintaining clear vegetated states in shallow lakes, but their role on methane (CH_4) dynamics is less explored. They might enhance methanogenesis by providing organic matter but they can also supply oxygen to the sediments increasing methanotrophy. They may also affect gas exchange by diminishing wind turbulence in the water column. We previously measured seasonal CO_2 and CH_4 partial pressure (pCO_2 and pCH_4) and diffusive fluxes from two clear vegetated and two turbid algal shallow lakes of the Pampean Plain, Argentina, and we reported that clear lakes had higher mean annual pCH_4 despite states having similar mean annual CH_4 diffusive flux. In this study we explore the contribution of physical and biological factors regulating surface pCH_4. Mean annual CH_4 diffusive fluxes and CH_4 fraction of oxidation (F_{ox}) were similar between states, implying a comparable mean annual CH_4 input. kCH_4 was significantly higher than kCO_2, suggesting occurrence of CH_4 microbubbles, yet kCH_4 was higher in turbid lakes than in clear lakes, implying a higher microbubble formation in turbid lakes. Furthermore, in turbid lakes there were positive relationships between k and wind speed, and between k and pCH_4, yet in clear lakes these relations were absent. Results suggest that submerged vegetation suppresses wind induced turbulence in clear vegetated lakes, decoupling kCH_4 from wind and reducing microbubble formation, therefore augmenting pCH_4 in their surface waters. Overall, physical rather than biological factors appear to control the observed differences in pCH_4 between states.

Keywords: methane, submerged macrophytes, gas exchange, microbubbles, turbulence, methane oxidation

OPEN ACCESS

Edited by:
Daniel F. McGinnis, Université de Genève, Switzerland

Reviewed by:
Baoli Wang, Tianjin University, China
Francois Clayer, Norwegian Institute for Water Research (NIVA), Norway

****Correspondence:***
Sofia Baliña
sofiabalinia@gmail.com

Specialty section:
This article was submitted to Biogeochemical Dynamics, a section of the journal Frontiers in Environmental Science

Received: *08 March 2022*
Accepted: *30 May 2022*
Published: *23 June 2022*

Citation:
Baliña S, Sánchez ML and del Giorgio PA (2022) Physical Factors and Microbubble Formation Explain Differences in CH_4 Dynamics Between Shallow Lakes Under Alternative States. Front. Environ. Sci. 10:892339. doi: 10.3389/fenvs.2022.892339

INTRODUCTION

Freshwater systems are a significant component of the global carbon cycle (Tranvik et al., 2018) and they emit substantial amounts of methane (CH_4) to the atmosphere (Bastviken et al., 2011). Within freshwater systems, shallow lakes are considered to be biogeochemical hot spots and are distributed worldwide (Downing 2010; Holgerson and Raymond 2016). In some regions, shallow lakes can present two contrasting states: a clear water state dominated by submerged macrophytes, with low turbidity and low phytoplankton biomass, and a turbid water state dominated by phytoplankton, with high turbidity and no submerged vegetation (Scheffer et al., 1993; Sánchez et al., 2015). Submerged vegetation plays a key role in maintaining clear vegetated states by preventing sediment

resuspension, by taking up nutrients from the water column, and by providing refuge for zooplankton, among others (Scheffer 2001; Hilt 2015). Their presence can also affect other processes, such as primary production, carbon burial rates and greenhouse gas (GHG) emissions (Hilt et al., 2017). In particular, the effect of submerged vegetation or phytoplankton on CH_4 dynamics is not well understood (Hilt et al., 2017). Submerged vegetation can enhance methanogenesis by providing macrophyte-derived carbon to the sediments (Emilson et al., 2018; Grasset et al., 2019), but phytoplankton-derived carbon has also been reported to enhance methanogenesis in sediments (Schwarz et al., 2008; West et al., 2012). Similarly, alternative states could have a differential effect on methane oxidation (MOX). The activity of methane oxidizing bacteria (MOB) depends mainly on, O_2 concentration and light penetration, where lower O_2 concentrations in combination with a reduction of light favors methanotrophs (Thottathil et al., 2018). Both submerged vegetation and phytoplankton can generate high oxygen concentrations and they can also diminish light penetration in the water column (Torremorell et al., 2009; Andersen et al., 2017). At the same time, it has been shown that submerged vegetation diminishes wind induced turbulence in the water column (Herb and Stefan 2005; Andersen et al., 2017), which could have a physical effect on gas exchange with the atmosphere, and this effect is not present in turbid phytoplanktonic lakes. Thus, it is not straightforward to predict potential biological—methanogenesis and methanotrophy—and physical - gas exchange with the atmosphere and also vertical and horizontal transport - differences in CH_4 dynamics between clear vegetated and turbid algal shallow lakes.

In a previous study we reported that clear vegetated shallow lakes from the Pampean Plain of Argentina had higher mean annual surface water CH_4 partial pressure (pCH_4) in comparison with turbid algal lakes (Baliña et al. under revision). However, we also reported that clear and turbid lakes presented similar mean annual CH_4 diffusive fluxes. The average CH_4 concentration in the water is the net balance between the rates of input to the water column, oxidation within the water column, and outflux to the atmosphere (Vachon et al., 2019; Noyce and Megonigal, 2021). Given that the average fluxes to the atmosphere were similar between states (Baliña et al. under revision), the differences in average pCH_4 could be the result of a physical effect due to differences in gas exchange, potentially combined with a biological effect, due to differences in the net balance between input and oxidation in the water column between the two states. CH_4 can be emitted from surface waters by diffusive flux, a strictly fickian process which depends on the concentration gradient at the water-air interface and the gas exchange velocity (k) and, in some cases, CH_4 can also be emitted in the form of microbubbles (Bastviken et al., 2004; Beaulieu et al., 2012). If CH_4 microbubbles are present, they can generate an additional flux of CH_4 to the atmosphere which will lead to increased measured k that is difficult to distinguish from that of purely diffusive k, and to a decoupling between CH_4 and CO_2 exchange velocities (Beaulieu et al., 2012; Prairie and del Giorgio 2013; McGinnis et al., 2015). This is a CH_4 emission pathway that is thought to relate positively to both water column turbulence and surface water CH_4 concentration (Prairie and del Giorgio 2013; McGinnis et al., 2015; Tang et al., 2016), yet it is currently difficult to predict whether these two contrasting lake states may be associated with an increased incidence of microbubbles.

In this study we assess both biological and physical factors influencing ambient surface pCH_4 in these shallow lakes: as biological factors, we explored potential differences in overall CH_4 oxidation between clear vegetated and turbid algal lakes, and by combining the patterns of oxidation and diffusive flux we infer potential differences in CH_4 input between states. As physical factors, we explored potential differences in kCH_4 between clear vegetated and turbid algal shallow lakes and also possible differences in the relationship between kCH_4 and wind, and between kCH_4 and pCH_4. In addition, we compared the patterns of kCO_2 and kCH_4 to infer differences in CH_4 microbubble dynamics between the two states.

MATERIALS AND METHODS

Study Area and Design

This study was carried out in the Pampean Plain (Buenos Aires, Argentina), a region with an exceptionally flat landscape that has a mean annual precipitation of 935 mm and mean annual temperature of 15.3°C (Allende et al., 2009). This region is characterized by the presence of hundreds of thousands of shallow lakes (Geraldi et al., 2011) that are eutrophic to hypereutrophic, polymictic (Diovisalvi et al., 2015), and that can be mostly found under two alternative states: a clear vegetated state dominated by submerged macrophytes, and a turbid algal state dominated by phytoplankton (Allende et al., 2009). For this study, we used data collected from four shallow lakes of the Pampean Plain: two in a clear vegetated state dominated by submerged macrophytes—La Segunda (SG) and Kakel Huincul (KH)—and other two in a turbid algal state, dominated by phytoplankton and with no submerged macrophytes—El Burro (BU) and La Salada Monasterio (SA) - (**Figure 1**). Lakes were sampled seasonally between 2018 and 2019, in winter (11–25 June 2018), spring (16–23 October 2019), summer (3–7 February 2019) and autumn (22–30 April 2019). In each field campaign physical, chemical, and biogeochemical parameters were measured (see specific parameters and related details below).

Baliña et al. (under revision) presented the environmental background data, pCH_4 and pCO_2, and flux data obtained for these lakes during the above-mentioned campaigns. Here we focus on the patterns of kCH_4 and kCO_2 derived from those diffusive fluxes and surface water pCH_4 and pCO_2, as well as on the isotopic signature of the surface water CH_4, which was used to derive CH_4 oxidation extent. Below we provide a summary of the methods used to obtain the surface water gas concentrations and diffusive fluxes (further details can be found in Baliña et al. (under revision)) and also the methods used to obtain the gas exchange velocities, the isotopic signature of surface water CH_4 and fresh CH_4 bubbles, and the calculation of CH_4 fraction of oxidation. Background information of the studied lakes can be found in **Supplementary Table S1**.

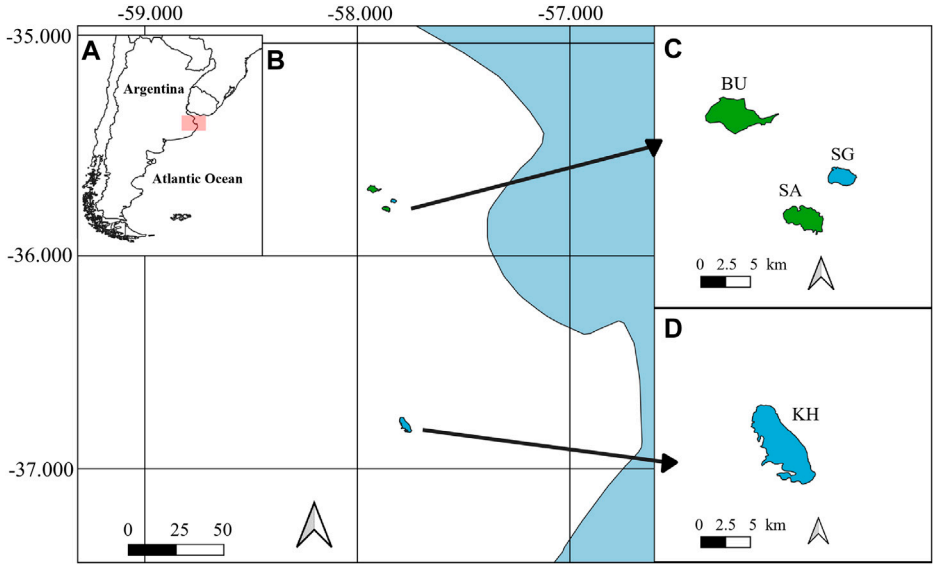


FIGURE 1 | (A) Map of Argentina, in red the study area. **(B)** Study area and the four studied shallow lakes. **(C)** La Segunda (SG), La Salada Monasterio (SA), El Burro (BU) and **(D)** Kakel Huincul (KH). Lakes in green correspond to the turbid algal lakes, whereas lakes in blue correspond to the clear vegetated lakes.

Environmental Parameters

In each shallow lake we measured surface water temperature and dissolved oxygen using a multi parameter HACH HQ30D portable sensor (HACH, United States). We also measured air temperature, atmospheric pressure, and wind speed using a Kestrel (4,000 Pocket Weather Tracker, Nielsen-Kellerman).

CH_4 and CO_2 Dissolved in the Water and Their Isotopic Signature

We took samples of surface waters to determine CH_4 and CO_2 partial pressure (p) in the water using the headspace technique, as described in Baliña et al. (under revision). Briefly, we filled two 60 ml syringes with 30 ml of water and 30 ml of atmospheric air, creating a 1:1 ratio of water: air. The syringes were then shaken for 2 min to ensure equilibration of the gas between the two phases. After equilibration, the 30 ml of air in the syringe were injected into a 30 ml glass pre-evacuated vial equipped with a crimped rubber stopper (Exetainer, Labco) for subsequent analysis in a cavity ringdown spectrometer (CRDS, Picarro G2201-i) (Maher et al., 2013) that determines pCH_4 and pCO_2 along with $\delta^{13}C$- CH_4 isotopic signature. To obtain the original p and isotopic signature of the CH_4 in the water, these data were subsequently corrected for the ambient air pCO_2 and pCH_4, the headspace ratio, *in situ* temperature of the water, water temperature after equilibration of the gas, the atmospheric pressure and the isotopic fractionation in the liquid:gas interface (Soued and Prairie 2020). pCH_4 and pCO_2 are reported as parts per million in volume (ppmv) and CH_4 isotopic data are reported in the standard delta notation (δ) expressed in per mil (‰) relative to the Vienna Pee Dee Belemnite standard (Whiticar 1999).

Diffusive Flux

Diffusive fluxes of CH_4 and CO_2 at the water-air interface were measured using a floating chamber (volume = 18.8 L, area = 0.1 m^2) equipped with a valve that allows to sample the chamber headspace, and also with an internal thermometer to track headspace temperature. We took samples from the chamber headspace at intervals of 5 min for 15 min, obtaining four time points. At each time point, we took two samples of air that were injected into 30 ml glass pre-evacuated vials equipped with crimped rubber stoppers (Exetainer, Labco), for subsequent analysis in a cavity ringdown spectrometer (CRDS, Picarro G2201-i). At each sampling time we also registered temperature. The diffusive flux of each gas (*Flux gas*) was determined in mmol m^{-2} d^{-1} following **Eq. 1**:

$$Flux\ gas = \left(\frac{s*V}{mV*A}\right)*t \quad (1)$$

Where s is the accumulation rate of gas in the chamber (ppmv min^{-1}), V is the volume of the chamber (L), mV is the molar volume of the gas (L $mmol^{-1}$) - which is corrected for the temperature in the chamber -, A is the chamber surface area (m^2), and t is a factor that converts minutes to days (1 day = 1,440 min) (DelSontro et al., 2016).

Isotopic Signature of Fresh Methane Bubbles

We captured fresh CH_4 bubbles to estimate the isotopic signature of fresh CH_4 that we subsequently used as a source endmember in the oxidation mass balance. We used an inverted funnel (area = 0.3 m^2) tied to a floating device that was deployed in the water. A glass bottle was filled with water from the lake and screwed to the

neck of the funnel. After this, sediments were stirred using an oar, causing the liberation of fresh CH_4 bubbles from the sediment through the water column and into the bottle (**Supplementry Figure S1**). We took two 30 ml air samples from the headspace that was generated in bottle and injected this air into 30 ml glass pre-evacuated vials equipped with crimped rubber stoppers (Exetainer, Labco), for subsequent analysis in a cavity ringdown spectrometer (CRDS, Picarro G2201-i). We determined δ^{13}C-CH_4 signature, as described for the gas dissolved in the water.

Estimation of the Extent of Water Column CH_4 Oxidation (F_{ox})

To explore possible differences in CH_4 oxidation between clear vegetated and turbid algal shallow lakes, we performed isotopic mass balances using two different models: a steady state open model (**Eq. 2**; Happell et al., 1994) and a non-steady state closed model (**Eq. 3**; Liptay et al., 1998). These models estimate a fraction of oxidation (F_{ox}) based on different assumptions. The first model assumes a steady state system whereas the second considers that the water body may be in a dynamic, not at steady state condition (Thottathil et al., 2018).

$$F_{ox} = \frac{(\delta^{13}C_{WT} - \delta^{13}C_{source})}{(\alpha - 1)*1000} \quad (2)$$

$$ln(1 - F_{ox}) = \frac{(ln(\delta^{13}C_{source} + 1000) - ln(\delta^{13}C_{WT} + 1000))}{(\alpha - 1)} \quad (3)$$

$\delta^{13}C_{source}$ is the isotopic signature of the source of methane, in this case the isotopic signature of the fresh CH_4 bubbles; $\delta^{13}C_{WT}$ is the isotopic signature of the CH_4 within the water column; and α is the isotopic fractionation factor related to microbial CH_4 oxidation. We used a value of $\alpha = 1.021$ following Coleman et al. (1981) and Thottathil et al. (2018). Additionally, we also calculated F_{ox} using values of $\alpha = 1.005$ and $\alpha = 1.031$ (Alperin et al., 1988; Whiticar 1999; Clayer et al., 2018) to better qualify the uncertainty around the selected α value, which is an intermediate value within the mentioned range.

Exchange Velocities Derived From Flux Measurements

The gas exchange velocity (k) is a rate equivalent to the depth of the water column that is equilibrated with the atmosphere per unit time (Prairie and del Giorgio 2013). This parameter was obtained using the measurements of diffusive flux and of gas dissolved in the surface waters, following **Eq. 4**:

$$k = \frac{Flux\ gas}{Kh*\Delta pGas} \quad (4)$$

Where *Flux gas* is the diffusive flux for CH_4 or CO_2 determined using **Eq. 1** (mmol $m^{-2}\,d^{-1}$), *Kh* is the Henry's constant correspondent to each gas corrected for atmospheric pressure and water temperature, and $\Delta pGas$ is the difference between the partial pressure of the respective gas in the water (P_w) and the partial pressure of the gas in equilibrium with the atmosphere (P_{eq}), i.e., $\Delta pGas\,(ppmv) = Pw - Peq$.

In order to allow comparison between gas exchange velocities, individual $k$$CH_4$ and $k$$CO_2$ were standardized to a Schmidt number of 600, following **Eq. 5**:

$$k_{600} = \frac{k_{CO2\ or\ CH4}}{(Sc_{CO2 or CH4}/600)^{-n}} \quad (5)$$

Where *Sc* is the Schmidt number of a given gas at a given temperature (Wanninkhof 1992), and n is a value that depends on wind speed. We used a value of n = 2/3 for ambient wind speeds <3.7 m s^{-1} and of n = 1/2 for ambient wind speeds >3.7 m s^{-1} (Guérin et al., 2007).

Statistical Analyses

To explore differences in mean annual CH_4 F_{ox} between states, we used a mixed generalized linear model with one fixed factor (state) and two random factors (season and lake). Since F_{OX} is a fraction we used the Beta distribution, which has a fixed domain between 0 and 1. We tested differences between k_{600} CO_2 and k_{600} CH_4 using a mixed general linear model with one fixed factor (gas, CO_2 or CH_4) and two random factors (season and lake). To test differences between states in k_{600} derived from CH_4 and k_{600} derived from CO_2, we used a mixed general linear model with one fixed factor (state) and two random factors (season and lake). To explore relations between k_{600} CH_4 vs. wind, k_{600} CH_4 vs. $p$$CH_4$, and k_{600} CO_2 vs. wind, we performed simple linear regressions for each state, including in all cases two random factors (season and lake).

We tested the assumptions for each model: for the F_{ox} model we analyzed the distribution of standardized residuals vs. predicted values to explore homogeneity of variances. For the rest of the models, residuals were tested to fit the assumptions of normality and homogeneity of variances. The F_{ox} model was carried out using the package "glmmTMB" (Brooks et al., 2017). The rest of the models were done using package "lmerTest 3.1-2" (Kuznetsova et al., 2017). Normality was checked with package "Stats 3.6.2" (Royston 1982) and homogeneity of variances was checked by exploring the relation between standardized residuals vs. predicted values and also with package "Car 3.0-8" (Fox and Sanford., 2018). If homogeneity of variances was not fulfilled, we modeled heteroscedasticity by means of three different functions: varIdent, varPower and varExp (Zuur et al., 2009) using package nlme 3.1-142 (Jose et al., 2019). All tests were performed at the 95% significance level using R version 3.6.2 in the RStudio environment version 1.2.5019 (R Core Team 2019). Figures were plotted with the package "ggplot2 3.3.2" (Hadley, 2016).

RESULTS

Clear vegetated lakes had three-fold higher mean annual $p$$CH_4$ than turbid algal lakes (1,181.7 ± 1,375.8 ppmv and 358.9 ± 390.4 ppmv, respectively) (p = 0.002, df = *1*, F = 10.6; **Figure 2A**; data from Baliña et al. (under revision)).

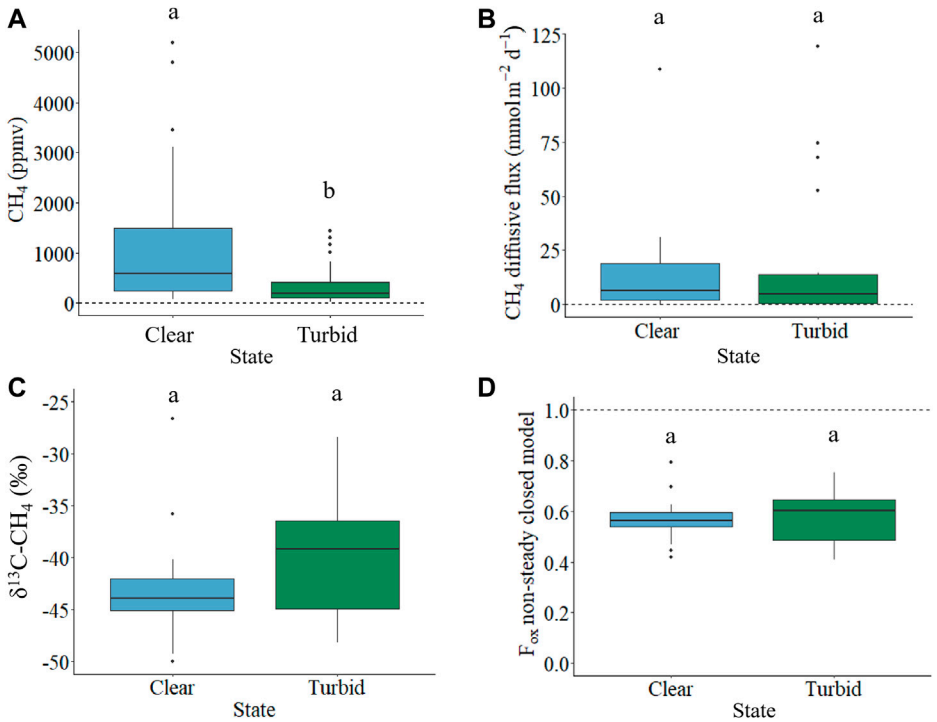


FIGURE 2 | (A) Mean annual surface water pCH_4 dissolved (ppmv), **(B)** mean annual CH_4 diffusive flux (mmol m^{-2} d^{-1}), **(C)** mean annual CH_4 isotopic signature (‰) and **(D)** mean annual Fraction of oxidation (F_{ox}) obtained with the non-steady closed model, of clear vegetated (blue) and turbid algal (green) shallow lakes, respectively. Different letters (a and b) imply significant differences between states within the respective panels. The dashed line in panel **(A)** corresponds to the mean annual atmospheric CH_4 partial pressure (1.71 ppmv), in panel **(B)** corresponds to a zero CH_4 diffusive flux and in panel **(D)** corresponds to an oxidation of 100%.

Nonetheless, clear vegetated and turbid algal lakes had similar mean annual CH_4 diffusive fluxes (14.4 ± 24.2 and 19.9 ± 33.5 mmol m^{-2} d^{-1}, respectively) (**Figure 2B**; data from Baliña et al. (under revision)). Mean annual $\delta^{13}C$-CH_4 was similar between clear vegetated and turbid algal shallow lakes and in both states and the isotopic signatures corresponded to enriched values related to fresh sediment CH_4 (**Figure 2C** and **Supplementary Table S2**). Our estimates of mean annual CH_4 fraction of oxidation (F_{ox}), obtained using the non-steady state closed model and assuming an average fractionation (α) of 1.021, were also very similar between clear vegetated and turbid algal lakes (average 0.57 ± 0.09 and 0.58 ± 0.11, respectively; **Figure 2C**). The steady state open model was not appropriate for these systems, since in a significant number of cases it yielded F_{ox} values higher than one (**Supplementary Figure S2**), as has been observed in other studies (Bastviken et al., 2002; Barbosa et al., 2018; Thottathil et al., 2018). Using α = 1.005 we obtained nonsensical F_{ox} values for both closed and open models, whereas using α = 1.031 we obtained logical F_{ox} values for both closed and open models that were in the range of the results obtained with α of 1.021 (**Supplementary Figure S3**).

There was a large range in measured k_{600} values based on either CO_2 or CH_4 across lakes (from 0.3 to 59.8 m d^{-1}), and although both agreed well for approximately 32% of observations, there was a high proportion of points that deviated significantly from the expected 1:1 relationship, and most of these points corresponded to turbid shallow lakes (**Figure 3**). The overall mean annual k_{600} CH_4 (12.7 ± 15.1 m d^{-1}) was significantly (6.4 times) higher than mean annual k_{600} CO_2 (1.98 ± 1.43 m d^{-1}), (p < 0.0001, df = *1*, F =

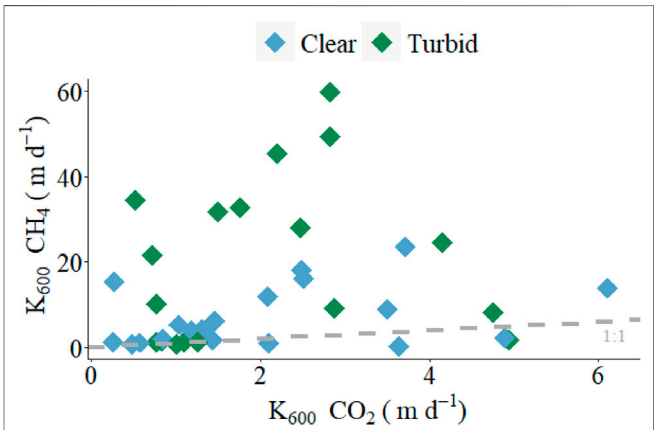


FIGURE 3 | Linear regression between k_{600} CH_4 (m d^{-1}) and k_{600} CO_2 (m d^{-1}). The dashed line represents the expected 1:1 relation between standardized exchange velocities. Blue diamonds correspond to clear vegetated lakes and green diamonds correspond to turbid algal lakes.

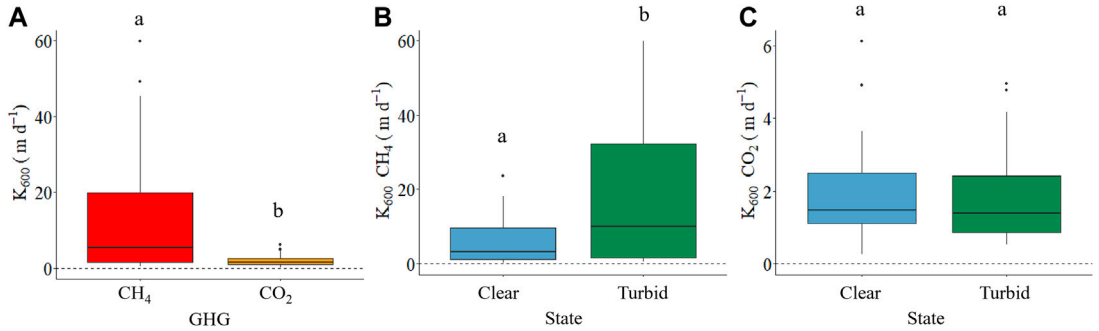


FIGURE 4 | Overall k_{600} of CH_4 and CO_2: (m d-1) **(A)**, k_{600} CH_4 (m d-1) for clear vegetated and turbid algal lakes **(B)** and k_{600} CO_2 (m d-1) for clear and turbid lakes **(C)**. Different letters (a and b) imply significant differences. The dotted line in the three panels corresponds to a zero-exchange velocity.

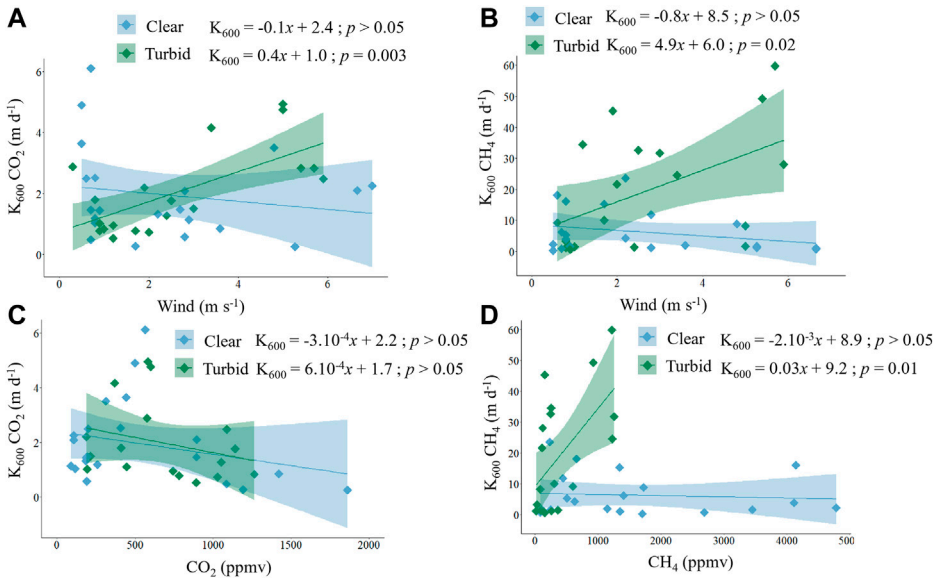


FIGURE 5 | Linear regressions between **(A)** k_{600} CH_4 and wind, **(B)** k_{600} CO_2 and wind, **(C)**k_{600} CH_4 and pCH_4, and **(D)** k_{600} CO_2 and pCO_2. Blue diamonds correspond to clear vegetated lakes while green diamonds correspond to turbid algal lakes. The shade corresponds to the standard error of the respective linear models and *p* values correspond to the slope of the regression model.

19.7; **Figure 4A**). There were also differences between states in the patterns of gas exchange: mean annual k_{600} CH_4 was 3 times higher in turbid lakes (19.3 ± 18.9 m d^{-1}) than in clear lakes (6.7 ± 7.0 m d^{-1}) (p = 0.0092, df = *1*, F = 7.5, **Figure 4B**), whereas mean annual k_{600} CO_2 was similar between clear and turbid lakes (2.0 ± 1.5 m d^{-1} and 2.0 ± 1.4 m d^{-1}, respectively, **Figure 4C**).

We explored the relationships between K_{600} and wind speed and also between K_{600} and CH_4 and CO_2 partial pressure in the water, separately for clear vegetated and turbid algal lakes. Mean annual wind speed was similar between clear vegetated and turbid algal lakes (**Supplementary Figure S4**). There was a significant positive relationship between k_{600} CO_2 and wind speed (**Figure 5A**) and also between k_{600} CH_4 and wind speed (**Figure 5B**), but in both cases these relationships were present only for turbid algal lakes and were not significant for clear vegetated lakes. These two relationships with wind in turbid lakes, however, are strikingly different: the slope of the k_{600} CH_4 vs. wind relationship (4.9 ± 1.9) is one order of magnitude higher than that of k_{600} CO_2 (0.4 ± 0.1), and the intercepts are significantly different as well (6 ± 7.7 vs. 1 ± 0.5, respectively). Regarding dissolved GHG, pCO_2 was weakly and negatively related to k_{600} CO_2 in both clear vegetated and turbid algal shallow lakes, and the relationship was similar for both states (**Figure 5C**). Likewise, there was a weak (but not significant) negative relationship between ambient pCH_4 and k_{600} CH_4 in clear vegetated lakes yet, interestingly, there was a strong significant positive relationship between pCH_4 and k_{600} CH_4 in turbid algal lakes (**Figure 5D**).

DISCUSSION

Surface water δ^{13}C-CH_4 corresponded to enriched methane in both clear vegetated and turbid algal shallow lakes (between −50‰ and −25‰), followed by also similar percentages of CH_4 oxidation (mean of 57%) and, therefore, implying a high methanotrophic activity in both states. A comparable range of δ^{13}C-CH_4 was reported for a subtropical shallow wetland from Australia (−53 and −39‰, Jeffrey et al., 2019) and a shallow Boreal lakes (−60 and −35‰, Desrosiers et al., 2021). A wider range of F_{ox}, also obtained using a non-steady state model, was reported for different habitat types within a shallow boreal lake (Desrosiers et al., 2021), with values ranging from 34% to 56% in *Brasenia* and *Typha* dominated habitats and down to 31% in open water areas. A wide range has also been reported for subtropical (15%–36%, Jeffrey et al., 2019), tropical (34%–100%; Barbosa et al., 2018), boreal (57%–75%; Bastviken et al., 2002) and temperate lakes (2%–97%; Thottathil et al., 2018) of varying size. This broad range of F_{ox} both within and across aquatic systems, highlights the complexity in the regulation of CH_4 oxidation. In this regard, the convergence in annual average F_{ox} between clear vegetated and turbid algal lakes despite their contrasting environmental conditions is remarkable.

Although there was significant seasonal variability in pCH_4 in both clear vegetated and turbid algal lakes (Baliña et al. (under revision)), this variation was centered around very different mean annual pCH_4 values for each state. Assuming that these annual means reflect an average steady state partial pressure of each lake state and are not varying greatly, then the amount of CH_4 exchanged at the water-air interface on an annual basis reflects the total CH_4 input to the water column (which includes CH_4 production in the sediments and water column, as well as lateral input) minus the CH_4 oxidized. Considering that annually the fraction of oxidation and the rates of diffusive flux were similar between states, we can infer that on an annual basis CH_4 input would be rather comparable between clear vegetated and turbid algal shallow lakes. CH_4 production in the sediments depends mainly on temperature, oxygen concentration and on the amount and type of organic matter (Megonigal et al., 2003; Duc et al., 2010). Both macrophyte and phytoplankton derived organic matter are known to favor methanogenesis (Emilson et al., 2018; Yan et al., 2019), but the extent to which the dominance of these different sources of organic matter may condition carbon cycling and methanogenesis at the ecosystem level is not well understood, with few studies having assessed this impact (Brothers et al., 2013). Although in this study we do not explicitly address CH_4 production, these results imply a comparable mean annual CH_4 input between clear vegetated and turbid algal states, which could be plausible since the characteristics of both states seem to favor sediment methanogenesis. Independent of sediment production, several authors have demonstrated that there is also a significant potential for CH_4 production in the water column (Grossart et al., 2011; Bogard et al., 2014; Günthel et al., 2019). Whereas there are studies that have explored possible isotopic signatures for this CH_4 (Günthel et al., 2020; Hartmann et al., 2020), there is to date no clear information of what the isotopic signature of this fresh pelagic CH_4 could be. Therefore, we could not include this source of CH_4 in the isotopic mass balance. Nonetheless, we consider that for the purpose of the present study it is sufficient to include a sedimentary methane source to derive a first order estimate of oxidation extent.

In our study, k_{600} CH_4 was 6.4 times higher than k_{600} CO_2. Previous studies have reported k_{600} CH_4 to be on average 1.8-fold higher than k_{600} CO_2 in two boreal lakes (Rantakari et al., 2015), 2.3-fold higher in a Canadian hydroelectric reservoir and boreal lakes (Prairie and del Giorgio 2013), 2.5-fold times higher in oligotrophic Lake Stechlin (McGinnis et al., 2015), and 2.5-fold higher in a tropical reservoir from Brazil (Paranaíba et al., 2018). In all cases, the differences between CH_4 and CO_2 exchange velocities were explained by the presence of CH_4 microbubbles, which result in a k_{600} CH_4 that is higher than that from diffusive exchange alone (Beaulieu et al., 2012; Prairie and del Giorgio 2013) and, therefore, generates a decoupling between k_{600} CH_4 and k_{600} CO_2 (Prairie and del Giorgio 2013; McGinnis et al., 2015). Moreover, we observed that turbid lakes had higher k_{600} CH_4 than clear lakes, which would suggest a differential CH_4 microbubble formation between states. CH_4 microbubbles are thought to be produced as a combination of CH_4 supersaturation and turbulence (Vagle et al., 2010; Prairie and del Giorgio 2013; McGinnis et al., 2015). Although clear vegetated lakes had a higher mean annual pCH_4 than turbid algal lakes, overall pCH_4 was high in both states, and even higher in comparison with other studies that reported CH_4 microbubble formation (Prairie and del Giorgio 2013; McGinnis et al., 2015; Tang et al., 2016). Therefore, both clear vegetated and turbid algal lakes could potentially harbor the production of CH_4 microbubbles in terms of the amount of CH_4 present in the water column. On the other hand, water column turbulence is substantially different between states, as evidenced by the different relationship that exists between k_{600} CO_2 and wind speed and as has been reported in previous studies (Herb and Stefan 2005; Andersen et al., 2017): in clear vegetated lakes submerged vegetation tends to suppress wind induced turbulence in the water column, whereas in turbid algal lakes the absence of submerged vegetation allows a higher wind induced turbulence. This might explain the observed apparent higher CH_4 microbubble formation in turbid algal lakes, leading to higher k_{600} CH_4 in comparison with clear vegetated lakes, in spite of average lower pCH_4.

Most models of diffusive gas exchange in lakes have positively linked k_{600} to wind speed (Sebacher et al., 1983; Raymond and Cole 2001; Guérin et al., 2007) and, if CH_4 microbubbles are present, k_{600} CH_4 is also expected to have a positive correlation with pCH_4 (Prairie and del Giorgio 2013). Our results suggest a fundamentally different response of CH_4 and CO_2 to wind forcing in turbid algal lakes, evidenced by the slope of the regressions, which also point towards CH_4 microbubble formation. In clear vegetated lakes, in contrast, neither k_{600} CH_4 nor k_{600} CO_2 were significantly related to wind, yet k_{600} CH_4 was nevertheless consistently higher than k_{600} CO_2, also implying CH_4 microbubble formation but with a different behavior towards wind turbulence. The positive and expected relationship between k_{600} CH_4 and pCH_4 was found only for turbid algal lakes and is consistent with a pattern of wind induced

microbubble formation that is enhanced by increasing supersaturation of CH_4. This was not the outcome for clear vegetated lakes, implying that this wind vs. pCH_4 interaction is largely suppressed in vegetated habitats. On the other hand, ambient pCO_2 was weakly and negatively related to k_{600} CO_2 in both states in a very similar manner, which is coherent with the expected role of gas exchange as a modulator of ambient gas concentrations in surface waters, as has been previously reported for lakes (Lapierre et al., 2013) and rivers (Rocher-Ros et al., 2019). Therefore, in turbid algal lakes the combination of wind and pCH_4 determine k_{600} CH_4, yet in clear vegetated lakes, gas exchange is largely decoupled from wind, and under this circumstance a reciprocal relationship is established between pCH_4 and gas exchange: the wind-independent and relatively constant k in clear vegetated lakes leads to high pCH_4 because it acts as a lid, yet pCH_4 also appears to influence k_{600} CH_4, because the high pCH_4 leads to higher k_{600} CH_4 relative to CO_2 through microbubble formation. Submerged vegetation therefore influences gas dynamics two-fold in these clear vegetated lakes: directly by modulating the effect of wind on water column turbulence and therefore on gas exchange velocity, as is the case on CO_2 exchange, but also indirectly, by altering the dynamics of microbubble formation and therefore of CH_4 exchange.

Previous studies have also reported a strong impact of aquatic vegetation on gas exchange in shallow lakes. Kosten et al. (2016) reported a lower CH_4 exchange velocity in the presence of free-floating vegetation in comparison with open water sites, where the higher pCH_4 detected below the floating vegetation was partly explained by the lower k. Likewise, Barbosa et al. (2020) reported that vegetated and open water habitats from a tropical floodplain lake had similar CH_4 diffusive fluxes but that vegetated habitats had higher pCH_4, which was linked to a higher k in open water sites. Martinsen et al. (2020) also reported a lower CO_2 exchange velocity in a small shallow lake when submerged macrophytes were more abundant and related this observation with a negative effect of vegetation on the mixing of the water column. In our case, k_{600} CO_2 did not differ in average magnitude between lake states, but as pointed out above, the relationship between k_{600} CO_2 and wind differed markedly between states. An almost complete decoupling between exchange velocity and wind has been reported in previous studies carried out in small lakes (Heiskanen et al., 2014; Tedford et al., 2014; Tan et al., 2021), where wind-based models (Cole and Caraco 1998; Crusius and Wanninkhof 2003; MacIntyre et al., 2010) did not adequately explain the observed patterns in gas exchange, and where other factors, such as convection, had a stronger influence on gas exchange velocities. In our study, wind speed was a good predictor for k_{600} CO_2 and k_{600} CH_4 but only in turbid algal lakes. In clear vegetated lakes, submerged vegetation seems to decouple this relationship, therefore the use of wind speed would not be a good predictor for exchange velocities in these systems.

Overall, our results imply a roughly comparable mean annual CH_4 input to the water column between lakes in turbid algal and clear vegetated states, the latter inferred from similar mean annual CH_4 diffusive fluxes and mean annual CH_4 fraction of oxidation. We also observed that mean annual pCH_4 in clear lakes was 3 times higher than in turbid lakes, while mean annual k_{600} CH_4 in turbid lakes was 3 times higher than in clear lakes. Furthermore, the higher k_{600} CH_4 in turbid lakes was associated with a positive relationship with wind and pCH_4, and these relationships were absent in clear vegetated shallow lakes. Therefore, the higher pCH_4 in clear vegetated lakes could be explained by their lower average k_{600} CH_4 and also by the absence

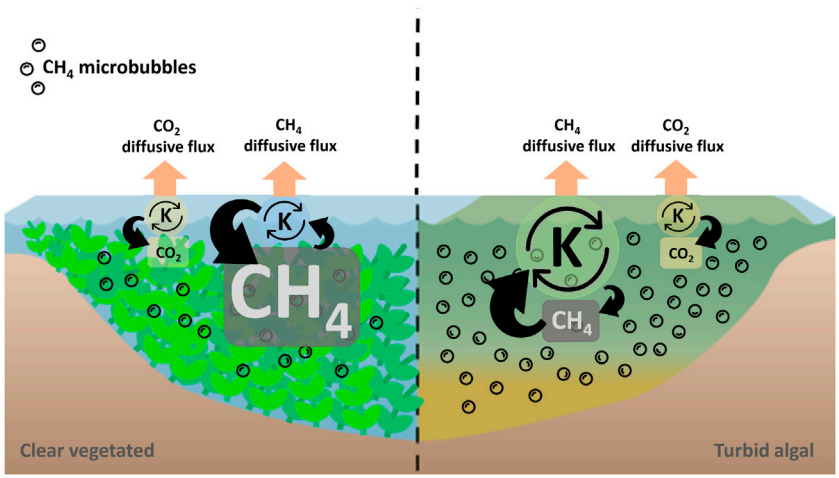


FIGURE 6 | Conceptual scheme of a plausible explanation for the observed results: states had similar mean annual CO_2 diffusive flux, pCO_2 and k_{600} CO_2. States also had similar mean annual CH_4 diffusive flux, but clear vegetated lakes had higher mean annual pCH_4 than turbid algal lakes. This difference in mean annual pCH_4 between states was explained by a lower mean annual k_{600} CH_4 in clear vegetated lakes, where submerged vegetation reduced wind induced turbulence in the water column, therefore diminishing CH_4 microbubbles formation. Overall, pCO_2 is controlled by k_{600} CO_2 in both states, as expected, but regulation of CH_4 is more complex: in clear lakes pCH_4 is mainly controlled by gas exchange (k_{600} CH_4) but there is also a minor control of pCH_4 over k_{600} CH_4, reflected in a consistently elevated k_{600} CH_4 relative to k_{600} CO_2 but that is independent of pCH_4 and wind. In turbid lakes, apparent k_{600} CH_4 is mainly controlled by wind and secondarily by pCH_4 through wind-driven CH_4 microbubble formation, whereas average pCH_4 is itself secondarily influenced by k_{600} CH_4.

of a relation between k_{600} CH_4 and wind, which further suggests a lower CH_4 microbubble formation. These patterns seem to be driven by a physical effect produced by the submerged vegetation over the mixing of the water column: a reduction of water column turbulence apparently leads to both a lower exchange velocity and also to a reduction of CH_4 microbubble formation, consequently leading to higher surface water pCH_4 in clear vegetated lakes (**Figure 6**). Furthermore, whereas pCO_2 is at least in part controlled by k_{600} CO_2, as expected, pCH_4 seems to be differentially controlled depending on the lake state: on one hand, in clear lakes pCH_4 is primarily controlled by gas exchange, yet k_{600} CH_4 is to some degree also influenced by pCH_4, since there is some degree of microbubble formation and k_{600} CH_4 is still systematically higher than k_{600} CO_2. In turbid algal lakes, on the other hand, pCH_4 appears to influence the apparent k_{600} CH_4 through wind-driven CH_4 microbubble formation, but there is also a control of k_{600} CH_4 over pCH_4 (**Figure 6**). Therefore, physical rather than biological processes - ie. methanogenesis and methanotrophy-seem to be controlling the differences observed in surface water mean annual pCH_4 between clear vegetated and turbid algal shallow lakes from the Pampean plain.

The observation that k_{600} CH_4 is systematically higher than k_{600} CO_2 is consistent with the formation and subsequent emission of CH_4 microbubbles, and similar observations have been reported for rivers (Beaulieu et al., 2012; Campeau et al., 2014), lakes (McGinnis et al., 2015; Rantakari et al., 2015; Jansen et al., 2020), and reservoirs (Prairie and del Giorgio 2013; Paranaíba et al., 2018), with enhancement values ranging from 1.8 to 2.5. Although this appears to be a widespread phenomenon, the data are still sparse because there are surprisingly few studies that have measured CH_4 air-water exchange in parallel to that of another gas that can be used as a reference. As a result, the CH_4 microbubble dynamics in inland waters remains poorly constrained (Jansen et al., 2020), and this adds a large degree of uncertainty to current models and budgets of freshwater CH_4 emissions that already include ebullitive, diffusive and plant mediated fluxes. Here we have shown that there is indeed an interaction between wind velocity and surface water CH_4 concentration in determining the relative enhancement of k_{600} CH_4 but that this combined effect is only present in turbid shallow lakes. In vegetated clear lakes, the presence of submerged macrophytes seems to greatly dampen wind-induced water column turbulence, and under this scenario, k_{600} CH_4 responds to neither wind speed nor to pCH_4. Had we sampled lakes in only one state, we may have perhaps concluded that pCH_4 regulates k, or that k regulates pCH_4, and yet both are occurring but under different habitat and climatic combinations. It is clear that the regulation of water-air CH_4 exchange is complex, and an improved understanding of this process will require parallel CH_4 and CO_2 - or another reference gas - measurements carried out in a wide range of habitat and climatic conditions.

DATA AVAILABILITY STATEMENT

The raw data supporting the conclusion of this article will be made available by the authors, without undue reservation.

AUTHOR CONTRIBUTIONS

SB contributed substantially to the data acquisition, laboratory, and statistical analyses, as well as to the writing of the manuscript. MLS contributed substantially to the data acquisition and to the drafting of the manuscript. PdG contributed substantially to the study's conception, to the analyses of the results, and the drafting of the manuscript.

FUNDING

This work was supported by the NSERC/HQ CarBBAS Industrial Research Chair, by Préstamo BID PICT RAICES 2017-2498 and by Préstamo BID PICT 2015-1509.

ACKNOWLEDGMENTS

We would like to thank several colleagues that were essential to carry out field work: F. Zolezzi, V. Rago, G. Chaparro, M. Saraceno, C. Miranda, S. Porcel and F. Rego. We also thank I. Izaguirre for academic and logistical support and L. Babino for statistical advice. We thank A. Parkes for the laboratory and logistics help through this entire project, P. Bodmer and P. Barbosa for their constructive comments on this manuscript and all the members of the CarBBAS laboratory for their helpful insights and discussions.

SUPPLEMENTARY MATERIAL

The Supplementary Material for this article can be found online at: https://www.frontiersin.org/articles/10.3389/fenvs.2022.892339/full#supplementary-material

REFERENCES

Allende, L., Tell, G., Zagarese, H., Torremorell, A., Pérez, G., Bustingorry, J., et al. (2009). Phytoplankton and Primary Production in Clear-Vegetated, Inorganic-Turbid, and Algal-Turbid Shallow Lakes from the Pampa Plain (Argentina). *Hydrobiologia* 624 (1), 45–60. doi:10.1007/s10750-008-9665-9

Alperin, M. J., Reeburgh, W. S., and Whiticar, M. J. (1988). Carbon and Hydrogen Isotope Fractionation Resulting from Anaerobic Methane Oxidation. *Glob. Biogeochem. Cycles* 2 (3), 279–288. doi:10.1029/gb002i003p00279

Andersen, M. R., Kragh, T., and Sand-Jensen., K. (20171862). Extreme Diel Dissolved Oxygen and Carbon Cycles in Shallow Vegetated Lakes. *Proc. R. Soc. B* 284, 20171427. doi:10.1098/rspb.2017.1427

Barbosa, P. M., Farjalla, V. F., Melack, J. M., Amaral, J. H. F., da Silva, J. S., and Forsberg, B. R. (2018). High Rates of Methane Oxidation in an Amazon

Floodplain Lake. *Biogeochemistry* 137 (3), 351–365. doi:10.1007/s10533-018-0425-2

Barbosa, P. M., Melack, J. M., Amaral, J. H. F., MacIntyre, S., Kasper, D., Cortés, A., et al. (2020). Dissolved Methane Concentrations and Fluxes to the Atmosphere from a Tropical Floodplain Lake. *Biogeochemistry* 148 (2), 129–151. doi:10.1007/s10533-020-00650-1

Bastviken, D., Tranvik, L. J., Downing, J. A., Crill, P. M., and Enrich-Prast, A. (2011). Freshwater Methane Emissions Offset the Continental Carbon Sink. *Science* 331 (Table 1), 50. doi:10.1126/science.1196808

Bastviken, D., Cole, J., Pace, M., and Tranvik, L. (2004). Methane Emissions from Lakes: Dependence of Lake Characteristics, Two Regional Assessments, and a Global Estimate. *Glob. Biogeochem. Cycles* 18 (4), a–n. doi:10.1029/2004GB002238

Bastviken, D., Ejlertsson, J., and Tranvik, L. (2002). Measurement of Methane Oxidation in Lakes: A Comparison of Methods. *Environ. Sci. Technol.* 36 (15), 3354–3361. doi:10.1021/es010311p

Beaulieu, J. J., Shuster, W. D., and Rebholz, J. A. (2012). Controls on Gas Transfer Velocities in a Large River. *J. Geophys. Res.* 117 (2), a–n. doi:10.1029/2011JG001794

Bogard, M. J., Del Giorgio, P. A., Boutet, L., Chaves, M. C. G., Prairie, Y. T., Merante, A., et al.Maria Carolina Garcia Chaves (2014). Oxic Water Column Methanogenesis as a Major Component of Aquatic CH4 Fluxes. *Nat. Commun.* 5 (May). doi:10.1038/ncomms6350

Brooks, M. E., Kristensen, K., Benthem, K. J. v., Magnusson, A., Berg, C. W., Nielsen, A., et al. (2017). GlmmTMB Balances Speed and Flexibility Among Packages for Zero-Inflated Generalized Linear Mixed Modeling. *R J.* 9 (2), 378–400. doi:10.32614/rj-2017-066

Brothers, S. M., Hilt, S., Attermeyer, K., Grossart, H. P., Kosten, S., Lischke, B., et al. (2013). A Regime Shift from Macrophyte to Phytoplankton Dominance Enhances Carbon Burial in a Shallow, Eutrophic Lake. *Ecosphere* 4 (11), art137. doi:10.1890/ES13-00247.1

Campeau, A., Lapierre, J.-f., Vachon, D., and Paul, G. (2014). Global Biogeochemical Cycles Boreal Landscape of Québec. *Glob. Biogeochem. Cycles* 28, 57–69. doi:10.1002/2013GB004685

Clayer, F., Moritz, A., Gélinas, Y., Tessier, A., and Gobeil, C. (2018). Modeling the Carbon Isotope Signatures of Methane and Dissolved Inorganic Carbon to Unravel Mineralization Pathways in Boreal Lake Sediments. *Geochimica Cosmochimica Acta* 229, 36–52. doi:10.1016/j.gca.2018.02.012

Cole, J. J., and Caraco, N. F. (1998). Atmospheric Exchange of Carbon Dioxide in a Low-Wind Oligotrophic Lake Measured by the Addition of SF6. *Limnol. Oceanogr.* 43 (4), 647–656. doi:10.4319/lo.1998.43.4.0647

Coleman, D. D., Risatti, J. B., and Schoell, M. (1981). Fractionation of Carbon and Hydrogen Isotopes by Methane-Oxidizing Bacteria. *Geochimica Cosmochimica Acta* 45 (7), 1033–1037. doi:10.1016/0016-7037(81)90129-0

Crusius, J., and Wanninkhof, R. (2003). Gas Transfer Velocities Measured at Low Wind Speed over a Lake. *Limnol. Oceanogr.* 48 (3), 1010–1017. doi:10.4319/lo.2003.48.3.1010

DelSontro, T., Boutet, L., St-Pierre, A., del Giorgio, P. A., and Prairie, Y. T. (2016). Methane Ebullition and Diffusion from Northern Ponds and Lakes Regulated by the Interaction between Temperature and System Productivity. *Limnol. Oceanogr.* 61, S62–S77. doi:10.1002/lno.10335

Desrosiers, K., DelSontro, T., and del Giorgio, P. A. (2021). Disproportionate Contribution of Vegetated Habitats to the CH4 and CO2 Budgets of a Boreal Lake. *Ecosystems*. doi:10.1007/s10021-021-00730-9

Diovisalvi, N., Bohn, V. Y., Piccolo, M. C., Perillo, G. M. E., Baigún, C., and Zagarese, H. E. (2015). Shallow Lakes from the Central Plains of Argentina: An Overview and Worldwide Comparative Analysis of Their Basic Limnological Features. *Hydrobiologia* 752 (1), 5–20. doi:10.1007/s10750-014-1946-x

Downing, J. A. (2010). Emerging Global Role of Small Lakes and Ponds: Little Things Mean a Lot. *Limnetica* 29 (1), 9–24. doi:10.23818/limn.29.02

Duc, N. T., Crill, P., and Bastviken, D. (2010). Implications of Temperature and Sediment Characteristics on Methane Formation and Oxidation in Lake Sediments. *Biogeochemistry* 100 (1), 185–196. doi:10.1007/s10533-010-9415-8

Emilson, E. J. S., Carson, M. A., Yakimovich, K. M., Osterholz, H., Dittmar, T., Gunn, J. M., et al. (2018). Climate-Driven Shifts in Sediment Chemistry Enhance Methane Production in Northern Lakes. *Nat. Commun.* 9 (1), 1801–1806. doi:10.1038/s41467-018-04236-2

Fox, J., and Sanford., W. (2018). Visualizing Fit and Lack of Fit in Complex Regression Models with Predictor Effect Plots and Partial Residuals. *J. Stat. Softw.* 87, 1–27. doi:10.18637/jss.v087.i09

Geraldi, Alejandra. M., Piccolo Maria, C., and Perillo, Gerardo. E. (2011). Lagunas Bonaerenses En El Paisaje. *Cienc. Hoy* 21 (123), 16–22.

Grasset, C., Abril, G., Mendonça, R., Roland, F., and Sobek, S. (2019). The Transformation of Macrophyte-derived Organic Matter to Methane Relates to Plant Water and Nutrient Contents. *Limnol. Oceanogr.* 64 (4), 1737–1749. doi:10.1002/lno.11148

Grossart, H.-P., Frindte, K., Dziallas, C., Eckert, W., and Tang, K. W. (2011). Microbial Methane Production in Oxygenated Water Column of an Oligotrophic Lake. *Proc. Natl. Acad. Sci. U.S.A.* 108 (49), 19657–19661. doi:10.1073/pnas.1110716108

Guérin, F., Abril, G., Serça, D., Delon, C., Richard, S., Delmas, R., et al. (2007). Gas Transfer Velocities of CO2 and CH4 in a Tropical Reservoir and its River Downstream. *J. Mar. Syst.* 66 (1–4), 161–172. doi:10.1016/j.jmarsys.2006.03.019

Günthel, M., Donis, D., Kirillin, G., Ionescu, D., Bizic, M., McGinnis, D. F., et al. (2019). Contribution of Oxic Methane Production to Surface Methane Emission in Lakes and its Global Importance. *Nat. Commun.* 10 (1), 1–10. doi:10.1038/s41467-019-13320-0

Günthel, M., Klawonn, I., Woodhouse, J., Bižić, M., Ionescu, D., Ganzert, L., et al. (2020). Photosynthesis-driven Methane Production in Oxic Lake Water as an Important Contributor to Methane Emission. *Limnol. Oceanogr.* 65 (12), 2853–2865. doi:10.1002/lno.11557

Hadley, W. (2016). *ggplot2: Elegant Graphics for Data Analysis*. New York: Springer-Verlag.

Happell, J. D., Chanton, J. P., and Showers, W. S. (1994). The Influence of Methane Oxidation on the Stable Isotopic Composition of Methane Emitted from Florida Swamp Forests. *Geochimica Cosmochimica Acta* 58 (20), 4377–4388. doi:10.1016/0016-7037(94)90341-7

Hartmann, J. F., Günthel, M., Klintzsch, T., Kirillin, G., Grossart, H.-P., Keppler, F., et al. (2020). High Spatiotemporal Dynamics of Methane Production and Emission in Oxic Surface Water. *Environ. Sci. Technol.* 54 (3), 1451–1463. doi:10.1021/acs.est.9b03182

Heiskanen, J. J., Mammarella, I., Haapanala, S., Pumpanen, J., Vesala, T., Macintyre, S., et al. (2014). Effects of Cooling and Internal Wave Motions on Gas Transfer Coefficients in a Boreal Lake. *Tellus B Chem. Phys. Meteorology* 66 (1), 22827. doi:10.3402/tellusb.v66.22827

Herb, W. R., and Stefan, H. G. (2005). Dynamics of Vertical Mixing in a Shallow Lake with Submersed Macrophytes. *Water Resour. Res.* 41 (2), 1–14. doi:10.1029/2003WR002613

Hilt, S., Brothers, S., Jeppesen, E., Veraart, A. J., and Kosten, S. (2017). Soren Brothers, Erik Jeppesen, Annelies J. Veraart, and Sarian KostenTranslating Regime Shifts in Shallow Lakes into Changes in Ecosystem Functions and Services. *BioScience* 67 (10), 928–936. doi:10.1093/biosci/bix106

Hilt, S. (2015). Regime Shifts between Macrophytes and Phytoplankton - Concepts beyond Shallow Lakes, Unravelling Stabilizing Mechanisms and Practical Consequences. *Limnetica* 34 (2), 467–480. doi:10.23818/limn.34.35

Holgerson, M. A., and Raymond, P. A. (2016). Large Contribution to Inland Water CO2 and CH4 Emissions from Very Small Ponds. *Nat. Geosci.* 9 (3), 222–226. doi:10.1038/ngeo2654

Jansen, J., Thornton, B. F., Cortés, A., Snöälv, J., Wik, M., MacIntyre, S., et al. (2020). Drivers of Diffusive CH₄ Emissions from Shallow Subarctic Lakes on Daily to Multi-Year Timescales. *Biogeosciences* 17 (7), 1911–1932. doi:10.5194/bg-17-1911-2020

Jeffrey, L. C., Maher, D. T., Johnston, S. G., Kelaher, B. P., Steven, A., and Tait, D. R. (2019). Wetland Methane Emissions Dominated by Plant-mediated Fluxes: Contrasting Emissions Pathways and Seasons within a Shallow Freshwater Subtropical Wetland. *Limnol. Oceanogr.* 64 (5), 1895–1912. doi:10.1002/lno.11158

Jose, Pinheiro., Douglas, Bates., Saikat., Deb. Roy., and Sarkar, Deepayan.the R Core Team (2019). Linear and Nonlinear Mixed Effects Models. Available at https://cran.rproject.org/web/packages/nlme/index.html.

Kosten, S., Piñeiro, M., de Goede, E., de Klein, J., Lamers, L. P. M., and Ettwig, K. (2016). Fate of Methane in Aquatic Systems Dominated by Free-Floating Plants. *Water Res.* 104, 200–207. doi:10.1016/j.watres.2016.07.054

Kuznetsova, A., Brockhoff, P. B., and Christensen, R. H. B. (2017). LmerTest Package: Tests in Linear Mixed Effects Models. *J. Stat. Soft.* 82 (13). doi:10.18637/jss.v082.i13

Lapierre, J.-F., Guillemette, F., Berggren, M., del Giorgio, P. A., and Del Giorgio, P. A. (2013). Increases in Terrestrially Derived Carbon Stimulate Organic Carbon Processing and CO2 Emissions in Boreal Aquatic Ecosystems. *Nat. Commun.* 4. doi:10.1038/ncomms3972

Liptay, K., Chanton, J., Czepiel, P., and Mosher, B. (1998). Use of Stable Isotopes to Determine Methane Oxidation in Landfill Cover Soils. *J. Geophys. Res.* 103 (97), 8243–8250. doi:10.1029/97jd02630

MacIntyre, S., Jonsson, A., Jansson, M., Aberg, J., Turney, D. E., and Miller, S. D. (2010). Buoyancy Flux, Turbulence, and the Gas Transfer Coefficient in a Stratified Lake. *Geophys. Res. Lett.* 37 (24), a–n. doi:10.1029/2010GL044164

Maher, D. T., Santos, I. R., Oakes, J. M., Erler, D. V., Carvalho, M. C., and Eyre, B. D. (2013). Novel Use of Cavity Ring-Down Spectroscopy to Investigate Aquatic Carbon Cycling from Microbial to Ecosystem Scales. *Environ. Sci. Technol.* 47 (22), 12938–12945. doi:10.1021/es4027776

Martinsen, K. T., Kragh, T., and Sand-Jensen, K. (2020). Carbon Dioxide Efflux and Ecosystem Metabolism of Small Forest Lakes. *Aquat. Sci.* 82 (1). doi:10.1007/s00027-019-0682-8

McGinnis, D. F., Kirillin, G., Tang, K. W., Flury, S., Bodmer, P., Engelhardt, C., et al. (2015). Enhancing Surface Methane Fluxes from an Oligotrophic Lake: Exploring the Microbubble Hypothesis. *Environ. Sci. Technol.* 49 (2), 873–880. doi:10.1021/es503385d

Megonigal, J. P., Hines, M. E., and Visscher, P. T. (2003). Anaerobic Metabolism: Linkages to Trace Gases and Aerobic Processes. *Treatise Geochem.* 8 (9), 317–424. doi:10.1016/B0-08-043751-6/08132-9

Noyce, G. L., and Megonigal, J. P. (2021). Biogeochemical and Plant Trait Mechanisms Drive Enhanced Methane Emissions in Response to Whole-Ecosystem Warming. *Biogeosciences* 18 (8), 2449–2463. doi:10.5194/bg-18-2449-2021

Paranaíba, José. R., Barros, Nathan., Mendonça, Raquel., Linkhorst, Annika., Isidorova, Anastasija., Roland, Fábio., et al. (2018). Spatially Resolved Measurements of CO2 and CH4 Concentration and Gas-Exchange Velocity Highly Influence Carbon-Emission Estimates of Reservoirs. *Environ. Sci. Technol.* 52 (2), 607–615. doi:10.1021/acs.est.7b05138

Prairie, Y., and del Giorgio, P. (2013). A New Pathway of Freshwater Methane Emissions and the Putative Importance of Microbubbles. *Iw* 3 (3), 311–320. doi:10.5268/IW-3.3.542

R Core Team. (2019). *R: A Language and Environment for Statistical Computing*. Vienna, Austria: R Foundation for Statistical Computing.

Rantakari, M., Heiskanen, J., Mammarella, I., Tulonen, T., Linnaluoma, J., Kankaala, P., et al. (2015). Different Apparent Gas Exchange Coefficients for CO2 and CH4: Comparing a Brown-Water and a Clear-Water Lake in the Boreal Zone during the Whole Growing Season. *Environ. Sci. Technol.* 49 (19), 11388–11394. doi:10.1021/acs.est.5b01261

Raymond, P. A., and Cole, J. J. (2001). Gas Exchange in Rivers and Estuaries: Choosing a Gas Transfer Velocity. *Estuaries* 24 (2), 312–317. doi:10.2307/1352954

Rocher-Ros, G., Sponseller, R. A., Lidberg, W., Mörth, C. M., and Giesler, R. (2019). Landscape Process Domains Drive Patterns of CO 2 Evasion from River Networks. *Limnol. Oceanogr. Lett.* 4 (4), 87–95. doi:10.1002/lol2.10108

Royston, J. P. (1982). An Extension of Shapiro and Wilk's W Test for Normality to Large Samples. *Source J. R. Stat. Soc. Ser. C Appl. Statistics)* 31, 115–124. doi:10.2307/2347973

Sánchez, M. L., Lagomarsino, L., Allende, L., and Izaguirre, I. (2015). Changes in the Phytoplankton Structure in a Pampean Shallow Lake in the Transition from a Clear to a Turbid Regime. *Hydrobiologia* 752 (1), 65–76. doi:10.1007/s10750-014-2010-6

Scheffer, M., Hosper, S. H., Meijer, M. L., Moss, B., and Jeppesen, E. (1993). Alternative Equilibria in Shallow Lakes. *Trends Ecol. Evol.* 8 (8), 275–279. doi:10.1016/0169-5347(93)90254-M

Scheffer, M. (2001). Alternative Attractors of Shallow Lakes. *Sci. World J.* 1, 254–263. doi:10.1100/tsw.2001.62

Schwarz, J. I. K., Eckert, W., and Conrad., R. (2008). Response of the Methanogenic Microbial Community of a Profundal Lake Sediment (Lake Kinneret, Israel) to Algal Deposition. *Limnol. Oceanogr.* 53 (1), 113–121. doi:10.4319/lo.2008.53.1.0113

Sebacher, D. I., Harriss, R. C., and Bartlett, K. B. (1983). Methane Flux across the Air-Water Interface: Air Velocity Effects. *Tellus* 35B, 103–109. doi:10.1111/j.1600-0889.1983.tb00014.x

Soued, C., and Prairie, Y. T. (2020). The Carbon Footprint of a Malaysian Tropical Reservoir: Measured versus Modelled Estimates Highlight the Underestimated Key Role of Downstream Processes. *Biogeosciences* 17 (2), 515–527. doi:10.5194/bg-17-515-2020

Tan, D., Li, Q., Wang, S., Yeager, K. M., Guo, M., Liu, K., et al. (2021). Diel Variation of CH4 Emission Fluxes in a Small Artificial Lake: Toward More Accurate Methods of Observation. *Sci. Total Environ.* 784, 147146. doi:10.1016/j.scitotenv.2021.147146

Tang, K. W., McGinnis, D. F., Ionescu, D., and Grossart, H.-P. (2016). Methane Production in Oxic Lake Waters Potentially Increases Aquatic Methane Flux to Air. *Environ. Sci. Technol. Lett.* 3 (6), 227–233. doi:10.1021/acs.estlett.6b00150

Tedford, E. W., MacIntyre, S., Miller, S. D., and Czikowsky, M. J. (2014). Similarity Scaling of Turbulence in a Temperate Lake during Fall Cooling. *J. Geophys. Res. Oceans* 119 (8), 4689–4713. doi:10.1002/2014JC010135

Thottathil, S. D., Reis, P. C. J., del Giorgio, P. A., and Prairie, Y. T. (2018). The Extent and Regulation of Summer Methane Oxidation in Northern Lakes. *J. Geophys. Res. Biogeosci.* 123 (10), 3216–3230. doi:10.1029/2018JG004464

Torremorell, A., Llames, M. E., Pérez, G. L., Escaray, R., Bustingorry, J., and Zagarese, H. (2009). Annual Patterns of Phytoplankton Density and Primary Production in a Large, Shallow Lake: The Central Role of Light. *Freshw. Biol.* 54 (3), 437–449. doi:10.1111/j.1365-2427.2008.02119.x

Tranvik, L. J., Cole, J. J., and Prairie, Y. T. (2018). The Study of Carbon in Inland Waters-From Isolated Ecosystems to Players in the Global Carbon Cycle. *Limnol. Oceanogr. Lett.* 3 (3), 41–48. doi:10.1002/lol2.10068

Vachon, D., Langenegger, T., Donis, D., McGinnis, D. F., and McGinnis, D. F. (2019). Influence of Water Column Stratification and Mixing Patterns on the Fate of Methane Produced in Deep Sediments of a Small Eutrophic Lake. *Limnol. Oceanogr.* 64 (5), 2114–2128. doi:10.1002/lno.11172

Vagle, S., McNeil, C., and Steiner, N. (2010). Upper Ocean Bubble Measurements from the NE Pacific and Estimates of Their Role in Air-Sea Gas Transfer of the Weakly Soluble Gases Nitrogen and Oxygen. *J. Geophys. Res.* 115 (12), 1–16. doi:10.1029/2009JC005990

Wanninkhof, R. (2014). Relationship between Wind Speed and Gas Exchange over the Ocean Revisited. *Limnol. Oceanogr. Methods* 12 (JUN), 351–362. doi:10.4319/lom.2014.12.351

West, W. E., Coloso, J. J., and Jones, S. E. (2012). Effects of Algal and Terrestrial Carbon on Methane Production Rates and Methanogen Community Structure in a Temperate Lake Sediment. *Freshw. Biol.* 57 (5), 949–955. doi:10.1111/j.1365-2427.2012.02755.x

Whiticar, Michael. J. (1999). Carbon and Hydrogen Isotope Systematics of Bacterial Formation and Oxidation of Methane. *Chem. Geol.* 161 (1), 291–314. doi:10.1016/s0009-2541(99)00092-3

Yan, X., Xu, X., Ji, M., Zhang, Z., Wang, M., Wu, S., et al. (2019). Cyanobacteria Blooms: A Neglected Facilitator of CH4 Production in Eutrophic Lakes. *Sci. Total Environ.* 651, 466–474. doi:10.1016/j.scitotenv.2018.09.197

Zuur, A. F., Ieno, E. N., Walker, N. J., Saveliev, A. A., and Smith, G. M. (2009). *Mixed Effects Models and Extensions in Ecology with R*. New York: Springer.

Conflict of Interest: The authors declare that the research was conducted in the absence of any commercial or financial relationships that could be construed as a potential conflict of interest.

Publisher's Note: All claims expressed in this article are solely those of the authors and do not necessarily represent those of their affiliated organizations, or those of the publisher, the editors and the reviewers. Any product that may be evaluated in this article, or claim that may be made by its manufacturer, is not guaranteed or endorsed by the publisher.

Copyright © 2022 Baliña, Sánchez and del Giorgio. This is an open-access article distributed under the terms of the Creative Commons Attribution License (CC BY). The use, distribution or reproduction in other forums is permitted, provided the original author(s) and the copyright owner(s) are credited and that the original publication in this journal is cited, in accordance with accepted academic practice. No use, distribution or reproduction is permitted which does not comply with these terms.

frontiers | Frontiers in Environmental Science

ORIGINAL RESEARCH
published: 24 June 2022
doi: 10.3389/fenvs.2022.833511

Trait-Based Model Reproduces Patterns of Population Structure and Diversity of Methane Oxidizing Bacteria in a Stratified Lake

Matthias Zimmermann[1,2], *Magdalena J. Mayr*[1,2†], *Damien Bouffard*[1], *Bernhard Wehrli*[1,2] *and Helmut Bürgmann*[1]*

[1]Eawag, Swiss Federal Institute of Aquatic Science and Technology, Surface Waters—Research and Management, Kastanienbaum, Switzerland, [2]Department of Environmental Systems Science, ETH Zürich, Zürich, Switzerland

OPEN ACCESS

Edited by:
Yves T. Prairie,
Université du Québec à Montréal, Canada

Reviewed by:
Ingeborg Bussmann,
Alfred Wegener Institute Helmholtz Centre for Polar and Marine Research (AWI), Germany
Annelies J. Veraart,
Radboud University Nijmegen, Netherlands

***Correspondence:**
Helmut Bürgmann
Helmut.Buergmann@eawag.ch

†Present Address:
Magdalena J. Mayr,
Division of Geological and Planetary Sciences, California Institute of Technology, Pasadena, CA, United States

Specialty section:
This article was submitted to Biogeochemical Dynamics, a section of the journal Frontiers in Environmental Science

Received: 11 December 2021
Accepted: 23 May 2022
Published: 24 June 2022

Citation:
Zimmermann M, Mayr MJ, Bouffard D, Wehrli B and Bürgmann H (2022) Trait-Based Model Reproduces Patterns of Population Structure and Diversity of Methane Oxidizing Bacteria in a Stratified Lake. Front. Environ. Sci. 10:833511. doi: 10.3389/fenvs.2022.833511

In stratified lakes, methane oxidizing bacteria are critical methane converters that significantly reduce emissions of this greenhouse gas to the atmosphere. Efforts to better understand their ecology uncovered a surprising diversity, vertical structure, and seasonal succession. It is an open question how this diversity has to be considered in models of microbial methane oxidation. Likewise, it is unclear to what extent simple microbial traits related to the kinetics of the oxidation process and temperature optimum, suggested by previous studies, suffice to understand the observed ecology of methane oxidizing bacteria. Here we incorporate niche partitioning in a mechanistic model of seasonal lake mixing and microbial methane oxidation in a stratified lake. Can we model MOB diversity and niche partitioning based on differences in methane oxidation kinetics and temperature adaptation? We found that our model approach can closely reproduce diversity and niche preference patterns of methanotrophs that were observed in seasonally stratified lakes. We show that the combination of trait values resulting in coexisting methanotroph communities is limited to very confined regions within the parameter space of potential trait combinations. However, our model also indicates that the sequence of community assembly, and variations in the stratification and mixing behavior of the lake result in different stable combinations. A scenario analysis introducing variable mixing conditions showed that annual weather conditions and the pre-existing species also affect the developing stable methanotrophic species composition of the lake. Both, effect of pre-existing species and the environmental impact suggest that the MOB community in lakes may differ from year to year, and a stable community may never truly occur. The model further shows that there are always better-adapted species in the trait parameter space that would destabilize and replace an existing stable community. Thus, natural selection may drive trait values into the specific configurations observed in nature based on physiological limits and tradeoffs between traits.

Keywords: niche partitioning, microbial kinetics, community assembly, methane affinity, temperature optimum, growth model, tradeoffs, competitive exclusion

INTRODUCTION

In recent years, considerable efforts have been made to better understand the ecology of methane oxidizing bacteria (MOB) in lakes. MOB are a diverse group of mainly *Alpha-* and *Gammaproteobacteria* that have the unique ability to use methane as their sole carbon and energy source (Hanson and Hanson, 1996). In lakes, these bacteria are an important sink for methane and significantly reduce methane emissions to the atmosphere (Kankaala et al., 2006; Conrad, 2009; Schubert et al., 2012; Zimmermann et al., 2021). This is a crucial process, as lake sediments are an important source of methane. Despite the activity of MOB, methane emission from lakes is responsible for about 75% of the emission of greenhouse gases from lacustrine systems (DelSontro et al., 2018) and its total emission might even offset the continental carbon sink (Bastviken et al., 2011). In seasonally or permanently stratified lakes with an anoxic hypolimnion MOB are found within the entire water column (Kojima et al., 2009; Tsutsumi et al., 2011; Mayr et al., 2020c). During stratification, methane oxidation strongly limits diffusive methane losses from such lakes. However, ebullition presents a shortcut to the atmosphere that allows significant amounts of methane to escape and often represents the dominant emission pathway, accounting for between 60% and 70% of total global emissions from lakes and reservoirs (DelSontro et al., 2018). The losses of stored methane during lake turnover appear to be again strongly limited by methane oxidation (Zimmermann et al., 2021).

Recent studies have brought to light the intriguing diversity, vertical structure and seasonal succession of MOB in stratified lakes (Mayr et al., 2020a, Mayr et al., 2020c; Reis et al., 2020; Rissanen et al., 2020; Martin et al., 2021). The fact that all MOB rely on methane and oxygen as primary resources, raises the question of how diversity within this functional group is maintained despite Hardin's competitive exclusion principle (Hardin, 1960). This is analogous to the situation of phytoplankton, which has been the inspiration of much research and the subject of much debate among ecologists as the "paradox of the plankton" (Hutchinson, 1961). For plankton, many explanations have been proposed, ranging from niche partitioning (Salcher, 2013), selective grazing and chaotic fluid motion to a dominance of stochastic processes (i.e., neutral theory) and many more (Roy and Chattopadhyay, 2007; Record et al., 2014). While we thus have a comprehensive general understanding of the ecological mechanisms that limit the competitive exclusion principle (Chesson, 2000; Maynard et al., 2020), the case of MOB diversity has not been thoroughly studied, and we propose that they can be an interesting test case for ecological theory. The potential for using trait-based approaches in prokaryotic microbial ecology has been highlighted (Martiny et al., 2015), noting in particular that many traits appear to be phylogenetically conserved, so that traits can frequently be related to taxonomic identities.

In our recent publications we have suggested that niche partitioning (species sorting) can at least partly explain the vertical (spatial) structuring of MOB in lakes (Mayr et al., 2020c) and that environmental drivers also partly explain temporal variability (Guggenheim et al., 2020). MOB niches may derive from various adaptations in MOB to temperature regimes and nutrient conditions, but also to the availability of the main substrate, i.e., through enzymes with variable substrate affinity or complementary metabolic costs. In MOB, there is a considerable body of evidence that adaptations to substrate availability plays a role for their ecology. MOB isolates are known to have a range of different affinities to methane (Knief and Dunfield, 2005; Dam et al., 2012) with high-affinity variants being able to oxidize methane at very low (e.g., atmospheric) levels. The particulate and soluble forms of methane monooxygenase (pMMO and sMMO) also differ in their kinetic properties, with sMMO exhibiting a lower methane affinity. Our previous research showed that both the observed vertical structures and seasonal succession of MOB community composition in a stratified lake were accompanied by differences in the methane oxidation kinetics (Mayr et al., 2020b) and potentially also temperature adaptation (Mayr et al., 2020a). Among the patterns observed in MOB populations were discrete population maxima above, within and below the oxycline under stable stratification (Mayr et al., 2020a), as well as in the epilimnion and anoxic hypolimnion (Guggenheim et al., 2020); on the temporal scale, succession and blooming of previously rare MOB taxa was observed during the autumn lake mixing (Mayr et al., 2020a). Statistical analyses of driving factors consistently pointed to the importance of the methane gradient and temperature, although other environmental factors as well as ecological interactions may play a role as well (Guggenheim et al., 2020).

In Zimmerman et al. (2021), we built a model to evaluate how MOB limited outgassing in seasonally stratified lakes during fall turnover. The approach was based on a mechanistic model to assess the dynamical development of the MOB biomass. Here, we build on this work to develop a trait-based model for MOB in a stratified lake. Trait-based models have a rich, yet recent, history in phytoplankton ecology (Litchman and Klausmeier, 2008) and were originally developed primarily to understand patterns of niche differentiation and diversity. The potential of such models to also improve our mechanistic understanding of biogeochemical processes has also been highlighted (Litchman et al., 2015; Zakharova et al., 2019). Traits that regulate both responses and effects are an interesting target for modeling. As a response trait, methane oxidation provides a growth advantage where methane is an abundant or perhaps the only available source of energy and carbon; and as an effect trait it may alter the availability of methane and oxygen in the system. On the other hand, pure response traits like temperature growth optima may still be related to biogeochemical effects if they are correlated with response traits. A key element of trait-based models is the concept of trade-offs between traits, i.e., limitations in the ability of organisms to optimize trait combinations arbitrarily. In lakes, trait-based models of MOB mostly followed a statistical approach to explain environmental drivers affecting MOB (Thottathil et al., 2019; Reis et al., 2020). Our approach instead follows an equation-based approach to study the diversity of MOB in a stratified lake.

Our previous work suggested that methane affinity and temperature growth optimum might be among the most important traits of MOB in stratified freshwater lakes. We here explored with the first trait-based mechanistic model of microbial methane oxidation, to what extent a model based on a minimal set of traits, i.e., just the two main parameters of methane oxidation kinetics and temperature optima, can reproduce observed patterns of MOB diversity. The microbial growth model specifically considers Monod-type methane oxidation kinetics associated with MOB "species" with three independent traits as suggested in Mayr et al. (2020a), Mayr et al. (2020c): maximum growth rates, methane half-saturation constants of the Monod-type kinetics and temperature dependence of methane oxidation. In order to limit complexity in this first attempt, we neglect further potential traits (such as kinetic or inhibitory effects of oxygen) as well as environmental drivers such as (micro) nutrient concentrations.

We further combine a 1D physical lake model with a simplified biogeochemical model for oxygen and methane to provide a realistic simulated lake environment. This model was developed with data available for Rotsee, a small, shallow, seasonally stratified eutrophic lake near the city of Lucerne, Switzerland. Our data and the modeled dynamics include the seasonal mixing of the lake as previously described (Schubert et al., 2012; Mayr et al., 2020a; Zimmermann et al., 2021). The model thus couples the trait-based approach directly with a physical and biogeochemical model of the lake's temperature and methane dynamics.

We then explored whether simulated MOB communities with species based on the three kinetic traits can qualitatively reproduce stable niche differentiation over the simulated vertical and temporal gradients of temperature, methane and oxygen of Rotsee simulated over several years. We assembled communities of 2, 3, and 4 species starting from trait combinations actually observed in the MOB populations of Rotsee. We explore the stability of such communities against new species with different trait combinations and changes in the simulated lake environment. Finally, we explore the spatiotemporal abundance patterns of the simulated species and compare them with observed population patterns.

METHODS

Basic Structure of the Physical and Biogeochemical Model

Our first objective was to reproduce the temporal evolution of the thermal structure in the water column of Lake Rotsee to derive physical parameters such as time and space varying temperature and vertical diffusion as well as dissipation coefficient. For this purpose, we calibrated the physical lake model Simstrat version 2.1.2 (Gaudard et al., 2019) to temperature observations in Lake Rotsee, Switzerland, that were available for multiple years. Assuming that we can neglect feedback of chemical and biological processes in the lake on the physical processes, we used this calibrated physical model to pre-calculate the physical framework of our biogeochemical model and thereby improved its computational efficiency.

Our second objective was to build a simple biogeochemical model that would on the one hand reproduce the concentrations of methane and oxygen, i.e., reproduce the observed seasonal dynamics of the biogeochemical boundary conditions for methane oxidation. On the other hand, we use this model of the lake to explore the population dynamics of different "species" (trait combinations) of methane oxidizing bacteria, and the conditions for stable coexistence of multiple species.

The model that we used for this second objective is based on the classical reaction-diffusion equation:

$$\partial_t u = D\nabla^2 u + R(u) \tag{1}$$

where u is the vector of concentrations, $R(u)$ describes the local reaction kinetics and D is the diagonal turbulent diffusion coefficient matrix. For numerical integration, we used a finite volume discretisation method that takes into account the lake bathymetry with a Crank-Nicolson integration scheme with Neumann boundary conditions (Moukalled et al., 2015). Areas A and volumes V for each grid cell of the finite volume discretization were derived from the lake bathymetry (Zimmermann et al., 2021). Numerical discretization and integration was implemented in Julia 1.2 (Bezanson et al., 2017) and is available on GitHub (see *Data Availability Statement*).

Using this diffusion-reaction system, we modelled methane, oxygen, and MOB species concentrations in the water column. The diffusion-coefficients were pre-calculated with the above mentioned physical model. Simulations were performed with a spatial resolution of 10 cm and time steps of 15 min. We used the same diffusion-reaction equation to model concentrations of organic matter, methane and oxygen in the sediment. For the sediment, the diffusion-coefficient was taken from available literature as described below (see section "*Methane Production in the Sediment*"). The complete set of additional processes that are part of the term $R(u)$ as well as the needed parameters (**Tables 1**, **2**) are discussed below. For a full set of equations, see **Supplementary Methods S1**.

Gas Exchange With the Atmosphere

We modelled the exchange of methane and oxygen with the atmosphere with the boundary layer model of Liss and Slater (1974).

$$F_{atm} = k\left(C - C_{eq}\right) \tag{2}$$

where F_{atm} is the flux into the atmosphere, C is the surface water concentration, C_{eq} is the equilibrium concentration and k is the transfer velocity. The temperature dependence of solubility of O_2 and CH_4 were considered. We used the surface-renewal model to calculate the transfer velocity based on the dissipation of turbulent kinetic energy (Zappa et al., 2007; MacIntyre et al., 2010; Read et al., 2012):

$$k = \eta(\epsilon\nu)^{1/4} Sc^{-n} \tag{3}$$

where ϵ is the rate of dissipation of turbulent kinetic energy near the air-water interface, ν is the kinematic viscosity, and η is an empirically derived, depth-dependent scaling coefficient. For this conceptual model, η was set to $1/(2\pi)$ based on theoretical

TABLE 1 | Set of the parameters used in the physical model.

Model aspect	Parameter	Value	Description	Reference
Physical model (Simstrat)	a_seiche	0.0038	fraction of wind energy to seiche energy	calibrated
	qNN	0.7	fit parameter for distribution of seiche energy	calibrated
	C10	F(wind)	wind drag coefficient	Wüest and Lorke (2003)
	f_wind	0.5	fraction of forcing wind to wind at 10 m (W10/Wf)	calibrated
	p_radin	0.99	fit parameter for absorption of IR radiation from sky	calibrated
	p_windf	1.04	fit parameter for convective and latent heat fluxes	calibrated
	Albsw	0.018	albedo for reflection of short-wave radiation	calibrated
	Absrp	0.44	light absorption coefficient	calibrated

TABLE 2 | Set of the parameters used in the biogeochemical model.

Model aspect	Parameter	Value	Description	References
Sediment model	k_{sed}	1.8×10^{-5} m s^{-1}	apparent sediment/water transfer velocity. Fitting parameter	calibrated
	D	12×10^{-6} m^2 h^{-1}	sediment diffusivity	Hofman et al. (1991)
	$F_{OM,sed}$	41 mmol C m^{-2} d^{-1}	sedimentation rate of organic matter	calibrated (Fiskal et al., 2019)
	$V_{max,sed}$	36 $days^{-1}$	maximum rate of methane production in the sediment	calibrated
	$K_{I,O_2,sed}$	50 nM	monod type inhibition constant of methane production by oxygen	calibrated
Water column	WBOD	3,190 µmol O_2 m^{-3} d^{-1}	oxygen consumption rate	Müller et al. (2012)
	k	$3.4 \times 10^{-6} \pm 1.41 \times 10^{-6}$ m s^{-1}	piston velocity	1-D physical model
Growth model	V_{max}	0.09–2.2 $days^{-1}$	maximum growth rate	Hanson and Hanson (1996), Knief and Dunfield (2005), Baani and Liesack (2008), Lofton et al. (2014), Milucka et al. (2015), Brand et al. (2016), Mayr et al., 2020a), Mayr et al. (2020c)
	K_{M,CH_4}	0.1–300 µM	monod constant for methane	Hanson and Hanson (1996), Knief and Dunfield (2005), Baani and Liesack (2008), Lofton et al. (2014)
	K_{M,O_2}	0.3 µM	monod constant for oxygen	this study (Milucka et al., 2015; Oswald et al., 2015)
	K_{I,O_2}	200 µM	monod type growth inhibition constant by oxygen	this study (Thottathil et al., 2019)
	Temperature dependence of r_{MOX}			Ratkowsky et al. (1983)
	T_{min}	1–12°C	minimum growth temperature	
	T_{opt}	5–25°C	optimal growth temperature	
	T_{max}	11–55°C	maximum growth temperature	
	y_{CCE}	0.3	carbon conversion efficiency	Leak and Dalton (1986)
	m_{anox}	0.0024 $days^{-1}$	mortality without oxygen	Roslev and King (1995)
	m_{ox}	0.022 $days^{-1}$	maximum mortality with oxygen	Roslev and King (1995)
	K_{mo,O_2}	100 µM	monod type saturation constant for oxygen dependency of mortality	

considerations (Soloviev et al., 2007). The rate of dissipation ϵ was pre-calculated for each time step by the physical model. We determined the Schmidt number *Sc* for methane and oxygen with an exponent of $n = -1/2$ (Wanninkhof, 2014).

The exchange of methane and oxygen with the atmosphere was implemented as a reaction term in the topmost cell of the spatially discrete diffusion-reaction system. Primary production was not considered, which is a deliberate simplification.

Water Column Oxygen Depletion

For eutrophic lakes in Switzerland, an average areal oxygen depletion rate in the water column of 0.9 g O_2 m^{-2} d^{-1} has been estimated (Müller et al., 2012). With an estimated sediment surface area of 0.49 km^2 and a total volume of 0.0044 km^3, we assumed a water column biochemical oxygen demand (WBOD) of 3,190 µmol O_2 m^{-3} d^{-1}. The water column biochemical oxygen demand was modelled as a constant reaction term in the diffusion-reaction system throughout the water column.

Methane Production in the Sediment

The methane production and flux from the sediment was parameterized with a simplified sediment model using a constant sedimentation velocity $F_{OM,sed}$ of organic material,

a methane production velocity $V_{max,sed}$ that is oxygen inhibited (K_{I,O_2}) and limited by the availability of organic material and an apparent constant exchange velocity with the water column (**Supplementary Method S1**). The input of organic matter to the sediment was implemented as reaction terms in the top-most cell of the sediment. Likewise, the exchange of methane and oxygen with the water column was added as a reaction term in the top-most cell of the sediment as well as the deepest cell of the water column. Temperature effects were not considered for this term as temperature fluctuations in the sediment are rather small and the effect of oxygen was assumed to be more important.

Growth Model for MOB

We assumed that methane oxidation rates were limited by methane, oxygen and temperature (Mayr et al., 2020a, Mayr et al., 2020c; Zimmermann et al., 2021). We used a Monod kinetics to describe limitation by methane. For oxygen, we assumed that MOB were able to grow at nanomolar oxygen concentrations (Milucka et al., 2015; Oswald et al., 2015) according to a Monod kinetics but were inhibited at higher oxygen concentrations (Thottathil et al., 2019). The sensitivity of pMMO to oxygen has been shown on isolated and purified enzymes and is most likely related to copper oxidation (Nguyen et al., 1998). We used a Ratkowski 2 model to formulate the temperature dependence of the methane oxidation rate (Ratkowsky et al., 1983). To our knowledge, there is no evidence on the exact shape of the temperature dependence of MOB growth rates but Ratkowski's growth rate model provides a common approach that has been successfully applied to describe the temperature dependence of a variety of bacterial species (Longhi et al., 2017). The combination of the three limiting factors leads to the following set of equations:

$$r_{MOX} = V_{max}(T)\frac{[CH_4]}{[CH_4]+K_{M,CH_4}}\frac{[O_2]}{[O_2]+K_{M,O_2}}\frac{K_{I,O_2}}{[O_2]+K_{I,O_2}} \quad (4)$$

$$V_{max}(T) = \left(b(T-T_{min})\left(1-exp[c(T-T_{max})]\right)\right)^2 \quad (5)$$

where K_{M,CH_4} is the half-saturation constant for methane, T_{min} and T_{max} are the minimum and maximum temperature at which the methane oxidation rate is zero. By solving the first derivative of **Eq. 5** at T_{opt}, i.e., where $V_{max}(T)$ has its maximum and the derivative is zero, we can calculate the coefficients b and c from the four parameters T_{min}, T_{max}, T_{opt} and $V_{max}(T_{opt})$:

$$c = \left[T_{min}LambertW(\gamma) - T_{opt}LambertW(\gamma) + T_{opt} - T_{max}\right] \Big/ \left[\left(T_{min}-T_{opt}\right)\left(T_{opt}-T_{max}\right)\right] \quad (6)$$

$$\gamma = -exp\left(\frac{T_{max}-T_{opt}}{T_{min}-T_{opt}}\right)\left(T_{max}-T_{opt}\right)\Big/\left(T_{opt}-T_{min}\right) \quad (7)$$

$$b = \sqrt{V_{max}\Big/\left(\left(T_{min}-T_{opt}\right)^2\cdot\left(exp\left(c\cdot\left(T_{opt}-T_{max}\right)\right)-1\right)^2\right)} \quad (8)$$

where $LambertW$ is the inverse function of $f(x) = xe^x$.

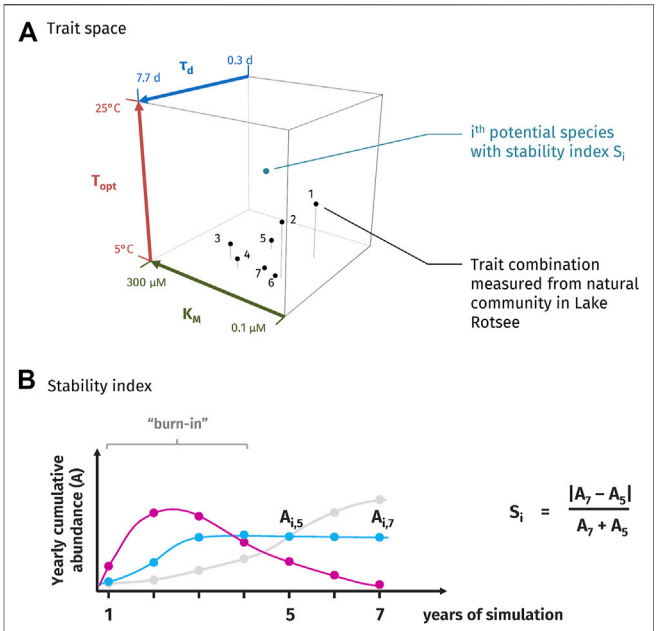


FIGURE 1 | Visualization of the methodological approach to analyze coexistence patterns in the model. **(A)** The 3-dimensional space of potential trait values for MOB is depicted as a cube. The range of trait values was derived to include trait values measured in Lake Rotsee (Mayr et al., 2020b). The affinity for methane is shown as the half-saturation constant for methane (high affinity = low K_M). The maximum growth rate is shown as doubling time. Most of the measured MOB assemblages in Lake Rotsee (shown in black) showed adaptation to low temperatures of 5–8°C and had slow methane oxidation rates of about 60 pmol cell^{-1} d^{-1} (full list of trait values in **Supplementary Table S1**). A single assemblage was abundant at higher temperatures of 16°C. However, we only have trait measurements of MOB assemblages from October to December, and we expect that there could be more trait combinations with adaptation to higher temperature earlier in the year and the range was accordingly set from 5 to 25°C. Similarly, other trait ranges were set somewhat in excess of measured trait combinations of assemblages, taking into account that traits of individual species can be averaged out in the assemblages **(B)** The stability index of a single species was calculated based on the difference between the yearly cumulative abundance in the fifth and seventh year of simulation. Lines illustrate the abundance of different MOB species in the model. The species in blue illustrates a species with a stable abundance after the initial "burn-in" phase. The species in pink illustrates an unstable species with decreasing concentrations. Another unstable species with increasing concentration is shown in grey.

Furthermore, we assumed that growth rates are directly proportional to methane oxidation rates, and we used typical values for the carbon use efficiency y_{CCE} (Leak and Dalton, 1986) as the fraction of oxidized methane that is incorporated into biomass. The growth rate r_{MOB} is therefore only a fraction of the methane oxidation rate:

$$\mu_{MOB} = y_{CCE}\cdot r_{MOX} - m \quad (9)$$

Mortality m was estimated from published laboratory experiments (Roslev and King, 1995) and was divided into a base mortality m_{anox} and an additional oxygen-dependent component:

$$m = m_{anox} + m_{ox}\frac{[O_2]}{[O_2] + K_{mo,O_2}} \quad (10)$$

Model Calibration

To calibrate the physical and biogeochemical model, we used PEST version 1.4 (Doherty, 2015). Meteorological data for the physical model were obtained from MeteoSwiss (see *Data Availability*). The primary calibration target was to reproduce available temperature profiles from 2014 to 2017. To calibrate the sediment model, we used seasonal methane profiles from 2016 (Mayr et al., 2020a; Zimmermann et al., 2021).

Mapping and Analysis of the Trait Space and Coexistence Patterns

Based on our hypothesis that methane oxidation kinetics and temperature adaptation are the main driver for niche partitioning of MOB in stratified lakes, we described each MOB species by three traits that form a three-dimensional trait space T (**Figure 1A**): its optimal temperature range, its affinity for methane and its maximum growth rate. Each point in this trait space T corresponds to a unique trait combination that describes a potential MOB species in the lake.

We used the above described biogeochemical model to explore the abundance and coexistence of single MOB species from the trait space T or whole communities of MOB species (multiple points in T). Based on preliminary explorations of the burn-in time of the model, we ran simulations for 7 years to allow the MOB species to establish their niches. For our simulation, we chose the meteorological forcing of a specific year and repeated these conditions in every year of the simulation. We thus simplified the problem by removing interannual variability and thereby focus on the development of population structure under realistic, but defined seasonal variations. For each species, we computed the annual cumulative abundance by simply adding up over depth and time.

To track survival or disappearance of species and long-term stability of the community, we defined a set of criteria. A species was considered a reoccurring member of the community if its annual cumulative abundance reached at least 10^3 cells in the last year of the simulation. For recurring members, we defined a stability index S_i where the stability S_i of a species i was calculated as the relative change of the cumulative abundance from year 5 to year 7 (**Figure 1B**):

$$S_i = \frac{|A_7 - A_5|}{A_7 + A_5} \quad (11)$$

This index was chosen as a simple proxy for stability that meets the following criteria: 1) the values range from 0 to 1, where 0 means stable (no change in abundance from year 5 to year 7) and 1 means unstable (extinction or infinitely many cells), and 2) the index is computationally efficient. If the simulation contained more than one species, we used the maximum value of all individual stabilities as the stability of the whole community. For a community, an overall stability index close to 0 indicates stable coexistence, whereas an overall stability index close to 1 indicates unstable coexistence.

To find and analyze trait combinations in multi-species communities that result in a stable coexistence, we generated maps of the stability index. To do so, we normalized each trait dimension (i.e., temperature optimum T_{Topt} , affinity for methane T_{KM} and maximum growth rate T_{Vmax}) and analyzed coexistence patterns in this normalized 3-dimensional trait space T (**Figure 1A**). The transformation from the normalized space T into actual trait values was performed as follows:

$$T_{opt} = 15 + 10 \cdot \begin{cases} (T_{Topt} - 0.5)2T_{Topt} \geq 0.5 \\ (T_{Topt} \cdot 2 - 1)T_{Topt} < 0.5 \end{cases} \quad [°C] \quad (12a)$$

$$T_{min} = 7 + \begin{cases} 5 \cdot (T_{Topt} - 0.5)2T_{Topt} \geq 0.5 \\ 6 \cdot (T_{Topt} \cdot 2 - 1)T_{Topt} < 0.5 \end{cases} \quad [°C] \quad (12b)$$

$$T_{max} = 33 + 22 \cdot \begin{cases} (T_{Topt} - 0.5) \cdot 2T_{Topt} \geq 0.5 \\ (T_{Topt} \cdot 2 - 1)T_{Topt} < 0.5 \end{cases} \quad [°C] \quad (12c)$$

$$K_M = 10^{(2.5-3.5 \cdot T_{KM})} \cdot 1000 \quad [\mu mol\, m^{-3}] \quad (13)$$

$$V_{max} = (0.1 + 1.9 \cdot T_{Vmax}) \cdot 10^{-5} \quad [s^{-3}] \quad (14)$$

Note, that K_M is normalized logarithmically while T_{opt} and V_{max} were normalized linearly. **Equations 12b**, **12c** describe our assumption on how temperature minimum and temperature maximum are situated around the temperature optimum. To our knowledge, there is no comprehensive dataset to derive this dependency and the two equations remain pragmatic assumptions.

We subdivided the normalized trait space into a grid with a resolution of 0.05 normalized trait units in every dimension. Each grid point in this trait space denotes a potential trait combination. The stability of a given point (a species) in T can be determined in isolation (single species) or tested in the presence of a community of n other species with different trait combinations.

In a first set of numerical experiments, we explored the stability of trait combinations and community compositions in an iterative way. For this purpose, we introduce the following nomenclature: T_n denotes the stability pattern of a whole community with n species that are known to be in a stable configuration and one additional species (n + 1). This allowed us to determine if the addition of a new species destabilizes a community that is otherwise stable, or if the new species can coexist with the previously stable community. For example, in T_0 every grid point denotes the stability of a single species with the trait combination at that specific grid point. In T_1, every grid point denotes the stability of the coexistence of the species at the grid point with a previously chosen, stable species from T_0. This allowed us to start out with a single stable species and iteratively explore which other species we can add to compose more and more complex stable communities.

In a second set of numerical experiments, the focus was on the effect of an additional species on a community that is known to be stable. According to the same principle, we define P_n as the stability pattern of only the already known, stable community with n species, when an additional species (n + 1) from the grid is added (i.e., without taking the stability of the added species into

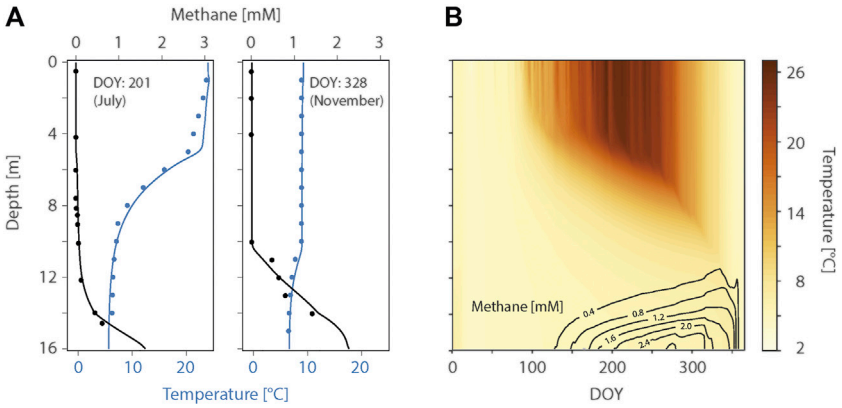


FIGURE 2 | Seasonal evolution of stratification, mixing and methane profiles in Lake Rotsee in 2016. **(A)** Typical profiles of measured (dots) and modelled (solid lines) temperatures and methane concentrations in 2016. Additional profiles are shown in **Supplementary Figure S1**. Log-scaled methane profiles are provided in **Supplementary Figure S4**. Methane profiles were computed without considering microbial methane oxidation, suggesting that the methane gradient is largely controlled by the physical stratification and mixing process rather than microbial activity. In July (left panel) the lake is stratified, and methane starts to accumulate in the hypolimnion. In November, lake cooling has deepened the mixed layer to about 10 m and transports methane from the hypolimnion into the mixed layer. **(B)** The seasonal evolution of lake temperatures simulated by the physical model is shown as a filled contour plot. The accumulation of methane predicted by the biogeochemical model is indicated by black contour lines that are labelled with methane concentrations in mM.

account). For example, in P_3 every grid point denotes the stability of the previously stable community of three species after addition of a fourth species with the trait combination at the grid point. The resulting stabilities associated with every grid-point in the trait spaces T_n and P_n were visualized using Wolfram Mathematica version 12.0.

Classification of Abundance Patterns

Based on the exploration of stability patterns (see *Results*), we determined a surface within the three dimensional trait space that covers trait combinations that are all coexisting with each other. The specific coexistence surface used for this exercise was selected to be close to the measured values of MOB assemblages in Rotsee. From this surface, we selected 1,564 species and ran a 7-year simulation. Because many of the 1,564 species will behave very similarly, our goal was to categorize the dominant abundance patterns. Due to the large number of observations and data points, classical statistical classification techniques are not suitable for this task. Instead, we used a technique that originates from the domain of unsupervised machine learning: self-organizing maps (SOM, Kohonen, 1982; Asan and Ercan, 2012). We used the implementation of the Julia package SOM.jl (see *Code Availability*) and trained eight neurons with all resulting abundance patterns to classify the dominant abundance patterns.

RESULTS AND DISCUSSION

Modelling Lake Stratification, Overturn and Methane Dynamics

The modelled development of stratification, mixing and methane concentrations qualitatively agreed well with field observations (**Figure 2**). The physical model overestimated surface water temperatures and underestimated water temperatures at the bottom of the lake (**Figure 2A**; **Supplementary Figure S1**). However, the mixed layer depths were in good agreement with the field observations, meaning that the stratification and mixing process was generally well reproduced. The modelled methane profiles qualitatively fitted well with measured methane profiles, which indicates that our biogeochemical model captured the most essential processes (**Figure 2A**; **Supplementary Figure S1**). Note that the aim of the model was not to reproduce the observations perfectly. For the purpose of this study, it was sufficient that the model was able to reproduce the general dynamics of the system (i.e., seasonal dynamics of stratification, accumulation of methane in the hypolimnion and subsequent lake overturn, which transports accumulated methane to the mixed layer) and to yield concentration values that are comparable to the observations (**Figure 2B**).

The modelled methane profiles within the water-column fitted well with observations even when we modelled methane profiles without considering microbial methane oxidation (**Figure 2A**; **Supplementary Figure S1**). This suggests that the shape of the methane gradient in the water-column (i.e., especially the position of the methane interface) is not a direct indication for microbial activity. In particular, the depth where methane concentrations started to increase matched well with the field observations suggesting that the position of the methane-oxygen counter gradient is largely controlled by the physical stratification and mixing process rather than microbial activity. Even though this indicates that microbial methane oxidation does not alter methane concentrations substantially, growth of methanotrophs is still supported by the flux of methane. The decreasing methane concentrations towards the mixed layer results in a flux of methane into the epilimnion. During stable stratification, this methane flux supports growth of methanotrophic bacteria right at the oxycline (Zimmermann et al., 2021). Without considering

microbial methane oxidation, the model overestimated methane concentrations in the epilimnion during the late overturn in autumn (**Supplementary Figure S1**). Increased concentrations result from the progressing thermocline deepening, which substantially increases the methane flux to the epilimnion. As shown in (Zimmermann et al., 2021), a rapidly growing assemblage of MOB in the epilimnion is able to oxidize almost all of this methane and keep methane concentrations low.

When the lake was completely mixed at the beginning of the year, the model predicted higher methane concentrations at the bottom of the lake than observed (**Supplementary Figure S1**). Even though water temperatures are low at this time, psychrophilic methanotrophs might be able to oxidize this methane (Trotsenko and Khmelenina, 2005). To our knowledge, however, there are no systematic measurements of MOB abundance and activity in stratified lakes during winter. Growth of MOB during this early, well-mixed phase might be an alternative explanation or might at least partially contribute to the methanotroph biomass observed in the anoxic hypolimnion during stable stratification (Oswald et al., 2016; Mayr et al., 2020a, 2020c; Zimmermann et al., 2021). At temperatures of about 5—6°C and without oxygen, this biomass might be well preserved for a considerable amount of time even when oxygen is no longer available in the hypolimnion (Roslev and King, 1995).

The sediment model is very simplified and needed substantial calibration. Our objective was to close our model with realistic sediment fluxes. In our model, the sediment water fluxes were on average 23 μmol m^{-2} d^{-1} (0.4 mg m^{-2} d^{-1}) with a peak in fall at about 55 μmol m^{-2} d^{-1} (0.9 mg m^{-2} d^{-1}). This flux was actually fitted to reproduce observed methane concentration in the hypolimnion. When compared to the literature, our model flux is in the lower range of the reported sediment-water methane fluxes. Huttunen et al. (2006) reported fluxes for eutrophic boreal lakes range over a wide range 0.44—76 mg m^{-2} d^{-1}. Similarly, the flux at temperature close to 4°C in Mindelsee ranged from 0.1 to 0.15 mmol m^{-2} d^{-1} (1.6–2.4 mg m^{-2} d^{-1}) while Bastkiven et al. (2008) indicated higher methane fluxes in the hypolimnion of three lakes in the United States (3–13 mmol m^{-2} d^{-1} (48–209 mg m^{-2} d^{-1}) for the hypolimnion). Steinsberger et al. (2017) also reported similar fluxes ranging from 0.08 to 4.24 mg m^{-2} d^{-1} for 5 Swiss lakes.

Configurations of Coexisting Species

We were interested in whether we can establish diversity and niche differentiation of MOB in our model, based on measured methane oxidation kinetics and temperature adaptation. We ran model simulations, which considered seven individual model species with trait value combinations derived from values determined for natural MOB assemblages in Rotsee water samples (Mayr et al., 2020b, **Supplementary Table S1**). While the measurements were obtained from mixed communities (**Supplementary Table S2**) and temperature optima were not determined experimentally, it appeared reasonable that average trait values of the community would approximate those of dominant species in each sample, and that these organisms would be adapted to the *in-situ* temperature, which was therefore used as the temperature optimum. Simulations with this set of species, however, did not result in a stable coexistence and niche differentiation in the model (**Supplementary Figure S2**). After the 7-year simulation period, only two of the seven simulated species were stable and dominated the MOB abundance whereas the other five species showed decreasing abundances or fell below the survival threshold (10^3 cells cumulative annual abundance). Therefore, we decided to systematically explore conditions for stable coexistence of MOB species in our model.

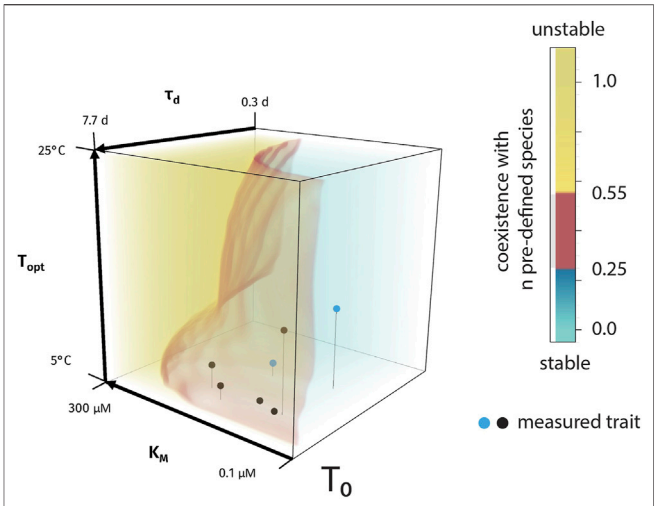


FIGURE 3 | Mapping coexisting communities of MOB in Lake Rotsee. The 3-dimensional space of potential trait values for MOB is depicted as a cube. Each point in the three-dimensional trait space is shaded according to the long-term recurrence of the respective trait-combination by itself or together with the pre-defined species of a stable assemblage. Here, we show the stability of single species in the simulated Rotsee. The arrows next to the axes label indicate increasing methane affinity, increasing adaptation to warm temperatures and increasing maximum methane oxidation rates, respectively. Regions of trait combinations with stable recurrence after 7 years are shaded in blue, regions of instable trait combinations in yellow. The transition between stable and unstable recurrence ($0.25 < S_i > 0.55$) is shaded in red. Seven trait combinations determined for MOB assemblages during a field campaign in Rotsee (Mayr et al., 2020b, **Supplementary Table S1**) are indicated as dots. In model simulations with all these seven species as a community, only two species remained stable and above the abundance threshold over the 7-year simulation (blue dots).

To search for combinations of MOB species that form a stable community in the model, we first examined each potential trait combination of a single species and determined which of these trait combinations resulted in a stable abundance in the lake (**Figure 3**). The resulting stability map for single species T_0 was monotonous in the sense that T_0 was split into two homogeneous regions: an unstable region towards low growth rates and low methane affinities and a stable region towards fast growth and high methane affinity. Interestingly, the transition between stability and instability was not gradual but limited to a thin, curved zone (red color in **Figure 3**).

The trait combinations determined from lake water samples (**Figure 3**, black dots) were all located within the stable region, which means that each individual species in this set would establish a stable abundance in the model. However, in

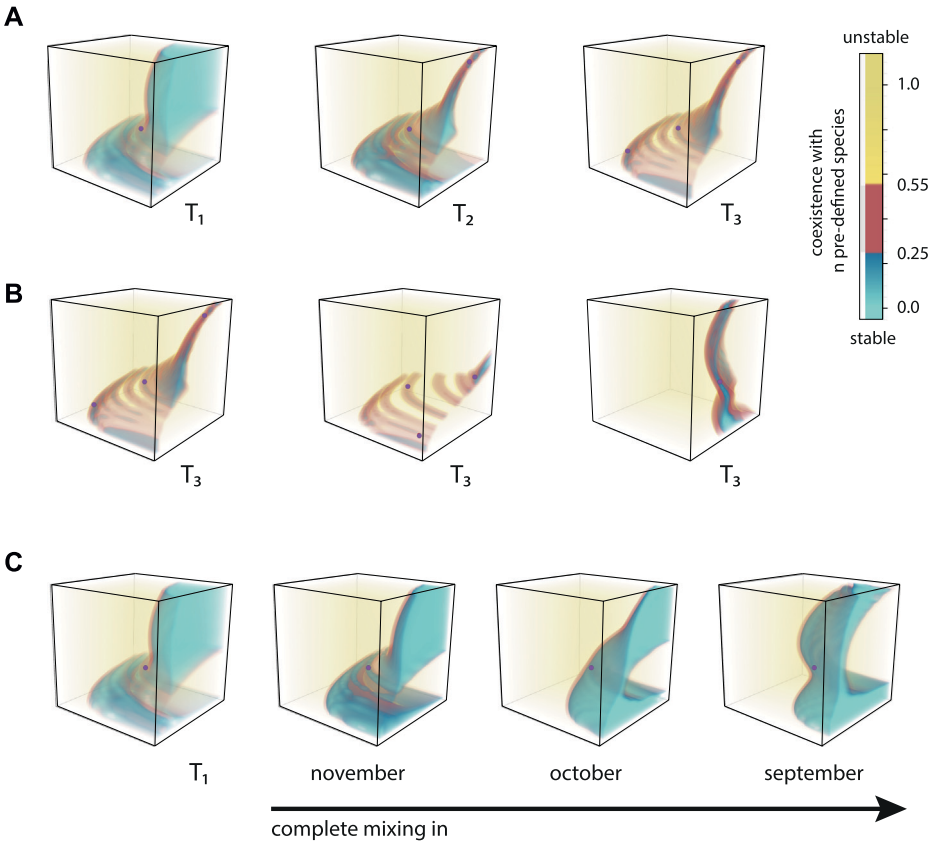


FIGURE 4 | (A) Regions of stable trait configurations with an increasing number of pre-defined species. The trait combination of the pre-defined species is indicated with purple dots. In T_1, a single species that was stable in T_0 is pre-defined, and the shading corresponds to the long-term coexistence of the pre-defined species with any second species in the trait space. In T_2, two coexisting species are pre-defined, and the shading corresponds to the long-term coexistence of the two pre-defined species with any third species in the trait space. The same principle applies to T_3. The banded pattern of emerging regions with stable coexistence is an artefact of the map resolution. **(B)** Depending on the selection process of species from T_1 to T_3, different configurations of stable communities emerge in T_3 (each point in the three-dimensional trait space is shaded according to the stability of the original community together with the species with the trait combination at that point). **(C)** Stability depends on the environmental conditions. We artificially introduced a strong wind-event into our simulations that completely mixed the water column in either September, October or November in each of the repeated 7 years of the simulation. Depending on the mixing behavior, the region of partners forming a stable community with a single pre-defined species (dark purple dot) has a different shape. To reduce distraction, axes labeling was omitted. The view and scaling is the same for all cubes and is equivalent to the cube in **Figure 3**.

combination with each other, some of the modelled species were not competitive under the model conditions. In the model, only two of the measured trait combinations were able to coexist (**Figure 3**, blue dots).

To explore which combinations of species would be able to coexist in the model, we assembled custom communities with the following procedure (illustrated in **Figure 4A**): We started by selecting a species with a custom trait combination close to the trait combinations measured for Lake Rotsee communities. Subsequently, we tested this trait combination against all other trait combinations for stable coexistence (**Figure 4A**, T_1). The resulting coexistence space T_1 consisted of confined regions (blue, **Figure 4A**) containing all possible stable partners. Interestingly, the stable regions were at some distance from the selected starting species, whereas the space in the immediate vicinity was largely unstable. This is in good agreement with Hardin's competitive exclusion principle (Hardin, 1960). Within the confines of the limited number of traits in our model, a competing species whose trait values differ only slightly will most likely either replace the original species, or is not competitive unless changes in several trait values compensate each other exactly. Species with more distant trait values are more likely to coexist because they can occupy a different niche.

Based on this analysis, we again selected one new species with a trait combination that formed a stable coexistence with the first trait combination. We then repeated the procedure of combining this pre-defined pair with all other trait combinations and determined the regions in the trait space that lead to a stably coexisting three-species assemblage (**Figure 4A**, T_2). This procedure can be repeated to combine several coexisting species from different regions of the trait space. We observed that the parameter space containing further partners which can coexist with the pre-defined assemblage shrinks as the number of coexisting species in the model increases (**Figure 4A**). The shrinking parameter space remains confined to

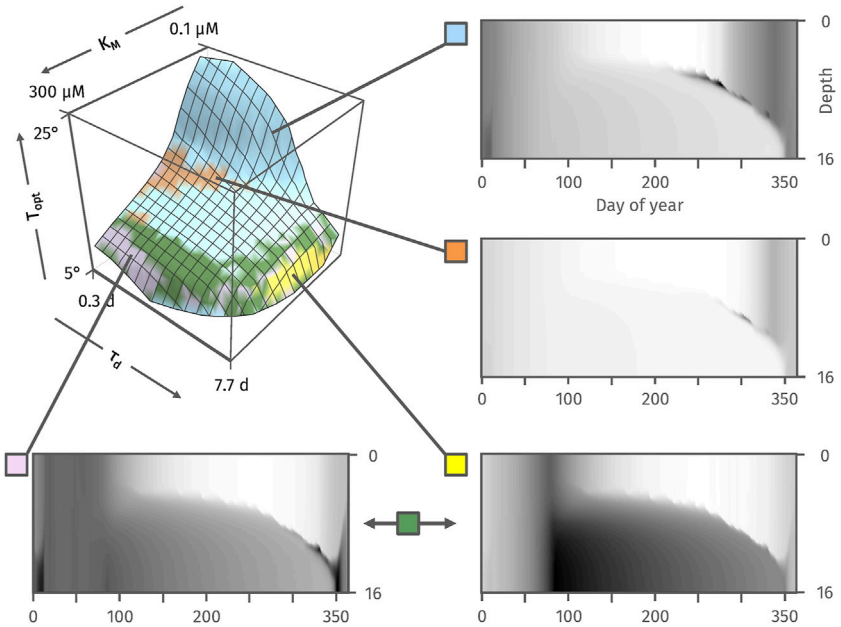


FIGURE 5 | Classification of normalized (0 = least abundant/white, 1 = most abundant/black) spatiotemporal abundance patterns using a self-organizing maps approach (Asan and Ercan, 2012). We ran a 7-year simulation with an initial set of 1,564 species whose trait combinations were sampled from a regular grid on the shown coexistence surface within the trait space. The coexistence surface approximates the regions of coexistence in **Figure 4A**, T_3. A self-organizing map with eight neurons was trained on all 1,564 normalized abundance patterns. We colored the surface of trait combinations to indicate the associated neuron that shows highest activation for the specific abundance pattern. Only five of the eight neurons specialized to a specific region on the surface. Each of the five neurons can reproduce the input/pattern to which it has specialized. The four clearly distinct abundance patterns are shown as heat maps (dark colors indicate high abundance, light colors indicate low abundance, i.e., white = 0, black = 1) representing abundance over depth and time in year 7 of the simulation. The neuron associated with the abundance pattern in green showed a combination of the two neighboring patterns.

a thin surface, indicating that the available niche space for additional partners is limited.

Within the trait space an unlimited number of configurations of coexisting species exists, which raises the question which trait distribution is effectively realized in nature. In our model, the shape of the region where coexisting trait combinations are located depended on the selection of pre-defined species (**Figure 4B**). This implies that there could be an exclusion mechanism, where the abundances of a few "founder" species in the beginning of the season already define which additional species are able to coexist with those already present.

To allow setting up reasonable criteria for stable coexistence, our lake model repeats the same meteorological conditions each simulated year, thus also the environmental conditions and the same mixing patterns unrealistically re-occur over the seven modelled years. We explored the potential impact of variable mixing conditions by artificially introducing mixing events at different times of the repeated annual cycle and evaluating the effect on the coexistence space with a single pre-existing species (T_1). This scenario analysis showed that the shape of regions of coexistence depended on the seasonal dynamics of lake stratification and mixing (**Figure 4C**). Different annual weather conditions will influence the stable species composition.

Both the effect of the pre-existing species and the environmental impact discussed above would suggest that under real-world conditions, the MOB community in lakes may differ from year to year, and a perennial stable community may never truly occur—instead changing conditions and species assemblies would continually open new niche spaces while other niches become obsolete. Multi-year Datasets on MOB communities in stratified lakes that would allow us to test if this prediction of our model is true in nature are currently not available. Longer-lasting modeling runs could include variable dynamics of annual warming, mixing and cooling. Such an extended approach could further explore the effects of the chaotic part in the annual oscillations on the long-term stability of the MOB community.

Abundance Patterns of Simulated Species in Space and Time

We analyzed abundance patterns of a large number of species (**Figure 5**) whose trait combinations were located on a coexistence surface that was selected to fall close to the measured trait combinations. Based on self-organizing map classification, we found at least 4 distinct abundance patterns (**Figure 5**, blue, orange, yellow, pink). One pattern was associated with species that were mainly abundant in the hypolimnion (**Figure 5**, pink), a pattern observed for example in the Methylococcales species ASV_4 in Rotsee (Mayr et al., 2020a). Two patterns showed an abundance maximum at the interface of the mixed layer and the hypolimnion during stratified conditions

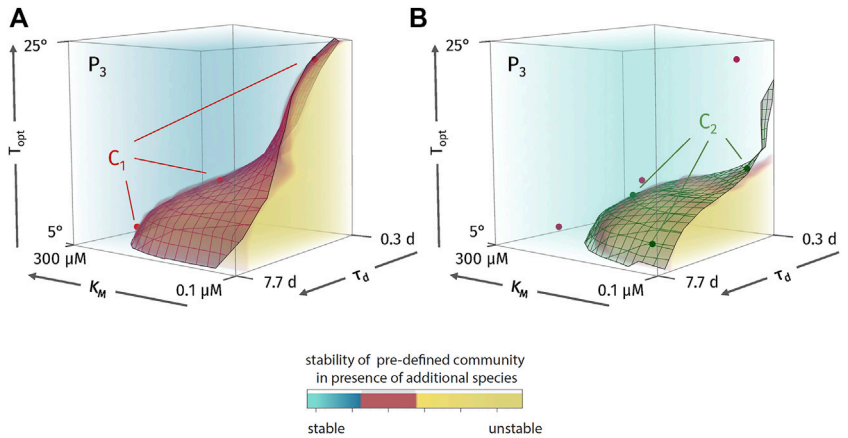


FIGURE 6 | (A) Stability space (P_3) of a stable community C_1 of three species (red dots) when an additional species is added. In P_3, each point in the three-dimensional trait space is shaded according to the stability of only the original community, when the species with the trait combination at that point is added to the community. The thin layer of coexistence in the stability space T_3 (**Figure 4B**, first cube on the left) is shown as an approximated smooth surface (red wire frame). Regions where the additional species would destabilize the original community are shaded in yellow. The stable community is destabilized and replaced by the addition of any "better adapted" species in this yellow region. **(B)** A stable community C_2 with three species (green dots) from the yellow region in panel **(A)**. The three species of community C_1 are shown as red dots. The thin layer of coexistence in the stability space T_3 (**Figure 4B**, second cube from the left) is shown as an approximated smooth surface (green wire frame). The stability space (P_3) of this community shows the same property of destabilization. Thus invasion or evolution of better adapted species would invariably lead to a contraction of the stable community (red arrows in panel **(A)**) towards a highly optimized community or ultimately even to a "superorganism." Compared to **Figure 4**, the trait-spaces are shown from a slightly tilted angle.

or in the mixed layer (**Figure 5**, blue, orange). Overall, these modelled patterns approximate the three main spatial niches quite well, which we proposed under stratified conditions (Epilimnion, Interface, Hypolimnion) previously (Mayr et al., 2020c). This indicates that the simple kinetic trait combinations used in our model suffice to reproduce this fundamental niche partitioning pattern of MOB in stratified lakes. Three patterns were further associated with species that became abundant in the mixed layer during different stages and different durations of the mixing period (**Figure 5**, blue, orange, pink). This matches observations from our previous study where we reported temporal succession of species dominating in the mixed layer during lake overturn (Mayr et al., 2020a). A pattern observed in nature, in Rotsee, e.g., for *Methylocystis* (Guggenheim et al., 2020), but not in our model was that of an abundance increase towards the lake surface during summer stratification. This indicates that certain traits or processes that determine the distribution of this taxon are not represented in our model. Overall, our custom assembled communities showed spatiotemporal abundance patterns remarkably similar to previously observed depth profiles and temporal dynamics of methanotroph species in Lake Rotsee (Mayr et al., 2020a). Considering the simple trait space used in the model, this finding is noteworthy and provides considerable support to the hypothesis that kinetic traits of the methane oxidation are a central adaptive strategy, and thus a basis for niche differentiation in freshwater methanotrophs.

Destabilizing a MOB Community

Moving from the stability pattern T_1 to T_3 reduces the stable trait space significantly (**Figure 4A**). Therefore, we hypothesize that with increasing number of community members, the region of stable trait configurations ultimately narrows down to a thin layer or surface. This would indicate that "stable" communities are actually easily disturbed if a new species invade them or if one of the members of the community acquires new trait values through adaptive evolution. In order to explore this idea further, we iteratively assembled a stable community C_1 of three species (**Figure 6A**, red dots) and determined its stability when added additional species. The region of additional species that would destabilize the original community covered the entire space on one side of the narrow layer of coexistence: the side towards higher growth rates, high affinity and adaptation to low temperatures. Members of the original community C_1 will be replaced by additional species with such trait combinations and therefore, the shape of the region with stable partners would change accordingly. We iteratively assembled a new stable community C_2 with species from the region that would destabilize the original community C_1 (**Figure 6B**). When we again determined the stability of this community C_2 after the addition of a new species, we observed the same distribution of stability and instability. Within our simplified model, unrestricted evolution towards optimized trait combinations would cause the surface of coexistence to shift gradually towards an increasingly optimized community and ultimately a "superorganism" that would outperform all other species. The observed diversity of the methanotrophic assemblage in real lakes points to a clear limitation of our model and to barriers precluding the evolution of such a superorganism, i.e., physiological limits or tradeoffs between and with additional traits. This further suggests that, if methane oxidation kinetics and adaptation to temperature are the dominant traits that explain coexistence and niche differentiation, the observed trait combinations should be aligned on a specific surface within the trait space T where

physiological restrictions and tradeoffs prevent further optimization of the trait values.

As noted earlier, trait values observed for MOB communities in Lake Rotsee did not result in a stable community in our model. Assuming that the three traits we modelled are the main explanatory variables for the observed niche differentiation, we would expect that observed trait values should be positioned at least approximately near one of the thin layers of potential coexistence. We approximated such a layer of coexistence that runs close to observed values (**Figure 4B**, first cube from the left) shown also as the smooth surface of community C_1 in **Figure 6A** (red wire frame). Even though the curvature of this surface roughly approximates the trait combinations actually observed in Lake Rotsee, several values diverged considerably, e.g., towards adaptation to lower temperature than allowed for stable coexistence (**Supplementary Figure S3**). As temperature optima were not measured but simply assumed to correspond to in-situ temperatures, it may not be surprising that we see such a divergence. The limited number of observations and the uncertainty associated with the measured values do not allow assessing how well kinetics and temperature adaptation can explain the observed trait distribution. Other traits not considered in our model may be important and may allow coexistence despite incompatible methane oxidation kinetics or temperature adaptation. Such additional traits could include oxygen tolerance (Nguyen et al., 1998), syntrophic strategies (Milucka et al., 2015; Skennerton et al., 2017), starvation metabolisms (Kalyuzhnaya et al., 2013) or acquisition strategies for other nutrients, such as nitrogen or copper (Auman et al., 2001; Semrau et al., 2013). Clearly, our physical and biogeochemical model is likewise a highly simplified representation of reality, that does not account for stochastic variability in the environment.

CONCLUSION AND OUTLOOK

With the observation of a fascinating diversity, vertical structure and seasonal succession of methane oxidizing bacteria in stratified lakes, the question arose how this diversity is maintained. Here we investigated with our trait-based mechanistic model of microbial methane oxidation if and how well we can reproduce and explain the observed patterns of lacustrine MOB diversity in a seasonally stratified lake.

With our model, we successfully recreate diversity and niche differentiation patterns of methanotrophs very similar to observed patterns in seasonally stratified lakes. This finding provides support to the hypothesis that the traits used in our model—kinetic traits of the methane oxidation and different temperature optima—are indeed central adaptive strategies, and thus a basis for niche differentiation in freshwater methanotrophs. However, in the model, the combination of trait values that allowed coexistence was rapidly confined to narrow regions in the parameter space as we increased the number of species, raising the question how these exact combinations would be realized in nature or whether there are mechanisms that widen these narrow regions. We argue that evolutionary convergence to the physiological limit that is inherent in the underlying biochemical and cellular systems is one mechanism that pushes trait values to these narrow regions on evolutionary time scales. In addition, the sequence of colonization or the annual variability of the stratification and mixing behavior of the lake may allow different stable configurations from year to year or on even shorter timescales, which may provide another way to maintain a higher diversity than expected from the competitive exclusion principle. Additional physiological traits (e.g., oxygen tolerance, symbiotic strategies or starvation tolerance) not considered here might be important for niche differentiation and may widen the space for coexistence.

The modeled environment was necessarily simplified; the data used to build our model of the Rotsee water column focused on the turnover period, and we have only a coarse representation of the methane-oxygen interface in the model. Specifically, we excluded the possible effects of nutrients (nitrogen, phosphorus), micronutrients such as copper (Guggenheim et al., 2019), and we neglected lateral exchange in our 1-D model (Thalasso et al., 2020). In particular, the parameterization of the sediment model can be questioned and improved as well. Adding more detail and expanding the kinetic parameter space will add more niches and more potential for a stable diversity of the MOB community. Nevertheless, our approach is the first attempt to combine a fundamentally realistic lake physical and biogeochemical model with a trait-based population model and thus provides the first opportunity to test the validity of a trait-based approach for MOB ecology against environmental data. Further, our model approach provides ample opportunity for future expansion, e.g., to test the importance of further traits, and for application in other lakes.

In this study, we have not yet analysed whether the trait-based approach for modelling methane oxidation affects the accuracy of the biogeochemical model. The question whether MOB diversity has to be taken into account when modelling methane emissions and microbial methane oxidation in lakes remains to be investigated. We found that the rough shape of the methane gradient in the studied lake is largely controlled by the physical stratification and mixing process, but, e.g., methane concentrations in the mixed layer during overturn would be overestimated without considering methane oxidation - and thus methane emissions would be overestimated. There may thus be a number of situations and research questions where knowledge of changes in methane oxidation kinetics, which our trait-based approach could provide, may be of importance. For example, the amount of outgassing of methane will depend on whether the most abundant MOB in the epilimnion in summer or in the mixed layer during lake overturn is a high affinity MOB or not. The improvement of incorporating trait diversity in a biogeochemical model may also become important when conditions change rapidly. Under such conditions, a trait-based model may predict how oxidation kinetics change and may provide a better system description. Finally, it would be interesting to explore if a high trait diversity results in more efficient methane oxidation in a system, especially if this diversity is independently controlled by other factors, such as, e.g., temperature, micronutrient availability or pollution.

DATA AVAILABILITY STATEMENT

The datasets presented in this study can be found in online repositories. The names of the repository/repositories and

accession number(s) can be found below: Physico-chemical data is available at the ETH Research Collection (https://doi.org/10.3929/ethz-b-000350091).

The source code of the physical model is available on GitHub (http://doi.org/10.5281/zenodo.3274379). The source code of the numerical discretization of the reaction-diffusion equation used for the biogeochemical model is available as a Julia package (https://github.com/zimmermm/FiniteVolumeRDS.jl). The actual implementation of the biogeochemical model as well as the microbial growth model for Lake Rotsee is available on GitHub (https://github.com/zimmermm/MOBDiversityModel).

AUTHOR CONTRIBUTIONS

MZ, MM, HB, and BW conceptualized the study. MZ and DB conceptualized the model. MZ developed the model under supervision of DB and with inputs by HB, MM, and BW. MM and MZ acquired the data. MZ wrote the first draft of the manuscript and created the figures. All authors contributed text during revisions of the manuscript and were involved in commenting and editing the paper. HB and BW acquired the funding.

FUNDING

The Swiss National Science Foundation (grant CR23I3_156759), ETH Zurich and Eawag funded this research. Open access funding provided by Swiss Federal Institute of Aquatic Science and Technology.

ACKNOWLEDGMENTS

We thank Karin Beck, Andreas Brand, Jason Day, Patrick Kathriner, Miro Meyer, Michael Plüss and Serge Robert for their help and advice in the field and the lab. We acknowledge the helpful discussions and feedback by Carsten Schubert, Blake Matthews and Anita Narwani. We thank Andreas Brand for his advice and support during the first phase of the project.

SUPPLEMENTARY MATERIAL

The Supplementary Material for this article can be found online at: https://www.frontiersin.org/articles/10.3389/fenvs.2022.833511/full#supplementary-material

REFERENCES

Asan, U., and Ercan, S. (2012). "An Introduction to Self-Organizing Maps," in *Computational Intelligence Systems in Industrial Engineering. Atlantis Computational Intelligence Systems*. Editor C. Kahraman (Paris: Atlantis Press), 6, 295–315. doi:10.2991/978-94-91216-77-0_14

Auman, A. J., Speake, C. C., and Lidstrom, M. E. (2001). nifH Sequences and Nitrogen Fixation in Type I and Type II Methanotrophs. *Appl. Environ. Microbiol.* 67, 4009–4016. doi:10.1128/AEM.67.9.4009-4016.2001

Baani, M., and Liesack, W. (2008). Two Isozymes of Particulate Methane Monooxygenase with Different Methane Oxidation Kinetics Are Found in Methylocystis Sp. Strain SC2. *Proc. Natl. Acad. Sci. U.S.A.* 105, 10203–10208. doi:10.1073/pnas.0702643105

Bastviken, D., Cole, J. J., Pace, M. L., and Van de Bogert, M. C. (2008). Fates of Methane from Different Lake Habitats: Connecting Whole-Lake Budgets and CH4emissions. *J. Geophys. Res.* 113, a–n. doi:10.1029/2007JG000608

Bastviken, D., Tranvik, L. J., Downing, J. A., Crill, P. M., and Enrich-Prast, A. (2011). Freshwater Methane Emissions Offset the Continental Carbon Sink. *Science* 331, 50. doi:10.1126/science.1196808

Bezanson, J., Edelman, A., Karpinski, S., and Shah, V. B. (2017). Julia: A Fresh Approach to Numerical Computing. *SIAM Rev.* 59, 65–98. doi:10.1137/141000671

Brand, A., Bruderer, H., Oswald, K., Guggenheim, C., Schubert, C. J., and Wehrli, B. (2016). Oxygenic Primary Production below the Oxycline and its Importance for Redox Dynamics. *Aquat. Sci.* 78, 727–741. doi:10.1007/s00027-016-0465-4

Chesson, P. (2000). Mechanisms of Maintenance of Species Diversity. *Annu. Rev. Ecol. Syst.* 31, 343–366. doi:10.1146/annurev.ecolsys.31.1.343

Conrad, R. (2009). The Global Methane Cycle: Recent Advances in Understanding the Microbial Processes Involved. *Environ. Microbiol. Rep.* 1, 285–292. doi:10.1111/j.1758-2229.2009.00038.x

Dam, B., Dam, S., Kube, M., Reinhardt, R., and Liesack, W. (2012). Complete Genome Sequence of Methylocystis Sp. Strain SC2, an Aerobic Methanotroph with High-Affinity Methane Oxidation Potential. *J. Bacteriol.* 194, 6008–6009. doi:10.1128/JB.01446-12

DelSontro, T., Beaulieu, J. J., and Downing, J. A. (2018). Greenhouse Gas Emissions from Lakes and Impoundments: Upscaling in the Face of Global Change. *Limnol. Oceanogr. Lett.* 3, 64–75. doi:10.1002/lol2.10073

Doherty, J. (2015). *Calibration and Uncertainty Analysis for Complex Environmental Models*. Australia: Watermark Numerical Computing Brisbane. Available at: https://doi.org/10.1111/gwat.12360.

Fiskal, A., Deng, L., Michel, A., Eickenbusch, P., Han, X., and Lagostina, L. (2019). Effects of Eutrophication on Sedimentary Organic Carbon Cycling in Five Temperate Lakes. *Biogeosciences* 16, 3725–3746. doi:10.5194/bg-16-3725-2019

Gaudard, A., Råman Vinnå, L., Bärenbold, F., Schmid, M., and Bouffard, D. (2019). Toward an Open Access to High-Frequency Lake Modeling and Statistics Data for Scientists and Practitioners – the Case of Swiss Lakes Using Simstrat v2.1. *Geosci. Model Dev.* 12, 3955–3974. doi:10.5194/gmd-12-3955-2019

Guggenheim, C., Brand, A., Bürgmann, H., Sigg, L., and Wehrli, B. (2019). Aerobic Methane Oxidation under Copper Scarcity in a Stratified Lake. *Sci. Rep.* 9, 4817. doi:10.1038/s41598-019-40642-2

Guggenheim, C., Freimann, R., Mayr, M. J., Beck, K., Wehrli, B., and Bürgmann, H. (2020). Environmental and Microbial Interactions Shape Methane-Oxidizing Bacterial Communities in a Stratified Lake. *Front. Microbiol.* 11, 579427. doi:10.3389/fmicb.2020.579427

Hanson, R. S., and Hanson, T. E. (1996). Methanotrophic Bacteria. *Microbiol. Rev.* 60, 439–471. doi:10.1128/mr.60.2.439-471.1996

Hardin, G. (1960). The Competitive Exclusion Principle. *Science* 131, 1292–1297. doi:10.1126/science.131.3409.1292

Hofman, P., de Jong, S., Wagenvoort, E., and Sandee, A. (1991). Apparent Sediment Diffusion Coefficients for Oxygen and Oxygen Consumption Rates Measured with Microelectrodes and Bell Jars: Applications to Oxygen Budgets in Estuarine Intertidal Sediments (Oosterschelde, SW Netherlands). *Mar. Ecol. Prog. Ser.* 69, 261–272. doi:10.3354/meps069261

Hutchinson, G. E. (1961). The Paradox of the Plankton. *Am. Nat.* 95, 137–145. doi:10.1086/282171

Huttunen, J. T., Väisänen, T. S., Hellsten, S. K., and Martikainen, P. J. (2006). Methane Fluxes at the Sediment-Water Interface in Some Boreal Lakes and Reservoirs. *Boreal Environ. Res.* 11 (1), 27–34.

Kalyuzhnaya, M. G., Yang, S., Rozova, O. N., Smalley, N. E., Clubb, J., Lamb, A., et al. (2013). Highly Efficient Methane Biocatalysis Revealed in a Methanotrophic Bacterium. *Nat. Commun.* 4, 2785. doi:10.1038/ncomms3785

Kankaala, P., Huotari, J., Peltomaa, E., Saloranta, T., and Ojala, A. (2006). Methanotrophic Activity in Relation to Methane Efflux and Total Heterotrophic Bacterial Production in a Stratified, Humic, Boreal Lake. *Limnol. Oceanogr.* 51, 1195–1204. doi:10.4319/lo.2006.51.2.1195

Knief, C., and Dunfield, P. F. (2005). Response and Adaptation of Different Methanotrophic Bacteria to Low Methane Mixing Ratios. *Environ. Microbiol.* 7, 1307–1317. doi:10.1111/j.1462-2920.2005.00814.x

Kohonen, T. (1982). Self-organized Formation of Topologically Correct Feature Maps. *Biol. Cybern.* 43, 59–69. doi:10.1007/BF00337288

Kojima, H., Iwata, T., and Fukui, M. (2009). DNA-based Analysis of Planktonic Methanotrophs in a Stratified Lake. *Freshw. Biol.* 54, 1501–1509. doi:10.1111/j.1365-2427.2009.02199.x

Leak, D. J., and Dalton, H. (1986). Growth Yields of Methanotrophs. *Appl. Microbiol. Biotechnol.* 23, 470–476. doi:10.1007/BF02346062

Liss, P. S., and Slater, P. G. (1974). Flux of Gases across the Air-Sea Nterface. *Nature* 247, 181–184. doi:10.1038/247181a0

Litchman, E., and Klausmeier, C. A. (2008). Trait-Based Community Ecology of Phytoplankton. *Annu. Rev. Ecol. Evol. Syst.* 39, 615–639. doi:10.1146/annurev.ecolsys.39.110707.173549

Litchman, E., Pinto, P. de. T., Edwards, K. F., Klausmeier, C. A., Kremer, C. T., and Thomas, M. K. (2015). Global Biogeochemical Impacts of Phytoplankton: a Trait-Based Perspective. *J. Ecol.* 103, 1384–1396. doi:10.1111/1365-2745.12438

Lofton, D. D., Whalen, S. C., and Hershey, A. E. (2014). Effect of Temperature on Methane Dynamics and Evaluation of Methane Oxidation Kinetics in Shallow Arctic Alaskan Lakes. *Hydrobiologia* 721, 209–222. doi:10.1007/s10750-013-1663-x

Longhi, D. A., Dalcanton, F., de Aragão, G. M. F., Carciofi, B. A. M., and Laurindo, J. B. (2017). Microbial Growth Models: A General Mathematical Approach to Obtain μ Max and λ Parameters from Sigmoidal Empirical Primary Models. *Braz. J. Chem. Eng.* 34, 369–375. doi:10.1590/0104-6632.20170342s20150533

MacIntyre, S., Jonsson, A., Jansson, M., Aberg, J., Turney, D. E., and Miller, S. D. (2010). Buoyancy Flux, Turbulence, and the Gas Transfer Coefficient in a Stratified Lake. *Geophys. Res. Lett.* 37, L24604 1–5. doi:10.1029/2010GL044164

Martin, G., Rissanen, A. J., Garcia, S. L., Mehrshad, M., Buck, M., and Peura, S. (2021). Candidatus Methylumidiphilus Drives Peaks in Methanotrophic Relative Abundance in Stratified Lakes and Ponds across Northern Landscapes. *Front. Microbiol.* 12, 669937. doi:10.3389/fmicb.2021.669937

Martiny, J. B. H., Jones, S. E., Lennon, J. T., and Martiny, A. C. (2015). Microbiomes in Light of Traits: A Phylogenetic Perspective. *Science* 350, aac9323. doi:10.1126/science.aac9323

Maynard, D. S., Miller, Z. R., and Allesina, S. (2020). Predicting Coexistence in Experimental Ecological Communities. *Nat. Ecol. Evol.* 4, 91–100. doi:10.1038/s41559-019-1059-z

Mayr, M. J., Zimmermann, M., Dey, J., Brand, A., Wehrli, B., and Bürgmann, H. (2020a). Growth and Rapid Succession of Methanotrophs Effectively Limit Methane Release during Lake Overturn. *Commun. Biol.* 3, 108. doi:10.1038/s42003-020-0838-z

Mayr, M. J., Zimmermann, M., Dey, J., Wehrli, B., and Bürgmann, H. (2020b). Lake Mixing Regime Selects Apparent Methane Oxidation Kinetics of the Methanotroph Assemblage. *Biogeosciences* 17, 4247–4259. doi:10.5194/bg-17-4247-2020

Mayr, M. J., Zimmermann, M., Guggenheim, C., Brand, A., and Bürgmann, H. (2020c). Niche Partitioning of Methane-Oxidizing Bacteria along the Oxygen–Methane Counter Gradient of Stratified Lakes. *ISME J.* 14, 274–287. doi:10.1038/s41396-019-0515-8

Milucka, J., Kirf, M., Lu, L., Krupke, A., Lam, P., Littmann, S., et al. (2015). Methane Oxidation Coupled to Oxygenic Photosynthesis in Anoxic Waters. *ISME J.* 9, 1991–2002. doi:10.1038/ismej.2015.12

Moukalled, F., Darwish, M., and Mangani, L. (2015). *The Finite Volume Method in Computational Fluid Dynamics : An Advanced Introduction with OpenFOAM and Matlab*. Berlin: Springer.

Müller, B., Bryant, L. D., Matzinger, A., and Wüest, A. (2012). Hypolimnetic Oxygen Depletion in Eutrophic Lakes. *Environ. Sci. Technol.* 46, 9964–9971. doi:10.1021/es301422r

Nguyen, H.-H. T., Elliott, S. J., Yip, J. H.-K., and Chan, S. I. (1998). The Particulate Methane Monooxygenase from Methylococcus Capsulatus (Bath) Is a Novel Copper-Containing Three-Subunit Enzyme. *J. Biol. Chem.* 273, 7957–7966. doi:10.1074/jbc.273.14.7957

Oswald, K., Milucka, J., Brand, A., Hach, P., Littmann, S., Wehrli, B., et al. (2016). Aerobic Gammaproteobacterial Methanotrophs Mitigate Methane Emissions from Oxic and Anoxic Lake Waters. *Limnol. Oceanogr.* 61, S101–S118. doi:10.1002/lno.10312

Oswald, K., Milucka, J., Brand, A., Littmann, S., Wehrli, B., Kuypers, M. M. M., et al. (2015). Light-dependent Aerobic Methane Oxidation Reduces Methane Emissions from Seasonally Stratified Lakes. *PLoS ONE* 10, e0132574. doi:10.1371/journal.pone.0132574

Ratkowsky, D. A., Lowry, R. K., McMeekin, T. A., Stokes, A. N., and Chandler, R. E. (1983). Model for Bacterial Culture Growth Rate throughout the Entire Biokinetic Temperature Range. *J. Bacteriol.* 154, 1222–1226. doi:10.1128/jb.154.3.1222-1226.1983

Read, J. S., Hamilton, D. P., Desai, A. R., Rose, K. C., MacIntyre, S., Lenters, J. D., et al. (2012). Lake-size Dependency of Wind Shear and Convection as Controls on Gas Exchange. *Geophys. Res. Lett.* 39, L094055 1–5. doi:10.1029/2012GL051886

Record, N. R., Pershing, A. J., and Maps, F. (2014). The Paradox of the "Paradox of the Plankton. *ICES J. Mar. Sci.* 71, 236–240. doi:10.1093/icesjms/fst049

Reis, P. C. J., Thottathil, S. D., Ruiz-González, C., and Prairie, Y. T. (2020). Niche Separation within Aerobic Methanotrophic Bacteria across Lakes and its Link to Methane Oxidation Rates. *Environ. Microbiol.* 22, 738–751. doi:10.1111/1462-2920.14877

Rissanen, A. J., Saarela, T., Jäntti, H., Buck, M., Peura, S., Aalto, S. L., et al. (2020). Vertical Stratification Patterns of Methanotrophs and Their Genetic Controllers in Water Columns of Oxygen-Stratified Boreal Lakes. *FEMS Microbiol. Ecol.* 97, fiaa252 1–16. doi:10.1093/femsec/fiaa252

Roslev, P., and King, G. M. (1995). Aerobic and Anaerobic Starvation Metabolism in Methanotrophic Bacteria. *Appl. Environ. Microbiol.* 61, 1563–1570. doi:10.1128/aem.61.4.1563-1570.1995

Roy, S., and Chattopadhyay, J. (2007). Towards a Resolution of 'the Paradox of the Plankton': A Brief Overview of the Proposed Mechanisms. *Ecol. Complex.* 4, 26–33. doi:10.1016/j.ecocom.2007.02.016

Salcher, M. M. (2013). Same Same but Different: Ecological Niche Partitioning of Planktonic Freshwater Prokaryotes. *J. Limnol.* 73, 74-87. doi:10.4081/jlimnol.2014.813

Schubert, C. J., Diem, T., and Eugster, W. (2012). Methane Emissions from a Small Wind Shielded Lake Determined by Eddy Covariance, Flux Chambers, Anchored Funnels, and Boundary Model Calculations: a Comparison. *Environ. Sci. Technol.* 46, 4515–4522. doi:10.1021/es203465x

Semrau, J. D., Jagadevan, S., DiSpirito, A. A., Khalifa, A., Scanlan, J., Bergman, B. H., et al. (2013). Methanobactin and MmoD Work in Concert to Act as the 'copper-Switch' in Methanotrophs. *Environ. Microbiol.* 15, 3077–3086. doi:10.1111/1462-2920.12150

Skennerton, C. T., Chourey, K., Iyer, R., Hettich, R. L., Tyson, G. W., and Orphan, V. J. (2017). Methane-fueled Syntrophy through Extracellular Electron Transfer: Uncovering the Genomic Traits Conserved within Diverse Bacterial Partners of Anaerobic Methanotrophic Archaea. *mBio* 8, e00530-17. doi:10.1128/mBio.00530-17

Soloviev, A., Donelan, M., Graber, H., Haus, B., and Schlüssel, P. (2007). An Approach to Estimation of Near-Surface Turbulence and CO2 Transfer Velocity from Remote Sensing Data. *J. Mar. Syst.* 66, 182–194. doi:10.1016/j.jmarsys.2006.03.023

Steinsberger, T., Schmid, M., Wüest, A., Schwefel, R., Wehrli, B., and Müller, B. (2017). Organic Carbon Mass Accumulation Rate Regulates the Flux of Reduced Substances from the Sediments of Deep Lakes. *Biogeosciences* 14 (13), 3275–3285. doi:10.5194/bg-14-3275-2017

Thalasso, F., Sepulveda-Jauregui, A., Gandois, L., Martinez-Cruz, K., and Gerardo-Nieto, O., Astorga-España, M. S., et al. (2020). Sub-oxycline Methane Oxidation Can Fully Uptake CH_4 Produced in Sediments: Case Study of a Lake in Siberia. *Sci. Rep.* 10, 3423. doi:10.1038/s41598-020-60394-8

Thottathil, S. D., Reis, P. C. J., and Prairie, Y. T. (2019). Methane Oxidation Kinetics in Northern Freshwater Lakes. *Biogeochemistry* 143, 105–116. doi:10.1007/s10533-019-00552-x

Trotsenko, Y. A., and Khmelenina, V. N. (2005). Aerobic Methanotrophic Bacteria of Cold Ecosystems. *FEMS Microbiol. Ecol.* 53, 15–26. doi:10.1016/j.femsec.2005.02.010

Tsutsumi, M., Iwata, T., Kojima, H., and Fukui, M. (2011). Spatiotemporal Variations in an Assemblage of Closely Related Planktonic Aerobic Methanotrophs. *Freshw. Biol.* 56, 342–351. doi:10.1111/j.1365-2427.2010.02502.x

Wanninkhof, R. (2014). Relationship between Wind Speed and Gas Exchange over the Ocean Revisited. *Limnol. Oceanogr. Methods* 12, 351–362. doi:10.4319/lom.2014.12.351

Wüest, A., and Lorke, A. (2003). Small-Scale Hydrodynamics in Lakes. *Annual Review of Fluid Mechanics* 35, 373–412. doi:10.1146/annurev.fluid.35.101101.161220

Zakharova, L., Meyer, K. M., and Seifan, M. (2019). Trait-based Modelling in Ecology: A Review of Two Decades of Research. *Ecol. Model.* 407, 108703. doi:10.1016/j.ecolmodel.2019.05.008

Zappa, C. J., McGillis, W. R., Raymond, P. A., Edson, J. B., Hintsa, E. J., Zemmelink, H. J., et al. (2007). Environmental Turbulent Mixing Controls on Air-Water Gas Exchange in Marine and Aquatic Systems. *Geophys. Res. Lett.* 34, L10601 1–6. doi:10.1029/2006GL028790

Zimmermann, M., Mayr, M. J., Bürgmann, H., Eugster, W., Steinsberger, T., Wehrli, B., et al. (2021). Microbial Methane Oxidation Efficiency and Robustness during Lake Overturn. *Limnol. Oceanogr. Lett.* 6, 320–328. doi:10.1002/lol2.10209

Conflict of Interest: The authors declare that the research was conducted in the absence of any commercial or financial relationships that could be construed as a potential conflict of interest.

Publisher's Note: All claims expressed in this article are solely those of the authors and do not necessarily represent those of their affiliated organizations, or those of the publisher, the editors and the reviewers. Any product that may be evaluated in this article, or claim that may be made by its manufacturer, is not guaranteed or endorsed by the publisher.

Copyright © 2022 Zimmermann, Mayr, Bouffard, Wehrli and Bürgmann. This is an open-access article distributed under the terms of the Creative Commons Attribution License (CC BY). The use, distribution or reproduction in other forums is permitted, provided the original author(s) and the copyright owner(s) are credited and that the original publication in this journal is cited, in accordance with accepted academic practice. No use, distribution or reproduction is permitted which does not comply with these terms.

frontiers | Frontiers in Environmental Science

ORIGINAL RESEARCH
published: 11 August 2022
doi: 10.3389/fenvs.2022.866152

The Effects of Engineered Aeration on Atmospheric Methane Flux From a Chesapeake Bay Tidal Tributary

Laura L. Lapham, Edward A. Hobbs, Jeremy M. Testa, Andrew Heyes, Melinda K. Forsyth, Casey Hodgkins, Curtis Szewczyk and Lora A. Harris*

Chesapeake Biological Laboratory, University of Maryland Center for Environmental Science, Solomons, MD, United States

Engineered aeration is one solution for increasing oxygen concentrations in highly eutrophic estuaries that undergo seasonal hypoxia. Although there are various designs for engineered aeration, all approaches involve either destratification of the water column or direct injection of oxygen or air through fine bubble diffusion. To date, the effect of either approach on estuarine methane dynamics remains unknown. Here we tested the hypotheses that 1) bubble aeration will strip the water of methane and enhance the air-water methane flux to the atmosphere and 2) the addition of oxygen to the water column will enhance aerobic methane oxidation in the water column and potentially offset the air-water methane flux. These hypotheses were tested in Rock Creek, Maryland, a shallow-water sub-estuary to the Chesapeake Bay, using controlled, ecosystem-scale deoxygenation experiments where the water column and sediments were sampled in mid-summer, when aerators were ON, and then 1, 3, 7, and 13 days after the aerators were turned OFF. Experiments were performed under two system designs, large bubble and fine bubble approaches, using the same observational approach that combined discrete water sampling, long term water samplers (OsmoSamplers) and sediment porewater profiles. Regardless of aeration status, methane concentrations reached as high as 1,500 nmol L^{-1} in the water column during the experiments and remained near 1,000 nmol L^{-1} through the summer and into the fall. Since these concentrations are above atmospheric equilibrium of 3 nmol L^{-1}, these data establish the sub-estuary as a source of methane to the atmosphere, with a maximum atmospheric flux as high as 1,500 µmol m^{-2} d^{-1}, which is comparable to fluxes estimated for other estuaries. Air-water methane fluxes were higher when the aerators were ON, over short time frames, supporting the hypothesis that aeration enhanced the atmospheric methane flux. The fine-bubble approach showed lower air-water methane fluxes compared to the larger bubble, destratification system. We found that the primary source of the methane was the sediments, however, *in situ* methane production or an upstream methane source could not be ruled out. Overall, our measurements of methane concentrations were consistently high in all times and locations, supporting consistent methane flux to the atmosphere.

Keywords: methane, aeration, eutrophication, estuary, OsmoSampler

OPEN ACCESS

Edited by:
Daniel F. McGinnis, Université de Genève, Switzerland

Reviewed by:
Peter Tango, United States Geological Survey (USGS), United States
Wei-Dong Zhai, Shandong University, China

****Correspondence:***
Laura L. Lapham
lapham@umces.edu

Specialty section:
This article was submitted to Biogeochemical Dynamics, a section of the journal Frontiers in Environmental Science

Received: *30 January 2022*
Accepted: *13 June 2022*
Published: *11 August 2022*

Citation:
Lapham LL, Hobbs EA, Testa JM, Heyes A, Forsyth MK, Hodgkins C, Szewczyk C and Harris LA (2022) The Effects of Engineered Aeration on Atmospheric Methane Flux From a Chesapeake Bay Tidal Tributary. Front. Environ. Sci. 10:866152. doi: 10.3389/fenvs.2022.866152

1 INTRODUCTION

The eutrophication of estuaries as a result of nutrient enrichment is a global phenomenon, with consequences that include deoxygenation and hypoxia (Diaz and Rosenberg, 2008). In fact, modeling and data analysis suggests that dissolved oxygen in estuaries will continue to decline into the future, primarily as a result of long-term warming (Breitburg et al., 2018; Ni et al., 2019; Whitney and Vlahos, 2021). The primary mitigation tool has been to enforce managed reductions of land-based nutrients in the United States (Linker et al., 2013) and in Europe (HELCOM, 2021), yet engineered solutions are also being considered (Conley et al., 2009; Lehtoranta et al., 2022). Engineered aeration efforts work by either destratifying the water column or directly injecting oxygen to the water (Harris et al., 2015; Stigebrandt et al., 2015; Koweek et al., 2020). This has also been commonly done in small lake systems (e.g., Martinez and Anderson, 2013; Hounshell et al., 2021) and reservoirs (McCord et al., 2016). While aeration should relieve the low oxygen problem to create habitat for metazoan life, prevent the noxious release of sulfide from sediments, and enhance coupled nitrification-denitrification, an additional potential consequence is that aeration could also enhance atmospheric methane emissions in estuaries. If this is true, methane emissions from estuaries that undergo aeration could be larger than currently considered in the global budget (Saunois et al., 2020). It is critical to constrain all sources of methane to the atmosphere since it is a powerful greenhouse gas (Forster et al., 2007; Dlugokencky, 2020). However, studies from an aerated freshwater reservoir show that the methane emissions were lower than a nearby natural reservoir (McClure et al., 2018; McClure et al., 2021). To date, this interplay between engineered aeration and methane fluxes in a natural estuary has not been rigorously tested.

Estuaries are dynamic environments, generating temporally and spatially-varying habitats in which methane producing and consuming processes occur. The primary source of methane is the underlying sediments, as in most organic rich environments (Martens and Berner, 1974; Reeburgh, 2007). However, there is an increasing appreciation for alternative sources such as demethylation of organic phosphonates (Karl et al., 2008), bacterial degradation of water column dissolved organic matter (Repeta et al., 2016) and/or production by phytoplankton (Bižić et al., 2020) that have not been fully explored in estuarine systems. In shallow-water, dynamic coastal and estuarine environments, methane can also be delivered with currents or tides from lateral sources (Bižić et al., 2020). While methane formed in the sediments can enter the water column through ebullition (Boudreau, 2012) or diffusion, nearly 85% of the methane produced within sediments is oxidized anaerobically before it reaches the sediment-water interface *via* microbially mediated reactions including sulfate reduction, nitrate reduction, and iron reduction (Froelich et al., 1979; Reeburgh, 2007). The remaining methane released from the sediments to the overlying water column can then be oxidized aerobically *via* methanotrophs (Hanson and Hanson, 1996). Thus a conceptual model for a healthy estuary shows a small methane flux to the atmosphere (**Figure 1A**). Alternatively, when estuarine waters are highly eutrophic, there is a breakdown in the aerobic biofilter in the water column and this results in an enhanced methane flux when the bottom waters go hypoxic and anoxic (Gelesh et al., 2016). Thus, under these conditions, there is a higher methane flux to the atmosphere (**Figure 1B**).

Under this simple conceptual model, it is enticing to speculate that if the bottom waters were re-oxygenated, this would return the aerobic biofilter to its normal state and lower the methane flux to the atmosphere. However, methane is a highly insoluble gas, and the mere addition of air bubbles (devoid of methane) and physical movement of the water during aeration could instead promote methane to dissolve into the rising bubbles and released to the atmosphere. In this case, the size of the air bubbles injected into the bottom waters could affect the magnitude of the atmospheric flux. For example, when the bubbles are large, the physical movement of the turbulent water would release large amounts of methane (**Figure 1C**). When the bubbles are small, there is the possibility for some of the oxygen to diffuse into the surrounding water (which is the goal of aeration systems) and promote aerobic methane oxidation (**Figure 1D**).

Oxygenated water columns are necessary for aerobic methane oxidizing bacteria to help control methane emissions to the atmosphere. In the simplest case of the open ocean where there are deep, well-oxygenated waters, nearly all the dissolved methane in the water column is oxidized (Leonte et al., 2017; Pohlman et al., 2017). Yet even in these systems, studies have shown there is a lag time for aerobic oxidation (Chan et al., 2019), with notable exceptions such as the rapid response of methanotrophs to methane released during events like the Deepwater Horizon oil spill (Kessler et al., 2011). Classic works have shown the highest rates of aerobic methane oxidation at the oxycline in arctic lakes (Rudd and Hamilton, 1978) suggesting that these organisms are facultative microaerophiles who work in these strong oxygen gradients (Oswald et al., 2015; Steinle et al., 2017). Aerobic methane oxidation can also proceed at high oxygen concentrations, especially when nitrogen is available. Under eutrophic conditions, when dissolved inorganic nitrogen concentrations >20 μM (M is used throughout as a symbol for mol L^{-1}), aerobic methane oxidation occurs at oxygen levels >31 μM; much higher than found in the oxyclines (Sansone and Martens, 1978). Along with nitrogen, micronutrients (especially copper) stimulate activity of methane oxidizing bacteria (Semrau et al., 2010). Not surprisingly the dissolved methane concentration in the environment has been shown to influence the rate of water column methane oxidation. For example, in Arctic waters, higher rates of methane oxidation were measured when higher concentrations of methane were available in summer (Mau et al., 2013). However, during the Deepwater Horizon oil spill, aerobic methane oxidation rates decreased over time after an initial spike, even though methane concentrations remained high (Crespo-Medina et al., 2014).

Here we present a study that quantified the effect of engineered aeration on air-water methane emissions from a eutrophic estuary. We leveraged a unique opportunity to manipulate whole ecosystem dissolved oxygen concentrations using two types of engineered destratification systems, that we

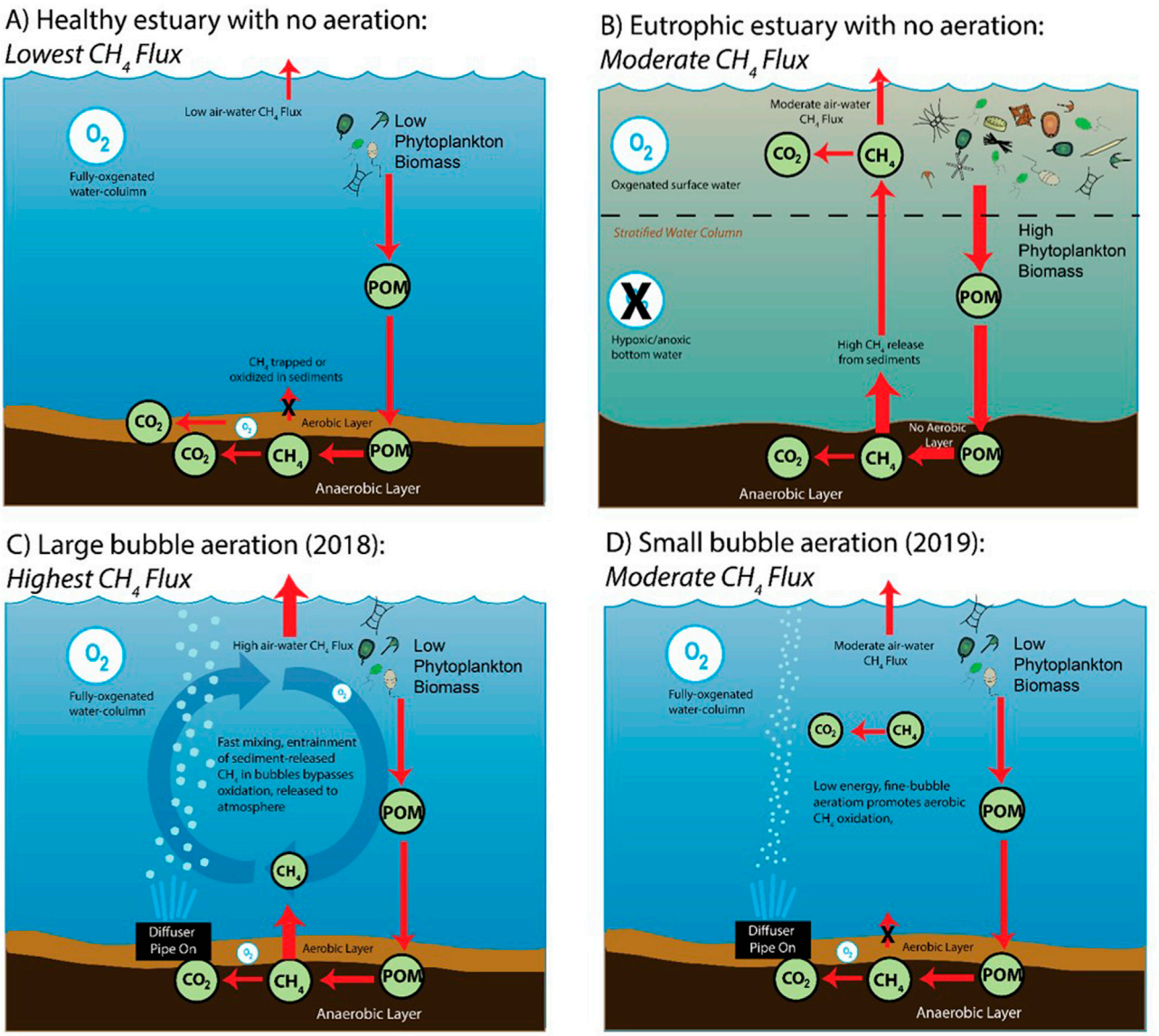


FIGURE 1 | Conceptual diagrams of methane dynamics in estuarine waters. With no aeration, **(A)** the lowest methane flux comes from a water column that is well oxygenated and **(B)** there is a moderate flux when waters are eutrophic. When aerated, the methane flux is **(C)** highest when there are large bubbles and **(D)** moderate when there are small bubbles.

distinguish based on the bubble size (large bubble and small bubble aeration). These systems provided an ideal opportunity to test the hypothesis that the physical disturbance introduced to a eutrophic system with bubbles will enhance the atmospheric methane flux (**Figures 1C,D**), regardless of oxygen concentration. We also surmised that the two different destratification systems would result in different methane fluxes to the atmosphere based on their bubble size; where the small bubbles would dissolve before reaching the air-water interface and not act as a transfer mechanism like larger bubbles. Furthermore, since the very idea behind engineered aeration is to add oxygen to the water column, we also hypothesized that aeration could enhance aerobic methane oxidation in the water column, which could act to lower the flux of methane to the atmosphere. To test our hypotheses, we conducted experimental manipulations of the aeration systems and sampled surface and bottom waters with aerators ON and then 1–13 days after the aerators were turned OFF. We hypothesized the source of methane in the water was the sediments, thus we also collected sediment cores at the same time. To put the discrete, experimental time points into a longer term context, we also present unique time-series measurements of methane concentrations in bottom waters across the whole estuary. Ultimately, this study contributes data to the growing literature of methane dynamics in shallow, eutrophic environments.

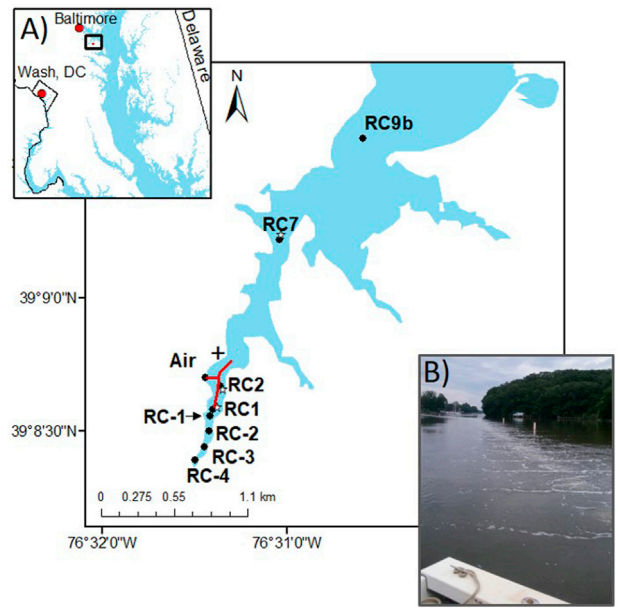


FIGURE 2 | Sample location map for Rock Creek. Red lines show location of the aeration tubes, black dots are water column and sediment station locations, white stars are OsmoSampler locations (very close to black dots), and black cross is location of dock where the benthic lander was deployed. **(A)** Location of Rock Creek (black square) in the northern Chesapeake Bay near Baltimore, Maryland. **(B)** Photo of bubbles breaking the surface in 2019 (photo by Laura Lapham).

2 MATERIALS AND METHODS

2.1 Field Description and Experimental Setup

The experiments were carried out in a 353-ha tidal tributary to the Chesapeake Bay found in Anne Arundel County, Maryland (**Figure 2**). Rock Creek's watershed is 80% residential and 20% forested. Due to the poor water quality over the past few decades (e.g., anoxia and extensive algal blooms), the county installed an engineered destratification system in 1988 to bring dissolved oxygen back to former levels (Harris et al., 2015). Herein, we call this the "large bubble aeration" system. Up until 2019, this system was made up of 138 ultra-coarse air diffusers distributed along a pipe that lines the middle creek channel with ~20 mm bubble size (CH2M_Hill, 2011), as described in design specifications reported by Dames and Moore (1988). The goal of the system was to vigorously overturn the water column in order to continuously introduce oxygen *via* de-stratification into the bottom waters, and the system was run continuously throughout the day. Every year, the aerators are turned on June 1 and turned off October 1, in order to minimize the effects of summertime hypoxia. An early study of this system determined that the zone of aeration influence was ~74 ha and that bottom waters remained oxic when diffusers were ON, but became anoxic within one tidal cycle when aerators were OFF (Harris et al., 2015; Harris et al., 2016). In spring 2019, the aeration system was upgraded to fine bubble diffusers to provide more oxygen to the water column, herein referred to as the "small bubble aeration" system. The goal of the diffusers is primarily to overturn the water to allow re-aeration to occur at the water surface, not to add oxygen from the bubbles themselves. There are two 213 m long diffusers emanating from the shore mainline, which provide air at a rate of 180 scfm (standard cubic feet per minute) in a continuous bubble pattern (0.26 scfm ft^{-1}) of bubbles 3 mm in diameter. The surface water expression of the new aeration system is shown in **Figure 2B**. With this new system, the county public works turns OFF the aerators every night to reduce neighborhood noise and energy consumption.

Over the course of 4 years (2016, 2018, 2019, 2021), the water column and sediments were sampled along the creek both within and outside the aeration zone and with both engineering designs (**Tables 1**, **2**). Stations within the aeration zone included RC1, which is located at the up-creek limit of aeration, and RC2 which is found mid-channel and directly in the aeration zone (**Figure 2**). RC7 is ~1 km downstream from the end of aeration, still within the zone of influence of aeration and where the creek widens, and RC9b is a background site, close to the mouth of the Patapsco River and outside the zone of influence of aeration (**Figure 2**). These stations were introduced in previous studies (Harris et al., 2015). Water depths are between 1.5–3.5 m. In 2021, four upstream stations were added to determine the river influence to the aeration zone (**Table 2**).

To study the effects of the aeration, our experimental approach was to sample while the aerators had been on for about 1 month, referred to as the "ON" sampling event, which occurred during the daylight hours. In the evening of the "ON" sampling, the aerators were turned off and waters sampled 1 day later (2016; large bubble aeration), 7 days later (2018; large bubble aeration), 13 days later (2019; small bubble aeration), and 3 days later (2021; small bubble aeration); these are referred to as the "OFF" sampling events (**Table 2**). After completion of the experiments, the aerators were turned back ON for the remainder of the season. By sampling at different time periods after aerators were turned OFF, the experiment addressed the question of the impact aeration had on methane flux from the Rock Creek estuary.

2.2 Sampling Description

During each field campaign, we collected water column hydrographic and chemical profiles, discrete water samples from the surface and bottom depths, and shallow (~30 cm) sediment cores *via* small boat. Water column temperature, salinity, and dissolved oxygen levels were recorded with a YSI

TABLE 1 | Station information.

Site	Latitude	Longitude	Water depth (m)
RC-4	39.13844	−76.52372	4
RC-3	39.13911	−76.52265	1.5
RC-2	39.14005	−76.52193	1.5
RC-1	39.14094	−76.52155	2.1
RC1	39.14133	−76.52122	2.1
RC2	39.14272	−76.52009	3.4
RC7	39.15108	−76.512	3.4
RC9b	39.15627	−76.50258	3.5

TABLE 2 | Overview of manipulation experiments.

Year	Date	Aeration status	Stations visited	System	CH_4[a] (nM)	DO[a] (mg L^{-1})	DIN[a] (μM)
2016	7/12/2016	ON	RC2,7	Large bubbles	324.1	4.0	21.2
	7/13/2016	OFF			351.1	2.3	20.3
2018	7/10/2018	ON	RC1,2,7,9b	Large bubbles	661.6	6.6	14.4
	7/11/2018	OFF			n.d	n.d	n.d
	7/11/2018	OFF			1,009.6	8.9	11.1
	7/17/2018	OFF			685.0	2.6	7.2
2019	7/9/2019	ON	RC1,2,7,9b	Small bubbles	337.2	6.6	27.8
	7/22/2019	OFF			834.1	6.2	4.9
2021	8/2/2021	ON	RC-4,-3,-2,-1,1,2,7,9b	Small bubbles	485.9	n.d	n.d
	8/6/2021	OFF			350.3	n.d	n.d

[a]*Methane, oxygen, and nitrogen values are averaged for stations RC1 and RC2 only. n.d. means not determined.*

EXO2 multiparameter sonde. In 2018, a benthic lander was placed at a dock (location shown as black cross in **Figure 2**) at the edge of the aeration zone that included continuous temperature, salinity, and dissolved oxygen sensors (YSI EXO2). Salinity is reported in practical salinity scale which has no units. Wind speeds were determined from a handheld anemometer (Weatherhawk, Windmate WM-200).

2.2.1. Discrete Water Column Samples

Water samples were collected for dissolved methane when the aerators were ON and OFF. Water samples were always taken within 1 m of the same GPS location. The sampling location is ~3 m off-axis to the aerators to ensure to not entangle the boat anchor. Therefore, when the aerators were ON, sampling never occurred in the bubble plume itself, always several meters away. Water column samples for dissolved methane concentrations were collected using published methods (Magen et al., 2014). Briefly, a submersible pump was placed at either 50 cm from the air-water interface, or 1 m from the sediment bottom and dispensed water into 125 mL glass serum vials by overfilling 5 times the vial volume and avoiding bubbles. The vials were then capped with thick butyl rubber septa and crimp sealed with aluminum rings. A 10 mL air (Ultra Zero Air purity, Airgas) headspace was given to the vials and then 0.5 mL 8 M KOH was added to arrest microbial activity during storage. The samples were stored upside down at 4°C until they could be measured back at the laboratory with a headspace equilibration technique. In 2021, water was collected with a slight modification to the method where the headspace equilibration step was conducted *in situ* and then the headspace physically separated from the water sample so no preservation was needed. Briefly, the submersible pump filled 120 mL into a 140 mL plastic syringe, bubble free. Then, 20 mL air (Ultra Zero Air purity, Airgas) was added and shook for 4 min to equilibrate. The temperature of the water was recorded for solubility calculations. Since this was a modification, we conducted efficiency tests using lab standards prior to the field campaign to verify 100% methane recovery from the method (**Supplementary Figure S1**). A complimentary water sample was also collected to quantify dissolved inorganic nitrogen (DIN) concentrations using published methods (Harris et al., 2015), in all years but 2021.

2.2.2. Sediments

Sediment cores were collected by hand off the side of the boat using a 6.5 cm diameter plexiglass cylinder attached to a pole. The cores were brought back to shore and immediately (within 1 h of sampling) sliced into 3 cm vertical sections and the sediment packed into 50 mL centrifuge tubes and stored at 4°C for later analysis of pore-water sulfate concentrations (Lapham et al., 2008b). A separate sample for dissolved methane in the pore-waters was also collected by subcoring each section with a 3 mL cut off plastic syringe and placing the material in a 13.5 mL glass serum vial, capped with butyl rubber septae and preserved with 3 mL 1 M KOH (Lapham et al., 2008b). Sediment samples were stored at −20°C until analysis.

2.2.3. Air Samples

At each station, a 140 mL plastic syringe was used to collect an air sample above the sampling site. In 2018, more air samples were collected over time because of opportunistic sampling. Notably, on the ON and OFF days, air samples were collected at all stations at dawn, during the day, and at dusk. Sampling in 2019 was synchronous with water and sediment sampling during the day only. The syringe was upwind of any boat traffic and flushed copiously to provide a clean sample, before any other sampling occurred and potentially contaminated the air. These air samples were stored at 23°C for less than 2 days before they were measured for methane concentrations and stable carbon isotope ratios.

2.2.4. Continuous Bottom Water Sampling

To capture the temporal variability of methane concentrations between sampling campaigns and after the aeration manipulation experiments were completed, bottom water was continuously collected using OsmoSamplers at RC1, RC2, and RC7. OsmoSamplers (**Supplementary Figures S2A,B**) are osmotically-driven pumps that continuously collect and store water in narrow bore copper capillary tubing (Jannasch et al., 2004). They have been used in numerous natural environments to quantify dissolved methane concentrations, including from deep water methane seeps (Lapham et al., 2008a; Wilson et al., 2015), estuaries (Gelesh et al., 2016), high altitude rivers (Buser-Young et al., 2021), high latitude wetlands (Buser-Young et al., 2022) and arctic lakes (McIntosh Marcek et al., 2021). Osmosis in the pumps

is created by an osmotic potential between a saturated brine chamber and freshwater chamber separated by semi-permeable membranes; no power is needed and there are no moving parts (Theeuwes and Yum, 1976; Jannasch et al., 2004). The osmotic pump is then connected to small-bore (0.082 cm inner diameter), long (up to 300 m) copper tubing coil, that is prefilled with freshwater. Water is then continuously drawn from the end of the copper tubing and stored in this tubing over time. The copper material is used so gases (i.e., methane) do not diffuse through it. The pumping rate is positively correlated to the surrounding water temperature and the number of membranes in the pump. For these deployments, two pump speeds were used. "Slow" pumps (8 membranes which pump 1 mL day^{-1}) were used for the long term collection of bottom water through the summer to give a temporal resolution of about 5 days (deployed for 9 months). "Fast" pumps (44 membranes which pump 5 mL day^{-1}) were used for a temporal high resolution of ~1 day (deployed for 1 week). For the slow pumps, we assume the sample stream undergoes plug flow; thus, dispersion within the tubing is minimal (Jannasch et al., 2004). For the fast pumps, plug flow may not be met, so we limited the deployment to a week. OsmoSamplers only collect water thereby precluding gas from affecting the sampler. The intakes are fitted with a 0.2 µm rhizone filter (Seeberg-Elverfeldt et al., 2005) to preclude microbes from the collection and alter the sample stream in the tubing during the deployment.

At the time of the deployment, the OsmoSamplers were attached to the copper coils and placed in a plastic crate (33 × 33 × 28 cm) under 16 kg weight and tied to a surface buoy (**Supplementary Figures S2C–E**). In 2018, the fast OsmoSampler sets were deployed at stations RC1, RC2, and RC7. In 2018, and 2019, slow OsmoSampler sets were also deployed at each of those stations along with Onset temperature and conductivity loggers. Because Rock Creek is a dynamic estuary, we used the conductivity detectors to verify the time-stamps in the OsmoSampler coils. OsmoSamplers were deployed from 9 July to 9 October 2018 and 18 June 2019 to 28 October 2019.

Upon recovery, the copper coils were sealed on either end with pliers and taken back to the lab to be stored at 4°C prior to further processing in the lab. The sensor data were downloaded. Within 1 week, the copper coils were unspooled and crimped into alternating lengths of 50 cm and 4.5 m using a wire crimping tool (Gelesh et al., 2016). The 50 cm sections were squeezed with a bench-top roller to flatten the copper tubing and force the liquid into 2 mL plastic tubes to immediately test for salinity using a handheld Extech RF20 refractometer. Because the coils were prefilled with freshwater before deployment, sectioning was terminated when zero salinity was observed for three samples in a row. These samples were also measured for chloride concentrations to compare to sensor conductivity measurements to verify time-stamps (Gelesh et al., 2016). The 4.5 m copper coil sections were squeezed using the bench-top hand roller which expressed sample liquid through a gastight adaptor and needle, and into a 13.5 mL glass sample vial at the opposite end, previously capped with a butyl rubber septum to prevent gas exchange, and flushed with helium. Each 4.5 m copper section contained approximately 2 mL of sample liquid that was transferred to the vials, resulting in an initial overpressure of approximately 2 mL. The dissolved CH_4 equilibrated with the helium headspace after shaking the vial for 2 min. Time stamps were calculated by adjusting pumping rates to *in situ* temperature, as shown in Gelesh et al. (2016). Unfortunately, the fast pumps only had 1 weeks' worth of tubing yet were deployed for 12 days due to weather delays. Thus, the pumps overpumped the coil and the first part of the deployment was lost.

2.3 Analytical Methods

For water column and sediment vial samples, the headspace was equilibrated with the dissolved methane from the aqueous sample and the headspace analyzed for the ppmv methane. For all samples, an aliquot of the headspace was extracted from the vials and injected onto a gas chromatograph (SRI 8610C multi-gas) equipped with a HayeSep D packed column and a Flame Ionization Detector in order to quantify methane concentrations (Magen et al., 2014). Certified standards (Airgas, Inc.) were used for the calibration curve. Analytical precision is 3% and all measurements were above detection limit of 2 ppmv. Resultant partial pressures were then used to calculate dissolved methane concentrations (in nM) in either the water column or the porewater using Henry's law according to equations in Magen et al. (2014) and porosity corrections according to Lapham et al. (2008a).

For sulfate and chloride concentrations in the sediment porewater samples, the tube containing whole sediment was centrifuged (3000 RPM, 30 min, 20°C, Sorvall© RT 6000D) and the resultant supernatant filtered with a 0.2 µm syringe filter. Samples were then diluted (1:135) in Milli-Q water and analyzed on a Dionex ICS 1000 ion chromatograph (IonPac AG22 4 × 50 mm guard column, IonPac AS22 4 × 250 mm analytical column, and ASRS 300 4 mm suppressor) with an AS40 Autosampler. Water samples from the 50 cm OsmoSampler sections were also measured for chloride with the same dilution to calculate salinity. Certified IAPSO seawater standard (Ocean Scientific International Ltd.) was used for the calibration curve. Analytical precision is 2% and all measurements were above detection limit of 0.05 mM for sulfate.

Air syringes were directly connected to the intake of a cavity ring down spectrometer (CRDS, Picarro 2201i) to measure for methane concentrations and methane stable carbon isotopes. For the water samples, 10 mL of degassed brine was added to the vials to displace the headspace and injected into the small sample isotope module (Picarro, Inc.) to introduce a small sample to the CRDS, similar to procedure in McIntosh Marcek et al. (2021). Isotope values were obtained through calibration with three Vienna Pee Dee Belemnite (VPDB) referenced standards (−23.9‰, −38.3‰, and −66.5‰ (±0.2‰); Isometric Instruments). Isotopic results are reported using the $\delta^{13}C$ notation in per mil (‰), where $\delta^{13}C = (R_{sample}/R_{standard} - 1) * 1{,}000$ and $R = {}^{13}C/{}^{12}C$. Analytical precision is 2% for concentrations and 4‰ for stable carbon isotope ratios.

2.4 Calculations

The air-water flux of CH_4, F, was determined for all discrete sampling campaigns using the updated flux equations presented Wanninkhof (2014):

$$F = k\left(C_w - C_{eq}\right) \quad (1)$$

where k is the gas transfer velocity (length time^{-1}), C_w is the measured surface water concentration, and C_{eq} is the CH_4 concentration in equilibrium with the atmosphere at *in situ* conditions (Yamamoto et al., 1976). There are several versions of **Eq. 1**, mostly based on wind speed. Here we employ the formulation and parameterization of Myllykangas et al. (2020), which reports a k value adapted from Raymond and Cole (2001):

$$k = 1.91\, e^{0.35u}\left(\frac{Sc}{600}\right)^{-0.5} \quad (2)$$

where u is the average wind speed and Sc is the Schmidt number for CH_4 in freshwater calculated from Wanninkhof (2014). Wind speeds were obtained from a nearby NOAA buoy (National Data Buoy Center BLTM2, Baltimore, MD) and averaged over the 3 days prior to sampling. Since the buoy is located 15 km away from Rock Creek, we compared the buoy to the handheld anemometer readings and found they compared within 7%. The buoy wind speed was used for all stations. Wind speeds varied between 2–3.2 m s^{-1}, which translated to k values varying between 3.8 and 5.9 cm h^{-1}, similar to values found in MacIntyre et al. (2010) in a lake system and mangrove dominated estuaries (Rosentreter et al., 2017). Air-water fluxes were then calculated using **Eq. 1** and reported as μmol CH_4 m^{-2} d^{-1}.

Since the calculated air-water flux is inherently based on assumptions of a stagnant boundary layer, the calculated air-water methane flux when the aerators are ON will be underestimated. To constrain this better when the aerators were ON, we calculated an air-water methane flux from direct bubble transport to surface water by applying the bubble radius of the system (3 mm, Mobley Engineering, Inc., personal communication) to an existing bubble model output to determine the mass transfer coefficient (**Figure 4** in McGinnis and Little, 2002). This mass transfer coefficient for the bubble radius in the system is 0.04 cm s^{-1} (or 144 cm h^{-1}) which was then used in **Eq. 1** to calculate a modified air-water methane flux for 2018 and 2019 at RC1 and RC2.

The sediment-water methane diffusive flux was calculated from Fick's first law:

$$J_{CH4-SWI} = -\varphi D_s \frac{dC}{dx} \quad (3)$$

where $J_{CH4\text{-}SWI}$ is the methane flux (μmol CH_4 cm^{-2} yr^{-1}) at the sediment-water interface, φ is the porosity (0.8), D_s is the sedimentary methane diffusion coefficient (cm^2 s^{-1}), x is the vertical sediment depth (cm) and dC/dx is the concentration gradient of methane. D_s was calculated for each station, corrected for tortuosity and *in situ* pressures (based on water depth), temperatures, and salinity (Millero, 1996), and was ~1.7 × 10^{-6} cm^2 s^{-1}. The gradient term was calculated between the uppermost porewater measurements; which usually started at 1.5 cm into the sediment. Thus, this gradient is most likely overestimated because it ignores any oxidation processes that might occur in that upper 1.5 cm of sediment. Using this gradient, the diffusive fluxes were then calculated for each station and time point with **Eq. 3**. For convenience, fluxes are reported as positive but represent flux out of sediment).

2.5 Box Model

We applied a simple box model to the flux data with the assumption that the sediments are the only source of methane to the water, and the atmospheric flux was the only sink of methane in the water. If the two balanced, then there would be no additional contributions to the methane budget in Rock Creek. If the fluxes did not balance, we could invoke additional microbial oxidation or production in the water column and/or advective transport of methane from up- or down-stream. To do this, at each station for 2018 and 2019, we subtracted the atmospheric methane flux from the sedimentary methane flux, then assigned the net difference as the water column methane inventory anomaly. For the aeration sites (RC1 and RC2), both air-water and sedimentary fluxes were averaged together. We should note that when the aerators are ON, we used the fluxes estimated from the stagnant boundary layer model which most likely underestimates the atmospheric flux.

2.6 Statistics

Student t-test was used in Excel (two-tailed, paired) to determine if the methane concentrations calculated from the discrete sampling events and the OsmoSampler samples were significantly similar. To create the paired methane dataset for this test, we extracted the OsmoSampler methane concentration that was sampled at the same time as the discrete methane measurement from the water column at each station. Please note that the OsmoSamplers average over 6–12 h. This comparison was done with the fast OsmoSamplers during 2018 (see **Section 3.6** for result).

3 RESULTS

3.1 Water Column Oxygen, Dissolved Inorganic Nitrogen, Temperature, and Salinity

The experimental design was intended to measure methane concentrations in well oxygenated, bubble-influenced waters when aerators were ON, and then hypoxic or anoxic waters without bubble transport when the aerators were turned OFF. Based on previous experiments in Rock Creek, the change to hypoxic conditions occurred within 1 day of turning off the aerators (Harris et al., 2015). However, for our manipulations, the goal was to observe changes over the longer term (up to 13 days) and the systems response. It is important to remember there was a 7-day difference between ON and OFF treatments in 2018 and 13-day difference in 2019.

In 2018 during aeration, the dissolved oxygen (DO) concentrations were ~7 mg L^{-1} at RC1 and RC2, and well mixed (**Figure 3** top panel). At RC7, the water column was still oxygenated (>4 mg L^{-1}; comparable to conditions at RC9b). After aerators were OFF for 7 days, RC1 and RC2 became hypoxic throughout the water column below 0.5 m, and the other stations had weakly stratified water columns, but with hypoxic bottom waters below 2.5 m.

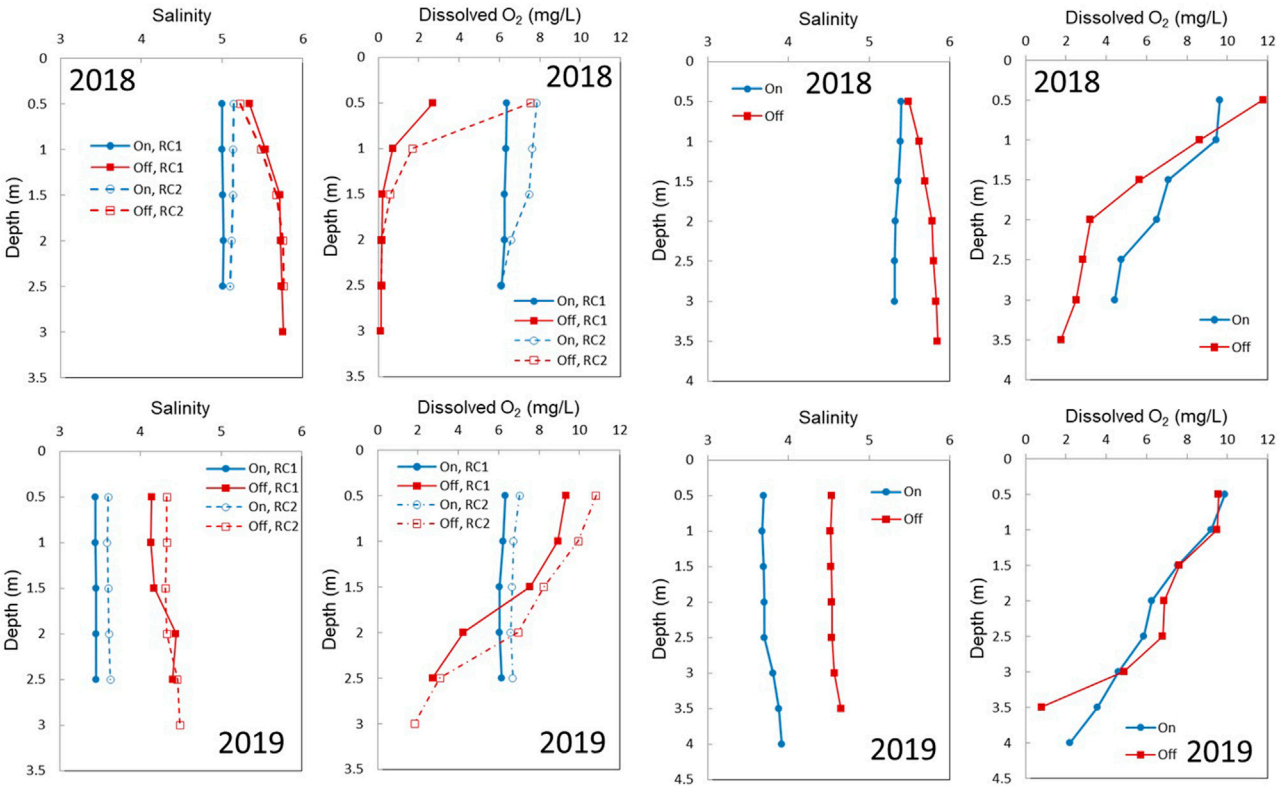


FIGURE 3 | Water column salinity and dissolved oxygen (O_2) profiles from 2018 (top panels) and 2019 (bottom panels) for stations within the aeration zone and stations outside the aeration zone. Blue symbols signify when aerators were ON and red when they were OFF.

Dissolved inorganic nitrogen concentrations averaged 14.4 μM (ranging between 0.8 and 19 μM for all stations) when aerators were ON and 7.2 μM (ranging between 3.7 and 12 μM) when aerators were OFF (**Table 2**). Salinity was ~5–5.5 (**Figure 3**). Water temperatures in 2018 varied between 26–30°C, and were similar for both ON and OFF treatments (data not shown).

In 2019, dissolved oxygen was relatively high in surface waters when the aerators were OFF at RC1 and RC2, giving way to oxygen-depleted conditions below 2 m (**Figure 3**). Dissolved inorganic nitrogen concentrations averaged 27.8 μM (ranging between 5 and 36 μM for all stations) when aerators were ON and 4.9 μM (ranging between 1 and 13 μM) when aerators were OFF (**Table 2**). Salinity was lower in 2019 than in 2018 and was nearly 3.5 when aerators were ON, and 4.5 when aerators were OFF (**Figure 3**). Water temperatures were between 26 and 29°C during the ON treatment and were warmer during OFF treatment (data not shown).

The tidal stage at each station varied over the discrete sampling time points (**Supplementary Figure S3**). In 2018 when aerators were ON, RC7 was sampled first at the ebbing tide, RC9b at low tide, and RC1 and RC2 at a high tide. When aerators were OFF, RC1 and RC2 were collected close to high tide or when waters were just beginning to ebb. RC7 and RC9b were sampled on the ebb tide. In 2019 when aerators were ON, RC9b, RC1, and RC2 were collected on flooding tide, and RC7 was collected right after high tide. When aerators were OFF, all stations were collected near the high tide.

3.2 Methane Concentrations and Stable Carbon Isotope Ratios in Water

Dissolved methane concentrations in surface and bottom water of Rock Creek varied over space and time (**Figure 4**). Overall, concentrations ranged between 150 and 1,500 nM, orders of magnitude higher than atmospheric equilibrium (which is ~3 nM), and were higher at stations RC1 and RC2, within the aeration zone, compared to stations closer to the Patapsco River (RC7, RC9b). In 2016, concentrations at RC2 and RC7 were around 400 nM throughout the period of measurements, regardless of aeration status (**Figure 4A**). In 2018, during aeration, the waters were relatively well mixed between surface and bottom waters (**Figure 4B**). Once aerators were turned OFF, there was an increase in bottom water methane at RC1 and RC2, and not much change at RC7 and RC9b. After 7 days, the surface waters were enriched in methane compared to the bottom water. In 2019, the concentrations between surface and bottom water followed expectations: during aeration, the water column was well mixed so there was little difference between surface and bottom waters and when aerators were turned OFF, methane

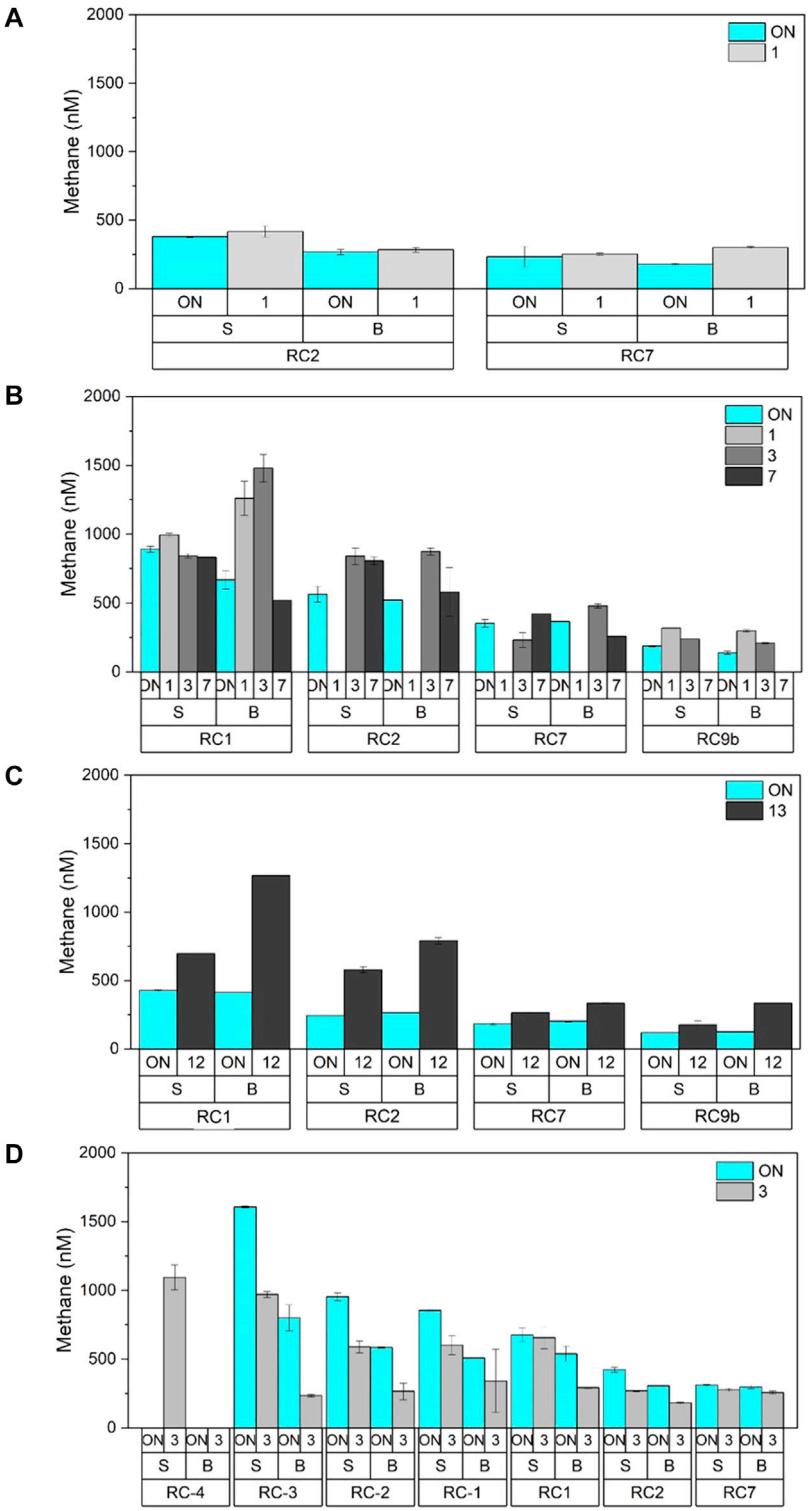


FIGURE 4 | Methane concentrations (colored bars) in surface (S) and bottom (B) water at all stations in **(A)** 2016, **(B)** 2018, **(C)** 2019, and **(D)** 2021. All blue colors represent the "ON" situation, and the gradients in gray color represent the number of days after aerators were turned off, which are described in each panel. Error bars represent standard error on replicate samples collected.

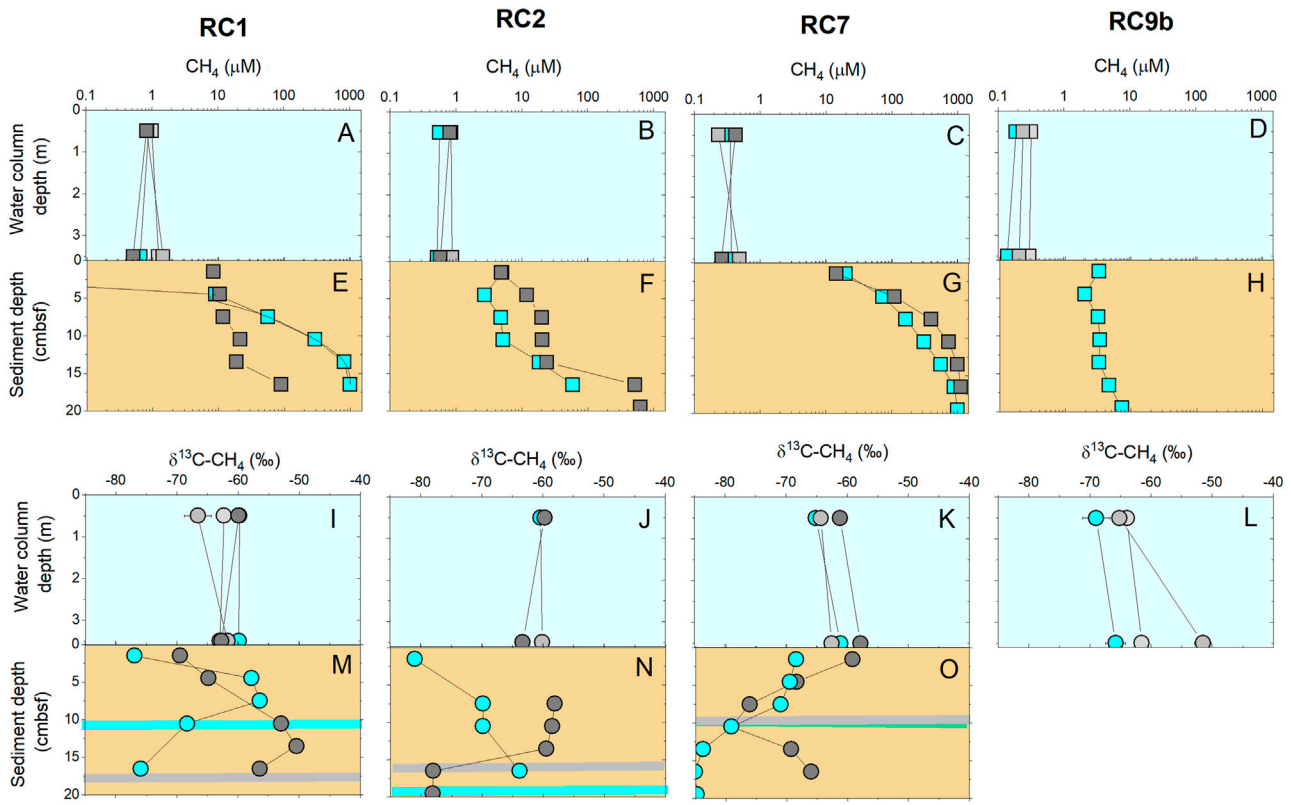


FIGURE 5 | In 2018, methane concentrations **(A–H)** and stable carbon isotopes **(I–O)** in water column (blue background) and in sediments (brown background). Blue symbol color denotes when aerators were on, and dark gray when they were off for 7 days. Horizontal bars in sediments **(M–O)** shows the movement of the sulfate-methane transition zone between ON (blue color) and OFF (gray color).

concentrations were higher in the bottom water than surface waters after 13 days (**Figure 4C**).

The 2021 field campaign was designed to resolve the upstream contribution of methane to the aeration zone. Overall, methane concentrations were lower than 2019 values but also showed the same pattern of higher concentrations at RC1 and RC2, than at RC7 (**Figure 4D**). At RC7, concentrations were similar between surface and bottom, and regardless of aeration status. At RC1 and RC2, methane concentrations were lower when aerators were OFF, which was unexpected. The other unexpected result was to record higher methane concentrations in surface waters than bottom waters during both ON and OFF periods (**Figure 4D**). Measurements made upstream of the aerators, which were only made in 2021, showed that surface waters were always higher than the bottom waters and that concentrations during the ON treatment were always higher than the OFF. Furthermore, methane concentrations were highest in the most upstream station, and declined downstream and into the estuary, such that water flowing into the aeration zone from upstream were enriched with methane relative to the aeration zone itself.

The water column methane concentrations are also presented in **Figures 5A–D**, **6A–D** as compilation figures showing the water column and sediments in a holistic view. Here we add to the water column concentration data the stable isotopic ratio of methane carbon to distinguish source of this methane (**Figures 5I–L**, **6I–L**). Regardless of station or aeration status, δ^{13}C-CH_4 values ranged from −69 to −51‰, with an average value of −61.4 ± 3.6‰, which is near the standard deviation of the method.

3.3 Sediment Porewater

Methane concentrations measured from the sediment porewaters increased with sediment depth (**Figures 5**, **6**, brown colored panels). Surface concentrations were at ~μM levels and increased to as high as 1,300 μM at the bottom of the core. In both years, concentrations were higher in the aeration zone (RC1 and RC2) and outside the aeration zone (RC7) compared to the background site (RC9b). Yet, there is variability in the sediment profiles. For example, at RC1 and RC2, sediment methane concentrations were lower in 2018 than in 2019, regardless of aeration status. After 13 days of no aeration, methane concentrations were higher in the sediments at RC2 and RC7. As noted, **Figures 5**, **6** also contain methane water column parameters for comparison purposes.

Methane increases in sediment porewaters are typically associated with a drawdown of sulfate in the surficial depths due to sulfate reducers outcompeting methanogens for substrates (Hoehler et al., 1994). Therefore, we also measured sulfate in porewater to help our understanding of anaerobic biogeochemical processing. Sulfate concentrations decreased downcore in all stations except RC9b although the depth of low sulfate (SO_4 < 0.5 mM) varied (**Supplementary**

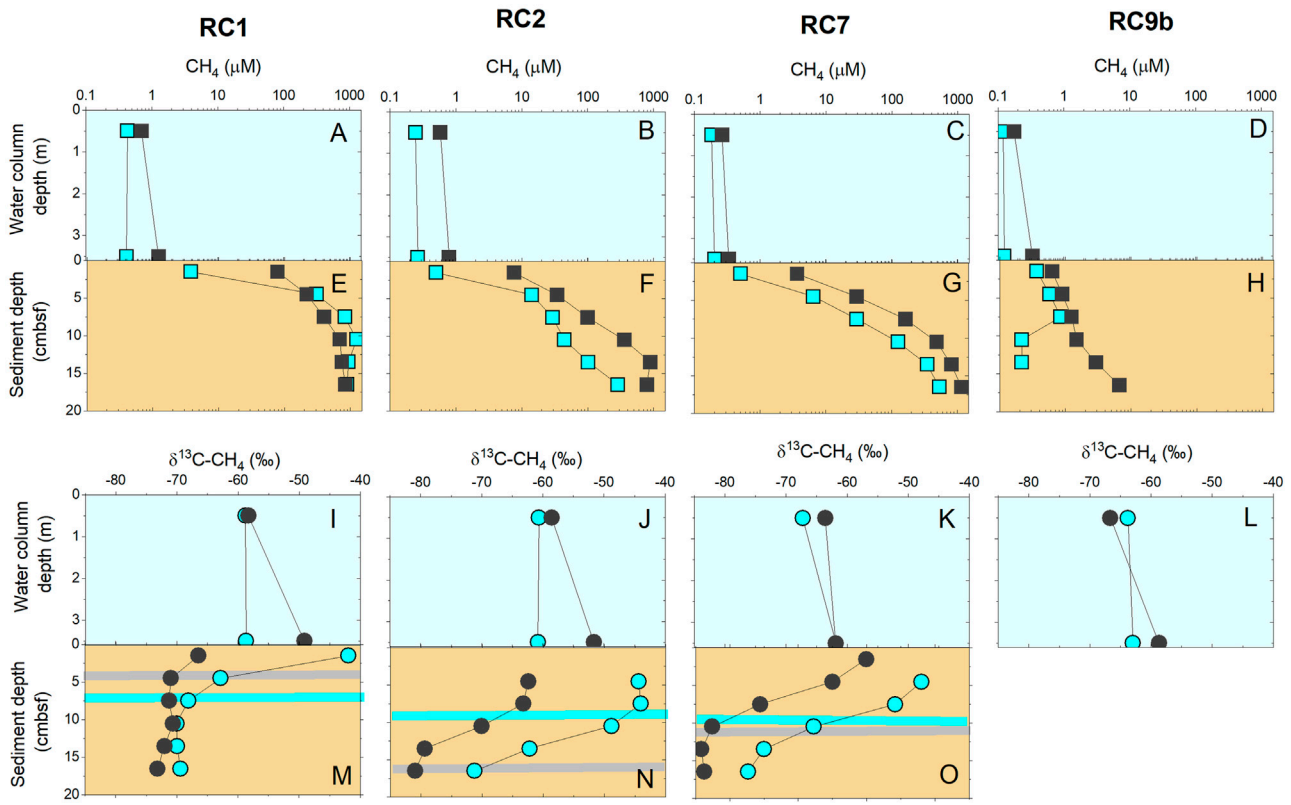


FIGURE 6 | In 2019, methane concentrations **(A–H)** and stable carbon isotopes **(I–O)** in water column (blue background) and in sediments (brown background). Blue symbol color denotes when aerators were on, and dark gray when they were off for 13 days. Horizontal bars in sediments **(M–O)** shows the movement of the sulfate-methane transition zone between ON (blue color) and OFF (gray color).

Figure S4). The depth of low sulfate typically coincides with the increase of methane, and is known as the sulfate methane transition (SMT) depth. The SMT is an area of active anaerobic methane oxidation *via* sulfate reduction (Jørgensen et al., 2020) and is a useful metric to show how active the anaerobic microbial community is in a sediment column (**Figures 5M–O**, **6M–O**). While we expected to see the SMT depth shoal when aeration was turned OFF, there was no consistent pattern of the depth of the SMT with aeration status for both years, although we will specifically present SMT depth patterns in each year below. Using the gradients from the top of the cores, the methane flux to the sediment-water interface varied across space and time, and ranged between 0.1 and 700 μmol m^{-2} d^{-1} (**Supplementary Figure S5**).

Chloride concentrations were also measured as a conservative tracer and as a way to validate any depletion of sulfate coming from sulfate reduction and not a consequence of groundwater. In 2018, while the chloride concentrations showed a slight increase in depth, the depth averages are as follows: 76 ± 8 mM (RC1, RC2), 100 ± 14 mM (RC7), and 85 ± 10 mM (RC9). Since these chloride values are within the range of what would be expected given the overlying water salinity, we represent any conservative mixing in terms of how it might affect sulfate concentrations. Given the rule of constant proportions, we calculated the range of sulfate values that would be estimated given those chloride concentrations (shaded rectangles in **Supplementary Figure S4**).

Methane stable carbon isotope ratios were measured to help distinguish the fate of methane formed in the sediment. Our measurements revealed two patterns in δ^{13}C-CH_4 values with depth: 1) δ^{13}C-CH_4 increasing with depth and 2) δ^{13}C-CH_4 peaks at intermediate depths associated with the SMT. In 2018, at RC1, the δ^{13}C-CH_4 values were similar during the ON and OFF conditions in that the surface was ^{13}C depleted (between −80 and −70‰), they became heavier with depth to as high as −50‰, and then decreased again to near surface sediment values (**Figure 5M**). The depth of the SMT deepened with aerators OFF. At RC2, during the ON condition, δ^{13}C-CH_4 values were ∼−80‰ and increased with depth in the core (**Figure 5N**). During the OFF condition, δ^{13}C-CH_4 values were around −60‰ in the shallow depths and quickly decreased to −80‰ at the SMT. At RC7, just outside the aeration zone, δ^{13}C-CH_4 values were ∼−70‰ at the surface when waters were aerated and decreased to −85‰ at the bottom of the core (**Figure 5O**). During the OFF situation, values showed a similar trend at the surface but then showed a mid-depth minimum of −80‰ at the SMT.

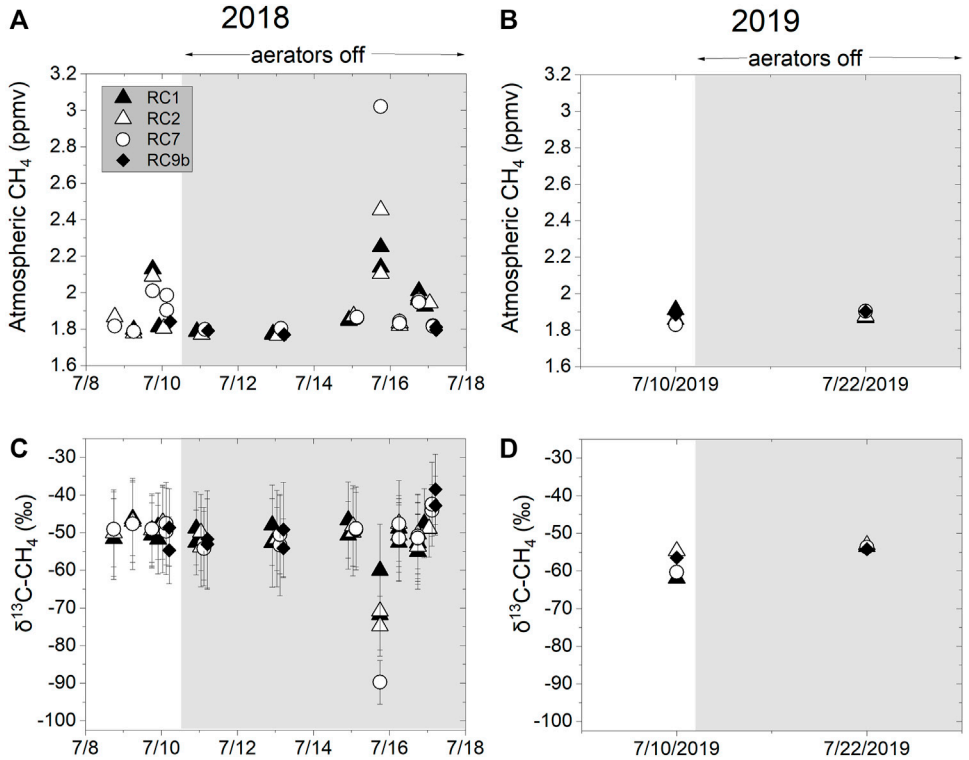


FIGURE 7 | Methane concentrations in air above the water in **(A)** 2018 and **(B)** 2019. δ^{13}C-CH_4 values in air above the water in **(C)** 2018 and **(D)** 2019. Shaded regions indicates when aerators were OFF.

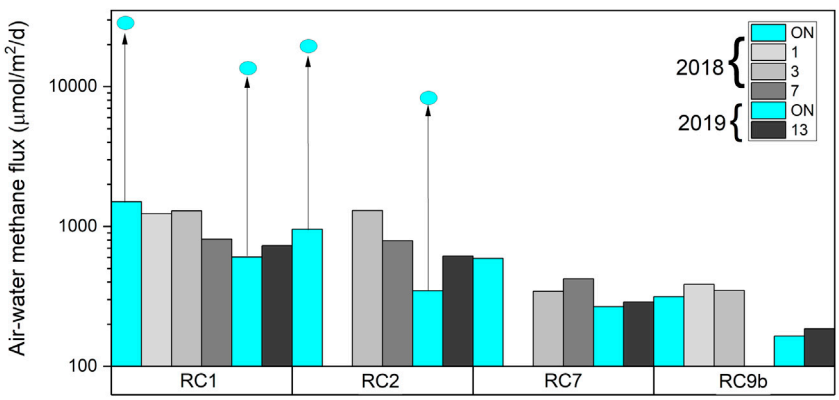


FIGURE 8 | Air-water methane flux for 2018 and 2019. Aerated waters are in blue, and non-aerated waters are shown in gray scale that corresponds to the number of days aerators were off. The bars indicate the flux calculated with the stagnant boundary layer model, whereas the extended arrows to the blue dots indicate the flux recalculated with bubble influence.

In 2019, the δ^{13}C-CH_4 value trends showed more consistency across the stations (**Figures 6M–O**). At RC1, values decreased at the surface from as high as −40 to ~ −70‰ where values remained for about 15 cm into the sediments (**Figure 6M**). RC2 and RC7 show almost the same isotope profiles where values decrease downcore, but the δ^{13}C-CH_4 values are ~10–15‰ higher when aerators were ON compared to when they were OFF (**Figures 6N,O**).

3.4 Methane Concentrations and Stable Carbon Isotope Ratios in Air and Air-Water Fluxes

Methane concentrations were measured in the air above each station during 2018 and 2019. In 2018, the average atmospheric methane concentration across all sites was 1.84 ± 0.06 ppmv, and

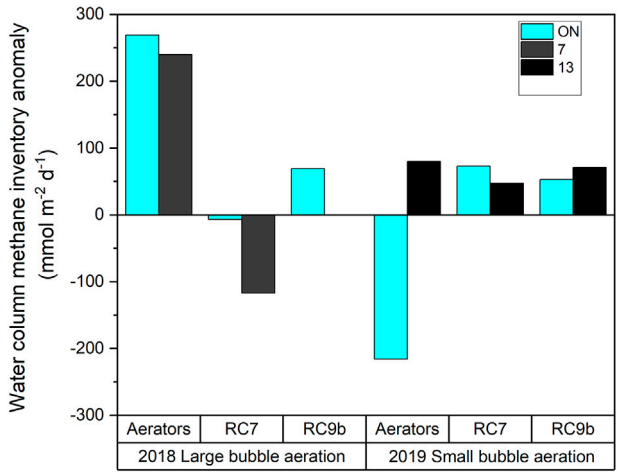


FIGURE 9 | Water column methane inventory anomaly assuming the sediments are the only source of methane to the water and the air-water interface is the only sink. A positive value means that there must be a source of methane to balance the source and sink, whereas the negative value means there must be a sink consuming methane.

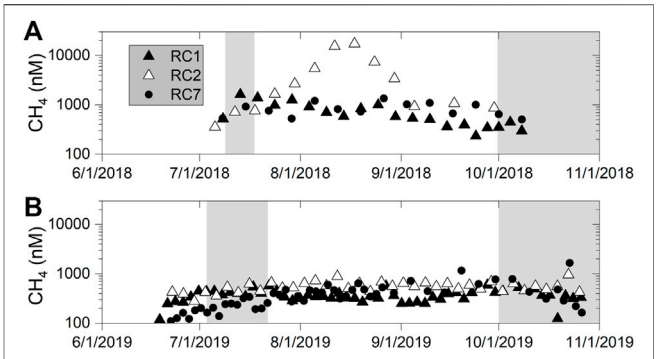


FIGURE 11 | Methane concentrations in bottom water in **(A)** 2018, and **(B)** 2019. Shaded region indicates when the aerators were turned off, otherwise, they were on.

didn't vary between ON and OFF conditions, except at the dawn sampling (**Figures 7A,B**). The average δ^{13}C-CH_4 value of the background methane was −51.4 ± 10‰ (**Figures 7C,D**). Dawn sampling on the ON and OFF days showed elevated methane concentrations, reaching as high as 3 ppmv at RC7 which had a δ^{13}C-CH_4 value of −90‰ (**Figures 7A,B**).

To calculate the air-water methane flux, we used two approaches. The first used the stagnant boundary layer model and most likely underestimates the flux for when the aerators are ON. Using this model, the air-water methane fluxes ranged between 300 and 1,500 μmol CH_4 m^{-2} d^{-1} (**Figure 8**). The flux was higher at RC1 and RC2 than other stations, regardless of aeration status or year. In 2018, the flux at the RC1 and RC2 was higher when aerators were ON after 7 days, whereas in 2019, the flux was lower when the aerators were ON. The second approach was only carried out when the aerators were ON and assumed methane was being stripped from the water as the aerator bubbles traveled up the water column. The calculated fluxes were much higher than the fluxes from the stagnant boundary layer (**Figure 8** extended arrows to blue dots). In 2018, at RC1 and RC2, air-water methane flux was 30,730 and 19,380 μmol CH_4 m^{-2} d^{-1}, respectively. In 2019, at RC1 and RC2, air-water methane flux was 14,669 and 8,342 μmol CH_4 m^{-2} d^{-1}, respectively.

3.5 Box Model Results

The sediment and air-water fluxes were used in the box model to determine if there are additional sources or sinks of methane beyond what is coming from the sediments and being lost to the atmosphere (**Figure 9**). In 2018, during large bubble aeration, there was a large source of methane (positive values in **Figure 9**) at the aerators, and actually a methane sink from RC7 when the aerators were off. In 2019, there was a methane source across all stations, regardless of aeration status, and this source was fairly

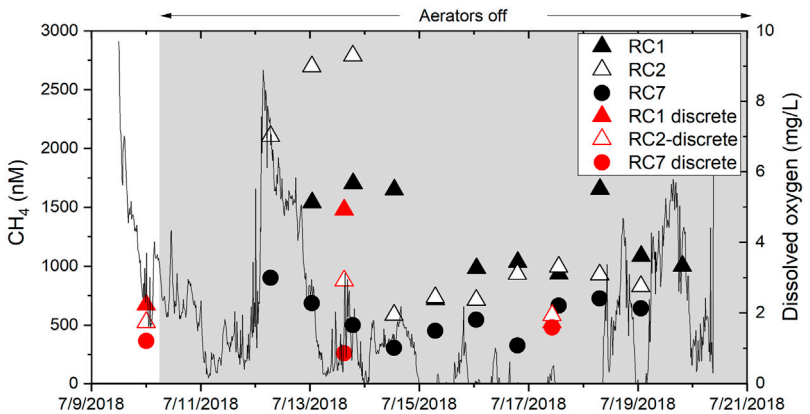


FIGURE 10 | Methane concentrations in high temporal resolution in bottom water from fast OsmoSamplers (black and white symbols) and discrete water samples (red symbols) in 2018 from stations RC1 (filled stars), RC2 (open stars), and RC7 (filled circles). Discrete samples overlap with OsmoSampler concentrations. Thin black line shows a dissolved oxygen record from sensors deployed in the bottom water off a nearby dock.

constant across the sites (**Figure 9**). The exception to this was at the aerators when they were ON; there was a large methane sink (negative value in **Figure 9**). However, since the atmospheric flux during the ON status is mostly likely underestimated, this exception is most likely a methane source too.

3.6 Time-Series Water Column Methane Measurements

Using OsmoSamplers, two separate records of dissolved methane concentrations from bottom water were obtained. The first was from the OsmoSampler deployment in 2018 that spanned 1-week using fast pumps with ~1 day resolution (**Figure 10**). The time stamps assigned were verified by comparing salinity (as calculated from chloride concentrations) in the OsmoSampler coils and the salinity from the sensor packages (**Supplementary Figure S6**). The salinity comparison shows relatively good agreement, especially at station RC7. The overall trend is similar between the sensor and OsmoSamplers at RC1 and RC2, but as we have observed in previous studies, the absolute salinity values did not match well at these stations (Gelesh et al., 2016). The highest methane concentrations came 3 days after the aerators were turned OFF at RC2 and reached almost 3,000 nM (**Figure 10**). Concentrations were also high at RC1 during this time. The timing of this methane peak came right after an event where dissolved oxygen (measured between stations RC2, and RC7) increased rapidly to ~8 mg L^{-1} oxygen (**Figure 10**). After 14 July 2018, methane concentrations decreased to less than 1,000 nM and were similar at all stations. Methane concentrations from OsmoSamplers were cross-checked with our discrete samples and we see no statistical difference between the two ($p = 0.72$); which is the first time this has been verified in field tests. Methane concentrations at RC7 remained lower than the other stations.

The second time-series record of methane concentration came from OsmoSamplers deployed through the summer and into the fall of 2018 and 2019, and contained slow pumps that give ~ weekly resolution (**Figure 11**). The temporal pattern was not the same each year. In 2018, at RC1 and RC2, the initial concentrations before aeration were lower (~400 nM), and then almost doubled when aerators were turned OFF (**Figure 11A**). Once they were turned back ON after our experiment, concentrations at RC1 continued to decrease at a rate of ~13 nM day^{-1} (linear fit with $R^2 = 0.8$); whereas at RC2, concentrations continued to increase through July and finally peak in August at 17,000 nM. Concentrations at RC2 then decreased and reached ~1,000 nM for the remainder of the timeseries. At RC7, concentrations didn't show much change with time and averaged 842 ± 265 nM. In 2019, we captured much higher temporal resolution with the samplers which started about 2 weeks before our experiment began (**Figure 11B**). Overall, concentrations were lower than in 2018 and ranged between 110 and 1,667 nM. There were concentration differences across sites, where methane concentrations at RC1 averaged 368 ± 100 nM; RC2 averaged 558 ± 136 nM; and RC7 averaged 400 ± 270 nM (**Figure 11B**). The bottom water temperature varied between 23–28°C in 2018 with some variability (**Supplmentary Figure S7**), whereas in 2019, the temperature gradually increased from ~23°C to a high of ~30°C in August and then decreased into the fall where a sudden decreased to less than 20°C occurred when the aerators were turned off (**Supplementary Figure S7**).

4 DISCUSSION

One solution to estuarine eutrophication is to artificially aerate the waters with bubble systems. This solution has benefits for reintroducing oxygen back into the water, but it could also have consequences for methane cycling. Previous studies have documented that the hypoxic or anoxic conditions in bottom waters that result from eutrophication also lead to the build-up of dissolved methane diffusing into the bottom waters from the sediments (Bange et al., 2010; Gelesh et al., 2016) which can result in a greater atmospheric flux. Thus, we hypothesized that when aerators are placed in such a system, the physical movement of all that water, with the fact that methane has low solubility, would enhance an atmospheric methane flux. To our knowledge, there is only one other study in a temperate lake that has studied oxygen effects on methane dynamics, and they found a remarkable decrease in methane build-up with engineered aeration (Hounshell et al., 2021), yet they did not quantify air-water flux. With our dataset, we were able to directly calculate this flux when the aerators were ON versus OFF to determine the impact of aeration in terms of methane dynamics. In addition to this, we also considered that the addition of oxygen to the water column might stimulate microbial aerobic methane oxidation which would somewhat control the release of methane at the air-water interface. Through our whole ecosystem manipulation experiment, we were able to address the following questions: 1) what is the effect of aeration on the atmospheric methane flux, 2) is Rock Creek an atmospheric methane source, 3) what is the source of water column methane in the Rock Creek, and 4) is aerobic methane oxidation enhanced in the water column? We also gained insights into complex biogeochemical processes and potential feedbacks occurring in this sub-estuary during and after aeration that sharpens our focus for future studies to further elucidate critical mechanisms related to dissolved oxygen dynamics and associated biogeochemical effects.

4.1 Aeration Enhanced Atmospheric Methane Flux

We hypothesized that the air-water methane flux would be higher during aeration then when the aerators were OFF. When we simply apply the stagnant boundary layer model to calculate the fluxes, we see that sites within the aeration zone (RC1 and RC2) had higher methane fluxes than downstream, regardless of aeration status (**Figure 8**). Yet these fluxes are most likely underestimates when the aerators are ON, as we see with the modified flux calculation (**Figure 8**, extended arrows to blue dots). We further hypothesized that under small bubble aeration, the flux would be lower than under large bubble aeration (**Figure 1**); which is what the fluxes showed in 2018 (large bubble aeration) versus 2019 (fine bubble aeration, **Figure 8**), supporting this hypothesis. The other observation was

TABLE 3 | Examples of estuarine flux of methane to the atmosphere.

Station	Air-water methane flux (mmol m^{-2} d^{-1})	References
Hudson River, NY Upper estuary	0.3	de Angelis and Scranton, (1993)
Hudson River, NY Lower estuary	0.6	de Angelis and Scranton, (1993)
Southern Baltic Sea	0.05–0.4	Bange et al. (1998)
European tidal estuaries	0.13	Middelburg et al. (2002)
Randers fjord, Denmark	0.04–0.4	Abril and Iversen (2002)
	0.002–4.9	Borges and Abril (2011)
Indian mangrove forest	0.01	Dutta et al. (2014)
Australian estuary	0.2	Maher et al. (2015)
Chesapeake Bay-June	0.2	Gelesh et al. (2016)
Chesapeake Bay-Sept	1.8	Gelesh et al. (2016)
Northwestern Borneo	0.001–7.6	Bange et al. (2019)
Chesapeake Bay, Rock Creek MD	0.2–1.5	This study

that in 2019, when the fine bubble aeration was installed, the air-water methane flux was lower during aeration then when the aerators were turned OFF. We have already stated that this flux is most likely underestimated. Future work would benefit from directly measuring this flux with floating chambers to more precisely quantify this flux.

4.2 Is Rock Creek an Atmospheric Methane Source?

Rock Creek is a source of atmospheric methane, regardless of aeration status, or site. The air-water methane flux from Rock Creek varied between 0.2 and 1.5 mmol m^{-2} d^{-1} (note change in units to compare to literature values), which was similar to fluxes measured from several estuaries (**Table 3**), and higher than those from oceanic environments, which vary between 0.0001 and 0.1 mmol m^{-2} d^{-1} (Bižić et al., 2020). Rock Creek methane fluxes are on par with a shallow subarctic lake which reached almost 0.4 mmol m^{-2} d^{-1} (Jansen et al., 2020), even though at times of ice-out, these lakes can release as much as 75 mmol m^{-2} d^{-1} (McIntosh Marcek et al., 2021). Surface water concentrations were also similar to those measured from an aerated eutrophic lake (Martinez and Anderson, 2013) suggesting methane is emitted in these aerated waters. A unique aspect to the work presented here is the high-frequency sampling over the warm season in Rock Creek which measured consistently high concentrations (400–1,000 nM) in the bottom water (**Figure 11**) that rival what has been measured in the anoxic bottom waters of the mainstem Chesapeake Bay in mid-summer (Gelesh et al., 2016) and further supports a sustained methane flux to the atmosphere. Thus this relatively shallow (~3 m) eutrophic estuary, may contribute more methane than previously thought, as was the case for streams and rivers (Stanley et al., 2016), and conforms to our understanding of coastal ecosystems as having an outsized influence on methane fluxes in a global context.

4.3 The Source of Methane: All From Sediments?

Sedimentary methanogenesis is likely the main source of methane to the water column of Rock Creek because the highest dissolved methane concentrations were measured in the sediments, and methane concentrations in the bottom water were typically higher than the surface water. Biogenic methane is also supported with the sedimentary porewater methane $\delta^{13}C\text{-}CH_4$ values in the deep sediments being < −70‰ (Whiticar, 1999). Yet, there was also evidence that methane produced in the deep sediments went through some degree of microbial oxidation before reaching the overlying water. The sediment porewater methane profiles showed classic concave-up shapes which are indicative of the anaerobic oxidation of methane (AOM) working in concert with sulfate reduction, as expressed here with the sulfate methane transition (SMT) depths (Jørgensen et al., 2019). AOM is also supported with the porewater methane isotopic composition data. In 2019, the porewater $\delta^{13}C\text{-}CH_4$ values also increased up the core through the SMT depth. This pattern indicates AOM; as the methane diffuses along the concentration gradient, microbial communities preferentially utilize ^{12}C and leave the ^{13}C behind (thereby values increase) as methane is oxidized (Whiticar, 1999). In 2019, this pattern is clear regardless of aeration status but there is a shift to more ^{13}C depleted values when aerators were OFF. This shift could represent enhanced microbial methane production when aerators were OFF but would need to be validated with other information such as diagenetic modeling (e.g., Martens et al., 1998). The 2019 sedimentary profiles, measured under the low-turbulence diffuse system, support our classic understanding of biogeochemical zonation (Froelich et al., 1979) and suggests that the sediments are diffusion dominated.

The pattern in 2018 was not as clear, possibly due to sediment disturbance with vigorous aeration. The destratification system employed during 2018 involved a high-volume through flow of air that leads to substantial physical disturbance of the water-column and sediments. Such disturbance at the aerators translated into variable porewater methane concentration and the isotope patterns, compared to outside the aeration zone (**Figure 5**). This implies that a simple, steady-state 1D, diffusion dominated interpretation of these profiles cannot be applied here because the destratification system could have driven substantial advective exchange between sediments and the water-column. It is interesting to note that at the aerators (RC1 and RC2), there was a depletion of ^{13}C up the core to the sediment-water interface. One way to inject such a depleted signature is by

methanogenesis which could happen in this agitated system by bubbling out deep methane during aeration or methanogenesis in the surface layers using non-competitive substrates (Alperin et al., 1988). More work would be needed to support or refute these possibilities.

Methane from the sediments can either diffuse into the overlying water or bubble out *via* ebullition (methane oversaturated porewaters forming bubbles). The methane released from both of those processes would have different isotopic signatures. For example, for bubbles to form in the sediments and efflux, the methane concentration must be above saturation which occurs in the sediments deeper than ~10 cmbsf, depending on the site and year (see **Figures 5**, **6**). At these depths, the $\delta^{13}C\text{-}CH_4$ values were between −80 and −85‰, so we would expect to see these values in the overlying water column (assuming a small amount of methane from the bubble equilibrates with the water). Bubbles captured in a shallow water column off North Carolina showed no isotopic fractionation when released to the water (Chanton and Martens, 1988). However, if the methane is diffusing into the water from the sediment surface, that methane would carry a $\delta^{13}C\text{-}CH_4$ value similar to the surface sediment methane signature. For 2018, the $\delta^{13}C\text{-}CH_4$ values of water column methane were always higher than the surface sediment, regardless of site or aeration status. This suggests that there could be some methane oxidation at the very sediment surface that we are missing in our sediment measurements. This was the same situation when the aerators were OFF in 2019. Perhaps future work could focus on the sediment-water interface as an area of intense methane oxidation, be it either aerobic or anaerobic.

The situation is a little different when the aerators were ON in 2019; the water column methane always had a lower $\delta^{13}C\text{-}CH_4$ value than the surficial sediments. This suggests that the methane was not simply diffusing in from the sediments, and that there must be another source of methane injecting isotopically depleted carbon; such as, sediment ebullition, methane being advected out of the sediments into the water column from the aerators, or microbial methane production in the water column. We don't have data to support or refute the advective release of methane out of the sediments other than to say that in 2019, the aeration was much finer and thus most likely less advective than in 2018 so it seems unlikely. Plus, since we were not focused on determining the ebullitive flux, its hard to evaluate. However, in 2018, we had evidence of an ebullitive flux of methane from the sediments. First, the methane in the air above Rock Creek waters had an average $\delta^{13}C\text{-}CH_4$ value of −50‰ which is slightly depleted in ^{13}C from the global, well-mixed value from the northern hemisphere of −47.4‰ (Lan et al., 2021). When this air $\delta^{13}C\text{-}CH_4$ value was compared to what was measured in the deep sediments, < −70‰, or in the water column, < −60‰, the ^{13}C depleted methane in air over Rock Creek waters can be explained with a small amount of biogenic methane from the sediments. Secondly, we measured a direct pulse of biogenic ($\delta^{13}C\text{-}CH_4$ = −80‰) methane in the air above RC7 at dawn when the aerators were OFF (**Figure 7**). This was most likely due to ebullition from the sediments directly reaching the atmosphere which was trapped in the air above the water due to the air inversion that occurs at dawn (Crill et al., 1988; Mukhophadhya et al., 2001). While this observation of high concentrations of methane in the morning air is not unexpected, it clearly documents how aqueous environments contribute to the atmospheric methane isotopic signal which has recently been shown to be enhanced in biogenic methane sources (Schaefer et al., 2016; Lan et al., 2021). It also clearly shows that in order to fully capture methane dynamics in this system, future work should quantify the bubble flux from the tributary, much like was done in the temperature lake in California (Martinez and Anderson, 2013).

4.4 Evidence for Methane Production in the Water Column

While we might have captured methane bubbling out of Rock Creek in 2018, that process is very heterogeneous and not continuous, and may not fully explain the water column $\delta^{13}C\text{-}CH_4$ values from 2019 ON status. We thus explore the possibility of water column methane production under aeration. There is growing evidence for an oxic production pathway in surface waters (see review in Bižić et al., 2020) that might be important. Most notably, it was concluded that 90% of methane in surface waters of a temperate lake was formed in the oxic surface waters, and not the sediments (Donis et al., 2017). However, a recent reevaluation of this work concluded that a sedimentary methane flux from the sediments flanking the lake in the shallow waters could explain the oversaturated surface waters (Peeters et al., 2019). In well stratified lakes, methane production in surface waters is shown to scale with sediment area and mixed layer volume (Günthel et al., 2019). Lakes are hydrodynamically very different from estuaries, making study comparisons to Rock Creek tenuous. Furthermore, the hydrodynamic conditions in destratification systems, such as in 2018, can create large cells of overturning water that may impact a much larger area of the tidal system (Gibbs and Howard-Williams, 2018). The lack of studies of sub-estuaries alone highlights the need to quantify the sources of methane from systems such as Rock Creek.

The box model, which balances sedimentary and air-water methane fluxes, shows that for most of the time, regardless of if aerators were ON or OFF, there is an additional methane source in the water column in 2019 (**Figure 11**). The observation that outside the aeration zone, RC7 and RC9, there is also an additional methane source could indicate the transport of methane from the Patapsco River, lateral inputs of water from across the creek as destratification cells pull in sources from a cross-section of the creek or simply upstream methane sources. Previous work in rivers also documented higher methane flux in upstream surface waters (de Angelis and Scranton, 1993; Abril and Iversen, 2002; Middelburg et al., 2002); as well as higher methane in smaller width creeks (Borges and Abril, 2011).

The further observation that there is a methane source regardless of the status of the aerators (either ON or OFF) suggests there is a bigger ecosystem response than just the influx of oxygen from the aerators. One possibility could be the presence of algal blooms which produce methane as a

byproduct (Bižić et al., 2020). Such blooms have been shown to occur before when aerators are turned OFF (Harris et al., 2015), and we also documented one right after the aerators were turned OFF in 2018 (**Figure 10**). Increased surface water oxygen levels were observed with an increase in particulate organic nitrogen and carbon, and iron (data not shown). The OsmoSamplers also captured a pulse of methane right after this oxygen pulse. If these blooms are a typical phenomenon right after turning the aerators OFF, it could explain why the methane fluxes were higher 3 days after turning aerators OFF in 2021 (**Figure 4D**) than when the aerators were ON. Future work could also directly quantify rates of methane production in aerobic waters.

4.5 Evidence for Aerobic Methane Oxidation in the Water Column?

While it seems clear that the aerators are enhancing a methane flux to the air above the creek, that the sediments are the main source of methane to the waters and there possibly is methane production in these aerated waters, we also considered if there is any microbially mediated oxidation in the surface waters that might offset this atmospheric flux. The idea here is that the waters are being oxygenated due to the aeration, as the oxygen data suggested happened during the experiment (**Figure 3**), and this oxygen is allowing for aerobic methane oxidation to happen. We have already speculated about a small potential oxidation process altering the $\delta^{13}C\text{-}CH_4$ from our surficial sedimentary methane values to the bottom water. Here, we focus solely on the water column. Since we didn't directly measure microbial rates, we need to rely on geochemical data. We did this in four ways. First, we interrogated the stable carbon isotopes of methane measured in the water column. The $\delta^{13}C\text{-}CH_4$ values give a bulk measure of what has happened to that methane since it was formed; the bulk methane signature would be more enriched in ^{13}C if it had been oxidized. In order to do this, we considered that the methane in the bottom water is the source for the methane in the surface water. **Figures 5**, **6** water column isotope profiles clearly show that in all cases, the surface water is always slightly ^{13}C depleted, if at all different, contrary to what would be found if aerobic methane oxidation was occurring. Secondly, we looked for a correlation between oxygen concentrations and methane concentrations. For this correlation, we surmised that if oxygen was controlling methane levels, we would see a linear relationship between the two. There was no correlation (**Supplementary Figure S8A**), which suggests oxygen is not the limiting factor for aerobic methane oxidation. Thirdly, we considered that maybe aerobic methane oxidation was limited by dissolved inorganic nitrogen (DIN), as has been proposed in the literature (Sansone and Martens, 1978). We surmise that if there is a negative relationship between DIN and water column methane concentrations, there could be evidence for aerobic methane oxidation. In other words, if methanotrophs were stimulated by DIN in an otherwise oxic water column, we would find low methane concentrations. This pattern did not emerge (**Supplementary Figure S8B**). And finally, in the box model approach described in **Section 4.3**, for most of the time in 2018 and 2019, there was a source of methane and not a sink. The exception was in 2019 when the aerators were ON. Taking all of this geochemical evidence into consideration, we conclude that we found little to no geochemical evidence for water column aerobic methane oxidation. Future work could focus on looking for microbial signature of oxidation in the water column.

4.6 Complicating Factors With Experimental Design

We have discussed the differences in atmospheric methane flux between the 2018 and 2019 aeration experiments to most likely be a factor of the bubble size during aeration. The large bubble aerators resulted in a larger flux of methane to the atmosphere than the small bubble aerators. However there were also differences between the 2 years in how long the aerators were turned OFF. Despite variability in the concentrations, we found almost no effect of aeration when the aerators were turned OFF for a few days (2016, 2021), but there was modest methane accumulation as oxygen was depleted for 3–7 days in 2018 and significant methane increases after 13 days in 2019. Thus, it appears that methane accumulation requires more than a day to emerge after deoxygenation, despite prior studies in Arctic lake systems (McIntosh Marcek et al., 2021) and in the Chesapeake Bay mainstem (Gelesh et al., 2016) that appear to indicate that methane is immediately released from sediments following deoxygenation. However, the temporal resolution of prior measures likely cannot capture day to day dynamics, and there are few, if any real-time measures of methane and oxygen in coastal systems to confirm the time-scale of methane responses to deoxygenation.

A second source of complication in our interpretations is that the experimental study is embedded in a system with background environmental variability. Thus, our "ON-OFF" study design using whole ecosystem manipulations does not offer a true controlled experimental system. For example, unlike previous work in Rock Creek (Harris et al., 2015), the waters did not go anoxic within 1 day in 2018 and 2019 and only at RC2 in 2018 did anoxia ever emerge. In 2018, there was also an influx of oxygen-rich water that appeared in the aeration zone within days after the aerators were turned OFF and when oxygen should have been depleted (seen in time series data on **Figure 10**). Although we did not measure methane during this event, the rapid increase in methane concentrations immediately after this pulse of tidally driven, oxygen-rich water could be the result of a rapid response to deoxygenation (that was not interrupted by the event) or an influx of methane rich water from upstream after the event. Our measurements in 2021 did indicate higher methane concentrations upstream of the aeration zone (~1,000 nM; **Figure 4D**), but these are substantially smaller than the concentrations measured after the event in 2018 (1,500 to 2,500 nM; **Figure 10**), suggesting that an upstream source is unlikely. Other potential inputs of methane are currently unknown, such as groundwater, and there are no substantial tidal wetlands that could serve as a methane source. Although

groundwater remains unlikely since chloride concentrations slightly increased with depth in sediment porewaters, our understanding of the drivers for the patterns remains elusive and long term observatories are needed.

Ecosystem responses to aeration beyond deoxygenation also likely feedback to influence methane dynamics in the estuary. Harris et al. (2015) reported a substantial algal bloom in Rock Creek within a week of the aerators being turned off, generating high surface water oxygen and organic matter concentrations. Given that Rock Creek has substantial light attenuation (Secchi Depth < 0.5), the vertical mixing induced by aerators likely keeps phytoplankton mixed below the photic layer, and when aerators are turned OFF, water-column stabilization allows for phytoplankton blooms. This is consistent with recent work in Chesapeake Bay that suggest that high chlorophyll-a packaging under low-light conditions combined with high nutrient concentrations allows for rapid algal growth when light becomes available (Buchanan, 2020). Methane concentrations reached the highest levels we measured at RC2 in 2018 (~2,700 nM), 3-days after an increase in particulate organic carbon of 700 μM after the aerators were turned OFF (data not shown). The consumption of this organic matter that likely followed may have generated substantial new methane, especially considering that oxygen concentrations were consistently below 32 μM (1 mg L^{-1}) for much of the following week (**Figure 10**). Given that the "destratification" approach used in 2018 was designed to physically mix and overturn the waters, such a phytoplankton response is likely. The "diffuse" approach used in 2019 involved much less physical disruption of the water-column (water-column salinity profiles were similar during ON and OFF), which may have prevented a phytoplankton response and also allowed for stable conditions that allowed the microbial communities to organize along expected redox conditions. This finding also points to an important impact of aerator design on our results, with differences in impact dependent on the mechanism of aeration and questions remain regarding how best to quantify mixing, oxygenation, and even water fluxes dependent on whether engineering impacted circulation (destratification design through large bubbles) versus diffusion of oxygen (small bubble aeration design).

5 CONCLUSION

There is evidence that the sediments are the main source of methane in Rock Creek as conceptualized in **Figure 1**, although we cannot rule out upstream creek waters or *in situ* production in the water column as additional sources. Our measurements suggest that aeration decreases the time frame available for aerobic methane oxidation in the water-column, thus connecting the sediment to the atmosphere more directly. This study did not allow for an in-depth examination of seasonal variations in methane sources and sinks, nor did it measure the impact of other complex factors on methane, such as shifting nutrient status and related microbial responses. Our experiments were also not intended to test aeration system design and operation (bubble size and density) in relation to methane flux, instead we used models to evaluate these impacts. Future work should 1) couple methane concentration and isotope data along with microbial rate measurements under various nutrient and oxygen conditions upstream and downstream of the aerators; 2) investigate seasonal changes to understand the complex factors controlling methane flux from this eutrophic estuary; and 3) characterize aerator design impacts on local hydrodynamics to better characterize physical effects on sediment transport and sediment-water exchange.

Keeping these recommendations in mind, the strength of our study can be distilled into two central findings we emphasize here: 1) The shallow, Rock Creek sub-estuary is a source of methane to the atmosphere, regardless of engineering intervention, and methane production and flux is likely enhanced as a consequence of eutrophication and 2) the strength of the methane flux is impacted by aeration bubble size design. Our conceptual model lays out the processes and impacts that are connected to these findings (**Figure 1**). The smallest fluxes occurred with the small bubble system (**Figure 9**), and we predict that continued implementation of this system combined with potential future oligotrophication could reduce methane fluxes. The largest fluxes occurred with the older, large bubble system that was intended to encourage destratification. The data support the hypothesis that aeration can lead to higher atmospheric methane fluxes and that aerator design is crucial to mitigating methane transfer. A key motivation for this study was to investigate the potential for unintended consequences of this engineering intervention in relation to greenhouse gas emissions. The dependency of the measured methane atmospheric fluxes on bubble size suggests that there is a path forward towards optimizing aerator design to reduce this consequence in eutrophic tidal waters (e.g., implement small bubble aeration). This study also adds to a growing body of literature quantifying methane fluxes in coastal waters. Regardless of aerator status or design, the current condition of Rock Creek as a eutrophic ecosystem characterized by high primary production of organic matter impacts its overall role as a source of methane to the atmosphere. As coastal water quality policies are implemented and managers seek both solutions and greater understanding of the complex biogeochemistry that impacts restoration trajectories in eutrophic systems, work on both engineering solutions and interpretation of restoration monitoring data would benefit from including methane dynamics and greenhouse gas impacts into holistic management frameworks.

DATA AVAILABILITY STATEMENT

The datasets presented in this study can be found in online repositories. The names of the repository/repositories and accession number(s) can be found below: https://www.ncei.noaa.gov/archive/accession/0244510.

AUTHOR CONTRIBUTIONS

LL, AH, JT, and LH conceived the idea; LL, CH, MF, CS, and EH conducted the experiment and analyzed samples; LL wrote the initial manuscript, and all authors contributed significant edits to the manuscript. We thank Mark Mobley for help with the bubble model, and the reviewers and editors who greatly improved this manuscript.

FUNDING

Financial support for this project was through U.S. National Science Foundation CBET-1706416 (LH, AH, JT, and LL), Maryland Sea Grant (NA14OAR4170090, SA75281450-O; LH and JT), and Maryland SeaGrant REU program (NSF grant OCE-1262374).

ACKNOWLEDGMENTS

We thank Anne Arundel county for access to the aerators, the residents of Rock Creek for allowing us to conduct the experiments in their backyard, and Janis Markusic for her support. The work could not have been done without the field help of Zachary Gotthardt, Lillian Henderson, and Brittany Clark and laboratory help of Maureen Strauss and Hadley McIntosh Marcek. We thank Dave Oliff at the Florida State University machine shop for building the fast OsmoSamplers. Work on this paper by Lapham was possible with the expertise and care of healthcare workers at the Johns Hopkins Breast Cancer Center and support from Marcia Lapham and Dr. Cédric Magen. Co-author Harris was supported by the Rock Creek team as a nursing mother in the field with patience, privacy, and good humor during boat work with co-authors Szewczyk and Testa. Lapham, Harris, and Testa depended on childcare provided by their communities and especially their spouses during the COVID-19 pandemic and are thankful to have had the time for this research. This is UMCES contribution #6188.

SUPPLEMENTARY MATERIAL

The Supplementary Material for this article can be found online at: https://www.frontiersin.org/articles/10.3389/fenvs.2022.866152/full#supplementary-material

REFERENCES

Abril, G., and Iversen, N. (2002). Methane Dynamics in a Shallow Non-tidal Estuary (Randers Fjord, Denmark). *Mar. Ecol. Prog. Ser.* 230, 171–181. doi:10.3354/meps230171

Alperin, M. J., Reeburgh, W. S., and Whiticar, M. J. (1988). Carbon and Hydrogen Isotope Fractionation Resulting from Anaerobic Methane Oxidation. *Glob. Biogeochem. Cycles* 2 (3), 279–288. doi:10.1029/gb002i003p00279

Bange, H. W., Dahlke, S., Ramesh, R., Meyer-Reil, L-A., Rapsomanikis, S., and Andreae, M. O. (1998). Seasonal Study of Methane and Nitrous Oxide in the Coastal Waters of the Southern Baltic Sea. *Estuar. Coast. Shelf Sci.* 47, 807–817.

Bange, H. W., Bergmann, K., Hansen, H. P., Kock, A., Koppe, R., Malien, F., et al. (2010). Dissolved Methane during Hypoxic Events at the Boknis Eck Time Series Station (Eckernförde Bay, SW Baltic Sea). *Biogeosciences* 7, 1279–1284. doi:10.5194/bg-7-1279-2010

Bange, H. W., Sim, C. H., Bastian, D., Kallert, J., Kock, A., Mujahid, A., et al. (2019). Nitrous Oxide (N2O) and Methane (CH4) in Rivers and Estuaries of Northwestern Borneo. *Biogeosciences* 16, 4321–4335.

Bižić, M., Grossart, H.-P., and Ionescu, D. (2020). "Methane Paradox," in *eLS* (Chichester: John Wiley & Sons).

Borges, A. V., and Abril, G. (2011). "Carbon Dioxide and Methane Dynamics in Estuaries," in *Treatise on Estuarine and Coastal Science*. Editors E. Wolanski and D. S. Mclusky (Waltham: Academic Press), 119–161. doi:10.1016/b978-0-12-374711-2.00504-0

Boudreau, B. P. (2012). The Physics of Bubbles in Surficial, Soft, Cohesive Sediments. *Mar. Petroleum Geol.* 38, 1–18. doi:10.1016/j.marpetgeo.2012.07.002

Breitburg, D., Levin, L. A., Oschlies, A., Grégoire, M., Chavez, F. P., Conley, D. J., et al. (2018). Declining Oxygen in the Global Ocean and Coastal Waters. *Science* 359 (46), 1–13. doi:10.1126/science.aam7240

Buchanan, C. (2020). A Water Quality Binning Method to Infer Phytoplankton Community Structure and Function. *Estuaries Coasts* 43 (4), 661–679. doi:10.1007/s12237-020-00714-3

Buser-Young, J. Z., Lapham, L., Thurber, A. R., Williams, K. H., and Colwell, F. S. (2021). Hidden Processes during Seasonal Isolation of a High-Altitude Watershed. *Front. Earth Sci.* 9 (6668199), 1–15. doi:10.3389/feart.2021.666819

Buser-Young, J. Z., Peck, E. K., Chace, P., Lapham, L. L., Vizza, C., and Colwell, F. S. (2022). Biogeochemical Dynamics of a Glaciated High-Latitude Wetland. *J. Geophys. Res. Biogeosci.* 127 (6), e2021JG006584. (accepted). doi:10.1029/2021JG006584

CH2M_Hill (2011). *Task4-Aeration Evaluation*. Annapolis: Maryland Department of Public Works.

Chan, E. W., Shiller, A. M., Joung, D. J., Arrington, E. C., Valentine, D. L., Redmond, M. C., et al. (2019). Investigations of Aerobic Methane Oxidation in Two Marine Seep Environments: Part 1—Chemical Kinetics. *J. Geophys. Res. Oceans* 124, 8852–8868. doi:10.1029/2019jc015594

Chanton, J. P., and Martens, C. S. (1988). Seasonal Variations in Ebullitive Flux and Carbon Isotopic Composition of Metahen in a Tidal Freshwater Estuary. *Glob. Biogeochem. Cycles* 2 (3), 289–298. doi:10.1029/gb002i003p00289

Conley, D. J., Bonsdorff, E., Carstensen, J., Destouni, G., Gustafsson, B. G., Hansson, L.-A., et al. (2009). Tackling Hypoxia in the Baltic Sea: Is Engineering a Solution? *Environ. Sci. Technol.* 43 (10), 3407–3411. doi:10.1021/es8027633

Crespo-Medina, M., Meile, C. D., Hunter, K. S., Diercks, A.-R., Asper, V. L., Orphan, V. J., et al. (2014). The Rise and Fall of Methanotrophy Following a Deepwater Oil-Well Blowout. *Nat. Geosci.* 7, 423–427. doi:10.1038/ngeo2156

Crill, P. M., Bartlett, K. B., Wilson, J. O., Sebacher, D. I., Harriss, R. C., Melack, J. M., et al. (1988). Tropospheric Methane from an Amazonian Floodplain Lake. *J. Geophys. Res.* 93 (D2), 1564–1570. doi:10.1029/jd093id02p01564

Dames and Moore (1988). The Rock Creek Estuary Study, Final Report. Prepared for the Anne Arundel County Watershed Management Program.

de Angelis, M. A., and Scranton, M. I. (1993). Fate of Methane in the Hudson River and Estuary. *Glob. Biogeochem. Cycles* 7 (3), 509–523. doi:10.1029/93gb01636

Diaz, R. J., and Rosenberg, R. (2008). Spreading Dead Zones and Consequences for Marine Ecosystems. *Science* 321 (5891), 926–929. doi:10.1126/science.1156401

Dlugokencky, E. (2020). *Global Methane Monthly Means*. [Online]. Available: https://www.esrl.noaa.gov/gmd/ccgg/trends_ch4/(Accessed January 1, 2021).

Donis, D., Flury, S., Stöckli, A., Spangenberg, J. E., Vachon, D., and McGinnis, D. F. (2017). Full-scale Evaluation of Methane Production under Oxic Conditions in a Mesotrophic Lake. *Nat. Commun.* 8 (1661), 1661–1712. doi:10.1038/s41467-017-01648-4

Dutta, M. K., Mukherjee, R., Jana, T. K., and Mukhopadhyay, S. K. (2014). Biogeochemical Dynamics of Exogenous Methane in an Estuary Assocaited to a Mangrove Biosphere; The Sundarbans, NE Coast of India. *Mar. Chem.* 170, 1–10.

Forster, P., Ramaswamy, V., Artaxo, P., Berntsen, T., Betts, R., Fahey, D. W., et al. (2007). *Changes in Atmospheric Constituents and in Radiative Forcing*. Cambridge, United Kingdom and New York, NY, USA: Cambridge University Press.

Froelich, P. N., Klinkhammer, G. P., Bender, M. L., Luedtke, N. A., Heath, G. R., Cullen, D., et al. (1979). Early Oxidation of Organic Matter in Pelagic Sediments

of the Eastern Equatorial Atlantic: Suboxic Diagenesis. *Geochim. Cosmochim. Acta* 43, 1075–1090. doi:10.1016/0016-7037(79)90095-4

Gelesh, L., Marshall, K., Boicourt, W., and Lapham, L. (2016). Methane Concentrations Increase in Bottom Waters during Summertime Anoxia in the Highly Eutrophic Estuary, Chesapeake Bay, U.S.A. *Limnol. Oceanogr.* 61 (S1), S253–S266. doi:10.1002/lno.10272

Gibbs, M. M., and Howard-Williams, C. (2018). "Physical Processes for In-Lake Restoration: Destratification and Mixing," in *Lake Restoration Handbook*. Editors D. P. Hamilton, K. J. Collier, J. M. Quinn, and C. Howard-Williams (Cham: Springer).

Günthel, M., Donis, D., Kirillin, G., Ionescu, D., Bizic, M., McGinnis, D. F., et al. (2019). Contribution of Oxic Methane Production to Surface Methane Emission in Lakes and its Global Importance. *Nat. Commun.* 10 (5497), 5497–5510. doi:10.1038/s41467-019-13320-0

Hanson, R. S., and Hanson, T. E. (1996). Methanotrophic Bacteria. *Microbiol. Rev.* 60 (2), 439–471. doi:10.1128/mr.60.2.439-471.1996

Harris, L. A., Hodgkins, C. L. S., Day, M. C., Austin, D., Testa, J. M., Boynton, W., et al. (2015). Optimizing Recovery of Eutrophic Estuaries: Impact of Destratification and Re-aeration on Nutrient and Dissolved Oxygen Dynamics. *Ecol. Eng.* 75, 470–483. doi:10.1016/j.ecoleng.2014.11.028

Harris, L. A., Day, M., and Hodgkins, C. (2016). *Rock Creek 2015 Water Quality Monitoring Results*. Technical report series No. TS-863-16. Solomons: University of Maryland Center for Environmental Science.

HELCOM (2021). *Baltic Sea Action Plan 2021 Update*. [Online]. Available: http://www.helcom.fi/(Accessed January 1, 2022).

Hoehler, T. M., Alperin, M. J., Albert, D. B., and Martens, C. S. (1994). Field and Laboratory Studies of Methane Oxidation in an Anoxic Marine Sediment: Evidence for a Methanogen-Sulfate Reducer Consortium. *Glob. Biogeochem. Cycles* 8 (4), 451–463. doi:10.1029/94gb01800

Hounshell, A. G., Mcclure, R. P., Lofton, M. E., and Carey, C. C. (2021). Whole-ecosystem Oxygenation Experiments Reveal Substantially Greater Hypolimnetic Methane Concentrations in Reservoirs during Anoxia. *Limnol. Oceanogr. Lett.* 6, 33–42. doi:10.1002/lol2.10173

Jannasch, H. W., Wheat, C. G., Plant, J. N., Kastner, M., and Stakes, D. S. (2004). Continuous Chemical Monitoring with Osmotically Pumped Water Samplers: OsmoSampler Design and Applications. *Limnol. Oceanogr. Methods* 2, 102–113. doi:10.4319/lom.2004.2.102

Jansen, J., Thornton, B. F., Cortés, A., Snöälv, J., Wik, M., MacIntyre, S., et al. (2020). Drivers of Diffusive CH4 Emissions from Shallow Subarctic Lakes on Daily to Multi-Year Timescales. *Biogeosciences* 17, 1911–1932. doi:10.5194/bg-17-1911-2020

Jørgensen, B. B., Beulig, F., Egger, M., Petro, C., Scholze, C., and Røy, H. (2019). Organoclastic Sulfate Reduction in the Sulfate-Methane Transition of Marine Sediments. *Geochim. Cosmochim. Acta* 254, 231–245. doi:10.1016/j.gca.2019.03.016

Jørgensen, B. B., Andren, T., and Marshall, I. P. G. (2020). Sub-seafloor Biogeochemical Processes and Microbial Life in the Baltic Sea. *Environ. Microbiol.* 22 (5), 1688–1706.

Karl, D. M., Beversdorf, L., Björkman, K. M., Church, M. J., Martinez, A., and Delong, E. F. (2008). Aerobic Production of Methane in the Sea. *Nat. Geosci.* 1, 473–478. doi:10.1038/ngeo234

Kessler, J. D., Valentine, D. L., Redmond, M. C., Du, M., Chan, E. W., Mendes, S. D., et al. (2011). A Persistent Oxygen Anomaly Reveals the Fate of Spilled Methane in the Deep Gulf of Mexico. *Science* 331 (6015), 312–315. doi:10.1126/science.1199697

Koweek, D. A., García-Sánchez, C., Brodrick, P. G., Gassett, P., and Caldeira, K. (2020). Evaluating Hypoxia Alleviation through Induced Downwelling. *Sci. Total Environ.* 719 (137334), 137334–137412. doi:10.1016/j.scitotenv.2020.137334

Lan, X., Nisbet, E. G., Dlugokencky, E. J., and Michel, S. E. (2021). What Do We Know about the Global Methane Budget? Results from Four Decades of Atmospheric CH4 Observations and the Way Forward. *Philos. Trans. R. Soc. Lond. Ser. A Phys. Sci. Eng.* 379 (20200440), 1–14. doi:10.1098/rsta.2020.0440

Lapham, L. L., Chanton, J. P., Martens, C. S., Higley, P. D., Jannasch, H. W., and Woolsey, J. R. (2008a). Measuring Temporal Variability in Pore-Fluid Chemistry to Assess Gas Hydrate Stability: Development of a Continuous Pore-Fluid Array. *Environ. Sci. Technol.* 42 (19), 7368–7373. doi:10.1021/es801195m

Lapham, L. L., Chanton, J. P., Martens, C. S., Sleeper, K., and Woolsey, J. R. (2008b). Microbial Activity in Surficial Sediments Overlying Acoustic Wipe-Out Zones at a Gulf of Mexico Cold Seep. *Geochem. Geophys. Geosyst.* 9 (6), Q06001. doi:10.1029/2008gc001944

Lapham, L. L., Strauss, M., Hobbs, E., Testa, J., Heyes, A., Forsyth, M., et al. (2021). *Methane (CH4) in Water, Methane (CH4) Stable Carbon Isotope Ratios, and Others in Rock Creek, Chesapeake Bay from 2016-07-12 to 2021-08-06 (NCEI Accession 0244510)*. Solomons: National Centers For Environmental Information. Available at: https://www.ncei.noaa.gov/archive/accession/0244510.

Lehtoranta, J., Bendtsen, J., Lännergren, C., Saarijärvi, E., Lindström, M., and Pitkänen, H. (2022). Different Responses to Artificial Ventilation in Two Stratified Coastal Basins. *Ecol. Eng.* 179 (106611), 1–13. doi:10.1016/j.ecoleng.2022.106611

Leonte, M., Kessler, J. D., Kellermann, M. Y., Arrington, E. C., Valentine, D. L., and Sylva, S. P. (2017). Rapid Rates of Aerobic Methane Oxidation at the Feather Edge of Gas Hydrate Stability in the Waters of Hudson Canyon, US Atlantic Margin. *Geochim. Cosmochim. Acta* 204, 375–387. doi:10.1016/j.gca.2017.01.009

Linker, L. C., Batiuk, R. A., Shenk, G. W., and Cerco, C. F. (2013). Development of the Chesapeake Bay Watershed Total Maximum Daily Load Allocation. *J. Am. Water Resour. Assoc.* 49 (5), 986–1006. doi:10.1111/jawr.12105

MacIntyre, S., Jonsson, A., Jansson, M., Aberg, J., Turney, D. E., and Miller, S. D. (2010). Buoyancy Flux, Turbulence, and the Gas Transfer Coefficient in a Stratified Lake. *Geophys. Res. Lett.* 37 (L24604), 1–5. doi:10.1029/2010gl044164

Magen, C., Lapham, L. L., Pohlman, J. W., Marshall, K., Bosman, S., Casso, M., et al. (2014). A Simple Headspace Equilibration Method for Measuring Dissolved Methane. *Limnol. Oceanogr.* 12, 637–650. doi:10.4319/lom.2014.12.637

Maher, D. T., Cowley, K., Santos, I. R., Macklin, P., and Eyre, B. D. (2015). Methane and Carbon Dioxide Dynamics in a Subtropical Estuary Over a Diel Cycle: Insights From Automated *in situ* Radioactive and Stable Isotope Measurements. *Mar. Chem.* 168, 69–79.

Martens, C. S., and Berner, R. A. (1974). Methane Production in the Interstitial Waters of Sulfate-Depleted Marine Sediments. *Science* 185 (4157), 1167–1169. doi:10.1126/science.185.4157.1167

Martens, C. S., Albert, D. B., and Alperin, M. J. (1998). Biogeochemical Processes Controlling Methane in Gassy Coastal Sediments-Part 1. A Model Coupling Organic Matter Flux to Gas Production, Oxidation and Transport. *Cont. Shelf Res.* 18, 1741–1770. doi:10.1016/s0278-4343(98)00056-9

Martinez, D., and Anderson, M. A. (2013). Methane Production and Ebullition in a Shallow, Artificially Aerated, Eutrophic Temperate Lake (Lake Elsinore, CA). *Sci. Total Environ.* 454-455, 457–465. doi:10.1016/j.scitotenv.2013.03.040

Mau, S., Blees, J., Helmke, E., Niemann, H., and Damm, E. (2013). Vertical Distribution of Methane Oxidation and Methanotrophic Response to Elevated Methane Concentrations in Stratified Waters of the Arctic Fjord Storfjorden (Svalbard, Norway). *Biogeosciences* 10, 6267–6278. doi:10.5194/bg-10-6267-2013

McClure, R. P., HamreHamre, K. D. A., Niederlehner, B. R., Munger, Z. W., Chen, S., Lofton, M. E., et al. (2018). Metalimnetic Oxygen Minima Alter the Vertical Profiles of Carbon Dioxide and Methane in a Managed Freshwater Reservoir. *Sci. Total Environ.* 636, 610–620. doi:10.1016/j.scitotenv.2018.04.255

McClure, R. P., Schreiber, M. E., Lofton, M. E., Chen, S., Krueger, K. M., and Carey, C. C. (2021). Ecosystem-Scale Oxygen Manipulations Alter Terminal Electron Acceptor Pathways in a Eutrophic Reservoir. *Ecosystems* 24, 1281–1298. doi:10.1007/s10021-020-00582-9

McCord, S. A., Beutel, M. W., Dent, S. R., and Schladow, S. G. (2016). Evaluation of Mercury Cycling and Hypolimnetic Oxygenation in Mercury-Impacted Seasonally Stratified Reservoirs in the Guadalupe River Watershed, California. *Water Resour. Res.* 52, 7726–7743. doi:10.1002/2016wr019061

McGinnis, D. F., and Little, J. C. (2002). Predicting Diffused-Bubble Oxygen Transfer Rate Using the Discrete-Bubble Model. *Water Res.* 36, 4627–4635. doi:10.1016/s0043-1354(02)00175-6

McIntosh Marcek, H. A., Lesack, L., Orcutt, B. N., Wheat, C. G., Dallimore, S., Geeves, K., et al. (2021). Continuous Dynamics of Dissolved Methane Over Two Years and its Carbon Isotopes (δ13C, Δ14C) in a Small Arctic Lake in the Mackenzie Delta. *J. Geophys. Res. Biogeosci.* 126 (3), 1–23. doi:10.1029/2020jg006038

Middelburg, J. J., Nieuwenhuize, J., Iversen, N., Høgh, N., de Wilde, H., Helder, W., et al. (2002). Methane Distribution in European Tidal Estuaries. *Biogeochemistry* 59, 95–119. doi:10.1023/a:1015515130419

Millero, F. (1996). *Chemical Oceanography*. Boca Raton, FL: CRC Books.

Mukhophadhya, S. K., Biswas, H., Das, K. L., De, T. K., and Jana, T. K. (2001). Diurnal Variation of Carbon Dioxide and Methane Exchange Above

Sundarbans Mangrove Forest, in NW Coast of India. *Indian J. Mar. Sci.* 30, 70–74.

Myllykangas, J.-P., Hietanen, S., and Jilbert, T. (2020). Legacy Effects of Eutrophication on Modern Methane Dynamics in a Boreal Estuary. *Estuaries Coasts* 43, 189–206. doi:10.1007/s12237-019-00677-0

Ni, W., Li, M., Ross, A. C., and Najjar, R. G. (2019). Large Projected Decline in Dissolved Oxygen in a Eutrophic Estuary Due to Climate Change. *J. Geophys. Res. Oceans* 124, 1–19. doi:10.1029/2019jc015274

Oswald, K., Milucka, J., Brand, A., Littmann, S., Wehrli, B., Kuypers, M. M. M., et al. (2015). Light-Dependent Aerobic Methane Oxidation Reduces Methane Emissions from Seasonally Stratified Lakes. *PLoS ONE* 10 (7), e0132574. doi:10.1371/journal.pone.0132574

Peeters, F., Encinas Fernandez, J., and Hofmann, H. (2019). Sediment Fluxes Rather than Oxic Methanogenesis Explain Diffusive CH4 Emissions from Lakes and Reservoirs. *Sci. Rep.* 9 (243), 243–310. doi:10.1038/s41598-018-36530-w

Pohlman, J. W., Greinert, J., Ruppel, C., Silyakova, A., Vielstädte, L., Casso, M., et al. (2017). Enhanced CO2 Uptake at a Shallow Arctic Ocean Seep Field Overwhelms the Positive Warming Potential of Emitted Methane. *Proc. Natl. Acad. Sci. U.S.A.* 114 (21), 5355–5360. doi:10.1073/pnas.1618926114

Raymond, P. A., and Cole, J. J. (2001). Gas Exchange in Rivers and Estuaries: Choosing a Gas Transfer Velocity. *Estuaries* 24 (2), 312–317. doi:10.2307/1352954

Reeburgh, W. S. (2007). Oceanic Methane Biogeochemistry. *Chem. Rev.* 107, 486–513. doi:10.1021/cr050362v

Repeta, D. J., Ferrón, S., Sosa, O. A., Johnson, C. G., Repeta, L. D., Acker, M., et al. (2016). Marine Methane Paradox Explained by Bacterial Degradation of Dissolved Organic Matter. *Nat. Geosci.* 9, 884–887. doi:10.1038/ngeo2837

Rosentreter, J. A., Maher, D. T., Ho, D. T., Call, M., Barr, J. G., and Eyre, B. D. (2017). Spatial and Temporal Variability of CO2 and CH4 Gas Transfer Velocities and Quantification of the CH4 Microbubble Flux in Mangrove Dominated Estuaries. *Limnol. Oceanogr.* 62, 561–578. doi:10.1002/lno.10444

Rudd, J. W. M., and Hamilton, R. D. (1978). Methane Cycling in a Eutrophic Shield Lake and its Effects on Whole Lake Metabolism. *Limnol. Oceanogr.* 23 (2), 337–348. doi:10.4319/lo.1978.23.2.0337

Sansone, F. J., and Martens, C. S. (1978). Methane Oxidation in Cape Lookout Bight, North Carolina. *Limnol. Oceanogr.* 23 (2), 349–355. doi:10.4319/lo.1978.23.2.0349

Saunois, M., Stavert, A. R., Poulter, B., Bousquet, P., Canadell, J. G., Jackson, R. B., et al. (2020). The Global Methane Budget 2000-2017. *Earth Syst. Sci. Data* 12, 1561–1623. doi:10.5194/essd-12-1561-2020

Schaefer, H., Fletcher, S. E. M., Veidt, C., Lassey, K. R., Brailsford, G. W., Bromley, T. M., et al. (2016). A 21-st Century Shift From Fossil-Fuel to Biogenic Methane Emissions Indicated by 13CH4. *Science* 352 (6281), 80–84. doi:10.1126/science.aad2705

Seeberg-Elverfeldt, J., Schlüter, M., Feseker, T., and Kölling, M. (2005). Rhizon Sampling of Porewaters Near the Sediment-Water Interface of Aquatic Systems. *Limnol. Oceanogr. Methods* 3, 361–371. doi:10.4319/lom.2005.3.361

Semrau, J. D., Dispirito, A. A., and Yoon, S. (2010). Methanotrophs and Copper. *FEMS Microbiol. Rev.* 34, 496–531. doi:10.1111/j.1574-6976.2010.00212.x

Stanley, E. H., Casson, N. J., Christel, S. T., Crawford, J. T., Loken, L. C., and Oliver, S. K. (2016). The Ecology of Methane in Streams and Rivers: Patterns, Controls, and Global Significance. *Ecol. Monogr.* 86 (2), 146–171. doi:10.1890/15-1027

Steinle, L., Maltby, J., Treude, T., Kock, A., Bange, H. W., Engbersen, N., et al. (2017). Effects of Low Oxygen Concentrations on Aerobic Methane Oxidation in Seasonally Hypoxic Coastal Waters. *Biogeosciences* 14, 1631–1645. doi:10.5194/bg-14-1631-2017

Stigebrandt, A., Liljebladh, B., de Brabandere, L., Forth, M., Granmo, Å., Hall, P., et al. (2015). An Experiment with Forced Oxygenation of the Deepwater of the Anoxic By Fjord, Western Sweden. *Ambio* 44 (1), 42–54. doi:10.1007/s13280-014-0524-9

Theeuwes, F., and Yum, S. I. (1976). Principles of the Design and Operation of Generic Osmotic Pumps for the Delivery of Semisolid or Liquid Drug Formulations. *Ann. Biomed. Eng.* 4 (4), 343–353. doi:10.1007/bf02584524

Wanninkhof, R. (2014). Relationship between Wind Speed and Gas Exchange Over the Ocean Revisited. *Limnol. Oceanogr. Methods* 12, 351–362. doi:10.4319/lom.2014.12.351

Whiticar, M. J. (1999). Carbon and Hydrogen Isotope Systematics of Bacterial Formation and Oxidation of Methane. *Chem. Geol.* 161, 291–314. doi:10.1016/s0009-2541(99)00092-3

Whitney, M. M., and Vlahos, P. (2021). Reducing Hypoxia in an Urban Estuary Despite Climate Warming. *Environ. Sci. Technol.* 55, 941–951. doi:10.1021/acs.est.0c03964

Wilson, R. M., Lapham, L. L., Riedel, M., Holmes, M. E., and Chanton, J. P. (2015). Observing Methane Hydrate Dissolution Rates Under Sediment Cover. *Mar. Chem.* 172, 12–22. doi:10.1016/j.marchem.2015.03.004

Yamamoto, S., Alcauskas, J. B., and Crozier, T. E. (1976). Solubility of Methane in Distilled Water and Seawater. *J. Chem. Eng. Data* 21 (1), 78–80. doi:10.1021/je60068a029

Conflict of Interest: The authors declare that the research was conducted in the absence of any commercial or financial relationships that could be construed as a potential conflict of interest.

Publisher's Note: All claims expressed in this article are solely those of the authors and do not necessarily represent those of their affiliated organizations, or those of the publisher, the editors and the reviewers. Any product that may be evaluated in this article, or claim that may be made by its manufacturer, is not guaranteed or endorsed by the publisher.

Copyright © 2022 Lapham, Hobbs, Testa, Heyes, Forsyth, Hodgkins, Szewczyk and Harris. This is an open-access article distributed under the terms of the Creative Commons Attribution License (CC BY). The use, distribution or reproduction in other forums is permitted, provided the original author(s) and the copyright owner(s) are credited and that the original publication in this journal is cited, in accordance with accepted academic practice. No use, distribution or reproduction is permitted which does not comply with these terms.

frontiers | Frontiers in Environmental Science

TYPE Original Research
PUBLISHED 09 September 2022
DOI 10.3389/fenvs.2022.880619

Check for updates

OPEN ACCESS

EDITED BY
Yves T. Prairie,
Université du Québec à Montréal, Canada

REVIEWED BY
Peter Regier,
Pacific Northwest National Laboratory (DOE), United States
Banwari Dandotiya,
Jiwaji University, India

*CORRESPONDENCE
Dag O. Hessen,
d.o.hessen@mn.uio.no

SPECIALTY SECTION
This article was submitted to Biogeochemical Dynamics, a section of the journal Frontiers in Environmental Science

RECEIVED 21 February 2022
ACCEPTED 23 August 2022
PUBLISHED 09 September 2022

CITATION
Valiente N, Eiler A, Allesson L, Andersen T, Clayer F, Crapart C, Dörsch P, Fontaine L, Heuschele J, Vogt RD, Wei J, de Wit HA and Hessen DO (2022), Catchment properties as predictors of greenhouse gas concentrations across a gradient of boreal lakes.
Front. Environ. Sci. 10:880619.
doi: 10.3389/fenvs.2022.880619

COPYRIGHT
© 2022 Valiente, Eiler, Allesson, Andersen, Clayer, Crapart, Dörsch, Fontaine, Heuschele, Vogt, Wei, de Wit and Hessen. This is an open-access article distributed under the terms of the Creative Commons Attribution License (CC BY). The use, distribution or reproduction in other forums is permitted, provided the original author(s) and the copyright owner(s) are credited and that the original publication in this journal is cited, in accordance with accepted academic practice. No use, distribution or reproduction is permitted which does not comply with these terms.

Catchment properties as predictors of greenhouse gas concentrations across a gradient of boreal lakes

Nicolas Valiente[1,2], Alexander Eiler[1], Lina Allesson[1], Tom Andersen[1], François Clayer[3], Camille Crapart[4], Peter Dörsch[5], Laurent Fontaine[1], Jan Heuschele[1], Rolf D. Vogt[3], Jing Wei[1], Heleen A. de Wit[1,3] and Dag O. Hessen[1]*

[1]Centre for Biogeochemistry in the Anthropocene, Department of Biosciences, Section for Aquatic Biology and Toxicology, University of Oslo, Oslo, Norway, [2]Division of Terrestrial Ecosystem Research, Center of Microbiology and Environmental Systems Science, University of Vienna, Vienna, Vienna, Austria, [3]Norwegian Institute for Water Research (NIVA), Oslo, Norway, [4]Centre for Biogeochemistry in the Anthropocene, Department of Chemistry, University of Oslo, Oslo, Norway, [5]Faculty of Environmental Sciences and Natural Resource Management, Norwegian University of Life Sciences, Aes, Norway

Boreal lakes are the most abundant lakes on Earth. Changes in acid rain deposition, climate, and catchment land use have increased lateral fluxes of terrestrial dissolved organic matter (DOM), resulting in a widespread browning of boreal freshwaters. This browning affects the aqueous communities and ecosystem processes, and boost emissions of the greenhouse gases (GHG) CH_4, CO_2, and N_2O. In this study, we predicted biotic saturation of GHGs in boreal lakes by using a set of chemical, hydrological, climate, and land use parameters. For this purpose, concentrations of GHGs and nutrients (organic C, -P, and -N) were determined in surface water samples from 73 lakes in south-eastern Norway covering wide ranges in DOM and nutrient concentrations, as well as catchment properties and land use. The spatial variation in saturation of each GHG is related to explanatory variables. Catchment characteristics (hydrological and climate parameters) such as lake size and summer precipitation, as well as NDVI, were key determinants when fitting GAM models for CH_4 and CO_2 saturation (explaining 71 and 54%, respectively), while summer precipitation and land use data were the best predictors for the N_2O saturation, explaining almost 50% of deviance. Our results suggest that lake size, precipitation, and terrestrial primary production in the watershed control the saturation of GHG in boreal lakes. These predictions based on the 73-lake dataset was validated against an independent dataset from 46 lakes in the same region. Together, this provides an improved understanding of drivers and spatial variation in GHG saturation in boreal lakes across wide gradients of lake and catchment properties. The assessment highlights the need to incorporate multiple explanatory parameters in prediction models of GHGs for extrapolation across the boreal biome.

KEYWORDS

catchment, lake interactions, boreal lake, methane biogeochemistry, land use, land cover change, brownification

1 Introduction

Boreal ecosystems are expected to be among the most affected biomes by climate change (Ruckstuhl et al., 2008). Regarding inland waters, boreal lakes are the most abundant lakes on Earth (Schindler, 1998). These lakes receive high loading of allochthonous dissolved organic matter (DOM) from the catchment (Dillon and Molot, 1997; Tranvik et al., 2009). As such, these lakes are crucial biogeochemical reactors: on the one hand, they sequester DOM by burial into lake sediments, while on the other hand, they are generally net heterotrophic and act as major conduits for greenhouse gas (GHGs) emissions (Hessen et al., 1990, 2017; Bastviken et al., 2004; Tranvik et al., 2009; Yang et al., 2015; de Wit et al., 2018).

In boreal watercourses the lateral fluxes of colored DOM have increased during the past 2–3 decades, mainly due to reduced deposition of acid rain (de Wit et al., 2007; Monteith et al., 2007), climate change (Mattsson et al., 2005), afforestation and land use changes (Palviainen et al., 2016; Škerlep et al., 2020). The increasing DOM is causing a widespread "browning" of these freshwater ecosystems (Finstad et al., 2016). In the boreal biome, changing climate will result in increased precipitation and runoff (Tranvik et al., 2009). In some regions of the northern hemisphere, like Fennoscandia (the common term for Finland, Norway and Sweden) in general, the proportion of forest cover has increased, leading to larger biomass pools (Fang et al., 2014). This increase in terrestrial biomass ("greening") has boosted the amount of allochthonous DOM that may be entering into surface waters (Larsen et al., 2011b), with increased rainfall and runoff further enhancing DOM catchment export (Tranvik et al., 2009; de Wit et al., 2016). Browning strongly affects light attenuation (Karlsson et al., 2009; Thrane et al., 2014; Allesson et al., 2021), nutrient dynamics (Dillon and Molot, 2005; Creed et al., 2018) and thus also primary productivity (Solomon et al., 2015; Hessen et al., 2017; Lau et al., 2021). The combined effect of increased DOM and increased light attenuation implies a decrease in photosynthesis, thus promoting the heterotrophy of these systems and the net emissions of GHGs derived from microbial mineralization of DOM (Yang et al., 2015).

A number of studies have addressed the main drivers of carbon dioxide (CO_2) and methane (CH_4) concentrations in boreal lakes, and how they are linked to DOM and lake productivity (Huttunen et al., 2003b; Bastviken et al., 2004; Juutinen et al., 2009; de Wit et al., 2018; Jahr, 2021) as well as catchment properties (Huttunen et al., 2003b; Li et al., 2020). Fewer studies have addressed nitrous oxide (N_2O) in boreal lakes. N_2O is an intermediate in the nitrification and denitrification (Trogler, 1999; Butterbach-Bahl et al., 2013) whose production depends on the availability of organic matter (OM), oxygen availability, and reactive nitrogen concentration (Yang et al., 2015; Kortelainen et al., 2020; Clayer et al., 2021). Hydrological parameters, such as lake size or runoff, have been recognized as key underlying factors determining which are the main biogeochemical C processes that are governing the production of GHGs (Jones et al., 2018). In the boreal zone, small lakes have been shown to have relatively higher sedimentation and GHG emission rates than larger lakes (Juutinen et al., 2009; Kankaala et al., 2013). Typically, small lakes are also characterized by higher concentrations of allochthonous OM (Xenopoulos et al., 2003; Einola et al., 2011) and shorter water residence times (Vachon et al., 2017). The residence time has also a strong influence on the quality of DOM. The longer the residence time, the more refractory the DOM becomes, and thus the proportion of C sequestered in the sediments increases relative to what is released as CO_2 or CH_4 (den Heyer and Kalff, 1998). Most of this production is microbial, yet for all gases the concentrations and emissions are also affected by uptake and conversions by methanogens, denitrifiers, and autotrophs, but also by abiotic factors affecting microbial activity (i.e., temperature, redox conditions). These biotic processes are labelled biogenic and, therefore, traceable (Jones and Grey, 2011). For CO_2, the concentrations will also be affected by other processes as photooxidation and in cases also inputs from tributaries and groundwater, yet integrated over the water column of boreal lakes, the biogenic activities generally are by far the most important (Hessen et al., 1990; Larsen et al., 2011a; Allesson et al., 2021).

The goal of this study was to model biotic saturation of GHGs in boreal lakes by using a set of chemical, hydrological, climate, and land use parameters. To date, only a limited number of studies have explored the influence of such factors in GHG saturations from boreal lakes. For this reason, we constructed predictive models for GHG saturation from this survey performed in 2019 (73 lakes) and tested them against an independent dataset of 46 lakes sampled from the epilimnion of lakes in mid-summer 2011 by somewhat different protocols but covering a similar area of southern Norway (Yang et al., 2015). This validation by an independent dataset is a novel take, and both these datasets differ from previous studies on basically lowland sites by encompassing an unusual range in DOM, from very clear, ultraoligotrophic alpine lakes to really brown lowland sites, surrounded by bogs and coniferous forests. The wide span in catchment properties is also reflected in the strong gradient in forest cover, precipitation and temperatures, helping to sort out the relative contribution from these potential drivers on the various GHGs. We tested the hypothesis that differences in GHG saturation can be predicted by water chemistry, catchment properties (hydrological and climate parameters),

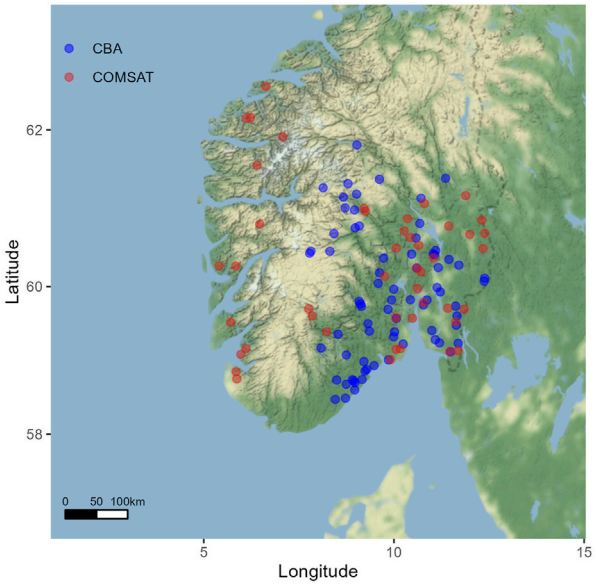


FIGURE 1
Lakes included in CBA (n = 73) and COMSAT (n = 46) surveys.

and land use variables. This approach aids to better predict the effect of on GHG emissions from pristine boreal lakes in climate change scenarios by combining well standardized watershed variables.

2 Material and methods

2.1 Field survey

Surface water samples were collected during autumn 2019 from 73 lakes in south-eastern Norway. This lake survey was conducted by the Centre for Biogeochemistry in the Anthropocene (CBA) at University of Oslo, hence these lakes are labelled "CBA dataset" hereafter. The lakes were selected as a subset of lakes monitored in a concomitant 1000-lake survey of the whole of Norway, conducted by the Norwegian Institute of Water research (NIVA). This synoptic survey repeated previous campaigns conducted in 1986 and 1995 (Henriksen et al., 1998). The CBA dataset span a wide range of water quality properties (e.g., DOM, nutrients) (Crapart et al., 2021), catchment properties, and land use (Lie, 2021). Sampling was performed in late fall, during or after lake overturn. Samples were collected approximately 4 m from the shore by means of a sampling rod with a sampling beaker. Composite water (≈2 L) was collected in a sampling bucket, with as minimal physical disturbance. Where feasible, the outlet of the lake was used as a sampling point. Due to logistical reasons, this was the only feasible way to sample all the lakes of this study. The lake edge may be more responsive to external inputs (i.e., precipitation, sunlight), likely acting more as a hotspot for GHG turnover compared to deeper sections of the lake. However, we believe that such bias is compensated in our models by including watershed hydrological characteristics (Section 2.4). In general, we assume that in these quite wind-exposed lakes, the gases are equally distributed in the epilimnion, but in sites with ebullition from the deepest part, we cannot exclude a non-homogenous distribution. In order to validate the models calibrated using the CBA dataset, a second dataset was used. This dataset, referred as COMSAT hereafter, includes 46 large southern Norwegian lakes sampled in the middle of the lakes by hydroplane in July and August 2011 (Thrane et al., 2014; Yang et al., 2015; Andersen et al., 2020). The selection of lakes was done with different constraints like size (>2 km^2) or water pH (>5), as detailed previously (Thrane et al., 2014). The locations of the lakes sampled in both campaigns are shown in Figure 1.

2.2 Chemical analysis

Water temperature (T), pH, and electrical conductivity (EC) were measured at the CBA lakes immediately after sample collection. From each site, 50 ml of unfiltered water was collected and stored at 10°C in polypropylene tubes. Upon arrival at the laboratory, these samples were frozen at −20°C until total organic carbon (TOC), total nitrogen (TN), and total phosphorus (TP) determination at the University of Oslo. TOC was measured by infrared CO_2 detection after catalytic high temperature combustion (Shimadzu TOC-VWP analyzer). TN was measured by detecting nitrogen monoxide by chemiluminescence using a TNM-1 unit attached to the Shimadzu TOC-VWP analyzer. TP was measured on an auto-analyzer as phosphate after wet oxidation with peroxodisulfate. We here use TOC as a proxy of DOM since this is by far the dominant constituent of DOM. By mass DOM is equivalent of DOC, and DOC make typically up some 95% of TOC in these boreal, low-productivity lakes (Larsen et al., 2011a; 2011b).

Concentrations of dissolved Argon (Ar), O_2, N_2, CH_4, CO_2, and N_2O were determined in duplicate for each lake water sample using the acidified headspace technique (Åberg and Wallin, 2014). From the surface of each lake, a volume of 30 ml was carefully collected directly into a syringe instead of collecting from the bucket to avoid potential disturbances (e.g., outgassing). Subsequently, a 20 ml headspace was created with atmospheric air in each syringe, before 0.6 ml of 3% HCl (≈1 M) was added. Syringes were closed and equilibrium was reached in the headspace at field temperature by shaking them for 3 min. Finally, 15 ml of the headspace gas was transferred into 12 ml evacuated vials and kept at room temperature until further analysis. Gas concentrations were determined at the Norwegian University of Life Sciences by automated gas chromatography (GC) analysis following the methodology

outlined by Yang et al. (2015). In brief, 2 ml of headspace gas were sampled (autosampler GC-Pal, CTC, Switzerland) and injected into a GC with He back-flushing (Agilent 7890A, Santa Clara, CA, United States). The GC was equipped with a 20-m wide-bore (0.53 mm) Poraplot Q column operated at 38°C and with He as carrier gas for separation of CH_4, CO_2, and N_2O from bulk gases (i.e., Ar, N_2, and O_2). N_2O and CH_4 were measured with an electron capture detector (ECD) operating at 375°C, and a flame ionization detector (FID), respectively. All other gases were measured with a thermal conductivity detector (TCD). Certified standards of CO_2, N_2O, and CH_4 in He were used for calibration (AGA, Germany), whereas N_2, O_2, and Ar were calibrated against air. The analytical precision for all gases was better than 1%.

2.3 Biogenic GHG saturation

Saturation relative to atmospheric equilibrium was calculated for all gases. For this purpose, Henry's law constants for 25°C were temperature adjusted to *in situ* water temperatures using the Clausius–Clapeyron equation with gas-specific solution enthalpies (Sander, 2015). Concentrations of GHGs in equilibrium with the atmosphere were calculated using the temperature adjusted Henry's law constants. The concentrations of GHGs in the surface water of the lakes were normalized relative to the concentration of dissolved Argon (Ar). Unlike Ar, which in water is only controlled by physical processes, O_2, N_2, CH_4, CO_2 and N_2O concentrations in water governed by both physical and biogenic processes (Aeschbach-Hertig et al., 1999). For this reason, the relative saturation of GHGs normalized to Ar was used as a proxy for the saturation of the biogenically derived lake GHG turnover (Yang et al., 2015). Thus, unless otherwise specified, hereafter the variables CH_4, CO_2 and N_2O are mentioned to refer to the normalized relative saturations of each GHG. A similar approach was used for the gas data collected during the COMSAT campaign (Thrane et al., 2014).

2.4 Catchment characteristics: Hydrological and climate parameters

Lake Altitude (in meters above sea level, m a.s.l.), lake surface (LakeArea in km^2), and catchment surface (CatchmentArea in km^2) were obtained using the "Lake database" (https://temakart.nve.no/tema/innsjodatabase) from the Norwegian Water Resources and Energy Directorate (NVE, https://www.nve.no). Drainage ratio (Drainage) was calculated as the ratio between catchment area and lake surface area, both in km^2. Lake depth (LakeDepth in m) was measured from an Airbus AS350 helicopter with an echosounder held within the top 0.5 m of the lake water column above the expected deepest point (Hindar et al., 2020). The remaining hydrological and climate parameters were compiled from the "NEVINA" database provided by the NVE (http://nevina.nve.no/). These were: specific runoff (Runoff in $L\ s^{-1}\ km^{-2}$); average inclination in the watershed (Slope in %); average annual air temperature (AnnualT in °C); average air temperature during the summer period (01/05–30/09) (SummerT in °C); average air temperature during the winter period (01/10–30/04) (WinterT in °C); average annual precipitation (AnnualP in mm); average precipitation during the summer period (SummerP in mm); and average precipitation during the winter period (WinterP in mm). Water residence time (Residence in yr) was estimated for each catchment from lake surface, lake depth, catchment surface, and specific runoff by assuming a cone-shaped morphometry for all lakes (Lindström et al., 2005).

2.5 Land use coverage

Land use data for each catchment were obtained from the Copernicus Land Monitoring Service (CLMS), using CORINE Land Cover (CLC) databases 2018 and 2012, for CBA and COMSAT, respectively (see (Feranec et al., 2007) for further details). In the CLC database the land use is classified into seven categories: agricultural areas (Cultivated), forested areas (Forest), human-derived and artificial impervious areas (Artificial), open areas with little or no vegetation (Fell), areas covered by glaciers and perpetual snow (Glacier), inland wetland areas (Peatland), and inland waterbodies in the watershed, including lake's surface itself (Waterbodies). The CLC databases were clipped and intersected with the catchment areas using the open-source software QuantumGIS (QGIS, version 3.20.1). The area covered by the different land use types were calculated as percentage of the total surface using QGIS field calculator. In addition, the average Normalized Difference Vegetation Index (NDVI) value was calculated for each catchment and year (2019 and 2011, for CBA and COMSAT, respectively) using the average values of the summer months (June, July, and August) obtained from Copernicus data (https://land.copernicus.eu/global/products/NDVI).

2.6 Statistical analysis

Data analysis was performed using the open-source software R version 4.1.0 (R Core Team, 2021). The package *raster* (Hijmans et al., 2015) was used to obtain average NDVI values per catchment. To determine significant differences in dissolved gas concentrations between CBA and COMSAT datasets, the Mann-Whitney test was used at a significance level of $p < 0.05$. Variables were checked for normality using the *bestNormalize* package (Peterson, 2021) and transformed to logarithmic, exponential, or square root where needed to reduce

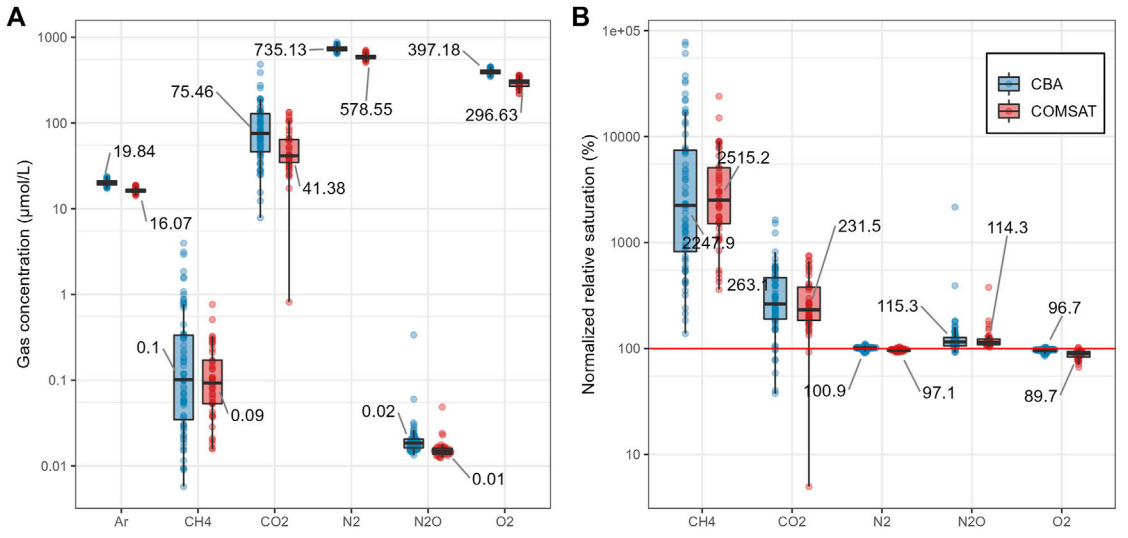


FIGURE 2
Surface water gas concentrations **(A)** and gas saturations **(B)** for CBA (blue) and COMSAT (red) datasets. Vertical axis are on a 10-base logarithmic scale. Data labels show median values for gas concentrations and saturations.

heteroscedasticity and obtain normally distributed residuals. However, variables were not standardized (i.e., mean centering and scaling) as comparisons of rescaled coefficients across datasets are problematic (King, 1986). A detailed list with the applied transformations is listed in the Supplementary Table S1. Once the transformations were performed, correlations were calculated using Spearman's correlation coefficients. In addition, principal component analysis (PCA) was performed for dimension reduction. This analysis was followed by K-means clustering. This non-hierarchical clustering method aims to partition the studied variables into *k* groups such that the sum of squares from points to the assigned cluster centres is minimized. Variation partitioning (function *varpart* in *vegan* package) (Oksanen et al., 2013) was used to evaluate the percentage of variance in biogenic GHG saturations that were in these clusters. Statistical modelling was carried out using the *mgcv* package (Wood and Wood, 2015) by fitting generalized additive models (GAM) to predict selected dependent variables (CH_4, CO_2, and N_2O). The selection of the predictive variable in the GAM models was performed by applying additional shrinkage on the null space of the penalty (*select* = *TRUE* argument in the mgcv:gam function) (Marra and Wood, 2011). To compare the contribution of each factor in explaining the total deviance of the model, we also formulated reduced models where we removed one of the terms at a time, as well as a null model. To be able to compare deviances, we fixed the smoothing parameters to the original model containing all terms (*sp* argument in the mgcv:gam function) and then calculated the contribution of each factor in the model as described previously (Ribic et al., 2010).

3 Results

3.1 Greenhouse gases

Across CBA lakes, the median surface concentrations of Ar, N_2, and O_2 were 19.8, 735, and 397 µmol/L, respectively. For GHGs, median concentrations were 0.10, 75.5, and 0.02 µmol/L for CH_4, CO_2, and N_2O, respectively (Figure 2A). GHG concentrations ranged widely across the CBA lakes, with CH_4 having a greater relative variability (CV = 183%) than N_2O (CV = 158%) and CO_2 (CV = 82.5%). On the contrary, Ar, N_2, and O_2 showed smaller coefficients of relative variation (7.6, 6.7, and 7.0%, respectively). The biogenic gas saturations were low for O_2 (median = 96.7%) and N_2 (median = 101%), while they were high for the GHGs: N_2O (median = 115%), CO_2 (median = 263%), and CH_4 (median = 2248%) (Figure 2B).

There were significant differences between all gas concentrations in the CBA data and the COMSAT datasets ($p < 0.05$, Mann-Whitney), except for CH_4 ($p = 0.50$) (Figure 2A). However, by comparing the relative biogenic gas saturations between both datasets, significant differences were found only for N_2 and O_2 ($p < 0.05$) (Figure 2B). The saturations of the biogenically derived CH_4 ($p = 0.74$), CO_2 ($p = 0.42$), and N_2O ($p = 0.86$) did not differ statistically between the two datasets.

3.2 Chemical-, catchment- and land use data

Besides varying in pH (4.4–7.9) and conductivity (0.39–151 µS/cm), CBA lakes varied widely in TOC from

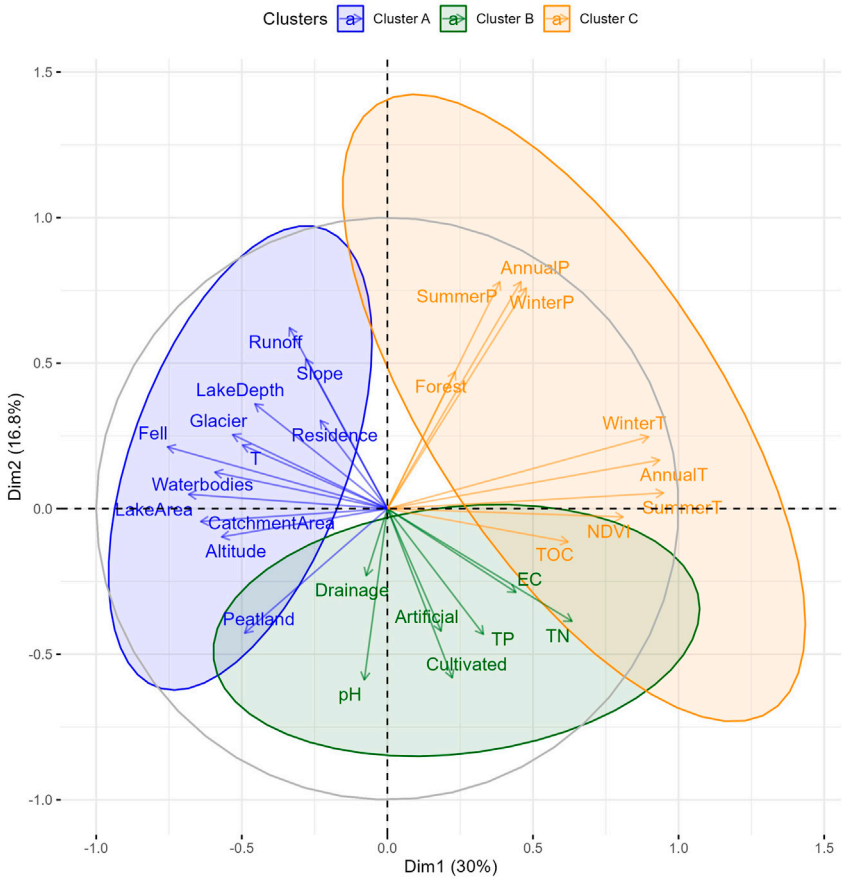


FIGURE 3
PCA analysis of the transformed variables depicting the two main principal components (PC) of parameter loading with the three defined clusters labeled in blue, green and orange (Clusters A, B and C, respectively). The two PCA axes explain 36.8% of total variability in the dataset.

2.54 to 116 mg/L (median = 13.3 mg/L), TN from 0.05 to 1.07 mg/L (median = 0.27 mg/L), and TP from 3.0 to 48.5 µg/L (median = 8.90 µg/L). A complete description of the chemical data can be found in the Supplementary Figure S1.

Catchment and Lake sizes varied from 0.02 to 369 km^2 (median = 0.93 km^2) and from 0.48 to 16,530 km^2 (median = 11.0 km^2), respectively. Drainage ratios varied from 2.76 to 405.8 (median = 24.6). The depths of the lakes ranged from 0.60 to 333 m (median = 12.0 m) and they are located at altitudes between 4 and 1,151 m a.s.l. (median = 190 m a.s.l.). Watershed slopes varied between 0.9 and 18.3% (median = 7.8%), while runoff values ranged from 8.0 to 41.8 L s^{-1} km^{-2} (median = 18.1 L s^{-1} km^{-2}). Estimated water residence times varied widely from 0.01 to 7.4 years (median = 0.29 years). Detailed information about the catchment variables is provided in the Supplementary Figure S2.

Most of the sampling sites in the CBA survey are first order lakes receiving drainage from pristine catchments. Forest was the main dominating land use type the watersheds (Forest, median = 83.7%), followed by inland waterbodies (Waterbodies; median = 3.7%) and agricultural land (Cultivated; median = 1.2%). Although generally comprising minor fractions of the catchment, peats and bogs (Peatland) and human-derived impervious surfaces (Artificial) reached coverages of up to 40.2 and 32.0%, respectively, in single catchments (see Supplementary Figure S3).

3.3 Explorative statistical analyses

Multivariate statistical analysis was performed on the transformed variables from the CBA dataset in order to explore whether the saturation of the biogenically derived GHGs significantly differed among explanatory variable groups. PCA of the transformed variables showed that 13 components were needed to explain 95% of the variance, with the first three components accounting for 59.1% of the total variance (30.0, 16.8, and 12.3%, respectively). Subsequent

K-means clustering analysis revealed three main groups of explanatory variables (Figure 3). The purpose of K-Means analysis is to group variables by minimizing data similarity between clusters, while maximizing data similarity within each cluster.

Cluster A (within the blue circle in Figure 3) includes water temperature measured during sampling (T) and non-forested land use (Waterbodies, Peatland, Fell, and Glacier), along with catchment physical properties (CatchmentArea, LakeArea and LakeDepth, Altitude, Residence, Slope, and Runoff). Cluster B (within the green circle in Figure 3) contains the water physicochemical parameters (pH and EC), nutrients (TN and TP), the coverage of Artificial and Cultivated land use types, as well as the Drainage ratio. Cluster C parameters (orange circle in Figure 3) are the biotic-related variables (Forest coverage, NDVI, and TOC) as well as climate factors in the watershed (temperature and precipitation).

Spearman rank-correlation analyses, using log transformed variables, provided information about internal correlation between the variables within the clusters, but also with the biogenic GHGs. Biogenic CH_4 normalized saturation was negatively correlated with lake size (LakeArea; $R = -0.78$; $p < 0.001$), watershed size (CatchmentArea; $R = -0.70$; $p < 0.001$), and lake depth (LakeDepth; $R = -0.50$; $p = 0.003$), whereas it was positively correlated with air temperature in the catchment (AnnualT; $R = 0.55$; $p < 0.001$) and NDVI ($R = 0.61$; $p < 0.001$). NDVI was positively correlated with average air temperature (AnnualT; $R = 0.69$; $p < 0.001$) (reflecting the altitude gradient) and thus Forest cover ($R = 0.53$; $p < 0.001$), whereas it was less negatively correlated with the percentage of water in the catchment (Waterbodies; $R = -0.54$; $p < 0.001$). The percentage of water in the watershed was also negatively correlated with the biogenic CO_2 normalized saturation ($R = -0.49$; $p = 0.004$), and as expected, positively correlated with lake size (LakeArea; $R = 0.75$; $p < 0.001$) and catchment size (CatchmentArea; $R = 0.64$; $p < 0.001$). Spearman's correlation plots are provided in Supplementary Figure S4.

Variation partitioning analyses (VPA) with transformed variables were carried out to assess relative contributions of the variables, grouped into the above defined clusters, to the biotic saturations of GHGs (Supplementary Figure S5). The combination of these variables explained 65.8% of the observed variation in biotic CH_4 saturation (Supplementary Figure S5A). The VPA showed that 38.1% of the total variation was shared between Cluster A, related mainly to catchment physical properties, and Cluster C, related to biotic and climate factors. Cluster A alone explained a large proportion of the variation (22.5%). The variance of biotic CO_2 saturation that could be explained by combining the whole set of variables was 39.7% (Supplementary Figure S5B). The largest explanatory value was shared by the three clusters (18.6%), explaining alone 4.4% (Cluster A) and 2.2% (Cluster B). Only 18.3% of the total variation of N_2O saturation was explained by the three clusters, with the variables within Cluster B providing most of the explanatory value to the spatial variation in biogenic N_2O saturation (11.4%) (Supplementary Figure S5C). This approach seems to be useful for CH_4 saturation. However, the high residuals observed for CO_2 and N_2O saturation makes the VPA not so informative about the contribution of each cluster to the total variation.

3.4 Modeling biogenic CH_4 saturation

Based on the explorative analyses (i.e., PCA, correlation, and VPA analyses), a stepwise selection was done to fit a GAM model (Model 1) to the transformed (i.e., log) normalized relative CH_4 saturation by minimizing the residual deviance. Lake surface (LakeArea; log), NDVI (exp) and average summer precipitation (SummerP; sqrt) were selected as independent variables, explaining 71.1% of the total variance with a $R^2_{adj} = 0.691$ (Table 1). LakeArea was the factor that explained the greatest variance by itself (26.9%), followed by SummerP (4.12%) and NDVI (4.10%) (Table 2). The variable selection is in line with the results from VPA, showing that clusters A (i.e., LakeArea) and C (i.e., SummerP and NDVI) explained a large proportion of the variation in CH_4 saturation. All independent variables were statistically significant ($p < 0.005$). Effective degrees of freedom (edf) for the factors were not close to 1. Therefore, smoothers were applied in the model with the default number of knots (k = 10), as shown in Figure 4. Validation of Model 1 with the COMSAT dataset, by comparing the predicted values (Y-axis) with the measured values (X-axis), resulted in a R^2_{adj} of 0.18 ($p < 0.005$). Diagnostics for Model 1 are provided in the Supplementary Figure S6.

3.5 Modeling biogenic CO_2 saturation

A second GAM model (Model 2) was fitted to the normalized relative CO_2 saturation (in log) following the approach described above. A deviance of 54.2% ($R^2_{adj} = 0.498$) was explained by selecting lake size (LakeArea; log), NDVI (exp), cultivated area (Cultivated; sqrt) and water temperature (T) as independent variables by stepwise method. LakeArea explained the highest variance (13.2%), followed by NDVI (8.39%), Cultivated (6.88%) and T (3.75%). All the variables were statistically significant ($p < 0.05$) (Table 2) and belonged to the three different clusters obtained in the PCA, in agreement with the VPA results for CO_2 saturation. In all the factors, edf were not close to one and therefore, smoothers were applied in the model with the default number of knots (k = 10) (Figure 5). Using COMSAT dataset to test the model gave a coefficient of determination (R^2_{adj}) of only 0.0075 ($p = 0.59$). Diagnostics for the Model 2 are shown in Supplementary Figure S7.

TABLE 1 Results of the generalized additive models (GAMs) calculated for biogenic saturation of CH_4, CO_2, and N_2O using both linear terms and smoothers (indicated with *s* before the variable). Edf: effective degrees of freedom. R^2_{adj}: R-squared adjusted for the number of predictors in the model. Dev: deviance explained by each model in %. AIC: Akaike information criterion.

Model	Response	Formula	edf	R^2_{adj}	Dev (%)	AIC	n
1	log (CH_4)	*s* (log (LakeArea)) + *s* (exp (NDVI)) + *s* (sqrt (SummerP))	5.67	0.691	71.1	73.660	71
2	log (CO_2)	*s* (log (LakeArea)) + *s*(T) + *s* (exp (NDVI)) + *s* (sqrt (Cultivated))	6.89	0.498	54.2	7.058	68
3	log (N_2O)	sqrt (Cultivated) + *s* (sqrt (SummerP)) + *s* (Forest) + *s* (sqrt (Artificial))	7.17	0.437	48.9	−199.88	68

TABLE 2 Output of each generalized additive models (GAM). Edf: effective degrees of freedom. Dev: deviance explained by each factor of the model in %.

Model	Variable	Estimate	Standard Error	*t*-Statistic	*p*-Value	Dev (%)
1 (CH_4)	Intercept	3.419	0.045	75.95	<2e-16	-
	Variable	**Edf**	**df residuals**	***F*-Statistic**	***p*-Value**	**Dev (%)**
	s (log (LakeArea))	2.336	9	7.476	<2e-16	26.9
	s (exp (NDVI))	0.879	9	0.809	0.00479	4.10
	s (sqrt (SummerP))	1.459	9	0.938	0.00463	4.12
Model	**Variable**	**Estimate**	**Standard Error**	***t*-Statistic**	***p*-Value**	**Dev (%)**
2 (CO_2)	Intercept	2.432	0.028	85.81	<2e-16	-
	Variable	**edf**	**df residuals**	***F*-Statistic**	***p*-Value**	**Dev (%)**
	s (log (LakeArea))	1.948	9	2.205	0.00003	13.2
	s (exp (NDVI))	1.838	9	1.157	0.00282	8.39
	s (sqrt (Cultivated))	0.883	9	0.837	0.00402	6.88
	s(T)	1.221	9	0.407	0.04804	3.75
Model	**Variable**	**Estimate**	**Standard Error**	***t*-Statistic**	***p*-Value**	**Dev (%)**
3 (N_2O)	Intercept	2.044	0.011	192.69	<2e-16	-
	sqrt (Cultivated)	0.020	0.006	3.489	0.00091	28.8
	Variable	**edf**	**df residuals**	***F*-Statistic**	***p*-Value**	**Dev (%)**
	s (sqrt (SummerP))	2.363	9	1.976	0.00027	15.6
	s (Forest)	2.084	9	1.287	0.00177	12.0
	s (sqrt (Artificial))	0.723	9	0.290	0.05034	12.0

3.6 Modeling biogenic N_2O saturation

Differences in normalized N_2O saturation (48.9%) were predicted by fitting a GAM model (Model 3) including as independent variables agricultural area (Cultivated; sqrt), average summer Precipitation (SummerP; sqrt), Forest area (Forest) and impervious land (Artificial; sqrt) (R^2_{adj} = 0.437). Variable selection was performed by stepwise method following the results from explorative analyses (i.e. PCA, correlation and VPA). In line with those, cultivated (Cluster C) was the factor explaining by itself the highest variance (28.8%), followed by SummerP (15.6%), Forest (12.0%) and Artificial (12.0%) (Table 2). Cultivated land showed an edf value close to 1, so smoother was removed from this variable (Figure 6). COMSAT dataset was used to validate the model and provided a R^2_{adj} of 0.49 ($p < 0.001$), which is similar to that obtained with the training dataset. Diagnostics for the Model 3 are provided in Supplementary Figure S8.

4 Discussion

4.1 Greenhouse gas saturation

The biogenic GHG saturation levels were in close accordance to those reported for boreal lakes in COMSAT dataset (Yang

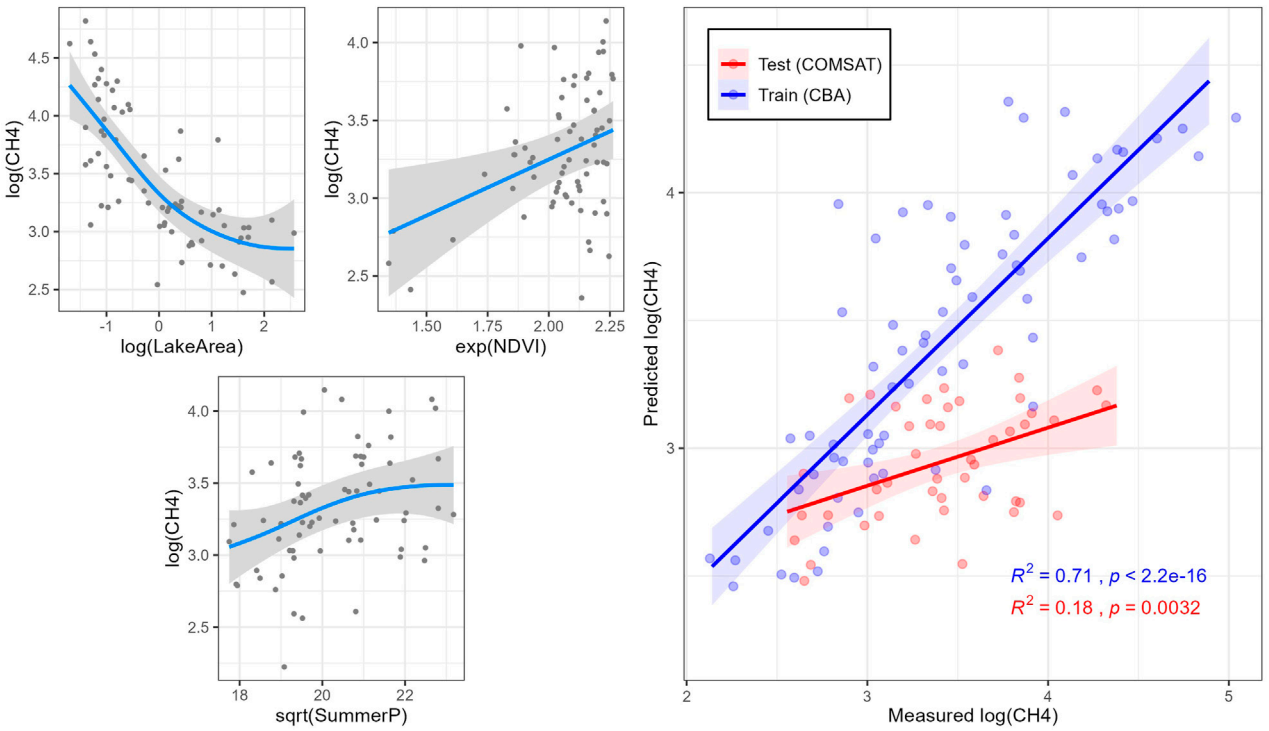


FIGURE 4
Simulations (blue lines) of normalized relative CH_4 saturations in the CBA dataset by generalized additive model (GAM) 1. On the right side, model training with CBA dataset (red) and test with COMSAT dataset (blue) for each model. Shaded gray areas indicate 95% confidence intervals.

et al., 2015). The biogenic oversaturation of CH_4, CO_2, and N_2O demonstrated a substantial impact of biogenic processes on GHG concentrations (Figure 2B). Methanogenesis and denitrification are microbially-mediated processes, which are affected by physical (e.g., temperature, rainfall) and chemical (e.g., nutrients) levels in the lake (Roland et al., 2017; Peña Sanchez et al., 2022). The well oxygenated waters of the study lakes (median = 96.7%, Figure 2B) are likely to constrain methanogenesis and promote methanotrophy in most of the water column. Still a pronounced CH_4 oversaturation (median = 2248%) was found, reflecting a pronounced methanogenesis in deep waters and sediments. In small lakes (<1 km^2), convective mixing in the epilimnion and deepening of the mixing layer may be the main mechanism transporting CH_4 to lake surface layers (Kankaala et al., 2013). Prior studies in small boreal lakes have noted the importance of convective cooling of water masses in autumn, where CH_4 effluxes exceed CH_4 oxidation in the water column (Kankaala et al., 2006). This is a possible explanation for the observed results, as our survey was conducted in autumn and 37 of the 73 lakes (51%) are classified as small. In large lakes (>1 km^2), CH_4 can be originated from shallow epilimnetic sediments (Bastviken et al., 2008) and be transported laterally from the littoral/riparian zone and the catchment area (López Bellido et al., 2013). It is important to bear in mind the possible bias in large lakes, as the sampling was performed from the littoral zone (Section 2.1). Nevertheless, the consistency between these datasets are noteworthy, even if the COMSAT lakes were sampled in the middle of the lakes in contrast to the littoral sampling of the current (CBA) dataset.

CO_2 exchange is mainly governed by biotic processes, specifically by the balance between photosynthesis and respiration. In boreal lakes, CO_2 oversaturation is to a large degree an effect of microbial respiration boosted by allochthonous C (Hessen et al., 1990), regulated by factors like catchment area or residence time (Larsen et al., 2011a). Our results showed CO_2 oversaturation in the CBA survey (median = 263.1%, Figure 2B) similar to those observed in the COMSAT survey (median = 231.5%). The lakes from the CBA survey were located in catchments dominated by coniferous forests, primarily spruce and pine. The positive correlation between CO_2 saturation and TOC concentrations (R = 0.3; p < 0.001) (Supplementary Figure S4) suggests in-lake CO_2 production by TOC mineralization. These results are in line with previous studies (Kortelainen et al., 2006; Whitfield et al., 2011). In addition, a positive correlation was found between CO_2 saturation and TN concentrations (R = 0.36; p < 0.001) (Supplementary Figure S4). Primary production in boreal lakes can be promoted by N availability (Elser et al., 2009). Nutrients also boost microbial activity, and our data demonstrate that boreal lakes

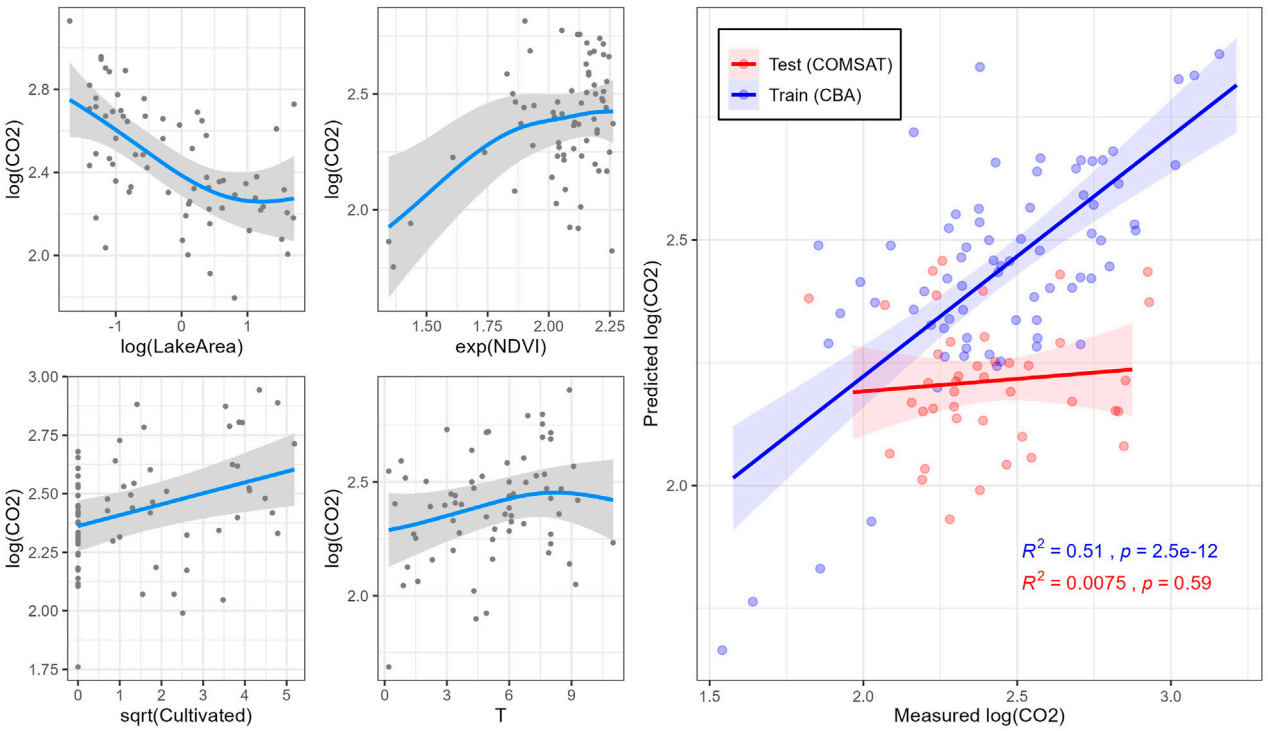


FIGURE 5
Simulations (blue lines) of normalized relative CO_2 saturations in the CBA dataset by generalized additive model (GAM) 2. On the right side, model training with CBA dataset (red) and test with COMSAT dataset (blue) for each model. Shaded gray areas indicate 95% confidence intervals.

generally retain net heterotrophy in spite of nutrient loading and potentially high primary production, in support of Huttunen et al. (2003a). These positive correlations with TOC and TN suggest the transport of bioavailable OM from catchment soils to lakes and in-lake breakdown of DOM is a main driver for dissolved CO_2 (Sobek et al., 2003; Whitfield et al., 2011). Furthermore, lateral export of DIC from soils to aquatic environments may contribute to lake CO_2 (Öquist et al., 2009; Vachon et al., 2017). In boreal catchments, DIC may derive from the dissolution of soil CO_2 as well as from mineral weathering (Nydahl et al., 2020). Water pH may regulate the CO_2 concentration by keeping a large proportion of the DIC as free CO_2 at low pH values, which in turn depends on the input of humic acids (Nydahl et al., 2019). Our results followed this trend, with a weak negative correlation between CO_2 saturation and pH (R = -0.21; p > 0.001) (Supplementary Figure S4).

Consistent with the literature (Huttunen et al., 2003a; Whitfield et al., 2011; Yang et al., 2015; Kortelainen et al., 2020), our research found N_2O oversaturation, but lower than CH_4 and CO_2. While being relatively low, the oversaturation of N_2O (median = 115.3%, Figure 2B) reflects the potential of boreal lakes as to act a net source for N_2O due to nitrification and denitrification processes. A positive correlation was found between N_2O saturation and TOC concentrations (R = 0.35; p < 0.001) (Supplementary Figure S4). Since DOM (or TOC) mainly derives from allochthonous sources, it suggests that N_2O concentration also depends on the transport of bioavailable OM from catchment soils. N_2O saturation in boreal lakes has been generally associated with agricultural land in the watershed (Kortelainen et al., 2020). Our results support this by a strong correlation between N_2O saturation and agricultural land cover (Cultivated) (R = 0.32; p < 0.001), but also with artificial impervious areas (Artificial) (R = 0.3; p < 0.001) (Supplementary Figure S4). In lakes, N_2O production and emissions is boosted by atmospheric N-deposition (Yang et al., 2015), as well as nitrate load from land to lakes (Huttunen et al., 2003b). This latter flux may be enhanced in the boreal landscape by rising temperatures leading to earlier floods due to snow melt (Blöschl et al., 2017) and consequent transport of nitrates to surface waters (Kortelainen et al., 2020).

4.2 Hydrological and climate determinants of GHG saturation

The generalized additive models (GAMs) calculated for biogenic saturation of GHG included either or both hydrological (LakeArea) and climate (SummerP, T) parameters as explanatory variables (Table 1). Variation

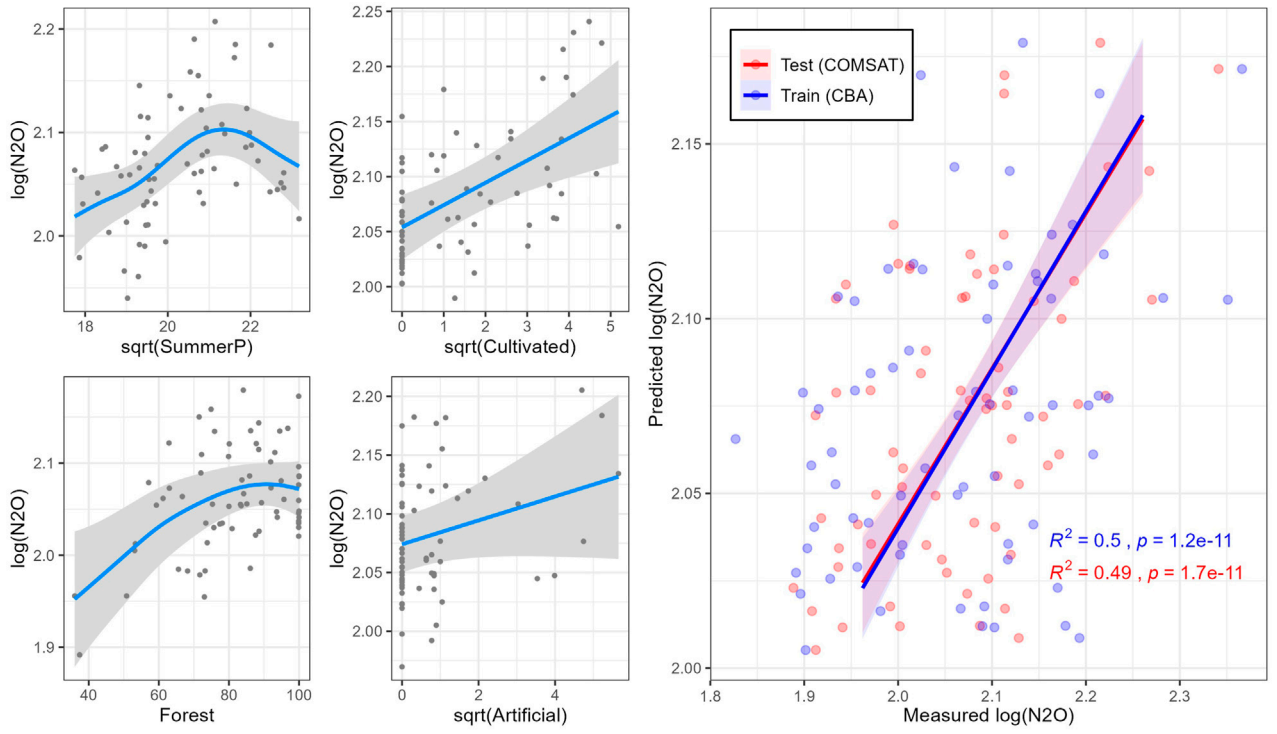


FIGURE 6
Simulations (blue lines) of normalized relative N_2O saturations in the CBA dataset by generalized additive model (GAM) 3. On the right side, model training with CBA dataset (red) and test with COMSAT dataset (blue) for each model. Shaded gray areas indicate 95% confidence intervals.

partitioning analyses indicated that hydrological parameters had the greatest contribution to biogenic CH_4 saturation (22.5%, Supplementary Figure S5A), supporting earlier studies (Kankaala et al., 2013; Li et al., 2020). In that sense, lake size (LakeArea) was the main explanatory factor for the spatial differences in biogenic CH_4 saturation (26.9% of the total deviance; Table 2), further supporting evidence from previous studies (Bastviken et al., 2004; Juutinen et al., 2009; Kankaala et al., 2013; Holgerson, 2015; Denfeld et al., 2020; Jahr, 2021). Biogenic CH_4 saturation level was negatively correlated with lake surface (LakeArea; Figure 4). This result may be explained by the fact that small lakes have a high perimeter/surface area ratio, which means that they receive relatively higher loads of allochthonous DOM relative to water volume (Holgerson and Raymond, 2016). The increased contribution of allochthonous DOM promotes microbial metabolism (Tranvik, 1998; Forsström et al., 2013). Therefore, littoral sediments can play a major role in increasing pelagic lacustrine CH_4 due to horizontal mixing in the surface layer (Juutinen et al., 2003; Rasilo et al., 2015; Bartosiewicz et al., 2016). This is also supported by the negative correlation found between log (CH_4) and log (LakeDepth) in (R = −0.50; Supplementary Figure S4). As stated, our sampling strategy may involve some bias in the results for large lakes. Lake size was also included as variable in the CO_2 saturation model (GAM model 2), showing a negative correlation between both (Figure 5). LakeArea explained 13.2% of the total deviance (Table 2) and was the sole catchment parameter included in the model (Figure 5). Compared to the CH_4 model, this predictor explained less deviance (22.5 vs. 13.2%) but it was still the strongest predictor in the model (Table 2). Our CO_2 model 2 predicted higher CO_2 saturations in lakes with smaller surface areas (LakeArea), in line with previous studies showing significantly higher CO_2 emissions in small lakes (Kortelainen et al., 2006), most likely as a result of increasing lateral OM fluxes (de Wit et al., 2018).

As climate parameters, the average precipitation during the summer period (SummerP) was selected as independent variable in the CH_4 model (Model 1; Table 1). It explained 4.12% of the total deviance (Table 2), showing a positive correlation to the variation in biogenic CH_4 saturation (Figure 4). Summer precipitation was orthogonal to the loading vectors, reflecting lake size within Cluster A (i.e., LakeArea, CatchmentArea, and LakeDepth; Figure 3).

Precipitation boosted GHG-production (cf. Model 3; Table 1), and more so for CH_4 than for N_2O saturation (Table 2 and Figure 6). These results are in line with previous studies showing that increased precipitation is associated with larger allochthonous DOM inputs to lakes (Rantakari and Kortelainen, 2005; Natchimuthu et al., 2014).

For the CO_2 saturation model (Model 2; Table 1), water temperature (T) was included as explanatory variable showing a positive correlation (Figure 5). By itself, it explained 3.75% of the total deviance (Table 2), being the only model where T was selected. Water temperature reflects on the seasonal changes in air temperature. It also strongly affects microbial metabolism and promotes mineralization in lake sediments (Gudasz et al., 2010). However, this trend may be the opposite depending on the season of the year in which sampling is performed because of phytoplankton activity (Tadonléké et al., 2012). Since the CBA sampling was conducted in late fall, close to lake overturn, we can rule out CO_2 uptake by phytoplankton as a main driver.

The stepwise selection of variables for the GAM models highlighted the importance of catchment characteristics (hydrological and climate parameters) in predicting biogenic GHG saturation from boreal lakes. In fact, both LakeArea and SummerP may be understood as proxies for water residence time in the watershed. Previous studies have noted that mineralization capacity of lakes at the catchment scale was closely correlated to the mean residence time of surface water in the watershed (Algesten et al., 2004). An inverse relationship between the rate of OM decay (i.e., biogenic CH_4 production) and residence time have been reported (Catalán et al., 2016). In that sense, higher decomposition rates are found in systems with short residence times, as a result of the constant renewal of the labile organic pool (Jones et al., 2018). Headwaters can be considered as hotspots for OM processing as they receive fresh allochthonous OM. Thus, the lability of the allochthonous OM decreases along the aquatic continuum (Clayer et al., 2021). Our results are consistent with those previous studies. Although our estimated water residence times (Residence) were not included as explanatory variables in the GAM models, significant negative correlations were found between Residence and normalized CH_4 saturation ($R = -0.34$; $p < 0.001$), and normalized N_2O saturation ($R = -0.27$; $p < 0.001$) (Supplementary Figure S4). Using TOC as proxy for OM inputs, the negative correlation observed between TOC and Residence ($R = -0.25$; $p < 0.001$) (Supplementary Figure S4) points to residence time as a key driver. This also implies that changes in precipitation and runoff also will affect GHG-metabolism in lakes via this mechanism.

4.3 The influence of terrestrial primary production on GHG saturations

Variables related to primary production in the catchment were also included in the generalized additive models (GAMs) calculated for biogenic saturation of GHG. In general, higher GHG saturations were found coupled to higher values of the primary production proxies in the catchment (i.e., NDVI, Cultivation and Forest cover). NDVI was selected as explanatory variable for CH_4 and CO_2 saturation models (Table 1). CH_4 model (Model 1) ranked NDVI as the third most explanatory variable (4.10% of the total deviance; Table 2), while it accounted for a higher deviance in the CO_2 model (8.39% of the total deviance; Table 2). NDVI is a proxy for terrestrial vegetation and primary production. NDVI was strongly correlated with TOC, AnnualT, and Forest cover (R of 0.43, 0.69, and 0.53, respectively; $p < 0.001$) (Supplementary Figure S4). Previous studies have shown a close link between NDVI in the watershed and levels of DOM/TOC in the runoff, suggesting that leachates from terrestrial primary production of litterfall are a major source of OM in boreal lakes (Larsen et al., 2011a; Finstad et al., 2016; Škerlep et al., 2020). The wide gradient of catchment NDVI and lake DOM is our studied lakes clearly reveals that the supply of allochthonous OM stimulates heterotrophic metabolism resulting in higher CH_4 and CO_2 saturations, which is observed in both models (Figures 4, 5).

Cultivation coverage was included in both CO_2 and N_2O saturation models (Table 1). It explained 6.88 and 28.8% of the total deviance explained in CO_2 and N_2O models, respectively (Table 2). The positive correlation between the agricultural land cover (Cultivated) and CO_2 concentrations in boreal lakes has been pointed out previously (Kortelainen et al., 2006), likely reflecting inputs of easily degradable DOM (Crapart et al., 2021) as well as nutrient loads from croplands (Rantakari and Kortelainen, 2005). For N_2O saturation, a positive correlation between N_2O saturation and agricultural land cover has previously been reported previously for boreal lakes (Kortelainen et al., 2020). Our research shows that agricultural land cover and TN are positively correlated ($R = 0.54$; $p < 0.001$) (Supplementary Figure S4). N from fertilizers applied in the watershed are microbially processed in lakes, producing N_2O as by-product of both nitrification and denitrification. N_2O saturation model (Model 3; Table 1) also included Forest and Artificial, explaining respectively 12.0 and 12.0% of the total deviance (Table 2). Higher proportions of these uses were associated with higher N_2O saturations in lake waters (Figure 6). Likewise, Forest and/or Artificial land cover seems to be associated with DOM inputs into lakes (Mattsson et al., 2005; Pellerin et al., 2006; Finstad et al., 2016), promoting processes such as denitrification (Liu et al., 2015). In forest dominated areas from the boreal landscape, soil N seems to leach from catchment soils directly into the lakes in form of nitrate (Khalili et al., 2010), which can be denitrified giving N_2O as a by-product.

4.4 Evaluation of biogenic GHG saturation models

Given the major role of boreal lakes for GHG-emissions (Tranvik et al., 2009), accurate models are needed to better predict biogenic GHG saturations in lakes across the boreal

landscape. In that sense, our GAM models were tested on the independent COMSAT dataset. Despite COMSAT lakes were all sampled in the middle of the lakes, our results showed that the datasets are basically consistent. In fact, the COMSAT lakes tend to be a bit lower in GHGs, which can be attributed to a somewhat larger area. The major levels and patterns in saturation of the three GHGs was basically consistent between the two datasets. In decreasing order, the trained models had the highest testing success for $N_2O > CH_4 > CO_2$. The N_2O model (Model 3; Table 1) was validated using COMSAT dataset, obtaining similar results as those obtained when using the training dataset (CBA) (Figure 6). The relatively low deviance explained by Model 3 (48.9%) probably reflects the low variability in biogenic N_2O concentrations, as well as the lack of likely key governing factors for the in lake biogeochemical N_2O production, such as N-deposition (Pregitzer et al., 2008; McCrackin and Elser, 2010; Kortelainen et al., 2013).

Despite the consistency in patterns and levels of saturation between the two independent datasets, the CH_4 saturation model (Model 1; Table 1) showed a poor correlation between predicted and measured biogenic CH_4 saturations with the COMSAT dataset (R^2_{adj} = 0.18) (Figure 4). This discrepancy could be attributed to the seasonality, the location, and the size of lakes sampled. The CBA lakes were sampled during fall turnover, while the COMSAT lakes were collected from the epilimnion during the summer stratification. The COMSAT survey covered a geographical gradient from western Norway (5.4°E) to the Norwegian-Swedish border (12.3°E). LakeArea distribution in the COMSAT dataset (median = 3.53 km^2) was also significantly larger ($p < 0.001$) than the LakeArea from CBA dataset (median = 0.93 km^2). Nevertheless, gas concentrations and especially biogenic saturations of GHGs were similar for both datasets (Figure 2). When the COMSAT dataset was restricted to lakes in central-eastern Norway (n = 33, longitude >7.7°E), the correlation between predicted and measured CH_4 saturations increased up to (R^2_{adj} = 0.39). It should also be noted that the western part of Norway is characterized as one of the rainiest parts of Europe. The original COMSAT dataset has values from SummerP to 919 mm, which may definitely affect the adjustment of CH_4 saturation model.

Also the CO_2 saturation model (Model 2; Table 1) showed only weak correlation between predicted and measured biogenic CO_2 saturation in the COMSAT dataset (R^2_{adj} = 0.008) (Figure 5). A feasible explanation for this discrepancy may be that samples for COMSAT were collected during the summer, when assimilation of CO_2 in the epilimnion is likely an important governing factor. The season of the year when sampling occurred may thus be a reason for the poor simulation of biogenic CO_2 saturation obtained when applying the model to the COMSAT dataset. In addition, LakeArea was the strongest predictor in the model and, as stated above, lake size distribution differed significantly between the CBA and COMSAT surveys. When COMSAT dataset was downscaled to lakes with a longitude above 7.7°E (n = 33), the adjustment was slightly better (R^2_{adj} = 0.10) but still far from that obtained with the training dataset (R^2_{adj} = 0.51).

These findings show the difficulties in achieving good models for predicting GHG saturations in boreal lakes. When modeling, increasing the number of variables used in the models may increase the variance explained, but complicate the interpretation and application of the models. Within the CBA dataset, we achieved robust predictions. Despite the patterns and levels of GHGs saturations are consistent between the two datasets, the generation of robust models predicting GHGs demands multiple explanatory parameters, including size and seasonality.

5 Conclusion

The purpose of the current study was to model biotic saturation of GHGs in boreal lakes by using a set of chemical, hydrological, climate, and land use parameters. Our models were trained on a dataset of boreal lakes (n = 73) sampled in 2019 and then validated with an additional dataset of boreal lakes (n = 46) sampled in 2011. Both these datasets encompass an extraordinary gradient in altitude, precipitation, temperature and not the least their content of organic matter, and allowed us to tease apart various drivers. We find that: i) hydrological and climate parameters are key drivers for predicting GHG saturation; ii) the influence of external OM inputs (i.e., terrestrial) plays a key role in biogeochemical cycling. Most of the variation in biogenic CH_4 saturation was explained by lake size: the larger the lake, the lower the CH_4 saturation. On the contrary, summer precipitation and NDVI exhibited a positive correlation with CH_4 saturation. Biogenic CO_2 saturation was mainly explained by lake size (negative correlation) followed by NDVI, proportion of cultivated area, and water temperature (positive correlation in all of them). For biogenic N_2O saturation, the differences in land use (cultivated, forest, and artificial area) were the strongest predictors showing a positive correlation, as well as summer precipitation. The insights given by our extraordinary range of catchment and lakes variables provides new insights in drivers of GHG-production in boreal lakes, which again improve predictions of impacts of climate change and human activities. The comparison of two independent datasets, and using one as a training dataset for model prediction, nevertheless demonstrate that predicting GHGs demands multiple explanatory parameters, including seasonality, for generation robust models.

Data availability statement

The datasets presented in this study can be found in online repositories. The names of the repository/repositories and accession number(s) can be found below: https://osf.io/r39ng/?view_only=e9a3b3de84794bfc9883db481cb9a483.

Author contributions

NV, AE, and DH conceived the idea. All authors were involved in either fieldwork and/or sample analysis, in the analysis of data and final writing. All authors contributed to the article and approved the submitted version.

Funding

The work has been funded by CBA, as well as EU-BioDiversa/Belmont Forum and The Research Council of Norway within ARCTIC-BIODIVER project ("Scenarios of freshwater biodiversity and ecosystem services in a changing Arctic"). University of Oslo provides funding for open access publication.

Acknowledgments

This study was carried out thanks to close cooperation between researchers from the Centre for Anthropocene Biogeochemistry (CBA, University of Oslo) and the Norwegian Institute for Water Research (NIVA). The authors acknowledge all of the participants involved in the CBA-100 lakes survey, NIVA for providing depth data, and especially to Per-Johan Færøvig and Berit Kaasa for their support with practicality issues in the labs.

Conflict of interest

The authors declare that the research was conducted in the absence of any commercial or financial relationships that could be construed as a potential conflict of interest.

Publisher's note

All claims expressed in this article are solely those of the authors and do not necessarily represent those of their affiliated organizations, or those of the publisher, the editors and the reviewers. Any product that may be evaluated in this article, or claim that may be made by its manufacturer, is not guaranteed or endorsed by the publisher.

Supplementary material

The Supplementary Material for this article can be found online at: https://www.frontiersin.org/articles/10.3389/fenvs.2022.880619/full#supplementary-material

References

Åberg, J., and Wallin, B. (2014). Evaluating a fast headspace method for measuring DIC and subsequent calculation of pCO2 in freshwater systems. *Inland Waters* 4, 157–166. doi:10.5268/IW-4.2.694

Aeschbach-Hertig, W., Peeters, F., Beyerle, U., and Kipfer, R. (1999). Interpretation of dissolved atmospheric noble gases in natural waters. *Water Resour. Res.* 35, 2779–2792. doi:10.1029/1999WR900130

Algesten, G., Sobek, S., Bergström, A.-K., Ågren, A., Tranvik, L. J., and Jansson, M. (2004). Role of lakes for organic carbon cycling in the boreal zone. *Glob. Chang. Biol.* 10, 141–147. doi:10.1111/j.1365-2486.2003.00721.x

Allesson, L., Koehler, B., Thrane, J.-E., Andersen, T., and Hessen, D. O. (2021). The role of photomineralization for CO_2 emissions in boreal lakes along a gradient of dissolved organic matter. *Limnol. Oceanogr.* 66, 158–170. doi:10.1002/lno.11594

Andersen, T., Hessen, D. O., Håll, J. P., Khomich, M., Kyle, M., Lindholm, M., et al. (2020). Congruence, but no cascade—pelagic biodiversity across three trophic levels in nordic lakes. *Ecol. Evol.* 10, 8153–8165. doi:10.1002/ece3.6514

Bartosiewicz, M., Laurion, I., Clayer, F., and Maranger, R. (2016). Heat-wave effects on oxygen, nutrients, and phytoplankton can alter global warming potential of gases emitted from a small shallow lake. *Environ. Sci. Technol.* 50, 6267–6275. doi:10.1021/acs.est.5b06312

Bastviken, D., Cole, J., Pace, M., and Tranvik, L. (2004). Methane emissions from lakes: Dependence of lake characteristics, two regional assessments, and a global estimate. *Glob. Biogeochem. Cycles* 18, 2238. doi:10.1029/2004GB002238

Bastviken, D., Cole, J. J., Pace, M. L., and Van de Bogert, M. C. (2008). Fates of methane from different lake habitats: Connecting whole-lake budgets and CH4 emissions. *J. Geophys. Res.* 113, 608. doi:10.1029/2007JG000608

Blöschl, G., Hall, J., Juraj, P., Perdigão Rui, A. P., Bruno, M., Berit, A., et al. (2017). Changing climate shifts timing of European floods. *Science* 357, 588–590. doi:10.1126/science.aan2506

Butterbach-Bahl, K., Baggs, E. M., Dannenmann, M., Kiese, R., and Zechmeister-Boltenstern, S. (2013). Nitrous oxide emissions from soils: How well do we understand the processes and their controls? *Phil. Trans. R. Soc. B* 368, 20130122. doi:10.1098/rstb.2013.0122

Catalán, N., Marcé, R., Kothawala, D. N., and Tranvik, Lars. J. (2016). Organic carbon decomposition rates controlled by water retention time across inland waters. *Nat. Geosci.* 9, 501–504. doi:10.1038/ngeo2720

Clayer, F., Thrane, J.-E., Brandt, U., Dörsch, P., and de Wit, H. A. (2021). Boreal headwater catchment as hot spot of carbon processing from headwater to fjord. *JGR. Biogeosciences* 126, e2021JG006359. doi:10.1029/2021JG006359

Crapart, C., Andersen, T., Hessen, D. O., Valiente, N., and Vogt, R. D. (2021). Factors governing biodegradability of dissolved natural organic matter in lake water. *Water* 13, 2210. doi:10.3390/w13162210

Creed, I. F., Bergström, A.-K., Trick, C. G., Grimm, N. B., Hessen, D. O., Karlsson, J., et al. (2018). Global change-driven effects on dissolved organic matter composition: Implications for food webs of northern lakes. *Glob. Chang. Biol.* 24, 3692–3714. doi:10.1111/gcb.14129

de Wit, H. A., Mulder, J., Hindar, A., and Hole, L. (2007). Long-term increase in dissolved organic carbon in streamwaters in Norway is response to reduced acid deposition. *Environ. Sci. Technol.* 41, 7706–7713. doi:10.1021/es070557f

de Wit, H. A., Valinia, S., Weyhenmeyer, G. A., Futter, M. N., Kortelainen, P., Austnes, K., et al. (2016). Current browning of surface waters will Be further

promoted by wetter climate. *Environ. Sci. Technol. Lett.* 3, 430–435. doi:10.1021/acs.estlett.6b00396

de Wit, H. A., Couture, R.-M., Jackson-Blake, L., Futter, M. N., Valinia, S., Austnes, K., et al. (2018). Pipes or chimneys? For carbon cycling in small boreal lakes, precipitation matters most. *Limnol. Oceanogr. Lett.* 3, 275–284. doi:10.1002/lol2.10077

den Heyer, C., and Kalff, J. (1998). Organic matter mineralization rates in sediments: A within- and among-lake study. *Limnol. Oceanogr.* 43, 695–705. doi:10.4319/lo.1998.43.4.0695

Denfeld, B. A., Lupon, A., Sponseller, R. A., Laudon, H., and Karlsson, J. (2020). Heterogeneous CO2 and CH4 patterns across space and time in a small boreal lake. *Inland Waters* 10, 348–359. doi:10.1080/20442041.2020.1787765

Dillon, P. J., and Molot, L. A. (1997). Effect of landscape form on export of dissolved organic carbon, iron, and phosphorus from forested stream catchments. *Water Resour. Res.* 33, 2591–2600. doi:10.1029/97WR01921

Dillon, P. J., and Molot, L. A. (2005). Long-term trends in catchment export and lake retention of dissolved organic carbon, dissolved organic nitrogen, total iron, and total phosphorus: The Dorset, Ontario, study, 1978–1998. *J. Geophys. Res.* 110, G01002. doi:10.1029/2004JG000003

Einola, E., Rantakari, M., Kankaala, P., Kortelainen, P., Ojala, A., Pajunen, H., et al. (2011). Carbon pools and fluxes in a chain of five boreal lakes: A dry and wet year comparison. *J. Geophys. Res.* 116, G03009. doi:10.1029/2010JG001636

Elser, J., Andersen, T., Baron Jill, S., Ann-Kristin, B., Mats, J., Marcia, K., et al. (2009). Shifts in lake N:P stoichiometry and nutrient limitation driven by atmospheric nitrogen deposition. *Science* 326, 835–837. doi:10.1126/science.1176199

Fang, J., Guo, Z., Hu, H., Kato, T., Muraoka, H., and Son, Y. (2014). Forest biomass carbon sinks in East Asia, with special reference to the relative contributions of forest expansion and forest growth. *Glob. Chang. Biol.* 20, 2019–2030. doi:10.1111/gcb.12512

Feranec, J., Hazeu, G., Christensen, S., and Jaffrain, G. (2007). Corine land cover change detection in Europe (case studies of The Netherlands and Slovakia). *Land Use Policy* 24, 234–247. doi:10.1016/j.landusepol.2006.02.002

Finstad, A. G., Andersen, T., Larsen, S., Tominaga, K., Blumentrath, S., de Wit, H. A., et al. (2016). From greening to browning: Catchment vegetation development and reduced S-deposition promote organic carbon load on decadal time scales in Nordic lakes. *Sci. Rep.* 6, 31944. doi:10.1038/srep31944

Forsström, L., Roiha, T., and Rautio, M. (2013). Responses of microbial food web to increased allochthonous DOM in an oligotrophic subarctic lake. *Aquat. Microb. Ecol.* 68, 171–184. doi:10.3354/ame01614

Gudasz, C., Bastviken, D., Steger, K., Premke, K., Sobek, S., and Tranvik, L. J. (2010). Temperature-controlled organic carbon mineralization in lake sediments. *Nature* 466, 478–481. doi:10.1038/nature09186

Henriksen, A., Skjelvåle, B. L., Mannio, J., Wilander, A., Harriman, R., Curtis, C., et al. (1998). Northern European lake survey, 1995: Finland, Norway, Sweden, Denmark, Russian kola, Russian karelia, scotland and wales. *Ambio* 27, 80–91.

Hessen, D. O., Andersen, T., and Lyche, A. (1990). Carbon metabolism in a humic lake: Pool sires and cycling through zooplankton. *Limnol. Oceanogr.* 35, 84–99. doi:10.4319/lo.1990.35.1.0084

Hessen, D. O., Håll, J. P., Thrane, J.-E., and Andersen, T. (2017). Coupling dissolved organic carbon, CO2 and productivity in boreal lakes. *Freshw. Biol.* 62, 945–953. doi:10.1111/fwb.12914

Hijmans, R. J., Van Etten, J., Cheng, J., Mattiuzzi, M., Sumner, M., Greenberg, J. A., et al. (2015). *Package 'raster.'* R package *734*.

Hindar, A., Garmo, Ø. A., Austnes, K., and Sample, J. E. (2020). *Nasjonal innsjøundersøkelse 2019*. Oslo, Norway: NIVA-rapport.

Holgerson, M. A. (2015). Drivers of carbon dioxide and methane supersaturation in small, temporary ponds. *Biogeochemistry* 124, 305–318. doi:10.1007/s10533-015-0099-y

Holgerson, M. A., and Raymond, P. A. (2016). Large contribution to inland water CO2 and CH4 emissions from very small ponds. *Nat. Geosci.* 9, 222–226. doi:10.1038/ngeo2654

Huttunen, J. T., Alm, J., Liikanen, A., Juutinen, S., Larmola, T., Hammar, T., et al. (2003a). Fluxes of methane, carbon dioxide and nitrous oxide in boreal lakes and potential anthropogenic effects on the aquatic greenhouse gas emissions. *Chemosphere* 52, 609–621. doi:10.1016/S0045-6535(03)00243-1

Huttunen, J. T., Juutinen, S., Alm, J., Larmola, T., Hammar, T., Silvola, J., et al. (2003b). Nitrous oxide flux to the atmosphere from the littoral zone of a boreal lake. *J. Geophys. Res.* 108, 4421. doi:10.1029/2002JD002989

Jahr, S. S. (2021). *A study of methane emissions from lakes in the 100 lakes survey*.

Jones, R. I., and Grey, J. (2011). Biogenic methane in freshwater food webs. *Freshw. Biol.* 56, 213–229. doi:10.1111/j.1365-2427.2010.02494.x

Jones, S. E., Zwart, J. A., Kelly, P. T., and Solomon, C. T. (2018). Hydrologic setting constrains lake heterotrophy and terrestrial carbon fate. *Limnol. Oceanogr. Lett.* 3, 256–264. doi:10.1002/lol2.10054

Juutinen, S., Alm, J., Larmola, T., Huttunen, J. T., Morero, M., Martikainen, P. J., et al. (2003). Major implication of the littoral zone for methane release from boreal lakes. *Glob. Biogeochem. Cycles* 17, 2105. doi:10.1029/2003GB002105

Juutinen, S., Rantakari, M., Kortelainen, P., Huttunen, J. T., Larmola, T., Alm, J., et al. (2009). Methane dynamics in different boreal lake types. *Biogeosciences* 6, 209–223. doi:10.5194/bg-6-209-2009

Kankaala, P., Huotari, J., Peltomaa, E., Saloranta, T., and Ojala, A. (2006). Methanotrophic activity in relation to methane efflux and total heterotrophic bacterial production in a stratified, humic, boreal lake. *Limnol. Oceanogr.* 51, 1195–1204. doi:10.4319/lo.2006.51.2.1195

Kankaala, P., Huotari, J., Tulonen, T., and Ojala, A. (2013). Lake-size dependent physical forcing drives carbon dioxide and methane effluxes from lakes in a boreal landscape. *Limnol. Oceanogr.* 58, 1915–1930. doi:10.4319/lo.2013.58.6.1915

Karlsson, J., Byström, P., Ask, J., Ask, P., Persson, L., and Jansson, M. (2009). Light limitation of nutrient-poor lake ecosystems. *Nature* 460, 506–509. doi:10.1038/nature08179

Khalili, M. I., Temnerud, J., Fröberg, M., Karltun, E., and Weyhenmeyer, G. A. (2010). Nitrogen and carbon interactions between boreal soils and lakes. *Glob. Biogeochem. Cycles* 24, 3668. doi:10.1029/2009GB003668

King, G. (1986). How not to lie with statistics: Avoiding common mistakes in quantitative political science. *Am. J. Political Sci.* 30, 666–687. doi:10.2307/2111095

Kortelainen, P., Larmola, T., Rantakari, M., Juutinen, S., Alm, J., and Martikainen, P. J. (2020). Lakes as nitrous oxide sources in the boreal landscape. *Glob. Change Biol.* 26, 1432–1445. doi:10.1111/gcb.14928

Kortelainen, P., Rantakari, M., Huttunen, J. T., Mattsson, T., Alm, J., Juutinen, S., et al. (2006). Sediment respiration and lake trophic state are important predictors of large CO2 evasion from small boreal lakes. *Glob. Chang. Biol.* 12, 1554–1567. doi:10.1111/j.1365-2486.2006.01167.x

Kortelainen, P., Rantakari, M., Pajunen, H., Huttunen, J. T., Mattsson, T., Juutinen, S., et al. (2013). Carbon evasion/accumulation ratio in boreal lakes is linked to nitrogen. *Glob. Biogeochem. Cycles* 27, 363–374. doi:10.1002/gbc.20036

Larsen, S., Andersen, T., and Hessen, D. O. (2011a). Predicting organic carbon in lakes from climate drivers and catchment properties. *Glob. Biogeochem. Cycles* 25, 3908. doi:10.1029/2010GB003908

Larsen, S., Andersen, T., and Hessen, D. O. (2011b). The pCO2 in boreal lakes: Organic carbon as a universal predictor? *Glob. Biogeochem. Cycles* 25, 3864. doi:10.1029/2010GB003864

Lau, D. C. P., Jonsson, A., Isles, P. D. F., Creed, I. F., and Bergström, A. (2021). Lowered nutritional quality of plankton caused by global environmental changes. *Glob. Chang. Biol.* 27, 6294–6306. doi:10.1111/gcb.15887

Li, M., Peng, C., Zhu, Q., Zhou, X., Yang, G., Song, X., et al. (2020). The significant contribution of lake depth in regulating global lake diffusive methane emissions. *Water Res.* 172, 115465. doi:10.1016/j.watres.2020.115465

Lie, R. O. (2021). *Effect of catchment characteristics on biodegradability of dissolved natural organic matter*.

Lindström, E. S., Agterveld, K.-V., and Zwart, G. (2005). Distribution of typical freshwater bacterial groups is associated with pH, temperature, and lake water retention time. *Appl. Environ. Microbiol.* 71, 8201–8206. doi:10.1128/AEM.71.12.8201-8206.2005

Liu, W., Wang, Z., Zhang, Q., Cheng, X., Lu, J., and Liu, G. (2015). Sediment denitrification and nitrous oxide production in Chinese plateau lakes with varying watershed land uses. *Biogeochemistry* 123, 379–390. doi:10.1007/s10533-015-0072-9

López Bellido, J., Tulonen, T., Kankaala, P., and Ojala, A. (2013). Concentrations of CO2 and CH4 in water columns of two stratified boreal lakes during a year of atypical summer precipitation. *Biogeochemistry* 113, 613–627. doi:10.1007/s10533-012-9792-2

Marra, G., and Wood, S. N. (2011). Practical variable selection for generalized additive models. *Comput. Statistics Data Analysis* 55, 2372–2387. doi:10.1016/j.csda.2011.02.004

Mattsson, T., Kortelainen, P., and Räike, A. (2005). Export of DOM from boreal catchments: Impacts of land use cover and climate. *Biogeochemistry* 76, 373–394. doi:10.1007/s10533-005-6897-x

McCrackin, M. L., and Elser, J. J. (2010). Atmospheric nitrogen deposition influences denitrification and nitrous oxide production in lakes. *Ecology* 91, 528–539. doi:10.1890/08-2210.1

Monteith, D. T., Stoddard, J. L., Evans, C. D., de Wit, H. A., Forsius, M., Høgåsen, T., et al. (2007). Dissolved organic carbon trends resulting from changes in atmospheric deposition chemistry. *Nature* 450, 537–540. doi:10.1038/nature06316

Natchimuthu, S., Panneer Selvam, B., and Bastviken, D. (2014). Influence of weather variables on methane and carbon dioxide flux from a shallow pond. *Biogeochemistry* 119, 403–413. doi:10.1007/s10533-014-9976-z

Nydahl, A. C., Wallin, M. B., Tranvik, L. J., Hiller, C., Attermeyer, K., Garrison, J. A., et al. (2019). Colored organic matter increases CO2 in meso-eutrophic lake water through altered light climate and acidity. *Limnol. Oceanogr.* 64, 744–756. doi:10.1002/lno.11072

Nydahl, A. C., Wallin, M. B., Laudon, H., and Weyhenmeyer, G. A. (2020). Groundwater carbon within a boreal catchment: Spatiotemporal variability of a hidden aquatic carbon pool. *J. Geophys. Res. Biogeosci.* 125, e2019JG005244. doi:10.1029/2019JG005244

Oksanen, J., Blanchet, F. G., Kindt, R., Legendre, P., Minchin, P. R., O'hara, R., et al. (2013). *Package 'vegan.'* Community ecology package. *version* 2, 1–295.

Öquist, M. G., Wallin, M., Seibert, J., Bishop, K., and Laudon, H. (2009). Dissolved inorganic carbon export across the soil/stream interface and its fate in a boreal headwater stream. *Environ. Sci. Technol.* 43, 7364–7369. doi:10.1021/es900416h

Palviainen, M., Laurén, A., Launiainen, S., and Piirainen, S. (2016). Predicting the export and concentrations of organic carbon, nitrogen and phosphorus in boreal lakes by catchment characteristics and land use: A practical approach. *Ambio* 45, 933–945. doi:10.1007/s13280-016-0789-2

Pellerin, B. A., Kaushal, S. S., and McDowell, W. H. (2006). Does anthropogenic nitrogen enrichment increase organic nitrogen concentrations in runoff from forested and human-dominated watersheds? *Ecosystems* 9, 852–864. doi:10.1007/s10021-006-0076-3

Peña Sanchez, G. A., Mayer, B., Wunderlich, A., Rein, A., and Einsiedl, F. (2022). Analysing seasonal variations of methane oxidation processes coupled with denitrification in a stratified lake using stable isotopes and numerical modeling. *Geochimica Cosmochimica Acta* 323, 242–257. doi:10.1016/j.gca.2022.01.022

Peterson, R. A. (2021). Finding optimal normalizing transformations via bestNormalize. *R J.* 13, 310–329. doi:10.32614/RJ-2021-041

Pregitzer, K. S., Burton, A. J., Zak, D. R., and Talhelm, A. F. (2008). Simulated chronic nitrogen deposition increases carbon storage in Northern Temperate forests. *Glob. Chang. Biol.* 14, 142–153. doi:10.1111/j.1365-2486.2007.01465.x

R Core Team (2021). *R: A language and environment for statistical computing*. Vienna, Austria: R Foundation for Statistical Computing. Available at: https://www.R-project.org/.

Rantakari, M., and Kortelainen, P. (2005). Interannual variation and climatic regulation of the CO2 emission from large boreal lakes. *Glob. Chang. Biol.* 11, 1368–1380. doi:10.1111/j.1365-2486.2005.00982.x

Rasilo, T., Prairie, Y. T., and del Giorgio, P. A. (2015). Large-scale patterns in summer diffusive CH4 fluxes across boreal lakes, and contribution to diffusive C emissions. *Glob. Change Biol.* 21, 1124–1139. doi:10.1111/gcb.12741

Ribic, C. A., Sheavly, S. B., Rugg, D. J., and Erdmann, E. S. (2010). Trends and drivers of marine debris on the Atlantic coast of the United States 1997–2007. *Mar. Pollut. Bull.* 60, 1231–1242. doi:10.1016/j.marpolbul.2010.03.021

Roland, F. A. E., Darchambeau, F., Morana, C., and Borges, A. V. (2017). Nitrous oxide and methane seasonal variability in the epilimnion of a large tropical meromictic lake (Lake Kivu, East-Africa). *Aquat. Sci.* 79, 209–218. doi:10.1007/s00027-016-0491-2

Ruckstuhl, K. E., Johnson, E. A., and Miyanishi, K. (2008). Introduction. The boreal forest and global change. *Phil. Trans. R. Soc. B* 363, 2243–2247. doi:10.1098/rstb.2007.2196

Sander, R. (2015). Compilation of Henry's law constants (version 4.0) for water as solvent. *Atmos. Chem. Phys.* 15, 4399–4981. doi:10.5194/acp-15-4399-2015

Schindler, D. W. (1998). A Dim Future for Boreal Waters and Landscapes: Cumulative effects of climatic warming, stratospheric ozone depletion, acid precipitation, and other human activities. *BioScience* 48, 157–164. doi:10.2307/1313261

Škerlep, M., Steiner, E., Axelsson, A.-L., and Kritzberg, E. S. (2020). Afforestation driving long-term surface water browning. *Glob. Change Biol.* 26, 1390–1399. doi:10.1111/gcb.14891

Sobek, S., Algesten, G., Bergström, A.-K., Jansson, M., and Tranvik, L. J. (2003). The catchment and climate regulation of pCO2 in boreal lakes. *Glob. Chang. Biol.* 9, 630–641. doi:10.1046/j.1365-2486.2003.00619.x

Solomon, C. T., Jones, S. E., Weidel, B. C., Buffam, I., Fork, M. L., Karlsson, J., et al. (2015). Ecosystem consequences of changing inputs of terrestrial dissolved organic matter to lakes: Current knowledge and future challenges. *Ecosystems* 18, 376–389. doi:10.1007/s10021-015-9848-y

Tadonléké, R. D., Marty, J., and Planas, D. (2012). Assessing factors underlying variation of CO2 emissions in boreal lakes vs. reservoirs. *FEMS Microbiol. Ecol.* 79, 282–297. doi:10.1111/j.1574-6941.2011.01218.x

Thrane, J.-E., Hessen, D. O., and Andersen, T. (2014). The absorption of light in lakes: Negative impact of dissolved organic carbon on primary productivity. *Ecosystems* 17, 1040–1052. doi:10.1007/s10021-014-9776-2

Tranvik, L. J. (1998). "Degradation of dissolved organic matter in humic waters by bacteria," in *Aquatic humic substances: Ecology and biogeochemistry*. Editors D. O. Hessen and L. J. Tranvik (Berlin, Heidelberg: Springer Berlin Heidelberg), 259–283. doi:10.1007/978-3-662-03736-2_11

Tranvik, L. J., Downing, J. A., Cotner, J. B., Loiselle, S. A., Striegl, R. G., Ballatore, T. J., et al. (2009). Lakes and reservoirs as regulators of carbon cycling and climate. *Limnol. Oceanogr.* 54, 2298–2314. doi:10.4319/lo.2009.54.6_part_2.2298

Trogler, W. C. (1999). Physical properties and mechanisms of formation of nitrous oxide. *Coord. Chem. Rev.* 187, 303–327. doi:10.1016/S0010-8545(98)00254-9

Vachon, D., Prairie, Y. T., Guillemette, F., and del Giorgio, P. A. (2017). Modeling allochthonous dissolved organic carbon mineralization under variable hydrologic regimes in boreal lakes. *Ecosystems* 20, 781–795. doi:10.1007/s10021-016-0057-0

Whitfield, C. J., Aherne, J., and Baulch, H. M. (2011). Controls on greenhouse gas concentrations in polymictic headwater lakes in Ireland. *Sci. Total Environ.* 410–411, 217–225. doi:10.1016/j.scitotenv.2011.09.045

Wood, S., and Wood, M. S. (2015). *Package 'mgcv.' R package version 1*, 729.

Xenopoulos, M. A., Lodge, D. M., Frentress, J., Kreps, T. A., Bridgham, S. D., Grossman, E., et al. (2003). Regional comparisons of watershed determinants of dissolved organic carbon in temperate lakes from the Upper Great Lakes region and selected regions globally. *Limnol. Oceanogr.* 48, 2321–2334. doi:10.4319/lo.2003.48.6.2321

Yang, H., Andersen, T., Dörsch, P., Tominaga, K., Thrane, J.-E., and Hessen, D. O. (2015). Greenhouse gas metabolism in Nordic boreal lakes. *Biogeochemistry* 126, 211–225. doi:10.1007/s10533-015-0154-8

frontiers | Frontiers in Environmental Science

TYPE Original Research
PUBLISHED 13 September 2022
DOI 10.3389/fenvs.2022.948529

Check for updates

OPEN ACCESS

EDITED BY
Huacheng Xu,
Chinese Academy of Sciences (CAS), China

REVIEWED BY
Wenxin Zhang,
Lund University, Sweden
Liudmila Shirokova,
UMR5563 Géosciences Environnement Toulouse (GET), France

*CORRESPONDENCE
George W. Kling,
gwk@umich.edu

SPECIALTY SECTION
This article was submitted to Biogeochemical Dynamics, a section of the journal Frontiers in Environmental Science

RECEIVED 20 May 2022
ACCEPTED 01 August 2022
PUBLISHED 13 September 2022

CITATION
Eugster W, DelSontro T, Laundre JA, Dobkowski J, Shaver GR and Kling GW (2022), Effects of long-term climate trends on the methane and CO_2 exchange processes of Toolik Lake, Alaska.
Front. Environ. Sci. 10:948529.
doi: 10.3389/fenvs.2022.948529

COPYRIGHT
© 2022 Eugster, DelSontro, Laundre, Dobkowski, Shaver and Kling. This is an open-access article distributed under the terms of the Creative Commons Attribution License (CC BY). The use, distribution or reproduction in other forums is permitted, provided the original author(s) and the copyright owner(s) are credited and that the original publication in this journal is cited, in accordance with accepted academic practice. No use, distribution or reproduction is permitted which does not comply with these terms.

Effects of long-term climate trends on the methane and CO_2 exchange processes of Toolik Lake, Alaska

Werner Eugster[1], Tonya DelSontro[2], James A. Laundre[3], Jason Dobkowski[4], Gaius R. Shaver[3] and George W. Kling[4]*

[1]ETH Zurich, Department of Environmental Systems Science, Zurich, Switzerland, [2]Department of Earth and Environmental Sciences, University of Waterloo, Waterloo, ON, Canada, [3]The Ecosystems Center, Marine Biological Lab, Woods Hole, MA, United States, [4]Department of Ecology and Evolutionary Biology, University of Michigan, Ann Arbor, MI, United States

Methane and carbon dioxide effluxes from aquatic systems in the Arctic will affect and likely amplify global change. As permafrost thaws in a warming world, more dissolved organic carbon (DOC) and greenhouse gases are produced and move from soils to surface waters where the DOC can be oxidized to CO_2 and also released to the atmosphere. Our main study objective is to measure the release of carbon to the atmosphere via effluxes of methane (CH_4) and carbon dioxide (CO_2) from Toolik Lake, a deep, dimictic, low-arctic lake in northern Alaska. By combining direct eddy covariance flux measurements with continuous gas pressure measurements in the lake surface waters, we quantified the k_{600} piston velocity that controls gas flux across the air–water interface. Our measured k values for CH_4 and CO_2 were substantially above predictions from several models at low to moderate wind speeds, and only converged on model predictions at the highest wind speeds. We attribute this higher flux at low wind speeds to effects on water-side turbulence resulting from how the surrounding tundra vegetation and topography increase atmospheric turbulence considerably in this lake, above the level observed over large ocean surfaces. We combine this process-level understanding of gas exchange with the trends of a climate-relevant long-term (30 + years) meteorological data set at Toolik Lake to examine short-term variations (2015 ice-free season) and interannual variability (2010–2015 ice-free seasons) of CH_4 and CO_2 fluxes. We argue that the biological processing of DOC substrate that becomes available for decomposition as the tundra soil warms is important for understanding future trends in aquatic gas fluxes, whereas the variability and long-term trends of the physical and meteorological variables primarily affect the timing of when higher or lower than average fluxes are observed. We see no evidence suggesting that a tipping point will be reached soon to change the status of the aquatic system from gas source to sink. We estimate that changes in CH_4 and CO_2 fluxes will be constrained with a range of +30% and –10% of their current values over the next 30 years.

KEYWORDS

Toolik Lake, long-term ecological research, LTER, methane flux, carbon dioxide flux, piston velocity, arctic trends, quantile regression

1 Introduction

A vast reservoir of organic matter is preserved in Arctic regions in permafrost, the permanently frozen ground at high latitudes (Schuur et al., 2015). Thawing of permafrost with climate warming exposes organic matter to decomposition, a process which has become a major concern as a positive and undesirable feedback of the Arctic to climate change (Tan and Zhuang, 2015; Elder et al., 2018; Elder et al., 2019; Elder et al., 2020). Greenhouse gases (GHG, here the sum of CO_2 and CH_4) produced by this terrestrial decomposition may be released directly to the atmosphere or they may be transferred by movement of groundwater or soil water into lakes and streams that drain the terrestrial landscape (e.g., Kling et al., 1991; Cole et al., 1994). In addition, newly-thawed dissolved and particulate organic carbon (C) on land can be transferred to surface waters where the C may be oxidized to CO_2 by microbes and sunlight (e.g., Cory et al., 2013; Cory et al., 2014). Open water bodies in the Arctic, which cover up to 48% of the earth surface in some regions of Alaska (Riordan et al., 2006; McGuire et al., 2009) and about 12%–14% of the surface area of the Alaskan North Slope, thus play an important role in greenhouse gas release to the atmosphere (Kling et al., 1991; Kling et al., 1992; McGuire et al., 2009; Cory et al., 2014; Garies and Lesack, 2020).

For over 110 years (see Krogh, 1910) the characteristics and controls of gas exchange across air-water interfaces have been examined, as described in several comprehensive studies and reviews (Brutsaert and Jirka, 1984; Liss and Merlivat, 1986; Jahne and Monahan, 1995; Wanninkhof et al., 2009; Garbe et al., 2014). The fundamental variable controlling gas flux is the gas transfer velocity (piston velocity) typically represented as k in a basic equation of gas flux (F) where $F = k(Cw - Co)$; Cw is the gas concentration beneath the water surface and Co, is the gas concentration at the water surface (modified for solubility or chemical enhancement, e.g., Wanninkhof et al., 2009). Depending on gas solubility and chemical enhancement, the physical-chemical controls on k have been studied from the water-side (less soluble and unreactive gases, e.g., Liss and Slater 1974) or from the air-side (more soluble and reactive gases, e.g., Johnson et al., 2011; Garbe et al., 2014). For gases of intermediate solubility or for processes that extend across the air-water interface (e.g., surface films, Yang et al., 2021, or the effects of wave breaking and bubble clouds, e.g., Deike and Melville, 2018), both air-side and water-side fluid dynamics may be important.

Formulations of k in gas flux models have over time increasingly recognized the role of turbulent kinetic energy (TKE), buoyancy flux (β), and energy dissipation (ε), especially in the hydrodynamic processes of surface waters, and this has improved model fits to empirical data (e.g., MacIntyre et al., 2001; Fredriksson et al., 2016; Esters et al., 2017). However, many studies still find deviations between model predictions and empirically-measured gas transfer velocities (e.g., Zappa et al., 2007; Heikensen et al., 2014), including our results in this paper. These deviations seem especially large at low wind speeds and in lakes (e.g., Read et al., 2012), and in a recent, comprehensive study Klaus and Vachon (2020) showed that existing models that predict k do better than using a mean value of k in only 2%–39% of lakes, and they could not explain what conditions led to the poor predictions of models.

Eugster et al. (2020a) examined the variability in gas fluxes from Toolik Lake, Alaska, using data from 2010–2015 and showed greater interannual than diel variation in CO_2 and CH_4 fluxes. In this paper, we focus on the gas exchange processes between lake surface waters and the near-surface atmosphere measured in detail during the 2015 ice-free season of Toolik Lake. We specifically examine the relationships of environmental conditions and drivers of gas transfer velocities computed with eddy covariance, and suggest that the enhancement of k compared to a range of model predictions, especially at low wind speeds in this small lake (1.5 km^2 area), are related to the characteristics and dissipation of atmospheric turbulence generated over land as it reaches the lake. We combine the information on environmental controls with a detailed trend analysis of potential driver variables, including rainfall and soil temperature that could influence the amount of C transferred from land to surface waters, that were monitored during the past (up to 33 years) by the Arctic Long-Term Ecological Research project (ARC LTER), also based at Toolik Lake (Hobbie and Kling, 2014). By projecting the past 30+ year trends into the future, and combining this information with the full 2010–2015 flux dataset (see Eugster et al., 2020a), we consider how CO_2 and CH_4 fluxes from deep lakes like Toolik might evolve over the next 30 years, from 2020–2050.

The paper is structured as follows: 1) methods and results of the gas flux measurements, 2) relationships of gas fluxes to environmental variables, 3) controls on gas fluxes, and 4) long-term trends of driver variables and expected trends in gas fluxes.

2 Materials and methods

2.1 Study site

Measurements were made on Toolik Lake (68°37.830′ N, 149°36.366′ W, WGS84 datum) at 719 m asl, and in the Toolik Field Station (TFS) environment. Toolik Lake is a relatively deep

glacial lake (maximum depth ≈26 m) located on the tundra north of the Alaskan Brooks Range with a surface area of 1.5 km^2 (Hobbie and Kling, 2014).

Six ice-free seasons (2010–2015) were covered with eddy covariance flux measurements (Section 2.2), the results of which were presented by Eugster et al. (2020a). In addition, in 2015 an equilibrator system with a dissolved gas extraction unit was used to continuously determine the gas mixing ratios in the Toolik lake surface waters (Section 2.3). And finally, long-term observations were made as a component of the ARC LTER project since the late 1980s. The location of the TFS meteorological station (68°37.698′ N, 149°35.759′ W, 722 m asl) is ~500 m southeast of the EC flux measurements.

Toolik lake is ice covered during 9–10 months of the year, with CO_2 and CH_4 accumulating under the ice (Kling et al., 1992), an aspect not covered here. Ice on and off dates are typically from mid-June to early July, and ice-on starts in the time period of end of August to late September. Because the Sun does not set at this northern latitude from 23 May to 19 July, there is no dark period of the day and "night" with darkness is not observed before August.

2.2 Eddy covariance flux instrumentation

The instrumentation and methods used in this study were presented in detail in Eugster et al. (2020a). Here we briefly summarize the key aspects of the EC measurements. Flux measurements were made with a three-dimensional ultrasonic anemometer-thermometer (CSAT3, Campbell Scientific, Logan, UT, United States) in combination with a closed-path integrated off-axis cavity output spectrometer (ICOS) for CH_4 (FMA, Los Gatos Research, Inc., San Jose, CA, United States) and a nondispersive infra-red gas analyzer for CO_2 and H_2O (Li-7000, Li-Cor Inc., Lincoln, NE, United States). Instruments were mounted on a floating platform (Supplementary Figure S1A) that was moored at approximately the same location every year ≈400 m from the nearest lake shore. Depth of the lake at this location was ≈12 m. The gap-filling of missing data up to four hours (up to 8 hours for 3-hourly resolved variables) was done by linear interpolation. For longer gaps the following approach was used: 1) the median diel cycle of all available years during the time-of-day of the gap, including a 1-day margin on both sides, was used as a reference; 2) then the beginning of the gap-filling time series was connected to the endpoint of the available data using an offset correction; and 3) finally, the endpoint of the gap was connected to the first valid data point after the gap *via* linear scaling. In addition, the pyranometer data were offset-corrected to obtain a mean 0 W m^{-2} nocturnal flux (this corrects for the offset associated with the instrument temperature of the pyranometer), after which all nocturnal values <0 W m^{-2} were set to zero. The main precipitation time series only captured liquid precipitation, hence frozen precipitation in summer (which tends to be a small component) was neglected until a second, heated rain gauge was installed on 19 June 2004. There was very good agreement of the rainfall amounts measured by both gauges [major axis regression slope of 0.0998%, 95% CI 0.995–1.001; Legendre and Legendre (1998)]. Thus, for the analysis here, the gaps in the long-term precipitation time series were filled by inserting the measurements from the newer rain gauge, with no attempt to fill the remaining (mainly winter) gaps. Thus, in the case of precipitation, our analysis is biased towards the warm season with predominantly liquid precipitation. For details on flux calculation, gap-filling of missing data, and the flux footprint of the EC measurements the reader is referred to Eugster et al. (2020a).

2.3 Equilibrator system with dissolved gas extraction unit

During the 2015 ice-free season an equilibrator system with automatic dissolved gas extraction unit was deployed on the EC float (Supplementary Figure S1A). The device used was a modified version of a prototype that Los Gatos Research, Inc., produced for us in 2012–2013, from which the commercial LGR Dissolved Gas Extraction Unit (https://www.lgrinc.com/documents/LGR_Dissolved%20Gas%20Extraction%20System.pdf) evolved. The basic principle (Supplementary Figure S2) is to pull water through a cylindrical Liqui-Cel device containing a gas-permeable membrane separating the water flow from the gas flow. The under-pressure generated by pulling water through the Liqui-Cel device increases the efficiency with which dissolved gases pass the membrane and are incorporated into the air strip-flow section of the device. The strip gas containing the gases extracted from the water are then analyzed by CH_4 and CO_2 analyzers (Supplementary Figures S1,S2), and the equilibrium gas mixing ratio (mol fraction or parts per million by volume) is then calculated using the flow rates of all components of the system, the initial gas mixing ratios in the air strip-flow, and the gas extraction efficiency of the Liqui-Cel membrane.

However, we were unable to achieve the expected accuracy of the equilibration mixing ratios of CO_2 and CH_4 in this configuration because we found no simple way to accurately determine the efficiency of the Liqui-Cel membrane. The reason might have been that Toolik lake has a substantial load of particulate organic matter (POM) in the water (DelSontro, 2011) and the main water filter system was unable to remove 100% of the POM before the water stream entered the Liqui-Cel device. We thus expected that the efficiency of the Liqui-Cel device was a non-trivial function of 1) its age, 2) the elapsed time since replacement of the main water filter, and 3) the POM load in the sample water stream. Thus, we remodeled our prototype to operate in conventional closed-loop equilibration mode

(Supplementary Figure S2 for the configuration used in this study).

Equilibrium gas mixing ratios were obtained by scaling the raw mixing ratio measurements obtained from the equilibrator device with the net difference between the gas flow from the Liqui-Cel membrane to the analyzers and the strip gas flow measured with a gas flow meter,

$$c_{eq} = \frac{c_{measured} \cdot F_{gas} - F_{stripgas} \cdot c_{ambient}}{F_{gas} - F_{stripgas}} \quad (1)$$

with ambient mixing ratio $c_{ambient}$ of 390 ppmv (parts per million by volume) for CO_2 and 1.85 ppmv for CH_4. The gas flow to the analyzer, Fgas, was $\approx 5.5 \cdot 10^{-4}$ m^3 s^{-1} (a 408 cm^3 sample cell refreshed every 7.4 s). The strip gas flow Fstripgas was continuously measured by the dissolved gas extraction unit (Supplementary Figures S1B,C). Due to the high variability of the raw mixing ratio measurements, a local polynomial regression smoothing (loess function in R) was applied in the computation of $c_{measured}$ to obtain the final equilibrium mixing ratio c_{eq}. Supplementary Figure S3 shows the data used for quality checking this procedure.

2.4 Long-term monitoring and trend analysis

In 1988 long-term meteorological measurements started, and the variables used in this study are shown in Supplementary Table S1. From the available variables, air temperature, barometric pressure, short-wave incoming radiation, lake depth, lake temperature, precipitation, relative humidity (RH), soil temperatures, and wind speed were used for trend analysis. For pre-1996 temperature and RH at 5 m height, we gap-filled from a local station when available, and to correct a degraded RH sensor an offset-correction was applied that sets the moving 7-days maximum to 100% and trims data to 100%. Vapor pressure deficit (VPD) was calculated from the air temperature Ta (in °C), relative humidity RH (in %) and barometric pressure Pa (in hPa) using the procedure by Buck (1981) to yield

$$VPD = \left(1 - \frac{RH}{100\%}\right) \cdot 6.1121 \cdot e^{\frac{17.502 \cdot Ta}{Ta} + 240.97} \cdot \left(1.0007 + 3.46 \cdot 10^{-6} \cdot P_a\right) \quad (2)$$

Snow depth and wind direction were not included in the trend analysis. Snow depth is only measured since 2014 (Supplementary Table S1) and moreover during the ice-free season an extensive snow cover is missing and thus it is not expected that this variable strongly influences summertime CO_2 and CH_4 fluxes. Wind direction also was excluded from the trend analysis because small trends in wind direction are not expected to influence lake–atmosphere GHG effluxes substantially.

For the trend analyses we used the Theil-Sen median slope estimator (Sen, 1968; Akritas et al., 1995) that takes account for the fact that time-series do not meet the model assumptions of ordinary least-square regression (the *x*-axis is not a random variable, and values are equally spaced in the time-series and do not follow a random normal distribution). This trend slope estimator was then combined with a quantile regression approach (Easterling, 1969; Lejeune and Sarda, 1988; Patel, 2021); within each year the quantiles of the available measurements are determined for each percentile of the empirical distribution for that year. Then the Theil-Sen median trend slope fit was calculated for each new time-series of the quantiles in each percentile of each year. This approach allows identification of trends that are not uniform across the entire gradient of values observed in a given time-series. To estimate the long-term overall trend of each monitored variable we then used only the percentiles with significant trends to obtain the median change per decade and its 95% confidence interval.

2.5 Statistical analyses

Statistical analyses were carried out with R version 4.1.2 (R Core Team, 2014). To compute the Theil-Sen median trend slope the trend package (Pohlert, 2020) was used, which provides the sens.slope function (Sen, 1968). Significance of the slope was determined using the nonparametric Mann-Kendall test provided by the mk.test function. Major axis (orthogonal) regression was computed using the lmodel2 function of the lmodel2 package (Legendre and Legendre, 1998).

3 Results

Six years of eddy covariance flux measurements of CH_4 and CO_2 during the ice-free season of Toolik lake (Eugster et al., 2020a) allow us to link interannual variability to trend estimates from the long-term ancillary monitoring data to estimate future development of these two most important GHG fluxes (see Section 4.2). The focus here is on the detailed process-level investigations from the 2015 ice-free season during which continuous dissolved gas mixing ratio measurements at fine temporal resolution were carried out, allowing us to assess the gas exchange processes and their short-term responses to variability in atmospheric meteorological and lake water conditions. These measured values allow for increased detail to be extracted from the record instead of using modeled GHG fluxes.

Equilibrium CO_2 mixing ratios of the Toolik lake surface water fluctuated around atmospheric mixing ratios throughout the season (Figure 1A), typically following a 12-h delay behind barometric pressure changes, whereas the water was supersaturated with CH_4 at all times (Figure 1B). The range

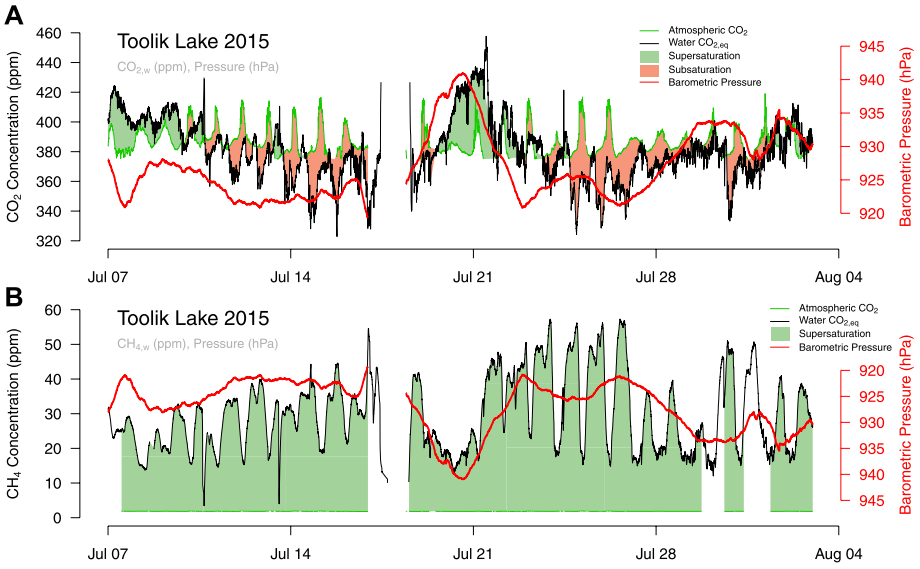


FIGURE 1
Timeseries of **(A)** CO_2 concentrations and **(B)** CH_4 concentrations in the atmosphere (green lines) and the surface water (black lines) during the ice-free seasons 2015. Supersaturation of the surface water is shown with a green area between the two concentrations, and subsaturation is shown with a red area. In addition, barometric pressure (bold red lines) are shown; note axes at right, and the inversed barometric pressure axis in **(B)**.

of equilibrium mixing ratios in the surface waters was much broader than in the atmosphere (Figure 2C), and the distribution of values was close to a normal distribution. In contrast, atmospheric mixing ratios followed a gamma distribution (Figure 2C) with a clear lower daytime boundary around 370 ppmv (Figure 2C), and a long tail towards higher mixing ratios at night. The CO_2 fluxes show a pronounced diel cycle (Figure 2B), but the timing is not synchronous with the diel cycle of the CO_2 mixing ratio (Figure 2A) or the cycle of primary production (driven by light; Miller et al., 1986). Above-average equilibrium CO_2 mixing ratios in the surface waters were observed during the period 0200–1600 h Alaska Daylight Time (AKDT) (Figure 2A), when substantially increased CO_2 fluxes were observed from 0000 to 0600 h AKDT (local midnight is at 0200 h AKDT), thus during the period of lowest net radiation input. Note that the Sun does not set during most of the summer season, and thus "night" does not imply complete darkness at Toolik Lake.

To examine the potential role of CO_2 uptake by photosynthesis, we measured chlorophyll *a* (an estimate of algal biomass), water column primary production, and concentrations of CO_2 (CO_2 measured with a syringe equilibration method, see Kling et al., 2000) at different depths in Toolik Lake. In 2015 at all depths measured near the surface (0.1, 1, 3 m) the CO_2 concentrations tended to increase as chlorophyll *a* or primary production increased (Supplementary Figure S4), which is the opposite of what we would expect if CO_2 drawdown from photosynthesis was important in determining surface water gas concentrations. Benthic fluxes of CO_2 or CH_4 were not measured in this study, in part because during the ice-free season this deep lake is stratified (Supplementary Figure S5) and any benthic flux would be essentially trapped in the hypolimnion during our period of measurements.

Dissolved CH_4 in Toolik Lake was supersaturated at all times (Figures 1B, 3C) with 10–58 ppmv higher equilibrium mixing ratios in surface waters than what was observed in the atmosphere. The diel cycle of atmospheric CH_4 mixing ratio (Figure 3A) almost mirrors the diel cycle of CO_2 flux (Figure 2B) with minimum equilibrium CH_4 mixing ratios in the surface waters from 0000 to 0600 h. CH_4 fluxes where slightly higher in the afternoon than in the early morning (Figure 3B).

3.1 Principal components of the drivers of CO_2 fluxes

A principal component analysis (PCA) of CO_2 flux measured during 2015 over Toolik Lake combined the potential driving variables at the same temporal resolution as CO_2 fluxes. This analysis includes meteorological variables, eddy flux variables, and temperature and gas mixing ratios in the water, including temperature of the upper mixing layer in the lake (0–4 m depth) and temperature near or below the typical summer thermocline (5 m depth). If arrows are shown perpendicular to each other, the variables are independent (uncorrelated) in the selected PCA

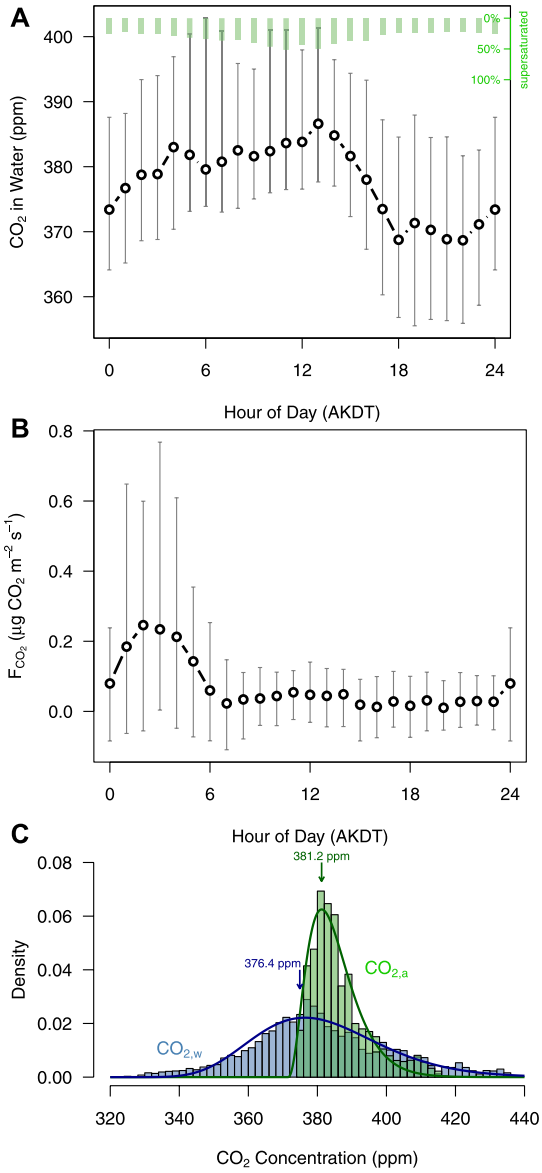


FIGURE 2
Diel cycles of **(A)** equilibrium surface water CO_2 concentration, **(B)** CO_2 flux across lake surface interface, and **(C)** the histograms of surface water ($CO_{2,w}$) and atmospheric ($CO_{2,a}$) concentrations. Arrows with values show the location of the maximum of the respective distribution. Error bars show the inter-quartal range (inner 50% of hourly data), and circles are hourly medians.

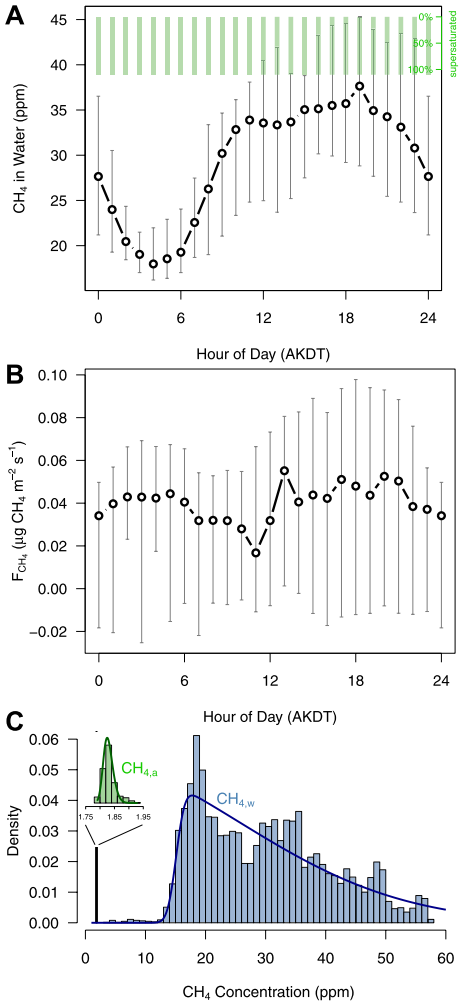


FIGURE 3
Diel cycles of **(A)** equilibrium surface water CH_4 concentration, **(B)** CH_4 flux across lake surface interface, and **(C)** the histograms of surface water ($CH_{4,w}$) and atmospheric ($CH_{4,a}$) concentrations. The distribution peaks are located at 1.825 and 17.8 ppm for $CH_{4,a}$ and $CH_{4,w}$, respectively. Error bars show the inter-quartal range (inner 50% of hourly data), and circles are hourly medians.

axes. Figure 4A shows CO_2 flux as the dominant variable in the second PCA axis. The two first PCA axes in Figure 4A explain a total of 59.5% of the variance in the selected dataset (42.4 % and 17.1%). F_{CO_2} increases as atmospheric CO_2 density (in mmol m^{-3}) increases, but is almost unrelated to CO_2 mixing ratio corrected for variability in density of air, which includes barometric pressure, air temperature, and atmospheric water vapor content. In contrast, the CO_2 mixing ratio gradient across the air-water interface, ΔCO_2 (in ppmv), has a weak, direct negative effect on F_{CO2}. The sign conventions of F_{CO2} and ΔCO_2 are that F_{CO2} is positive when gas evades from the water to the atmosphere, and ΔCO_2 is positive when the equilibration mixing ratio of CO_2 in the surface water is higher than the corresponding atmospheric value.

The transfer of CO_2-rich waters from depths lower in the epilimnion or the metalimnion toward the lake surface will enhance flux to the atmosphere. This is seen in Figure 4A as the first temperature below the typical thermocline (water temperature at 5 m depth) correlates positively with ΔCO_2,

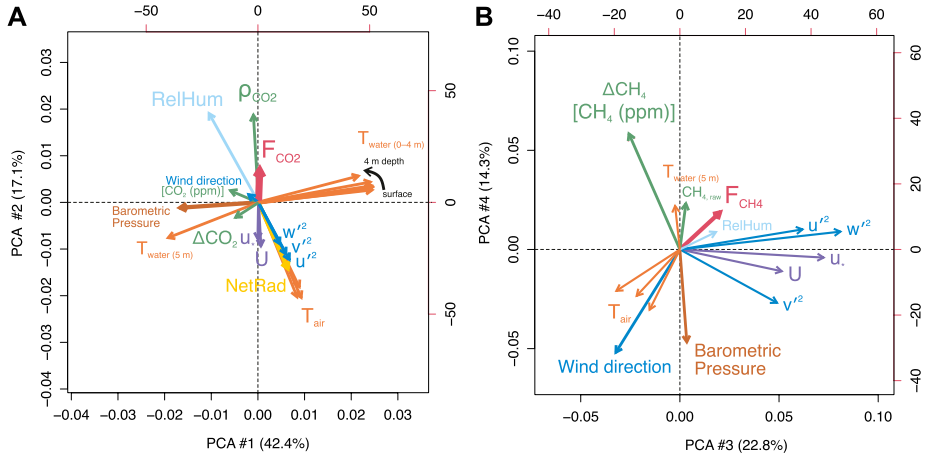


FIGURE 4
Principal component biplots of **(A)** CO_2 flux and **(B)** CH_4 flux with the most relevant potential driver variables. The CO_2 flux (F_{CO2}) already appears prominently in PCA #2, thus the first two PCAs are displayed in **(A)**, whereas the CH_4 flux (F_{CH4}) only appears in PCA #3, hence the third and fourth PCAs are shown in **(B)**, and the percentage of explained variance is modified by excluding PCAs #1 and #2 from the total in **(B)**. U is the mean horizontal wind speed, and u_* the friction velocity (downward-directed momentum flux); u'^2, v'^2, and w'^2 are the turbulent variances of horizontal along-wind, across wind, and vertical wind fluctuations, respectively. ρ_{CO2} is the CO_2 density in air (mmol m^{-3}).

whereas the epilimnion temperatures down to 4 m depth are negatively correlated with ΔCO_2. There is a slight but important increase in correlation between the epilimnion temperatures and F_{CO2} with increasing depth, indicating that temperature effects at the thermocline where CO_2 is typically higher (Supplementary Figure S5) are more important for F_{CO2} than is the surface temperature.

Increasing wind speed (U) and turbulence (u_*, u'^2, v'^2, w'^2) all reduce—not increase—F_{CO2}, almost in perfect agreement with net radiation, which represents atmospheric stability over the water surface. With increases in net radiation, wind speed and turbulence also increase. Atmospheric stability is negative ($z/L < 0$ and $Ri < 0$; e.g., Stull, 1988 and Supplementary Figure S6) most times of the day, except in the afternoon when it is in the near-neutral to slightly unstable range (ca. 1200–2100 h AKDT; data not shown). This indicates the important difference of a lake surface from a terrestrial surface, where over land atmospheric stability is negative when net radiation is high, but positive (stable) at night during times where the lake surface water temperatures are warmer than the terrestrial atmosphere. These conditions where a cooler atmosphere overlies a warmer surface water, leading to convection in the water, lead to the substantial peak in F_{CO2} at night between 0000 and 0600 h AKDT (Figure 2B), whereas barometric pressure has no influence on F_{CO2}. In summary, CO_2 effluxes from Toolik Lake are strongly governed by environmental drivers and thus are a key component in the second PCA axis, indicating a close link between F_{CO2} and the observed driver variables.

3.2 Principal components of the drivers of CH_4 fluxes

In contrast to CO_2 efflux from Toolik Lake, the CH_4 fluxes are much less coupled with the same driver variables (Figure 4B) that influence CO_2 evasion (Figure 4A). The first two PC axes (explaining 59.5% of the data subset used in this analysis) do not include F_{CH4}, thus we only inspect PC axes 3 and 4 which explain 22.8% and 14.3% of the remaining variance, respectively (Figure 4B). For F_{CH4} the wind direction has a strong influence with northerly directions (direction towards 360°) reducing F_{CH4}. This reflects the local daytime foreland–mountain wind system with northwesterly winds (from the coast to the Brooks range) typically prevailing from 0800 to 1400 h AKDT, and south-easterly dominance (winds from the mountains to the foreland of the North Slope) from 1500 to 0600 h AKDT.

However, in contrast to CO_2, equilibrium methane mixing ratios in the water are supersaturated at all times (Figure 3) by a median 27.3 ppmv (95% CI 13.2–51.3 ppmv), and thus both atmospheric CH_4 mixing ratio and the gradient measured acros s the water interface have almost no influence on F_{CH4} (the two arrow are almost at a right angle with F_{CH4} in Figure 4B, indicating statistical independence). However, not quite as expected, air temperature (represented by three redundant measurements) has a negative effect on F_{CH4} with warmer air temperatures reducing CH_4 evasion from the lake. According to Figure 4B warmer air temperatures are associated with lower wind speed and atmospheric turbulence. Also barometric pressure has an influence as high pressure tends to suppress

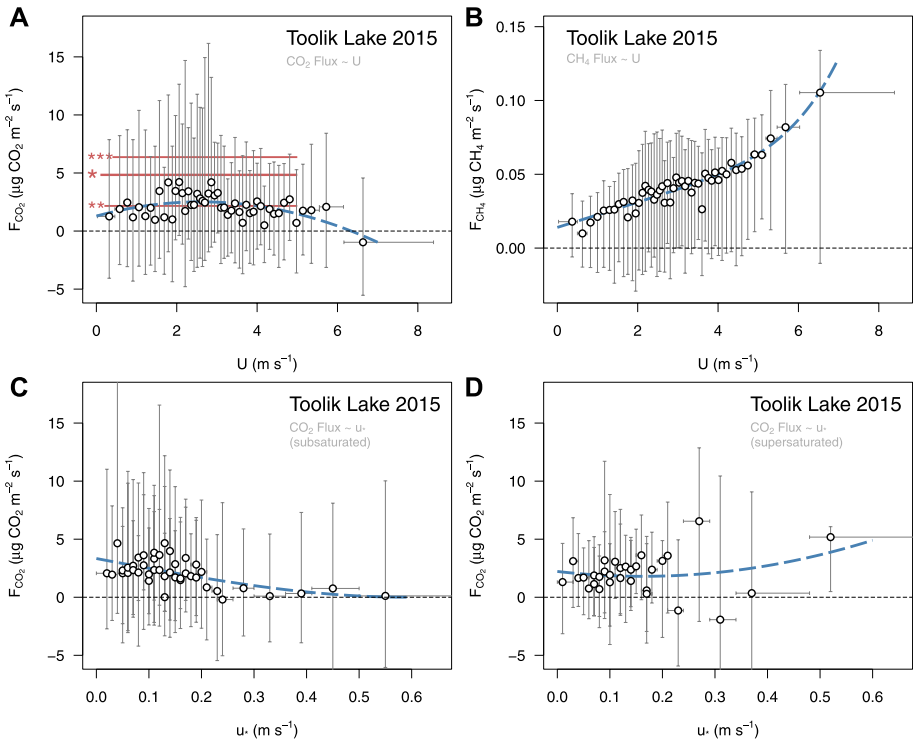


FIGURE 5
CO_2 flux **(A)** and CH_4 flux **(B)** at 5-min resolution as a function of mean horizontal wind speed, and CO_2 flux as a function of friction velocity u_* with subsaturated water **(C)** and supersaturated water **(D)**. The red line with in **(A)** shows the Eugster et al. (2003) average flux level determined over a few days (*), during stratified conditions (**), and during convective periods (***). Vertical error bars show the inter-quartile range of values (inner 50% of data), whereas the horizontal whiskers show the entire size of the associated bin.

F_{CH4}. Higher wind speeds and turbulence only have a weak enhancing effect on F_{CH4}, but it is clearly in contrast to F_{CO2} where the same variables seem to reduce F_{CO2}. Net radiation (and thus atmospheric stability) and water temperatures of the epilimnion were unrelated with F_{CH4}; only the upper metalimnion temperature (5 m depth) seems to positively influence F_{CH4}. In the biweekly sampled CH_4 mixing ratio profiles the peak CH_4 mixing ratio is often found at the depth of the thermocline (Supplementary Figure S5), whereas in contrast to the substantial CO_2 storage in the metalimnion there is no such CH_4 storage in deeper waters of Toolik lake.

The diel variation of CH_4 mixing ratio in the water is substantial (Figure 3A), with the lowest median of 18.0 ppmv at 0400 h AKDT and the highest median of 37.6 ppmv at 1900 h AKDT. This range, however, does not translate to a clear diel cycle in F_{CH4} (Figure 3B) because the water is strongly supersaturated with CH_4 at all times. Median fluxes during low and high water mixing ratio periods of the day are all on the order of 0.02–0.06 μg CH_4 m^{-2} s^{-1}, with no strong pattern in diel variation (Figure 3B).

3.3 Flux–gradient relationships across the lake surface interface

The CO_2 efflux from Toolik Lake is almost insensitive to mean horizontal wind speed (U) (see also Zappa et al., 2007) (Figure 5A; all regression fits to Toolik Lake data are given in Supplementary Table S2). It even appears that the highest observed wind speeds in 2015 actually reduced the CO_2 flux slightly (Figure 5A). If the data are analyzed separately for conditions with subsaturated (Figure 5C) vs. supersaturated (Figure 5D) CO_2 mixing ratios in the lake surface waters, and U is replaced by the friction velocity u_* (representing mechanical turbulence directly driving the gas flux), then CO_2 effluxes are highest under lower turbulence conditions ($u_* < 0.2$ m s^{-1}) when conditions are subsaturated, and become net neutral at $u_* \geq 0.2$ m s^{-1} (Figure 5C). In contrast, if the surface waters are supersaturated with CO_2, then CO_2 fluxes are similar to the subsaturated condition at low u_*, but become higher and more variable at $u_* \geq 0.2$ m s^{-1} (Figure 5C). This is consistent with surface waters that are supersaturated because increased stirring (*via* increasing u_*) should more completely outgas the surplus CO_2 in the surface waters.

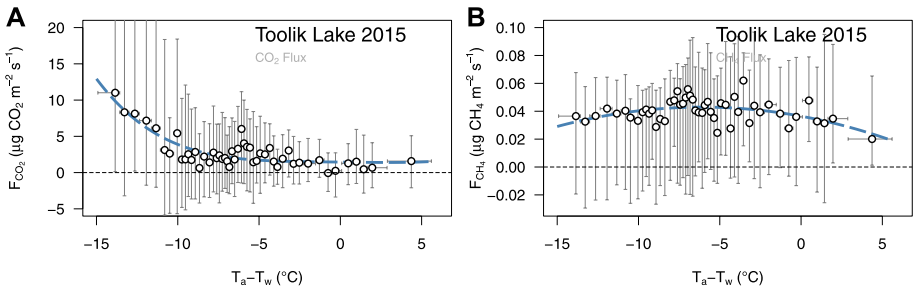


FIGURE 6
Effect of water–air temperature differences on **(A)** CO_2 fluxes and **(B)** on CH_4 fluxes at 5-min resolution. Vertical error bars show the inter-quartile range of values (inner 50% of data), whereas the horizontal whiskers show the entire size of the associated bin.

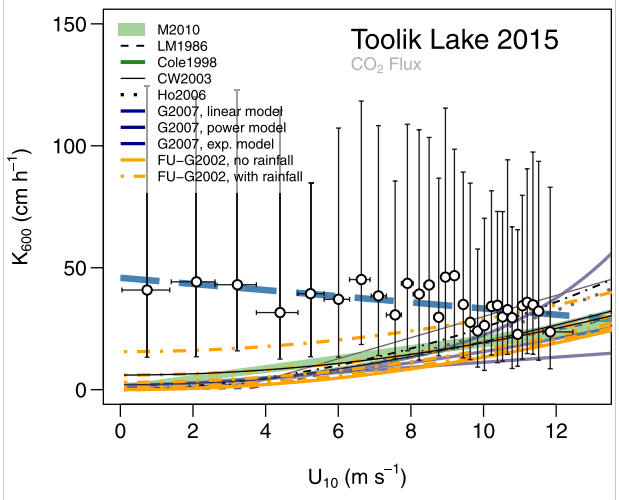


FIGURE 7
Comparison of measured piston velocities normalized to k_{600} for CO_2 flux–gradient relationships at 5-min resolution with a selection of models to estimate the fluxes from simpler water–air gradient measurements. Open circles show the median of each bin, approximated by a dashed blue line. Vertical error bars show the inter-quartile range of values (inner 50% of data), whereas the horizontal whiskers show the entire size of the associated bin. Models used are: M2010: MacIntyre et al. (2010), range given by the buoyancy flux term; LM 1986: Liss and Merlivat (1986); Cole 1998: Cole and Caraco (1998); CW 2004: Crusius and Wanninkhof (2003); Ho 2006: Ho et al. (2006); G2007: Guérin et al. (2007) with three versions (linear, power, and exponential model); and FU-G2002: Frost and Upstill-Goddard (2002), solid line without precipitation, and dashed lines with 0.05, 0.15, and 0.30 mm h^{-1} rainfall. See Table S3 for K_{600} model equations used. The U_{10} values derived for the 10-m height from local measurements and then enlarged by Charnock's relationship that relates true u_* to U_{10} (Figure 10A).

A more direct and clear relationship of CO_2 efflux from Toolik lake was found when the temperature difference between the water surface and the air was used as a reference (Figure 6A). In the range where T_w is colder or less than 5°C warmer than the air, the CO_2 fluxes appear weakly driven by the temperature difference. But at $T_w > (T_a + 5°C)$ an exponential increase of CO_2 efflux with increasing temperature difference was found (Figure 6A).

Methane fluxes do not show the same response to the temperature gradient between water and air (Figure 6B). If the water is 5°C colder than the air, the CH_4 effluxes were low and steadily increased to an optimum when the water temperature was around 8°C warmer than the air. If the difference was even larger, then CH_4 efflux decreased slightly (Figure 6B).

In this study we measured both concentrations in water and air, and fluxes of CO_2 and CH_4 fluxes (an advance since the beginning of air–sea exchange measurements, see Wanninkhof et al., 2009). Contrastingly, if only gas gradients are measured across the water–air interface, e.g., by syringe sampling, then the piston velocity normalized to a Schmidt number of 600 (k_{600}) must be estimated from horizontal wind speed measurements, although some authors claim that the relation to horizontal wind speed often is weak (Zappa et al., 2007). Most of the models used to predict k_{600} from wind speed at 10 m height (U_{10}) are derived for open ocean environments with a large fetch without obstacles. Over an inland lake with limited surface area such as Toolik, these models of k_{600} inadequately reflect the local conditions. Figure 7 shows that our direct measurements of the k_{600} piston velocity for CO_2 are almost constant, the highest values occur at low U_{10}, and only at $U_{10} > 10$ m s^{-1} do our estimates fall in the range of k_{600} that any model, including the MacIntyre et al. (2010) model that considers the buoyancy flux term, would predict for a stratified lake (Supplementary Table S3). This can be interpreted with the fact that it is actually u_*, not U_{10}, that drives vertical turbulent exchange of gases along the gradient between water surface and atmosphere. If measurements are made over a small lake, then the distance travelled over the lake surface is too short to bring u_* into equilibrium with U_{10}. There is a much higher level of turbulent mixing present in air masses that travelled over rough terrestrial tundra, and thus u_* remains relatively high in comparison to U_{10}.

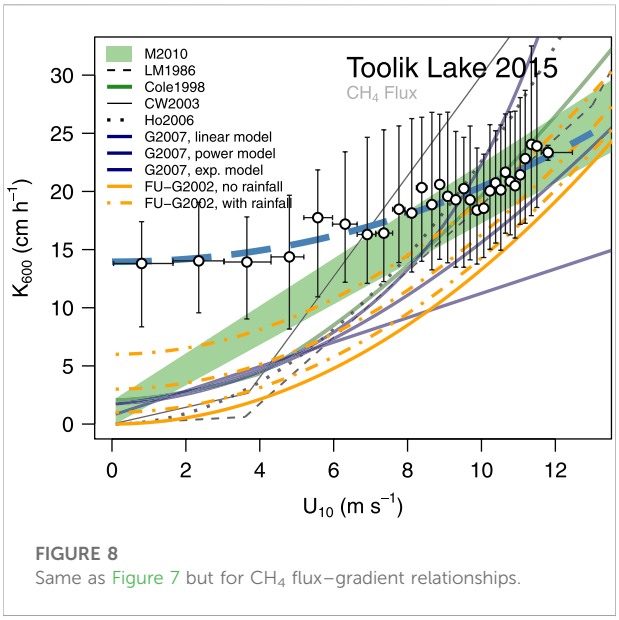


FIGURE 8
Same as Figure 7 but for CH_4 flux–gradient relationships.

The k_{600} piston velocity for CH_4 differs from that of CO_2 and shows the expected exponential increase with increasing U_{10} (Figure 8). However, there is a substantially higher turbulent exchange efficiency at low U_{10} than expected from models, with k_{600} around 14 cm h^{-1} even at very calm wind conditions (Figure 8). At U_{10} > 6 m s^{-1} the k_{600} for CH_4 then merges with the predicted values that most models provide (Figure 8).

The high turbulent exchange efficiency at low wind speeds, and the rather weak dependence of k_{600} on U_{10} in general, result in an almost constant CO_2 efflux (Figure 9A) and CH_4 efflux (Figure 9B) and mostly independent of the air-water difference in gas mixing ratio.

Figure 10A clearly shows that the u_*-to-U_{10} relationship is substantially enhanced over Toolik Lake as compared to what would be expected over the open ocean (red dashed line in Figure 10A). At U_{10} < 2 m s^{-1}, u_* is rather constant around 0.08 m s^{-1}, which is a factor 2–5× higher than what the Charnok relationship predicts (Figure 10A). Moreover, at low wind speeds the turbulent mixing not only depends on the mean U_{10} during an average interval, but also on the history of U_{10} during the previous interval. Over Toolik Lake the threshold of equal antecedent wind speeds is around $U_{10} \approx$ 5 m s^{-1} (Figure 10B); if U_{10} is below that threshold, it is most likely that U_{10} was higher with more turbulent mixing during the previous time interval, and if U_{10} was above that threshold, the U_{10} in the previous time interval was most likely lower.

3.4 Long-term trends of driver variables affecting CO_2 and CH_4 fluxes

Long-term trends are available for a few monitoring variables that cover the period from 1988 (or later) to 2020. For CO_2 and CH_4 gas exchange over Toolik Lake we focus on the long-term trends of lake depth (Figure 11A), lake surface water temperature (Figure 11B), horizontal wind speed (Figure 11C), rainfall (Figure 12), air temperature (Figure 13A), relative humidity (Figure 13B), short-wave incoming radiation (Figure 13C), barometric pressure (Figure 13D), and soil temperatures at the surface (in moss at the transition from green active tissue to brown peat) and at the deepest level recorded (1.5 m depth, corresponding to the maximum extension of the thawed active layer in summer) (Figure 14).

Because trends tend to be weak or statistically insignificant at annual aggregation of the long-term monitoring variables, all trends were determined *via* quantile regression that determines the trend slope for each quantile of the full dataset collected in each observation year. In this way, opposing trends at low, intermediate, or high values (quantiles) of the respective monitoring variable can be detected. Depending on the variable and expectation, we either tested the significance of the trend with a one-sided test (for existence of monotonically increasing or decreasing trends), or with a two-sided test to determine if any trend is significantly different from a null trend. Lake depth (Figure 11A) significantly decreased in all quantiles by −8.5 cm per decade, thereby reducing the water pressure on the lake bottom sediments which could increase the flux of gases produced at saturation in the sediments and released as bubbles to the water body (particularly the insoluble CH_4), and potentially thus increase the GHG efflux from organic sediments. However, we have observed very few ebullition events for CH_4 in Toolik Lake, which are the most expected events resulting from changing air pressure (Eugster et al., 2020a).

Lake water temperature did not show any significant trend during the warm season (Figure 11B), only winter conditions with surface water temperatures <2°C show a significant warming trend on the order of 0.1°C per decade (Figure 11B). Wind speed shows a decreasing trend at the lower 50% of the wind speed distribution, whereas wind speeds in the typical gentle breeze range (Beaufort 3, 3.6–5.1 m s^{-1} according to WMO, Hasse and Isemer, 1986; Arguez and Vose, 2011) remained almost unchanged in the past 33 years. Only the 1% most extreme wind speeds have increased more substantially by 0.3 m s^{-1} per decade, but this trend is not significant when we test for greater than normal wind speed extremes.

There is a highly significant increasing trend of rainfall events. On a daily basis the number of hours with precipitation has increased since 1988, both at the annual scale (Figure 12A) and during the terrestrial growing season months (May–September, Figure 12B). For days with up to 4 h of precipitation the increase in rainfall hours closely follows the + 5% increase curve during the growing season and follows the + 4% increase in the range of 4–7 h day^{-1}. The trend on days with >7 h of precipitation is less dramatic, although still statistically significantly compared to a null trend.

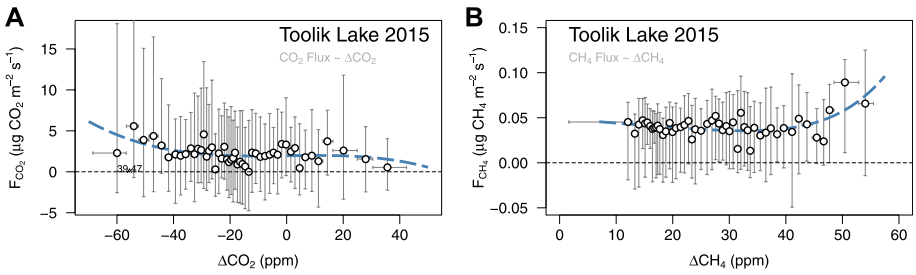


FIGURE 9
Relationships between measurements of the water–air **(A)** CO_2 gradient (ΔCO_2) and **(B)** CH_4 gradient (ΔCH_4) and their respective flux across the water interface. Positive Δ values indicate that the mixing ratio in water is above the equilibrium mixing ratio in the air.

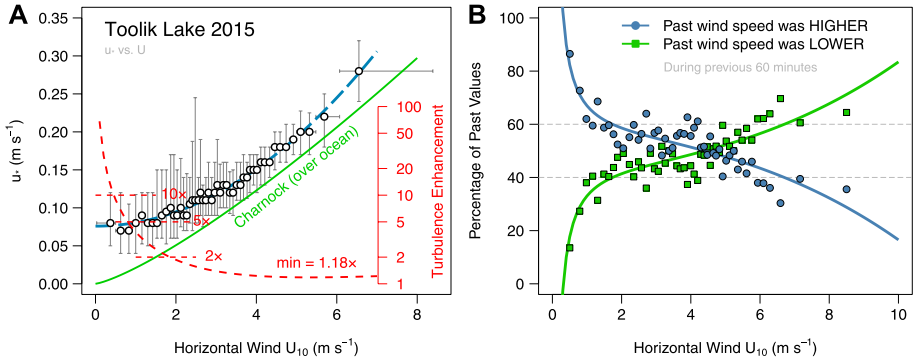


FIGURE 10
Turbulent mixing **(A)** (expressed by friction velocity u_* as a function of horizontal wind speed) is substantially enhanced over limited-sized Toolik Lake as compared to the widely-used Charnock-relationship over open ocean water surfaces. Moreover, **(B)** variability of horizontal wind speed over Toolik Lake is high, with past wind speeds (last 60 min) typically having been greater than actual wind speeds <4.4 m s^{-1}. The red dashed line in **(A)** shows the ratio between measurements (fit to group means) and the expected u_* according to Charnock.

Interestingly, the increasing duration of rain events is associated with significantly decreasing amounts of rainfall (−0.15 mm h^{-1} per decade; Figure 12C). This combination of prolonged rainfall events with lower precipitation amounts may reduce the risk of terrestrial flushing or erosion due to strong storms, and reduce the terrestrial export of DOC, thus supplying the lake with less carbon to be respired to CO_2 and CH_4.

During the warm season no significant trends in air temperature were found (Figure 13A). Significantly increasing air temperatures only affect winter temperatures < −8°C (Figure 13A), but the trend is rather substantial with a 1.2°C increase per decade.

Trends of relative humidity measured at 5 m a.g.l (above ground level) were separately determined for temperatures above and below freezing (Figure 13B). Above freezing, the high relative humidity (>85%) showed no significant trends. This is in line with the observed rainfall trends with prolonged duration of rainfall events, which tend to dominate conditions with high relative humidity. Although statistically significant, the decreasing trend in relative humidity at humidity values < ~80% is only a −1.6% reduction per decade, a value that most likely does not strongly affect GHG fluxes from Toolik lake.

Short-wave incoming radiation (Figure 13C) showed a roughly +0.5% increase over 33 years of measurements, which corresponds to a short-wave radiation increase of 9.0 [0.7–21.6] W m^{-2} per decade. This decadal trend is 3.3 times the estimate of the human-caused radiative forcing in 2019 as compared to 1750 [2.72 (1.96–3.48) W m^{-2}; IPCC AR6 WGI (2021; p.13: A.4.1)], but is in agreement with the global brightening that replaced the trend towards global dimming when the Toolik Lake long-term measurements were initiated in 1988 (Wild, 2005; Wild et al., 2012).

Barometric pressure has significantly increased at all quantiles by an average 1.4 [1.1–2.2] hPa per decade (Figure 13D), against a background range of ~900–1,000 hPa. Converted to a water column pressure this corresponds to a 1.43 cm increase in water level per decade. This increase in

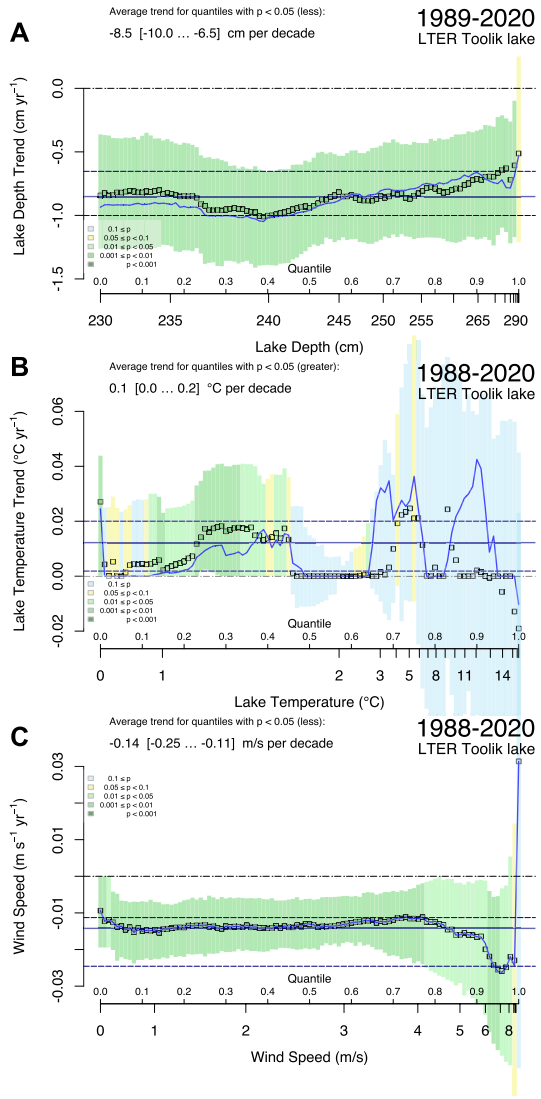


FIGURE 11
Quantile regression trend estimates of **(A)** lake depth, **(B)** lake temperature, and **(C)** horizontal wind speed at 5 m a.g.l. Black squares show the best estimate of the Theil-Sen median trend slope for each percentile of the observed range of quantiles. Color bands show the 95% confidence interval of the slope estimate with color coding from green (significant at $p < 0.05$ to yellow (marginally significant, $p < 0.1$) and light blue for insignificant slopes. The analysis was carried out on gap-filled timeseries. For comparison, the best estimates without gap-filling are shown with the solid blue line. A significant downward trend of the lake depth was observed, whereas the warming trend of lake surface waters is only significant at the lower 45% of temperature observations, that is, winter (under ice) temperatures < 1–2°C.

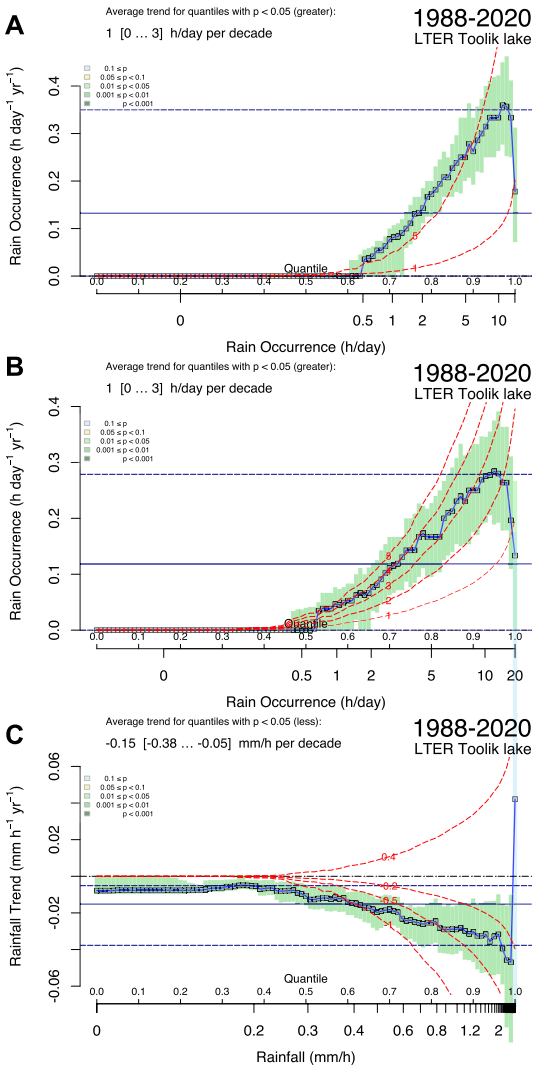


FIGURE12
Quantile regression trend estimates of **(A)** increasing occurrence of hours with rainfall, **(B)** as in **(A)** but restricted to the growing season months May–September, and **(C)** rainfall amount. Display as in Figure 11, with the addition of red dashed lines indicating equal percentage of change.

barometric pressure counteracts the effect of the decreasing lake depth trend, but its magnitude is only one sixth of the concurrent decreasing trend in lake depth (Figure 11A).

Soil temperatures from the air-moss interface down to 1.5 m depth show a very consistent warming trend ranging from the lowest values at the soil surface (i.e., in the moss layer) of 0.7–1.0°C per decade (Figures 14A, B) to 1.1°C per decade at 1.5 m depth (Figures 14C, D), which is the transition zone from the maximum extent of the summer active-layer thaw and the permafrost. The warming trend is significant and consistent across all soil depths for temperatures < −1°C and > 1–5°C, but around the freezing point there is no significant trend seen at any depth (Figure 14). This lack of trend at the freezing point is regulated by the physics of the phase transition from solid ice to liquid water; the phase transition remains near 0.0°C irrespective of climate warming trends, but the response is how much heat content is stored in either the deeper permafrost soil or in the seasonally-thawed active layer.

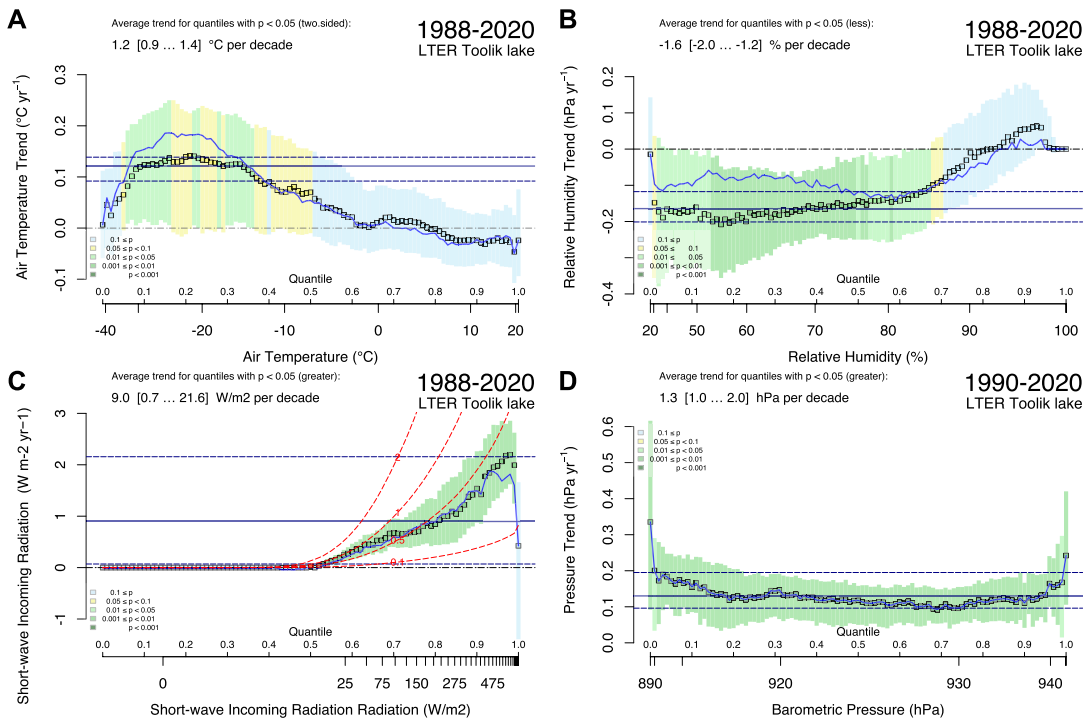


FIGURE 13
Quantile regression trend estimates of **(A)** air temperatures (two-sided test), **(B)** decreasing relative humidity at temperatures above freezing, **(C)** increasing global radiation, and **(D)** increasing barometric pressure. Display as in Figure 11.

4 Discussion

During the study period, CH_4 was always supersaturated (with respect to the atmosphere) in Toolik Lake surface waters (Figure 3), and there was a consistent flux of CH_4 from the lake to the atmosphere. CO_2 concentrations fluctuated close to atmospheric values, and fluxes to the atmosphere were low but consistently positive (Figure 1). These results are generally consistent with prior results of eddy covariance measurements from Toolik Lake (Eugster et al., 2003; Eugster et al., 2020a). At some times barometric pressure was positively related to dissolved CO_2 and negatively related to dissolved CH_4 in surface waters (Figure 1). Higher atmospheric pressure could increase the partial pressure of CO_2 or CH_4 in the water, but the mixing ratios in water would not change unless the air mass also had a different mixing ratio of these gases. Lower atmospheric pressures may release gases close to saturation in lake sediments, but as mentioned above we found very few if any bubbles in the water column of Toolik Lake (Eugster et al., 2020a).

In the diel cycle CO_2 concentrations were slightly lower during the evening hours, but as with CH_4 there was no obvious relationship between CO_2 concentrations and CO_2 flux to the atmosphere (Figure 2). CO_2 efflux was typically highest at night from 0000 to 0600 h, which has been attributed to greater convective mixing at the lake surface when air temperatures are cooler than lake temperatures (Eugster et al., 2003; Eugster et al., 2020a). Vertical profiles of CO_2 concentrations (Supplementary Figure S5) clearly show increasing concentrations with depth during summer stratification, indicating a near-surface source of CO_2 to be entrained by mixing and support greater flux to the atmosphere. Diel variations in CH_4 mixing ratios were not obviously related to the CH_4 efflux from the lake, which was more or less constant over the day (Figure 3). The difference between higher nighttime fluxes of CO_2 but not CH_4 (Figure 2,3) may be related to the lack of obvious increases in CH_4 concentration with depth (Supplementary Figure S4), and thus the lack of a near-surface supply of CH_4 to the surface during convective mixing at night when air temperatures decrease relative to surface water temperatures.

Natural or deliberate fertilization of lakes can increase algal biomass and rates of algal drawdown of CO_2 during photosynthesis, as demonstrated for a fertilized arctic lake near Toolik (Kling et al., 1992). In that same study results showed no indication of algal drawdown of CO_2 contributing to diel or seasonal variation of dissolved CO_2 concentrations or to atmospheric fluxes in ultra-oligotrophic Toolik Lake. In addition, here we show that the relationships between dissolved CO_2 concentrations and primary production or chlorophyll *a* in surface waters are positive (Supplementary Figure S4), and thus the opposite of expected if

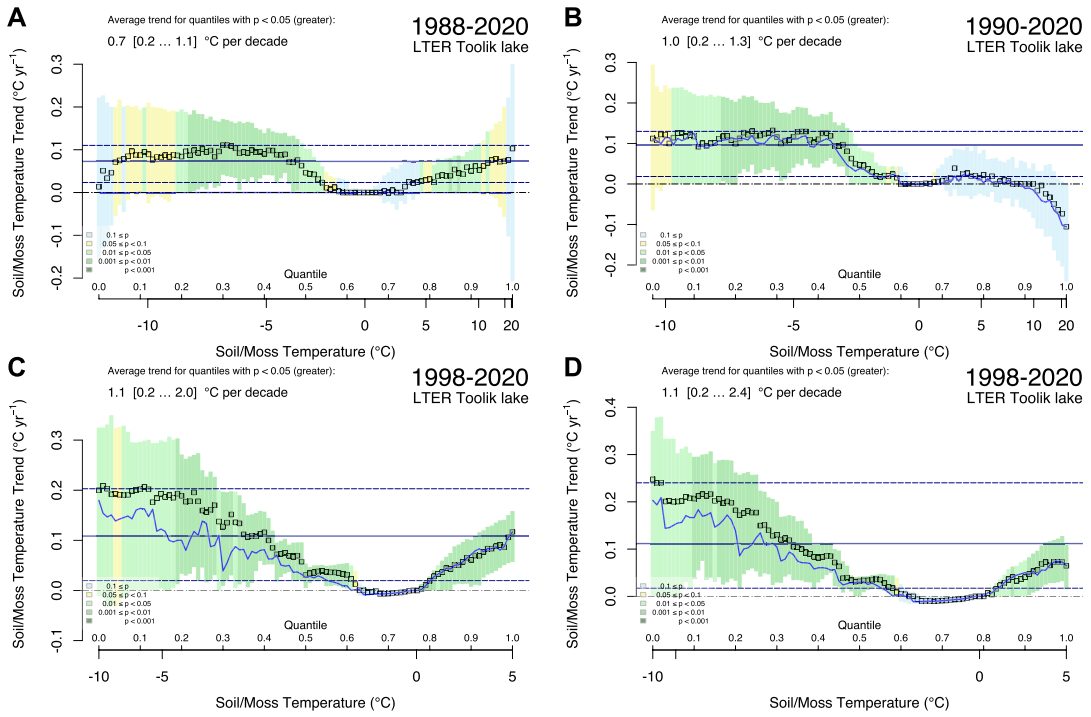


FIGURE 14
Quantile regression trend estimates of **(A,B)** moss temperatures of two replicates (two-sided test), and **(C,D)** soil temperatures at 1.5 m depth (typical maximum depth of active layer). Display as in Figure 11.

photosynthetic drawdown of CO_2 was important or could affect CO_2 efflux. There is also no clear drawdown of CO_2 concentrations during the middle of the day (1000–1400 h) when photosynthesis would be strongest. Even on short time scales it is unlikely that photosynthetic uptake would substantially influence dissolved CO_2 concentrations and thus gas exchange in this ultra-oligotrophic lake. For example, the highest rates of primary production shown in Supplementary Figure S4 would consume CO_2 at ~0.2 µmol L^{-1} hr^{-1} against a background concentration of ~20–50 µmol CO_2 L^{-1} (Supplementary Figure S4). At the same time, there is an input of CO_2 from bacterial respiration in surface waters of at least half the algal uptake rate (Crump et al., 2003). This input of CO_2 is considered a minimum value because it assumes 100% bacterial growth efficiency of respired CO_2 per C incorporated into bacterial cells. If a typical bacterial growth efficiency of 50% was used, then bacterial respiration alone could resupply the maximum photosynthetic uptake of CO_2.

4.1 Gas exchange velocities

Perhaps the most intriguing finding of this study is that measured piston velocities (k) for both CO_2 and CH_4 at wind speeds <10 m s^{-1} exceed what flux models would predict (Figures 7, 8), and the friction velocities (u_*) at all wind speeds exceed the expected values given the Charnock relationship (Charnock, 1955; Figure 10A). Even updated Charnock relationships (Edson et al., 2013; Jimenez and Dudhia, 2018) that predict increased wind stress at a given U_{10} still underestimate our measured u_*, especially at lower wind speeds (Figure 10A). Thus the higher friction velocity imparted to the water surface in our study should generate greater TKE in the surface water to enhance gas exchanges (k in Figures 7, 8).

There are several possible explanations for the high gas transfer velocities we measured at medium to low wind speeds (<10 m s^{-1}, Figures 7, 8). First, Munk (1947) proposed that flow over the ocean is laminar up to the Kelvin-Helmholtz instability around 6.5 m s^{-1} and only becomes turbulent at higher wind speeds (Supplementary Figures S6, S7). Fetch is unlimited over the open ocean, and hence even at low wind speeds an equilibrium can establish between the atmospheric flow and the ocean depending on the previous status of the atmospheric and ocean turbulence (Supplementary Figure S6). Contrastingly, smaller lakes have a limited fetch and are thus more influenced by the surrounding, relatively rough landscape that generates more atmospheric turbulence, and the previous status is always “turbulent” under such conditions (Supplementary Figures S6, S7). There is no wind sheltering at Toolik Lake due to the low canopy structure of the surrounding tundra, but topographical rises of 20 m within 100 m of

the shoreline are common and hills can be 30 m above the lake surface within 300 m of the lake shore. This complex terrain, coupled with a lack of wind sheltering to reduce wind speed and turbulence in the air mass reaching the lake (e.g., Markfort et al., 2010), act to generate more TKE in the atmosphere over the lake than is typically generated at the same wind speeds in smooth landscapes or over large lakes or oceans.

Second, the memory effect of turbulent mixing in the atmosphere brings well-mixed conditions from the rough terrestrial surface to the smooth lake water body, but in this small lake even a kilometer of fetch is unlikely sufficient to bring the turbulence state of the near-surface atmosphere into equilibrium with the water surface. However, at the same time the "young" waves generated when the fetch is small are typically shorter and steeper than waves closer to equilibrium with wind speeds in large lakes or oceans, and this steepness can increase the gas exchange (Edson et al., 2013) and increase the form stress on the water surface (Sullivan et al., 2018).

Third, the smaller, shorter waves that develop over shorter-fetch waters for a given wind speed are less likely to break than are larger waves and thus less likely to inject bubbles into the surface water. Bubble-mediated gas exchange is biased toward invasion (Woolf and Thorpe, 1991), and bubbles generated during wave breaking reintroduce atmosphere into the near surface and that reduces gas exchange (e.g., Emerson and Bushinsky, 2016). Note that as wind speed and wave height increase the bubble-mediated gas invasion will also increase, thereby reducing our measured *k* values compared to model predictions; this behavior is seen in Figures 7, 8.

Fourth, open-water surface roughness tends to increase at shallower depths (e.g., Taylor and Yelland, 2001), which leads to increased surface drag over shallow waters typically unaccounted for in models (Jiménez and Dudhia, 2018). Taken together, these processes tend to increase the measured k values compared to values predicted from models, including those developed for use in lakes and that incorporate buoyancy flux (e.g., MacIntyre et al., 2010). At present, we have no clear means of separating the individual contributions of these potential explanations for the higher than predicted gas exchange velocities we measured.

It is also unclear at present why there is a difference between the flux behavior of CO_2 and CH_4 (e.g., Figures 5–9). Although both of these gases are low enough in solubility to be generally controlled by water-side dynamics (Wanninkhof et al., 2009; Garbe et al., 2014), recent work has highlighted that bubble-dynamics vary between gases (Goddijn-Murphy et al., 2016; Rosentreter et al., 2017), and even gas solubility and transfer is differentially affected in response to films on the water surface (Mesarchaki et al., 2015).

4.2 Summary of environmental drivers of fluxes

A PCA indicated a strong coupling of CO_2 fluxes with environmental variables (meteorological variables, eddy flux variables, and temperature and gas mixing ratios in the water, including temperature of the upper mixing layer in the lake, 0–4 m depth, and temperature near or below the typical summer thermocline at 5 m depth). An increased dissolved CO_2 mixing ratio does not automatically increase the CO_2 efflux from the lake. It seems to represent the important transfer of CO_2-rich waters at the bottom of the epilimnion or in the metalimnion (Supplementary Figure S5) being transferred into the upper epilimnion, thereby increasing CO_2 mixing ratio, but not directly F_{CO2} (Figure 4).

The CH_4 fluxes are much less coupled with the same driver variables (Figure 4B) that influence CO_2 evasion (Figure 4A). We only inspected PC axes 3 and 4 where F_{CH4} plays a role and which explain 22.8% and 14.3% of the remaining variance (after PC1 and PC2), respectively (Figure 3B). It is probably the constantly high supersaturation of CH_4 (Figure 3A) that leads to a constant CH_4 efflux with a minor diel cycle (Figure 3B), and this makes F_{CH4} much less dependent on environmental variables than is F_{CO2} (Figure 4A).

4.3 Interannual flux variability

The process-level relationships between GHG mixing ratios in the surface waters and the eddy-covariance flux measurements of CO_2 and CH_4 were only available from summer 2015, but seasonal flux measurements were carried out at Toolik lake during the ice-free seasons 2010–2015. In Eugster et al. (2020a) we provided a detailed comparison of interannual variability of the seasonal fluxes. In summary, the 2012 season provided the highest CO_2 and CH_4 effluxes with 1.3 g CO_2 m^{-2} day^{-1} (30 mmol m^{-2} day^{-1} and 3.2 mg CH_4 m^{-2} day^{-1} (0.20 mmol m^{-2} day^{-1}), respectively. During the 2010 season with the lowest CO_2 efflux only 30% of the 2015 efflux was observed, and in the case of CH_4 the following 2011 season had the lowest efflux which was 35% of the 2015 maximum flux. This high interannual variability is not easily explained by the long-term trends of the monitored variables that influence gas exchange across the water surface in the short term and at the process-level. However, given that carbon input (CO_2, CH_4, DOC, and POC) to the lake from streams can be quite variable and can affect microbial processing of DOC to CO_2 or CH_4 (e.g., Kling et al., 2000; Crump et al., 2003, Crump et al., 2007), it is possible that variable inputs of carbon to the lake affect the interannual variability more than meteorological variables that govern gas exchange. Wu et al. (2013) have also reported that diffusive gas fluxes from two lakes were primarily attributable (30%–45%) to inputs and respiration of terrestrial DOC.

A linear, mixed-effect model combining the Eugster et al. (2020a) data with the monitoring variables used in this paper, suggests different processes governing the variability of the

TABLE 1 Linear mixed effect model for CO_2 flux during the Toolik lake ice-free seasons 2010–2015. Predictor variables aggregated to 3-h averages or sums (rainfall) were normalized to look at relative importance (estimate of response slopes). Insignificant effects and those influencing CO_2 flux by less than ± 1% are not included. Effects influencing CO_2 flux by more than ± 10% are shown with bold face font. Stepwise forward selection was used to find the best model. Fixed effects were sorted within each significance level according to their relative importance (Estimate).

Variable	Estimate	Std. Error	df	T	Value Pr(>|t|)
soil_10 cm.gf	**0.265**	**0.033**	**4031.0**	**7.9290**	**<0.0001*****
vpd.gf	0.032	0.009	4023.0	3.6590	0.0003***
wind_sp_5 m.gf:soil_moss.gf	0.025	0.005	4031.0	5.2990	<0.0001***
U:soil_10 cm.gf	0.015	0.001	4034.0	11.5510	<0.0001***
soil_moss.gf:soil_10 cm.gf	0.013	0.002	4021.0	5.3250	<0.0001***
wind_sp_5 m.gf:soil_50 cm.gf	0.012	0.004	4014.0	3.3190	0.0009***
rain.mean.gf.n04:air_temp_5 m.gf	0.010	0.003	4027.0	3.7000	0.0002***
soil_10 cm.gf:soil_20 cm.gf	−0.018	0.004	4022.0	−4.2460	<0.0001***
soil_5 cm.gf	−0.022	0.006	4019.0	−3.8850	0.0001***
soil_100 cm.gf	−0.043	0.013	4028.0	−3.2990	0.0010***
wind_sp_5 m.gf	**−0.100**	**0.019**	**4023.0**	**−5.2310**	**<0.0001*****
wind_sp_5 m.gf:soil_10 cm.gf	**−0.119**	**0.017**	**4023.0**	**−7.2260**	**<0.0001*****
USTAR:soil_moss.gf	−0.032	0.011	4017.0	−3.0090	0.0026**
soil_20 cm.gf	−0.037	0.014	4021.0	−2.6630	0.0078**
(Intercept)	**−1.002**	**0.330**	**14.8**	**−3.0340**	**0.0085****
soil_10 cm.gf:soil_150 cm.gf	0.032	0.013	4024.0	2.4090	0.0160*
soil_50 cm.gf	−0.025	0.010	4007.0	−2.4570	0.0141*
soil_moss.gf	−0.037	0.018	4024.0	−2.0850	0.0371*
rain.mean.gf.n04	**−0.377**	**0.156**	**4019.0**	**−2.4100**	**0.0160***

TABLE 2 Linear mixed effect model for CH_4 flux during the Toolik lake ice-free seasons 2010–2015. Predictor variables aggregated to 3-h averages or sums (rainfall) were normalized to look at relative importance (estimate of response slopes). Insignificant effects and those influencing CH_4 flux by less than ± 1% are not included. Effects influencing CH_4 flux by more than ± 10% are shown with bold face font. Stepwise forward selection was used to find the best model. Fixed effects were sorted within each significance level according to their relative importance (Estimate).

Variable	Estimate	Std. Error	df	t	Value Pr(>|t|)
soil_moss.gf	0.039	0.006	2956.0	6.2090	<0.0001***
vpd.gf	0.016	0.005	3042.0	3.4720	0.0005***
soil_5 cm.gf:soil_100 cm.gf	0.013	0.002	3042.0	7.0480	<0.0001***
vpd.gf:soil_5 cm.gf	0.011	0.001	3040.0	12.6510	<0.0001***
rain.mean.gf.n04:soil_20 cm.gf	−0.013	0.003	3044.0	−3.8810	<0.0001***
soil_5 cm.gf	−0.066	0.008	3045.0	−8.7300	<0.0001***
USTAR:rain.mean.gf.n04	**−0.113**	**0.031**	**3045.0**	**−3.7130**	**0.0002*****
USTAR	**−0.230**	**0.050**	**3046.0**	**−4.6170**	**0.0000*****
(Intercept)	**−1.632**	**0.092**	**20.8**	**−17.7760**	**0.0000*****
soil_150 cm.gf	−0.023	0.008	3045.0	−2.7200	0.0066**
soil_20 cm.gf	0.019	0.008	3046.0	2.3760	0.0175*
U:soil_150 cm.gf	0.017	0.007	3043.0	2.3050	0.0212*
USTAR:soil_5 cm.gf	−0.012	0.005	3046.0	−2.4420	0.0147*
soil_100 cm.gf	0.024	0.015	3046.0	1.6460	0.0998
U	0.016	0.009	3044.0	1.7670	0.0773

CO_2 fluxes (Table 1) versus the CH_4 fluxes (Table 2). The mixed-effect model shows that warm soil temperatures at 10 cm depth increase CO_2 fluxes by 26.5 ± 3.3% (Table 1), but rainfall 12 h ahead reduces CO_2 fluxes substantially by −37.7% ± 15.6%. It is possible that at warm times or in warm years that soil temperatures tend to increase organic matter decomposition

in soil and thus increase the transport of CO_2 and CH_4 to the lake, or to increase the production of DOC and POC that feed into Toolik Lake. But rainfall, especially heavier rainfall intensities, are expected to increase effluxes of CO_2 and CH_4 from the lake (Guérin et al., 2007). Stronger winds, and stronger winds in combination with warmer 10-cm soil temperatures, also exert a negative effect on CO_2 fluxes on the order of −10% (Table 1). From other ecosystems it is also known that the near-surface soils are the most important substrate for respiration, in combination with soil temperature but with a dominance of availability of organic matter (e.g., Robinson et al., 2022). In arctic tundra there is substantial organic peat available across the upper soil profile, and thus the importance of the 10-cm conditions (and not the moss or 5 cm temperature) for respiration and decomposition may be most relevant as soils warm and eventually thaw in the Arctic.

The driving forces for CH_4 effluxes include a set of variables that each contribute only a minor percentage to the flux: warmer moss temperatures (i.e., temperature measured at the transition from green living moss matter to brown moss peat), a dry atmosphere (higher vapor pressure deficits, VPD), and warm temperatures in the topsoil (5 cm) in combination with warmer temperatures near the bottom of the active layer (100 cm). A strong negative effect is quite prominent when we observe turbulent mixing above the water surface (u_*) (−23.0 ± 0.5%, Table 2) or high u_* in combination with rainfall intensity 12 h ahead (−11.3% ± 3.1%, Table 2). That the processes affecting CH_4 fluxes differ from those affecting CO_2 is not surprising given the differences in relationships with physical forcing between the two gases (e.g., Figures 4–8). In addition, CH_4 is only produced under anaerobic conditions and will be oxidized to CO_2 when it is exposed to an aerobic environment.

4.4 Expected trends of CO_2 and CH_4 fluxes until 2050

To translate the past and present functional relationships between CO_2 and CH_4 fluxes and their environmental driving forces into the future, we analyze changes in the observed long-term monitoring variables and how they correlate with the GHG fluxes in Toolik Lake. Because the trends of most variables are looking roughly 30 years into the past, our projection is an estimate for conditions 30 years into the future (i.e., a time horizon of 2050). This extrapolation of trends over the last 30 years assumes that, in general, human activities leading to GHG emissions today will continue to increase at the same pace as in the last 30 years (the business as usual or RCP8.5 scenarios). This assumption is made in part because downscaled, regional predictions of future climate for the North Slope of Alaska are unavailable (see Hobbie and Kling, 2014). But projecting the trend observed during the past 30 + years to the next 30 years is not the same as using an IPCC scenario for predictions. Thus, with continued warming the IPCC projections expect that both CO_2 and CH_4 emissions to the atmosphere will increase in the years to come, despite the low confidence (or too little data) in the potential role of Arctic warming (IPCC AR6 WGI, 2021).

In summary, the relevant long-term trends in monitored potential driver variables of CO_2 and CH_4 fluxes are 1) the decreasing trend in lake depth, 2) the increasing trend in barometric pressure, 3) the decreasing trend of the lower 50% of wind speeds, 4) the 4%–5% increase in daily hours with rainfall in combination with the decreasing trend of rainfall intensity (precipitation amount per hour), 5) the increasing global radiation with global brightening since the early 1990s, and 6) the increasing soil temperatures above and below freezing (but not near the freezing point) across the entire 1.5 m depth profile equipped with temperature sensors. Not included in this discussion are 1) photosynthesis, 2) air temperatures that only show significant warming during the winter and thus outside the ice-free period covered with GHG flux measurements in this study, and 3) relative humidity that does not appear to have a strong influence on GHG effluxes from Toolik Lake. Wind direction trends were not included in this analysis (see Eugster et al., 2020a for wind direction analyses).

Starting with substrate availability for CO_2 and CH_4 production in Toolik Lake, the warming trend of the soil and increasing permafrost thaw (Turetsky et al., 2020) is probably an important positive feedback that will increase carbon inputs from land *via* stream inflow, groundwater, and overland flow to lakes in permafrost terrain (Hobbie and Kling, 2014; Vonk et al., 2015). If part of this increased input of C is in the form of particulate C that settles to the lake bottom, decreasing trends of lake depth might then amplify the outgassing of carbon gases produced from this particulate organic matter (less pressure to keep insoluble gases in the sediments). However, our earlier study (Eugster et al., 2020a) found no relevant role of CO_2 and CH_4 production in the bottom sediments of Toolik Lake, as deduced from the lack of evidence for ebullition. Moreover, the cold hypolimnion temperatures around 5–6°C even in peak summer limit biological activity and thus decomposition of C-rich substrates deposited in the lake bottom sediments. A study by Bayer et al. (2019) suggests that future gas fluxes from permafrost lakes are dependent on carbon inputs from the catchment.

The increasing trend in barometric pressure counteracts the effect of the decreasing trend in lake depth; that is, as the former reduces outgassing of GHGs from the bottom sediments, the latter promotes outgassing when the hydrostatic pressure on GHGs produced in lake sediments decreases. The net result would be toward enhanced outgassing because the magnitude of the barometric pressure trend is only one sixth of the opposing pressure trend exerted by lake depth. Hence we expect that a long-term trend of increasing barometric pressure may influence the short-term timing of GHG efflux from the lake, but the more

important lake depth change most likely influences any long-term change in GHG fluxes derived from gases lost from lake bottom sediments.

Because of the weak relationship with CO_2 flux and either U_{10} or u_*, a reduction of wind speeds below 1 m s^{-1} or above 5 m s^{-1} only slightly reduces the average F_{CO2} level of 2.5 µg CO_2 m^{-2} s^{-1}; at the highest wind speeds there is one data point showing that the CO_2 flux is reduced to near zero (Figure 5A). An assessment of the trend of increasing wind speeds on global ocean gas exchange with the atmosphere (Wanninkhof and Trenanes, 2017) suggested a slight increase in flux to the atmosphere, and more pronounced effects at lower wind speeds. That study did not consider gas fluxes from inland waters, which would generally experience lower wind speeds than do oceans. However, our results indicate that wind speed may be a poor predictor of and underestimate gas effluxes, which could be considered in future predictions of gas fluxes from all surface waters.

The unexpected increasing trend of daily hours with precipitation but decreasing trend in rainfall intensity (mm h^{-1}) indicates that the risk of storm erosion and thus transport of particulate organic matter to the inlet stream and further to Toolik Lake should decrease compared to the past. This could impose an important negative feedback on substrate availability for heterotrophic respiration in Toolik Lake that could even reduce the GHG fluxes from the lake. However, this potential effect must be balanced against the possibility of erosion and carbon inputs to the lake due to thermokarst failures, which are increasing in many arctic areas most likely due to permafrost thaw (Lewkowicz and Way, 2019). In addition, Cherry et al. (2014) predicted a wetter future for the Toolik region, which could increase the amount of DOC exported from land and respired within the lake (Kling et al., 2000, Kling et al., 2014). Finally, rainfall can enhance gas flux when raindrops add mixing energy to the water surface (Ho et al., 2004; Harrison et al., 2010), and longer periods of rainfall, independent of rain intensity, may thus increase gas fluxes. Overall, the effect of changes in precipitation on lake gas fluxes are complex and difficult to predict.

Increasing short-wave incoming radiation of course means more energy available at the Earth's surface, which reduces atmospheric stability of the near-surface boundary layer and increases turbulent mixing in the atmosphere and thus the transfer of energy to the water surface that affects gas exchange (Erickson, 1993). At the same time, light-energy inputs warm surface waters, and increase buoyancy and water column stability, thus reducing TKE that can drive gas exchange across the lake surface (Imberger, 1985). On land, some of the energy will be used to increase soil heat flux; this is not in the set of long-term monitoring variables, but is key for the heat required to sustain the observed warming trends both below and above freezing in soils as discussed above. At present it is unclear how light energy increases will affect the balance between higher turbulence on land versus lower turbulence in surface waters with respect to controlling gas exchange.

The brightening of the atmosphere (Wild, 2005) reflected by the significantly increasing trend of short-wave incoming radiation has the potential to increase CO_2 fluxes, but most likely has no substantial effect on CH_4 fluxes. In case of the CO_2 fluxes we observed a positive influence of large T_w to T_a differences (Figure 6A), which most likely would be further amplified by increasing radiation inputs. In addition, increased photon flux to surface waters will increase photomineralization of DOC to CO_2 (Cory et al., 2014; Cory and Kling, 2018). Although greater solar radiation has the potential to increase algal photosynthesis, it is unlikely to be important in ultra-oligotrophic arctic lakes (Supplementary Figure S4). However, the warming trend in lake surface temperature (Figure 11B) was not significant at summer temperatures, but a significant warming trend of 0.1°C per decade under the ice cover (water temperature <2°C; Figure 11B) has the potential to increase under-ice microbial respiration, leading to a greater release of GHG accumulating under the ice during winter. However, this warming trend is quite weak and therefore unlikely to strongly impact microbial respiration under ice in the next 30 years.

Given the combined and often complex and counterbalancing effects of changing environmental drivers of gas flux, it is unlikely that Toolik Lake GHG fluxes will reach a tipping point where the system changes state from a source of gas to the atmosphere to a gas sink. The trends in drivers appear to be statistically significant but of low magnitude, most likely modifying present-day CO_2 and CH_4 effluxes in the range of an estimated factor 0.9–1.3. The lower value (0.9) is derived from an average reduction of –0.14 m s^{-1} in mean wind speed of 3.0 m s^{-1} per decade (–0.42 m s^{-1} in 30 years), which translates to almost unchanged F_{CO2} and a −10% change in F_{CH4} (based on Supplementary Table S2, Figures 5A,5B). The upper estimate (1.3) is derived from changes in the terrestrial environment that may stimulate organic matter respiration and transport to surface waters; for example, moss temperatures (Figure 14A) increasing by 0.7°C per decade (2.1°C in 30 years) above the average temperature of 7.0°C for conditions >0°C. If this temperature increase is linearly related to the inflow of increased CO_2 and CH_4 to the lake as permafrost thaws (and not including DOC transport and subsequent oxidation), we expect a −30% increase in fluxes from the lake.

It is unclear how the identified trends in environmental drivers and the estimated impacts on GHG fluxes apply to other lakes. However, there may be some similarities in response because many of the processes that influence gas fluxes described here (e.g., rainfall and carbon loading, temperature and respiration, photomineralization of DOC) occur in all surface waters. We suggest that lakes deep enough to stratify seasonally may behave similarly to Toolik Lake, while shallower lakes or wetlands may respond differently to

environmental change (e.g., greater ebullition than observed in Toolik). In addition, catchment differences in vegetation and surface topography may contribute to highly site-specific responses of lakes to changing environmental conditions.

5 Conclusion

We investigated the flux–gradient relationships between gas mixing ratios of CO_2 and CH_4 measured in lake surface waters during the ice-free season 2015 at Toolik Lake, estimated the relative strength of potential environmental driving forces governing CO_2 and CH_4 effluxes, and then combined this newly gained process-level knowledge with long-term trends of meteorological and soil temperature data to make predictions of how gas fluxes may change in the coming decades. In contrast to expectations, the flux–gradient relationship of CO_2 mixing ratio differences across the air-water interface had an influence on F_{CO2} only if the water surface was at least 8–10°C warmer than the air. Otherwise F_{CO2} was surprisingly constant over a wide range of horizontal wind speed. F_{CH4} showed a typical exponential increase in flux over the full range of observed wind speeds. Overall, the relationship between wind speed and gas exchange coefficients (k) represented by several models compared poorly to our measured values of k for both CO_2 and CH_4. The models substantially under-predict our measured k values for CO_2 and CH_4 at low to medium wind speeds (<8–10 m s^{-1}), above which our k computed from direct measurements converges on the range of values predicted by most models, especially models specific for lakes that include the effects of buoyancy flux. We attribute these higher gas exchange velocities at low wind speeds to the characteristics of the atmospheric turbulence generated on land and carried over water in this tundra lake, and how that affects surface roughness, wave-breaking, and bubble-mediated gas exchange at low wind speeds. Increased turbulence and a higher u_*-to-U_{10} ratio over smaller lakes as compared to oceans increased both F_{CO2} and F_{CH4} at low wind speeds well beyond the level expected over the ocean.

Combining the analysis of the effects of environmental drivers on gas flux with the 30 + year long-term trends of driver variables monitored by the LTER program we found both flux-enhancing and flux-reducing effects. The warming trend across the whole 1.5 m soil profile equipped with temperature sensors tends to enhance both CO_2 and CH_4 fluxes, whereas rainfall intensity tends to reduce F_{CO2}, and also F_{CH4} if in combination with low u_*. High u_* alone also reduces F_{CH4}, whereas in the case of F_{CO2} it is rather increased horizontal wind speed than u_* that reduces fluxes.

We argue that the biological processing of carbon-rich substrate that becomes available for decomposition as the tundra soil warms (e.g., Robinson et al., 2022) is key for understanding future trends in GHG fluxes (see also Wu et al., 2013), whereas the variability and long-term trends of the physical and meteorological variables primarily affect the timing when higher or lower than average fluxes are observed. When all aspects are taken into account, we see no strong evidence that a tipping point will be reached to change the status of the system substantially (e.g., source to sink). Instead we suggest that CO_2 and CH_4 fluxes should not increase by more than ~30% by 2050, and we do not expect them to decrease by more than ~ −10% within the next 30 years. This range of −10% to +30% characterizes the limitations of the study, including the variance shown for the relationships of environmental variables and gas fluxes. However, we suggest that lakes in the Arctic will remain a clear and strong source of CO_2 and CH_4 fluxes despite their relatively small area in the terrestrial landscape.

Data availability

The long-term meteorological data used in this study can be downloaded from University of Alaska's Toolik Field Station Environmental Data Center (https://www.uaf.edu/toolik/edc/monitoring/abiotic/met-data-query.php). The CO_2 and CH_4 flux data used in this study are available from: Eugster et al. (2020b). See also Eugster et al. (2020a). Turbulence and flux data from eddy flux platform on Toolik Lake, Alaska 2009–2015 from Environmental Data Initiative, http://dx.doi.org/10.6073/pasta/919cd028d73ef4f8427d951148f974ec. Gap-filling data from: Shaver (2016).

Author contributions

WE and GK designed the study, collected and analyzed data, and prepared the manuscript. JL contributed to data collection and analysis. TD, JL, and GS contributed data. All authors contributed comments on the manuscript.

Acknowledgments

We acknowledge support from the Arctic LTER grants NSF-DEB-1637459, 1026843, 1754835, NSF-PLR 1504006, and supplemental funding from the NSF-NEON and OPP-AON programs. WE acknowledges additional funding received from ETH Zurich scientific equipment grants 0-43350-07 and 0–43683–11. Many thanks also go to numerous technical assistants working at Toolik Lake, and to Toolik Field Station staff members for their support.

Dr. Werner Eugster, an esteemed scientist and our colleague and dear friend for decades, passed away in May 2022. We dedicate this paper to Werner—it was his brainchild, and he continued to contribute to it in his last days. Werner was a world leader in the fields of micrometeorology and eddy covariance studies, and a kind and tireless mentor for us and many other scientists. We miss him.

Conflict of interest

The authors declare that the research was conducted in the absence of any commercial or financial relationships that could be construed as a potential conflict of interest.

Publisher's note

All claims expressed in this article are solely those of the authors and do not necessarily represent those of their affiliated organizations, or those of the publisher, the editors and the reviewers. Any product that may be evaluated in this article, or claim that may be made by its manufacturer, is not guaranteed or endorsed by the publisher.

Supplementary material

The Supplementary Material for this article can be found online at: https://www.frontiersin.org/articles/10.3389/fenvs.2022.948529/full#supplementary-material

References

Akritas, M. G., Murphy, S. A., and Lavalley, M. P. (1995). The Theil-Sen estimator with doubly censored data and applications to astronomy. *J. Am. Stat. Assoc.* 90, 170–177. doi:10.1080/01621459.1995.10476499

Arguez, A., and Vose, R. S. (2011). The definition of the standard WMO climate normal: The key to deriving alternative climate normals. *Bull. Am. Meteorol. Soc.* 92, 699–704. doi:10.1175/2010bams2955.1

Bayer, T. K., Gustafsson, E., Brakebusch, M., and Beer, C. (2019). Future carbon emission from boreal and permafrost lakes are sensitive to catchment organic carbon loads. *J. Geophys. Res. Biogeosci.* 124, 1827–1848. doi:10.1029/2018JG004978

W. Brutsaert and G. H. Jirka (Editors) (1984). *Gas transfer at water surfaces* (Springer Netherlands). doi:10.1007/978-94-017-1660-4

Buck, A. L. (1981). New equations for computing vapor pressure and enhancement factor. *J. Appl. Meteor.* 20, 1527–1532. doi:10.1175/1520-0450(1981)020<1527:nefcvp>2.0.co;2

Charnock, H. (1955). Wind stress on a water surface. *Q. J. R. Meteorol. Soc.* 81, 639–640. doi:10.1002/qj.49708135027

Cherry, J. E., Déry, S. J., Cheng, Y., Stieglitz, M., Jacobs, A. S., and Pan, F. (2014). "Climate and hydrometeorology of the Toolik lake region and the kuparuk river basin," in *Alaska's changing arctic*. Editors J. Hobbie and G. Kling (Oxford University Press). doi:10.1093/acprof:osobl/9780199860401.003.0002

Cole, J. J., and Caraco, N. F. (1998). Atmospheric exchange of carbon dioxide in a low-wind oligotrophic lake measured by the addition of SF_6. *Limnol. Oceanogr.* 43, 647–656. doi:10.4319/lo.1998.43.4.0647

Cole, J. J., Caraco, N. F., Kling, G. W., and Kratz, T. K. (1994). Carbon dioxide supersaturation in the surface waters of lakes. *Science* 265, 1568–1570. doi:10.1126/science.265.5178.1568

Cory, R. M., Crump, B. C., Dobkowski, J. A., and Kling, G. W. (2013). Surface exposure to sunlight stimulates CO_2 release from permafrost soil carbon in the Arctic. *Proc. Natl. Acad. Sci. U. S. A.* 110, 3429–3434. doi:10.1073/pnas.1214104110

Cory, R. M., Ward, C. P., Crump, B. C., and Kling, G. W. (2014). Sunlight controls water column processing of carbon in arctic fresh waters. *Science* 345, 925–928. doi:10.1126/science.1253119

Cory, R. M., and Kling, G. W. (2018). Controls on DOM degradation along the aquatic continuum: The influence of interactions between light, chemistry, and biology. *Limnol. Oceanogr. Lett.* 3 (3), 102–116. doi:10.1002/lol2.10060

Crump, B. C., Kling, G. W., Bahr, M., and Hobbie, J. E. (2003). Bacterioplankton community shifts in an arctic lake correlate with seasonal changes in organic matter source. *Appl. Environ. Microbiol.* 69, 2253–2268. doi:10.1128/aem.69.4.2253-2268.2003

Crump, B. C., Adams, H. E., Hobbie, J. E., and Kling, G. W. (2007). Biogeography of bacterioplankton in lakes and streams of an Arctic tundra catchment. *Ecology* 88, 1365–1378. doi:10.1890/06-0387

Crusius, J., and Wanninkhof, R. (2003). Gas transfer velocities measured at low wind speed over a lake. *Limnol. Oceanogr.* 48, 1010–1017. doi:10.4319/lo.2003.48.3.1010

Deike, L., and Melville, W. K. (2018). Gas transfer by breaking waves. *Geophys. Res. Lett.* 45, 10482–10492. doi:10.1029/2018GL078758

DelSontro, T. S. (2011). *Quantifying methane emissions from reservoirs: From basin-scale to discrete analyses with a focus on ebullition dynamics*. Ph.D. thesis. Switzerland: ETH Zurich, 154pp.

Easterling, R. G. (1969). Discrimination intervals for percentiles in regression. *J. Am. Stat. Assoc.* 64, 1031–1041. doi:10.1080/01621459.1969.10501034

Edson, J. B., Jampana, V., Weller, R. A., Bigorre, S. P., Plueddemann, A. J., Fairall, C. W., et al. (2013). On the exchange of momentum over the open ocean. *J. Phys. Oceanogr.* 43, 1589–1610. doi:10.1175/JPO-D-12-0173.1

Elder, C. D., Xu, X., Walker, J., Schnell, J. L., Hinkel, K. M., Townsend-Small, A., et al. (2018). Greenhouse gas emissions from diverse Arctic Alaskan lakes are dominated by young carbon. *Nat. Clim. Chang.* 8, 166–171. doi:10.1038/s41558-017-0066-9

Elder, C. D., Schweiger, M., Lam, B., Crook, E. D., Xu, X., Walker, J., et al. (2019). Seasonal sources of whole-lake CH_4 and CO_2 emissions from interior alaskan thermokarst lakes. *J. Geophys. Res. Biogeosci.* 124, 1209–1229. doi:10.1029/2018jg004735

Elder, C. D., Thompson, D. R., Thorpe, A. K., Hanke, P., Anthony, K. M. W., and Miller, C. E. (2020). Airborne mapping reveals emergent power law of arctic methane emissions. *Geophys. Res. Lett.* 47, e2019GL085707. doi:10.1029/2019gl085707

Emerson, S., and Bushinsky, S. (2016). The role of bubbles during air-sea gas exchange. *J. Geophys. Res. Oceans* 121, 4360–4376. doi:10.1002/2016JC011744

Erickson, D. J., III. (1993). A stability-dependent theory for air-sea gas exchange. *J. Geophys. Res.* 98, 8471–8488. doi:10.1029/93jc00039

Esters, L., Landwehr, S., Sutherland, G., Bell, T. G., Christensen, K. H., Saltzman, E. S., et al. (2017). Parameterizing air-sea gas transfer velocity with dissipation. *J. Geophys. Res. Oceans* 122, 3041–3056. doi:10.1002/2016JC012088

Eugster, W., DelSontro, T., Shaver, G. R., and Kling, G. W. (2020a). Interannual, summer, and diel variability of CH_4 and CO_2 effluxes from Toolik Lake, Alaska, during the ice-free periods 2010–2015. *Environ. Sci. Process. Impacts* 22, 2181–2198. doi:10.1039/d0em00125b

Eugster, W., Kling, G. W., Jonas, T., McFadden, T., Weust, A., MacIntyre, S., et al. (2003). CO_2 exchange between air and water in an arctic Alaskan and mid-latitude Swiss lake: The importance of convective mixing. 108 (D12), 4362. doi:10.1029/2002JD002653

Eugster, W., Kling, G., and Laundre, J. (2020b). Turbulence and flux data from eddy flux platform on Toolik Lake, Alaska 2009-2015. ver 1. Environmental data initiative. Available at: https://doi.org/10.6073/pasta/919cd028d73ef4f8427d951148f974ec (Accessed August 19, 2022).

Fredriksson, S. T., Arneborg, L., Nilsson, H., Zhang, Q., and Handler, R. A. (2016). An evaluation of gas transfer velocity parameterizations during natural convection using DNS. *J. Geophys. Res. Oceans* 121, 1400–1423. doi:10.1002/2015JC011112

Frost, T., and Upstill-Goddard, R. C. (2002). Meteorological controls of gas exchange at a small English lake. *Limnol. Oceanogr.* 47, 1165–1174. doi:10.4319/lo.2002.47.4.1165

Garbe, C. S., Rutgersson, A., Boutin, J., de Leeuw, G., Delille, B., Fairall, C. W., et al. (2014). "Transfer across the air-sea interface," in *Ocean-atmosphere interactions of gases and particles*. Editors P. S. Liss and M. T. Johnson (Springer Earth System Sciences). doi:10.1007/978-3-642-25643-1_2

Garies, J. A. L., and Lesack, L. F. W. (2020). Ice-out and freshet fluxes of CO_2 and CH_4 across the air–water interface of the channel network of a great Arctic delta, the Mackenzie. *Polar Res.* 39, 3528. doi:10.33265/polar.v39.3528

Goddijn-Murphy, L., Woolf, D. K., Callaghan, A. H., Nightingale, P. D., and Shutler, J. D. (2016). A reconciliation of empirical and mechanistic models of the air-sea gas transfer velocity. *J. Geophys. Res. Oceans* 121, 818–835. doi:10.1002/2015JC011096

Guérin, F., Abril, G., Serça, D., Delon, C., Richard, S., Delmas, R., et al. (2007) Gas transfer velocities of CO_2 and CH_4 in a tropical reservoir and its river downstream. *J. Mar. Syst.* 66, 161–172. doi:10.1016/j.jmarsys.2006.03.019

Harrison, E. L., Veron, F., Ho, D. T., Reid, M. C., Orton, P., and McGillis, W. R. (2012). Nonlinear interaction between rain- and wind-induced air-water gas exchange. *J. Geophys. Res.* 117, C03034. doi:10.1029/2011JC007693

Hasse, L., and Isemer, H. J. (1986). Annual migration of the North Atlantic zero heat flux line. *Naturwissenschaften* 73, 550–551. doi:10.1007/bf00368163

Heiskanen, J. J., Mammarella, I., Haapanala, S., Pumpanen, J., Vesala, T., MacIntyre, S., et al. (2014). Effects of cooling and internal wave motions on gas transfer coefficients in a boreal lake. *Tellus B Chem. Phys. Meteorology* 66 (1), 22827. doi:10.3402/tellusb.v66.22827

Ho, D., Law, C. S., Smith, M. J., Schlosser, P., Harvey, M., and Hill, P. (2006). Measurements of air–sea gas exchange at high wind speeds in the Southern Ocean: Implications for global parameterizations. *Geophys. Res. Lett.* 33, L16611. doi:10.1029/2006GL026817

Ho, D. T., Zappa, C. J., McGillis, W. R., Bliven, L. F., Ward, B., Dacey, J. W. H., et al. (2004). Influence of rain on air-sea gas exchange: Lessons from a model ocean. *J. Geophys. Res.* 109, C08S18. doi:10.1029/2003JC001806

Hobbie, J. E., and Kling, G. W. (Editors) (2014). *Alaska's changing arctic: Ecological consequences for tundra, streams, and lakes* (New York, USA: Oxford University Press), 331~pp.

Imberger, J. (1985). The diurnal mixed layer1. *Limnol. Oceanogr.* 30, 737–770. doi:10.4319/lo.1985.30.4.0737

IPCC AR6 WGI (2021). *Climate change 2021: The physical science basis*. Intergovernmental Panel on Climate Change IPCC. Cambridge, United Kingdom: Cambridge University Press, 3949pp. doi:10.1017/9781009157896

Jahne, B., and Monahan, E. C. (Editors) (1995). *Air-water gas transfer: Selected papers from the third international symposium on air-water gas transfer* (Hanau, Germany: Aeon Verlag), 900.

Jiménez, P. A., and Dudhia, J. (2018). On the need to modify the sea surface roughness formulation over shallow waters. *J. Appl. Meteorol. Climatol.* 57, 1101–1110. doi:10.1175/JAMC-D-17-0137.1

Johnson, M. T., Hughes, C., Bell, T. G., and Liss, P. S. (2011). "A Rumsfeldian analysis of uncertainty in air–sea gas exchange,". *Gas transfer at water surfaces*. Editors S. Komori, W. McGillis, and R. Kurose (Kyoto University Press), 464–485.

Klaus, M., and Vachon, D. (2020). Challenges of predicting gas transfer velocity from wind measurements over global lakes. *Aquat. Sci.* 82 (53), 53–17. doi:10.1007/s00027-020-00729-9

Kling, G. W., Adams, H. E., Bettez, N. D., Bowden, W. B., Crump, B. C., Giblin, A. E., et al. (2014). "Land-water interactions,". *A changing arctic: Ecological consequences for tundra, streams, and lakes*. Editors J. E. Hobbie and G. W. Kling (Oxford University Press), 143–172.

Kling, G. W., Kipphut, G. W., and Miller, M. C. (1991). Arctic lakes and streams as gas conduits to the atmosphere: Implications for tundra carbon budgets. *Science* 251, 298–301. doi:10.1126/science.251.4991.298

Kling, G. W., Kipphut, G. W., and Miller, M. C. (1992). The flux of CO_2 and CH_4 from lakes and rivers in arctic Alaska. *Hydrobiologia* 240, 23–36. doi:10.1007/bf00013449

Kling, G. W., Kipphut, G. W., Miller, M. C., and O'Brien, W. J. (2000). Integration of lakes and streams in a landscape perspective: The importance of material processing on spatial patterns and temporal coherence. *Freshw. Biol.* 43, 477–497. doi:10.1046/j.1365-2427.2000.00515.x

Krogh, A. (1910). Some experiments on the invasion of oxygen and carbonic oxide into Water[1]. *Skand. Arch. Fur Physiol.* 23, 224–235. doi:10.1111/j.1748-1716.1910.tb00599.x

Legendre, P., and Legendre, L. (1998). *Numerical ecology*. Amsterdam: Elsevier, 853~pp.

Lejeune, M. G., and Sarda, P. (1988). Quantile regression: A nonparametric approach. *Comput. Statistics Data Analysis* 6, 229–239. doi:10.1016/0167-9473(88)90003-5

Lewkowicz, A. G., and Way, R. G. (2019). Extremes of summer climate trigger thousands of thermokarst landslides in a High Arctic environment. *Nat. Commun.* 10, 1329. doi:10.1038/s41467-019-09314-7

Liss, P. S., and Merlivat, L. (1986). "Air–sea gas exchange rates: Introduction and synthesis," in *The role of air–sea exchange in geochemical cycling*. Editor P. Buat-Ménard (Dordrecht, Holland: D. Reidel), 113–127.

Liss, P., and Slater, P. (1974). Flux of gases across the air-sea interface. *Nature* 247, 181–184. doi:10.1038/247181a0

MacIntyre, S., Eugster, W., and Kling, G. W. (2001). "The critical importance of buoyancy flux for gas flux across the air-water interface," in *Gas transfer at water surfaces*. Editors M. A. Donelan, W. M. Drennan, E. S. Saltzman, and R. Wanninkhof (American Geophysical Union).

MacIntyre, S., Jonsson, A., Jansson, M., Aberg, J., Turney, D. E., and Miller, S. D. (2010). Buoyancy flux, turbulence, and the gas transfer coefficient in a stratified lake. *Geophys. Res. Lett.* 37, L24604. doi:10.1029/2010GL044164

Markfort, C. D., Perez, A. L. S., Thill, J. W., Jaster, D. A., Porté-Agel, G., and Stefan, H. G. (2010). Wind sheltering of a lake by a tree canopy or bluff topography. *Water Resour. Res.* 46, W03530. doi:10.1029/2009WR007759

McGuire, A. D., Anderson, L. G., Christensen, T. R., Dallimore, S., Guo, L., Hayes, D. J., et al. (2009). Sensitivity of the carbon cycle in the Arctic to climate change. *Ecol. Monogr.* 79, 523–555. doi:10.1890/08-2025.1

Mesarchaki, E., Kräuter, C., Krall, K. E., Bopp, M., Helleis, F., Williams, J., et al. (2015). Measuring air–sea gas-exchange velocities in a large-scale annular wind–wave tank. *Ocean Sci.* 11, 121–138. doi:10.5194/os-11-121-2015

Miller, M. C., Spatt, P., Westlake, P., Yeakel, D., and Hater, G. R. (1986). Primary production and its control in Toolik lake, Alaska. *Arch. Hydrobiol. Suppl.* 74, 97–131.

Munk, W. H. (1947). A critical wind speed for air–sea boundary processes. *J. Mar. Res.* 6, 203–218. Available at: https://images.peabody.yale.edu/publications/jmr/jmr06-03-04.pdf.

Patel, D. (2021). "Quantile regression support vector machine (QRSVM) model for time series data analysis," in *Soft computing and its engineering applications* (Springer Singapore). doi:10.1007/978-981-16-0708-0_6

Pohlert, T. (2020) trend: Non-Parametric trend tests and change-point detection. R package version 1.1.4.

R Core Team (2014). R: A language *and environment for statistical computing*. Vienna, Austria.

Read, J. S., Hamilton, D. P., Desai, A. R., Rose, K. C., MacIntyre, S., Lenters, J. D., et al. (2012). Lake-size dependency of wind shear and convection as controls on gas exchange. *Geophys. Res. Lett.* 39, L09405. doi:10.1029/2012gl051886

Riordan, B., Verbyla, D., and McGuire, A. D. (2006). Shrinking ponds in subarctic Alaska based on 1950–2002 remotely sensed images. *J. Geophys. Res.* 111, G04002. doi:10.1029/2005jg000150

Robinson, S. I., O'Gorman, E. J., Frey, B., Hagner, M., and Mikola, J. (2022). Soil organic matter, rather than temperature, determines the structure and functioning of subarctic decomposer communities. *Glob. Change Biol.* 28, 3929–3943. doi:10.1111/gcb.16158

Rosentreter, J. A., Maher, D. T., Ho, D. T., Call, M., Barr, J. G., and Eyre, B. D. (2017). Spatial and temporal variability of CO_2 and CH_4 gas transfer velocities and quantification of the CH_4 microbubble flux in mangrove dominated estuaries. *Limnol. Oceanogr.* 62, 561–578. doi:10.1002/lno.10444

Schuur, E. A. G., McGuire, A. D., Schädel, C., Grosse, G., Harden, J. W., Hayes, D. J., et al. (2015). Climate change and the permafrost carbon feedback. *Nature* 520, 171–179. doi:10.1038/nature14338

Sen, P. K. (1968). Estimates of the regression coefficient based on kendall's tau. *J. Am. Stat. Assoc.* 63, 1379–1389. doi:10.1080/01621459.1968.10480934

Shaver, G. (2016). Hourly weather data from the Arctic LTER Moist Acidic Tussock Experimental plots from 1990 to 1999, Toolik Field Station, North Slope, Alaska. ver 5. Environmental data initiative. Available at: https://doi.org/10.6073/pasta/431942c31aad96a5d0314939d68e2421 (Accessed August 19, 2022).

Stull, R. B. (1988). *An introduction to boundary layer meteorology*. Dordrecht: Kluwer Academic Publishers, 670.

Sullivan, P., Banner, M. L., Morison, R. P., and Peirson, W. (2018). Turbulent flow over steep steady and unsteady waves under strong wind forcing. *J. Phys. Oceanogr.* 48, 3–27. doi:10.1175/JPO-D-17-0118.1

Tan, Z., and Zhuang, Q. (2015). Arctic lakes are continuous methane sources to the atmosphere under warming conditions. *Environ. Res. Lett.* 10, 054016. doi:10.1088/1748-9326/10/5/054016

Taylor, P. K., and Yelland, M. J. (2001). The dependence of sea surface roughness on the height and steepness of the waves. *J. Phys. Oceanogr.* 31, 572–590. doi:10.1175/1520-0485(2001)031<0572:tdossr>2.0.co;2

Turetsky, M. R., Abbott, B. W., Jones, M. C., Anthony, K. W., Olefeldt, D., Schuur, E. A. G., et al. (2020). Carbon release through abrupt permafrost thaw. *Nat. Geosci.* 13, 138–143. doi:10.1038/s41561-019-0526-0

Vonk, J. E., Tank, S. E., Mann, P. J., Spencer, R. G. M., Treat, C. C., Striegl, R. G., et al. (2015). Biodegradability of dissolved organic carbon in permafrost soils and

aquatic systems: A meta-analysis. *Biogeosciences* 12, 6915–6930. doi:10.5194/bg-12-6915-2015

Wanninkhof, R., Asher, W. E., Ho, D. T., Sweeney, C., and McGillis, W. R. (2009). Advances in quantifying air-sea gas exchange and environmental forcing. *Ann. Rev. Mar. Sci.* 1, 213–244. doi:10.1146/annurev.marine.010908.163742

Wanninkhof, R., and Triñanes, J. (2017). The impact of changing wind speeds on gas transfer and its effect on global air-sea CO_2 fluxes. *Glob. Biogeochem. Cycles* 31, 961–974. doi:10.1002/2016GB005592

Wild, M., Gilgen, H., Roesch, A., Ohmura, A., Long, C. N., Dutton, E. G., et al. (2005). From dimming to brightening: Decadal changes in solar radiation at earth's surface. *Science* 308, 847–850. doi:10.1126/science.1103215

Wild, M., Roesch, A., and Ammann, C. (2012). Global dimming and brightening – evidence and agricultural implications. *Cab. Rev.* 7, 1–7. doi:10.1079/PAVSNNR20127003

Woolf, D., and Thorpe, S. (1991). Bubbles and the air-sea exchange of gases in near-saturation conditions. *J. Mar. Res.* 49, 435–466. doi:10.1357/002224091784995765

Wu, H., Peng, C., Lucotte, M., Soumis, N., Ge´linas, Y., Duchemin, E., et al. (2013). A coupled two-dimensional hydrodynamic and terrestrial input model to simulate CO_2 diffusive emissions from lake systems. *Geosci. Model Dev. Discuss.* 6, 3509–3556. doi:10.5194/gmdd-6-3509-2013

Yang, M., Smyth, T. J., Kitidis, V., Brown, I. J., Wohl, C., Yelland, M. J., et al. (2021). Natural variability in air–sea gas transfer efficiency of CO_2. *Sci. Rep.* 11, 13584. doi:10.1038/s41598-021-92947-w

Zappa, C. J., McGillis, W. R., Raymond, P. A., Edson, J. B., Hintsa, E. J., Zemmelink, H. J., et al. (2007). Environmental turbulent mixing controls on air-water gas exchange in marine and aquatic systems. *Geophys. Res. Lett.* 34, L10601. doi:10.1029/2006gl028790

frontiers | Frontiers in Environmental Science

TYPE Original Research
PUBLISHED 20 September 2022
DOI 10.3389/fenvs.2022.833688

Check for updates

OPEN ACCESS

EDITED BY
Laodong Guo,
University of Wisconsin–Milwaukee,
United States

REVIEWED BY
Mark Alexander Lever,
ETH Zürich, Switzerland
Guangbin Zhang,
Institute of Soil Science (CAS), China

*CORRESPONDENCE
Shoji D. Thottathil,
shoji.thottathil@gmail.com

†PRESENT ADDRESS
Paula C. J. Reis,
Institut National de la Recherche Scientifique—Eau Terre Environnement,
Québec City, Canada

‡These authors have contributed equally to this work and share first authorship

SPECIALTY SECTION
This article was submitted to Biogeochemical Dynamics, a section of the journal Frontiers in Environmental Science

RECEIVED 12 December 2021
ACCEPTED 06 September 2022
PUBLISHED 20 September 2022

CITATION
Thottathil SD, Reis PCJ and Prairie YT (2022), Variability and controls of stable carbon isotopic fractionation during aerobic methane oxidation in temperate lakes.
Front. Environ. Sci. 10:833688.
doi: 10.3389/fenvs.2022.833688

COPYRIGHT
© 2022 Thottathil, Reis and Prairie. This is an open-access article distributed under the terms of the Creative Commons Attribution License (CC BY). The use, distribution or reproduction in other forums is permitted, provided the original author(s) and the copyright owner(s) are credited and that the original publication in this journal is cited, in accordance with accepted academic practice. No use, distribution or reproduction is permitted which does not comply with these terms.

Variability and controls of stable carbon isotopic fractionation during aerobic methane oxidation in temperate lakes

Shoji D. Thottathil[1]*‡, Paula C. J. Reis[2†‡] and Yves T. Prairie[2]

[1]Department of Environmental Science, School of Engineering and Sciences, SRM University-AP, Amaravati, Andhra Pradesh, India, [2]Groupe de Recherche Interuniversitaire en Limnologie, Département des Sciences Biologiques, Université du Québec à Montréal, Montréal, QC, Canada

The aerobic oxidation of methane (CH_4) by methanotrophic bacteria (MOB) is the major sink of this highly potent greenhouse gas in freshwater environments. Yet, CH_4 oxidation is one of the largest uncertain components in predicting the current and future CH_4 emissions from these systems. While stable carbon isotopic mass balance is a powerful approach to estimate the extent of CH_4 oxidation *in situ*, its applicability is constrained by the need of a reliable isotopic fractionation factor (α_{ox}), which depicts the slower reaction of the heavier stable isotope (^{13}C) during CH_4 oxidation. Here we explored the natural variability and the controls of α_{ox} across the water column of six temperate lakes using experimental incubation of unamended water samples at different temperatures. We found a large variability of α_{ox} (1.004–1.038) with a systematic increase from the surface to the deep layers of lake water columns. Moreover, α_{ox} was strongly positively coupled to the abundance of MOB in the γ-proteobacteria class (γ-MOB), which in turn correlated to the concentrations of oxygen and CH_4, and to the rates of CH_4 oxidation. To enable the applicability in future isotopic mass balance studies, we further developed a general model to predict α_{ox} using routinely measured limnological variables. By applying this model to $\delta^{13}C$-CH_4 profiles obtained from the study lakes, we show that using a constant α_{ox} value in isotopic mass balances can largely misrepresent and undermine patterns of the extent of CH_4 oxidation in lakes. Our α_{ox} model thus contributes towards more reliable estimations of stable carbon isotope-based quantification of CH_4 oxidation and may help to elucidate large scale patterns and drivers of the oxidation-driven mitigation of CH_4 emission from lakes.

KEYWORDS

methane, aerobic oxidation, isotopic mass balance, fractionation factor, lakes

Introduction

Freshwater aquatic systems are important sources of methane (CH_4)—a highly potent greenhouse gas—to the atmosphere (Bastviken et al., 2011; Saunois et al., 2016). However, large uncertainties exist in the estimates of global inland water CH_4 emissions, partly due to the lack of a clear understanding on the various processes driving CH_4 saturation and emission in aquatic environments. Aerobic methane oxidation (MOX), for example, plays a central role in regulating the global CH_4 budget by biologically mitigating CH_4 emissions from various natural (e.g., wetlands, rivers, lakes, and ocean) and anthropogenic (e.g., rice paddy fields, landfills) sources (King, 1992; Guérin and Abril, 2007; Reeburgh, 2007; Bastviken et al., 2008; Chanton et al., 2009; Chanton et al., 2011; Serrano-Silva et al., 2014; Cai et al., 2016; Sawakuchi et al., 2016; Li et al., 2022). Despite its pivotal role in controlling CH_4 emissions, accurate quantification of MOX is constrained methodologically and often represents one of the largest uncertain components in the budgets of various CH_4 sources. While experimental incubations of isolated samples (soil, sediment, or water) and tracking the decrease in CH_4 concentration over time is the most often used method, *in situ* estimations based on the stable isotopic composition of CH_4 offers a non-invasive whole-ecosystem technique to estimate the extent of CH_4 oxidation (Happell et al., 1994; Tyler et al., 1997; Liptay et al., 1998; Bastviken et al., 2002; Chanton et al., 2008; Chanton et al., 2011; Zhang et al., 2012; Preuss et al., 2013; Sawakuchi et al., 2016; Gebert and Streese-Kleeberg, 2017; Sparrow et al., 2019; Komiya et al., 2020; Bakkaloglu et al., 2021).

The stable carbon isotopic signature of CH_4 ($\delta^{13}C\text{-}CH_4$) is extensively used for isotopic mass balance-based oxidation estimations. This approach relies on the behaviour of the two stable carbon isotopes (^{12}C and ^{13}C) in terms of mass, steric properties, and diffusion rates leading to unequal behaviour in the rates of transport and at the enzyme bonding sites of CH_4-oxidizing bacteria (MOB or methanotrophic bacteria). As a result of the slightly faster diffusion and oxidation of ^{12}C, the residual CH_4 pool gets enriched in ^{13}C (Barker and Fritz, 1981; Jahnke et al., 1999; Whiticar, 1999; De Visscher et al., 2004; Templeton et al., 2006; Gebert and Streese-Kleeberg, 2017). From the shift in the $\delta^{13}C$ signature of CH_4 at the point of sampling ($\delta^{13}C\text{-}CH_{4\text{-}sample}$) relative to the anoxic source ($\delta^{13}C\text{-}CH_{4\text{-}source}$), the fraction of CH_4 oxidized (f_{ox}) can be estimated using either open system models at steady state (Happell et al., 1994; Tyler et al., 1997) or non-steady state Rayleigh model for closed systems (Liptay et al., 1998).

Due to the slightly faster uptake of ^{12}C relative to ^{13}C by MOB, the first order rate constant (k) of the oxidation of $^{12}CH_4$ is greater than that of $^{13}CH_4$; therefore, the ratio of $^{12}k/^{13}k$ represents the isotopic fractionation factor (α_{ox}). In practice, the α_{ox} is determined from the incubation of samples at a desired temperature, with or without CH_4 amendments (Chanton and Liptay, 2000; Börjesson et al., 2001; Bastviken et al., 2002; Börjesson et al., 2007; Chanton et al., 2008; Aghdam et al., 2018; Obersky et al., 2018; Sparrow et al., 2019; Fjelsted et al., 2020; but *see* Gebert and Streese-Kleeberg, 2017). From the concomitant change in the concentration ($[CH_4]$) and stable isotopic signature ($\delta^{13}C\text{-}CH_4$) of CH_4 during the incubation, the fractionation factor α_{ox} can be derived from the slope (β) of the regression between ln $[CH_4]$ and ln ($\delta^{13}C\text{-}CH_4$ + 1000) (approximate Rayleigh approach, Mahieu et al., 2006) as:

$$\propto_{ox} = \frac{\beta}{1+\beta} \quad (1)$$

While the isotopic method is a simple and powerful tool to estimate CH_4 oxidation *in situ*, an accurate α_{ox} value associated with oxidation in the given ecosystem is important in ensuring reliable estimations of the amount of CH_4 consumed by methanotrophy. The use of inaccurate α_{ox} can induce large differences in the f_{ox} estimate (see, Cabral et al., 2010; Capanema and Cabral, 2012; Gebert and Streese-Kleeberg, 2017). It is thus critical to use suitable fractionation factors that are appropriate for each environment or for each place and time within a system.

Even though α_{ox} is often used as a constant, experimentally determined stable carbon isotopic fractionation factors for methanotrophic bacterial cultures and various terrestrial and aquatic environments together vary widely (1.003–1.049; Coleman et al., 1981, Bergamaschi et al., 1998, Bastviken et al., 2002, Venkiteswaran and Schiff, 2005, Chanton et al., 2008, Templeton et al., 2006; Gebert and Streese-kleeberg, 2017; Aghdam et al., 2018; Obersky et al., 2018; Sparrow et al., 2019; Fjelsted et al., 2020; Bakkaloglu et al., 2021). This large variability of α_{ox} across environments can be attributed to diverse mechanisms; from the supply of CH_4 to the oxidizing zone to the rate of enzyme-catalysed oxidation of CH_4 by MOB. In an environment with abundant CH_4 supply, the irreversible conversion of dissolved CH_4 to the cellular carbon pool of MOB controls the isotopic fractionation—a process dependent on the diffusion and dissolution of CH_4 in the system, enzyme activity of the MOB, and the rate of CH_4 oxidation (Templeton et al., 2006). Since the above factors can be regulated by a variety of environmental conditions such as temperature, production and diffusion of CH_4 to oxidation zone, and MOB cell abundance, strong links between these variables and α_{ox} are expected. For example, an inverse relationship between temperature and α_{ox} is often observed for the forests and landfill soil environments (Tyler et al., 1994; Jahnke et al., 1999; Chanton and Liptay, 2000; Chanton et al., 2008; Nihous et al., 2010; Gebert and Streese-Kleeberg, 2017). The underlying mechanism behind such a pattern is suggested to be the increased oxidation rate at elevated temperature resulting in little fractionation, while low MOX rate is associated with greater discrimination of ^{13}C. However, it should be also noted that an

increase of α_{ox} with temperature was observed in enriched methanotrophic bacterial cultures (Coleman et al., 1981), which was supported by field estimates in the Alaskan soils (King et al., 1989) and European landfills (Bergamaschi et al., 1998). Furthermore, temperature response of α_{ox} is highly inconsistent in aquatic environments; from a complete absence of temperature effect in large lakes and reservoirs (Bastviken et al., 2002; Venkiteswaran and Schiff, 2005) to an inverse relationship between temperature for a small temperate lake (Venkiteswaran and Schiff, 2005). These inconsistent temperature responses in various environments suggest that there may be factors other than MOX rates at play to regulate α_{ox} variability. Experimental studies in terrestrial systems and/or methanotrophic bacterial cultures have shown that in addition to MOX rates, α_{ox} is dependent on the availability of CH_4 and oxygen (O_2), and the abundance of MOB (Börjesson et al., 2001; Templeton et al., 2006; Chanton et al., 2008; Gebert and Streese-Kleeberg, 2017).

Despite the long-recognised potential of isotopic mass balance in estimating CH4 oxidation in lakes (Bastviken et al., 2002), this approach is not extensively used in freshwater systems compared to terrestrial environments such as forest soils, landfills, and rice paddy fields. The number of $\delta^{13}C$-CH_4 measurements has been increasing recently to derive greater insights on aquatic CH_4 dynamics (Schubert et al., 2010; Blees et al., 2014; Rinta et al., 2015; Morana et al., 2015; Cadieux et al., 2016; Begum et al., 2021). Yet, only very few studies have derived the extent of CH_4 oxidation based on isotopic data (Kankaala et al., 2007; Itoh et al., 2015; Thottathil et al., 2018; Grasset et al., 2020; Soued and Prairie, 2022) and studies that experimentally determined αox are even lesser (Bastviken et al., 2002; Venkiteswaran and Schiff, 2005; Itoh et al., 2015). Nevertheless, these studies showed variable α_{ox} values for lakes and reservoirs; between 1.018 and 1.021 for three Swedish boreal lakes (Bastviken et al., 2002), between 1.019 and 1.021 in a small temperate pond, 1.013–1.014 in temperate reservoirs (Venkiteswaran and Schiff, 2005), and 1.010 in a subtropical reservoir (Itoh et al., 2017). Since the number of αox estimates are limited in lakes, knowledge of the natural variability and environmental control of α_{ox} in these ecosystems is critically lacking. Methanotrophy in lakes is controlled by a suite of environmental factors including temperature, pH, total phosphorus (TP), total nitrogen (TN), and dissolved organic carbon (DOC) through regulating MOB population, supply of substrates (CH_4 and O_2), and by affecting water column light attenuation (Crevecoeur et al., 2019; Thottathil et al., 2019; Guggenheim et al., 2020; Reis et al., 2020; Sawakuchi et al., 2021; Kashi et al., 2022; Nijman et al., 2022). As response to these multiple environmental factors, MOX rates in freshwater lakes vary widely (Bastviken et al., 2002; Bastviken et al., 2008; Thottathil et al., 2019; Denfeld et al., 2016; Sawakuchi et al., 2021; D'Ambrosio and Harrison, 2021). However, whether α_{ox} values equally vary along with the MOX rates and/or how multiple environmental factors simultaneously shape the isotopic fractionation during CH_4 oxidation in highly dynamic environments such as freshwater lakes remain elusive.

Here, we explicitly examine the variability and controls of stable carbon isotopic fractionation during aerobic CH_4 oxidation in temperate lakes. Given the wide variability of MOX rate, we hypothesize that, 1) the inter- and intra-lake variability of α_{ox} can be large in the stratified water column of lakes, and 2) the environmental variables relevant in shaping the rate of CH_4 oxidation and MOB abundance (e.g., temperature, pH, and concentrations of CH_4, O_2, nutrients, and DOC), are also relevant in regulating isotopic fractionation factor. To test these hypotheses, we conducted extensive incubation experiments with unamended lake water samples obtained from the stratified water column of six Canadian Shield lakes in southeastern Quebec during the summer stratification period. Using this unique dataset, we show that α_{ox} variability in freshwater lakes is large and comparable to the variability observed in terrestrial environments and is modulated by the abundance of a specific MOB group as well as by the rates of CH_4 oxidation, which are in turn regulated by a suite of environmental factors. Furthermore, we developed an empirical model using routinely measured limnological variables that can be used to estimate α_{ox} in a wide range of freshwater environments. Finally, we show that CH_4 oxidation extent in lakes can be significantly misrepresented at both seasonal and spatial scales if the variability of α_{ox} is poorly constrained.

Materials and methods

Study area and sampling strategy

We sampled six northern temperate lakes of variable morphometry (surface area: 0.008–0.44 km^2; maximum depth: 4.3–20.3 m) during the summer stratification period (June to October) of 2016. Details on the limnological features of study lakes, sampling strategy, and experimental setups were given elsewhere (Thottathil et al., 2019; Reis et al., 2020). In each study lake, a single station was sampled onboard a small aluminium boat anchored at the deepest point located based on the known bathymetry (https://crelaurentides.org/dossiers/eau-lacs/atlasdeslacs). We performed the water column profiling at 1 m interval for temperature, pH, and O_2 using a multiparameter probe (Yellow Spring Instruments, YSI; OH, United States). Along with the YSI-profiling, the water samples were collected for dissolved CH_4 measurements from discrete depths at 1 m intervals using a continuous flow submersible pump (Proactive Environmental Products, FL, United States) attached to the YSI. At each discrete depth, water was allowed to pump for more than 5 minutes before initiating the sampling for dissolved CH_4 using headspace equilibration method and the YSI was monitored continuously to ensure that pump was placed at the desired depth throughout the

sampling. For the headspace equilibration, a 60 ml syringe was connected to the pump outlet through a two-way luer-lock valve in such a way that water is directly transferred to the syringe without getting exposed to the air and subsequent degassing. After filling two 60 ml syringes, 30 ml water was removed and the equivalent volume of ultrapure zero air (Praxair Canada Inc., Canada) was transferred to the syringe from a small pressurized zero air tank through a needle (23 G1, Becton–Dickinson) injected through a rubber septum of the zero-air tank outlet. The headspace was equilibrated manually for 2 min by vigorous shaking and the equilibrated headspace gas was then transferred into 12-ml pre-evacuated exetainer vials (Labco Ltd., United Kingdom) using a needle. The water sample for the incubation experiment (~40 L) was collected in flexible cubitainers (VWR International, Canada) from two to three depths of the oxygenated layer of the water column of each lake using a submersible pump. The pump outlet was placed at the bottom of the cubitainers and filled slowly without bubbling and allowed to overflow for several minutes to replace the entire volume of the cubitainers and closed without trapping air bubbles. Except for the surface samples, the sampling depths for the incubation experiments were chosen differently in each lake due to large difference in total depth and the extent of stratification. Our sampling depths represented the surface mixed layer (surface), metalimnion (intermediate), and the deepest oxic waters in the hypolimnion or above the sediment (deep). This approach allowed us to cover a range of environmental conditions in terms of O_2 and CH_4 concentrations, as well as in terms of general water column chemistry (pH, TP, TN, and DOC) which are important drivers of the MOB community and CH_4 oxidation (Sawakuchi et al., 2016; Crevecoeur et al., 2019; Thottathil et al., 2019; Guggenheim et al., 2020; Reis et al., 2020; Sawakuchi et al., 2021; Kashi et al., 2022; Nijman et al., 2022).

From the depths chosen for incubation experiments, samples for TN and TP were collected in duplicates directly into acid washed (10% Hydrochloric acid) and oven-dried (at 200°C) 50 ml screwcap tubes. For DOC, water samples were first collected into 60 ml plastic syringes directly from the submersible pump outlet and subsequently filtered through a 0.45 µm syringe filters (Sarstedt AG & Co., Germany) into acid-washed 40 ml glass vials. The vials were sealed with plastic caps lined with Teflon and rubber septa. All samples were kept cold in the dark until analyses. Except for L. Triton and L. en Coeur, where the water column was weakly stratified and therefore only two depths (surface and deep) were sampled, in all other lakes three depths (surface, intermediate, and deep) were sampled for the experiment. Thus, a total of 16 samples were collected from six lakes for the experimental incubations.

Experimental setup

In the laboratory, water from the cubitainers were dispersed into thirty 500 ml glass flasks, allowed to overflow and plugged air-tight using silicon stoppers without trapping air bubbles. A set of ten flasks were placed in temperature-controlled incubators set at three different temperatures: surface samples were at 10, 20, and 25°C; intermediate and deep water samples were incubated at 5, 10, and 20°C. All experiments were performed using unamended lake water samples since the addition of CH_4 and/or O_2 may yield higher than actual fractionation effect (Templeton et al., 2006). The first time point sampling for concentration and the stable carbon isotopic signature of CH_4 ($\delta^{13}C\text{-}CH_4$) was collected after about 3 h of acclimatization period in the incubators and a total of three to five time point samplings were conducted for each set of incubation. In order to examine presence of O_2 in the incubation flasks for the aerobic oxidation, the concentration of O_2 was monitored in two out of ten incubation flasks using optical O_2 sensors spots and a fiber optic meter (PreSens GmbH, Regensburg, Germany). At each time point, two flasks were removed from the incubation system and two 30 ml sub-samples were withdrawn from each flask using 60 ml plastic syringes attached with a long needle to ensure that water was withdrawn from the bottom of the flask to avoid the contact of water with the air. The headspace (30 ml) was created by adding zero air into the syringes from a pressurized tank using a needle attached the luer-lock valve of the syringe and piercing through the rubber septa at the outlet of the regulated pressure valve. The headspace was equilibrated for 2 minutes by vigorous shaking and the equilibrated headspace was transferred into 12 ml pre-evacuated exetainer vials.

Measurement of CH_4 concentration, $\delta^{13}C\text{-}CH_4$ values, methanotrophic bacteria abundance, and environmental variables

The partial pressure and $\delta^{13}C$ signature of CH_4 in the headspace-equilibrated samples were measured using a Cavity Ring Down Spectrometer (CRDS) equipped with Small Sample Isotopic Module (SSIM, Picarro G2201-*i*, Picarro Inc., CA, United States). For high concentration samples (i.e., headspace concentration > 200 ppm), CH_4 concentration was first measured using gas chromatograph (GC) with a flame ionization detector (GC-2014, Shimadzu, Kyoto, Japan) then the isotopic measurements were performed after dilution using zero air *via* SSIM. The original pCH_4 in the water was calculated using the headspace ratio, incubation temperature, and temperature of the water in the syringe during equilibration using appropriate solubility constants (Yamamoto et al., 1976). The standard curve for $\delta^{13}C\text{-}CH_4$ signature was prepared using certified isotopic standards obtained from Isometric Instruments, Canada (Liso1: −66.5 ± 0.2‰, Tiso1: −38.3 ± 0.2‰, and Hiso1: −23.9 ± 0.2‰) and values are reported in delta (δ) notation expressed in ‰ relative to the standard Vienna Pee Dee Belemnite.

To estimate the abundance of MOB cells, 40 ml water samples collected at the start of the incubation were fixed

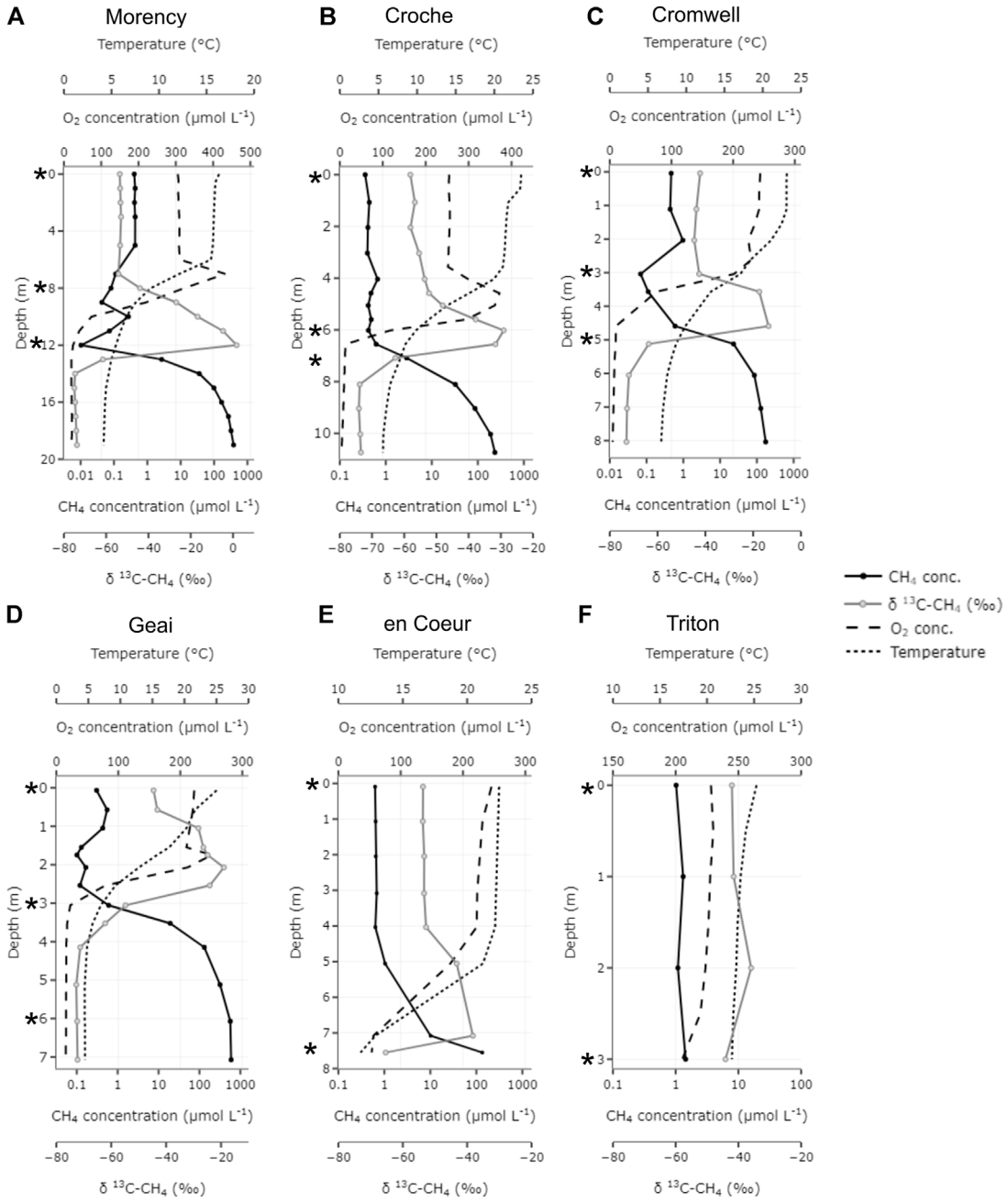


FIGURE 1
Vertical distribution of temperature, dissolved oxygen, methane concentration and stable carbon isotopic signature (^{13}C-CH_4) in each study lake **(A–F)**. Symbol (*) in the Y-axis panel indicate the sampling depths for experimental incubations.

with buffered paraformaldehyde and filtered through 0.2 µm polycarbonate filters (Millipore GTTP, 25 mm). The filters were kept frozen until microscopic analysis through Catalysed Reporter Deposition—Fluorescence *In Situ* Hybridization (CARD-FISH) with probes for aerobic MOB belonging to α- and γ-proteobacteria and epifluorescence microscopy (see Reis et al., 2020 for details). We used extensively applied CARD-FISH probes (Malpha450, Mgamma84, and Mgamma705) to detect MOB cells and the effectiveness of these probes for detecting α-MOB and γ-MOB cells were described previously (see Figure 1; and Supplementary Material in Reis et al., 2022).

The concentration of TP was measured after potassium persulfate digestion of unfiltered samples following ammonium molybdate colorimetric method (Wetzel and

Likens, 2000). For the measurement of TN, unfiltered samples were first digested using alkaline persulfate and analysed using a continuous flow analyser (ALPKEM Flow Solution 3100) equipped with a cadmium reactor (Patton and Kryskalla, 2003). The concentration of DOC was measured after sodium persulfate digestion of filtered water samples using a Total Organic Carbon analyzer (OI 1010, OI Analytical, TX, United States).

Calculations and statistical analyses

To estimate the kinetic isotopic fractionation during CH_4 oxidation, first we calculated the slope of the regression between ln [CH_4] and ln (δ^{13}C-CH_4 + 1000) for each incubation and then the fractionation factor (α_{ox}) was derived from the slope following Eq. 1 (*see* Introduction). This estimation is based on the "Simplified Rayleigh approach" recommended for incubation experiments using unamended and unlabelled CH_4 (Mahieu et al., 2006). In this approach, the range of CH_4 concentration has been shown to have a limited influence on the error of α_{ox}. Since our experiments are conducted over a large range of CH_4 concentrations, error associated with CH_4 concentrations will be minimal with the Simplified Rayleigh approach and therefore can be compared across the experiments. Moreover, this approximation of α_{ox} was shown to be superior to the Coleman method (Coleman et al., 1981) since its difference to the original Rayleigh method is relatively smaller (<0.05%) than that of the Coleman method (up to 5%).

Further, we explored the environmental control of α_{ox} using multiple regression analysis with Least Square Regression method. We used the incubation temperature, pH, concentrations of DOC, O_2, CH_4, TN, TP, cell abundance of α-MOB and γ-MOB, and MOX rates as candidate independent variables and only statistically significant variables were selected in the final model. The final environmental model was applied to the data collected in 2014 and 2015 in the same study lakes to explore the implications of our model on the seasonal and vertical variability of α_{ox} and the fraction of CH_4 oxidized (f_{ox}). First, we estimated the seasonality in f_{ox} in the surface layers of the study lakes using closed system model (Eq. 2).

$$\ln\ (1 - f_{ox}) = \frac{\left[\ln\left(\delta^{13}CH_{4source} + 1000\right) - \ln\left(\delta^{13}CH_{4sample} + 1000\right)\right]}{\propto_{ox} - 1} \quad (2)$$

where $\delta^{13}C\text{-}CH_{4sample}$ is the seasonal $\delta^{13}C\text{-}CH_4$ data obtained from our study lakes during May–November 2015 and $\delta^{13}C\text{-}CH_{4\text{-}source}$ is a fixed value for each lake. For the comparison, we used modelled α_{ox} along with a fixed value of 1.020 which is the average α_{ox} estimated in the previous studies for the northern lakes (Bastviken et al., 2002; Venkiteswaran and Schiff, 2005). Secondly, we estimated the vertical variability of α_{ox} using data obtained from three of our study lakes during the summer 2014.

We used Analysis of Variance (ANOVA) and Tukey's HSD (Honest Significant Difference) to explore the variations in the water chemistry, CH_4 concentrations, stable isotopic signature, and α_{ox} across depth zones. All the statistical analyses were performed with JMP® Pro software version 14.0 (SAS Institute, United States) and graphs were plotted using ggplot2 (v3.3.3), cowplot (v1.1.1) and plotly (v4.10.0) packages (Wickham, 2016; Wilke et al., 2019; Sievert, 2020) in R software (v4.0.4) or using Grapher™ (Golden Software LLC, United States).

Results

Environmental conditions, concentration and $\delta^{13}C$ signature of CH_4, and methanotrophic bacteria abundance

All sampling lakes, but L. Triton, were thermally stratified and the vertical distribution of CH_4 concentration and $\delta^{13}C\text{-}CH_4$ values were mirror images of each other with lowest CH_4 concentration and most enriched $\delta^{13}C\text{-}CH_4$ values coinciding in the metalimnion (Figure 1). Since we sampled the thermally stratified water column for the experiment, various chemical variables (pH, TN, TP, and DOC) at the beginning of the incubations varied largely across layers (Supplementary Figure S1). Similarly, the initial CH_4 concentration in the incubations varied widely with significant difference across depth zones; surface and intermediate layers showed a narrower range (0.27–0.59 and 0.06–0.36 μmol L^{-1}, respectively) than the deep layer (0.25–30.02 μmol L^{-1}; Figure 2A). While initial $\delta^{13}C\text{-}CH_4$ values showed a narrower range in the surface (−55.48‰ to −26.07‰) and deep layer (−55.79‰ to −26.76‰), the intermediate layer exhibited a much larger variability (−49.04‰ to −15.32‰) (Figure 2B). The abundance of α-MOB and γ-MOB at the start of each incubation also varied widely; the abundance of γ-MOB ranged from 1.05 × 10^2 to 8.11 × 10^4 cells ml^{-1} (average: 1.13 × 10^4 cells ml^{-1}) and α-MOB abundance ranged from 8.27 × 10^2 to 2.37 × 10^4 cells ml^{-1} (average: 6.93 × 10^3 cells ml^{-1}; Figures 2C,D). While the abundance of α-MOB was unrelated to the concentration of O_2 and only slightly related to the CH_4 concentrations, the abundance of γ-MOB increased with decreasing O_2 concentrations and positively correlated with CH_4 concentrations (Supplementary Figure S2). Furthermore, γ-MOB abundance was strongly positively and linearly correlated with TP (R^2 = 0.74, p < 0.0001) and TN (R^2 = 0.64, p < 0.0001), but unrelated to DOC (Supplementary Figure S3). On the other hand, abundance of α-MOB was not significantly linearly related to the above variables, except a weak positive

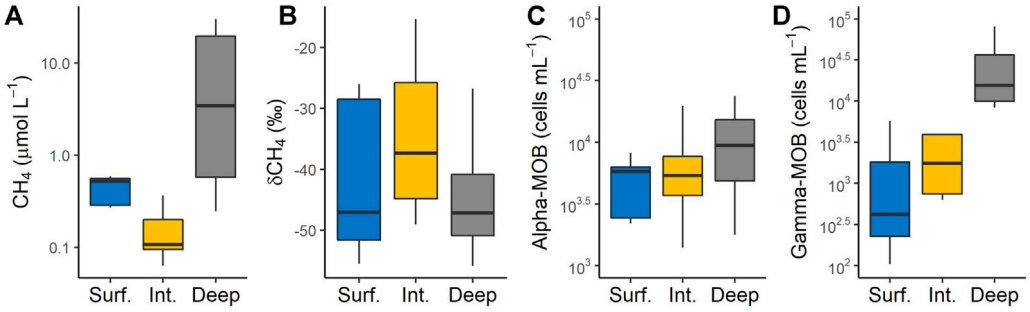


FIGURE 2
Variability of methane (CH_4) concentration **(A)**, stable carbon isotopic signature of CH_4 ($\delta^{13}C$-CH_4) **(B)**, abundance of α **(C)** and γ **(D)** groups of methanotrophic bacteria (α-MOB and γ-MOB, respectively) at the start of the incubation experiments across all study lakes. Surf., Surface layer; Inter., Intermediate layer; Deep, Deeper layer. The boxplots represent the median, first and third quartiles (hinges) and the 1.5 × interquartile range (whiskers).

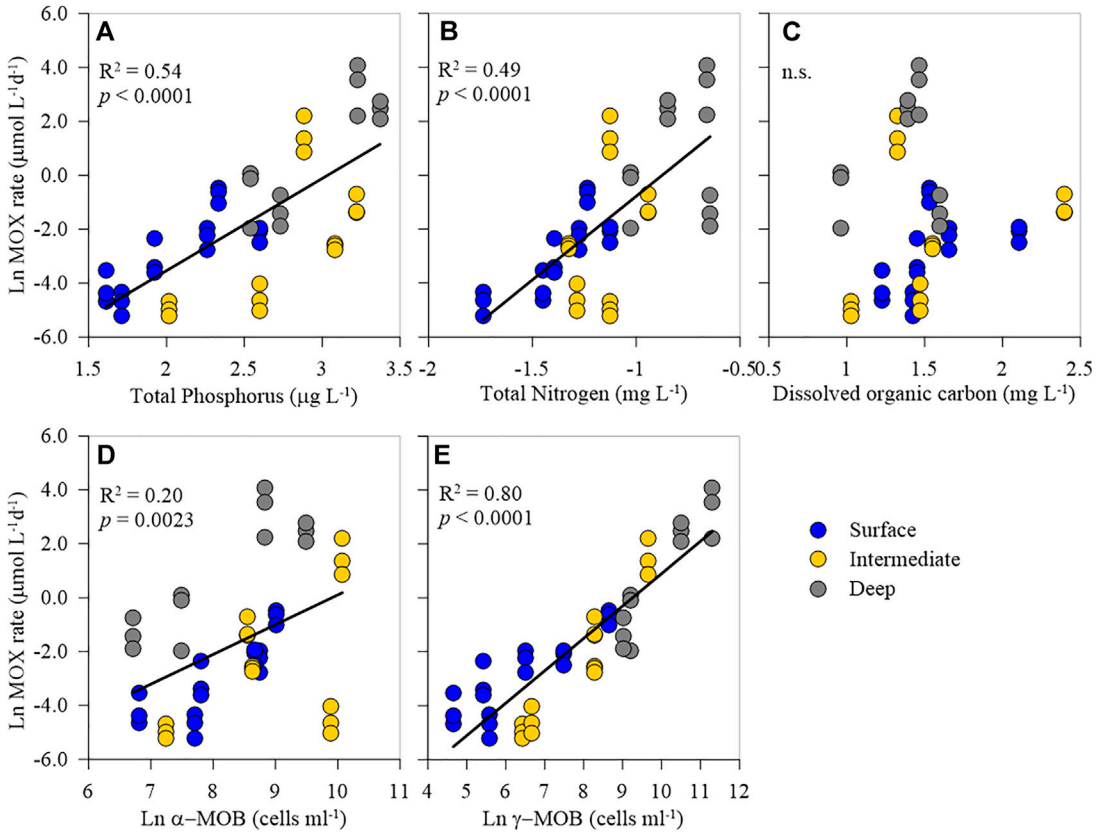


FIGURE 3
Relationships between methane oxidation rate (MOX) and total phosphorus **(A)**, total nitrogen **(B)**, dissolved organic carbon **(C)**, and abundance of α-MOB **(D)** and γ-MOB **(E)**.

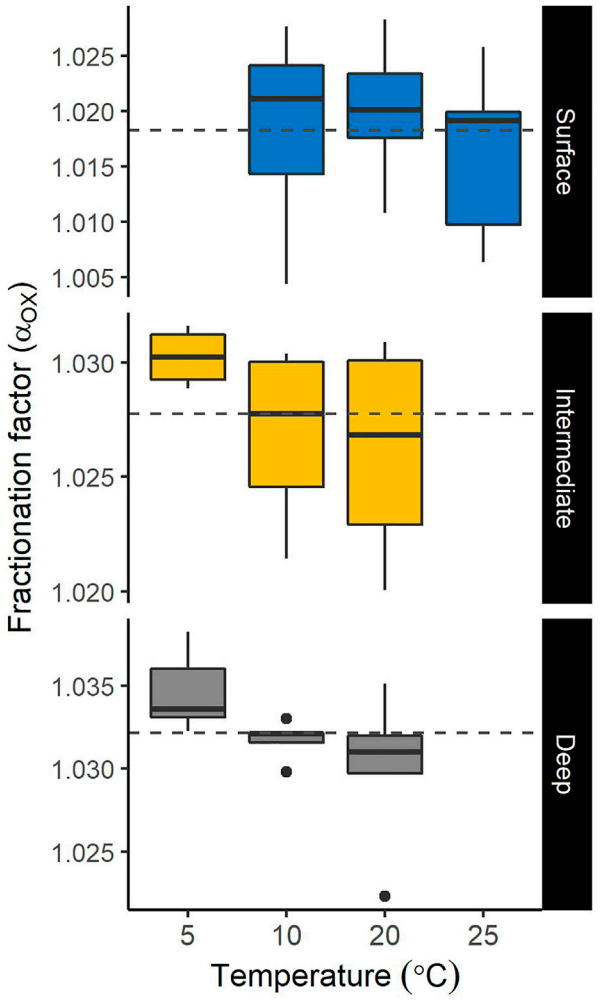


FIGURE 4
Variation of the isotopic fractionation factor (α_{ox}) during aerobic CH_4 oxidation across different layers and incubation temperatures in the study lakes. Note that α_{ox} estimations from all lakes are pooled for a given incubation temperature. Horizontal dashed lines represent the average for each layer across all incubation temperatures. The boxplots represent the median, first and third quartiles (hinges) and the 1.5 × interquartile range (whiskers).

correlation with TP (R^2 = 0.31, p < 0.0001; Supplementary Figure S3).

Methane oxidation rate and patterns of isotopic fractionation factor

A total of 48 incubation experiments encompassing samples from six different lakes, two-three depths from each system, and three different incubation temperatures were conducted. The MOX rates across our study lakes, depth layers, and incubation temperature ranged widely from 0.01 to 59.71 μmol L^{-1} d^{-1} with consistently high rates in the deep layer (16.27 ± 20.33 μmol L^{-1} d^{-1}) than in the surface (0.13 ± 0.18 μmol L^{-1} d^{-1}) and intermediate layer (0.11 ± 0.15 μmol L^{-1} d^{-1}). The MOX rate was highly positively correlated with the concentrations of TP (R^2 = 0.64; p < 0.0001) and TN (R^2 = 0.55; p < 0.0001) while unrelated to DOC (Figures 3A–C). Furthermore, MOX rate was strongly positively correlated with γ-MOB abundance (R^2 = 0.84; p < 0.0001; Figure 3E), while weakly correlated with the abundance of α-MOB (R^2 = 0.33; p < 0.0001; Figure 3D).

For the water samples from the deeper layers of L. Geai, the initial O_2 concentrations were quite low (<26 μmol O_2 L^{-1}). Given the measured MOX rate (55.8, 47.7, and 31.3 μmol L^{-1} d^{-1} at 20, 10, and 5°C respectively) and assuming a CH_4:O_2 stoichiometry of 1:1.8 for aerobic CH_4 oxidation (Naguib 1976), incubations would have run out of O_2 before the second time point sampling within 12 h. Therefore, those results were excluded to limit our analysis to the controls of isotopic fractionation factor during strict aerobic oxidation. Hence, a total of 45 α_{ox} estimations representing the water column of six temperate lakes were used for further statistical analysis to understand the controls of α_{ox}. During the incubation, declines in CH_4 concentration were generally mirrored by the $\delta^{13}C$-CH_4 value and the isotopic fractionation factor (α_{ox}) was estimated for each depth and incubation temperature (Supplementary Figure S4). Across the water column of the six study lakes, two—three depths, and different incubation temperatures (5–25°C), α_{ox} varied from 1.004 to 1.038 (Figure 4; Supplementary Table S1). Notably, this large variability of α_{ox} observed in our experiments is not only introduced by the difference in incubation temperature, but the sampling depth also mattered substantially. For instance, α_{ox} varied from 1.011 to 1.028 for the surface samples of all lakes incubated at 20°C, while for the intermediate and deep layer samples at the same temperature, α_{ox} values varied from 1.020 to 1.031 and 1.030 to 1.032, respectively (Supplementary Table S1). Moreover, combining our estimates at different temperatures by layers showed a remarkably low α_{ox} in the surface (1.018 ± 0.007) relative to the intermediate (1.028 ± 0.004) and the deep (1.032 ± 0.004) layers (Figure 4). However, a strong decrease in α_{ox} with increasing temperature was generally observed for the intermediate and deep layers (Figure 4). Except for the surface layer of shallow L. Triton, where α_{ox} strongly negatively correlated with temperature, a hump-shaped relationship between α_{ox} and temperature was observed for the surface of other lakes (Supplementary Figure S5). Together, temperature was negatively correlated with α_{ox} (R^2 = 0.12; p = 0.0190; Supplementary Figure S5). For a given depth where MOX rate is high and an increase of MOX rate was observed with increasing temperature, a general decline of α_{ox} with increasing temperature and therefore MOX rate was evident (Supplementary Figure S6). This pattern suggests that in several cases, particularly in the

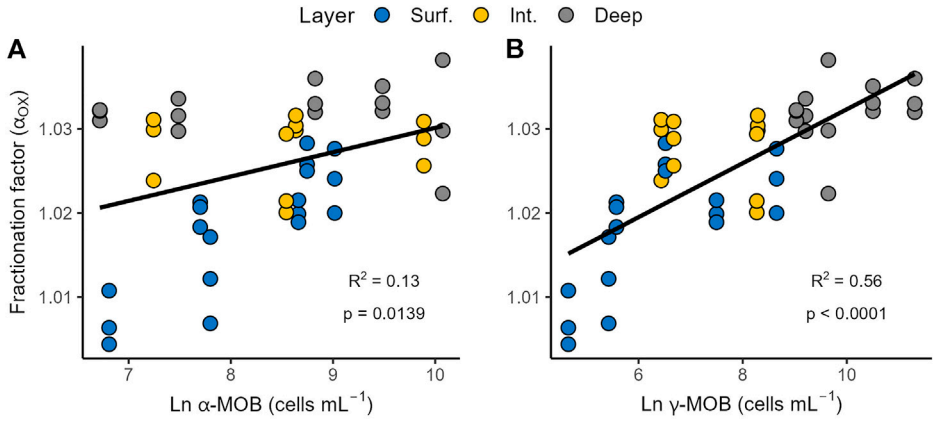


FIGURE 5
Relationships between carbon stable isotopic fractionation factor (α_{ox}) and the abundance of α-MOB **(A)** and γ-MOB **(B)** in the study lakes.

intermediate and deep layers, MOX rate was strongly negatively correlated to the isotopic fractionation (Supplementary Figure S6).

We explored the regulation of α_{ox} in the water column of our study lakes; α_{ox} was most significantly correlated with γ-MOB abundance ($R^2 = 0.56$, $p < 0.0001$), while only weakly correlated with α-MOB ($R^2 = 0.13$, $p = 0.0139$; Figure 5). We developed a simple predictive model for α_{ox} using multiple regression. Among all the tested variables, γ-MOB abundance (cells ml^{-1}) and MOX rate (μmol L^{-1} d^{-1}) emerged as the predictive variables in the multiple regression model (both MOB abundance and MOX rate were highly statistically significant; $p < 0.0001$) and the resulting model took the form of:

$$\alpha_{ox} = 0.965 + (-0.003 \times \mathrm{Ln\,MOX\,rate}) + (0.007 \times \mathrm{Ln}\,\gamma - \mathrm{MOB}) \quad (3)$$

$p < 0.0001$, $n = 45$

While this simple model explains MOB abundance and MOX rates as the key drivers of α_{ox}, MOB abundance and MOX rates are not frequently measured variables and therefore may not be suitable as a predictive model for α_{ox} to be applied in the isotopic mass balance of other systems. Therefore, we further explored the data to develop a predictive model for α_{ox} using routinely measured limnological variables. To do so, we have included all measured variables such as temperature, pH, concentrations of O_2, CH_4, DOC, TP, TN, and Chlorophyll *a* in the statistical analysis. However, the final multiple regression model with statistically significant predictive variables took the form of:

$$\alpha_{ox} = 1.0698 + (0.0067 \times \mathrm{Ln}\,TP) + (-0.0059 \times pH) + (-0.0144 \times \mathrm{Ln}\,DOC) + (-0.0002 \times Temperature) \quad (4)$$

$R^2 = 0.78$; $p < 0.0001$; $n = 45$, where TP and DOC are in μg L^{-1} and mg L^{-1}, respectively and temperature is in °C (Supplementary Figure S7). All the parameter estimates of the model were statistically significant; $p < 0.0001$ for DOC and pH, $p = 0.00025$ for TP, and $p = 0.02045$ for temperature.

Variability of modelled α_{ox} and implications to f_{ox} estimates

Further, we used the temperature, pH, TP, and DOC data of the surface layer of the study lakes in 2015 to predict the fractionation factor by applying the α_{ox} model (Eq. 4). We observed a clear seasonality in the estimated α_{ox} values with lower values consistently observed during the peak summer stratification period (Figure 6). Across our study lakes, modelled αox varied widely with a larger seasonal variability in L. Morency (1.003–1.025) and L. Croche (1.009–1.025) compared to L. Geai (1.015–1.028) and L. Cromwell (1.016–1.027), while the seasonal α_{ox} variability was minimal in L. en Coeur and L. Triton (1.010–1.019 and 1.019–1.029, respectively). Subsequently, the variability of the extent of oxidation (i.e., f_{ox}) was different across lakes; much pronounced in some lakes (Morency, Croche, and Geai) while moderate in the others (Figure 6). Further, we compared f_{ox} estimates derived from the modelled α_{ox} with a fixed value of 1.020 previously used for temperate lakes (Bastviken et al., 2002). Our comparison indicates that using a fixed α_{ox} clearly masks seasonality and can substantially misrepresent oxidation estimates at ecosystem scale. Similarly, when we applied the α_{ox} model to water column profiles performed in 2014, we observed a large variability of α_{ox} with depth (Figure 7), but the extent of the variability was different across lakes. α_{ox} ranged from 1.019 to 1.044 in L. Morency, while the variability was only

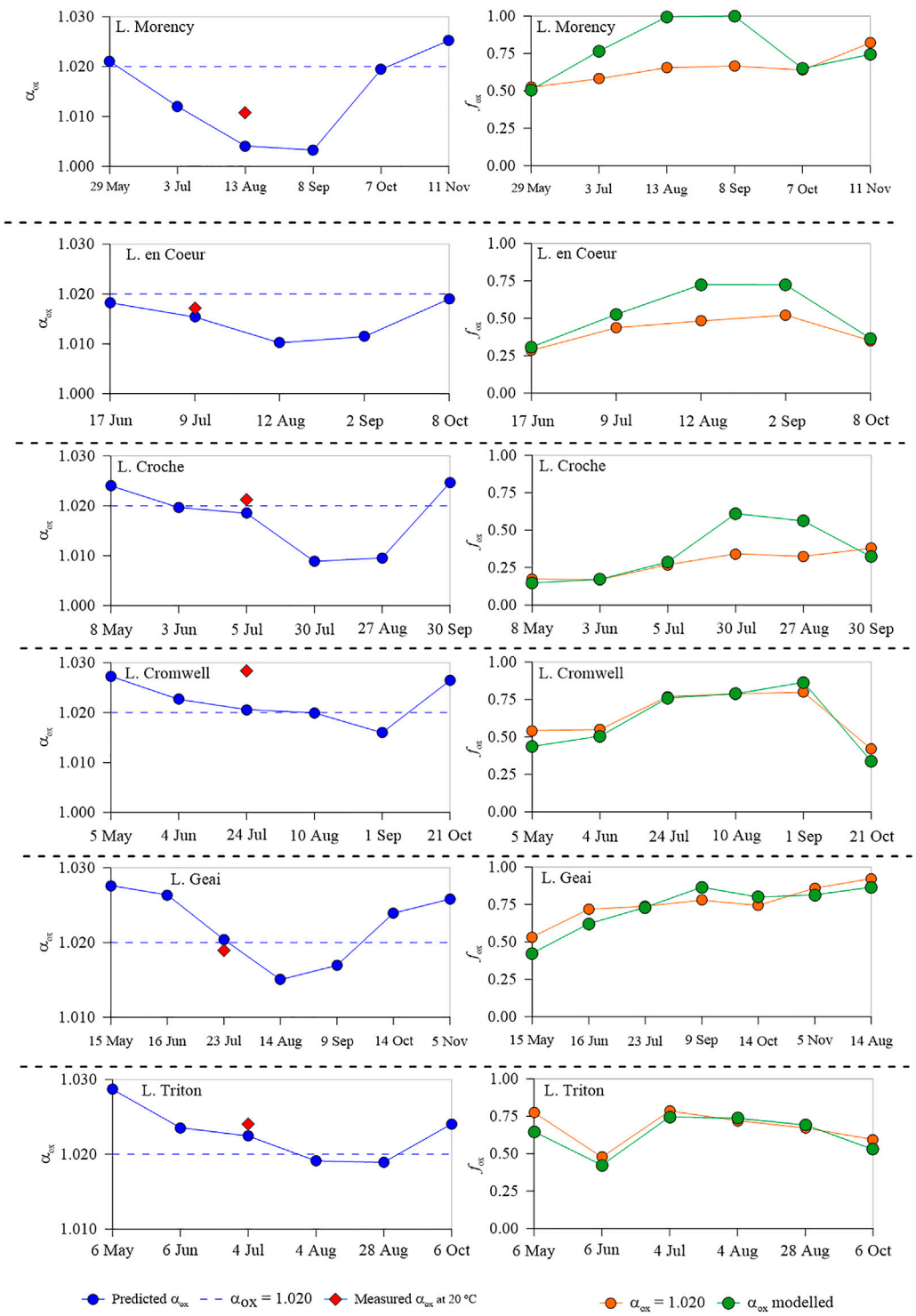


FIGURE 6
Seasonal variation in predicted α_{ox} (left panel) and fraction of CH_4 oxidised (f_{ox}) (right panel) estimated using a fixed α_{ox} of 1.020 or the modelled α_{ox} in the surface layers of each study lake.

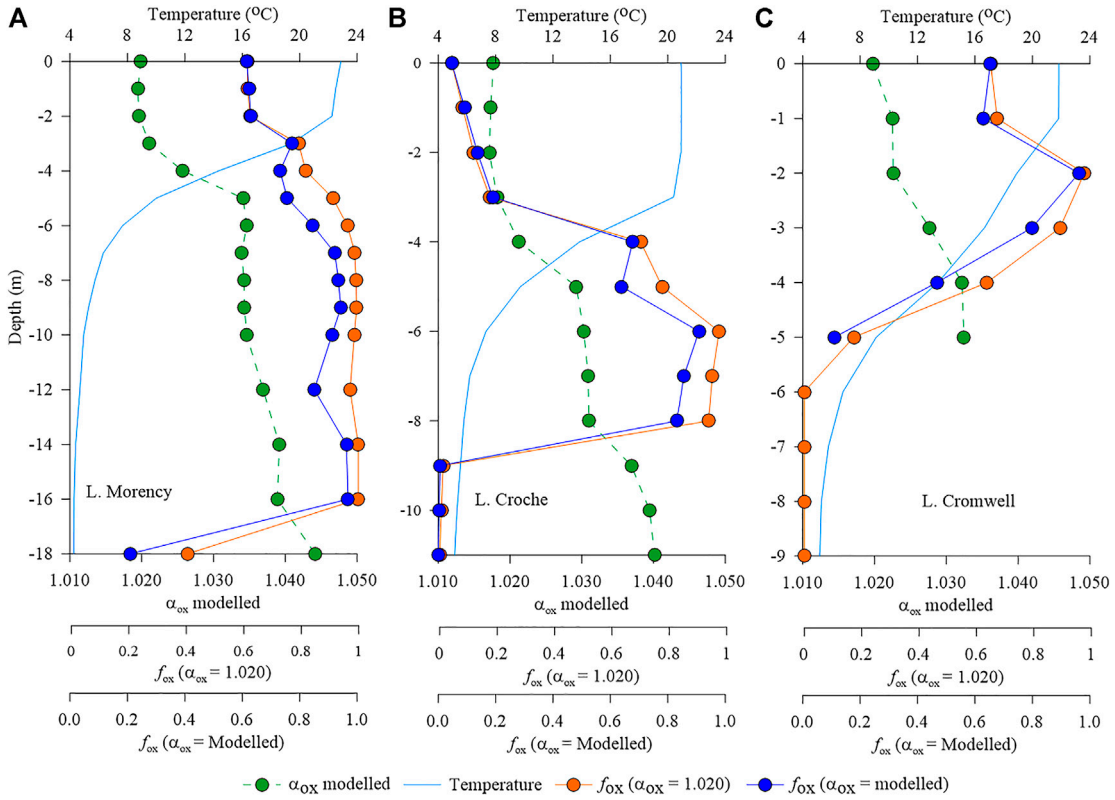


FIGURE 7
Vertical variation in modelled α_{ox}, the fraction of CH_4 oxidised (f_{ox}) estimated using a fixed α_{ox} of 1.020, and f_{ox} estimated using modelled α_{ox} in **(A)** L. Morency, **(B)** L. Croche and **(C)** L. Cromwell.

marginal (1.020–1.032) in L. Cromwell. Overall, our estimation showed a large spatial and temporal variability of α_{ox} across lakes and therefore shows that inaccurate α_{ox} values can cause large errors in the estimation of CH_4 oxidation.

Discussion

The estimation of CH_4 oxidation using stable isotopic approach fundamentally relies on the isotopic fractionation factor. Despite the growing number of stable isotopic measurements of CH_4 in inland waters (Bastviken et al., 2002; Kankaala et al., 2007; Schubert et al., 2010; Rinta et al., 2015; Sawakuchi et al., 2016; Thottathil et al., 2018; Grasset et al., 2020; Begum et al., 2021), the use of isotopic mass balance to estimate the extent of CH_4 oxidation is restricted to very few studies, and wherever attempted, a single α_{ox} was applied across systems (Bastviken et al., 2002; Sawakuchi et al., 2016; Thottathil et al., 2018; Grasset et al., 2020). Our extensive experimental incubations of unamended water samples from six temperate lakes have shown wide variability of α_{ox} in natural conditions. Furthermore, we show that α_{ox} variability in lake water column is predominantly shaped by the dominant group in the methanotrophic bacterial assemblage (γ-MOB) and MOX rates. However, in a practical point of view, we further developed a model for predicting α_{ox} in natural waters using routinely measured limnological variables that are in turn known to regulate γ-MOB assemblage and MOX rates.

Variability and patterns of α_{ox} in freshwater lakes

The existing data show a large variability of α_{ox} (1.005–1.049) in terrestrial environments (landfill, rice paddy field, and soil) and in various methanotrophic bacterial cultures (Coleman et al., 1981; Bergamaschi, 1997; Templeton et al., 2006; Chanton et al., 2008; Gebert and Streese-kleeberg, 2017; Aghdam et al., 2018; Obersky et al., 2018; Sparrow et al., 2019; Fjelsted et al., 2020; Bakkaloglu et al., 2021). Unlike these systems, only a few experimentally determined α_{ox} values exist for aquatic systems: 1.009 in a subtropical reservoir (Itoh et al., 2015), 1.013–1.021 in experimentally flooded boreal reservoir (Venkiteswaran and Schiff, 2005), and 1.018 to 1.021 in three

boreal lakes (Bastviken et al., 2002). However, given that MOX rates vary several orders of magnitude across lakes (Bastviken et al., 2002; Thottathil et al., 2019; Denfeld et al., 2016; Sawakuchi et al., 2021; D'Ambrosio and Harrison, 2021) and considering that MOX rate is often coupled with isotopic fractionation (Chanton et al., 2008; Gebert and Streese-Kleeberg, 2017), existing estimates (1.009–1.021) likely underrepresent the extent of α_{ox} variability in lakes. Unlike previous studies, we estimated the isotopic fractionation factor across and within several lakes covering large environmental gradients and range in methanotrophic activity. Therefore, our study revealed a large and previously unrealised variability of α_{ox} (1.004–1.038; Figure 4) during aerobic CH_4 oxidation in aquatic environments.

Our experimentally determined α_{ox} values for six temperate lakes encompass nearly the full spectrum of variability shown across methanotrophic bacterial cultures and diverse terrestrial environments (1.003–1.049; Bergamaschi, 1997; Chanton et al., 2008, Templeton et al., 2006; Bakkaloglu et al., 2021). Based on concurrently measured deep-water profiles of CH_4 and $\delta^{13}CH_4$, α_{ox} values were estimated to be 1.008 in the temperate L. Lugano (Blees et al., 2014), 1.037 in the boreal L. Mekkojarvi (Kankaala et al., 2007), and between 1.02 and 1.06 in three Arctic lakes (Cadieux et al., 2016). Unlike these data from different systems, our extensive estimates within the water column of temperate lakes showed a systematic vertical shift in α_{ox} with significantly lower values in the surface relative to a few meters below (Figure 4). This systematic variability of α_{ox} can be attributed to the observed increase of MOB abundance. While inhibition of CH_4 oxidation at high O_2 levels combined with low CH_4 supply reduce methanotrophic activity in the surface layers, "optimal O_2" concentration (~15 μmol L^{-1}; Thottathil et al., 2019) and high CH_4 supply enhance MOB growth, particularly γ-MOB abundance in the deep layer (Zigah et al., 2015; Reis et al., 2020). Together, the vertical distribution of α_{ox} in the water column of our study lakes shows greater discrimination of heavier isotopes (^{13}C) at high MOB abundance while relatively less discrimination in the surface layer where MOB abundance is relatively low.

Studies in terrestrial environments shown that for a given site, α_{ox} generally decreases with increasing MOX rate which is in turn linked to temporal changes in temperature (Chanton et al., 2008; Gebert and Streese-Kleeberg, 2017). Therefore, the low α_{ox} in the surface layer where MOX rate is low and high α_{ox} in the deeper layer where MOX rate is high in lakes seems contradictory to the pattern observed in the terrestrial environments. However, at a fixed MOB abundance for a given water layer, temperatures generally enhanced the MOX rates, which resulted in lower α_{ox} (Figure 4; Supplementary Figures S5, S6). This is particularly pronounced in the intermediate and deep layers where MOX rate and MOB abundance are consistently high (Supplementary Figure S6). Thus, our data in general is in accordance with the pattern observed in the terrestrial environment where higher MOX rates lead to lower discrimination against heavier isotope and therefore lower values of α_{ox} (Chanton et al., 2008; Gebert and Streese-Kleeberg, 2017). However, for a given layer of the stratified water column, α_{ox} can be highly sensitive to the factors affecting the temporal changes in CH_4 oxidation besides temperature (substrate supply, nutrients, etc.) and these need to be accounted for precise α_{ox} estimates. Together, our study clearly shows that using literature-derived α_{ox} values, or assuming a single isotopic fractionation factor over space and time within or across systems can lead to miscalculation of oxidation extent in lakes.

The emergence of γ-MOB as a key predictor of α_{ox} in the lake water column is an important outcome of this study. Notably, the correlation between γ-MOB and α_{ox} was evident within each layer of the water column—even in the surface waters where γ-MOB abundance was generally low (Figure 5). Although previous studies have linked isotopic fractionation to MOB abundance in growth medium with pure and/or mixed methanotrophic cultures (Templeton et al., 2006; Feisthauer et al., 2011), our study establish such connection in natural, unamended samples. It should be noted that the abundance of γ-MOB was higher than the abundance of α-MOB (Figure 2) in our study lakes, particularly in the deeper layer of stratified lakes where multiple environmental factors (low pH, high TP concentration, and strong counter gradients of CH_4 and O_2; Figure 1; Supplementary Figure S1) support the proliferation of γ-MOB cells (Reis et al., 2020; Nijman et al., 2021). Under these ideal environmental conditions, the greater γ-MOB abundance and higher CH_4 oxidation rates result in higher isotopic fractionation. This is further evident from the stronger correlation between γ-MOB abundance and MOX rates than that between α-MOB abundance and MOX rates in our study lakes (Figure 3). However, the stronger relationship between γ-MOB abundance and α_{ox} (Figure 5) does not necessarily indicate a greater discrimination against the heavier isotope (^{13}C-CH_4) in γ-MOB cells than in α-MOB cells. In systems or environments where α-MOB is dominant over γ-MOB and MOX rate is regulated by α-MOB abundance, changes in α-MOB abundance are expected to drive α_{ox} variation. Our estimates suggest that under ideal conditions, enhanced uptake of lighter carbon (^{12}C) can result in α_{ox} values as high as 1.038, corroborating previous observation that where there is an ideal condition for methanotrophic growth (i.e., excess CH_4 availability and optimal O_2 oxygen concentration), α_{ox} values should approach its maximum (Templeton et al., 2006). Our data shows that in the stratified lakes, such condition often exists in the deep layers of the water columns resulting in large increase of α_{ox} from the surface to deeper layers. Further, multiple regression analysis suggested that γ-MOB abundance and MOX rates essentially control the variability of isotopic fractionation in the water column of our study lakes (Eq. 3), where α_{ox} was shown to decrease with increasing oxidation rates while increases with γ-MOB abundance. While the depth-wise variation of α_{ox} suggests an increase of isotopic fractionation with MOX rates (Figure 4), the multiple regression analysis shows an inverse

relationship between α_{ox} and MOX rates consistent with studies from various terrestrial environments (Templeton et al., 2006; Chanton et al., 2008; Gebert and Streese-Kleeberg, 2017). This suggest that for a given γ-MOB cell abundance, an increase in MOX rate induced by increased in temperature and CH_4 concentration, and/or "optimal O_2" supply would essentially result in less discrimination against heavier isotope.

Modelling α_{ox} with routinely measured limnological variables

While the α_{ox} model depicts that the abundance of γ-MOB and MOX rates are the most important drivers of isotopic fractionation (Eq. 3), we analysed the data further to develop a more "practical model" that enables the prediction of α_{ox} using routinely measured limnological variables (Eq. 4; Supplementary Figure S7). Temperature emerged as a statistically significant parameter ($p = 0.0245$) in explaining the variability of isotopic fractionation. Systematic decrease of α_{ox} with increasing temperature was often observed in terrestrial environments for temperature range of 5–25°C (Tyler et al., 1994; Chanton et al., 2008; Gebert and Streese-Kleeberg, 2017). Despite a comparable temperature range for our incubations, inverse relationship between temperature and α_{ox} was weak in our model where all measurements were combined. Yet, for samples where MOX rates were generally high and substantially enhanced by temperature, strong temperature response was observed (Supplementary Figure S6). For instance, small (0.017 km^2) and shallow (maximum depth: 4.2 m) unstratified L. Triton where MOX rate was highest among all surface samples, a strikingly strong temperature dependence of α_{ox} (Supplementary Figure S5) with a slope (-7.6×10^{-4} and -1.6×10^{-3}) comparable with the values reported for soil environments (-4.0×10^{-6} to -1.7×10^{-4}; Chanton et al., 2008) was observed. Although we lack estimates from similar systems, a previous study in a similarly sized boreal lake (0.024 km^2) in the Experimental Lakes Area, Ontario (Canada) showed a comparable pattern with strong temperature dependence of α_{ox} (slope: -2.0×10^{-4}; Venkiteswaran and Schiff, 2005). Thus, these data suggest a comparable temperature dependence of α_{ox} in small lakes and soil environments, while the pattern is different for the surface layers of larger lakes (Supplementary Figure S5). However, further studies are needed to confirm whether there exists systematic shift in the temperature response of α_{ox} in the continuum from soil to small and large lakes. In addition to small L. Triton, for most of the deep layer samples where MOX rates were relatively high, increasing incubation temperature resulted in a general decrease of α_{ox} (Figure 4; Supplementary Figure S6). This temperature response of α_{ox} that we observed for most our samples is likely linked to the increasing MOX rates with temperature; where a strong positive relationship with temperature and MOX rate was observed, an inverse relationship between temperature and α_{ox} was evident (Supplementary Figure S6) indicating that for a given sample, enhanced CH_4 oxidation with temperature is associated with less isotopic discrimination. Our result is therefore consistent with the inverse relationship between site specific seasonal temperature changes and α_{ox} observed for various terrestrial environments (Tyler et al., 1994; Chanton et al., 2008; Gebert and Streese-Kleeberg, 2017).

Despite the narrow pH range in our data, pH was a highly significant variable ($p < 0.0001$) in shaping overall variability of isotopic fractionation. Given that in our study lakes α_{ox} is shaped by γ-MOB abundance, the emergence of pH in the model is consistent with the effect that pH exerts on bacterial communities in general and on MOB community structure in lakes (Newton et al., 2011; Ren et al., 2015; Crevecoeur et al., 2019; Guggenheim et al., 2020). The pH effect on bacterial abundance can be direct since even small changes in pH can impose strong physiological changes, likely induce changes in competition for resources, and affect the net growth of the population (Madigan et al., 2011; Ren et al., 2015). Furthermore, at the ecosystem-scale, pH also exerts indirect effects on bacterial communities acting as an integrative factor of multiple environmental variables including nutrients and substrate availability (Ren et al., 2015; Crevecoeur et al., 2019; Guggenheim et al., 2020). Therefore, we believe that the effect of pH shown in these studies must be relevant for MOB communities in our study lakes, thereby emerging as a proxy of γ-MOB abundance, which directly controls α_{ox}. However, we acknowledge that our understanding on the effect pH on MOB communities and isotopic fractionation is still limited and future studies are warranted to confirm the trend shown here.

The "practical model" for α_{ox} showed a highly significant negative relationship between α_{ox} and DOC concentrations ($p < 0.0001$; Supplementary Figure S7). Although this pattern corroborates the role of DOC in shaping MOB community in northern lakes (Samad and Bertilsson, 2017; Crevecoeur et al., 2019), uncoupling of DOC and MOB abundance (Supplementary Figure S3) in our study lakes warrants other explanations for the DOC-α_{ox} relationship in the model. It should be noted that DOC concentration was positively correlated with MOX rates in the surface and intermediate layers, while a hump-shaped relationship was found in the deep layer (Supplementary Figure S8). This positive relationship between MOX rate and DOC in the upper layers can be attributed to the strong negative relationship between DOC and O_2 concentrations which is in turn induced by higher heterotrophic bacterial respiration of organic carbon with increasing DOC concentration (Supplementary Figure S8). Since high O_2 concentration inhibits CH_4 oxidation (Rudd et al., 1976; Thottathil et al., 2019), observed decrease of O_2 concentration with the increasing concentration of DOC is likely to relive the methanotrophic community from O_2 inhibition and

thereby enhances the oxidation rate. However, it should be noted that O_2 is not selected as a predictive variable in the α_{ox} model. Therefore, DOC not only integrates the effect of O_2, but also accounts for other potential factors such as the light attenuation-mediated enhancement of MOB activity (Dumestre et al., 1999; Murase and Sugimoto, 2005; Sawakuchi et al., 2016; Thottathil et al., 2018). Together, we suggest that increasing DOC concentration and thereby MOX rates resulted in less discrimination against the heavier isotope as shown in the model (Eq. 3); therefore, in our "practical model" DOC should be interpreted as proxy of CH_4 oxidation.

Unlike temperature, pH, and DOC, the model showed a strong positive correlation between TP and α_{ox} (Supplementary Figure S7; $p = 0.0003$). Note that TP was correlated with the abundance of MOB, particularly with γ-MOB (Supplementary Figure S3) suggesting a greater role of P-availability in enhancing the methanotrophic abundance; a pattern previously shown for ice-covered boreal lake water column (Denfeld et al., 2016; Sawakuchi et al., 2021) and subtropical lake sediment (Nijman et al., 2022). Therefore, the positive correlation between TP and α_{ox} indicates that TP in our "practical model" is a proxy of the abundance of dominant methanotrophic group (i.e., γ-MOB). The identification of TP as a strong regulator of MOX rates and α_{ox} has important implications. For example, a recent study reported strong correlation between the extent of oxidation (i.e., f_{ox}) and TP across lake mesocosms (Grasset et al., 2020). Since CH_4 oxidation is known to be light inhibited (Dumestre et al., 1999; Murase and Sugimoto, 2005), the authors attributed this pattern to enhanced methanotrophic activity due to greater light attenuation in the P-amended mesocosms where phytoplankton biomass increased substantially (Grasset et al., 2020). However, our data suggests that the role of TP on CH_4 oxidation can be rather direct by stimulating CH_4 oxidation as shown in recent studies (Sawakuchi et al., 2021; Kashi et al., 2022; Nijman et al., 2022). Hence, our model suggests that overlooking the effect of TP and assuming a single α_{ox} for the mass balance calculation across systems with different trophic status could underestimate the f_{ox}. It is interesting to note that despite the covariation of TP and TN in our study lakes, TN is not a significant predictive variable in the multiple regression analysis. This is in accordance with the recent study showing that MOB community is P-limited as evident from the increase of P content of the MOB biomass despite the elevated phosphorus and nitrogen levels in the experimental incubations (Nijman et al., 2022). Along with the above study, our data suggests that strong correlation between TP and MOB abundance is not just due to their concomitant increase with depth but caused due to the strong role of P in stimulating MOX rates and increasing MOB abundance in lakes. The γ-MOB abundance is positively correlated with α_{ox} in our model (Eq. 3); therefore, the strong correlation between α_{ox} and TP in our "practical model" suggests TP as a proxy of γ-MOB abundance and its increase leads to greater isotopic fractionation.

The importance of using appropriate α_{ox} values

By applying our environmental model of α_{ox} to water column profiles, we found that α_{ox} and consequently the seasonal variability of f_{ox} was much more pronounced in some lakes (Morency, Croche, and Geai) than in others (Figures 6, 7). Therefore, assuming a single α_{ox} value to all lakes would largely misrepresent the oxidation extent and thereby lead to errors in the estimation of ecosystem-scale CH_4 oxidation rates. For instance, assuming a constant α_{ox} of 1.020 throughout the year in the epilimnion of L. Morency would underestimate the f_{ox} by up to 34% during August–September period and underestimate by up to 8% in the spring and autumn period (Figure 6). Similarly, applying an α_{ox} of 1.020 throughout the water column overestimates f_{ox} by up to 10% in the deeper layers of our study lakes (Figure 7). These potential errors in the f_{ox} estimation induced solely by the difference in α_{ox} value is comparable with the error estimations reported previously (Cabral et al., 2010; Capanema and Cabral, 2012). Together, our "practical α_{ox} model" with routinely measured limnological variables allows more accurate estimation of f_{ox} *via* $\delta^{13}C\text{-}CH_4$ mass balance and enable to derive large-scale patterns of CH_4 oxidation across freshwater aquatic systems without the biases induced by the variability of α_{ox}.

Conclusion

In conclusion, we show a large variability in the stable carbon isotopic fractionation during aerobic CH_4 oxidation in freshwater lakes with a systematic increase of α_{ox} from the surface to deep layers of the water column. Our study showed that the rates of CH_4 oxidation and the abundance of γ-MOB explain the variability of α_{ox} in temperate lake water columns. However, we suggest that the observed relationship between γ-MOB abundance and α_{ox} is due to the dominance of this MOB group in the temperate lake water column and does not necessarily suggest a group specific difference in isotopic fractionation. For a given γ-MOB abundance, α_{ox} decreased with increasing MOX rates—a pattern consistent with the data from various terrestrial environments suggesting that with increasing CH_4 oxidation rate, there is less discrimination against the heavier stable isotope (^{13}C). For practical purposes, we developed a general model of α_{ox} by integrating the effect of various factors on experimentally derived α_{ox} values using routinely measured limnological variables. We showed that applying a single α_{ox} value in CH_4 stable isotopic mass balances can misrepresent its within lake variability, thereby hampering the detection of existing spatial and temporal patterns in the extent of CH_4 oxidation across lakes. Our model of α_{ox} in conjunction with the growing

number of $\delta^{13}C\text{-}CH_4$ measurements should help to elucidate large scale patterns and drivers of the oxidation-driven mitigation of CH_4 emission from freshwater aquatic systems.

Data availability statement

The original contributions presented in the study are included in the article/Supplementary Material, further inquiries can be directed to the corresponding author.

Author contributions

ST and PR developed the research idea and conducted experiments. ST analyzed and plotted data and wrote the first version of the manuscript, and PR analyzed and plotted data, reviewed, and edited the manuscript. YP contributed to analyzing data, reviewed and edited the manuscript, supervised the research, and acquired funding.

Funding

This study was supported by Natural Sciences and Engineering Research Council of Canada Discovery grants to YP and is a contribution to UNESCO Chair in Global Environmental Change. ST and PR were supported by doctoral scholarships from Fonds de recherche Nature et Technologies du Québec, Canada.

Acknowledgments

We thank the reviewers for their helpful comments. We thank Katherine Velghe for the assistance in the laboratory. We also thank the staff at the Station de biologie des Laurentides (Université de Montréal) for assistance.

Conflict of interest

The authors declare that the research was conducted in the absence of any commercial or financial relationships that could be construed as a potential conflict of interest.

Publisher's note

All claims expressed in this article are solely those of the authors and do not necessarily represent those of their affiliated organizations, or those of the publisher, the editors and the reviewers. Any product that may be evaluated in this article, or claim that may be made by its manufacturer, is not guaranteed or endorsed by the publisher.

Supplementary material

The Supplementary Material for this article can be found online at: https://www.frontiersin.org/articles/10.3389/fenvs.2022.833688/full#supplementary-material

References

Aghdam, E. F., Fredenslund, A. M., Chanton, J., Kjeldsen, P., and Scheutz, C. (2018). Determination of gas recovery efficiency at two Danish landfills by performing downwind methane measurements and stable carbon isotopic analysis. *Waste Manag.* 73, 220–229. doi:10.1016/j.wasman.2017.11.049

Bakkaloglu, S., Lowry, D., Fisher, R. E., France, J. L., and Nisbet, E. G. (2021). Carbon isotopic characterisation and oxidation of UK landfill methane emissions by atmospheric measurements. *Waste Manag.* 132, 162–175. doi:10.1016/j.wasman.2021.07.012

Barker, J. F., and Fritz, P. (1981). Carbon isotope fractionation during microbial methane oxidation. *Nature* 293 (5830), 289–291. doi:10.1038/293289a0

Bastviken, D., Cole, J. J., Pace, M. L., and Van de Bogert, M. C. (2008). Fates of methane from different lake habitats: Connecting whole-lake budgets and CH4 emissions. *J. Geophys. Res.* 113 (G2). doi:10.1029/2007jg000608

Bastviken, D., Ejlertsson, J., and Tranvik, L. (2002). Measurement of methane oxidation in lakes: a comparison of methods. *Environ. Sci. Technol.* 36 (15), 3354–3361. doi:10.1021/es010311p

Bastviken, D., Tranvik, L. J., Downing, J. A., Crill, P. M., and Enrich-Prast, A. (2011). Freshwater methane emissions offset the Continental Carbon Sink. *Science* 331 (6013), 50. doi:10.1126/science.1196808

Begum, M. S., Bogard, M. J., Butman, D. E., Chea, E., Kumar, S., Lu, X., et al. (2021). Localized pollution impacts on greenhouse gas dynamics in three anthropogenically modified Asian river systems. *J. Geophys. Res. Biogeosci.* 126, e2020JG006124. doi:10.1029/2020jg006124

Bergamaschi, P., Lubina, C., Königstedt, R., Fischer, H., Veltkamp, A. C., and Zwaagstra, O. (1998). Stable isotopic signatures (δ13C, δD) of methane from European landfill sites. *J. Geophys. Res.* 103 (D7), 8251–8265. doi:10.1029/98jd00105

Bergamaschi, P. (1997). Seasonal variations of stable hydrogen and carbon isotope ratios in methane from a Chinese rice paddy. *J. Geophys. Res.* 102 (D21), 25383–25393. doi:10.1029/97jd01664

Blees, J., Niemann, H., Wenk, C. B., Zopfi, J., Schubert, C. J., Kirf, M. K., et al. (2014). Micro-aerobic bacterial methane oxidation in the chemocline and anoxic water column of deep south-Alpine Lake Lugano (Switzerland). *Limnol. Oceanogr.* 59 (2), 311–324. doi:10.4319/lo.2014.59.2.0311

Börjesson, G., Chanton, J., and Svensson, B. H. (2001). Methane oxidation in two Swedish landfill covers measured with carbon-13 to carbon-12 isotope ratios. *J. Environ. Qual.* 30 (2), 369–376. doi:10.2134/jeq2001.302369x

Börjesson, G., Samuelsson, J., and Chanton, J. (2007). Methane oxidation in Swedish landfills quantified with the stable carbon isotope technique in combination with an optical method for emitted methane. *Environ. Sci. Technol.* 41 (19), 6684–6690. doi:10.1021/es062735v

Cabral, A. R., Capanema, M. A., Gebert, J., Moreira, J. F., and Jugnia, L. B. (2010). Quantifying microbial methane oxidation efficiencies in two experimental landfill biocovers using stable isotopes. *Water Air Soil Pollut.* 209 (1), 157–172. doi:10.1007/s11270-009-0188-4

Cadieux, S. B., White, J. R., Sauer, P. E., Peng, Y., Goldman, A. E., and Pratt, L. M. (2016). Large fractionations of C and H isotopes related to methane oxidation in Arctic lakes. *Geochimica Cosmochimica Acta* 187, 141–155. doi:10.1016/j.gca.2016.05.004

Cai, Y., Zheng, Y., Bodelier, P. L., Conrad, R., and Jia, Z. (2016). Conventional methanotrophs are responsible for atmospheric methane oxidation in paddy soils. *Nat. Commun.* 7 (1), 11728–11810. doi:10.1038/ncomms11728

Capanema, M. A., and Cabral, A. R. (2012). Evaluating methane oxidation efficiencies in experimental landfill biocovers by mass balance and carbon stable isotopes. *Water Air Soil Pollut.* 223 (9), 5623–5635. doi:10.1007/s11270-012-1302-6

Chanton, J., Abichou, T., Langford, C., Hater, G., Green, R., Goldsmith, D., et al. (2011). Landfill methane oxidation across climate types in the US. *Environ. Sci. Technol.* 45 (1), 313–319. doi:10.1021/es101915r

Chanton, J., and Liptay, K. (2000). Seasonal variation in methane oxidation in a landfill cover soil as determined by an *in situ* stable isotope technique. *Glob. Biogeochem. Cycles* 14 (1), 51–60. doi:10.1029/1999gb900087

Chanton, J. P., Powelson, D. K., Abichou, T., Fields, D., and Green, R. (2008). Effect of temperature and oxidation rate on carbon-isotope fractionation during methane oxidation by landfill cover materials. *Environ. Sci. Technol.* 42 (21), 7818–7823. doi:10.1021/es801221y

Chanton, J. P., Powelson, D. K., and Green, R. B. (2009). Methane oxidation in landfill cover soils, is a 10% default value reasonable? *J. Environ. Qual.* 38 (2), 654–663. doi:10.2134/jeq2008.0221

Coleman, D. D., Risatti, J. B., and Schoell, M. (1981). Fractionation of carbon and hydrogen isotopes by methane-oxidizing bacteria. *Geochimica Cosmochimica Acta* 45 (7), 1033–1037. doi:10.1016/0016-7037(81)90129-0

Crevecoeur, S., Ruiz-González, C., Prairie, Y. T., and Del Giorgio, P. A. (2019). Large-scale biogeography and environmental regulation of methanotrophic bacteria across boreal inland waters. *Mol. Ecol.* 28 (18), 4181–4196. doi:10.1111/mec.15223

D'Ambrosio, S. L., and Harrison, J. A. (2021). Methanogenesis exceeds CH_4 consumption in eutrophic lake sediments. *Limnol. Oceanogr. Lett.* 6 (4), 173–181. doi:10.1002/lol2.10192

De Visscher, A., De Pourcq, I., and Chanton, J. (2004). Isotope fractionation effects by diffusion and methane oxidation in landfill cover soils. *J. Geophys. Res.* 109 (D18), D18111. doi:10.1029/2004jd004857

Denfeld, B. A., Ricão Canelhas, M., Weyhenmeyer, G. A., Bertilsson, S., Eiler, A., and Bastviken, D. (2016). Constraints on methane oxidation in ice-covered boreal lakes. *J. Geophys. Res. Biogeosci.* 121 (7), 1924–1933. doi:10.1002/2016jg003382

Dumestre, J. F., Guézennec, J., Galy-Lacaux, C., Delmas, R., Richard, S., and Labroue, L. (1999). Influence of light intensity on methanotrophic bacterial activity in Petit Saut Reservoir, French Guiana. *Appl. Environ. Microbiol.* 65 (2), 534–539. doi:10.1128/aem.65.2.534-539.1999

Feisthauer, S., Vogt, C., Modrzynski, J., Szlenkier, M., Krüger, M., Siegert, M., et al. (2011). Different types of methane monooxygenases produce similar carbon and hydrogen isotope fractionation patterns during methane oxidation. *Geochimica Cosmochimica Acta* 75 (5), 1173–1184. doi:10.1016/j.gca.2010.12.006

Fjelsted, L., Christensen, A. G., Larsen, J. E., Kjeldsen, P., and Scheutz, C. (2020). Closing the methane mass balance for an old closed Danish landfill. *Waste Manag.* 102, 179–189. doi:10.1016/j.wasman.2019.10.045

Gebert, J., and Streese-Kleeberg, J. (2017). Coupling stable isotope analysis with gas push-pull tests to derive *in situ* values for the fractionation factor α_{ox} associated with the microbial oxidation of methane in soils. *Soil Sci. Soc. Am. J.* 81 (5), 1107–1114. doi:10.2136/sssaj2016.11.0387

Grasset, C., Sobek, S., Scharnweber, K., Moras, S., Villwock, H., Andersson, S., et al. (2020). The CO2-equivalent balance of freshwater ecosystems is non-linearly related to productivity. *Glob. Chang. Biol.* 26 (10), 5705–5715. doi:10.1111/gcb.15284

Guérin, F., and Abril, G. (2007). Significance of pelagic aerobic methane oxidation in the methane and carbon budget of a tropical reservoir. *J. Geophys. Res.* 112 (G3). doi:10.1029/2006jg000393

Guggenheim, C., Freimann, R., Mayr, M. J., Beck, K., Wehrli, B., and Bürgmann, H. (2020). Environmental and microbial interactions shape methane-oxidizing bacterial communities in a stratified lake. *Front. Microbiol.* 11, 579427. doi:10.3389/fmicb.2020.579427

Happell, J. D., Chanton, J. P., and Showers, W. S. (1994). The influence of methane oxidation on the stable isotopic composition of methane emitted from Florida swamp forests. *Geochimica Cosmochimica Acta* 58 (20), 4377–4388. doi:10.1016/0016-7037(94)90341-7

Itoh, M., Kobayashi, Y., Chen, T. Y., Tokida, T., Fukui, M., Kojima, H., et al. (2015). Effect of interannual variation in winter vertical mixing on CH4 dynamics in a subtropical reservoir. *J. Geophys. Res. Biogeosci.* 120 (7), 1246–1261. doi:10.1002/2015jg002972

Itoh, M., Kojima, H., Ho, P. C., Chang, C. W., Chen, T. Y., Hsiao, S. S. Y., et al. (2017). Integrating isotopic, microbial, and modeling approaches to understand methane dynamics in a frequently disturbed deep reservoir in Taiwan. *Ecol. Res.* 32, 861–871. doi:10.1007/s11284-017-1502-z

Jahnke, L. L., Summons, R. E., Hope, J. M., and Des Marais, D. J. (1999). Carbon isotopic fractionation in lipids from methanotrophic bacteria II: The effects of physiology and environmental parameters on the biosynthesis and isotopic signatures of biomarkers. *Geochimica Cosmochimica Acta* 63 (1), 79–93. doi:10.1016/s0016-7037(98)00270-1

Kankaala, P., Taipale, S., Nykänen, H., and Jones, R. I. (2007). Oxidation, efflux, and isotopic fractionation of methane during autumnal turnover in a polyhumic, boreal lake. *J. Geophys. Res.* 112 (G2), G02033. doi:10.1029/2006jg000336

Kashi, N. N., Hobbie, E. A., Varner, R. K., Wymore, A. S., Ernakovich, J. G., and Giesler, R. (2022). Nutrients alter methane production and oxidation in a thawing permafrost mire. *Ecosystems*, 1–16. doi:10.1007/s10021-022-00758-5

King, G. M. (1992). "Ecological aspects of methane oxidation, a key determinant of global methane dynamics," in *Advances in microbial ecology*. Editor K. C. Marshall (Boston, MA: Springer), 12, 431–468.

King, S. L., Quay, P. D., and Lansdown, J. M. (1989). The $^{13}C/^{12}$ C Kinetic isotopic effect for soil oxidation of methane at ambient atmospheric concentrations. *J. Geophys. Res.* 94 (18), 273277–273318.

Komiya, S., Yazaki, T., Kondo, F., Katano, K., Lavric, J. V., McTaggart, I., et al. (2020). Stable carbon isotope studies of CH4 dynamics via water and plant pathways in a tropical Thai paddy: Insights into diel CH4 transportation. *J. Geophys. Res. Biogeosci.* 125 (9), e2019JG005112. doi:10.1029/2019jg005112

Li, S., Chen, Y., Yu, F., Zhang, Y., Liu, K., Zhuo, X., et al. (2022). Reducing methane emission by promoting its oxidation in rhizosphere through nitrogen-induced root growth in paddy fields. *Plant Soil* 474, 541–560. doi:10.1007/s11104-022-05360-1

Liptay, K., Chanton, J., Czepiel, P., and Mosher, B. (1998). Use of stable isotopes to determine methane oxidation in landfill cover soils. *J. Geophys. Res.* 103 (D7), 8243–8250. doi:10.1029/97jd02630

Madigan, M. T., Martinko, J. M., Stahl, D. A., and Clark, D. P. (2011). *Brock biology of microorganisms*. 13th ed. San Francisco, CA: Pearson Benjamin Cummings.

Mahieu, K., De Visscher, A., Vanrolleghem, P. A., and Van Cleemput, O. (2006). Carbon and hydrogen isotope fractionation by microbial methane oxidation: Improved determination. *Waste Manag.* 26 (4), 389–398. doi:10.1016/j.wasman.2005.11.006

Morana, C., Borges, A. V., Roland, F. A. E., Darchambeau, F., Descy, J.-P., and Bouillon, S. (2015). Methanotrophy within the water column of a large meromictic tropical lake (Lake Kivu, East Africa). *Biogeosciences* 12, 2077–2088. doi:10.5194/bg-12-2077-2015

Murase, J., and Sugimoto, A. (2005). Inhibitory effect of light on methane oxidation in the pelagic water column of a mesotrophic lake (Lake Biwa, Japan). *Limnol. Oceanogr.* 50 (4), 1339–1343. doi:10.4319/lo.2005.50.4.1339

Naguib, M. (1976). Stoichiometry of methane oxidation in the methane-oxidizing strain M102 under the influence of various CH_4/O_2 mixtures. *Z. Allg. Mikrobiol.* 16, 437–444. doi:10.1002/jobm.3630160604

Newton, R. J., Jones, S. E., Eiler, A., McMahon, K. D., and Bertilsson, S. (2011). A guide to the natural history of freshwater lake bacteria. *Microbiol. Mol. Biol. Rev.* 75 (1), 14–49. doi:10.1128/mmbr.00028-10

Nihous, G. C., Obersky, L., Rafiee, R., Cabral, A. R., Golding, S. D., and Clarke, W. P. (2010). Notes on the temperature dependence of carbon isotope fractionation by aerobic CH4-oxidising bacteriaMethodology to determine the extent of anaerobic digestion, composting and CH4 oxidation in a landfill environment. *Isotopes Environ. health studies Waste Manag.* 4676 (2), 133364–140373. doi:10.1016/j.wasman.2018.02.029

Nijman, T., Amado, A. M., Bodelier, P. L., and Veraart, A. J. (2022). Relief of phosphate limitation stimulates methane oxidation. *Front. Environ. Sci.* 10, 202. doi:10.3389/fenvs.2022.804512

Nijman, T. P. A., Davidson, T. A., Weideveld, S. T. J., Audet, J., Esposito, C., Levi, E. E., et al. (2021). Warming and eutrophication interactively drive changes in the methane-oxidizing community of shallow lakes. *ISME Commun.* 1, 32–36. doi:10.1038/s43705-021-00026-y

Patton, C., and Kryskalla, J. (2003) Methods of analysis by the U.S. Geological Survey National Water Quality Laboratory – evaluation of alakaline persulfate digestion as an alternative to Kjedahl digestion for determmination of total and dissolved nitrogen and phosphorus. Water-Resources Investigations Report 2003-4174

Obersky, L., Rafiee, R., Cabral, A. R., Golding, S. D., and Clarke, W. P. (2018) Methodology to determine the extent of anaerobic digestion, composting and CH4 oxidation in a landfill environment. *Waste Manag.* 76, 364–373. doi:10.1016/j.wasman.2018.02.029

Preuss, I., Knoblauch, C., Gebert, J., and Pfeiffer, E. M. (2013). Improved quantification of microbial CH_4 oxidation efficiency in arctic wetland soils using

carbon isotope fractionation. *Biogeosciences* 10 (4), 2539–2552. doi:10.5194/bg-10-2539-2013

Reeburgh, W. S. (2007). Oceanic methane biogeochemistry. *Chem. Rev.* 107 (2), 486–513. doi:10.1021/cr050362v

Reis, P. C. J., Thottathil, S. D., and Prairie, Y. T. (2022). The role of methanotrophy in the microbial carbon metabolism of temperate lakes. *Nat. Commun.* 13 (1), 43–49. doi:10.1038/s41467-021-27718-2

Reis, P. C. J., Thottathil, S. D., Ruiz-González, C., and Prairie, Y. T. (2020). Niche separation within aerobic methanotrophic bacteria across lakes and its link to methane oxidation rates. *Environ. Microbiol.* 22 (2), 738–751. doi:10.1111/1462-2920.14877

Ren, L., Jeppesen, E., He, D., Wang, J., Liboriussen, L., Xing, P., et al. (2015). pH influences the importance of niche-related and neutral processes in lacustrine bacterioplankton assembly. *Appl. Environ. Microbiol.* 81 (9), 3104–3114. doi:10.1128/aem.04042-14

Rinta, P., Bastviken, D., van Hardenbroek, M., Kankaala, P., Leuenberger, M., Schilder, J., et al. (2015). An inter-regional assessment of concentrations and δ 13 C values of methane and dissolved inorganic carbon in small European lakes. *Aquat. Sci.* 77 (4), 667–680. doi:10.1007/s00027-015-0410-y

Rudd, J. W., Furutani, A., Flett, R. J., and Hamilton, R. D. (1976). Factors controlling methane oxidation in shield lakes: The role of nitrogen fixation and oxygen concentration 1. *Limnol. Oceanogr.* 21 (3), 357–364. doi:10.4319/lo.1976.21.3.0357

Samad, M. S., and Bertilsson, S. (2017). Seasonal variation in abundance and diversity of bacterial methanotrophs in five temperate lakes. *Front. Microbiol.* 8, 142. doi:10.3389/fmicb.2017.00142

Saunois, M., Bousquet, P., Poulter, B., Peregon, A., Ciais, P., Canadell, J. G., et al. (2016). The global methane budget 2000-2012. *Earth Syst. Sci. Data* 8, 697–751. doi:10.5194/essd-8-697-2016

Sawakuchi, H. O., Bastviken, D., Sawakuchi, A. O., Ward, N. D., Borges, C. D., Tsai, S. M., et al. (2016). Oxidative mitigation of aquatic methane emissions in large Amazonian rivers. *Glob. Chang. Biol.* 22 (3), 1075–1085. doi:10.1111/gcb.13169

Sawakuchi, H. O., Martin, G., Peura, S., Bertilsson, S., Karlsson, J., and Bastviken, D. (2021). Phosphorus regulation of methane oxidation in water from ice-covered lakes. *JGR. Biogeosciences* 126 (9), e2020JG006190. doi:10.1029/2020jg006190

Schubert, C. J., Lucas, F. S., Durisch-Kaiser, E., Stierli, R., Diem, T., Scheidegger, O., et al. (2010). Oxidation and emission of methane in a monomictic lake (Rotsee, Switzerland). *Aquat. Sci.* 72 (4), 455–466. doi:10.1007/s00027-010-0148-5

Serrano-Silva, N., Sarria-Guzmán, Y., Dendooven, L., and Luna-Guido, M. (2014). Methanogenesis and methanotrophy in soil: a review. *Pedosphere* 24 (3), 291–307. doi:10.1016/s1002-0160(14)60016-3

Sievert, C. (2020). *Interactive web-based data visualization with R, plotly, and shiny*. Florida: Chapman and Hall/CRC.

Soued, C., and Prairie, Y. T. (2022). Patterns and regulation of hypolimnetic CO_2 and CH_4 in a tropical reservoir using a process-based modeling approach. *JGR. Biogeosciences* 127, e2022JG006897. doi:10.1029/2022jg006897

Sparrow, K. J., Chanton, J. P., Green, R. B., Scheutz, C., Hater, G. R., Wilson, L. C., et al. (2019). Stable isotopic determination of methane oxidation: When smaller scales are better. *Waste Manag.* 97, 82–87. doi:10.1016/j.wasman.2019.07.032

Templeton, A. S., Chu, K. H., Alvarez-Cohen, L., and Conrad, M. E. (2006). Variable carbon isotope fractionation expressed by aerobic CH 4-oxidizing bacteria. *Geochimica Cosmochimica Acta* 70 (7), 1739–1752. doi:10.1016/j.gca.2005.12.002

Thottathil, S. D., Reis, P. C., del Giorgio, P. A., and Prairie, Y. T. (2018). The extent and regulation of summer methane oxidation in northern lakes. *J. Geophys. Res. Biogeosci.* 123 (10), 3216–3230. doi:10.1029/2018jg004464

Thottathil, S. D., Reis, P. C., and Prairie, Y. T. (2019). Methane oxidation kinetics in northern freshwater lakes. *Biogeochemistry* 143 (1), 105–116. doi:10.1007/s10533-019-00552-x

Tyler, S. C., Bilek, R. S., Sass, R. L., and Fisher, F. M. (1997). Methane oxidation and pathways of production in a Texas paddy field deduced from measurements of flux, δl3C, and δD of CH4. *Glob. Biogeochem. Cycles* 11 (3), 323–348. doi:10.1029/97gb01624

Tyler, S. C., Crill, P. M., and Brailsford, G. W. (1994). Fractionation of methane during oxidation in a temperate forested soil. *Geochimica Cosmochimica Acta* 58 (6), 1625–1633. doi:10.1016/0016-7037(94)90564-9

Venkiteswaran, J. J., and Schiff, S. L. (2005). Methane oxidation: isotopic enrichment factors in freshwater boreal reservoirs. *Appl. Geochem.* 20 (4), 683–690. doi:10.1016/j.apgeochem.2004.11.007

Wetzel, R. G., and Likens, G. E. (2000). *Limnological analyses*. 3rd ed. New York, NY: Springer.

Whiticar, M. J. (1999). Carbon and hydrogen isotope systematics of bacterial formation and oxidation of methane. *Chem. Geol.* 161 (1), 291–314. doi:10.1016/s0009-2541(99)00092-3

Wickham, H. (2016). *ggplot2: Elegant graphics for data analysis*. New York, NY: Springer.

Wilke, C. O., Wickham, H., and Wilke, M. C. O. (2019). Package 'cowplot'. Streamlined plot theme and plot annotations for 'ggplot2. R package version 1.0.0. Available at: https://CRAN.R-project.org/package=cowplot.

Yamamoto, S., Alcauskas, J. B., and Crozier, T. E. (1976). Solubility of methane in distilled water and seawater. *J. Chem. Eng. Data* 21 (1), 78–80. doi:10.1021/je60068a029

Zhang, G., Ji, Y., Ma, J., Xu, H., Cai, Z., and Yagi, K. (2012). Intermittent irrigation changes production, oxidation, and emission of CH4 in paddy fields determined with stable carbon isotope technique. *Soil Biol. Biochem.* 52, 108–116. doi:10.1016/j.soilbio.2012.04.017

Zigah, P. K., Oswald, K., Brand, A., Dinkel, C., Wehrli, B., and Schubert, C. J. (2015). Methane oxidation pathways and associated methanotrophic communities in the water column of a tropical lake. *Limnol. Oceanogr.* 60, 553–572. doi:10.1002/lno.10035

frontiers | Frontiers in Environmental Science

TYPE Original Research
PUBLISHED 03 October 2022
DOI 10.3389/fenvs.2022.895531

Check for updates

OPEN ACCESS

EDITED BY
Yves T. Prairie,
Université du Québec à Montréal, Canada

REVIEWED BY
Alistair Grinham,
The University of Queensland, Australia
François Birgand,
North Carolina State University, United States
Jean-Francois Lapierre,
Université de Montréal, Canada
Sydney Moyo,
Rhodes College, United States

*CORRESPONDENCE
Kerri Finlay,
Kerri.Finlay@uregina.ca

†PRESENT ADDRESS
Jackie R. Webb,
Centre for Regional and Rural Futures (CeRRF), Faculty of Science, Engineering and Built Environment, Deakin University, NSW, Australia;
Gavin L. Simpson,
Department of Animal Science, Aarhus University, Aarhus, Denmark

SPECIALTY SECTION
This article was submitted to Biogeochemical Dynamics, a section of the journal Frontiers in Environmental Science

RECEIVED 14 March 2022
ACCEPTED 04 August 2022
PUBLISHED 03 October 2022

CITATION
Jensen SA, Webb JR, Simpson GL, Baulch HM, Leavitt PR and Finlay K (2022), Seasonal variability of CO_2, CH_4, and N_2O content and fluxes in small agricultural reservoirs of the northern Great Plains.
Front. Environ. Sci. 10:895531.
doi: 10.3389/fenvs.2022.895531

COPYRIGHT
© 2022 Jensen, Webb, Simpson, Baulch, Leavitt and Finlay. This is an open-access article distributed under the terms of the Creative Commons Attribution License (CC BY). The use, distribution or reproduction in other forums is permitted, provided the original author(s) and the copyright owner(s) are credited and that the original publication in this journal is cited, in accordance with accepted academic practice. No use, distribution or reproduction is permitted which does not comply with these terms.

Seasonal variability of CO_2, CH_4, and N_2O content and fluxes in small agricultural reservoirs of the northern Great Plains

Sydney A. Jensen [1], Jackie R. Webb [1†], Gavin L. Simpson [2†], Helen M. Baulch [3], Peter R. Leavitt [1,2] and Kerri Finlay [1,2*]

[1]Biology Department, University of Regina, Regina, SK, Canada, [2]Institute of Environmental Change and Society, University of Regina, Regina, SK, Canada, [3]School of Environment and Sustainability and Global Institute for Water Security University of Saskatchewan, Saskatoon, SK, Canada

Inland waters are important global sources, and occasional sinks, of CO_2, CH_4, and N_2O to the atmosphere, but relatively little is known about the contribution of GHGs of constructed waterbodies, particularly small sites in agricultural regions that receive large amounts of nutrients (carbon, nitrogen, phosphorus). Here, we quantify the magnitude and controls of diffusive CO_2, CH_4, and N_2O fluxes from 20 agricultural reservoirs on seasonal and diel timescales. All gases exhibited consistent seasonal trends, with CO_2 concentrations highest in spring and fall and lowest in mid-summer, CH_4 highest in mid-summer, and N_2O elevated in spring following ice-off. No discernible diel trends were observed for GHG content. Analyses of GHG covariance with potential regulatory factors were conducted using generalized additive models (GAMs) that revealed CO_2 concentrations were affected primarily by factors related to benthic respiration, including dissolved oxygen (DO), dissolved inorganic nitrogen (DIN), dissolved organic carbon (DOC), stratification strength, and water source (as $\delta^{18}O_{water}$). In contrast, variation in CH_4 content was correlated positively with factors that favoured methanogenesis, and so varied inversely with DO, soluble reactive phosphorus (SRP), and conductivity (a proxy for sulfate content), and positively with DIN, DOC, and temperature. Finally, N_2O concentrations were driven mainly by variation in reservoir mixing (as buoyancy frequency), and were correlated positively with DO, SRP, and DIN levels and negatively with pH and stratification strength. Estimates of mean CO_2-eq flux during the open-water period ranged from 5,520 mmol m^{-2} $year^{1}$ (using GAM-predictions) to 10,445 mmol m^{-2} $year^{-1}$ (using interpolations of seasonal data) reflecting how extreme values were extrapolated, with true annual flux rates likely falling between these two estimates.

KEYWORDS

agricultural pond, seasonality, greenhouse gas fluxes, CO_2 equivalent (CO_2-eq), methane, nitrous oxide, carbon dioxide

1 Introduction

Inland waters are often sources of greenhouse gases (GHG) to the atmosphere as a result of net emissions of carbon dioxide (CO_2), methane (CH_4), and nitrous oxide (N_2O) (Cole et al., 2007; Tranvik et al., 2009; DelSontro et al., 2018). However, recent research, including that on hard-water prairie ecosystems, suggests that the magnitude, spatial extent, and timing of emissions varies greatly among locales (Finlay et al., 2010; Finlay et al., 2015; Webb et al., 2019a; Webb et al., 2019b; Finlay et al., 2019). Major drivers of GHGs have been shown to be linked to nutrient status (carbon, nitrogen, and phosphorus), primary productivity, surface area, temperature, and latitude (Downing 2010; Deemer et al., 2016; Holgerson and Raymond 2016; DelSontro et al., 2018). Complete accounting of the role of inland waters in the global carbon budget needs to better characterize such temporal variability in different regions and waterbody types, particularly with respect to the cumulative effects of main greenhouse gases.

Waterbodies in agricultural areas are of particular interest in greenhouse gas dynamics as they have elevated nutrient loading reflecting elevated fertilizer application and livestock densities to meet the growing demand of global human populations (Tilman 1999; Earles et al., 2012; Baumann et al., 2017). Small agricultural reservoirs (also referred to as dams, impoundments, or dugouts) appear to vary dramatically in terms of the magnitude and direction of GHG fluxes. For example, Australian farm reservoirs emit large amounts of CO_2 and CH_4 to the atmosphere, but only small quantities of N_2O (Ollivier et al., 2018; Ollivier et al., 2019). In contrast, agricultural reservoirs of the northern Great Plains of North America are often sinks for CO_2 (52% of sites) and N_2O (67%), but are consistent net sources of CH_4 (Webb et al., 2019a; Webb et al., 2019b). Unfortunately, most of these surveys are based on single samples in late-summer (August) samples (Maberly 1996; Dillon and Molot 1997; Baehr and DeGrandpre 2004; Ducharme-Riel et al., 2015; Denfeld et al., 2016; Finlay et al., 2019), raising questions of the role of seasonal variability in influencing net annual carbon sources.

Understanding the mechanistic controls of aquatic CO_2, CH_4, and N_2O concentrations is critical for upscaling efforts, predictions of future climate change effects, and management opportunities to use these systems as carbon offsets (Bastviken et al., 2004; DelSontro et al., 2016). Temporal dynamics of CO_2 are usually correlated with changes in either microbial metabolism or the supply of inorganic carbon to freshwaters (Chapin et al., 2006; Dubois et al., 2009; McDonald et al., 2013; Bogard and Giorgio 2016; Wilkinson et al., 2016). In boreal ecosystems, the main pathway of CO_2 production and consumption is through photosynthesis (*P*, consumption) and respiration (R, production), with CO_2 evasion occurring when $P < R$ (Chapin et al., 2006; Bogard and Giorgio 2016). However, this metabolic control can be overridden in non-boreal systems due to substantial inputs of inorganic C (e.g., DIC in runoff or groundwater) or changes in pH and carbonate chemistry (Dubois et al., 2009; Finlay et al., 2010; McDonald et al., 2013; Bogard and Giorgio 2016; Wilkinson et al., 2016). For example, in small prairie hardwater systems, CO_2 concentration are regulated by a complex interaction between primary production, DIC content, nutrient status, stratification intensity, groundwater fluxes, and regional edaphic conditions (Webb et al., 2019b). Together, these models suggest that seasonal variation in the interaction among control factors is likely to create significant temporal variation in net CO_2 fluxes.

Methane is produced by methanogenic bacteria through the anaerobic degradation of organic matter, most often in the anoxic or hypoxic sediments of waterbodies (Glass and Orphan 2012). This CH_4 can be released to the atmosphere through diffusion, ebullition, or plant-mediated fluxes. Rates of CH_4 production are highly dependent on temperature ($Q_{10} \sim 4$; range 1–35) (Yvon-Durocher et al., 2014; DelSontro et al., 2016), whereas CH_4 can be consumed by methane-oxidizing bacteria ("methanotrophy") under oxic conditions (King 1992; Duc et al., 2010). Gas concentrations are also influenced by other factors including organic carbon availability and quality (Segers 1998; Bridgham et al., 2006), mineral nutrient availability, and productivity (Deemer et al., 2016; DelSontro et al., 2018; Ollivier et al., 2018; Beaulieu et al., 2019) and competitive inhibition by sulfur-reducing bacteria (Lovley and Klug 1983; Webb et al., 2019b). Landscape models of farm reservoirs suggest that lowest CH_4 concentrations occur with DO supersaturation, low sediment C:N ratios, reduced dissolved inorganic nitrogen (DIN) concentrations, intermediate water residence time, elevated groundwater inflow, and higher conductivity levels (Webb et al., 2019b). Taken together, these observations suggest that seasonal CH_4 production in agricultural ponds will reach a maximum in late summer, when temperature, productivity, thermal stratification and deepwater anoxia are greatest.

Production of N_2O arises as an intermediary product during nitrification (Quick et al., 2019), incomplete denitrification (Firestone and Davidson 1989; Glass and Orphan 2012), or dissimilatory nitrate reduction to NH_4^+ (DNRA; Scott et al., 2008), whereas denitrification consumes N_2O (Quick et al., 2019). Previous research suggests that temporal controls of N_2O flux include DO saturation, organic carbon availability, nitrogen availability and speciation, pH, and temperature (Baulch et al., 2011; Gooding & Baulch 2017; Quick et al., 2019; Zhang et al., 2021). Spatial analysis of variation in N_2O emissions from small agricultural reservoirs reveals N_2O concentrations were lowest when thermal stratification was strong, phytoplankton biomass (as Chl-*a*) was elevated, and DO was supersaturated (Webb et al., 2019a). Although N_2O emissions from prairie wetlands are known to be high in spring (Pennock et al., 2010) when DOC and NOx is abundant, there have been few systematic studies of the controls of seasonal variation in the regulation of N_2O fluxes.

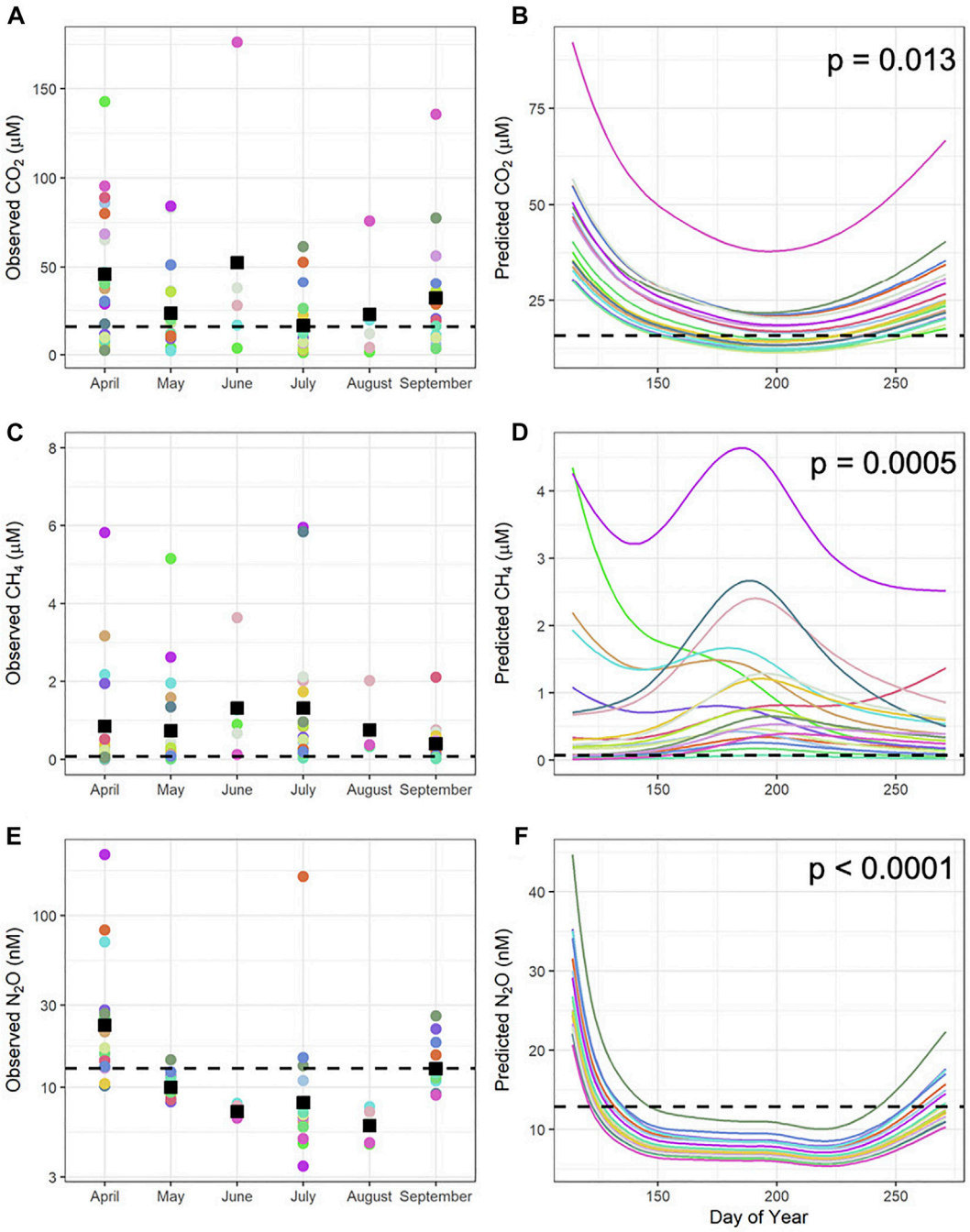


FIGURE 1
Seasonal carbon dioxide (CO_2, **(A,B)**), methane (CH_4, **(C,D)**), and nitrous oxide (N_2O, **(E,F)**) concentrations from 20 reservoirs in 2018. Left column: Raw observed GHG data for all three gases. Each coloured circle is one reservoir. The black squares represent the monthly mean. This data was used to inform the models. Right column: The modelled seasonal gas concentration from a generalized additive model (GAM) of all three gases. Each coloured line represents a single reservoir. *p*-values for the GAM are located at the top of each plot. Black dashed line in both panels represents the calculated (from ppm) atmospheric concentration of each gas. The colour in the left panel corresponds to the coordinating colour in the right panel. Deviance explained = 36.6% for CO_2, 88.7% for CH_4, and 90.2% for N_2O.

Thus, while previous research provides some mechanistic predictions for GHG fluxes from small waterbodies, it is difficult to anticipate how all three gases will sum to a CO_2-equivalent (CO_2-eq) flux over the entire open water season. This study presents a seasonal and diel assessment of the magnitude of CO_2, CH_4, and N_2O concentration and diffusive flux, and the factors

TABLE 1 Physical and environmental parameters measured in the 20 reservoirs monthly in 2018. All parameters, excluding max depth, Secchi depth, and buoyancy frequency were measured using the YSI multi-parameter probe at 0.5 m below the water surface, excluding deep dissolved oxygen which was taken 0.5 m above the sediment. Presented as mean ± standard deviation (SD). Superscript letters denote significant differences between months based on ANOVA and post-hoc Tukey test. DO = Dissolved Oxygen.

	Units	Month	Mean (SD)
Surface Temperature	°C	April[a]	7.98 (4.38)
		May[b]	15.6 (2.6)
		July[c]	22.7 (1.5)
		September[a]	6.99 (0.9)
Max Depth	Meters	April[a]	1.57 (1.3)
		May[a]	1.92 (0.8)
		July[a]	2.14 (0.9)
		September[a]	1.73 (0.7)
Secchi Depth	Meters	April[a]	0.481 (0.1)
		May[a]	0.591 (0.4)
		July[a]	0.824 (0.5)
		September[a]	0.556 (0.5)
Buoyancy Fraquency	s^{-2}	April[b]	0.001 (0.002)
		May[a]	0.006 (0.005)
		July[a]	0.01 (0.008)
		September[b]	0 (0)
pH	Unitless	April[a]	8.29 (0.8)
		May[ab]	8.71 (0.5)
		July[ab]	8.94 (0.6)
		September[b]	8.62 (0.4)
Surdace DO	%Saturation	April[a]	90.4 (30.1)
		May[a]	92.9 (20.7)
		July[a]	94.6 (44.3)
		September[a]	81.0 (22.1)
Deep DO	%Saturation	April[a]	67.2 (43.4)
		May[ab]	39.3 (38.6)
		July[b]	11.3 (19.0)
		September[a]	665.5 (29.1)
Conductivity	µS cm^{-1}	April[a]	737 (590.5)
		May[ab]	1,178 (891.2)
		July[ab]	1728 (1,533.4)
		September[a]	1824 (1721.9)

TABLE 2 Carbon and nutrient concentrations for each month in the 20 reservoirs in 2018. Presented as mean ± standard deviation (SD). Superscript letters denote significant differences based on ANOVA and post-hoc Tukey test. DIC = dissolved inorganic carbon. DOC = dissolved organic carbon. TDP = total dissolved phosphorus. SRP = soluble reactive phosphorus. TDN = total dissolved nitrogen. NO_x = nitrate and nitrite concentration. NH_3 = ammonia concentration. Chl-*a* = chlorophyll a concentration. Dissolved inorganic nitrogen (DIN) is the sum of NO_x and NH_3.

	Units	Month	Mean (SD)
DIC	mg C L^{-1}	April[a]	30.5 (11.8)
		May[ab]	40.5 (13.5)
		July[b]	47.2 (22.9)
		September[b]	56.0 (26.4)
DOC	mg C L^{-1}	April[a]	20.1 (6.5)
		May[ab]	23.6 (8.0)
		July[ab]	26.3 (9.5)
		September[b]	31.3 (12.0)
TDP	µg P L^{-1}	April[a]	569 (816.1)
		May[b]	340 (468.3)
		July[b]	426 (860.4)
		September[a]	315 (500.0)
SRP	µg P L^{-1}	April[a]	381 (446.3)
		May[b]	293 (445.7)
		July[b]	343 (677.4)
		September[a]	265 (484.1)
TDN	µg N L^{-1}	April[a]	3,421 (3,218.0)
		May[a]	1913 (706.6)
		July[a]	2,694 (1899.1)
		September[a]	3,197 (3,197.4)
NO_x	µg N L^{-1}	April[a]	644 (1,054.1)
		May[b]	22.7 (27.2)
		July[ab]	277 (675.3)
		September[b]	37.3 (49.7)
NH_3	µg N L^{-1}	April[a]	496 (924.9)
		May[a]	118 (126.4)
		July[a]	126 (143.2)
		September[a]	544 (874.1)
Chl-*a*	µg L^{-1}	April[a]	41.9 (53.5)
		May[a]	25.5 (23.0)
		July[a]	38.4 (67.3)
		September[a]	75.1 (80.7)

controlling the seasonal concentrations of these GHGs across 20 agricultural reservoirs in the northern Great Plains, the largest farming region in Canada. This study builds on previous work which found that some regional lakes sequester CO_2 (Finlay et al., 2009; Finlay et al. 2010; Finlay et al. 2015; Finlay et al. 2019), as well as previous spatial surveys of 101 agricultural reservoirs that found highly variable fluxes of CO_2 and CH_4, but general undersaturation of N_2O (Webb et al., 2019a; Webb et al., 2019b). The goals of this study were to: 1) quantify the change in concentrations of CO_2, CH_4, and N_2O on seasonal and diel timescales in agricultural reservoirs; 2) identify the seasonal drivers of CO_2, CH_4, and N_2O concentrations in these agricultural reservoirs, and; 3) estimate the total annual CO_2 equivalence contribution of GHG to the atmosphere from these systems. Based on earlier work, we anticipated that the reservoirs would be consistent sinks for CO_2 and N_2O, with only notable release in spring and late fall (Finlay et al., 2015; Finlay et al., 2019), that GHG release varied inversely with stratification

intensity (Webb et al., 2019a), and that CH_4 may be the main control of net CO_2-eq exchanges in these systems (Pennock et al., 2010; Webb et al., 2019b).

2 Methods

Twenty constructed agricultural reservoirs were chosen for this study (Figure 1). Agricultural reservoirs, known regionally as "dugouts", typically have a rectangular construction, with steep sloping sides (1.5:1) and a maximum depth of 4–6 m (Webb et al., 2019b). All reservoirs are located in southern Saskatchewan, Canada, within a 150 km radius of the City of Regina (50° 27′ 10.19″ N, −104° 36' 14.39″ W), as a previous survey of 100 regional reservoirs did not identify significant spatial component to regulation of GHG concentrations (Webb et al., 2019a; Webb et al., 2019b). Sites were selected to encompass a wide range of physical and chemical parameters (Table 1 and Table 2) based on data collected in 2017. Reservoirs were sampled four times during 2018; in late April when 75% of ice cover had melted, mid-May when sites were entirely ice-free, mid-July, and at the end of September prior to October ice formation. Five sites were also sampled in June and August to evaluate the effect of increased temporal resolution on determination of seasonal patterns in GHG content and fluxes.

2.1 Field collection

2.1.1 Seasonal sampling

During each sampling period, samples were collected within a 10-day interval, and all collections were made during daylight hours. Each site was sampled from a canoe, anchored near the center of the reservoir over the deepest water. Water temperature (°C), DO (mg L^{-1}, % saturation), conductivity (μS cm^{-1}), and pH were measured using a Yellow Springs Instrument (YSI) multi-parameter probe at ~0.5-m depth intervals from the surface to the bottom. The probe was calibrated monthly using three standard solutions for pH, whereas DO saturation was calibrated at each sampling location. Atmospheric pressure (mm Hg) was estimated at each site using the YSI probe. Depth of the reservoir was taken using a Norcross Hawkeye handheld depth finder. Water clarity was measured using a 20-cm diameter Secchi disk.

Water samples were collected using a submersible pump with an intake deployed at ~0.5-m depth. Whole water was screened through 80-μm mesh to remove large zooplankton and particulate matter and combined into a pre-rinsed cleaned carboy. Samples were transported back to the laboratory for chemical analyses.

GHG concentration of water was sampled on site using the headspace extraction method of Webb et al. (2019a). This process involves using a submersible pump to fill a 1.2-L glass serum bottle to overflow using water from ~0.5-m depth, ensuring that there were no bubbles present, and sealing the bottle with a two-way rubber stopper. A 60-ml sample of atmospheric air was added to the bottle while 60-ml of water was removed to maintain constant pressure in the bottle. The bottle was then shaken vigorously for 2 min to equilibrate the air and water. Two replicate gas samples were extracted from the headspace using an air-tight syringe and put into 12-ml pre-evacuated Exetainer vials with double wadded caps. This process was repeated in duplicate to collect four samples per date. A sample of atmospheric air was also collected and placed in a 12-ml pre-evacuated Exetainer vial with double wadded cap. All gas samples were stored at room temperature until analysis within 2 months of collection. While methane ebullition is known to contribute significantly to methane emissions, this analysis only focuses on diffusive flux of greenhouse gases. Methane ebullition is known to be very patchy both spatially and temporally, and seasonal changes in bubble flux is currently not well constrained.

2.1.2 Diel sampling

Four reservoirs were selected for diel monitoring to assess daily variability in CO_2, CH_4, and N_2O concentrations. Samples were collected at 4-h intervals over 24 h (6 total), beginning ~10: 00 h, between 26 June and 01 August 2018. Each diel cycle involved GHG sampling and YSI readings as described above. Water samples were collected at the 0-h, 12-h, and 24-h marks to determine changes in water chemistry throughout the 24-h period. Additionally, a YSI multi-parameter probe was deployed in each site for the entire 24-h period, taking readings for water temperature, DO, pH, and conductivity at 10-min intervals. Sites were selected from a set of previously sampled sites to include a wide range of physical and chemical parameters. Secondarily, sites were selected based on ease of access and availability of services for the field team.

2.2 Laboratory analysis

At the laboratory, water samples were stored at 4°C and filtered within 24 h of collection. Sufficient water to visibly discolour a Whatman 1.2-μm GF/C filter was filtered was recorded, and filtrate was frozen (−10°C) in sealed darkened film canisters until analysis for chlorophyll pigments.

Greenhouse gas samples were analyzed at the Global Institute for Water Security, University of Saskatchewan. Headspace gas samples were analyzed for the dry molar fraction of CO_2, CH_4, and N_2O using a fully calibrated Scion 456 Gas Chromatograph (Bruker Ltd.) with Combipal autosampler (CTC Analytics–PAL System), using argon as the carrier gas. A flame ionization detector was used for methane samples (<100,000 ppmv). A thermal conductivity detector was used for CO_2 and high level CH_4 concentrations (>100,000 ppmv). N_2O was measured using a micro-electron capture detector and argon/methane (90/10) as

a makeup gas (injector temperature 60°C, column temperature 60°C, detector temperature 350°C). All gases were calibrated using mixed gas standards (Praxair) with the addition of a single gas N_2O standard (0.1 ppmv; Scotty).

Water chemistry and water isotope samples were analyzed at the Institute for Environmental Change and Society at the University of Regina. Water chemistry samples were analyzed for soluble reactive phosphorus (SRP), total dissolved nitrogen (TDN), nitrate and nitrite (NO_x), ammonia (NH_3), dissolved organic carbon (DOC), and dissolved inorganic carbon (DIC). DOC and DIC were analyzed using standard analytic procedures on a Shimadzu model 5000 A total carbon analyzer (Finlay et al., 2009; Webb et al., 2019b). Dissolved nitrogen (TDN, NO_x, NH_3) and dissolved phosphorus (TDP, SRP) were measured using standard procedures on a Lachat QuikChem 8,500 (APHA-AWWA/WEF 1998; Bergbusch et al., 2021). Chl-*a* concentration was standard trichromatic spectrophotometric methods (Jeffrey and Humphrey 1975; Finlay et al., 2009). Water was analyzed for $\delta^{18}O\text{-}H_2O$ using a Picarro L2120-I cavity ring-down spectrometer (CRDS), and $\delta^{18}O$ inflow was calculated using coupled isotope tracer methods as an estimate of water source (winter vs. summer precipitation, groundwater, Yi et al., 2008; Webb et al., 2019a; Haig et al., 2020).

2.3 Numerical analyses

The squared Brunt-Väisälä buoyancy frequency (s^{-2}) was calculated as a measure of maximum stratification strength within the water column. This approach uses the greatest density gradient from the vertical water temperature profiles taken at intervals of 0.5 m (0.25 m in shallower waterbodies) using the rLakeAnalyzer package (Read et al., 2011) in R (version 4.0.5; R Core Team, 2021) (Webb et al., 2019b).

The dry molar fractions of CO_2, CH_4, and N_2O were corrected for dilution and converted to concentrations according to the solubility coefficients and atmospheric partial pressure of each gas and the salinity of the water. Four replicate gas concentrations for each site were averaged for CO_2, CH_4, and N_2O to estimate mean concentrations for each sampling period. We removed an extreme CH_4 outlier for in one reservoir seen during April (93.5 μM) and assumed an ebullitive event that was captured in the associated water sample.

The concentration of each of the gases were used to estimate the diffusive flux for CO_2, CH_4, and N_2O. The diffusive flux (f_C) was calculated using the gas transfer velocity (k_c), gas concentration of the water (C_{water}), and the ambient air concentration (C_{air}) using the following equation (Eq. 1):

$$f_C = k_c (C_{water} - C_{air}) \quad (1)$$

The ambient air concentration of each gas was taken as the average over the sampling period at the Mauna Loa NOAA station from April to September 2018, inclusive. The average concentrations were 408.94 μatm (or ppm) for CO_2, 1.86 μatm (or ppm) for CH_4, and 0.33 μatm (or ppm) for N_2O, and corrected for the barometric pressure for each sampling effort. The diffusive flux was calculated using the gas transfer velocity as measured on similar agricultural reservoirs in 2017 (Webb et al. 2019a; Webb et al. 2019b). We did not estimate ebullitive CH_4 fluxes, although we recognize this will lead to an underestimation of the true total CH_4 efflux.

Integrating seasonal GHG flux across all gases is challenging, owing to temporal variability and the assumptions required to extrapolate between sampling dates. Here, we calculated total CO_2-eq flux using several methods to bound true values. First, the "July only" procedure used only the daily CO_2-eq value observed in July multiplied over the total number of ice-free days to extrapolate over the entire open water period (e.g., metanalysis in DelSontro et al., 2018). Second, the "Seasonal" protocol used the CO_2-eq values measured in April, May, July, and September for the respective intervals summed over the entire open water period (e.g., Striegl and Michmerhuizen 1998; Finlay et al., 2019). Third, we calculated a "Predicted" flux using the generalized additive models (GAMs) of the smoothed seasonal splines to interpolate fluxes on each date between sampling periods. For this last method, we took both the mean smooth value and the upper 95% credible interval ("Upper CI") to estimate mean and maximum seasonal CO_2-eq flux. Given the lack of consistent diel trend (see Section 3.4 below), we used measured flux rates from daytime determinations only. In all cases, the CO_2-eq flux was calculated by first converting the moles of diffusive flux value to grams of diffusive flux, and then multiplying by the sustained global warming potential (45 and 270 for CH_4 and N_2O, respectively) if the diffusive flux value was positive, and by the sustained global cooling potential (203 and 349 for CH_4 and N_2O, respectively) if the diffusive flux value was negative (Neubauer and Megonigal 2015).

Generalized additive models (Wood 2006; Wood et al., 2016) were used to assess the seasonal trends in CO_2, CH_4, and N_2O concentration in the reservoirs, as they are particularly useful for estimating linear, nonlinear, and nonmonotonic relationships between response variables and predictors (Webb et al., 2019a; b; Swarbrick et al., 2019). All modelling was done using the *mgcv* package (Wood 2011; Wood 2016) for R (version 4.0.5; R Core Team, 2021). GAMs were also used to link CO_2, CH_4, and N_2O concentrations to various biotic and abiotic predictive parameters to identify which factors might regulate changes in GHG concentrations in agricultural reservoirs. Covariates included those thought to control seasonal variation in GHG levels during the open-water period and were based on spatial analysis of these agricultural reservoirs (Webb et al., 2019a; Webb et al., 2019b). Variables included nutrient content (DOC, DIN,

SRP), production (Chl-*a*, DO), and stratification strength (buoyancy frequency). The CO_2 model additionally included water sources (as $\delta^{18}O$ of inflow), specifically groundwater, rainfall, or snowmelt (Yi et al., 2008; Haig et al., 2020). Conductivity was additionally included in the CH_4 model as a proxy for ionic content and, in this region, sulfate concentrations ($r^2_{cond\text{-}SO4}$ = 0.64, p < 0.01). Similarly, pH was included in the N_2O model because of its known effects on N_2O production and consumption processes (Quick et al., 2019). Site identity (ID) was included as a random effect in the model, to account for the differences between individual sites.

A Gamma distribution was used with a log-link function, for positive, continuous responses of CO_2 and CH_4. We used a gammals distribution for N_2O concentrations to model the log mean and log scale parameter (or standard deviation/variance) for the probability density function. The gammals distribution was used because two sites exhibited high, outlying N_2O concentrations compared to the rest, so this allowed for grouping (high and low) of sites separately from the rest of the sites to inform a non-normal distribution. Sites were put into the high group if 25% or more of their N_2O concentrations were outliers. Basis size, dispersion of residuals, homogeneity of variance, and the relationship between the observed and predicted response were assessed in each model to ensure assumptions were not violated. Residual marginal likelihood (REML) was used for selection of smoothness parameters (Wood, 2011). To help with model selection, the double penalty approach of Marra and Wood (2011) was used. An additional penalty is applied to the perfectly smooth parts of the basis (the functions in the penalty null space) of each smooth function in the model, which allows entire smooths to be effectively penalised out of the model, while accounting for the selection procedure in the statistical tests applied to model terms. Parameters predicting CO_2, CH_4, and N_2O concentrations were considered significant at 95% confidence level (α = 0.05) for each waterbody.

3 Results

3.1 Water quality

Physical and environmental parameters of the 20 reservoirs exhibited a wide range of values among sites and over the season (Table 1). The mean monthly max depth (mean = 1.88 m, standard deviation (SD) = 0.92), Secchi depth (0.61 ± 0.43 m), DO saturation (89.5 ± 31.2%), and Chl-*a* (44.8 ± 61.1 μg L^{-1}) of the reservoirs did not change significantly between any month (ANOVA, p-value > 0.05). Mean surface water temperature was low in April (mean = 7.98°C, SD = 4.38), reached a maximum in July (mean = 22.7°C, SD = 1.47), and declined again in September (mean = 6.99°C, SD = 0.87, ANOVA post-hoc Tukey test, p-value < 0.001). The pH of the surface water was lowest in April (mean = 8.29, SD = 0.84), reached a maximum in July (mean = 8.94, SD = 0.61), and decreased again in September (mean = 8.62, SD = 0.44, ANOVA post-hoc Tukey test, p-value = 0.014). Conductivity increased from April (mean = 737 μS cm^{-1}, SD = 591) to September (mean = 1824 μS cm^{-1}, SD = 1722, ANOVA post-hoc Tukey test, p-value = 0.029). Salinity also increased from April (mean = 0.53 ppt, SD = 0.42) to September (mean = 1.25 ppt, SD = 1.11, ANOVA post-hoc Tukey test, p-value = 0.033).

Water chemistry parameters were highly variable both between months and among reservoirs (Table 2). Soluble reactive phosphorus (seasonal mean = 320 μg P L^{-1}, SD = 515), TDN (2,793 ± 2,141 μg N L^{-1}) and NH_3 (seasonal mean = 316 μg N L^{-1}, SD = 654) concentrations did not have a significant change between monthly means (ANOVA post-hoc Tukey test, p-value = 0.001). DOC concentrations also increased from April (mean = 20.1 mg C L^{-1}, SD = 6.54) to September (mean = 31.3 mg C L^{-1}, SD = 12.0, ANOVA post-hoc Tukey test, p-value = 0.004). The concentration of NO_x was highest initially following ice-off in April (mean = 644 μg N L^{-1}, SD = 1,054, ANOVA post-hoc Tukey test, p-value = 0.009).

3.2 Seasonal greenhouse gas concentration and flux

Temporal variation in concentrations of CO_2, CH_4, and N_2O (Figure 1A) was identified as significant seasonal trends when analyzed by GAMs for all gases (Figure 1B). The concentrations of each of the gases was highly variable between reservoirs, yet there were common trends for each gas. For example, concentrations of CO_2 were greatest immediately following ice-off in April (mean = 45.8 μM, SD = 39.3), declined during spring and summer (May–mean = 23.5 μM, SD 23.6, July–mean = 16.5 μM, SD 17.0), then increased again in fall (mean = 32.0 μM, SD 31.2, GAM, p-value = 0.013, deviance explained = 49%). In contrast, CH_4 concentration were initially low in the spring (April–mean = 0.849 μM, SD = 1.54; May–mean = 0.73 μM, SD = 1.28), but increased into a mid-summer peak (mean = 1.32 μM, SD = 1.70) before decreasing in fall (mean = 0.40 μM, SD = 0.47, GAM, p-value = 0.0005, deviance explained = 91.4%). Finally, concentration of N_2O exhibited a strong pulse during ice-off in April (mean = 35.2 nM, SD = 50.3), followed by a sharp decrease to low values in spring and summer

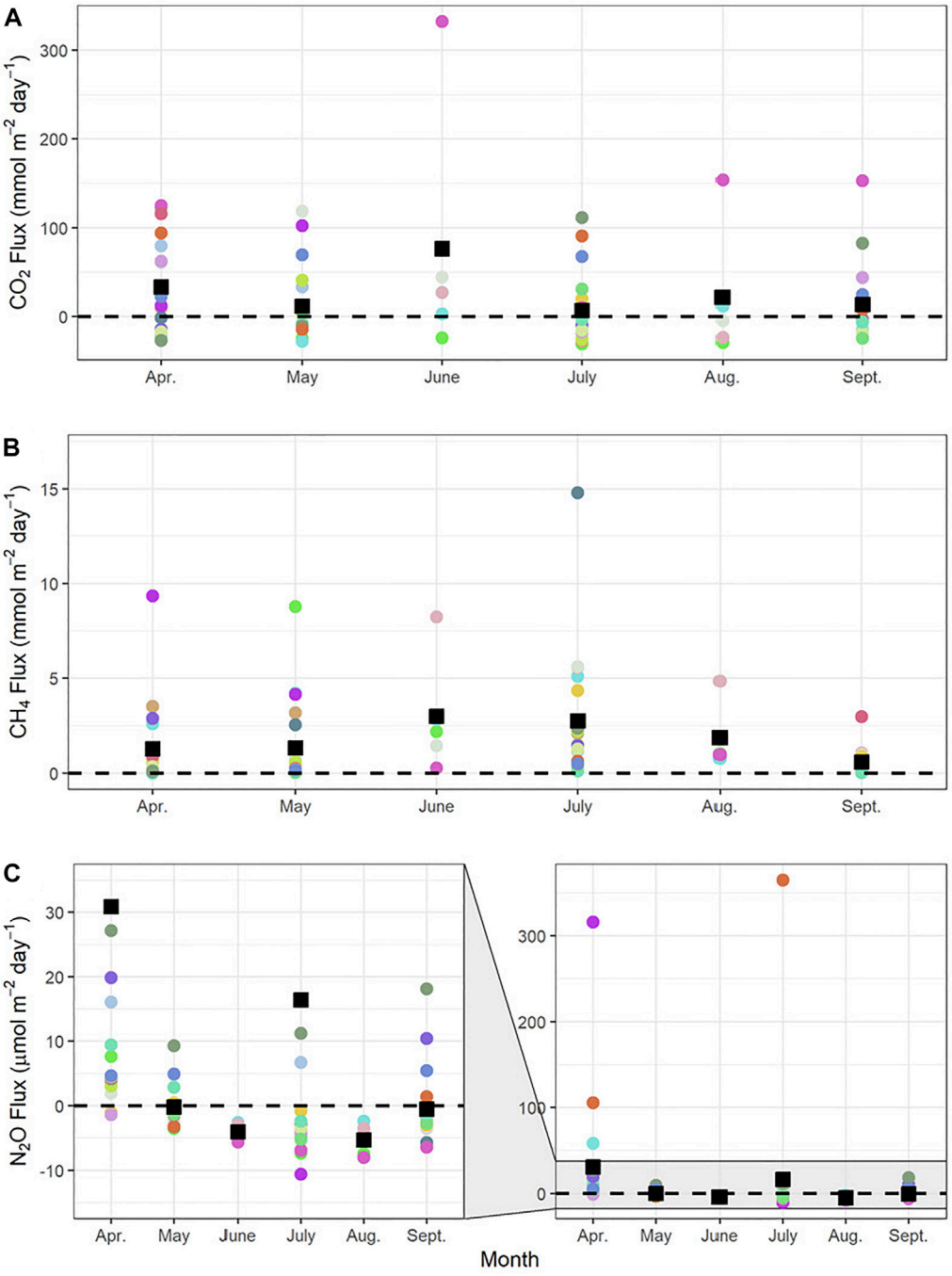


FIGURE 2
(A) Carbon Dioxide (CO_2) **(B)** methane (CH_4), and **(C)** nitrous oxide (N_2O) flux for the sampling period. Each coloured circle represents a single reservoir, while the black square represents the monthly mean. Black dashed line atmospheric equilibrium, where values above indicate loss of gas to the atmosphere and values below indicate removal of gas from the atmosphere. One outlying CH_4 value in April was omitted (value = 100 mmol m-2 day-1) as it is assumed that an ebullition event was captured.

(May–mean = 10.1 nM, SD = 1.5; July–mean = 15.4 nM, SD = 36.1), before rising slightly again prior to ice formation (mean = 13.3 nM, SD = 4.31, GAM, p-value < 0.0001, deviance explained = 89.5%).

Estimates of diffusive fluxes of CO_2, CH_4, N_2O were all highly variable among sites (Figure 2). Despite among-site variation, diffusive flux of CO_2 varied little between months (ANOVA, p-value = 0.161), with the overall mean (= SD) of 19.7 ±

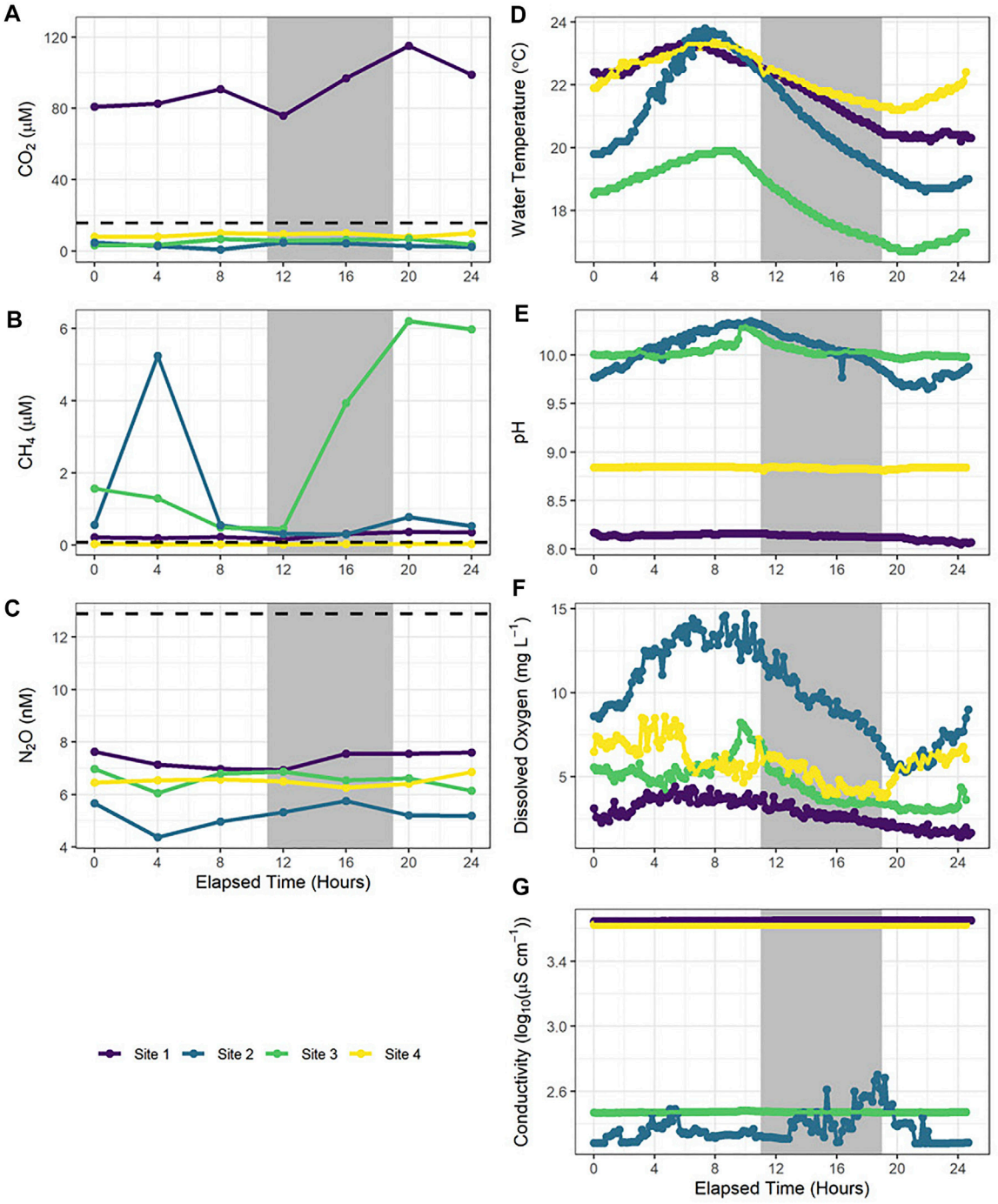


FIGURE 3
Greenhouse gas **(A–C)** and water quality parameters **(D–G)** in four reservoirs measured over a 24-h period. Each coloured line is representative of one site. The grey shaded regions are the average night-time period. Elapsed time is time from the initiation of the 24-h period. Earliest start was 09:50, while the latest start was 11:24. Temperature **(D)**, DO (dissolved oxygen **(E)**), pH **(F)** and conductivity **(G)** readings were taken every 10 min, while greenhouse gas concentrations were collected every 4 h. CO_2 = carbon dioxide **(A)**. CH_4 = methane **(B)**. N_2O = nitrous oxide **(C)**. See 24-h averages of nutrient, Chl-*a* and carbon concentrations in Supplementary Table S1.

56.6 mmol m^{-2} day^{-1}. Similar patterns were recorded for the diffusive flux of CH_4, with no seasonal difference between monthly means (ANOVA, *p*-value = 0.654) and an overall flux of 2.9 ± 10.9 mmol m^{-2} day^{-1}. Diffusive flux of N_2O was variable among sites but not months (ANOVA, *p*-value = 0.361), with an overall mean diffusive N_2O flux of 9.7 ± 52.9 µmol m^{-2} day^{-1}.

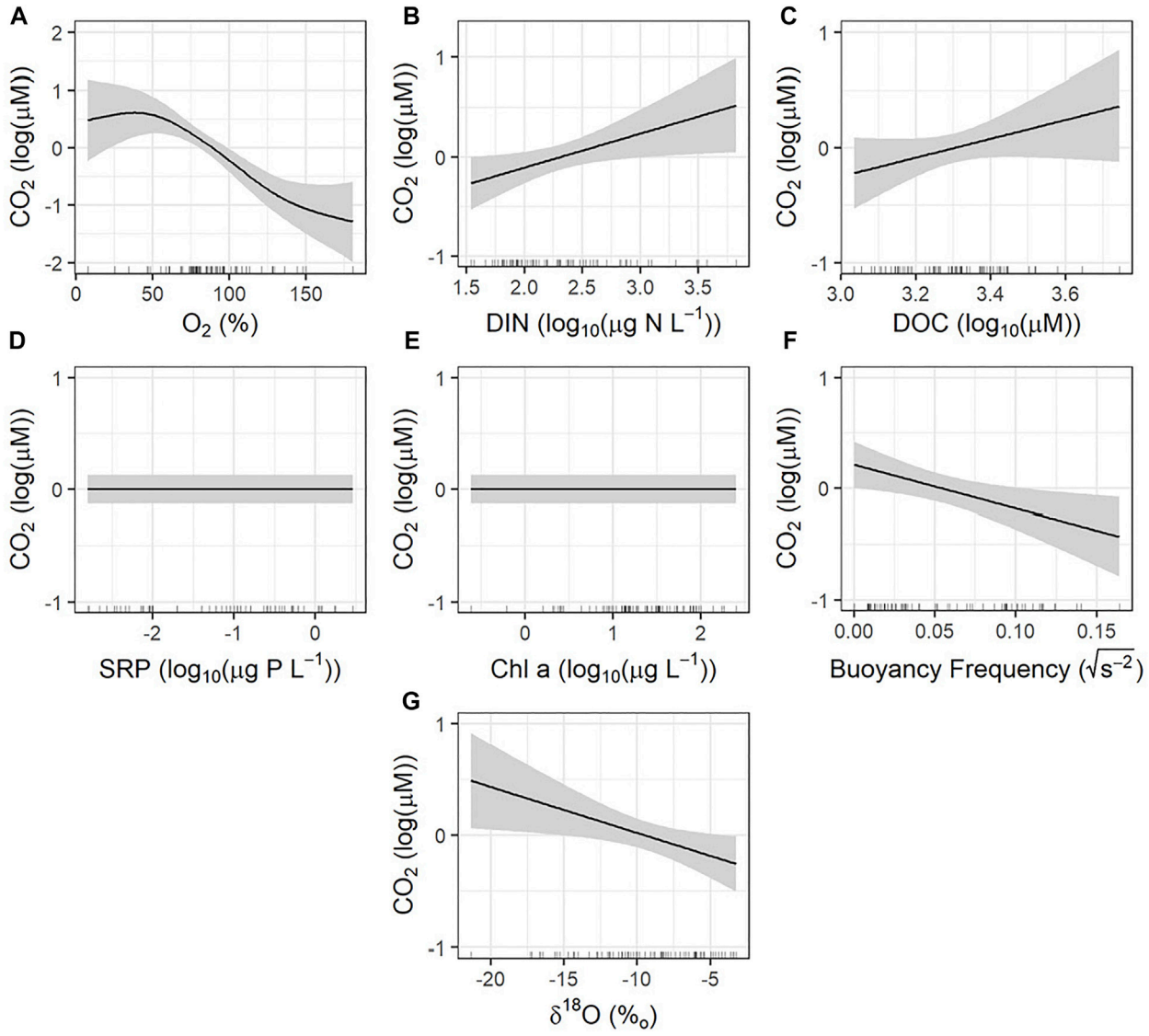


FIGURE 4
Partial effects plots from generalized additive models assessing the seasonal controls of carbon dioxide (CO_2). Model deviance explained was 63.9%. Shaded region represents the 95% confidence interval. The rug along the *x*-axis indicates the distribution of observations. **(A)** Dissolved oxygen saturations; significant. **(B)** Dissolved inorganic nitrogen concentration; significant. **(C)** Dissolved organic carbon concentration; significant. **(D)** Soluble reactive phosphorus concentration; not significant. **(E)** Chl-*a* concentration; not significant. **(F)** Buoyancy frequency (stratification strength); significant. **(G)** $d_{18}O$ inflow (measure of water source); significant.

3.3 Diel water chemistry

Most water quality parameters did not change substantially during the diel cycle (Figure 3). In general, temperature was greater during the day and lower at night, although there were up to 4°C differences among sites (Figure 3D). Similarly, while DO exhibited some high frequency variation, concentrations were generally lower at night than in the day (Figure 3E). In contrast, few trends were observed for conductivity, and pH exhibited diel cycle (elevated in day) at only one site with elevated Chl-*a* values and high diel changes in DO. Nutrients (TN, TP, SRP, DOC, DIC) and Chl-*a* did not exhibit any observable changes during the diel cycle in any sites, while NO_x concentration and ammonia concentration only exhibited notable variation at one site with high DIN levels (Supplementary Table S1).

3.4 Diel greenhouse gas concentration and flux

Concentrations of CO_2, CH_4, and N_2O showed no consistent trends during a 24-h period in the four

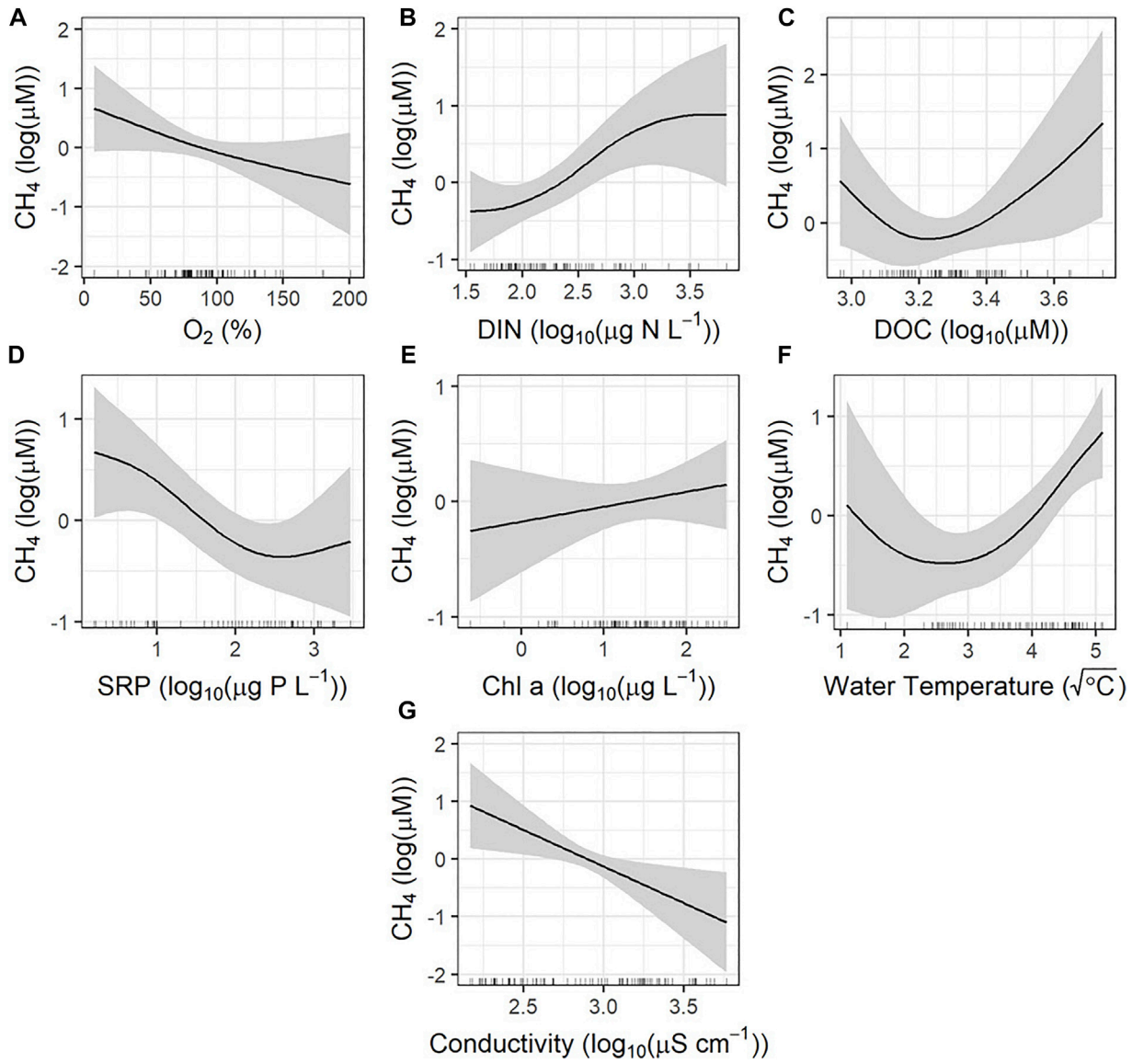


FIGURE 5
Partial effects plots from generalized additive models assessing the seasonal controls of methane (CH_4). Model deviance explained was 74.5%. Shaded region represents the 95% confidence interval. The rug along the *x*-axis indicates the distribution of observations. **(A)** Dissolved oxygen saturations; significant. **(B)** Dissolved inorganic nitrogen concentration; significant. **(C)** Dissolved organic carbon concentration; significant. **(D)** Soluble reactive phosphorus concentration; significant. **(E)** Chl-*a* concentration; not significant. **(F)** Water temperature; significant. **(G)** Conductivity; significant.

reservoirs sampled (Figure 3). At three sites, CO_2 concentrations were consistently undersaturated over the diel cycle, while values were supersaturated at the fourth site yet no more variable through time. CH_4 concentrations at two sites remained low throughout the diel cycle, while the other two basins showed inconsistent but elevated variation during the 24 h study period. Overall, N_2O concentrations were consistently low and undersaturated during the diel cycle.

3.5 Seasonal greenhouse gas controls

Seasonal changes in CO_2 concentration in the reservoirs were explained best by a GAM using the pH of surface water as the sole predictor (Supplementary Figure S2). This model explained 89.1% of deviance in CO_2 and was characterized by a strong negative relationship with CO_2 above pH of 8. When pH was not included in the model, variation in CO_2 was explained best by a combination of DO saturation (Figure 4A), DIN concentration

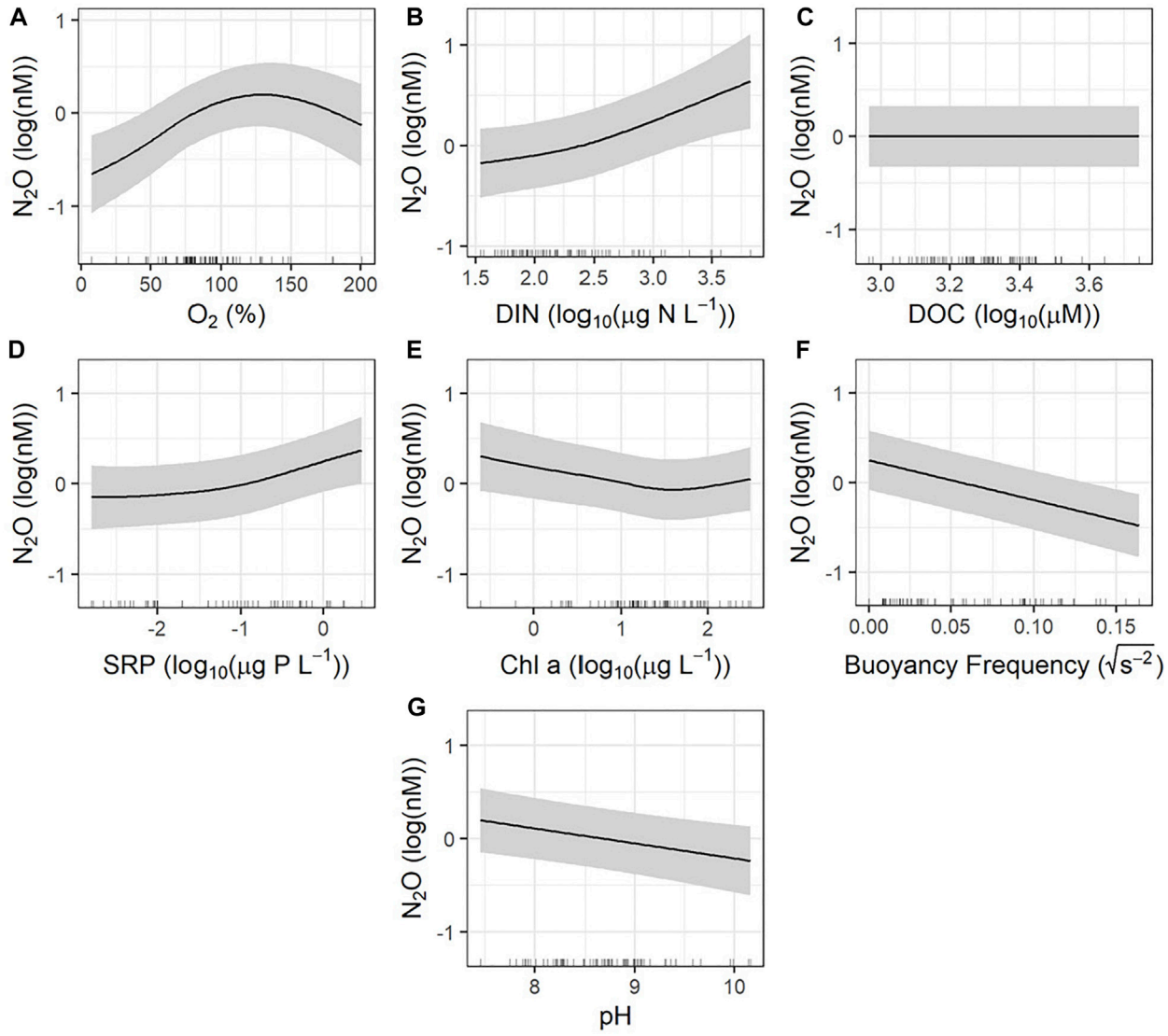


FIGURE 6
Partial effects plots from generalized additive models assessing the seasonal controls of nitrous oxide (N_2O). Model deviance explained was 87.4%. Shaded region represents the 95% confidence interval. The rug along the *x*-axis indicates the distribution of observations. **(A)** Dissolved oxygen saturations; significant. **(B)** Dissolved inorganic nitrogen concentration; significant. **(C)** Dissolved organic carbon concentration; not significant. **(D)** Soluble reactive phosphorus concentration; significant. **(E)** Chl-*a* concentration; significant. **(F)** Buoyancy frequency (stratification strength); significant. **(G)** pH; significant.

(Figure 4B), DOC levels (Figure 4C), buoyancy frequency (Figure 4F), and water source (as $\delta^{18}O$; Figure 4G). Dissolved oxygen, buoyancy frequency, and $\delta^{18}O$ exhibited significant negative relationships with variation in CO_2 concentration, while DIN and DOC had positive relationships. Overall, this model explained 63.9% of deviance in the CO_2 levels.

Seasonal changes in CH_4 concentrations were explained best by a combination of DO saturation (Figure 5A), concentrations of DIN (Figure 5B), DOC (Figure 5C), and SRP (Figure 5D), as well as surface water temperature (Figure 5F), and conductivity (Figure 5G). Dissolved oxygen, SRP, and conductivity exhibited significant negative relationships with the seasonal CH_4 concentration, while DIN, DOC, and surface water temperature exhibited significant positive relationships with methane levels. Model deviance explained was 74.5% of variation in CH_4 levels.

Regulation of seasonal variation in N_2O concentrations was also complex, with significant effects of changes in DO saturation (Figure 6A), DIN concentration (Figure 6B), SRP concentration (Figure 6D), Chl-*a* concentration (Figure 6E), buoyancy

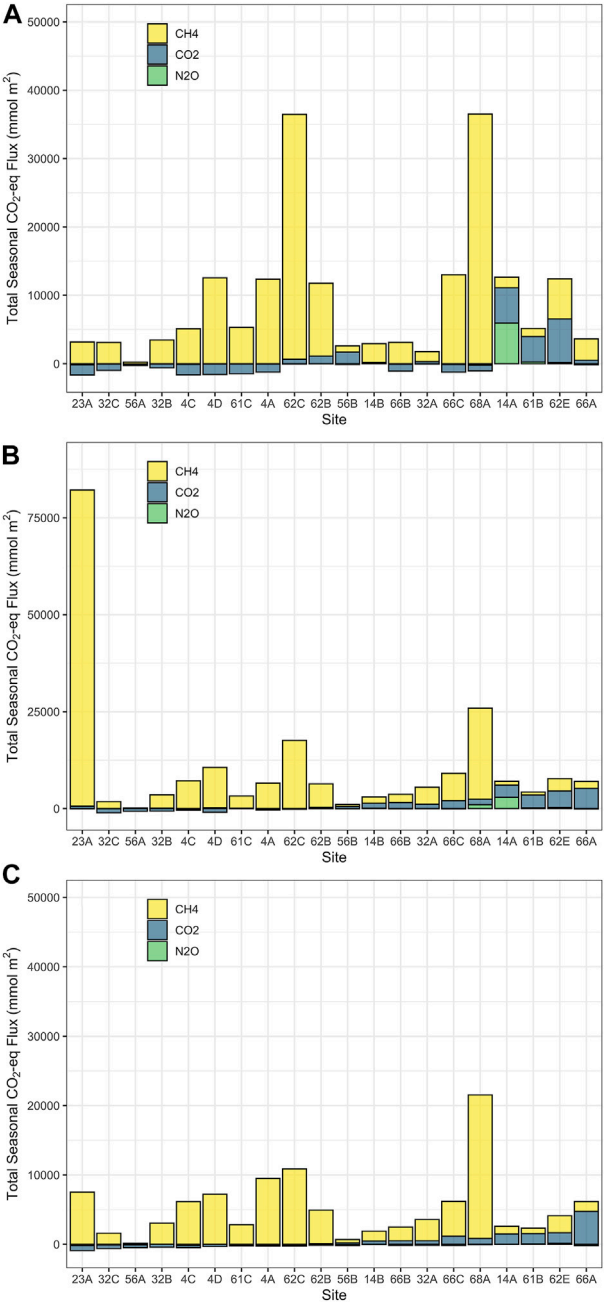


FIGURE 7
Calculated CO_2-eq fluxes based on three different estimates: **(A)** Using GHG fluxes measured in July and extrapolating over the entire open-water season; **(B)** Using GHG fluxes measured on four dates (April, May, July and Sept) in 2018 and interpolating between sampling dates; **(C)** Mean predicted flux using GAMs from Figure 1 to interpolate gas flux between sampling dates.

frequency (Figure 6F), and pH of the surface water (Figure 6G). Variation in N_2O levels were related positively to changes in DO, DIN, and SRP, and negatively to variation in Chl-*a*, buoyancy frequency, and pH, while the model explained 87.4% of the deviance in N_2O levels.

3.6 Seasonal CO_2-eq flux

Estimates of total CO_2-eq flux over the open-water period varied dependent on the method used to estimate *in situ* GHG concentrations (Figure 7), but all were within an order of magnitude of each other. Mean seasonal CO_2-eq flux was comparable between the "July-only" (9,811 ± 10,269 mmol m^{-2}, Figure 7A) and "seasonal" methods (10,446 ± 17,893 mmol m^{-2}, Figure 7B), and were roughly twice the fluxes predicted using GAMs (5,027 ± 4,806 mmol m^{-2}, Figure 7C). All methods suggest that methane was the dominant GHG responsible for CO_2-eq flux, and contributed more than 50% to total GHG efflux in 16 of 20 sites (Figure 7, yellow bars). While the mean seasonal values were comparable among methods, there were some discrepancies within individual sites. For example, Site 23 A demonstrated extremely high CO_2-eq flux, attributable to one very high CH_4 measurement in April. This likely reflected an ebullition event at this time that was not captured when the "July-only" method was used, and which was constrained using the GAM-predicted method.

4 Discussion

Evaluation of temporal variability and controls of GHG in 20 agricultural reservoirs in the northern Great Plains indicated that while CO_2, CH_4, and N_2O flux exhibited few diel trends (Figures 3A–C), all GHG exhibited pronounced seasonality during the ice-free period regulated by complex interactions between microbial metabolism, allochthonous carbon inputs, and physico-chemical features (Webb et al., 2019a; Webb et al., 2019b). As predicted, all sites demonstrated peaks of CO_2 and N_2O in spring, as well as a second, lower peak of CO_2 during fall (Pennock et al., 2010; Webb et al., 2019a; Webb et al., 2019b), whereas CH_4 content was maximal in mid-summer (Figure 1), consistent with studies of Yvon-Durocher et al. (2014) and DelSontro et al. (2018). Contrary to predominantly planktonic controls identified in earlier regional GHG studies (Finlay et al., 2015; Wiik et al., 2018; Finlay et al., 2019), seasonal variation in CO_2 concentrations were correlated with temperature and organic carbon availability, indicating effects of benthic respiration (Figure 4). Similarly, CH_4 levels were correlated to changes in temperature, while a negative correlation with conductivity suggests inhibition of methanogenesis by sulfate-reducing bacteria in ion-rich waters (Figure 5). In contrast, N_2O concentrations appeared to be controlled mainly by variation in reservoir stratification or mixing (Figure 6). Taken together these findings suggest that

the response of small farm reservoirs to future climate change will depend strongly on which climatic parameters (temperature, evaporation, runoff, wind) are most affected by atmospheric heating. In particular, factors that regulate mid-summer CH_4 release appear to be paramount in determining whether small reservoirs hold potential as net CO_2-eq sources or sinks in the coming decades.

4.1 Carbon dioxide

CO_2 concentration in agricultural reservoirs was high in the spring, low throughout the summer, and began to increase again in fall (Figure 1B). This seasonal pattern was consistent with that observed in boreal and other hard-water systems, where CO_2 accumulates under the ice in the winter, causing a pulse of CO_2 released in the spring following ice off (Baehr and DeGrandpre 2002; Finlay et al., 2015; Denfeld et al., 2016). Depressed CO_2 in summer is attributed to isolation of surface waters leading to elevated photosynthetic rates that increase pH and deplete dissolved pCO_2 to values below atmospheric values (Huotari et al., 2009; Holgerson 2015). Conversely, elevated fall CO_2 concentrations appear to reflect loss of water-column stratification, and release of hypolimnetic CO_2 which had been accumulated during the summer period of stratification (Huotari et al., 2009; Holgerson 2015; Webb et al., 2019b; Finlay et al., 2019). Agricultural reservoirs in this study have a high relative depth (5.6 ± 3.1%), and thus exhibit a high resistance to vertical mixing (Wetzel and Likens 1991; Holgerson et al., 2022) during summer. As elevated primary production sinks into the hypolimnion and decomposes during summer, CO_2 is released leading to supersaturation of this gas in deep water (Huotari et al., 2009; Finlay et al., 2019).

Seasonally, pronounced negative correlations between CO_2 concentration and DO saturation (Figure 4A) and positive correlations between CO_2 and both DIN and DOC (Figure 4C) are indicative of metabolic controls of CO_2 concentrations (Holgerson 2015; Balmer and Downing 2017; Vachon et al., 2019). The metabolic stoichiometry between CO_2 and DO is well documented (Vachon et al., 2019) and represent autotrophic and heterotrophic processes occurring both in the water column or emanating from the sediments (Roulet et al., 1997; Jonsson et al., 2003; Rantakari and Kortelainen 2005; Kortelainen et al., 2006; Holgerson 2015). Here, the significant positive relationship between CO_2 concentration and DIN levels (Figure 4B), as well as DOC levels (Figure 4C), and lack of significant relationship with Chl-*a* (Figure 4E) suggests that elevated nutrient content stimulated microbial respiration rather than primary production, such as seen in other artificial waterbodies and prairie lakes (Ollivier et al., 2018; Wiik et al., 2018; Webb et al., 2019b; Peacock et al., 2019), and natural temporary wetland ponds (Holgerson 2015). As shown in mesocosm fertilization experiments, moderate eutrophication of shallow prairie waters first elevates primary production and DO saturation, then leads to water-column anoxia due to build-up of dissolved and particulate organic matter (Donald et al., 2011; Bogard et al., 2020). Consistent with this mechanism, monitored reservoirs exhibited low ratios of dissolved N:P characteristic of N-limited regional lakes (Donald et al., 2011) (Table 2), while on-going whole-reservoir fertilization experiments show that N fertilization both increases surface water Chl-*a* levels and causes deep water supersaturation of CO_2 (C.A.C. Gushulak and P.R. Leavitt, unpublished data). At present, it is unclear whether the relationships observed in this or other studies reflect water column processes or the disproportionate effect of warm sediments in these shallow water bodies.

The negative correlation between CO_2 concentration and buoyancy frequency, a measure of stratification strength (Figure 4F), is consistent with the effects of seasonal thermal stratification in isolating deeper waters and constraining CO_2 loss to the atmosphere (Huotari et al., 2009; Holgerson 2015). Here, CO_2 concentrations are elevated both in spring after ice melting allows release of the winters' accumulation of respired CO_2 (Baehr and DeGrandpre 2002; Finlay et al., 2015; Denfeld et al., 2016), as well as in fall after when cooling air temperatures erode thermal stratification and release hypolimnetic CO_2 (Huotari et al., 2009; Holgerson 2015). Between these intervals, agricultural reservoirs can exhibit thermal stratification that isolates respired CO_2 derived from sediments and prevents accumulation in surface waters. In general, this pattern contrasts findings from a spatial survey of prairie farm reservoirs in 2017 that found a significant positive relationship between CO_2 concentration and buoyancy frequency (Webb et al., 2019b). We speculate that this difference arose because sampling for Webb et al. (2019b) took place during the summer and would have mainly captured variation in the degree of thermal stratification among sites, rather than the sharp seasonal patterns of water column mixing exhibited in this study.

CO_2 concentration and $\delta^{18}O$ exhibited a pronounced negative relationship (Figure 4G) suggesting that elevated inflow of snowmelt or groundwater resulted in higher CO_2 concentrations in these farm reservoirs, consistent with observations in the 2017 spatial study (Webb et al., 2019b). In general, regional farmers site the reservoirs in existing lowland or wetland areas, often with direct contact to shallow aquifers, or with abundant overland runoff. In this region, snowmelt in spring is both the main source of overland flow (Pomeroy et al., 2007), and the mechanism recharging shallow aquifers (Haig et al., 2020) and, in both cases, exhibited highly depleted $\delta^{18}O$ values relative to rainwater sources (Haig et al., 2020; Haig et al., 2021). Further, this groundwater has high concentrations of both DOC and DIC, and is frequently supersaturated with CO_2 (Macpherson 2009; Webb et al., 2019b). Seasonal monitoring of piezometers for water isotopes, CO_2 levels and dissolved C

concentrations will be required to further resolve this mechanism.

We did not observe consistent diel fluctuations of CO_2 concentrations in the four reservoirs sampled (Figure 3). Previous studies have shown that CO_2 concentrations are typically lower during the daytime when primary production exceeds respiration (P > R), but increase overnight due to continued respiration (Liu et al., 2016; Raymond et al., 2013; Wiik et al., 2019). The magnitude in the shifts of CO_2 concentration is often linked to the water-column productivity, with the largest diel changes observed in systems with the highest productivity (Hanson et al., 2003; Morales-Pineda et al., 2014; Shao et al., 2015; Wiik et al., 2018). Here Chl-*a* concentrations ranged from 2.9 to 296 μg L^{-1}, therefore, a strong diel change in CO_2 concentration would be expected in the more productive sites. Lack of pronounced variation through the day may reflect the high pH of these systems which would favour rapid conversion of CO_2 to bicarbonate (HCO_3^-) and carbonate (CO_3^{2-}). Furthermore, the high total alkalinity (241.3 ± 159.4 mg L^{-1}) of the systems likely resisted diel variation in pH in all but one reservoir (Figure 3D), as diel changes in CO_2 were much less than the total reservoir content of DIC (Dodds 2002; Stets et al., 2017).

4.2 Methane

CH_4 concentrations showed a marked peak during July-August (Figure 1B) similar to those seen high latitude wetlands (Pickett-Heaps et al., 2011), aquaculture ponds (Yang et al., 2015), shallow urban basins (van Bergen et al., 2019), and prairie wetlands (Bansal et al., 2016). In general, this interval corresponds to the period of greatest water temperatures and is consistent with peak CH_4 levels occurring when water temperatures are greatest in this study (Figure 5F) and the observation that metabolism of methanogenic bacteria is greater in warmer waters (Segers 1998). Such a positive relationship of CH_4 and temperature has been observed in other shallow systems including prairie wetland ponds (Bansal et al., 2016), urban ponds (van Bergen et al., 2019), natural temporary wetlands (Holgerson 2015), and sites with abundant *Phragmites* growth (Kim et al., 1998). Methane ebullition was not included in our study; however, we acknowledge that this process can contribute significantly to GHG fluxes from inland water and may also vary seasonally.

Dissolved CH_4 is expected to be more abundant under anoxic conditions (Glass and Orphan 2012), therefore, the significant negative relationship with DO saturation was expected (Figure 5A). Such a trend is common in diverse ecosystems, including boreal lakes (Kankaala et al., 2013), natural temporary wetland ponds (Holgerson 2015), and our earlier spatial survey of prairie farm reservoirs (Webb et al., 2019b).

The strong negative relationship between CH_4 concentration and conductivity (Figure 5G) was also observed in the 2017 spatial study, which is likely attributed to sulfate limiting methanogenesis (Webb et al., 2019b). Sulfate-reducing bacteria have been shown to outcompete methanogenic bacteria at sulfate concentrations as low as 60 μM in freshwater sediments in oligotrophic lakes (Lovley and Klug 1983), and as low as 200 μM in eutrophic lakes (Winfrey and Zeikus 1977; Lovley et al., 1982). A linear regression showed that conductivity and sulfate are highly related in these agricultural reservoirs ($r^2 = 0.64$, p-value < 0.01). Based on this calculation, the sulfate concentration ranges from 0.33 to 35.9 mM in these agricultural reservoirs. Surface water conductivity significantly increased over the open water season (Table 1) and is likely one of the mechanisms driving down the CH_4 concentrations in fall.

Nutrient (DOC, DIN, and SRP) levels were also important predictors of CH_4 concentrations in agricultural reservoirs (Figures 5B,C,E), although solute concentrations did not appear to be correlated to primary production as Chl-*a* (Supplementary Figure S2.1). As noted above, effects of allochthonous nutrients may be felt mainly through changes in the redox potential and dissolved oxygen content of these shallow ecosystems, rather than via augmentation of primary production. In particular, elevated production (Figure 5E) and sedimentation of labile organic matter may have favoured decomposition and anoxia in sediments, thereby improving habitat and substrate for methanogenesis (Smith et al., 1999; Anderson et al., 2002; Ollivier et al., 2019). The pronounced negative relationship between CH_4 and SRP may suggest that there is competition for substrate between methanogenesis, and denitrification at high P levels, consistent with the increase in N_2O concentration is seen at high SRP concentrations (Figure 6D). Such a mechanism has also been observed in anaerobic wetland sediment slurry incubations (Kim et al., 2015).

CH_4 concentrations did not show a consistent diel trend in the four reservoirs sampled, despite obvious variation in both temperature and DO in the surface water (Figure 3). In contrast, distinct diel patterns of CH_4 production have been seen in other systems where gas levels increase following sunrise, peak in the early afternoon, then decline quickly a stable low level at night (Neue et al., 1997; Kim et al., 1998; Xing et al., 2004). In general, mid-day maxima were seen here only in ponds with greatly elevated CH_4 levels, possibly suggesting that the absence of strong diurnal maxima in some sites reflects a generally low abundance of methanogenic bacteria in some reservoirs. While speculative, we suggest that differences in the influx of groundwater- or sub-surface sulfate ($SO_4^=$) may explain the variation in absolute and relative CH_4 levels during a 24 h cycle (see below), where the presence of sulfur-reducing bacteria can inhibit methanogenesis (Lovley and Klug 1983; Pennock et al., 2010).

4.3 Nitrous oxide

Although freshwaters are often significant emitters of N_2O (Beaulieu et al., 2008; Beaulieu et al., 2011; DelSontro et al., 2018), patterns and controls of the seasonality of N_2O concentrations are poorly understood. The seasonal trend observed here shows that following an initial pulse in N_2O production immediately following ice melt in the spring, these reservoirs were often undersaturated in N_2O for much of the ice-free period (Figure 1B). These low N_2O values may be attributed to complete denitrification of dissolved NO_3^- to di-nitrogen gas (N_2), similar to patterns seem in some lakes (Piña-Ochoa and Álvarez-Cobelas 2006), including Lake Kasumiguara, a shallow eutrophic lake that does not have an anaerobic zone (Hashimoto et al., 1993). Widespread undersaturation of N_2O was also observed in regional farm reservoirs during 2017 (Webb et al., 2019a); however, this study provides the first evidence that N_2O undersaturation last much of the summer, a finding which has not previously been recorded for nitrogen-rich agricultural landscapes. Better understanding of the mechanisms controlling this process may be important to regulating net CO_2-eq fluxes from small water bodies in the continental interiors that represent much of the global agricultural regions.

The significant relationships seen between DO saturation, DIN (NO_x + NH_3), Chl-*a*, and buoyancy frequency (Figure 6) were similar to those seen spatial surveys of agricultural reservoirs (Webb et al., 2019a). This finding suggests that mechanisms relating to productivity and mixing are controlling N_2O concentrations in reservoirs both seasonally and spatially (Webb et al., 2019a). The pulse of N_2O in the spring may be explained by the build-up of N_2O under ice over the winter season, which is a common observation in prairie and boreal lakes (Soued et al., 2016; Cavaliere and Baulch, 2018). The lack of atmospheric exchange (during ice cover) combined with ongoing N_2O producing processes such as nitrification and denitrification (Cavaliere and Baulch, 2018), without the competing factor of primary productivity for DIN (NO_x was elevated in April, Table 2), may explain the higher N_2O levels. The switch to N_2O undersaturation coincides with a decline in NO_x concentration owing to elevated algal uptake, along with the onset of temporary water column stratification and a decline in the DO saturation in the deep waters (Table 1) where complete denitrification can proceed. Complete denitrification leads to the consumption of N_2O in the process of producing N_2 (Quick et al., 2019), which suggests that the conditions in agricultural reservoirs favour complete denitrification during most of the open-water period. Additionally, the significant positive relationship between N_2O concentrations and SRP may be driven by direct, or indirect effects, via impacts of SRP on algal biomass and carbon production, or via direct effects on N_2O producing microbes.

N_2O concentration in the four reservoirs sampled on a diel timescale remained under-saturated throughout the 24 h cycle. This pattern is similar to that seen in an arid zone alpine pond which remained undersaturated in N_2O for most of the diel cycle (Molina et al., 2021). Previous studies have diel variation in N_2O concentrations, primarily in rivers and streams, although comparisons among these site exhibit little common diel pattern among habitats. For example, some studies show clear diel patterns with greater concentrations observed during nighttime relative to those during the daytime (Rosamond et al., 2011; Wu et al., 2018a; Wu et al., 2018b), while other locations show a peak during the day (Molina et al., 2021) as well as a peak during the nighttime (Rosamond et al., 2011). One study found a sharp decrease in N_2O concentration during the nighttime (Harrison et al., 2005) and others did not find a consistent diel trend (Baulch et al., 2012).

4.4 Seasonal CO_2 equivalent budget

We calculated areal CO_2-eq flux for the farm ponds to range from an average 32.0 mmol m^{-2} day^{-1} using the GAM-predicted flux, to 66.5 mmol m^{-2} day^{-1} using the seasonal method, over the 157-days open-water season. These values are somewhat lower than the mean (129 mmol m^{-2} day^{-1}) but well within the range (−10 to 1,462 mmol m^{-2} day^{-1}) of the daily flux estimates in the 2017 spatial survey (Webb et al., 2019a; Webb et al., 2019b). Similar to findings from previous studies (DelSontro et al., 2018; Ollivier et al., 2019), we observed that CH_4 was the major driver of CO_2-eq flux (average 91.5% across all methods), while N_2O contributed the least (0.73%). The contribution of CH_4 to total CO_2-eq flux is likely to be even higher when ebullition is also considered (DelSontro et al., 2016; Rosentreter et al., 2021).

Findings from this study show that all three GHGs exhibited significant seasonal trends, thereby suggesting that extrapolation from a single date to the entire open-water period may produce inaccurate estimates of the total CO_2 equivalent (CO_2-eq) flux from these systems. In our study, the seasonal trends of each GHG (Figure 1), combined with the fact that CH_4 is typically the dominant gas contributing to CO_2-eq flux (Figure 7) would suggest that extrapolating measurements in mid-summer are likely to overestimate seasonal flux. The GAM-predicted seasonal fluxes were, on average, half of that of the other two methods, likely because the modeled fluxes constrained occasional extreme effluxes GHG and avoided excessive extrapolation through time series. For example, the exceptionally high estimate of seasonal flux at site 23 A in Figure 7B reflects a pulse of CH_4 in April (observed CH_4 = 90.7 μM) which was not included in the July-only flux calculations, and was constrained in the GAM models. Depending on whether this extreme point was interpolated to the next sampling date or not, estimated CO_2-eq flux differed during the spring period by up to 72,800 mmol m^{-2} depending on whether elevated values were (~75,600 mmol m^{-2}) or were not (2,800 mmol m^{-2}) used to estimate vernal fluxes. Although ebullition can occur due to changes in production, water depth, or meteorological conditions (DelSontro et al., 2016), observed elevated values are unlikely to persist over the 3-week spring interval. Conversely, GAM

predicted values missed the likely-real pulsed efflux, and thereby likely underestimated seasonal fluxes. Overall, the "seasonal" calculation also likely overestimates CO_2-eq flux by inflating short-term emissions, while the July-only calculation will miss seasonal trends, and the use of the GAM smooths may dampen any short-term pulses of GHG efflux and lose the contribution of these to the seasonal flux rates. Reconciling these discrepancies to provide the best estimate of total open-water GHG fluxes will require continuous monitoring of GHG with sondes, now possible for CO_2, but still limited for CH_4 and N_2O due to more limited sensor sensitivity.

This study shows that agricultural reservoirs exhibit significant seasonal trends in the concentrations of all major GHGs, and that the concentrations of these gases are regulated by a combination of physical, chemical, and biological mechanisms. Additionally, it was found that inclusion of estimates of this seasonal variability may be essential to accurately total CO_2-eq fluxes to the atmosphere. However, reconciling accurate net GHG over the annual scale will only truly be overcome through increased GHG monitoring via *in situ* sensors to capture extreme changes in water conditions (such as at ice off). The Northern Great Plains, as the largest agricultural area of Canada, is an area where agricultural water management is ongoing. Reservoirs in the landscape mediate substantive fluxes, although more work is required to reduce error in estimation of annual efflux from these often-eutrophic reservoirs. Perhaps more importantly, the Northern Great Plains are a region of extremely high variability in factors known to influence GHG efflux, and upscaling efforts aimed at understanding the role of inland waters in GHG efflux need to account for spatial variability in solutes, including sulfate.

Data availability statement

The datasets presented in this study can be found in online repositories. The names of the repository/repositories and accession number(s) can be found below: https://github.com/finlay4k/Jensen_dugout_seasonality.git.

Author contributions

SJ, JW, GS, PL, HB, and KF designed research; SJ performed research and drafted the paper; HB contributed new reagents/analytic tools; JW, PL, GS, HB, and KF contributed towards ideas and data analysis; SJ developed generalized additive models. All authors revised and approved the final manuscript.

Funding

Financial support for data collection and analyses were provided in part by Government of Saskatchewan (Award 200160015), Natural Sciences and Engineering Research Council of Canada Discovery grants (to KF, GS, HB, and PL), the Canada Foundation for Innovation (Award RGPIN–2018-0490), University of Regina.

Acknowledgments

We thank Shaeya Cluff, Ann King, and Mackenzie Metz for fieldwork assistant and all landowners for their generous cooperation in volunteering their reservoirs for this research. This research took place on Treaty 4 and 6 territories, traditional areas of Cree, Saulteaux, Lakota, Dakota, and Nakota peoples, and homeland of the Métis.

Conflict of interest

The authors declare that the research was conducted in the absence of any commercial or financial relationships that could be construed as a potential conflict of interest.

Publisher's note

All claims expressed in this article are solely those of the authors and do not necessarily represent those of their affiliated organizations, or those of the publisher, the editors and the reviewers. Any product that may be evaluated in this article, or claim that may be made by its manufacturer, is not guaranteed or endorsed by the publisher.

Supplementary material

The Supplementary Material for this article can be found online at: https://www.frontiersin.org/articles/10.3389/fenvs.2022.895531/full#supplementary-material

References

Anderson, D. M., Glibert, P. M., and Burkholder, J. M. (2002). Harmful algal blooms and eutrophication: Nutrient sources, composition, and consequences. *Estuaries* 25, 704–726. doi:10.1007/bf02804901

Baehr, M. M., and DeGrandpre, M. D. (2002). Under-ice CO_2 and O_2 variability in a freshwater lake. *Biogeochemistry* 61, 95–113. doi:10.1023/a:1020265315833

Baehr, M. M., and DeGrandpre, M. D. (2004). *In situ* pCO_2 and O_2 measurements in a lake during turnover and stratification: Observations and modeling. *Limnol. Oceanogr.* 49, 330–340. doi:10.4319/lo.2004.49.2.0330

Balmer, M. B., and Downing, J. A. (2017). Carbon dioxide concentrations in eutrophic lakes: Undersaturation implies atmospheric uptake. *Inland Waters* 1, 125–132. doi:10.5268/IW-1.2.366

Bansal, S., Tangen, B., and Finocchiaro, R. (2016). Temperature and hydrology affect methane emissions from prairie pothole wetlands. *Wetlands* 36, 371–381. doi:10.1007/s13157-016-0826-8

Bastviken, D., Cole, J., Pace, M., and Tranvik, L. (2004). Methane emissions from lakes: Dependence of lake characteristics, two regional assessments, and a global estimate. *Glob. Biogeochem. Cycles* 18, n/a. doi:10.1029/2004gb002238

Baulch, H. M., Dillon, P. J., Maranger, R., and Schiff, S. L. (2011). Diffusive and ebullitive transport of methane and nitrous oxide from streams: Are bubble-mediated fluxes important? *J. Geophys. Res.* 116, G04028. doi:10.1029/2011JG001656

Baulch, H. M., Dillon, P. J., Maranger, R., Venkiteswaran, J. J., Wilson, H. F., and Schiff, S. L. (2012). Night and day: Short-term variation in nitrogen chemistry and nitrous oxide emissions from streams. *Freshw. Biol.* 57, 509–525. doi:10.1111/j.1365-2427.2011.02720.x

Baumann, M., Gasparri, I., Piquer-Rodríguez, M., Pizarro, G. G., Griffiths, P., Hostert, P., et al. (2017). Carbon emissions from agricultural expansion and intensification in the Chaco. *Glob. Chang. Biol.* 23, 1902–1916. doi:10.1111/gcb.13521

Beaulieu, J. J., Arango, C. P., Hamilton, S. K., and Tank, J. L. (2008). The production and emission of nitrous oxide from headwater streams in the Midwestern United States. *Glob. Chang. Biol.* 14, 878–894. doi:10.1111/j.1365-2486.2007.01485.x

Beaulieu, J. J., Tank, J. L., Hamilton, S. K., Wollheim, W. M., Hall, R. O., Mulholland, P. J., et al. (2011). Nitrous oxide emission from denitrification in stream and river networks. *Proc. Natl. Acad. Sci. U. S. A.* 108, 214–219. doi:10.1073/pnas.1011464108

Beaulieu, J. J., DelSontro, T., and Downing, J. A. (2019). Eutrophication will increase methane emissions from lakes and impoundments during the 21st century. *Nat. Commun.* 10, 1375. doi:10.1038/s41467-019-09100-5

Bergbusch, N. T., Hayes, N. M., Simpson, G. L., Swarbrick, V. J., Quiñones-Rivera, Z. J., and Leavitt, P. R. (2021). Effects of nitrogen removal from wastewater on phytoplankton in eutrophic prairie streams. *Freshw. Biol.* 66, 2283–2300. doi:10.1111/fwb.13833

Bogard, M. J., and Giorgio, P. A. (2016). The role of metabolism in modulating CO_2 fluxes in boreal lakes. *Glob. Biogeochem. Cycles* 30, 1509–1525. doi:10.1002/2016GB005463

Bogard, M. J., Vogt, R. J., Hayes, N. M., and Leavitt, P. R. (2020). Unabated nitrogen pollution favors growth of toxic cyanobacteria over chlorophytes in most hypereutrophic lakes. *Environ. Sci. Technol.* 54, 3219–3227. doi:10.1021/acs.est.9b06299

Bridgham, S. D., Megonigal, J. P., Keller, J. K., Bliss, N. B., and Trettin, C. (2006). The carbon balance of North American wetlands. *Wetlands* 26, 889–916. doi:10.1672/0277-5212(2006)26[889:tcbona]2.0.co;2

Cavaliere, E., and Baulch, H. M. (2018). Denitrification under lake ice. *Biogeochemistry* 137 (3), 285–295. doi:10.1007/s10533-018-0419-0

Chapin, F. S., Woodwell, G. M., Randerson, J. T., Rastetter, E. B., Lovett, G. M., Baldocchi, D. D., et al. (2006). Reconciling carbon-cycle concepts, terminology, and methods. *Ecosystems* 9, 1041–1050. doi:10.1007/s10021-005-0105-7

Cole, J. J., and Caraco, N. F. (1998). Atmospheric exchange of carbon dioxide in a low-wind oligotrophic lake measured by the addition of SF6. *Limnol. Oceanogr.* 43 (4), 647–656. doi:10.4319/lo.1998.43.4.0647

Cole, J., Prairie, Y., Caraco, N., McDowell, W. H., Tranvik, L. J., Striegl, R. G., et al. (2007). Plumbing the global carbon cycle: Integrating inland waters into the terrestrial carbon budget. *Ecosystems* 10, 172–185. doi:10.1007/s10021-006-9013-8

Deemer, B. R., Harrison, J. A., Li, S., Beaulieu, J. J., DelSontro, T., Barros, N., et al. (2016). Greenhouse gas emissions from reservoir water surfaces: A new global synthesis. *BioScience* 66, 949–964. doi:10.1093/biosci/biw117

DelSontro, T., Boutet, L., St-Pierre, A., Giorgio, P., and Prairie, Y. (2016). Methane ebullition and diffusion from northern ponds and lakes regulated by the interaction between temperature and system productivity. *Limnol. Oceanogr.* 61, S62–S77. doi:10.1002/lno.10335

DelSontro, T., Beaulieu, J. J., and Downing, J. A. (2018). Greenhouse gas emissions from lakes and impoundments: Upscaling in the face of global change. *Limnol. Oceanogr. Lett.* 3, 64–75. doi:10.1002/lol2.10073

Denfeld, B. A., Kortelainen, P., Rantakari, M., Sobek, S., and Weyhenmeyer, G. A. (2016). Regional variability and drivers of below ice CO_2 in boreal and subarctic lakes. *Ecosystems* 19, 461–476. doi:10.1007/s10021-015-9944-z

Dillon, P. J., and Molot, L. A. (1997). Dissolved organic and inorganic carbon mass balances in central Ontario lakes. *Biogeochemistry* 36, 29–42. doi:10.1023/a:1005731828660

Dodds, W. K. (2002). "Aquatic chemistry controlling nutrient cycling: Redox and O2," in *Freshwater Ecology*. Editors J. H. Thorp, J. A. Stanford, R. Stein, and R. G. Wetzel (Academic Press), 202–228.

Donald, D. B., Bogard, M. J., Finlay, K., and Leavitt, P. R. (2011). Comparative effects of urea, ammonium, and nitrate on phytoplankton abundance, community composition, and toxicity in hypereutrophic freshwaters. *Limnol. Oceanogr.* 56, 2161–2175. doi:10.4319/lo.2011.56.6.2161

Downing, J. (2010). Emerging global role of small lakes and ponds: Little things mean a lot. *Limnetica* 29, 9–24. doi:10.23818/limn.29.02

Dubois, K., Carignan, R., and Veizer, J. (2009). Can pelagic net heterotrophy account for carbon fluxes from eastern Canadian lakes? *Appl. Geochem.* 24, 988–998. doi:10.1016/j.apgeochem.2009.03.001

Duc, N. T., Crill, P., and Bastviken, D. (2010). Implications of temperature and sediment characteristics on methane formation and oxidation in lake sediments. *Biogeochemistry* 100, 185–196. doi:10.1007/s10533-010-9415-8

Ducharme-Riel, V., Vachon, D., del Giorgio, P. A., and Prairie, Y. T. (2015). The relative contribution of winter under-ice and summer hypolimnetic CO_2 accumulation to the annual CO_2 emissions from northern lakes. *Ecosystems* 18 (4), 547–559. doi:10.1007/s10021-015-9846-0

Earles, J. M., Yeh, S., and Skog, K. E. (2012). Timing of carbon emissions from global forest clearance. *Nat. Clim. Chang.* 2, 682–685. doi:10.1038/nclimate1535

Finlay, K., Leavitt, P., Wissel, B., and Prairie, Y. (2009). Regulation of spatial and temporal variability of carbon flux in six hard-water lakes of the northern Great Plains. *Limnol. Oceanogr.* 54, 2553–2564. doi:10.4319/lo.2009.54.6_part_2.2553

Finlay, K., Leavitt, P., Patoine, A., Patoine, A., and Wissel, B. (2010). Magnitudes and controls of organic and inorganic carbon flux through a chain of hard-water lakes on the northern Great Plains. *Limnol. Oceanogr.* 55, 1551–1564. doi:10.4319/lo.2010.55.4.1551

Finlay, K., Vogt, R., Bogard, M., Wissel, B., Tutolo, B., Simpson, G., et al. (2015). Decrease in CO_2 efflux from northern hardwater lakes with increasing atmospheric warming. *Nature* 519, 215–218. doi:10.1038/nature14172

Finlay, K., Vogt, R., Simpson, G., and Leavitt, P. (2019). Seasonality of pCO_2 in a hard-water lake of the northern Great Plains: The legacy effects of climate and limnological conditions over 36 years. *Limnol. Oceanogr.* 64, 11113. doi:10.1002/lno.11113

Firestone, M. K., and Davidson, E. A. (1989). Microbiological basis of NO and N_2O production and consumption in soil. *Exch. Trace Gases Between Terr. Ecosyst. Atmos.* 47, 7–21.

Glass, J. B., and Orphan, V. J. (2012). Trace metal requirements for microbial enzymes involved in the production and consumption of methane and nitrous oxide. *Front. Microbiol.* 3, 61. doi:10.3389/fmicb.2012.00061

Gooding, R. M., and Baulch, H. M. (2017). Small reservoirs as a beneficial management practice for nitrogen removal. *J. Environ. Qual.* 46 (1), 96–104. doi:10.2134/jeq2016.07.0252

Haig, H. A., Hayes, N. M., Simpson, G. L., Yi, Y., Wissel, B., Hodder, K. R., et al. (2020). Comparison of isotopic mass balance and instrumental techniques as estimates of basin hydrology in seven connected lakes over 12 years. *J. Hydrology X* 6, 100046. doi:10.1016/j.hydroa.2019.100046

Haig, H. A., Hayes, N. M., Simpson, G. L., Yi, Y., Wissel, B., Hodder, K. R., et al. (2021). Effects of seasonal and interannual variability in water isotopes (δ^2H, $\delta^{18}O$) on estimates of water balance in a chain of seven prairie lakes. *J. Hydrology X* 10, 100069. doi:10.1016/j.hydroa.2020.100069

Hanson, P. C., Bade, D. L., Carpenter, S. R., and Kratz, T. K. (2003). Lake metabolism: Relationships with dissolved organic carbon and phosphorus. *Limnol. Oceanogr.* 48 (3), 1112–1119. doi:10.4319/lo.2003.48.3.1112

Harrison, J. A., Matson, P. A., and Fendorf, S. E. (2005). Effects of a diel oxygen cycle on nitrogen transformations and greenhouse gas emissions in a eutrophied subtropical stream. *Aquat. Sci.* 67, 308–315. doi:10.1007/s00027-005-0776-3

Hashimoto, S., Sun, H. Y., Nakamura, T., Nojiri, Y., and Otsuki, A. (1993). Seasonal variations in dissolved nitrous oxide concentrations in a eutrophic shallow lake without anaerobic layer. *Geochem. J.* 27, 117–123. doi:10.2343/geochemj.27.117

Holgerson, M. A., Richardson, D. C., Roith, J., Bortolotti, L. E., Finlay, K., Hornback, D. J., et al. (2022). Classifying mixing regimes in ponds and shallow lakes. *Water Resour. Res.* 58, e2022WR032522. In press. doi:10.1029/2022WR032522

Holgerson, M. (2015). Drivers of carbon dioxide and methane supersaturation in small, temporary ponds. *Biogeochemistry* 124, 305–318. doi:10.1007/s10533-015-0099-y

Holgerson, M., and Raymond, P. (2016). Large contribution to inland water CO_2 and CH_4 emissions from very small ponds. *Nat. Geosci.* 9, 222–226. doi:10.1038/ngeo2654

Huotari, J., Ojala, A., Peltomaa, E., Pumpanen, J., Hari, P., and Vesala, T. (2009). Temporal variations in surface water CO_2 concentration in a boreal humic lake basaed on high-frequency measurements. *Boreal Environ. Res.* 14, 48–60.

Jeffrey, S. W., and Humphrey, G. F. (1975). New spectrophotometric equations for determining chlorophylls a, b, c1 and c2 in higher plants, algae and natural phytoplankton. *Biochem. Physiol. Pflanz.* 167, 191–194. doi:10.1016/s0015-3796(17)30778-3

Jonsson, A., Karlsson, J., and Jansson, M. (2003). Sources of carbon dioxide supersaturation in clearwater and humic lakes in northern Sweden. *Ecosystems* 6, 224–235. doi:10.1007/s10021-002-0200-y

Kankaala, P., Huotari, J., Tulonen, T., and Ojala, A. (2013). Lake-size dependent physical forcing drives carbon dioxide and methane effluxes from lakes in a boreal landscape. *Limnol. Oceanogr.* 58, 1915–1930. doi:10.4319/lo.2013.58.6.1915

Kim, J., Verma, S. B., Billesbach, D. P., and Clement, R. J. (1998). Diel variation in methane emission from a midlatitude prairie wetland: Significance of convective throughflow in *Phragmites australis*. *J. Geophys. Res.* 103, 28029–28039. doi:10.1029/98jd02441

Kim, S. Y., Veraart, A. J., Meima-Franke, M., and Bodelier, P. L. E. (2015). Combined effects of carbon, nitrogen and phosphorus on CH_4 production and denitrification in wetland sediments. *Geoderma* 259, 354–361. doi:10.1016/j.geoderma.2015.03.015

King, G. M. (1992). Ecological aspects of methane oxidation, a key determinant of global methane dynamics. *Adv. Microb. Ecol.* 12, 431–468. doi:10.1007/978-1-4684-7609-5_9

Kortelainen, P., Rantakari, M., Huttenen, J. T., Mattsson, T., Alm, J., Juutinen, S., et al. (2006). Sediment respiration and lake trophic state are important predictors of large CO_2 evasion from small boreal lakes. *Glob. Chang. Biol.* 12, 1554–1567. doi:10.1111/j.1365-2486.2006.01167.x

Liu, H., Zhang, Q., Katul, G. G., Cole, J. J., Chapin, F. S., III, and MacIntyre, S. (2016). Large CO_2 effluxes at night and during synoptic weather events significantly contribute to CO_2 emissions from a reservoir. *Environ. Res. Lett.* 11 (6), 064001. doi:10.1088/1748-9326/11/6/064001

Lovley, D. R., Dwyer, D. F., and Klug, M. J. (1982). Kinetic analysis of competition between sulfate reducers and methanogens for hydrogen in sediments. *Appl. Environ. Microbiol.* 43, 1373–1379. doi:10.1128/aem.43.6.1373-1379.1982

Lovley, D. R., and Klug, M. J. (1983). Sulfate reducers can outcompete methanogens at freshwater sulfate concentrations. *Appl. Environ. Microbiol.* 45, 187–192. doi:10.1128/aem.45.1.187-192.1983

Maberly, S. C. (1996). Diel, episodic and seasonal changes in pH and concentrations of inorganic carbon in a productive lake. *Freshw. Biol.* 35, 579–598. doi:10.1111/j.1365-2427.1996.tb01770.x

Macpherson, G. L. (2009). CO_2 distribution in groundwater and the impact of groundwater extraction on the global C cycle. *Chem. Geol.* 264, 328–336. doi:10.1016/j.chemgeo.2009.03.018

Marra, G., and Wood, S. N. (2011). Practical variable selection for generalized additive models. *Comput. Stat. Data Anal.* 55, 2372–2387. doi:10.1016/j.csda.2011.02.004

McDonald, C., Stets, E., Striegl, R., and Butman, D. (2013). Inorganic carbon loading as a primary driver of dissolved carbon dioxide concentrations in the lakes and reservoirs of the contiguous United States. *Glob. Biogeochem. Cycles* 27, 285–295. doi:10.1002/gbc.20032

Molina, V., Eissler, Y., Fernandez, C., Cornejo-D'Ottone, M., Dorador, C., Bebout, B. M., et al. (2021). Greenhouse gases and biogeochemical diel fluctuations in a high-altitude wetland. *Sci. Total Environ.* 768, 144370. doi:10.1016/j.scitotenv.2020.144370

Morales-Pineda, M., Cózar, A., Laiz, I., Úbeda, B., and Gálvez, J. A. (2014). Daily, biweekly, and seasonal temporal scales of pCO_2 variability in two stratified Mediterranean reservoirs. *J. Geophys. Res. Biogeosci.* 119, 509–520. doi:10.1002/2013JG002317

Neubauer, S. C., and Megonigal, J. P. (2015). Moving beyond global warming potentials to quantify the climatic role of ecosystems. *Ecosystems* 18 (6), 1000–1013. doi:10.1007/s10021-015-9879-4

Neue, H. U., Wassmann, R., Kludze, H. K., Bujun, W., and Lantin, R. S. (1997). Factors and processes controlling methane emissions from rice fields. *Nutr. Cycl. Agroecosyst.* 49, 111–117. doi:10.1023/a:1009714526204

Ollivier, Q. R., Maher, D. T., Pitfield, C., and Macreadie, P. I. (2018). Punching above their weight: Large release of greenhouse gases from small agricultural dams. *Glob. Chang. Biol.* 25, 721–732. doi:10.1111/gcb.14477

Ollivier, Q. R., Maher, D. T., Pitfield, C., and Macreadie, P. I. (2019). Winter emissions of CO_2, CH_4, and N_2O from temperate agricultural dams: Fluxes, sources, and processes. *Ecosphere* 10. doi:10.1002/ecs2.2914

Peacock, M., Audet, J., Jordan, S., Smeds, J., and Wallin, M. B. (2019). Greenhouse gas emissions from urban ponds are driven by nutrient status and hydrology. *Ecosphere* 10, e02643. doi:10.1002/ecs2.2643

Pennock, D., Yates, T. T., Bedard-Haughn, A., Phipps, K., Farrell, R., and McDougal, R. (2010). Landscape controls on N_2O and CH_4 emissions from freshwater mineral soil wetlands of the Canadian Prairie Pothole Region. *Geoderma* 155, 308–319. doi:10.1016/j.geoderma.2009.12.015

Pickett-Heaps, C. A., Jacob, D. J., Wecht, K. J., Kort, E. A., Wofsy, S. C., Diskin, G. S., et al. (2011). Magnitude and seasonality of wetland methane emissions from the Hudson Bay Lowlands (Canada). *Atmos. Chem. Phys.* 11, 3773–3779. doi:10.5194/acp-11-3773-2011

Piña-Ochoa, E., and Álvarez-Cobelas, M. (2006). Denitrification in aquatic environments: A cross-system analysis. *Biogeochemistry* 81, 111–130. doi:10.1007/s10533-006-9033-7

Pomeroy, J., Gray, D., Brown, T., Hedstrom, N., Quinton, W., Granger, R., et al. (2007). The cold regions hydrological model: A platform for basing process representation and model structure on physical evidence. *Hydrol. Process.* 21, 2650–2667. doi:10.1002/hyp.6787

Quick, A. M., Reeder, W. J., Farrell, T. B., Tonina, D., Feris, K. P., and Benner, S. G. (2019). Nitrous oxide from streams and rivers: A review of primary biogeochemical pathways and environmental variables. *Earth. Sci. Rev.* 191, 224–262. doi:10.1016/j.earscirev.2019.02.021

R Core Team (2021). *R: A language and environment for statistical computing*. Available at: https://www.R-project.org/.

Rantakari, M., and Kortelainen, P. (2005). Interannual variation and climatic regulation of the CO_2 emission from large boreal lakes. *Glob. Chang. Biol.* 11, 1368–1380. doi:10.1111/j.1365-2486.2005.00982.x

Raymond, P. A., Hartmann, J., Lauerwald, R., Sobek, S., McDonald, C., Hoover, M., et al. (2013). Global carbon dioxide emissions from inland waters. *Nature* 503, 355–359. doi:10.1038/nature12760

Read, J. S., Hamilton, D. P., Jones, I. D., Muraoka, K., Winslow, L. A., Kroiss, R., et al. (2011). Derivation of lake mixing and stratification indices from high-resolution lake buoy data. *Environ. Model. Softw.* 26, 1325–1336. doi:10.1016/j.envsoft.2011.05.006

Rosamond, M. S., Thuss, S. J., Schiff, S. L., and Elgood, R. J. (2011). Coupled cycles of dissolved oxygen and nitrous oxide in rivers along a trophic gradient in southern ontario, Canada. *J. Environ. Qual.* 40, 256–270. doi:10.2134/jeq2010.0009

Rosentreter, J. A., Borgest, A. V., Deemer, B. R., Holgerson, M. A., Liu, S., Song, C., et al. (2021). Half of global methane emissions come from highly variable aquatic ecosystem sources. *Nat. Geosci.* 14, 225–230. doi:10.1038/s41561-021-00715-2

Roulet, N. T., Crill, P., Comer, N., Dove, A., and Boubonniere, R. (1997). CO_2 and CH_4 flux between a boreal beaver pond and the atmosphere. *J. Geophys. Res.* 102, 29313–29319. doi:10.1029/97JD01237

Scott, J. T., McCarthy, M. J., Gardner, W. S., and Doyle, R. D. (2008). Denitrification, dissimilatory nitrate reduction to ammonium, and nitrogen fixation along a nitrate concentration gradient in a created freshwater wetland. *Biogeochemistry* 87, 99–111. doi:10.1007/s10533-007-9171-6

Segers, R. (1998). Methane production and methane consumption: A review of processes underlying wetland methane fluxes. *Biogeochemistry* 41, 23–51. doi:10.1023/a:1005929032764

Shao, C., Chen, J., Stepien, C. A., Chu, H., Ouyang, Z., Bridgeman, T. B., et al. (2015). Diurnal to annual changes in latent, sensible heat, and CO_2 fluxes over a laurentian Great lake: A case study in western Lake Erie. *J. Geophys. Res. Biogeosci.* 120, 1587–1604. doi:10.1002/2015JG003025

Smith, V. H., Tilman, G. D., and Nekola, J. C. (1999). Eutrophication: Impacts of excess nutrient inputs on freshwater, marine, and terrestrial ecosystems. *Environ. Pollut.* 100, 179–196. doi:10.1016/s0269-7491(99)00091-3

Soued, C., del Giorgio, P. A., and Maranger, R. (2016). Nitrous oxide sinks and emissions in boreal aquatic networks in Québec. *Nat. Geosci.* 9, 116–120. doi:10.1038/ngeo2611

Stets, E. G., Butman, D., McDonald, C. P., Stackpoole, S. M., DeGrandpre, M. D., and Striegl, R. G. (2017). Carbonate buffering and metabolic controls on carbon dioxide in rivers. *Glob. Biogeochem. Cycles* 31, 663–677. doi:10.1002/2016gb005578

Striegl, R. G., and Michmerhuizen, C. M. (1998). Hydrologic influence on methane and carbon dioxide dynamics at two north-Central Minnesota lakes. *Limnol. Oceanogr.* 43, 1519–1529. doi:10.4319/lo.1998.43.7.1519

Swarbrick, V. J., Simpson, G. L., Glibert, P. M., and Leavitt, P. R. (2019). Differential stimulation and suppression of phytoplankton growth by ammonium enrichment in eutrophic hardwater lakes over 16 years. *Limnol. Oceanogr.* 64 (S1), S130–S149. doi:10.1002/lno.11093

Tilman, D. (1999). Global environmental impacts of agricultural expansion: The need for sustainable and efficient practices. *Proc. Natl. Acad. Sci. U. S. A.* 96, 5995–6000. doi:10.1073/pnas.96.11.5995

Tranvik, L. J., Downing, J. A., Cotner, J. B., Loiselle, S. A., Striegl, R. G., Ballatore, T. J., et al. (2009). Lakes and reservoirs as regulators of carbon cycling and climate. *Limnol. Oceanogr.* 54, 2298–2314. doi:10.4319/lo.2009.54.6_part_2.2298

Vachon, D., Sadro, S., Bogard, M. J., Lapierre, J.-F., Baulch, H. M., Rusak, J. A., et al. (2019). Paired O_2-CO_2 measurements provide emergent insights into aquatic ecosystem function. *Limnol. Oceanogr. Lett.* 5, 287–294. doi:10.1002/lol2.10135

van Bergen, T. J., Barros, N., Mendonça, R., Aben, R. C., Althuizen, I. H., Huszar, V., et al. (2019). Seasonal and diel variation in greenhouse gas emissions from an urban pond and its major drivers. *Limnol. Oceanogr.* 64 (5), 2129–2139. doi:10.1002/lno.11173

Webb, J. R., Hayes, N. M., Simpson, G. L., Leavitt, P. R., Baulch, H. M., and Finlay, K. (2019a). Widespread nitrous oxide undersaturation in farm waterbodies creates an unexpected greenhouse gas sink. *Proc. Natl. Acad. Sci. U. S. A.* 116, 9814–9819. doi:10.1073/pnas.1820389116

Webb, J. R., Leavitt, P. R., Simpson, G. L., Baulch, H. M., Haig, H. A., Hodder, K. R., et al. (2019b). Regulation of carbon dioxide and methane in small agricultural reservoirs: Optimizing potential for greenhouse gas uptake. *Biogeosciences* 16, 4211–4227. doi:10.5194/bg-16-4211-2019

Wetzel, R. G., and Likens, G. E. (1991). *Limnological analyses*. 3rd ed. Springer Science.

Wiik, E., Haig, H., Hayes, N., Finlay, K., Simpson, G., Vogt, R., et al. (2018). Generalized additive models of climatic and metabolic controls of subannual variation in pCO_2 in productive hardwater lakes. *J. Geophys. Res. Biogeosci.* 123, 1940–1959. doi:10.1029/2018JG004506

Wilkinson, G. M., Buelo, C. D., Cole, J. J., and Pace, M. L. (2016). Exogenously produced CO_2 doubles the CO_2 efflux from three north temperate lakes. *Geophys. Res. Lett.* 43, 1996–2003. doi:10.1002/2016gl067732

Winfrey, M. R., and Zeikus, J. G. (1977). Effect of sulfate on carbon and electron flow during microbial methanogenesis in freshwater sediments. *Appl. Environ. Microbiol.* 33, 275–281. doi:10.1128/aem.33.2.275-281.1977

Wood, S. N. (2006). *Generalized additive models: An introduction with R*. Chapman and Hall/CRC.

Wood, S. N. (2011). Fast stable restricted maximum likelihood and marginal likelihood estimation of semiparametric generalized linear models. *J. Roy. Stat. Soc. B Stat. Methodol.* 73, 3–36. doi:10.1111/j.1467-9868.2010.00749.x

Wood, S. (2016). Package 'mgcv'. Accessed 23 June 2018. Available from: https://cran.r-project.org/web/packages/mgcv/mgcv.pdf.

Wood, S. N., Pya, N., and Säfken, B. (2016). Smoothing parameter and model selection for general smooth models. *J. Am. Stat. Assoc.* 111, 1548–1563. doi:10.1080/01621459.2016.1180986

Wu, S., Chen, J., Li, C., Kong, D., Yu, K., Liu, S., et al. (2018a). Diel and seasonal nitrous oxide fluxes determined by floating chamber and gas transfer equation methods in agricultural irrigation watersheds in southeast China. *Environ. Monit. Assess.* 190, 122. doi:10.1007/s10661-018-6502-0

Wu, S., Hu, Z., Hu, T., Chen, J., Yu, K., Zou, J., et al. (2018b). Annual methane and nitrous oxide emissions from rice paddies and inland fish aquaculture wetlands in southeast China. *Atmos. Environ.* 175, 135–144. doi:10.1016/j.atmosenv.2017.12.008

Xing, Y., Xie, P., Yang, H., Ni, L., Wang, Y., and Tang, W. (2004). Diel variation of methane fluxes in summer in a eutrophic subtropical lake in China. *J. Freshw. Ecol.* 19, 639–644. doi:10.1080/02705060.2004.9664745

Yang, P., He, Q., Huang, J., and Tong, C. (2015). Fluxes of greenhouse gases at two different aquaculture ponds in the coastal zone of southeastern China. *Atmos. Environ. X.* 115, 269–277. doi:10.1016/j.atmosenv.2015.05.067

Yi, Y., Brock, B. E., Falcone, M. D., Wolfe, B. B., and Edwards, T. W. D. (2008). A coupled isotope tracer method to characterize input water to lakes. *J. Hydrol. X.* 350, 1–13. doi:10.1016/j.jhydrol.2007.11.008

Yvon-Durocher, G., Allen, A. P., Bastviken, D., Conrad, R., Gudasz, C., St-Pierre, A., et al. (2014). Methane fluxes show consistent temperature dependence across microbial to ecosystem scales. *Nature* 507, 488–491. doi:10.1038/nature13164

Zhang, W., Li, H., Xiao, Q., and Li, X. (2021). Urban rivers are hotspots of riverine greenhouse gas (N_2O, CH_4, CO_2) emissions in the mixed-landscape Chaohu lake basin. *Water Res.* 189, 116624. doi:10.1016/j.watres.2020.116624

frontiers | Frontiers in Environmental Science

TYPE Original Research
PUBLISHED 05 October 2022
DOI 10.3389/fenvs.2022.889289

Check for updates

OPEN ACCESS

EDITED BY
Tonya DelSontro,
University of Waterloo, Canada

REVIEWED BY
Pascal Bodmer,
Université du Québec à Montréal, Canada
Roberta Bittencourt Peixoto,
Federal University of Rio de Janeiro, Brazil

*CORRESPONDENCE
Joseph Rabaey,
Rabae005@umn.edu

SPECIALTY SECTION
This article was submitted to Biogeochemical Dynamics, a section of the journal Frontiers in Environmental Science

RECEIVED 04 March 2022
ACCEPTED 14 September 2022
PUBLISHED 05 October 2022

CITATION
Rabaey J and Cotner J (2022), Pond greenhouse gas emissions controlled by duckweed coverage.
Front. Environ. Sci. 10:889289.
doi: 10.3389/fenvs.2022.889289

COPYRIGHT
© 2022 Rabaey and Cotner. This is an open-access article distributed under the terms of the Creative Commons Attribution License (CC BY). The use, distribution or reproduction in other forums is permitted, provided the original author(s) and the copyright owner(s) are credited and that the original publication in this journal is cited, in accordance with accepted academic practice. No use, distribution or reproduction is permitted which does not comply with these terms.

Pond greenhouse gas emissions controlled by duckweed coverage

Joseph Rabaey[1]* and James Cotner[2]

[1]Department of Ecology, Evolution and Behavior, University of Minnesota Twin Cities, Saint Paul, MN, United States, [2]Department of Biological Sciences, University of Bergen, Bergen, Norway

Freshwaters are significant contributors of greenhouse gases to the atmosphere, including carbon dioxide (CO_2), methane (CH_4), and nitrous oxide (N_2O). Small waterbodies such as ponds are now recognized to have disproportionate greenhouse gas emissions relative to their size, but measured emissions from ponds have varied by several orders of magnitude. To assess drivers of variation in pond greenhouse gas dynamics, we measured concentrations and emissions of CO_2, CH_4, and N_2O across 26 ponds in Minnesota, United States, during the ice-free season. The studied ponds differed in land-use, from urban stormwater ponds to natural forested ponds. The ponds were all sources of greenhouse gases, driven by large CH_4 emissions (mean 704 [sd 840] mg CH_4-C m^{-2} d^{-1}). CO_2 fluxes were variable, but on average a sink (mean −25.9 [sd 862] mg CO_2-C m^{-2} d^{-1}), and N_2O emissions were generally low (mean 0.398 [sd 0.747] mg N_2O-N m^{-2} d^{-1}). Duckweed coverage on the water surfaces ranged from 0% to 100% coverage, and had the largest influence on water chemistry and greenhouse gas dynamics across the ponds. Duckweed covered ponds (ponds with greater than 85% coverage) had higher phosphorus levels and increased anoxia compared to ponds without duckweed (ponds with less than 12% coverage), leading to higher CH_4 concentrations and overall greenhouse gas emissions in the duckweed ponds. Duckweed ponds had a mean emission rate in CO_2 equivalents of 30.9 g C m^{-2} d^{-1} compared to 11.0 g C m^{-2} d^{-1} in non-duckweed ponds.

KEYWORDS

floating macrophytes, stormwater ponds, gas fluxes, carbon dioxide (CO2), methane (CH4), nitrous oxide (N2O), freshwaters, climate change

Introduction

Freshwater lakes and reservoirs are important sites of biogeochemical activity and emissions of the major greenhouse gases carbon dioxide (CO_2), methane (CH_4), and nitrous oxide (N_2O). While freshwater lakes cover less than 4% of the earth's non-glaciated land area (Verpoorter et al., 2014), they are estimated to annually emit over 0.5 Pg C of CO_2 (DelSontro et al., 2018) and 0.3 Pg C of CH_4 (Rosentreter et al., 2021) to the atmosphere. However, small waterbodies such as ponds remain a major uncertainty in freshwater emission estimates, and ponds are increasingly recognized as disproportionately large emitters of greenhouse gases relative to their size (Holgerson

& Raymond, 2016). Ponds, which tend to be < 5 ha in size (Richardson et al., 2022), comprise over 90% of freshwater lakes by number (Downing et al., 2006) and 20% by surface area (Verpoorter et al., 2014). This makes them one of the most common terrestrial-aquatic interfaces on the landscape, and thus key hotspots of biogeochemical cycling (McClain et al., 2003).

Ponds can receive high loads of allochthonous organic carbon from the watershed relative to their small volume, and this coupled with autochthonous carbon from production can lead to high decomposition and respiration rates (van Bergen et al., 2019). High respiration rates in the water column and the sediments can consume oxygen and create anoxia, which can lead to anaerobic CO_2 and CH_4 production (Duc et al., 2010). Ponds tend to be especially prolific sources of CH_4 emissions, given that anoxia and shallow depths can limit CH_4 water-column oxidation and increase ebullition (Lazar et al., 2014; Kifner et al., 2018), a process whereby CH_4 bubbles are released from the sediment. CH_4 can account for much of the warming potential of pond emissions (Holgerson & Raymond, 2016; Gorsky et al., 2019), especially given that over a 100-year period CH_4 has a warming potential about 37 times higher than CO_2 (Derwent, 2020), or 84 times higher on a 20-years time period (Myhre et al., 2013). Denitrification under hypoxic and anoxic conditions can produce N_2O, a greenhouse gas with 265 times the warming potential of CO_2 over a 100-year period (Myhre et al., 2013). Denitrification potential can be high in ponds with large nitrogen inputs (Bettez & Groffman, 2012), though this may not always lead to elevated N_2O production as complete denitrification can consume N_2O while producing N_2 (Blaszczak et al., 2018).

While recent studies have shown ponds to have the potential for extremely high greenhouse gas emissions, pond emission rates vary by several orders of magnitude, even within individual studies (Grinham et al., 2018; Gorsky et al., 2019; Peacock et al., 2019; Audet et al., 2020). This extreme variation hinders evaluating pond emissions at larger scales, and thus their role in freshwater emissions as a whole. Mechanisms driving variation in pond gas emissions are largely not understood, and there remains a lack of spatially and temporally representative pond greenhouse gas measurements (Koschorreck et al., 2020).

Much of the variation in pond greenhouse gas dynamics could stem from the many physical and biological differences in ponds across different environments. Dominant macrophyte and algal communities can vary significantly across pond ecosystems, and macrophytes are known to play a significant role in both CO_2 and CH_4 fluxes in aquatic ecosystems. Emergent macrophytes can directly transport gases from the sediments to the atmosphere, and can increase CH_4 emissions (Desrosiers et al., 2022). Submersed macrophytes can also increase CH_4 emissions by influencing methanogenesis and CH_4 ebullition, even in oxygenated waters (Hilt et al., 2022). The effect of floating macrophytes on greenhouse gas emissions has not been well-studied, though large floating macrophytes such as water hyacinth have been shown to reduce CO_2 emissions through increased photosynthesis (Attermeyer et al., 2016). While water hyacinth largely grows in tropical and sub-tropical waterbodies, small floating macrophytes, such as duckweed (family Lemnaceae) are practically ubiquitous in waterbodies worldwide (Tippery & Les, 2020), and are especially prevalent in small pond ecosystems (Hillman, 1961). Duckweed can form mats covering the entire surface of small ponds, and shade out other rooted macrophytes (Hillman, 1961). Despite the effects duckweed can have in aquatic ecosystems, little is known about how duckweed may directly influence greenhouse gas production and emissions in ponds.

In addition to differing macrophyte communities among different ponds, ponds can vary greatly in land-use from human-constructed ponds deigned for certain uses, to natural ponds in pristine watersheds. While natural ponds (Holgerson, 2015) and urban constructed ponds (Herrero Ortega et al., 2019; Audet et al., 2020; Goeckner et al., 2022) have been evaluated separately, no studies have compared natural and constructed ponds directly in the same study. Urban ponds often receive more nutrients and particles transported in stormwater runoff compared to natural ponds, which increases autochthonous production and eutrophication. Land-use and watershed properties may also directly impact the macrophyte communities of ponds, with eutrophication leading to the disappearance of submersed aquatic vegetation and the dominance of floating macrophytes (Khan & Ansari, 2005).

To evaluate the effects of floating macrophytes and environmental characteristics on pond greenhouse gas dynamics, this study measured both daytime concentrations and emissions of CO_2, CH_4, and N_2O in 26 ponds during the growing season. It was hypothesized that factors influencing oxygen loss, such as surface duckweed coverage, would have the largest impact on pond greenhouse gas emissions, given the particular importance of anaerobic processes for the formation of CH_4 and N_2O. Physical and chemical properties were measured in ponds with and without duckweed coverage, as well as both constructed and natural ponds. To gain a complete view of greenhouse gas dynamics in the ponds, surface and bottom concentrations of CO_2, CH_4, N_2O were measured, as well as emission rates from floating chamber measurements for CO_2 and CH_4.

Materials and methods

Study sites

The 26 ponds in this study were all located within a 40-mile radius within the metropolitan area of St. Paul and Minneapolis, Minnesota, United States. The ponds varied in land use type, from stormwater ponds in urban environments to natural forested ponds in preserves and parks. Ponds were divided

Physical and biogeochemical processes driving methane sources, sinks and emissions in aquatic systems: The past, present and future under global change

Topic editors

Daniel F. McGinnis — University of Geneva, Switzerland
Yves T. Prairie — Université du Québec à Montréal, Canada
Hans-Peter Grossart — University of Potsdam, Germany
Tonya DelSontro — University of Waterloo, Canada

Citation

McGinnis, D. F., Prairie, Y. T., Grossart, H.-P., DelSontro, T., eds. (2023). *Physical and biogeochemical processes driving methane sources, sinks and emissions in aquatic systems: The past, present and future under global change.* Lausanne: Frontiers Media SA. doi: 10.3389/978-2-8325-2622-4

into two categories based on origin, "natural" ponds and "constructed" ponds. While the complete history of some ponds was unknown, ponds were classified as constructed if there were known human alterations to the pond. All constructed ponds in this study are functioning stormwater ponds, managed for water regulation or the reduction of nutrient and metal exports. Daily aerial imagery at 3 m resolution from Planet Labs (Planet Team, 2017) was used to examine pond inundation, surface area, canopy cover, and floating macrophyte coverage. All ponds remain inundated year-round, and pond surface area did not detectably change within the study period. Canopy cover within a 50 m buffer around each pond was estimated using the area covered by mature trees within the buffer, using imagery from the same day each pond was sampled. Pond surface area ranged from 0.04 to 1.5 ha and pond max depth ranged from 0.3 to 1.8 m deep (Table 1).

The ponds were all sampled once between mid-July and mid-August 2021. Ponds were sampled between 10:30 in morning and 14:00 in the afternoon, to remove as much hourly variation as possible. While diel cycles have been shown to influence both CO_2 and CH_4 emissions, both sample time and sample date did not show a significant trend with measured emissions (Supplementary Figure S1). Nonetheless, diel studies have shown that daytime fluxes of CO_2 underestimate total daily fluxes while overestimating total CH_4 fluxes (van Bergen et al., 2019; Sieczko et al., 2020). Percent cover of floating macrophytes on each pond was estimated using aerial imagery. Since surface area coverage of macrophytes can change day to day with wind speed and direction, the maximum percent cover within a week period around the sample date for each pond was used. Visual estimates of floating macrophyte coverage were also taken onsite during sampling to verify the areal estimates and assess types of floating macrophytes. Floating macrophytes were almost exclusively duckweed (*lemna* sp.) and watermeal (*wolffia* sp.), here-on referred to as "duckweed".

Surface water samples were collected in the middle of each pond and used to measure total phosphorus (TP), dissolved organic carbon (DOC), total dissolved nitrogen (TDN), nitrate/nitrite (NO_3/NO_2), and ammonium (NH_4). TP was measured using the molybdenum blue reaction with acid-persulfate digestion (Murphy & Riley, 1962). For DOC, TDN, NO_3/NO_2 and NH_4 analysis water samples were passed through a muffled 0.45 µm filter. DOC and TDN was measured using a Shimadzu TOC-L model high temperature carbon-analyzer with a TNM-L module (Shimadzu Corp., Kyoto, Japan). NO_3/NO_2 was measured using colorimetric analysis by the cadmium reduction method, and NH_4 was measured using colorimetric analysis by the salicylate/nitroprusside method using a Lachat 8500 FIA (Lachat Instruments, Loveland Colorado, United States). Spectral scans of water samples and DOC concentrations were also used to calculate specific ultraviolet absorbance at 254 nm ($SUVA_{254}$) as a measure of DOC aromaticity (Weishaar et al., 2003).

Profiles were taken at the deepest point of each pond to measure water temperature, dissolved oxygen (DO), pH, chlorophyll a (chl a), and conductivity (Manta probe, Eureka Water Probes, Austin Texas, United States). Measurements were taken every 5 s, and profiles were taken slow enough to allow for measurements every 0.05–0.1 m. DO profiles were used to calculate the anoxic fraction of the pond, defined as the fraction of sediment exposed to anoxic conditions (anoxic sediment area/pond surface area) (Nürnberg, 1995). DO values under 2 mg L^{-1} were considered anoxic (Nürnberg, 1995). The anoxic sediment area was determined using DO profiles and pond hypsographic curves determined from bathymetry. As an example, in a 1.5 m-deep pond in which the DO profile was less than 2 mg L^{-1} within 0.5 m of the bottom of the pond, all sediment at a depth of 1 m or greater was considered the anoxic sediment area. Bathymetry of ponds was acquired from maps or previous measurements, however for six ponds bathymetry was not available. For these ponds bathymetry was estimated using functions in the LakeAnalyzer R package (Read et al., 2011).

Water temperature profiles were used to calculate relative thermal resistance to mixing (RTRM) as a measure of stratification strength. RTRM (unitless value) was calculated for the whole water column by taking the difference of the densities of the surface water layer (using surface water temperature) and bottom water layer (using temperature ~5 cm above sediment) and dividing by the difference in densities of water at 4 and 5°C (Birge, 1916). An RTRM >1 implies that the water column is stably stratified (more stable at higher values), while an RTRM ≤1 implies the water column is unstable and will mix (i.e. the density difference between water layers is less than the density difference between water at 4 and at 5°C). A value of zero implies the water layers are the same density.

Greenhouse gas sampling

Greenhouse gas emissions of CO_2 and CH_4 were measured using a floating chamber technique (Erkkilä et al., 2018; Grinham et al., 2018; Gorsky et al., 2019). N_2O fluxes proved to be too low to get reliable emission rates using the floating chamber, and therefore N_2O emissions were estimated from surface water and atmospheric concentrations. The floating chamber was constructed from an inverted white 5-gallon bucket, with a headspace volume of 10.02 L within the chamber. The chamber was wrapped in Styrofoam to float on the surface of the water, with 3 cm extending below the water surface to reduce turbulence. The floating chamber was connected directly to a portable greenhouse gas analyzer (DX4040 FTIR Gas Analyzer, Gasmet Technologies Oy, Vantaa, Finland) *via* inlet and outlet

tubing to create a closed loop system. To measure CH_4 and CO_2 emissions, the float was placed on the surface of the water and the pressure was allowed to equilibrate through the outlet port. The float was then connected to the gas analyzer, and the analyzer began pulling air through the loop with an approximate pumping rate of 1.5 L min^{-1}. No alterations were made to the water surface before placing the chamber, and the chamber was placed on top of any floating macrophytes (such as duckweed) or algal mats on the surface of the pond as well as open water. Gas measurements were taken every 5 s, and incubations lasted at least 5 min, and up to 10 min if rates were low. Chamber incubations were taken at three locations on each pond, one near the shoreline, one at the deep spot, and one in between those two points. Ponds were sampled with either a kayak or canoe, with the chamber floating freely connected by approximately 2 m of tubing. If the boat had to be anchored due to wind, the anchor was placed far away from the floating chamber to avoid ebullition events caused by disturbing the sediment.

Concentrations of CO_2, CH_4, and N_2O in both the surface water and bottom water were measured using the headspace technique (McAuliffe, 1971). Surface samples were collected 5–10 cm below the surface, and bottom water samples were collected approximately 10 cm above the sediment using a Van Dorn water sampler. Van Dorn sampling was done slowly and carefully to not produce bubbles or cause turbulence, and after retrieval one end was opened to directly collect the bottom water sample. For all samples, 125 ml of water was collected in a 140 ml plastic syringe. Any bubbles formed when drawing water collected in the top of the syringe, and then were removed by reducing the syringe volume to 105 ml. Atmospheric air (32.5 ml) was introduced into the syringe and then vigorously shaken for 2 minutes. Thereafter, 30 ml of the headspace was transferred into a separate syringe, and immediately injected onsite into the Gasmet portable gas analyzer, equipped with a closed loop injection system (Wilkinson et al., 2019).

Greenhouse gas calculations

The diffusive flux for all gases across the air-water interface can be expressed as:

$$\boldsymbol{F} = \boldsymbol{k} \times (\boldsymbol{C_w} - \boldsymbol{C_{sat}}) \quad (1)$$

Where F is the gas flux, k is the gas transfer velocity, C_w is the concentration of gas in the surface water, C_{sat} is the concentration of gas in the surface water at equilibrium with the overlying atmosphere. For CO_2 and CH_4, gas flux (F) was calculated directly with the floating chamber measurements. For CO_2, concentrations always increased or decreased linearly over time, and a simple linear regression method was used to calculate the flux based on the slope of linear increase (Xiao et al., 2014). For CH_4, ebullition led to a non-linear increase in CH_4 concentration when bubbling occurred (example shown in Supplementary Figure S2). With the 5 s measurement resolution, emission from ebullition events could be separated from the diffusive flux due to the high sampling frequency, as shown by Xiao et al. (2014). First, the CH_4 diffusion rate was calculated by fitting a linear regression to a long straight segment of the sample curve (Supplementary Figure S2). Multiplying this diffusion rate by the total sample time gave the CH_4 concentration in the chamber due to diffusion. CH_4 concentration due to ebullition was the surplus CH_4 concentration, calculated by subtracting the diffusion concentration and original background concentration from the total concentration at the sampling endpoint (Supplementary Figure S2). The Ideal Gas Law was used to convert concentrations to mass, and all emission rates for CO_2 and CH_4 are expressed in mg of carbon (i.e. CO_2-C, CH_4-C).

As shown by Eq. 1, the rate of gas flux will change over time as the concentration changes inside the floating chamber (as C_{sat} increases or decrease). While linear models are often used calculating gas fluxes from floating chambers (e.g. Xiao et al., 2014; Attermeyer et al., 2016; Gorsky et al., 2019), it has been shown that exponential models may be more appropriate, and linear models may underestimate fluxes by 10—30% for short incubations (5—25 min), and by over 50% for hour long incubations (Xiao et al., 2016). To test the use of a linear or exponential model, emission rates were calculated using both linear and exponential models for every CO_2 incubation ($n = 75$) and every CH_4 incubation where ebullition did not occur ($n = 26$), and model goodness of fits were compared using coefficient of determination R^2. Contrary to the results from Xiao et al. (2016), the linear models had a higher R^2 value for most incubations, and initial slope values did not significantly differ between linear and exponential models (Supplementary Table S1). Therefore, linear models were chosen to calculate CO_2 and CH_4 emission rates from the float chambers.

To calculate the concentration of CO_2, CH_4, and N_2O in the surface and bottom water, gas concentrations in the sample headspace were first calculated using the following equation (Wilkinson et al., 2019):

$$\boldsymbol{X_{headspace}} = \left(\frac{\boldsymbol{V_l} - \boldsymbol{V_s}}{\boldsymbol{V_s}}\right)\Delta\boldsymbol{X} + \boldsymbol{X_0} \quad (2)$$

Where $X_{headspace}$ is the concentration of the sample headspace, V_l is the volume of the closed loop system, V_s is the volume of the injected sample, ΔX is the change in gas concertation after sample injection, and X_0 is the initial gas concentration. Inputs from the added atmospheric air was subtracted out from the headspace concentration using onsite measurements of atmospheric gas concentrations (usually around 400 ppm CO_2, 2 ppm CH_4 and 0.33 ppm N_2O). The partial pressure of gas in the headspace was used to calculate the moles of dissolved gas in the water (mol_{aq})

according to Henry's law, and this was added to the moles of gas in the headspace ($mol_{headspace}$) and divided by the original sample volume to find the concentration of gas in the original sample (C_w) (Johnson et al., 1990):

$$mol_{aq} = P_{headspace} \times K_H \quad (3)$$

$$mol_{headspace} = \frac{P_{headspace}}{RT} \times V_{headspace} \quad (4)$$

$$C_w = \frac{mol_{aq} + mol_{headspace}}{V_w} \quad (5)$$

Where $P_{headspace}$ is the partial pressure of gas in the headspace (atm), K_H is Henry's constant (mol l^{-1} atm^{-1}), R is the universal gas constant (0.082, L·atm mol^{-1} K^{-1}), T is the temperature (K), $V_{headspace}$ is the volume of the headspace (L), and V_w is the volume of the water sample (L). Henry's constants were calculated for each gas: CO_2 (Weiss, 1974), CH_4 (Wiesenburg & Guinasso, 1979), and N_2O (Weiss & Price, 1980) and corrected for water temperature and pressure. Constants were also corrected for salinity, as particularly the bottom waters of urban ponds can have high salinity due to road salt inputs. The highest recorded conductivity in the study ponds was 10,000 µS cm^{-1}. Conductivity for each sample was converted to salinity using equations from Fofonoff and Millard Jr (1983), and Hill et al. (1986). Molar concentrations for all gases were then expressed in mg of carbon or nitrogen (i.e. CO_2-C, CH_4-C, N_2O-N).

Using Eq. 1, the estimate C_w, and calculating C_{sat} according to Henry's law, the gas transfer velocity (k) was estimated for each pond. Since CO_2 chamber fluxes were often influenced by floating macrophyte photosynthesis, CH_4 diffusion fluxes and surface concentrations were used with Eq. 1 to calculate k values specific to CH_4 and the sample temperature. k coefficients were then normalized to k_{600} values for comparison among gases and at different water temperatures, with the following equation (Jähne et al., 1987):

$$k_{600} = k_{g,T}\left(\frac{600}{Sc_{g,T}}\right)^{-n} \quad (6)$$

Where $k_{g,T}$ and $Sc_{g,T}$ are the gas transfer velocity and Schmidt number of a given gas (in this case CH_4) and temperature (Wanninkhof, 1992). Temperature specific Sc values were calculated using equations in Wanninkhof (1992), and an n of 2/3 was used for all calculations, as this factor is appropriate for a smooth liquid surface (Deacon, 1981). These site-specific k_{600} values were then used to estimate emissions for N_2O, based on N_2O surface concentrations and using Eq. 1.

For each site, equilibrium concentrations of each gas were calculated with Eq. 3, using the gas and temperature specific K_H (mol l^{-1} atm^{-1}) and the partial pressure of the gas in the atmosphere measured at each site.

To evaluate the total greenhouse gas effect of emitted gases, gas emissions (floating chamber method for CO_2, CH_4, concentration method of N_2O) were then converted to CO_2eq (mg C m^{-2} d^{-1}) on a mass basis by multiplying the CH_4 emissions by 37 (Derwent, 2020) and N_2O emissions by 265 (Myhre et al., 2013).

Data analysis and statistics

To test for differences in the chamber emission estimates among the three sample sites (near-shore, intermediate point, and the deep point) on each pond, linear mixed effect models were used with ponds included as a random effect (Zuur et al., 2009). For the rest of analyses, chamber emission estimates from the three sample sites were averaged, to provide a single mean CO_2 and CH_4 emission rate for each pond. To evaluate individual relationships among all greenhouse gas metrics and environmental variables, a Pearson correlation matrix was used. Relationships among all variables were first visually inspected with scatter plots to check for a linear relationship, and then correlations were calculated with the raw values. Environmental variables included surface area, max depth, TP, DOC, $SUVA_{254}$, TDN, NH_4, chl. a, anoxic fraction, RTRM, duckweed coverage, and canopy coverage.

To further investigate the effect of duckweed on pond greenhouse gas emissions, ponds were classified as "duckweed ponds" and "non-duckweed ponds" using a k-means cluster analysis of pond duckweed coverage, resulting in 10 duckweed ponds and 16 non-duckweed ponds. Unequal variance t-tests were used for all comparisons between natural/constructed categories and duckweed/non-duckweed categories, as variances were not homogeneous between categories for many variables. To test for interactions among the categorical variables (natural/constructed and duckweed/non-duckweed), two-way anova tests were used. p-values < 0.05 were considered significant for all analyses. All statistics were performed using R statistical software (R 4.4.1, R Core Team 2021). The lme4 package was used for mixed effect models along with the lmerTest package to test for significant differences between sampling sites, and the stats package was used for the unequal variance t-tests, k-means cluster analysis, and two-way anova tests.

Results

Pond characteristics

The 26 ponds varied widely in water chemistry and physical characteristics (Table 1). The ponds were generally small and shallow with a mean (range) surface area of 0.51 (0.04–1.5) ha and a mean max depth of 1.2 m (0.3–1.8). Most ponds were high in total phosphorus (TP) (mean 150 [44—470] µg L^{-1}), dissolved organic carbon (DOC) (mean 12 [7.1–20] mg L^{-1})), and total

TABLE 2 Differences in environmental variables between duckweed ponds and non-duckweed ponds. Ponds were categorized as duckweed or non-duckweed by *k*-means clustering, with duckweed ponds having an average coverage of 96%, and non-duckweed ponds having an average coverage of 3%.

Variable	Duckweed ponds mean (sd)	Non-duckweed ponds mean (sd)	*p*-value (significance at $p < 0.05$)
TP (ug L^{-1})	206 (106.9)	111.6 (50.5)	0.023*
Surface DO (mg L^{-1})	6.6 (1.68)	8.11 (1.69)	0.037*
Anoxic Fraction	0.642 (0.197)	0.237 (0.164)	0.000049*
RTRM	92.1 (44.9)	66.7 (47.4)	0.18
Canopy Cover in 50 m Buffer (%)	51.6 (21.1)	40.9 (23.4)	0.24

TABLE 3 Mean (range) concentrations and emissions of CO_2, CH_4, and N_2O for the 26 study ponds.

			k_{600} values using CH_4 fluxes	Flux (based on float measurements for CO_2/CH_4, based on concentrations for N_2O)			Flux in CO_2 equivalents	
Gas	Surface Conc. (mg L^{-1})	Bottom Conc. (mg L^{-1})	k_{600} (m d^{-1})	Total Emissions (mg m^{-2} d^{-1})	Diffusive (mg m^{-2} d^{-1})	Ebullition (mg m^{-2} d^{-1})	Emissions CO_2eq (mg m^{-2} d^{-1})	% of total CO_2eq
CO_2-C	2.03 (0.274–6.78)	10.3 (0.280–49.6)		-25.9 (-2000—1940)			-25.9 (-2000—1940)	4.00 (-12.0–57.3)
CH_4-C	0.250 (0.00889–0.968)	1.38 (0.0144–6.03)	1.12 (0.240–2.82)	704 (6.50–3,658)	219 (6.50–896)	484 (0–2,760)	26,000 (240–135,000)	94.5 (35.2–111)
N_2O-N	0.000501 (0.0000773–0.00130)	0.000313 (8.24e-08 - 0.00109)		0.398 (-0.302—3.60)			105 (-80.1–953)	1.4 (-2.16 - 10.7)
						Total Flux in CO_2eq	26,100 (683–135,000)	

dissolved nitrogen TDN) (mean 0.79 [0.26–1.7] mg L^{-1}). All but one pond (New Seminary) had undetectable levels of NO_2/NO_3 (below 10 μg L^{-1}). Most ponds showed evidence of stratification, with relative thermal resistance to mixing (RTRM) greater than one in all ponds (mean RTRM of 77, range of 6.8–180).

Natural ponds and constructed ponds did not significantly differ in TP levels (p = 0.66), but natural ponds did have significantly higher levels of DOC and TDN (p = 0.045, 0.016). On average, natural ponds had a larger surface area than constructed ponds (0.92 vs. 0.32 ha, p = 0.017), but constructed ponds had a deeper max depth (1.3 vs. 0.97 m, p = 0.14), though not significantly.

Duckweed coverage on the ponds ranged from 0 to 100%, though most ponds had either close to no duckweed present or almost full duckweed coverage (Table 1). Ponds were split into two duckweed categories using *k*-means cluster analysis, and duckweed ponds had an average duckweed coverage of 95.5% (n = 10), while non-duckweed ponds had an average duckweed coverage of 2.84% (n = 16). Compared to non-duckweed ponds, duckweed ponds had significantly higher TP concentrations (p = 0.023), significantly lower surface oxygen concentrations (p = 0.037), and a significantly larger anoxic fraction ($p < 0.001$; Table 2). There were no significant interactions for environmental variables or greenhouse gas metrics between the natural/constructed and duckweed/non-duckweed categories.

Greenhouse gas concentrations and emissions

Both concentrations in the surface and bottom water and emissions varied by several orders of magnitude across the ponds for each greenhouse gas (Table 3). In the surface water, mean concentrations of gases across all ponds were 2.03 mg CO_2-C L^{-1}, 0.250 mg CH_4-C L^{-1}, and 0.501 μg N_2O-N L^{-1}. Mean concentrations in the bottom water were 10.3 mg CO_2-C L^{-1}, 1.38 mg CH_4-C L^{-1}, and 0.313 μg N_2O-N L^{-1} (Table 3). The difference between surface and bottom concentrations was significant for each gas, with CO_2 concentrations significantly higher in the bottom water (mean difference 8.24 mg CO_2-C L^{-1}, p = 0.002), CH_4 concentrations significantly higher in the bottom water (mean difference 1.13 mg CH_4-C L^{-1}, p = 0.002), and N_2O concentrations significantly lower in the bottom water (mean difference -0.188 μg N_2O-N L^{-1}, p = 0.017). Equilibrium concentrations were on average 162 μg L^{-1} for CO_2-C,

TABLE 4 Pearson correlation coefficients between environmental variables and greenhouse gas metrics for all ponds (n = 26 for all variables). * indicates significance (*p < 0.05, **p < 0.01, ***p < 0.001).

	Area	Max depth	TP	DOC	$SUVA_{254}$	TDN	Ammonium	Chl. a	Anoxic fraction	RTRM	Duckweed	Canopy
Surface Area (ha)	1											
Max Depth (m)	−0.046	1										
TP (μg L^{-1})	−0.132	−0.128	1									
DOC (mg L^{-1})	0.181	−0.003	0.083	1								
$SUVA_{254}$ (L mg-M^{-1})	−0.395*	0.049	0.182	−0.204	1							
TDN (mg L^{-1})	0.127	−0.29	0.21	0.749***	−0.488*	1						
Ammonium-N (mg L^{-1})	−0.115	−0.17	0.344	0.074	−0.008	0.227	1					
Chl. a (μg L^{-1})	0.16	0.25	0.319	0.221	−0.231	0.221	0.138	1				
Anoxic Fraction	0.237	0.016	0.545**	0.478*	0.051	0.458*	0.078	0.374	1			
RTRM	0.273	0.444*	0.321	−0.019	0.036	-0.194	−0.241	0.275	0.362	1		
Duckweed Coverage (%)	0.205	−0.255	0.561**	0.323	0.028	0.395*	0.148	0.224	0.765***	0.239	1	
Canopy cover 50 m buffer (%)	0.678***	0.212	0.105	0.165	−0.177	0.111	0.055	0.256	0.347	0.272	0.267	1
Surface CO_2 Conc. (mg L^{-1})	−0.075	0.091	0.547**	0.145	0.307	0.212	0.451*	0.02	0.553**	0.094	0.362	0.053
Surface CH_4 Conc. (mg L^{-1})	0.418*	−0.03	0.639***	0.278	0.093	0.278	0.226	0.29	0.683***	0.532**	0.678***	0.344
Surface N_2O Conc	0.018	0.193	−0.232	0.032	-0.075	0.038	−0.27	−0.098	−0.116	-0.085	−0.247	0.281
Bottom CO_2 Conc. (mg L^{-1})	−0.053	0.518**	0.047	−0.079	0.430*	−0.183	0.004	0.232	0.421*	0.264	0.227	0.145
Bottom CH_4 Conc. (mg L^{-1})	0.046	0.512**	0.377	−0.134	0.187	−0.123	−0.04	0.453*	0.460*	0.487*	0.387	0.18
Bottom N_2O Conc. (mg L^{-1})	−0.262	−0.491*	−0.138	−0.152	−0.034	0.048	-0.037	−0.455*	−0.544**	-0.467*	−0.331	−0.214
Emission CO_2 (mg m^{-2} d^{-1})	−0.07	−0.03	−0.422*	−0.233	0.139	−0.172	0.039	−0.490*	−0.394*	−0.480*	−0.554**	−0.095
Emission CH_4 Tot. (mg m^{-2} d^{-1})	0.208	−0.336	0.677***	0.119	0.143	0.195	0.147	0.27	0.475*	0.26	0.530**	0.078
Emission CH_4 Eb. (mg m^{-2} d^{-1})	0.159	−0.354	0.606**	0.059	0.154	0.129	0.029	0.188	0.368	0.213	0.434*	0.008
Emission CH_4 Dif. (mg m^{-2} d^{-1})	0.289	−0.218	0.716***	0.251	0.085	0.323	0.420*	0.423*	0.651***	0.323	0.664***	0.243

0.034 μg L^{-1} for CH_4-C, and 0.24 μg L^{-1} for N_2O-N, meaning that the ponds were generally super saturated with all three greenhouse gases. In the surface water, CO_2 concentrations were on average 11-fold supersaturated, CH_4 concentrations were on average 7,000-fold supersaturated, and N_2O concentrations were on average 2-fold supersaturated.

Emission rates using the floating chamber method did not significantly vary by location within each pond (Supplementary

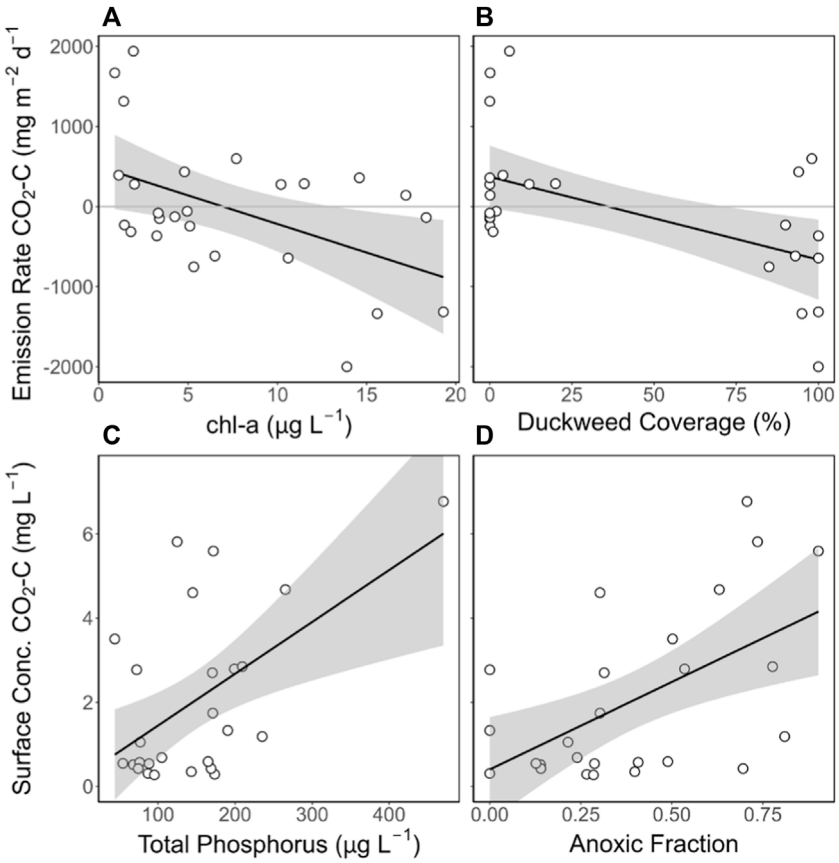


FIGURE 1
CO_2 emissions from the floating chamber and CO_2 surface concentrations were significantly correlated with different variables. Scatterplots show significant correlations for all ponds (n = 26) between **(A)** CO_2 emission rate and chl-a (y = -71.28 + 496.25, R^2 = 0.22, p = 0.016) **(B)** CO_2 emission rate and duckweed coverage (y = -10.34 + 371.83, R^2 = 0.31, p = 0.0033) **(C)** CO_2 surface concentration and total phosphorus (y = 0.01x + 0.21, R^2 = 0.30, p = 0.0039), and **(D)** CO_2 surface concentration and anoxic fraction (y = 4.15x + 0.41, R^2 = 0.38, p = 0.001).

Figure S3), with no significant differences between the shallow, middle and deep locations (p = 0.245, 0.782, and 0.315 for CO_2 emission, CH_4 diffusion, and CH_4 ebullition, respectively). Though not significant, CH_4 ebullition emissions were highest at the near-shore shallow location, while CH_4 diffusion emissions were highest at the deep point location (Supplementary Figure S3). When all three floating chamber incubations were averaged to get a mean rate for each pond the mean emission rates for CO_2 and CH_4 were −25.9 mg CO_2-C m^{-2} d^{-1} and 705 mg CH_4-C m^{-2} d^{-1}, with mean rates of 219 mg CH_4-C m^{-2} d^{-1} for diffusion and 484 mg CH_4-C m^{-2} d^{-1} for ebullition. Using surface concentrations and calculated k_{600} values, the average emission rate for N_2O was 0.398 mg N_2O-N m^{-2} d^{-1}. The mean k_{600} across all ponds was 1.12 m d^{-1} but ranged from 0.240—2.82 m d^{-1} (Table 3). k_{600} did not significantly correlate with any environment variables but was lower in duckweed ponds compared to non-duckweed ponds (0.924 vs 1.24 m d^{-1}), though not significantly (p = 0.251).

The mean total daytime emission rate for all three greenhouse gases in CO_2 equivalents was 26,100 mg C m^{-2} d^{-1}, with CH_4 accounting for over 94% of the total emissions in CO_2 equivalents on average. CO_2 accounted for about 4% of the total emissions in CO_2 equivalents, but ranged from a sink of −12%–57%. N_2O accounted for 2.4% of the total emissions in CO_2 equivalents, ranging from a sink of −2.2%–11% (Table 3).

Predictors of greenhouse gases

CO_2 emission rates from the floating chamber method was significantly negatively correlated with TP, chl. a, anoxic fraction, RTRM, and duckweed coverage, with the strongest correlations being duckweed, and chl. a (Table 4; Figure 1). However, surface concentrations of CO_2 were significantly positively correlated with TP and anoxic fraction, as well as ammonium concentration (Table 4; Figure 1).

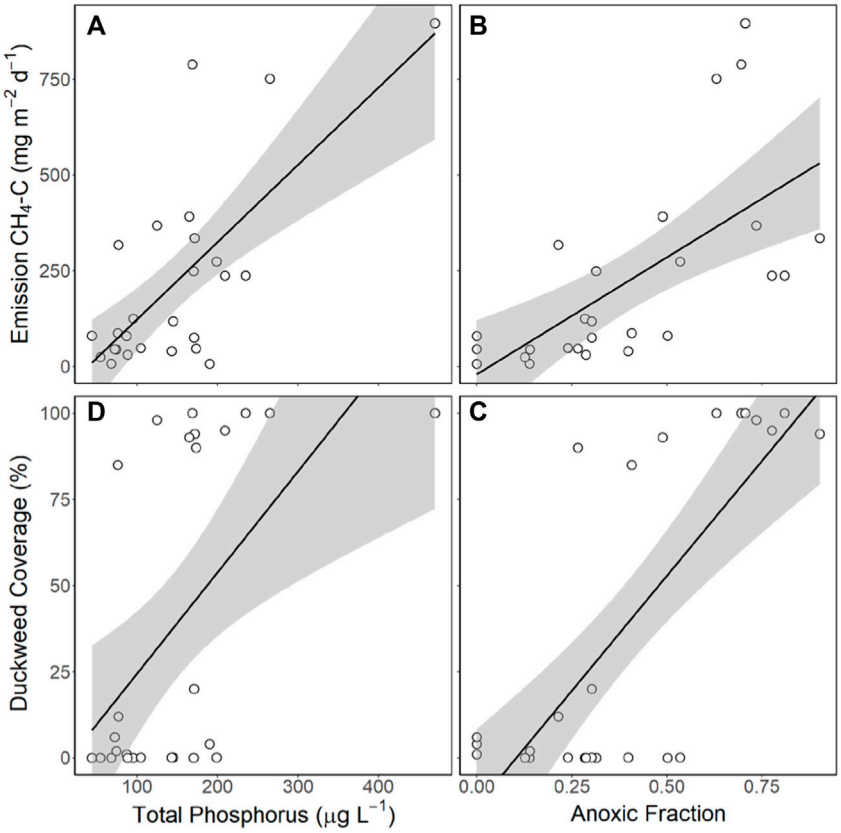


FIGURE 2
CH_4 emissions and duckweed coverage were both significantly correlated with total phosphorus and anoxic fraction. Scatterplots show significant correlations for all ponds (n = 26) between **(A)** CH_4 emission rate and total phosphorus (y = 2.02x−79.33, R^2 = 0.51, p < 0.0001) **(B)** CH_4 emission rate and anoxic fraction (y = 611.34x−20.85, R^2 = 0.44, p = 0.0002 **(C)** duckweed coverage and total phosphorus (y = 0.29x−4.94, R^2 = 0.32, p = 0.0028), and **(D)** duckweed coverage and anoxic fraction (y = 133.3x - 13.87, R^2 = 0.51, p < 0.0001).

CH_4 emission rates and surface concentrations correlated with similar variables, with surface CH_4 concentrations significantly positively correlated with surface area, TP, RTRM, anoxic fraction, and duckweed coverage. For emission rates of CH_4, total emission, ebullition, and diffusion were all significantly positively correlated with TP, anoxic fraction, and duckweed coverage, with ebullition also negatively correlated with maximum depth, and diffusion also positively correlated with ammonium and chl-a (Table 4; Figure 2).

N_2O surface concentrations were not significantly correlated with any environmental variables. All three greenhouse gas bottom concentrations were correlated with maximum depth (positively for CO_2 and CH_4, negatively for N_2O). CO_2 bottom concentration was also positively correlated with SUVA values, and N_2O bottom concentration was negatively correlated with chl-a, anoxic fraction, and RTRM (Table 4).

Duckweed coverage was significantly correlated with many of the greenhouse gas metrics, as well as significantly positively correlated with TP and anoxic fraction (Table 4; Figure 2). Duckweed ponds had significantly higher CH_4 emissions for both total emission (p = 0.04) and diffusion (p = 0.0085), but not ebullition (p = 0.095). Duckweed ponds also had significantly lower CO_2 emissions (p = 0.0055; Figure 3). For greenhouse gas concentrations, duckweed ponds had significantly higher CH_4 surface concentrations (p = 0.004), and significantly lower N_2O bottom concentrations (p = 0.043; Figure 4).

Discussion

Greenhouse gas concentrations and emissions

Most of the 26 ponds in this study were super-saturated with all three greenhouse gases during the study period. Concentrations of greenhouse gases in the surface water were comparable to other recent studies of pond greenhouse gases, including ponds in Connecticut (mean of

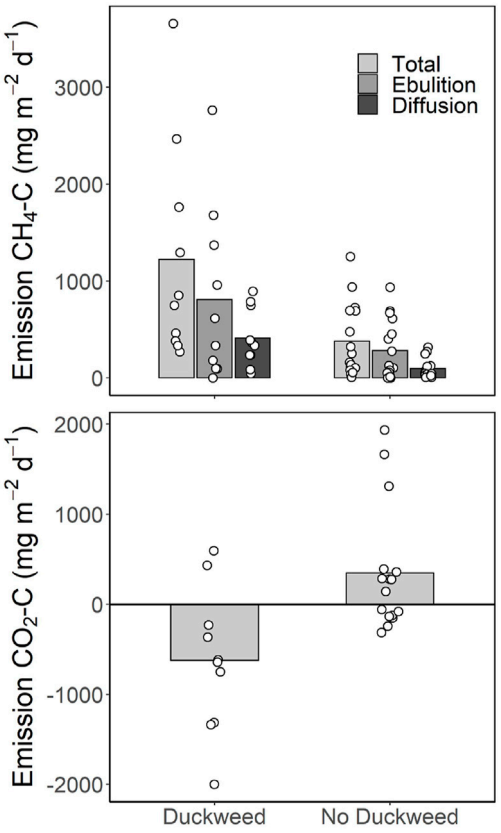


FIGURE 3
Daily emission rates of CH_4 and CO_2 for duckweed and non-duckweed ponds. Significant differences between duckweed ponds and non-duckweed ponds are total CH_4 emission (p = 0.04), diffusion CH_4 emission (p = 0.0085), and CO_2 emission (p = 0.0055).

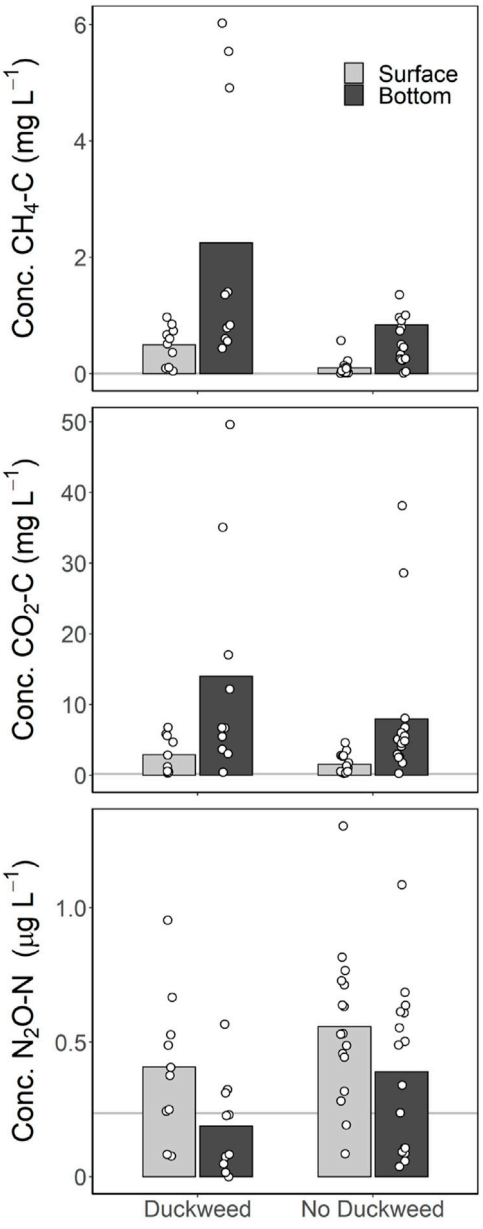


FIGURE 4
Surface and bottom concentrations of CH_4, CO_2, and N_2O for duckweed and non-duckweed ponds. Significant differences between duckweed ponds and non-duckweed ponds are surface CH_4 concentration (p = 0.0040), and bottom N_2O concentration (p = 0.043). Grey horizontal lines represent the equilibrium concentration.

4.32 mg CO_2-C L^{-1} and 0.396 mg CH_4-C L^{-1} (Holgerson, 2015)), and ponds in Denmark (mean of 1.94 mg CO_2-C L^{-1}, 0.044 mg CH_4-C L^{-1}, and 0.8 µg N_2O-N L^{-1} (Audet et al., 2020)). However, surface concentrations of CO_2 and CH_4 were higher than values typically reported for lakes. In a survey of 1,835 lakes, the mean CO_2 concentration of the upper 10% of the samples were 16-fold above atmospheric equilibrium, while the average of all lakes was about 2-fold above equilibrium (Cole et al., 1994). For the ponds in this study, the highest surface CO_2 concentration was 40-fold above atmospheric equilibrium, while the average of all 26 ponds was 11-fold above equilibrium. For CH_4, a survey of surface methane concentrations from 48 lakes had a mean concentration of 8.3 µg CH_4-C L^{-1} with 27.9 µg CH_4-C L^{-1} as the highest concentration (Bastviken et al., 2004). The ponds in this study had an average surface concentration of 250 µg CH_4-C L^{-1}, showing ponds can be extreme hotspots of CH_4 production. These high CH_4 concentrations may also signal the lack of CH_4 oxidation in ponds, potentially driven by anoxia and/or a lack of other oxidants such as nitrate, or shallow depth that allows for rapid transport of CH_4 from the sediment to the surface (Bastviken et al., 2004). Surface N_2O concentrations were not much higher than atmospheric equilibrium, and four of the 26 ponds were undersaturated in surface N_2O. These ponds overall had lower surface N_2O

concentrations compared to many lakes. A study of 15 Swiss lakes found an average of 434% saturation for surface N_2O (Mengis et al., 1997), while the ponds in this study had an average saturation of 209%.

Bottom water concentrations of CO_2 and CH_4 were on average much higher than surface concentrations, while N_2O concentrations were often lower in the bottom waters. While all ponds were less than 1.8 m deep, all ponds still showed evidence of stratification, with relative thermal resistance to mixing (RTRM) greater than one in all ponds during the day. Thus, many ponds had substantial storage of CO_2 and CH_4 in the bottom waters, as well as undersaturation of N_2O. Bottom water concentrations of greenhouse gases are less often measured or reported for lakes and ponds, but the ponds in this study had high concentrations of CO_2 and CH_4 that compare to or exceeded anoxic hypolimnion concentrations of stratified lakes. Hypolimnion concentrations of CO_2 from northern lakes can reach 3.6 to 5.4 mg CO_2-C L^{-1} (Ducharme-Riel et al., 2015), while these study ponds had a maximum bottom CO_2 concentration of 49 mg CO_2-C L^{-1} (mean 10.3 mg CO_2-C L^{-1}). The highest hypolimnion CH_4 concentrations in a study of three Wisconsin lakes in late summer ranged from 3.6—8.4 mg CH_4-C L^{-1} (Bastviken et al., 2008), while the highest bottom concentrations in these study ponds was 6 mg CH_4-C L^{-1} (mean 1.38 mg CH_4-C L^{-1}). This shows that some small ponds can still build up large concentrations of CO_2 and CH_4 in the bottom waters, which likely are emitted during fall turnover or other mixing events. Intermittently mixed ponds may mix during the night or early morning when the surface water cools (Holgerson et al., 2022), and nighttime emissions could be higher due to mixing events in some of these ponds. N_2O concentrations were on average lower in the bottom waters compared to the surface waters, and 14 of the 26 ponds were undersaturated in the bottom waters, compared to only four ponds undersaturated in the surface waters. This pattern agrees with many findings for lakes and reservoirs, where N_2O concentrations peak in the surface water or oxic-anoxic interface, and are undersaturated in the permanently anoxic part of the hypolimnion (Mengis et al., 1997; Beaulieu et al., 2015).

CO_2 using floating chamber estimates suggested that the ponds are a net sink (Table 3), though these ponds were sampled during the day and in the peak growing season and this likely does not reflect overall daily or annual CO_2 fluxes from these ponds. Fluxes of CO_2 would likely be the lowest during day when photosynthesis is high and would peak during the night when respiration predominates. Therefore, the daily CO_2 fluxes measured in these ponds are likely underestimated due to the lack of nighttime measurements. The negative fluxes of CO_2 contrasted with the CO_2 supersaturation in the surface waters of most ponds, due to duckweed creating a CO_2 sink above the surface of the duckweed covered ponds. Despite middle floating chamber incubations and surface concentrations being measured in the same spots, using surface concentrations to estimate CO_2 fluxes would have greatly overestimated daytime CO_2 emissions for the duckweed covered ponds.

Fluxes of CH_4 were always positive, and the CH_4 emission rates from these ponds were extremely high for freshwater ponds and lakes. CH_4 emissions have been shown to peak during the day and regress at night (Sieczko et al., 2020), and daytime sampling of these ponds may overestimate daily emission rates. Nonetheless, ponds may mix at night due to convective cooling unlike larger lakes (Andersen et al., 2017), which may lead to higher emissions during nighttime as gases escape from the bottom waters. CH_4 emissions also peak during the growing season (van Bergen et al., 2019), and therefore the CH_4 emission rates found in these study ponds may represent the peak emission rates that these ponds experience. However, mixing during the shoulder seasons could also lead to the release of CH_4 from the bottom waters, and fall and spring CH_4 emission rates can be higher than other seasons (Riera et al., 1999; Jansen et al., 2019). Mean total CH_4 emissions from these ponds were among the highest reported for studies involving multiple ponds (Table 5). Diffusive CH_4 emission were high compared to a global assessment of lakes and ponds, where waterbodies less than 1 ha in size had a mean diffusive emission rate of 21.8 mg CH_4-C m^{-2} d^{-1} (Holgerson & Raymond, 2016). However, emissions were similar to diffusive CH_4 emissions found in Virginia stormwater ponds (mean 271.8 mg CH_4-C m^{-2} d^{-1}) (Gorsky et al., 2019). Ebullition CH_4 emissions are less often measured in ponds, and ebullition rates are highly variable both spatially and temporally. Ebullition CH_4 emissions from these study ponds were higher than mean ebullition fluxes in Canadian ponds (mean 55.2, max 204 mg CH_4-C m^{-2} d^{-1}) (DelSontro et al., 2016), but within a similar range of ponds across Canada and Missouri (highest median pond ebullition rate of 485 mg CH_4-C m^{-2} d^{-1}) (Baron et al., 2022). Ebullition rates can be strongly correlated with temperature (DelSontro et al., 2016), and sampling in mid-summer during the day likely facilitated the peak ebullition rates observed from these ponds.

The mean gas transfer velocity, k_{600}, of the study ponds was high but many of the ponds fell within the range of other measurements of k_{600} in small, shallow waterbodies (Xiao et al., 2014; Holgerson et al., 2017). Many studies that use a literature value of k_{600} to calculate greenhouse gas fluxes based on surface concentrations use a k_{600} value of less than 1 m d^{-1} for small waterbodies, such as the 0.36 m d^{-1} used by Holgerson and Raymond (2016). The high average k_{600} in these ponds of 1.12 m d^{-1} was driven by a few ponds with exceptional large k_{600} values (up to 2.82 m d^{-1}), and the median value of 0.89 m d^{-1} is closer to what studies assuming a constant k_{600} may use for small waterbodies. Gas transfer velocities can be extremely variable, and the high k_{600} values seen in these ponds may mean that assuming a low constant k_{600} could underestimate greenhouse gas emissions based on surface water concentrations.

TABLE 5 Average daily greenhouse gas emissions reported from recent studies including multiple ponds. All rates converted to mg C/N m^{-2} d^{-1}, for comparison.

References	Region	Number of ponds	Method	Pond types	Surface area range (ha)	Max depth range (m)	Mean (range) emission rate mg CO2-C m^{-2} d^{-1}	Mean (range) emission rate mg CH4-C m^{-2} d^{-1}	Methane emission pathway	Mean (range) emission rate mg N2O-N m^{-2} d^{-1}
Audet et al. (2020)	Denmark	37	Headspace Conc	Artificial	0.0135–0.652	Up to 1.5	628	15	Diffusion only	0.19
Gorsky et al. (2019)	Virginia, United States	15	Floating Chambers	Artificial	0.07–10.56	1.45–4.75	409 (-394.7–1924)	271.8 (5.4–1,373)	Diffusion only	0.079 (-0.506—0.87)
Grinham et al. (2018)	Australia	22	Floating Chambers	Artificial	0.021–5.68			234.9 (13.5–1753)	Ebulition plus diffusion	
Peacock et al. (2019)	Sweden	40	Headspace Conc	Artificial			752 (-187—3,449)	30.3 (0.4–174)	Diffusion only	
Peacock et al. (2021)	Sweden	16	Floating Chambers	Artificial and Natural	0.004–0.415	0.04–0.78	994	30.9	Diffusion only	
Goeckner et al. (2022)	Florida, United States	5	Floating Chambers	Artificial	0.622–1.885	1.8–7.2	1,622 (338–3,627)	35.8 (11–96.8)	Diffusion only	
This study	Minnesota, United States	26	Floating Chambers for CO2 CH4, concentration for N2O	Artificial and Natural	0.04–1.5	0.3–1.8	-25.9 (-2000—1940)	704 (6.50–3,658)	Ebulition plus diffusion	0.398 (-0.302—3.60)

Environmental predictors of greenhouse gases

CO_2 concentrations and emissions correlated with similar variables, but in opposite directions. While surface CO_2 concentrations were significantly positively correlated with TP, CO_2 emissions were significantly negatively correlated with TP. This is likely due to a relationship between duckweed and TP, with phosphorus facilitating duckweed growth (Lasfar et al., 2007), that then reduces CO_2 emissions. Neither CO_2 concentrations nor emissions were correlated with DOC concentration, a relationship that has been found in many lakes (Raymond et al., 2013). Surface CO_2 concentrations did correlate negatively with surface oxygen concentrations (r^2 = 0.46, p = 0.00014), a relationship that has been shown to best predict CO_2 concentrations in ponds (Kankaala et al., 2013; Holgerson, 2015). Low oxygen is likely consequence of the combination of high rates of aerobic respiration in ponds, where sediment respiration can affect the whole water column (Holgerson, 2015), and low ventilation rates, especially in the systems that were protected from wind and with high abundance of duckweed.

Both CH_4 concentrations and emissions were predicted by similar variables. CH_4 diffusion and TP concentration was the strongest correlation among any greenhouse gas metric and any environmental variable, and TP also correlated with ebullition rates and surface CH_4 concentrations. This trend agrees with previous research that showed higher CH_4 emissions in more eutrophic lakes and ponds (DelSontro et al., 2016, 2018; Beaulieu et al., 2019). While it is unknown if high phosphorus levels stimulate CH_4 production directly, excess phosphorus likely helps create conditions conducive to CH_4 production, including stimulating algal growth, which when degraded can lead to more labile organic matter and increased anoxia (Davidson et al., 2018). The pond anoxic fraction was also significantly positively correlated with all CH_4 gas metrics. As methanogenesis is primarily an anoxic process, more anoxic water can lead to increased CH_4 formation in the water column and the sediments, as well as decreased methane oxidation (Bastviken et al., 2004).

While no environmental variables correlated with surface N_2O, N_2O concentrations from the ponds in this study compare well to other studies that have not found significant N_2O emissions from ponds (Singh et al., 2005; Audet et al., 2020). Despite high nutrients in these ponds, many which are hyper-eutrophic based on phosphorus concentrations (Carlson, 1977), there was almost no detectable levels of NO_3/NO_2 in any of the ponds, which can be a strong driver of N_2O emissions (Mccrackin & Elser, 2010; Beaulieu et al., 2015; Wang et al., 2021). Furthermore, almost all of the ponds were stratified to

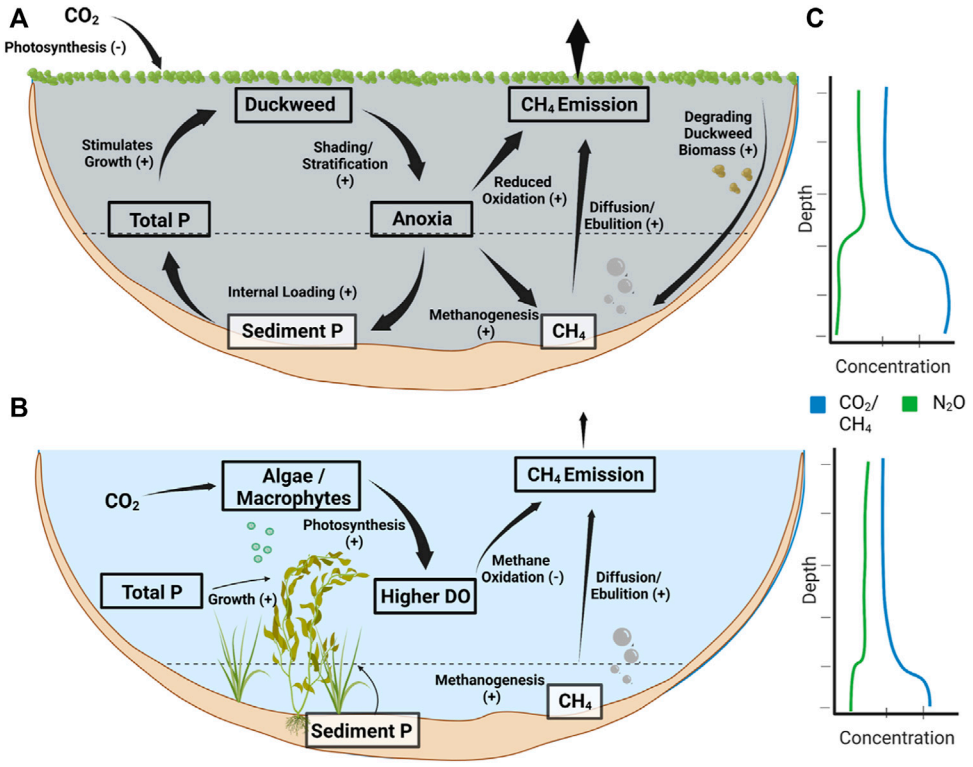


FIGURE 5
A conceptual diagram of the effect of duckweed on pond greenhouse gas emissions. **(A)** Duckweed can create a positive feedback loop that promotes anoxia, phosphorus loading, and further duckweed growth. While duckweed can consume CO_2, high phosphorus levels and increased anoxia can promote CH_4 production, reduce CH_4 oxidation, and lead to high CH_4 emissions. **(B)** Non-duckweed ponds have photosynthesis occurring within the water column, leading to higher DO, more methane oxidation, and less methane production. **(C)** Conceptual profiles of dissolved gases in duckweed and non-duckweed ponds.

some degree during the day, similar to conditions in Canadian farm ponds that became N_2O sinks in late summer (Webb et al., 2019).

There was no significant difference in greenhouse gas concentrations or emissions between constructed ponds and natural ponds, which was likely due to very similar water chemistry on average between natural and constructed ponds. There were no significant differences in TP among constructed and natural ponds, highlighting that most ponds are often highly eutrophic, even among different land use types. While there can be many reasons why constructed ponds may function differently compared to natural ponds (Clifford & Heffernan, 2018), constructed ponds can vary greatly in physical and chemical characteristics just like natural ponds, potentially mitigating differences between the two at larger scales.

Impacts of duckweed

Duckweed coverage had a discernable effect on the physical and chemical states among ponds, as well as a significant effect on all three greenhouse gases. Among the 26 ponds, conditions either supported the complete coverage of duckweed over the pond surface, or ponds were not suitable for duckweed to have significant growth. Conditions for duckweed growth may depend on terrestrial canopy cover to block wind, as well as available nutrients (Hillman, 1961) (Table 4). Very few ponds had only partial duckweed coverage, though larger ponds with duckweed often had some open water if there was any wind. Duckweed coverage had clear effects on oxygen levels, with duckweed ponds having significantly less surface oxygen and a larger anoxic fraction (Tables 3, 4). Duckweed mats are known to reduce oxygen levels in small waterbodies (Pokorny & Rejm, 1983; Ceschin et al., 2019), likely due to duckweed shading out photosynthetic organisms in the water column and leading to almost no oxygen production within the pond. A blanket of duckweed coverage could also reduce atmospheric exchange of oxygen, and duckweed ponds did have slightly lower mean gas transfer velocity, though not significantly. Stratification was also stronger in duckweed ponds, though not significantly (Table 4), and this could also play a role in developing a more

anoxic hypolimnion. Duckweed ponds were also significantly higher in TP (Tables 3, 4), likely due to increased anoxia which led to a positive feedback loop by stimulating further duckweed growth (Lasfar et al., 2007). Greater anoxia can stimulate higher rates of internal loading of phosphorus from the sediments (Taguchi et al., 2020) (Figure 5).

Through these physical and chemical effects on the water column, duckweed coverage created two distinct states among the 26 ponds in this study. The increased anoxia and high phosphorus concentrations promoted by duckweed coverage also coincided with increased CH_4 emissions from duckweed ponds (Figure 2), and duckweed ponds had mean CH_4 emissions over twice that of non-duckweed ponds for each of total, ebullitive, and diffusive emissions (Figure 3). Degrading duckweed may also create a large pool of labile organic matter in duckweed ponds similar to submersed macrophytes (Hilt et al., 2022), which could further promote methanogenesis and ebullition (West et al., 2012; Zhou et al., 2019). Duckweed ponds were on average CO_2 sinks, despite having higher CO_2 concentrations in the surface waters compared to non-duckweed ponds (Figures 3, 4). Though duckweed ponds were a daytime CO_2 sink, higher CO_2 concentrations may mean that these ponds release more CO_2 during the night, potentially offsetting the CO_2 captured by the duckweed. Further, CH_4 accounted for over 95% of the total emission rate in CO_2eq on average for these ponds, showing that CH_4 dominates the emissions in small ponds. Overall duckweed ponds had about three times the emission rate in CO_2 equivalents compared to non-duckweed ponds (mean 31 vs. 11 g C m^{-2} d^{-1}).

Duckweed ponds also had higher concentrations of CH_4 and CO_2 in the bottom waters, though not significantly. Duckweed ponds did have significantly lower concentrations of N_2O in the bottom waters, with most bottom waters of duckweed ponds undersaturated. This could again be due to anoxic conditions in the hypolimnion of duckweed ponds, which has been linked to undersaturated N_2O (Beaulieu et al., 2015).

Implications and management

Floating macrophyte coverage, including duckweed, is increasing worldwide in recent decades, correlated with expanding urbanization and increased eutrophication of aquatic systems (Kleinschroth et al., 2021). While not all floating macrophytes may create similar dynamics, other floating macrophytes that shade out water column oxygen production could lead higher anoxia, higher phosphorus concentrations, and higher CH_4 emissions as seen in the ponds in this study. For urban stormwater ponds, floating macrophytes may undermine the goal of capturing and preventing nutrients from flowing into downstream waterways by increasing internal loading of from phosphorus-rich sediments (Taguchi et al., 2020). Further, duckweed and other floating macrophytes may be causing an unforeseen increase in greenhouse gas emissions from both constructed and natural ponds.

In constructed ponds, management of duckweed and other floating macrophytes can be difficult, as weed control can be costly and labor intensive (Kleinschroth et al., 2021). Duckweed may be utilized as an obvious "indicator" of degraded conditions in constructed ponds, likely signaling high nutrients, poor water quality, and high greenhouse gas emissions, and duckweed has already been used as an indicator of pollution and heavy metal contamination (Garg & Chandra, 1994). While canopy cover blocking wind may be an important influencer of duckweed growth, data for this study suggest phosphorus levels may be one of the most important drivers of duckweed coverage. While management of stormwater ponds already often focuses on reducing nutrient levels, the duckweed state in ponds may act similarly to stable states seen in shallow lakes (Scheffer et al., 1993), where duckweed takes over as the dominant primary producer, and the ensuing degraded water quality state is more resistant to reduced nutrient levels. Oxygen depletion may be the largest factor in increasing CH_4 emissions caused by duckweed, and increasing oxygenation in ponds may limit phosphorus loading as well as reduce greenhouse gas emissions.

Conclusion

The ponds in this study had high concentrations and emissions of greenhouse gases, especially CH_4, that were similar to other recent studies of ponds. While no differences in nutrient levels or greenhouse gas concentrations were found between natural and constructed ponds, duckweed had a distinct impact on pond physical and chemical characteristics, as well as greenhouse gas dynamics. Duckweed ponds had CH_4 emission rates nearly three times as high as non-duckweed ponds. Duckweed ponds had lower CO_2 and N_2O emissions, but overall had higher emissions in CO_2eq due to methane. Globally increasing duckweed and other floating macrophyte coverage worldwide may be increasing greenhouse gas emissions from ponds and can be an indicator of degraded water quality conditions.

Data availability statement

The datasets presented in this study are located in the Environmental Data Initiative (EDI) Repository. (Rabaey and Cotner, 2022) https://doi.org/10.6073/pasta/370cca808d5d1991ddb7f2b9f2b6c107.

Author contributions

JR and JC conceived and designed the analysis, JR completed data collection, performed data analysis, and drafted the manuscript. JC aided in data interpretation and revising the manuscript.

Funding

Research funding was provided by the University of Minnesota College of Biological Sciences, the Bell Museum of Natural History, and the NSF Department of Environmental Biology (DEB), grant number 1722507.

Acknowledgments

Thank you to Miriam Arroyo for aiding in fieldwork and data collection. Thank you to the Belwin Conservancy, Dodge Nature Center, Ordway Field Station, and Cedar Creek Ecosystem Reserve for access and use of study ponds. Research funding was provided by the University of Minnesota College of Biological Sciences, as well as the Bell Museum of Natural History.

Conflict of interest

The authors declare that the research was conducted in the absence of any commercial or financial relationships that could be construed as a potential conflict of interest.

Publisher's note

All claims expressed in this article are solely those of the authors and do not necessarily represent those of their affiliated organizations, or those of the publisher, the editors and the reviewers. Any product that may be evaluated in this article, or claim that may be made by its manufacturer, is not guaranteed or endorsed by the publisher.

Supplementary material

The Supplementary Material for this article can be found online at: https://www.frontiersin.org/articles/10.3389/fenvs.2022.889289/full#supplementary-material

References

Andersen, M. R., Kragh, T., Sand-jensen, K., and Andersen, M. R. (2017). *Extreme diel dissolved oxygen and carbon cycles in shallow vegetated lakes*. The Royal Society B, 284.

Attermeyer, K., Flury, S., Jayakumar, R., Fiener, P., Steger, K., Arya, V., et al. (2016). Invasive floating macrophytes reduce greenhouse gas emissions from a small tropical lake. *Sci. Rep.* 6, 20424. doi:10.1038/srep20424

Audet, J., Carstensen, M. V., Hoffmann, C. C., Lavaux, L., Thiemer, K., and Davidson, T. A. (2020). Greenhouse gas emissions from urban ponds in Denmark. *Inland Waters* 10 (3), 373–385. doi:10.1080/20442041.2020.1730680

Baron, A. A. P., Dyck, L. T., Amjad, H., Bragg, J., Kroft, E., Newson, J., et al. (2022). Differences in ebullitive methane release from small, shallow ponds present challenges for scaling. *Sci. Total Environ.* 802, 149685. doi:10.1016/j.scitotenv.2021.149685

Bastviken, D., Cole, J. J., Pace, M. L., and van de-Bogert, M. C. (2008). Fates of methane from different lake habitats: Connecting whole-lake budgets and CH4 emissions. *J. Geophys. Res.* 113 (2), 1–13. doi:10.1029/2007JG000608

Bastviken, D., Cole, J., Pace, M., and Tranvik, L. (2004). Methane emissions from lakes: Dependence of lake characteristics, two regional assessments, and a global estimate. *Glob. Biogeochem. Cycles* 18 (4), 1–12. doi:10.1029/2004GB002238

Beaulieu, J. J., DelSontro, T., and Downing, J. A. (2019). Eutrophication will increase methane emissions from lakes and impoundments during the 21st century. *Nat. Commun.* 10 (1), 1375–1377. doi:10.1038/s41467-019-09100-5

Beaulieu, J. J., Nietch, C. T., and Young, J. L. (2015). Controls on nitrous oxide production and consumption in reservoirs of the Ohio River Basin. *J. Geophys. Res. Biogeosci.* 120 (10), 1995–2010. doi:10.1002/2015JG002941

Bettez, N. D., and Groffman, P. M. (2012). Denitrification potential in stormwater control structures and natural riparian zones in an urban landscape. *Environ. Sci. Technol.* 46 (20), 10909–10917. doi:10.1021/es301409z

Birge, E. A. (1916). *The work of the wind in warming a lake*. Notes from the Laboratory of the Wisconsin Geological and Natural History Survey.

Blaszczak, J. R., Steele, M. K., Badgley, B. D., Heffernan, J. B., Hobbie, S. E., Morse, J. L., et al. (2018). Sediment chemistry of urban stormwater ponds and controls on denitrification. *Ecosphere* 9 (6). doi:10.1002/ecs2.2318

Carlson, R. E. (1977). A trophic state index for lakes1. *Limnol. Oceanogr.* 22 (2), 361–369. doi:10.4319/lo.1977.22.2.0361

Ceschin, S., Abati, S., Traversetti, L., Spani, F., del Grosso, F., and Scalici, M. (2019). Effects of the invasive duckweed lemna minuta on aquatic animals: Evidence from an indoor experiment. *Plant Biosyst. - Int. J. Deal. All Aspects Plant Biol.* 153 (6), 749–755. doi:10.1080/11263504.2018.1549605

Clifford, C. C., and Heffernan, J. B. (2018). Artificial aquatic ecosystems. *Water* 10, 1096. doi:10.3390/w10081096

Cole, J. J., Caraco, N. F., , et al.Cole, J. J., Caraco, N. F., Kling, G. W., Kratz, T. K. (1994). Carbon dioxide supersaturation in the surface waters of lakes. *Science* 265 (5178), 1568–1570. doi:10.1126/science.265.5178.1568

Davidson, T. A., Audet, J., Jeppesen, E., Landkildehus, F., Lauridsen, T. L., Søndergaard, M., et al. (2018). Synergy between nutrients and warming enhances methane ebullition from experimental lakes. *Nat. Clim. Chang.* 8 (2), 156–160. doi:10.1038/s41558-017-0063-z

Deacon, E. L. (1981). Sea-air gas transfer: The wind speed dependence. *Bound. Layer. Meteorol.* 21, 31–37. doi:10.1007/bf00119365

DelSontro, T., Beaulieu, J. J., and Downing, J. A. (2018). Greenhouse gas emissions from lakes and impoundments: Upscaling in the face of global change. *Limnol. Oceanogr. Lett.* 3 (3), 64–75. doi:10.1002/lol2.10073

DelSontro, T., Boutet, L., St-Pierre, A., del Giorgio, P. A., and Prairie, Y. T. (2016). Methane ebullition and diffusion from northern ponds and lakes regulated by the interaction between temperature and system productivity. *Limnol. Oceanogr.* 61, S62–S77. doi:10.1002/lno.10335

Derwent, R. G. (2020). Global warming potential (GWP) for methane: Monte Carlo analysis of the uncertainties in global tropospheric model predictions. *Atmosphere* 11 (5), 486. doi:10.3390/ATMOS11050486

Desrosiers, K., Delsontro, T., and del Giorgio, P. A. (2022). Disproportionate contribution of vegetated habitats to the CH4 and CO2 budgets of a boreal lake. *Ecosystems*. doi:10.1007/s10021-021-00730-9

Downing, J. A., McDowell, W. H., Kortelainen, P., Caraco, N. F., Tranvik, L. J., Cole, J. J., et al. (2006). The global abundance and size distribution of lakes, ponds, and impoundments. *Limnol. Oceanogr.* 51 (5), 2388–2397. doi:10.4319/lo.2006.51.5.2388

Duc, N. T., Crill, P., and Bastviken, D. (2010). Implications of temperature and sediment characteristics on methane formation and oxidation in lake sediments. *Biogeochemistry* 100 (1), 185–196. doi:10.1007/s10533-010-9415-8

Ducharme-Riel, V., Vachon, D., del Giorgio, P. A., and Prairie, Y. T. (2015). The relative contribution of winter under-ice and summer hypolimnetic CO2 accumulation to the annual CO2 emissions from northern lakes. *Ecosystems* 18 (4), 547–559. doi:10.1007/s10021-015-9846-0

Erkkilä, K. M., Ojala, A., Bastviken, D., Biermann, T., Heiskanen, J., Lindroth, A., et al. (2018). Methane and carbon dioxide fluxes over a lake: Comparison between eddy covariance, floating chambers and boundary layer method. *Biogeosciences* 15 (2), 429–445. doi:10.5194/bg-15-429-2018

Fofonoff, N. P., and Millard, R. D., Jr. (1983). Algorithms for computation of fundamental properties of seawater. *Unesco Tech. Pap. Mar. Sci.* 44, 44.

Garg, P., and Chandra, P. (1994). The duckweed wolffia globosa as an indicator of heavy metal pollution: Sensitivity to cr and cd. *Environ. Monit. Assess.* 29, 89–95. doi:10.1007/bf00546781

Goeckner, A. H., Lusk, M. G., Reisinger, A. J., Hosen, J. D., and Smoak, J. M. (2022). Florida's urban stormwater ponds are net sources of carbon to the atmosphere despite increased carbon burial over time. *Commun. Earth Environ.* 3 (1), 53. doi:10.1038/s43247-022-00384-y

Gorsky, A. L., Racanelli, G. A., Belvin, A. C., and Chambers, R. M. (2019). Greenhouse gas flux from stormwater ponds in southeastern Virginia (USA). *Anthropocene* 28, 100218. doi:10.1016/j.ancene.2019.100218

Grinham, A., Albert, S., Deering, N., Dunbabin, M., Bastviken, D., Sherman, B., et al. (2018). The importance of small artificial water bodies as sources of methane emissions in Queensland, Australia. *Hydrol. Earth Syst. Sci.* 22 (10), 5281–5298. doi:10.5194/hess-22-5281-2018

Herrero Ortega, S., Romero González-Quijano, C., Casper, P., Singer, G. A., and Gessner, M. O. (2019). Methane emissions from contrasting urban freshwaters: Rates, drivers, and a whole-city footprint. *Glob. Chang. Biol.* 25 (12), 4234–4243. doi:10.1111/gcb.14799

Hill, K. D., Dauphinee, T. M., and Woods, D. J. (1986). The extension of the practical salinity scale 1978 to low salinities. *IEEE J. Ocean. Eng.* 11 (1), 109–112. doi:10.1109/JOE.1986.1145154

Hillman, W. S. (1961). The Lemnaceae, or duckweeds. A review of the descriptive and experimental literature. *Bot. Rev.* 27, 221–287. doi:10.1007/bf02860083

Hilt, S., Grossart, H., McGinnis, D. F., and Keppler, F. (2022). Potential role of submerged macrophytes for oxic methane production in aquatic ecosystems. *Limnol. Oceanogr.* doi:10.1002/lno.12095

Holgerson, M. A. (2015). Drivers of carbon dioxide and methane supersaturation in small , temporary ponds. *Biogeochemistry* 124, 305–318. doi:10.1007/s10533-015-0099-y

Holgerson, M. A., Farr, E. R., and Raymond, P. A. (2017). Gas transfer velocities in small forested ponds. *JGR. Biogeosciences* 122 (5), 1011–1021. doi:10.1002/2016JG003734

Holgerson, M. A., and Raymond, P. A. (2016). Large contribution to inland water CO 2 and CH 4 emissions from very small ponds. *Nat. Geosci.* 9, 222–226. doi:10.1038/NGEO2654

Holgerson, M. A., Richardson, D. C., Roith, J., Bortolotti, L. E., Finlay, K., Hornbach, D. J., et al. (2022). Classifying mixing regimes in ponds and shallow lakes. *Water Resour. Res.* 58 (7). doi:10.1029/2022WR032522

Jähne, B., Münnich, K. O., Bösinger, R., Dutzi, A., Huber, W., and Libner, P. (1987). On the parameters influencing air-water gas exchange. *J. Geophys. Res.* 92, 1937–1949. doi:10.1029/jc092ic02p01937

Jansen, J., Thornton, B. F., Jammet, M. M., Wik, M., Cortés, A., Friborg, T., et al. (2019). Climate-sensitive controls on large spring emissions of CH 4 and CO 2 from northern lakes. *J. Geophys. Res. Biogeosci.* 124, 2379–2399. doi:10.1029/2019jg005094

Johnson, K., Hughes, J., Donaghay, P., and Sieburthm, John. (1990). Bottle-calibration static head space method for the determination of methane dissolved in seawater. *Anal. Chem.* 62, 2408–2412. doi:10.1021/ac00220a030

Kankaala, P., Huotari, J., Tulonen, T., and Ojala, A. (2013). Lake-size dependent physical forcing drives carbon dioxide and methane effluxes from lakes in a boreal landscape. *Limnol. Oceanogr.* 58 (6), 1915–1930. doi:10.4319/lo.2013.58.6.1915

Khan, F. A., and Ansari, A. A. (2005). Eutrophication: An ecological vision. *Botanical Rev.* 71 (4), 449–482. doi:10.1663/0006-8101(2005)071[0449:eaev]2.0.co;2

Kifner, L. H., Calhoun, A. J. K., Norton, S. A., Hoffmann, K. E., and Amirbahman, A. (2018). Methane and carbon dioxide dynamics within four vernal pools in Maine, USA. *Biogeochemistry* 139 (3), 275–291. doi:10.1007/s10533-018-0467-5

Kleinschroth, F., Winton, R. S., Calamita, E., Niggemann, F., Botter, M., Wehrli, B., et al. (2021). Living with floating vegetation invasions. *Ambio* 50 (1), 125–137. doi:10.1007/s13280-020-01360-6

Koschorreck, M., Downing, A. S., Hejzlar, J., Marcé, R., Laas, A., Arndt, W. G., et al. (2020). Hidden treasures: Human-made aquatic ecosystems harbour unexplored opportunities. *Ambio* 49 (2), 531–540. doi:10.1007/s13280-019-01199-6

Lasfar, S., Monette, F., Millette, L., and Azzouz, A. (2007). Intrinsic growth rate: A new approach to evaluate the effects of temperature, photoperiod and phosphorus-nitrogen concentrations on duckweed growth under controlled eutrophication. *Water Res.* 41 (11), 2333–2340. doi:10.1016/j.watres.2007.01.059

Lazar, J. G., Addy, K., Welsh, M. K., Gold, A. J., and Groffman, P. M. (2014). Resurgent beaver ponds in the northeastern United States: Implications for greenhouse gas emissions. *J. Environ. Qual.* 43 (6), 1844–1852. doi:10.2134/jeq2014.02.0065

McAuliffe, C. (1971). Cas chromatographic determination of solutes by multiple phase equilibrium. *Chem. Technol.* 1, 46–51.

McClain, M. E., Boyer, E. W., Dent, C. L., Gergel, S. E., Grimm, N. B., Groffman, P. M., et al. (2003). Biogeochemical hot spots and hot moments at the interface of terrestrial and aquatic ecosystems. *Ecosystems* 6 (4), 301–312. doi:10.1007/s10021-003-0161-9

Mccrackin, M. L., and Elser, J. J. (2010). Atmospheric nitrogen deposition influences denitrification and nitrous oxide production in lakes. *Ecology* 91 (2), 528–539. doi:10.1890/08-2210.1

Mengis, M., Gächter, R., and Wehrli, B. (1997). Sources and sinks of nitrous oxide (N2O) in deep lakes. *Biogeochemistry* 38 (3), 281–301. doi:10.1023/A:1005814020322

Murphy, J., and Riley, J. P. (1962). A modified single solution method for the determination of phosphate in natural waters. *Anal. Chim. Acta* 27, 31–36. doi:10.1016/s0003-2670(00)88444-5

Myhre, G., Shindell, D., Bréon, F.-M., Collins, W., Fuglestvedt, J., Huang, J., et al. (2013). "Anthropogenic and natural radiative forcing," in *Climate change 2013 the physical science basis: Working group I contribution to the fifth assessment report of the intergovernmental panel on climate change*. Editors T. F. Stocker, D. Qin, G.-K. Plattner, M. Tignor, S. K. Allen, J. Boschung, et al. (Cambridge: Cambridge University Press), 659–740. doi:10.1017/CBO9781107415324.018

Nürnberg, G. K. (1995). Quantifying anoxia in lakes. *Limnol. Oceanogr.* 40 (6), 1100–1111. doi:10.4319/lo.1995.40.6.1100

Peacock, M., Audet, J., Bastviken, D., Cook, S., Evans, C. D., Grinham, A., et al. (2021). Small artificial waterbodies are widespread and persistent emitters of methane and carbon dioxide. *Glob. Chang. Biol.* 27 (20), 5109–5123. doi:10.1111/gcb.15762

Peacock, M., Audet, J., Jordan, S., Smeds, J., and Wallin, M. B. (2019). Greenhouse gas emissions from urban ponds are driven by nutrient status and hydrology. *Ecosphere* 10 (3), e02643. doi:10.1002/ecs2.2643

Planet Team (2017). In Planet application program interface: In space for life on earth. Available at https://api.planet.com.

Pokorny, J., and Rejm, E. (1983). Oxygen regime in A fishpond with duckweeds (Lemnaceae) and ceratophyllum. *Aquatic Botany*, 17.

Rabaey, J. S., and Cotner, J. B. (2022). *Greenhouse gas and water chemistry data from ponds in the twin-cities area of Minnesota, 2021 ver 1. Environmental Data Initiative.*

Raymond, P. A., Hartmann, J., Lauerwald, R., Sobek, S., McDonald, C., Hoover, M., et al. (2013). Global carbon dioxide emissions from inland waters. *Nature* 503 (7476), 355–359. doi:10.1038/nature12760

Read, J. S., Hamilton, D. P., Jones, I. D., Muraoka, K., Winslow, L. A., Kroiss, R., et al. (2011). Derivation of lake mixing and stratification indices from high-resolution lake buoy data. *Environ. Model. Softw.* 26 (11), 1325–1336. doi:10.1016/J.ENVSOFT.2011.05.006

Richardson, D. C., Holgerson, M. A., Farragher, M. J., Hoffman, K. K., King, K. B. S., Alfonso, M. B., et al. (2022). A functional definition to distinguish ponds from lakes and wetlands. *Sci. Rep.* 12 (1), 10472. doi:10.1038/s41598-022-14569-0

Riera, J. L., Schindler, J. E., and Kratz, T. K. (1999). Seasonal dynamics of carbon dioxide and methane in two clear-water lakes and two bog lakes in northern Wisconsin, U.S.A. *Can. J. Fish. Aquat. Sci.* 56 (2), 265–274. doi:10.1139/f98-182

Rosentreter, J. A., Borges, A. v., Deemer, B. R., Holgerson, M. A., Liu, S., Song, C., et al. (2021). Half of global methane emissions come from highly variable aquatic ecosystem sources. *Nat. Geosci.* 14, 225–230. doi:10.1038/s41561-021-00715-2

Scheffer, M., Hosper, S. H., Meijer, M.-L., Moss, B., and Jeppesen, E. (1993). Alternative Equilibria in Shallow Lakes. *Reviews* 11 (3), 220–226.

Sieczko, A. K., Thanh Duc, N., Schenk, J., Pajala, G., Rudberg, D., Sawakuchi, H. O., et al. (2020). Diel variability of methane emissions from lakes. *Proc. Natl. Acad. Sci. U. S. A.* 117 (35), 21488–21494. doi:10.1073/pnas.2006024117

Singh, V. P., Dass, P., Kaur, K., Billore, S. K., Gupta, P. K., and Parashar, D. C. (2005). Nitrous oxide fluxes in a tropical shallow urban pond under influencing factors. *Curr. Sci.* 88 (3), 478–483.

Taguchi, V. J., Olsen, T. A., Natarajan, P., Janke, B. D., Gulliver, J. S., Finlay, J. C., et al. (2020). Internal loading in stormwater ponds as a phosphorus source to downstream waters. *Limnol. Oceanogr. Lett.* 5 (4), 322–330. doi:10.1002/lol2.10155

Tippery, N. P., and Les, D. H. (2020). *Tiny plants with enormous potential: Phylogeny and evolution of duckweeds*, 19–38. doi:10.1007/978-3-030-11045-1_2

van Bergen, T. J. H. M., Barros, N., Mendonça, R., Aben, R. C. H., Althuizen, I. H. J., Huszar, V., et al. (2019). Seasonal and diel variation in greenhouse gas emissions from an urban pond and its major drivers. *Limnol. Oceanogr.* 64 (5), 2129–2139. doi:10.1002/lno.11173

Verpoorter, C., Kutser, T., Seekell, D. A., and Tranvik, L. J. (2014). A global inventory of lakes based on high-resolution satellite imagery. *Geophys. Res. Lett.* 41 (18), 6396–6402. doi:10.1002/2014GL060641

Wang, G., Xia, X., Liu, S., Zhang, S., Yan, W., and McDowell, W. H. (2021). Distinctive Patterns and Controls of Nitrous Oxide Concentrations and Fluxes from Urban Inland Waters. *Environ. Sci. Technol.* 55, 8422–8431. doi:10.1021/acs.est.1c00647

Wanninkhof, R. (1992). Relationship between wind speed and gas exchange over the ocean. *J. Geophys. Res.* 97 (C5), 7373–7382. doi:10.1029/92JC00188

Webb, J. R., Hayes, N. M., Simpson, G. L., Leavitt, P. R., Baulch, H. M., and Finlay, K. (2019). Widespread nitrous oxide undersaturation in farm waterbodies creates an unexpected greenhouse gas sink. *Proc. Natl. Acad. Sci. U. S. A.* 116 (20), 9814–9819. doi:10.1073/pnas.1820389116

Weishaar, J. L., Aiken, G. R., Bergamaschi, B. A., Fram, M. S., Fujii, R., and Mopper, K. (2003). Evaluation of specific ultraviolet absorbance as an indicator of the chemical composition and reactivity of dissolved organic carbon. *Environ. Sci. Technol.* 37 (20), 4702–4708. doi:10.1021/es030360x

Weiss, R. F. (1974). Carbon Dioxide in Water and Seawater: The Solubility of a Non-Ideal Gas. *Mar. Chem.* 2, 203–215. doi:10.5194/bg-13-841-2016

Weiss, R. F., and Price, B. A. (1980). Nitrous Oxide Solubility in Water and Seawater. *Mar. Chem.* 8, 347–359.

West, W. E., Coloso, J. J., and Jones, S. E. (2012). Effects of algal and terrestrial carbon on methane production rates and methanogen community structure in a temperate lake sediment. *Freshw. Biol.* 57 (5), 949–955. doi:10.1111/j.1365-2427.2012.02755.x

Wiesenburg, D. A., and Guinasso, N. L. (1979). Equilibrium Solubilities of Methane, Carbon Monoxide, and Hydrogen in Water and Sea Water. *J. Chem. Eng. Data* 24 (4), 356–360. doi:10.1021/je60083a006

Wilkinson, J., Bors, C., Burgis, F., Lorke, A., and Bodmer, P. (2019). Measuring CO2 and CH4 with a portable gas analyzer: Closed-loop operation, optimization and assessment. *PLoS ONE* 13 (4), e0193973. doi:10.1371/journal.pone.0193973

Xiao, S., Wang, C., Wilkinson, R. J., Liu, D., Zhang, C., Xu, W., et al. (2016). Theoretical model for diffusive greenhouse gas fluxes estimation across water-air interfaces measured with the static floating chamber method. *Atmos. Environ.* 137, 45–52. doi:10.1016/j.atmosenv.2016.04.036

Xiao, S., Yang, H., Liu, D., Zhang, C., Lei, D., Wang, Y., et al. (2014). Gas transfer velocities of methane and carbon dioxide in a subtropical shallow pond. *Tellus B Chem. Phys. Meteorology* 66 (1), 23795. doi:10.3402/tellusb.v66.23795

Zhou, Y., Zhou, L., Zhang, Y., Garcia de Souza, J., Podgorski, D. C., Spencer, R. G. M., et al. (2019). Autochthonous dissolved organic matter potentially fuels methane ebullition from experimental lakes. *Water Res.* 166, 115048. doi:10.1016/j.watres.2019.115048

Zuur, A. F., Ieno, E. N., Walker, N. J., Saveliev, A. A., and Smith, G. M. (2009). *Mixed effects modelsand extensions in ecologywith R*. Springer.

frontiers | Frontiers in Environmental Science

TYPE Original Research
PUBLISHED 19 October 2022
DOI 10.3389/fenvs.2022.884133

Check for updates

OPEN ACCESS

EDITED BY
Yves T Prairie,
Université du Québec à Montréal, Canada

REVIEWED BY
Danny Ionescu,
Leibniz-Institute of Freshwater Ecology and Inland Fisheries (IGB), Germany
Yongcui Deng,
Nanjing Normal University, China

*CORRESPONDENCE
Sarah B. Cadieux,
cadies@rpi.edu

SPECIALTY SECTION
This article was submitted to Biogeochemical Dynamics, a section of the journal Frontiers in Environmental Science

RECEIVED 25 February 2022
ACCEPTED 06 September 2022
PUBLISHED 19 October 2022

CITATION
Cadieux SB, Schütte UME, Hemmerich C, Powers S and White JR (2022), Exploring methane cycling in an arctic lake in Kangerlussuaq Greenland using stable isotopes and 16S rRNA gene sequencing.
Front. Environ. Sci. 10:884133.
doi: 10.3389/fenvs.2022.884133

COPYRIGHT
© 2022 Cadieux, Schütte, Hemmerich, Powers and White. This is an open-access article distributed under the terms of the Creative Commons Attribution License (CC BY). The use, distribution or reproduction in other forums is permitted, provided the original author(s) and the copyright owner(s) are credited and that the original publication in this journal is cited, in accordance with accepted academic practice. No use, distribution or reproduction is permitted which does not comply with these terms.

Exploring methane cycling in an arctic lake in Kangerlussuaq Greenland using stable isotopes and 16S rRNA gene sequencing

Sarah B. Cadieux[1,2]*, Ursel M. E. Schütte[3], Chris Hemmerich[4], Sarah Powers[5] and Jeffrey R. White[2,5]

[1]Earth and Environmental Sciences, Rensselaer Polytechnic Institute, Troy, NY, United States, [2]Earth and Atmospheric Sciences, Indiana University, Bloomington, IN, United States, [3]Institute for Arctic Biology, University of Alaska Fairbanks, Fairbanks, AK, United States, [4]Center for Genomics and Bioinformatics, Indiana University, Bloomington, IN, United States, [5]O'Neill School of Public and Environmental Affairs, Indiana University, Bloomington, IN, United States

Lakes are currently responsible for a significant amount of total natural methane emission. Microbial oxidation of methane plays a central role in Arctic carbon cycling, potentially reducing methane emissions from lakes, though little is known about methane cycling in the water column of Arctic lakes. We previously detected surprisingly large enrichments of heavy carbon and hydrogen isotopes of methane in three small lakes in Greenland suggesting unusually efficient methanotrophic communities in these Arctic lakes. Using stable isotope and 16S rRNA gene sequencing we determined carbon and hydrogen isotopes and microbial community composition down the water column of Teardrop lake, under open-water conditions. We found that isotopic values of methane in Teardrop lake were again highly enriched ^{13}C and ^{2}H at 4 m depth with –13.2‰ and –27.1‰ values for carbon and hydrogen isotopes, respectively. Methane concentrations slightly increased at the depth interval with isotope enrichment, not typical of classic methanotrophy. Consistent with isotopic enrichment of the heavy isotopes we detected the highest relative abundance of putative methanotrophs, in particular *Methylovulum* at 4 m. The highest relative abundance of putative methanogens was detected at 3 m as well as at 5 m. At the same depth interval, temperature and oxidation reduction potential also increase, supporting increased microbial activity within the water column. Based on geochemical and microbial observations, we suggest that the methane cycling in Teardrop lake is decoupled from a traditional depth dependent model where the dominant source of methane is in the anoxic sediments. Instead, methane in the water column is likely from a combination of anoxic sediment, littoral transport and oxic methanogenesis in the mid-water column, and recycling of carbon within the water column is leading to extreme isotope enrichments. Thus, understanding linkages between depth-dependent microbial dynamics and methane biogeochemistry are necessary to constrain the sensitivity of the methane cycle to future climate change.

KEYWORDS

methane oxidation, methanotrophs, isotopes, lake, arctic, methane cycling

1 Introduction

Lakes are currently responsible for 6%–16% of total natural emissions of methane (Bastviken et al., 2004; Rosentreter et al., 2021), an important greenhouse gas, with about 25% greater radiative forcing than CO_2 on a per molecule basis over a period of 100 years (Whalen, 2005; Etminan et al., 2016). As the climate continues to warm, methane production and emissions from freshwater environments are expected to increase (Tan and Zhuang, 2015). In the Arctic, small lakes (< 10 km^2) represent approximately half of the total area of surface water environments (Abnizova et al., 2012) and emit more methane per unit area than larger lakes (Downing, 2010). Microbial production of methane by methanogens is dependent upon anoxia, temperature and the amount and quality of organic substrates (Liikanen et al., 2003; Kankaala et al., 2006; Duc et al., 2010; Borrel et al., 2011). Microbial oxidation of methane plays a central role in carbon cycling, potentially reducing emissions of methane from lakes where warming climate has increased biogenic methane production. In northern lakes, up to 88% of the methane produced is oxidized by methanotrophs (Lopez Bellido et al., 2009), lowering concentrations of methane in surface waters, and thereby attenuating the positive feedback potential from biogenic methane.

In lakes, methane is primarily produced in anoxic sediments by methanogenic archaea. A depth-dependent model for methane cycling assumes methane is predominantly produced within anoxic sediments and is exported into the water column by ebullition or diffusion. However, recent studies suggest that methane is also produced in oxic conditions leading to an oversaturation in oxic waters (Keppler et al., 2006; Tang et al., 2016; Günthel et al., 2019; Bizic et al., 2020). For example, in Lake Cromwell, oxic methane production accounted for 20% of methane emissions (Bogard et al., 2014). Additionally, methane has the potential to be introduced into the lake water column by lateral transport from peripheral water bodies, littoral sediments and *in situ* biological production in addition to profundal sediments (Günthel et al., 2019). Therefore, it is possible then to have cyclic production and consumption of methane happening simultaneously within the water column.

The fraction of in-lake methane production that is oxidized before emission varies greatly from negligible to nearly complete. Methane oxidation rates in aquatic systems are likely dependent on a suite of environmental variables, including methane concentration, dissolved O_2 concentration, water temperature and light. Incubation experiments suggest that methane concentration is often a major factor affecting methane oxidation rate (Loften et al., 2014; Shelley et al., 2014). However, methanotrophs can also adapt to low methane concentrations (Mau et al., 2013). In many lakes, the highest methanotrophic activity is associated with depths where dissolved O_2 concentrations are very low, suggesting partial inhibition of methanotrophic activity at high O_2 concentrations (Kankaala et al., 2013; Blees et al., 2014; Martinez-Cruz et al., 2015). Several studies have shown no effect of temperature on methane oxidation rate; however, others suggest that methane oxidation is temperature dependent (Duc et al., 2010; Shelley et al., 2014). Additionally, light has been suggested to inhibit methane oxidation in the euphotic zone (Murase and Sugimoto, 2005), potentially leading to increased methane emissions. Recent studies found a decline of methane emissions with increasing dissolved organic carbon concentration and lake color, potentially the result of increased methanotrophic activity under low light (Rasilo et al., 2015). However, in shallow lakes with light penetration below the oxycline, increased methane oxidation can occur due to coupling with *in situ* production of oxygen by photosynthesis, known as cryptic photosynthetic oxygen production (Milucka et al., 2015; Oswald et al., 2015, 2016; Brand et al., 2016). The localized photosynthetic oxygen production might in turn support methanotrophy that suppresses methane emissions.

In freshwater environments, methane oxidation is carried out by type I and type II methanotrophs, primarily by aerobic methane oxidizing bacteria, such as *Methylobacter*, *Methylosoma*, *Methylovulum*, *Methylosoma*, *Methylosarcina* and *Methylomicrobium* (He et al., 2012; Oswald et al., 2017). Methanotrophs have been observed throughout the water column and sediments and their abundance is influenced by methane concentration, temperature, depth, dissolved oxygen, dissolved phosphate concentration and season. Abundance of methanotrophs generally increases with depth and relative abundance is higher in the winter compared to the summer (Samad and Bertilsson, 2017). While microbial communities in aquatic polar environments are receiving increased interest (Comeau et al., 2012; Stoeva et al., 2014; Vick-Majors et al., 2014; Osudar et al., 2016; Ruuskaanen et al., 2018; Bomberg et al., 2019; Butler et al., 2019; Vigneron et al., 2019; Møller et al., 2020; Somers et al., 2020; Emerson et al., 2021), most studies focusing on the role of microbial communities in methane cycling are based on lake sediments (He et al., 2012, 2022; Martinez-Cruz et al., 2017; Colby et al., 2020; Møller et al., 2020; Zandt et al., 2020). For example, carbon acquisition in lake sediments is driven predominantly by *Methylobacter*, *Methylosoma*, *Methylosoma* (He et al., 2012), and *Methylobacter* has been shown to acquire carbon in anaerobic sediments (Martinez-Cruz et al., 2017). Microbial methane cycling in the water column is less well understood.

Isotopic signatures of methane are useful indicators of microbial methane processes, including microbial methane oxidation. During anoxic biogenic methanogenesis a kinetic isotope effect yields methane that is depleted in ^{13}C and ^{2}H relative to precursor substrates (Whiticar et al., 1986; Balabane

et al., 1987; Valentine et al., 2004). However, oxic methane production, such as methyl-phosphonate demethylation, has been shown to have minimal fractionation (Taenzer et al., 2020), whereas isotopic fractionation from other oxic methane production pathways have not been reported (Bizic et al., 2020; Wang et al., 2021). Methanotrophy exhibits a kinetic isotope effect that leaves the residual methane pool isotopically enriched in ^{13}C and ^{2}H (Coleman et al., 1981; Happell et al., 1994; Templeton et al., 2006; Kinnaman et al., 2007). The isotope discrimination during oxidation can yield residual methane pools that are enriched by < 1‰–30‰ for $\delta^{13}C_{CH4}$ and 3‰–200‰ for $\delta^{2}H_{CH4}$ (Coleman et al., 1981; Happela et al., 1994; Bastviken et al., 2002).

Isotopic measurements of C and H of dissolved methane in small Greenlandic lakes under both ice-free and ice-covered conditions from 2013–2014 revealed surprisingly large ranges for both $\delta^{13}C$ and $\delta^{2}H$. Under open-water conditions, $\delta^{13}C$ ranged from −68.7‰ to +7.4‰ and $\delta^{2}H$ from −370‰ to +250‰, while under ice covered conditions, $\delta^{13}C$ ranged from −72.2‰ to −33.2‰ and $\delta^{2}H$ from -388‰ to -29‰. The most enriched ^{13}C and ^{2}H isotopic values were observed in a single lake, Teardrop lake, under open-water conditions, coinciding with a metalimnetic oxygen minimum at 4 m depth in summer 2013. The enrichment in ^{13}C and ^{2}H was associated with low methane concentrations, as is characteristic with consumption of methane by microbial oxidation of methane (Coleman et al., 1981; Happell et al., 1994; Templeton et al., 2006; Kinnaman et al., 2007). Isotope excursions have been demonstrated in other Arctic lakes at mid-water column depths, with carbon isotope values as high as +1.4‰ reported in shallow Canadian lakes (Thottathil et al., 2018, 2019). Similarly, in these lakes, the most enriched carbon isotope values of methane were associated with low methane concentrations near the oxycline, supporting the potential of highly efficient methanotrophic communities at intermediate water depth.

In order to study water column methane oxidation in greater detail, we returned to Teardrop lake in summer 2015 and expanded the scope of the investigation to include more detailed water column chemistry, stable isotopic signatures of dissolved methane, and a characterization of the microbial communities with depth. We have had success in identifying spatial agreement between methane, sulfur and nitrogen gradients and changes in the microbial community using amplicon-based sequencing targeting the 16S rRNA genes and aqueous geochemistry in these lakes (Schütte et al., 2016). Our objectives were to answer the following questions: 1) is extreme isotopic enrichment ^{13}C and ^{2}H of dissolved methane observed in subsequent years, or was the phenomenon in 2013 a unique occurrence? And 2) if enrichment in ^{13}C and ^{2}H is observed, what microbial communities are present? Could microbial community composition explain the isotope enrichment in ^{13}C and ^{2}H of dissolved methane? Climate change has the potential to increase methane emissions from freshwater systems, which would in turn induce further climate change, resulting in a positive climate feedback. Understanding linkages between microbial communities and methane biogeochemistry are necessary to constrain the sensitivity of the methane cycle to future climate predictions.

2 Materials and methods

2.1 Site description

The ice-free margin of southwest Greenland is characterized by a low continental climate and is strongly influenced by the high-pressure system over the Greenland Ice Sheet (Bennike, 2000). In Kangerlussuaq, the average annual temperature is −5°C from 2008 to present, the maximum temperature measured was 15.4°C in June of 2018, and the minimum temperature measured was −44.9°C in February of 2015. The average rainfall is 243 mm. Teardrop lake (informal name) is located ~5 km from the terminal moraine of the Russell Glacier (Figure 1). It is a relatively small lake, with a surface area of 0.97 ha, volume of 34,000 m^3 and maximum depth of 5.25 m. Teardrop is a moderately brackish, mesotrophic lake, with mean conductivity of 2,740 µS $cm^{-1}$and mean dissolved organic carbon of 97.6 mg L^{-1} (Cadieux et al., 2016). Under open-water conditions in 2013, the pH was alkaline and buffered, ranging from 8.98 to 9.3. Currently, Teardrop lake is a hydrologically closed basin, with no direct inflow or outflow channel. Due to continuous permafrost, groundwater seepage is assumed to be limited. While many lakes in the Kangerlussuaq region are cold monomictic (Anderson et al., 2001), Teardrop lake is a dimictic lake, exhibiting ice cover from late October to early June (Cadieux et al., 2016).

2.2 Sampling and in situ analysis

Water samples and measurements were taken at two depth profiles located in the deepest basin of Teardrop lake (Figure 1C) in August of 2015. Profiles were similar between the two locations, noted East and West (Supplementary Figures S1,S2). Herein, we will present findings from the East sampling station located in the center of the basin at the maximum depth point. Dissolved oxygen (D. O., mg L^{-1}), pH, specific conductivity (µS cm^{-1}) and oxidation reduction potential (ORP, mV) were measured using a YSI 6039 Data Sonde (Yellow Springs Inc., Yellow Springs, OH, United States) deployed at 0.5 m depth intervals down to maximum depth. Photosynthetically active radiation

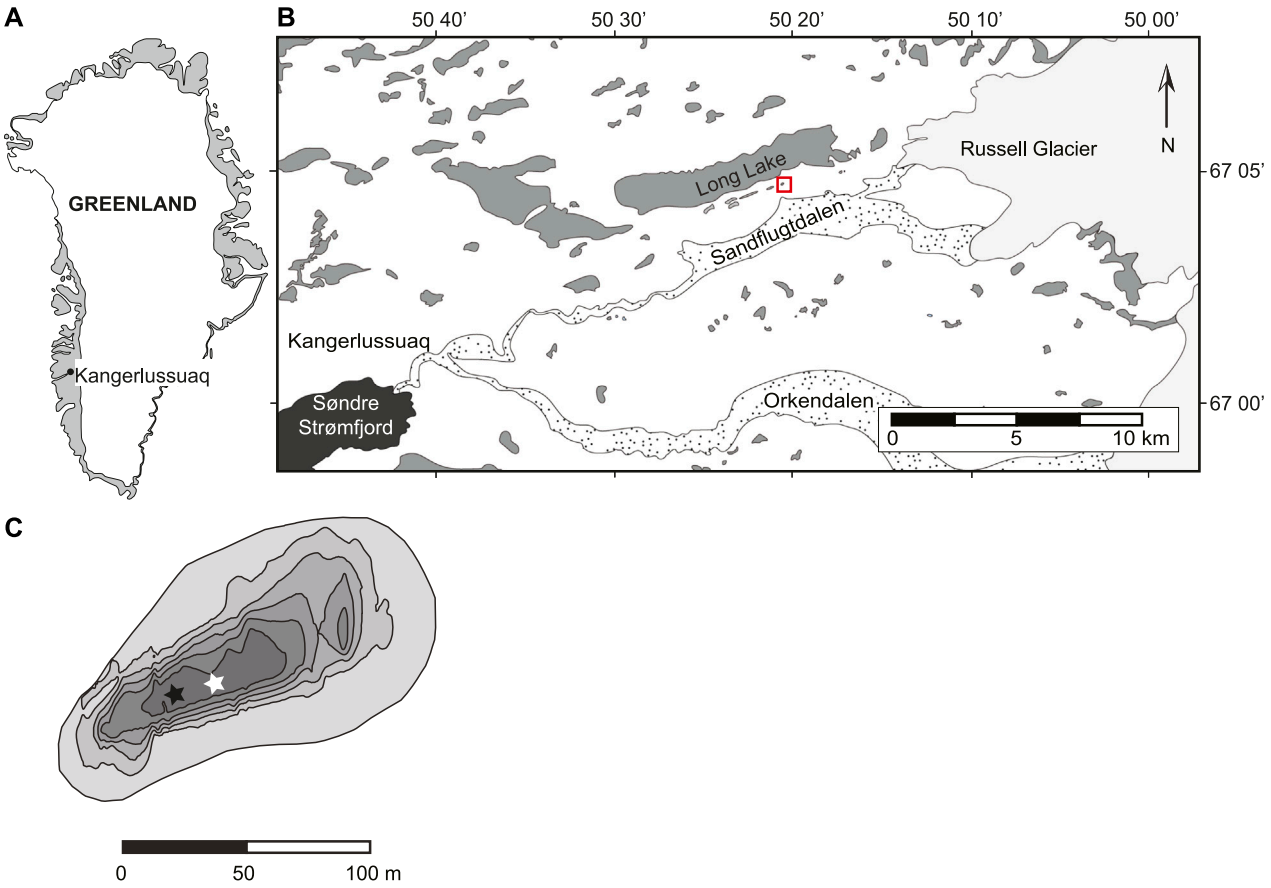


FIGURE 1
Figure 1: Maps of **(A)** Greenland showing Kangerlussuaq; **(B)** zoom in of Kangerlussuaq region. Red box highlights Teardrop lake; **(C)** Teardrop lake bathymetry (contour interval = 1 m) showing sample locations. White star shows East sampling location (discussed in paper); black star shows West sampling location. Modifed from Cadieux et al., 2016.

(PAR) was measured using a Li-Cor LI193 Spherical Quantum Sensor. Water samples were taken with a submersible pump at 0.5 m–1 m intervals throughout the water column at each location, with the exception for methane, where only one sample was obtained from the well-mixed epilimnion and the remainder of the water column was sampled at 0.5 m intervals.

For methane, 1 L of water at each interval was immediately stripped in the field using a headspace-equilibrium technique to extract methane gas from water (Westendorp, 1985). Headspace gas was displaced into a Cali-5-Bond bag using surficial water (Cadieux et al., 2016, 2017). For chlorophyll, 250 ml of water was filtered onto a 0.7 nm glass filter, and the filter was transferred to an amber bottle and remained frozen until analysis. Additionally, 1 L of water was collected into sterile HDPE Nalgene bottles and filtered through 0.22 µm Isopore Membrane Filters (Millipore SiGMa, Burlington, MA) for microbial analysis. Filters were frozen until analysis.

2.3 Chemical analysis

Chlorophyll-a concentrations were determined using acetone pigment extraction in aqueous acetone solution and spectrophotometric determination of chlorophyll a with pheophytin correction at Indiana University (APHA, 2012). Concentrations of dissolved aqueous methane were measured on a Gas Chromatography Flame Ionization Detector (GC-FID) at Indiana University. Stable C and H isotopes of methane were analyzed using continuous-flow gas chromatography-oxidation/pyrolysis isotope ratio mass spectrometry (GC-ox/pyr-IRMS) with a laboratory-built gas pre-concentrator interfaced with a ThermoFinnigan GCC and Delta Plus XP IRMS at the Stable Isotope Research Facility (SIRF) at Indiana University in Bloomington Indiana (Cadieux et al., 2016). Carbon isotope values are referenced to Vienna Pee Dee Belemnite standard (VPDB) and hydrogen isotope values are referenced to Vienna Standard Mean Ocean

Water (VSMOW) by comparison with pure methane where the isotopic composition has been measured by off-line combustion. Instrument uncertainty of $\delta^{13}C$ and $\delta^{2}H$ from the GC-C-IRMS was calculated as 0.4‰ and 10‰ respectively, which is one standard deviation for repeated measurements of the gas standards analyzed during sample runs.

2.4 Microbial community composition

Genomic DNA was extracted using the PowerWater DNA isolation kit (MOBIO laboratories, Carlsbard, CA). Amplification of the 16S rRNA genes was performed using the forward primer 515f and a barcoded reverse primer 806r (Caporaso et al., 2012, http://www.earthmicrobiome.org). Each reaction was 25 µl in volume with 5 µl 5′ HF Buffer (New England BioLabs), 1.5 µl of 50 mM $MgCl_2$, 0.5 ml 10 mM dNTPs, 0.5 µl of each 10 mM primer (Integrated DNA Technologies, Coraville, IA) 0.25 µl of 2,000 U/ml Phusion DNA Polymerase (New England Biolabs), 10 ng–20 ng of DNA, and 15.75 µl PCR water. Amplification was performed using an initial incubation step at 94°C for 3 min followed by 35 cycles of 94°C for 45 s, 50°C for 1 min, 72°C for 1.5 min and a final extension step at 72°C for 10 min. PCR amplicons were cleaned using the PCR purification kit (QIAgen, Valencia, CA). Amplicons were pooled in an equimolar mixture and the pool was cleaned an additional time using the Agencourt AMPure XP (Beckman Coulter, Brea, CA). Sequences were generated on the MiSeq Illumina platform using MiSeq Reagent Kit v2 (300 cycles, PE 300 bp, Illumina Inc., San Diego, CA) and custom-made sequencing primers (http://www.earthmicrobiome.org).

After quality control amplicon sequence variants (ASVs) were generated using the DADA2 (Callahan et al., 2016) subcommand from within QIIME2 (Bolyen et al., 2019) release 2018.2 with the parameters "--p-trunc-len-f 200--p-trunc-len-r 95". A portion of the Mothur MiSeq SOP (Kozich et al., 2013) was then followed to align reads to the RDP training set v.9 and remove reads identified as anything other than bacteria or archaea. Remaining reads were imported back into QIIME2 and chimeras were removed using the "vsearch uchime-denovo" subcommand. ASVs were classified using the "classify-sklearn" command in QIIME2 against release 138 of the Silva SSU database (Quast et al., 2013) and a rooted tree was generated using the phylogeny subpackage with default parameters. Shannon entropy and Faith pd diversity measures were generated within QIIME 2. We used these sequence data to assess changes in microbial community composition based on differences in relative abundances with depth in Teardrop lake. Recent studies have pointed out that using differences in relative abundances without determining changes in total abundance through e.g., qPCR can be misleading when inferring changes in microbial community composition in the environment (Aitchison 1982; Gloor et al., 2017; Knight et al., 2018; Morton et al., 2019). An increase in the relative abundance of e.g., methanotrophs can be associated with low absolute numbers of methanotrophs at a particular location suggesting that the relevance of this function may still be limited. Furthermore, changes in the relative abundance of one taxa results in compensatory changes in at least one other taxa as the relative abundances of the microbial taxa are not independent from one another (Aitchison 1982; Gloor et al., 2017). Many different underlying scenarios for changes in the microbial community lead to the same relative abundances of taxa (Morton et al., 2019). However, in this study we assessed the changes in microbial community composition in combination with changes in multiple geochemical parameters. This approach has allowed us to investigate linkages between inferred microbial functional groups and corresponding geochemical processes.

Phytoplankton samples were concentrated *via* sedimentation and settling using an Utermoehl settling chamber. Taxa present were identified, and plankton enumeration was done using a nanoplankton counting chamber at 200x magnification ensuring a minimum of 200 organisms were counted for each sample depth. Colony forming phytoplankton were enumerated and individual cells were counted from a minimum of 10 organisms to generate an average cell count. This multiplication factor was used to generate cells per milliliter (APHA, 2012).

3 Results

At the time of sampling in August 2015, the temperature in the lake ranged from 14.1°C at the surface to 10.2°C at the bottom, with a slight increase of 0.6°C from 3.5 m–4.0 m depth (Figure 2A). The lake was well-mixed from surface to 3.5 m depth, with uniform pH, specific conductivity, D. O and ORP. At 3.5 m depth, pH decreased from 9.3 to 8.7 and D.O. decreased from 12.6 mg L^{-1} to 0.6 mg L^{-1} (115%–5.3%). Specific conductivity increased with depth from 1,545 µS cm^{-1} to 2,318 µS cm^{-1}. ORP also increased from 121.1 mV to 136.2 mV at 4.5 m, but decreased to 120.7 mV at the sediment water interface (Figure 2B). Light penetrated through the entire water column, with 1.3% of PAR surface irradiance remaining at the sediment water interface (Figure 3C). Chlorophyll concentrations were highest at the sediment water interface, and varied throughout the water column, ranging from 0.74 µg/L to 3.9 µg/L.

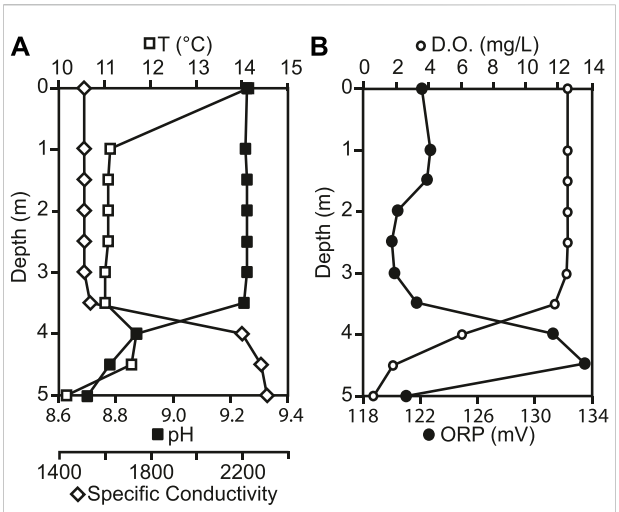


FIGURE 2
(A) Changes in temperature (T), pH, specific conductivity, **(B)** dissolved oxygen (D. O.), and Redox Potential (ORP) down the water column.

The overall microbial community composition changed throughout the water column with two distinct changes, one at 3 m and one below 4.5 m (Figure 4). Both Shannon diversity and Faith pd indicated highest diversity of the microbial community at 5 m; microbial diversity and community composition were similar at the West and East depth profiles (Supplementary Figures S3-S5). These shifts in community composition are consistent with changes in ORP and dissolved oxygen (Figure 2B). The community composition in the upper water column showed higher relative abundances of *Luteolibacter*, *Polynucleobacter*, *Burkholderiaceae*, *Candidatus Limnoluna*, and *hgcl* clade (family *Sporichthyaceae*) among others (Figure 4). At 3 m *GKS98* freshwater group, family *Alcaligenaceae* increased in relative abundance and taxa such as *NS11-12* marine group (order *Sphingobacteriales*), *Pseudarcicella*, *Flavobacterium*, and *Algoriphagus* decreased in relative abundance. Below 3 m besides an increase in the relative abundance of *Pedobacter* and a decrease in the relative abundance of *Polynucleobacter* the community composition was surprisingly similar to the composition in the upper water column. The most distinct change in microbial community composition occurred below 4.5 m with a sharp decrease in the number of taxa with a relative abundance of over 1% and a decrease in the relative abundance of *Luteolibacter*, *Pedobacter*, *NS11-12* marine group, *Pseudarcicella*, and *Sporichthyaceae*. In contrast the relative abundance of *Hgcl* clade increased. The phytoplankton population was dominated by Cyanobacteria, in particular *Aphanocapsa*, with concentrations increasing from 1.4×10^4 cells/ml at 3.5 m to 2.9×10^4 cells/ml at 5.0 m (Figure 3A,B). Other cyanobacteria exhibited lower concentrations ranging from 50 cells/ml to just below 250 cells/ml. The most abundant other cyanobacteria included *Dolichospermum*, *Aphanizomenon*, and *Chroococcus* at the surface, with *Chroococcus* being the most abundant throughout the water column. The second most abundant group of phytoplankton was *Chlorophyta* with *Oocystis* the most abundant at the surface. *Sphaerocystis* showed an increase in abundance at 3 m and the *Micratinium* increased from 2 m–4 m.

Methane concentrations were greatest at the sediment-water interface (27.2 µM) and decreased up the water column to 4.0 µM (Figure 5C). A slight increase in concentration occurred from 4.5 m to 3.5 m. Corresponding with the increase in methane concentration at 4.0 m is an isotope enrichment for both $\delta^{13}C$ (−13.2‰) and $\delta^{2}H$ (−101‰). Carbon and hydrogen isotope values of methane are statistically significantly related throughout the water column (Figure 5C). The putative methanotrophs we detected included *Methylovulum*, *Methylobacter*, *Crenothrix*, and *Methylomonaceae* (Figure 5A; Supplementary Figure S6). Consistent with an increased isotope enrichment of $\delta^{13}C$ at 4 m we detected the highest relative abundance of putative methanotrophs (0.038). The combined geochemical evidence of isotope enrichment and redox change supports the increase in the relative abundances of putative methanotrophs and methanotrophy. This lessens the concern of solely using relative abundances to assess changes in microbial community composition (Aitchison 1982; Gloor et al., 2017; Knight et al., 2018; Morton et al., 2019). Differences in methanotrophs with depth was in particular due to changes in the relative abundance of *Methylovulum*, making up 90% of all the putative methanotrophs detected at 4 m. Below 4 m the overall relative abundance of putative methanotrophs decreased to below 1%, but the relative abundance of *Methylobacter* and *Crenothrix* increased. The overall relative abundance of putative methanogens ranged from 0.07%–0.22% across the water column (Figure 5B, Supplementary Figure S7). *Methanobacterium*, *Methanosaeta*, and *Methanoregula* made up among others the community of putative methanogens throughout the water column. Surprisingly, the highest relative abundance of putative methanogens was detected at 3 m and also at 5 m with *Methanobacterium* making up most of the relative abundance of putative methanogens at 3 m and *Methanobacterium*, *Methanosaeta*, *Methanospirillum*, *Methanoregula*, and Methanolinea being the putative methanogens with the highest relative abundance.

Nitrite is the most abundant nitrogen species throughout the water column, with median concentration 295.5 µM, 20 times greater than nitrate concentrations (median

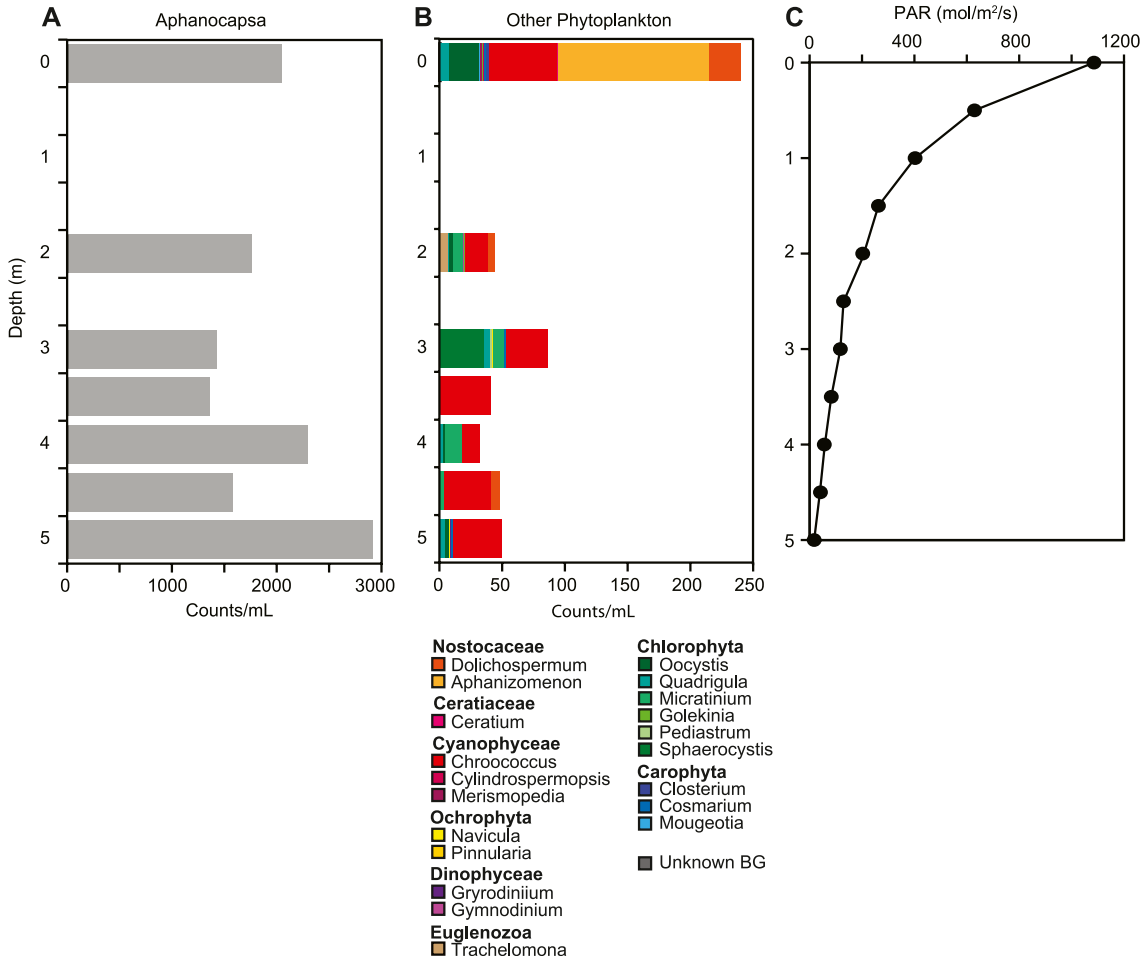


FIGURE 3
Changes in phytoplankton **(A,B)** and **(C)** photosynthetically active radiation (PAR) down the water column. Aphanocapsa was the most dominant phytoplankton. Phytoplankton were determined by visual analysis and counting.

14.5 µM, Figure 6D). Nitrogen concentrations were overall uniform throughout the water column, with a slight increase in nitrite from 3.5 m to 4.0 m depth, and slight decrease in both nitrate and ammonia from 3.5 m to 4.0 m depth. Putative denitrifiers overall had the highest relative abundances (0.4–0.5, Figure 6B) followed by putative dissimilatory nitrate reducers ranging in relative abundance between < 0.001 and 0.009 at 5 m (Figure 6C, Supplementary Figure S9) and putative ammonia oxidizers ranging from < 0.001 to 0.001 (Figure 6A, Supplementary Figure S10). Consistent with the uniform concentrations of nitrate throughout the water column, the relative abundances of putative denitrifiers did not change with depth (Figure 6B, Supplementary Figure S9). In contrast, putative ammonia oxidizers showed the highest relative abundances at 3.5 m and 4.5 m (Figure 6A). The decrease in the relative abundances of putative ammonia oxidizers and dissimilatory nitrate reducers (DNRA) at 4.0 m corresponds to the shift in nitrogen concentration at that depth (Figure 6C, Supplementary Figure S11). The geochemical evidence supports changes in microbial functional groups involved in nitrogen cycling throughout the water column in Teardrop lake. This lessens the concern of solely using relative abundances to assess changes in the microbial community composition (Aitchison 1982; Gloor et al., 2017; Knight et al., 2018; Morton et al., 2019). We did detect very low relative abundances of *Candidatus Anammoximicrobium* up to 3.5 m and again at 5.0 m indicating that the potential for anaerobic ammonia oxidation exists in Teardrop lake.

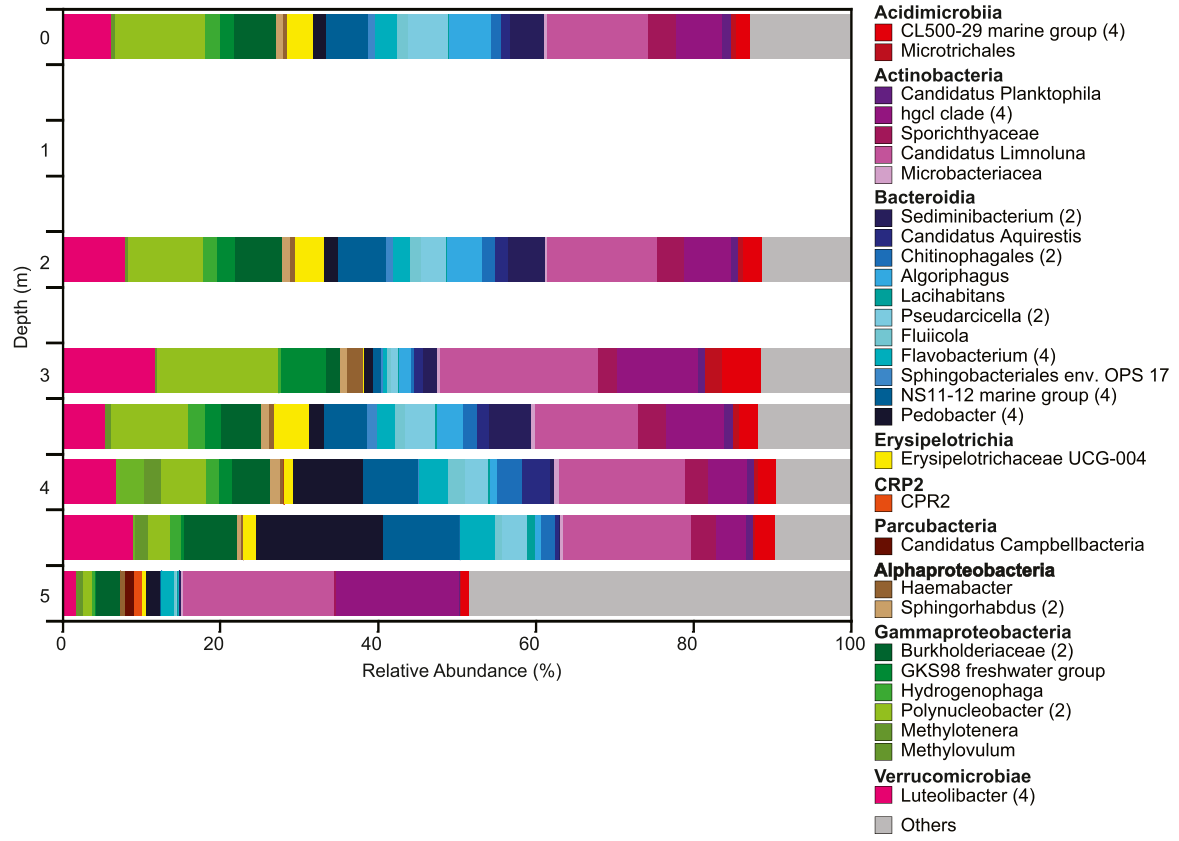


FIGURE 4
Depth profile of microbial community composition down the water column based on changes in the relative abundances of 16S rRNA gene sequences. All ASVs with a relative abundance > 1% are shown. ASVs with identical identification were combined into the same taxonomic group. ASVs with a relative abundance < 1% are combined in the category 'others'. The number of ASVs included in each taxonomic group is included with the number given after the taxonomic name. If no number is given, the group only contains one ASV.

4 Discussion

4.1 Geochemical, isotopic and genomic evidence of traditional methane cycling

The traditional conceptual model of methane cycling in northern lakes involves methane production in anoxic sediments that is transported vertically up the water column by ebullition and diffusion, with oxidative removal along the transport path that generates a concentration profile of dissolved methane that decreases up the water column (Wik et al., 2016; Thottathil and Prairie, 2021). Our results for dissolved methane in Teardrop lake exhibited this general pattern - methane concentrations decreased from a maximum just above the sediment/water interface to a minimum in the upper water column. Oxidative removal of methane along the path was also likely. Dissolved oxygen was clinograde, reaching hypoxic conditions at the sediment-water interface. Oxidation of methane by aerobic methanotrophic bacteria was likely occurring throughout the water column as evidenced by the inverse relationship between dissolved oxygen and dissolved methane concentrations throughout, the change in methane isotopic signature, and the presence of methanotrophs throughout the water column (Figure 5). Dissolved oxygen concentrations were sufficient to support methanotrophy throughout the water column which is consistent with an increase in relative abundance of putative methanotrophs we observed below 3.5 m (Figure 5). Additionally, a strong positive correlation was observed between $\delta^{13}C$ and $\delta^{2}H$ of dissolved methane (n = 12, R = 0.93, p < 0.001; Supplementary Figure S12), characteristic of residual methane following aerobic methanotrophic activity (Whiticar and Faber, 1985; Happell et al., 1994; Whiticar, 1999; Bastviken et al., 2002; Alstad and Whiticar, 2011; Wik et al., 2020). The average slope of enrichment of ^{13}C and ^{2}H of dissolved methane, calculated

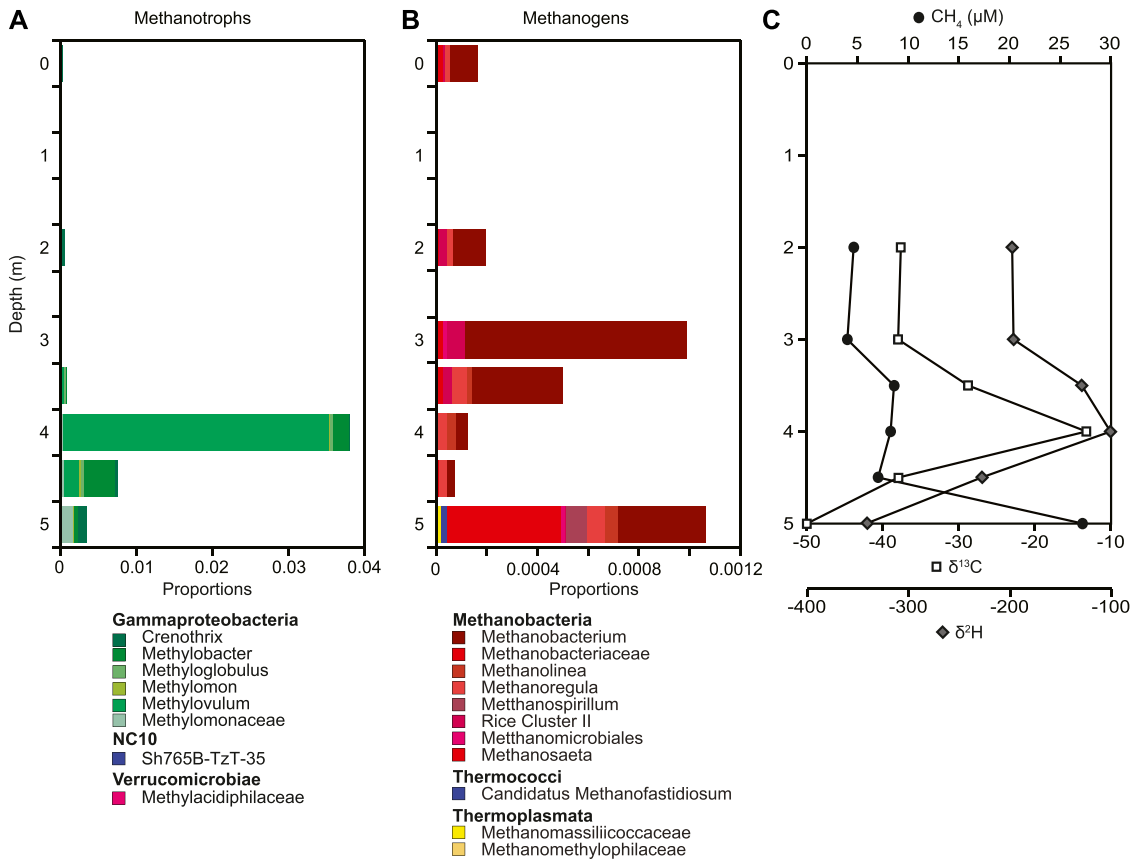


FIGURE 5
Depth profiles of **(A)** putative methanogen relative abundances, **(B)** putative methanotroph relative abundances based on 16S rRNA gene sequences, as well as **(C)** concentration and stable C and H isotope composition of dissolved methane down the water column. The number of ASVs included in each taxonomic group is included with the number given after the taxonomic name. If no number is given, the group only contains one ASV.

as $\delta^2H/\delta^{13}C$ (5.2) is similar to the slope of projected oxidation predicted by previous experimental studies, which range from 5.9 to 13 (Coleman and Risatti, 1981; Whiticar, 1999; Kinnaman et al., 2007). These results are consistent with previous findings from Teardrop lake, other Greenlandic lakes in this area (Cadieux et al., 2016), and other Arctic freshwater environments (Wik et al., 2020).

Putative methanotrophic communities were present throughout the water column of Teardrop lake and were similar to other lacustrine systems. Gammaproteobacteria, the dominant putative methanotrophs observed here, were also the most abundant taxa in high oxidation zones in several other lacustrine systems (Carini et al., 2005; Blees et al., 2014; Oswald et al., 2015, 2016; Zigah et al., 2015). In neighboring Potentilla lake, where microbial communities were collected under ice in late winter, we detected high relative abundances of *Gammaproteobacteria* known to be type I methanotrophs, including *Crenothrix* and *Methylobacter*, which dominated between 4 m and 5 m depth (Schütte et al., 2016). In Teardrop lake, *Methylovulum* was the dominant type I methanotroph, and exhibited the highest relative abundance at 4 m. *Beijerinckiaceae* (*Alphaproteobacteria*) including *Methylobacterium* were present in low relative abundance in Teardrop lake. However, Tamas et al. (2014) reported that members of *Beijerinckiaceae* lost their capabilities of methanotrophy and are not methanotrophs. Others report that *Methylobacterium* is methylotrophic and not methanotrophic (Dedysh et al., 2004; Theisen and Murrell, 2005). Most other studies of Arctic lakes described methanotroph community composition mainly in lake sediments rather than from the water column (He et al., 2012, 2022). Consistent with our results, He et al. (2012) found the methanotrophic community in an Arctic lake in Alaska to be dominated by members of the *Gammaproteobacteria*. In contrast, studies from boreal lake systems found that *Gammaproteobacteria*, in particular *Candidatus*

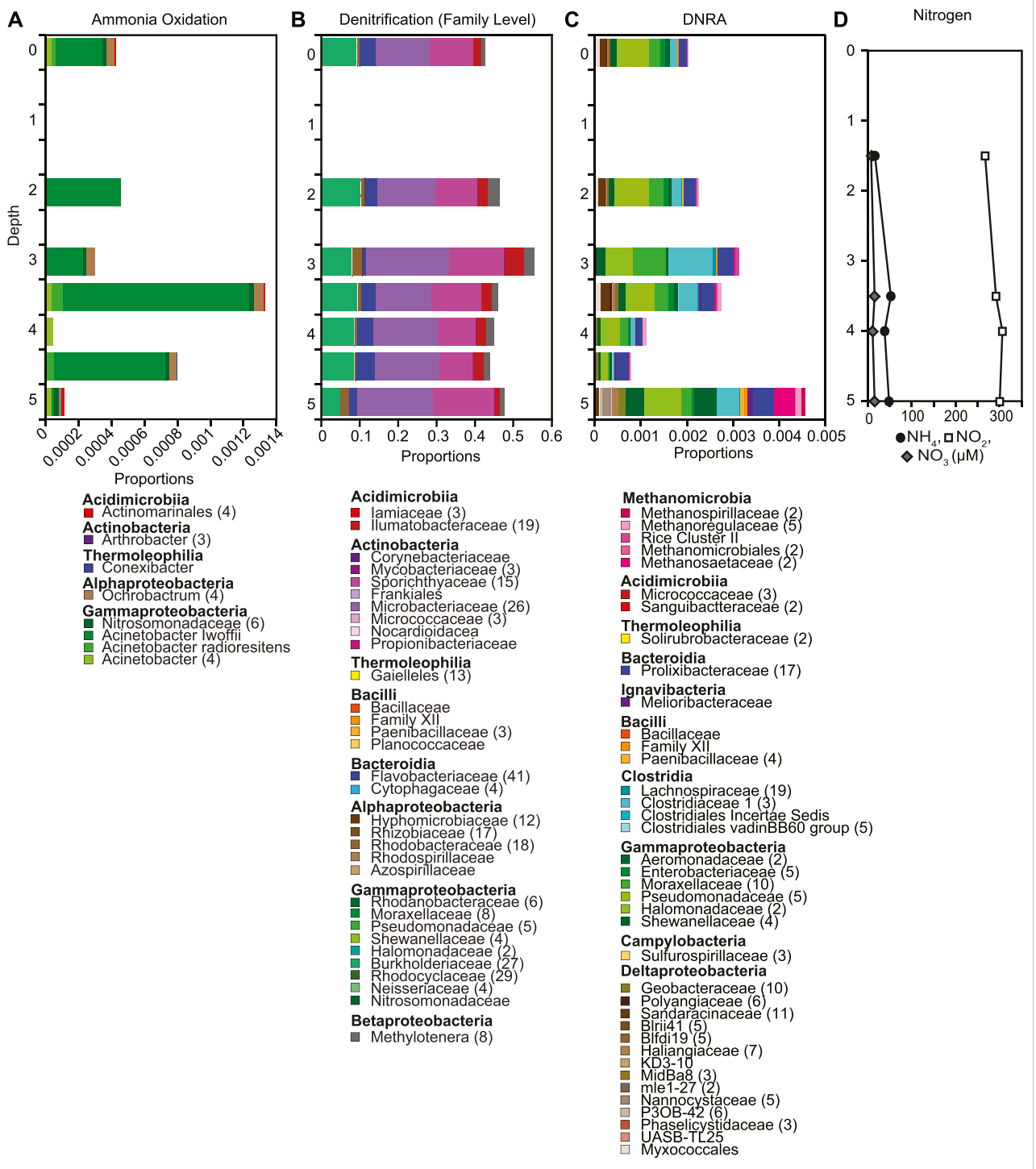


FIGURE 6
Depth profiles of putative **(A)** ammonia oxidizers, **(B)** denitrifiers, **(C)** DNRA based on 16S rRNA gene sequences, as well as **(D)** concentrations of nitrate, nitrite and ammonia down the water column. **(A–C)**. The number of ASVs included in each taxonomic group is included with the number given after the taxonomic name. If no number is given, the group only contains one ASV.

Methylumidiphilus within the order *Methylococcales*, had high relative abundances throughout the lake, but *Alphaproteobacteria* known to be type II methanotrophs had high relative abundance in surface water where methane concentrations were comparatively low (0 μM–1 μM) (Martin et al., 2021). In comparison, methane concentrations in Teardrop

lake were elevated throughout the water column (2 μM–27 μM), consistent with the ubiquitous presence of type I methanotrophs, which have been suggested to have lower methane affinity compared to type II methanotrophs (Martin et al., 2021).

4.2 Decoupled methane cycle at intermediate depth

Coexisting with a traditional methane cycle functioning throughout the water column, we found evidence of methane cycling centered between 3 and 5 m depth that may be decoupled from the full water column cycle. Extreme isotope enrichment of ^{13}C and ^{2}H of dissolved methane centered at 4 m depth may result from methanogenesis coupled tightly to methanotrophy in what approaches closed-system characteristics. Microbial oxidation of methane under these conditions leads to a systematic enrichment in both ^{13}C and ^{2}H of the residual un-oxidized methane pool (Whiticar and Faber, 1985; Happell et al., 1994; Whiticar, 1999; Bastviken et al., 2002; Alstad and Whiticar, 2011; Wik et al., 2020). At the time of sampling in August 2015, dissolved methane in Teardrop lake at 3 m–4 m depth was isotopically enriched by as much as 36‰ for ^{13}C and 279‰ for ^{2}H relative to bottom waters at 5 m depth. The lake was weakly thermally stratified and likely approaching holomixis. However, a slight increase in temperature was observed at 4 m depth, potentially supporting increased microbial processes leading to a thermal discontinuity or temporary biogenic meromixis. Oxidation-reduction potential was also elevated within this zone by 15 mV. A subsurface maximum in the isotopic enrichment of ^{13}C and ^{2}H in dissolved methane is an unusual pattern relative to other local lakes that we first observed in Teardrop lake in 2013 (Cadieux et al., 2016). However, this pattern has recently been reported in a German lake (Lake Stechlin; Hartmann et al., 2018), as well as group of northern freshwater lakes in the Canadian Shield (i.e., Morency Lake, Croche Lake, Cromwell Lake, Gelil Lake), with $\delta^{13}C$ mid-depth values as high as +1.7‰ and is attributed to localized elevated methanotrophic activity (Thottathil et al., 2019).

Photosynthesis in the euphotic zone of lakes is known to fuel aerobic methane oxidation as the addition of dissolved oxygen can stimulate methane oxidation and rates of oxygen production can be of the same magnitude as methane oxidation (Oswald et al., 2015). In Teardrop lake, the entire water column was euphotic, with photosynthesis likely occurring at all depths, including 3.5 m–4.5 m depth. Additionally, we observed concentrated layers of potential microbial growth suspended throughout the lake at mid-depths, supported by increased phytoplankton counts at 3 m (Figure 3). These suspended microbial communities could contribute to enhanced oxygenic photosynthesis. At the major methane isotope excursion at 4 m, there was no observable increase in dissolved oxygen, as oxygen is saturated and not a limiting factor. However, there was a 10% increase in ORP to +134 mV between 4.5 m and 3.5 m confirming sufficient concentration of dissolved oxygen to meet terminal electron acceptor demand from aerobic methanotrophy.

Corresponding with the extreme isotope enrichment in ^{13}C and ^{2}H of methane at 4 m was an increase in the relative abundance of putative methanotrophs. The putative methanotrophic community was dominated by type I methanotrophs belonging to the *Gammaproteobacteria*. Despite being microaerophilic, incubation studies suggest that Gamma-MOB also have a high tolerance for dissolved oxygen (Reis et al., 2020). *Methylovulum* had the highest relative abundance at 4 m in Teardrop lake. The change in relative abundances of putative methanotrophs with depth was consistent with changes in putative methylotrophic bacteria. Methylotrophic bacteria such as *Methylotenera* and *Methylobacterium* were present throughout the water column, but showed a significant increase at 4 m consistent with the increase in methanotrophs (i.e., relative abundance of 0.002 at 3 m to 0.312 at 4 m for *Methylotenera*; Supplementary Figure S8). Recent studies have shown that methylotrophs can co-feed with methanotrophs (Krause et al., 2016). The presence of methylotrophs can lead to a change in gene expression and the production of a different enzyme that results in the release of methanol that methylotrophs can then metabolize (Krause et al., 2016). Metagenomic analysis of methanotrophs in Arctic lake sediments showed that methanotrophs also have the capability to produce methanol (He et al., 2022). This suggests that methylotrophs in Teardrop lake have the capability to co-feed with methanotrophs and that the increase in relative abundance of methanotrophs at 4 m may help account for the increase of methylotrophs at that depth.

In Teardrop lake, methane concentrations increased at the interval corresponding with extreme isotope enrichment of ^{13}C and ^{2}H, which is not typical of classic methanotrophy. Production and accumulation of methane in oxic waters, known as the "methane paradox," has been documented in other lakes, globally (Keppler et al., 2006; Bogard et al., 2014; Tang et al., 2014, 2016; Günthel et al., 2019; Bizic et al., 2020; Bizic 2021; Wang et al., 2021) and could lead to a mid-water-depth increase in methane concentrations. Putative methanogens were identified both above and below the zone of ^{13}C and ^{2}H isotope enrichment of methane at 3 m and 5 m, though relative abundances were overall low. Methanogenesis in oxic water has been demonstrated to be driven by acetoclastic production (Bogard et al., 2014). We only detected two ASVs classified as *Methanosaeta* known to be capable of acetoclastic production with increased relative abundance at 5 m (Fournier and Gogarten 2008). All other putative methanogens we detected carry out hydrogenotrophic and/or methylotrophic methanogenesis (Vanwonterghem et al., 2016). Isotopic composition of methane above and below the interval of isotopic excursion ranged between −37‰ and −38‰ for $\delta^{13}C$ and −100‰

to −227‰ for δ^2H, which is closer to the isotopic range from acetoclastic methanogenesis than to that from hydrogenotrophic methanogenesis (Whiticar 1999). Additionally, accumulation of methane in oxygenated freshwater systems, though lower than archaeal methanogenic production rates, has been associated with the presence of phytoplankton including cyanobacteria, which readily convert fixed inorganic carbon into methane under both light and dark conditions (Bizic et al., 2020, 2021; Hartmann et al., 2020; Bizic 2021). Potential pathways include association of archaeal methanogens with cyanobacteria (Berg et al., 2014), demethylation of methylophosphates (Yao et al., 2016) under phosphorus starvation (Bizic et al., 2020), and a connection to the photosynthetic electron transfer chain in cyanobacteria (Bizic et al., 2020, 2021). In Teardrop lake, phytoplankton were present throughout the water column, with highest abundance especially of the cyanobacteria, *Anabaena*, at the surface, but a marked increase of *Aphanocapsa* at 4 m and other phytoplankton at 3 m depth. If methanogenesis in the oxic water column is associated with algal activity, the increased abundance of more labile organic matter could potentially promote methanogenesis. Microbial degradation of methylphosphate to methane has been shown to result in minimal fractionation (Taenzer et al., 2020), but isotopic fractionation from other oxic methane production pathways has not been reported (Bizic et al., 2020; Wang et al., 2021). Therefore, we are unable to use isotopic signatures of methane to confirm if oxic methane production is occurring in Teardrop Lake.

In addition to mid-depth methanogenesis, methane in surface intervals may also derive from different source areas than the anoxic sediments of deeper waters. One possibility is lateral transport of methane from littoral sediments, which has been reported in other lakes, and can amount to 30%–40% of methane emitted during the summer stratification (Günthel et al., 2020). Though in lower relative abundance, we detected putative methanogens throughout the water column (Figure 5). Teardrop lake is a hydrologically closed basin, with no inputs from other water bodies. Lateral methane source areas are limited to shallow littoral sediments. Carbon isotopic composition of porewater methane collected from littoral sediments in 2013 ranged from −48.6 to −36.5‰ (Cadieux et al., 2016), within the range of epilimnetic waters in Teardrop lake. The dissolved methane in profundal sediments of Teardrop lake was more depleted in ^{13}C and enriched in ^2H relative to the methane in littoral sediments, suggesting different microbial production pathways (Cadieux et al., 2016). Partial oxidation of porewater methane or more isotopically enriched methanogenic substrates in littoral sediments can also contribute to differences in the isotopic composition of dissolved methane between littoral and profundal sediments in small Arctic lakes (Thompson et al., 2018).

Biogeochemical cycles in lakes are often coupled, and driven by underlying microbial community interactions (Wetzel, 2001). In particular, methane and nitrogen cycling are known to be coupled (Bodelier and Steenbergh, 2014; Zhu et al., 2016; Jing et al., 2020). Under anaerobic conditions, methane oxidation occurs using alternative electron acceptors such as nitrate and nitrite instead of oxygen (Valentine, 2002; Oswald et al., 2017). Nitrogen concentrations have been found to both inhibit and stimulate methanotrophic activity and methane oxidation. For example, ammonium-based fertilization has been found to stimulate the growth and activity of methane oxidizers in rice patties (Bodelier et al., 2000; Krüger and Frenzel, 2003), however, ammonium concentrations > 4 mM have also been found to repress methane oxidation in littoral lake sediments (Bosse et al., 1993). Ammonium concentrations in Teardrop lake are 3 orders of magnitude below the threshold for inhibition and unlikely to influence methane oxidation. Methanotrophic bacteria have also been suggested to co-oxidize ammonia when nitrite is present (Harrits and Hanson, 1980). Nitrite concentrations in Teardrop lake exceeded nitrate concentrations, which has also been reported in other local Greenlandic lakes (Cadieux et al., 2016, 2017; Schütte et al., 2016). In Teardrop lake, nitrite concentrations increased slightly at 4 m where extreme isotope enrichment of ^{13}C and ^2H was observed associated with a drop in the relative abundance of putative ammonia oxidizers (Figure 6A), but concentrations remained overall stable throughout the water column. Additionally, the presence of nitrate has been suggested to stimulate methane oxidation rates under oxic conditions, with *Methylotenera* being capable of denitrification (van Grinsven et al., 2020). Relative proportions of putative denitrifiers were overall constant in Teardrop lake, though the putative methylotroph *Methylotenera* increased at 4 m–2.5% (Supplementary Figure S9). This increase in the relative abundance of *Methylotenera* was mostly driven by one ASV. Despite not finding clear linkages between methane and nitrogen biogeochemical cycles in Teardrop lake, it is possible that the extreme isotope enrichment of ^{13}C and ^2H in dissolved methane resulted from alternative co-cycling of nutrients.

4.3 Implications

Arctic lakes are likely to represent a growing net source of methane to the atmosphere with rapid warming of northern landscapes (Wik et al., 2016; Li and Xue, 2021). Measurements of global atmospheric $\delta^{13}C\text{-}CH_4$ suggest a rapidly increasing microbial source (Lan et al., 2021) that may account for up to 85% of the recent growth in atmospheric methane (Tollefson, 2022). Identification and inclusion of the key biogeochemical processes in climate models is a significant challenge (Lan et al., 2021). In the last 10 years, the methane paradox has been unfolding in the literature, demonstrating that methane in oxic water is not exclusively from transport from anoxic sources, and oxic methane production may account for 18%–90% of surface emissions (Keppler et al., 2006; Grossart et al., 2011; Bogard et al., 2014; Tang et al., 2014, 2016; Günthel et al., 2019, 2020). We suggest

that, in Teardrop lake, methane in the water column may derive from a combination of sources: anoxic sediments, lateral transport from littoral areas and oxic methanogenesis in the mid-water column. Additionally, there is evidence for tight carbon recycling within a limited depth interval of the water column, leading to extreme isotope enrichment in ^{13}C and ^{2}H of the dissolved methane pool. Our work from Teardrop lake highlights the challenge in predicting potential methane emissions from small, shallow water bodies. Most conceptual models of greenhouse gas emissions from northern landscapes utilize large lakes and assume methane emissions from conventional anoxic sources (IPCC 2013; Saunois et al., 2016). Feedbacks involving small lakes have been lacking (Rasilo et al., 2015). As permafrost thaw rapidly expands with warming climate, smaller thermokarst lakes are increasing in number and area in the Arctic (Abnizova et al., 2012; Gao et al., 2013). It is important to integrate methane cycling of small Arctic lakes into the conceptual modeling framework for greenhouse gas emissions from the terrestrial biosphere.

Data availability statement

Data is available through the National Center for Biotechnology Information Sequence Read Archive. BioProject ID is PRJNA879411.

Author contributions

SC, US, and JW contributed to conception and design of the study. JW collected field samples. SC performed chemical and isotopic analyses. US performed microbial analyses. SP performed chlorophyll and plankton analyses. CH performed bioinformatics. SC and US wrote the first draft of the manuscript. SC, US, JW, SP and CH wrote sections of the manuscript. All authors contributed to manuscript revision, read, and approved the submitted version.

Funding

The Funding for this project is from NASA Astrobiology Science and Technology for Exploring Planets (ASTEP) Program #NNX11AJ01G.

Acknowledgments

Robert Whitticar and Lisa Pratt for assistance with collecting field samples.

Conflict of interest

The authors declare that the research was conducted in the absence of any commercial or financial relationships that could be construed as a potential conflict of interest.

Publisher's note

All claims expressed in this article are solely those of the authors and do not necessarily represent those of their affiliated organizations, or those of the publisher, the editors and the reviewers. Any product that may be evaluated in this article, or claim that may be made by its manufacturer, is not guaranteed or endorsed by the publisher.

Supplementary material

The Supplementary Material for this article can be found online at: https://www.frontiersin.org/articles/10.3389/fenvs.2022.884133/full#supplementary-material.

References

Abnizova, A., Siemens, J., Langer, M., and Boike, J. (2012). Small ponds with major impact: The relevance of ponds and lakes in permafrost landscapes to carbon dioxide emissions. *Glob. Biogeochem. Cycles* 26, 4237. doi:10.1029/2011GB004237

Aitchison, J. (1982). The statistical analysis of compositional data. *J. R. Stat. Soc. Ser. B* 44, 139–160. doi:10.1111/j.2517-6161.1982.tb01195.x

Alstad, K. P., and Whiticar, M. J. (2011). Carbon and hydrogen isotope ratio characterization of methane dynamics for Fluxnet Peatland Ecosystems. *Org. Geochem.* 42 (5), 548–558. doi:10.1016/j.orggeochem.2011.03.004

American Public Health Association (2012). *Standard methods for the examination of water and wastewater*. 22nd Edition. Washington, D.C: American Public Health Association, American Water Works Association and the Water Environment Federation.

Anderson, N. J., Harriman, R., Ryves, D. B., and Patrick, S. T. (2001). Dominant factors controlling variability in the ionic composition of West Greenland lakes. *Arct. Antarct. Alp. Res.* 33, 418–425. doi:10.1080/15230430.2001.12003450

Balabane, M., Galimov, E. M., Hermann, M., and Letolle, R. (1987). Hydrogen and carbon isotope fractionation during experimental production of bacterial methane. *Org. Geochem.* 11, 115–119. doi:10.1016/0146-6380(87)90033-7

Bastviken, D., Cole, J., Pace, M., and Tranvik, L. (2004). Methane emissions from lakes: Dependence of lake characteristics, two regional assessments, and a global estimate. *Glob. Biogeochem. Cycles* 18. doi:10.1029/2004GB002238

Bastviken, D., Ejlertsson, J., and Tranvik, L. (2002). Measurement of methane oxidation in lakes: A comparison of methods. *Environ. Sci. Technol.* 36, 3354–3361. doi:10.1021/es010311p

Bennike, O. (2000). Palaeoecological studies of Holocene lake sediments from west Greenland. *Palaeogeogr. Palaeoclimatol. Palaeoecol.* 155, 285–304. doi:10.1016/s0031-0182(99)00121-2

Berg, A., Lindblad, P., and Svensson, B. H. (2014). Cyanobacteria as a source of hydrogen for methane formation. *World J. Microbiol. Biotechnol.* 30 (2), 539–545. doi:10.1007/s11274-013-1463-5

Bizic, M., Klintzsch, T., Ionescu, D., Hindiyeh, M. Y., Günthel, M., Muro-Pastor, A. M., et al. (2020). Aquatic and terrestrial cyanobacteria produce methane. *Sci. Adv.* 6 (3), eaax5343. doi:10.1126/sciadv.aax5343

Bizic, M. (2021). Phytoplankton photosynthesis: An unexplored source of biogenic methane emission from oxic environments. *J. Plankton Res.* 43 (6), 822–830. doi:10.1093/plankt/fbab069

Blees, J., Niemann, H., Weck, C. B., Zopfi, J., Schubert, C. J., Kirf, M. K., et al. (2014). Micro-aerobic bacterial methane oxidation in the chemocline and anoxic water column of deep south-Alpine Lake Lugano (Switzerland). *Limnol. Oceanogr.* 59 (2), 311–324. doi:10.4319/lo.2014.59.2.0311

Bodelier, P. L. E., Roslev, P., Henckel, T., and Frenzel, P. (2000). Stimulation by ammonium-based fertilizers of methane oxidation in soil around rice roots. *Nature* 403, 421–424. doi:10.1038/35000193

Bodelier, P. L. E., and Steenbergh, A. K. (2014). Interactions between methane and the nitrogen cycle in light of climate change. *Curr. Opin. Environ. Sustain.* 9 (10), 26–36. doi:10.1016/j.cosust.2014.07.004

Bogard, M. J., del Giorgio, P. A., Boutet, L., Chaves, M. C., Prairie, Y. T., Merante, A., et al. (2014). Oxic water column methanogenesis as a major component of aquatic CH_4 fluxes. *Nat. Commun.* 5, 5350. doi:10.1038/ncomms6350

Bolyen, E., Rideout, J. R., Dillon, M. R., Bokulich, N. A., Abnet, C. C., Al-Ghalith, G. A., et al. (2019). Reproducible, interactive, scalable and extensible microbiome data science using QIIME 2. *Nat. Biotechnol.* 37, 852–857. doi:10.1038/s41587-019-0209-9

Bomberg, M., Claesson, L. L., Lamminmäki, T., and Kontula, A. (2019). Highly diverse aquatic microbial communities separated by permafrost in Greenland show distinct features according to environmental niches. *Front. Microbiol.* 10, 1583. doi:10.3389/fmicb.2019.01583

Borrel, G., Jezequel, D., Biderre-Petit, C., Morel-Desrosiers, N., Morel, J. P., Peyret, P., et al. (2011). Production and consumption of methane in freshwater lake ecosystems. *Res. Microbiol.* 162, 832–847. doi:10.1016/j.resmic.2011.06.004

Bosse, U., Frenzel, P., and Conrad, R. (1993). Inhibition of methane oxidation by ammonium in the surface layer of a littoral sediment. *FEMS Microbiol. Ecol.* 13, 123–134. doi:10.1111/j.1574-6941.1993.tb00058.x

Brand, A., Bruderer, H., Oswald, K., Guggenheim, C., Schubert, C. J., and Wehrli, B. (2016). Oxygenic primary production below the oxycline and its importance for redox dynamics. *Aquat. Sci.* 78, 727–741. doi:10.1007/s00027-016-0465-4

Butler, T. M., Wilhelm, A. C., Dwyer, A. C., Webb, P. N., Baldwin, A. L., and Techtmann, S. M. (2019). Microbial community dynamics during lake ice freezing. *Sci. Rep.* 9, 6231. doi:10.1038/s41598-019-42609-9

Cadieux, S. B., White, J. R., and Pratt, L. M. (2017). Exceptional summer warming leads to contrasting outcomes for methane cycling in small Arctic lakes of Greenland. *Biogeosciences* 14, 559–574. doi:10.5194/bg-14-559-2017

Cadieux, S. B., White, J. R., Sauer, P. E., Peng, Y., Goldman, A. E., and Pratt, L. M. (2016). Large fractionations of C and H isotopes related to methane oxidation in Arctic lakes. *Geochimica Cosmochimica Acta* 187, 141–155. doi:10.1016/j.gca.2016.05.004

Callahan, B., McMurdie, P., Rosen, M., Han, A. W., Johnson, A. J. A., and Holmes, S. P. (2016). DADA2: High-resolution sample inference from Illumina amplicon data. *Nat. Methods* 13, 581–583. doi:10.1038/nmeth.3869

Caporaso, J. G., Lauber, L. C., Walters, W. A., Berg-Lyons, D., Huntley, J., Fierer, N., et al. (2012). Ultra-high-throughput microbial community analysis on theIllumina HiSeq and MiSeq platforms. *ISME J.* 6, 1621–1624. doi:10.1038/ismej.2012.8

Carini, S., Bano, N., LeCleir, G., and Joye, S. B. (2005). Aerobic methane oxidation and methanotroph community composition during seasonal stratification in Mono Lake, California (USA). *Environ. Microbiol.* (7), 1127–1138. doi:10.1111/j.1462-2920.2005.00786.x

Colby, G. A., Ruuskanen, M. O., St. Pierre, K. A., Louis, St.V. L., Poulain, A. J., and Aris-Brosou, S. (2020). Warming climate is reducing the diversity of dominant microbes in the largest high Arctic lake. *Front. Microbiol.* 11, 561194. doi:10.3389/fmicb.2020.561194

Coleman, D. D., Risatti, J. B., and Schoell, M. (1981). Fractionation of carbon and hydrogen isotopes by methane-oxidizing bacteria. *Geochimica Cosmochimica Acta* 45, 1033–1037. doi:10.1016/0016-7037(81)90129-0

Coleman, D. D., Risatti, J. B., and Schoell, M. (1981). Fractionation of carbon and hydrogen isotopes by methane-oxidizing bacteria. *Geochimica Cosmochimica Acta* 45, 1033–1037. doi:10.1016/0016-7037(81)90129-0

Comeau, A., Harding, T., Galand, P. E., Vincent, W. F., and Lovejoy, C. (2012). Vertical distribution of microbial communities in a perennially stratified Arctic lake with saline, anoxic bottom waters. *Sci. Rep.* 2, 604. doi:10.1038/srep00604

Dedysh, S. N., Dunfield, P. F., and Trotsenko, Y. A. (2004). Methane utilization by Methylobacterium species: New evidence but still no proof for an old controversy. *Int. J. Syst. Evol. Microbiol.* 54 (6), 1919–1920. doi:10.1099/ijs.0.63493-0

Downing, J. A. (2010). Emerging global role of small lakes and ponds: Little things mean a lot. *Limnetica* 29, 9–24. doi:10.23818/limn.29.02

Duc, N. T., Crill, P., and Bastviken, D. (2010). Implications of temperature and sediment characteristics on methane formation and oxidation in lake sediments. *Biogeochemistry* 100, 185–196. doi:10.1007/s10533-010-9415-8

Emerson, J. B., Varner, R. K., Wik, M., Parks, D. H., Neumann, R. B., Johnson, J. E., et al. (2021). Diverse sediment microbiota shape methane emission temperature sensitivity in Arctic lakes. *Nat. Commun.* 12, 5815. doi:10.1038/s41467-021-25983-9

Etminan, M., Myhre, G., Highwood, E. J., and Shine, K. P. (2016). Radiative forcing of carbon dioxide, methane and nitrous oxide: A significant revision of the methane radiative forcing. *Geophys. Res. Lett.* 43 (24), 2614–12623. doi:10.1002/2016gl071930

Fournier, G. P., and Gogarten, J. P. (2008). Evolution of acetoclastic methanogenesis in methanosarcina via horizontal gene transfer from cellulolytic clostridia. *J. Bacteriol.* 190 (3), 1124–1127. doi:10.1128/JB.01382-07

Gao, X., Schlosser, C. A., Sokolov, A., Anthony, K. W., Zhuang, Q., and Kicklighter, D. (2013). Permafrost degradation and methane: Low risk of biogeochemical climate-warming feedback. *Environ. Res. Lett.* 8 (3), 035014. doi:10.1088/1748-9326/8/3/035014

Gloor, G. B., Macklaim, J. M., Pawlowsky-Glahn, V., and Egozcue, J. J. (2017). Microbiome datasets are compositional: And this is not optional. *Front. Microbiol.* 8, 2224. doi:10.3389/fmicb.2017.02224

Grossart, H. P., Frindte, K., Dziallas, C., Eckert, W., and Tang, K. W. (2011). Microbial methane production in oxygenated water column of an oligotrophic lake. *Proc. Natl. Acad. Sci. U. S. A.* 108, 19657–19661. doi:10.1073/pnas.1110716108

Günthel, M., Donis, D., Kirillin, G., Ionescu, D., Bizic, M., McGinnis, D. F., et al. (2019). Contribution of oxic methane production to surface methane emission in lakes and its global importance. *Nat. Commun.* 10, 5497. doi:10.1038/s41467-019-13320-0

Günthel, M., Klawonn, I., Woodhouse, J., Bizic, M., Ionescu, D., Ganzert, L., et al. (2020). Photosynthesis-driven methane production in oxic lake water as an important contributor to methane emission. *Limnol. Oceanogr.* 65, 2853–2865. doi:10.1002/lno.11557

Happell, J. D., Chanton, J. P., and Showers, W. S. (1994). The influence of methane oxidation on the stable isotopic composition of methane emitted from Florida swamp forests. *Geochimica Cosmochimica Acta* 58, 4377–4388. doi:10.1016/0016-7037(94)90341-7

Harrits, S. M., and Hanson, R. S. (1980). Stratification of aerobic methane-oxidizing organisms in lake mendota, madison, Wisconsin1. *Limnol. Oceanogr.* 25 (3), 412–421. doi:10.4319/lo.1980.25.3.0412

Hartmann, J. F., Gentz, T., Schiller, A., Greule, M., Grossart, H.-P., Ionescu, D., et al. (2018). A fast and sensitive method for the continuous *in situ* determination of dissolved methane and its δ^{13}C-isotope ratio in surface waters. *Limnol. Oceanogr. Methods* 16, 273–285. doi:10.1002/lom3.10244

Hartmann, J. F., Günthel, M., Klintzsch, T., Kirillin, G., Grossart, H.-P., Keppler, F., et al. (2020). High spatiotemporal dynamics of methane production and emission in oxic surface water. *Environ. Sci. Technol.* 54, 1451–1463. doi:10.1021/acs.est.9b03182

He, R., Wang, J., Pohlman, J. W., Jia, Z., Chu, Y. X., Wooller, M. J., et al. (2022). Metabolic flexibility of aerobic methanotrophs under anoxic conditions in Arctic lake sediments. *ISME* 16 (1), 78–90. doi:10.1038/s41396-021-01049-y

He, R., Wooller, M. J., Pohlman, J. W., Quensen, J., Tiedje, J. M., and Leigh, M. B. (2012). Shifts in identity and activity of methanotrophs in Arctic lake sediments in response to temperature changes. *Appl. Environ. Microbiol.* 78 (13), 4715–4723. doi:10.1128/AEM.00853-12

Jing, H., Wang, R., Jiang, Q., Zhang, Y., and Peng, X. (2020). Anaerobic methane oxidation coupled to denitrification is an important potential methane sink in deep-sea cold seeps. *Sci. Total Environ.* 748, 142459. doi:10.1016/j.scitotenv.2020.142459

Kankaala, P., Huotari, J., Peltomaa, E., Saloranta, T., and Oiala, A. (2006). Methanotrophic activity in relation to methane efflux and total heterotrophic bacterial production in a stratified, humic, boreal lake. *Limnol. Oceanogr.* 51, 1195–1204. doi:10.4319/lo.2006.51.2.1195

Kankaala, P., Huotari, J., Tulonen, T., and Ojala, A. (2013). Lake-size dependent physical forcing drives carbon dioxide and methane effluxes from lakes in a boreal landscape. *Limnol. Oceanogr.* 38, 1915–1930. doi:10.4319/lo.2013.58.6.1915

Keppler, F., Hamilton, J. T., Brass, M., and Rockmann, T. (2006). Methane emissions from terrestrial plants under aerobic conditions. *Nature* 439, 187–191. doi:10.1038/nature04420

Kinnaman, F. S., Valentine, D. L., and Tyler, S. C. (2007). Carbon and hydrogen isotope fractionation associated with the aerobic microbial oxidation of methane, ethane, propane and butane. *Geochimica Cosmochimica Acta* 71, 271–283. doi:10.1016/j.gca.2006.09.007

Knight, R., Vrbanac, A., Taylor, B. C., Aksenov, A., Callewaert, C., Debeliu, J., et al. (2018). Best practices for analysing microbiomes. *Nat. Rev. Microbiol.* 16, 410–422. doi:10.1038/s41579-018-0029-9

Kozich, J. J., Westcott, S. L., Baxter, N. T., Highlander, S. K., and Schloss, P. D. (2013). Development of a dual-index sequencing strategy and curation pipeline for analyzing amplicon sequence data on the MiSeq Illumina sequencing platform. *Appl. Environ. Microbiol.* 79 (17), 5112–5120. doi:10.1128/aem.01043-13

Krause, S. M., Johnson, T., Samadhi Karunaratne, Y., Fu, Y., Beck, D. A., Chistoserdova, L., et al. (2016). Lanthanide-dependent cross-feeding of methane-derived carbon is linked by microbial community interactions. *Proc. Natl. Acad. Sci. U. S. A.* 114 (2), 358–363. doi:10.1073/pnas.1619871114

Krüger, M., and Frenzel, P. (2003). Effects of N-fertilization on CH_4 oxidation and production, and consequences for CH_4 emissions from microcosms and rice fields. *Glob. Change Biol.* 9, 773–784. doi:10.1046/j.1365-2486.2003.00576.x

Lan, X., Basu, S., Schwietzke, S., Bruhwiler, L. M., Dlugokencky, E. J., Michel, S. E., et al. (2021). Improved constraints on global methane emissions and sinks using $\delta^{13}C$-CH_4. *Glob. Biogeochem. Cycles* 35 (6), e2021GB007000. doi:10.1029/2021gb007000

Li, L., and Xue, B. (2021). Methane emissions from northern lakes under climate change: A review. *SN Appl. Sci.* 3 (12), 883–912. doi:10.1007/s42452-021-04869-x

Liikanen, A., Huttunen, J. T., Murtoniemi, T., Tanskanene, H., Vaisanen, T., Silvola, J., et al. (2003). Spatial and seasonal variation in greenhouse and nutrient dynamics and their interactions in the sediment of a boreal eutrophic lake. *Biogeochemistry* 65, 83–103. doi:10.1023/a:1026070209387

Loften, D. D., Whalen, S. C., and Hershey, A. E. (2014). Effect of temperature on methane dynamics and evaluation of methane oxidation kinetics in shallow Arctic Alaskan lakes. *Hydrobiologia* 721, 209–222. doi:10.1007/s10750-013-1663-x

López Bellido, J., Tulonen, T., Kankaala, P., and Ojala, A. (2009). CO_2 and CH_4 fluxes during spring and autumn mixing periods in a boreal lake (Pääjärvi, southern Finland). *J. Geophys. Res.* 114, G04007. doi:10.1029/2009JG000923

Martin, G., Rissanen, A. J., Garcia, S. L., Mehrshad, M., Buck, M., and Peura, S. (2021). Candidatus Methylumidiphilus drives peaks in methanotrophic relative abundance in stratified lakes and ponds across northern landscapes. *Front. Microbiol.* 12, 669937. doi:10.3389/fmicb.2021.669937

Martinez-Cruz, K., Lewis, M-C., Herriott, I. C., Sepulveda-Jauregui, A., Walter Anthony, K., Thalasso, F., et al. (2017). Anaerobic oxidation of methane by aerobic methanotrophs in sub-Arctic lake sediments. *Sci. Total Environ.* 607-608, 23–31. doi:10.1016/j.scitotenv.2017.06.187

Martinez-Cruz, K., Sepulveda-Jauregui, A., Walter Anthony, K., and Thalasso, F. (2015). Geographic and seasonal variation of dissolved methane and aerobic methane oxidation in Alaskan lakes. *Biogeosciences* 12, 4595–4606. doi:10.5194/bg-12-4595-2015

Mau, S., Blees, J., Helmke, E., Niemann, H., and Damm, E. (2013). Vertical distribution of methane oxidation and methanotrophic response to elevated methane concentrations in stratified waters of the Arctic fjord Storfjorden (Svalbard, Norway). *Biogeosciences* 10, 6267–6278. doi:10.5194/bg-10-6267-2013

Milucka, J., Kirf, M., Lu, L., Krupke, A., Lam, P., Littmann, S., et al. (2015). Methane oxidation coupled to oxygenic photosynthesis in anoxic waters. *ISME J.* 9, 1991–2002. doi:10.1038/ismej.2015.12

Møller, T. E., van der Bilt, G. G. M., Roerdink, D. L., and Jørgensen, S. L. (2020). Microbial community structure in Arctic lake sediments reflect variations in holocene climate conditions. *Front. Microbiol.* 11, 1520. doi:10.3389/fmicb.2020.01520

Morton, J. T., Marotz, C., Washburne, A., Silverman, J., Zaramela, L. S., Edlund, A., et al. (2019). Establishing microbial composition measurement standards with reference frames. *Nat. Commun.* 10, 2719. doi:10.1038/s41467-019-10656-5

Murase, J., and Sugimoto, A. (2005). Inhibitory effect of light on methane oxidation in the pelagic water column of a mesotrophic lake (Lake Biwa, Japan). *Limnol. Oceanogr.* 50, 1339–1343. doi:10.4319/lo.2005.50.4.1339

Osudar, R., Liebner, S., Alawi, M., Yang, S., Bussmann, I., and Wagner, D. (2016). Methane turnover and methanotrophic communities in arctic aquatic ecosystems of the Lena Delta, Northeast Siberia. *FEMS Microbiol. Ecol.* 92 (8), fiw116. doi:10.1093/femsec/fiw116

Oswald, K., Graf, J., Littmann, S., Tienken, D., Brand, A., Wehrli, B., et al. (2017). *Crenothrix* are major methane consumers in stratified lakes. *ISME J.* 11, 2124–2140. doi:10.1038/ismej.2017.77

Oswald, K., Jegge, C., Tischer, J., Berg, J., Brand, A., Miracle, M. R., et al. (2016). Methanotrophy under versatile conditions in the water column of the ferruginous meromictic Lake La Cruz (Spain). *Front. Microbiol.* 7, 1762. doi:10.3389/fmicb.2016.01762

Oswald, K., Milucka, J., Brand, A., Littmann, S., Wehril, B., Kuypers, M. M. M., et al. (2015). Light-dependent aerobic methane oxidation reduces methane emissions from seasonally stratified lakes. *PLoS ONE* 10 (7), e0132574. doi:10.1371/journal.pone.0132574

Quast, C., Pruesse, E., Yilmaz, P., Gerken, J., Schweer, T., Yarza, P., et al. (2013). The SILVA ribosomal RNA gene database project: Improved data processing and web-based tools. *Nucleic Acids Res.* 41 (D1), D590–D596. doi:10.1093/nar/gks1219

Rasilo, T., Prairie, Y. T., and Del Giorgio, P. A. (2015). Large-scale patterns in summer diffusive CH_4 fluxes across boreal lakes, and contribution to diffusive C emissions. *Glob. Change Biol.* 21, 1124–1139. doi:10.1111/gcb.12741

Reis, P. C. J., Thottathil, S. D., Ruiz-Gonzales, C. l., and Prairie, Y. T. (2020). Niche separation within aerobic methanotrophic bacteria across lakes and its link to methane oxidation rates. *Environ. Microbiol.* 22 (2), 738–751. doi:10.1111/1462-2920.14877

Rosentreter, J. A., Borges, A. V., Deemer, B. R., Holgerson, M. A., Liu, S., Song, C., et al. (2021). Half of global methane emissions come from highly variable aquatic ecosystem sources. *Nat. Geosci.* 14, 225–230. doi:10.1038/s41561-021-00715-2

Ruuskanen, M. O., St. Pierre, K. A., Louis, St.V. L., Aris-Brosou, S., and Poulain, A. J. (2018). Physicochemical drivers of microbial community structure in sediments of lake hazen, nunavut, Canada. *Front. Microbiol.* 9, 1138. doi:10.3389/fmicb.2018.01138

Samad, M. S., and Bertilsson, S. (2017). Seasonal variation in abundance and diversity of bacterial methanotrophs in five temperate lakes. *Front. Microbiol.* 8, 142. doi:10.3389/fmicb.2017.00142

Saunois, M., Bousquet, P., Poulter, B., Peregon, A., Ciais, P., Canadell, J. G., et al. (2016). The global methane budget 2000-2012. *Earth Syst. Sci. Data* 8, 697–751. doi:10.5194/essd-8-697-2016

Schütte, U. M. E., Cadieux, S. B., Hemmerich, C., Pratt, L. M., and White, J. R. (2016). Unanticipated geochemical and microbial community structure under seasonal ice cover in a dilute, dimictic Arctic lake. *Front. Microbiol.* 7, 1035. doi:10.3389/fmicb.2016.01035

Shelley, F., Grey, J., and Trimmer, M. (2014). Widespread methanotrophic primary production in lowland chalk rivers. *Proc. R. Soc. B* 281, 20132854. doi:10.1098/rspb.2013.2854

Somers, D. J., Strock, K. E., and Saros, J. E. (2020). Environmental controls on microbial diversity in arctic lakes of west Greenland. *Microb. Ecol.* 80, 60–72. doi:10.1007/s00248-019-01474-9

IPCC (2013). *Climate change 2013: The physical science basis. Contribution of working group I to the fifth assessment report of the intergovernmental panel on climate change*. Editors T. F. Stocker, D. Qin, G.-K. Plattner, M. Tignor, S. K. Allen, J. Boschung, et al. (Cambridge, United Kingdom and New York, NY, USA: Cambridge University Press), 1535. doi:10.1017/CBO9781107415324

Stoeva, M. K., Aris-Brosou, S., Che´telat, J., Hintelmann, H., Pelletier, P., and Poulain, A. J. (2014). Microbial community structure in lake and wetland sediments from a high arctic polar desert revealed by targeted transcriptomics. *PLoS ONE* 9 (3), e89531. doi:10.1371/journal.pone.0089531

Taenzer, L., Carini, P. C., Masterson, A. M., Bourquie, B., Gaube, J. H., and Leavitt, W. D. (2020). Microbial methane from methylphosphonate isotopically records source. *Geophys. Res. Lett.* 74. doi:10.1029/2019GL085872

Tamas, I., Smirnova, A. V., He, Z., and Dunfield, P. F. (2014). The (d)evolution of methanotrophy in the beijerinckiaceae – a comparative genomics analysis. *ISME J.* 8, 369–382. doi:10.1038/ismej.2013.145

Tan, Z., and Zhuang, Q. (2015). Arctic lakes are continuous methane sources to the atmosphere under warming conditions. *Environ. Res. Lett.* 10, 054016. doi:10.1088/1748-9326/10/5/054016

Tang, K. W., McGinnis, D. F., Frindte, K., Brüchert, V., and Grossart, H.-P. (2014). Paradox reconsidered: Methane oversaturation in well-oxygenated lake waters. *Limnol. Oceanogr.* 59, 275–284. doi:10.4319/lo.2014.59.1.0275

Tang, W. K., McGinnis, D. F., Ionescu, D., and Grossart, H.-P. (2016). Methane production in oxic lake waters potentially increases aquatic methane flux to air. *Environ. Sci. Technol. Lett.* 3, 227–233. doi:10.1021/acs.estlett.6b00150

Templeton, A. S., Chu, K.-H., Alvarez-Cohen, L., and Conrad, M. E. (2006). Variable carbon isotope fractionation expressed by aerobic CH_4-oxidizing bacteria. *Geochimica Cosmochimica Acta* 70, 1739–1752. doi:10.1016/j.gca.2005.12.002

Theisen, A. R., and Murrell, J. C. (2005). Facultative methanotrophs revisited. *J. Bacteriol.* 187 (13), 4303–4305. doi:10.1128/JB.187.13.4303-4305.2005

Thompson, H. A., Pratt, L. M., and White, J. R. (2018). Spatial variation in stable isotopic composition of organic matter of macrophytes and sediments from a small Arctic Lake in West Greenland. *Arct. Antarct. Alp. Res.* 50 (1), ID1420282. doi:10.1080/15230430.2017.1420282

Thottathil, S. D., and Prairie, Y. T. (2021). Coupling of stable carbon isotopic signature of methane and ebullitive fluxes in northern temperate lakes. *Sci. Total Environ.* 777, 146117. doi:10.1016/j.scitotenv.2021.146117

Thottathil, S. D., Reis, P. C. J., del Giorgio, P. A., and Prairie, Y. T. (2018). The extent and regulation of summer methane oxidation in northern lakes. *J. Geophys. Res. Biogeosci.* 123, 3216–3230. doi:10.1029/2018JG004464

Thottathil, S. D., Reis, P. C. J., and Prairie, Y. T. (2019). Methane oxidation kinetics in northern freshwater lakes. *Biogeochemistry* 143, 105–116. doi:10.1007/s10533-019-00552-x

Tollefson, J. (2022). Scientists raise alarm over 'dangerously fast' growth in atmospheric methane. *Nature*. Epub ahead of print. doi:10.1038/d41586-022-00312-2

Valentine, D. L. (2002). Biogeochemistry and microbial ecology of methane oxidation in anoxic environments: A review. *Ant. Van Leeuwenhoek* 81, 271–282. doi:10.1023/A:1020587206351

Valentine, D. L., Chidthaisong, A., Rice, A., Reeburgh, W. S., and Tyler, S. C. (2004). Carbon and hydrogen isotope fractionation by moderately thermophilic methanogens 1. *Geochimica Cosmochimica Acta* 68, 1571–1590. doi:10.1016/j.gca.2003.10.012

van Grinsven, S., Sinninghe Damsté, J. S., Harrison, J., and Villanueva, L. (2020). Impact of electron acceptor availability on methane-influenced microorganisms in an enrichment culture obtained from a stratified lake. *Front. Microbiol.* 11, 715. doi:10.3389/fmicb.2020.00715

Vanwonterghem, I., Evans, P., Parks, D. H., Jensen, P. D., Woodcroft, B. J., Hugenholtz, P., et al. (2016). Methylotrophic methanogenesis discovered in the archaeal phylum Verstraetearchaeota. *Nat. Microbiol.* 1, 16170. doi:10.1038/nmicrobiol.2016.170

Vick-Majors, T., Priscu, J. C., and Amaral-Zettler, L. A. (2014). Modular community structure suggests metabolic plasticity during the transition to polar night in ice-covered Antarctic lakes. *ISME J.* 8, 778–789. doi:10.1038/ismej.2013.190

Vigneron, A., Lovejoy, C., Cruaud, P., Kalenitchenko, D., Culley, A., and Vincent, W. F. (2019). Contrasting winter versus summer microbial communities and metabolic functions in a permafrost thaw lake. *Front. Microbiol.* 10, 1656. doi:10.3389/fmicb.2019.01656

Wang, Q., Alowaifeer, A., Kerner, P., Balasubramanian, N., Patterson, A., Christian, W., et al. (2021). Aerobic bacterial methane synthesis. *Proc. Natl. Acad. Sci. U. S. A.* 118, e2019229118. doi:10.1073/pnas.2019229118

Westendorp, R. G. (1985). A quantitation method for dynamic headspace analysis using multiple runs. *J. Chromatogr. Sci.* 23, 521–524. doi:10.1093/chromsci/23.11.521

Wetzel, R. G. (2001). *Limnology: lake and river ecosystems*. 3rd ed. San Diego: Elsevier. doi:10.1016/C2009-0-02112-6

Whalen, S. C. (2005). Biogeochemistry of methane exchange between natural wetlands and the atmosphere. *Environ. Eng. Sci.* 22, 73–94. doi:10.1089/ees.2005.22.73

Whiticar, M. J. (1999). Carbon and hydrogen isotope systematics of bacterial formation and oxidation of methane. *Chem. Geol.* 161, 291–314. doi:10.1016/S0009-2541(99)00092-3

Whiticar, M. J., and Faber, E. (1985). Methane oxidation in sediment and water column environments – isotope evidence. *Org. Geochem.* 10, 759–768. doi:10.1016/s0146-6380(86)80013-4

Whiticar, M. J., Faber, E., and Schoell, M. (1986). Biogenic methane formation in marine and freshwater environments: CO_2 reduction vs. acetate fermentation-isotope evidence. *Geochim. Cosmochim. Acta* 50, 693–709. doi:10.1016/0016-7037(86)90346-7

Wik, M., Thornton, B. F., Varner, R. K., McCalley, C., and Crill, P. M. (2020). Stable methane isotopologues from northern lakes suggest that ebullition is dominated by sub-lake scale processes. *J. Geophys. Res. Biogeosci.* 125 (10), e2019JG005601. doi:10.1029/2019jg005601

Wik, M., Varner, R. K., Anthony, K. W., MacIntyre, S., and Bastviken, D. (2016). Climate-sensitive northern lakes and ponds are critical components of methane release. *Nat. Geosci.* 9 (2), 99–105. doi:10.1038/ngeo2578

Yao, M., Henny, C., and Maresca, J. A. (2016). Freshwater bacteria release methane as a byproduct of phosphorus acquisition. *Appl. Environ. Microbiol.* 82 (23), 6994–7003. doi:10.1128/AEM.02399-16

Zandt, M. H., Frank, J., Yilmaz, P., Cremers, G., Jetten, M. S. M., and Welte, C. U. (2020). Long-term enriched methanogenic communities from thermokarst lake sediments show species-specific responses to warming. *FEMS Microbes* 1 (1). doi:10.1093/femsmc/xtaa008

Zhu, J., Wang, Q., Yuan, M., Tan, G. A., Sun, F., Wang, C., et al. (2016). Microbiology and potential applications of aerobic methane oxidation coupled to denitrification (AME-D) process: A review. *Water Res.* 90, 203–215. doi:10.1016/j.watres.2015.12.020

Zigah, P. K., Oswald, K., Brand, A., Dinkel, C., Wehrli, B., and Schubert, C. J. (2015). Methane oxidation pathways and associated methanotrophic communities in the water column of a tropical lake. *Limnol. Oceanogr.* 60, 553–572. doi:10.1002/lno.10035

frontiers | Frontiers in Environmental Science

TYPE Original Research
PUBLISHED 03 November 2022
DOI 10.3389/fenvs.2022.865862

Check for updates

OPEN ACCESS

EDITED BY
Tonya DelSontro,
University of Waterloo, Canada

REVIEWED BY
Sarah Beth Cadieux,
Rensselaer Polytechnic Institute, United States
Peter Douglas,
McGill University, Canada
Regina Gonzalez Moguel,
McGill University, Canada

*CORRESPONDENCE
Teresa Einzmann,
teresa.einzmann@unibas.ch
Moritz Schroll,
moritz.schroll@geow.uni-heidelberg.de

†These authors have contributed equally to this work and share first authorship

SPECIALTY SECTION
This article was submitted to Biogeochemical Dynamics, a section of the journal Frontiers in Environmental Science

RECEIVED 30 January 2022
ACCEPTED 12 October 2022
PUBLISHED 03 November 2022

CITATION
Einzmann T, Schroll M, Kleint JF, Greule M and Keppler F (2022), Application of concentration and 2-dimensional stable isotope measurements of methane to constrain sources and sinks in a seasonally stratified freshwater lake.
Front. Environ. Sci. 10:865862.
doi: 10.3389/fenvs.2022.865862

COPYRIGHT
© 2022 Einzmann, Schroll, Kleint, Greule and Keppler. This is an open-access article distributed under the terms of the Creative Commons Attribution License (CC BY). The use, distribution or reproduction in other forums is permitted, provided the original author(s) and the copyright owner(s) are credited and that the original publication in this journal is cited, in accordance with accepted academic practice. No use, distribution or reproduction is permitted which does not comply with these terms.

Application of concentration and 2-dimensional stable isotope measurements of methane to constrain sources and sinks in a seasonally stratified freshwater lake

Teresa Einzmann[1,2*†], Moritz Schroll[1*†], Jan F. Kleint[1,3], Markus Greule[1] and Frank Keppler[1,4]

[1]Institute of Earth Sciences, Heidelberg University, Heidelberg, Germany, [2]Department of Environmental Sciences, University of Basel, Basel, Switzerland, [3]Department of Geosciences, MARUM – Center for Marine Environmental Sciences, University of Bremen, Bremen, Germany, [4]Heidelberg Center for the Environment (HCE), Heidelberg University, Heidelberg, Germany

Methane (CH_4) emissions from aquatic systems have recently been comprised to account for up to 50% of global CH_4 emissions, with lakes representing one of the largest CH_4 sources within this pool. However, there is large uncertainty associated with CH_4 emissions from freshwater environments to the atmosphere, because of a lack of understanding in the spatial and temporal dynamics of CH_4 sources and sinks, as well as underlying mechanisms and processes. In this study, we investigated the concentrations and stable carbon ($\delta^{13}C$-CH_4) and hydrogen ($\delta^{2}H$-CH_4) isotope composition of CH_4 in a small eutrophic lake (Lake Willersinnweiher) with seasonal stratification and its spatial and temporal variation. We found that while supersaturation of CH_4 in the entire water column was present throughout the whole year, the isotopic composition of CH_4 in sediment and water column varied depending on lake stratification, physiochemical conditions, and lake depth. During the stratification period, isotopic characteristics of pelagic surface water CH_4 differed from littoral and sedimentary CH_4, suggesting likely mixing of CH_4 from different sources including vertical and lateral input as well as groundwater input and potentially oxic methane production in the mixed surface water layer. Aerobic CH_4 oxidation indicated by a strong increase in both $\delta^{13}C$-CH_4 and $\delta^{2}H$-CH_4 values at the bottom of the oxycline was found to significantly reduce upward migrating CH_4 released at the sediment-water interface. In the sediment, stable isotope characteristics of CH_4 showed an increasing dominance of the acetoclastic CH_4 formation pathway from the pelagic towards the littoral area. Furthermore, the occurrence of sulfate-dependent anaerobic methane oxidation in the sediment was suggested by an increase in $\delta^{13}C$-CH_4 and $\delta^{2}H$-CH_4 values. During the mixing period, the isotopic CH_4 composition of the water column was distinctively less negative than during the stratification period potentially resulting from a greater impact of groundwater CH_4 input compared to the stratification period. Our findings implicate that the application of concentrations and dual isotope measurements of CH_4 is a

promising approach for constraining CH_4 sinks and sources in Lake Willersinnweiher and potentially other small lakes to clearly disentangle the complex CH_4 dynamics in lakes both spatially and seasonally.

KEYWORDS

$\delta^{13}C$-CH_4 values, δ^2H-CH_4 values, methane sources, methane sinks, lake, stable isotopes, stratification

Introduction

Lakes and other freshwater systems cover only a small area of the earth's continental land surface (>3%; Downing et al., 2006), but play an important role in the global carbon cycle and greenhouse gas emissions to the atmosphere (Oswald et al., 2015). Amongst aquatic systems, lakes constitute one of the largest sources of CH_4 emission, releasing 23–142 Tg CH_4 yr^{-1} to the atmosphere (Rosentreter et al., 2021). Thus, CH_4 cycles in lakes and their fluxes to the atmosphere have been investigated extensively in recent years (e.g. Casper et al., 2000; Bastviken et al., 2004; Natchimuthu et al., 2016; Donis et al., 2017; Peeters et al., 2019) and global lake CH_4 emissions were found to be dominated by small lakes (surface area <1 km^2) (Thottathil et al., 2022). Nevertheless, many key factors regarding CH_4 sources and sinks in lakes and their spatial and temporal variability remain unknown (Duc et al., 2010; Loken et al., 2019). Methane dynamics in lacustrine environments are complex and dependent on various biological production and consumption mechanisms as well as different transport pathways, impacting the distribution and accumulation of CH_4 in the water column (Günthel et al., 2019) (Figure 1). In particular, the source of CH_4 supersaturation in the surface water layer has been intensely debated in recent years. Whilst some research groups support lateral (riverine, littoral) and vertical CH_4 input from anoxic sources as the main mechanisms behind this observation (Fernández et al., 2016; Peeters et al., 2019; Peeters and Hofmann, 2021), others provide evidence for CH_4 production under oxic conditions as a potentially important process in the surface water layer of lakes (Grossart et al., 2011; Tang et al., 2016; Donis et al., 2017; Günthel et al., 2019; Hartmann et al., 2020; Thottathil et al., 2022). However, the large discrepancies in estimations of the contribution of oxic CH_4 production to surface water CH_4 emissions, varying from negligible contributions (Peeters and Hofmann, 2021) to a contribution of oxic methanogenesis to surface water emissions of up to 90% (Donis et al., 2017), reveal a lack of understanding of the processes contributing to surface supersaturation and their spatial and temporal variability. Although the determination of dissolved CH_4 concentrations and CH_4 fluxes is helpful to establish the magnitude of emissions, it cannot resolve the responsible pathways and production mechanisms (Cadieux et al., 2016). Measurement of stable carbon and hydrogen isotopes of CH_4 (expressed as $\delta^{13}C$-CH_4 and δ^2H-CH_4 values) are known to assist with identifying sources and sinks of CH_4 (e.g., Waldron et al., 1999; Whiticar, 2020; Douglas et al., 2021).

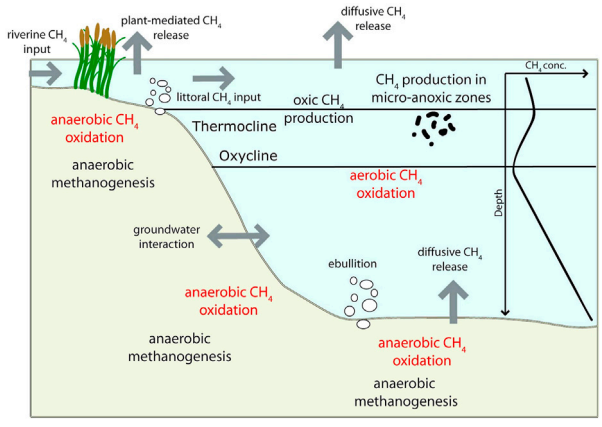


FIGURE 1
Overview of sources and sinks of CH_4 as well as transport processes (transport direction indicated by grey arrows) and a typical concentration profile of CH_4 in the lacustrine environment during thermal stratification. Modified after Tang et al. (2016).

In aquatic systems, biogenic CH_4 production has until recently been assumed to be solely performed by anaerobic methanogenic archaea occurring in the anoxic sediment and water column (e.g. Lessner, 2009). Microbial methanogenesis leads to the formation of ^{13}C and ^2H depleted CH_4. In anoxic sediment, methanogenesis typically involves two metabolic pathways using competitive substrates: Carbon dioxide (CO_2) reduction *via* H_2 (hydrogenotrophic) and acetate fermentation (acetoclastic). Methane production through CO_2 reduction generates $\delta^{13}C$-CH_4 values ranging from −110 to −60‰ and δ^2H-CH_4 values from −250 to −150‰, whereas acetoclastic methanogenesis generates $\delta^{13}C$-CH_4 values varying from −60 to −40‰ and δ^2H-CH_4 values from −400 to −250‰ (Whiticar, 1999; Belle et al., 2015). However, the δ^2H-CH_4 values were found not be exclusively controlled by the methanogenic formation pathway, but other variables such as CH_4 oxidation and δ^2H-H_2O values also have significant impact on the stable hydrogen isotope composition of CH_4 (e.g., Waldron et al., 1999; Douglas et al., 2021).

The observation of CH_4 oversaturation in the oxic surface mixed water layer of aquatic systems challenges the view of methanogenesis exclusively occurring under anoxic conditions (Donis et al., 2017; Bižić et al., 2020a; Hartmann et al., 2020).

Recent research has shown that CH_4 production is possible under oxic conditions, both in terrestrial environments, e.g. plants and fungi (Keppler et al., 2006; Lenhart et al., 2012), as well as in aquatic environments, e.g. phytoplankton and cyanobacteria (Lenhart et al., 2015; Bižić et al., 2020b). Recently, Ernst et al. (2022) proposed a reaction mechanism for CH_4 formation potentially occurring on a cellular level across all living organisms through the interaction of reactive oxygen species with free iron and methylated sulfur and nitrogen compounds in living cells. Furthermore, the authors found that increased levels of oxidative stress enhanced CH_4 production in all of the investigated organisms, providing a possible explanation not only for CH_4 emissions under oxic conditions but also for the large variability of emission rates observed for many organisms in aquatic and terrestrial environments. However, the related $\delta^{13}C$ and $\delta^{2}H$ isotopic patterns of CH_4 produced in the oxic environment remain yet to be clarified.

Aerobic CH_4 oxidation (MOx) as a counteracting mechanism to CH_4 production is usually observed mainly at the oxic-anoxic interface in aquatic systems where high CH_4 concentrations and dissolved oxygen are present. MOx is generally characterized by an increase in $\delta^{13}C$-CH_4 and $\delta^{2}H$-CH_4 values, since methanotrophic bacteria prefer to oxidize the light carbon and hydrogen stable isotopes, leading to a relative enrichment of ^{13}C and ^{2}H in the CH_4 pool (Barker and Fritz, 1981; Whiticar, 1999). In the anoxic sediment, anaerobic oxidation of CH_4 (AOM) through electron acceptors other than oxygen can be observed leading to an enrichment in ^{13}C and ^{2}H of CH_4, however other isotopic effects discussed later might obscure this typical isotope enrichment. AOM coupled to sulfate reduction is a common and widely described process in the ocean, oxidizing >90% of CH_4 produced in oceanic sediment (Knittel and Boetius, 2009). Due to usually low sulfate concentrations in freshwater systems, sulfate-dependent AOM only occurs in some specific lake environments.

Tsunogai et al. (2020) suggested that the relation between the original carbon and hydrogen isotopic composition of CH_4 can be inferred from the relation between $\delta^{13}C$-CH_4 and $\delta^{2}H$-CH_4 values of residual CH_4, irrespective of the isotopic fractionation caused by CH_4 oxidation. Therefore, they introduced a novel stable isotope indicator $\Delta(2,13)$, which corrects for the kinetic isotope fractionation effect associated to oxidation by using the ratio of hydrogen to carbon stable isotopes during microbial oxidation and thus can help in characterizing sources of CH_4 in a system. Through the application of dual stable isotopes and flux measurements, model predictions can be complemented and provide a better comprehension of processes occurring in the system and disentangling production and consumption mechanisms.

So far, application of dual isotope and concentration measurements has only found limited use in aquatic environments and an overview of dual stable isotope characterization of limnic CH_4 processes is missing. Therefore, we analyzed the $\delta^{13}C$-CH_4 and $\delta^{2}H$-CH_4 values as well as CH_4 concentrations in Lake Willersinnweiher - a seasonally stratified, eutrophic lake in southwestern Germany - and furthermore applied the novel $\Delta(2,13)$ indicator. Detailed profiles of the water column and pore water of the sediments were collected during the stratified and non-stratified lake periods in order to gain a better understanding of the CH_4 sources and sinks and the diffusive and ebullitive processes involved in CH_4 cycling of the lake. We aim to isotopically characterize different sources of CH_4 to the lake and thus to disentangle the contribution of these sources to the complex CH_4 cycling at Lake Willersinnweiher both spatially and temporally.

Material and methods

Site description and geochemical characterization

Lake Willersinnweiher is situated in the plain of the Upper Rhine Graben (Germany), northwest of Ludwigshafen (49.499950 °N; 8.397138 °E) and covers an area of 17 ha (Figure 2). It is one of four gravel pit lakes and has neither a surface inflow nor outflow, thereby making inflowing groundwater its main source of water and solutes (Wollschläger et al., 2007). Lake Willersinnweiher is composed of a shallower northeastern basin with a maximum water depth of 14 m and a deeper southwestern basin with a maximum water depth of 20 m. The average water depth in the lake is 8 m (Sandler, 2000).

Geochemically, Lake Willersinnweiher can be characterized as an eutrophic hardwater lake with an average water residence time of 3.7 years and experiences seasonal water stratification during summer (stratification period) (Wollschläger et al., 2007). From November/December to March/April, the water column of Lake Willersinnweiher is fully mixed (mixing period). This leads to fully oxic conditions during the mixing period in the lake with O_2 reaching the upper few millimeters of the sediment (Schröder, 2004). With warming temperatures in spring, thermal stratification starts to build up and reaches a maximum in late summer, leading to the formation of a warm, fully oxygenated epilimnion and the anoxic hypolimnion separated by a thermocline at the upper boundary of the metalimnion and a chemocline/oxycline at the lower boundary of the metalimnion. Chlorophyll-a measurements show a peak in algal activity at the thermocline and at the transition from metalimnion to hypolimnion. As thermal stratification weakens in October due to decreasing temperatures, characteristics of mixing are observed throughout the entire water column reflecting the transition to whole lake circulation prevailing during winter.

Sulfate (SO_4^{2-}) concentrations in the lake are unusually high for a freshwater environment (~2 mmol L^{-1}) and are the result of

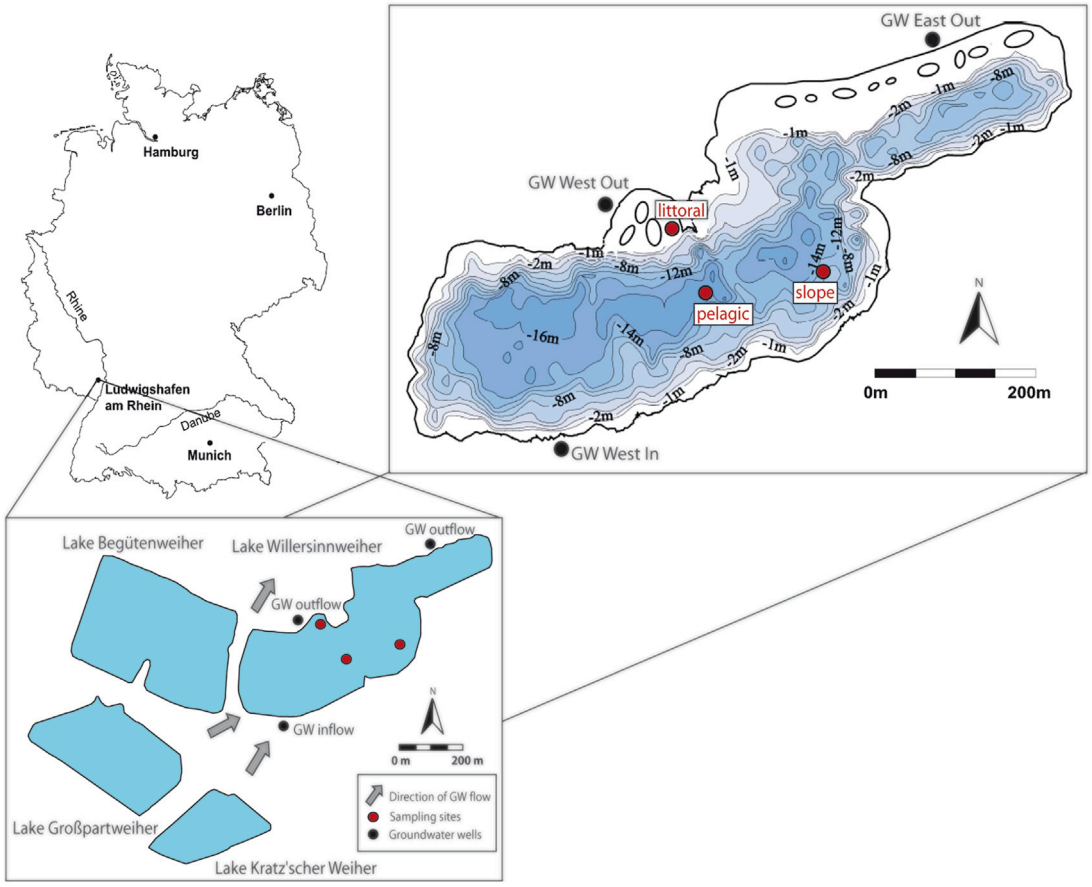


FIGURE 2
Location of Lake Willersinnweiher and the three adjacent lakes in Germany modified after Kleint et al. (2021). Lake sampling sites (pelagic, slope and littoral) and groundwater sampling sites (GW West In, GW West Out, GW East Out) are shown as red and black dots, respectively. Groundwater flow direction was modified after Wollschläger et al. (2007).

sulfate-rich groundwater inflow at the southwestern shore of the lake (Schröder, 2004). Hence, due to high SO_4^{2-} concentrations in Lake Willersinnweiher, the potential for sulfate-dependent AOM is high compared to most other limnic environments. The main process of organic matter turnover in Lake Willersinnweiher is degradation *via* sulfate reduction (Kleint et al., 2021). This results in the production of sulfide (S^{2-}) in the lake sediment, causing diffusive release into the bottom water and consequently leading to euxinic conditions in the hypolimnion during the stratification period. Pyrite oxidation in the Quaternary river sediments of the Rhine cause high SO_4^{2-} concentrations in the catchment upstream of the lake (Schröder, 2004; Isenbeck-Schröter et al., 2016). A detailed review of geochemical processes in the lake water and sediment of Lake Willersinnweiher can be found in a recent study by Kleint et al. (2021).

Eutrophic conditions in the lake are caused by agriculture and land use in the vicinity of the lake, resulting in the release of nutrients into the groundwater, which ultimately reach the lake (Laukenmann, 2002). Groundwater flow in the area of Lake Willersinnweiher is generally directed from southwest to northeast with low flow velocities due to a nearly horizontal groundwater table. Inflowing groundwater at the southwestern shore has already passed at least one of the adjacent smaller lakes upstream of Lake Willersinnweiher (Wollschläger et al., 2007).

Field methods

Sampling of the lake water and sediment was performed at three different sites in the southwestern basin. The pelagic sampling site in the center of the lake has a water depth of 16 m, the slope site is 9 m and the littoral site about 1.5 m deep. Groundwater sampling was carried out at three wells surrounding the lake (*see* Figure 2). The lake water, groundwater and sediment were sampled in July 2020 during

the stratification period and in March 2021 during the mixing period.

Changes in lake water parameters (temperature, pH, dissolved oxygen and chlorophyll-a) with depth were recorded using an Exo1 multiparameter probe (*Xylem Analytics*, Norway). The probe was calibrated for each of the monitored parameters prior to each sampling session.

Samples of the water column were taken at different depth levels using a submersible pump (COMET-Pumpen Systemtechnik GmbH & Co. KG, Germany) and prepared for measurement of CH_4 concentration and isotopic composition using a headspace technique (Kampbell et al., 1989). Samples collected for dissolved ion and dissolved inorganic carbon (DIC) analysis were filtered through a 0.2 µm filter into falcon tubes (Corning, United States). Samples for cation analysis were acidified with 150 µl of 6 M nitric acid.

For pore-water analysis, two sediment cores (core length ~21–29 cm) were taken at each site with a manually operated gravity corer. Pore-water was extracted from one of the cores immediately after sampling in defined intervals using rhizons (*Rhizosphere Research Products*, Netherlands) with a pore-size of 0.15 µm. For measurement of sedimentary CH_4 concentration and its isotopic composition, the sediment of the second core was subsampled in the same intervals as the pore-water by transferring 3 ml of lake sediment with a cut-off plastic syringe into glass vials. The sediment was treated with 5 ml of sodium hydroxide (1 M NaOH) and subsequently the vials were crimped with a lid containing a butyl rubber septum and shaken vigorously to impede any further microbial activity. In the laboratory, the sediment samples were shaken for ~10 min to equilibrate porewater CH_4 and the gas headspace. Afterwards, the headspace was extracted for further analysis. The sediment samples were dried in an oven at 105°C for several days to determine their water content and porosity.

Groundwater wells were sampled using a submersible pump (MP1, Grundfos GMBH, Germany) after pumping until groundwater parameters showed steady values (~30 min). Groundwater samples were prepared in the same way as lake water samples.

Ebullitive CH_4 was sampled for its isotopic composition in November 2020 and September 2021 by deploying an in-house built bubble trap consisting of inverted plastic funnels. A gravity corer was dropped into the sediment in order to release gas bubbles trapped in the sediment. Released gas bubbles were collected with the bubble traps directly under the lake surface and the accumulated gas was analyzed for CH_4 concentration as well as its carbon and hydrogen isotopic composition. The collection of ebullitive CH_4 *via* this method was only performed in November 2020 and September 2021 at the littoral and slope sites, whereas at the pelagic site, it was not possible to collect gas bubbles at the surface after dropping the weight into the sediment.

Gas samples for measurement of δ^{13}C-CH_4 and δ^2H-CH_4 values released to the atmosphere *via* diffusion were taken between March and September 2021 using a floating chamber. The floating chamber consisted of a plastic body with a volume of 8.6 L, two tubes equipped with three-way valves in order to take samples and a floatable ring made from polyethylene that kept the chamber afloat and the edges of the chamber in the water at a depth between 2 and 3 cm. Samples were collected when the chamber was placed in the water and after 15 and 30 min. All gas samples collected from the water column, sediment, groundwater and *via* the floating chamber were analyzed for their CH_4 concentrations, δ^{13}C-CH_4 and δ^2H-CH_4 values in the laboratory.

Laboratory methods

All laboratory analyses were performed at the Institute of Earth Sciences at Heidelberg University, Germany.

δ^{13}C and δ^2H stable isotope analysis of CH_4 and DIC

The natural stable isotopic composition of CH_4 is expressed in the conventional δ-notation in permil (‰) *versus* Vienna Peedee Blemnite (V-PDB) for carbon and Vienna Standard Mean Ocean Water (V-SMOW) for hydrogen. The δ-notation is defined as the relative difference of isotope ratios of a sample compared to the standard substance, hence the $^{13}C/^{12}C$ ratio of a sample compared to V-PDB (δ^{13}C value) and the $^2H/^1H$ ratio of a sample compared to V-SMOW (δ^2H value) (Eq. 1):

$$\delta_S = \frac{R_S - R_{Std}}{R_{Std}} = \frac{R_S}{R_{Std}} - 1 \quad (1)$$

A Delta^{PLUS} XL IRMS (*Thermo Fisher Scientific*, Bremen, Germany) was used to analyze δ^{13}C-CH_4, δ^2H-CH_4 and δ^{13}C-DIC values in the headspace samples. For ^{13}C-DIC analysis, the water sample was first acidified with a few drops of hydrochloric acid (≥25% HCl) in order to transform all DIC to CO_2 prior to sampling the headspace gas. The IRMS was coupled to a HP 6890N GC (*Agilent Technologies*, United States) *via* a GC Combustion III Interface (GC-C; *ThermoFisher Scientific*, United States) with an oxidation reactor at 960°C and a thermo conversion reactor (GC-TC) at 1450°C for carbon and hydrogen stable isotopic analysis, respectively. The GC was equipped with a CP-PoraPLOT Q capillary column (length: 27.5 m; inner diameter 0.25 mm; film thickness: 8 µm; *Varian*, United States). For δ^{13}C-CH_4 and δ^2H-CH_4 measurements, the GC-C/TC-IRMS was linked to a cryogenic pre-concentration unit, whereas for δ^{13}C-DIC an A200S autosampler was applied (*CTC Analytics*, Switzerland).

For CH_4 measurements with the pre-concentration unit, the headspace gas samples were transferred to an evacuated 40 ml sample loop. Methane was trapped on HayeSep D at −125°C, separated from other remaining compounds by GC, and then

introduced into the IRMS system *via* the interface described above. All $\delta^{13}C$ and $\delta^{2}H$ values were corrected using two CH_4 reference standards (*Isometric instruments*, Canada) with $\delta^{13}C$-CH_4 values of −42.32‰ and −66.35‰ and $\delta^{2}H$-CH_4 values of −190.6‰ and −149.9‰, respectively, that were calibrated against International Atomic Energy Agency (IAEA) and National Institute of Standards and Technology (NIST) reference substances. Sample values were normalized according to Paul et al. (2007).

Analysis of CH_4 *via* gas chromatography

Pore-water, water column and groundwater samples were analyzed using a gas chromatograph (14B GC-FID, Shimadzu, Japan) equipped with a flame ionization detector for CH_4 concentrations ranging from 100 ppbv to 50 ppmv and a gas chromatograph (GC-2010 BID, Shimadzu, Japan) equipped with a barrier discharge ionization detector for CH_4 concentrations higher than 50 ppmv. The 14B GC-FID was fitted with a stainless-steel column (length: 2 m; inner diameter: 1/8 inches) filled with a molecular sieve 5A (60–80 mesh; pore-size: 5 Å diameter). The GC oven temperature was isothermal at 125°C. Two reference standards (2.192 ppmv and 9.655 ppmv) were also analyzed for quality control. The GC-2010 BID was fitted with a stainless-steel ShinCarbon ST packed column (80/100 mesh; length: 2 m; diameter: 0.53 mm). The GC oven temperature was programmed to hold at 30°C for 6.5 min, rise to 75°C at a rate of 10°C/min and then to 180°C at a rate of 30°C/min. The GC-2010 BID was calibrated using several standards ranging from 50 ppmv to 97% CH_4. A 1000 ppmv CH_4 standard was analyzed for quality control.

DIC, SO_4^{2-} and S^{2-} analysis

For determination of the dissolved inorganic carbon (DIC) concentration, a TOC-V CPH (*Shimadzu*, Japan) was used. The instrument was calibrated by repeated analysis of an in-house standard solution prior to each measurement. The SO_4^{2-} concentration was analyzed by a Dionex™ ICS-1100 Ion Chromatography System (ThermoFisher Scientific, United States). The measurement precision for each element was <3% and derived from long-term repeated analysis of reference material SPS-NUTR-WW1. The S^{2-} concentration within the water column, pore-water and groundwater samples was determined photometrically (DREL 2800, Hach, United States) immediately after returning to the laboratory from sampling in the field. The samples were prepared using the Spectroquant® Sulfide Reagent Test (Merck, Germany) and measured at a wavelength of 665 nm. The concentrations of cations in the water samples were determined using an Inductively Coupled Plasma Optical Emission Spectrometer (ICP-OES 720, Agilent Technologies, United States). For quality control, the reference material SPS-SW2 was analyzed along with the samples with a measurement precision for each element <2%.

The ionic balance was determined by the sum of major cation and anion concentrations in order to qualitatively control the results of total dissolved ion composition analysis. Results of ionic balance calculations showing a deviation less than 5% displayed good quality control of the measurements.

Application of stable isotopes of methane

Methane formation and consumption processes are associated with a kinetic isotope effect leading to a change in its isotopic composition. The magnitude of this kinetic isotope effect is expressed in the isotope fractionation factor α. Processes of CH_4 formation can be distinguished by determining the apparent carbon isotopic fractionation factor $\alpha_{CH4\text{-}CO2}$ between CH_4 and CO_2 according to Eq. 2:

$$\alpha_{CH4-CO2} = \frac{\delta^{13}C - CO_2 + 1000}{\delta^{13}C - CH_4 + 1000} \quad (2)$$

In order to calculate the $\delta^{13}C$-CO_2 values from $\delta^{13}C$-DIC values the methodology as described by Gonzalez Moguel et al. (2021) was used. Shortly, in a first step the DIC concentrations as well as the pH values in the respective depth were used to calculate the distribution of CO_3^{2-}, HCO_3^- and dissolved CO_2. Using this species distribution and the isotope fractionation factors between gaseous CO_2 and dissolved CO_2, HCO_3^- and CO_3^{2-} as reported by Zhang et al. (1995), dissolved $\delta^{13}C$-CO_2 values were calculated. An $\alpha_{CH4\text{-}CO2}$ between 1.050 and 1.060 indicates acetoclastic methanogenesis whilst between 1.060 and 1.090 shows predominance of hydrogenotrophic methanogenesis (Thottathil and Prairie, 2021).

Isotopic fractionation factors $^{13}\alpha$ for carbon and $^{2}\alpha$ for hydrogen during CH_4 oxidation were determined using the Rayleigh model for closed systems according to Bastviken et al. (2002) (Eq. 3):

$$\ln(1-f) = \frac{[\ln(\delta_P + 1000) - ln(\delta_{Ox} + 1000)]}{[\alpha - 1]} \quad (3)$$

where f is the fraction of CH_4 being oxidized, δ_P the carbon/hydrogen isotopic value of CH_4 in the near-bottom water and the zone of CH_4 production in the sediment, respectively, and δ_{Ox} the carbon/hydrogen isotopic value of CH_4 in the oxidation zone in the aerobic water column or the anoxic sediment, respectively. During CH_4 oxidation, a gradual enrichment of the heavier isotope in the residual CH_4 compared to initial $\delta^{13}C$-CH_4 and $\delta^{2}H$-CH_4 values occurs due to kinetic fractionation. The magnitude of this enrichment is expressed by the isotope fractionation ε (Eq. 4).

$$\varepsilon = \alpha - 1 \quad (4)$$

The Keeling plot method was used to determine the $\delta^{13}C$-CH_4 and $\delta^{2}H$-CH_4 values of CH_4 released from the

water column to the atmosphere (Keeling, 1958). For a detailed description of the Keeling plot method, we refer the reader to Pataki et al. (2003) and Keppler et al. (2016). Briefly, a graphical approach based on the Keeling plot method was used to estimate stable isotope source values of CH_4. Here, the inverse CH_4 mixing ratios of the three individual measurements during sampling of diffusion (*x*-axis) are plotted against their respective $\delta^{13}C\text{-}CH_4$ or $\delta^{2}H\text{-}CH_4$ values measured *via* GC-C-IRMS (*y*-axis). Then a linear regression was employed and the intercept of this linear regression with the *y*-axis reflects the $\delta^{13}C\text{-}CH_4$ or $\delta^{2}H\text{-}CH_4$ source value. Reported errors are based on the standard error of the linear regression.

A novel stable isotope indicator $\Delta(2, 13)$ was applied, which was introduced by Tsunogai et al. (2020), to characterize sources of CH_4 by correcting for changes in the isotopic composition of CH_4 due to the progression of oxidation (Eq. 5).

$$\Delta(2, 13) = \delta^2 H - \Lambda \, x \, \delta^{13} C \tag{5}$$

The Λ value thereby corresponds to the ratio of stable hydrogen vs. stable carbon isotope fractionation ε_H and ε_C, respectively, during microbial CH_4 oxidation (Eq. 6), and thus corrects for the kinetic isotope effect associated with oxidation.

$$\Lambda = \frac{\varepsilon_H}{\varepsilon_C} \tag{6}$$

To calculate the $\Delta(2, 13)$ values, the Λ value for Lake Willersinnweiher needs to be known. Hence, a MOx incubation experiment was performed in the month of July 2021 with water from a depth of 6 m (Supplementary Figure S1). Lake water was filled into acid washed and autoclaved vials and incubated without any further treatment for 20 days in the dark at the lake temperature (15°C). Temporal sampling of CH_4 was performed three times in triplicate during the incubation period *via* the headspace technique (Kampbell et al., 1989). The $\delta^{13}C\text{-}CH_4$ and $\delta^{2}H\text{-}CH_4$ was subsequently analyzed and Λ was then estimated from the slope of the linear regression between the changes in $\delta^{13}C\text{-}CH_4$ and $\delta^{2}H\text{-}CH_4$ values analyzed at the different intervals during the incubation yielding a result of $\Lambda = 9.3 \pm 0.3$ (Supplementary Figure S1). In order to calculate $\Delta(2, 13)$, the concentration-weighted mean isotopic value of the lake water samples was used.

Results

Dissolved CH_4 concentrations and isotopic composition of CH_4 in the sediment

Sediment porewater profiles of CH_4 concentrations at the pelagic site showed an increase with greater sediment depth during the stratification period with maximum concentrations ranging around 1 mmol L^{-1}, which were accompanied by $\delta^{13}C\text{-}CH_4$ values of −80 to −75‰ and $\delta^{2}H\text{-}CH_4$ values of −314 to −328‰ (Figure 3D). A brief shift towards more positive isotopic values of CH_4 within a few centimeters in the upper sediment occurred, where $\delta^{13}C\text{-}CH_4$ values showed a maximum increase of 11‰, however $\delta^{2}H\text{-}CH_4$ data is missing for this depth interval due to problems in collecting samples. The upper sediment core at the pelagic site was characterized by decreasing CH_4 concentrations towards the sediment surface. Sulfate concentrations decreased with depth in the upper few centimeters (3–5 cm) of the sediment while simultaneously a rise in S^{2-} concentrations was recorded in the same depth interval (Figure 3E). Also, DIC concentrations in the pore-water increased with depth and showed lowest $\delta^{13}C$-DIC values of around −14‰ in the upper part and an enrichment in ^{13}C with increasing sediment depth to −9‰ (Figure 3F).

At the slope site an increase in CH_4 concentrations with depth was observed accompanied by $\delta^{13}C\text{-}CH_4$ values varying from −77 to −69‰ and $\delta^{2}H\text{-}CH_4$ values ranging from −338 to −271‰ (Figure 4D). Similarly to the pelagic site, a decrease in SO_4^{2-} and an increase in S^{2-} concentration with depth was recorded (Figure 4E), whereas DIC concentrations increased towards the bottom of the sediment core coinciding with an overall decrease in $\delta^{13}C$-DIC values (Figure 4F).

At the littoral site, profiles of the sediment porewater showed CH_4 concentrations of up to 1.3 mmol L^{-1} (Figure 5D). ^{13}C-enriched CH_4 values compared to the pelagic and slope sites around −58 to −52‰ were found during the stratification period along with $\delta^{2}H\text{-}CH_4$ values ranging from −333 to −256‰ (Figure 5D). Similar to the deeper sites, a shift towards a more positive isotopic signal particularly in $\delta^{2}H\text{-}CH_4$ values was recorded in the upper sediment layers, whereas $\delta^{13}C\text{-}CH_4$ values showed a gradual increase from −57‰ at 3 cm to −51‰ at 9 cm sediment depth.

During the mixing period, porewater CH_4 at the pelagic site showed highly variable $\delta^{13}C\text{-}CH_4$ values throughout the entire sediment core varying from −39 to −75‰, whereas $\delta^{2}H\text{-}CH_4$ showed a rather uniform distribution ranging between −234 and −266‰, respectively (Figures 3J–L). Methane concentrations were at a much higher level than during the stratification period at the pelagic site, increasing to 3.1 mmol L^{-1} in the lower part of the core. In contrast, the littoral sediment recorded significantly lower CH_4 concentrations around 0.3 mmol L^{-1} during the mixing period (Figure 5J). For the slope site no CH_4 data is available for the mixing period. Similar to the stratification period, SO_4^{2-} concentrations decreased in the upper part of the pelagic sediment and stayed at very low levels in the lower part of the core (Figure 3K). No increase in S^{2-} concentration was observed in the sediment of the three investigated sites during the mixing period. DIC concentrations showed a similar trend as during the stratification period and increased with sediment

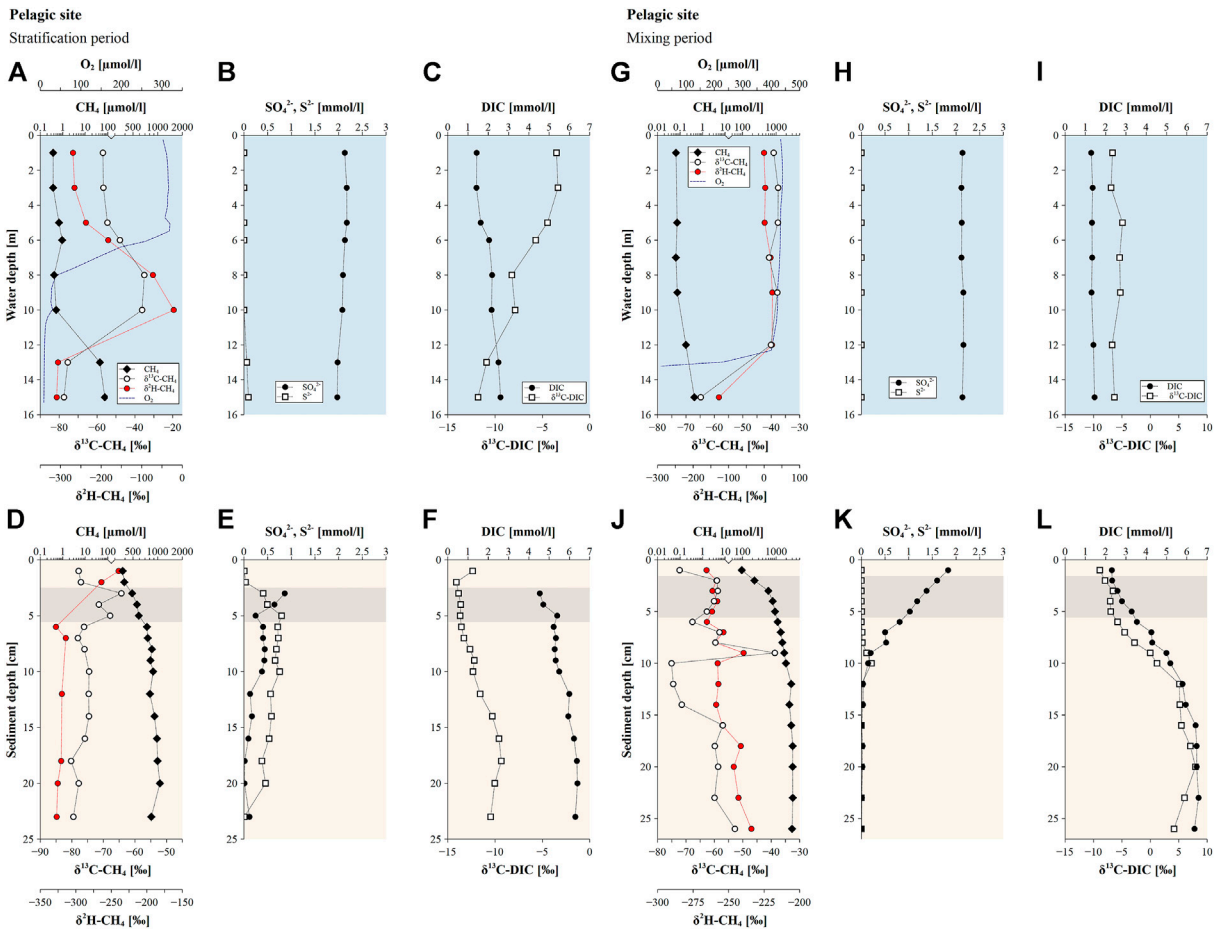


FIGURE 3
Methane (CH_4) concentrations, $\delta^{13}C$-CH_4 and $\delta^{2}H$-CH_4 values along with sulfate, sulfide, dissolved organic carbon (DIC) concentrations and $\delta^{13}C$-DIC values observed at the pelagic site during **(A–F)** the stratification period (July 2020) and **(G–L)** the mixing period (March 2021). Blue graph background colors indicate profiles in the water column, orange background colors show profiles of sediment cores and grey highlighted sediment depths indicate the occurrence of the SMTZ.

depth accompanied by increasing $\delta^{13}C$-DIC values (Figure 3L).

Dissolved CH_4 concentrations and isotopic composition of CH_4 in the water column

In the lake water column, CH_4 concentrations showed a decrease from the hypolimnion towards the surface water accompanied by an enrichment in ^{13}C-CH_4 and ^{2}H-CH_4 during the stratification period (Figure 3A). Methane in the bottom water of Lake Willersinnweiher showed $\delta^{13}C$-CH_4 and $\delta^{2}H$-CH_4 values of −77‰ and −309‰, respectively, and increased to $\delta^{13}C$-CH_4 values of −56‰ and −269‰, respectively, in the surface water layer during the stratification period. Methane concentrations in the surface water ranged from 0.37 to 0.67 µmol L^{-1} with highest concentrations found at the littoral site (Figure 5A). DIC concentrations rose from 1.4 mmol L^{-1} in the surface water to 2.6 mmol L^{-1} in the bottom water, while $\delta^{13}C$-DIC showed a decrease from −4 to −12‰ throughout the water column from top to bottom (Figure 3C).

A pronounced zone of low CH_4 concentrations was observed at the pelagic site during the stratification period in the lower metalimnion, showing a maximum decline in CH_4 of 0.52 µmol L^{-1} from 6 to 8 m water depth (Figure 3A). This minimum in CH_4 concentrations coincided with maximum $\delta^{13}C$-CH_4 and $\delta^{2}H$-CH_4 values in the water column.

A local peak in CH_4 concentrations in the oxic upper water column was found at a water depth of 6 m during the stratification period at the pelagic site, showing a maximum increase of 0.56 µmol L^{-1} compared to surface water CH_4

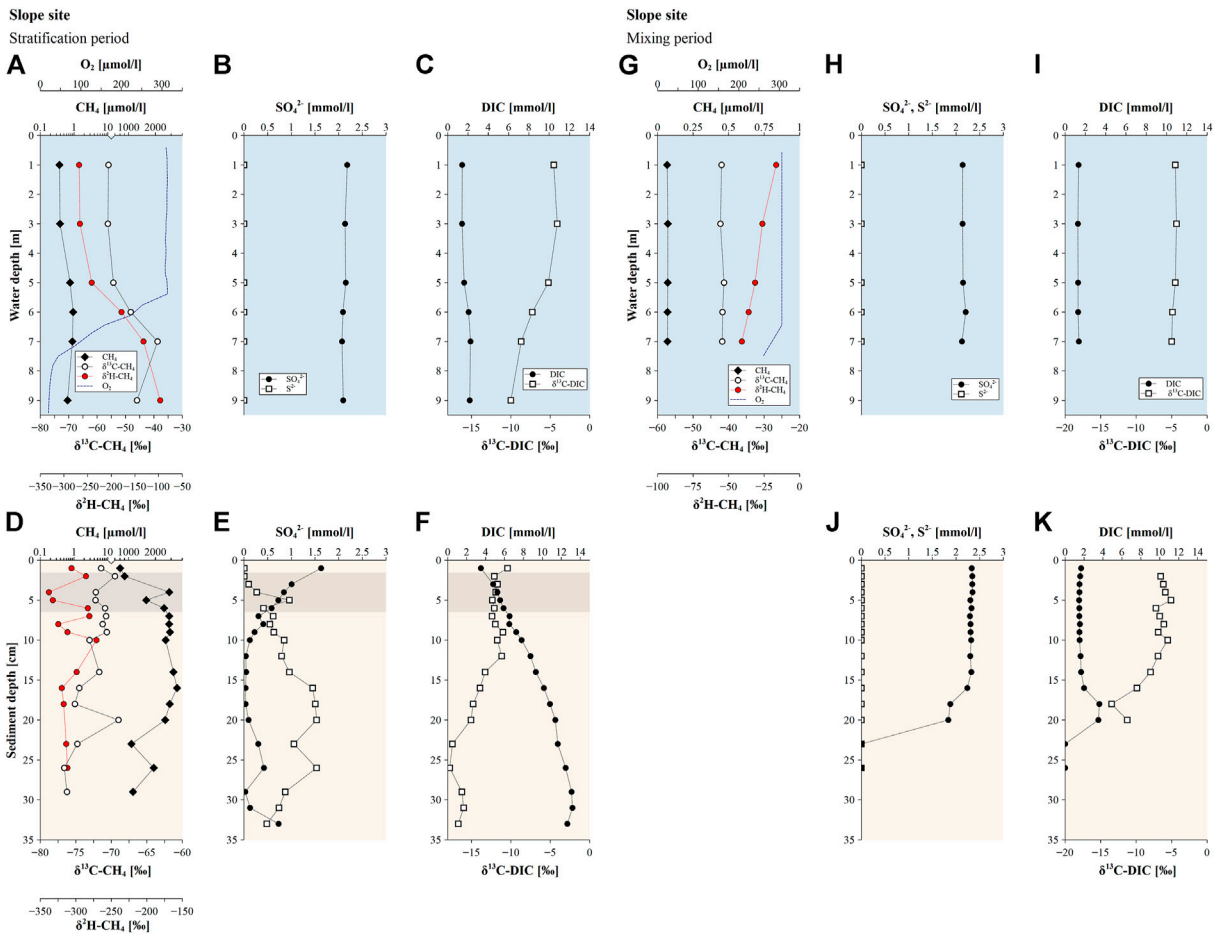


FIGURE 4
Methane (CH_4) concentrations, $\delta^{13}C$-CH_4 and $\delta^{2}H$-CH_4 values along with sulfate, sulfide, dissolved organic carbon (DIC) concentrations and $\delta^{13}C$-DIC values observed at the slope site during **(A–F)** the stratification period (July 2020) and **(G–K)** the mixing period (March 2021). No sediment CH_4 data available for March 2021 at the slope site. Blue background colors indicate profiles in the water column, orange background colors show profiles of sediment cores and grey highlighted sediment depths indicate the occurrence of the SMTZ.

concentrations during the stratification period (Figure 3A). This was accompanied by an increase in the $\delta^{13}C$-CH_4 and $\delta^{2}H$-CH_4 values of about 9‰ and 83‰, respectively, compared to surface water values, resulting in $\delta^{13}C$-CH_4 values of −48‰ and $\delta^{2}H$-CH_4 values of −83‰ at 6 m water depth.

The slope site showed similar surface water CH_4 concentrations (0.37–0.39 µmol L^{-1}) and isotopic compositions ($\delta^{13}C$-CH_4 of -56‰ and $\delta^{2}H$-CH_4 of -268‰) as the pelagic site and recorded an increase in the concentration with depth up to 0.94 µmol L^{-1}, which was accompanied by an increase in $\delta^{13}C$-CH_4 and $\delta^{2}H$-CH_4 values of 17‰ and 136‰, respectively (Figure 4A). The littoral site displayed CH_4 enriched in ^{13}C-CH_4 and ^{2}H-CH_4 ($\delta^{13}C$-CH_4 and $\delta^{2}H$-CH_4 values of −51 and −263‰) in the surface water (Figure 5A) compared to the pelagic and slope sites.

During the mixing period, distinctively lower CH_4 concentrations around 0.07 µmol L^{-1} at the pelagic site throughout almost the entire water column were characterized by $\delta^{13}C$-CH_4 values of −39‰ and +11‰ for $\delta^{2}H$-CH_4 values (Figure 3G). The bottom water showing CH_4 concentrations of 0.4 µmol L^{-1} recorded more negative isotopic values of −65‰ and −127‰. The concentration of DIC in the water column stayed at the same level throughout the water column and the carbon isotopic pattern recorded a minor shift towards slightly more positive values from −7 to −5‰ at intermediate water depths (Figure 3I). While CH_4 concentrations and $\delta^{13}C$-CH_4 values at the slope and littoral site were similar to those found at

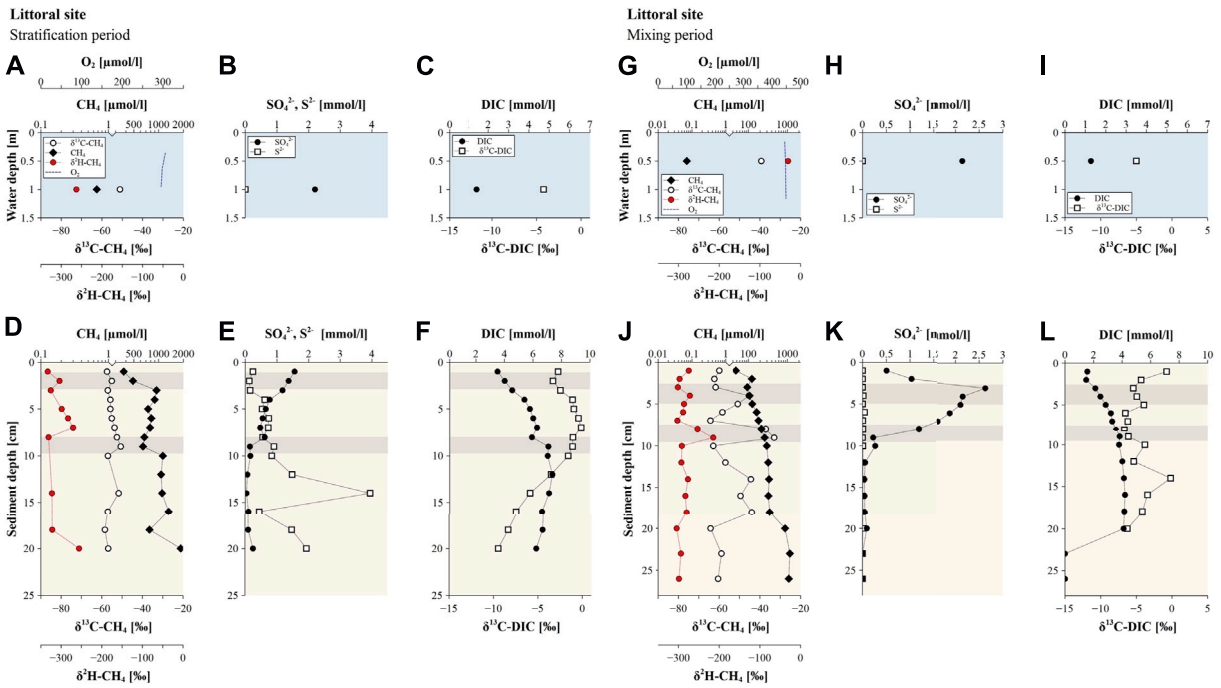


FIGURE 5
Methane (CH_4) concentrations, $\delta^{13}C$-CH_4 and $\delta^{2}H$-CH_4 values along with sulfate, sulfide, dissolved organic carbon (DIC) concentrations and $\delta^{13}C$-DIC values observed at the slope site during **(A–F)** the stratification period (July 2020) and **(G–L)** the mixing period (March 2021). Blue background colors indicate profiles in the water column, orange background colors show profiles of sediment cores and grey highlighted sediment depths indicate the occurrence of the SMTZ.

the pelagic site, $\delta^{2}H$-CH_4 values were more negative varying around −30‰ (Figures 4G, 5G).

Isotopic fractionation factors in the sediment and water column

The apparent carbon isotopic fractionation factor $\alpha_{CH4\text{-}CO2}$ between CH_4 and CO_2 (Eq. 2) in the sediment was determined for sediment depths where CH_4 concentrations were highest, therefore most likely indicating the occurrence of methanogenesis in these depths. The $\alpha_{CH4\text{-}CO2}$ was found to be lowest at the littoral site (1.047) and rose with increasing lake depth (1.058 at the slope site and 1.066 at the pelagic site) during the stratification period (Supplementary Table S1). During the mixing period, the pelagic and littoral site exhibited a $\alpha_{CH4\text{-}CO2}$ of 1.070 and 1.047, respectively.

Isotopic fractionation factors associated with CH_4 oxidation (Eq. 3) were determined in the upper sediment layers of the three sampled locations where a zone of decreasing CH_4 was observed. During the stratification period, isotopic fractionation in these zones was found to range from 1.005 to 1.031 for $^{13}\alpha$ and from 1.042 to 1.124 for $^{2}\alpha$ (Table 1). During the mixing period, $^{13}\alpha$ varied from 1.051 to 1.087 and $^{2}\alpha$ from 1.015 to 1.169. In the water column, an isotopic fractionation factor was determined for the zone between the upper and the lower metalimnion at the pelagic site in which a decrease in CH_4 concentrations was apparent for the stratification period, where an $^{13}\alpha$ of 1.009 and an $^{2}\alpha$ of 1.057 was calculated. An isotopic fractionation factor for the mixing period could not be calculated since no changes in the isotopic composition of

TABLE 1 Isotopic fractionation factors for carbon ($^{13}\alpha$) and hydrogen ($^{2}\alpha$) calculated for the for zones of decreasing CH_4 concentrations in the water column (bottom water to lower metalimnion) and in the upper sediment during the stratification period (July 2020) and for the upper sediment during the mixing period (March 2021).

		$^{13}\alpha$	$^{2}\alpha$
July 2020	Pelagic water column	1.009	1.057
	Pelagic sediment	1.031	—
	Slope sediment	1.005	1.042
	Littoral sediment	1.012	1.124
March 2021	Pelagic sediment	1.051	1.015
	Slope sediment	—	—
	Littoral sediment	1.087	1.169

TABLE 2 δ^{13}C-CH_4 and δ^{2}H-CH_4 values of diffusively released CH_4 from the lake surface water into the atmosphere.

Month	Site	$\delta^{13}C\text{-}CH_{4\ diffusion}$ [‰]	$\delta^{2}H\text{-}CH_{4\ diffusion}$ [‰]
March 2021	pelagic	−37 ± 1	1 ± 34
May 2021		−56 ± 1	—
June 2021		−59 ± 1	−310 ± 8
July 2021		−52 ± 1	−208 ± 3
August 2021		−54 ± 1	−250 ± 25
September 2021		−53 ± 1	−271 ± 4
March 2021	slope	−42 ± 1	26
May 2021		−53 ± 2	—
June 2021		−58 ± 1	−306 ± 13
July 2021		−53 ± 2	−205 ± 14
August 2021		−53 ± 1	—
September 2021		−52 ± 1	−220 ± 11
March 2021	littoral	−36 ± 8	—
May 2021		—	—
June 2021		—	—
July 2021		−53 ± 1	−250 ± 14
August 2021		−51 ± 1	−195 ± 22
September 2021		−55 ± 2	−224 ± 4

SD corresponds to the slope uncertainty in the linear regression of the Keeling plot.

CH_4 was observed in the water column and similar CH_4 concentrations throughout the entire water column were recorded (Figure 3G).

Concentration and isotopic composition of diffusive and ebullitive CH_4

Methane released *via* diffusion from the lake surface water into the atmosphere during the stratification period (May to September) recorded similar $\delta^{13}C\text{-}CH_4$ values at each of the three sampled sites, varying between −52 and −58‰ (Table 2). $\delta^{2}H\text{-}CH_4$ values were more variable ranging from −195 to −310‰ at the different sites, whereby the pelagic and slope site showed in July the most positive values during the stratification period (−208 ± 3 and −205 ± 14‰, respectively) and the littoral site in August (−195 ± 22‰). During the mixing period, CH_4 emitted from the lake was considerably enriched in the heavier isotopes at all investigated sites compared to the stratification period. $\delta^{13}C\text{-}CH_4$ values ranged from −36 to −42‰ and $\delta^{2}H\text{-}CH_4$ values from 1 to 26‰.

The concentrations and isotopic composition of ebullitive CH_4 were analyzed for the littoral and slope site of the lake in November 2020 and September 2021 (Supplementary Table S2). Ebullitive CH_4 was not collected for analysis in July 2020 and March 2021 due to logistical reasons. Nevertheless, the stratified lake period is represented by the data from September 2021, whereas the mixing period is represented by the data from November 2020.

In September during thermal stratification, CH_4 concentrations in gas bubbles in the littoral area reached 80.8 ± 4.5%. In November, CH_4 concentrations of ebullitive CH_4 were in the range of 62.1 ± 7.4% and 66.8 ± 3.2% at the littoral and slope site, respectively. $\delta^{13}C\text{-}CH_4$ values at the littoral site were more negative in September compared to November with −58 ± 1‰ and −50 ± 12‰, respectively. In contrast, $\delta^{2}H\text{-}CH_4$ values in September and November at the littoral site were very similar with −323 ± 3‰ and −326 ± 4‰. At the slope site, $\delta^{13}C\text{-}CH_4$ values were more negative compared to the littoral site with −64 ± 11‰, but $\delta^{2}H\text{-}CH_4$ values were in a similar range compared to the littoral site with values of −318 ± 1‰.

Groundwater methane

Groundwater in the area of Lake Willersinnweiher showed highly variable CH_4 concentrations, $\delta^{13}C\text{-}CH_4$ and $\delta^{2}H\text{-}CH_4$ values and was strongly enriched in $^{2}H\text{-}CH_4$ and $^{13}C\text{-}CH_4$ (Table 3). During the stratification period, inflowing groundwater yielded a CH_4 concentration of 1.01 μmol L^{-1} with an isotopic composition enriched in ^{13}C and ^{2}H ($\delta^{13}C\text{-}CH_4$ value of −24‰ and $\delta^{2}H\text{-}CH_4$ value of +106‰). Outflowing groundwater of the southwestern basin showed slightly lower CH_4 concentrations of 0.95 μmol L^{-1} along with $\delta^{13}C\text{-}CH_4$ and $\delta^{2}H\text{-}CH_4$ values of +18‰ and +582‰, respectively. CH_4 concentrations of groundwater flowing out of the northeastern basin were 0.77 μmol L^{-1} during the

TABLE 3 Methane concentration and its stable isotopic composition of the three different groundwater wells during the stratification period (July 2020) and the mixing period (March 2021).

	CH_4 [µmol l^{-1}]	$\delta^{13}C$ [‰]	$\delta^{2}H$ [‰]
July 2020			
GW inflow SW Basin	1.01	−24	+106
GW outflow SW Basin	0.95	+18	+582
GW outflow NE Basin	0.77	−50	−187
March 2021			
GW inflow SW Basin	1.97	−19	—
GW outflow SW Basin	2.71	−37	+24
GW outflow NE Basin	30.89	−58	−245

stratification period accompanied by $\delta^{13}C$-CH_4 values of −50‰ and $\delta^{2}H$-CH_4 values of −187‰. Between the two outflowing groundwater wells in the western and eastern part of Lake Willersinnweiher a disparity in CH_4 concentrations and stable isotope values is worth noticing. This observation is probably caused as outflowing groundwater in the western part consists of a mixture of outflowing groundwater from the lake and groundwater with properties similar to inflowing groundwater, that also passed subjacent lakes, due to its location and groundwater flow direction (*see* Figure 2). During the mixing period, groundwater at the three wells showed CH_4 concentrations of 1.97 and 2.71 µmol L^{-1} for inflowing and outflowing groundwater of the southwestern basin, respectively, and even 30.89 µmol L^{-1} for groundwater flowing out of the northeastern basin. Groundwater outflow of the southwestern basin showed a $\delta^{13}C$-CH_4 value of −37‰ and a $\delta^{2}H$-CH_4 value of +24‰. The isotopic composition of groundwater at the other two groundwater wells was in the range of values reported during the stratification period (Table 3).

Discussion

Methanogenesis in the sediment

Methanogenesis is the last step in the microbial degradation of organic matter and is performed by methanogenic archaea in the anaerobic environment (Conrad, 2005). However, in presence of other electron donors (such as SO_4^{2-}), organic matter degradation *via* sulfate reduction is favored over methanogenesis. This is most likely the case for Lake Willersinnweiher, where sulfate-reducing bacteria are believed to thermodynamically outcompete methanogenic archaea for available carbon compounds and H_2 in the upper sediment due to high SO_4^{2-} concentrations in the lake water (Kleint et al., 2021). In aquatic systems with high SO_4^{2-} concentrations, anaerobic methanogenesis is therefore restricted to greater sediment depths, where SO_4^{2-} concentrations are low (Holmer and Storkholm, 2001; Reeburgh, 2007; Schubert et al., 2011). Methanogenesis in Lake Willersinnweiher is suggested to occur in zones of the deeper sediment where CH_4 in the sediment accumulated (Figures 3D, 4D, 5D). Hydrogenotrophic methanogenesis as the dominant process of CH_4 production in the sediment during the stratification period was indicated by relatively negative $\delta^{13}C$-CH_4 values (ranging from around −80 to −75‰) observed in the lower sediment of the pelagic and slope site, where maximum CH_4 concentrations were recorded (Figure 3D). Whereas the associated $\delta^{2}H$-CH_4 values of around −321 to −246‰ were rather negative for this type of methanogenesis (Whiticar, 1999). However, $\delta^{2}H$-CH_4 values in this environment are likely mostly linked to the $\delta^{2}H$ value of the source water (Waldron et al., 1999; Douglas et al., 2021) and seem to be less indicative of the methanogenic pathway compared to $\delta^{13}C$-CH_4 values as $\delta^{2}H$-CH_4 values are less studied and influenced by more factors. Above that a mixing of the hydrogenotrophic and acetoclastic pathway is possible (Sugimoto and Wada, 1995; Walter et al., 2008). During methanogenesis, hydrogen originating from ambient water is incorporated into the CH_4 molecule, thus $\delta^{2}H$-CH_4 values are mostly dependent on the hydrogen isotopic composition of the water (Sugimoto and Wada, 1995). Plotting sedimentary $\delta^{13}C$-CH_4 values against $\delta^{2}H$-CH_4 values and classifying them after Whiticar (2020) indicated an overlap of the two different methanogenic pathways at the pelagic and slope site (Figure 6). For the littoral site, a dominance of acetoclastic methanogenesis seems to be implied due to less negative $\delta^{13}C$-CH_4 values compared to the pelagic and slope site.

Furthermore, based on the carbon isotopic shift between CH_4 and CO_2, we determined apparent carbon isotopic fractionation factors associated to anaerobic methanogenesis, which is an indicator to distinguish between the hydrogenotrophic and acetoclastic pathway. At the pelagic site, an $\alpha_{CH4\text{-}CO2}$ of 1.066 supports the dominance of hydrogenotrophic methanogenesis during the stratification period (Supplementary Table S1). The $\alpha_{CH4\text{-}CO2}$ decreased towards the littoral site, indicating an increasing contribution of the acetoclastic pathway. Overlapping characteristics were hence especially visible at the slope site, where $\delta^{13}C$-CH_4 values around −75‰ point to hydrogenotrophic methanogenesis whereas the calculated $\alpha_{CH4\text{-}CO2}$ of 1.058 is representative for acetoclastic CH_4 formation. The proposed increasing dominance of acetoclastic methanogenesis from the pelagic towards the littoral area is based on the isotopic values of sedimentary CH_4 observed at Lake Willersinnweiher and might be coupled to changes in sediment temperatures and differences in organic matter availability with varying lake depth (Thottathil and Prairie, 2021). However, further investigations are needed to gain more insight into the occurrence and distribution of

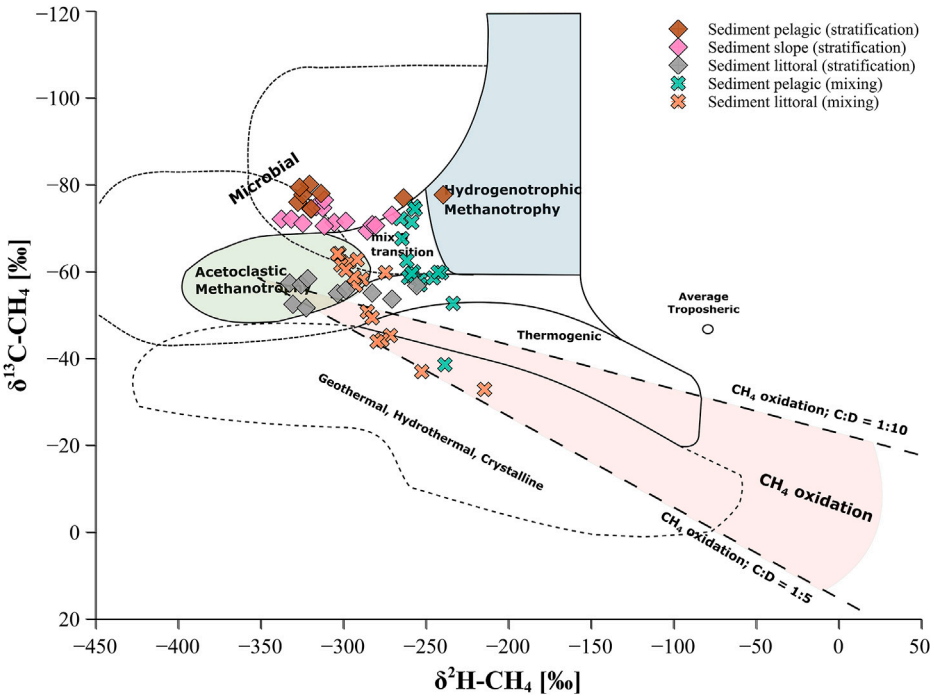


FIGURE 6
2-dimensional isotope plot of sedimentary CH_4 data from the stratification and mixing period implemented into the classification of methanogenic pathways modified after (Whiticar, (2020). The dotted lines represent the range of ratios of ^{13}C and ^{2}H (C:D) enrichment during anaerobic CH_4 oxidation as reported by Martens et al. (1999), Holler et al. (2009) and Rasigraf et al. (2012).

the different methanogenic pathways in the sediment of Lake Willersinnweiher.

During the mixing period, the observed $\alpha_{CH4\text{-}CO2}$ of 1.070 for the pelagic site (Supplementary Table S1) was higher than during the stratification period suggesting a higher dominance of hydrogenotrophic CH_4 formation. This might possibly reflect the limited availability of fresh organic material in the lake. However, higher sedimentary CH_4 concentrations found at the pelagic site during the mixing period compared to the stratification period (Figures 3D,J) seemed to contradict the expected decrease of CH_4 concentrations due to lower primary production in winter and therefore reduced organic matter availability. This indicated that processes other than microbial activity in the sediment must have contributed to the high observed sedimentary CH_4 concentrations and isotopic pattern in the sediment at the pelagic site and highlights the complex interaction of the occurring processes influencing the sedimentary CH_4 cycle. However, we suggest that infiltrating groundwater as a potential CH_4 source might also play an important role at Lake Willersinnweiher since it yielded very high CH_4 concentrations characterized by extremely positive isotopic $\delta^{13}C\text{-}CH_4$ and $\delta^{2}H\text{-}CH_4$ values both for inflowing and outflowing groundwater (Table 3). Mixing of groundwater and lake sediment CH_4 might potentially skew the calculated fractionation factors for the mixing period, hence these have to be considered with caution and can only be used as a preliminary indicator for the methanogenic pathway.

Anaerobic methane oxidation in the sediment

The shift to more positive $\delta^{13}C\text{-}CH_4$ and $\delta^{2}H\text{-}CH_4$ values partially observed in the upper sediment layers during the stratification period was most likely caused by the anaerobic oxidation of CH_4 coupled to SO_4^{2-}reduction. The occurrence of sulfate-dependent AOM in Lake Willersinnweiher was described in a recent study by Kleint et al. (2021) and we therefore refer the reader to this study for more detailed discussion on this process at Lake Willersinnweiher. Here we want to give a brief summary on sulfate-dependent AOM at Lake Willersinnweiher and discuss the associated isotopic effects of this process. In the sediment, upward rising CH_4 and downward diffusing SO_4^{2-} meet in the so-called sulfate-methane transition zone (SMTZ), where anaerobic methanotrophic archaea in syntrophic association with sulfate-reducing bacteria are able to reverse methanogenesis and oxidize CH_4 using SO_4^{2-} (Boetius et al., 2000). In most freshwater environments, low SO_4^{2-}

concentrations usually preclude sulfate-dependent AOM, whereas in the oceans, sulfate-dependent CH_4 oxidation is a widely described and common process due to high SO_4^{2-} concentrations in the ocean water (Knittel and Boetius, 2009). Since Lake Willersinnweiher shows high SO_4^{2-} concentrations, compared to other lakes, as a result of sulfate-rich groundwater input, sulfate-dependent AOM is possible.

Indicative of AOM might furthermore be the observation of DIC enriched in ^{12}C in the upper lake sediment compared to the lower sediment during the stratification period since ^{12}C-CH_4 is preferably oxidized by the microorganisms, thereby providing HCO_3^- relatively enriched in ^{12}C to the sedimentary DIC pool (Schubert et al., 2011). With increasing sediment depth, microbial hydrogenotrophic CH_4 production caused a depletion in isotopically light DIC, thus leading to DIC enriched in ^{13}C-DIC in the sediment pore-water.

Zones in the lake sediment where sulfate-dependent AOM was presumed to take place were not always characterized by a clear shift towards less negative $\delta^{13}C$-CH_4 and δ^2H-CH_4 values (Figures 3J, 5D), as one might typically expect for CH_4 oxidation or restrained to a few centimeters within the upper sediment at the investigated sites of Lake Willersinnweiher. Plotting sedimentary $\delta^{13}C$-CH_4 values against δ^2H-CH_4 values shows a progression of the littoral sediment data of the mixing period within a predicted CH_4 oxidation line between a ratio of C:D of 1: 5 and 1:10 (e.g., Wang et al., 2016; Whiticar, 2020), referring to an enrichment of CH_4 in hydrogen isotopes 5–10 times more than in carbon isotopes during AOM (Figure 6). This observation is in good accordance with previously reported C:D ratios during AOM ranging between 6.4 and 10 (Martens et al., 1999; Holler et al., 2009; Feisthauer et al., 2011; Rasigraf et al., 2012). However, this trend was less pronounced at the other two sites, limiting the use of carbon and hydrogen stable isotopes of CH_4 to characterize AOM in the lake sediment. Nevertheless, carbon and hydrogen isotopic fractionation factors $^{13}\alpha$ and $^2\alpha$ were also determined to identify the occurrence of potential AOM in the respective zones of the sediment. The calculated carbon isotopic fractionation factors $^{13}\alpha$ values for the observed enrichment in ^{13}C-CH_4 and ^2H-CH_4 and associated with AOM in the sediment (1.002–1.019, Table 1) were on the lower end of $^{13}\alpha$ values determined for AOM in marine and brackish environments and in laboratory studies (1.009–1.039, Whiticar and Faber, 1986; Holler et al., 2009; Knittel and Boetius, 2009). The hydrogen isotopic fractionation factors $^2\alpha$ (1.033–1.057) determined for Lake Willersinnweiher were substantially lower than $^2\alpha$ modelled for aquatic environments and found in *in vitro* experiments (1.109–1.315, Whiticar and Faber, 1986; Alperin et al., 1988; Holler et al., 2009). It is important to mention that natural systems might differ significantly from modelled conditions and *in vitro* experiments, thus leading to discrepancies in isotopic fraction factors. Furthermore, it must be noted that isotopic fractionation factors of AOM determined from *in situ* isotopic signatures, as in the case of Lake Willersinnweiher, have to be considered with caution since AOM and methanogenesis might overlap in the sediment and carbon isotope equilibrium effects caused by forward and backward AOM influence the isotopic composition of the CH_4 pool in opposite ways (Holler et al., 2009; Yoshinaga et al., 2014; Chang et al., 2019). A study by Wegener et al. (2021) furthermore showed, that the accumulation of ^{13}C and ^2H-depleted CH_4 in zones of AOM was driven under low sulfate conditions (similar to SO_4^{2-} concentrations found in lake Willersinnweiher) because of intracellular reactions associated with the enzymatic AOM mechanism. They found that the reactions in the enzymatic AOM pathway became more reversible and thus closer to equilibrium at low SO_4^{2-} conditions driving the formation of ^{13}C and ^2H depleted CH_4. The lack of a clear enrichment in the heavier isotopes of CH_4 in sediment zones where AOM is presumed to occur in Lake Willersinnweiher might therefore be resulting from the above-mentioned isotopic effects.

Due to AOM in the lake sediment, the diffusive release of CH_4 at the sediment-water interface is reduced in Lake Willersinnweiher (Kleint et al., 2021). Our concentration depth profiles of CH_4 in the sediment show a decreasing gradient towards the sediment water interface, caused by CH_4 diffusion into the bottom water and most likely AOM. Significant decreases in sedimentary CH_4 concentrations observed particularly at the slope and littoral site were suggested to be related to AOM as they coincided with an enrichment in ^{13}C-CH_4 and ^2H-CH_4 (Figures 4D, 5D). Methane diffusion from the sediment into the bottom water significantly elevated hypolimnic CH_4 concentrations (up to 74 µmol L^{-1} at the pelagic site). The negative isotope values of hypolimnic CH_4 of −77‰ and −309‰ for $\delta^{13}C$-CH_4 and δ^2H-CH_4 values, respectively, during the stratification period (Figure 3A) fell well within the range of $\delta^{13}C$-CH_4 and δ^2H-CH_4 values found in sediment depths where anaerobic methanogenesis is presumed to occur, hence suggesting anaerobic CH_4 production in the sediment as its origin.

During the mixing period, shifts towards more positive $\delta^{13}C$-CH_4 and δ^2H-CH_4 values in the upper sediment at the pelagic and littoral site suggested the occurence of AOM in the sediment (Figures 3J, 5J). Furthermore, decreasing CH_4 concentrations and increasing SO_4^{2-} concentrations towards the sediment surface might be indicative of the occurrence of sulfate-dependent AOM (Figures 3J,K, 5J,K). The apparent lack of S^{2-} accumulation in the sediment might be caused by re-oxidation of sulfide to sulfate *via* manganese oxides in the sediment pore-water as described by Kleint et al. (2021). The determined fractionation factors associated to AOM during the mixing period (1.051–1.087 for $^{13}\alpha$ and 1.015–1.169 for $^2\alpha$, Table 1) do not reflect typical fractionation factors for AOM, however as discussed above, these fractionation factors have to be considered cautiously as different isotopic effects can influence the isotopic composition of CH_4 in the SMTZ. Furthermore, a

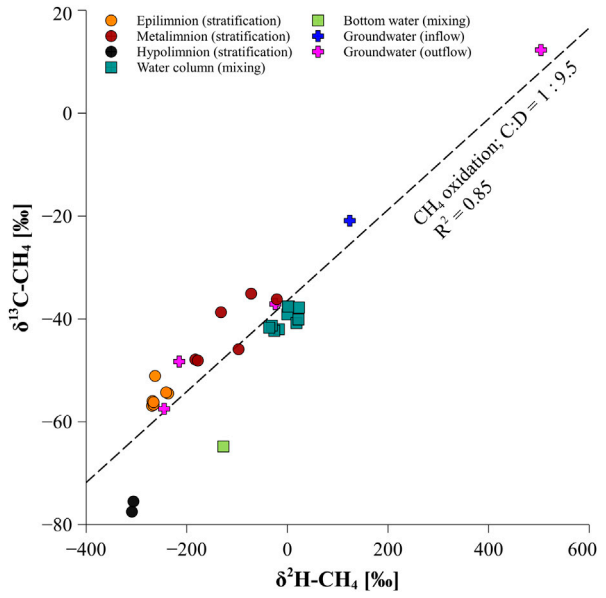


FIGURE 7
2-dimensional isotope plot of water column and groundwater CH_4 data from the stratification and mixing period. The dotted line represents the ratio of ^{13}C to ^{2}H (C:D) enrichment during CH_4 oxidation in the water column and groundwater at lake Willersinnweiher.

mixture with other CH_4 sources, e.g., groundwater CH_4 input, might affect the carbon and hydrogen isotopic composition of sedimentary CH_4 since mixing of groundwater and sedimentary CH_4 might lead to an increase in sedimentary $\delta^{13}C$-CH_4 and $\delta^{2}H$-CH_4 values due to the very enriched ^{13}C and ^{2}H isotopic composition of groundwater CH_4. AOM most likely reduced the release of CH_4 at the sediment-water interface, however diffusion from the uppermost sediment layers into the bottom water layer caused elevated CH_4 concentrations in the bottom water.

Aerobic methane oxidation in the water column

During the stratification period, a strong increase in the isotopic composition of CH_4 ($\delta^{13}C$-CH_4 values of −35‰ and $\delta^{2}H$-CH_4 values of −72‰, Figure 3A) along with a decrease in CH_4 concentrations at the bottom of the oxycline in the water column compared to surface water CH_4 suggested MOx of sedimentary released CH_4. The enrichment in the $\delta^{13}C$-CH_4 and $\delta^{2}H$-CH_4 signal is caused by the preference of methanotrophic organisms to metabolize light atoms ^{12}C and ^{1}H of CH_4, leading to an enrichment in ^{13}C-CH_4 and ^{2}H-CH_4 of the remaining CH_4 (Silverman and Oyama, 1968; Barker and Fritz, 1981; Coleman et al., 1981). From the 2-dimensional isotope plot it can be inferred that MOx occurs in the metalimnion during the stratification period since the metalimnic stable isotope data are distributed along a gradient showing a stronger enrichment of ^{2}H compared to ^{13}C during MOx with a C:D ratio of 9.5 (Figure 7). This observation fits well within similar reported C:D ratios during MOx ranging between 5.9 and 14.9 (Coleman et al., 1988; Kinnaman et al., 2007; Powelson et al., 2007; Feisthauer et al., 2011; Wang et al., 2016). In comparison, epilimnic water samples plot did not show this progression, hence implying that $\delta^{13}C$-CH_4 and $\delta^{2}H$-CH_4 values there are most likely not or less affected by MOx.

The carbon isotopic fractionation factor $^{13}\alpha$ of 1.009 determined for the observed enrichment in Lake Willersinnweiher furthermore suggested the occurrence of MOx at this depth as it is in the range of $^{13}\alpha$ determined for MOx in experimental studies (1.003–1.039; Templeton et al., 2006). The estimated $^{2}\alpha$ of 1.057 on the other hand is substantially lower than values determined for MOx in closed cultures (1.103–1.325; Alperin et al., 1988). However, a higher $^{2}\alpha$ than $^{13}\alpha$ (factor of ~9.5) at Lake Willersinnweiher confirms the larger isotopic fractionation generally observed for stable hydrogen isotopes compared to stable carbon isotopes during microbial oxidation. The isotopic partitioning between hydrogen isotopes is greater than between carbon isotopes because of a larger mass difference between ^{2}H and ^{1}H than between ^{13}C and ^{12}C (e.g., Wang et al., 2016). This leads to a stronger enrichment in hydrogen isotopes than in carbon isotopes during oxidation.

The zone of MOx at the oxic-anoxic interface in Lake Willersinnweiher during the stratification period acts as a barrier and effectively limits the release of sedimentary produced CH_4 into the surface mixed water layer to minimum concentrations (Kleint et al., 2021). The occurrence of MOx at the bottom of the oxycline indicated by maximum $\delta^{13}C$-CH_4 and $\delta^{2}H$-CH_4 values suggests that CH_4 oxidizing bacteria are most active at low O_2 levels and their presence is restricted as O_2 concentrations rise in the upper water body (Schubert et al., 2010; Thottathil et al., 2019). At the littoral site, the isotopic composition of the water column agrees well with sedimentary $\delta^{13}C$-CH_4 and $\delta^{2}H$-CH_4 values, suggesting that MOx did not occur here. The apparent absence of MOx at the littoral sampling site might be caused by fully oxygenated conditions in the shallow water column. Another controlling factor of MOx might be the availability of light in the photic zone of the water column. Murase and Sugimoto (2005) showed that MOx was inhibited under light conditions, whereas a linkage between a light driven supply of O_2 through photosynthesis and MOx was found in a study by Oswald et al. (2015), implying that MOx is dependent on light availability.

MOx leads to the formation of CO_2, which is converted to HCO_3^- according to the bicarbonate buffer system due to a prevailing pH of 8.5–7.3 in the water column of the lake. This contributed to an increase in DIC concentrations in the metalimnion, which was accompanied by decreasing $\delta^{13}C$-DIC

values (Figure 3C) caused by CH_4 oxidizing organisms and their preference for $^{12}CH_4$ consumption leading to the production of ^{12}C enriched DIC. However, increased DIC concentrations might also originate from the degradation of organic matter. Organic material is generally characterized by relatively negative $\delta^{13}C$ values, consequently causing the trend to more negative $\delta^{13}C$-DIC values with depth as degradation proceeds and inorganic carbon is released from the sediment into the water column.

During the mixing period, constant CH_4 concentrations as well as similar $\delta^{13}C$-CH_4 and $\delta^{2}H$-CH_4 values in the water column, except between a depth of 12 and 15 m, where stable isotope values of CH_4 became more enriched, did not suggest MOx (Figure 3G). Since almost the entire water column was fully oxygenated, this might have prevented efficient MOx as methane oxidizing bacteria were found to be sensitive to high O_2 concentrations (Thottathil et al., 2019). However, MOx could still have occurred in the lake water column in the absence of O_2, $\delta^{13}C$-CH_4 and $\delta^{2}H$-CH_4 gradients due to mixing and thus might contribute to CH_4 enriched in ^{13}C and ^{2}H during the mixing period compared to the stratification period. Plotting $\delta^{13}C$-CH_4 values against $\delta^{2}H$-CH_4 values further suggests the occurrence of MOx during the mixing period as the data points show a distribution along the gradient of isotope enrichment (Figure 7). Beyond this the enrichment in ^{13}C and ^{2}H of lake water CH_4 during the mixing period ($\delta^{13}C$-CH_4 values of −39‰ and $\delta^{2}H$-CH_4 values of +11‰) compared to lake water values from the stratification period, the enrichement might also have originated from the input of groundwater CH_4 since inflowing and outflowing groundwater recorded extremely positive $\delta^{13}C$-CH_4 and $\delta^{2}H$-CH_4 values (Table 3). Groundwater CH_4 might therefore have constituted an important source to lake water CH_4 during the mixing period and contributed to the shift towards more positive $\delta^{13}C$-CH_4 and $\delta^{2}H$-CH_4 values of lake water during the mixing period, when CH_4 concentrations in the water column were much lower compared to the stratification period and the relative importance of groundwater on lake water CH_4 thus increases.

Methane supersaturation in the surface water layer

During the stratification period, fully oxygenated conditions in the epilimnion of Lake Willersinnweiher likely prevented efficient MOx in the upper water column, thus leading to the accumulation of CH_4 in the surface mixed water layer. The surface water of Lake Willersinnweiher with CH_4 concentrations ranging from 0.3 to 0.6 µmol L^{-1} during the stratification period was oversaturated compared to the atmosphere, since water in equilibrium with the atmosphere shows CH_4 concentrations of ~3 nmol L^{-1} (Wiesenburg and Guinasso, 1979).

During the stratification period, the $\delta^{13}C$-CH_4 and $\delta^{2}H$-CH_4 values of CH_4 in the pelagic surface water were around −56‰ and −270‰, respectively. These values were significantly different from hypolimnic $\delta^{13}C$-CH_4 values of −77‰ and $\delta^{2}H$-CH_4 values −323‰. This difference raises the question for the source of CH_4 supersaturation in the surface water layer (Figure 8A). The isotopic signatures of surface water CH_4 is likely altered by the mixing of different CH_4 pools, e.g., through littoral and vertical input, ebullition, groundwater interactions and internal oxic CH_4 production (e.g., Tang et al., 2016; Hartmann et al., 2020).

Vertical input of CH_4 from the sediment is strongly reduced in the lower metalimnion through MOx (Figure 3A). However, sedimentary CH_4 might still migrate into the upper water layer and become enriched in ^{13}C and ^{2}H through MOx, resulting in less negative surface water $\delta^{13}C$-CH_4 and $\delta^{2}H$-CH_4 values compared to hypolimnic values. Transport of CH_4 from the littoral sediment to pelagic lake areas comprises an important source especially in small lakes with organic rich littoral zones, where CH_4 deriving from the sediment can be distributed in the surface water layer of the entire lake through turbulences, e.g., induced by wind activity (Tang et al., 2014). As thermal stratification builds up in the Lake Willersinnweiher, around 0.3 µmol L^{-1} higher CH_4 concentrations can be observed in the littoral area of Lake Willersinnweiher than in the epilimnion of the pelagic and slope sites during the stratification period. Sediments in the littoral zone are usually not isolated through thermal stratification from the overlying water column compared to pelagic sites, thus often resulting in higher CH_4 concentrations in littoral waters (Loken et al., 2019). Higher sediment temperatures and disruption by waves fuel CH_4 production and release in the littoral zone during summer (Hofmann et al., 2010). A similar pattern of spatiotemporal CH_4 distribution was observed in other lakes and highlights the importance of the littoral area considering CH_4 emission to the atmosphere (Wang et al., 2006; Tsunogai et al., 2020). During maximum stratification, the isotopic CH_4 pattern of littoral surface water showed a $\delta^{13}C$-CH_4 value of −51‰ which is different from the values observed for the pelagic and slope sites ($\delta^{13}C$-CH_4 value of −56‰), whereas $\delta^{2}H$-CH_4 values were rather similar around −265‰, suggesting that sources of CH_4 in the surface water might differ between the littoral and deeper sites (Figure 8A). However, it is possible that mixing of littoral and vertical CH_4 input caused the observed more negative isotopic values of surface water CH_4 in the pelagic zone of the lake compared to the littoral area. A further potential source of CH_4 in the surface water layer of aquatic system is oxic CH_4 production despite the long-standing paradigm defining methanogenesis as a process occurring only under anoxic conditions (Grossart et al., 2011; Tang et al., 2014, 2016; Donis et al., 2017; Günthel et al., 2019; Hartmann et al., 2020;

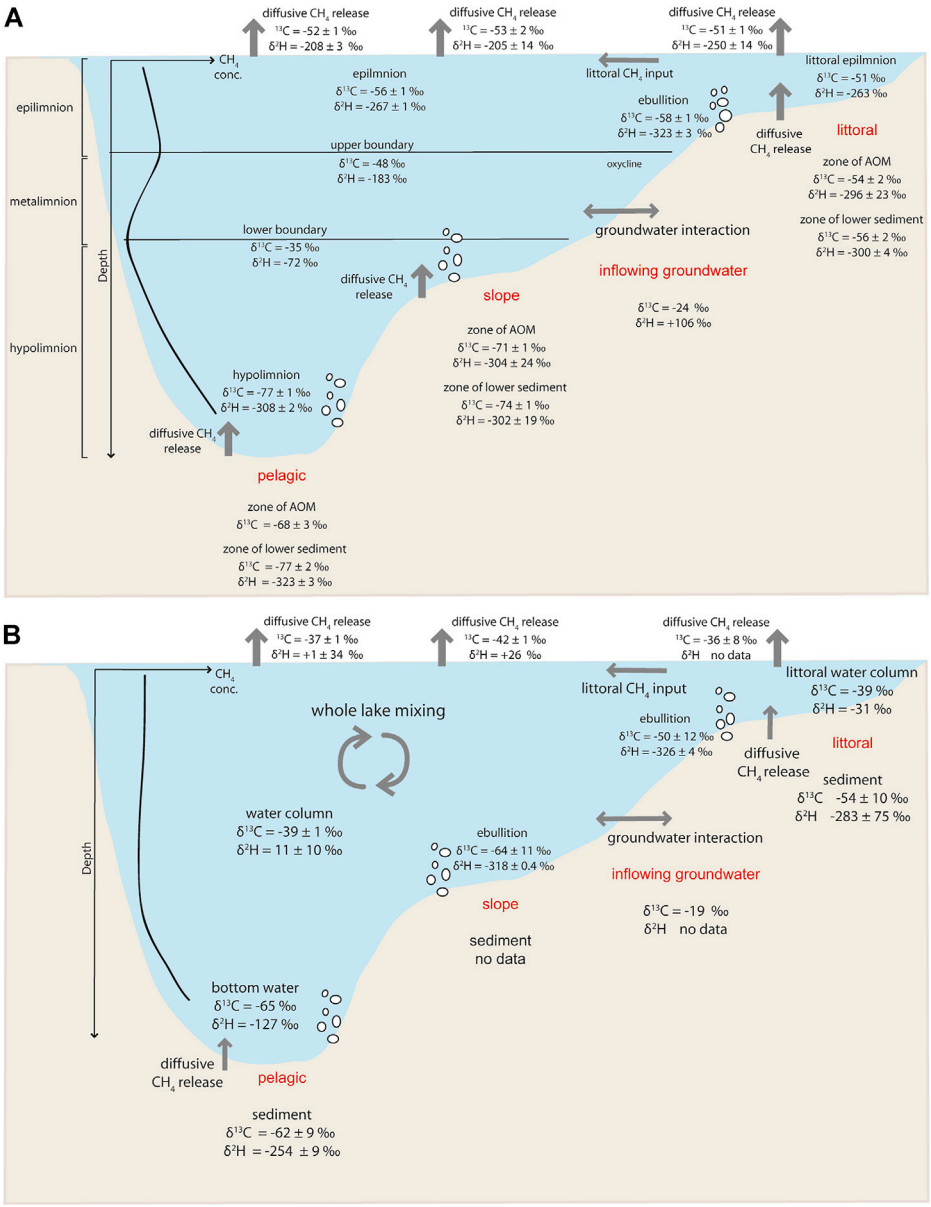


FIGURE 8
Methane cycling in Lake Willersinnweiher showing CH_4 sources and sinks with $\delta^{13}C$-CH_4 and $\delta^{2}H$-CH_4 values (where available) as well as transport mechanisms (grey) of different water layers (black) observed at the three investigated sites during **(A)** the stratification period (July 2020, for diffusive release at water-air interface data from July 2021 is shown and for ebullition data from September 2021) and **(B)** the mixing period (March 2021 and for ebullition data from November 2020 is shown).

Thottathil et al., 2022). In Lake Willersinnweiher, CH_4 in the oxic upper water column peaked at a water depth of 6 m during the stratification period, which was accompanied by an increase in the $\delta^{13}C$-CH_4 and $\delta^{2}H$-CH_4 values to −48‰ and −183‰, respectively, compared to surface water $\delta^{13}C$-CH_4 values of −57‰ and $\delta^{2}H$-CH_4 values of −269‰ (Figure 3A). Although the isotopic signature of CH_4 produced in the oxic water column is hitherto unknown, Hartmann et al. (2020) proposed that oxic CH_4 production might cause an enrichment in ^{13}C in the CH_4 pool in the lake surface layer. More recently, $\delta^{13}C$ mass balance estimates by Thottathil et al. (2022) supported this finding by stating that CH_4 produced from oxic sources is relatively enriched in ^{13}C compared to anoxic sources with $\delta^{13}C$-CH_4 values ranging between −64 and −38‰. More positive $\delta^{13}C$-CH_4 values in the surface mixed layer compared to sedimentary $\delta^{13}C$-CH_4 values have also been

found in other oxic lakes such as Lake Stechlin (−50‰; Tang et al., 2014), Lake Cromwell (−40‰; Bogard et al., 2014) and Lake Lugano (−55‰; Blees et al., 2014). These isotopic values are in line with the observed increase in δ^{13}C-CH_4 values to around −48‰ in the upper metalimnion during the stratification period in Lake Willersinnweiher. The slight enrichment in ^{13}C might be due to different precursors and pathways of *in situ* oxic CH_4 production compared to anoxic methanogenesis and/or an interplay of co-occurring MOx. (Donis et al., 2017). Beyond δ^{13}C-CH_4 values, better constraints on δ^{2}H-CH_4 values of oxic CH_4 production would assist in the characterization of *in situ* produced CH_4 in the oxic environment as well as the possible influence of MOx in the observation of enriched stable isotope values of CH_4.

The exact pathways of CH_4 formation in the oxic water column are not fully understood to date. However recently, Ernst et al. (2022) suggested a reaction mechanism for CH_4 formation associated to the interaction of reaction oxygen species with free iron and methylated sulfur and nitrogen compounds occurring on a cellular level across all living organisms and that increasing the level of oxidative stress enhanced the production of CH_4. Moreover, it has been discovered that cyanobacteria produce CH_4 (Bižić et al., 2020b) and that light as well as temperature yield a significant control over oxic CH_4 production rates by influencing phytoplankton communities (Klintzsch et al., 2020). Furthermore, the role of submerged macrophytes for oxic methane production has so far been ignored, but might also contribute significantly (Hilt et al., 2022). Hence, oxic CH_4 production is most likely closely coupled to primary production, potentially contributing to an increase in CH_4 concentrations in the surface water layer during the stratification period as it was also observed at Lake Willersinnweiher. A peak in chlorophyll-α co-occurring with maximum CH_4 concentrations in the upper metalimnion at Lake Willersinnweiher might support a linkage between CH_4 production and algal activity as proposed already in other studies (Grossart et al., 2011; Bogard et al., 2014; Tang et al., 2016; Hartmann et al., 2020; Thottathil et al., 2022). Nevertheless, Donis et al. (2017) suggested that the accumulation of CH_4 at the thermocline can be caused by physical processes in the water column and the highest production rates of CH_4 can be found in the surface water layer.

Beyond the 2-dimensional stable isotope approach, we applied a novel stable isotopic indicator $\Delta(2,13)$ introduced by Tsunogai et al. (2020) which corrects for fractionation effects caused by CH_4 oxidation, to isotopically characterize different sources of CH_4 to the lake and disentangle the sources of CH_4 to the lake surface water layer. Since the $\Delta(2,13)$ indicator has been introduced only recently more research is necessary to reliably assess its strengths and weaknesses to constrain CH_4 sources and sinks in aquatic systems. Hence, we only briefly discuss the application of this parameter in this section (for a more detailed description see Supplementary Annotations A1). $\Delta(2,13)$ values of the surface water layer showed good agreement at the pelagic and slope site (266 ± 4‰ and 260 ± 5‰, respectively) but differed distinctively from the littoral water column and sediment (214 ± 2‰ and 219 ± 33‰) (Supplementary Figure S2A). This might imply a different CH_4 source to the pelagic and slope surface water layer compared to the littoral site, making littoral input as the main CH_4 source in the entire lake surface water layer unlikely and potentially indicating internal oxic CH_4 production as an important source during the stratification period. However, it is important to note that $\Delta(2,13)$ only corrects for the fractionation effects caused by CH_4 oxidation and does not account for fractionation due to mixing of different CH_4 sources. Hence, mixing of vertically migrating sedimentary CH_4 and littoral CH_4 input might cause the observed shift in the epilimnic $\Delta(2,13)$ values of the pelagic and slope site compared to the littoral site.

Infiltrating groundwater might further contribute to CH_4 supersaturation in the surface water layer of Lake Willersinnweiher and most likely influenced lake water CH_4 during the entire year due to the lake's direct accessibility to the upper aquifer and high groundwater CH_4 concentrations around 1 μmol L^{-1} (Wollschläger et al., 2007). Possibly, groundwater CH_4 yielding less negative δ^{13}C-CH_4 and δ^{2}H-CH_4 values could also have contributed to the observed enrichment in ^{13}C and ^{2}H at the upper thermocline. So far the origin of the groundwater CH_4 remains unclear and different possibilities have been proposed to explain the source of CH_4 in the inflowing groundwater and its unusually positive isotopic signature including CH_4 production in a contamination site through oxidative biodegradation of hydrocarbons such as volatile chlorinated organic compounds, in organic-rich sediments from old branches of the Rhine river or in aquifers located upstream of Lake Willersinnweiher (Wollschläger et al., 2007; Kleint et al., 2021). Only limited data about groundwater CH_4 concentrations and δ^{13}C-CH_4 values are available to date and groundwater that enriched in ^{13}C-CH_4 and ^{2}H-CH_4 seems to be only a rare occurrence (Schloemer et al., 2016). The highly enriched isotopic values of infiltrating groundwater might point to intense AOM since the groundwater is suboxic. The oxidation might therefore be coupled to the reduction of other electron acceptors such as nitrate, nitrite, manganese and iron (Kleint et al., 2021). Methane oxidation causing the highly enriched isotopic composition of groundwater CH_4 might also be supported by the 2-dimensional isotope plot, revealing a distribution of inflowing and outflowing groundwater along the gradient of CH_4 oxidation at Lake Willersinnweiher (Figure 7).

Mixing of lake and groundwater might lead to a change towards more positive isotope values in the lake water column, however the impact of groundwater CH_4 on lake water CH_4 is hard to estimate based on the current dataset and more detailed research concerning groundwater CH_4 in the area of Lake

Willersinnweiher is desirable. Due to lower primary productivity and lower CH_4 concentrations in the lake during the mixing period we suggest that groundwater input might be an important source of CH_4 to the lake especially during the mixing period. This might also contribute to the less negative isotopic composition of lake water CH_4 observed during the mixing period (Figures 3G, 4G, 5G).

Supersaturation of CH_4 in the surface water leads to CH_4 release into the atmosphere during the stratification period. Additionally, the surface water was also oversaturated with CH_4 during the mixing period (70 nmol L^{-1}, Figures 3G, 4G, 5G), highlighting that Lake Willersinnweiher emits CH_4 all year round. Methane can be emitted *via* plant-mediated processes, diffusion or ebullitive transport (Bastviken et al., 2004), however since plant-coverage at Lake Willersinnweiher is negligible, plant-mediated release of CH_4 to the atmosphere is considered to be of minor importance. Methane emitted *via* diffusion from the surface water into the atmosphere showed a great range in the isotopic composition over 1 year with most positive values found at the three investigated sites during the mixing period (δ^{13}C-CH_4 of −42 to −37‰ and δ^2H-CH_4 of +1 to +26‰) and distinctively lower values observed during the stratification period (δ^{13}C-CH_4 of −59 to −51‰ and δ^2H-CH_4 of −310 to −195‰, Table 2). These isotopic values reflect the isotopic composition of lake surface water, which is enriched in the heavier isotopes during the mixing period. Especially during the mixing period, ^{13}C-CH_4 and ^{2}H-CH_4 were much more enriched compared to previously reported values (e.g., from Thottathil and Prairie, 2021 ranging from −58.8‰ to −43.5‰), highlighting the potential impact and importance of diffusive CH_4 emissions from lakes with similar properties, such as high sulfate concentrations, for regional and/or global isotope source apportionment studies.

We found that in Lake Willersinnweiher, δ^{13}C-CH_4 and δ^2H-CH_4 values of CH_4 released *via* ebullition displayed temporal and spatial disparities (Figure 8). At the deeper sampling site, CH_4 transported *via* ebullition yielded more negative δ^{13}C-CH_4 values (−64 ± 11‰) when compared to δ^{13}C-CH_4 values at the littoral site (−50 ± 12‰ during the mixing period in November 2021). These differences in the isotopic composition were most likely induced by CH_4 formation taking place mainly *via* the hydrogenotrophic and acetoclastic pathways at the slope and littoral sites, respectively, as discussed above. Ebullition plays a particularly important role in the littoral area of aquatic systems since the potential for CH_4 transported *via* gas bubbles rises to reach the surface water with decreasing water depth. In particular, CH_4 release to the atmosphere *via* ebullition likely represents an important pathway and has been found to vary significantly spatially and temporally (West et al., 2016; Thottathil and Prairie, 2021). Interestingly, δ^2H-CH_4 values only show small differences between the littoral and slope site at Lake Willersinnweiher (326 ± 4‰ for the littoral site and 318 ± 1‰ for the slope site, Figure 8B). In previous studies, changes in the δ^2H-CH_4 values of CH_4 emitted *via* ebullition were attributed to changes in the δ^2H values of water (e.g. due to evaporation in shallow lakes), which is a hydrogen source for methanogens (Wik et al., 2020). As Lake Willersinnweiher is a distinctively deeper lake (average depth of 8 m), this effect might only play a minor role and therefore have a smaller influence on δ^2H-CH_4 values. However, Douglas et al. (2021) showed that even though the δ^2H-H_2O values highly influenced δ^2H-CH_4 values, other processes such as methane oxidation and the type of the methanogenic pathway might also contribute to the isotopic composition of CH_4. Furthermore, sulfate-dependent AOM in the sediments of lake Willersinnweiher might play an important role regarding the isotopic composition of CH_4 released *via* ebullition and therefore might affect δ^{13}C-CH_4 values and to a lesser extent δ^2H-CH_4 values (Wegener et al., 2021). However, the influence of AOM is hard to estimate as AOM most probably takes place heterogeneously throughout the sediment. In November, when there is less organic matter input than in September (which is also indicated by the lower CH_4 concentrations within the gas bubbles, Supplementary Table S2), pockets of CH_4 within the sediment might be subject to heterogeneously occurring AOM, which might contribute to the relatively high variability of δ^{13}C-CH_4 values. During the uprise of gas bubbles in the water column, CH_4 partly dissolves into the water (e.g. McGinnis et al., 2006). However, isotope fractionation associated with dissolution of CH_4 was found to be small and most likely lower than the variability of the measured isotope values (Fuex, 1980; Bergamaschi, 1997). Additionally, the surface water layer showed isotopic values enriched in ^{13}C and ^{2}H compared to the gas bubbles (δ^{13}C-CH_4 of −56‰ and δ^2H-CH_4 of −270‰ for lake surface water and δ^{13}C-CH_4 of −64 ± 11‰ and δ^2H-CH_4 of −318 ± 1‰ for ebullitive CH_4). We therefore conclude that ebullition is not the main source of surface water CH_4 supersaturation in the pelagic area of the lake.

Conclusion

We investigated the sources and sinks of CH_4 in a seasonally stratified freshwater lake using concentration measurements of CH_4 and dual isotope analysis. Our main findings are presented in Figures 8A,B for the stratification period and the mixing period:

- δ^{13}C-CH_4 and δ^2H-CH_4 values of sedimentary CH_4, anaerobic methanogenesis at the three investigated sites indicated a mix of the hydrogenotrophic and acetoclastic pathway at the pelagic and slope site and an increasing dominance of the acetoclastic methanogenesis towards the shallower littoral site. During the mixing period, the dominance of hydrogenotrophic methanogenesis

potentially increased at the pelagic and slope sites. Throughout the whole year, sulfate-dependent AOM caused shifts towards heavier δ^{13}C-CH_4 and δ^{2}H-CH_4 values in the upper sediment and reduced the diffusive release of CH_4 at the sediment-water interface.
- MOx efficiently consumed upward migrating CH_4 in the water column during thermal stratification of the lake, indicated by a strong enrichment of ^{13}C-CH_4 and ^{2}H-CH_4 values.
- Supersaturation of CH_4 in the surface water was present both during the stratification period and the mixing period, whereas supersaturation during the stratification period was significantly higher than supersaturation during the mixing period. Supersaturation of CH_4 in the pelagic area of the lake possibly originated from the vertical and lateral input of sedimentary and littoral CH_4, however oxic CH_4 production might also supply CH_4 to the surface water layer of the lake and might contribute to a local peak in concentrations at the upper thermocline during the stratification period. On the contrary, CH_4 input from groundwater with unusually positive δ^{13}C-CH_4 and δ^{2}H-CH_4 values and CH_4 diffusion from the littoral sediment were most likely the main source of lake water CH_4 during the mixing period, leading to rather positive isotopic δ^{13}C-CH_4 and δ^{2}H-CH_4 values in the water column.
- Methane released from the water into the atmosphere *via* diffusion covered a wide range from −59 to −36‰ for δ^{13}C-CH_4 and −310 to +26‰ for δ^{2}H-CH_4 values during the stratification period and mixing of the water column during the mixing period, highlighting the potential importance of diffusive CH_4 emissions from lakes with similar properties for regional and/or global isotope source apportionment studies.

Our study provides an overview of the isotopic characteristics of CH_4 sources and sinks in a seasonally stratified lake and gives new insight into the sources contributing to CH_4 supersaturation in the surface water layer of lacustrine systems. It furthermore outlines the potential for disentangling different sources and sinks both spatially and temporally based on their isotopic signature, especially considering the still highly debated contribution of oxic CH_4 production to lake water CH_4 concentrations. This clearly highlights the need for a multiparameter approach including the investigation of stable isotopes when researching the complex CH_4 dynamics in an aquatic system since only then can a complete understanding of the involved processes be achieved.

Data availability statement

The experimental data used in this study are available from heiDATA, which is an institutional repository for research data of the Heidelberg University (https://doi.org/10.11588/data/KLFDVF). Requests to access the datasets should be directed to teresa.einzmann@unibas.ch.

Author contributions

FK, TE, and MS conceived the study. TE and MS performed the field measurements and experiments under supervision of FK. TE and MS analyzed the data and visualized the results. MG validated stable isotope measurements of methane and analyzed stable carbon isotope measurements of dissolved inorganic carbon. TE, MS, FK, and JK discussed the results. The manuscript was written under the lead of TE and MS, with contribution of all authors.

Funding

This study was supported by DFG (German Research Foundation, project KE 884/16-2).

Acknowledgments

We thank Stefan Rheinberger, Silvia Rheinberger and Christian Scholz for analytical support. We are grateful to Bernd Knape for technical support in the laboratory and field. We thank Kai Ernst, Hannah Geisinger, Martin Lienenlüke, Iva Ralenekova and Timo Schreiter for help with field work and support in data analysis.

Conflict of interest

The authors declare that the research was conducted in the absence of any commercial or financial relationships that could be construed as a potential conflict of interest.

Publisher's note

All claims expressed in this article are solely those of the authors and do not necessarily represent those of their affiliated organizations, or those of the publisher, the editors and the reviewers. Any product that may be evaluated in this article, or claim that may be made by its manufacturer, is not guaranteed or endorsed by the publisher.

Supplementary material

The Supplementary Material for this article can be found online at: https://www.frontiersin.org/articles/10.3389/fenvs.2022.865862/full#supplementary-material

References

Alperin, M. J., Reeburgh, W. S., and Whiticar, M. J. (1988). Carbon and hydrogen isotope fractionation resulting from anaerobic methane oxidation. *Glob. Biogeochem. Cycles* 2, 279–288. doi:10.1029/GB002i003p00279

Barker, J. F., and Fritz, P. (1981). Carbon isotope fractionation during microbial methane oxidation. *Nature* 293, 289–291. doi:10.1038/293289a0

Bastviken, D., Cole, J., Pace, M., and Tranvik, L. (2004). Methane emissions from lakes: Dependence of lake characteristics, two regional assessments, and a global estimate. *Glob. Biogeochem. Cycles* 18, 1–12. doi:10.1029/2004GB002238

Bastviken, D., Ejlertsson, J., and Tranvik, L. (2002). Measurement of methane oxidation in lakes: A comparison of methods. *Environ. Sci. Technol.* 36, 3354–3361. doi:10.1021/es010311p

Belle, S., Verneaux, V., Millet, L., Parent, C., and Magny, M. (2015). A case study of the past CH_4 cycle in lakes by the combined use of dual isotopes (carbon and hydrogen) and ancient DNA of methane-oxidizing bacteria: Rearing experiment and application to lake remoray (eastern France). *Aquat. Ecol.* 49, 279–291. doi:10.1007/s10452-015-9523-6

Bergamaschi, P. (1997). Seasonal variations of stable hydrogen and carbon isotope ratios in methane from a Chinese rice paddy. *J. Geophys. Res.* 102, 25383–25393. doi:10.1029/97jd01664

Bižić, M., Grossart, H., and Ionescu, D. (2020a). "Methane paradox," in *eLS* (Chichester: John Wiley & Sons). doi:10.1002/9780470015902.a0028892

Bižić, M., Klintzsch, T., Ionescu, D., Hindiyeh, M. Y., Günthel, M., Muro-Pastor, A. M., et al. (2020b). Aquatic and terrestrial cyanobacteria produce methane. *Sci. Adv.* 6, eaax5343–10. doi:10.1126/sciadv.aax5343

Blees, J., Niemann, H., Wenk, C. B., Zopfi, J., Schubert, C. J., Kirf, M. K., et al. (2014). Micro-aerobic bacterial methane oxidation in the chemocline and anoxic water column of deep south-Alpine Lake Lugano (Switzerland). *Limnol. Oceanogr.* 59, 311–324. doi:10.4319/lo.2014.59.2.0311

Boetius, A., Ravenschlag, K., Schubert, C. J., Rickert, D., Widdel, F., Gieseke, A., et al. (2000). A marine microbial consortium apparently mediating anaerobic oxidation of methane. *Nature* 407, 623–626. doi:10.1038/35036572

Bogard, M. J., del Giorgio, P. A., Boutet, L., Chaves, M. C. G., Prairie, Y. T., Merante, A., et al. (2014). Oxic water column methanogenesis as a major component of aquatic CH_4 fluxes. *Nat. Commun.* 5, 5350. doi:10.1038/ncomms6350

Cadieux, S. B., White, J. R., Sauer, P. E., Peng, Y., Goldman, A. E., and Pratt, L. M. (2016). Large fractionations of C and H isotopes related to methane oxidation in Arctic lakes. *Geochimica Cosmochimica Acta* 187, 141–155. doi:10.1016/j.gca.2016.05.004

Casper, P., Maberly, S. C., Hall, G. H., and Finlay, B. J. (2000). Fluxes of methane and carbon dioxide from a small productive lake to the atmosphere. *Biogeochemistry* 49, 1–19. doi:10.1023/a:1006269900174

Chang, P.-C., Yang, T. F., Wallmann, K., Matsumoto, R., Hu, C.-Y., Chen, H. W., et al. (2019). Carbon isotope exchange during anaerobic oxidation of methane (AOM) in sediments of the northeastern South China Sea. *Geochimica Cosmochimica Acta* 246, 138–155. doi:10.1016/j.gca.2018.11.003

Coleman, D. D., Risatti, J. B., and Schoell, M. (1981). Fractionation of carbon and hydrogen isotopes by methane-oxidizing bacteria. *Geochimica Cosmochimica Acta* 45, 1033–1037. doi:10.1016/0016-7037(81)90129-0

Conrad, R. (2005). Quantification of methanogenic pathways using stable carbon isotopic signatures: A review and a proposal. *Org. Geochem.* 36, 739–752. doi:10.1016/j.orggeochem.2004.09.006

Donis, D., Flury, S., Stöckli, A., Spangenberg, J. E., Vachon, D., and McGinnis, D. F. (2017). Full-scale evaluation of methane production under oxic conditions in a mesotrophic lake. *Nat. Commun.* 8, 1661. doi:10.1038/s41467-017-01648-4

Douglas, P. M. J., Stratigopoulos, E., Park, S., and Phan, D. (2021). Geographic variability in freshwater methane hydrogen isotope ratios and its implications for global isotopic source signatures. *Biogeosciences* 18, 3505–3527. doi:10.5194/bg-18-3505-2021

Downing, J. A., Prairie, Y. T., Cole, J. J., Duarte, C. M., Tranvik, L. J., Striegl, R. G., et al. (2006). The global abundance and size distribution of lakes, ponds and impoundments. *Limnol. Oceanogr.* 51, 2388–2397. doi:10.4319/lo.2006.51.5.2388

Duc, N. T., Crill, P., and Bastviken, D. (2010). Implications of temperature and sediment characteristics on methane formation and oxidation in lake sediments. *Biogeochemistry* 100, 185–196. doi:10.1007/s10533-010-9415-8

Ernst, L., Steinfeld, B., Barayeu, U., Klintzsch, T., Kurth, M., Grimm, D., et al. 2022, methane formation driven by reactive oxygen species across all living organisms *Nature*, 603, 482, doi:10.1038/s41586-022-04511-9

Feisthauer, S., Vogt, C., Modrzynski, J., Szlenkier, M., Krüger, M., Siegert, M., et al. (2011). Different types of methane monooxygenases produce similar carbon and hydrogen isotope fractionation patterns during methane oxidation. *Geochimica Cosmochimica Acta* 75, 1173–1184. doi:10.1016/j.gca.2010.12.006

Fernández, J. E., Peeters, F., and Hofmann, H. (2016). On the methane paradox: Transport from shallow water zones rather than *in situ* methanogenesis is the major source of CH4 in the open surface water of lakes. *J. Geophys. Res. Biogeosci.* 121, 2717–2726. doi:10.1002/2016JG003586

Fuex, A. N. (1980). Experimental evidence against an appreciable isotopic fractionation of methane during migration. *Phys. Chem. Earth* 12, 725–732. doi:10.1016/0079-1946(79)90153-8

Gonzalez Moguel, R., Bass, A. M., Garnett, M. H., Pilote, M., Keenan, B., Matveev, A., et al. (2021). Radiocarbon data reveal contrasting sources for carbon fractions in thermokarst lakes and rivers of eastern Canada (nunavik, quebec). *J. Geophys. Res. Biogeosci.* 126, 1–16. doi:10.1029/2020JG005938

Grossart, H.-P., Frindte, K., Dziallas, C., Eckert, W., and Tang, K. W. (2011). Microbial methane production in oxygenated water column of an oligotrophic lake. *Proc. Natl. Acad. Sci. U. S. A.* 108, 19657–19661. doi:10.1073/pnas.1110716108

Günthel, M., Donis, D., Kirillin, G., Ionescu, D., Bižić, M., McGinnis, D. F., et al. (2019). Contribution of oxic methane production to surface methane emission in lakes and its global importance. *Nat. Commun.* 10, 5497. doi:10.1038/s41467-019-13320-0

Hartmann, J. F., Günthel, M., Klintzsch, T., Kirillin, G., Grossart, H.-P., Keppler, F., et al. (2020). High spatiotemporal dynamics of methane production and emission in oxic surface water. *Environ. Sci. Technol.* 54, 1451–1463. doi:10.1021/acs.est.9b03182

Hilt, S., Grossart, H. P., McGinnis, D. F., and Keppler, F. (2022). Potential role of submerged macrophytes for oxic methane production in aquatic ecosystems. *Limnol. Oceanogr.* doi:10.1002/lno.12095

Hofmann, H., Federwisch, L., and Peeters, F. (2010). Wave-induced release of methane: Littoral zones as source of methane in lakes. *Limnol. Oceanogr.* 55, 1990–2000. doi:10.4319/lo.2010.55.5.1990

Holler, T., Wegener, G., Knittel, K., Boetius, A., Brunner, B., Kuypers, M. M. M., et al. (2009). Substantial $^{13}C/^{12}C$ and D/H fractionation during anaerobic oxidation of methane by marine consortia enriched in vitro. *Environ. Microbiol. Rep.* 1, 370–376. doi:10.1111/j.1758-2229.2009.00074.x

Holmer, M., and Storkholm, P. (2001). Sulphate reduction and sulphur cycling in Lake sediments: A review. *Freshw. Biol.* 46, 431–451. doi:10.1046/j.1365-2427.2001.00687.x

Isenbeck-Schröter, M., Aeschbach, W., Al Najem, S., Freundt, F., and Schmidt, G. (2016). Trace - TiefenReservoir-Analyse und Charakterisierung von der Erdoberfläche: Geochemisch-isotopisches Multimethoden-Konzept zur Charakterisierung tiefer Aquifere: Abschlussbericht TRACE Teil B. *Tech. Inf. Hann.* 95. doi:10.2314/GBV:871282461

Kampbell, D. H., Wilson, J. T., and Vandegrift, S. A. (1989). Dissolved oxygen and methane in water by a GC headspace equilibration technique. *Int. J. Environ. Anal. Chem.* 36, 249–257. doi:10.1080/03067318908026878

Keeling, C. D. (1958). The concentration and isotopic abundances of atmospheric carbon dioxide in rural areas. *Geochimica Cosmochimica Acta* 13, 322–334. doi:10.1016/0016-7037(58)90033-4

Keppler, F., Hamilton, J. T. G., Braß, M., and Röckmann, T. (2006). Methane emissions from terrestrial plants under aerobic conditions. *Nature* 439, 187–191. doi:10.1038/nature04420

Keppler, F., Schiller, A., Ehehalt, R., Greule, M., Hartmann, J., and Polag, D. (2016). Stable isotope and high precision concentration measurements confirm that all humans produce and exhale methane. *J. Breath. Res.* 10, 016003. doi:10.1088/1752-7155/10/1/016003

Kinnaman, F. S., Valentine, D. L., and Tyler, S. C. (2007). Carbon and hydrogen isotope fractionation associated with the aerobic microbial oxidation of methane, ethane, propane and butane. *Geochimica Cosmochimica Acta* 71, 271–283. doi:10.1016/j.gca.2006.09.007

Kleint, J. F., Wellach, Y., Schroll, M., Keppler, F., and Isenbeck-Schröter, M. (2021). *The impact of seasonal sulfate–methane transition zones on methane cycling in a sulfate-enriched freshwater environment: Limnology and Oceanography*, 1–19. doi:10.1002/lno.11754

Klintzsch, T., Langer, G., Wieland, A., Geisinger, H., Lenhart, K., Nehrke, G., et al. (2020). Effects of temperature and light on methane production of widespread marine phytoplankton. *J. Geophys. Res. Biogeosci.* 125. doi:10.1029/2020jg005793

Knittel, K., and Boetius, A. (2009). Anaerobic oxidation of methane: Progress with an unknown process. *Annu. Rev. Microbiol.* 63, 311–334. doi:10.1146/annurev.micro.61.080706.093130

Laukenmann, S. (2002). *Transport und Austausch redoxsensitiver Elemente zwischen Freiwasser und Sediment in einem eutrophen Hartwassersee*

(Willersinnweiher/Ludwigshafen), unter besonderer Berücksichtigung des geochemischen Verhaltens von Uran. Heidelberg, BW: Ruprecht-Karls-Universität Heidelberg, 125. doi:10.11588/heidok.00002919

Lenhart, K., Bunge, M., Ratering, S., Neu, T. R., Schuttmann, I., Greule, M., et al. (2012). Evidence for methane production by saprotrophic fungi. *Nat. Commun.* 3, 1046–1048. doi:10.1038/ncomms2049

Lenhart, K., Klintzsch, T., Langer, G., Nehrke, G., Bunge, M., Schnell, S., et al. (2015). Evidence for methane production by marine algae (Emiliana huxleyi) and its implication for the methane paradox in oxic waters. *Biogeosciences Discuss.* 12, 20323–20360. doi:10.5194/bgd-12-20323-2015

Lessner, D. J. (2009). "Methanogenesis biochemistry," in *eLS*. doi:10.1002/9780470015902.a0000573.pub2*Chichester*

Loken, L. C., Crawford, J. T., Schramm, P. J., Stadler, P., Desai, A. R., and Stanley, E. H. (2019). Large spatial and temporal variability of carbon dioxide and methane in a eutrophic lake. *J. Geophys. Res. Biogeosci.* 124, 2248–2266. doi:10.1029/2019JG005186

Martens, C. S., Albert, D. B., and Alperin, M. J. (1999). Stable isotope tracing of anaerobic methane oxidation in the gassy sediments of Eckernfoerde Bay, German Baltic Sea. *Am. J. Sci.* 299, 589–610. doi:10.2475/ajs.299.7-9.589

McGinnis, D. F., Greinert, J., Artemov, Y., Beaubien, S. E., and Wüest, A. (2006). Fate of rising methane bubbles in stratified waters: How much methane reaches the atmosphere? *J. Geophys. Res.* 111, C09007. doi:10.1029/2005JC003183

Murase, J., and Sugimoto, A. (2005). Inhibitory effect of light on methane oxidation in the pelagic water column of a mesotrophic lake (Lake Biwa, Japan). *Limnol. Oceanogr.* 50, 1339–1343. doi:10.4319/lo.2005.50.4.1339

Natchimuthu, S., Sundgren, I., Gålfalk, M., Klemedtsson, L., Crill, P., Danielsson, Å., et al. (2016). Spatio-temporal variability of lake CH_4 fluxes and its influence on annual whole lake emission estimates. *Limnol. Oceanogr.* 61, S13–S26. doi:10.1002/lno.10222

Oswald, K., Milucka, J., Brand, A., Littmann, S., Wehrli, B., Kuypers, M. M. M., et al. (2015). Light-dependent aerobic methane oxidation reduces methane emissions from seasonally stratified lakes. *PLoS ONE* 10, e0132574. doi:10.1371/journal.pone.0132574

Pataki, D. E., Ehleringer, J. R., Flanagan, L. B., Yakir, D., Bowling, D. R., Still, C. J., et al. (2003). The application and interpretation of Keeling plots in terrestrial carbon cycle research. *Glob. Biogeochem. Cycles* 17, 1022. doi:10.1029/2001gb001850

Peeters, F., Fernandez, J. E., and Hofmann, H. (2019). Sediment fluxes rather than oxic methanogenesis explain diffusive CH_4 emissions from lakes and reservoirs. *Sci. Rep.* 9, 243. doi:10.1038/s41598-018-36530-w

Peeters, F., and Hofmann, H. (2021). Oxic methanogenesis is only a minor source of lake-wide diffusive CH_4 emissions from lakes. *Nat. Commun.* 12, 1206. doi:10.1038/s41467-021-21215-2

Powelson, D. K., Chanton, J. P., and Abichou, T. (2007). Methane oxidation in biofilters measured by mass-balance and stable isotope methods. *Environ. Sci. Technol.* 41, 620–625. doi:10.1021/es061656g

Rasigraf, O., Vogt, C., Richnow, H. H., Jetten, M. S., and Ettwig, K. F. (2012). Carbon and hydrogen isotope fractionation during nitrite-dependent anaerobic methane oxidation by Methylomirabilis oxyfera. *Geochimica Cosmochimica Acta* 89, 256–264. doi:10.1016/j.gca.2012.04.054

Reeburgh, W. S. (2007). Oceanic methane biogeochemistry. *Chem. Rev.* 107, 486–513. doi:10.1021/cr050362v

Rosentreter, J. A., Borges, A. V., Deemer, B. R., Holgerson, M. A., Liu, S., Song, C., et al. (2021). Half of global methane emissions come from highly variable aquatic ecosystem sources. *Nat. Geosci.* 14, 225–230. doi:10.1038/s41561-021-00715-2

Sandler, B. (2000). *Die Wirkung von Sanierungs- und Restaurierungsmaßnahmen auf die Nährstoffströme und die biotische Dynamik eines anthropogenen Gewässers am Beispiel des Willersinnweihers/Ludwigshafen*. Heidelberg, BW: Ruprecht-Karls-Universität Heidelberg, 190.

Schloemer, S., Elbracht, J., Blumenberg, M., and Illing, C. J. (2016)., 67. Germany, 118–132. doi:10.1016/J.APGEOCHEM.2016.02.005Distribution and origin of dissolved methane, ethane and propane in shallow groundwater of Lower Saxony, Germany*Appl. Geochem.*

Schröder, H. (2004). *Saisonale Redoxfronten im Kopplungsbereich zwischen Schwefel- Eisen- und Mangankreislauf im System Seewasser – sediment – Grundwasser des Willersinnweihers*. Heidelberg, BW: Ruprecht-Karls-Universität Heidelberg, 122. doi:10.11588/heidok.00004894

Schubert, C. J., Lucas, F. S., Durisch-Kaiser, E., Stierli, R., Diem, T., Scheidegger, O., et al. (2010). Oxidation and emission of methane in a monomictic lake (Rotsee, Switzerland). *Aquat. Sci.* 72, 455–466. doi:10.1007/s00027-010-0148-5

Schubert, C. J., Vazquez, F., Lösekann-Behrens, T., Knittel, K., Tonolla, M., and Boetius, A. (2011). Evidence for anaerobic oxidation of methane in sediments of a freshwater system (Lago di Cadagno). *FEMS Microbiol. Ecol.* 76, 26–38. doi:10.1111/j.1574-6941.2010.01036.x

Silverman, M. P., and Oyama, V. I. (1968). Automatic apparatus for sampling and preparing gases for mass spectral analysis in studies of carbon isotope fractionation during methane metabolism. *Anal. Chem.* 40, 1833–1837. doi:10.1021/ac60268a001

Sugimoto, A., and Wada, E. (1995). Hydrogen isotopic composition of bacterial methane: CO_2/H_2 reduction and acetate fermentation. *Geochimica Cosmochimica Acta* 59, 1329–1337. doi:10.1016/0016-7037(95)00047-4

Tang, K. W., McGinnis, D. F., Frindte, K., Brüchert, V., and Grossart, H.-P. (2014). Paradox reconsidered: Methane oversaturation in well-oxygenated lake waters. *Limnol. Oceanogr.* 59, 275–284. doi:10.4319/lo.2014.59.1.0275

Tang, K. W., McGinnis, D. F., Ionescu, D., and Grossart, H.-P. (2016). Methane production in oxic lake waters potentially increases aquatic methane flux to air. *Environ. Sci. Technol. Lett.* 3, 227–233. doi:10.1021/acs.estlett.6b00150

Thottathil, S. D., and Prairie, Y. T. (2021). Coupling of stable carbon isotopic signature of methane and ebullitive fluxes in northern temperate lakes. *Sci. Total Environ.* 777, 146117. doi:10.1016/j.scitotenv.2021.146117

Thottathil, S. D., Reis, P. C. J., and Prairie, Y. T., 2022, Magnitude and drivers of oxic methane production in small temperate lakes, doi:10.1021/acs.est.2c01730

Thottathil, S. D., Reis, P. C. J., and Prairie, Y. T. (2019). Methane oxidation kinetics in northern freshwater lakes. *Biogeochemistry* 143, 105–116. doi:10.1007/s10533-019-00552-x

Tsunogai, U., Miyoshi, Y., Matsushita, T., Komatsu, D. D., Ito, M., Sukigara, C., et al. (2020). Dual stable isotope characterization of excess methane in oxic waters of a mesotrophic lake. *Limnol. Oceanogr.* 65, 2937–2952. doi:10.1002/lno.11566

Waldron, S., Lansdown, J. M., Scott, E. M., Fallick, A. E., and Hall, A. J. (1999). The global influence of the hydrogen isotope composition of water on that of bacteriogenic methane from shallow freshwater environments. *Geochimica Cosmochimica Acta* 63, 2237–2245. doi:10.1016/S0016-7037(99)00192-1

Walter, K. M., Chanton, J. P., Chapin, F. S., Schuur, E. A. G., and Zimov, S. A. (2008). Methane production and bubble emissions from arctic lakes: Isotopic implications for source pathways and ages. *J. Geophys. Res.* 113, G00A08. doi:10.1029/2007JG000569

Wang, D. T., Welander, P. V., and Ono, S. (2016). Fractionation of the methane isotopologues 13CH4, 12CH3D, and 13CH3D during aerobic oxidation of methane by *Methylococcus capsulatus* (Bath). *Geochimica Cosmochimica Acta* 192, 186–202. doi:10.1016/j.gca.2016.07.031

Wang, H., Lu, J., Wang, W., Yang, L., and Yin, C. (2006). Methane fluxes from the littoral zone of hypereutrophic Taihu Lake, China. *J. Geophys. Res.* 111, 17109. doi:10.1029/2005JD006864

Wegener, G., Gropp, J., Taubner, H., Halevy, I., and Elvert, M. (2021). Sulfate-dependent reversibility of intracellular reactions explains the opposing isotope effects in the anaerobic oxidation of methane. *Sci. Adv.* 7, eabe4939. doi:10.1126/sciadv.abe4939

West, W. E., Creamer, K. P., and Jones, S. E. (2016). Productivity and depth regulate lake contributions to atmospheric methane. *Limnol. Oceanogr.* 61, S51–S61. doi:10.1002/lno.10247

Whiticar, M. J. (1999). Carbon and hydrogen isotope systematics of bacterial formation and oxidation of methane. *Chem. Geol.* 161, 291–314. doi:10.1016/S0009-2541(99)00092-3

Whiticar, M. J., and Faber, E. (1986). Methane oxidation in sediment and water column environments - isotope evidence. *Org. Geochem.* 10, 759–768. doi:10.1016/S0146-6380(86)80013-4

Whiticar, M. J. (2020). "The biogeochemical methane cycle," in *Hydrocarbons, oils and lipids: Diversity, origin, chemistry and fate*. Editor H. Wilkes (Cham: Springer International Publishing), 669–746. doi:10.1007/978-3-319-90569-3_5

Wiesenburg, D. A., and Guinasso, N. L., Jr. (1979). Equilibrium solubilities of methane, carbon monoxide, and hydrogen in water and sea water. *J. Chem. Eng. Data* 24, 356–360. doi:10.1021/je60083a006

Wik, M., Thornton, B. F., Varner, R. K., McCalley, C., and Crill, P. M. (2020). Stable methane isotopologues from northern lakes suggest that ebullition is dominated by sub-lake scale processes. *J. Geophys. Res. Biogeosci.* 125. doi:10.1029/2019JG005601

Wollschläger, U., Ilmberger, J., Isenbeck-Schröter, M., Kreuzer, A. M., von Rohden, C., Roth, K., et al. (2007). Coupling of groundwater and surface water at Lake Willersinnweiher: Groundwater modeling and tracer studies. *Aquat. Sci.* 69, 138–152. doi:10.1007/s00027-006-0825-6

Yoshinaga, M. Y., Holler, T., Goldhammer, T., Wegener, G., Pohlman, J. W., Brunner, B., et al. (2014). Carbon isotope equilibration during sulphate-limited anaerobic oxidation of methane. *Nat. Geosci.* 7, 190–194. doi:10.1038/NGEO2069

Zhang, J., Quay, P. D., and Wilbur, D. O. (1995). Carbon isotope fractionation during gas-water exchange and dissolution of CO_2. *Geochimica Cosmochimica Acta* 59 (1), 107–114. doi:10.1016/0016-7037(95)91550-D

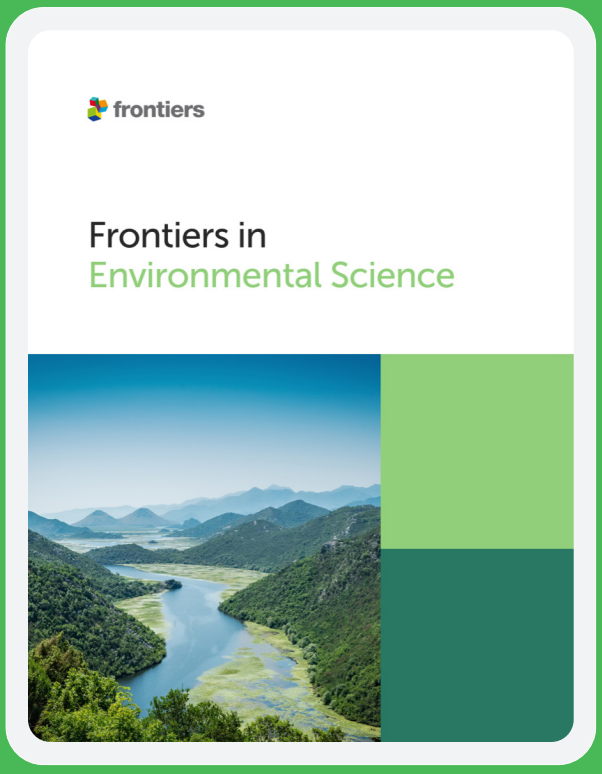
Frontiers in Environmental Science

Explores the anthropogenic impact on our natural world

An innovative journal that advances knowledge of the natural world and its intersections with human society. It supports the formulation of policies that lead to a more inhabitable and sustainable world.

Discover the latest Research Topics

See more →



Frontiers

Avenue du Tribunal-Fédéral 34
1005 Lausanne, Switzerland
frontiersin.org

Contact us

+41 (0)21 510 17 00
frontiersin.org/about/contact